Acta Chemica Scandinavica A 36 (1982) 1–5

Microwave Spectra and Structure of Six Isotopic Species of 1-Chlorophosphaethene, $CH_2=PCl$

BØRGE BAK, NIELS ARNT KRISTIANSEN and HENRIK SVANHOLT

Chemical Laboratory V, The H. C. Ørsted Institute, University of Copenhagen, DK-2100 Copenhagen Ø

Six isotopic species of 1-chlorophosphaethene, $CH_2=PCl$, have been produced by pyrolysis of CH_3OPCl_2, methyldichlorophosphite, $^{13}CH_3OPCl_2$ and CD_3OPCl_2. Vapor-phase microwave spectra (26.5 – 39.7 GHz) of $CH_2=P^{35,37}Cl$, $^{13}CH_2=P^{35,37}Cl$ and $CD_2=P^{35,37}Cl$ have been recorded and analyzed in a rigid rotor approximation (ground-level rotational constants A_o, B_o, C_o with inertial defects). Planar rigid models have been derived reproducing B_o, C_o for all six species almost within the experimental errors. The acceptable models have C=P distances close to 1.655 Å, P–Cl distances close to 2.060 Å and an angle CPCl = 103.3°. The angles around carbon are as in ethylene to within a degree.

In a "flow" system described earlier[1] CH_3OPCl_2, methyldichlorophosphite, splits off CH_3Cl at *ca.* 50 mTorr on a hot (825 °C) quartz surface as seen by microwave (mw) detection. However, the so far unknown stoichiometric moiety, POCl, the phosphorous analogue of nitrosyl chloride, has not yet been identified by us in mw spectra of products of pyrolysis recorded for the 26.5–39.7 GHz region. Over a 750–850 °C range of temperature the immediate results were spectra of readily identified $HC\equiv P$(I)[2] and $CH_2=PCl$(II)[3a] together with a new spectral series, L, of equidistant (~1655 MHz) line-groups (width ~10–15 MHz). The molecule, M(L), giving rise to L was shown to be a symmetric top (linear Stark effect) not containing chlorine since no chlorine isotope effect was noticed. L was finally assigned to P_4O_7 by subsequently replacing CH_3OPCl_2 by CD_3OPCl_2 (99 % enriched) and $^{13}CH_3OPCl_2$ (90 %) in our pyrolyses. In both cases expected isotopic shifts for I and II were observed whereas L was simply repeated. Thus, M(L) contains at most P and O. Its final identification as P_4O_7 will be reported in a separate paper.[3b] Here, rotational constants of the title compounds (Table 1) will be used to derive an approximate structure of II based on fewer structural elements from other molecules than earlier.[3a] Our observed mw spectra still involve unassigned lines mainly occurring at lower temperature (POCl?). However, the present paper is a necessary prequisite in a search for mw absorption by further species.

PREPARATIONS

Small-scale preparations of $^{12}CH_3OPCl_2$, $^{13}CH_3OPCl_2$ and $^{12}CD_3OPCl_2$ were performed in accordance with Ref. 4 adjusted to vacuum-line operations. Vapors of 20 mmol of $CH_3OH-{}^{13}CH_3OH-CD_3OH$ were condensed into 20 mmol of freshly distilled and magnetically stirred PCl_3 at –78 °C. The temperature was raised slowly (16 h) under stirring. An evolution of HCl(gas) started at –25 °C indicating the beginning of the reaction $CH_3OH+PCl_3\rightarrow CH_3OPCl_2+HCl$, the final volume of HCl at 20 °C corresponding to 100 % conversion. The reaction vessel was again cooled to –78 °C and HCl removed by pumping. Vial-to-vial separation was performed at bath temperature 0 °C (stirring). The pertinent vapor pressures (v.p.) are 40 m Torr (PCl_3), 30 mTorr (CH_3OH) and 15 mTorr (CH_3OPCl_2), the v.p. of $(CH_3O)_2PCl$ being unknown. Sample fractions of v.p. between 17 and 5 mTorr were collected and redistilled. Quantities of 800 mg (~6 mmol) of constant boiling CH_3OPCl_2, $^{13}CH_3OPCl_2$ and $^{12}CD_3OPCl_2$ (v.p. 15–16 mTorr at 0 °C) were obtained. Ref. 4 has v.p. = 15.5 mTorr. However, in pyrolyses the samples have to be kept at –50 °C (v.p. = 0.5 mTorr) to produce a necessary pressure in front of the oven.

0302-4377/82/010001-05$02.50

Tables 1. Isotopic species (ISOTOPES), percent enrichment (PERCENT), number of observed transitions N, rotational constants A_o, B_o, C_o(MHz) and inertial defects I.D. (u.Å.^{2}) for ground level. ROTFIT data treatment.[a]

ISOTOPES	PERCENT	N^b	A_o	B_o	C_o	I.D.
$^{12}CH_2=P-^{35}Cl$	75	11	22704(20)[c]	4667.26(7)[c]	3865.448(68)[c]	0.20(2)
$^{12}CH_2=P-^{37}Cl$	25	7	22662(34)	4539.04(10)	3775.72(10)	0.21(4)
$^{13}CH_2=P-^{35}Cl$	68	12	22118(16)	4559.177(55)	3774.048(55)	0.21(2)
$^{13}CH_2=P-^{37}Cl$	22	8	22065(38)	4433.51(12)	3685.92(12)	0.22(4)
$CD_2=P-^{35}Cl$	75	12	19652(6)	4322.593(26)	3537,424(26)	0.23(1)
$CD_2=P-^{37}Cl$	25	8	19549(27)	4205.26(11)	3456.94(11)	0.16(4)

[a] Ref. 6. [b] Includes resolved quadrupole components. [c] Ref. 3a has $A_o=22711.17$, $B_o=4667.23$, $C_o=3865.45$ MHz. No. experimental frequencies.

Prior to any pyrolyses PCl_3 was seen to be present in the samples (mw lines at 31407.0 and 36641.8 MHz at 1000 V/cm). This might be due to contamination in spite of the separations but more likely to equilibration such as $2CH_3OPCl_2$ (liq.) $\leftrightarrow(CH_3O)_2PCl+PCl_3$. Thus, the applied samples are more complicated than desirable. CH_3PCl_2 was absent. Table 1 summarizes the isotopic species studied, their abundance and, for sake of convenience, their final rotational constants and inertial defects.

MW SPECTRA. ROTATIONAL CONSTANTS

$K_{-1}=0$ and 1 μ_a-transitions were recorded at 1000 V/cm square-wave amplitude, $K_{-1}=2$ transitions at 300 V/cm (Table 2). The multiplet structure (when observed) due to the ^{35}Cl and ^{37}Cl quadrupoles was predictable and in fair agreement with experiment when based on quadrupole coupling constants for $NO^{35}Cl$ and $NO^{37}Cl$.[5] For unresolved patterns (^{37}Cl species; ^{35}Cl species with $K_{-1}=0$ and 1) positions of maximum intensity are reported in Table 2 both under F_A and ν_{RED}. This introduces errors of an estimated ±0.5 MHz. The r.m.s. deviations of Table 2 are of this order or less. The fits, $\nu_{RED}-\nu_{CALC}$, and the rotational constants were obtained using ROTFIT[6] in a rigid rotor approximation. The calculated inertial defects are of the same order as for $CH_2=NCN$.[7]

STRUCTURE OF $CH_2=P-Cl$

Pioneering work on the production of $CH_2=PCl$ by pyrolysis of CH_3PCl_2 (as different from CH_3OPCl_2) has been published in 1976 by Kroto and collaborators[3a] with a preliminary rigid planar model (rotational constants B_M, C_M) obtained by fitting the C=P distance and the angle α (Fig. 1) to the observed B_o and C_o of $CH_2=P^{35}Cl$ with a view to guarantee correct identification of the new species. The fit had $|B_o-B_M|\sim|C_o-C_M|\leq 5$ MHz.[3a] Knowing B_o and C_o for 6 isotopic species we want to draw more material into a derived structure. No r_s-structure can, of course, be obtained since only ($|a|$, $|b|$)=(1.252705, 0.147619) for chlorine and ($|a|$, $|b|$)=(1.604012, 0.783055) for carbon can be calculated (nominal numbers in the inertial system of $CH_2=P^{35}Cl$ (Fig. 1)). The resulting C···Cl distance is 2.926 Å. It should be reproduced approximately in any suggested structure. The "M_5" structure of Table 3 has C···Cl=2.924 Å. The

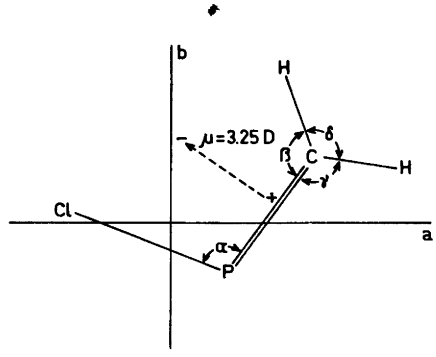

Fig. 1. 1-Chlorophosphaethene, $CH_2=PCl$, in the inertial system of $CH_2=P-^{35}Cl$. Bond angles α, β, γ, δ. Dipole moment $\mu=3.25$ Debye (D) from Ref. 15 with $\mu_a=2.68$ D and $\mu_b=1.84$ D. No experimental determination in this paper.

Table 2. Observed frequencies F_A (MHz) of μ_a-type transitions of 6 isotopic species of 1-chlorophosphaethene in the ground level. Frequencies corrected (see text) for chlorine quadrupole coupling effects ν_{RED}. Calculated frequencies ν_{CALC} based on a rigid rotor fit. ROTFIT r.m.s.[a]

	F_A				ν_{RED}	$\nu_{RED}-\nu_{CALC}$	r.m.s.
$^{12}CH_2=P^{35}Cl$							
$3_{13}\rightarrow4_{14}$	32476.25				32476.25	−0.241	0.1618
$3_{03}\rightarrow4_{04}$	33871.16				33871.16	0.086	
$3_{22}\rightarrow4_{23}$	34108.17	34109.75	34112.43	34113.72	34110.88	0.377	
$3_{21}\rightarrow4_{22}$	34367.68	34369.02	34371.78	34373.17	34370.28	0.019	
$3_{12}\rightarrow4_{13}$	35680.31				35680.31	−0.241	
$^{12}CH_2=P^{37}Cl$							
$3_{13}\rightarrow4_{14}$	31686.14				31686.14	−0.390	0.5621
$3_{03}\rightarrow4_{04}$	33024.50				33024.50	0.174	
$3_{22}\rightarrow4_{23}$	33239.23	33242.38			33241.23	0.543	
$3_{21}\rightarrow4_{22}$	33473.81	33476.42			33475.47	0.063	
$3_{12}\rightarrow4_{13}$	34736.70				34736.70	−0.389	
$^{13}CH_2=P^{35}Cl$							
$3_{13}\rightarrow4_{14}$	31712.53				31712.53	−0.174	0.2955
$3_{03}\rightarrow4_{04}$	33076.31	33077.44			33077.14	0.029	
$3_{22}\rightarrow4_{23}$	33310.58	33311.84	33314.72	33715.91	33313.21	0.336	
$3_{21}\rightarrow4_{22}$	33566.05	33567.46	33570.13	33571.49	33568.64	−0.017	
$3_{12}\rightarrow4_{13}$	34849.88				34849.88	−0.174	
$^{13}CH_2P^{37}Cl$							
$3_{13}\rightarrow4_{14}$	30937.17				30937.17	−0.136	0.6277
$3_{03}\rightarrow4_{04}$	32245.64	32246.23			32246.07	−0.250	
$3_{22}\rightarrow4_{23}$	32457.81	32461.84			32460.38	0.786	
$3_{21}\rightarrow4_{22}$	32688.72	32691.82			32690.69	−0.264	
$3_{12}\rightarrow4_{13}$	33924.80				33924.80	−0.136	
$CD_2=P^{35}Cl$							
$3_{13}\rightarrow4_{14}$	29813.03				29813.03	0.018	0.1309
$3_{03}\rightarrow4_{04}$	31148.44				31148.44	−0.151	
$3_{22}\rightarrow4_{23}$	31414.65	31416.48	31418.74	31419.48	31417.25	0.037	
$3_{21}\rightarrow4_{22}$	31705.89	31707.62	31710.14	31711.71	31708.59	−0.101	
$3_{12}\rightarrow4_{13}$	32949.58				32949.58	0.107	
$4_{14}\rightarrow5_{15}$	37215.74				37215.74	0.071	
$CD_2P^{37}Cl$							
$3_{13}\rightarrow4_{14}$	29100.05				29100.05	−0.388	0.4513
$3_{03}\rightarrow4_{04}$	30384.10				30384.10	0.401	
$3_{22}\rightarrow4_{23}$	30626.00	30629.50			30628.20	0.213	
$3_{21}\rightarrow4_{22}$	30891.81	30894.16			30893.30	0.254	
$3_{12}\rightarrow4_{13}$	32089.74				32089.74	−0.434	
$4_{14}\rightarrow5_{15}$	36329.35				36329.35	−0.037	

[a] Ref. 6.

Table 3. Geometric parameters GP of planar rigid models M_i of $CH_2=PCl$ isotopic species (ISOTOPES). Distances in Å, angles in degrees. Model rotational constants B_{Mi}, C_{Mi} (MHz), experimental rotational constants B_o, C_o (Table 1). Quality of fit measured by $Q \sim |B_o - B_{Mi}|_{max} \sim |C_o - C_{Mi}|_{max}$ (MHz).

ISOTOPES	B_o, C_o	B_o, C_o	B_o, C_o	B_o, C_o	B_{M5}	C_{M5}
$CH_2=P^{35}Cl$	Engaged	Engaged	Engaged	Engaged	4667.3880	3865.5317
$CH_2=P^{37}Cl$	"	"	"	"	4539.0330	3775.5814
$^{13}CH_2=P^{35}Cl$	"	"	"	"	4559.2519	3774.1451
$^{13}CH_2=P^{37}Cl$	"	"	"	"	4433.3029	3685.8612
$CD_2=P^{35}Cl$	Not engaged	"	"	"	4322.6082	3537.5159
$CD_2=P^{37}Cl$	"	"	"	"	4205.2156	3456.8434
GP Fig. 1	M_1	M_2	M_3	M_4	M_5	
C=P	1.6543	1.6616	1.6548	1.6556	1.6548	
P−Cl	2.0609	2.0552	2.0600	2.0600	2.0600	
C−H, D(cis)	1.090 (ass.)	1.085 (ass.)	1.085 (ass.)	1.13	1.085	
C−H, D(trans)	1.090 (ass.)	1.085 (ass.)	1.085 (ass.)	1.14	1.085	
α	103.3	103.5	103.3	103.3	103.3	
β	120 (ass.)	120 (ass.)	121.9	115.8	121.9 (ass.)	
γ	123 (ass.)	123 (ass.)	121.6	121.8	121.6(ass.)	
δ	117 (ass.)	117 (ass.)	116.5	122.4	116.5	
Q	0.2	1.0	0.4	0.6	0.2	

structures derived (Table 3) aimed at a least square fit[8] to the observed B_o and C_o values (Table 1). Details are available on request. M_1 involves only data for species with almost equal zero-point energies. In M_2, data for the structurally different deuterated species get involved. This is compensated for by very slight changes in C=P, P−Cl and α, the dominating structural parameters (GP), and a slightly inferior "fit parameter" $Q=1$ MHz. In M_3 the angles β and γ (Fig. 1) have been included among the variables. The fit parameter Q is improved ($Q=0.4$ MHz), the distribution of angles in the methylene group being close to the distributions in related molecules (Table 4). An attempt to include all 7 GP was less successful (M_4). Finally, supposing $\beta=121.9°$ and $\gamma=121.6°$, varying C=P, C−Cl, α and C−H(D), *cis* and *trans*, resulted in M_5. We consider M_5 our ultimate model, its main merit being that its rotational constants B_{M5}, C_{M5} (Table 3) with A_{M5}'s taken as 22702, 22659, 22119, 22072, 19651 and 19545 respectively, from top to bottom of Table 3, reproduce observed frequencies of 6 isotopic species fairly accurately ($I_a(M_i)=I_c(M_i)-I_b(M_i)-$I.D.).

DISCUSSION. SUGGESTED EXPERIMENTS.

The geometric parameters (GP) of, for example, model M_5 can now be discussed in terms of GP from other molecules. The angles β, γ and δ have already been put on a satisfactory comparative basis (Table 4). Table 5 documents that the P=C distance is, indeed, in good agreement with other data. This is more problematic to illustrate for the P−Cl distance. It is noted, though, that the C−Cl distance of

Table 4. Value of angles β, γ and δ (Fig. 1) for ethylene, vinyl chloride and 1-chlorophosphaethene.

	$CH_2=CH_2$[16]	$CH_2=CHCl$[13]	$CH_2=PCl$[a]
β(cis)	121.08	119.53	121.9
γ(trans)	121.08	121.07	121.6
δ	117.83	119.53	116.5

[a] This paper, M_5. See text.

Table 5. Comparison of C,N and C,P bond lengths (Å) horizontally Δ_h (C−N/C=N/C≡N and C−P/C=P/C≡P) and vertically Δ_V (C−N/C−P, C=N/C=P and C≡N/C≡P).

		Δ_h		Δ_h	
	CH_3NH_2[9]		$CH_2=NH$[10]		$HC\equiv N$[11]
	1.471	0.198	1.273	0.116	1.156
Δ_V	0.392		0.387		0.386
	CH_3PH_2[12]		$CH_2=PCl$[a]		$HC\equiv P$[2]
	1.863	0.203	1.660	0.118	1.542

[a] This paper.

$CH_2=CHCl$[13] is 1.726 Å. Since the covalent radii of carbon and nitrogen differ by *ca.* 0.055 Å[14] the N−Cl distance in hypothetical $CH_2=N-Cl$ would be 1.671 Å. Adding $\Delta_v=0.387$ from Table 5, a P−Cl distance of 2.058 Å is predicted in (almost too) good agreement with the experiment.

By an *ab initio* geometry optimization of $CH_2=PCl$ on a STO-3G basis Thomson[15] calculated a P=C length of 1.65 Å, a P−Cl length of 2.11 Å and $\alpha=99.2°$. His estimate of the height of the barrier to in-plane inversion was *ca.* 5 kcal/mol. The predicted dipole moment was 3.25 Debye. Its predicted orientation could be seen from the indicated relative charge distribution,[15] the result being shown as the dotted vector of Fig. 1. This suggests that it might be worth-while to search for μ_b-transitions in the mw spectrum. Work in the infrared is also suggested since vibrational frequencies would help correcting our mw data for the effect of zero-point energy.

Acknowledgements. Thanks are due to G. O. Sørensen of this laboratory for permission to use his programs ROTFIT and LINDA. The Danish Research Council for Natural Sciences has supported this work.

REFERENCES

1. Bak, B., Larsen, N. W. and Svanholt, H. *Acta Chem. Scand. A 31* (1977) 755.
2. Gier, T. E. *J. Am. Chem. Soc. 83* (1961) 1769; Tyler, J. K. *J. Chem. Phys. 40* (1964) 1170 and Ref. 3.
3. a. Hopkinson, M. J., Kroto, H. W., Nixon, J. F. and Simmons, P. C. *J. Chem. Soc. Chem. Commun.* (1976) 513; b. Bak, B., Kristiansen, N. A. and Svanholt, H. *J. Mol. Struct. 70* (1981) *In press.*
4. Marten, D. R. and Pizzolato, P. J. *Inorganic Synthesis IV*, McGraw-Hill, New York 1953, p. 63.
5. Endo, K., Shimada, S., Morita, S. and Kamura, Y. *Nippon Kagaku Kaishi 1* (1979) 1.
6. Sørensen, G. O. *Program ROTFIT*(available). This laboratory.
7. Bak, B. and Svanholt, H. *Chem. Phys. Lett.* 75 (1980) 528.
8. Sørensen, G. O. *Program LINDA* (available). This laboratory.
9. Tagakiu, K. and Kojima, T. *J. Phys. Soc. Jpn. 30* (1971) 1145.
10. Person, R., Jr. and Lovas, F. J. *J. Chem. Phys. 66* (1977) 4149.
11. Winnewisser, G., Maki, A. G. and Johnson, D. R., *J. Mol. Spectrosc. 39* (1971)149.
12. Kojima, T., Breig, E. L. and Lin, C. C. *J. Chem. Phys. 35* (1961) 2139.
13. Kivelson, D. and Wilson, E. B., Jr. *J. Chem. Phys. 32* (1960) 205.
14. Bak, B. and Hansen-Nygaard, L. *J. Chem. Phys. 33* (1960) 418.
15. Thomson, C. *J. Chem. Soc. Chem. Commun.* (1977) 322.
16. Duncan, J. L. and Wright, I. J. *J. Mol. Spectrosc. 42* (1972) 251; 463.

Received April 14, 1981.

Acta Chemica Scandinavica A 36 (1982) 7–13

The Crystal Structure of Hexakis(dimethylsulfoxide)zinc(II) Perchlorate and the Structure of the Hexakis(dimethylsulfoxide)-zinc(II) Ion in Dimethylsulfoxide Solution

INGMAR PERSSON

Inorganic Chemistry 1, Chemical Center, University of Lund, P.O. Box 740, S-220 07 Lund 7, Sweden

The compound $[Zn(DMSO)_6](ClO_4)_2$ crystallizes in the trigonal space group $P31c$ (No. 159) with $a=12.006(3)$, $c=12.578(9)$ Å and $Z=2$. The X-ray investigation was based on 817 independent reflections collected with an automatic single-crystal diffractometer of the type CAD-4, using Mo$K\alpha$-radiation. The structure consists of discrete hexakis-(dimethylsulfoxide)zinc(II) complex ions and perchlorate ions. The zinc atom coordinates six DMSO molecules through the oxygen atoms, forming an almost regular octahedron. A structural investigation of the hexakis(dimethylsulfoxide)zinc(II) ions has also been performed in dimethylsulfoxide solution, using a large-angle $\theta-\theta$ diffractometer for X-ray diffraction measurements on liquids. The average Zn–O bond length is 2.110 Å in the solid state and 2.127(5) Å in dimethylsulfoxide solution, the corresponding Zn–S distances are 3.135 Å and 3.147(3) Å, respectively.

The configuration of zinc(II) is usually either octahedral or tetrahedral.[1] With most unidentate ligands coordinating *via* oxygen octahedral complexes are formed. Many structural investigations of crystals containing the hexaaquazinc(II) ions, $Zn(OH_2)_6^{2+}$, have been reported.[2–8] The structure of the hexaaquazinc(II) ion has also been determined in concentrated aqueous solutions.[9,10] The average Zn–O bond length in this ion is 2.09 Å in both crystals and solutions. Also organic ligands coordinating *via* oxygen, such as pyridine *N*-oxide, form regular octahedral structures[11] with an average Zn–O bond length of 2.102 Å.

The solvation of the divalent d^{10} ions, zinc(II), cadmium(II) and mercury(II) in dimethylsulfoxide solution has previously been studied by means of calorimetry, large angle X-ray diffraction on solutions and Raman and infrared spectroscopy.[12,13] For cadmium(II) and mercury(II) the structures have been determined in both solid state and solution.[13–15] For zinc(II), spectroscopic measurements show that the dimethylsulfoxide is coordinated *via* the oxygen atom.[13] The preparation of the compound $[Zn(DMSO)_6](ClO_4)_2$ has been described previously.[16] Judging from the empirical formula, the zinc(II) ion probably coordinates six DMSO molecules in an octahedral configuration. The coordination geometry of the DMSO solvated zinc(II) ion in solution plays a fundamental part in the discussion of the thermodynamics of the complex formation of zinc(II) in DMSO solution.[17]

In an earlier paper,[13] it was reported that the solubility of $[Zn(DMSO)_6](ClO_4)_2$ in DMSO is only 0.29 M. This concentration is too low to allow a study of the solvate structure by means of X-ray diffraction measurements. It is, however, possible to prepare a supersaturated 0.70 M solution. With this solution the structure of the zinc(II) DMSO solvate can be determined.

EXPERIMENTAL

Preparation of crystals. The crystals were prepared and analyzed as described previously.[16] They are slightly hygroscopic; single-crystals decompose in air to powder in two days. The crystals also react with organic compounds such as stopcock and silicon grease and different types of glue. Epoxy glues work satisfactorily, however. The density of the crystals was determined by the displacement method with benzene.

X-Ray data collection. Weissenberg photograms revealed the Laue class $\bar{3}m$ and the systematic

0302-4377/82/010007-07$02.50

absences: $hh2\bar{h}l$; $l=2n+1$ indicating the space groups $P\bar{3}1c$ or $P31c$.

The intensity data were collected by an automatic single-crystal diffractometer of type CAD-4, at 246 ± 1 K, in order to avoid extensive decomposition of the crystal. Zr-filtrated Mo$K\alpha$-radiation ($\lambda=0.71300$ Å) was used. A hexagonal prismatic crystal with all edges $\simeq0.20-0.25$ mm was used. The unit cell dimensions were obtained from the θ values of 25 reflections. Crystal data: $a=12.006(3)$, $c=12.578(9)$ Å, $V=1570.2(2)$ Å^3, $Z=2$, $D_m=1.54(2)$, $D_x=1.55$ g cm^{-3}, μ(Mo$K\alpha$)$=14.1$ cm^{-1}.

The $\omega-2\theta$ scan technique was employed, with a scan interval $\Delta\omega=1.00+0.15\tan\theta$. The background measurements were performed by increasing $\Delta\omega$ with 1/4 on both sides. 2141 independent reflections in the range $3°\leq\theta\leq32°$ were measured. Among these, 7 strong reflections were deleted because they were too intense for the counter. Another 810, with $I<3\sigma_c(I)$ were deleted as being too weak. The values of $\sigma_c(I)$ were based on counting statistics. Three reflections were selected as standard. The fluctuations in the intensities of the standard reflections were irregular and less than 8 %. The values of I and $\sigma_c(I)$ were corrected for Lorentz, polarization and absorption effects.

X-Ray data collection from solutions. The X-ray scattering of Mo$K\alpha$-radiation ($\lambda=0.71069$ Å) from the free surface of the DMSO solution was measured as described in previous papers.[18,19] The solution was enclosed in an air-tight shield, with cylindrical beryllium windows for the X-rays. The scattered intensity was measured at discrete points between the θ values 1.0 and 62.5°, where 2θ is the scattering angle. Intervals of 0.1° for $1.0°\leq\theta\leq20.0°$ and 0.25° for $20.0°\leq\theta\leq62.5°$ were used. 40 000 counts were accumulated twice for each point, corresponding to a statistical error of 0.35 %. All measurements were performed at 25 ± 1 °C.

Preparation of the solution. The DMSO solution investigated was prepared by dissolving $[Zn(DMSO)_6](ClO_4)_2$ in DMSO at around 90 °C. The solution was cooled to room temperature very slowly. The 0.70 M solution obtained was metastable and had to be handled with care. On shaking, solid $[Zn(DMSO)_6](ClO_4)_2$ immediately precipitated. The absorption coefficient, μ, of the solution was 6.1 cm^{-1}.

Computer programs. The computer programs used for determining the crystal structure are the same as listed elsewhere.[20] All calculations of the structures in solution were made by the KURVLR and PUTSLR computer programs.[21] All calculations were carried out on a UNIVAC 1100/80 computer at the Computer Center, University of Lund.

STRUCTURE DETERMINATION OF THE SOLID SOLVATE

In the space group $P31c$ (no. 159), the zinc ions were placed in $z=0.25$ (2(b)), which fixed the origin. The chlorine atoms were given z coordinates close to 0.00 and 0.75 in the special positions 2(a) and 2(b), respectively. This was in accordance with the Patterson map. From a difference Fourier map, the positions of the sulfur, oxygen and carbon atoms in the DMSO molecules could be identified. With these atoms isotropic, full-matrix least-squares refinements, minimizing $\Sigma w(|F_o|-|F_c|)^2$, gave $R=0.14$($R_w=0.18$).

The conventional R-value is defined as $R=\Sigma(|F_o|-|F_c|)/\Sigma|F_o|$, and the weighted as $R_w=(((\Sigma w|F_o|-|F_c|)^2)/\Sigma w|F_o|^2)^{1/2}$. A refinement in the space group $P\bar{3}1c$ was unsuccessful.

At this stage a difference Fourier map revealed the positions of three oxygen atoms in each perchlorate ion. The remaining oxygen, on the three-fold axis, could not be located, presumably due to a very high temperature coefficient. In the following calculations, a high, fixed value was therefore given to this coefficient. Reflections with $\theta>23°$ are all very weak and were therefore excluded in the final refinements. This resulted in $R=0.073$ and $R_w=0.089$ for the remaining 817 independent reflections. A total of 92 parameters, including two scale factors, were varied in the final refinements. In the last cycle the shifts in the parameters were less than

Table 1. Final fractional atomic positional parameters with estimated standard deviations in parentheses.

Atom	x	y	z
Zn	1/3	2/3	1/4
O1	0.1699(12)	0.6293(12)	0.1584(10)
S1	0.1518(4)	0.7406(4)	0.1313(4)
C1	0.0728(25)	0.6995(22)	0.0043(16)
C2	0.0204(19)	0.7261(22)	0.2137(15)
O2	0.2198(12)	0.5045(13)	0.3443(10)
S2	0.0890(5)	0.4722(5)	0.3815(4)
C3	0.0806(23)	0.4209(24)	0.5164(17)
C4	0.9815(19)	0.3237(24)	0.3240(19)
Cl1	0	0	0.0019(14)
Cl2	2/3	1/3	0.2639(10)
O11	0.1145(26)	0.0121(23)	0.0481(15)
O12	0	0	0.897(7)
O21	0.6653(25)	0.2166(27)	0.2217(19)
O22	2/3	1/3	0.369(7)

Table 2. Final anisotropic thermal parameters ($Å^2$) with estimated standard deviations in parentheses. The temperature factor expression used is $\exp[-\beta_{11}h^2-\cdots-2\beta_{12}hk-\cdots]$. The isotropic temperature coefficients are given in $Å^2$.

	β_{11}	β_{22}	β_{33}	β_{12}	β_{13}	β_{23}
Zn	0.0051(1)	0.0051(2)	0.005(2)	0.0026(1)	0	0
O1	0.0097(13)	0.0097(13)	0.0081(10)	0.0055(11)	−0.0012(9)	0.0000(9)
S1	0.0073(4)	0.0079(5)	0.0069(3)	0.0039(4)	−0.0002(3)	0.0037(6)
C1	0.0183(32)	0.0162(26)	0.0074(16)	0.0115(25)	−0.0039(18)	0.0010(17)
C2	0.0111(22)	0.0139(26)	0.0084(15)	0.0085(20)	0.0024(14)	−0.0011(16)
O2	0.0114(15)	0.0104(14)	0.0068(9)	0.0067(13)	0.0000(9)	0.0007(9)
S2	0.0100(6)	0.0120(6)	0.0087(4)	0.0058(5)	0.0031(4)	0.0038(4)
C3	0.0165(30)	0.0189(33)	0.0064(13)	0.0125(28)	0.0054(16)	0.0047(17)
C4	0.0079(20)	0.0166(31)	0.0114(20)	0.0046(21)	−0.0013(16)	−0.0016(19)
Cl1	0.0097(5)	0.0097(5)	0.0185(10)	0.0048(2)	0	0
Cl2	0.0082(4)	0.0082(4)	0.0118(8)	0.0041(2)	0	0
O11	11.4(6)					
O12	25.0					
O21	12.6(8)					
O22	25.0					

1 % of the e.s.d.'s. The weighting scheme was $w=1/\sigma_c^2+0.040|F_o|^2+3.00$ which, according to a weight analysis, gave a satisfactory error distribution. The largest remaining peak found in the final difference Fourier map was 1.35 e $Å^{-3}$. This peak was close to the position of the sulfur atom, the distance being 0.85 Å. Definite H atom positions could not be ascertained. The scattering factors used in the calculations were taken from International Tables for X-Ray Crystallography, Vol. IV. The final refined parameter values are given in Tables 1 and 2.

DESCRIPTION AND DISCUSSION OF THE STRUCTURE

The structure consists of hexakis(dimethylsulfoxide)zinc(II) cations, $Zn(DMSO)_6^{2+}$, with a three-fold axis, and of perchlorate ions, ClO_4^-. A stereoscopic view of the molecular geometry of the DMSO solvated zinc(II) ion is given in Fig. 1, and a stereoscopic view of the unit cell in Fig. 2. Some intramolecular distances and angles are listed in Table 3.

The $Zn(DMSO)_6^{2+}$ complex. Each zinc(II) ion coordinates six DMSO molecules through the

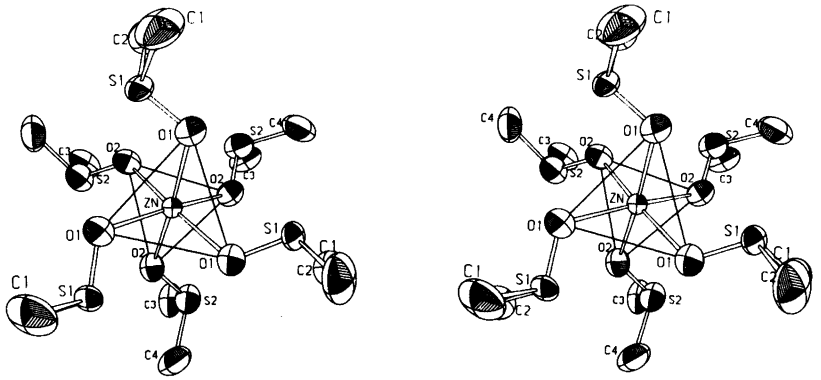

Fig. 1. A stereoscopic view of the $Zn(DMSO)_6^{2+}$ cation. All atoms are represented by 50 % probability ellipsoids.

Table 3. Some intramolecular atomic distances (Å) and angles (degrees) in $Zn(DMSO)_6(ClO_4)_2$(s). Estimated standard deviations are given in parentheses.

Zn–O1	2.121(13)	O1–Zn–O1	93.3(5)
Zn–O2	2.098(13)	O2–Zn–O2	91.2(5)
		O1–Zn–O2	85.2(5)
Zn–S1	3.115(4)	O1–Zn–O2	90.4(5)
Zn–S2	3.154(5)	O1–Zn–O2	176.1(5)
S1–O1	1.496(13)	Zn–O1–S1	117.8(7)
S1–C1	1.796(22)	Zn–O2–S2	122.0(8)
S1–C2	1.820(20)		
S2–O2	1.492(13)	O1–S1–C1	104.5(9)
S2–C3	1.790(23)	O1–S1–C2	106.9(9)
S2–C4	1.750(24)	C1–S1–C2	99.6(10)
C11–O11	1.43(3)	O2–S2–C3	104.9(10)
C11–O12	1.31(9)	O2–S2–C4	106.3(9)
C12–O21	1.48(3)	C3–S2–C4	98.9(12)
C12–O22	1.32(9)		
		O11–C11–O11	104.7(12)
		O11–C1–O12	113.9(10)
		O12–C12–O12	109.4(11)
		O12–C12–O22	109.5(11)

oxygen atoms. The resulting coordination polyhedron around the zinc(II) ion is a slightly distorted octahedron with an average Zn–O bond length of 2.110 Å, Table 3. The sulfur atoms also form a somewhat irregular octahedron around zinc, with an average Zn–S distance of 3.135 Å. The slight distortion of the octahedron around zinc is shown by a torsion angle of 57.3° along the three-fold axis and a distance of 0.017 Å between the zinc atom and the centre of gravity of the oxygen octahedron.

The average S–O and S–C distances within the pyramidal DMSO molecule are 1.494 and 1.790 Å, respectively, which agree well with distances found for other solvates where DMSO is coordinated *via* oxygen.[22] The S–O bond is slightly longer and consequently weaker than in crystalline DMSO.[23] This is also indicated by the Raman and infrared spectra[13] which show a lowering of the S–O stretch frequency on the coordination of DMSO *via* oxygen. The S–C bond is, on the other hand, shorter, and consequently stronger, in the coordinated DMSO. Consistent with this, the S–C stretching frequency is higher in coordinated than in free DMSO.[13]

The average Zn–O–S angle is 120°, Table 3, a value found for the M–O–S angle in many DMSO solvates. It is obvious that the hybridization around the oxygen atom in DMSO determines this angle. The angles within the coordinated DMSO molecules are much the same as in other DMSO complexes[14,15,24,25] and in free DMSO.[23]

The ClO_4^- ion. The four oxygen positions 011,

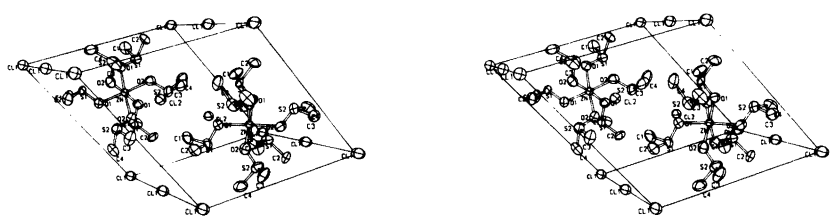

Fig. 2. A stereoscopic view of the trigonal unit cell.

012, 021 and 022 belong to the two perchlorate ions. Two of these, 011 and 021, are situated around a three-fold axis and fairly well-defined. The bond lengths Cl–O for these oxygens are 1.43 and 1.48 Å (Table 3), *i.e.* close to the bond lengths generally found in perchlorates, 1.42–1.43 Å.[26] The other two oxygen positions 012 and 022 are on the three-fold axis. Disordered perchlorate ions are also found, *e.g.*, in the structure of $AgClO_4 \cdot 2DMSO$,[24] $[Cd(DMSO)_6](ClO_4)_2$,[14] $[Hg(DMSO)_6](ClO_4)_2$,[15] $Hg(ClO_4)_2 \cdot 4DMSO$.[25] A survey of such structures is given in Ref. 24.

STRUCTURE DETERMINATION IN SOLUTION

Data reduction and correction. The measured intensities were corrected for the background and normalized to a stoichiometric unit of volume, V, corresponding to the average volume per zinc(II) ion in the solution. The normalization was done by comparing the high angle region of the corrected intensities with the sum of the independent coherent scattering and the fraction of the incoherent scattering reaching the counter. No corrections for the absorption were applied.

RHF scattering factors, f, were used[27] for the neutral atoms and zinc(II). For hydrogen, the spherical form factors proposed by Stewart *et al.* were employed.[28] No absorption corrections were necessary. Anomalous dispersion corrections, $\Delta f'$ and $\Delta f''$, were applied to all atoms.[27] The incoherent scattering factors, I_{incoh}, were taken from the same sources as before.[29] Corrections for the Breit-Dirac factor in the form appropriate for a radiation counter, $(\lambda/\lambda')^3$, where $\lambda' = \lambda + \Delta\lambda$ and $\Delta\lambda = \frac{h}{mc}(1-\cos 2\theta)$, were applied.[27] The reduced intensity curves, $i(s)$, and the electronic radial distribution functions, $D(r)$, with M = Zn, were calculated as described previously.[13] Small spurious peaks below 1.5 Å in the $[D(r)_{obs} - D(r)_{calc}]$ function which could not be related to interatomic distances, were removed by a Fourier transformation procedure.[3] The calculation of intramolecular intensity contributions to the reduced intensity curve and the electronic radial distribution function were carried out as described previously.[21,30]

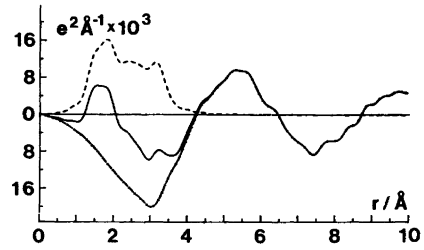

Fig. 3. The function $D(r) - 4\pi r^2\rho_o$ (solid line) compared with sums of calculated peak shapes of the refined model (dashed line). The parameter values used are given in Table 4 and in the text. The difference is shown by the dashed-dotted lines.

RESULTS

Intensity curve and radial distribution (RDF). The electronic radial distribution function (RDF), $D(r) - 4\pi r^2\rho_o$, is given in Fig. 3. The peak found at about 3.2 Å in the radial distribution function (RDF) fits with the zinc–sulfur distance, found in the solid state of $[Zn(DMSO)_6](ClO_4)_2$, Table 3.

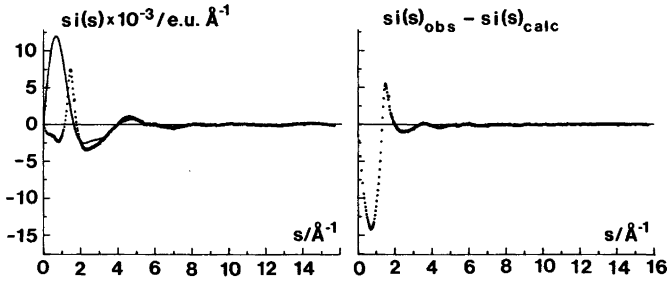

Fig. 4. Reduced intensities, $i(s)$, multiplied with s, for 0.7 M $Zn(DMSO)_6^{2+}$ solution (left). Experimental values are denoted by dots (the six first are obtained by extrapolation) and values calculated for the refined model by a solid line. The difference between experimental and calculated values, $si_{obs}(s) - si_{calc}(s)$, is also shown (right).

The expected zinc–oxygen distance at about 2.1 Å could not be seen in the RDF, however.

The intramolecular DMSO distances should occur at about 1.48(S–O), 1.81(S–C), 2.66(O–C) and 2.77 Å(C–C). The peak at 1.6–1.7 Å, Fig. 4 is due to the S–O and S–C distances. Expected Cl–O and O–O distances within the tetrahedral ClO_4^- ion are 1.43 and 2.33 Å, respectively.[26] The broad peaks at 5–6 and 9–10 Å are certainly due to interactions between DMSO molecules.[31]

The sum of all calculated intramolecular reduced intensity contributions, $i_{calc}(s)$, is compared with experimental $i_{obs}(s)$ curves in Fig. 4, after multiplication by s.

Least-squares refinements. This procedure was carried out as described previously.[13] The model finally selected consisted of the following parts.

1. In the $Zn(DMSO)_6^{2+}$ complex, the distances Zn–O and Zn–S, d, the coefficients b of their temperature factors $\exp(-bs^2)$, and the number of distances, n, were refined. Also the contribution from the O–O interactions was introduced, assuming an octahedral arrangement around the zinc atom.

2. Intramolecular DMSO bond distances and temperature factor coefficients were taken from a study of liquid DMSO.[31] These distances agree very well with the values found in solid and gaseous state.[23,32] In this way, all DMSO molecules, bonded as well as non-bonded, were accounted for.

3. The same parameters as before were used for the perchlorate ion.[13]

The parameter values from the refinements in the range $5.50 \leq s \leq 15.25$ Å^{-1} are summarized in Table 4. The standard deviations given are those calculated in the least-squares procedure.

Table 4. Least-squares refinement of the 0.70 M zinc(II) perchlorate DMSO solution. The refined parameters d=distance (Å), b=temperature factor coefficient (Å^2) and n=number of distances per metal atom are obtained in the range $5.50 \leq s \leq 15.25$ of the reduced intensity curve. Estimated standard deviations are given in parentheses for refined parameters.

Complex	Interaction	Parameter	
$Zn(DMSO)_6^{2+}$	Zn–O	d	2.127(5)
		b	0.0148(9)
	Zn–S	d	3.147(3)
		b	0.0158(6)
	Zn–O and Zn–S	n	6.0(1)
ClO_4^-	Cl–O	d	1.425
		b	0.0010
		n	4
DMSO	S–O	d	1.496
	S–C	d	1.805
	S–O and S–C	b	0.0017

DISCUSSION

The zinc(II) ion coordinates six DMSO molecules through the oxygen atoms in an octahedral configuration. A zinc(II) solvate of the same type is formed with pyridine-N-oxide.[11] In the solid solvates, the Zn–O distances are 2.110 and 2.102 Å, respectively. The Zn–O distance of 2.127 Å found in the zinc(II) solvate in DMSO solution is very close to the values found in the solid.

Zinc(II) is a hard acceptor preferring hard donor atoms like oxygen. The bonds formed are of a mainly electrostatic character. Among the important oxygen ligands coordinated is water. In all crystalline zinc(II) hydrates investigated, six water molecules are octahedrally coordinated.[2–8] The average Zn–O distance ranges from 2.078 to 2.107 Å, with an overall average of 2.092 Å. This value is very close to the distances found in the hexahydrated zinc(II) ion in aqueous solution, 2.08 and 2.092 Å.[9,10]

The Zn–O distances in the hexahydrates are significantly shorter than in the DMSO and pyridine-N-oxide hexasolvates. Water is thus more strongly bonded than organic solvents coordinating *via* oxygen. The oxygen in solvents such as DMSO and pyridine *N*-oxide thus acts as a less hard donor than the water oxygen.

From the average bond lengths of the zinc(II) hydrates and solvates, the ionic radius of the zinc (II) ion in octahedral configuration can be derived. The radii of oxygen are taken as 1.35 Å in the organic solvates where oxygen is two-coordinated and as 1.36 Å in the hydrates where oxygen is three-coordinated.[33] From the solid hexasolvates a value of $r(Zn^{2+})=0.76$ Å is calculated and from the DMSO hexasolvate in solution $r(Zn^{2+})=0.78$ Å. From the hydrates in solid phase and solution $r(Zn^{2+})=0.73$ Å is found. The value calculated from oxide and fluoride structures by Shannon and Prewitt,[33] 0.745 Å, is very close to the value derived from the present measurements.

The enthalpy change of the transfer[12] $Zn^{2+}(aq) \rightarrow Zn^{2+}(DMSO)$, $\Delta H_{tr}^{\circ} = -60$ kJ mol^{-1}, indicates that the solvation of the zinc(II) ion is favoured in DMSO relative to water, in spite of the fact that the Zn–O bonds are shorter and consequently stronger in water than in DMSO. An obvious explanation of this apparent contradiction is that more energy has to be spent in water to break the solvent structure. This difference must evidently be >60 kJ, the value of ΔH_{tr}°. It should be noted that for mercury(II), the bond distances Hg–O are about the same,[13] 2.40 Å, in aqueous and DMSO solution, while the value of $\Delta H_{tr}^{\circ} = -76$ kJ mol^{-1}.

Acknowledgements. My thanks are due to Dr. Åke Oskarsson for his continuous readiness to help during the crystallographic part of this work. I am also most indebted to Professor Oliver Lindqvist and Mr. Åke Iverfeldt who recorded the data of the zinc(II) perchlorate in DMSO solution on the X-ray diffractometer for liquids of the Department of Inorganic Chemistry, University of Göteborg. Professor Sten Ahrland is gratefully thanked for his stimulating and continuous interest in this investigation.

REFERENCES

1. Wells, A. F. *Structural Inorganic Chemistry*, 4th Ed., Oxford 1975.
2. Yü, S. H. and Beevers, C. A. *Z. Kristallogr. 82* (1932) 297.
3. Montgomery, H. and Lingafelter, E. C. *Acta Crystallogr. 17* (1964) 1295.
4. Ferrari, A., Braibanti, A., Manotti Lanfredi, A. M. and Tiripicchio, A. *Acta Crystallogr. 22* (1967) 240.
5. Ray, S., Zalkin, A. and Templeton, D. H. *Acta Crystallogr. B 29* (1973) 2741.
6. Black, W. H., Griffith, E. A. H. and Robertson, B. E. *Acta Crystallogr. B 31* (1975) 615.
7. Whitnall, J., Kennard, C. H. L., Nimmo, J. and Moore, F. H. *Cryst. Struct. Commun. 4* (1975) 717.
8. Gupta, M. P. and Agrawal, J. L. *Cryst. Struct. Commun. 6* (1977) 103.
9. Bol, W., Gerrits, G. J. A. and van Panthaleon van Ek, C. L. *J. Appl. Crystallogr. 3* (1970) 486.
10. Ohtaki, H., Yamaguchi, T. and Maeda, M. *Bull. Chem. Soc. Jpn. 49* (1976) 701.
11. O'Connor, C. J., Sim, E. and Carlin, R. L. *Inorg. Chem. 16* (1977) 3314.
12. Ahrland, S., Kullberg, L. and Portanova, R. *Acta Chem. Scand. A 32* (1978) 251.
13. Sandström, M., Persson, I. and Ahrland, S. *Acta Chem. Scand. A 32* (1978) 607.
14. Sandström, M. *Acta Chem. Scand. A 32* (1978) 519.
15. Sandström, M. and Persson, I. *Acta Chem. Scand. A 32* (1978) 95.
16. Ahrland, S. and Björk, N. O. *Acta Chem. Scand. A 28* (1974) 823.
17. Ahrland, S., Björk, N. O. and Portanova, R. *Acta Chem. Scand. A 30* (1976) 270.
18. Johansson, G. *Acta Chem. Scand. 20* (1966) 553.
19. Johansson, G. *Acta Chem. Scand. 25* (1971) 2787, 2799.
20. Svensson, C. *Diss.*, Institute of Technology, Lund 1978.
21. Johansson, G. and Sandström, M. *Chem. Scr. 4* (1973) 195.
22. Persson, I. *Diss.*, University of Lund, Lund 1980.
23. Viswamitra, M. A. and Kannan, K. K. *Nature 209* (1966) 1016.
24. Björk, N. O. and Cassel, A. *Acta Chem. Scand. A 30* (1976) 235.
25. Sandström, M. *Acta Chem. Scand. A 32* (1978) 527.
26. Berglund, B., Thomas, J. O. and Tellgren, R. *Acta Crystallogr. B 31* (1975) 1842.
27. *International Tables of X-Ray Crystallography*, Kynoch Press, Birmingham 1968 and 1974, Vols. 3 and 4.
28. Stewart, R. F., Davidson, E. R. and Simpson, W. T. *J. Chem. Phys. 42* (1965) 3175.
29. Sandström, M. and Johansson, G. *Acta Chem. Scand. A 31* (1977) 132.
30. Levy, H. A., Danford, M. D. and Narten, A. H. *Data Collection and Evaluation with an X-Ray Diffractometer Designed for Study of Liquid Structure*, Report ORNL-3960, Oak Ridge National Laboratory, Oak Ridge 1966.
31. Ahrland, S., Hansson, E., Iverfeldt, Å. and Persson, I. *Acta Chem. Scand. A 35* (1981) 275.
32. Bastiansen, O. and Viervoll, H. *Acta Chem. Scand. 2* (1948) 702.
33. Shannon, R. D. and Prewitt, C. T. *Acta Crystallogr. B 25* (1969) 925.

Received May 5, 1981.

Acta Chemica Scandinavica A 36 (1982) 15–19

A Calorimetric Study of Copper(II) Chloride Complexes in Aqueous Solution

ROBERT ARNEK,[a] IGNASI PUIGDOMENECH[a] and MANUEL VALIENTE[b]

[a] The Royal Institute of Technology, Department of Inorganic Chemistry, S-100 44 Stockholm, Sweden and [b] Universitat Autónoma, Departamento Quimica Analitica, Bellaterra-Barcelona, Spain

The complex formation between copper(II) and chloride ion in 5 M $Na(ClO_4,Cl)$ medium at 25 °C has been investigated with a flow microcalorimetric technique. By using equilibrium constants determined earlier, the enthalpy changes for the formation of the species $CuCl^+$, $CuCl_2$ and $CuCl_3^-$ were obtained.

The weak complex formation between copper(II) and chloride ion in aqueous solution has been investigated mainly by spectrophotometric methods.[1-17] Other methods which have been used are ion-exchange,[22] ion exchange paper chromatography,[23] kinetics,[2] solvent extraction[25] and calorimetry.[10,16,18-21] Some of the results, obtained under conditions similar to those in the present investigation, are given in Table 1. The β_n and ΔH_n values refer to the reactions $Cu^{2+} + nCl^- \rightleftarrows CuCl_n^{(2-n)}$ with $n = 1-4$. The existence of these complexes was first established by Bjerrum[1] already in 1946 and has been confirmed by later investigators.[8]

The main objective of the present work has been to determine reliable ΔH-values for the formation

Table 1. Some literature data for the system Cu(II) chloride at 25 °C.

Ref.	Method	Medium	β_1 M^{-1}	β_2 M^{-2}	β_3 M^{-3}	β_4 M^{-4}	ΔH_1 kJ mol^{-1}
2	spectr.	1 M $HClO_4$	1.30±0.03	0.23±0.15	–	–	–
5, 18	spectr. calorim.	2 M $NaClO_4$	1.22	–	–	–	6.6
23	paper chromat.	3 M $HClO_4$	0.94±0.05	0.16±0.07	0.05±0.08	–	–
19	calorim.	2 M $NaClO_4$	0.96±0.01	–	–	–	8.2±0.2
24	kinetics	1 M $NaClO_4$	1.30±0.27	–	–	–	–
10	spectr. calorim.	3 M $NaClO_4$	0.87±0.08	–	–	–	9.3±0.2
21	calorim.	3 M $LiClO_4$	0.83	–	–	–	12.1
11	spectr.	4 M $NaClO_4$	1.52±0.02	–	–	–	–
		5 M $NaClO_4$	1.86±0.04	–	–	–	–
12	spectr.	5 M $NaClO_4$	4.0±0.7	4.7±0.6	1.96±0.25	0.23±0.05	–
14	spectr.	4 M $NaClO_4$	1.3±0.1	–	–	–	–
		6 M $NaClO_4$	1.85±0.1	–	–	–	–
15	spectr.	5 M $NaClO_4$	1.5	0.63	0.088	0.0032	–
16	spectr. calorim.	4 M $LiClO_4$	0.92±0.07	–	–	–	13.6
17	spectr.	3 M $NaClO_4$	0.99±0.15	0.40±0.06	–	–	–

0302-4377/82/010015-05$02.50

of copper(II) chloride complexes in 5 M $Na(ClO_4, Cl)$ medium.

Several difficulties are encountered when weak complexes, such as those between copper(II) and chloride, are studied. The most serious of these is introduced by the need to substitute ligand (Cl^-) for a great part of medium – in this case perchlorate – in order to promote complex formation. Assignment of activity coefficients to facilitate interpretation of the data is complicated by this variation of the medium.

Another difficulty, when studying weak complexes with calorimetry, derives from the small heat effect obtained. However, the technique used in this investigation, flow microcalorimetry, is, from our experience, well suited for the measurement of small heat effects with good accuracy.

EXPERIMENTAL

Chemicals. The *copper(II) perchlorate* stock solution was prepared[26] from CuO (Merck *p.a.*) and perchloric acid (Merck *p.a.*). The solution was analyzed for copper by electrodeposition[27] and for H^+ potentiometrically.

Sodium perchlorate stock solution was prepared[28] from Na_2CO_3 (Merck *p.a.*) and perchloric acid (Merck *p.a.*).

Sodium chloride (Merck *p.a.*) was recrystallized in water, the crystals were dried at 200 °C and stored in a desiccator.

The compositions of the solutions used in the calorimetric measurements were

Solution *a* 5 M $NaClO_4$
$\simeq$0.015 M $HClO_4$

Solution *b* *A* M $Cu(ClO_4)_2$
$(5-2A)$ M $NaClO_4$
$\simeq$0.015 M $HClO_4$

Solution *c* *B* M NaCl
$(5-B)$ M $NaClO_4$
$\simeq$0.015 M $HClO_4$

The solutions were acidified to suppress the hydrolysis of copper(II).

Apparatus. For the measurements an LKB Flow microcalorimeter (10700-1) was used. The thermal output was amplified by a Keithley 150 B Microvolt amplifier and recorded on a potentiometric recorder. The reactants were passed through the mixing cell by means of two peristaltic pumps (LKB Vario Perpex II). The pumps were calibrated frequently by weighing the amount of water pumped in a known amount of time. It was found that the flow rates changed less than 0.2 % during an experiment, usually about five hours. The flow, $\phi(cm^3\ h^{-1})$, of the mixing reactants covered a range of values between 1.5 and 25 $cm^3\ h^{-1}$.

The mixing cell used was a 24-carat gold channel, about 0.7 cm^3 in volume. The detector sensitivity was 0.07 $\mu V/\mu W$ and the calibration current had an accuracy of ± 0.1 %.

Calorimetric procedure. The calorimetric measurements were performed in the following way. The base line output potential was taken when solution *a* (ionic medium) and solution *c* (chloride solution) were pumped through the cell. When a stable base line was obtained, solution *a* was replaced by solution *b* (copper(II) solution). In this way the heat of dilution of chloride into the medium was automatically corrected for. The base line shift obtained then had to be corrected for the heat of dilution of the metal ion [copper(II)], which had to be determined in separate experiments.

For copper(II) concentrations less than about 0.40 M, it was found that

$$\Delta H_{dilution}(J\ mol^{-1}) = -1030\Delta[Cu^{2+}]$$

where $\Delta[Cu^{2+}]$ is the difference between the final and initial copper(II) concentration when a $Cu(ClO_4)_2$ solution (medium 5 M ClO_4^-) is diluted in 5 M $NaClO_4$.

RESULTS AND CALCULATIONS

The calorimetric data obtained are collected in Table 2. The range of copper concentration covered is 0.004 – 0.35 M and of chloride 0.03 – 3.5 M. The measured heat effect corrected for the heats of dilution is Q_{exp}.

The calorimetric data were treated with the least-squares computer program LETAGROP/KALLE[30] and also with a new version of LETAGROP,[31] linked with SUBHTF[32] (a subroutine form of HALTAFALL).

The results of the calculations are given in Table 3. The ΔH-values were obtained using the equilibrium constants given by Bjerrum and Skibsted.[15] A poorer fit to the experimental data was obtained

Table 2. Calorimetric data for the $Cu^{2+}-Cl^-$ system in 5 M $Na(ClO_4,Cl)$ at 25 °C. Q_{calc} is the heat effect calculated with the β and ΔH_β values in Table 3.

$[Cu^{2+}]$ M	ϕ_{Cu} ml/h	$[Cl^-]$ M	ϕ_{Cl} ml/h	Q_{exp} J/h	$Q_{calc}-Q_{exp}$ J/h
0.394	11.69	0.300	1.43	1.78	+0.02
	22.76		4.42	5.25	+0.06
	19.33		4.32	5.10	0.00
	11.57		4.30	4.66	−0.02
	6.87		4.53	4.20	−0.01
	14.42		10.53	9.39	+0.01
	5.55		4.28	3.70	+0.05
	5.03		4.37	3.70	−0.04
	4.69		7.66	4.82	−0.08
	4.75		4.53	3.69	−0.04
0.0146	5.26		4.96	0.188	−0.003
	4.99		6.59	0.203	0.000
	5.29		8.35	0.229	0.000
	5.00	1.00	1.72	0.299	−0.011
0.0734	5.00		1.72	1.35	+0.03
0.0146	11.46		4.66	0.724	+0.006
	4.58		4.85	0.466	−0.008
	4.66		11.46	0.57	+0.01
	11.46	3.00	4.66	1.58	+0.04
	11.44	5.00	4.63	2.04	+0.06
	4.58	3.00	4.85	0.86	0.00
0.0365	11.85	5.00	6.40	5.86	−0.02
0.0146	4.67	3.00	11.48	0.965	+0.021
	4.58	5.00	4.85	1.01	0.00
0.0365	10.05		18.46	5.80	0.00
0.0146	4.66		11.46	1.09	0.00

when the equilibrium constants given by Schwing-Weill[12] were used.

From the present data it was not possible to determine ΔH for the formation of $CuCl_4^{2-}$. It is seen from Fig. 1 that $CuCl_4^{2-}$ does not exist in noticeable amounts in the region studied by us.

In the calculations, it has been assumed that the activity coefficients are constant, although part of the experimental data have been obtained in a region where a large fraction of the medium ions has been replaced by chloride ions. The good fit of the data over the whole concentration range gives some support to this assumption.

Some ΔH_1-values that have been reported in the literature are listed in Table 1. Several of these values[16,21] are comparable to the ΔH_1-value determined by us. This agreement may be coincidental however; in the earlier investigations[16,21] it was assumed that only the monoligated complex was formed. Furthermore the ionic media used were not the same as used by us.

It is of interest to note as well that the present investigation of the Cu(II)−Cl system seems to be the first in which the ΔH for the formation of $CuCl_2$ and $CuCl_3^-$ as well as $CuCl^+$ has been determined.

In Table 4 the thermodynamic parameters $\Delta G°$, $\Delta H°$ and $\Delta S°$ for the formation of $Cu^{2+}-Cl^-$ complexes are given.

In Table 5 the log K and $\Delta H°$-values for some metal−chloride complexes are compared. The trend

Table 3. Results from the calculations made with the LETAGROP program on data of Table 2. The given uncertainties are 3σ. The calculations gave $\sigma(Q_{calc}-Q_{exp})=0.032$ J.

β_i	ΔH_i kJ mol^{-1}
$\beta_1=1.5^a$	$\Delta H_1=12.30\pm0.1$
$\beta_2=0.63^a$	$\Delta H_{\beta2}=23.0\pm1.5$
$\beta_3=0.088^a$	$\Delta H_{\beta3}=11\pm4$

[a] From Ref. 15.

in the stepwise log K and $\Delta H°$ values for Cu(II) is similar to the trend observed in these parameters for Zn(II) and is to be expected for the interaction between a typical (a)-acceptor ("hard") and the

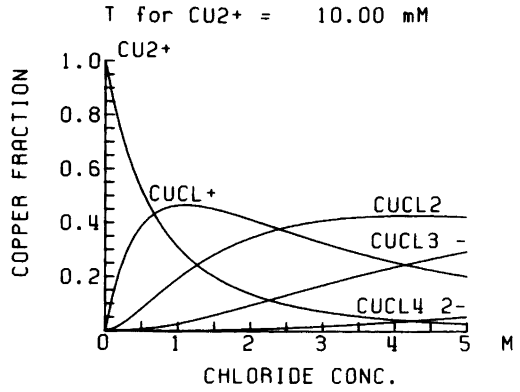

Fig. 1. Distribution of copper species as a function of chloride concentration in 5 M Na(ClO_4,Cl) at 25 °C. Plot produced by the SOLGASWATER [29] program with the equilibrium constants from Ref. 15.

Table 4. Calculated values of $\Delta G°$, $\Delta H°$, and $\Delta S°$ for the stepwise complex formation $Cu^{2+}-Cl^-$ in 5 M Na(ClO_4,Cl) at 25 °C.

Complex	K M^{-1}	$\Delta G°$ kJ mol^{-1}	$\Delta H°$ kJ mol^{-1}	$\Delta S°$ J mol^{-1}K^{-1}
$CuCl^+$	1.5[a]	−1.0	12.3	44.6
$CuCl_2$	0.42[a]	+2.2	10.7	28.5
$CuCl_3^-$	0.14[a]	+4.9	−12.0	−56.7

[a] From Ref. 15.

Table 5. log K and ΔH-values for the stepwise formation of chloride complexes of Zn(II), Cd(II), Hg(II) and Cu(II) at 25 °C.

Metal ion	Complex	log K	ΔH kJ mol^{-1}	Medium	Ref.
Zn^{2+}	$ZnCl^+$	0.147	17±2	4 M $LiClO_4$	33
	$ZnCl_2$	0.418	12±1.4		
	$ZnCl_3^-$	0.212	−3.4±7		
Cd^{2+}	$CdCl^+$	1.58	−0.42	3 M $NaClO_4$	34
	$CdCl_2$	0.64	0.08		
	$CdCl_3^-$	0.18	7.74		
	$CdCl^+$	1.77	−2.8	4 M Li(ClO_4,Cl)	35
	$CdCl_2$	0.70	−2.7		
	$CdCl_3^-$	0.64	6.28		
	$CdCl_4^{2-}$	−0.55	24.7		
Hg^{2+}	$HgCl^+$	7.07	−24.2±1.0	3 M $NaClO_4$	36
	$HgCl_2$	6.91	−27.2±1.5		
	$HgCl_3^-$	1.08	−4.3±0.9		
	$HgCl_4^{2-}$	1.09	−6.2±1.0		
Cu^{2+}	$CuCl^+$	0.18	12.3±0.1	5 M Na(ClO_4,Cl)	This work
	$CuCl_2$	−0.38	10.7±1.5		
	$CuCl_3^-$	−0.85	−12±4		

chloride ion. For comparison, data are also given in the Table for a representative (b)-acceptor, Hg(II) and for a "mild" (b)-acceptor, Cd(II).

It should also be added that the analysis of the Cu(II)−Cl thermodynamic data summarized in Table 4 could possibly be further refined. One could attempt to take into account the proportion of inner and outer sphere complexes formed.[37] However, attempts that have been made to estimate the formation constant for outer and inner sphere $CuCl^+$ complexes[20,21] are somewhat speculative. Therefore we have not considered it worthwhile to reinterpret our thermodynamic data for $Cu^{2+}-Cl^-$ by estimating the proportion of inner and outer sphere complexes which must necessarily be based on an uncertain estimate of their respective formation constants.

Acknowledgements This work has been supported by the Swedish Natural Science Research Council. Dr. J. Marinsky is thanked for the linguistic revision.

REFERENCES

1. Bjerrum, J. *K. Dan. Vidensk. Selsk. Mat.-Fys. Medd. 22* (1946) No. 18.
2. McConnell, H. and Davidson, N. *J. Am. Chem. Soc. 72* (1950) 3164.
3. Näsanen, R. *Acta Chem. Scand. 4* (1950) 140.
4. Kruh, R. *J. Am. Chem. Soc. 76* (1954) 4865.
5. Lister, M. W. and Rosenblum, P. *Can. J. Chem. 38* (1960) 1827.
6. Mironov, V. E., Makashev, Yu. A., Mavrina, I. Ya. and Kryzhanovskii, M. M. *Russ. J. Inorg. Chem. 15* (1970) 668 (Russian page 1301).
7. Libus, Z. *Inorg. Chem. 12* (1973) 2972.
8. Schwing-Weill, M.-J. *Bull. Soc. Chim. Fr.* (1973) 823.
9. Khan, M. A. *Thesis*, Université L. Pasteur, Strasbourg 1975.
10. Blokhin, V. V., Razmyslova, L. I., Shalaevskaya, M. I., Makashev, Yu. A. and Mironov, V. E. *Russ. J. Phys. Chem. 48* (1974) 275 (Russian page 469).
11. Ashurst, K. G. *National Institute for Metallurgy*, Report 1712, Randburg, South Africa 1975.
12. Khan, M. A. and Schwing-Weill, M.-J. *Inorg. Chem. 15* (1976) 2202.
13. Carlsson, B. and Wettermark, G. *J. Inorg. Nucl. Chem. 38* (1976) 1525.
14. Koneva, T. N. and Fedorov, V. A. *Russ. J. Inorg. Chem. 21* (1976) 616 (Russian page 1132).
15. Bjerrum, J. and Skibsted, L. H. *Acta Chem. Scand. A 31* (1977) 673.
16. Koneva, T. N., Fedorov, V. A. and Trofinov, G. L. *Russ. J. Phys. Chem. 51* (1977) 470 (Russian page 793).
17. Sjöberg, S. *Acta Chem. Scand. A 31* (1977) 729.
18. Kennedy, M. B. and Lister, M. W. *Can. J. Chem. 44* (1966) 1709.
19. Almemark, M. and Arnek, R. *Unpublished results.*
20. Blokhin, V. V., Regulin, G. K., Anufrienko, V. F., Makashev, Yu. A. and Mironov, V. E. *Russ. J. Phys. Chem. 44* (1970) 1512 (Russian page 2654).
21. Blokhin, V. V., Razmyslova, L. I., Makashev, Yu. A. and Mironov, V. E. *Russ. J. Phys. Chem. 48* (1974) 82 (Russian page 151).
22. Morris, D. F. C. and Short, E. L. *J. Chem. Soc.* (1962) 2672.
23. Grimaldi, M. and Liberti, A. *J. Chromatogr. 15* (1964) 510.
24. Hutchinson, M. H. and Higginson, W. C. E. *J. Chem. Soc. Dalton Trans. 12* (1973) 1247.
25. Sato, T. and Kato, T. *J. Inorg. Nucl. Chem. 39* (1977) 1205.
26. Berecki-Biedermann, C. *Ark. Kemi 9* (1956) 175.
27. Vogel, A. I. *Textbook of Quantitative Inorganic Analysis*, 4th Ed., Longman, London 1978, p. 532.
28. Biedermann, G. *Ark. Kemi 9* (1956) 277.
29. Eriksson, G. *Anal. Chim. Acta 112* (1979) 375.
30. Arnek, R. *Ark. Kemi 32* (1970) 81.
31. Sundstrand, S. *MODFNK, the use of LETAGROP for ones own model functions. Draft.* 1975.
32. Puigdomenech, I. and Wallin, T. *SUBHTF, a subtroutine form of the HALTAFALL program.* TRITA-OOK-2012, 1980.
33. Fedorov, V. A., Chernikova, G. E. and Mironov, V. E. *Zh. Neorg. Khim. 15* (1970) 2100.
34. Gerding, P. and Jönsson, I. *Acta Chem. Scand. 22* (1968) 2247.
35. Fedorov, V. A., Kripin, L. I. and Mironov, V. E. *Russ. J. Inorg. Chem. 17* (1972) 641 (Russian page 1233).
36. Arnek, R. *Ark. Kemi 24* (1965) 531.
37. Ahrland, S. *Coord. Chem. Rev. 8* (1972) 21.

Received May 15, 1981.

Acta Chemica Scandinavica A 36 (1982) 21 – 30

Thermodynamics and Kinetics for the Equilibration between Monohydroxo and Dihydroxo Bridged Binuclear Tetraammine Chromium(III) Complexes. Synthesis and Isolation of the Monohydroxo Bridged Species

FINN CHRISTENSSON and JOHAN SPRINGBORG

Chemistry Department, Royal Veterinary and Agricultural University, Thorvaldsensvej 40, DK-1871 Copenhagen V, Denmark

The binuclear ion $[(NH_3)_4Cr(OH)_2Cr(NH_3)_4]^{4+}$ (diol) equilibrates in acid solution according to Scheme 1.

The kinetics and equilibria have been studied in 1 M (Na,H)ClO_4 in the temperature range 25 – 34.4 °C and the hydrogen ion concentration range 0.001 – 1.0 M. The results were:

$k_1(25\,°C) = 1.21 \times 10^{-4} s^{-1}$; $E_a = 89$ kJ mol^{-1}.
$k_{-1}(25\,°C) = 3.80 \times 10^{-4} s^{-1}$; $E_a = 83$ kJ mol^{-1}.
$k_{-2}(25\,°C) = 2.7 \times 10^{-6} s^{-1}$; $E_a = 126$ kJ mol^{-1}.
$k_2/K_{a3}(25\,°C) = 4.9 \times 10^{-5} s^{-1} M^{-1}$; $E_a(k_2) - \Delta H°(K_{a3}) = 84$ kJ mol^{-1}.
$K_1(25\,°C) = k_1/k_{-1} = 0.318$; $\Delta H° = +6$ kJ mol^{-1}.

The acid dissociation constants of the diaqua monool *cis,cis*-$[(H_2O)(NH_3)_4Cr(OH)Cr(NH_3)_4(H_2O)]^{5+}$, were found to be K_{a1} (25 °C) = 0.0176 M, $\Delta H° = 49$ kJ mol^{-1} and K_{a2} (25 °C) = 3.2×10^{-8} M. Solid salts of both aquahydroxo monool and diaqua monool have been prepared.

It was shown recently that both isomers (Δ,Λ and Δ,Δ – Λ,Λ) of the dihydroxo bridged cation $[(en)_2Cr(OH)_2Cr(en)_2]^{4+}$ (diol) very rapidly attain equilibrium with their corresponding monohydroxo bridged isomers $[(H_2O)(en)_2Cr(OH)Cr(en)_2(OH)]^{4+}$ (monool).[1,2] The reduced robustness of these systems is somewhat surprising when compared to the corresponding bis(tetraaqua)chromium(III) system,[3] for which the rate constants are orders of magnitude smaller than those in the ethylenediamine

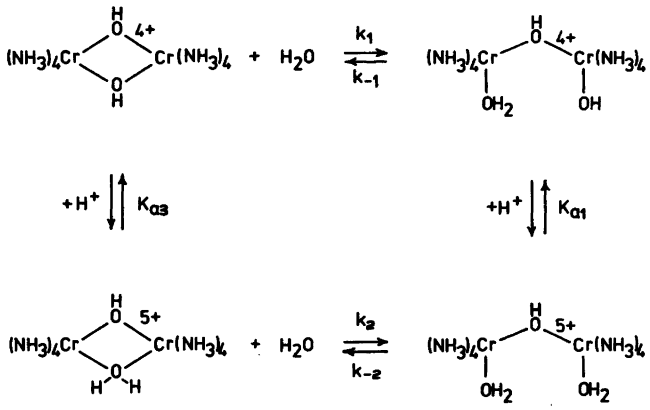

Scheme 1.

0302-4377/82/010021-10$02.50

systems. The reasons for this difference are not immediately obvious, and studies on related hydroxo- and dihydroxo-bridged binuclear chromium(III) systems are clearly required for a better understanding of the factors which determine the kinetic and thermodynamic properties of such systems. We have therefore extended our previous studies on the bis(ethylenediamine)chromium(III) systems to include the tetraamminechromium(III) system, and the present work describes our results for the latter.

RESULTS

Preparations. It is now more than fifty years since Dubsky[4] prepared salts of the dihydroxo bridged cation $[(NH_3)_4Cr(OH)_2Cr(NH_3)_4]^{4+}$, diol, by heating solid *cis*-$[Cr(NH_3)_4(OH)(H_2O)]SO_4.H_2O$. In the present work the diol is converted to its parent monohydroxo-bridged species, monools, as follows: When $[(NH_3)_4Cr(OH)_2Cr(NH_3)_4](ClO_4)_4.2H_2O$ was dissolved in 1 M $HClO_4$ at 55 °C the solution changed colour within minutes from purple to reddish owing to the equilibration reaction between the diol and the two monools, *i.e.* diaqua monool and aquahydroxo monool. The equilibrium between diol and aquahydroxo monool, eqn. (1), is shifted to the left.

$$[(NH_3)_4Cr(OH)_2Cr(NH_3)_4]^{4+} + H_2O \underset{k_{-1}}{\overset{K_1}{\rightleftarrows}} \underset{k_1}{} \quad (1)$$

cis,cis-$[(H_2O)(NH_3)_4Cr(OH)Cr(NH_3)_4(OH)]^{4+}$

Since the aquahydroxo monool reacts with acid giving the cation *cis,cis*-$[(H_2O)(NH_3)_4Cr(OH)Cr(NH_3)_4(H_2O)]^{5+}$, diaqua monool, it follows that the equilibrium is shifted toward monool in strong acid. It is important in this connection to emphasize that further acid hydrolysis of the monools, such as bridge cleavage to give the monomeric species *cis*-$[Cr(NH_3)_4(H_2O)_2]^{3+}$, is much slower than cleavage of the first hydroxo bridge in the diol. The equilibrated acid mixture therefore contains diol and a large amount of monool, mainly as diaqua monool, and a crude tetrachlorozincate chloride salt of the latter was isolated using fractional reprecipitation (yield 79 %). From this salt a pure aquahydroxo monool salt, *cis,cis*-$[(H_2O)(NH_3)_4Cr(OH)Cr(NH_3)_4(OH)][ZnCl_3(OH)].(ClO_4)_2$, was prepared and from the latter a pure diaqua monool salt, *cis,cis*-$[(H_2O)(NH_3)_4Cr(OH)Cr(NH_3)_4(H_2O)][ZnCl_4]_2Cl$, could be obtained. The visible absorption spectra in 1.0 M $HClO_4$ of these two salts are identical, confirming that they are pure.

Assignment of structures. The dihydroxo bridged structure of the diol cation, $[(NH_3)_4Cr(OH)_2Cr(NH_3)_4]^{4+}$, was proposed more than half a century ago by Dubsky,[4] and has since been established by X-ray single-crystal structure analysis of the dithionate salt and the bromide salt.[5]

The monools can exist as the three isomers *cis,cis,trans,trans* and *cis,trans* where *cis* and *trans* refer to the position of H_2O or OH relative to the bridge. The proposed assignment *cis,cis* is derived from the geometry of the diol and the well-known tendency of chromium(III) mainly to undergo thermal substitution without steric change.

The hydroxo-bridged structure of the monools is supported by several observations. The acid-base properties clearly establish the presence of two terminal (nonbridging) hydroxo groups. Strong evidence for the proposed structure is also provided by the observation that an aqueous solution of the monool at pH ≈ 5 reforms diol, which can be isolated nearly quantitatively (90 %) as the tetrachlorozincate salt. The ligand-field parameters, Δ, for the three monools are in agreement with the structure assignment. From the spectral data given in Table 1, the Δ values for the diaqua monool, the aquahydroxo monool and the dihydroxo monool, respectively, are calculated to be 19.46, 19.25 and 18.73 kK (1 kK = 1000 cm^{-1}). The observed decrease in Δ on the replacement of H_2O by OH^- is consistent with the spectrochemical series. Furthermore, the replacement of one H_2O by OH^- per Cr(III) corresponds to a decrease in Δ of 0.73 kK, and this is in excellent agreement with the corresponding decrease of 0.67 kK obtained from the Δ values[6] of *cis*-$[Cr(NH_3)_4(H_2O)_2]^{3+}$ and *cis*-$[Cr(NH_3)_4(OH)_2]^{+}$ (Δ = 20.16 kK and 18.83 kK, respectively). Finally, it should be mentioned that the thermodynamic and kinetic results described below fully confirm the structural assignments.

The ligand-field spectra (extrapolated to the time of dissolution) of solutions of diol perchlorate salt in perchlorate medium with $[H^+]$ varying from 1.0 to 10^{-5} M were identical within experimental accuracy (Table 1), confirming the absence of a terminal non-bridging hydroxo group. This result further implies that protonation of the diol to give a μ-aqua-μ-hydroxo dimer must be negligible for solutions with $[H^+] \leq 1.0$ M. Protonation of one hydroxo bridge will certainly change the ligand

Table 1. Spectral data at 25 °C and ionic strength 1.0 M.

Cation	Medium	$(\varepsilon,\lambda)_{max}$	$(\varepsilon,\lambda)_{max}$
$[(NH_3)_4Cr(OH)_2Cr(NH_3)_4]^{4+}$	1 M $NaClO_4$ [a]	(124.5, 536.0)	(67.3, 386.5)
cis,cis-$[(H_2O)(NH_3)_4Cr(OH)Cr(NH_3)_4(H_2O)]^{4+}$	1 M(H,Na)ClO_4 [b,e]	(98.0, 514.0)	(62.7, 380.0)
cis,cis-$[(H_2O)(NH_3)_4Cr(OH)Cr(NH_3)_4(OH)]^{4+}$	Pyridine buffer [c,e]	(97.7, 519.5)	(77.4, 385.5)
cis,cis-$[(OH)(NH_3)_4Cr(OH)Cr(NH_3)_4(OH)]^{4+}$	Ammonia buffer [d,e]	(100.0, 534.0)	(91.0, 402.0)

[a] Measured on the perchlorate salt. Identical values were obtained in 1 M $HClO_4$. [b] Calculated from spectra measured in 1 M $HClO_4$ and in pyridine buffer. See text. [c] Buffer solutions with the composition 0.1 M pyridine, 0.76 M $HClO_4$, 0.24 M $NaClO_4$, and 0.1 M pyridine, 0.24 M $HClO_4$, 0.76 M $NaClO_4$ gave identical values. [d] Buffer solutions with the composition 0.9 M NH_3, 0.1 M NH_4ClO_4, 0.9 M $NaClO_4$, and 1 M NH_3, 1 M NH_4ClO_4 gave identical values. [e] All measurements made on the aquahydroxo monool salt.

field spectrum considerably, and accordingly a lower estimate for the acid dissociation constant, K_{a3}, of the μ-aqua-μ-hydroxo species of $K_{a3} \geq 30$ M can be made if it is assumed that protonation to the extent of more than 3 % would have changed the spectrum measurably.

Spectra of the diaqua monool salt (extrapolated back to the time of dissolution) were recorded at unit ionic strength, maintained constant with $NaClO_4$, and with $[H^+]$ varying from 1.0 M to 10^{-10} M. The absorption curves changed with $[H^+]$ and all observations were consistent with the assumption that the monools in this $[H^+]$ region attain the two acid-base equilibria, (2) and (3).

$$[(H_2O)(NH_3)_4Cr(OH)Cr(NH_3)_4(H_2O)]^{5+} \overset{K_{a1}}{\rightleftarrows} [(H_2O)(NH_3)_4Cr(OH)Cr(NH_3)_4(OH)]^{4+} + H^+ \quad (2)$$

$$[(H_2O)(NH_3)_4Cr(OH)Cr(NH_3)_4(OH)]^{4+} \overset{K_{a2}}{\rightleftarrows} [(OH)(NH_3)_4Cr(OH)Cr(NH_3)_4(OH)]^{3+} + H^+ \quad (3)$$

The absorption spectra for solutions of the diaqua monool salt were unchanged but different from each other in the two pH regions $4.4 \leq pH \leq 5.1$ (pyridine buffer) and $9.3 \leq pH \leq 10.2$ (ammonia buffer), respectively, and therefore represent the spectra of the cations

cis,cis-$[(H_2O)(NH_3)_4Cr(OH)Cr(NH_3)_4(OH)]^{4+}$
and
cis,cis-$[(OH)(NH_3)_4Cr(OH)Cr(NH_3)_4(OH)]^{3+}$

(Table 1). The spectrum of the diaqua monool cation, *cis,cis*-$[(H_2O)(NH_3)_4Cr(OH)Cr(NH_3)_4(H_2O)]^{5+}$, was calculated from the spectrum of the diaqua monool salt in 1 M $HClO_4$ and the spectrum of the aquahydroxo monool species using the value for K_{a1} determined below.

Thermodynamic measurements. The equilibrium constant for the equilibrium between monool and diol, K_1 in eqn. (1), and the first acid-dissociation constant for the diaqua monool, K_{a1} in eqn. (2), were determined simultaneously from spectrophotometric measurements. The second acid-dissociation constant for the diaqua monool, K_{a2} in eqn. (3), was determined potentiometrically.

The spectra of acidic solutions initially containing monool or diol changed with time and became constant within one to seven hours at 25 °C. The spectral changes were accompanied by well-defined isosbestic points, and for each $[H^+]$ value the final spectra were identical for solutions initially containing monool and diol, respectively, as shown in Fig. 1. The final spectra clearly indicated an equi-

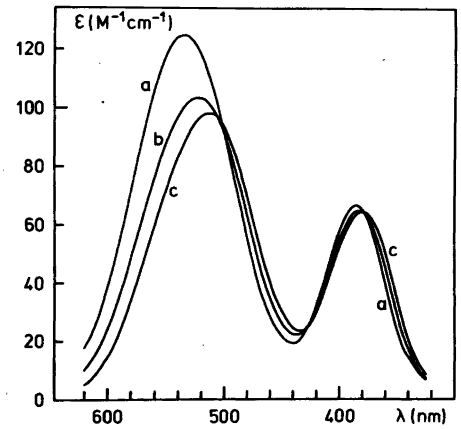

Fig. 1. Visible absorption spectra at 25 °C of 4×10^{-3} M solutions of $[(NH_3)_4Cr(OH)_2Cr(NH_3)_4](ClO_4)_4$ (a) and at equilibrium (b) and of $[(H_2O)(NH_3)_4Cr(OH)Cr(NH_3)_4(H_2O)](ZnCl_4)_2Cl$ (c) in 0.1 M $HClO_4$ 0.9 M $NaClO_4$.

Table 2. Kinetic and thermodynamic results[a] for the ammine system at ionic strength 1.0 M (Na, H)ClO_4.

Temp. °C	$k_1 \times 10^4$ s^{-1}	$k_{-1} \times 10^4$ s^{-1}	$k_2/K_{a3} \times 10^5$[b] $s^{-1}\,M^{-1}$	$k_{-2} \times 10^6$[b] s^{-1}	K_1	K_{a1} M	pK_{a2}
25.0	1.208(14)	3.80(4)	4.9(5)	2.7(3)	0.318(11)	0.0176(9)	7.50(5)
34.4	3.63(5)	10.58(15)	13.7(14)	12.7(13)	0.343(13)	0.0319(18)	–

[a] Activation parameters for k_1 and k_{-1} are given in Tables 3 and 4, and ΔH° and ΔS° values for K_1 and K_{a1} are given in Table 5. [b] $\Delta H^\ddagger(k_2) - \Delta H^\circ(K_{a3}) = 82(11)$ kJ mol^{-1} and $\Delta S^\ddagger(k_2) - \Delta S^\circ(K_{a3}) = -53(35)$ J $mol^{-1}\,K^{-1}$. $\Delta H^\ddagger(k_{-2}) = 123(11)$ kJ mol^{-1} and $\Delta S^\ddagger(k_{-2}) = +63(35)$ J $mol^{-1}\,K^{-1}$.

librated solution and all observations were in agreement with the stoichiometry expressed by eqns. (1) and (2).

The spectra of the pure monool mixture and of the pure diol species, and the spectra of the equilibrium solutions were measured in the $[H^+]$ region $1.0 \geq [H^+] \geq 10^{-5}$ M. It is easily seen that all these spectra allow a determination of the equilibrium constants K_1 and K_{a1} as described in the experimental section. The results are given in Table 2.

The second acid-dissociation constant for the diaqua monool was determined by glass electrode measurements. Solutions of monool made from pure monool salts are not suitable for this purpose since both of the isolated salts contain zinc(II) whose hydroxo complex formation would seriously complicate the measurements. The problem was solved by preparing the solutions of monool *in situ* by allowing a solution of diol perchlorate (0.01 M) in 0.01 M $HClO_4$, 0.99 M $NaClO_4$ to equilibrate at 25 °C. The equilibrium solution contains 32 % monool and 68 % diol, as calculated from K_1 and K_{a1} determined above, and since the diol does not exhibit acid-base properties in this pH region, K_{a2} could be determined from pH measurements on partially neutralized solutions. However, because of a rather rapid equilibration reaction between monool and diol, a normal titration could not be performed. Each point on the titration curve had therefore to be determined using a freshly prepared equilibrated solution. pH at the time of the addition of base was then calculated by a linear extrapolation based on pH measurements within the first five to ten minutes. From four such series of measurements the value $pK_{a2} = 7.50(5)$ [25 °C, $I = 1.0$ M ($NaClO_4$)] was then calculated.

Kinetic measurements. The kinetics for the equilibration reaction between monool and diol were investigated spectrophotometrically at two temperatures (25.0 and 34.4 °C) and at ionic strength 1.0 M [(Na,H)ClO_4]. In all experiments pseudo first-order conditions were employed, *i.e.* the change in $[H^+]$ during the reactions was never greater than 3 %. The change of absorbancy with time followed first-order kinetics for at least $3t_{\frac{1}{2}}$. Pseudo first-order rate constants for the reactions initially containing monool, $k_{obs}(M)$, and diol, $k_{obs}(D)$, respectively, were calculated from eqn. (5) using non-linear regression analysis.

Kinetic measurements on solutions initially prepared from diol were made in the $[H^+]$ region $10^{-3} \leq [H^+] \leq 1.0$ M. Strongly acidic solutions contain mainly monool at equilibrium (95 % monool at pH = 0), and kinetic measurements on solutions initially prepared from monool cannot be accurate in this region. Measurements on solutions initially containing monool were therefore made in the $[H^+]$ region $10^{-2} \leq [H^+] \leq 0.25$ M.

The variation of k_{obs} with $[H^+]$ is seen in Fig. 2 to be similar for the k_{obs} values obtained for solutions initially containing diol, k_{obs} (D), or monool, k_{obs} (M), and this is consistent with first-order reversible kinetics.

As established above, the stoichiometry of the equilibrium mixture can be described by the equilibrium between diol and aquahydroxo monool [eqn. (1)], and the acid-base equilibrium between the diaqua- and aquahydroxo monools [eqn. (2)]. However, the rate-expression derived from these equilibria alone is insufficient for a complete interpretation of the kinetic data, and an additional, acid-catalyzed reaction path must be included as shown in Scheme 1. From this reaction scheme the rate-expression (4) is derived:

$$k_{calc} = k_{calc}(D) = k_{calc}(M)$$
$$= k_1 + \frac{[H^+]k_2}{K_{a3}} + \frac{K_{a1}k_{-1} + [H^+]k_{-2}}{K_{a1} + [H^+]}$$
$$= k_1 + \frac{[H^+]K_1k_{-2}}{K_{a1}} + \frac{K_{a1}K_1^{-1}k_1 + [H^+]k_{-2}}{K_{a1} + [H^+]} \quad (4)$$

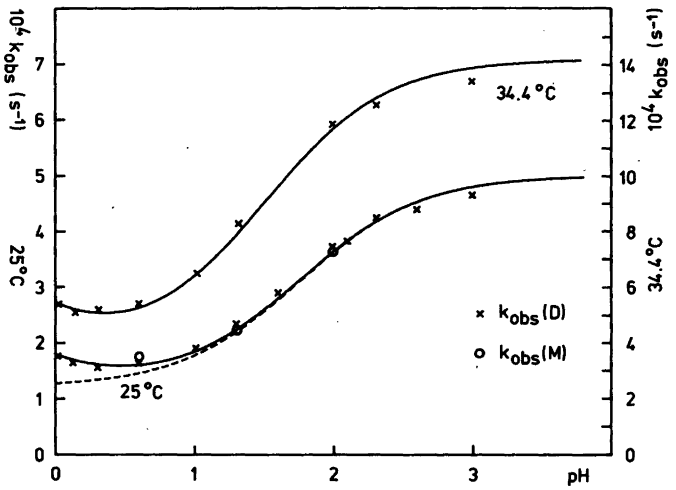

Fig. 2. The observed rate constants for the equilibration reaction between monool and diol as a function of pH=-log[H^+]. The solid lines represent the calculated values of k_{obs} for the proposed acid catalyzed reaction mechanism with K_{a1} and K_1 taken from Table 2. The broken line represents calculated values of k_{obs} at 25 °C, but without the acid catalyzed terms of eqn. (4), *i.e.* k_2 and k_{-2} have been set equal to zero.

assuming that $K_{a3} \gg [H^+]$, *i.e.* assuming that the protonation of the diol is stoichiometrically negligible as can be concluded from the spectral data for diol in strongly acidic media, and using the relations $K_{a3}/K_2 = K_{a1}/K_1$, $K_1 = k_1/k_{-1}$ and $K_2 = k_2/k_{-2}$.

Two of the parameters, K_1 and K_{a1}, in this equation have been determined thermodynamically as described above, and using these values (Table 2) our problem is then reduced to the determination of the two rate constants, k_1 and k_{-2}. This was done by the method of non-linear regression analysis and gave the parameter values shown in Table 2. It is seen (Fig. 2) that the values of k_{calc} and k_{obs} agree excellently, and also it is noted that all parameters are well defined (Table 2). This means that the thermodynamic results are consistent with the kinetic results, thereby providing strong support for the proposed reaction mechanism.

The results also support the observation mentioned above that $K_{a3} \gg 1$, but it is not possible to determine either K_{a3} or K_2 on the basis of the present data, and this is a consequence of the fact that the concentration of the μ-aqua-μ-hydroxo

Table 3. Comparison of kinetic data for the bridge-cleavage reactions of different diols. 25 °C and ionic strength 1.0 M (H, Na)ClO_4.

Diol	$k_1 \times 10^4$ s^{-1}	$\Delta H^{\neq}$ kJ mol^{-1}	$\Delta S^{\neq}$ J mol^{-1} K^{-1}	Ref.
Δ,Λ-$[(en)_2Cr(OH)_2Co(en)_2]^{4+}$	69(9)[138(17)][c]	78(3)	−25(12)[−20(12)][c]	7,8[a]
Δ,Λ-$[(en)_2Cr(OH)_2Cr(en)_2]^{4+}$	69(5)	79.9(19)	−18(7)	1[a]
Δ,Δ-Λ,Λ-$[(en)_2Cr(OH)_2Cr(en)_2]^{4+}$	46.1(19)	85.0(13)	−4(5)	2[a]
$[(NH_3)_4Cr(OH)_2Cr(NH_3)_4]^{4+}$	1.21(2)	86.7(15)	−29(5)	This work
Δ,Δ-Λ,Λ-$[(phen)_2Cr(OH)_2Cr(phen)_2]^{4+}$	0.69(3)	99(3)	+7(11)	9[b]

[a] Calculated from data at $t = 0.8$ and 20.0 °C in the quoted references. [b] From O^{18} exchange data in 0.1 M (H, Na)NO_3 and calculated from data given in the reference. [c] If it is assumed that the bridge cleavage in the mixed system essentially occurs with Cr−O bond-breaking, the k_1 value should be corrected with a statistical factor of 2 when compared with the remaining complexes giving the values in square brackets.

Table 4. Comparison of kinetic data for the reaction of aquahydroxo monool to diol. 25 °C and ionic strength 1 M (Na,H)ClO_4.[a]

Aquahydroxo monool	$k_{-1} \times 10^4$ s^{-1}	$\Delta H^{\neq}$ kJ mol^{-1}	$\Delta S^{\neq}$ J mol^{-1} K^{-1}	K_{a1} M	Ref.
Δ,Δ-Λ,Λ-$[(H_2O)(en)_2Cr(OH)Cr(en)_2(OH)]^{4+}$	207(8)	87.2(13)	15(5)	0.29(4)	2[a]
Δ,Λ-$[(H_2O)(en)_2Cr(OH)Cr(en)_2(OH)]^{4+}$	93(7)	84(2)	−0.69(7)	0.33(2)	1[a]
Δ,Λ-$[(H_2O)(en)_2Cr(OH)Co(en)_2(OH)]^{4+}$	18(2)	78(3)	−37(12)	0.05(2)[b]	7,8[a]
cis,cis-$[(H_2O)(NH_3)_4Cr(OH)Cr(NH_3)_4(OH)]^{4+}$	3.80(4)	80.6(15)	−40(5)	0.0176(9)	This work

[a] The parameters given here have been calculated from data at $t = 0.8$ and 20.0 °C from these references (see also comments on Table 5). K_{a1} is the acid-dissociation constant of the diaquamonools. [b] For the mixed system K_{a1} has been measured at 0.8 °C.

species is always stoichiometrically negligible in the $[H^+]$ region used in this study. Activation parameters for the rate constants k_1, k_{-1} and k_{-2} as well as values for the terms $\{\Delta H^{\neq}(k_2) - \Delta H^{\circ}(K_{a3})\}$ and $\{\Delta S^{\neq}(k_2) - \Delta S^{\circ}(K_{a3})\}$ are given in Tables 2, 3, and 4.

DISCUSSION

Kinetic and thermodynamic parameters for the equilibria between monools and diol have been reported previously for the two ethylenediamine diols[1,2] Δ,Λ-$[(en)_2Cr(OH)_2Cr(en)_2]^{4+}$ and Δ,Δ-Λ,Λ-$[(en)_2Cr(OH)_2Cr(en)_2]^{4+}$, and for the heterobinuclear diol[7,8] $(+)_D$-Λ,Δ-$[(en)_2Cr(OH)_2Co(en)_2]^{4+}$. The ammonia system and the above-mentioned ethylenediamine systems show several common features. For each of these systems, equilibrium between the monools and the diol is established fairly rapidly, although somewhat faster in the ethylenediamine systems than in the ammonia system. For all the complexes the equilibrium constant K_1 for the equilibrium between aquahydroxo monool and diol has a value around 1, and the diaqua monools are all unusually acidic, having pK_{a1} values in the region 0.5 − 2. However, the ammonia system differs from the ethylenediamine systems by the significant acid-catalyzed contribution to the equilibration reaction between monool and diol.

The literature contains two other related but less detailed studies: Results for the 1,10-phenanthroline-diol system[9] have been obtained from a study of the acid cleavage reaction of the diol Δ,Δ-Λ,Λ-$[(phen)_2Cr(OH)_2Cr(phen)_2]^{4+}$ to give monomeric diaqua species. In the latter study the monool species was neither isolated nor characterized. However, evidence was presented that the equilibrium constant K_1 for this system is much less than unity, and with this presumption an estimate for k_1 was obtained from O^{18} exchange studies.

The kinetics for the equilibrium between the aqua diol, $[(H_2O)_4Cr(OH)_2Cr(H_2O)_4]^{4+}$, and its corresponding monool have been studied at ionic strength 2.0 and at several temperatures, and the kinetic data were interpreted in terms of a mechanism similar to that shown in Scheme 1, *i.e.*, with an acid-catalyzed and an uncatalyzed reaction path.[3] The equilibrium constants, K_1 and K_{a1}, were not determined independently of the k_{obs} values, *i.e.* from A_0 and A_∞ values (although estimates for the ratio K_1/K_{a1} were obtained for ionic strengths higher than $I = 2.0$). All four parameters in eqn. (4) were therefore fitted on the basis of k_{obs} data alone. However, we have made some preliminary calculations using the data for 25 °C given in Ref. 3. These calculations clearly showed that the k_{obs} data do not require the inclusion of an acid-catalyzed reaction path. Because of this ambiguity in the interpretation of the kinetic data in the aqua system, this system will not be included in the following discussion.

Comparing the pK_a values of *cis,cis*-$[(H_2O)(NH_3)_4Cr(OH)Cr(NH_3)_4(H_2O)]^{5+}$ with those of *cis*-$[Cr(NH_3)_4(H_2O)_2]^{3+}$ ($pK_{a1} = 4.96$ and $pK_{a2} = 7.53$ in 1 M $NaClO_4$ at 25 °C)[10], two notable differences are apparent. Firstly, the diaquamonool is a much stronger acid than the parent monomeric diaqua complex, and secondly, the difference between pK_{a1} and pK_{a2} is larger (more than two pK units) for the hydroxo-bridged system, despite the fact that the two protolytic groups are more remote in the bridged complexes.

The lower pK_{a1} value for the monool can, to some extent, be explained in terms of charge effects,

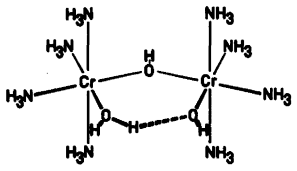

Fig. 3. The proposed hydrogen-bond stabilized structure of the aquahydroxo monool.

since we are comparing complexes with 5+ and 3+ charges, respectively. However, a charge effect alone cannot account fully for the observed difference, since on comparing the diaqua monool with the equally charged *cis*-aqua erythro ion, *cis*-$[(NH_3)_5Cr(OH)Cr(NH_3)_4(H_2O)]^{5+}$ ($pK_a = 3.5$ in 1 M $NaClO_4$, 25 °C),[11] it is seen that substitution of one water by ammonia increases pK_a by 1.5 (when comparing the acid strength of the aquaerythro with pK_{a1} for the diaqua monool, a statistical correction factor of 0.3 should be added to the latter).

As suggested previously in connection with the ethylenediamine monools,[1,2] which exhibit the same kind of 'anomalous' acid-base properties, the increased acid strength of the diaqua monools can be explained as being due to the existence of a hydrogen bond-stabilized conformation of the corresponding bases, aquahydroxo monools, as shown in Fig. 3. A similar internal hydrogen-bond stabilization might also be operative in the diaqua- and in the dihydroxo complexes, but the very symmetrical conformation in the aquahydroxo complex with H_2O donating hydrogen to OH is likely to be much more stable than those of the latter. pK_a for the 4+ charged aquahydroxo monool is almost identical to that for the 2+ charged mononuclear aquahydroxo species. This is in keeping with the discussion above, since in this case the effects of charge and of hydrogen-bond stabilization work in opposite directions.

The combined effects of charge and of hydrogen-bond stabilization of the aquahydroxo monools therefore qualitatively fully account for the exceptionally small values of pK_{a1}, as well as the large difference between pK_{a1} and pK_{a2}. The values of pK_{a1} for the *meso* and *racemic* isomers of the ethylenediamine monools are almost equal but more than one pK unit less than that of the ammonia monool (Table 5). This is paralleled by a similar but significantly smaller difference in the pK_{a1} values for the parent monomeric cations: *cis*-$[Cr(en)_2(H_2O)_2]^{3+}$ and *cis*-$[Cr(NH_3)_4(H_2O)_2]^{3+}$ ($pK_{a1} = 4.75$ and 4.96, respectively, 25 °C, $I = 1.0$ M).[10] In terms of the proposals made above, the large difference in pK_{a1} therefore could imply that in the ammonia system the hydrogen-bond stabilized conformation is less predominant than in the ethylenediamine systems, and some support for this proposal is provided by the thermodynamic parameters, $\Delta H°$ and $\Delta S°$. The formation of the hydrogen-bond stabilized structure in Fig. 3, from the non-hydrogen-bond stabilized conformation

Table 5. Comparison of thermodynamic parameters[a] for different monools and diols. 25 °C and ionic strength 1.0 M (H, Na)ClO_4.

Diol	K_1	$\Delta H°$ kJ mol^{-1}	$\Delta S°$ J mol^{-1} K^{-1}	K_{a1} M	$\Delta H°$ kJ mol^{-1}	$\Delta S°$ J mol^{-1} K^{-1}	pK_{a2}	Ref.
Δ,Λ-$[(en)_2Cr(OH)_2Cr(en)_2]^{4+}$	0.75(2)	−3.1(9)	−13(3)	0.33(2)[c]	+12(3)	+30(9)	7.94[d]	1[b,c]
Δ,Δ-Λ,Λ-$[(en)_2Cr(OH)_2Cr(en)_2]^{4+}$	0.22(3)	−1.9(4)	−19(13)	0.29(4)	+12(5)	+30(18)	6.87[e]	2[b]
$[(NH_3)_4Cr(OH)_2Cr(NH_3)_4]^{4+}$	0.318(11)	+6(4)	+11(14)	0.0176(9)	+49(6)	+129(20)	7.50(5)	This work
Δ,Λ-$[(en)_2Cr(OH)_2Co(en)_2]^{4+}$	4[g]	–	–	0.049(17)[d]	–	–	~8[g]	7,8
Δ,Δ-Λ,Λ-$[(phen)_2Cr(OH)_2Cr(phen)_2]^{4+}$	$\ll 1$[f]	–	–	–	–	–	–	9

[a] K_1 is the equilibrium constant for the equilibrium between aquahydroxomonool and diol, and K_{a1} and K_{a2} are the acid-dissociation constants for the corresponding diaquamonools. [b] Calculated from data given at 0.8 and 20 °C in these references. The standard deviation for the equilibrium constants have been calculated from the data in these references and from the original data material of these studies. [c] For the calculations of K_{a1} the value[15] $K_{a1} = 0.30$ at 20 °C has been used together with the data given in Ref. 1. [d] For $t = 0.8$ °C. [e] For $t = 20$ °C. [f] Estimated from O^{18} exchange data and spectrophotometric measurements in 0.1 M (Na, H)ClO_4.[9] [g] Estimated from unpublished data.

is certainly associated with a negative ΔH° and a negative ΔS°, and in agreement with this it is observed that the greater acid strength of the ethylenediamine system is accompanied by a decrease in ΔH° which is greater than the decrease in $T\Delta S^\circ$ (Table 5).

From the data in Table 3 it is seen that the rate constant, k_1, for the bridge cleavage reaction of the different diols decreases in the order Δ,Λ-en > $\Delta,\Delta-\Lambda,\Lambda$-en > NH_3 > 1,10-phen, and this order is followed by an increase in $\Delta H^{\neq}$. This relationship between k_1 and $\Delta H^{\neq}$ is normal for series of reactions of chromium(III) reactions.

The data given in Table 3 for the mixed diol, $\Delta,\Lambda-[(en)_2Cr(OH)_2Co(en)_2]^{4+}$, place this complex in the above sequence close to the *meso* ethylenediamine diol, both with respect to k_1 and $\Delta H^{\neq}$, which might suggest that in the mixed diol the k_1 path is essentially associated with Cr–O bond cleavage.

In the following discussion concerning the reaction of aquahydroxo monool to give diol, with rate constant k_{-1}, the data for the mixed CrCo system are included even though k_{-1} for the mixed system is a composite term due to the fact that ring-closure can occur both *via* $Cr-OH_2$ and $Co-OH_2$ bond-breaking. K_{a1} for the mixed system is also a composite term since deprotonation to form aquahydroxo monool can occur at two different metal centres. The following discussion should therefore be read with these reservations in mind. However, since bridge cleavage in the mixed diol probably occurs by Cr–O bond cleavage as suggested above, it seems probable, following the principle of microscopic reversibility, that k_{-1} is essentially associated with $Cr-OH_2$ bond-breaking.

From the data in Table 4 it is seen that the rate constant for diol formation, k_{-1}, for the ammonia monool and the three ethylenediamine monools decreases in the order $\Delta,\Delta-\Lambda,\Lambda-CrCr > \Delta,\Lambda-CrCr > \Delta,\Lambda-CrCo > NH_3-CrCr$. This order is at the same time the order of decreasing acid strength, K_{a1}, of the corresponding monools, and therefore, following the discussion above, it is the order of decreasing internal hydrogen-bond stabilization of the aquahydroxo monools. In order to explain this apparent correlation between k_{-1} and K_{a1}, we consider the possible effect on k_{-1} of the formation of hydrogen-bond stabilized conformations of the aquahydroxo monools.

Firstly, it is clearly reasonable to assume that the hydrogen-bond stabilized conformation resembles the transition state more than other conformations and should therefore contribute to k_{-1} by an enhancement of $\Delta S^{\neq}$. Simultaneously, the internal hydrogen bond has to be broken and this bond-breaking will contribute to k_{-1} in terms of increasing $\Delta H^{\neq}$. We therefore expect increasing $\Delta S^{\neq}$ to be associated with increasing $\Delta H^{\neq}$ and this is in good agreement with the experimental result of Table 4.

From the above discussion it is not possible to predict any relationship between k_{-1} and the degree of hydrogen-bond stabilization. The observation that increasing k_{-1} values are associated with increasing $\Delta S^{\neq}$ values is in the present case seen to be caused by a larger increase in $T\Delta S^{\neq}$. We therefore conclude that an increased hydrogen-bond stabilization of the aquahydroxo monool may be responsible for a simultaneous increase of K_{a1} and of the activation parameters $\Delta H^{\neq}$ and $\Delta S^{\neq}$ for the monool→diol reaction.

The equilibration reaction between monool and diol in the ammonia system proceeds *via* two reaction paths, the uncatalyzed reaction path (k_1 and k_{-1}) discussed above and an acid-catalyzed path (k_2/K_{a3} and k_{-2}) involving protonation of the diol hydroxo bridge. The acid-catalyzed contribution to k_{obs} is significant at low pH as shown in Fig. 2 and is ~30 % at pH = 0 (25 °C). A corresponding acid-catalysis term was not found in the ethylenediamine systems or the phenanthroline system and, as discussed before, the occurrence of an acid-catalyzed reaction path in the aqua system is not clearly established.

The rate of the reaction of the diaqua monool to give the aqua-bridged intermediate (k_{-2}) is ~100 times smaller than that of the aquahydroxo monool to give diol. This is not surprising since coordinated water is certainly a poorer nucleophile than coordinated hydroxide. Both reactions involve displacement of coordinated water but the activation parameters, $\Delta H^{\neq}$, are significantly different. This suggests an associative mechanism for both the k_{-1} and k_{-2} pathways, since in terms of an essentially dissociative mechanism the rate of chromium–water bond-breaking to form the transition state would probably be rather similar for the two monools and should thus lead to similar $\Delta H^{\neq}$ values.

An associative mechanism is clearly in keeping with the discussion above in connection with k_{-1}, and it is also in agreement with the well-documented fact that the water-exchange reactions of chromium(III) ammines, $[Cr(NH_3)_{6-n}(H_2O)_n]^{3+}$, are essentially associative.[12,13] The rate constant

for exchange of one water in *cis*-$[Cr(NH_3)_4(H_2O)_2]^{3+}$ is 5.9×10^{-5} s^{-1} at 25 °C ($I = 1.0$ M), and the activation parameters are $\Delta H^{\neq} = 95.0$ kJ mol^{-1} and $\Delta S^{\neq} = -7(6)$ J mol^{-1} K^{-1}.[14] Comparing these values with those for k_{-2}, it is seen that the nucleophilicity of water is tremendously decreased on coordination, reflected by a very large $\Delta H^{\neq}$ (k_{-2}) value. However, despite this, k_{-2} is only a factor of 20 less than the rate of water exchange, and this is due to a proximity effect, *i.e.* a very large $\Delta S^{\neq}(k_{-2})$ value.

EXPERIMENTAL

Materials. The complex $[(NH_3)_4Cr(OH)_2Cr(NH_3)_4](ClO_4)_4.2H_2O$ was prepared as described in the literature.[6] All chemicals were of analytical grade. CO_2-free distilled water was used for all spectrophotometric and potentiometric measurements.

Instruments. A Zeiss DMR 21 spectrophotometer was used for all spectrophotometric measurements in the visible region. For the spectrophotometric data given above the molar absorptivity ε is given in l mol^{-1} cm^{-1} and the wavelength λ in nm. The molarity of solutions of the binuclear complexes is in all cases defined in terms of the number of mol of complex, rather than the number of mol of chromium(III), per litre of solution.

The pH measurements were made with a GK 2301 C combined glass and calomel electrode in conjunction with a PHM 61 digital pH-meter (Radiometer, Copenhagen). The saturated potassium chloride electrolyte in the calomel electrode was replaced with 1 M sodium chloride in order to avoid precipitation of $KClO_4$ in the boundary between the medium and the electrode.

Analysis. Zink analyses were made by atomic absorption spectrophotometry. Chromium analyses by atomic absorption spectrophotometry were performed by Karen Jørgensen, Chemistry Dept. I, H. C. Ørsted Institute. H, N, Br and Cl analyses were performed by the microanalytical laboratory at the H. C. Ørsted Institute.

Preparations. 1. μ-Hydroxo-[*cis*-tetraammineaquachromium(III)] (*cis*-tetraamminehydroxochromium(III) trichlorohydroxozincate diperchlorate, *cis,cis*-$[(H_2O)(NH_3)_4Cr(OH)Cr(NH_3)_4(OH)][ZnCl_3(OH)].(ClO_4)_2$. Solid $[(NH_3)_4Cr(OH)_2Cr(NH_3)_4](ClO_4)_4.2H_2O$ (20.0 g, 28.2 mmol) was added to hot (55 °C) 1 M $HClO_4$ (120 ml). The diol salt dissolved within one minute and the colour changed from purple to reddish within minutes. The solution was kept at 55 °C for 15 min and to the resulting red solution was then added a saturated solution of $NaClO_4$ (35 ml) with stirring and cooling in ice for about ½ hour. The resulting precipitate of unreacted diol perchlorate salt (2.0 g) was filtered off. Addition of an ice-cold mixture of 12 M HCl (20 ml) and 4 M Li_2ZnCl_4 (40 ml) to the cold filtrate caused almost instantaneous precipitation of a crude diaqua monool salt, *cis,cis*-$[(H_2O)(NH_3)_4Cr(OH)Cr(NH_3)_4(H_2O)][ZnCl_4]_2Cl$, which was contaminated with a small amount of diol salt. The precipitate was filtered off, washed thoroughly with 96 % ethanol and dried in the air (yield 16.5 g, 79 %). This crude product (16.5 g) was dissolved in water (140 ml) at 0 °C and ice-cold 6 M LiCl (35 ml) and then a saturated (20 °C) solution of sodium perchlorate (35 ml) were added with cooling in an ice-bath and stirring. After 15 min a very small amount of purple diol salt was filtered off. 2 M sodium acetate (35 ml) was then added to the filtrate with continued stirring and cooling in ice, and red crystals precipitated almost immediately. The precipitate was isolated as above. The yield was 11.9 g (62 %) of a pure salt.

Anal $[(H_2O)(NH_3)_4Cr(OH)Cr(NH_3)_4(OH)][ZnCl_3(OH)].(ClO_4)_2$: Cr, H, N, Zn, Cl (ionic) and Cl (covalent). The salt is light-sensitive and was therefore stored in the dark. Visible absorption spectra are given in Table 1. The salt is soluble in water and in strong acids such as hydrochloric acid and perchloric acid.

2. μ-Hydroxo-bis(*cis*-tetraammineaquachromium(III))ditetrachlorozincate chloride, *cis,cis*-$[(H_2O)(NH_3)_4Cr(OH)Cr(NH_3)_4(H_2O)][ZnCl_4]_2Cl$ Pure *cis,cis*-$[(H_2O)(NH_3)_4Cr(OH)Cr(NH_3)_4(OH)][ZCl_3(OH)].(ClO_4)_2$ (5.0 g, 7.35 mmol) was dissolved at 0 °C in 1 M HCl (100 ml) and to the stirred solution was then added 4 M Li_2ZnCl_4 (25 ml) with cooling in ice. Red crystals of the diaqua monool precipitated almost immediately. The precipitate was filtered off and washed with 96 % ethanol and dried in the air. The yield was 5.3 g (97 %) of a pure salt. Anal. $[(H_2O)(NH_3)_4Cr(OH)Cr(NH_3)_4(H_2O)](ZnCl_4)_2.Cl$: Cr, H, N, Zn, and Cl.

Potentiometric determination of the second acid-dissociation constant K_{a2} *of the diaquamonool.* A 1.00×10^{-2} M solution of $[(NH_3)_4Cr(OH)_2Cr(NH_3)_4](ClO_4)_4.2H_2O$ in 10^{-2} M $HClO_4$, 0.99 M $NaClO_4$ was kept at 25 °C for 3 h. This gave an equilibrated solution containing 67.6 % diol and 32.4 % monool as calculated from the values of K_{a1} and K_1 given in Table 2. Aliquots of this equilibrium solution were then added to the appropriate volume of thermostatted 10^{-2} M NaOH, 0.99 M $NaClO_4$ with vigorous stirring.

Reliable readings on the pH-meter could be obtained about 30 s after the time of mixing. The measurements were continued over a period of 10 min and the pH at the time of mixing was determined by linear extrapolations which typically showed Δ pH/Δ min ≈ 0.02. The definition pH =

$-\log[H^+]$ was employed throughout, and concentration pH standards were made in the actual salt medium. pK_{a2} was calculated from 5 such series of measurements in the pH range of 7.0 to 7.9 (Table 2).

Spectra and treatment of spectral data. Spectra of monool and diol salts in the various media were obtained as recently described in detail for the *meso* ethylenediamine system.[1]

Kinetic measurements were made under pseudo first-order conditions, *i.e.* the change in hydrogen-ion concentration during a kinetic run never exceeded 3 %. Pseudo first-order rate constants, k_{obs}, were calculated from the absorbance A as function of time t by means of non-linear regression analysis, using the expression (5) where A_o is the

$$A = A_\infty + (A_o - A_\infty)\exp(-k_{obs}t) \quad (5)$$

absorbance at $t=0$ and A_∞ is the absorbance at equilibrium. The rate constants were calculated on the basis of absorbances measured at wavelengths 560 and 540 nm, and duplicate kinetic runs were always made. The activation parameters $\Delta H^{\neq}$ and $\Delta S^{\neq}$ were calculated from eqn. (6),

$$k_r = (kT/h)\exp(-\Delta H^{\neq}/RT + \Delta S^{\neq}/R) \quad (6)$$

The equilibrium constants K_{a1} and K_1 were calculated from ε_o and ε_∞ values obtained for solutions initially containing diol [ε_o(D) and ε_∞(D)] or monool [ε_o(M) and ε_∞(M)], the ε-values being measured at the four wavelengths 560, 540, 400 and 380 nm. At 560 and 540 nm, ε_o and ε_∞ values were calculated using A_o and A_∞ values from the kinetic calculation [eqn. (5)]. At 400 and 380 nm A_o values were obtained by linear extrapolation back to the time of dissolution and A_∞ values were measured at $t = 7t_{\frac{1}{2}}$. The variation in the observed ε-values with the hydrogen-ion concentration, at a given wavelength and temperature, can be expressed by eqns. (7)–(9), where ε_1, ε_2 and ε_3 are the

$$\varepsilon_o(D) = \varepsilon_1 \quad (7)$$

$$\varepsilon_o(M) = \frac{\varepsilon_2 \cdot K_{a1} + \varepsilon_3[H^+]}{K_{a1} + [H^+]} \quad (8)$$

$$\varepsilon_\infty(M) = \varepsilon_\infty(D) = \frac{\varepsilon_1 K_{a1} + \varepsilon_2 K_{a1} K_1 + \varepsilon_3[H^+]K_1}{K_{a1} + K_{a1}K_1 + [H^+]K_1} \quad (9)$$

molar absorption coefficients of diol, aquahydroxo monool and diaqua monool, respectively. These parameters together with K_{a1} and K_1 were then fitted using least-square non-linear regression analysis. The calculations were made simultaneously for data obtained at the two temperatures 25.0 and 34.4 °C. Data for ε_o and ε_∞ were obtained for solutions with $[HClO_4]$ varying from 1 to 10^{-3} M. In some experiments the actual concentration of hydrogen ion deviated from the stoichiometric concentration of perchloric acid due to the acid-base equilibrium [eqn.(2)]. These deviations were never greater than 3 % and were accounted for in the final calculations.

Acknowledgements. The authors wish to thank Dr. Martin Hancock for revising the English manuscript, and Dr. Ole Mønsted for valuable comments.

REFERENCES

1. Springborg, J. and Toftlund, H. *Acta Chem. Scand. A 30* (1976) 171.
2. Christensson, F., Toftlund, H. and Springborg, J. *Acta Chem. Scand. A 34* (1980) 317.
3. Thompson, G. *Lawrence Radiation Laboratory Report*, UCRL-11410, Berkeley, California, 1964.
4. Dubsky, J. V. *J. Prakt. Chem. 90* (1914) 61.
5. Cline, S., Kallesøe, S., Hodgson, D. and Pedersen, E. *Inorg. Chem. To be published.*
6. Springborg, J. and Schäffer, C. E. *Inorg. Synth. 18* (1978) 75.
7. Springborg, J. and Schäffer, C. E. *Inorg. Chem. 15* (1976) 1744.
8. Springborg, J. and Schäffer, C. E. *Acta Chem. Scand. A 30* (1976) 787.
9. Wolcott, D. and Hunt, J. B. *Inorg. Chem. 7* (1968) 755.
10. Mønsted, L. and Mønsted, O. *Acta Chem. Scand. A 30* (1976) 202.
11. Bjerrum, J., Schwarzenbach, G. and Sillén, L. G. *Stability Constants of Metal-Ion Complexes*, Part I. The Chemical Society, 1st Ed., London 1957, 2nd Ed., London 1964, 3rd Ed., London 1971.
12. Mønsted, L. *Acta Chem. Scand. A 32* (1978) 377 and references therein.
13. Mønsted, O. *Acta Chem. Scand. A 32* (1978) 297.
14. Mønsted, L. and Mønsted, O. *Acta Chem. Scand. A 34* (1980) 259.
15. Springborg, J. *Unpublished results.*

Received April 30, 1981.

Acta Chemica Scandinavica A 36 (1982) 31 – 38

Solvent Effects on the Racemization of Optically Active Biphenyl Derivatives

LARS BALTZER and NILS-ÅKE BERGMAN

Department of Organic Chemistry, University of Göteborg and Chalmers University of Technology, S-412 96 Göteborg, Sweden

The biphenyl derivative 2,2′-dihydroxy-6,6′-dinitrobiphenyl has been synthesized. As a minor by-product 2-hydroxy-2′-methoxy-6,6′-dinitrobiphenyl was also obtained. The inversion rates of the former and its dianion and of the anion of the latter have been measured in a range of solvents.

A large rate increase is observed for the dianion of 2,2′-dihydroxy-6,6′-dinitrobiphenyl when the solvent is changed from water to 95 mol % of dimethyl sulfoxide in water. The effect is interpreted as being due to desolvation of the dianion by dimethyl sulfoxide.

The kinetic solvent isotope effect on the inversion of the dianion has been measured. In water the effect is negligible, and added dimethyl sulfoxide has no effect on the isotopic rate ratio. In methanol $k^{OH}/k^{OD} = 0.93 \pm 0.02$. The effect is somewhat more pronounced in 25 mol % of dimethyl sulfoxide in methanol, $k^{OH}/k^{OD} = 0.83$. The increase in the strength of the effect is probably due to increased fractionation because of desolvation.

The biphenyl frame-work has provided a very useful model system for a large variety of investigations. A multiplicity of derivatives has been used for the study of steric,[1] salt[2] and solvent effects.[3] A particularly beautiful example is the elucidation of the nature of steric isotope effects with protium and deuterium.[4] In view of the very simple and well-known geometry of the biphenyl inversion reaction we decided to use it for our study of hydrogen-bond types of interaction between oxyanions and hydroxylic solvents. In an earlier investigation,[5] the rate of racemization of the dianion of 6-nitrodifenic acid was determined in light and heavy water. The results were interpreted in terms of the fractionation theory[6] and a model was suggested where the numbers of solvating molecules in the initial and transition states were given.

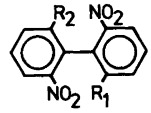

I $R_1 = R_2 = O^-$
II $R_1 = R_2 = OH$
III $R_1 = O^-, R_2 = OCH_3$
IV $R_1 = OH, R_2 = OCH_3$
V $R_1 = R_2 = OCH_3$

Scheme 1.

In order to extend the study, an optically active biphenyl derivative, 2,2′-dihydroxy-6,6′-dinitrobiphenyl (II), with the possibility of more concentrated charges in the ortho positions, has been synthesized and the range of solvents has been extended. A study of this kind provides some insight into the phenomena of solvation in sterically hindered systems, and the results obtained should be useful in discussing other sterically hindered systems where our knowledge of the solvation is very limited, *e.g.*, the transition states of chemical reactions.

EXPERIMENTAL

2,2′-Dimethoxy-6,6′-dinitrobiphenyl (V) was prepared according to the method of Adams and Finger[7] with the following modifications. Methylation of 2-chloro-3-nitrophenol was carried out according to Brändström.[8] Ullman coupling of 2-chloro-3-nitroanisole was performed in a melt, according to standard procedures.[9] The compound V so obtained, consisted of yellow crystals, m.p. 228 – 230 °C (lit.[7] 226 – 228 °C).

2,2′-Dihydroxy-6,6′-dinitrobiphenyl (II) was obtained from V by cleavage of the alkyl aryl ether using $AlCl_3$ in the dry.[10] The compound V (1.8 g) was carefully ground in a mortar with 4 g of $AlCl_3$,

0302-4377/82/010031-08$02.50

under nitrogen. The material was put in a round-bottomed flask equipped with a drying tube, and the flask was heated at 90 °C overnight. The reactants were again ground in the mortar with an additional portion of $AlCl_3$, 1 g, and heated at 110 °C for two hours. The contents of the flask were poured onto ice. The mixture was made basic and filtered, the deeply red filtrate acidified and filtered to give yellow crystals. Esterification with acetyl chloride, chromatography on silica gel with dichloromethane followed by hydrolysis of the two products in 0.5 M NaOH in 50% ethanol–water (v/v) gave the following yields: the compound II, 180 mg (11%) m.p. 295 °C and IV, 30 mg m.p. 223 °C. Some unreacted starting material (0.6 g) could also be recovered. An attempt to cleave the ether groups by BBr_3[11] was unsuccessful.

Resolution of II and IV. The crude product after cleavage with $AlCl_3$ was considered pure enough for this step. In order to resolve the compounds they were converted into diastereomeric esters[12] with the acid chloride of (+)-2-phenylbutyric acid (Norse Laboratories, Inc.). The acid chloride was prepared by treatment of the acid with excess of freshly distilled $SOCl_2$,[13] and the optical activity of the obtained acid chloride was $[\alpha]_D^{25} = +94.5$ (*c.* 2.25, benzene). The mixture of diastereomeric esters was separated by HPLC using a stainless steel column (30 cm, 7.7 mm I.D.) packed with silica gel (Porsil, Waters Ass.) and cyclohexane–acetone 9:1 (v/v) as eluent. Base-line separation was nearly achieved but due to low solubility in suitable solvents no attempt was made to estimate optical purity. The optically active esters were hydrolyzed as described above. Melting point of (+)- II, 267 °C (decomposes). Optical activity of (+)- II: $[\alpha]_D^{20} = +675$ (*c.* = 0.114, methanol).

The identity of II was established from mass spectrometric analysis and by NMR. The identity of IV was established from NMR. Both compounds were those expected from the synthetic procedure.

Solvents from the following manufacturers were used without further purification. Methanol (May & Baker, Methanol Anhydrous, water less than 0.01%, w/w), methanol-*O*-*d* (Ciba-Geigy 99.7 atom % D) and in later runs 99.9 atom % D, *ultrapur* (when the first-mentioned quality was withdrawn from the market), DMSO (Riedel-de Haën, getrocknet für Analyse, less than 0.01% water, w/w), DMSO-d_6 (Ciba-Geigy 99.5 atom % D) and deuterium oxide (Ciba-Geigy 99.7 atom % D). Light water was deionized, distilled and boiled out under nitrogen. Ethanol (Kemetyl AB, absolute ethanol, 99.5%) and *t*-butanol (FLUKA, *tert*-butyl alcohol, *puriss. p.a.*) were purified according to the method of Bjerrum and Lund.[14] To test the water content of some of the solvents, the commercial methanol and the purified ethanol and *t*-butanol were subjected to Karl Fischer titration. In no case did the water content exceed 0.012% (w/w).

Base solutions were prepared in the following way. Sodium hydroxide from commercially available ampoules, sodium deuteroxide by dilution of a commercially available solution, (Merck, Natronlauge-d_1) with deuterium oxide. Sodium methoxide and ethoxide and potassium *t*-butoxide by dissolving clean sodium or potassium metal in the respective solvent. Preparation of base solutions was carried out under nitrogen. All base solutions were titrated against 0.1 M HCl or potassium hydrogen phthalate. Mixed solvents were prepared by weight and base solutions were diluted by weight.

The kinetic runs were performed in three different ways depending on the reaction rate and on the optical density of the solutions. The reactions in water and a few of the reactions in DMSO–water were followed in a polarimeter cell of a Zeiss Digital Polarimeter Old 5, that was connected to an automatic data collecting assembly. When the solutions were too coloured to allow the polarimeter to read accurately the optical rotation of the reaction solution, sealed ampoules had to be used during the reaction, and when the reactions had half-lives of 20 min or less the reaction solution was kept in a gas-tight bottle sealed with a septum and the samples were collected with a Hamilton syringe. In the ampoule and gas-tight bottle experiments the aliquots were acidified and the optical rotation of the undissociated compound was determined.

Treatment of data. The rate constants were calculated with a least-squares program or with the program PROGAEXP that fits an exponential expression to the experimental data. This program was used in the polarimetric runs.

Check experiments. On some occasions racemizations were run for more than ten half-lives in order to check the kinetics. No deviations from first-order kinetics could be detected. Several of the kinetic runs were followed by UV/VIS spectroscopy to detect any deterioration of the substrate. Only in one solvent, ethanol, did this occur. These reactions were therefore not monitored for more than one half-life, and the results from them should be treated with some caution.

The maximum of the longest wave-length absorption of I appears at 395 ± 5 nm in water, methanol, ethanol and *t*-butanol. It is sensitive to the DMSO content in the binary mixtures, and it is red-shifted as much as 50 nm at high DMSO concentrations. In *t*-butanol solutions of predominant DMSO content a new absorption band is observed at 495 ± 5 nm. Its intensity grows with x_{DMSO}. The band is also seen in *t*-butanol in the presence of excess of crown-ether. The significance of the new absorption is not known.

Table 1. Racemization of I in different solvent systems. Counterion: Na^+ (K^+ in *t*-BuOH and mixtures of it). Temperature 333.15 K.

Solvent	Mol fraction DMSO	$k \times 10^{-5}/s^{-1}$ [a]
H_2O–DMSO	0	0.172±0.003
	0	2.26±0.02 [b]
	0	2.31±0.02 [b,c]
	0.251	1.31±0.06
	0.500	7.49
	0.516	7.72
	0.751	24.9
	0.954	100
D_2O–DMSO	0	0.165±0.009
	0	2.20±0.02 [b]
	0	2.24±0.02 [b,c]
	0.249	1.30
	0.251	1.29
	0.503	7.06
	0.752	25.7
	0.951	89.1
MeOH–DMSO	0	0.927±0.002
	0.246	3.20
	0.251	3.27
	0.253	3.21
	0.259	3.43
	0.265	3.80
	0.606	15.6
	0.820	32.2
	0.947	57.7
	0.950	74.9
MeOD–DMSO	0	0.992±0.009
	0.247	3.90
	0.264	4.15
	0.591	15.0
	0.793	27.6
t-BuOH–DMSO	0	8.40±0.07
	0	145±6 [d]
	0.131	7.52
	0.263	7.77
	0.507	20.9
	0.761	78.3
EtOH	0	1.17

[a] The values are mean values of at least two runs and error limits correspond to maximum deviation from the mean value. Single measurements are given without error limits. In most runs the error limits within one run are less than 2%, but at high DMSO concentrations the reproducibility probably is not better than ±5% because of the dramatic effect of fortuitous water. [b] Temperature 353.15 K. [c] In the excess of cryptand 2.2.1. [d] In the presence of 18-crown-6.

In order to investigate the influence of the ionic strength on the rate of the reaction of I in water, some runs were performed with varying concentration of NaOH (0.05–0.15 M). No significant variation of the rate could be detected within the studied concentration interval.

RESULTS

The rate of racemization of I has been determined in a number of solvents and the results are given in Table 1. The rate increases by a factor of 600, relative to that in water, when the reaction is run in 95 mol% of dimethyl sulfoxide (DMSO) in water. Comparing methanol, ethanol and tertiary butanol the rate increases in a way that parallels their respective basicities. The importance of ion-pairing to the rate of racemization has also been investigated and in all solvents but those including butanol, it has been found to be negligible. The conclusion was drawn from kinetic runs (water) in the presence of cation complexing agents, the rates being indistinguishable from those obtained in the absence of such agents, and from electronic spectra.

In methanol and ethanol, the spectra were identical before and after addition of a crown ether or a cryptand. In *t*-butanol a batochromic shift is observed on addition of crown ether.

The effect on the rate of reaction by substitution of deuterium for protium in the hydroxylic positions of the solvent molecules has been determined in water, methanol and their mixtures with DMSO, Table 2. The effect in water is very weak, and addition of DMSO does not have any significant influence on the isotopic rate ratio, the apparent difference at high mol fractions of DMSO (Table 1) being probably due to the large uncertainty in the determinations. In methanol, however, the isotope

Table 2. Kinetic solvent isotope effect on the racemization of I in various solvents. Temperature 333.15 K.

Solvent	Mol fraction DMSO	k^{OH}/k^{OD}
L_2O	0	1.042±0.07
L_2O	0	1.027±0.018 [a]
MeOH–DMSO	0	0.93±0.02
	0.25	0.83
	0.60	~1

[a] Temperature 353.15 K.

Table 3. Racemization of II and III. Counterion Na^+ with III. Solvent $H_2O-DMSO$. Temperature 353.15 K.

Substrate	Mol fraction of DMSO	$k \times 10^{-5}/s^{-1}$ [a]
II	0	0.028
	0.99	0.0893
III	0	0.871 ± 0.022
	0.503	20.0

[a] See footnote [a] in Table 1.

effect is pronounced, giving $k^{OH}/k^{OD} = 0.93 \pm 0.02$, and in 25 mol % of DMSO in methanol the rate constant ratio is decreased even further.

For comparison with I, the rate of racemization of 2,2'-dihydroxy-6,6'-dinitrobiphenyl (II) and 2-hydroxy-2'-methoxy-6,6'-biphenyl anion (III) have been studied in some solvents and the results are given in Table 3. The biphenol, II, is slower than I by a factor of 80 at 353 K in water, and in mixtures of DMSO and water of mol fractions of DMSO larger than 0.95, the reaction of I is more than 1100 times faster. The reaction rate of III is slightly slower than that of I in water at 353 K, and the rate in an equimolar mixture of DMSO and water is increased by a factor of 23 relative to the former solvent. For comparison, the corresponding increase for I at 353 K amounts to a factor of 44.

DISCUSSION

The solvent effect on the rate of racemization of biphenyl derivatives is generally very small. In one investigation the rates in widely different solvents were all within a factor of five.[3] The large increase presented here is therefore indicative of specific solute–solvent interactions. In the following, solvent effects and solvent isotope effects on the rate of racemization, together with spectroscopic data, will be used to assign numbers of hydrogen-bonded solvating molecules to the reactant and transition states.

Solvent effects. The role of DMSO in mixtures with hydroxylic solvents is to act as an acceptor of hydrogen bonds from its cosolvent and to desolvate the anions. The rate increase in the racemization of I is consequently interpreted in these terms.

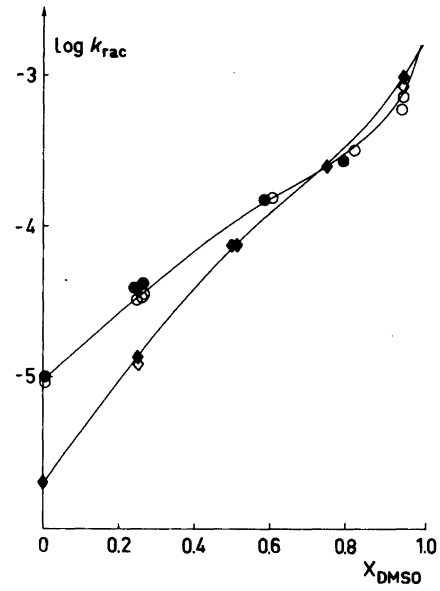

Fig. 1. Variation of the logarithm of the rate constant for racemization of I in mixtures of hydroxylic solvents with DMSO. Temperature 333.15 K. ●, MeOD/DMSO; ○, MeOH/DMSO; ◆, H_2O/DMSO; ◇, D_2O/DMSO.

The charged oxygen atoms of I are solvated by a number of hydroxylic molecules. In the inversion reaction, the ortho substituents have to pass each other and a sterically hindered transition state is reached in the process. Some of the solvating molecules are then scraped off. In the pure hydroxylic solvent the reactant carries more solvent molecules than the transition state and is more destabilized on addition of DMSO to the solution. The result is that when the DMSO content is increased in the solution, the rate of the reaction is enhanced (Fig. 1). If this interpretation is correct a similar effect would also be expected in hydrogen bonding solvents where the hydrogen-bond donating ability is weaker than in water. The results from kinetic runs in some alcohols, Table 1, are in agreement with this prediction.

Comparison with II and III that have fewer hydrogen-bond accepting sites than I also corroborates our hypotesis. The racemization rate of II is not enhanced much, only a factor of three on transfer from water to 99 mol % DMSO–water (Table 3), an increase that is of the same magnitude as those already reported for substrates without specific interactions with the solvent. The anion III

has only one charged oxygen atom and should be solvated by about half as many molecules as I. If that is so, the number of solvent molecules that will have to be scraped off is also expected to be half the number for I. A rate increase for III is therefore anticipated that is weaker than that of I, corresponding to a decrease in the free-energy of activation by half the amount for I. This is qualitatively born out, Table 3.

However, one must realize at this point that the making or breaking of hydrogen bonds should contribute to the enthalpy of activation, a quantity that is unknown to us. Without any knowledge of the activation parameters the question might be raised whether we are, in fact, dealing with an entropy effect. An increase in the activation entropy of 59 J/mol K would account for the variation in rate between water and DMSO (Fig. 1) observed for compound I. This is not very likely to be the explanation as entropies of activation in the biphenyl system are generally negative and small, -21 to -63 J/mol K. Thus, it seems unlikely that the solvent effects on the rate should be mainly entropy effects, but a minor contribution may be included.

Another alternative explanation might be that there is some strong interaction between DMSO and the transition state of I that accelerates the racemization. The rationalization for such an argument would be found in the fact that large polarizable anions show solvent activity coefficients of less than unity in dipolar solvents, when hydroxylic ones are used as reference solvents.[15]

Experimental evidence which makes this explanation rather unlikely comes from a comparison of the rate of racemization of I in *t*-butanol and DMSO, respectively, (for possible pitfalls with respect to the *t*-butanol results, see above). In a plot of log k_{rac} *versus* the mol fraction of DMSO, x_{DMSO}, Fig. 1, an extrapolation to $x_{DMSO}=1$ gives a good measure of the rate in pure DMSO. The rate in DMSO coincides very closely with that in *t*-butanol in the presence of excess crown ether. Unless it is a pure coincidence, the only explanation appears to be that *t*-butanol is a very weak hydrogen-bonding solvent and that I is practically unsolvated in both solvents. In that case, the conclusion is inescapable that polarization of the transition state contributes negligibly to the reaction rate, *t*-butanol and DMSO being too different as solvents, with respect to most physical properties,[16] to give similar rates otherwise.

Salt effects. Apart from a non-specific "medium" effect, here of negligible magnitude (see Experimental), chelate formation with a cation may occur when negatively charged groups are situated in the ortho positions of the two rings. A slower reaction is expected with the chelate than with the free dianion. The rate of racemization of I in *t*-butanol with the potassium ion as counter-ion is increased 17 times when 18-crown-6 is added in excess, (Table 1). We take this as proof of a tendency for chelate formation between I and the potassium ion.

Provided that the inversion rate of the chelate is negligible the observed rate constant in such a case is [2a]

$$k_{obs} = k_{rac}\frac{1}{1+K[M^+]}$$

where $[M^+]$ is the concentration of cations, K is the equilibrium constant for chelate formation,

$$K = \frac{[IM^+]}{[I][M^+]}$$

In the presence of excess of a powerful complexing agent, no chelation with I occurs, $k_{obs}=k_{rac}$, and comparison with the observed rate constant in the absence of complexing agent, allows calculation of K. In the present case it has been determined as $K = 230 \pm 30\ M^{-1}$.

In the absence of a complexing agent the rate is enhanced when the mol fraction of DMSO in *t*-butanol is increased above 0.25 and approaches that in pure DMSO, as estimated from the methanol and water mixtures with DMSO, (Table 1).

In water, the addition of cryptand (2,2,1) does not significantly change the rate of reaction. The electronic spectra of I in methanol and ethanol are not affected by the addition of crown ether. We conclude that chelate formation is of negligible importance in these solvents, but would like to add that here the sodium ion has been the counter-ion.

Solvent isotope effects. To elucidate the possible use of fractionation theory to assign numbers of molecules to solvating positions, the kinetic solvent isotope effect on the rate of racemization of I has been determined in water, methanol and their mixtures with DMSO, Table 2. Adapted to the present conditions, the theoretical expression describing the rate-constant ratio for the

racemization reaction in isotopic solvents is given by (1).[5]

$$k^{OH}/k^{OD} = \prod_i \phi_{Ri} / \prod_j \phi_{Tj} \quad (1)$$

The k's are the rate constants for racemization in deuterated (OD) or protiated (OH) solvent. The fractionation factors ϕ are given for each fractionating position in the reactant (R) and the transition state (T). The interpretation may be expected to be complicated since all parameters are expected to change on going into DMSO mixtures. The magnitude of ϕ can, for the present purpose, be given the simplified meaning that it is lower the stronger the hydrogen bond is.

The solvent isotope effect in water is very weak, a surprising fact at first, but probably due to cancellation between the denominator and the numerator of eqn. 1. Addition of DMSO does not alter the magnitude of the isotope effect and, as mentioned above, the apparent effect at high mol fractions of DMSO merely reflects the experimental difficulties at those solvent compositions.

In methanol the effect is clearly perceivable and in 25 mol % of DMSO in methanol the rate constant ratio decreases even more, but at 60 mol % of DMSO the effect is gone (Table 2). In methanol there is undoubtedly a difference in fractionation in the solvation shell of the reactant and the transition state. The effect is not impressive, however, so it is quite possible that some of the solvating molecules are still present when the transition state is reached, giving rise to some cancellation and diminishing the effect. The reason why the solvent isotope effect is strengthened when a dipolar solvent is added is that the contribution to the kinetic solvent isotope effect (1) from the reactant, compared to the transition state, is increased because of desolvation.

Such behaviour has been noted before[17] and is not restricted to desolvation by a dipolar non-hydroxylic solvent. The same effect is achieved by a steric obstacle that keeps the solvent away from the hydrogen-bonding sites, as can be deduced from the run in water where the isotope effect is nearly invisible in spite of the fact that it is very likely that there should be appreciable fractionation in the solvation shell of I. The evidence for this comes from an NMR experiment where an isotope effect on the chemical shift of the hydroxylic hydrogens has been established on addition of 0.61 M of I.[18] There are two reasons for an isotope effect to occur on the chemical shift of hydrogen. One is an anharmonicity effect[19] that occurs in systems with strong hydrogen bonds. The other reason is isotopic fractionation.[20] Under the assumption that the potential well does not exhibit anharmonicity we may conclude that fractionation occurs.

Solvation model. From the results in the mixed solvents, some conclusions may be drawn about the detailed solvation of I.

Recollecting that in the transition-state theory[21] any by-product in the formation of the activated complex appears in the denominator of the expression for the observed rate, we have

$$\text{Rate} = k_o \times \frac{f_I}{f_S^p f_{\neq}} \times \frac{[(+)\text{-I}]}{[S]^p}$$

In the present case the by-products may be identified with the p hydroxylic solvent molecules, S, that are scraped off in the coplanar conformation of I. The symbol f stands for activity coefficient and k_o is the rate constant in the standard state. We choose the pure hydroxylic solvent as standard state.

Taking logarithms of the pseudo first-order observed rate constant (k_{obs}),[22] we find

$$\log (k_{obs}/k_o) = -p \log a_S + \log(f_I/f_{\neq})$$

A plot of $\log (k_{obs}/k_o)$ *versus* $\log a_S$ should give a slope of $-p$. The second term is also a function of the composition of the solvent. In the limit as the composition of the solvent tends toward that of the pure hydroxylic solvent, the slope should be affected very little by the activity-coefficient ratio.

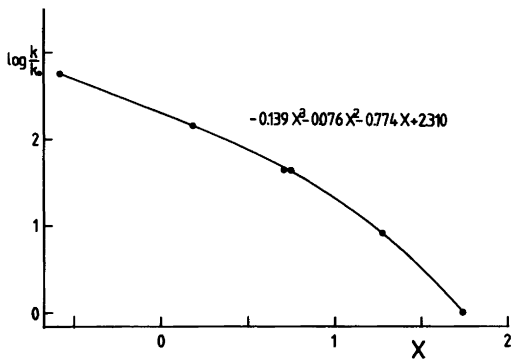

Fig. 2. Plot of $\log k/k_o$ *versus* $x = \log a_{H_2O}$. $k = k_{obs}$ and k_o (rate constant in H_2O) are obtained from Table 1. a_{H_2O} is calculated from literature data, see text. The solid curve is given by the polynomial.

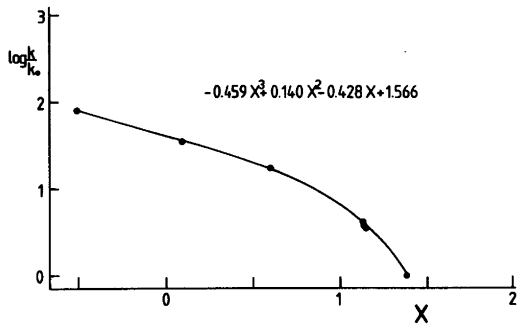

Fig. 3. Plot of $\log k/k_o$ *versus* $x = \log a_{MeOH}$. $k = k_{obs}$ and k (rate constant in MeOH) are obtained from Table 1. a_{MeOH} is calculated from literature data, see text. The solid curve is given by the polynomial.

The results for the DMSO–water mixtures are presented in Fig. 2 and those for the DMSO–methanol mixtures are given in Fig. 3. The activity (a_S), in a mixture of a hydroxylic solvent with DMSO has been defined as $a_S = [\text{hydroxylic solvent}] \times f_S$, f_S being the activity coefficient of the hydroxylic solvent in that mixture.[23,24] The concentration of the hydroxylic solvent in a given mixture has been calculated from published density data.[25,26] The experimental data are fitted to polynomials from which the slopes at $x_{DMSO} = 0$ are obtained.

In DMSO–water $p = 2.3$ and for DMSO–methanol, $p = 2.7$. For simplicity, the solvation numbers are assumed to be integers (2 and 3).

The upper limit of the solvation number of I is set by the number of available electron pairs on the charged oxygen atoms. The lower limit is zero, but, from the NMR experiment (see above) where an isotope effect on the chemical shift of the hydroxylic hydrogens was obtained, it is obvious that the reactant must carry solvating molecules. From the absence of a kinetic solvent isotope effect in water we conclude that this is true also for the transition state.

A further restriction on the solvation numbers arises from the symmetry of the activated complex where the oxygens are at a maximum distance from each other. The solvation shells are independent of each other and the number of solvating molecules should thus be an even number.

This rather simple picture sums up to a detailed model of the solvation of I. In water the reactant carries 6 or 4 molecules of water and the transition state 4 or 2, respectively. In methanol the corresponding figures are 5 for the reactant and 2 for the transition state. The underlying assumption that the solvation numbers have to be integers is, of course, an open question.

Acknowledgements. We would like to thank Professor Lars Melander for his interest in the present work and for many fruitful duscussions concerning problems in connection with it. Financial support from the Swedish Natural Science Research Council is gratefully acknowledged.

REFERENCES

1. Shriner, R. L., Adams, R. and Marvel, C. S. In Gilman, H., Ed., *Organic Chemistry An Advanced Treatise*, 2nd Ed., Wiley, New York 1958, Chapter 4; Bott, G., Field, L. D. and Sternhall, S. *J. Am. Chem. Soc. 102* (1980) 5618.
2. a. Berntsson, P. and Carter, R. E. *Acta Chem. Scand. 22* (1968) 2141; b. Berntsson, P., Wanger, M. and Carter, R. E. *Acta Chem. Scand. 21* (1967) 879; Graham, W. H. and Leffler, J. E. *J. Phys. Chem. 63* (1959) 1274; Leffler, J. E. and Graybill, B. M. *J. Phys. Chem. 63* (1959) 1457.
3. Leffler, J. E. and Graham, W. H. *J. Phys. Chem. 63* (1959) 687.
4. Carter, R. E. and Melander, L. *Adv. Phys. Org. Chem. 10* (1973) 1.
5. Bergman, N.-Å. and Baltzer, L. *Acta Chem. Scand. A 31* (1977) 343.
6. Gold, V. *Trans. Faraday Soc. 56* (1960) 255; Kresge, A. J. *Pure Appl. Chem. 8* (1964) 243. For a recent text on the subject see Melander, L. and Saunders, W. H., Jr. *Reaction Rates of Isotopic Molecules*, Wiley, New York 1980, Chapter 7.
7. Adams, R. and Finger, G. C. *J. Am. Chem. Soc. 61* (1939) 2828.
8. Brändström, A. *Preparative Ion Pair Extraction*, Swedish Academy of Pharmaceutical Sciences, Stockholm 1976, p. 155.
9. Fanta, P. E. *Chem. Rev. 64* (1964) 613.
10. Becker, H.-D. *Acta Chem. Scand. 16* (1962) 78.
11. Baumgarten, H. E. *Org. Synth. Coll. Vol. 5* (1973) 412.
12. Knauf, A. E., Shildneck, P. R. and Adams, R. *J. Am. Chem. Soc. 56* (1934) 2109.
13. Samdahl, B. and Berg, B. *Bull. Soc. Chim. Fr.* (1949) 461, 463.
14. Fieser, L. F. *Experiments in Organic Chemistry*, D. C. Heath and Company, Boston 1957, p. 286.
15. Parker, A. J. *Chem. Rev. 69* (1969) 1.
16. Reichardt, C. *Solvent Effects in Organic Chemistry*, Verlag Chem., New York 1979, p. 270.
17. Baltzer, L. and Bergman, N.-Å. *J. Chem. Soc. Perkin Trans. 2 To be published.*

18. Baltzer, L. *Unpublished results.*
19. Altman, L. J., Laungani, D., Gunnarsson, G., Wennerström, H. and Forsén, S. *J. Am. Chem. Soc. 100* (1978) 8264.
20. Saunders, M. *Personal communication.*
21. Glasstone, S., Laidler, K. J. and Eyring, H. *The Theory of Rate Processes*, McGraw-Hill, New York and London 1941, p. 184.
22. A similar treatment of acid catalysis in strongly acidic solutions has been used by Bunnett, J. F. *J. Am. Chem. Soc. 83* (1961) 4956, 4968, 4973, 4978.
23. Cox, B. G. and McTigue, P. T. *Aust. J. Chem. 20* (1967) 1815.
24. Quitzsch, K., Ulbrecht, H. and Geischer, G. *Z. Phys. Chem. Leipzig 234* (1967) 33.
25. Tommila, E. *Acta Chem. Scand. 20* (1966) 923.
26. Tommila, E. and Savolainen, M. *Acta Chem. Scand. 20* (1966) 946.

Received May 5, 1981.

Acta Chemica Scandinavica A 36 (1982) 39–45

Isotope Effects in Proton-transfer Reactions. VIII.* Isotope Effects in the Proton-transfer from (−)-Menthone to Methoxide Ion in Methanol and Methanol–Dimethyl Sulfoxide Solutions

BO ANHEDE, LARS BALTZER and NILS-ÅKE BERGMAN

Department of Organic Chemistry, University of Göteborg and Chalmers University of Technology, S-412 96 Göteborg, Sweden

The primary kinetic and solvent isotope effects on the proton transfer from (−)-menthone to methoxide ion in methanol and methanol–dimethyl sulfoxide have been determined. The primary isotope effect at 25 °C is somewhat stronger in methanol ($k_H/k_D = 7.15 \pm 0.09$) than in 10 mol % methanol–90 mol % dimethyl sulfoxide ($k_H/k_D = 5.96 \pm 0.08$) but no clear maximum in the primary kinetic isotope effect is observed when the amount of DMSO in the solvent is varied. The kinetic solvent isotope effect at 25 °C varies from $k^{MeOD}/k^{MeOH} = 2.04$ in methanol to 1.43 in 10 mol % methanol–90 mol % dimethyl sulfoxide. The variation is explained in terms of the fractionation theory with a gradual decrease of the fractionation factors and the number of solvating molecules when the amount of dimethyl sulfoxide in the solution is increased.

Solvent effects on proton-transfer reactions have recently been subject to a considerable interest. The influence of the solvent on the magnitude of the primary kinetic isotope effect and Brönsted's β for simple proton-transfer reactions have been explored.[1,2] Solvent motions coupled to the proton-transfer have been considered both in connection with experimental results[3] and from a theoretical point of view.[4]

Since the discovery of the exceptional properties of the non-hydroxylic solvent dimethyl sulfoxide (DMSO) in the solvation of ionic species this solvent is frequently used in order to change the degree of solvation in a reaction.

The present paper presents an investigation of the change of the kinetic primary isotope effect and of the kinetic solvent isotope effect of a proton-transfer reaction in mixtures of a hydroxylic (methanol) and a non-hydroxylic (DMSO) solvent. The model reaction which has been studied is the methoxide-ion catalyzed epimerization of (−)-menthone–(+)-isomenthone (Scheme 1). This reaction has been rather extensively studied and a very recent investigation treats the kinetics of the reaction in the given media in detail.[6]

A study of the reaction in water–DMSO mixtures showed that the primary kinetic isotope effect for the reaction passes through a maximum ($k_H/k_D = 6.45$) at about 35 mol % DMSO–65 mol % water.[7]

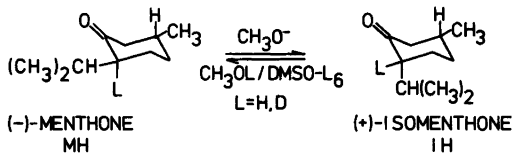

Scheme 1.

RESULTS

The rate constants for the epimerization of (−)-menthone in mixtures of methanol and DMSO are given in Table 1. The rate of epimerization is increased by a factor of about 200 over the interval

*For Part VII of this series see: Bergman, N.-Å. and Källsson, I. *Acta Chem. Scand. A 30* (1976) 421.

0302-4377/82/010039-07$02.50

Table 1. Epimerization of (−)-menthone in mixtures of methanol and dimethyl sulfoxide. Temperature 25.00±0.05 °C. Substrate concentraton $\sim 3 \times 10^{-5}$ M.

mol % DMSO	[MeONa]/M	$k/M^{-1}s^{-1}$ [a]
0	0.154−0.187	$(8.670 \pm 0.050) \times 10^{-3}$
14.9	0.151, 0.152	$(1.413 \pm 0.015) \times 10^{-2}$
27.0	0.0290	$(2.310 \pm 0.047) \times 10^{-2}$
28.0	0.0946	$(2.411 \pm 0.019) \times 10^{-2}$
41.3	0.0709	$(4.696 \pm 0.058) \times 10^{-2}$
50.3	0.0228	$(7.333 \pm 0.080) \times 10^{-2}$
57.6	0.0473	$(1.203 \pm 0.011) \times 10^{-1}$
59.7	0.0154	$(1.303 \pm 0.006) \times 10^{-1}$
70.0	0.00542	$(2.552 \pm 0.028) \times 10^{-1}$
74.5	0.0073	$(3.775 \pm 0.150) \times 10^{-1}$
79.8	0.00343	$(5.942 \pm 0.023) \times 10^{-1}$
80.0	0.00344	$(6.073 \pm 0.034) \times 10^{-1}$
90.0	0.00207	2.108±0.037
91.0	0.0029	1.996±0.145

[a] The values are weighted averages from at least 3 runs and the error limits are $\pm 2\sigma$. Uncertainty in the concentration of the base is included.

Table 2. Epimerization of (−)-menthone-*d* in mixtures of methanol and dimethyl sulfoxide. Temperature 25.00±0.05 °C. Substrate concentration $\sim 3 \times 10^{-5}$ M.

mol % DMSO	[MeONa]/M	$k/M^{-1}s^{-1}$ [a]
0	0.164−0.187	$(1.213 \pm 0.008) \times 10^{-3}$
14.9	0.151	$(2.004 \pm 0.027) \times 10^{-3}$
28.0	0.0946	$(3.481 \pm 0.030) \times 10^{-3}$
41.3	0.0709	$(6.649 \pm 0.117) \times 10^{-3}$
50.3	0.0228	$(1.058 \pm 0.016) \times 10^{-2}$
59.7	0.0154	$(1.921 \pm 0.008) \times 10^{-2}$
70.0	0.00542	$(3.697 \pm 0.056) \times 10^{-2}$
79.8	0.00343	$(8.993 \pm 0.022) \times 10^{-2}$
80.0	0.00344	$(9.052 \pm 0.042) \times 10^{-2}$
90.0	0.00207	$(3.534 \pm 0.055) \times 10^{-1}$

[a] The values are weighted averages from at least 3 runs and the error limits are $\pm 2\sigma$. Uncertainty in the concentration of the base is included.

0−90 mol % DMSO. This increase is somewhat less than for the same reaction in corresponding mixtures of water−DMSO.[7]

The second-order rate constants for epimerization of deuterated (−)-menthone are given in Table 2. Most of these rate constants were obtained by running a 50:50 mixture of (−)-menthone and (−)-menthone-*d*. (In fact, deuterated (−)-menthone contains deuterium in the 6 position too, but the influence of these deuterium atoms is neglected and deuterated (−)-menthone will be referred to a (−)-menthone-*d*.) The change in optical rotation as a function of time was then analyzed using the computer program PROGAEXP to determine the best fit of a two-exponential expression to the experimental data. Provided that the reaction is followed long enough to get good accuracy in k_D this is a convenient method in as much as k_H/k_D could be obtained without interexperimental errors.

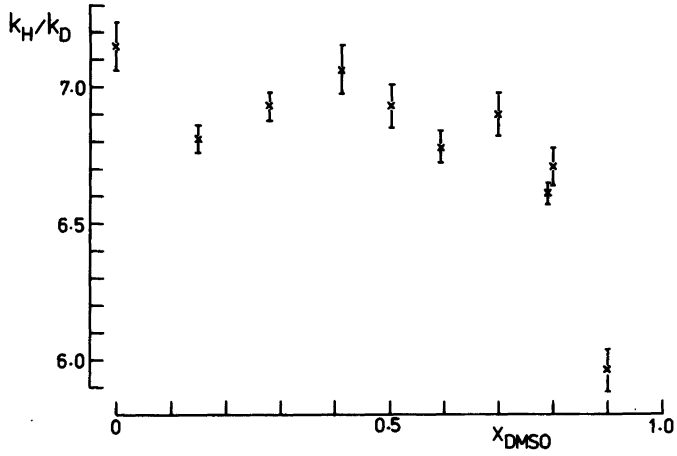

Fig. 1. Primary kinetic isotope effect for proton abstraction from (−)-menthone in mixtures of methanol −DMSO. Temperature 25.00±0.05 °C.

Table 3. Epimerization of (−)-menthone in mixtures of methanol-*O-d* and dimethyl sulfoxide-d_6. Temperature 25.00±0.05 °C. Substrate concentration ~3×10^{-5} M.

mol % DMSO-d_6	[MeONa]/M	k/M^{-1}s^{-1} [a]
0	0.1456	$(1.835 \pm 0.031) \times 10^{-2}$
0	0.119	$(1.696 \pm 0.035) \times 10^{-2}$
15.4	0.0683	$(2.767 \pm 0.036) \times 10^{-2}$
24.2	0.0534	$(3.684 \pm 0.054) \times 10^{-2}$
27.0	0.0287	$(4.445 \pm 0.096) \times 10^{-2}$
50.1	0.0152	$(1.282 \pm 0.023) \times 10^{-1}$
68.6	0.00435	$(3.963 \pm 0.070) \times 10^{-1}$
74.5	0.0051, 0.0072	$(6.570 \pm 0.190) \times 10^{-1}$
90.1 [b]	0.00163	2.988±0.083
90.2 [b]	0.00166	2.974±0.090
90.4 [b]	0.00157	3.127±0.222
91	0.00224	2.664±0.080

[a] The values are weighted averages from at least 3 runs and the error limits are $\pm 2\sigma$. Uncertainty in the base concentration is included. [b] DMSO-h_6 was used since DMSO-d_6 of good quality was not available at the time for these runs. The rate of exchange of protons in the DMSO is believed to be slow in comparison to the rate of the reaction studied.

The method was checked by running (−)-menthone and (−)-menthone-*d* separately, giving the same result.

As has been shown,[6] the rate of enolate ion formation for (−)-menthone in methanol-*O-d* is somewhat higher than the corresponding rate for (+)-isomenthone. This implies that k_{obs} in light media starting with (−)-menthone is not exactly equal to the rate constant for formation of the enolate ion but as the deviation amounts to only some few percent no correction for this has been made in the present investigation. The k_H/k_D values in methanol−DMSO are given in Fig. 1.

The reaction was also studied in mixtures of methanol-*O-d*−DMSO-d_6 and the rate constants are given in Table 3. The kinetic solvent isotope effect was calculated directly for runs with the same methanol−DMSO composition. For runs with nearly the same composition, linear interpolation was performed in order to adjust the rate constants to an intermediate composition. The variation of the solvent isotope effect with increasing content of DMSO is shown in Fig. 2.

DISCUSSION

As can be seen from Table 1 the rate increase in the inversion of methone going from methanol to a mixture containing 90 mol % DMSO amounts to a factor of about 200. This is rather normal for ketones in mixtures of a hydroxylic solvent and DMSO. It is, however, somewhat less than the corresponding factor for, *e.g.*, cyanocarbon acids over the corresponding composition range.[8,9] The reason for this could at least qualitatively be explained by a possible destabilization of the developing enolate ion in the transition state[10] analogous to the known destabilization of the

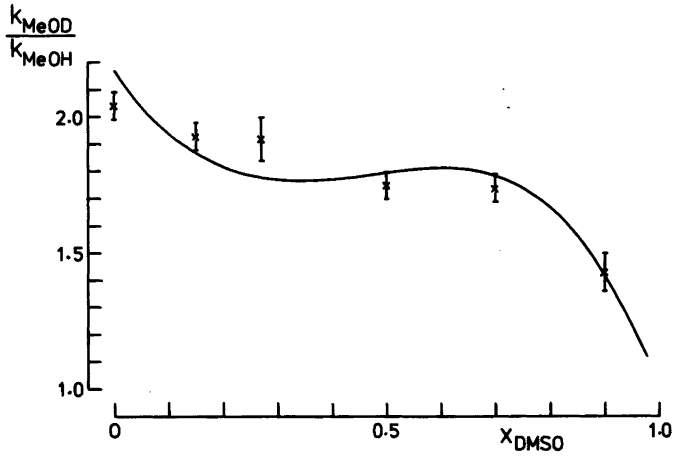

Fig. 2. Kinetic solvent isotope effect for proton abstraction from (−)-menthone in mixtures of methanol−DMSO. The solid line shows the theoretical curve (see text). Temperature 25.00±0.05 °C.

methoxide ion in DMSO mixtures with hydroxylic solvents.

The primary kinetic isotope effect is determined by the properties of the isotopic reactants and the corresponding transition states of the rate-determining step.[11] A maximum in the isotope effect will be observed when cancellation of the zero-point energy difference between the isotopic reactants is at a minimum in the transition state. This has been suggested to occur for a reaction

$$AH + B \rightleftharpoons A + BH$$

when $\Delta pK = pK_{HA} - pK_{HB}$ equals zero, *i.e.*, $\Delta G^\circ = 0$.[12]

For the present system there is no straightforward way of obtaining ΔpK in different mixtures of methanol and DMSO. One way to estimate ΔpK is to use the H_--function.[7,13]

The use of the H_--function in determining Brönsted's β for a reaction in mixtures of DMSO and water has been questioned by Cox and Gibson [1] who found that both rates and isotope effects for simple proton-transfer reactions varied considerably as the solvent composition was altered. No correlation between the kinetic isotope effects and the overall energy changes for the reactions could be established.

The range of ΔpK for the present system could, however, be estimated to about 7 pK units ranging from $\Delta pK = 4$ in methanol to $\Delta pK = -3$ in DMSO. These figures could be obtained by assuming a $pK_a = 22$ of menthone in methanol and $pK_a = 18.3$ of methanol in methanol.[14] The corresponding values in DMSO being for menthone $pK_a = 26$ (*cf.* $pK_a = 26.3$ for phenyl isopropyl ketone in DMSO [15]) and for methanol $pK_a = 29.1$.

These figures mean that in terms of ΔpK the transition state for the proton transfer changes from being slightly product-like in methanol to slightly reactant-like in DMSO.

As can be seen from Fig. 1 there is, however, no clear maximum in the k_H/k_D values but rather a somewhat irregular decrease as the amount of DMSO in the solvent is increased. Nevertheless, the rather strong isotope effect is an indication that the proton must be about half transferred in the transition state. The largest k_H/k_D values in the present investigation are found at positive ΔpK values and it is interesting to note that also in the epimerization of methone in water–DMSO the isotope-effect maximum lies at about $\Delta pK = +2.7$ It seems thus rather plausible that the k_H/k_D curve obtained in the present investigation could be part of an isotope-effect maximum curve.

The solvent isotope effect as depicted in Fig. 2 shows a dramatic change from methanol to pure DMSO.

Solvent isotope effects are most conveniently discussed in terms of fractionation theory.[16] For the present case the expression for the limiting rate constant (k^{OD}) in heavy medium relative to the one (k^{OH}) in light medium will be

$$k^{OD}/k^{OH} = \prod_i \phi_i^*/\prod_i \phi_i^R$$

where ϕ_i^* and ϕ_i^R denote the fractionation factor for an exchangeable hydrogen in the transition and reactant states, respectively. The only positions with exchangeable hydrogens in the reactant are the OH-positions in the solvation shell of the methoxide ion, the fractionation factor of which is usually denoted ϕ_{OMe}. The number of methanol molecules solvating the methoxide ion in methanol is usually assumed to be three.

Very little is known about the relative importance of functional-group solvation in the transition-state but one model of the transition state which should be considered is shown in Scheme 2.

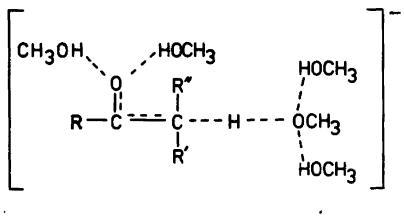

Scheme 2.

The solvation of the two partly negatively charged oxygen atoms is thought to take place *via* two methanol molecules on each oxygen atom. The transition state could, according to the magnitude of the primary kinetic isotope effect, be considered as rather symmetric and a partial negative charge on the carbonyl oxygen atom is thus likely.

The resulting expression for the solvent isotope effect should thus be,

$$k^{OD}/k^{OH} = (\phi^*)^4/\phi_{OMe}^3$$

under the assumption of four equal fractionation factors in the transition state and three for the methoxide ion. This expression is valid for pure methanol-*O*-*d*–methanol and gives with the experimental value $k^{OD}/k^{OH}=2.04$ and ϕ_{OMe} the result $\phi^*=0.95$.

For analysis of the results in mixtures of methanol and DMSO the fractionation factor of methoxide ion in these mixtures has to be known. A very recent investigation[17] has shown that there is a decrease from $\phi_{OMe}=0.74$ in methanol to $\phi_{OMe}=0.38$ in 75 mol % DMSO – 25 mol % methanol. The change of ϕ_{OMe} over the studied solvent composition is given by:

$$\phi_{OMe}=-0.40x^2-0.20x+0.75$$

The expression is obtained by a least-squares fit to the experimental data[17] and x denotes the mol fraction of DMSO. It is reasonable to assume a decrease even in the ϕ^* value when the DMSO content in the mixture is increased. This decrease could, however, be estimated to be somewhat less pronounced. Assuming a second-degree dependence of ϕ^* (as well as of ϕ_{OMe} above) and assuming linear change with x of the number of methanol molecules solvating the methoxide ion and the transition state gives the general expression (1). From this expression and the experimental values for k^{OD}/k^{OH} (ax^2+bx+c) can be calculated for a number of x-values. The so determined points are fitted to a second-degree polynomial (with the method of least squares). This procedure yields $a=0.21$, $b=-0.35$ and $c=0.98$ which, inserted in expression (1), gives the theoretical curve in Fig. 2.

$$k^{OD}/k^{OH}=\frac{(ax^2+bx+c)^{4(1-x)}}{(-0.40x^2-0.20x+0.75)^{3(1-x)}} \quad (1)$$

It is important to realize that the precise course of the theoretical solvent isotope effect curve is very sensitive to small deviations in the measured rate constants. However, the general shape is judged as reliable because test calculations with reasonably altered values, around the experimental ones, produce curves of similar shape.

It is also possible to construct curves of a similar shape using other assumptions regarding the form of ϕ^* as well as of the solvation of the activated complex. Our assumptions, though, seem natural and are not contradicted by the experimental results.

The denominator in (1) has the attractive feature of being essentially constant over the interval $x=0$ -0.5 (Fig. 3). Neglecting any "medium" effect, a deviation from the value in methanol of k^{OD}/k^{OH} in this region would have to be attributed to fractionation in the solvating positions surrounding the transition state. The numerator of (1) gives the contribution from the transition state and is given in Fig. 3. It might be argued that the drop in k^{OD}/k^{OH} is

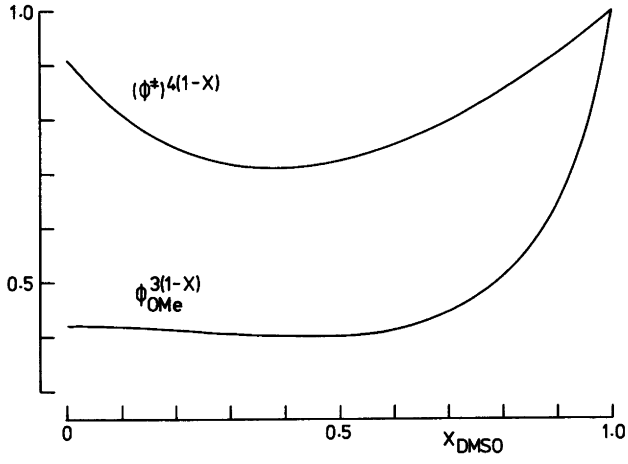

Fig. 3. Variation of the contributions from the transition state and the methoxide ion to the kinetic solvent isotope effect.

not a transition-state contribution but is merely reflecting the error limits in ϕ_{OMe} or reflecting the crudeness in our assumption that the methoxide ion is linearly desolvated with x. However, to account for the decrease in the isotope effect at, for instance, $x_{DMSO}=0.4$, a ϕ_{OMe} of 0.68 would have to be used instead of 0.61 or a mean solvation number for methanol of 1.28 instead of 1.80 and, in view of the large errors that would have to be assumed, our interpretation is presented with some confidence. A "medium" effect on the isotope effect may also be suggested but it has been shown that medium effects are small in proton-transfer reactions.[18]

The increase in fractionation of the transition state is probably an effect of desolvation. The number of occupied hydrogen-bonding sites is descreased, but at the same time the fractionation factors deviate more from unity. The result is that the product of $\phi^{\ddagger}$'s gives a lower value in 50 mol % DMSO than in methanol. The balance between the numerical values of the fractionation factors and the number of sites gives for the methoxide-ion fractionation, as mentioned above, a constant contribution to the overall isotope effect in the range $x_{DMSO}=0-0.5$. For the transition state the fractionation factor product goes through a minimum at roughly 40 mol % DMSO. An analogous increase in fractionation caused by desolvation has been observed in the case of sterically hindered oxyanions.[19] Although the interpretation of the isotope effects is complicated under these conditions, we believe that the magnitude of the drop of the numerator of eqn. (1) is a measure of the strength of the interactions between the solvent and the transition state.

From Fig. 3 it is obvious that a solvent of about 40 mol % of DMSO in methanol should provide a potential source for studying such effects for methoxide-catalyzed reactions.

It would be interesting to carry the analysis one step further, trying to ascribe the contribution from solvation to different parts of the transition state.

In general, substrates exhibiting similar degree of steric hindrance would be expected to give rise to a larger contribution from solvation of the methoxy oxygen the more reactant-like the transition state. The functional-group contribution would be more conspicuous the more product-like the transition state is, although large differences between different functional groups are anticipated. If solvation of the transition state is on the whole unimportant the kinetic solvent isotope effect would be expected to be of a constant magnitude on going from 0 to 50 mol % of DMSO in methanol.

Table 4. Kinetic solvent isotope effects on the methoxide-catalyzed proton abstraction from (−)-menthone and (+)-2-methyl-3-phenylpropionitrile in methanol and in 54 mol % DMSO in methanol.

Substrate	k^{OD}/k^{OH}	
	Methanol	54 mol % DMSO
Menthone (25 °C)	2.04	1.75
2-Methyl-3-phenyl-propionitrile (60 °C)	2.09[a]	1.76

[a] From Ref. 20.

For the present system it is reasonable to assume a rather symmetric transition state making both functional-group solvation and methoxy−oxygen solvation of some importance.

For a reaction with a very unsymmetric transition state such as the methoxide-catalyzed proton-abstraction from 2-methyl-3-phenylpropionitrile in methanol[8] the situation is somewhat different. The highly product-like transition state in this reaction would suggest functional-group solvation to be of main importance.

In order to compare the two reactions we have therefore measured the kinetic solvent isotope effect of 2-methyl-3-phenylpropionitrile in 54 mol % of DMSO in methanol, and the results are presented in Table 4.

The results for the two very different reactions are virtually the same showing a pronounced drop in the kinetic solvent isotope effect when the solvent is changed from methanol to 54 mol % of DMSO in methanol. A compensation for the difference in temperature will change the values only slightly. In the case of 2-methyl-3-phenylpropionitrile dominant methoxy solvation is ruled out by the very unsymmetric transition state and the drop in the kinetic solvent isotope effect must thus be assigned to the functional group.

Clearly, more work is needed before our understanding of solvent fractionation is complete but we suggest that determination of kinetic solvent isotope effects at the two solvent compositions mentioned above may be a useful tool for elucidating in detail the solvation of transition states.

EXPERIMENTAL

(−)-Menthone was synthesized and separated from the small amounts of (+)-isomenthone also formed according to Ref. 21.

Deuterated (−)-menthone and (+)-isomenthone were prepared from (−)-menthone by equilibration in methanol-*O-d* with sodium methoxide as catalyst. The solution was poured out onto ice with enough hydrochloric acid to neutralize the methoxide. The equilibrium mixture was extracted with ether. The ether layer was dried with $CaSO_4$ (Sikkon, Fluka AG) and the ether was evaporated. The procedure was repeated until NMR showed complete deuteration in position 2. The deuterated (−)-menthone and (+)-isomenthone were separated by HPLC in the same way as undeuterated material according to Ref. 21.

The solvents of listed quality were obtained from the following manufacturers and used without further purification.

Methanol. Anhydrous, $H_2O < 0.01\%$ w/w, May & Baker.

Dimethyl sulfoxide. $H_2O < 0.01\%$, Riedel-de Haën AG.

Methanol-O-d. >99.5 atom % D, CIBA.

Dimethyl sulfoxide-d_6. >99.5 atom % D, CIBA.

All handling of the solvents was carried out under nitrogen in order to avoid uptake of moisture.

Base solutions were made by dissolving sodium in methanol under nitrogen. The concentration of sodium methoxide was determined by titration against potassium hydrogen phthalate using phenolphthalein as indicator.

All glass apparatus was cleaned with chromic acid, washed with water, dilute ammonia, and then carefully rinsed with distilled water and finally dried at 120 °C for at least 24 h.

The polarimeter cell was rinsed with anhydrous methanol and then flushed with a stream of nitrogen prior to each kinetic run.

Kinetic runs were performed on a Zeiss OLD 5 digital polarimeter which can be read to 0.001°. The reactions were carried out in a thermostatted 10 cm polarimeter cell. The temperature was maintained by a Hetotherm Ultrathermostat 02 Pt 623 UO together with a Hetofrig cooling bath. The temperature in the thermostat bath was read on a thermometer, which could be read to 0.01 °C. In the circulation water, immediately after the cell, was mounted a REC Platinum resistance sensing element connected to a Fluke 8300 A digital voltmeter/ohmmeter readable to 0.01 ohm corresponding to 0.03 °C in the temperature range around 25 °C. This system was calibrated against a Hewlett-Packard quartz thermometer 2801 A which was calibrated against the resistance thermometer normal of National Testing Institute, Borås, Sweden. Data from the polarimeter and from the voltmeter were collected on discettes in a Compucorp 625 Mark II desktop computer interfaced on line. The data were then analyzed using the computer program PROGAEXP.

Acknowledgements. The authors wish to thank Professor Lars Melander for his interest in the present work and for reading the manuscript prior to publication. Technical assistance by Dr. Inger Källsson with some of the polarimeter measurements is gratefully acknowledged. Financial support from the Swedish Natural Science Research Council is gratefully acknowledged.

REFERENCES

1. Cox, B. G. and Gibson, A. *J. Chem. Soc. Perkin Trans. 2* (1977) 1812.
2. Cox, B. G. and Natarajan, R. *J. Chem. Soc. Perkin Trans. 2* (1977) 2021.
3. Caldin, E. F. and Wilson, C. J. *Symp. Faraday Soc. 10* (1975) 121.
4. Melander, L. and Bergman, N.-Å. *Acta Chem. Scand. A 30* (1976) 703.
5. Buncel, E. and Wilson, H. *Adv. Phys. Org. Chem. 14* (1977) 133.
6. Bergman, N.-Å. *Acta Chem. Scand. A 33* (1979) 577.
7. Bell, R. P. and Cox, B. G. *J. Chem. Soc. B* (1970) 194.
8. Melander, L. and Bergman, N.-Å. *Acta Chem. Scand. 25* (1971) 2264.
9. Bergman, N.-Å. and Källsson, I. *Acta Chem. Scand. A 30* (1976) 411.
10. Jaiswal, D. K., Jones, J. R. and Fuchs, R. *J. Chem. Soc. Perkin. Trans. 2* (1976) 102.
11. Melander, L. and Saunders, W. H., Jr. *Reaction Rates of Isotopic Molecules*, Wiley, New York 1980.
12. Bell, R. P. and Goodall, D. M. *Proc. R. Soc. London Ser. A 294* (1966) 273.
13. Ref. 11, p. 135.
14. Ritchie, C. D. In Coetzee, J. F. and Ritchie, C. D., Eds., *Solute-Solvent Interactions*, Dekker, New York 1969, Chapter 4.
15. Ritchie, C. D. In Coetzee, J. F. and Ritchie, C. D., Eds., *Solute-Solvent Interactions Vol. 2*, Dekker, New York 1976, Chapter 12.
16. Ref. 11, Chapter 7.
17. Baltzer, L. and Bergman, N.-Å. *J. Chem. Soc. Perkin Trans. 2. To be published.*
18. Gold, V. and Morris, K. P. *J. Chem. Soc. Perkin Trans. 2* (1980) 1421.
19. Baltzer, L. and Bergman, N.-Å. *Acta Chem. Scand. A 36* (1982) 31.
20. Bergman, N.-Å. and Melander, L. *Acta Chem. Scand. A 28* (1974) 747.
21. Bergman, N.-Å. and Hall, B. *Acta Chem. Scand. B 33* (1979) 148.

Received May 5, 1981.

Acta Chemica Scandinavica A 36 (1982) 47–53

Equilibrium and Structural Studies of Silicon(IV) and Aluminium(III) in Aqueous Solution. 4. A Potentiometric Study of Polynuclear Aluminium(III) Hydroxo Complexes with Gallic Acid in Hydrolyzed Aluminium(III) Solutions

LARS-OLOF ÖHMAN and STAFFAN SJÖBERG

Department of Inorganic Chemistry, University of Umeå, S-901 87 Umeå, Sweden

Equilibria between aluminium(III), gallic acid ($C_7H_6O_5$,H_3L) and OH^- were studied within the limits $-\lg[H^+] \lesssim 4$; $0.003 \leq B \leq 0.028$ M; $0.0007 \leq C \leq 0.031$ M and $0.025 \leq C/B \lesssim 3$ where B and C stand for the total concentrations of aluminium and gallic acid, respectively. The measurements were performed as potentiometric (glass electrode) titrations in 0.6 M Na(Cl) at 25 °C. Besides binary hydrolytic species $AlOH^{2+}$ and $Al_3(OH)_4^{5+}$ and mononuclear aluminium-gallic acid complexes $AlHL^+$ and AlL, all data could be explained with the complexes $Al_4L_3^{3+}$ and $Al_3(OH)_4(H_2L)^{4+}$ (tentative structures). The equilibrium constants with standard deviations are given. Data were analyzed with the least squares program LETAGROPVRID. A solid phase $AlL \cdot 4H_2O$ (or $Al(OH)(HL) \cdot 3H_2O$) was identified and an approximate solubility product of this phase was calculated.

In part 1 of this series, equilibria in the three component system $Al^{3+} - OH^-$-gallic acid (3,4,5-trihydroxy benzoic acid, H_3L) were studied at 25 °C in 0.6 M Na(Cl) medium. With $3 \leq C/B \leq 25$ (B,C denote the total concentration of aluminium and gallic acid, respectively) data were explained with binary as well as ternary complexes. Besides the mononuclear species $AlHL^+$, AlL (or Al(OH)HL), AlL_2^{3-}, and AlL_3^{6-}, a dinuclear proton series $Al_2(OH)_2(HL)_3^{2-} - Al_2(OH)_2L_3^{5-}$ was proposed.

For quotients $3 \leq C/B \leq 4$ a white, noncrystalline precipitate was formed within the range $4 \lesssim -\lg[H^+] \lesssim 5.5$. At still lower quotients, where the hydrolysis of Al^{3+} becomes more pronounced, stable potentials were difficult to obtain after the dissolution of the precipitate ($-\lg[H^+] \gtrsim 5.5$). This fact is probably due to the slow kinetics in hydrolyzed Al^{3+}-solutions. It was also found that additional effects, caused by ternary species other than those mentioned above, were found in slightly acidic solutions before the onset of the precipitation.

The aim of the present investigation was to interpret the complexing ability of gallic acid in these slightly acidic, hydrolyzed, Al^{3+}-solutions. The composition of the precipitate was also determined as well as an approximate value of its solubility product.

EXPERIMENTAL

Chemicals and analysis. All solutions used were prepared and analyzed as described earlier.[1] *Tropolone* ($C_7H_6O_2$) (Fluka, purum), used for quantitative precipitation of Al(III) in the precipitate study, was sublimed in vacuum.

Apparatus. The thermostat, cell arrangement and experimental details, including special precautions to protect the weakly acidic solutions from oxygen in the emf measurements, are fully described in Ref. 1.

The apparatus used to study the composition of the precipitate comprised: A thermobalance (Netzsch, type 409), to determine water content (135 °C) and Al content (800 °C), and an IR-spectrophotometer (Beckman IR 4240) to ensure that the same solid phase was formed from solutions of different compositions.

0302-4377/82/010047-07$02.50

METHOD

The titration procedures, calibrations and the assumptions made in connection with the use of the glass electrode were the same as described earlier.[1] Each titration was performed at a constant C/B ratio where the initial concentrations of B and C were varied within the limits $0.003 \leq B \leq 0.028$ M and $0.0007 \leq C \leq 0.031$ M, covering the C/B ratios: 2.6, 2, 1, 0.5, 0.3, 0.2, 0.1, 0.05 and 0.025. To test reproducibility and reversibility of equilibria, both forward (addition of OH^-) and backward (addition of H^+) titrations were performed. To obtain more data points in the most interesting areas some dilution experiments (titrations with pure medium solution) were also performed. Owing to the formation of precipitate ($C/B \geq 0.3$) or very slow attainment of equilibria ($C/B \leq 0.2$) the available $-\lg h$ range was restricted to an upper limit of 3.8–4.2.

Data treatment. In order to visualize experimental results, data sets $Z_B(\lg h)$ were calculated and some of them are given in Fig. 1. Z_B is defined as the average number of OH^- reacted per aluminium and is given by the relation $Z_B = (h - H - k_w h^{-1})/B$. H denotes the total concentration of protons calculated over the zero level H_2O, Al^{3+}, H_3L. The term $k_w h^{-1}$, where k_w is the ionic product of water, can be neglected in the present study. The different types of equilibria which must be considered in the present study can be divided into groups as follows:

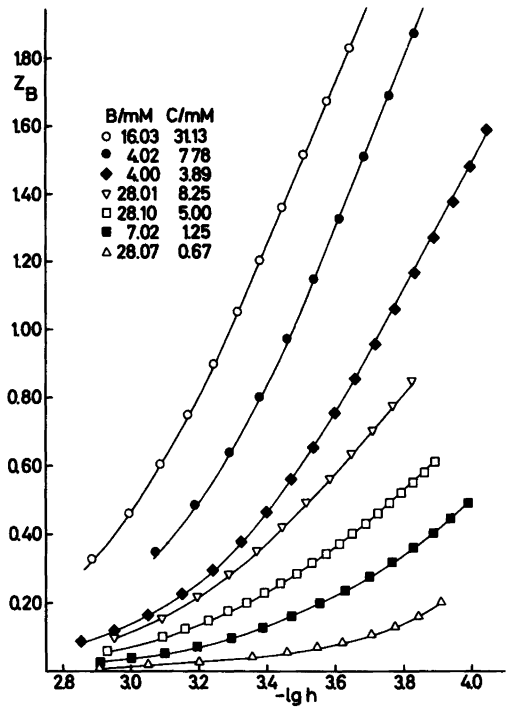

Fig. 1. A part of experimental data plotted as curves $Z_B(-\lg h)$, where $Z_B = (h - H - k_w h^{-1})B^{-1}$. All symbols represent initial concentrations. The full curves have been calculated using the set of proposed constants in Table 1.

(i) the binary gallic acid equilibria

$$H_3L \rightleftarrows H_2L^- + H^+ ; \beta_{-101} \quad (1)$$

$$H_3L \rightleftarrows HL^{2-} + 2H^+ ; \beta_{-201} \quad (2)$$

$$H_3L \rightleftarrows L^{3-} + 3H^+ ; \beta_{-301} \quad (3)$$

(ii) the hydrolytic equilibria of Al^{3+}, which within the actual concentration ranges of B and $\lg h$ in this study are

$$H_2O + Al^{3+} \rightleftarrows AlOH^{2+} + H^+ ; \beta_{-110} \quad (4)$$

$$4H_2O + 3Al^{3+} \rightleftarrows Al_3(OH)_4^{5+} + 4H^+ ; \beta_{-430} \quad (5)$$

$$32H_2O + 13Al^{3+} \rightleftarrows Al_{13}O_4(OH)_{24}^{7+} + 32H^+ ; \beta_{-32\,13\,0} \quad (6)$$

Accurate values for these formation constants were evaluated from a separate study of the system $H^+ - Al^{3+} - CO_2(g)$ at 25 °C in 0.6 M Na(Cl) (Öhman and Forsling).[2] It can be noted that this study gave no evidence for the formation of $Al_2(OH)_2^{4+}$.

(iii) three component equilibria of the general form

$$pH^+ + qAl^{3+} + rH_3L \rightleftarrows (H^+)_p(Al^{3+})_q(H_3L)_r^{p+3q} ; \beta_{pqr} \quad (7)$$

In the Part 1 investigation, formation constants for binary as well as ternary mononuclear and polynuclear complexes were determined. These constants, in addition to those under (i) and (ii), are given in Table 1. In the following calculations these constants are considered as known and no attempts will be made to vary them.

In the evaluarion of the experimental data, the least squares computer program LETAGROPVRID,[3] version ETITR,[4] was applied. *pqr*-triplets and corresponding equilibrium constants that "best" fit the experimental data were determined by minimizing the error squares sum $U = \Sigma(H_{calc} - H)$.[2] In Part 1 the minimized function was $U = \Sigma((H_{calc} - H)/C)$.[2] As in the present study, C varies between 0.0007–0.031 M, small differences in $H_{calc} - H$ would yield large contributions to U at low C and would thus give too much weight to these data. The LETAGROP calculations also give

Table 1. Binary and ternary complexes in the three-component system $Al^{3+}-OH^{-}$-gallic acid. The formation constants are related according to the reaction $pH^{+}+qAl^{3+}+rH_3L \rightleftarrows H_pAl_q(H_3L)_r^{p+3q}$, where H_3L stands for gallic acid.

p	q	r	Tentative structure	$\lg(\beta_{pqr}\pm 3\sigma)$	Ref.
−1	0	1	H_2L^{-}	−4.152±0.002	1
−2	0	1	HL^{2-}	−12.590±0.005	1
−3	0	1	L^{3-}	−23.674±0.007	1
−1	1	0	$Al(OH)^{2+}$	−5.52±0.04	2
−4	3	0	$Al_3(OH)_4^{5+}$	−13.57±0.02	2
−32	13	0	$Al_{13}O_4(OH)_{24}^{7+}$	−109.2±0.12	2
−2	1	1	$Al(HL)^{+}$	−4.933±0.009	1
−3	1	1	AlL or Al(OH)(HL)	−9.43±0.02	1
−6	1	2	AlL_2^{3-}	−21.98±0.03	1
−9	1	3	AlL_3^{6-}	−37.69±0.02	1
−8	2	3	$Al_2(OH)_2(HL)_3^{2-}$	−22.65±0.04	1
−9	2	3	$Al_2(OH)_2(HL)_2L^{3-}$	−27.81±0.07	1
−10	2	3	$Al_2(OH)_2(HL)(L)_2^{4-}$	−32.87±0.03	1
−11	2	3	$Al_2(OH)_2L_3^{5-}$	−39.56±0.05	1
−5	3	1	$Al_3(OH)_4(H_2L)^{4+}$	−12.52±0.01	
−9	4	3	$Al_4(L)_3^{3+}$	−20.25±0.05	This
−3	1	1	$AlL\cdot 4H_2O(s)$	−6.2±0.5	work

standard deviations $\sigma(H)$, $\sigma(\beta_{pqr})$ and $3\sigma(\log \beta_{pqr})$. For the definitions of these errors the reader is referred to Sillén.[5] The computations were performed on a Cyber 172 computer.

DATA, CALCULATIONS AND RESULTS

The analysis of data, comprising 24 titrations with 496 experimental points, was started with a

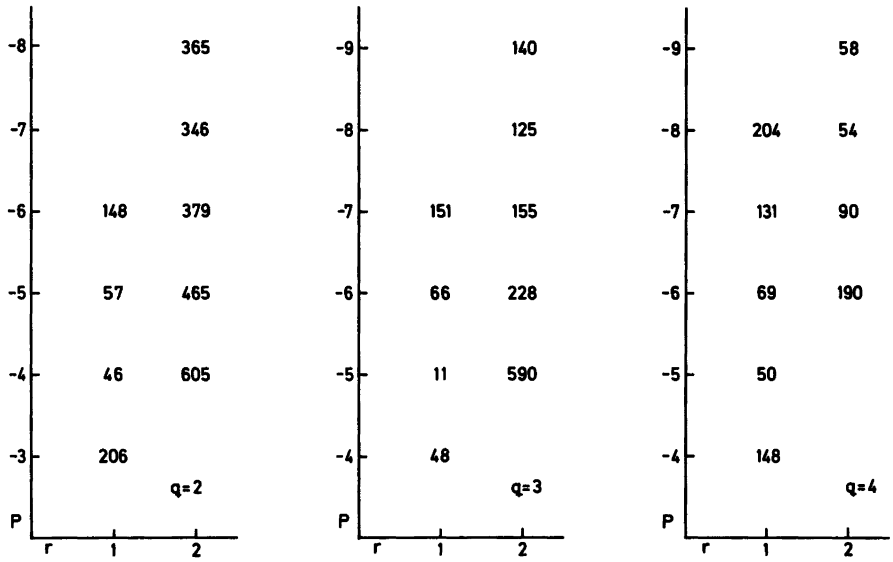

Fig. 2. Result of a *pqr*-analysis in the area $C/B<3$ and $-\lg h \lesssim 4$. The figures give the error squares sums $U_H(pr)_q$ assuming one new complex. Binary and ternary complexes listed in the upper part of Table 1 have been assumed to be known. The calculations are based on 496 points giving $U_H(00)_0=714$.

residual calculation using the results from Refs. 1 and 2. These residuals clearly indicated that one or more additional complexes must be present. From the very strong concentration dependence it could further be concluded that the additional complexes were probably polynuclear. In order to explain the data, we tested the very simple hypothesis that only one additional complex, $H_pAl_q(H_3L)_r^{p+3q}$, was present. The search for the composition and the equilibrium constant for this complex was performed as a *pqr*-analysis (systematic testing of *pqr* combinations) using the LETAGROPVRID program and the criteria for best explanation was the error squares sum $U=\Sigma(H_{calc}-H)$.[2] The result of this analysis is given in Fig. 2 and it was found that the lowest value of U was obtained for the complex $H_{-5}Al_3(H_3L)^{4+}$ with $\lg(\beta_{-531}\pm3\sigma)=-12.47\pm0.013$.

The fit to experimental data was very good for quotients $C/B\lesssim0.5$; however, at higher quotients systematic effects remained to be explained. In order to interpret this upper range we introduced another ternary complex into the model. Since the remaining residuals seemed to be strongly dependent on the constant value chosen for the complex $H_{-5}Al_3(H_3L)^{4+}$ we found it necessary to perform this search as a covariation between $H_{-5}Al_3(H_3L)^{4+}$ and the new $H_pAl_q(H_3L)_r^{p+3q}$ complex. No sharp pit could be obtained for any single additional complex. However, the best fit was found assuming $\lg(\beta_{-531}\pm3\sigma)=-12.52\pm0.010$ together with $H_{-9}Al_4(H_3L)_3^{3+}$; $\lg(\beta_{-943}\pm3\sigma)=-20.25\pm0.049$, giving $U=3.9$ and $\sigma(H)=0.09\times10^{-3}$ M. The best tri- and pentanuclear species found were $H_{-6}Al_3(H_3L)_2^{3+}$ and $H_{-12}Al_5(H_3L)_4^{3+}$ giving $U=4.6$ and 4.1, respectively. It is interesting to note that all three complexes belong to the same series $Al_nL_{n-1}^{3+}$, with $n=3$, 4 and 5.

The conclusion we have drawn from this search is (see Discussion) that $H_{-9}Al_4(H_3L)_3^{3+}$ is a type of average complex but that the remaining residuals are too small to permit more detailed analysis. Our final model for the complexation in the quotient range $C/B\lesssim3$ and $-\lg h\lesssim4$ is therefore: $H_{-5}Al_3(H_3L)^{4+}$ with $\lg(\beta_{-531}\pm3\sigma)=-12.52\pm0.010$ and $H_{-9}Al_4(H_3L)_3^{3+}$ with $\lg(\beta_{-943}\pm3\sigma)=-20.25\pm0.049$.

Determination of the composition of the precipitate. The white precipitate formed in the region $4\lesssim-\lg h\lesssim5.5$ for $C/B\lesssim4$ was prepared from solutions of different C/B quotients, filtered off through a Jena G4 glass filter, dried by boiling off residues of water

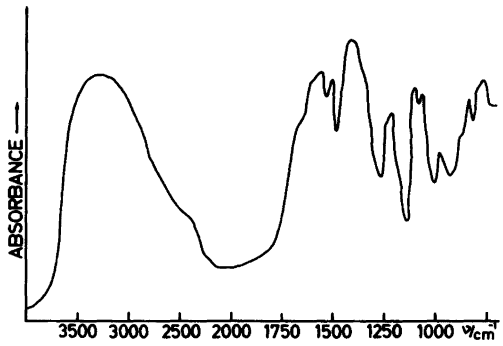

Fig. 3. IR spectrum of the solid $H_{-3}Al(H_3L)\cdot4H_2O$.

in vacuum at 25 °C and examined by IR technique using KBr as pellet material. All solids gave the same spectra (Fig. 3) proving that the precipitate formed was the same independent of C/B quotient in solution. In attempts to take powder photographs of the solid, no lines were obtained and it was concluded that the precipitate was quite amorphous. To examine the Al content of the solid a thermobalance was used. A known amount was held at 800 °C for 24 h and the residue (a perfectly white powder, insoluble in conc. HCl) was assumed to be Al_2O_3. The result obtained was that the precipitate contained 11.2 % Al.

To determine the number of protons bound and the amount of gallic acid, a known amount was dissolved in a standardized hydrochloric acid, Al^{3+} was precipitated with tropolone, the solid ($Al(C_7H_5O_2)_3$) formed filtered off and a known volume of the solution titrated potentiometrically using the ordinary precautions to protect it from oxygen. The resulting titration curve was identical to an ordinary gallic acid-OH^- titration curve and it was possible to determine the gallic acid content to be 61 % of the solid. From the same curve, H was determined to be $-3\times$ Al over our zero level. Finally, from the weight of the dried $Al(C_7H_5O_2)_3$, the aluminium content was checked and found to be 11.1 %, in good agreement with the thermogravimetric analysis.

The remaining part (28 %) of the solid could consist of Na^+, Cl^- or H_2O but tests for Na^+ (atomic emission) as well as for Cl^- (spot test with Ag^+ after dissolution in $HClO_4$) were negative. In order to determine the water content, the solid phase was analyzed thermogravimetrically, this time at 135 °C for 6 h in an atmosphere of argon. The

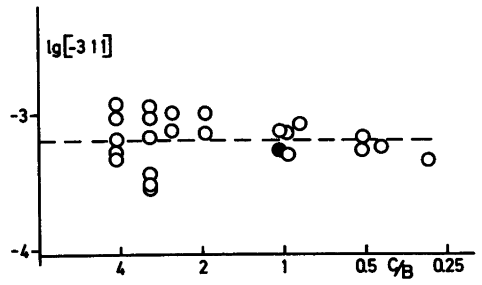

Fig. 4. Approximate solubility product of $H_{-3}Al(H_3L)\cdot 4H_2O$ calculated as an average of the concentration of the complex (−3,1,1) in the last measured point in solution (unfilled symbols). The filled symbol represents the calculated value obtained after a 24 h equilibration time within the precipitation area.

sample lost 27 % of its weight without being discoloured afterwards. A simple stoichiometric analysis of the results obtained then gave the composition $H_{-3}Al(H_3L)\cdot 4H_2O$ (calc. Al: 10.2 %, L^{3-}:62.8 %, H_2O:27.1 %).

Approximate solubility product of $H_{-3}Al(H_3L)\cdot 4H_2O$. The point of initial precipitation was clearly evident from the recorded potential. When precipitation occurred, the potential began drifting and no steady value was obtained even after several hours. This behaviour was found to be a reliable indication of the onset of precipitation provided $C/B \gtrsim 0.3$. In order to determine the solubility product, defined according to the equilibria (10),

$$Al^{3+} + H_3L + 4H_2O \rightleftarrows H_{-3}Al(H_3L)\cdot 4H_2O(s) + 3H^+; k_s \quad (10)$$

a separate titration with $C/B=1$ was performed where the precipitate was allowed to equilibrate with the solution. During a 24 h period, E was continuously measured. No stable potential was obtained; in fact, a constant drift of about 0.05 mV per hour was found, indicating equilibria (10) to be very sluggish or some misbehaviour of the glass electrode. At the present time no efforts have been made to equilibrate the solid phase for longer periods. This probably would yield an accurate value of k_s, provided the extreme oxygen sensitivity of gallic acid, under the conditions needed for this examination, can be eliminated.

However, in an attempt to give an approximate value of k_s for freshly precipitated $H_{-3}Al(H_3L)$, the concentration of the −3,1,1 species (AlL or Al(OH)-HL) was calculated in the last stable point (no precipitate present) in each titration. These points (in total 23 of which 5 are from the alkaline side of the precipitate) are all $\lesssim 0.1$ lg h units from the precipitation limit. In Fig. 4 the calculated values of [AIL] are plotted as a function of C/B, and as can be seen [AIL] seems to be constant within the C/B range in question, giving lg $k_s = -6.2 \pm 0.5$. If it is assumed that equilibrium with the precipitate is reached within 24 h, the value −6.1 in lg k_s is obtained (filled symbol in Fig. 4).

DISCUSSION

The present study completes the investigation of the ability of gallic acid to form complexes with the Al^{3+} ion. A compilation of proposed complexes and corresponding formation constants from this and the Part 1 investigation is given in Table 1.

In the present study evidence for the formation of ternary polynuclear complexes is given. The distribution diagrams in Fig. 5 show that the complexes with p,q,r notations −5,3,1 and −9,4,3 are both formed in significant amounts (~25 % of B). It can also be noted that these species are formed within concentration ranges where hydrolysis of the Al^{3+} ion must be taken into consideration in the evaluation of the equilibrium model.

It has also been shown that a solid phase with the composition $H_{-3}Al(H_3L)\cdot 4H_2O$, is formed, and an approximate solubility product of this phase has been calculated. In Fig. 6, the approximate existence area of this solid is visualized.

Concerning the structures of the species formed, an investigation of this kind gives no direct information. Applying such aspects on the problem, however, often make the interpretation of data easier. In Ref. 1 we made comparisons with some crystal data and with other investigated Al^{3+}-organic acid systems and found it conceivable that the complexation took place between Al^{3+} and two *ortho*-coordinated phenolic groups. The same approach concerning the complex $H_{-5}Al_3(H_3L)^{4+}$, however, leads to very unrealistic structures. If, on the other hand, we assume that the complex is a carboxylate complex it is possible to write it as $Al_3(OH)_4(H_2L)^{4+}$, thus confirming the connection found earlier in several systems between the binary hydrolysis and the ternary species formed. The fact

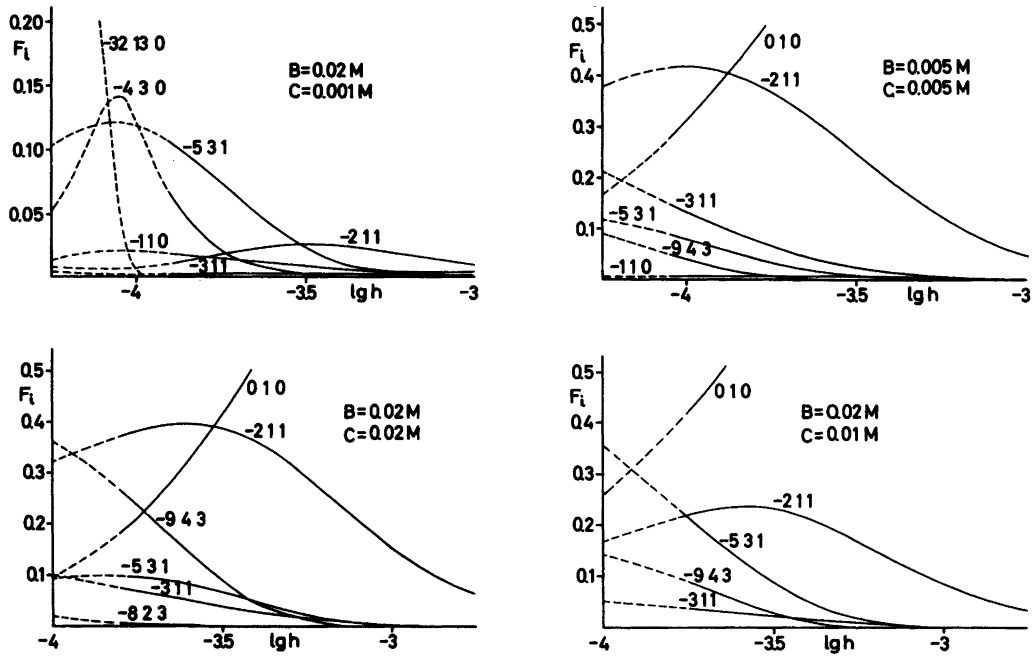

Fig. 5. Distribution diagrams $F_i(\lg h)_{B,C}$. F_i is defined as the ratio between aluminium(III) in a species and total aluminium(III). The calculations have been performed using the computer program SOLGASWATER[6] with constants given in Table 1. In order to make the figures clear the species Al^{3+} has been omitted in part of the diagrams.

that a complex of the same composition is obtained in the system $Al^{3+}-OH^{-}-CO_2(g)$ $(Al_3(OH)_4(HCO_3)^{4+})$, also provides strong support for this idea.

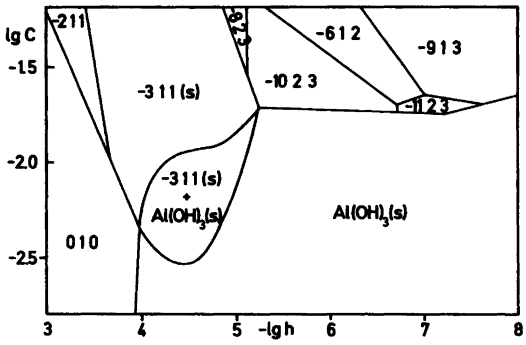

Fig. 6. Predominance area diagram for the different aluminium(III) gallic acid species. The equilibrium constants for $Al(OH)_2^+$, $Al(OH)_3^0$, $Al(OH)_4^-$ and the solubility product for $Al(OH)_3$ are those given by Baes and Mesmer.[7] The calculation is performed at a total aluminium concentration of 10 mM using the computer program SOLGASWATER.[6]

Having *o*-diphenolic complexation at high *C/B* quotients and carboxylic complexation at low quotients then makes it reasonable to assume that both sites should be active in some middle quotient range. Such behaviour would then strongly promote the occurrence of chain complexes of different lengths. If we consider those tri-, tetra- and pentanuclear complexes giving the best fit in the quotient range $0.5 \lesssim C/B \lesssim 2$, they could all be written as $Al_n(L)_{n-1}^{3+}$; $n=3$, 4, 5. As a consequence, we have decided to regard the best fitting species, $Al_4(L)_3^{3+}$, as a type of average complex, giving the mean length of the chains in solution.

With regard to the solid phase, we find it plausible that its building blocks are the complex $(-3,1,1)$, *i.e.* AlL or Al(OH)(HL), found in solution. The four water molecules (or three water molecules and one hydroxyl ion) found, probably completes the oxygen octahedron around Al^{3+}. Extensive work is now in progress to prepare a single crystal of this phase for X-ray determination.

Acknowledgements. We thank Professor Nils Ingri for much valuable advice, for his great interest

and for all the facilities placed at our disposal. The English of the present paper has been corrected by Dr. Michael Sharp. The work forms part of a program financially supported by the Swedish Natural Science Research Council.

REFERENCES

1. Öhman, L.-O. and Sjöberg, S. *Acta Chem. Scand. A 35* (1981) 201.
2. Öhman, L.-O. and Forsling, W. *Acta Chem. Scand. A 35* (1981) 795.
3. Ingri, N. and Sillén, L. G. *Ark. Kemi 23* (1964) 97.
4. Arnek, R., Sillén, L. G. and Wahlberg, O. *Ark. Kemi 31* (1969) 353; Brauner, P., Sillén, L. G. and Whiteker, R. *Ark. Kemi 31* (1969) 365.
5. Sillén, L. G. *Acta Chem. Scand. 16* (1962) 159; Sillén, L. G. and Warnqvist, B. *Ark. Kemi 31* (1969) 341.
6. Eriksson, G. *Anal. Chim. Acta 112* (1979) 375.
7. Baes, C. F. and Mesmer, R. E. *The Hydrolysis of Cations*, Wiley, New York 1976, p. 112.

Received May 8, 1981.

Acta Chemica Scandinavica A 36 (1982) 55–62

The Structure of the Tetraiodothallate(III) Ion in its Tetrabutylammonium Salt and in a Dichloromethane Solution

JULIUS GLASER,[a] PETER L. GOGGIN,[b], MAGNUS SANDSTRÖM[a] and VLADIMIR LUTSKO[a,*]

[a] Department of Inorganic Chemistry, Royal Institute of Technology, S-100 44 Stockholm, Sweden and [b] Department of Inorganic Chemistry, The University, Bristol BS8 1TS, England

The crystal structure of $[N(C_4H_9)_4][TlI_4]$ has been determined by single crystal X-ray diffraction methods. The orange-red compound crystallises in the monoclinic space group $P2_1$ (No. 4) with cell parameters $a=11.746(2)$ Å, $b=21.079(6$ Å, $c=11.699(3)$ Å, $\beta=98.23(2)°$, and $Z=4$. The structure is built up of discrete tetrabutylammonium ions and almost regular tetrahedral tetraiodothallate(III) complex ions with Tl–I bond lengths between 2.723(4) and 2.840(5) Å.

A ruby-red 0.77 M solution of $[N(C_5H_{11})_4][TlI_4]$ in dichloromethane was investigated by X-ray diffraction. Tetrahedral TlI_4^- ions with a Tl–I bond length of 2.771(3) Å were found to occur in the solution.

Vibrational spectra of solid $[N(C_4H_9)_4][TlI_4]$ at both room temperature and liquid nitrogen temperature are reported and discussed.

A comparison is made of bond lengths of the d^{10} ions Tl(III), Hg(II), Cd(II), and Zn(II) in tetrahedral tetrahalide complexes and in their octahedrally hydrated cations.

The formation of Tl(III) halide complexes TlX_n^{3-n} (X=Cl, Br or I) has been extensively studied.[1] Although examples with Cl or Br have been reported where $n>4$[(2–6)] there are none for iodides.

Crystalline $KTlBr_4\cdot 2H_2O$, $RbTlBr_4\cdot H_2O$, $CsTlBr_4$, $NH_4TlBr_4\cdot 2H_2O$ and the corresponding tetraiodothallates(III) are all isomorphous and have been reported to contain planar TlX_4^- ions.[7] However, the validity of these early conclusions is doubtful because a recent single crystal X-ray study has shown that in $KTlBr_4\cdot 2H_2O$ the anion is tetrahedral.[8] Crystal structure determinations show tetrahedral TlX_4^- ions in $MTlCl_4$ (M=K,Tl(I), Rb, NH_4),[9] in Tl(I)Tl(III)Br_4[10] and in $[C_5H_5NH][TlI_4]C_5H_5N$,[11]* and had been inferred from vibrational spectra of crystalline salts.[12]

Vibrational spectra of TlX_4^- salts in solution have also been interpreted on the basis of anions with T_d symmetry.[13,14]

As part of a structural study of thallium(III) halide complexes in crystalline solids[5,6,8,9c,15] and in solutions[16,17] the vibrational spectra of the TlI_4^- ion in dichloromethane solution and in $[NBu_4]TlI_4$(s) have been re-examined. Since the stretching bands for the solid and for the solution showed some differences, as well as the Tl NMR chemical shifts,[17] it was decided to determine the structure of this anion in both phases by means of X-ray diffraction.

EXPERIMENTAL

Preparations. The compounds were prepared by stirring TlI (8.2g), I_2 (6.35g) and either $[N(C_4H_9)_4]I$ (9.2g) or $[N(C_5H_{11})_4]I$ (10.6g) with dichloromethane (100 cm^3) for 2 h, during which time all but a little TlI dissolves to give a ruby red solution. The solution was filtered and diethylether was added to effect crystallization. Yields were practically quantitative. $[N(C_4H_9)_4][TlI_4]$ orange-red needles, m.p. 136–137 °C (lit. 117–118 °C);[18] found % C=20.4, % H=4.0, % N=1.25: $C_{16}H_{36}NI_4Tl$ requires % C=20.15, % H=3.8, % N=1.45. $[N(C_5H_{11})_4][TlI_4]$ orange-red needles, m.p. 138 °C; found %

* Permanent address: Institute for Physico-Chemical Research, Byelorussian State University, 220080 Minsk-80, USSR.

* A complete report of this determination has not, however, been published.

0302-4377/82/010055-08$02.50

C=23.95, % H=4.3, % N=1.45: $C_{20}H_{44}NI_4Tl$ requires % C=23.75, % H=4.4, % N=1.4.

Vibrational Spectra. Infrared spectra were obtained with a Nicolet 7199 Fourier transform infrared spectrometer using a "Globar" source, 6.25 μm thick Mylar beam splitter and polyethylene-windowed triglycine sulphate detector. Spectra of the solid tetrabutylammonium salt, as a compressed pellet in polyethylene, were measured at ambient temperature and, using a Specac cryostat, at liquid nitrogen temperature. Data collection was sufficient for spectra to be computed at 2 cm^{-1} resolution, but somewhat degraded by use of a Happ-Genzel apodisation function.[19] The infrared spectrum of a dichloromethane solution was also recorded, using a cell with high density polyethylene windows and 0.2 mm spacer.

Raman spectra were excited with 647.1 nm radiation (0.4 W) from a Coherent Radiation Laboratories Model 52 krypton-ion laser and were measured with a Coderg T800 triple monochromator at 2 cm^{-1} resolution or better using photomultiplier (EMI 5998 A) detection and d.c. amplification. For measurement of the spectrum of the solid at liquid nitrogen temperature a Coderg Cryocirc cryostat was used.

The Crystal. A needle of $[N(C_4H_9)_4][TlI_4]$ was cut and ground to a sphere of diameter 0.20 mm and sealed into a thin-walled glass capillary. The crystal was found to have monoclinic symmetry by film methods. A least-squares refinement on 25 reflexions centered on the diffractometer gave the unit cell parameters $a=11.746(2)$ Å, $b=21.079(6)$ Å, $c=11.699(3)$ Å, and $\beta=98.23(2)°$. The density, estimated by flotation to 2.2(1) g cm^{-3}, corresponds to four formula units in the cell which gives a calculated density of 2.21 g cm^{-3}.

Intensity data were collected at room temperature on a Syntex $P2_1$ automatic four-circle diffractometer using the ω scan technique. All 2777 hkl and $hk\bar{l}$ reflexions up to $2\theta=40°$ (Mo$K\alpha$ radiation) were measured. Only $0k0$ reflexions with $k=2n+1$ were systematically absent.

The Solution. A ruby-red 0.767 M solution (density 1.582(4) g cm^3) of $[N(C_5H_{11})_4]$ TlI_4 in dichloromethane was prepared. The tetrapentylammonium salt was used due to its higher solubility in dichloromethane (about 1.0 M at 25 °C). The solution was contained in a sealed thin-walled spherical glass-bubble. The diffracted intensity of Mo$K\alpha$ X-ray radiation was measured at 25 ± 1 °C from the surface of the solutions in the same way as described previously.[20]

No decomposition could be observed during the measurements, but a brown precipitate was slowly formed after a few weeks exposure to daylight.

DATA TREATMENT

The Crystal Data. The reduction to scaled F_o values was performed as described previously,[21]

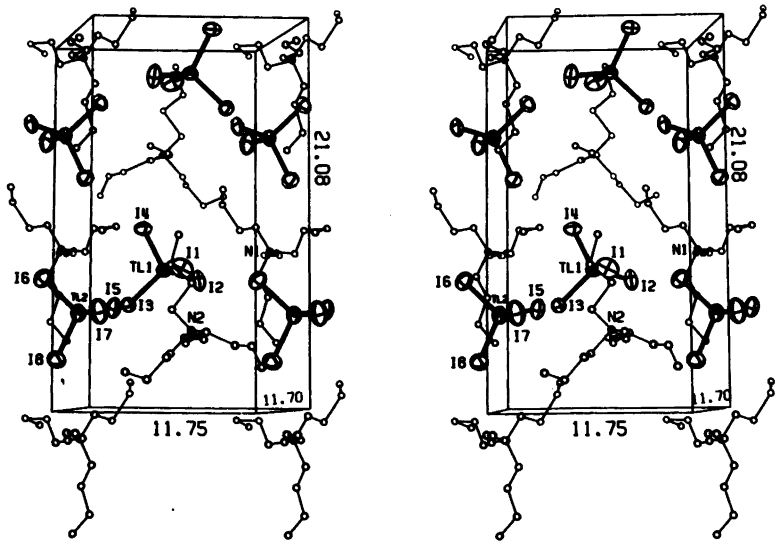

Fig. 1. A stereoscopic view of the monoclinic unit cell of $[N(C_4H_9)_4][TlI_4]$, showing the packing of the complex ions. The size of the thermal ellipsoids corresponds to 40 % probability, but all C and N atoms have for clarity been given the isotropic parameter value $U=0.013$ Å^2. The lengths of the unit cell edges are given in Å.

Table 1. Final fractional atomic positional parameters for the heavy atoms. Estimated standard deviations are given in parentheses.

Atom	x	y	z
Tl1	0.4855(2)	0.6240(1)	0.7113(2)
I1	0.5216(4)	0.6280(2)	0.4834(3)
I2	0.6879(3)	0.6447(2)	0.8612(3)
I3	0.3188(3)	0.7164(2)	0.7328(3)
I4	0.3942(3)	0.5102(2)	0.7589(4)
Tl2	0.9841(2)	0.7574(1)	0.2111(2)
I5	0.1767(3)	0.7383(2)	0.3650(3)
I6	0.8232(3)	0.6680(2)	0.2424(3)
I7	0.0385(3)	0.7593(3)	0.9920(4)
I8	0.8931(3)	0.8763(2)	0.2606(4)

using computer programs and scattering factors from the same sources. The semi-empirical absorption correction method[22a] was applied, the linear absorption coefficient was 100.3 cm^{-1}. The largest relative variation in the transmission factors was from 1 to 0.71.

The positions of the heavy atoms were found by direct methods applied on the non-centrosymmetrical space group $P2_1$. An isotropic least-squares refinement of their parameters gave $R=0.14$ ($R_w=0.20$).* Successive Fourier maps and refinements revealed possible positions of all nitrogen and carbon atoms. However, for some of the carbon atoms (mostly terminal ones) refinement of their parameters led to unreasonable bond lengths and angles to neighbouring atoms, and they were therefore kept constant ($U=0.10$ Å^2) at the values obtained from the Fourier maps. The least-squares refinements were made using the Gauss-Seidel blocked method and were based on a minimization of

* Definitions in Ref. 21.

Table 2. Final anisotropic thermal parameters with estimated standard deviations in parentheses. The expression used is $\exp[-2\pi^2(U_{11}h^2a^{*2}+\cdots+2U_{12}hka^*b^*+\cdots)]$.

Atom	U_{11}	U_{22}	U_{33}	U_{12}	U_{13}	U_{23}
Tl1	0.084(1)	0.061(1)	0.083(1)	0.000(1)	0.013(1)	0.005(1)
I1	0.183(4)	0.146(4)	0.056(2)	0.026(3)	0.009(2)	0.019(2)
I2	0.061(2)	0.176(4)	0.117(3)	0.008(2)	0.014(2)	−0.035(3)
I3	0.074(2)	0.078(2)	0.149(3)	0.005(2)	0.002(2)	−0.010(2)
I4	0.129(3)	0.069(2)	0.149(4)	−0.015(3)	0.015(3)	0.015(2)
Tl2	0.064(1)	0.099(1)	0.071(1)	−0.002(1)	0.005(1)	0.003(1)
I5	0.064(2)	0.142(3)	0.088(2)	−0.012(2)	0.001(2)	0.018(2)
I6	0.088(2)	0.104(3)	0.085(2)	−0.016(2)	−0.010(2)	0.013(2)
I7	0.102(3)	0.194(5)	0.110(3)	0.016(3)	0.035(2)	0.019(3)
I8	0.096(3)	0.093(3)	0.161(4)	0.001(2)	−0.009(2)	−0.043(3)

Table 3. Some interatomic distances in Å and angles in degrees. Estimated standard deviations are given in parentheses.

Tl1 – I1	2.760(4)[a]	2.791(4)[b]	I1 – Tl1 – I2	111.7(1)[a]
Tl1 – I2	2.779(4)	2.804(4)	I1 – Tl1 – I3	106.0(1)
Tl1 – I3	2.797(4)	2.811(4)	I1 – Tl1 – I4	110.2(1)
Tl1 – I4	2.718(4)	2.741(4)	I2 – Tl1 – I3	112.4(1)
			I2 – Tl1 – I4	109.6(1)
			I3 – Tl1 – I4	107.0(1)
Tl2 – I5	2.712(4)	2.723(4)	I5 – Tl2 – I6	109.6(1)
Tl2 – I6	2.730(4)	2.738(4)	I5 – Tl2 – I7	109.9(1)
Tl2 – I7	2.730(5)	2.757(5)	I5 – Tl2 – I8	107.5(1)
Tl2 – I8	2.818(4)	2.840(5)	I6 – Tl2 – I7	113.3(1)
			I6 – Tl2 – I8	107.3(1)
			I7 – Tl2 – I8	109.1(1)

[a] Non-corrected values. [b] Corrected for thermal motion assuming the I atom to ride on the Tl atom.

$\Sigma w\{|F_o|-|F_c|\}^2$, including reflexions with $|F_o|>3.92\ \sigma(F_o)$. The weighting function used was $w=1/\{\sigma^2(F_o)+(0.03\ F_o)^2\}$ which gave $S=1.64$.*

The final cycle (187 parameters, the heavy atoms anisotropic, ten atoms not refined) led to $R=0.054$ ($R_w=0.071$) for 2046 independent reflexions. The largest shift for any parameter was less than 0.3 of its estimated standard deviation.

The probable absolute configuration was established by comparing the R_w values for the two possible enantiomers ($R_w=0.075$ for the other configuration) according to Hamilton.[22b] The two highest residual peaks in the final difference Fourier map were of height 1.0 e Å^{-3} and corresponded to alternative positions of two terminal carbon atoms. No hydrogen atoms were located.

The final parameter values of the heavy atoms are listed in Tables 1 and 2. Calculated bond lengths and angles in the two TlI_4 units are given in Table 3.** The thermal motion correction was performed using the algorithm described in Ref. 22c.

The Solution Data. The data treatment was essentially carried out as described before.[20] An additional empirical correction for the intensity loss in the glass bubble was made by measuring intensities from a standard solution within and without the glass bubble. The corrected experimental intensities were normalized to a stoichiometric unit of volume V containing one thallium atom. The reduced intensity curve, $i_{obs}(s)$ multiplied by s, is shown in Fig. 2. By a Fourier transformation the radial distribution curve was obtained, Fig. 3. The modification function used was $M(s)=\{f^2_{Tl}(0)/f^2_{Tl}(s)\}\exp\{-0.008\ s^2\}$ where f is the scattering factor and the scattering variable is $s=(4\pi/\lambda)\sin\theta$.

For each type of distinct intramolecular interaction between atoms p and q, its contribution to the reduced intensity was calculated according to eqn. (1), where the scattering factors have been corrected for anomalous dispersion effects.

$$i_{calc}(s)= n_{pq}f_p(s)f_q(s)\frac{\sin sr_{pq}}{sr_{pq}}\exp(-\tfrac{1}{2}l^2_{pq}s^2) \quad (1)$$

In the high-angle region where the intramolecular part of the scattered reduced intensity dominates,[20] least-squares refinements could be performed of the three parameters r_{pq} (the distance), n_{pq} (the number of distances per Tl atom), and l^2_{pq} (the mean-square variation in the distance) within the Tl–I species. The intramolecular contributions from the solvent molecules CH_2Cl_2 and from the $(C_5H_{11})_4N^+$ cations were calculated using values from crystal structures[23,24] and mean amplitudes from electron diffraction studies of related compounds.[25]

* Definitions in Ref. 21.

** Full listings of parameter values and structure factors are available from the authors on request.

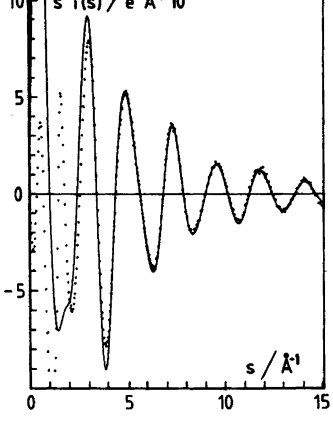

Fig. 2. A comparison (see text) of experimental (dots) and calculated (line) reduced intensities, multiplied by s, for the 0.77 M $[N(C_5H_{11})_4]TlI_4$ solution in dichloromethane.

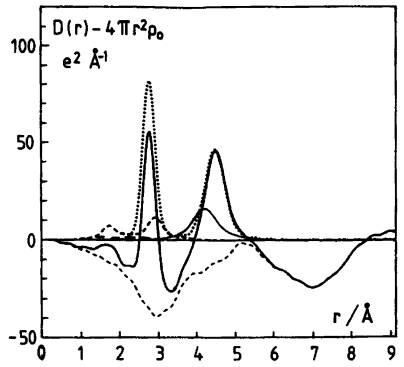

Fig. 3. The experimental difference distribution function, $D(r)-4\pi r^2\rho_o$, is represented by the heavy solid line. Calculated peak-shapes corresponding to interactions within TlI_4^- (dotted line), CH_2Cl_2 molecules (short dashes), $N(C_5H_{11})_4^+$ (long dashes), and to the estimated I–C interactions (solid line), are subtracted from the experimental curve to give the lower dashed line.

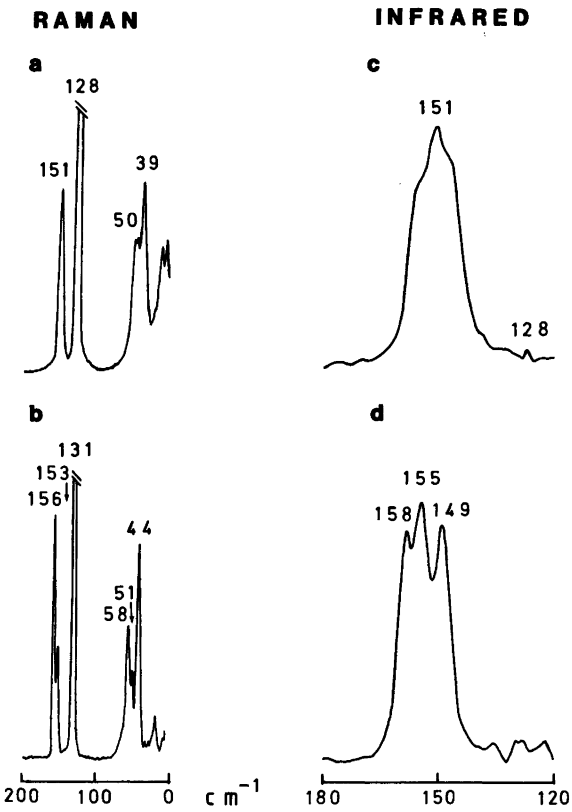

Fig. 4. IR and Raman spectra of solid $[N(C_4H_9)_4][TlI_4]$: (a) Raman at 293 K, (b) Raman at *ca.* 100 K, (c) IR at 293 K, (d) IR at *ca.* 100 K.

RESULTS AND DISCUSSION

The Crystal Structure. The two crystallographically independent TlI_4^--entities in the asymmetric part of the unit cell are in contact in the *x*-direction (Fig. 1) forming zig-zag chains surrounded by the tetrabutylammonium ions. The closest intermolecular contacts between the TlI_4 groups are I4–I8 4.379(5) Å (4.437)* and I3–I5 4.409(5) Å (4.455)*. Several I–C distances occur around 3.9 Å.

The Tl–I bond lengths range from 2.712(2.723)** to 2.816 (2.840)** Å, Table 3, which agrees well with previously reported values, 2.734–2.774 Å.[11] The symmetry is approximately tetrahedral with I–Tl–I angles between 106.0(1) to 112.4(1)°.

The two different tetrabutylammonium ions show some signs of disorder, as mentioned above, and do not give precise atomic positions. The average bond lengths obtained are C–N 1.57 and C–C 1.58 Å, and the average angles N–C–C, C–N–C, and C–C–C are all equal 109(3)°.

Vibrational Spectra of Solid $[N(C_4H_9)_4][TlI_4]$. Although spectra of this[12a] and some related solid salts[12b] have been reported previously, the Raman spectrum obtained at room temperature (Fig. 4a) shows low wavenumber features more clearly than hitherto. The spectrum appears to be in agreement with the predictions for an isolated regular tetrahedral ion with four fundamentals 151 (T_2), 128 (A_1), 50 (T_2) and 39 (E) cm^{-1}. However, the Tl–I stretching feature observed in the i.r. shows distinct shoulders (Fig. 4*c*) resulting from irregularity as observed in the crystal structure and consequent removal of degeneracy.

On cooling to liquid nitrogen temperature the effects of the asymmetry become much more distinct

* Corrected for thermal motion assuming independent motion.

** Corrected for thermal motion assuming I to ride on Tl.

in the IR spectrum and are now clearly seen in the Raman spectrum (Figs. 4d and 4b).

Full factor group analysis for the $P2_1$ space-group[26] predicts there will be 16 Tl−I stretching modes active in both IR and Raman spectra. If correlation forces are negligible, the number might be expected to reduce to 8, four for each type of $[TlI_4]^-$ anion. Of course, because the distortions from tetrahedral regularity are not very large a relationship to the spectrum of a T_d anion is to be expected; thus the nature of the lowest wavenumber stretching co-ordinates will closely resemble that of the A_1 mode of the T_d system and although the Raman spectrum is dominated by a very intense band at 128 cm^{-1} (130.8 cm^{-1} in the low temperature spectrum) only a very weak infrared-active counterpart is detected (Figs. 4a−4c). Even at a resolution of 0.5 cm^{-1} no splitting of this Raman band into two features derived from the distinct types of $[TlI_4]^-$ is observed.

The three Tl−I stretching features in the IR spectrum are observed at 158.1, 154.6, and 149.3 cm^{-1}, but only two Raman bands are seen in the same region (at 156.5 and 153.0 cm^{-1}). Although the wavenumbers of the Raman bands do not coincide exactly with any of the IR bands they do presumably relate to similar normal co-ordinates. The point of particular interest is that the Raman feature relating to one of the components derived from the T_2 mode of the T_d ion is absent. In an ion of C_{2v} symmetry this effect could be rationalised in terms of a destructive Fermi resonance between the A_1 symmetric and asymmetric stretching modes if both have significant intrinsic intensity in both IR and Raman spectra.[27] This could result in the lower wavenumber A_1 feature having very high Raman intensity but very low i.r. intensity, with the high wavenumber A_1 mode showing the reverse intensity behaviour. In the present case, however, all modes are of the same symmetry species. Therefore, it is not clear to us why there should be such a marked intensity partitioning between two of the modes considering an individual $[TlI_4]^-$ ion. We note, however, that $[NBu_4][InI_4]$ shows identical behaviour.[28]

In the deformation region of the low-temperature Raman spectrum we presume that 57.8 and 51.2 cm^{-1} are deformations derived from T_2 and that 44.0 cm^{-1} is related to the E mode of a regular ion; unfortunately we were unable to obtain i.r. spectra of sufficient quality for meaningful comparison in this wavenumber range.

The Solution Structure. The radial distribution curve (*Fig. 3*) shows a minor peak at about 1.7 Å, mainly due to intramolecular C−Cl interactions in the CH_2Cl_2 molecules, and two major peaks at 2.78 and 4.5 Å. By comparison with the crystal structure, and in agreement with vibrational spectra[14] the latter are identified as being essentially due to Tl−I and I−I interactions, respectively. Their parameters have been refined by least-squares methods and a summary of the results is given in Table 4. In order to give a more realistic error estimate, including effects of systematic errors, the standard deviations given are increased to account also for the variation obtained in the parameter values when various *s*-intervals of the intensity data were used for the refinements.

Column A in *Table 4* gives the result from refinements without any intermolecular interactions included. The Tl−I distance obtained, 2.775(3) Å, corresponds closely to the average value from the crystal structure, 2.756[2.776]* Å. The number of Tl−I and I−I distances is also consistent with a tetrahedral structure. For regular tetrahedral symmetry, however, the expected I−I distance should be $\sqrt{8/3} \times r(\mathrm{Tl-I}) = 4.532(5)$ Å. The value obtained for this refined model, 4.491(5) Å, is significantly shorter.

However, the non-coordinating solvent promotes the formation of ion-pairs. In the crystal structure,

* Corrected for thermal motion assuming riding motion of I versus Tl. Note that an uncorrected distance r_{pq} is obtained as $|\langle \mathbf{r}_q \rangle - \langle \mathbf{r}_p \rangle|$ in a crystal structure determination, but as $|\langle \mathbf{r}_q - \mathbf{r}_p \rangle|$ for a solution (the brackets denote mean values and $\mathbf{r}$ denotes a vector). When comparing bond lengths from solution studies with interatomic distances from crystal structures, the latter should therefore be corrected for thermal motion effects.

Table 4. Parameter values (see text) obtained by least-squares refinement for the TlI_4^- complex ion in solution. The estimated standard deviations are given in parentheses.

Interaction	Parameter values	A	B
Tl−I	r (Å)	2.775(3)	2.771(3)
	n	3.9(1)	4.0(1)
	l^2 (Å^2)	0.0062(5)	0.0072(5)
I−I	r (Å)	4.491(5)	4.53(1)
	n	6.0(5)	6 (fixed)
	l^2 (Å^2)	0.040(4)	0.038(4)

Table 5. Bond lengths in Å for some d^{10} ions in octahedral hexaaqua complexes and in tetrahedral tetrahalocomplexes. The crystal structure values marked with (*) are corrected for thermal riding motion. The solvent is water except for TlI_4^-. Values for which references are not given are quoted from Ref. 32.

	$[M(H_2O)_6]$		$[MCl_4]$		$[MBr_4]$		$[MI_4]$	
	Crystal	Solution	Crystal	Solution	Crystal	Solution	Crystal	Solution
Tl(III)	*2.23(2)[33]	2.235(5)[16]	*2.433(3)[7]	2.43(1)[6]	*2.554(3)[8]	2.564(2)[16]	*2.776	2.771(3)
Hg(II)	*2.349(6)	2.41(1)	2.46_4	2.47(1)	2.58_7	2.610(5)	2.77–2.78	2.785(3)
Cd(II)	2.28[34]	2.292(5)[35]	2.45_4[36]	–	2.588(2)[45]	–	*2.790(3)[37]	2.790(3)[30]
Zn(II)	2.08[38]	2.093(15)[39]	2.25[40]	2.29(1)[41]	2.39[42]	2.40(1)[41]	2.60_5[43]	–

there are on the average six I–C distances shorter than 4.5 Å (13 less than 5 Å) for each iodine atom. Assuming six I–C distances at 4.5 Å with an estimated variation $l = 0.2$ Å, *cf.* eqn. (1), to occur in the solution, another set of refinements was performed (Table 4, column B). The ratio $r(I-I)/r(Tl-I) = 1.635$ (4) then obtained corresponds closely to the tetrahedral value 1.633. This is consistent with the vibrational spectra of $[N(C_5H_{11})_4]TlI_4$ in dichloromethane solution, which displayed a single symmetrical stretching band: at 153 cm^{-1} in IR (after solvent subtraction) and at 130 cm^{-1} in Raman.[14]

The parameter values in Table 4, column B, have been used in a calculation of reduced intensities, $i_{calc}(s)$. Together with the constant contributions from the solvent as mentioned above, these values are compared with the experimental values in Fig. 2. The agreement is satisfactory in the high-angle regions ($s > 5$ Å) used in the refinements.

Peak shapes, calculated by Fourier transformation of the $i_{calc}(s)$ values, are subtracted from the distribution curve in Fig. 3. The difference curve is relatively smooth, without any sharp peaks. The broad feature remaining between 4 to 6 Å is mostly due to the solvent structure,[29] but probably also to distances from the ion-pair formation, not accounted for in the model.

Comparisons with other d^{10} *ions.* The root-mean-square variation in the distances (Table 4, column B) $l(Tl-I)$ 0.085(3) Å and $l(I-I)$ 0.20(1) Å, are comparable to the corresponding values obtained by X-ray diffraction for HgI_4^{2-}, 0.10(1) and 0.24(2) Å,[20] and for CdI_4^{2-}, 0.084(7) and 0.19(1) Å.[30] Calculated vibrational amplitudes from spectroscopic data are of the same magnitude, for HgI_4^{2-} 0.070 and 0.195 Å, and for CdI_4 0.075 and 0.190 Å,[31] respectively. In Table 5, a comparison is made of bond lengths in the tetrahalo complex ions of Tl(III), Hg(II), Cd(II), and Zn(II), and in their octahedral hexaaqua complexes. It is interesting to note that the metal-ligand bond lengths for the tetraiodo complexes of Tl(III), Hg(II) and Cd(II) are virtually equal, although there is a marked difference in their hydrates, reflecting the different acceptor properties of the cations.[44] The very soft acceptor Hg^{2+} forms markedly longer bonds with the hard donor H_2O, than the less soft Tl^{3+} ion does. The Cd^{2+} ion has an intermediate character, which is discernible also for the tetrachloride complexes.

The relative decrease in bond length when the softness of the ligand decreases from the soft donor I^- to the hard H_2O is, as expected, most pronounced for the hardest acceptor Zn^{2+}.

Acknowledgements. The authors wish to thank Dr. Georg Johansson for providing results prior to publication and the Swedish Natural Science Research Council for economic support. We also wish to thank the S.R.C. for grants towards spectroscopic equipment.

REFERENCES

1. Lee, A. G. *The Chemistry of Thallium*, Elsevier, Amsterdam 1971.
2. Shriver, D. F. and Wharf, I. *Inorg. Chem. 8* (1969) 2167 and references therein.
3. Rath, H. J. *Thesis*, Universität Erlangen-Nürnberg, 1972.
4. Grunwald, B. *Thesis*, Universität Erlangen-Nürnberg, 1977.
5. Glaser, J. *Acta Chem. Scand. 34* (1980) 141.
6. Glaser, J. *Thesis*, Royal Inst. of Technology, Stockholm 1981.
7. Watanabe, T., Sarto, Y., Shiono, R. and Atoji, M. *Struct. Rept. 11* (1947–48) 393.
8. Glaser, J. *Acta Chem. Scand. 34* (1980) 157.

9. a. Thiele, G. and Rink, W. *Z. Anorg. Allg. Chem. 414* (1975) 231; b. Thiele, G., Grunwald, B., Rink, W. and Breitinger, D. *Z. Naturforsch. Teil B 34* (1979) 1512; c. Glaser, J. *Acta Chem. Scand. A 34* (1980) 75.
10. Hazell, A. C. *J. Chem. Soc.* (1963) 3459.
11. Drew, M. G. B., Lewis, D. F. and Walton, R. A. *Inorg. Nucl. Chem. Lett. 6* (1970) 163.
12. a. Spiro, T. G. *Inorg. Chem. 6* (1967) 569; b. Adams, D. M. and Morris, D. M. *J. Chem. Soc. A* (1968) 694.
13. Davies, E. D. and Long, D. A. *J. Chem. Soc. A* (1968) 2050.
14. Andrews, S. P., Badger, P. E. R., Goggin, P. L., Hurst, N. W. and Rattray, A. J. M. *J. Chem. Res. (S)* (1978) 1401.
15. Glaser, J. *Acta Chem. Scand. A 33* (1979) 789.
16. Glaser, J. and Johansson, G. *In press.*
17. Glaser, J. and Henriksson, U. *J. Am. Chem. Soc. 103* (1981) 6642.
18. Cotton, F. A., Johnson, B. F. G. and Wing, R. M. *Inorg. Chem. 4* (1965) 502.
19. Berkie, J. E. In Durig, J. R., Ed., *Analytic Applications of FT-IR to Molecular and Biological Systems*, Reidel, Dordrecht 1980, p. 25.
20. a. Sandström, M. and Johansson, G. *Acta Chem. Scand. A 31* (1977) 132; b. Sandström, M., Persson, I. and Ahrland, S. *Ibid. A 32* (1978) 607.
21. Sandström, M. and Persson, I. *Acta Chem. Scand. A 32* (1978) 95.
22. a. Kopfmann, G. and Huber, R. *Acta Crystallogr. A 24* (1968) 348; North, A. C. T., Phillips, D. C. and Scott Matthews, F. *Ibid.* 351; b.Hamilton, U. C. *Acta Crystallogr. 18* (1965) 502; c. Busing, W. R. and Levy, H. A. *Acta Crystallogr. 17* (1964) 142; Busing, W. R., Martin, K. O. and Levy, H. A. *Function and Error Program*, Report ORNL-TM-306, Oak Ridge National Laboratory, Oak Ridge 1965.
23. Kawaguchi, T., Tanaka, K., Takeuchi, T. and Watanabé, T. *Bull. Chem. Soc. Jpn. 46* (1973) 62.
24. Goggin, P. L., King, P., Sandström, M. and Woodward, P. *J. Chem. Soc. Dalton Trans. In press.*
25. Cyvin, S. J. *Molecular Vibrations and Mean Square Amplitudes*, Elsevier, Amsterdam 1968, p. 226.
26. Adams, D. M. and Newton, D. C. *Tables for Factor Group and Point Group Analysis*, Beckman R. I. I. C. Ltd., Croydon 1970.
27. Overend, J. In Davies, M., Ed., *Infrared Spectroscopy and Molecular Structure*, Elsevier, Amsterdam 1963, p. 351.
28. Goggin, P. L. *Unpublished work.*
29. Goggin, P. L. and Sandström, M. *To be published.*
30. Pocev, S., Triolo, R. and Johansson, G. *Acta Chem. Scand. A 33* (1979) 179.
31. Mohan, S. *Acta Ciencia Indica 4* (1978) 371.
32. Sandström, M., *Thesis*, Royal Institute of Technology, Stockholm 1978 (available on request).
33. Glaser, J. and Johansson, G. *Acta Chem. Scand. A 35* (1981) 639.
34. Caminiti, R., Johansson, G. and Sandström, M. *To be published.*
35. Caminiti, R. and Johansson, G. *Acta Chem. Scand. To be published.*
36. Oleksyn, B. J., Stadnicka, K. M. and Hodorowicz, S. A. *Acta Crystallogr. B 34* (1978) 811.
37. Kallel, A., Bats, J. W. and Daoud, A. *Acta Crystallogr. B 37* (1981) 676.
38. Ray, S., Zalkin, A. and Templeton, D. H. *Acta Crystallogr. B 29* (1973) 2741.
39. Bol, W., Gerrits, G. J. A. and van Panthaleon van Eck, C. L. *J. Appl. Crystallogr. 3* (1970) 486.
40. McGinnety, J. A. *Inorg. Chem. 13* (1974) 1057.
41. Maeda, M. and Johansson, G. *To be published.*
42. Morosin, B. and Lingafelter, E. C. *Acta Crystallogr. 12* (1959) 744.
43. Orioli, P. L. and Lip, C. H. *Cryst. Struct. Commun. 3* (1974) 477.
44. a. Ahrland, S., Chatt, J. and Davies, N. R. *Q. Rev. Chem. Soc. 12* (1958) 265; b. Pearson, R. G. *J. Chem. Educ. 45* (1968) 581, 643.
45. Bart, J. C. J., Bassi, I. W. and Calcaterra, M. *Phosphorus Sulfur 9* (1981) 347.

Received May 19, 1981.

Acta Chemica Scandinavica A 36 (1982) 63–68

The Crystal Structure and Electron Density Distribution of Tetraformohydrazide at 110 K

TOR OTTERSEN,[a] JAN ALMLÖF[a] and JØRGEN CARLÉ[b]

[a] Department of Chemistry, University of Oslo, Blindern, Oslo 3, Norway and [b] Marine Chemistry Section, Chemical Laboratory II, The H. C. Ørsted Institute, Universitetsparken 5, DK-2100 Copenhagen, Denmark.

The deformation electron density in tetraformohydrazide (TFH) has been determined by $X-X_{HO}$ Fourier synthesis and by *ab initio* Hartree-Fock calculations. The structure has been refined to a final R_w of 3.8 %. The general features of the difference maps are the same with both methods. The most striking feature of the maps is the low electron density in the N–N bond, showing little or no increase compared to the free-atom densities.

The present work is part of a series of investigations on bonding and electron density distributions in molecules containing the N–C=O and N–N moieties. The effect of hydrogen bonding has been studied in some detail both by experimental and theoretical methods.[1-3] Changes introduced by various substitutions have also been systematically investigated. The X-ray study of 1,2-diformohydrazide[3] showed that even for H-atoms realistic nuclear positions can be obtained, and this opens a possibility to obtain accurate experimental deformation densities from X-ray data alone. Deformation density distributions in a series of related molecules have been investigated and compared with theoretical distributions.[4-6] Within this series the effect of basis set changes in the theoretical investigations has also been investigated.[6]

An earlier X-ray study of TFH[7] showed a molecular configuration with torsional angles about the N–N bond of 90° in agreement with the structure of 1,2-dimethyl-1,2-diformohydrazide,[2] whereas 1,2-diformohydrazide is planar.[3] The N–N bond should be affected by this non-planarity, and the conjugation over the N–C=O moieties should also be influenced by the competition of two such groups for the N lone-pair.

In order to study these effects and also to get more information about the deformation density distribution in the N–C=O and N–N moieties, the present investigation was undertaken. TFH crystallizes in a non-centrosymmetric space group, which introduces some complications to the calculation of difference Fourier syntheses. By this study one would therefore gain experience concerning the calculation of deformation densities for such space groups.

EXPERIMENTAL

19.0 g (0.20 mol) sodium diformamide[8] was ground together with 4.4 g (0.05 mol) 1,2-diformohydrazide[9] and the mixture suspended in 55 ml anhydrous CH_2Cl_2. 22.9 g (0.20 mol) methanesulfonyl chloride dissolved in 16 ml anhydrous CH_2Cl_2 was added in one portion while stirring, and the heterogeneous reaction mixture was refluxed with stirring for 12 h. The white solid material was filtered off and extracted with acetone for 7 h in a Soxleth apparatus. By concentrating the acetone extract to *ca.* 50 ml, the TFH precipitated as a white solid. Further concentration of the acetone extract gave only very minor amounts of TFH. Recrystallization from acetone gave 2.6 g (36 % yield based on 1,2-diformohydrazide) of pure TFH as white cubic crystals applicable for X-ray crystallography.

NMR spectra were obtained on Varian T-60A (^{1}H) and Bruker WH90 FT (^{13}C) instruments, and data are given in ppm measured relative to TMS. The mass spectrum was recorded on an AEI-MS902 instrument with ion source temperature 100 °C (70 eV, direct sample insertion). ^{1}H NMR (4 % in DMSO-d_6): δ 9.27 (4H, s). ^{13}C NMR (9 % in DMSO-d_6): δ 161.6. Mass spectrum *m/e*, (%): 116(2), 88(45), 70(9), 60(48), 46(11), 45(18), 44(100),

0302-4377/82/010063-06$02.50

42(22), 40(36). The spectrum showed no molecular ion. The *m/e* 116, 88 and 60 were shown by high resolution to have the composition $C_3H_4N_2O_3$, $C_2H_4N_2O_2$ and CH_4N_2O, respectively.

Data collection and reduction. A crystal of dimensions $0.20 \times 0.20 \times 0.35$ mm was selected for data collection on a Syntex-Pl four-circle diffractometer equipped with a modified Enraf-Nonius low-temperature device (liquid nitrogen). The temperature at the crystal site was 110 ± 1 K. The angular coordinates of 15 reflections with 2θ values between 40 and 70° were used in a least-squares calculation to determine the crystal orientation and cell dimensions (see Crystal data).

The intensities of 874 reflections ($2\theta_{max} = 136°$) were recorded using a $\theta/2\theta$ scan, graphite monochromatized MoK_α radiation, and a scintillation detector. Since the number of symmetry-independent reflections is small, no attempts were made to exclude low-intensity reflections from the measurements, as was done in similar studies.[3,10] Each reflection was scanned from $2\theta(\alpha_1) - 1.4°$ to $2\theta(\alpha_2) + 1.9°$ for reflections with $2\theta \leq 50°$, and from $2\theta(\alpha_1) - 1.0°$ to $2\theta(\alpha_2) + 1.1°$ for reflections with $2\theta \geq 50°$, with a scan speed variable from 1.0°/min to 2.0°/min (2θ) depending on the intensity of the reflection as measured in a 3 s preliminary scan.

Three check reflections, measured after every sixty reflections, showed no systematic variations throughout the data collection. Estimated standard deviations of the net intensities were calculated as:

$$\sigma(I) = [(B_1 + B_2) \times \left(\frac{\text{scan time}}{2 \text{ background time}}\right)^2 + I_s + 10^{-4} \times I_s^2]^{\frac{1}{2}}$$

where B_1 and B_2 are the two background counts and I_s is the integrated intensity. The factor 10^{-4} accounts for the observed mean-square deviation of the check reflections. Of the 874 reflections measured, the 730 having net intensities $> 2\sigma(I)$ were used in the refinement.

Lorentz and polarization corrections were applied to the net intensities. The polarization factor includes polarization by the monochromator crystal.[11] The intensity data were corrected for truncation errors.[12] Using the notation of Ref. 12, the correction is given by:

$$I_{corr} = I/[A_1C_1 + A_2C_2 + (\lambda_a - \lambda_b)\{A_1[I_1(\lambda_a) + I_1(\lambda_b)] + A_2[I_2(\lambda_a) + I_2(\lambda_b)]\}]$$

The line widths ($W_1 = 2.9 \times 10^{-4}$ Å and $W_2 = 3.2 \times 10^{-4}$ Å) and intensity ratio $A_2/A_1 = 0.499$) were obtained from Compton and Allison,[13] and the wavelength values used are $\lambda_1 = 0.70926$ and $\lambda_2 = 0.71354$ Å. The maximum correction is $I_{corr} = I/0.935$.

The estimated errors in intensities due to absorption were all in the range 3–5 %, and it was therefore regarded unnecessary to apply absorption corrections. Checks on the data during the refinement procedure indicated no effects from secondary extinction.

CRYSTAL DATA (at 110 K)

Space group $I4\bar{2}m$, $a = 6.443(1)$ [6.492(4)], $c = 7.475(1)$ [7.545(4)], $V = 310.36(9)$ Å^3 [318.0], $M = 144.06$, $Z = 2$, $D_{calc} = 1.541$ g cm^{-3}, $F(000) = 148$, $\mu = 1.509$ cm^{-1}. The numbers in brackets are results from the earlier room-temperature study.

REFINEMENT

The quantity $\Sigma w(F_{obs} - K|F_{calc}|)^2$ was minimized in full-matrix least-squares refinements with $w = 1/\sigma^2(F_{obs})$. Starting positional parameters were obtained from the earlier study.[7] The atomic scattering factors used were those calculated by Doyle and Turner[14] for C, N and O; the contracted spherical scattering factor calculated by Stewart, Davidson and Simpson[15] was used for H.

The $\sin\theta/\lambda$ cut-off value was varied systematically, refinements were performed with minimum cut-off values of 0.0, 0.50, 0.65, 0.75 and 0.85 Å^{-1}. Hydrogen parameters were not refined for cut-off limits above 0.65 Å^{-1}. In some of the refinements with low-order data the hydrogens were refined with anisotropic temperature factors in order to obtain a better agreement between F_{obs} and F_{calc}. A refinement was also performed with a maximum cut-off of 0.85 Å^{-1}. Some data from the refinements are given in Table 1.

The heavy-atom parameters converged to their final values for the 0.75 Å^{-1} cut-off in agreement with the results for previous investigations.[3,10]

As found earlier, the maximum deviation from the "true" nuclear position occurred for the 0.50 Å^{-1} cut-off. This behaviour is now rather well established and seems to reflect real features of the electron density distribution in the X–H bond. For cut-off values above 0.50 Å^{-1} the refined H position shifts towards a more reasonable value. In the present case the C–H bond lengthens to 1.02(5) Å for the 0.65 Å^{-1} cut-off. This is still too short, but the low scattering power of H at high angles increases the standard deviation of the H parameters to the extent that the use of higher cut-off values is fairly meaningless.

Table 1. Some results from refinements using various parts of the data set. Estimated standard deviations are given in parentheses.

$\sin\theta/\lambda$ cut-off ($Å^{-1}$)	reflections	parameters	R(%)	R_w(%)	R_t(%)[a]	Goodness of fit	Scale for F_o	C–H(Å)
<0.85	259	23	2.80	3.63	4.81	4.25	0.06502(1)	0.986(15)
–	730	23	3.81	3.98	3.81	2.88	0.06582(1)	0.977(11)
–	730	20	3.79	4.00	3.79	2.89	0.06583(1)	0.973(11)
>0.50	668	20	3.54	2.72	2.88	1.56	0.06782(1)	0.781(20)
>0.65	604	20	3.76	2.75	3.80	1.30	0.06764(1)	1.023(51)
>0.75	544	17	4.22	3.13	3.66	1.22	0.06707(1)	
>0.85	471	17	4.57	3.61	3.60	1.17	0.06568(2)	

[a] R_t is the R-factor for the whole data set.

Final atomic parameters from some of the refinements are given in Table 2. The estimated standard deviations in the molecular parameters were calculated from the full correlation matrix. The values of the correlation coefficients involving H were all less than 0.30.

THE STRUCTURE

Molecular parameters are given in Fig. 1. The torsional angle around the N–N bond is crystallographically determined to 90°, with planar configurations around the N atoms. The configuration around the C–N bond is similar to that in diformohydrazide,[3] with the oxygen atoms *cis*-planar relative to the N–N bond. The introduction of two new formyl groups leads to decrease in the N–N–C angle of 1.0°. The angles around N are equivalent to those found in 1,2-dimethyl-1,2-diformohydrazide,[2] which has a similar configuration as TFH with torsional angles around the N–N bond close to 90°, but with the oxygens anti-planar to the N–N bond.

In Table 3 the bond lengths are compared with those obtained in similar structures. The values differ widely from those reported earlier for TFH.[7] Some reasons for these discrepancies may be found in the low overdetermination ratio and the refinement technique used in the earlier investigation.

The C–N and C=O bond lengths obtained in the present study imply a low degree of conjugation

Table 2. Parameters from some of the refinements. S is the cut-off value for $\sin\theta/\lambda$ in $Å^{-1}$. The anisotropic temperature factor is given by $\exp(-[B_{11}h^2+\cdots+B_{23}kl])$. E.s.d.'s (in parentheses) are in units of the last digits given.

	S	X	Z	$B_{11}(B)$	B_{33}	B_{12}	B_{13}
O	>0.75	0.24913(7)	0.10071(8)	0.01396(10)	0.00576(5)	−0.01652(20)	−0.00041(8)
	>0.65	0.24923(6)	0.10076(7)	0.01387(8)	0.00576(4)	−0.01637(16)	−0.00034(7)
	<0.85	0.24914(12)	0.10079(11)	0.01442(17)	0.00608(13)	−0.01548(38)	−0.00078(22)
N	>0.75	0.0	0.09208(7)	0.00598(5)	0.00270(4)	−0.00098(14)	0.0
	>0.65	0.0	0.09207(6)	0.00597(5)	0.00258(4)	−0.00104(13)	0.0
	<0.85	0.0	0.09244(16)	0.00673(15)	0.00234(14)	−0.00102(53)	0.0
C	>0.75	0.13412(6)	0.18042(6)	0.00787(6)	0.00355(4)	−0.00319(13)	−0.00113(6)
	>0.65	0.13415(5)	0.18039(5)	0.00780(5)	0.00354(4)	−0.00325(12)	−0.00117(6)
	<0.85	0.13423(13)	0.17987(14)	0.00822(14)	0.00441(14)	−0.00204(41)	−0.00159(23)
H	>0.65	0.1253(59)	0.3168(69)	2.06(47)			
	>0.50	0.1198(25)	0.2834(27)	2.01(26)			
	<0.85	0.1213(20)	0.3108(21)	0.0119(33)	0.0018(25)	−0.0107(107)	0.0035(47)

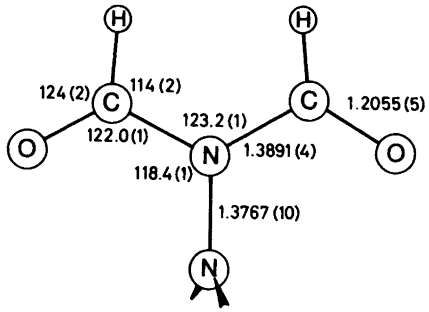

Fig. 1. Bond distances and angles in tetraformohydrazide.

over the N−C=O fragment. The reason for this must be twofold; the lack of hydrogen bonding in the present case and the two formyl groups competing for the nitrogen lone-pair. Earlier studies have shown that hydrogen bonding has a marked effect on the conjugation of N−C=O groups; for a review see Refs. 1 and 2. The reduced participation of the N lone-pair in the conjugation is evidenced by the differences between the bond lengths in TFH and in dimethyl-diformohydrazide.

In conclusion, the molecular parameters obtained in the present study are found to confirm and enhance the conclusions drawn from earlier investigations.

Deformation electron density. TFH crystallizes in a non-centrosymmetric space group. A difference density map calculated in the standard way, assuming the same phases for F_{obs} and F_{calc}, will therefore suffer from considerable errors.[6,16] The difference densities were therefore calculated in the same way as for acetamide.[6] A low-order refinement (<0.85 Å^{-1}) with 259 observed reflections was performed in order to obtain atomic parameters for computing the scale and phases of F_{obs}. For this purpose, a good fit between observed and calculated intensities is more important than the physical significance of the parameters, and anisotropic temperature factors were therefore refined for the hydrogen atoms. The final F_{calc}, on the contrary, were computed from atomic parameters refined with high-order data (>0.75 Å^{-1} for the heavy atoms, >0.65 Å^{-1} for hydrogen). The low-order subset of data was used in all calculations of deformation densities.

The mean difference in phase angles between F_{obs} and F_{calc} is 1.16°, and the corresponding r.m.s. phase difference is 2.55°. These values are small compared with those found for acetamide,[6] 2.3 and 3.7°, respectively, and for lithium formate monohydrate,[17] 3.3 and 7.2°. However, results from other, similar investigations indicate that the absolute values of these phase differences do not necessarily reflect the effect their omission would have on the densities.

The resulting $X-X_{HO}$ map is shown in Fig. 2. The densities in bonds and lone-pairs increased with 10−40 % compared to the map calculated with the standard method.

A difference map based on the low-order parameters showed densities in the bond and lone-pair regions of up to 50 % of those shown in Fig. 2. Ideally for the purpose of this parameter set this difference should show zero value at all points, since the parameters are used to calculate the phases of F_{obs}. However, since all interesting regions in TFH are situated on symmetry elements where the e.s.d. of the density is relatively high, no attempts were made to obtain a better fit for the low-order refinement, as was done for acetamide.

Deformation electron densities are often readily accessible to theoretical calculations. Systems of the size of TFH may easily be treated with compa-

Table 3. Some bond lengths obtained in a series of related molecules.

	C=O	C−N	N−N
TFH (present work)	1.2055(5)	1.3891(4)	1.3767(10)
TFH (previous work [7])	1.214(5)	1.325(4)	1.346(6)
Diformohydrazide [3]	1.2380(2)	1.3316(2)	1.3797(2)
Dimethyldiformohydrazide [2]	1.222(3)	1.356(2)	1.386(2)
Hexahydropyridazinedione [4]	1.245(1)	1.346(1)	1.398(1)
Carbonohydrazide [10]	1.2458(3)	1.3581(3)	1.4103(3)
		1.3574(3)	1.4156(3)
Hexahydro-dimethylpyridazinedione [18]	1.230(1)	1.366(1)	1.406(1)
	1.232(1)	1.366(1)	

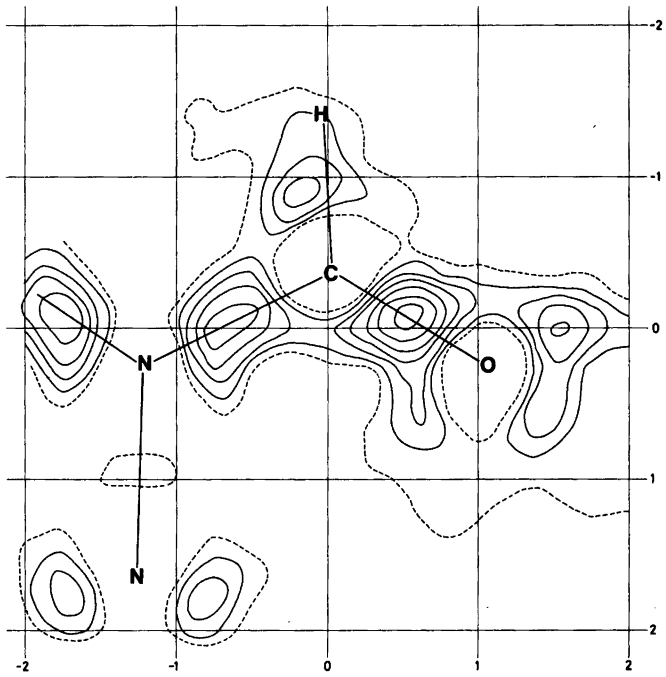

Fig. 2. Experimental deformation density in the symmetry plane of the molecule.

ratively accurate calculations on the Hartree-Fock level of approximation. The question then arises whether that approximation is applicable for the study of problems related to electron density distributions.

Defining a fluctuation potential as the difference between the exact Hamiltonian and the sum of Hartree-Fock operators for the electrons of a system

$$H' = H - \sum_{i} F(i)$$

it may be shown that, in a perturbational approach, the Hartree-Fock electron density is correct up to the second order in the fluctuation potential. The Hartree-Fock method should therefore be rather well suited for the present type of investigation.

In a previous study on diformohydrazide, it was found that a polarized basis of roughly triple-zeta quality produced rather reliable deformation densities. The same basis set was therefore used in the present investigation (*i.e.* 9*s*5*pld* contracted to 5*s*3*p*1*d* for C, N and O, and 5*slp* contracted to 3*slp* for H). The entire basis set for the calculation thus comprised 224 contracted basis functions. From the calculated wavefunctions the electron density

$$\rho(r_1) = \int \psi^*(r_1, r_2 \cdots r_n)\psi(r_1, r_2 \cdots r_n)\, dv_2 dv_3 \cdots dv_n$$

was evaluated. The deformation density was obtained by subtracting densities for the atoms, calculated in the same way and with the same basis set. This procedure ensures a close cancellation of errors introduced by the different approximations used in the calculations. The resulting theoretical deformation density is shown in Fig. 3. Both the experimental and the theoretical deformation densities conform well with those obtained earlier for similar structures.[4-6,10] The peak heights in the C=O bonds vary from 0.4 to 0.6 e Å^{-3}, and in the C–N bonds from 0.4 to 0.55 e Å^{-3}. The largest difference between the experimental and theoretical densities is found in the oxygen lone-pair region, where the theoretical densities are significantly higher than the experimental ones. Similar discrepancies have been noted in previous studies on related compounds.[4,6] The basis set used in the present calculations probably gives somewhat overestimated lone-pair densities (*cf.* Ref. 6 for a systematic investigation of this effect), but this does not seem to explain the whole discrepancy. According to the theoretical maps, the oxygen lone-pairs are very

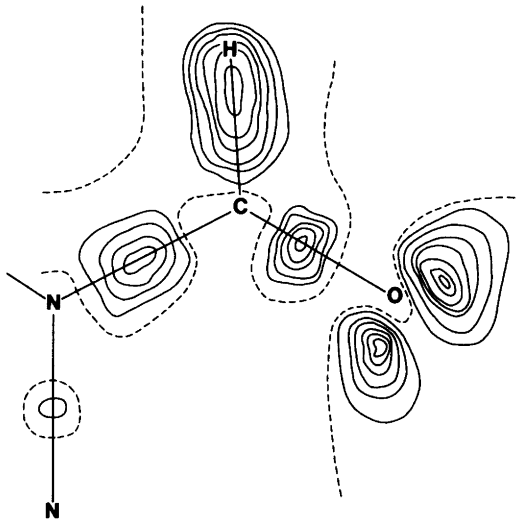

Fig. 3. Theoretical deformation density in the symmetry plane of the molecule.

contracted and close to the nucleus. It seems likely, therefore, that the high-order atomic parameters are still affected by these density distributions, which accordingly will appear with reduced amplitude in the difference maps.

When comparing the present results with those obtained earlier, the differences are rather small and probably insignificant, in particular when diformohydrazide is concerned. The particularly low densities previously found in the N–N bonds are observed in the present case also. A detailed discussion of the deformation density in TFH in relation to the previous findings is therefore considered superfluous.

REFERENCES

1. Ottersen, T. *Adv. Mol. Relaxation Processes 9* (1969) 105.
2. Ottersen. T. *Acta Chem. Scand. A 32* (1978) 127.
3. Hope, H. and Ottersen, T. *Acta Crystallogr. B 34* (1978) 3623.
4. Ottersen, T. and Almlöf, J. *Acta Chem. Scand. A 32* (1978) 219.
5. Hope, H. and Ottersen, T. *Acta Crystallogr. B 35* (1979) 370
6. Ottersen, T., Almlöf, J. and Hope, H. *Acta Crystallogr. B 36* (1980) 1147.
7. Hinderer, A. and Hess, H. *Chem. Ber. 107* (1974) 492.
8. Allenstein, E. and Beyl, E. *Chem. Ber. 100* (1967) 3551.
9. Schöfer, G. and Schwar, N. *J. Prakt. Chem. 51* (1895) 180.
10. Ottersen, T. and Hope, H. *Acta Crystallogr. B 35* (1979) 373.
11. Hope, H. *Acta Crystallogr. A 27* (1971) 392.
12. Denne, W. A. *Acta Crystallogr. A 33* (1977) 438.
13. Compton, A. H. and Allison, S. K. *X-Rays in Theory and Experiments*, Macmillan, London 1935.
14. Doyle, P. A. and Turner, P. S. *Acta Crystallogr. A 24* (1968) 390.
15. Stewart, R. F., Davidson, E. R. and Simpson, W. T. *J. Chem. Phys. 42* (1965) 3175.
16. Coppens, P. *Acta Crystallogr. B 30* (1974) 255.
17. Thomas, J. O., Tellgren, R. and Almlöf, J. *Acta Crystallogr. B 31* (1975) 19.
18. Ottersen, T. and Sørensen, U. *Acta Chem. Scand. A 31* (1977) 808.

Received May 20, 1981.

Acta Chemica Scandinavica A 36 (1982) 69–77

Tentative Assignments of Fundamental Vibrations of Thio- and Selenoamides. VIII. 1,2-Dimethyl-3-pyrazolidineselone, a Cyclic Selenohydrazide. Selenation of the Thioamide Group in Theory and Practice

U. ANTHONI,[a] G. BORCH,[b] P. KLÆBOE[c] and P. H. NIELSEN[a]

[a] Chemical Laboratory II, The H. C. Ørsted Institute, DK-2100 Copenhagen, Denmark, [b] Chemistry Department A, The Technical University of Denmark, DK-2800 Lyngby, Denmark and [c] Department of Chemistry, University of Oslo, Oslo 3, Norway

As a continuation of our investigation on the molecular vibrations of a cyclic thiohydrazide, 1,2-dimethyl-3-pyrazolidinethione, the IR and Raman spectra of the corresponding selenium analogue, 1,2-dimethyl-3-pyrazolidineselone, have been recorded from 40–4000 cm^{-1}. The vibrational assignment was assisted by a normal coordinate analysis with a force field partly transferred from the sulfur compound. The scope and limitations of the methods of selenation, *i.e.* comparison of the spectra of compounds containing a thioamide grouping with the corresponding selenium analogoues, are evaluated. On the basis of CNDO/2 calculations it is concluded that the electronic structures are subject to considerable changes on selenation contrary to what is commonly assumed.

An empirical classification of the IR bands in spectra of compounds containing a thioamide group, *e.g.* thioamides, thioureas and thiosemicarbazides, may often be obtained by a comparison with the spectra of the corresponding selenium analogues. Most of the bands appear almost unchanged in intensity, shape, and frequency and would as a first approximation be expected to originate in vibrations other than the CS bond. Some bands appear to have retained their intensity and shape, but are displaced towards lower frequencies as expected for vibrations due mainly to the CS group. It is often observed that the spectra are virtually superimposable in many regions, and that only a few bands show major shifts towards lower frequencies. On this basis we proposed[1] the term 'selenation' as a method for identification of bands characteristic for the thioamide grouping by comparison with the spectra of the corresponding selenium compound and stated that the method 'almost works like an isotopic substitution'. In this paper we want to investigate the foundation and limitations of the method.

The method was rapidly adopted by other authors.[2] Normal coordinate analyses (NCA) on dithio- and diselenocarbamates[3,4] served to clarify the relative importance of changes in geometry, mass and force field induced in the molecule on selenation. The NCA also showed that borderline cases with small selenation shifts were found whenever strong coupling occurs between vibrations of the thioamide group and the remaining molecule. Recently, in a paper dealing with the IR spectra of tetramethylthiourea and tetramethylselenourea[5] we have summarised the deficiencies of the selenation method as follows. (i) Selenation shifts may be missed because bands of different origin interfere. (ii) Bands displaying selenation shifts with unaltered shape and intensity may nevertheless originate in different vibrations. (iii) Selenation shifts may be caused not only by electronic but also by steric changes following substitution of sulfur by selenium. However, many of the above-mentioned problems are eliminated by considering selenation shifts of a large number of compounds containing the same thioamide group-

0302-4377/82/010069-09$02.50

ing which was done in the original work[1] and in a study of dithiocarbamates.[6] Selenation of only a few compounds of a given type unassisted by NCA may be quite insufficient for an ample classification of the relevant bands (see *e.g.* a recent paper[7] on benzimidazole-, benzoxazole- and benzothiazole-2-thiones). Some authors[8-15] have extended the concept of selenation to imply (i) that the electronic structure of analogous sulfur and selenium compounds are very similar and (ii) that only slight modifications are needed in transferring the force field for a given sulfur compound to the analogous selenium compound. Both statements will be discussed below.

In the previous communication[16] the vibrational spectrum of a cyclic thiohydrazide, 1,2-dimethyl-3-pyrazolidinethione (DMPT), was discussed in some detail. In the present paper the investigation is extended to the selenium analogue, 1,2-dimethyl-3-pyrazolidineselone (DMPS). These results provide a firm basis for an evaluation of the selenation method applied to thiohydrazides. To illustrate the electronic and steric effects of selenation we have carried out CNDO/2 calculations on DMPT and DMPS. An attempt is made to correlate the changes in force field from DMPT to DMPS with the calculated changes in electronic density of the two compounds.

STRUCTURE

Experimental data on the structure of selenoamides or -hydrazides have to our knowledge not been reported. Though most of the geometrical parameters needed for this study could be transferred from similar molecules (DMPT, selenoureas) we still do not know with certainty how the CN bond length in compounds containing the thioamide grouping is influenced by substituting selenium for sulfur. For example, the CN bond length increases in selenourea[17] (1.34–1.45 Å) relative to thiourea[18-20] (1.33–1.34 Å) but decreases in selenourea solvates[21] (1.31–1.32 Å). Varying changes are also observed when complex compounds of ethylenethiourea and ethyleneselenourea[22,23] are compared. X-Ray analyses of closely related thio- and selenosemicarbazones[24,25] indicate an increased CN bond length in the CSe–NH_2 group (1.37 Å) relative to CS–NH_2 (1.33 Å) while the other thioureide CN bond is almost unchanged. The CN bond lengths in tetramethylthiourea[26] (1.37 Å) and tetramethylselenourea[5] (1.347 Å) are not influenced by hydrogen bonding as in the above-mentioned examples but in these cases sterical hindrance prevents the planarity of the thio- and selenoureide groups. The trends observed for the CN bond lengths in diselenocarbamates relative to dithiocarbamates[27-29] also seem difficult to generalise.

Since the crystal structure for 5-(*p*-chlorophenyl)-DMPT is known[16] a sample of the corresponding selenium compound, 5-(*p*-chlorophenyl)-DMPS, was prepared and turned out to be isostructural with the sulfur compound. The details of this investigation will be published elsewhere, but the most important results of the X-ray structure determination will be summarised here. The CSe bond length was found to be 1.824(4) Å not far from the mean value in selenourea[17] (1.86 Å), selenourea solvate21 (1.867 Å) and selenosemicarbazones[25] (1.83(2) Å). Rather unexpectedly all other bond lengths and interbond angles were found to be identical within the experimental error. The thiohydrazide CN bond length, in particular, is 1.314(3) Å in 5-(*p*-chlorophenyl)-DMPT and 1.306(6) Å in the corresponding selenium compound. The fact that the geometrical structures of 5-(*p*-chlorophenyl)-DMPT and -DMPS are identical apart from the CS/CSe bonds does not necessarily mean that the electronic structures are also identical. Thus, the CNDO/2 calculations indicate that selenation of the thiohydrazide group introduces both electronic and steric effects. However, the effects can be mutually compensating or too small to influence the CN bond lengths significantly.

EXPERIMENTAL

Perkin-Elmer spectrometers 180, 225 and 580 were used to study the IR spectrum in the 180–4000 cm^{-1} range. The pure liquids were supported between KBr and CsI plates. Solutions in CCl_4 and CS_2 were run in standard cells of different thicknesses. The far IR spectra were recorded with a fast scan Fourier transform interferometer (model 114c) from Bruker using 1 mm PET cells. Beam splitters of Mylar of 3.5 and 12 nm thickness were employed to cover the region 600–50 cm^{-1}. The Raman spectra were recorded with a Cary model 81 spectrometer equipped with an Argon ion laser source using blue and green lines in both 180 and 90° illumination modes. The preparation and properties of DMPS and 5-(*p*-chlorophenyl)-DMPS will be reported elsewhere. All samples used for the spectroscopical measurements were carefully fractionated and show satisfactory elemental analyses.

NORMAL COORDINATE ANALYSIS

The normal vibrations were calculated for DMPS using the same method as for DMPT.[16] Initially a calculation was performed with the force field of DMPT but with the mass and geometry found for DMPS. The shifts calculated by this method are reproduced in Table 1. It allows a provisional assignment since most of the fundamentals in the range 100 – 3000 cm^{-1} are predicted within 10 cm^{-1} and only eight deviated up to 30 cm^{-1} from the experimental values. The result indicated that the force fields of DMPT and DMPS were indeed, very similar, but not quite identical. To avoid a laborious isotopic substitution of DMPS we now decided to vary only the force constants pertaining to the selenohydrazide group and transfer the remaining force field from DMPT. This approach was justified by the following considerations: (i) The CNDO/2 calculation showed that changes in electron density on selenation are restricted to the selenohydrazide group. (ii) The PED (potential energy distribution) of the eight fundamentals not correctly predicted indicated significant contributions also from this part of the molecule. (iii) It proved possible to obtain a good fit in this way and the force field obtained was compatible with the CNDO/2 results.

The force constants included in the iterative procedure were primarily the five stretching, the six in-plane bending (with $H_{\varepsilon_1} = H_{\varepsilon_2}$ as in DMPT) and the ΔCSe out-of-plane bending force constants of the N – N(CH′3) – CSe – C chain. Since the CNDO/2 calculation indicated small changes in electron density around the $CH_2(-CSe)$ group the relevant force constants were also included, however, almost without effect as expected. Unfortunately the force constants for CH′3 – N – N and N – N – CS deformation (H_{ε_2} and H_{ε_3}) depend heavily upon the location of the fundamentals below 200 cm^{-1} which is subject to considerable uncertainty. In order to secure a well-conditioned and physically significant convergence of the least-square iterative process, these force constants were fixed to the values found for DMPT, while H_{ε_1} was still allowed to vary. The iteration was designed to obtain the best possible fit between the observed and calculated selenation shifts (see Table 1) rather than to obtain agreement between observed and calculated frequencies. Furthermore the shifts were introduced in the iteration with weights reflecting their trustworthiness, as estimated from a consideration of their IR and Raman spectra. For example, some of the fundamentals couple rather heavily with overtones and/or combination modes occurring in the same region and cannot be attributed to definite selenation shifts.

The final force field is not unique, though experience from 30 calculations with different approximations indicate that the direction and magnitude of all the major shifts are correct. The final values are the following (designation and units as in Ref. 16): K_D 3.0; K_{L_2} 3.6; K_A 5.1; K_{B_2} 7.6; K_{P_2} 4.7; H_{μ_1} 0.7; H_{μ_2} 2.9; H_{μ_3} 1.6; H_{ε_1} 0.4; H_{ω_1} 1.6; H_{δ_2} 0.49; H_Δ 0.33; $H_{\gamma_3^\circ} = H_{\gamma_4^\circ}$ 0.66; $F_{\gamma_3^\circ\gamma_4^\circ}$ 0.05. All other values were transferred from DMPT. The agreement between the calculated and the observed shifts (Table 1) are considered satisfactory with two exceptions. The downwards shifts of *ca.* 10 cm^{-1} of ν_{21} and ν_{22} are difficult to reproduce by the NCA. Explorative calculations show that agreement can only be reached if the force constant for NN stretching, K_A, is lowered considerably. This seems improbable, since almost all the NN stretching character at the same time is transferred from ν_{20} to ν_{22}. The calculation reproduced in Table 1 is a likely compromise. The calculated shift is also much too small for ν_{33}, and again a better fit seems to be dependent upon a lowered value for K_A. The exact value found for K_{B_2}, the force constant for C^3N stretching, depends heavily upon the calculated shift for ν_{11}, and the slight increase found here is probably not significant.

RESULTS AND DISCUSSION

IR spectra of DMPS and DMPT as liquids in the spectral region 180 – 4000 cm^{-1} are given in Fig. 1. The spectra clearly show the great similarity which is the basis for the use of the selenation technique. Some important selenation shifts have been indicated on the figure to facilitate comparison in the low-frequency range where the correlation is not obvious. The numerical material is collected in Table 1, which lists all pertinent results in a manner similar to that used for DMPT in the previous paper.[16] Since the spectra of DMPS and DMPT are very similar, it is unnecessary to give a detailed account of the results obtained here for DMPS. Instead we shall concentrate on the concept of selenation, *i.e.* whether comparison of the IR spectra of DMPT and DMPS can be used profitably in identifying the vibrations originating in the thio- and selenohydrazide groupings.

Table 1. Observed and calculated vibrational frequencies (cm^{-1}) of 1,2-dimethylpyrazolidine-3-selone, tentative assignments of the spectra, and description of the fundamentals.[a]

Frequency					Selenation shifts[d]				
IR, obs.		Raman, obs.		Calc.[c]	Obs.			Calc.[e]	Assignment and description (PED, %)[f]
liquid	CCl_4/CS_2 solution	liquid	pol.[b]		IR liq.	IR sol.	Raman liq.		
				2988				0(0)	ν_1, $\nu_{as}CH_3$ (99)
2989m	2986m	2986m,sh	0.7	2985	+4	+3	−1	0(0)	ν_2, $\nu_{as}CH_3$ (99)
				2972				0(0)	ν_3, $\nu_{as}CH_2$ (98)
				2967				0(0)	ν_4, $\nu_{as}CH_3'$ (99)
2964m	2968m	2969m	0.5	2964	+2	+3	+2	0(0)	ν_5, $\nu_{as}CH_3'$ (99)
				2958				0(0)	ν_6, $\nu_{as}CH_2$ (98)
				2930				0(0)	ν_7, ν_sCH_2 (98)
2926m,sh	2930m	2926m,sh	0.3	2929	−4	+4	−2	0(0)	ν_8, ν_sCH_3' (99)
2910m	2910m	2909m	0.3	2918	−10	−6	−11	0(0)	ν_9, ν_sCH_2 (99)
2860m	2861m	2861w,sh	0.3	2862	0	+1	−6	0(0)	ν_{10}, ν_sCH_3 (100)
2791mw	2792mw	2792w			−1	0	0		$2 \cdot \nu_{19}$
1516vs,br	1505vs,br	1513vs	0.5	1510	*+15*	*+12*	*+10*	*+12(0)*	ν_{11}, $\nu C^3N(61)$, $\delta_{as}CH_3'$ (15)
1471m	1472m,sh	1463w,sh		1462	+7	+6	−3	−2(0)	ν_{12}, $\nu C^3N(6)$, $\delta_{as}CH_3'$ (60), δCH_2 (24)
	1457s			1458		+3		−1(0)	ν_{13}, $\delta_{as}CH_3$ (77)
1450s	1450s	1448m,sh	0.7	1455	−1	+2	−2	0(0)	ν_{14}, $\delta_{as}CH_3$ (99)
				1446				+3(0)	ν_{15}, $\delta_{as}CH_3'$ (83)
	1436vw	1435m,sh				+1	−3		
				1432				+1(0)	ν_{16}, δCH_2 (88)
1424s	1425s	1424m	0.6	1418	0	0	−2	−3(−2)	ν_{17}, δCH_2 (80)
1416s,sh	1414s			1415	0	+2		0(0)	ν_{18}, δ_sCH_3 (98)
1392s	1392s	1390s	0.4	1388	+1	+1	−5	−3(0)	ν_{19}, $\nu C^3N(7)$, δ_sCH_3' (95)
1385s,sh									
1340w	1344w	1339vw		1344	0	0	−5	−3(−2)	ν_{20}, *νNN(16)*, *νCSe(5)*, $\nu C^3N(5)$, ν/δring (64)
1300s	1303m			1310	*−12*	*−10*		*−7(0)*	ν_{21}, t/ωCH$_2$ (74)
	1296s	1297m	0.3	1309		*−10*	*−9*	*0(−3)*	ν_{22}, *νNN(18)*, t/ωCH$_2$ (41), ν/δring (29)
1255m	1255s	1255vw	0.2		−4	−3	−2		
1239m	1240m	1236vw,sh			−9	−7	−9		
1224m	1224m	1224w	0.6	1226	*−8*	*−9*	*−8*	*−7(−3)*	ν_{23}, ω/tCH$_2$ (35), ν/δring (40), ρCH$_3$ (28)
1187s	1188s	1184w	0.5	1191	+1	+3	−4	−5(0)	ν_{24}, ω/tCH$_2$ (70), ρCH$_3$ (23)
1174m,sh	1174m,sh	1174m,sh		1165	0	0	−1	−3(−2)	ν_{25}, *νNNCSe(6)*, νring (31), ρCH$_3$ (38), ω/tCH$_2$ (21)
1130m,sh	1130m,sh	1127vw,sh		1128	−1	−3	−5	−9(−1)	ν_{26}, *νNNCSe(7)*, ρCH$_3$ (43), νring (29) *and* $\nu_{34}+\nu_{41}$
1113s	1114s	1111w,sh			−5		−10		

1095m,sh		1095w,sh		1102	0		−1	+2(0)	ν_{27}, $\rho CH_3'$ (56), ν/δring (19)
1089s	1089s	1087w	0.5	1099	*+13*	*+13*	*+3*	*+11(−1)*	ν_{28}, $\rho CH_3'$ (90)
1064s	1066s	1062w	0.7	1058	+5	+6	−2	−2(−1)	ν_{29}, νCC(45), ρCH_2 (34)
1054m,sh	1054m	1054vw,sh							
1038m,sh	1040w,sh	1039vw,sh		1042	*−5*	*−3*	*−3*	*−4(−4)*	ν_{30}, *νNCSe (6)*, $\rho CH_3'$ (21), νring (52)
1005m,sh	1006m								
1001m	1001m	1002vw	0.7	992	*−4*	*−3*	*−5*	*−4(0)*	ν_{31}, ρCH_2 (70), νring (17)
968w	967w	966vw	0.7		−3	−4	−8		
938m	939m	933vw,sh		943	*−1*	*−1*	*−6*	*−6(−1)*	ν_{32}, *νNN (5)*, ρCH_2 (58), νring (24)
924m	925m	921vw	0.3		−2	−1	−5		
874m	875m	874s	0.4	901	*−17*	*−16*	*−19*	*−3(−3)*	ν_{33}, *νNN (18)*, *νCSe (4)*, νring (40), ρCH_2 (22)
773m	772m	773w	0.4	783	*−13*		*−14*	*−17(−18)*	ν_{34}, *νCSe(14)*, *νNN(10)*, *$\nu C^3N(5)$*, νring(25), δring(51)
695vw,sh		690m,sh	0.3		−7		−13		
683w	687w	685s	0.2	686	*−6*	*−5*	*−8*	*−5(−4)*	ν_{35}, *νCSe(5)*, *νNN(5)*, *$\nu C^3N(6)$*, νring(45), δring (21)
635m	635m	635m	0.2	630	*−4*	*−4*	*−7*	*−8(−2)*	ν_{36}, *νNN(11)*, νring (53), δring (45)
	540w,sh	540vw,sh				−2	−4		
526m	524m	525mw	0.6	549	+8	+7	+4	−4(−1)	ν_{37}, $\Delta CH_3-N<^{N}_{C}$(60), νring (27) *and* $\nu_{42}+\nu_{43}$
					−20	*−17*	*−23*		$\Delta CSe(23)$, $\Delta CH_3-N<^{N}_{C}$(25), ρCH_2 (53) *and*
468w	470w	468w	0.5	476				*−14(−7)*	ν_{38}, $\nu_{41}+\nu_{46}$
458w	457w	458w	0.6		*+6*	*+5*	*+8*		
418w	421w	419w	0.5	408	*−4*	*−2*	*−5*	*−13(−7)*	ν_{39}, $\Delta CSe(43)$, $\Delta CH_3-N<^{N}_{C}$(24), δring (36), νring (23)
	365vw,sh	365w,sh		375			−5	−3(−1)	ν_{40}, $\Delta CSe(13)$, ρCH_2 (43), ν/δring (26)
354w	352m	352w	0.5	346	*+5*	*+3*	*+2*	*+8(+39)*	ν_{41}, *νCSe(22)*, *νNN(8)*, $\delta CH_3-N</CH_3'-N<$ (36), ν/δring (32)
321ms	325s	320s	0.3	305	*−110*	*−107*	*−114*	*−124(−129)*	ν_{42}, *νCSe(36)*, *δCSe(22)*, ν/δring (37)
216m	222m	221w,sh		225	*−51*		*−47*	*−43(−45)*	ν_{43}, *δCSe(41)*, *νCSe(7)*, *νNN(6)*, $\delta CH_3'-N<$ (39)
204m,sh	207m	209m	0.6	200	+2		+6	−2(−2)	ν_{44}, τCH_3 (66)
174w		170vw		170			0	0(0)	ν_{45}, τCH_3 (92)
	110w	110w		120			−8	+2(−1)	ν_{46}, δring
	55m			48				−19(−1)	ν_{47}, δring
				19				−3(−2)	ν_{48}, δring

[a] The following abbreviations have been used: s, strong; m, medium; w, weak; br, broad; sh, shoulder. Weak and very weak bands not assigned to fundamentals have in most instances been omitted. [b] Approximate depolarisation ratio ($\rho=0.75$ corresponds to a fully depolarised band). [c] Using the final converged force field partly transferred from DMPT. [d] Shifts (cm^{-1}) of corresponding bands (*i.e.* with similar PED) in DMPS and DMPT ($\nu_{DMPS}-\nu_{DMPT}$). Values in italics are believed to be significant trends. [e] Calculated selenation shifts using the force field mentioned in note *c*. The part of the shift originating only in changes of mass and geometry is given in parenthesis (calculated using the geometry and mass of DMPS but the force field of DMPT). [f] Abbreviations: ν = stretch; δ = deformation; Δ = out-of-plane deformation; ρ = rock; ω = wag; t = twist; τ = torsion; s = symmetric, and as = antisymmetric. Vibrations of the pyrazolidine ring and the attached heavy atoms are designated 'ring' or using the following nomenclature: N^1-CH_3, N^2-CH_3', C^3Se. The potential energy distribution (PED, $x_{ik}=100F_{ii}L^2_{ik}/\lambda_k$) is stated only for significant contributions. The PED corresponding to the selenohydrazide group is underlined.

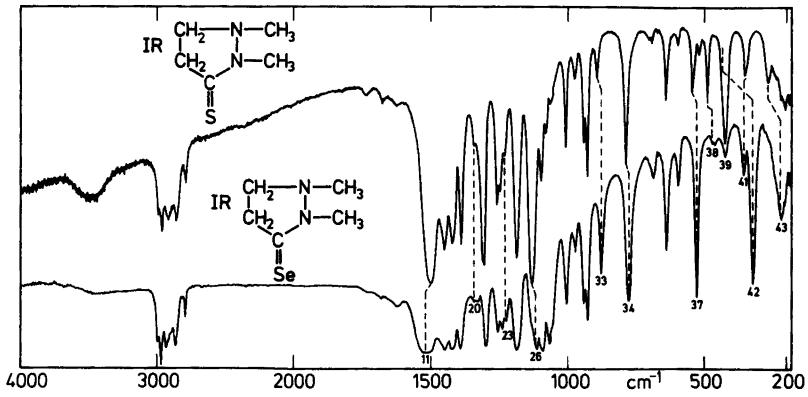

Fig. 1. IR spectra of DMPT (top) and DMPS (bottom) in the liquid state. The numbering refers to the assigned fundamentals of DMPS; the corresponding bands in DMPT are indicated with a hatched line.

To avoid possible misunderstandings the terms used below will be briefly defined. Selenation of DMPT involves: (i) A mass change from (mainly) ^{32}S to a mixture of selenium isotopes mostly in the range ^{76}Se to ^{82}Se, (ii) a geometry change, according to the X-ray results confined to the length of the CS/CSe bond and (iii) a change in force field due to the electronic and steric effects of selenium relative to sulfur. The results of selenation are the following: (i) A change in position of bands described by the selenation shift, $\nu_{DMPS} - \nu_{DMPT}$. (ii) A change in PED of the normal vibrations. As long as the changes are small we talk about corresponding bands in DMPT and DMPS, in other words, the concept of group frequencies is valid. (iii) Changes in intensity, form and depolarisation ratio may occur, especially as a result of different Fermi interactions with overtones and combination modes. In this case a visual identification of corresponding bands in DMPT is difficult or impossible.

Visual identification of corresponding bands in DMPS and DMPT. A necessary prerequisite for using the selenation method is the establishment of a one-to-one correspondence between the bands of DMPS and DMPT *e.g.* by superposition of the spectra. Moreover, at this stage we try to identify the fundamentals from eventual overtones and combination modes by intensity considerations. The number of accidentally degenerate fundamentals ($\nu_1 - \nu_3$, $\nu_4 - \nu_6$, $\nu_7 - \nu_8$ and $\nu_{15} - \nu_{16}$) is identical in DMPS and DMPT and presents no problem. The occurrence of Fermi resonance with near-lying overtones and combination modes makes the identification of ν_{23}, ν_{26}, ν_{37} and ν_{38} difficult (see Table 1). In the case of *e.g.* ν_{23}, this does not invalidate the selenation method since the form and intensity of the triad of bands between 1220 and 1260 cm^{-1} are very similar in the IR spectra of DMPT and DMPS (see Fig. 1).

The ν_{37} of DMPS is different. In the spectrum of DMPT it is observed at 548 cm^{-1} with medium intensity followed by a weak Fermi enhanced combination mode at 522 cm^{-1}. In the IR spectrum of DMPS the intensity distribution is exactly opposite, and ν_{37} is observed as a medium strong band at 526 cm^{-1} with a very weak shoulder at 540 cm^{-1}. The obvious conclusion is that ν_{37} is displaced from 548 cm^{-1} in DMPT to 526 cm^{-1} in DMPS, *i.e.* displays a selenation shift of 22 cm^{-1} as indicated on Fig. 1. Comparison with Raman data reveals that this is probably not correct. In the Raman spectrum of DMPT, ν_{37} is found at 521 cm^{-1} with medium intensity accompanied by two weak satellites at 538 and 544 cm^{-1}, while in DMPS it is a medium weak band at 525 cm^{-1} followed by a weak combination mode at 540 cm^{-1}. In our opinion this example demonstrates convincingly that a visual identification of corresponding bands by the selenation method cannot be regarded as definite without supporting data from either Raman spectra or *e.g.* spectra of deuterium substituted compounds. In the present case the results of the NCA also identifies ν_{37} as originating in a vibration unperturbed by selenation, supporting the interpretation given here.

Apparently corresponding bands in DMPS and DMPT. Even when the fundamentals are correctly identified and have similar characteristics (form,

intensity, depolarisation ratio *etc.*) in DMPT and DMPS they may nevertheless have quite different PED's and thus are only apparently corresponding. The fundamentals $\nu_{38}-\nu_{43}$ in DMPS (and DMPT) with significant contributions from CSe stretching, in-plane and out-of-plane bending are obvious examples of this complication as can be verified by comparing the PED's of Table 1 with those for DMPT reported previously.[16] As an outstanding example we want to point out that ν_{41} in DMPS, although containing a 25 % contribution from CSe stretching, only displays a very small shift (2–5 cm^{-1}) relative to a band with almost the same strength, intensity and form in DMPT (ν_{42}) which has no contribution at all from vibrations of the thiohydrazide group. This demonstrates that selenation shifts may be absent even in bands with high contribution from the thiohydrazide group provided that the PED changes in a suitably way.

Measurement of the selenation shifts. From the results in Table 1 it can be concluded that the selenation shifts are subjected to small variations when calculated from the IR and from the Raman spectra, and the shifts may even go in opposite directions (*e.g.* ν_{12}, ν_{24} and ν_{29}). In the case of Fermi resonance with neighbouring overtones and/or combination modes (ν_{26}, ν_{37} and ν_{38}) definite shifts cannot be calculated from the data. Even the direction of the selenation shift may be difficult to assess with certainty unless the shift is prominent (ν_{38}). In Table 1 significant trends are given in italics and have also been attributed increased weight in the NCA.

Mass and geometry effects in selenation. In Table 1 the calculated selenation shifts are listed together with the part of the shift originating solely from changes in mass and geometry, 'the mass-geometry shift.' We shall briefly discuss some major selenation shifts mainly of this origin. The fundamentals ν_{34} and ν_{35} found at 786–789 and 689–693 cm^{-1}, respectively, in DMPT are displaced on selenation to 772–773 and 683–687 cm^{-1}, respectively. Since the calculated mass-geometry shifts are of similar magnitude the obvious conclusion is that the observed selenation shifts have this origin. However, a closer inspection reveals that the change in force field by change reproduces the same selenation shifts, but with a quite different PED on the fundamentals. In our opinion this example demonstrates that a coincidence between experimental selenation shifts and calculated mass-geometry shifts may very well be fortuitous. Similar remarks

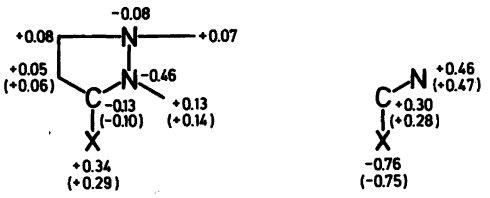

Fig. 2. The CNDO/2 charge density for DMPT (X=S) and, in parenthesis, for DMPS (X=Se). If only one figure is given, the charge densities are identical. The σ-densities are shown to the left while the π-densities of the NCX group are shown to the right.

apply to the fundamentals $\nu_{38}-\nu_{43}$ of DMPS relative to the corresponding bands in DMPT. An interesting example is ν_{41} in which a major shift predicted by change in mass and geometry (+39 cm^{-1}) is almost compensated by the accompanying changes in force field. The 25 % contribution from CSe stretching to this fundamental would never have been suspected from experimental results alone, but is understandable from the NCA results.

Force field changes on selenation. From *ab initio* calculations[30] it is known that substitution of sulfur with selenium introduces a steric effect, the size increasing from S to Se, and a polarisability effect, the Se atom being more polarisable than the S atom. Both in S and Se compounds the lowest empty *d*-orbitals serve to polarise the basis set while the $(3d)^{10}$ orbitals of Se are essentially core orbitals. In order to explore whether similar differences are operative for DMPT and DMPS, CNDO/2 calculations were performed. The charge densities (Fig. 2) show that the π-distribution of the thioamide group in DMPT corresponds to a superposition of the familiar structures $N^+=C-S^-$ and C^+-S^- while the σ-electrons are displaced in the opposite direction. The densities in the remaining part of the molecule are identical in DMPS and DMPT and need no further discussion. On selenation of the thioamide group, however, small but characteristic changes occur in the electron density.

Due to the increased size of Se relative to S a rehybridisation occurs. Electron density (0.06e) is transferred to the *p*- and *d*-orbitals directed towards carbon to increase the overlap density of the lengthened bond. The decrease in density of the hardly overlapping 2*s*-orbitals of carbon (0.03e) simultaneously with an increased p_π-density (0.02e) also adds to a better stabilisation of the CSe bond in DMPS.

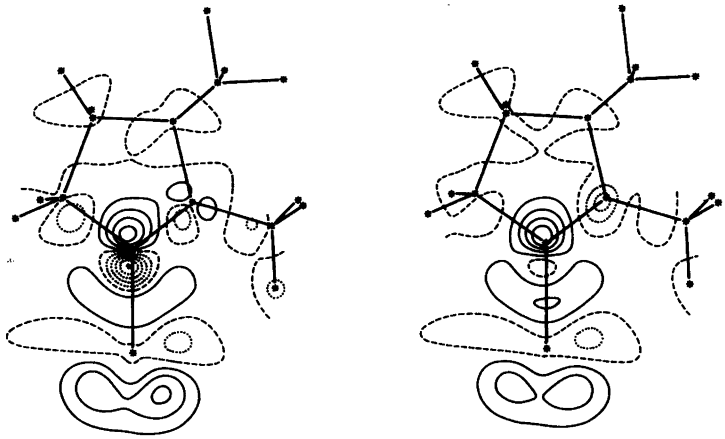

Fig. 3. Difference map (DMPS − DMPT) of the total molecular density in the NCS/NCSe plane (left) and in a plane 0.62 Å above this plane (right) as calculated by the CNDO/2 method. Solid, dashed and dotted lines represent positive, zero and negative difference densities, respectively, plotted linearly with a spacing of 0.001 electron/Å^3. The molecules have been arranged with coincident atoms of the rings and the methyl groups, *i.e.* the sulfur atom of DMPT is located on the C − Se bond drawn on the difference maps.

Some of the electron density necessary for stabilisation of the CSe bond (0.03e) is removed from the neighbouring CH_2, N and CH_3' groups. These changes in steric demands and *d*-orbital stabilisation compare well to those expected from *ab initio* results (*cf.* also thiophene[31]). The polarisability effect is documented by the difference density contours in Fig. 3, displaying the changes in electron density of DMPT on selenation. The changes in a plane through the NCSe group show how the large selenium atom polarises the electrons along the $-CH_2-C-N-CH_3'$ chain. The regions near Se display a consistent decrease, those further removed a corresponding increase in density. The sterically proximate CH_3' group induces a counter-polarisation of Se relative to S as expected. The changes in a plane corresponding to the π-electrons of the NCSe group also show the polarisation of Se from the CH_3' group, but otherwise only reflect the increased electron density of carbon at the expense of N and Se already noted above.

The gross features of the changes in force field and electron density on selenation seem consistent. The NCA indicates that all stretching force constants of the C − CX − N(CH_3') − N (X = S, Se) chain decrease except that of the central CN bond which perhaps increases slightly. The decrease in the force constant for CX stretching from DMPT to DMPS is mainly a consequence of the diminished overlap of the longer CSe bond, which cannot be fully compensated for even from the flow of electrons from the contiguous parts of the molecule and the rehybridisation of C and Se. The diminished electron density is responsible for the decrease in the force constants for C − C, N − CH_3', and N − N stretching. The slight increase in the force constant for stretching of the central CN bond is either not significant or arises from an increased density due to polarisation, not incompatible with the curves of Fig. 3. The latter density contours also support the NCA results that the force constants for in-plane bending around the central $\overset{C}{N}>C=X$ atom increase while that for $CH_3'NC$ deformation decreases. The remaining changes in force constants on selenation are small as are the changes in electron density.

Acknowledgements. This research was supported by grants from the Danish Natural Science Research Council and the Norwegian Research Council for Science and the Humanities.

REFERENCES

1. Jensen, K. A. and Nielsen, P. H. *Acta Chem. Scand. 20* (1966) 597.
2. Hallam, H. E. and Jones, C. M. *Spectrochim. Acta A 25* (1969) 1791.
3. Jensen, K. A., Dahl, B. M., Nielsen, P. H. and Borch, G. *Acta Chem. Scand. 25* (1971) 2029, 2039.

4. Jensen, K. A., Dahl, B. M., Nielsen, P. H. and Borch, G. *Acta Chem. Scand. 26* (1972) 2241.
5. Anthoni, U., Borch, G., Klæboe, P. and Nielsen, P. H. *Spectrochim. Acta A 34* (1978) 955.
6. Pilipenko, A. T. and Melnikova, N. V. *Russ. J. Inorg. Chem. 14* (1969) 236.
7. Devillanova, F. A. and Verani, G. *Aust. J. Chem. 33* (1980) 279.
8. Dwarakanath, K. and Sathyanarayana, D. N. *Indian J. Pure Appl. Phys. 17* (1979) 171.
9. Dwarakanath, K. and Sathyanarayana, D. N. *Indian J. Chem. A 18* (1979) 302.
10. Dwarakanath, K. and Sathyanarayana, D. N. *Bull. Chem. Soc. Jpn. 52* (1979) 2699.
11. Dwarakanath, K., Sathyanarayana, D. N. and Anagnostopoulos, A. *Indian J. Chem. A 16* (1978) 834.
12. Gayathri Devi, K. R., Sathyanarayana, D. N. and Volka, K. *Spectrochim. Acta A 34* (1978) 1137.
13. Durgaprasad, G., Sathyanarayana, D. N. and Patel, C. C. *Bull. Chem. Soc. Jpn. 44* (1971) 316.
14. Dwarakanath, K., Sathyanarayana, D. N. and Volka, K. *Bull. Soc. Chim. Belg. 87* (1978) 667.
15. Sathyanarayana, D. N., Volka, K. and Geetharani, K. *Spectrochim. Acta A 33* (1977) 517.
16. Anthoni, U., Borch, G., Klæboe, P., Lerstrup, K. and Nielsen, P. H. *Acta Chem. Scand. In press.*
17. Rutherford, J. S. and Calvo, C. *Z. Kristallogr. 128* (1969) 229.
18. Goldschmith, G. J. and White, J. W. *J. Chem. Phys. 31* (1959) 1175.
19. Elcombe, M. M. and Taylor, J. C. *Acta Crystallogr. 24* (1968) 410.
20. Mullen, D. and Hellner, E. *Acta Crystallogr. B 34* (1978) 2789.
21. Hauge, S. *Acta Chem. Scand. A 33* (1979) 317.
22. Vikane, O. *Acta Chem. Scand. A 29* (1975) 763.
23. Vikane, O. *Acta Chem. Scand. A 29* (1975) 787.
24. Restivo, R. and Palenik, G. *Acta Crystallogr. B 26* (1970) 1397.
25. Conde, A., Lopez-Castro, A. and Marques, R. *Acta Crystallogr. B 28* (1972) 3464.
26. Zvonkova, Z. V., Astakhova, L. I. and Glushkova, V. P. *Kristallografiya 5* (1960) 547; (English translation p. 526).
27. Bonamico, M. and Dessy, G. *J. Chem. Soc. A* (1971) 264.
28. Esperås, S., Husebye, S. and Rolandsen, Å. *Acta Chem. Scand. A 29* (1975) 608.
29. Gould, R. O., Jones, C. L., Savage, W. J. and Stephenson, T. A. *J. Chem. Soc. Dalton Trans.* (1976) 908.
30. Lehn, J.-M., Demuynck, J. and Wipff, G. *Helv. Chim. Acta 60* (1977) 1239.
31. Gelius, U., Roos, B. and Siegbahn, P. *Theor. Chim. Acta 27* (1972) 171.

Received May 20, 1981.

Acta Chemica Scandinavica A 36 (1982) 79–82

^{43}Ca NMR Relaxation Times and Quadrupole Coupling Constants for Some Small Calcium Complexes

TORBJÖRN DRAKENBERG

Div. of Physical Chemistry 2, Chemical Center, University of Lund, Box 740, S-220 07 Lund 7, Sweden

The ^{43}Ca spin-lattice relaxation times have been measured for the calcium complexes with EDTA, EGTA and a cyclic ligand. The ^{43}Ca quadrupole coupling constant was calculated for each complex, using correlation times calculated from ^{13}C relaxation times. An increase in the quadrupole coupling constant by a factor of four is found on going from the Ca-EDTA to the Ca-EGTA complex. This is interpreted as being due to differences in the symmetry of the complexes.

^{43}Ca NMR studies have up to recently been very scarce[1-3] although the calcium ion is recognised to be of importance in many physiological processes.[4] The calcium ion with a spin $I \neq 0$, ^{43}Ca ($I = 7/2$) has a very low natural abudance (0.14 %) and also a sensitivity that is less than for *e.g.* ^{13}C.[5] This explains the lack of interest shown in the past. However, very recently a few studies have appeared in which enriched ^{43}Ca was used to study calcium–protein interaction.[8-12] It has even been possible to observe the ^{43}Ca NMR signal from calcium strongly bound to some small proteins.[13]

The interpretation of ^{43}Ca NMR data is somewhat hampered by the lack of knowledge about the ^{43}Ca NMR relaxation time, T_1, for various systems. Therefore a study of the spin-lattice relaxation time of ^{43}Ca bound to various small ligands has been initiated. The following complexes for which the metal exchange is slow on the NMR time scale have been studied: Ca-EDTA (EDTA-ethylenediaminetetraaceticacid), CA-EGTA [EGTA-ethyleneglycol-bis(β-ethylamine)-*N*,*N*′-tetraacetic acid], Ca-I.

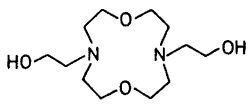

I

EXPERIMENTAL

Ligand I was a gift from Prof. J. Dale (Ref. 15) and EDTA and EGTA were obtained from Merck and Sigma, respectively.

The ^{43}Ca NMR studies were carried out at 17.16 MHz with a home made spectrometer with a magnetic field of 6T using horizontally arranged 17 mm O.D. samples. All samples were made up from ^{43}Ca enriched (60 %, Oak Ridge Natl. Lab., USA) calcium perchlorate in water solutions. The calcium concentration varied from 0.5 to 4 mM and the ligand concentration was 2–4 mM. The ^{43}Ca T_1 measurements were made using the inversion recovery method, using 10 000 pulse sequences with a 180° pulse length of 36 μs and a delay between the sequences of at least 3 times T_1.

^{13}C NMR measurements were made on a Varian XL-100 spectrometer using *ca.* 40 mM concentration of complexes with natural abudance calcium in 12 mm O.D. NMR tubes. The T_1 measurements were made using the fast inversion recovery method[16] with 10 000 pulse sequences, a 180° pulse width of 180 μs, and a delay between the sequences of 0.5 s. All T_1 values were obtained from a non-linear least squares fit to the experimental data, using three adjustable parameters. The given uncertainties are three times the standard deviation.

RESULTS

^{43}Ca NMR spectra from solutions of one of the ligands (EDTA,EGTA or ligand I) and an excess of Ca^{2+} showed two signals, when a sufficiently

0302-4377/82/010079-04$02.50

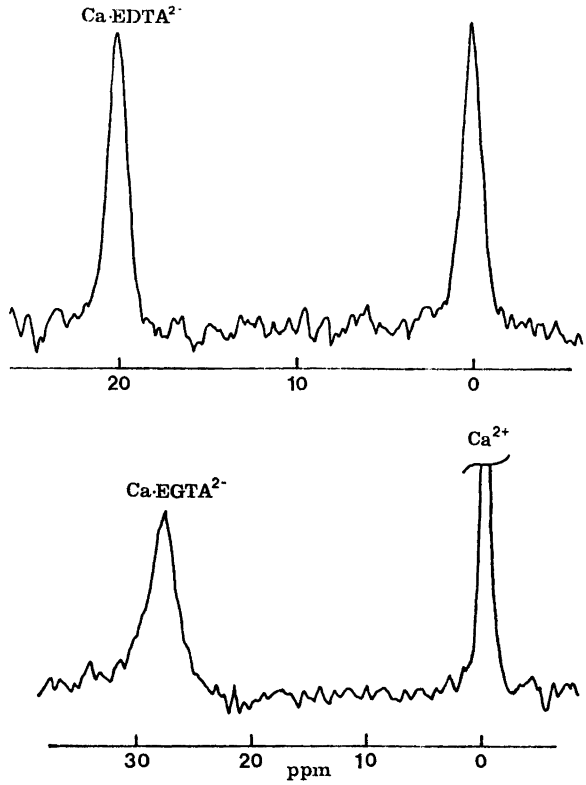

Fig. 1. ^{43}Ca NMR spectrum at 17.16 MHz from a solution containing 2mM ^{43}Ca and 1 mM of either EGTA or EDTA. 10^4 70° pulses, with a 1 s repetition time, were accumulated for each spectrum.

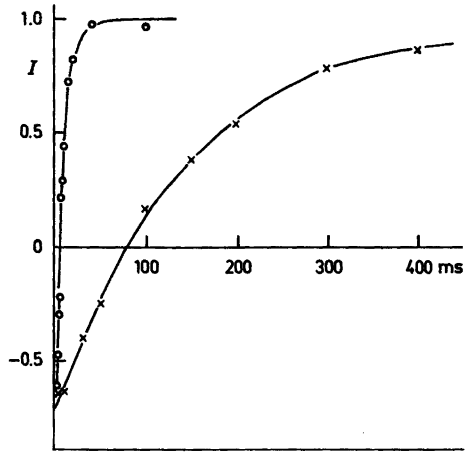

Fig. 2. The ^{43}Ca signal intensity as a function of the delay time in the inversion recovery experiment. $I = I_0(1 - k\exp(-\tau/T_1)$ The solid curves are the calculated best fit. ×, Ca-EDTA; O, Ca-EGTA.

high pH (8, 10 and 10 for EDTA, EGTA and ligand I, respectively) was used. Even at elevated temperature no broadening of the signals could be detected, showing that the exchange between free and complexed calcium ions is very slow (Fig. 1). For solutions with total calcium and ligand concentrations of 4 mM the spin lattice relaxation time was measured using the inversion recovery method. (Fig. 2) The resulting relaxation times, as well as the chemical shifts, are given in Table 1.

In order to obtain the correlation times of the various complexes, the carbon-13 spin lattice relaxation times for all the carbons, except the carbonyles, were measured for solutions that had a complex concentration of 40 mM. The large difference in concentration between the ^{43}Ca and ^{13}C solutions was a compromise due to the high cost of ^{43}Ca and the sensitivity of ^{13}C, however a doubling of the concentration for the ^{13}C experiment had no significant effect on the ^{13}C T_1's. The correlation times, τ_c, was calculated from

Table 1. Chemical shifts and relaxation times of ^{43}Ca in some complexes.

Ligand	δ^b(ppm)	T_1 (ms)	χ^a(MHz)
EGTA	27.9	7.1±1.4	2.1
EDTA	20.0	150±10	0.5
I	4.7	22±7	1.4

[a] Quadrupole coupling constants defined as $\chi=\frac{e^2qQ}{h}\left(1+\frac{\eta}{3}\right)^{\frac{1}{2}}$. [b] Chemical shift from 1 mM $Ca(ClO_4)_2$ in H_2O, positive to higher frequency.

$$1/T_1=\gamma_H^2\gamma_C^2\hbar^2r^{-6}\tau_c$$

where γ_H and γ_C are the gyromagnetic ratio for protons and carbon-13, respectively, $\hbar$ is Planck's constant and r the proton–carbon bond distance (1.09 Å). The measured relaxation times and the calculated correlation times are summarized in Table 2.

The correlation times calculated from the ^{13}C T_1 data and the ^{43}Ca relaxation times were used to calculate the quadrupole coupling constant, χ, for ^{43}Ca in the various complexes from

$$1/T_1=\frac{2\pi^2}{49}\cdot\chi^2\tau_c$$

where T_1 is the ^{43}Ca spin lattice relaxation time,

$$\chi=\frac{e^2qQ}{h}\cdot\left(1+\frac{\eta^2}{3}\right)^{\frac{1}{2}}$$

(the quadrupole coupling constant), and the other parameters are as defined above.

DISCUSSION

Very little is known about the effect of various ligands on the chemical shift of ^{43}Ca. In contrast to the effect of a carboxyl group on the ^{113}Cd chemical shift, which is upfield, Robertson *et al.*[6] have reported a downfield shift of 2 ppm due to complexation with Z-D-Gla-D-Gla-OMe. This, however, also contradicts the results reported by Lutz *et al.*, who found an upfield shift for both formate and lactate solutions.[2]

Table 2. Carbon-13 relaxation times (mean values) and correlation times for some Ca-complexes.

Ligand	T_1 (s)	τ_c (s)
EGTA	0.29±0.05	8.0×10^{-11}
EDTA	0.4±0.05	5.8×10^{-11}
I	0.42±0.1	5.6×10^{-11}

The chemical shifts of ^{43}Ca in the complexes studied in the present work (Table 1) are in agreement with the accepted effect of a nitrogen ligand on the ^{113}Cd chemical shift.[13] However, as expected the ^{43}Ca shifts are smaller than the ^{113}Cd shifts. These ^{43}Ca shifts are so small that they will probably not be very important, especially not in studies of protein–metal interactions, because the linewidth of the signals from protein bound ^{43}Ca are of the order of 10^3 Hz (~60 ppm at our field).[13]

As can be seen from Table 1 there is a significant variation in the ^{43}Ca relaxation rate in the various complexes. The ^{43}Ca relaxation can safely be assumed to be totally dominated by the quadrupolar relaxation. Reasonable estimates of the relaxation rate due to other mechanisms result in rates that are at least a factor of 100 slower than the observed ones. Therefore the differences in the relaxation rates among the complexes can be explained by either a difference in the quadrupole coupling constant, χ, and/or a difference in the correlation time, τ_c.

The ^{13}C relaxation rates show clearly that the overall correlation times sensed by the carbon nuclei are very similar for all three complexes (Table 2), ruling out this as a possible explanation for the observed variation in the ^{43}Ca relaxation rate. However, there could still exist a local mobility in the Ca-EDTA complex which would not be sensed by the carbons, but would strongly affect the calcium nucleus. There is some evidence that the Ca-EDTA complex in water solution is a mixture of two forms,[17–22] where the metal is either penta- or hexa-coordinated to the EDTA ligand, as illustrated by Scheme 1.

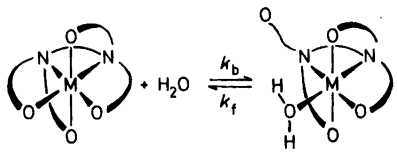

Scheme 1.

In the penta coordinated complex the sixth site on the metal is occupied by a water molecule. It could well be anticipated that the water exchange might be fast without affecting the carbon correlation time. Such a water exchange could be coupled to a nitrogen inversion, which for the Pb-EDTA complex has been shown to be fast on the NMR time scale.[23] Very recently Harada *et al.*[22] used an ultrasonic absorption method to measure the water exchange rate in the alkaline earth complexes with EDTA. They found a rate constant, k_f, of 3.6×10^7 s^{-1} for the Ca EDTA complex. Since this exchange is much slower than the inverse of the rotation correlation time of the complex the effective symmetry brought about by the water exchange cannot be the cause of the difference between the relaxation behaviour of ^{43}Ca in Ca-EDTA and Ca-EGTA.

Consequently, we must assume that the observed longer relaxation time for ^{43}Ca in the Ca-EDTA complex, as compared to the other two complexes, is caused by an effective symmetry in the Ca-EDTA complex, resulting in a field gradient that is smaller than for the other complexes. It is not unreasonable to assume that small changes in the geometry of the complex might have a pronounced effect on the field gradient. Maybe it is even so that this is the type of variation one should expect.

Acknowledgements. The author thanks Prof. S. Forsén for helpful discussions, Prof. J. Dale for the kind gift of ligand I and Dr. R. E. Carter for linguistic criticism. This work was financed by the Swedish Natural Sciences Research Council.

REFERENCES

1. Bryant, R. G. *J. Am. Chem. Soc. 91* (1969) 1870.
2. Lutz, O., Schwenk, A. and Uhl, A. *Z. Naturforch. A 30* (1975) 1122.
3. Lindman, B., Forsén, S. and Lilja, H. *Chem. Scr. 11* (1977) 91.
4. Wasserman, R. H., Corradino, R. A., Carifoli, E., Kretsinger, R. H., MacLennan, D. A. and Siegel, F. L., Eds., *Calcium Binding Proteins and Calcium Function*, North-Holland, New York 1977.
5. Lindman, B. and Forsén, S. In Harris and Mann, Eds., *NMR and the Periodic Table*, Academic, New York 1979.
6. Robertson, P., Jr., Hiskey, R. G. and Koehler, K. A. *J. Biol. Chem. 253* (1978) 5880.
7. Farmer, R. M. and Popov, A. I. *Inorg. Nucl. Chem. Lett. 17* (1981) 51.
8. Parello, J., Lilja, H., Cavé, A. and Lindman, B. *FEBS Lett. 87* (1978) 191.
9. Reimarsson, P., Parello, J., Drakenberg, T., Gustavsson, H. and Lindman, B. *FEBS Lett. 108* (1979) 439.
10. March, H. C., Robertsen, P., Jr., Scott, M. E., Koehler, K. A. and Hiskey, R. G. *J. Biol. Chem. 254* (1979) 4628.
11. Andersson, T., Drakenberg, T., Forsén, S., Wieloch, R. and Lindström, M. *FEBS Lett. 123* (1981) 115.
12. Andersson, T., Drakenberg, T., Forsén, S. and Thulin, E. *FEBS Lett. 125* (1981) 39.
13. Andersson, T., Swärd, M., Drakenberg, T. and Forsén, S. *J. Am. Chem. Soc. In press.*
14. Forsén, S., Thulin, E. and Lilja, H. *FEBS Lett. 104* (1979) 123.
15. Amble, E. and Dale, J. *Acta Chem. Scand. B 33* (1979) 698.
16. Levy, G. C., Ed., *Topics in Carbon-13 NMR Spectroscopy*, Wiley, New York 1974, Vol. 1.
17. Bhat, T. R. and Krishnamurthy, M. *J. Inorg. Nucl. Chem. 25* (1963) 1147.
18. Brunetti, A. P., Nancollas, G. H. and Smith, P. N. *J. Am. Chem. Soc. 91* (1969) 4680.
19. Wilkins, R. G. and Yelin, R. E. *J. Am. Chem. Soc. 92* (1970) 1191.
20. Higgins, W. E. C. and Samuel, B. *J. Chem. Soc. A* (1980) 1579.
21. Grant, M. W., Dodgen, H. W. and Hunt, J. P. *J. Am. Chem. Soc. 93* (1971) 6828.
22. Harada, S., Funaki, Y. and Yasunga, T. *J. Am. Chem. Soc. 102* (1980 136.
23. Day, R. J. and Reilley, C. H. *Inorg. Chem. 36* (1964) 1073.

Received April 23, 1981.

Acta Chemica Scandinavica A 36 (1982) 83–87

The Preparation, Resolution, and Characterization of Tris(1,2-ethanediamine)iridium(III) Complexes

FRODE GALSBØL and BIRGITTE S. RASMUSSEN

Chemistry Department I, Inorganic Chemistry, H. C. Ørsted Institute, University of Copenhagen, Universitetsparken 5, DK-2100 Copenhagen Ø, Denmark

$[Ir(en)_3]^{3+}$ (en = 1,2-ethanediamine) is obtained in *ca.* 70 % yield as the double salt $2[Ir(en)_3]Cl_3.LiCl.6H_2O$ by reaction of $IrCl_3.4H_2O$ with an aqueous solution of en at 170 °C followed by recrystallization from LiCl-solution. The complex ion is resolved *via* the diastereoisomer $Li\{(-)[Ir(en)_3]\}\{(+)\text{-tart}\}_2.3H_2O$ [(+)-tart = (+)-tartrate anion]. The isomer $(+)[Ir(en)_3]^{3+}$ is assigned the absolute configuration Δ by the method of active racemates. This assignment agrees with Werner's criterion of least soluble diastereoisomers. The compounds are characterized by their electronic and circular dichroism spectra and their optical rotation. $Li\{(+)_{589}[Co(en)_3]\}\{(+)\text{-tart}\}_2.3H_2O$ has also been prepared.

Tris(1,2-ethanediamine)iridium(III) bromide was first reported by Werner *et al.*[1] who prepared this compound in 17 % yield by the reaction of 1,2-ethanediamine(en) with $Na_3[Ir(NO_2)_4Cl_2].2H_2O$ (170 °C for 10 h) together with *cis*-$[Ir(en)_2(NO_2)_2]^+$ in 30 % yield. The $Na_3[Ir(NO_2)_4Cl_2].2H_2O$ was prepared[2] in *ca.* 30 % yield from $Na_2[IrCl_6].6H_2O$. Lebedinski[3] prepared the iodide from $Na_3[IrCl_6].12H_2O$ and en (140 °C for 15 h, no yield specified). Mathieu[4] modified the method of Werner but did not specify the yield. Later Lebedinski's method was modified by Watt *et al.*[5] to give 43 % yield of $[Ir(en)_3]I_3$. The extremely soluble chloride has not been prepared directly before. In the present paper we describe a procedure which gives a *ca.* 70 % yield of the double salt $2[Ir(en)_3]Cl_3.LiCl.6H_2O$.

Werner[1] resolved the tris(1,2-ethanediamine)iridium(III) ion with sodium-3-nitro-(+)-camphor (Nanic). However, the solubility of the precipitated diastereoisomer, $(-)[Ir(en)_3](nic)_3$, is so low that purification by recrystallization is impracticable, and furthermore some disagreement exists[4] about the amount of resolving agent to be used. By the present method $(-)[Ir(en)_3]^{3+}$ is precipitated as the tartrate double salt $Li\{(-)[Ir(en)_3]\}\{(+)\text{-tart}\}_2.3H_2O$ which is then purified before conversion to the chloride. This method is analogous to the ones published earlier[6] for the resolution of $[Rh(en)_3]Cl_3$ and $[Cr(en)_3]Cl_3$.

EXPERIMENTAL

Materials. Iridium(III) chloride hydrate (*ca.* 4 mol H_2O/mol Ir) was obtained from Johnson, Matthey and Co. and 1,2-ethanediamine (*puriss. p.a.*) from Fluka. All other chemicals were of analytical or reagent grade and were used without further purification.

Instrumentation. Absorption spectra were recorded on a Cary 118C spectrophotometer and circular dichroism on a Roussel-Jouan Dichrographe III. Optical rotation was measured using a Perkin-Elmer polarimeter 141 and X-ray powder diffraction photographs were taken with a Hägg-Guinier focusing camera XDC 700 calibrated with silicon and using Cu$K\alpha$ radiation.

Synthetic Procedures

1. Bis{tris(1,2-ethanediamine)iridium(III) chloride} lithium chloride, hexahydrate. 3.5 ml of anhydrous 1,2-ethanediamine (52 mmol, 29 % excess) and 6 ml of water are mixed in a pyrex test tube, and carbon dioxide (which appears to catalyze the reaction) is bubbled through the solution over a period of 1 min. After 5 min, 5.0 g of $IrCl_3.4H_2O$ (13.5 mmol) is added in 1 g portions. (It is sometimes necessary to moderate the reaction by cooling the tube under the water tap). The mixture is then heated cautiously to boiling and boiled for a few minutes.

0302-4377/82/010083-05$02.50

The solution is reheated twice with a few minutes' interval. The test tube is then sealed and placed in an autoclave containing a little water. The autoclave is kept in an oven at 170 °C for 25 h and then allowed to cool to room temperature together with the oven. The ampoule is cooled in icewater and cautiously opened (slight overpressure) by melting off the top. The contents are diluted with 20 ml of water, and 0.5 g of active carbon is added. After standing for 1 h, the mixture is filtered (Whatman No. 50) and washed with water until the filtrate is colourless. The yellow filtrate is acidified with 12 M HCl (*ca.* 0.7 ml) and evaporated to *ca.* half volume on a rotating vacuum evaporator (RVE) to expel the carbon dioxide. Then $LiOH.H_2O$ is added until the solution is basic (*ca.* 0.7 g), and the solution is evaporated to dryness on an RVE (final bath temperature 90 °C). The LiCl, excess ethanediamine and organic by-products are extracted by boiling with 100 ml of absolute ethanol. The resulting precipitate is filtered and washed with three 10 ml portions of absolute ethanol. The residue is dissolved in 20 ml of water by heating, 1 ml of 12 M HCl is added, and the acidic solution is evaporated to dryness on an RVE (final bath temperature 90 °C). LiCl is again removed by extraction with 100 ml of boiling absolute ethanol followed by filtration and washing with absolute ethanol. The light yellow residue (*ca.* 7 g) is dissolved in the minimum volume* (*ca.* 13 ml) of boiling half saturated LiCl-solution (23 g of LiCl in 100 ml of water) and allowed to stand overnight. The precipitate is filtered, washed successively with 1 ml portions of icecold water, 50 % v/v ethanol, and 96 % ethanol, and dried in air. Yield 4.5 g (60 %) of $2[Ir(en)_3]Cl_3.LiCl.6H_2O$. (Found: C 13.01; N 15.12; H 5.58; Cl 22.45. Calc. for $LiIr_2C_{12}N_{12}H_{60}Cl_7O$: C 13.01; N 15.17; H 5.46; Cl 22.39.)

A second crop of crystals is obtained in the following way: the combined filtrate and washings are evaporated to dryness on an RVE. LiCl is extracted with 100 ml of boiling absolute ethanol followed by filtration and washing with absolute ethanol. The residue is dissolved in the minimum volume (*ca.* 5 ml) of half saturated LiCl-solution and allowed to stand overnight. The precipitate is filtered, washed successively with 0.5 ml portions of icecold water, 50 % v/v ethanol, and 96 % ethanol, and dried in air. Yield 0.7 g (9 %).

2. Tris(1,2-ethanediamine)iridium(III) chloride, hydrate. A column of 20 g of Dowex 50W X2 cation exchanger (H^+-form, 200–400 mesh, *ca.* 20 cm long, and *ca.* 1.2 cm diameter) is washed with 50 ml of 4 M HCl followed by 5 ml of water. A solution of 3.0 g of $2[Ir(en)_3]Cl_3.LiCl.6H_2O$ in 100 ml of water is applied and the column is washed with 50 ml of water before it is eluted with 80 ml of 0.2 M HCl. All these eluates are discharged. The complex ion is eluted with 80 ml of 4 M HCl followed by 5 ml of water. The eluate is evaporated to dryness on an RVE and the flask and solid residue ($2[Ir(en)_3]Cl_3.HCl.6H_2O$) are heated to 160 °C for 1 h to expel the hydrogen chloride. The residue is dissolved in 4 ml of water. The solution is filtered and the filter washed with another 1 ml of water. The filtrate is heated and ethanol (*ca.* 16 ml) is added with reflux until the solution starts to become turbid. The solution is allowed to stand for crystallization and the product is isolated by filtration, washed with two 2 ml portions of a mixture of 3 ml of ethanol and 1 ml of water and air-dried. Yield *ca.* 2.4 g (83 %) of $[Ir(en)_3]Cl_3.aq.$* (Found: C 13.53; N 15.62; H 5.42; Cl 19.94 *i.e.* C:N:H:Cl = 6.00:5.94:28.6:3.00.)

3. Resolution of the tris(1,2-ethanediamine)iridium(III) ion. A 2.80 g sample of $2[Ir(en)_3]Cl_3.LiCl.6H_2O$ (5.05 mmol), 1.15 g of (+)-tartaric acid (7.66 mmol), and 0.64 g of $LiOH.H_2O$ (15.3 mmol) are placed in a 25 ml conical flask and dissolved in 5 ml of boiling water. A clear solution is formed and is allowed to cool by standing for 5 min. 2.5 ml of ethanol is added and the solution is reheated to boiling. The flask is stoppered and the solution is allowed to stand for about one day at room temperature with occasional shaking. The crystal cake is then broken up and allowed to stand for a further 2 h. The precipitate is filtered (the mother liquor is retained for later use), washed with three 1.5 ml portions of 96 % ethanol, and dried in air. Yield 1.85 g of crude $Li\{(-)[Ir(en)_3]\}\{(+)\text{-tart}\}_2.3H_2O$.

The mother liquor is evaporated to dryness on an RVE (final bath temperature 90 °C). The residue is dissolved in 3 ml of 12 M HCl by heating to boiling, and 20 ml of absolute ethanol is added (a large white crystalline precipitate is formed). The mixture is heated to boiling, and the suspension is allowed to stand for two hours at room temperature before the precipitate is filtered, washed with three 1 ml portions of ethanol, and placed in an oven for 1 h at 160 °C to remove hydrogen chloride. The yield of crude $(+)[Ir(en)_3]Cl_3$ is 1.1 g. This product is dissolved in 1.1 ml of boiling water and the solution is allowed to stand for crystallization. If a small amount of precipitate (*ca.* 0.1 g) is not formed within one day, two drops of 96 % ethanol is added. After another 30 min the small precipitate which has formed is filtered off. To the filtrate is added 4 ml of 96 % ethanol, which immediately results in considerable precipitation. The mixture is allowed to stand for two hours before the precipitate is filtered, washed with three 0.5 ml portions

* $[Ir(en)_3]Cl_3$ is extremely soluble in water.

* The content of water of crystallization is somewhat variable.

of 96 % ethanol, and dried in air. Yield 0.85 g (63 %) of $(+)[Ir(en)_3]Cl_3.2H_2O$.* (Found: C 13.71; N 16.12; H 5.45; Cl 22.56; Li 0.39 *i.e.* C:N:H:Cl:Li = 6.00: 6.05:28.4:3.34:0.30.) λ (nm)/$\Delta\varepsilon_{extr.}$ (1 mol^{-1} cm^{-1}): 271/−0.85, 253/−0.34, 232/−0.84.

The crude tartrate double salt is dissolved in 3.6 ml of boiling water and the solution is allowed to stand for five minutes before the addition of 1.8 ml of 96 % ethanol. The mixture is reheated to boiling and allowed to stand overnight for crystallization. After filtration the precipitate is washed twice with 0.5 ml portions of 50 % v/v ethanol, once with 1 ml of 96 % ethanol, and dried in air. Yield 1.6 g (87 %) of $Li\{(-)[Ir(en)_3]\}\{(+)\text{-tart}\}_2.3H_2O$ (Found: C 22.91; N 11.62; H 5.38. Calc. for $LiIrC_{14}N_6H_{38}O_{15}$: C 23.05; N 11.52; H 5.25.)

The recrystallized tartrate double salt (1.6 g, 2.2 mmol) is dissolved in 1 ml of boiling 12 M HCl and 10 ml of absolute ethanol is added. A large white crystalline precipitate is formed. The mixture is heated to boiling, and the suspension is allowed to stand for 2 h. The precipitate is filtered, washed with three 1 ml portions of 96 % ethanol, and placed in an oven for one hour at 160 °C. The residue (1.0 g) is dissolved in the minimum volume (*ca.* 1 ml) of boiling water, after which four times this volume of 96 % ethanol is added. After two hours the precipitate is filtered, washed three times with 1 ml portions of ethanol, and dried in air. Yield 0.67 g (57 %) of $(-)[Ir(en)_3]Cl_3.2H_2O$.* (Found: C 13.70; N 16.16; H 5.40; Cl 21.79; Li 0.35 *i.e.* C:N:H:Cl:Li = 6.00:6.07:28.2:3.23:0.27.)

4. $(+)_{589}$-Tris(1,2-ethanediamine)cobalt(III) chloride, monohydrate. $(+)_{589}$-Tris(1,2-ethanediamine)cobalt(III) chloride *d*-tartrate, pentahydrate was prepared by the partial asymmetric synthesis of Broomhead *et al.*[7] and recrystallized twice from hot water. After filtration the crystals are washed with 40 % ethanol and dried in air. λ(nm)/$\Delta\varepsilon_{extr.}$ (1 mol^{-1} cm^{-1}): 490/1.82, 432/−0.25, 350/0.26.

A 40.0 g sample of this product (78 mmol) is dissolved in 20 ml of hot 12 M HCl. 250 ml of absolute ethanol is added dropwise to the solution with stirring. The precipitate is filtered, washed with three 30 ml portions of ethanol, and air-dried. The crude product is dissolved in 12 ml of hot water. On cooling to room temperature under stirring some crystals separate. Under continuous stirring 70 ml of absolute ethanol is then added dropwise to the mixture. After filtration the crystals are washed with three 20 ml portions of ethanol and dried in air. Yield 23.6 g (83 %) of $(+)_{589}[Co(en)_3]Cl_3.H_2O$ (Found: C 19.67; N 23.17; H 7.36; Cl 29.25. Calc. for $CoC_6N_6H_{26}Cl_3O$: C 19.82; N 23.11; H 7.21; Cl 29.25.) λ(nm)/$\Delta\varepsilon_{extr.}$ (1 mol^{-1} cm^{-1}): 488/1.93, 428/−0.14, 349/0.25.

5. Active racemate. A 1.0907 g sample of $(+)_{589}[Co(en)_3]Cl_3.H_2O$ (3.00 mmol) and 1.5406 g of $(+)[Ir(en)_3]Cl_3.2H_2O$ (2.93 mmol) are each dissolved in the minimum amount of water (*ca.* 1 ml) at room temperature. The two solutions are heated to 50 °C, mixed, and allowed to stand for 6 h for crystallization. After filtration the crystals are washed with 0.5 ml of ice-cold water, 0.5 ml of 50 % v/v ethanol, and 1 ml of ethanol and dried in air. Yield 1.2 g (*ca.* 40 %) of $\{(+)_{589}[Co(en)_3](+)\text{-}[Ir(en)_3]\}Cl_6.6H_2O$.* (Found: C 15.15; N 17.35; H 6.53; Cl 24.43; Co 6.16; Li 0.31 *i.e.* C:N:H:Cl:Co:Li = 12.00:11.78:61.6:6.56:0.994:0.43.)

6. Lithium $(+)_{589}$-tris(1,2-ethanediamine)cobalt (III) (+)-tartrate, trihydrate. $[Co(en)_3]Cl_3$ was prepared by the method of Work[8] and recrystallized from water. 10.0 g of the recrystallized product (25 mmol), 5.64 g of (+)-tartaric acid (38 mmol) and 3.16 g of $LiOH.H_2O$ are dissolved in 25 ml of boiling water and the solution is allowed to stand overnight with occasional shaking until the crystals start to separate. The crystal cake is broken up. The crystals are filtered, washed with three 10

* The product is contaminated with LiCl.

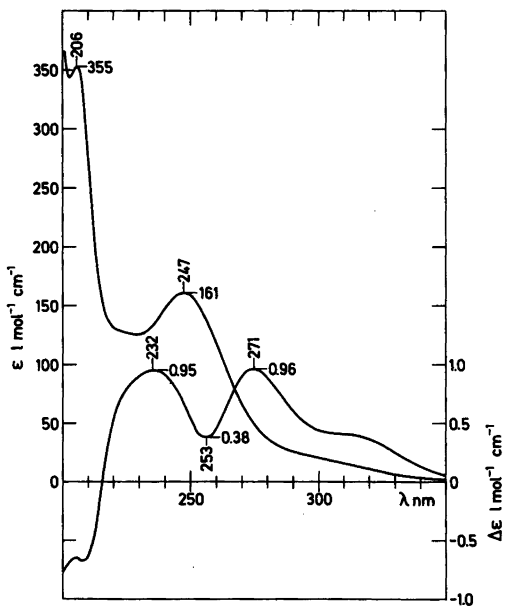

Fig. 1. The absorption spectrum of $2[Ir(en)_3]Cl_3.LiCl.6H_2O$ and the circular dichroism spectrum of $(-)[Ir(en)_3]Cl_3.2H_2O$.

* The product is contaminated with LiCl. If necessary it can be purified by the ion exchange procedure described in section 2.

Table 1. Unit cell dimensions determined from X-ray powder photographs. All crystals are indexed as belonging to the hexagonal crystal system.

Compound	*a*, Å	*c*, Å	*V*, Å^3
$[Co(en)_3]Cl_3.aq$[9]	11.44_3	15.48_3	1756
$\{(+)_{589}[Co(en)_3](+)[Ir(en)_3]\}Cl_6.aq$	11.56_2	15.51_1	1796
$[Ir(en)_3]Cl_3.aq$	11.63_6	15.42_8	1809

ml portions of 40 % ethanol and dried in air. The crude product (5.1 g) is dissolved in 30 ml of boiling water. 5 g of LiCl is added and the solution is filtered. To the hot filtrate 20 ml of ethanol is added with stirring. After stirring for a few hours the precipitate is filtered, washed with three 5 ml portions of 40 % ethanol, and dried in air. Yield: 3.0 g (40 %) of $Li\{(+)_{589}[Co(en)_3]\}\{(+)\text{-tart}\}_2.3H_2O$ (Found: C 27.83; N 14.27; H 6.81; Co 9.89. Calc. for $LiCoC_{14}N_6H_{38}O_{15}$: C 28.20; N 14.09; H 6.42; Co 9.88.) λ(nm)/$\Delta\varepsilon_{extr.}$ (1 mol^{-1} cm^{-1}): 491/1.80, 434/−0.31, 348/0.27.

RESULTS

The isomer $(+)[Ir(en)_3]^{3+}$ is assigned the absolute configuration Δ, using the method of active racemates,[9] by correlation with $\Lambda(+)_{589}$-$[Co(en)_3]^{3+}$ the absolute configuration of which has been determined[10] by X-ray single crystal methods: the racemic compounds $[Ir(en)_3]Cl_3.aq$ and $[Co(en)_3]Cl_3.aq$ and the active racemate $\{(+)_{589}$-$[Co(en)_3](+)[Ir(en)_3]\}Cl_6.aq$ have almost identical X-ray powder photographs (Table 1), differing from those of the optically active compounds.* This assignment agrees with Werner's criterion of least soluble diastereoisomers.[12] The least soluble diastereoisomers $Li\{act[M(en)_3]\}\{(+)\text{-tart}\}_2.3H_2O$ (M = Cr[6], Co, Rh[6], and Ir) all have the absolute configuration Λ. The members of this series are isomorphous (Table 2).* The Co and Ir compounds have not been described before.

The molar rotations are given in Table 3. With the exception of the two lowest wavelengths the results for $(-)[Ir(en)_3]Cl_3.2H_2O$ are in agreement with the values published for the bromide.[4]

The absorption spectrum of $2[Ir(en)_3]Cl_3.LiCl.6H_2O$ is shown in Fig. 1. The $^1A_{1g} \rightarrow {}^3T_{1g}(O_h)$ transition is seen at *ca.* 310 nm as a "foot" on the low energy side of the $^1A_{1g} \rightarrow {}^1T_{1g}(O_h)$ band and the $^1A_{1g} \rightarrow {}^1T_{2g}(O_h)$ transition appears as a shoulder at *ca.* 225 nm. The spectrum is in accordance with the results published by Jørgensen[14] and by DeArmond and Hillis.[15] Fig. 1 also shows the circular dichroism (CD) spectrum of $\Lambda(-)[Ir(en)_3]Cl_3.2H_2O$. The contour differs from that of the CD spectra of the corresponding Rh and Co complexes in that it is all positive in the $d-d$ transition range. A comparison with the CD spectrum[16] of $\Delta(+)[Ir\{(-)chxn\}_3$-$\lambda\lambda\lambda]^{3+}$ reveals that the transitions to the $E(D_3)$ and $A_2(D_3)$ excited levels of $T_{1g}(O_h)$ parentage and the

*(+)[Co(en)$_3$]Cl$_3$.aq is tetragonal (a=9.67$_6$ Å, c = 16.29$_5$ Å) and (+)[Ir(en)$_3$]Cl$_3$.aq is cubic (a=21.71$_3$ Å) like the rhodium analog (a=21.70$_5$ Å, Ref. 11 a=21.67$_5$ Å, space group $F4_132$).

*Kushi *et al.*[13] have published the crystal structure of the Cr compound (a=7.86 Å, b=16.99 Å, c=9.22 Å, β = 100.4°, space group $P2_1$).

Table 2. Unit cell dimensions determined from X-ray powder photographs. All crystals belong to the monoclinic crystal system and the indexing of all powder photographs is very similar. The chromium compound belongs[13] to space group $P2_1$.

Compound	*a*, Å	*b*, Å	*c*, Å	β,°	*V*, Å^3
$Li\{(+)_{589}[Cr(en)_3]\}\{(+)\text{-tart}\}_2.3H_2O$	7.85_5	16.98_1	9.22_2	100.2_7	1210
$Li\{(+)_{589}[Co(en)_3]\}\{(+)\text{-tart}\}_2.3H_2O$	7.83_8	16.89_4	9.21_6	100.5_5	1200
$Li\{(-)_{589}[Rh(en)_3]\}\{(+)\text{-tart}\}_2.3H_2O$	7.87_1	16.99_2	9.21_2	100.4_6	1212
$Li\{(-)_{589}[Ir(en)_3]\}\{(+)\text{-tart}\}_2.3H_2O$	7.87_7	17.00_7	9.20_2	100.5_7	1212

Table 3. Molar rotations ($[M]=(100\alpha)/(cl)$ deg. l mol^{-1} cm^{-1}) in aqueous solution at 25 °C.

	313 nm	364 nm	436 nm	546 nm	578 nm	589 nm
$Li\{(-)[Ir(en)_3]\}\{(+)\text{-tart}\}_2.3H_2O$; $c\approx 2.7\times10^{-3}$ M	−672	−383	−350	−220	−197	−182
$(-)[Ir(en)_3]Cl_3.2H_2O$; $c\approx 3.8\times10^{-3}$ M	−983	−678	−577	−367	−327	−311
$(+)[Ir(en)_3]Cl_3.2H_2O$; $c\approx 4.2\times10^{-3}$ M	907	616	525	333	298	287

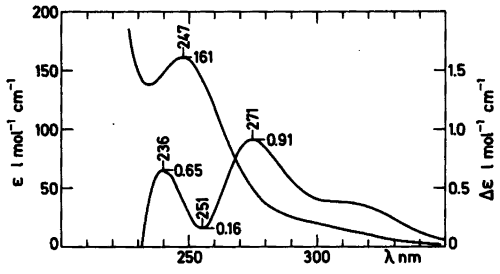

Fig. 2. The absorption and circular dichroism spectra of $Li\{(-)[Ir(en)_3]\}\{(+)\text{-tart}\}_2.3H_2O$.

transition to the $E(D_3)$ excited level of $T_{2g}(O_h)$ parentage are all situated *ca.* 2000 cm^{-1} lower in energy.

Fig. 2 shows the absorption and CD spectra of $Li\{(-)[Ir(en)_3]\}\{(+)\text{-tart}\}_2.3H_2O$. The low wavelength part of the CD spectrum has a lower intensity than that found for the chloride and the band at *ca.* 235 nm has narrowed considerably. This is due partly to a narrow CD band of the (+)-tartrate ion appearing at 216 nm ($\Delta\varepsilon=2.2$ l mol^{-1} cm^{-1}) and partly to ion-pairing effects.

REFERENCES

1. Werner, A. and Smirnoff, A. P. *Helv. Chim. Acta 3* (1920) 472.
2. Werner, A. and de Vries, O. *Justus Liebigs Ann. Chem. 364* (1909) 77.
3. Lebedinski, V. V. *Izv. Inst. Izuch. Platiny Drugikh Blagorodn. Met: Akad. Nauk. SSSR 4* (1926) 235; *Chem. Abstr. 21* (1927) 3571.
4. Mathieu, J.-P. *J. Chim. Phys. Phys.-Chim. Biol. 33* (1936) 78.
5. Watt, G. W., Sharif, L. E. and Helvenston, E. P. *Inorg. Chem. 1* (1962) 6.
6. Galsbøl, F. *Inorg. Synth. 12* (1970) 269.
7. Broomhead, J. A., Dwyer, F. P. and Hogarth, J. W. *Inorg. Synth. 6* (1960) 186.
8. Work, J. B. *Inorg. Synth. 2* (1946) 221.
9. Andersen, P., Galsbøl, F. and Harnung, S. E. *Acta Chem. Scand. 23* (1969) 3027.
10. Saito, Y., Nakatsu, K., Shiro, M. and Kuroya, H. *Bull. Chem. Soc. Jpn. 30* (1957) 795.
11. Whuler, A., Brouty, C., Spinat, P. and Herpin, P. *C. R. Acad. Sci. Ser. C 284* (1977) 117.
12. Werner, A. *Ber. Dtsch. Chem. Ges. 45* (1912) 1228.
13. Kushi, Y., Kuramoto, M. and Yoneda, H. *Chem. Lett.* (1976) 339.
14. Jørgensen, C. K. *Acta Chem. Scand. 10* (1956) 500.
15. DeArmond, M. K. and Hillis, J. E. *J. Chem. Phys. 54* (1971) 2247.
16. Galsbøl, F. *Acta Chem. Scand. A 32* (1978) 757.

Received April 28, 1981.

Acta Chemica Scandinavica A 36 (1982) 89 – 92

Short Communications

Preparation of *cis*-Dinitrobis(trimethylenediamine)cobalt(III) Nitrite Using Dimethylsulfoxide as Solvent

MASAYUKI MUTO [a,*] and
CHIEKO NAKAO [b]

[a] Chemistry Department A, Technical University of Denmark, Building 207, DK-2800 Lyngby, Denmark and [b] Department of Chemistry, Faculty of Education, Wakayama University, 1-1 Masago, Wakayama 640, Japan

One of the authors has reported the preparation of several cobalt(III) complexes using dimethylsulfoxide (DMSO) as a solvent.[1-3] It is of interest that there is some difference between ligand substitution reactions in water and in non-aqueous solvent and that even a complex difficult or troublesome to synthesize in water can be synthesized easily in non-aqueous solvent. In this paper we report that *cis*-isomer of dinitrobis[trimethylenediamine(= 1,3-diaminopropane)]cobalt(III) nitrite is selectively synthesized using DMSO as a solvent.

The *trans*-$[Co(NO_2)_2(tn)_2]^+$ (tn: trimethylenediamine = 1,3-diaminopropane) was first synthesized by Werner and Lindenberg,[4] whereas two studies were recently reported on the *cis*-form, one by Kawaguchi and Kawaguchi[5] and the other by Čelap *et al.*[6] In the former[5] the complex was obtained from *trans*-$[CoCl_2(tn)_2]Cl$ and sodium nitrite in water, while in the latter[6] from $[CoCO_3(tn)_2]$-$Cl \cdot H_2O$ and sodium nitrite in 12 % acetic acid aqueous solution. However, the data reported in the two investigations differ, particularly the UV ansorption spectra.

Previous investigators have found that the *cis*-isomer has a much higher solubility in water than the *trans*-form. Moreover evidence was presented that in an aqueous solution the *cis-trans* equilibrium is rapidly established at room temperature. Because water and non hydrogen-bonded solvents often show mutually exclusive solubilities, we attempted to synthesize the *cis*-isomer by precipitating it from a DMSO solution. These experiments, resulting in a convenient method of preparation for the *cis*-complex, form the subject of the present communication.

Experimental. Preparation. To 3 g (7.4 mmol) powdered $Na_3[Co(NO_2)_6]$ suspended in 10 ml of DMSO 1.1 g (14.8 mmol) trimethylenediamine was added. The mixture was heated on a water bath, whereby the suspended complex reacted gradually with the amine and after a while, an orange yellow crystalline precipitate was formed. The reaction was completed within 15 – 20 min. The precipitate was filtered off, washed several times with ethanol and then with ether, finally, dried *in vacuo*. Yield was *ca.* 1.4 g.

Found: C, 21.04; H, 5.95; N, 27.18 %. Calc. for $[Co(NO_2)_2(tn)_2]NO_2$: C, 20.88; H, 5.84; N, 27.40 %.

The *trans*-isomer was synthesized in the usual way.[4]

Thin-layer chromatography. As an adsorbent, cation-exchange cellulose P-41 pretreated with 5 M sodium chloride solution was used. The development was carried out at room temperature using a 0.5 M sodium chloride solution.

Spectral measurement. The visible and UV spectra were recorded with a Hitachi 124 spectrophotometer, and the IR spectra with a Hitachi EPI-L spectrophotometer.

The ^1H NMR spectra were obtained with a Japan Electrooptics JNM-60 spectrometer.

Results and discussion. Preparation of complex. In this study DMSO was used as a solvent. With dimethylformamide, instead of DMSO, a mixture of *cis*- and *trans*-form was found to be precipitated.

Thin-layer chromatography. The solution of our complex yields only spot at an R_f value of 0.5, and the filtrate shows a spot at 0.7 accompanied by a very faint spot at 0.5. On the other hand, the *trans* complex synthesized in the usual way[4] shows a spot at 0.7. The *cis*-isomer being the more polar of the two would be expected to have a lower R_f value than the *trans*-isomer. This suggests that the main product of the synthesis is, in fact, the *cis*-isomer.

Visible and UV spectra. The absorption curve of our complex is similar to that of the *cis*-isomer in Ref. 6. The IR spectrum of the proposed *cis*-isomer of Ref. 5 corresponds closely to that of the *trans*-

*On leave of absence from Wakayama University.

0302-4377/82/010089-02$02.50

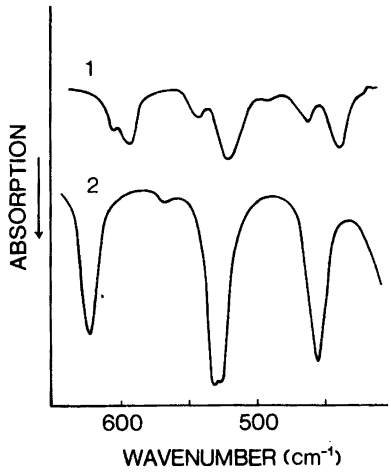

Fig. 1. Infrared absorption spectra in the 400 – 650 cm^{-1} region. (1) *cis*-$[Co(NO_2)_2(tn)_2]NO_2$ and *trans*-$[Co(NO_2)_2(tn)_2]NO_2$.

isomer. The first absorption band of the *trans*-isomer seems to split into two (21.2 and 22.3 kK), but the *cis*-isomer has a single maximum at 22.1 kK. A difference of the same kind arises with the *cis*-isomer and *trans*-isomer of $[Co(NO_2)_2(en)_2]NO_2$.[7]

IR spectra. As shown in Fig. 1, the spectrum of *trans*-isomer shows a slightly split $Co-N(NH_2)$ stretching at about 530 cm^{-1}, whereas in that of our complex two bands are observed. The *trans*-isomer further exhibits two bands attributable to NO_2 wagging (610 cm^{-1}) and $Co-N(NO_2)$ stretching (450 cm^{-1}) each of which is clearly split into two bands in the spectrum of our complex.

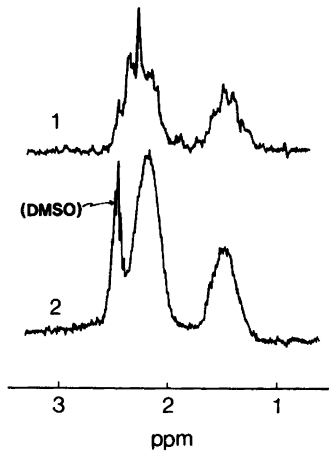

Fig. 2. Proton nuclear magnetic resonance spectra in dimethylsulfoxide-d_6. (1) *cis*-$[Co(NO_2)_2(tn)_2]NO_2$ and (2) *trans*-$[Co(NO_2)_2(tn)_2]NO_2$.

^1H NMR spectra. The ^1H NMR spectra were assigned by comparing with $[Co(tn)_3]^{3+}$. The spectrum of our complex is shown in Fig. 2 together with *trans*-isomer. The *trans*-isomer gives two singlets which correspond respectively to the single species of β-methylene proton at 1.50 ppm and α,α'-methylene proton at 2.22 ppm, the ratio of their areas being 1:2, which show the symmetrical configuration of the *trans*-form. In the corresponding parts of the spectrum of our complex complicated patterns are observed as would be expected for the *cis*-isomer.

The results described support strongly our conclusion that the complex prepared by us – as well as that described in Ref. 6, but not the complex presented in Ref. 5 – consists mainly of the *cis*-dinitrobis(trimethylenediamine)cobalt(III) nitrite.

Acknowledgement. The authors wish to acknowledge Professor F. Woldbye's kindness in giving us the opportunity to carry out this work in the Chemistry Department A, of the Technical University of Denmark.

1. Muto, M., Baba, T. and Yoneda, H. *Bull. Chem. Soc. Jpn. 41* (1968) 2918.
2. Muto, M., Yamaguchi, M. and Yoneda, H. *Bull. Chem. Soc. Jpn. 43* (1970) 3935.
3. Yoneda, H., Muto, M. and Tamaki, K. *Bull. Chem. Soc. Jpn. 44* (1971) 2863.
4. Werner, A. and Lindenberg, G. *Justus Liebigs Ann. Chem. 386* (1921) 265; *Gmelins Handbuch, Cobalt Teil B*, p. 222.
5. Kawaguchi, H. and Kawaguchi, S. *Bull. Chem. Soc. Jpn. 43* (1970) 2103.
6. Ćelap, M. B., Maliner, M. J. and Radivojiša, P. N. *Inorg. Chem. 14* (1975) 2965.
7. Shimura, Y. and Tsuchida, R. *Bull. Chem. Soc. Jpn. 29* (1956) 311.

Received July 23, 1981.

Synthesis and Properties of Di-μ-hydroxo-bis[bis(trimethylenediamine)chromium(III)] Salts

TROELS LAIER, BENTE NIELSEN and JOHAN SPRINGBORG

Chemistry Department, Royal Veterinary and Agricultural University, Thorvaldsensvej 40, DK-1871 Copenhagen V, Denmark

In previous studies from this laboratory it was shown that the diols $[(NH_3)_4Cr(OH)_2Cr(NH_3)_4]^{4+}$ and $[(en)_2Cr(OH)_2Cr(en)_2]^{4+}$ (en = 1,2-ethanediamine) obtain equilibrium with their respective parent monohydroxo-bridged complexes, and the thermodynamics and kinetics of these equilibria have been studied in detail.[1-3] Continuing these studies we are now investigating other Cr(III) diols and wish here to report the synthesis of a trimethylenediamine diol and the results of its hydrolysis in acid solution. (tn = trimethylenediamine = 1,3-propanediamine).

The compound *cis*-$[Cr(tn)_2(OH)(H_2O)]S_2O_6$ was obtained from *cis*-$[Cr(tn)_2Cl_2]Cl$ *via* Ag(I) assisted hydrolysis to give, initially, the *cis*-diaqua complex. On heating (140 °C, 45 min), *cis*-$[Cr(tn)_2(OH)(H_2O)]S_2O_6$ yields the dihydroxo-bridged complex $[(tn)_2(OH)_2(tn)_2](S_2O_6)_2$, the diol, nearly quantitatively. This dithionate salt is rather insoluble in water and was therefore converted to the more soluble bromide salt, $[(tn)_2Cr(OH)_2Cr(tn)_2]Br_4.2H_2O$. The perchlorate salt, $[(tn)_2Cr(OH)_2Cr(tn)_2](ClO_4)_4.H_2O$, was obtained from the bromide salt by reprecipitation with sodium perchlorate.

The chemical properties of these salts provide unambiguous evidence for the proposed dihydroxo-bridged structure. The cation gives a neutral reaction and shows no buffer capacity in the region $2 \leq pH \leq 10$ as determined by glass-electrode measurements. Furthermore, the visible absorption spectrum shows no dependence on $[H^+]$ in the region $10^{-9} \leq [H^+] \leq 0.1$ M. These results clearly exclude[1-3] structures having terminal hydroxo groups, and when taken in conjunction with the elemental analyses they strongly support the proposed diol structure.

By analogy with its ethylenediamine analogue[1-6] the cation $[(tn)_2Cr(OH)_2Cr(tn)_2]^{4+}$ can exist in two isomeric forms, *viz.* a *meso* (Δ,Λ) and a *racemic* (Δ,Δ − Λ,Λ) form. However, the configuration of the present cation has not yet been established.

The spectra of aqueous neutral or acidic solutions of the diol changed with time, but constant spectra were never obtained. The spectral changes were interpreted on the basis of an initial, relatively fast reaction followed by one or more much slower reactions. Using the method of Guggenheim,[7] linear plots were obtained for at least three half-lifes. Pseudo first-order rate constants, k_{obs}, calculated for the initial fast reaction, gave k_{obs} (25 °C) = 6(1) $\times 10^{-4}$ s^{-1} in both 0.01 M $HClO_4$, 0.09 M $NaClO_4$ and in 0.1 M $NaClO_4$ (pH ≈ 5). Following our recent results for the corresponding ammonia[3] and ethylenediamine[1,2] systems, we interpret the initial reaction as a bridge-cleavage as shown in eqn. (1) (amine ligands omitted). Therefore $k_{obs} =$

$$Cr(OH)_2Cr^{4+} + H_2O \underset{k_{-1}}{\overset{k_1}{\rightleftharpoons}} (H_2O)Cr(OH)Cr(OH)^{4+} \quad (1)$$

$k_1 + k_{-1} = 6(1) \times 10^{-4}$ s^{-1} is of the same order of magnitude as the value (5.0×10^{-4} s^{-1}) recently reported[3] for the ammonia system.

By analogy with its ammonia and ethylenediamine analogues[1-3] the trimethylenediamine diol is a very weak acid ($pK_a \approx 12$), and it reacts instantaneously and reversibly with hydroxide ions to give a blue complex which is probably a μ-hydroxo-μ-oxo dimer.[1-3] The blue oxo-bridged complex reacts in aqueous solution (1 M NaOH, 25 °C) within seconds to give a red solution. No doubt the reaction involves bridge cleavage, but other reactions probably also take place and well-defined products were not isolated.

Experimental. Materials. *cis*-$[Cr(tn)_2Cl_2]Cl.$ 0.75 H_2O was prepared as described previously.[8] All other chemicals were of analytical grade.

Analysis. C, N, H, Cl, and Br analyses were made by the microanalytical laboratory at the H. C. Ørsted Institute, University of Copenhagen.

Spectra. A Zeiss DMR 21 spectrophotometer was used for spectral measurements in the visible region. For the spectral data the absorbancy ε is given in 1 mol^{-1} cm^{-1} and the wavelength λ is given in nm.

Preparations. 1. *cis*-aquahydroxobis(trimethylenediamine)chromium(III) dithionate. *cis*-$[Cr(tn)_2(OH)(H_2O)]S_2O_6$.

A suspension of *cis*-$[Cr(tn)_2Cl_2]Cl.$ 0.75 H_2O (3.80 g, 11.9 mmol) and $AgNO_3$ (6.06 g, 35.7 mmol) in ice-cold 0.001 M HNO_3 (12 ml) was stirred vigorously with cooling in ice for 10 min. Precipitated silver chloride was filtered off and washed with 0.001 M HNO_3 (5 ml). To the combined filtrates was then added, with continued cooling in ice and stirring, a hot (80 − 90 °C) solution of $Na_2S_2O_6.2H_2O$ (3.8 g, 15.7 mmol) in water (10 ml). After further cooling for 10 min pyridine (6 ml) was added dropwise and red crystals of *cis*-$[Cr(tn)_2(OH)(H_2O)]S_2O_6$ precipitated. The precipitate was

0302-4377/82/010091-02$02.50

filtered off, washed with 50 % ethanol, then 96 % ethanol and finally with diethyl ether. Drying in the air gave 2.8 g (59 %) of crude *cis*-$[Cr(tn)_2(OH)(H_2O)]S_2O_6$.

2. Di-μ-hydroxo-bis[bis(trimethylenediamine)-chromium(III)] bromide. $[(tn)_2Cr(OH)_2Cr(tn)_2]Br_4.2H_2O$.

Solid *cis*-$[Cr(tn)_2(OH)(H_2O)]S_2O_6$ (2.8 g, 7.1 mmol) was heated (140 °C) for 45 min to give 2.4 g of purple diol dithionate. The crude dithionate salt was added to a saturated solution of NH_4Br (30 ml) at room temperature and the suspension was stirred thoroughly for ½ h. The dithionate salt dissolved and reddish-purple crystals of the bromide salt separated. The bromide salt was filtered off, washed with 50 % ethanol, 96 % ethanol and then with diethyl ether. Drying in the air gave 0.95 g of a crude bromide salt. A pure salt was obtained by reprecipitation. The bromide (0.95 g) was dissolved in 0.01 M HBr (30 ml) at room temperature and filtered through a fine porosity sintered glass filter, and then a saturated solution of NH_4Br (30 ml) was added. Crystals of the bromide salt separated within minutes and after 10 min the product was filtered off, washed with 96 % ethanol, ethyl ether and then dried in the air. This gave 0.85 g (30 %) of pure $[(tn)_2Cr(OH)_2Cr(tn)_2]Br_4.2H_2O$. The visible absorption spectrum did not change upon further recrystallisation. Anal. $[Cr_2(tn)_4(OH)_2]Br_4.2H_2O$: C, H, N, Br. Spectral data at 25 °C: $(\varepsilon,\lambda)_{max}=(170,533)$; (89,387). $(\varepsilon,\lambda)_{min}=(27.6,442)$; (0.1 M $HClO_4$). $(\varepsilon,\lambda)_{max}=(169,533)$; (89,387). $(\varepsilon,\lambda)_{min}=(28.0,443)$. (0.1 M $NaClO_4$, pH ≈ 5). $(\varepsilon,\lambda)_{max}=(169,533)$; (90,387). $(\varepsilon,\lambda)_{min}=(28.0,443)$. (0.1 M NH_3, 0.1 M NH_4Cl).

3. Di-μ-hydroxo-bis[bis(trimethylenediamine)-chromium(III)] perchlorate, $[(tn)_2Cr(OH)_2Cr(tn)_2](ClO_4)_4.H_2O$.

To a solution of diol bromide (0.5 g, 0.63 mmol) in water (10 ml) at room temperature was added a saturated solution of $NaClO_4$ in water (10 ml). The perchlorate salt precipitated immediately and quantitatively. The precipitate was filtered off and washed with 96 % ethanol and when with diethyl ether. After drying in the air the perchlorate salt was dissolved in water (45 ml), reprecipitated by adding a saturated solution of $NaClO_4$ in water (8 ml) and then isolated as described above. Yield 0.47 g (88 %). Anal. $[Cr_2(tn)_4(OH)_2](ClO_4)_4.H_2O$: C, H, N, Cl. The spectral data in water were identical to those given above for the bromide salt. The perchlorate salt is only slightly soluble in perchlorate media and the kinetic measurements have been made in 0.1 M perchlorate media.

1. Springborg, J. and Toftlund, H. *Acta Chem. Scand. A 30* (1976) 171.
2. Christensson, F., Springborg, J. and Toftlund, H. *Acta Chem. Scand. A 34* (1980) 317.
3. Christensson, F. and Springborg, J. *Acta Chem. Scand. A 36* (1982) 21.
4. Beutler, A., Güdel, H. V., Snellgrove, T. R., Chapuis, G. and Schenk, K. J. *J. Chem. Soc. Dalton Trans.* (1979) 983.
5. Kaas, K. *Acta Crystallogr. B 32* (1976) 2021.
6. Cline, S. J., Scaringe, R. P., Hatfield, W. E. and Hodgson, D. J. *J. Chem. Soc. Dalton Trans.* (1977) 1662.
7. Guggenheim, E. A. *Philos. Mag. 2* (1926) 538.
8. Pedersen, E. *Acta Chem. Scand. 24* (1970) 3362.

Received September 9, 1981.

Acta Chemica Scandinavica A 36 (1982) 93–94

Letter

On the Molecular Structure and Bonding in Germanocenes. The Molecular Structure of Bis(pentamethylcyclopentadienyl)germanium; a Retraction

LIV FERNHOLT,[a] ARNE HAALAND,[a]* PETER JUTZI,[b] RAGNHILD SEIP,[a] JAN ALMLØF,[a] KNUT FÆGRI, Jr.,[a] EIVIND KVÅLE,[a] HANS P. LÜTHI,[c] BIRGITTE E. R. SCHILLING[a] and KJELL TAUGBØL[a]

[a] Department of Chemistry, University of Oslo, Blindern, Oslo 3, Norway, [b] Fakultät für Chemie der Universität Bielefeld, D-4800 Bielefeld, Germany and [c] Department of Inorganic Chemistry, University of Zürich, CH-8057, Zürich, Switzerland

In 1980 we published the results of a gas electron diffraction investigation of decamethylgermanocene, $(\eta\text{-}C_5Me_5)_2Ge$.[1] The mean Ge–C bond distance was reported to be about 2.32 Å. In this letter we first present the preliminary results of a similar investigation of 1,1'-dimethylgermanocene, $(\eta\text{-}C_5H_4Me)_2Ge$, where the mean Ge–C bond distance is found to be about 0.2 Å longer. Secondly, we describe the results of *ab initio* molecular orbital calculations on $(\eta\text{-}C_5H_5)_2Ge$ and $(\eta\text{-}C_5Me_5)_2Ge$ which give optimum Ge–C bond distances of 2.63 and 2.59 Å, respectively. Finally we present analytical results which show the reported structure of $(C_5Me_5)_2Ge$ to be invalid, and suggest that the sample used consisted of the previously unknown compound $(C_5Me_5)GeCl$.

The sample of $(C_5H_4Me)_2Ge$ was prepared from GeI_2 and $K(C_5H_4Me)$ and purified by repeated extractions as described by Stobart *et al.*[2] It consisted of a yellow viscous oil. The electron diffraction pattern was recorded with reservoir and nozzle temperatures of about 90 °C. After completion of the electron diffraction experiments the reservoir was found to contain a deep yellow to orange solid residue which we believe to consist partly of polymerization products[2,3] and partly of non-volatile impurities. The electron diffraction pattern was consistent from plate to plate and thus offered no indication for the presence of volatile impurities.

The electron diffraction data were found to be consistent with an angular sandwich structure similar to those found for $(C_5H_5)_2Sn$ and $(C_5H_5)_2Pb$ in the gas phase[4] and for $(C_5H_5)_2Sn$,[5] $(C_5Me_5)_2Sn$[6] and $(C_5Me_5)_2Pb$[5] in the solid phase. The mean Ge–C bond distance was found to be 2.53(2) Å, much longer than that reported for $(C_5Me_5)_2Ge$, 2.322(6) Å.[1] In the latter compound the ligand rings were reported to be parallel or nearly parallel, in $(C_5H_4Me)_2Ge$ the angle between the ring planes is found to be 35(10)°.

The M–Cl bond distances of monomeric gaseous $PbCl_2$,[7] $SnCl_2$[8] and $GeCl_2$[9] are 2.441(1), 2.347(7) and 2.184(4) Å, respectively, indicating that the bonding radius of Pb(II) is about 0.09 Å greater than that of Sn(II) which in turn is about 0.16 Å greater than that of Ge(II). Since the mean M–C bond distances in gaseous $(C_5H_5)_2Pb$ and $(C_5H_5)_2Sn$ are 2.778(5) and 2.706(8) Å, respectively, the mean Ge–C bond distance of 2.53 Å found in $(C_5H_4Me)_2Ge$ appears normal, while that reported for $(C_5Me_5)_2Ge$ appears abnormally short. The large difference is also at variance with results for $(C_5Me_5)_2Sn$,[6] $(C_5Me_5)_2Fe$[10] and $(C_5Me_5)_2Co$[10] which all have bond distances differing from those of the unsubstituted metallocenes by less than 0.02 Å.

We therefore decided to carry out *ab initio* molecular orbital calculations on $(C_5H_5)_2Ge$ and $(C_5Me_5)_2Ge$ to see whether the large difference between the Ge–C bond distances in the two compounds could be reproduced and explained. The calculations were carried out with a double-zeta basis set. The molecular symmetries were assumed to be D_{5h} and the ligand geometries kept constant while the metal-ring distance was varied. Similar calculations on another main group metallocene, $(C_5H_5)_2Mg$, yield an optimum Mg–C bond distance which is 0.06 Å greater than the experimental.[11]

Calculations with a valence shell electron configuration equal to that found for $(C_5H_5)_2Sn$,[6] gave results in accordance with the *aufbau* principle and was assumed to represent the ground state. The optimum Ge–C bond distance was found to be 2.63 Å in $(C_5H_5)_2Ge$ and 2.59 Å in $(C_5Me_5)_2Ge$.

Since it is known that $(C_5Me_5)_2Mn$ is in a

0302-4377/82/010093-02$02.50

different electronic state from $(C_5H_5)_2Mn$ and the Mn–C distance consequently 0.25 Å shorter,[10] we also carried out calculations on some alternative electron configurations. But these turned out to yield much higher energies and longer Ge–C bond distances than the ground state. In conclusion, the *ab initio* calculations provided no support for the existence of very different Ge–C bond distances in germanocenes, and increased our suspicion that the reported structure of $(C_5Me_5)_2Ge$ was incorrect.

The sample of $(C_5Me_5)_2Ge$ had been synthesized from $GeCl_2$ and $Li(C_5Me_5)$ and purified by recrystallization as described by Jutzi *et al.*[6] It consisted of pale yellow crystals which melted at 90 to 94 °C.[1] The electron diffraction data were recorded with reservoir and nozzle temperatures of about 140 °C. After completion of the experiment no residue remained in the reservoir, and the diffraction pattern was consistent from plate to plate. In sum: the sample appeared in every way to consist of *one* pure compound.

Only after the completion of the molecular orbital calculations did it occur to us that the reaction between $GeCl_2$ and $Li(C_5Me_5)$ might have been incomplete, and that our sample might have contained significant amounts of $(C_5Me_5)GeCl$. This compound has not been mentioned in the literature, but the analogous compound $(\eta$-$C_5H_5)SnCl$ is known, and the crystal structure has been determined by Noltes *et al.*[12] In this compound the mean Sn–C bond distance is about 0.1 Å shorter than in $(C_5H_5)_2Sn$ and the Sn–Cl bond distance about 0.3 Å longer than in $SnCl_2$: Comparison suggests that both the Ge–C and Ge–Cl bond distances in $(C_5Me_5)GeCl$ may be around 2.3 Å.

Neutron activation analysis has now shown that the sample used in our study of $(C_5Me_5)_2Ge$ contained stoichiometric amounts of Cl. Standardization against a sample of $GeCl_4$ shows that the Cl to Ge molar ratio is 1.00 ± 0.02. *The reported structure of $(C_5Me_5)_2Ge$ is therefore invalid.* We now intend to investigate the reaction between $GeCl_2$ and $Li(C_5Me_5)$ more closely and hope to be able to report results in the near future.

Note added in proof. Elemental analysis of the sample by Ilse Beetz, Kronach, West Germany, has given the following results: 49.52% C, 6.21% H, 14.51% Cl. Calculated for $C_{10}H_{15}GeCl$: 49.37% C, 6.22% H and 14.57% Cl.

1. Fernholt, L., Haaland, A., Jutzi, P. and Seip, R. *Acta Chem. Scand. A 34* (1980) 585.
2. Bonny, A., McMaster, A. D. and Stobart, S. R. *Inorg. Chem. 17* (1978) 935.
3. Scibelli, J. V. and Curtis, M. D. *J. Am. Chem. Soc. 95* (1973) 924.
4. Almenningen, A., Haaland, A. and Motzfeldt, T. *J. Organomet. Chem. 7* (1967) 97.
5. Atwood, J. L., Hunter, W. E., Cowley, A. H., Jones, R. A. and Stewart, C. A. *J. Chem. Soc. Chem. Commun.* (1981) 925.
6. Jutzi, P., Kohl, F., Hofmann, P., Krüger, C. and Tsay, Y.-H. *Chem. Ber. 113* (1980) 757.
7. Hargittai, I., Tremmel, J., Vadja, E., Ishchenko, A. A., Ivanov, A. A., Ivashkevich, L. S. and Spiridonov, V. P. *J. Mol. Struct. 42* (1977) 147.
8. Ishchenko, A. A., Ivashkevish, L. S., Zasorin, E. Z., Spiridonov, V. P. and Ivanov, A. A. *Abstract 6th Austin Symposium on Gas Phase Molecular Structure*, Austin, Texas 1976.
9. Schultz, G., Tremmel, J., Hargittai, I., Berecz, I. Bohátka, S., Kagramanov, N. D., Maltsev, A. K. and Nefedov, O. M. *J. Mol. Struct. 55* (1979) 207.
10. Haaland, A. *Acc. Chem. Res. 11* (1979) 415 and references therein.
11. Almløf, J., Fægri, K., Jr. and Lüthi, H. P. *Unpublished results.*
12. Bos, K. D., Bulten, E. J., Noltes, J. G. and Spek, A. L. *J. Organomet. Chem. 99* (1975) 71.

Received November 12, 1981.

Acta Chemica Scandinavica A 36 (1982) 95–99

X-Ray Diffraction Studies of Solid Solutions of $M_3(PO_4)_2$ in $Co_3(PO_4)_2$

ANDERS G. NORD

Section of Mineralogy, Swedish Museum of Natural History, P.O. Box 50007, S-104 05 Stockholm 50, Sweden

Solid solutions of $M_3(PO_4)_2$ in $Co_3(PO_4)_2$ have been prepared and equilibrated at 1070 K (M = Mg, Mn, Fe, Ni, Cu, Zn, or Cd). Approximate homogeneity ranges have been determined, and the monoclinic unit cell dimensions are given. The crystallographic properties of the $(Co_{1-z}M_z)_3(PO_4)_2$ solid solutions and the corresponding $(Mg_{1-z}M_z)_3(PO_4)_2$ phases are closely related [$Co_3(PO_4)_2$ is isostructural with $Mg_3(PO_4)_2$]. However, the results indicate that certain $(Co_{1-z}M_z)_3(PO_4)_2$ compositions crystallize with anomalous symmetries so that at least some atoms are incompatible with the space group symmetry reported for pure cobalt orthophosphate.

For structural chemists, geochemists and mineralogists it is of fundamental interest to correlate crystallographic properties of solid solutions such as solubility ranges, unit cell dimensions, cation radii and intra-crystalline cation distributions. Studies with this aim have been published on some important oxosalt structure types, mostly silicates, containing divalent-metal cations like Fe^{2+}, Mg^{2+}, Mn^{2+} and Ca^{2+}, ubiquitous in nature. However, practically all these studies concern only tetrahedral and, in particular, octahedral cationic environments. I have therefore started such investigations on structures containing also five-coordinated M^{2+} cations. To a major extent solid solutions with the "γ-$Zn_3(PO_4)_2$" structure have been used. This crystal structure was determined in 1963 by Calvo;[1] it is here described in the monoclinic space group $P2_1/n$ (No. 14). Two thirds of its cations occupy five-coordinated sites, called M(1), while the rest reside in six-coordinated octahedral sites, M(2).

Two pure orthophosphates are isomorphous with "γ-$Zn_3(PO_4)_2$": The crystal structure of $Mg_3(PO_4)_2$ was published by Nord and Kierkegaard.[2] Later a note on the $Co_3(PO_4)_2$ structure was published,[3] and a detailed structural investigation by Anderson *et al.* appeared shortly afterwards.[4] Some studies based on $(Mg_{1-z}M_z)_3(PO_4)_2$ solid solutions and with the aims mentioned above have already been published.[5-7] An iron-containing magnesium orthophosphate has also been found as a rare mineral, *farringtonite*.[8,9] The present study was undertaken to determine, at least roughly, the homogeneity ranges at about 1070 K for $(Co_{1-z}M_z)_3(PO_4)_2$ solid solutions with M^{2+} cations similar in size to Co^{2+}, *i.e.* M = Mg, Mn, Fe, Ni, Cu, Zn or Cd, each series henceforward abbreviated Co/M. The monoclinic unit cell dimensions have been accurately determined. Finally, these data are discussed in relation to earlier results obtained on the $(Mg_{1-z}M_z)_3(PO_4)_2$ solid solutions.[5-7]

EXPERIMENTAL DETAILS

The preparation of all pure $M_3(PO_4)_2$ orthophosphates involved in this study has already been described.[10] The purity was always checked by X-ray diffraction. Each solid solution between $Co_3(PO_4)_2$ and the $M_3(PO_4)_2$ compound in question was then prepared by heating pellets of stoichiometric mixtures of the two phosphates in an electric furnace. Whenever iron or manganese was included, the sample was heated in an evacuated and sealed Ø 5 mm silica tube to prevent the oxidation of Fe^{2+} or Mn^{2+}. All other mixtures were heated in air in small, open, silica tubes. The heating continued for one month to ensure homogeneity and chemical equilibrium (*cf.* Ref. 7), whereupon the samples were quenched in cold water.

0302-4377/82/020095-05$02.50

The equilibrium temperature, about 1070 K (800 ± 10 °C), was the same as in the earlier mentioned studies of $(Mg_{1-z}M_z)_3(PO_4)_2$ solid solutions. This temperature was chosen because it is easily maintained, it is within a temperature region of considerable interest to geochemists and mineralogists, and finally the solid solutions are formed within reasonable time.

X-Ray powder diffraction data of each sample were obtained at 298 K (25 ± 1 °C) with an XDC-700 Guinier-Hägg type focusing camera ($r = 50.00$ mm) using strictly monochromatized Cr$K\alpha_1$ radiation ($\lambda = 2.28975$ Å). Potassium chloride ($a = 6.29294$ Å [11]) was always used as an internal standard.

UNIT CELL DIMENSIONS

The visually observed readings of the Guinier photographs were corrected using the internal standard technique as described by Westman and Magnéli.[12] The dimensions of the monoclinic unit cell for all Co/M compounds were refined by a traditional least-squares procedure on a NOVA 4/X computer (program CELREF by A. G. Nord); 25–30 unambiguously single-indexed reflections were used in each refinement. The results are given in Table 1, which also indicates the homogeneity ranges, within ±3 atom per cent, for the Co/M solid solution series. The observed change in unit cell volume with composition for each Co/M series is mainly due to the changes in the monoclinic b axis length, while a, c and the β angle change comparatively little. For clarity, the unit cell volumes V ($Z = 2$) for the $(Co_{1-z}M_z)_3(PO_4)_2$ phosphates have been plotted *versus* the composition z in Fig. 1. Note that Vegard's law is clearly not obeyed in some cases.

Each Co/M series may be sorted into one of three groups: (1) low solubility of M^{2+} in $Co_3(PO_4)_2$ [M = Ni or Cd], (2) moderate solubility of the incorporated cation [M = Cu, Fe or Mn], and (3) complete or almost complete solubility of $M_3(PO_4)_2$ in cobalt orthophosphate over the whole composition range [M = Zn or Mg]. The Co/M series are

Table 1. Unit cell dimensions ($Z = 2$) at 298 K for some $(Co_{1-z}M_z)_3(PO_4)_2$ solid solutions, equilibrated at 1070 K.

z	a (Å)	b (Å)	c (Å)	β (°)	V (Å^3)
$Co_3(PO_4)_2$					
	7.556(1)	8.374(1)	5.062(1)	94.03(2)	319.6(1)
$(Co_{1-z}Cd_z)_3(PO_4)_2$					
0.03	7.566(2)	8.406(2)	5.064(2)	93.89(2)	321.4(2)
$(Co_{1-z}Mn_z)_3(PO_4)_2$					
0.05	7.575(4)	8.392(3)	5.072(3)	94.00(6)	321.6(4)
0.10	7.587(2)	8.419(2)	5.073(1)	93.96(2)	323.3(2)
0.15	7.593(3)	8.434(3)	5.075(2)	93.94(2)	324.2(3)
0.20	7.596(4)	8.445(4)	5.079(2)	93.92(4)	325.0(3)
0.25	7.603(2)	8.458(3)	5.079(2)	93.90(3)	325.9(2)
0.30	7.609(5)	8.470(5)	5.080(3)	93.86(5)	326.6(4)
$(Co_{1-z}Fe_z)_3(PO_4)_2$					
0.05	7.573(5)	8.389(3)	5.071(2)	94.00(5)	321.3(4)
0.10	7.574(2)	8.392(2)	5.072(1)	94.08(2)	321.6(2)
0.20	7.581(2)	8.405(1)	5.077(1)	94.06(2)	322.7(1)
0.30	7.590(2)	8.421(1)	5.081(1)	94.09(2)	323.9(1)
0.40	7.597(1)	8.428(1)	5.088(1)	94.09(2)	325.0(1)
$(Co_{1-z}Cu_z)_3(PO_4)_2$					
0.10	7.565(2)	8.326(2)	5.074(1)	93.72(2)	318.9(1)
0.15	7.569(3)	8.295(4)	5.080(2)	93.55(3)	318.3(3)
0.20	7.573(3)	8.264(2)	5.085(1)	93.30(3)	317.8(3)
0.25	7.578(3)	8.237(2)	5.093(1)	93.00(4)	317.4(3)
$(Co_{1-z}Ni_z)_3(PO_4)_2$					
0.05	7.558(3)	8.365(2)	5.067(1)	93.99(3)	319.5(2)
0.10	7.553(2)	8.346(2)	5.069(1)	93.92(2)	318.8(2)
0.15	7.557(5)	8.349(5)	5.074(3)	93.93(5)	319.3(5)

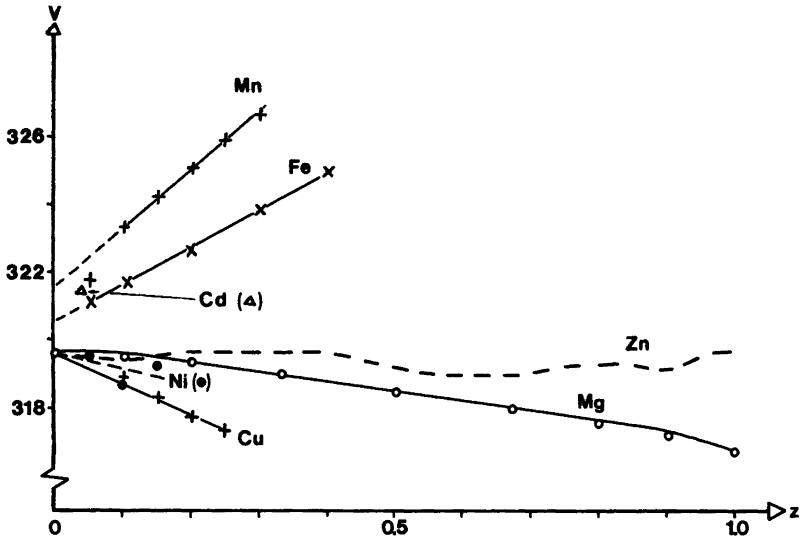

Fig. 1. Unit cell volumes V (in Å^3) *versus* composition z for the $(Co_{1-z}M_z)_3(PO_4)_2$ solid solutions. The Co/Mg data are based on Ref. 6, and the Co/Zn data, indicated by a dashed curve, on Ref. 15.

discussed below in the order mentioned. The divalent cation radii cited within parentheses (r_M) are those published by Shannon and Prewitt[13] for octahedral coordination with oxygen ligands (r_{Co} is 0.74 Å for Co^{2+}). All solubility ranges are given at about 1070 K.

Ni^{2+} is the smallest of the cations involved in this study ($r_{Ni}=0.70$ Å). The solubility in $Co_3(PO_4)_2$ is surprisingly low, considering that Ni^{2+} and Co^{2+} oxosalt compounds are often isostructural (*e.g.* see Ref. 10); there is, however, a pronounced difference in crystal field stabilization energy between the two cations.[14] Cd^{2+} is the largest cation to be incorporated in cobalt orthophosphate ($r_{Cd}=0.95$ Å). The solubility of cadmium is very slight, probably as a result of the size effect. The Co/Cu orthophosphates clearly obey Vegard's law. The unit cell volume smoothly decreases as the slightly smaller copper ions ($r_{Cu}=0.73$ Å) replace cobalt. Divalent iron ($r_{Fe}=0.77$ Å) and manganese ($r_{Mn}=0.82$ Å) have a solubility in $Co_3(PO_4)_2$ around 35 atom per cent. The unit cell volume in each series (Co/Fe and Co/Mn) increases linearly with the composition z. However, both curves show discontinuities in the vicinity of pure $Co_3(PO_4)_2$. This effect will be discussed in the next section.

The magnesium and zinc (γ-phase) orthophosphates are isomorphous with cobalt orthophosphate, and it is therefore natural that Mg^{2+} and Zn^{2+} are the most soluble cations in $Co_3(PO_4)_2$. The former ion ($r_{Mg}=0.72$ Å) is, in fact, continuously soluble over the whole composition range (at 1070 K). The unit cell dimensions have already been published,[6] and they are included in Fig. 1. As regards zinc ($r_{Zn}=0.75$ Å), up to 97 % of the cobalt may be replaced by this metal. The Co/Zn "cell volume" curve (Fig. 1) is almost linear. The slight discontinuities will be looked into more closely in a forthcoming paper on γ-$(Zn_{1-z}M_z)_3(PO_4)_2$ solid solutions.[15]

DISCUSSION

The crystal structure of $Co_3(PO_4)_2$ is built up of distorted trigonal bipyramids, $M(1)O_5$, and almost regular $M(2)O_6$ octahedra and PO_4 tetrahedra.[2,4,10] The Co/M solid solutions and $Co_3(PO_4)_2$ are isostructural or at least closely related. The homogeneity region for each Co/M series at 1070 K is rather similar to that of the corresponding Mg/M series (see Table 2). Ca^{2+} is too large to be incorporated in $Co_3(PO_4)_2$. Neither can calcium replace magnesium in $Mg_3(PO_4)_2$.[16] However, as pointed out earlier, the cobalt and magnesium orthophosphates are isostructural, and Co^{2+} and Mg^{2+} are similar in size. X-Ray diffraction studies of $Co_2Mg(PO_4)_2$ and $(Co_{0.5}Mg_{0.5})_3(PO_4)_2$ have

Table 2. Approximate homogeneity ranges, in atom per cent, for the $(Co_{1-z}M_z)_3(PO_4)_2$ and $(Mg_{1-z}M_z)_3(PO_4)_2$ solid solution series at about 1070 K. The cation radii, r_M, are from Shannon and Prewitt [13] for octahedral M^{2+} coordination of oxygen ligands.

Cation	r_M/Å	Homogeneity ranges (atom %) Co/M[a]	Mg/M[b]
Ni^{2+}	0.70	15	10
Mg^{2+}	0.72	100	–
Cu^{2+}	0.73	25	15
Co^{2+}	0.74	–	100
Zn^{2+}	0.75	97	97
Fe^{2+}	0.77	40	60
Mn^{2+}	0.82	30	33
Cd^{2+}	0.95	3	10
Ca^{2+}	1.00	0	0[c]

[a] This work. [b] Ref. 6. [c] Ref. 16.

also shown that the cation distribution was close to random but with a slight predominance for Co^{2+} at the M(1) sites.[7] These facts may, partly, explain the similar solubility ranges for Co/M and Mg/M. A difference, though, is noted for Cu^{2+}: the solubility in $Co_3(PO_4)_2$ is moderate, but low in magnesium orthophosphate. The latter fact is curious, since Cu^{2+} has a large tendency to enter into very distorted environments such as five-coordinated sites. Another significant difference is noted for Fe^{2+}, where the solubility situation is reversed: greater solubility in $Mg_3(PO_4)_2$ than in $Co_3(PO_4)_2$. This effect is consistent with the results of cation distribution studies performed on $(Mg_{1-z}M_z)_3(PO_4)_2$ solid solutions, which show that the M(1) site preference order in this structure is $Co^{2+} > Fe^{2+} > Mg^{2+}$, although with very small differences.[6] In Mg/Fe, iron therefore has better possibilities to enter into the more numerous five-coordinated M(1) sites, while in Co/Fe the converse is true: Co^{2+} preferentially occupies the M(1) sites thus leaving the less numerous M(2) sites for the major part of the Fe^{2+} ions. However, there is also another effect observed in the Co/Fe phases to take into consideration, which will be discussed below.

In contrast to the Mg/M series,[6] it is obvious that some of the Co/M solid solution series slightly disobey Vegard's law, *viz.* Co/Zn, Co/Fe and Co/Mn. The two latter series display similar anomalies: the plots of unit cell volume *versus* composition z for the two $(Co_{1-z}M_z)_3(PO_4)_2$ series are principally linear but show a discontinuity close to $z=0$ (Fig. 1). I assume that, upon substitution of some cobalt for Fe^{2+} or Mn^{2+}, the structure changes slightly so that at least some of the atoms no longer conform to the centrosymmetric space group reported for pure cobalt orthophosphate. Atomic displacements may be implied by a superstructure or by some other symmetry change. However, experiments with a Giebe-Scheibe piezoelectric tester could not produce any definite results as regards the existence or not of a center of symmetry in Co/Mn or Co/Fe. Some Co/Fe Guinier photographs have been evaluated by means of a computer-controlled film scanner. For each phase only two very weak reflections out of thirty-two (at $d \approx 2.97$ Å and $d \approx 2.56$ Å) could not be indexed assuming $P2_1/n$ symmetry. [These two reflections do not originate from an impurity of $Fe_3(PO_4)_2$ which might otherwise be suspected, considering the preparation method.] Any structural changes must therefore be very slight; this is also indicated by the small irregular increases in the unit cell dimensions close to $z=0$.

Mössbauer spectroscopy studies of some Co/Fe compounds have also been performed.[17] The preliminary results show three distinct Fe^{2+} doublets in each spectrum. Two of the doublets (one strong and one weak) closely correspond to those obtained in an earlier study of some $(Mg_{1-z}Fe_z)_3(PO_4)_2$ and γ-$(Zn_{1-z}Fe_z)_3(PO_4)_2$ solid solutions, isomorphous with $Mg_3(PO_4)_2$ and $Co_3(PO_4)_2$.[5] The third "extra" doublet of Co/Fe is quite strong and with much lower quadrupole splitting. The above results thus indicate that the Co/Fe phases contain at least three crystallographically non-equivalent M^{2+} cation positions rather than two as in pure cobalt orthophosphate.

Finally, another difference in structural behaviour between $Co_3(PO_4)_2$ and $Mg_3(PO_4)_2$ will be pointed out. Pure and iron-doped magnesium orthophosphate contracts to a denser high-pressure phase at about 25 kbar;[18] the new structure is that of the mineral *sarcopside*[19] or nickel orthophosphate.[20] However, when high pressures are applied to pure and iron-doped $Co_3(PO_4)_2$, another phase is formed.[17] The X-ray powder diffraction patterns of the two latter compounds are similar, but the high-pressure structure in question is so far unknown. Further Mössbauer and neutron diffraction studies of some $(Co_{1-z}Fe_z)_3(PO_4)_2$ phases are in progress.

Acknowledgements. I am most grateful to Professors Eric Welin (Swedish Museum of Natural History) and Peder Kierkegaard (Arrhenius Laboratory, Stockholm) for the excellent laboratory and computing facilities they have placed at my disposal. I am also indebted to Dr. Sven Westman who carefully revised the English of this article.

REFERENCES

1. Calvo, C. *J. Phys. Chem. Solids 24* (1963) 141.
2. Nord, A. G. and Kierkegaard, P. *Acta Chem. Scand. 22* (1968) 1466.
3. Nord, A. G. *Acta Chem. Scand. A 28* (1974) 150.
4. Anderson, J. B., Kostiner, E., Miller, M. C. and Rea, J. R. *J. Solid State Chem. 14* (1975) 372.
5. Annersten, H., Ericsson, T. and Nord, A. G. *J. Phys. Chem. Solids 41* (1980) 1235.
6. Nord, A. G. and Stefanidis, T. *Mater. Res. Bull. 15* (1980) 1183.
7. Nord, A. G. and Stefanidis, T. *Z. Kristallogr. 153* (1980) 141.
8. DuFresne, E. R. and Roy, S. K. *Geochim. Cosmochim. Acta 24* (1961) 198.
9. Fuchs, L. H., Olsen, E. and Gebert, E. *Am. Mineral. 58* (1973) 949.
10. Nord, A. G. and Kierkegaard, P. *Chem. Scr. 15* (1980) 27.
11. Hambling, P. G. *Acta Crystallogr. 6* (1953) 98.
12. Westman, S. and Magnéli, A. *Acta Chem. Scand. 11* (1957) 1587.
13. Shannon, R. D. and Prewitt, C. T. *Acta Crystallogr. B 25* (1969) 925.
14. Burns, R. G. *Mineralogical Applications of Crystal Field Theory*, Univ. Press, Cambridge 1970.
15. Nord, A. G. and Stefanidis, T. *Mat. Res. Bull. In press.*
16. Ando, J. *Bull. Chem. Soc. Jpn. 31* (1957) 201.
17. Nord, A. G., Stefanidis, T., Annersten, H. and Ericsson, T. *To be published.*
18. Annersten, H. and Nord, A. G. *Acta Chem. Scand. A 34* (1980) 389.
19. Moore, P. B. *Am. Mineral. 57* (1972) 24.
20. Calvo, C. and Faggiani, R. *Can. J. Chem. 53* (1975) 1516.

Received June 4, 1981.

Acta Chemica Scandinavica A 36 (1982) 101 – 108

The Crystal Structure of 1,10-Phenanthrolinium Pentafluoroperoxoniobate(V), $(C_{12}H_{10}N_2)[NbF_5(O_2)]$

ROLF STOMBERG

Department of Inorganic Chemistry, CTH/GU, Chalmers Tekniska Högskola, S-412 96 Göteborg, Sweden

Crystals of $(C_{12}H_{10}N_2)[NbF_5(O_2)]$ are triclinic, space group $P\bar{1}$ (No. 2), with $a=9.467(1)$ Å, $b=10.374(2)$ Å, $c=7.594(1)$ Å, $\alpha=102.38(1)°$, $\beta=113.11(1)°$, $\gamma=92.92(1)°$, $V=662.4(2)$ Å^3 and $Z=2$. With an automatic single crystal X-ray diffractometer using Mo$K\alpha$ radiation 5142 independent reflexions were registered. Least-squares refinement of structural and thermal parameters yielded a final R-value of 0.029.

The crystals are composed of 1,10-phenanthrolinium and pentafluoroperoxoniobate(V) ions, held together by ionic and hydrogen bond forces, the shortest hydrogen bond distance, N–H···F, being 2.566(7) Å. The anion has a pentagonal bipyramidal arrangement of ligands, the peroxo group and three fluorine atoms forming the pentagonal plane, while the other two fluorine atoms occupy the apical positions of the bipyramid. The symmetry of the anion is almost C_{2v}.

The anions are disordered in the crystal and have two main orientations, with occupation numbers 0.60 and 0.40, respectively. The differently orientated anions have the same niobium and apical fluorine atom positions within the limits of experimental errors, while the approximately coplanar pentagonal planes are mutually twisted 61°.

Weighted average bond distances within the anions are: Nb–O 1.89 Å, O–O 1.47 Å, Nb–$F_{equatorial}$ 2.00 Å and Nb–F_{apical} 1.92 Å.

In their study of 8-hydroxyquinolinium pentafluoroperoxoniobate(V) trihydrate, $(C_9H_8NO)_2[NbF_5(O_2)]\cdot 3H_2O$, Ružić-Toroš *et al.* claim to have observed a rather short peroxo oxygen bond distance, 1.17(9) Å, and a population parameter of only 0.3 for one of the peroxo oxygen atoms.[1] It is the author's experience that O–O distances in transition metal peroxo compounds as short as at least 0.1 Å less the normal value of 1.49 Å may be observed, especially when dealing with rather unstable compounds (see *e.g.* Refs. 2–5 and references therein). Different occupation numbers for the two oxygen atoms of a peroxo group have, however, not been observed. A reinvestigation of the structure of $(C_9H_8NO)_2[NbF_5(O_2)]\cdot 3H_2O$, using single crystal diffractometer data was therefore undertaken.[6] Preliminary results indicate disorder but not significant decomposition during the data collection. For comparison, it was thought worthwhile to determine the structure of the corresponding 1,10-phenanthrolinium complex, which turned out to be $(C_{12}H_{10}N_2)[NbF_5(O_2)]$.

EXPERIMENTAL

Preparation. Niobium(V) oxide was dissolved in an excess of boiling 38 % hydrofluoric acid. The stoichiometric amount of 1,10-phenanthroline and an excess of hydrogen peroxide were added. By evaporation of the solvent at room temperature, well-developed, pale yellow transparent crystals were obtained.

Data collection. Intensities were recorded at room temperature with a SYNTEX $P2_1$ automatic four-circle single crystal X-ray diffractometer using graphite–monochromatized Mo$K\alpha$ radiation. The crystal, having the dimensions $0.35\times0.39\times0.49$ mm, was coated with a thin layer of epoxy resin. The ω-2θ scan method was used, and the 2θ scan speed was allowed to vary between 2–8°/min, depending on the intensity of the measured reflexion. Data were collected for $2\theta\leq65°$. Three test reflexions, measured after each fiftieth reflexion, showed no significant difference in intensity during the data collection. A profile analysis based on the Lehmann-Larsen method[7] was applied to the 96-step profile collected for each reflexion.

0302-4377/82/020101-08$02.50

A total of 5142 independent reflexions were measured. Of these, 4648 having $I_o \geq 2\sigma(I_o)$ were regarded as being observed and were used in the subsequent calculations. The intensities were corrected for Lorentz and polarization effects but not for absorption.

The unit cell parameters were determined from a least-squares fit of refined diffractometer setting angles for 15 reflexions.

CRYSTAL DATA

1,10-Phenanthrolinium pentafluoroperoxoniobate (V) $(C_{12}H_{10}N_2)[NbF_5(O_2)]$; F.W. = 402.12
Space group $P\bar{1}$ (No. 2)
$a = 9.467(1)$ Å, $b = 10.374(2)$ Å, $c = 7.594(1)$ Å,
$\alpha = 102.38(1)°$, $\beta = 113.11(1)°$, $\gamma = 92.92(1)°$,
$V = 662.4(2)$ Å^3, $Z = 2$, $D_c = 2.016$ g cm^{-3}
$\mu(\text{Mo}K\alpha) = 9.4$ cm^{-1}, $\lambda(\text{Mo}K\alpha) = 0.71069$ Å.

List of structure factors and thermal parameters are available from the author upon request.

STRUCTURE DETERMINATION

The Patterson function showed a large peak at (0.521, 0.545, 0.177) taken to be an Nb – Nb vector. If $P\bar{1}$ is assumed to be the correct space group, Nb thus occupies the general position 2*i* with the approximate coordinates (0.261, 0.273, 0.089). With F_o-signs based on the niobium coordinates, a Fourier summation was undertaken. In the resulting Fourier map, the 22 non-hydrogen atoms were located, giving a plausible structure with a pentagonally bipyramidal coordination about niobium. Successive full-matrix least-squares and Fourier calculations reduced the *R*-value to 0.045. All coordination distances to niobium and bond distances within the 1,10-phenanthrolinium ion had normal values at this stage. The obtained peroxo oxygen bond distance of 1.9 Å as well as too short an F(1)···F(1) packing distance showed, however, that the proposed model was not completely correct, despite the low *R*-value.

At an early stage of the structure determination, it was observed that the pentagonal ring atoms O(1), O(2), F(1), F(2) and F(3) had higher *B*-values ($B = 6-9$ Å^{-2}) than the apically situated atoms F(4) and F(5) ($B = 4$ Å^{-2}) as well as the other atoms ($B = 2.6-4.1$ Å^{-2}). Furthermore, a difference synthesis, excluding the ring atoms of the anion, showed broad peaks extending in the equatorial plane in a direction perpendicular to the niobium-ligand atom direction (see Fig. 1). This had been

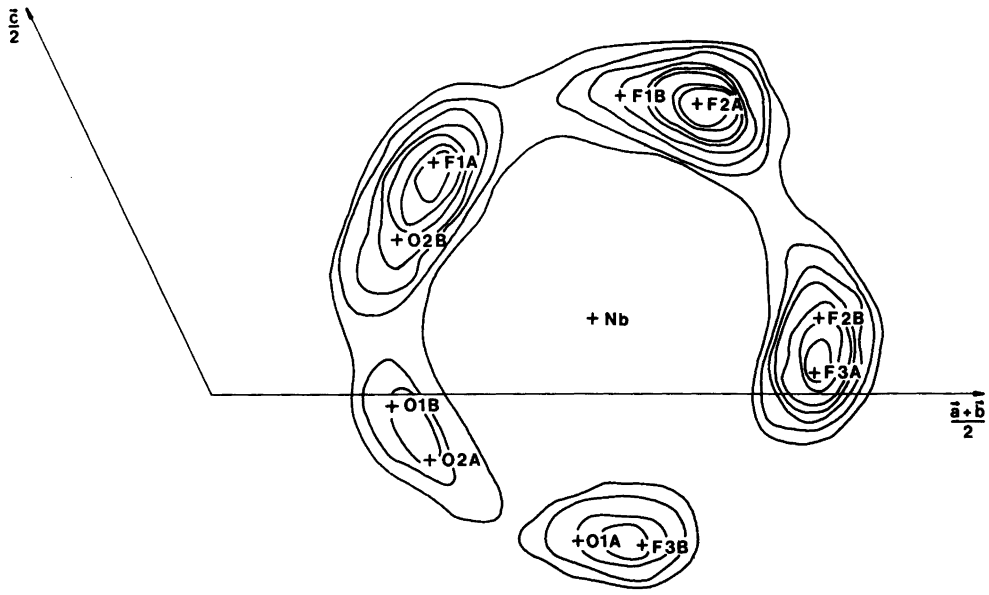

Fig. 1. Section of the electron density difference map. The equatorial atoms F(1), F(2), F(3), O(1) and O(2) were not included in the F_c's ($R = 0.22$). Contours at integral multiples of 1 e Å^{-3}, beginning at 1 e Å^{-3}. Contours about Nb have been omitted. The final atomic positions are indicated by crosses.

taken to be due to anisotropy. Despite large thermal vibrations, the average atomic positions should, however, have led to acceptable interatomic distances among the five ring atoms. Since this was not the case, several models were tried, using space group $P\bar{1}$ as well as $P1$, consistent with the observed peak extension in the equatorial plane of the anion. One model, which had two orientations of the anion with refined occupation numbers of 0.6 and 0.4, respectively, could be successfully refined. The atoms in the pentagonal planes of the two overlapping anions, A and B, could be separated by the least-squares method, while the corresponding niobium and apical fluorine atoms, being too close, could not. A difference map revealed all hydrogen atoms. Refinement of all positional parameters as well as isotropic thermal parameters for the hydrogen atoms and anisotropic ones for all others gave a final R-value of 0.029 ($R=\Sigma\|F_o|-|F_c\|/\Sigma|F_o|$). A difference synthesis calculated after

Table 1. Atomic coordinates, expressed as fraction of the cell edges, for $(C_{12}H_{10}N_2)[NbF_5(O_2)]$. All atoms occupy the general position 2*i* of space group $P\bar{1}$. A and B denote different anions. $U_{eq}=\frac{1}{3}\sum_i\sum_j U_{ij}a_i^*a_j^*a_ia_j \cos\alpha_{ij}$. Occupation numbers are 0.6 and 0.4 for atoms marked with A and B, respectively.

Atom	*x*	*y*	*z*	$U_{eq}/Å^2$ ($U_{iso}/Å^2$ for H)
Nb	0.26168(2)	0.27460(2)	0.09021(3)	0.039
F(1A)	0.2125(5)	0.2139(4)	0.2900(6)	0.087
F(1B)	0.3662(8)	0.3589(7)	0.3767(8)	0.092
F(2A)	0.4102(3)	0.4101(3)	0.3640(5)	0.055
F(2B)	0.4050(7)	0.4190(5)	0.0923(13)	0.110
F(3A)	0.3814(5)	0.4043(4)	0.0245(6)	0.086
F(3B)	0.2198(8)	0.2385(6)	−0.1909(9)	0.085
F(4)	0.4307(2)	0.1739(2)	0.1375(3)	0.068
F(5)	0.1325(2)	0.4117(2)	0.1000(3)	0.059
O(1A)	0.1641(7)	0.2158(6)	−0.1881(7)	0.082
O(1B)	0.1034(12)	0.1206(9)	−0.0161(19)	0.121
O(2A)	0.0954(7)	0.1418(5)	−0.0868(9)	0.094
O(2B)	0.1619(9)	0.1710(7)	0.1955(13)	0.097
N(1)	0.2602(2)	0.5478(2)	0.5436(3)	0.041
N(2)	0.3720(2)	0.6656(2)	0.3022(3)	0.040
C(1)	0.2095(3)	0.4907(3)	0.6541(4)	0.049
C(2)	0.1337(3)	0.5614(4)	0.7603(4)	0.056
C(3)	0.1144(3)	0.6906(3)	0.7507(4)	0.053
C(4)	0.1692(3)	0.7506(3)	0.6338(4)	0.046
C(5)	0.2431(2)	0.6748(2)	0.5280(3)	0.037
C(6)	0.1543(4)	0.8869(3)	0.6264(5)	0.058
C(7)	0.2078(4)	0.9417(3)	0.5146(5)	0.058
C(8)	0.2815(3)	0.8669(2)	0.4030(4)	0.046
C(9)	0.2993(3)	0.7337(2)	0.4089(3)	0.037
C(10)	0.3397(4)	0.9240(3)	0.2878(5)	0.057
C(11)	0.4147(4)	0.8516(3)	0.1860(5)	0.057
C(12)	0.4286(3)	0.7203(3)	0.1948(4)	0.048
H(N1)	0.288(5)	0.476(5)	0.457(8)	0.121(18)
H(N2)	0.384(3)	0.582(3)	0.294(4)	0.027(7)
H(C1)	0.218(4)	0.395(3)	0.633(5)	0.035(8)
H(C2)	0.096(4)	0.524(4)	0.843(5)	0.053(10)
H(C3)	0.073(4)	0.747(3)	0.841(5)	0.036(8)
H(C6)	0.110(3)	0.934(3)	0.719(5)	0.033(8)
H(C7)	0.193(4)	1.033(3)	0.498(5)	0.037(9)
H(C10)	0.302(5)	1.011(5)	0.252(7)	0.090(15)
H(C11)	0.450(4)	0.903(3)	0.117(5)	0.040(9)
H(C12)	0.468(5)	0.690(4)	0.136(7)	0.089(16)

Table 2. Bond distances and angles in $(C_{12}H_{10}N_2)[NbF_5(O_2)]$. A and B denote different anions.

Distance/Å			
Nb–F(1A)	1.962(4)	C(4)–C(6)	1.439(4)
Nb–F(1B)	1.971(6)	C(5)–C(9)	1.433(3)
Nb–F(2A)	2.127(3)	C(6)–C(7)	1.347(5)
Nb–F(2B)	1.963(6)	C(8)–C(7)	1.430(4)
Nb–F(3A)	1.980(4)	C(8)–C(9)	1.409(3)
Nb–F(3B)	1.958(6)	C(8)–C(10)	1.410(4)
Nb–F(4)	1.913(2)	C(11)–C(10)	1.378(4)
Nb–F(5)	1.931(2)	C(11)–C(12)	1.388(4)
Nb–O(1A)	1.884(5)	N(2)–C(9)	1.368(3)
Nb–O(1B)	1.924(10)	N(2)–C(12)	1.337(5)
Nb–O(2A)	1.872(6)	N(1)–H(N1)	1.00(5)
Nb–O(2B)	1.883(8)	N(2)–H(N2)	0.87(3)
O(1A)–O(2A)	1.483(8)	C(1)–H(C1)	0.98(3)
O(1B)–O(2B)	1.440(16)	C(2)–H(C2)	0.97(4)
N(1)–C(1)	1.337(3)	C(3)–H(C3)	1.02(3)
N(1)–C(5)	1.360(3)	C(6)–H(C6)	1.00(3)
C(2)–C(1)	1.400(4)	C(7)–H(C7)	0.99(3)
C(2)–C(3)	1.375(5)	C(10)–H(C10)	1.04(4)
C(4)–C(3)	1.417(4)	C(11)–H(C11)	0.96(3)
C(4)–C(5)	1.408(3)	C(12)–H(C12)	0.72(5)
Angle/°			
F(1A)–Nb–F(2A)	75.3(2)	N(1)–C(1)–C(2)	120.2(3)
F(1A)–Nb–F(3A)	149.1(2)	C(1)–C(2)–C(3)	118.8(3)
F(1A)–Nb–F(4)	90.2(1)	C(2)–C(3)–C(4)	120.6(3)
F(1A)–Nb–F(5)	89.0(1)	C(3)–C(4)–C(5)	118.5(2)
F(1A)–Nb–O(1A)	129.7(2)	C(3)–C(4)–C(6)	121.4(3)
F(1A)–Nb–O(2A)	83.2(2)	C(4)–C(5)–N(1)	118.7(2)
F(2A)–Nb–F(3A)	73.8(2)	N(1)–C(5)–C(9)	122.0(2)
F(2A)–Nb–F(4)	85.2(1)	C(5)–C(4)–C(6)	120.1(2)
F(2A)–Nb–F(5)	79.9(1)	C(4)–C(6)–C(7)	120.2(3)
F(2A)–Nb–O(1A)	154.3(2)	C(6)–C(7)–C(8)	121.1(3)
F(2A)–Nb–O(2A)	157.8(2)	C(7)–C(8)–C(9)	120.0(2)
F(3A)–Nb–F(4)	88.2(1)	C(7)–C(8)–C(10)	121.5(2)
F(3A)–Nb–F(5)	84.7(1)	C(5)–C(9)–C(8)	119.2(2)
F(3A)–Nb–O(1A)	80.9(2)	C(5)–C(9)–N(2)	122.3(2)
F(3A)–Nb–O(2A)	127.4(2)	C(4)–C(5)–C(9)	119.3(2)
F(4)–Nb–F(5)	164.8(1)	C(9)–C(8)–C(10)	118.5(2)
F(4)–Nb–O(1A)	99.1(2)	C(8)–C(10)–C(11)	120.7(2)
F(4)–Nb–O(2A)	100.6(2)	F(3B)–Nb–F(4)	90.8(2)
F(5)–Nb–O(1A)	93.1(2)	F(3B)–Nb–F(5)	98.5(2)
F(5)–Nb–O(2A)	94.4(2)	F(3B)–Nb–O(1B)	79.6(4)
O(1A)–Nb–O(2A)	46.5(3)	F(3B)–Nb–O(2B)	124.1(3)
F(1B)–Nb–F(2B)	79.8(3)	F(4)–Nb–O(1B)	94.8(3)
F(1B)–Nb–F(3B)	158.3(3)	F(4)–Nb–O(2B)	92.7(2)
F(1B)–Nb–F(4)	84.7(2)	F(5)–Nb–O(1B)	98.7(3)
F(1B)–Nb–F(5)	82.2(2)	F(5)–Nb–O(2B)	92.0(2)
F(1B)–Nb–O(1B)	121.8(4)	O(1B)–Nb–O(2B)	44.4(5)
F(1B)–Nb–O(2B)	77.4(3)	C(1)–N(1)–C(5)	123.2(2)
F(2B)–Nb–F(3B)	78.7(3)	C(10)–C(11)–C(12)	118.9(3)
F(2B)–Nb–F(4)	86.2(2)	C(11)–C(12)–N(2)	120.5(2)
F(2B)–Nb–F(5)	83.8(2)	C(9)–N(2)–C(12)	122.9(2)
F(2B)–Nb–O(1B)	158.4(5)	C(8)–C(9)–N(2)	118.5(2)
F(2B)–Nb–O(2B)	157.2(4)		

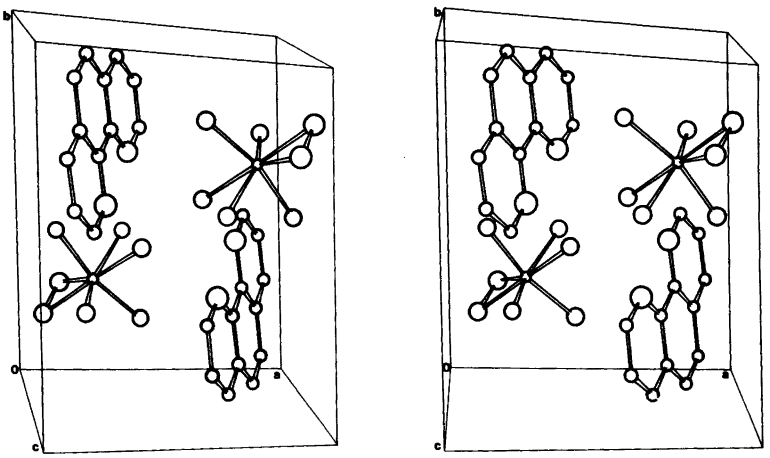

Fig. 2. Stereoscopic drawing of the unit cell of $(C_{12}H_{10}N_2)[NbF_5(O_2)]$. Only the orientation A of the anion is shown.

the final cycle of refinement showed no peak higher than 0.53 e/Å^3.

The weighting scheme used was that of Cruickshank:[8] $w=(a+|F_o|+c|F_o|^2+d|F_o|^3)^{-1}$ with $a=20$, $c=0.02$ and $d=0.0004$. The atomic scattering factors for Nb, F, O and H were taken from the *International Tables for X-Ray Crystallography, Vol. III*, as was the dispersion correction applied to Nb, while those for N and C are from Cromer *et al.*[9]

Calculations were carried out on an IBM 360/65 computer using the crystallographic programmes described by Lindgren.[10]

RESULTS AND DISCUSSION

The positional parameters as well as U_{eq} (or U_{iso}) are given in Table 1. A stereoscopic view of the unit cell content is shown in Fig. 2. Bond distances and angles are given in Table 2 and Figs. 3 and 4 and interionic distances in Table 3.

The crystals of 1,10-phenanthrolinium pentafluoroperoxoniobate(V), $(C_{12}H_{10}N_2)[NbF_5(O_2)]$, consist of 1,10-phenanthrolinium and pentafluoroperoxoniobate(V) ions held together by ionic and hydrogen bond forces.

The 1,10-phenanthrolinium ion is planar. The distances from the non-hydrogen atoms defining

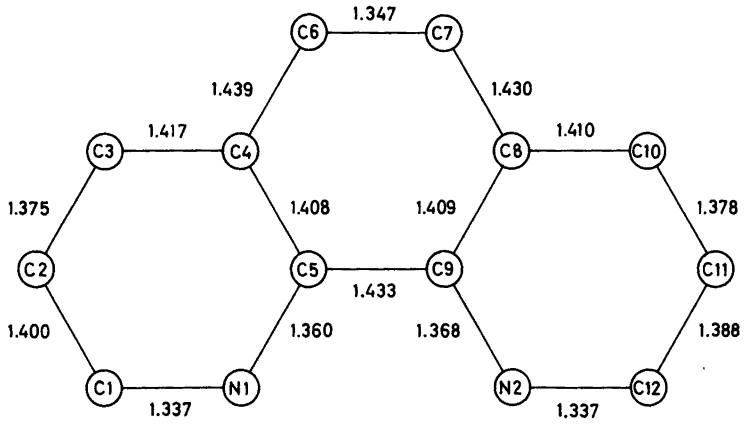

Fig. 3. The ion $C_{12}H_{10}N_2^{2+}$.

this plane to the plane are given in Table 4. Corresponding bond distances in the two hetero rings are equal, the largest difference of 0.012 Å being 3σ. One C–N distance is shorter than the other in both hetero rings, the mean distance * being 1.337(0) Å for the shorter and 1.364(4) Å for the longer one. One C–C distance, C(6)–C(7), is shorter than the other C–C distances, which can be divided into four groups with mean distances of 1.434(4) Å, 1.411(4) Å, 1.394(6) Å and 1.376(2) Å. All bond distances and angles in the 1,10-phenanthrolinium ion agree well with other observations for this ion and 1,10-phenanthroline.[11–14]

The pentafluoroperoxoniobate(V) anions are disorderly orientated in the crystal. Two main orientations, denoted A and B, with occupancies 0.6 and 0.4, respectively, were observed. The two anions $[NbF_5(O_2)]^{2-}$ have a pentagonal bipyramidal arrangement of ligands (Fig. 4), a configuration observed in several transition metal peroxo complexes (see, *e.g.*, Refs. 4, 5, 15–18). The consistency of this geometry for the pentafluoromonoperoxometallates is evident from Table 5 in Ref. 17, listing interatomic distances in some compounds of this type, and is further supported by the values obtained in the present investigation (see Table 5). The distances

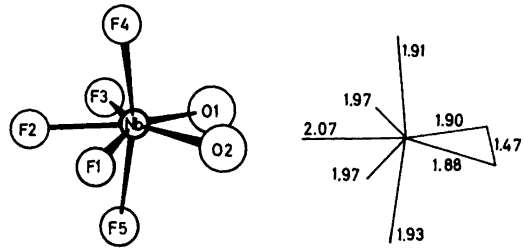

Fig. 4. The ion $[NbF_5(O_2)]^{2-}$. Average distances (weighted mean) are given.

from the equatorial plane, defined by F(1), F(2), F(3), O(1) and O(2), to these atoms and to Nb, F(4) and F(5) are given in Table 4. F(2), F(4), F(5), Nb and the midpoint between O(1) and O(2) form a plane too. The angle between these planes is 90.5° in the A anion and 87.3° in the B anion. Hence, the point symmetry of $[NbF_5(O_2)]^{2-}$ is almost C_{2v}.

The disorder of the anions A and B can be described in the following way. Neither the central atom positions nor those of the apical atoms in A could be distinguished from the corresponding ones in B.* The equatorial pentagonal planes form an

* R.m.s. deviation from the mean is given in parenthesis.

* As a consequence of this, the interatomic distances involving these atoms [Nb, F(4) and F(5)] are probably more uncertain than can be judged from the e.s.d.'s.

Table 3. Interionic distances in $(C_{12}H_{10}N_2)[NbF_5(O_2)]$. A and B denote different anions. Distances of less than 3.2 Å have been included.

Distance/Å			
F(1B)···N(1)	2.566(7)	F(3A)···C(12^{ii})	3.057(5)
F(1B)···N(2^{i})	2.782(7)	F(3A)···N(2)	3.086(5)
F(1B)···F(2A^{i})	2.879(8)	F(3A)···F(3A^{ii})	3.105(9)
F(1B)···C(1)	3.151(7)	F(3A)···C(12)	3.194(5)
F(2A)···F(2A^{i})	2.430(6)	F(3B)···C(1^{iii})	3.081(7)
F(2A)···N(1)	2.609(4)	F(4)···C(5^{i})	3.177(3)
F(2A)···N(2)	2.806(3)	F(5)···N(2)	3.059(3)
F(2A)···N(2^{i})	2.865(4)	F(5)···N(1)	3.065(3)
F(2A)···N(1^{i})	2.903(3)	F(5)···C(2^{iv})	3.098(3)
F(2B)···N(2)	2.811(7)	F(5)···C(3^{iv})	3.197(3)
F(2B)···C(12)	3.029(6)	O(2B)···C(3^{iv})	3.169(8)
F(2B)···F(3A^{ii})	3.156(8)	O(2B)···C(10^{v})	3.190(8)
F(3A)···C(1^{iii})	3.000(5)		

Symmetry codes

i	$(1-x,1-y,1-z)$
ii	$(1-x,1-y,\bar{z})$
iii	$(x,y,z-1)$
iv	$(\bar{x},1-y,1-z)$
v	$(x,y-1,z)$

Table 4. Displacements (Å) of the atoms from certain least-squares planes in $(C_{12}H_{10}N_2)[NbF_5(O_2)]$. Defining atoms are

Plane I F(1A), F(2A), F(3A), O(1A) and O(2A)
Plane II F(1B), F(2B), F(3B), O(1B) and O(2B)
Plane III N1, N2, C1–C12

Atom	Plane I	Atom	Plane II	Atom	Plane III
F(1A)	−0.034	F(1B)	−0.032	N(1)	−0.008
F(2A)	0.036	F(2B)	0.035	C(1)	−0.022
F(3A)	−0.028	F(3B)	−0.029	C(2)	−0.006
O(1A)	0.004	O(1B)	0.008	C(3)	0.006
O(2A)	0.022	O(2B)	0.018	C(4)	0.015
Nb	−0.076	Nb	0.019	C(5)	0.013
F(4)	−1.971	F(4)	−1.887	C(6)	−0.012
F(5)	1.839	F(5)	1.919	N(2)	0.024
				C(12)	−0.004
				C(11)	−0.028
				C(10)	−0.003
				C(8)	0.011
				C(9)	0.022
				C(7)	−0.007

angle of 3.3° with one another, and the pentagons are mutually twisted 61°. This disorder differs from that observed for $Na_2[NbF_5(O_2)]\cdot 2H_2O$,[17] $(NH_4)_3[TiF_5(O_2)]$[19,20] and $(C_9H_8NO)_2[NbF_5(O_2)]\cdot 3H_2O$.[6]

The $Nb-F_{equatorial}$ bond distances, 1.958–2.127 Å, are somewhat longer than the $Nb-F_{apical}$ bond distances, 1.913–1.931 Å. This compares well with the corresponding distances in $Na_2[NbF_5(O_2)]\cdot H_2O$[15] and $Na_3[HF_2][NbF_5(O_2)]$.[16] A possible explanation to these differences is given in Ref. 15.

The Nb–O distances, 1.872–1.924 Å, are normal Nb–O single bond distances, observed ones in $Na_2[NbF_5(O_2)]\cdot H_2O$,[15] $Na_3[HF_2][NbF_5(O_2)]$[16] and $Na_2[NbF_5(O_2)]\cdot 2H_2O$[17] being 1.928, 1.924–1.940 and 1.933–1.962 Å, respectively. Additional Nb–F and Nb–O distances can be found in Ref. 21 and references therein.

The peroxo oxygen bond distances, 1.483 and

Table 5. The lengths of the edges (Å) of the pentagonal bipyramidal coordination polyhedra. The designation of the edges conforms to Fig. 3 in Ref. 17. Compare with Table 5 in Ref. 17.

Edge		Distance/Å		Distance/Å
a	F(1A)···F(2A)	2.501(5)	F(1B)···F(2B)	2.523(10)
b	F(2A)···F(3A)	2.471(5)	F(2B)···F(3B)	2.487(9)
c	F(3A)···O(1A)	2.508(7)	F(3B)···O(1B)	2.485(13)
d	O(1A)···O(2A)	1.483(8)	O(1B)···O(2B)	1.440(16)
e	O(2A)···F(1A)	2.546(8)	O(2B)···F(1B)	2.411(10)
f	F(4)···F(1A)	2.745(5)	F(4)···F(1B)	2.618(7)
g	F(4)···F(2A)	2.739(4)	F(4)···F(2B)	2.649(6)
h	F(4)···F(3A)	2.710(5)	F(4)···F(3B)	2.757(7)
i	F(4)···O(1A)	2.889(6)	F(4)···O(1B)	2.824(11)
j	F(4)···O(2A)	2.914(7)	F(4)···O(2B)	2.747(8)
k	F(5)···F(1A)	2.727(4)	F(5)···F(1B)	2.565(7)
l	F(5)···F(2A)	2.610(3)	F(5)···F(2B)	2.601(7)
m	F(5)···F(3A)	2.636(5)	F(5)···F(3B)	2.945(6)
n	F(5)···O(1A)	2.770(5)	F(5)···O(1B)	2.925(10)
o	F(5)···O(2A)	2.790(6)	F(5)···O(2B)	2.744(8)

1.440 Å, compare well with other observations (see Table 7 in Ref. 4 and Table 5 in Ref. 17).

The niobium atom is displaced 0.076 and 0.019 Å from the equatorial planes. Such small displacements have been observed for the $[NbF_5(O_2)]^{2-}$ ion in other compounds[15-17] and for other transition metal peroxo compounds, when, as in this case, the apical positions are occupied by identical ligands. When the apical atoms are different, or are differently coordinated, the central atom is in most cases displaced by 0.2–0.5 Å (see Table 6 in Ref. 4).

The short distances between F(1B) and N(1) and between F(2A) and N(1) indicate rather strong hydrogen bonding. The small distance of 2.430 Å between F(2A) and $F(2A^i)$ is energetically not a plausible distance and therefore not judged to really exist. It is supposed to be a consequence of the disorder, which might be more complicated though not observed in the final electron density difference map. It should also be noted that the fluorine atoms involved in the shortest $Nb-F_{equatorial}$ and $Nb-F_{apical}$ distances, respectively, have only one intermolecular neighbouring atom, while those involved in the longest ones have three or four such neighbouring atoms.

Acknowledgement. I wish to express by gratitude to Mrs. Solveig Olson for technical assistance.

REFERENCES

1. Ružić-Toroš, Z., Kojić-Prodić, B., Gabela, F. and Sljukić, M. *Acta Crystallogr. B 33* (1977) 692.
2. Stomberg, R. *Ark. Kemi 24* (1965) 283.
3. Stomberg, R. *Acta Chem. Scand. 24* (1970) 2024.
4. Svensson, I.-B. and Stomberg, R. *Acta Chem. Scand. 25* (1971) 898.
5. Larking, I. and Stomberg, R. *Acta Chem. Scand. 26* (1972) 3708.
6. Stomberg, R. *Acta Chem. Scand. To be published.*
7. Lehmann, M. S. and Larsen, F. K. *Acta Crystallogr. A 30* (1974) 580.
8. Cruickshank, D. W. J. *Crystallographic Computing*, Munksgaard, Copenhagen 1970, p. 195.
9. Cromer, D. T. and Waber, J. T. *Acta Crystallogr. 18* (1965) 104.
10. Lindgren, O. *Thesis*, University of Göteborg and Chalmers University of Technology, Göteborg 1977.
11. Mathern, G. and Weiss, R. *Acta Crystallogr. B 27* (1971) 1582.
12. Thevenet, G. and Rodier, N. *Acta Crystallogr. B 34* (1978) 1280.
13. Thevenet, G., Rodier, N. and Khodadad, P. *Acta Crystallogr. B 34* (1978) 2594.
14. Viossat, B. and Rodier, N. *Acta Crystallogr. B 37* (1981) 56.
15. Stomberg, R. *Acta Chem. Scand. A 34* (1980) 193.
16. Stomberg, R. *Acta Chem. Scand. A 35* (1981) 389.
17. Stomberg, R. *Acta Chem. Scand. A 35* (1981) 489.
18. Larking, I. and Stomberg, R. *Acta Chem. Scand. 24* (1970) 2043.
19. Stomberg, R. and Svensson, I.-B. *Acta Chem. Scand. A 31* (1977) 635.
20. Massa, W. and Pausewang, G. *Mater. Res. Bull. 13* (1978) 361.
21. Pakhomov, V. I. and Kaidalova, T. A. *Kristallografiya 19* (1974) 733.

Received May 22, 1981.

Acta Chemica Scandinavica A 36 (1982) 109–115

Crystal Structure Analyses of 1,4,7,10,13,16-Hexaoxacyclooctadecane and its Complexes with Lithium Perchlorate Dihydrate and Lithium Thiocyanate Dihydrate at −150 °C

P. GROTH

Department of Chemistry, University of Oslo, Oslo 3, Norway

Crystals were grown at room temperature and cooled rapidly to about −150 °C, the temperature at which data were collected on an automatic four-circle diffractometer. The cyclic hexaether of the perchlorate complex adopts the non-angular D_{3d} conformation, while that of the (2:1) thiocyanate complex is the biangular [8, 10]. In both structures the (18-crown-6) ring skeleton, which is too large for the small Li^+ ion, is effectively narrowed by the encapsulated water molecules. They have the double role of acting as coordinating agents towards Li^+ and hydrogen bond donors towards the ether oxygens, and are creating geometries compatible with the coordination preferences for the lithium cation.

1,4,7,10,13,16-Hexaoxacyclooctadecane (18-crown-6), in its complexes with K^+ and larger cations, adopts a centrosymmetric non-angular D_{3d} conformation [1] [Fig. 1(a)]. This conformation is also found in several crystalline "adducts" or molecular complexes.[2–4] An exception is one involving the NH_2 group of benzenesulfonamid [5] where the cyclic hexaether has the centrosymmetric biangular [99] * conformation shown in Fig. 1(b). In the absence of cations or protic adduct-formers, 18-crown-6 crystallizes in a completely different non-angular centrosymmetric conformation [1] [Fig. 1(c)]. Among the complexes with smaller cations than K^+, that of hydrated sodium thiocyanate has been investigated by X-rays.[1] The crystal structure reveals that a part of the ring is deformed in a highly irregular manner, which brings one ether oxygen into an apical ligand position 1.95 Å out of the mean plane of the other five, giving the triangular [3, 5, 10] conformation illustrated in Fig. 2. In order to explore whether the hexaether may adopt other conformations, compatible with the coordination preferences for

* A shorthand notation for conformational type, consisting of a series of numbers within brackets, each giving the number of bonds in one "side", starting with the shortest. The direction around the ring is so chosen that the following number is smallest possible.

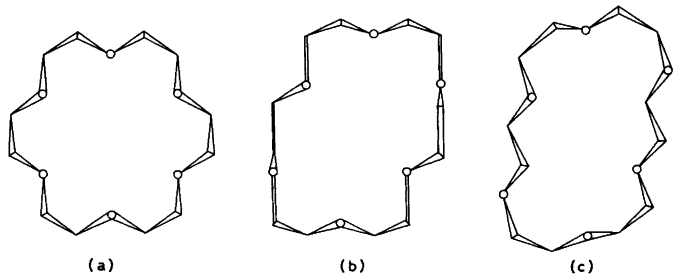

Fig. 1. Crystal structures of 1,4,7,10,13,16-hexaoxacyclooctadecane (a) as a 1:1 complex with KSCN, (b) as a 1:2 complex with benzenesulfonamide and (c) in the uncomplexed state.

0302-4377/82/020109-07$02.50

Table 1. Crystal data for $LiClO_4 \cdot (CH_2-CH_2-O)_6 \cdot 2H_2O$ (I) and $(iSCN)_2 \cdot (CH_2-CH_2-O)_6 \cdot 2H_2O$ (II).

	Space group	a (Å)	b (Å)	c (Å)	β(°)	Z	D_m g cm^{-3}	D_x g cm^{-3}	Number of observed reflections
(I)	$P2_1/c$	17.006(2)	7.058(1)	20.849(3)	128.72(9)	4	1.35	1.38	2451
(II)	$P2_1/n$	9.533(4)	16.252(6)	13.855(3)	100.49(3)	4	1.30	1.35	3019

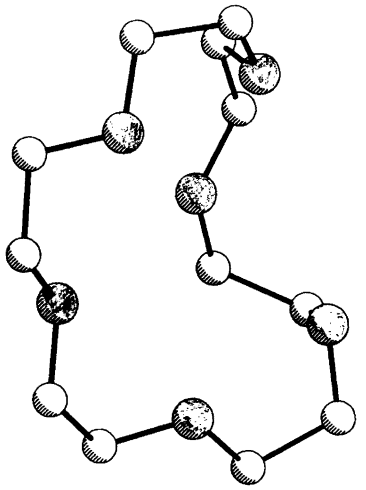

Fig. 2. The conformation of the (18-crown-6) ether in the complex with $NaSCN \cdot H_2O$.

Table 2. Final fractional coordinates with estimated standard deviations for $LiClO_4 \cdot (CH_2CH_2O)_6 \cdot 2H_2O$. Hn1 and Hn2 are bonded to Cn. HWn1 and HWn2 are bonded to OWn.

ATOM	X	Y	Z
O1	.95779(15)	.19546(31)	.82799(12)
O2	.83631(16)	.52934(32)	.73138(13)
O3	.62757(16)	.50520(33)	.62996(13)
O4	.55134(15)	.25203(31)	.67652(12)
O5	.66803(16)	-.07807(30)	.77742(12)
O6	.88242(16)	-.05268(31)	.88776(13)
C1	.99423(24)	.38406(51)	.83619(20)
C2	.93217(25)	.48147(49)	.75452(21)
C3	.77452(26)	.62421(49)	.65405(19)
C4	.67729(25)	.67639(48)	.63675(18)
C5	.53077(26)	.53823(53)	.60841(21)
C6	.48603(24)	.34845(55)	.59974(20)
C7	.51247(24)	.06960(49)	.67266(20)
C8	.57451(25)	-.01988(51)	.75607(20)
C9	.73023(25)	-.17035(50)	.85512(19)
C10	.82730(25)	-.22293(48)	.87345(19)
C11	.97096(24)	-.08886(48)	.89616(19)
C12	1.01886(24)	.09697(50)	.90465(19)
CL	.74365(6)	1.14011(13)	.50375(5)

Table 2. Continued.

O7	.83349(20)	1.22193(43)	.57282(18)
O8A	.67125(48)	1.15095(93)	.51907(41)
O9A	.69249(48)	1.21084(98)	.42292(35)
O10A	.75199(51)	.93038(74)	.49896(36)
O8B	.70112(66)	1.03170(96)	.52852(48)
O9B	.67918(52)	1.29481(92)	.45260(43)
O10B	.77508(51)	1.04815(91)	.46393(33)
OW1	.21810(18)	.69080(32)	.16181(14)
OW2	.24587(17)	.88426(33)	.31032(13)
LI+	.29898(50)	.70072(99)	.27950(37)
HW11	.2556	.7063	.1370
HW12	.1865	.8193	.1442
HW21	.2600	.8600	.3600
HW22	.1800	.8600	.2800
H11	1.0659	.3734	.8582
H12	.9901	.4569	.8751
H21	.9230	.3949	.7123
H22	.9674	.5995	.7583
H31	.7608	.5384	.6099
H32	.8093	.7412	.6563
H41	.6337	.7492	.5841
H42	.6914	.7554	.6827
H51	.4869	.6090	.5553
H52	.5379	.6129	.6526
H61	.4795	.2739	.5559
H62	.4180	.3645	.5850
H71	.5140	-.0129	.6345
H72	.4414	.0832	.6517
H81	.5381	-.1324	.7552
H82	.5866	.0740	.7973
H91	.6957	-.2871	.8535
H92	.7435	-.0829	.8987
H101	.8135	-.2931	.8257
H102	.8675	-.3059	.9235
H111	.9526	-.1570	.8464
H112	1.0189	-.1681	.9461
H121	1.0872	.0745	.9209
H122	1.0252	.1748	.9478

cations too small to fill the ring cavity of the D_{3d} conformation, crystal structure analyses of the complexes (I) and (II) have been carried out.

$$LiClO_4 \cdot (CH_2 \cdot CH_2 \cdot O)_6 \cdot 2H_2O \quad \text{(I)}$$

$$(LiSCN)_2(CN_2 \cdot CH_2 \cdot O)_6 \cdot 2H_2O \quad \text{(II)}$$

Attempts to make a crystalline (1:1) complex with LiSCN were unsuccessful. The crystals of (I) and (II) were grown at room temperature and cooled

Table 3. Final fractional coordinates with estimated standard deviations for $(LiSCN)_2(CH_2CH_2O)_6 \cdot 2H_2O$. Hn1 and Hn2 are bonded to Cn. HWn1 and HWn2 are bonded to OWn.

ATOM	X	Y	Z
O1	1.21353(13)	.08299(7)	.31287(9)
O2	.97310(13)	.11503(7)	.23233(9)
O3	.75311(13)	-.02572(7)	.25739(9)
O4	.85546(13)	-.13582(7)	.64292(9)
O5	1.10904(12)	-.10744(7)	.56389(8)
O6	1.27975(12)	.04038(7)	.62778(8)
C1	1.17791(20)	.13240(11)	.38984(13)
C2	1.04154(20)	.10071(12)	.91484(13)
C3	.73972(20)	.09753(11)	.85415(13)
C4	.75509(20)	.00749(12)	.35385(13)
C5	.69840(20)	-.10978(11)	.75136(14)
C6	.70976(20)	-.14276(11)	.65277(14)
C7	.89314(20)	-.18341(11)	.56407(13)
C8	1.05251(20)	-.18756(11)	.57316(13)
C9	1.26139(19)	-.10637(11)	.58903(13)
C10	1.31360(19)	-.02324(12)	.56440(13)
C11	1.38566(19)	.04771(11)	.71547(13)
C12	1.33992(19)	.11156(12)	.78130(13)
S1	.08664(5)	.39875(2)	.56458(3)
S2	.46203(5)	.23633(3)	.58897(3)
N1	.07235(17)	.25724(10)	.67956(12)
N2	.75032(18)	.19123(10)	.64257(12)
C13	.07999(18)	.31544(11)	.63212(13)
C14	.63137(22)	.21037(11)	.62040(13)
LI1+	1.05536(33)	.03398(19)	.29235(23)

Table 3. Continued.

LI2+	.45034(35)	.33910(19)	.20265(23)
OW1	.00647(12)	.39272(7)	.36926(8)
OW2	.92110(13)	.08285(8)	.19085(10)
HW11	-.0877	.9447	.3666
HW12	.0450	.9269	.4299
HW21	.9821	.1359	.1663
HW22	.8320	.0666	.1676
H11	1.1653	.1909	.9674
H12	1.2557	.1291	.9486
H21	1.0202	.1304	.9739
H22	1.0500	.0404	.9291
H31	.7148	.1258	.8041
H32	.7858	.1204	.9208
H41	.6592	-.0002	.8724
H42	.8289	-.0218	.9024
H51	.5963	-.1084	.7597
H52	.7557	-.1432	.8042
H61	.6480	-.1105	.5998
H62	.6796	-.2018	.6481
H71	.8542	-.1565	.4999
H72	.8531	-.2402	.5650
H81	1.0810	-.2267	.5296
H82	1.0918	-.2068	.6463
H91	1.3021	-.1500	.5505
H92	1.2922	-.1178	.6607
H101	1.2683	-.0023	.4954
H102	1.4195	-.0256	.5698
H111	1.4788	.0642	.6977
H112	1.3969	-.0065	.7504
H121	1.3193	.1645	.7444
H122	1.4172	.1295	.8395

rapidly to about −150 °C, the temperature at which data were collected on an automatic four-circle diffractometer (Mo$K\alpha$-radiation, $2\theta_{max}=50°$). Crystal data for the two compounds are given in Table 1. No corrections for absorption or secondary extinction were made (maximum crystal size 0.4 × 0.5 × 0.3 mm). The structures were (solved by direct methods[6] and refined by full-matrix least squares technique.[7,*] Weights in least squares were obtained from the standard deviations in intensities, $\sigma(I)$, taken as $\sigma(I)=[C_T+(0.02C_N)^2]^{\frac{1}{2}}$ where C_T is the total number of counts, and C_N the net count. Standard deviations in bond distances and angles

*All programs used (except those for phase determination) are included in this reference.

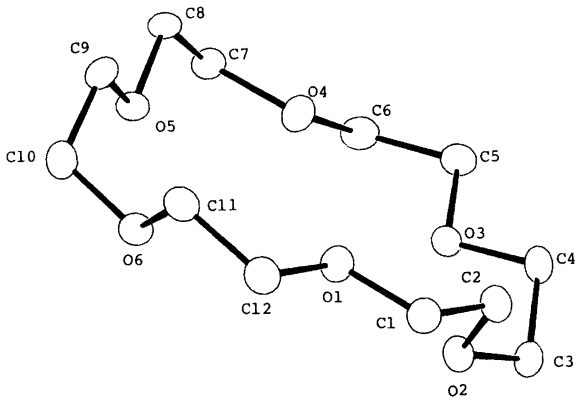

Fig. 3. Schematic drawing showing the [8, 10] conformation of the cyclic hexaether in the complex with $(LiSCN)_2 \cdot 2H_2O$.

Table 4. Bond distances and angles and dihedral angles for $LiClO_4 \cdot (CH_2CH_2O)_6 \cdot 2H_2O$ with estimated standard deviations.

DISTANCE	(Å)	DISTANCE	(Å)
O1 - C1	1.433(4)	O1 - C12	1.428(4)
O2 - C2	1.421(4)	O2 - C3	1.426(4)
O3 - C4	1.430(4)	O3 - C5	1.429(4)
O4 - C6	1.426(4)	O4 - C7	1.426(4)
O5 - C8	1.418(4)	O5 - C9	1.423(4)
O6 - C10	1.436(4)	O6 - C11	1.426(4)
C1 - C2	1.496(5)	C3 - C4	1.501(5)
C5 - C6	1.494(5)	C7 - C8	1.497(5)
C9 - C10	1.490(5)	CL - O7	1.410(3)
CL - O8A	1.455(7)	CL - O9A	1.419(5)
CL -O10A	1.496(5)	CL - O8B	1.357(7)
CL - O9B	1.438(6)	CL -O10B	1.397(5)
OW1 - O9A	2.968(7)	OW1 -O10B	2.877(6)
OW1 - O6	2.882(3)	OW2 - O1	2.852(3)
OW2 - O8A	2.903(7)	OW2 - O8B	2.944(9)
OW1 - LI+	1.922(6)	OW2 - LI+	1.906(7)
LI+ - O3	2.070(7)	LI+ - O4	2.124(7)

ANGLE	(°)	ANGLE	(°)
O1 - C1 - C2	110.3(3)	C1 - O1 - C12	111.2(2)
O1 - C12 - C11	109.5(3)	O2 - C2 - C1	109.8(3)
C2 - O2 - C3	111.9(2)	O2 - C3 - C4	108.0(3)
O3 - C4 - C3	108.1(3)	C4 - O3 - C5	112.8(3)
O3 - C5 - C6	106.9(3)	O4 - C6 - C5	108.2(3)
C6 - O4 - C7	111.1(3)	O4 - C7 - C8	110.5(3)
O5 - C8 - C7	108.9(3)	C8 - O5 - C9	112.3(2)
O5 - C9 - C10	108.7(3)	O6 - C10 - C9	108.6(3)
C10 - O6 - C11	112.2(2)	O6 - C11 - C12	108.2(3)
O7 - CL - O8A	106.2(3)	O7 - CL - O9A	122.4(3)
O7 - CL -O10A	112.7(3)	O7 - CL - O8B	109.7(4)
O7 - CL - O9B	106.4(4)	O7 - CL -O10B	103.0(3)
O8A - CL - O9A	105.6(4)	O8A - CL -O10A	101.3(4)
O9A - CL -O10A	106.4(4)	O8B - CL - O9B	111.7(5)
O8B - CL -O10B	117.2(5)	O9B - CL -O10B	108.0(4)
OW1 - LI+ - OW2	110.1(3)	OW1 - LI+ - O4	105.3(3)
OW2 - LI+ - O3	108.2(3)	OW2 - LI+ - O4	116.1(3)

DIHEDRAL ANGLE	(°)
C11 - C12 - O1 - C1	172.6(3)
C12 - O1 - C1 - C2	177.4(2)
O2 - C2 - C1 - O1	73.2(3)
C3 - O2 - C2 - C1	179.5(3)
C4 - C3 - O2 - C2	-177.5(3)
O3 - C4 - C3 - O2	-63.1(3)
C5 - O3 - C4 - C3	-176.4(3)
C6 - C5 - O3 - C4	177.5(3)
O4 - C6 - C5 - O3	59.3(3)
C7 - O4 - C6 - C5	179.5(3)
C8 - C7 - O4 - C6	-172.8(3)
O5 - C8 - C7 - O4	-73.0(3)
C9 - O5 - C8 - C7	-178.1(3)
C10 - C9 - O5 - C8	-178.8(3)
O6 - C10 - C9 - O5	68.7(3)
C11 - O6 - C10 - C9	-173.1(3)
C12 - C11 - O6 - C10	175.9(3)
O6 - C11 - C12 - O1	-70.3(3)

Table 5. Bond distances and angles and dihedral angles for $(LiSCN)_2(CH_2CH_2O)_6 \cdot 2H_2O$ with estimated standard deviations.

DISTANCE	(Å)	DISTANCE	(Å)
O1 - C1	1.424(2)	O1 - C12	1.431(2)
O2 - C2	1.443(2)	O2 - C3	1.432(2)
O3 - C4	1.439(2)	O3 - C5	1.443(2)
O4 - C6	1.425(2)	O4 - C7	1.435(2)
O5 - C8	1.437(2)	O5 - C9	1.435(2)
O6 - C10	1.431(2)	O6 - C11	1.436(2)
C1 - C2	1.496(3)	C3 - C4	1.506(3)
C5 - C6	1.496(3)	C7 - C8	1.498(3)
C9 - C10	1.506(3)	C11 - C12	1.498(3)
S1 - C13	1.653(2)	S2 - C14	1.648(2)
N1 - C13	1.162(2)	N2 - C14	1.162(2)
LI1+ - OW1	1.966(3)	LI1+ - OW2	1.899(4)
LI1+ - O3	2.073(3)	LI1+ - O4	1.995(3)
LI2+ - OW1	1.996(3)	LI2+ - O2	1.991(3)
LI2+ - N1	2.011(4)	LI2+ - N2	1.998(4)
OW1 - O5	2.803(2)	OW1 - O6	2.755(2)

ANGLE	(°)	ANGLE	(°)
O1 - C1 - C2	108.4(1)	C1 - O1 - C12	112.0(1)
O1 - C12 - C11	108.4(1)	O2 - C2 - C1	108.6(1)
C2 - O2 - C3	112.7(1)	O2 - C3 - C4	113.6(2)
O3 - C4 - C3	109.6(1)	C4 - O3 - C5	110.4(1)
O3 - C5 - C6	108.2(1)	O4 - C6 - C5	107.0(1)
C6 - O4 - C7	114.5(1)	O4 - C7 - C8	108.3(1)
O5 - C8 - C7	109.8(1)	C8 - O5 - C9	111.2(1)
O5 - C9 - C10	108.1(1)	O6 - C10 - C9	113.2(1)
C10 - O6 - C11	112.1(1)	O6 - C11 - C12	109.5(1)
S1 - C13 - N1	178.6(2)	S2 - C14 - N2	179.1(2)

DIHEDRAL ANGLE	(°)
C11 - C12 - O1 - C1	169.3(1)
C12 - O1 - C1 - C2	177.3(1)
O2 - C2 - C1 - O1	-66.7(2)
C3 - O2 - C2 - C1	-171.4(1)
C4 - C3 - O2 - C2	-77.9(2)
O3 - C4 - C3 - O2	-62.4(2)
C5 - O3 - C4 - C3	-171.0(1)
C6 - C5 - O3 - C4	-175.4(1)
O4 - C6 - C5 - O3	56.3(2)
C7 - O4 - C6 - C5	165.3(1)
C8 - C7 - O4 - C6	-165.7(1)
O5 - C8 - C7 - O4	-67.9(2)
C9 - O5 - C8 - C7	172.6(1)
C10 - C9 - O5 - C8	175.4(1)
O6 - C10 - C9 - O5	69.9(2)
C11 - O6 - C10 - C9	86.2(2)
C12 - C11 - O6 - C10	-176.6(1)
O6 - C11 - C12 - O1	65.2(2)

and dihedral angles are calculated from the correlation matrix of the final least squares refinement. Hydrogen atoms were included in the structure factor calculations, but not refined. Anisotropic temperature factors were introduced for all non-hydrogen atoms. Methylene hydrogen positions were calculated while those of the water molecules were localized in difference Fourier maps.

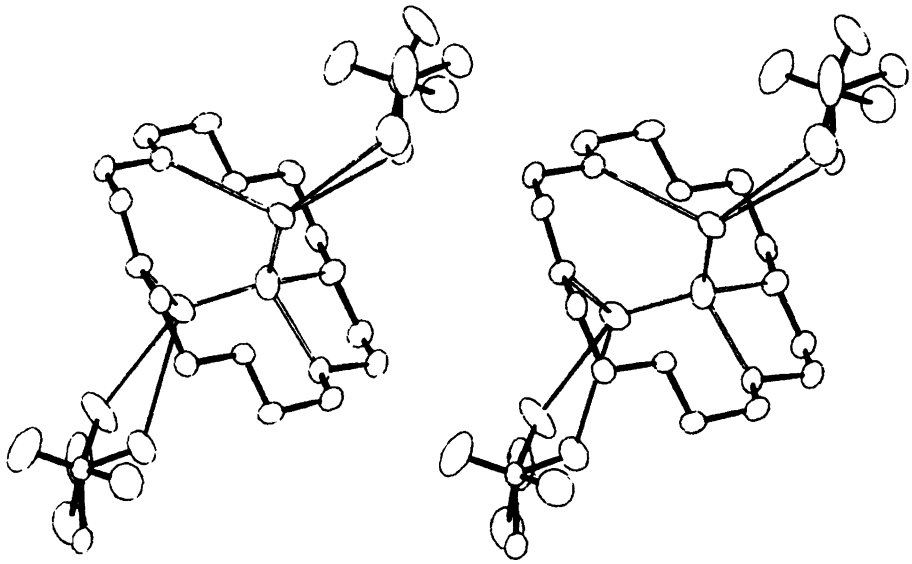

Fig. 4. Stereoscopic view of the complex $LiClO_4 \cdot (CH_2CH_2O)_6 \cdot 2H_2O$.

The final R value for the perchlorate complex was 5.4% ($R_w = 4.8\%$) for 2451 observed reflections. Corresponding values for the thiocyanate complex were $R = 3.0\%$ and $R_w = 3.4\%$ for 3019 observed reflections. Maximum root mean squares anisotropic thermal amplitudes range from 0.17 to 0.40 Å [for (I)] and from 0.15 to 0.22 Å [for (II)].

Final fractional coordinates for (I) are listed in Table 2, and the corresponding values for (II) may be found in Table 3. Bond distances and angles and dihedral angles for (I) and (II), respectively, are given in Table 4 and Table 5.

The torsional angles of Table 4 reveal that the cyclic hexaether of the perchlorate complex adopts the non-angular D_{3d} conformation shown in Fig. 1(a), while those of Table 5 for the thiocyanate complex correspond to the biangular conformation, [8, 10], illustrated in Fig. 3.

Fig. 4 is a stereoscopic view of the complex (I). It may be seen that three oxygens of the perchlorate anion are disordered, and Table 4 shows that these three accept hydrogen bonds from the two water molecules. In addition, two of the crown ether oxygens serve as hydrogen bond acceptors. The

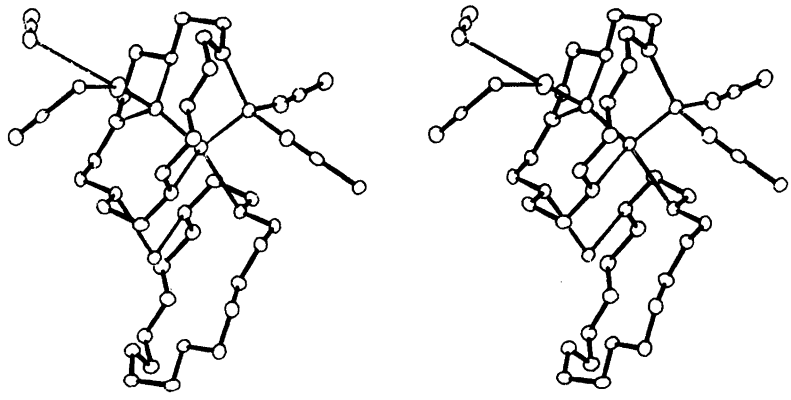

Fig. 5. Stereoscopic view of the complex $(LiSCN)_2(CH_2CH_2O)_6 \cdot 2H_2O$.

lithium cation is coordinated to both water molecules and two ring oxygens. The hydrogen bonds create chains of alternating dihydrated complexes and perchlorate anions.

A stereoscopic view of the (2:1) lithium thiocyanate complex, (II), is presented in Fig. 5. Each lithium cation has four-fold coordination. One is coordinated to two ether oxygens and two water molecules, the other to one ether oxygen, one water molecule and two nitrogens of the thiocyanate anions. Two different ring oxygens in symmetry-related cyclic hexaethers serve as hydrogen bond acceptors for one of the water molecules, while the sulphur atoms of SCN^- accept those of the other. These bonds create a somewhat complicated three-dimensional network.

In both structures the (18-crown-6) ring skeleton, which is too large for the small Li^+ ion, is effectively narrowed by the encapsulated water molecules with the double role of acting as coordinating agents towards Li^+ and hydrogen bond donors towards the ether oxygens. Whether a ring deformation alone, in the absence of any uncharged substrate particles, is able to establish a geometry compatible with the coordination preferences for Li^+, remains to be seen.

Corresponding bond lengths and bond angles of Table 4 and Table 5 do not deviate significantly. They also agree, within error limits, with earlier findings.[1]

Lists of thermal parameters and observed and calculated structure factors are available from the author.

REFERENCES

1. Dunitz, J. D., Dobler, M., Seiler, P. and Phizackerley, R. P. *Acta Crystallogr. B 30* (1974) 2733.
2. Kaufmann, R., Knöchel, A., Kopf, J., Oehler, J. and Rudolph, G. *Chem. Ber. 110* (1977) 2249.
3. Goldberg, I. *Acta Crystallogr. B 31* (1975) 754.
4. Knöchel, A., Kopf, J., Oehler, J. and Rudolph, G. *Inorg. Nucl. Chem. Lett. 14* (1978) 61.
5. Knöchel, A., Kopf, J., Oehler, J. and Rudolph, G. *Chem. Commun.* (1978) 595.
6. Germain, G., Main, P. and Woolfson, M. M. *Acta Crystallogr. A 29* (1971) 368.
7. Groth, P. *Acta Chem. Scand. 27* (1973) 1837.

Received May 22, 1981.

Acta Chemica Scandinavica A 36 (1982) 117–123

Hydrogen Isotope Disproportionation and Fractionation Equilibria in H_2O-D_2O Solvent System. I. Fractionation of Deuterium between Trihalomethanes and Water

PIRKETTA SCHARLIN

Department of Chemistry and Biochemistry, University of Turku, SF-20500 Turku 50, Finland

The equilibrium constant of the isotope disproportionation reaction between H_2O and D_2O in liquid phase has been calculated from isotope fractionation factor measurements carried out with trichloromethane, bromodichloromethane and tribromomethane in different H_2O-D_2O mixtures. A value of 3.76(6) was obtained for the equilibrium constant $K(HDO)^2$. The statistical value is $K(HDO)^2=4$. The effect of a breakdown of the postulate of the geometric mean on the isotope fractionation equilibria of substrates with one exchangeable hydrogen is discussed.

The isotope disproportionation equilibrium $H_2O+D_2O=2$ HDO is important in the treatment of solvent isotope effects in mixtures of H_2O and D_2O. In the simple theory of solvent isotope effects[1-3] one of the assumptions made is that the postulate of the geometric mean[4] (PGM) governs the isotope disproportionation equilibria involved. According to the PGM, the equilibrium constant of the reaction $H_2O+D_2O=2$ HDO has already at ordinary temperatures its classisal value 4, which is determined by symmetry considerations alone. By means of the PGM the calculations can be appreciably simplified. The correct value of the equilibrium constant of the isotope disproportionation reaction of water both in gas and liquid phase has occupied the mind of scientists ever since the discovery of deuterium.[5-21] It has been shown that the PGM does not hold for the mixtures of H_2O and D_2O. A breakdown of the PGM in the isotope disproportionation reaction of water has straightforward consequences for the isotope fractionation equilibria in the H_2O-D_2O solvent system. In particular, knowledge of the exact value of the equilibrium constant is of great importance for the theory of solvent deuterium isotope effects. In spite of the importance of the isotope disproportionation equilibrium of liquid water there has, however, been quite a lot of discordance in the values of the equilibrium constant of this reaction. Besides, most of the experimental studies carried out are associated with the gas phase. The aim of this work was to acquire more experimental information about the hydrogen isotope disproportionation in the liquid phase and about the effect of a breakdown of the PGM on the istope fractionation equilibria in the H_2O-D_2O solvent system. An indirect method was used to determine the value of equilibrium constant of the isotope disproportionation reaction of liquid water. The method is based on the fact that for the deuterium isotope fractionation in a substrate with only one exchangeable hydrogen, the deviations from the PGM are confined to the solvent water and are reflected in the dependence of the fractionation factor upon the deuterium isotope mol fraction of water.

EXPERIMENTAL

Materials. Trichloromethane (E. Merck AG, *pro analysi*) was used as received. Bromodichloromethane (EGA-Chemie KG) and tribromomethane (E. Merck AG, reinst) were distilled once before use.

Deuteriotrichloromethane, deuteriobromodichloromethane and deuteriotribromomethane were prepared by shaking trihalomethane and deuterium oxide at 25 °C with NaOD as catalyst. The reactions were followed by ^1H NMR spectroscopy (a 60 MHz

0302-4377/82/020117-07$02.50

Perkin-Elmer Model R 10 spectrometer). The deuterium oxide portions "worsened" in the reactions were replaced by fresh portions of D_2O, the procedure being repeated five times in all. In each portion of D_2O the deuterium excess over trihalomethane was about threefold. The deuteriotrihalomethanes were dried over anhydrous $MgSO_4$ and distilled. The final degree of deuteriation was determined by ^1H NMR spectroscopy and was found to be 99.7 % for the deuteriotrichloromethane, 99.1 % for the deuteriobromodichloromethane and 98.9 % for the deuteriotribromomethane.

The deuterium oxide used in the experiments was a product of Norsk Hydro-elektrisk Kvaelstofaktieselskab. The deuterium isotope mol fraction of D_2O was reported to be 0.998.

For the equilibration experiments the sodium hydroxide – sodium deuteroxide solutions, in which the deuterium isotope mol fraction of water varied between 0.1 – 0.9, were usually prepared by weight from pure light and heavy water, adding a suitable amount of NaOL (L=H, D) just before the equilibrations. When calculating the solvent deuterium isotope mol fraction of each solution, the increase of H_2O or D_2O coming from the added catalyst solution was taken into consideration. For the equilibrations of trichloromethane, aqueous NaOL-solutions were prepared by mixing aqueous NaOH- and NaOD-solutions in suitable volumetric ratios. To calculate the deuterium isotope mol fraction of water in the mixed solutions, the densities of the NaOH- and NaOD-solutions were determined. The aqueous sodium hydroxide solution was prepared from a standard Titrisol solution (E. Merck AG) by dilution with distilled water. The corresponding sodium deuteroxide solution was made by diluting a stock solution of NaOD with deuterium oxide. The stock solution was prepared by dissolving metallic sodium in deuterium oxide under toluene in a separating funnel. The base concentration of the sodium deuteroxide solution was determined by titration with a known acid solution.

For IR-measurements the reference solutions of trihalomethanes in CCl_4 were prepared by adding suitable amounts of CHX_3 and CDX_3 (X=Cl, Br) to 2 cm^3 portions of carbon tetrachloride with the aid of an Agla micrometer syringe. The total volume of CLX, in each solution was 0.05 – 0.06 cm^3. The mol fraction of CDX_3 in the CLX_3-solutions varied between 0 – 0.997. The molar volumes of a trihalomethane and the corresponding deuteriotrihalomethane were assumed to be equal.

Equilibration experiments. In the equilibrations the substrate – catalyst – water mixtures were shaken in 50 cm^3 separating funnels surrounded by a jacket for water circulation. The system was held at a constant temperature of 25.0 °C within ±0.1 °C with water circulating from a Lauda thermostat. The time of equilibration was maintained about ten times longer than the time that was found necessary just to attain the equilibrium. In the equilibrations the suitable concentration of catalyst was in the range 0.001 – 0.01 mol dm^{-3}, the volume of catalyst – water solution was 40 cm^3, the amount of substrate varied in the range of 0.00067 – 0.0031 mol and the time of equilibration was between 1 – 2 h depending on the trihalomethane. After the equilibrium was reached, 10 cm^3 samples were taken from the equilibrium mixtures by means of a semiautomatic pipette. The samples were transferred to 25 cm^3 separating funnels containing an acid solution for neutralization of the sample and carbon tetrachloride (1 cm^3) for extraction of the equilibrated substrate. From each equilibrium mixture 3 – 10 samples were taken. After extraction the deuterium content of the substrate was determined by IR measurements.

IR measurements. The measurements were made with a Perkin-Elmer Model 180 IR spectrophotometer using sealed KBr cells of a fixed path length of 0.1 mm. Before the IR analysis the extracts from the equilibrium mixtures were dried over anhydrous $MgSO_4$. The spectra of the extracts were recorded immediately after the spectra of the reference solutions. The characteristic absorbtion peaks used in the analysis were those arising from the C – H and C – D deformation vibrations of the trihalomethanes: 1213 and 907 cm^{-1} for $CLCl_3$, 1205, 1164, 898 and 866 cm^{-1} for $CLCl_2Br$ and 1140, 860 and 845 cm^{-1} for $CLBr_3$. For each of the three trihalomethanes examined in this work, a good linear correlation was found to exist between the

Table 1. Mol ratios of deuterium and protium in trichloromethane equilibrated in different H_2O – D_2O mixtures and the experimental fractionation factors $\phi'(CHCl_3)$ at 298.2 K.

$x(D;L_2O)$ [a]	$\frac{n(D;CLCl_3)}{n(H;CLCl_3)}$ [b]	$\phi'(CHCl_3)$ [b]
0.0993	0.1290(5)	1.171(5)
0.199	0.2751(13)	1.109(6)
0.298	0.4762(16)	1.120(4)
0.398	0.7284(7)	1.102(1)
0.498	1.086(7)	1.097(7)
0.597	1.634(8)	1.102(6)
0.697	2.455(11)	1.067(5)
0.797	4.42(2)	1.126(6)
0.897	9.49(16)	1.091(19)

[a] $x(D;L_2O)$ is the deuterium isotope mole fraction of water. [b] Mean values of 8 – 10 determinations with standard errors of mean.

Table 2. Mol ratios of deuterium and protium in bromodichloromethane equilibrated in different H_2O-D_2O mixtures and the experimental fractionation factors $\phi'(CHCl_2Br)$ at 298.2 K.

$x(D;L_2O)^a$	$\frac{n(D;CLCl_2Br)_b}{n(H;CLCl_2Br)}$	$\phi'(CHCl_2Br)^b$
0.103	0.1338(7)	1.165(6)
0.204	0.2830(18)	1.104(7)
0.284	0.4331(12)	1.092(3)
0.401	0.715(3)	1.068(4)
0.475	0.955(3)	1.056(4)
0.610	1.672(11)	1.069(7)
0.699	2.54(2)	1.093(8)
0.807	4.46(4)	1.067(8)
0.897	9.47(11)	1.088(12)

[a] $x(D;L_2O)$ is the deuterium isotope mol fraction of water. [b] Mean values of 8 determinations with standard errors of mean.

Table 3. Mol ratios of deuterium and protium in tribromomethane equilibrated in different H_2O-D_2O mixtures and the experimental fractionation factors $\phi'(CHBr_3)$ at 298.2 K.

$x(D;L_2O)^a$	$\frac{n(D;CLBr_3)_b}{n(H;CLBr_3)}$	$\phi'(CHBr_3)^b$
0.105	0.1266(7)	1.079(5)
0.108	0.1301(17)	1.074(13)
0.202	0.274(3)	1.081(9)
0.214	0.291(2)	1.070(7)
0.316	0.488(6)	1.056(11)
0.333	0.527(9)	1.056(16)
0.397	0.684(3)	1.039(4)
0.402	0.700(6)	1.041(8)
0.500	1.029(4)	1.029(4)
0.506	1.057(5)	1.032(5)
0.599	1.534(6)	1.027(4)
0.601	1.554(6)	1.031(3)
0.693	2.308(14)	1.023(6)
0.704	2.439(13)	1.025(5)
0.800	4.128(7)	1.032(2)
0.802	4.175(19)	1.031(3)
0.897	8.96(8)	1.028(8)

[a] $x(D;L_2O)$ is the deuterium isotope mol fraction of water. [b] Mean values of 3 – 4 determinations with standard errors of mean.

mol fractions of CDX_3 and the absorbances measured from the spectra of the reference solutions. The correlation coefficients for the straight lines were in the range of 0.9953 – 0.9999. The results from the equilibrations of the trihalomethanes are listed in Tables 1 – 3.

DISCUSSION

Calculation of $K(HDO)^2$. When a substrate SH containing one exchangeable hydrogen is dissolved in water of arbitrary deuterium content, the following equilibria are set up: disproportionation equilibrium (1) between isotopically different waters, isotopic fractionation equilibrium (2) between the substrate and the solvent water, and isotopic exchange equilibria (3) and (4), which are not independent ones, but can be presented by combinations of equilibria (1) and (2).

$$H_2O + D_2O = 2\ HDO \quad (1)$$

$$SH + \tfrac{1}{2}\ D_2O = SD + \tfrac{1}{2}\ H_2O \quad (2)$$

$$SH + D_2O = SD + HDO \quad (3)$$

$$SH + HDO = SD + H_2O \quad (4)$$

In the following approach it is assumed that in the expressions of equilibrium constants the activities can be replaced by mol fractions. The equilibrium constants of the equilibria (1) and (2) are expressed by eqns. (5) and (6). The fractionation factor $\phi'(SH)$,

$$K(HDO)^2 = \frac{x(HDO)^2}{x(H_2O)x(D_2O)} \quad (5)$$

$$\phi(SH) = \frac{x(SD)}{x(SH)}\left[\frac{x(H_2O)}{x(D_2O)}\right]^{\frac{1}{2}} \quad (6)$$

which is an experimentally determinable quantity, is defined according to eqn. (7), where n is the amount of deuterium or protium in SL or L_2O, L = H, D and $x(D;L_2O)$ is the deuterium isotope mol fraction of solvent water. In terms of mol fractions of isotopic water species, the deuterium isotope mol fraction of water can be expressed by eqn. (8). Using eqn. (8) and the fact that $x(D_2O)+x(HDO)+x(H_2O)=1$, eqns. (9) and (10) are obtained for $x(HDO)$ and $x(H_2O)$. When equations (5), (9) and (10) are solved

$$\phi'(SH) = \frac{n(D;SL)}{n(H;SL)} : \frac{n(D;L_2O)}{n(H;L_2O)} = \frac{x(SD)}{x(SH)} \times \frac{1-x(D;L_2O)}{x(D;L_2O)} \quad (7)$$

$$x(D;L_2O) = x(D_2O) + \tfrac{1}{2}x(HDO) \quad (8)$$

$$x(HDO) = 2[x(D;L_2O) - x(D_2O)] \quad (9)$$

$$x(H_2O) = 1 - 2x(D;L_2O) + x(D_2O) \quad (10)$$

$$\phi(\mathrm{SH}) = \phi'(\mathrm{SH})\frac{x(\mathrm{D};\mathrm{L_2O})}{1-x(\mathrm{D};\mathrm{L_2O})} \times$$

$$\sqrt{\frac{2[1-x(\mathrm{D};\mathrm{L_2O})][4-K(\mathrm{HDO})^2]+K(\mathrm{HDO})^2-\sqrt{\mathrm{F}\{K(\mathrm{HDO})^2;x(\mathrm{D};\mathrm{L_2O})\}}}{2x(\mathrm{D};\mathrm{L_2O})[4-K(\mathrm{HDO})^2]+K(\mathrm{HDO})^2-\sqrt{\mathrm{F}\{K(\mathrm{HDO})^2;x(\mathrm{D};\mathrm{L_2O})\}}}} \qquad (11)$$

where $\mathrm{F}\{K(\mathrm{HDO})^2;\ x(\mathrm{D};\mathrm{L_2O})\} = K(\mathrm{HDO})^4 + 4K(\mathrm{HDO})^2[4-K(\mathrm{HDO})^2]x(\mathrm{D};\mathrm{L_2O})[1-x(\mathrm{D};\mathrm{L_2O})]$

simultaneously, the mol fractions of the three isotopic water species are obtained in terms of $K(\mathrm{HDO})^2$ and $x(\mathrm{D};\mathrm{L_2O})$. The expressions for these mol fractions together with eqns. (6) and (7) lead to eqn. (11) for the computation of the equilibrium constants $K(\mathrm{HDO})^2$ and $\phi(\mathrm{SH})$.*

The results obtained when the experimental data from Tables 1 – 3 are applied to eqn. (11) are listed in Table 4. The calculations were performed with a UNIVAC 1108 computer. The mean of the three $K(\mathrm{HDO})^2$ values from Table 4 is $K(\mathrm{HDO})^2 = 3.76(6)$. When this value is used for the equilibrium constant of reaction (1), values for the mol fractions of the different water species in the water of the deuterium isotope mol fraction $x(\mathrm{D};\mathrm{L_2O})$, listed in Table 5, are obtained.

Effect of Value of $K(HDO)^2$ *on* $\phi(SH)$. All equilibria described by (2) contain the ratio $[x(\mathrm{D_2O})/x(\mathrm{H_2O})]^{\frac{1}{2}}$, *cf.* eqn. (6). If the PGM were to be valid in regard to the $\mathrm{H_2O}-\mathrm{D_2O}$ mixtures, the ratio of the mol fractions could be expressed by eqn. (12). Actually the right side of eqn. (12) must be expressed by eqn. (13), where $x(\mathrm{HDO}) = K(\mathrm{HDO}) \times [x(\mathrm{H_2O})x(\mathrm{D_2O})]^{\frac{1}{2}}$. Solving the quadratic equation that results from eqn. (13), an exact equation (14) is obtained for the ratio $[x(\mathrm{D_2O})/x(\mathrm{H_2O})]^{\frac{1}{2}}$.

Table 4. Equilibrium constants of the isotope disproportionation reaction $\mathrm{H_2O}+\mathrm{D_2O}=2\ \mathrm{HDO}$, $K(\mathrm{HDO})^2$, and isotope fractionation reaction $\mathrm{SH}+\frac{1}{2}\ \mathrm{D_2O}=\mathrm{SD}+\frac{1}{2}\ \mathrm{H_2O}$, $\phi(\mathrm{SH})$, in the liquid state at 298.2 K.

SH	$\phi(\mathrm{SH})$	$K(\mathrm{HDO})^2$	Data in Table
$CHCl_3$	1.107(7)	3.79(7)	1
$CHCl_2Br$	1.083(9)	3.77(7)	2
$CHBr_3$	1.041(3)	3.73(5)	3

Table 5. Values for mol fractions of different water species in water of the deuterium isotope mol fraction $x(\mathrm{D};\mathrm{L_2O})$ when $K(\mathrm{HDO})^2 = 3.76$.

$x(\mathrm{D};\mathrm{L_2O})$	$x(\mathrm{H_2O})$	$x(\mathrm{HDO})$	$x(\mathrm{D_2O})$
0.0	1.0000	0.0000	0.0000
0.10	0.8105	0.1790	0.0105
0.20	0.6416	0.3168	0.0416
0.30	0.4927	0.4145	0.0927
0.40	0.3636	0.4729	0.1636
0.50	0.2539	0.4923	0.2539
0.60	0.1636	0.4729	0.3636
0.70	0.0927	0.4145	0.4927
0.80	0.0416	0.3168	0.6416
0.90	0.0105	0.1790	0.8105
1.00	0.0000	0.0000	1.0000

$$\left[\frac{x(\mathrm{D_2O})}{x(\mathrm{H_2O})}\right]^{\frac{1}{2}} = \frac{x(\mathrm{D};\mathrm{L_2O})}{1-x(\mathrm{D};\mathrm{L_2O})} \qquad (12)$$

$$\frac{x(\mathrm{D};\mathrm{L_2O})}{1-x(\mathrm{D};\mathrm{L_2O})} = \frac{2x(\mathrm{D_2O})+x(\mathrm{HDO})}{2x(\mathrm{H_2O})+x(\mathrm{HDO})} \qquad (13)$$

*A referee has pointed out that eqn. (11) can be simplified to

$$\phi(\mathrm{SH}) = \phi'(\mathrm{SH})\left\{\frac{\sqrt{[2x(\mathrm{D};\mathrm{L_2O})-1]^2K(\mathrm{HDO})^2+16x(\mathrm{D};\mathrm{L_2O})[1-x(\mathrm{D};\mathrm{L_2O})]}}{4[1-x(\mathrm{D};\mathrm{L_2O})]} - \frac{[2x(\mathrm{D};\mathrm{L_2O})-1]K(\mathrm{HDO})}{4[1-x(\mathrm{D};\mathrm{L_2O})]}\right\}.$$

The computations have not been repeated with this version since it was found that the above equation gives the same values of $K(\mathrm{HDO})^2$ and $\phi(\mathrm{SH})$ as those obtained from computations with eqn. (11).

$$\left[\frac{x(D_2O)}{x(H_2O)}\right]^{\ddagger} = \frac{[2x(D;L_2O)-1]K(HDO)}{4[1-x(D;L_2O)]} + \frac{\sqrt{[2x(D;L_2O)-1]^2K(HDO)^2+16x(D;L_2O)[1-x(D;L_2O)]}}{4[1-x(D;L_2O)]} \quad (14)$$

$$\left[\frac{x(D_2O)}{x(H_2O)}\right]^{\ddagger}_{real} = \gamma\left[\frac{x(D_2O)}{x(H_2O)}\right]^{\ddagger}_{PGM} = \gamma\frac{x(D;L_2O)}{1-x(D;L_2O)} \quad (15)$$

$$\gamma = \frac{[2x(D;L_2O)-1]K(HDO)}{4x(D;L_2O)} + \frac{\sqrt{[2x(D;L_2O)-1]^2K(HDO)^2+16x(D;L_2O)[1-x(D;L_2O)]}}{4x(D;L_2O)} \quad (16)$$

$$\gamma = [-0.06144(12)]x(D;L_2O) + 1.03086(7) \quad (r = -0.99997) \quad (17)$$

$$\left[\frac{x(D_2O)}{x(H_2O)}\right]^{\ddagger} = [1.03086 - 0.06144x(D;L_2O)] \times \frac{x(D;L_2O)}{1-x(D;L_2O)} \quad (18)$$

To find out direct deviations from the PGM, it is convenient to express the ratio $[x(D_2O)/x(H_2O)]^{\ddagger}$ in the form of eqn. (15) in which the coefficient γ for different values of $x(D;L_2O)$ can be calculated from eqn. (16). Applying then the method of linear least squares to values $[x(D;L_2O),\gamma]$, an expression (17) is obtained for the coefficient γ. The exact equation (14) can thus be expressed in an approximate form (18), which, when compared with eqn. (12), shows direct deviations from the PGM with different values for $x(D;L_2O)$. Combining eqns. (6), (7) and (18), a relationship (19) is obtained between the experimentally determinable fractionation factor $\phi'(SH)$ and the real fractionation factor $\phi(SH)$.

$$\phi'(SH)/\phi(SH) = 1.03086 - 0.06144x(D;L_2O) \quad (19)$$

The ratio $\phi'(SH)/\phi(SH)$ is independent of the size of the fractionation factor itself and thus it presents the dependence of the fractionation factor $\phi'(SH)$ of any substrate of type SH on the deuterium content of solvent water. The correction of $\phi'(SH)$ to obtain $\phi(SH)$ is given by $1/[1.03086-0.06144x(D;L_2O)]$ varying from 0.970 at $x(D;L_2O)=0$ to 1.032 at $x(D;L_2O)=1$, *i.e.*, 6% over the whole range of $x(D;L_2O)$.

When $x(D;L_2O)=0.5$, the ratio $[x(D_2O)/x(H_2O)]^{\ddagger}=1$ whether the PGM is valid or not. Thus the fractionation factor $\phi'(SH)$ measured in equimolar mixtures of H_2O and D_2O should be quite close to the equilibrium constant $\phi(SH)$. Also the mean value of $\phi'(SH)$, when measurements of $\phi'(SH)$ are carried out evenly over the whole range of $x(D;L_2O)$, should be only slightly different from $\phi(SH)$. The mean values of the experimental fractionation factors $\phi'(CHX_3)$ calculated from the values in Tables 1–3 are $\bar{\phi}'(CHCl_3)=1.109(10)$, $\bar{\phi}'(CHCl_2Br)=1.089(11)$ and $\bar{\phi}'(CHBr_3)=1.044(5)$. The values of $\bar{\phi}'(CHX_3)$ seem to be quite close to the real $\phi(CHX_3)$ values (Table 4). The same cannot be said about the values of $\phi'(CHX_3)$ measured at solvent deuterium isotope mol fractions of about 0.5: $\phi'(CHCl_3)=1.097(7)$ at $x(D;L_2O)=0.498$, $\phi'(CHCl_2Br)=1.056(4)$ at $x(D;L_2O)=0.475$ and $\phi'(CHBr_3)=1.029(4)$ at $x(D;L_2O)=0.500$ and $\phi'(CHBr_3)=1.032(5)$ at $x(D;L_2O)=0.506$. Taking into account the scattering in the measured $\phi'(CHX_3)$ values, it is clear that the correction for $\phi'(SH)$ using eqn. (19) will be relevant only when the experimental data are sufficiently accurate.

$$\left[\frac{x(D_2O)}{x(H_2O)}\right]^{\ddagger} = \frac{x(D;L_2O)[1-x(;L_2O)+\frac{1}{4}K(HDO)^2x(D;L_2O)]}{[1-x(D;L_2O)]\cdot\frac{1}{2}K(HDO)} \quad (20)$$

Albery and Davies[22] derived an approximate eqn. (20) for small departures from the PGM when $\frac{1}{2}K(HDO)$ is near unity. When $K(HDO)^2$ is fixed at 3.76, which is the value obtained in this work, the approximate eqn. (20) will be essentially the same as eqn. (18) obtained in this work.

The correlation between fractionation factor $\phi'(SH)$ and the deuterium isotope mol fraction of solvent water can also be expressed by means of a relative fractionation factor $\phi_r(SH)$, defined by eqn.

Table 6. Relative fractionation factor ϕ_r(SH) with different values for the deuterium isotope mol fraction of water, $x(D;L_2O)$, when $K(HDO)^2 = 3.76$.

$x(D;L_2O)$	ϕ_r(SH)	$x(D;L_2O)$	ϕ_r(SH)	$x(D;L_2O)$	ϕ_r(SH)
0.10	0.9937	0.40	0.9755	0.70	0.9578
0.20	0.9875	0.50	0.9695	0.80	0.9519
0.30	0.9815	0.60	0.9636	0.90	0.9460

$$\phi_r(SH) = \frac{\phi'(SH)}{\phi_0(SH)} = \frac{\frac{1}{2}x(HDO)}{x(H_2O)} \times \frac{1 - x(D;L_2O)}{x(D;L_2O)} \quad (21)$$

(21) as reported by Gold.[13] ϕ_0(SH) is the limit value for the fractionation factor ϕ'(SH) when $n(D;L_2O)/n(H;L_2O) \rightarrow 0$. The value of ϕ_r(SH) at different deuterium isotope mol fractions of water can be calculated from eqn. (21) using the values from Table 5 for $x(H_2O)$ and x(HDO). The values for ϕ_r(SH) are listed in Table 6. A good linear correlation (22) was found to exist between the relative fractionation factor ϕ_r(SH) and the deuterium isotope mol fraction of water, when the method of linear least squares was applied to the values in Table 6. Because the relative fractionation factor is independent of the size of the fractionation factor itself, eqn. (22) presents the dependence of the

$$\phi_r(SH) = [-0.0595(2)]x(D;L_2O) + 0.9994(1) \quad (r = -0.99997) \quad (22)$$

fractionation factor of any substrate of type SH on the deuterium isotope mol fraction of water. Only if the PGM were to be valid for the isotope disproportionation reaction of water, *i.e.*, if $K(HDO)^2 = 4$, the experimental fractionation factor ϕ'(SH) would be constant over the whole range of $x(D;L_2O)$. The dependence of ϕ'(SH) upon the deuterium isotope mol fraction of water, when $K(HDO)^2 = 3.76$, is illustrated in Fig. 1. When $x(D;L_2O)$ is expressed in terms of the mol fractions of the different water species, and eqn. (5) is applied to eqn. (21), an expression (23) is obtained for the relative fractionation factor ϕ_r(SH). Also the relative fractionation factor ϕ_r(SH) would be independent of the deuterium isotope mol fraction of water only if $K(HDO)^2$ had its statistical value of 4. As can be seen from eqn. (23), the value of ϕ_r(SH) would be unity

$$\phi_r(SH) = \frac{1}{2}\frac{K(HDO)^2 x(D_2O) + 2x(HDO)}{2x(D_2O) + x(HDO)} \quad (23)$$

over the whole range of $x(D;L_2O)$. The value of $1 - \phi_r$(SH) at $x(D;L_2O) = 1$ presents the error that can be introduced in the measurements of the fractionation factors if the deviations from the PGM are neglected.[18] From eqn. (22) a value of 0.94 can be calculated for ϕ_r(SH) with $x(D;L_2O) = 1$, and thus the error will be about 6%.

In summary, the experimental results obtained in this work support the view that at present the use of

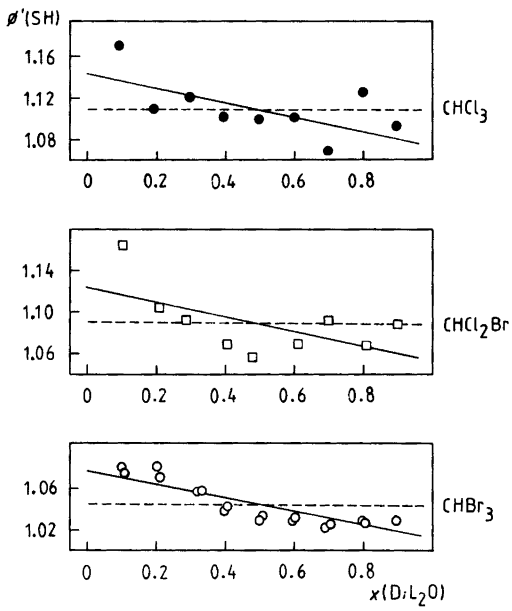

Fig. 1. Dependence of fractionation factor ϕ'(SH) upon the deuterium isotope mol fraction of water, $x(D;L_2O)$, when $K(HDO)^2 = 3.76$. The fractionation factors ϕ'(SH) for drawing the unbroken straight lines were calculated using the ϕ_r(SH) values from Table 6 so that each ϕ'(SH) at $x(D;L_2O) = 0.5$ was to be the mean value of the experimental fractionation factors measured for the trihalomethanes (Tables 1, 2 and 3). The broken lines for ϕ'(SH) represent the situation if the PGM were to be valid for the disproportionation reaction of water, *i.e.* if $K(HDO)^2 = 4$.

the PGM in the isotope disproportionation equilibrium of water provides a good approximation in the treatment of solvent isotope effects in mixtures of H_2O and D_2O. The exact value of the equilibrium constant becomes important if the experimental accuracy is essentially improved. It seems, however, that if the fractionation factor measurements with substrates of type SH are carried out at either end of the range of deuterium isotope mol fraction of water, they should be corrected.

Acknowledgements. Financial aid from the Emil Aaltonen Foundation, and from the Finnish Cultural Foundation is gratefully acknowledged.

REFERENCES

1. Schaleger, L. L., Salomaa, P. and Long, F. A. In Conway, B. E. and Barradas, R. G., Eds., *Chemical Physics of Ionic Solutions*, Wiley, New York 1966, Chapter 13.
2. Gold, V. *Adv. Phys. Org. Chem. 7* (1969) 259.
3. Salomaa, P. *Acta Chem. Scand. 23* (1969) 2095.
4. Bigeleisen, J. *J. Chem. Phys. 23* (1955) 2264.
5. Nelson, W. E. and Butler, J. A. V. *J. Chem. Soc.* (1938) 958.
6. Urey, H. C. *J. Chem. Soc.* (1947) 562.
7. Holmes, J. R., Kivelson, D. and Drinkard, W. C. *J. Chem. Phys. 37* (1962) 150.
8. Pyper, J. W. and Long, F. A. *J. Chem. Phys. 41* (1969) 2213.
9. Papousek, D. and Pliva, J. *Collect. Czech. Chem. Commun. 29* (1964) 1973; *via* Weston, R. E., Jr. *J. Chem. Phys. 42* (1965) 2635.
10. Friedman, L. and Shiner, V. J., Jr. *J. Chem. Phys. 44* (1966) 4693.
11. Pyper, J. W., Newbury, R. S. and Barton, G. W., Jr. *J. Chem. Phys. 46* (1967) 2253.
12. Kresge, A. J. and Chiang, Y. *J. Chem. Phys. 49* (1968) 1439.
13. Gold, V. *Trans. Faraday Soc. 64* (1968) 2770.
14. Hulston, J. R. *J. Chem. Phys. 50* (1969) 1483.
15. Wolfsberg, M. *J. Chem. Phys. 50* (1969) 1484.
16. Jones, N. A., Friesen, R. D. and Pyper, J. W. *Rev. Sci. Instrum. 41* (1970) 1828.
17. Gold, V. and Tomlinson, C. *Chem. Commun.* (1970) 472.
18. More O'Ferral, R. A., Koeppl, G. W. and Kresge, A. J. *J. Am. Chem. Soc. 93* (1971) 9.
19. Van Hook, W. A. *Chem. Commun.* (1972) 479.
20. Pyper, J. W. and Christensen, L. D. *J. Chem. Phys. 62* (1975) 2596.
21. Pyper, J. W., Dupzyk, R. J., Friesen, R. D., Bernasek, S. L., May, C. A., Echeverria, A. W. and Tolman, L. F. *Int. J. Mass Spectrom. Ion Phys. 23* (1977) 209.
22. Albery, W. J. and Davies, M. H. *Trans. Faraday Soc. 65* (1969) 1059.

Received June 2, 1981.

Acta Chemica Scandinavica A 36 (1982) 125–135

On the Structures of the Hydrated Thallium(III) Ion and its Bromide Complexes in Aqueous Solution

JULIUS GLASER and GEORG JOHANSSON

Department of Inorganic Chemistry, Royal Institute of Technology (KTH), S-100 44 Stockholm, Sweden

From X-ray diffraction measurements on concentrated aqueous solutions of thallium(III) and different concentrations of bromide, the structures of the $TlBr_n(H_2O)_m^{3-n}$ ($n=0,2,3,4$) complexes have been determined. The hydrated thallium(III) ion, present in acid solutions of $Tl(ClO_4)_3$, is shown to contain six equidistant water molecules with a Tl–O bond length of 2.235(5) Å. The second complex, $TlBr_2^+$, is linear with a Tl–Br distance of 2.481(2) Å and is probably associated with four water molecules leading to an octahedral species $TlBr_2(H_2O)_4^+$. For the third complex, $TlBr_3$, the data are consistent with a planar triangular geometry with a Tl–Br bond length of 2.512(2) Å. Two water molecules are probably bonded to this complex, leading to a trigonal–bipyramidal $TlBr_3(H_2O)_2$ species. The $TlBr_4^-$ complex is tetrahedral with the Tl–Br bond length 2.564(2) Å. For large bromide to thallium ratios the formation of higher species $TlBr_n^{3-n}$ ($n>4$) is indicated. Polynuclear species have not been found to be present in the solutions investigated.

The thallium(III) bromide complexes, which are among the most stable complexes known,[1] have been extensively investigated by several different methods.[2] The presence of $TlBr^{2+}$, $TlBr_2^+$, $TlBr_3$, and $TlBr_4^-$ is well-established for dilute aqueous solutions.[3–6] The existence of higher species, such as $TlBr_5^{2-}$ or $TlBr_6^{3-}$, has for a long time been a matter of controversy.[2] Thus, potentiometric,[3–5] solubility,[4b] and calorimetric measurements[3,6] have been interpreted to show that the formation of higher complexes is negligible. NMR measurements on concentrated aqueous solutions have been claimed to indicate that $Tl_2Br_9^{3-}$ is the dominant species at high bromide concentrations.[7] A recent NMR study of the same system[8] has been found to be consistent with only one higher complex formed, probably $TlBr_6^{3-}$, with the very small formation constant $K_{4,6}=[TlBr_6^{3-}]/([TlBr_4^-][Br^-]^2)=2\times 10^{-3}\ M^{-2}$.

Very little is known about the structures of the aqua and bromide complexes of Tl(III) in solution. It has been suggested that in aqueous solutions of $Tl(ClO_4)_3$ only two water molecules are strongly bound to Tl^{3+}.[9,10] For the $TlBr_4^-$ ion Raman spectra in CH_2Cl_2 and also in ethanolic and in aqueous solutions have been found to be consistent with a tetrahedral structure.[11]

The thallium(III) bromide complexes have well-separated regions of existence (Fig. 1). It is possible, therefore, to prepare solutions in which one single complex dominates and, since the complexes are also highly soluble, this makes them favorable for a structure determination by means of diffraction methods. The compositions of the solutions used for the present investigation are given in Fig. 1 and in Table 1. They were chosen to contain a maximal amount of each of the different complexes $TlBr_2^+$ (in BR2), $TlBr_3$ (in BR3), $TlBr_4^-$ (in $BR4_1$ and $BR4_2$), and of the hydrated metal ion (in TL1 and TL2). The $TlBr^{2+}$ complex could not be investigated because of the spontaneous reduction of Tl(III) by the bromide ion in the corresponding solution.

The stability constants used for the calculation of the distribution of complexes in Fig. 1 were derived for the concentrations used here by a procedure described in a previous paper.[8]

EXPERIMENTAL

Stock solutions were prepared and analyzed as described previously.[12] The compositions of the

0302-4377/82/020125-11$02.50

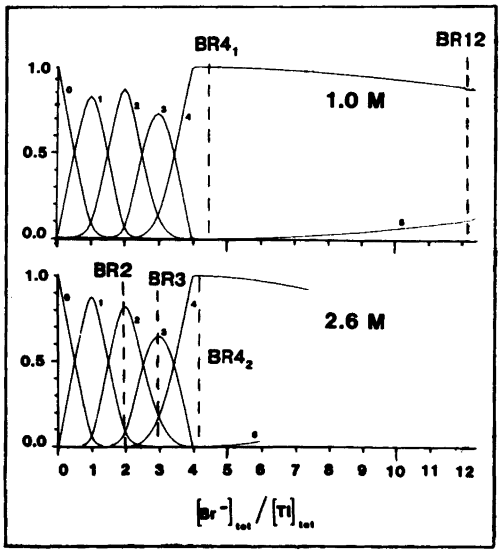

Fig. 1. Fraction of Tl(III) present as $TlBr_n^{3-n}$ as a function of the bromide to thallium ratio (from Ref. 8) for two different total thallium concentrations. The compositions of the solutions, investigated in the present work, are indicated by the broken lines (the lines for the perchlorate solutions TL1 and TL2 coincide with the vertical axes).

solutions used for the X-ray scattering measurements are given in Table 1. The amount of Tl(I) was always less than 0.3 % of the total thallium concentration. The scattered radiation ($\lambda_{MoK\alpha}=0.7107$ Å) monochromatized by a focusing single crystal of lithium fluoride placed in the diffracted beam, was measured as a function of the scattering angle in a $\theta-\theta$ diffractometer described previously.[13] The intensities were measured at discrete points at intervals of 0.1° for $1°<\theta<21°$ and 0.25° for $21°<\theta<70°$, corresponding to the s range 0.3 $Å^{-1}<s=4\pi\lambda^{-1}\sin\theta<16.7\,Å^{-1}$. Typically 10^5 counts were accumulated for each point. A complete data collection was performed twice for each solution.

Raman spectra were recorded using a Cary 82 (Ar, 4881 Å line) and a Coderg T800 (Kr, 5682 Å line) laser spectrophotometer.

DATA TREATMENT

After recalculation to a common slit width the intensity data were corrected for multiple scattering and polarization and were normalized to a stoichiometric unit of colume containing one Tl atom. The normalization was done by comparing observed intensities with the calculated sum of independent coherent and incoherent scattering in the high angle part of the intensity curve. The integration method[14] usually gave the same value for the scaling factor. Reduced intensities $i(s)$ were calculated from the expression $i(s)=I(s)-\sum_i n_i f_i^2(s)$, where $I(s)$ are the normalized observed intensities after subtraction of the incoherent scattering and f_i are the scattering factors of the atoms. The summation is taken over all atoms in the stoichiometric unit of volume.

The scattering factors for neutral atoms were taken from the International Tables for X-Ray Crystallography (1974).[15] Intensity contributions from water molecules were calculated using the molecular scattering factors for H_2O given by Narten *et al.*[16]

The incoherent scattering values were those given by Cromer *et al.*,[17a] Cromer[17b] and Compton *et al.*[17c] All calculations were carried out with the aid of computer programs decribed in a previous paper.[18] Radial distribution functions (RDF's), $D(r)$ and $D(r)-4\pi r^2\rho_o$, were calculated with a sharpening function

Table 1. Compositions (in mol/l) of the investigated solutions.

Solution	Tl	Br	Li	H^+	ClO_4	H_2O	Ratio Br/Tl
TL1	1.00	–	–	2.68	5.68	42.3	0
TL2	2.10	–	–	2.65	8.95	35.9	0
BR2	2.74	5.48	–	0.13	2.87	41.5	2.0
BR3	2.59	7.77	–	–	–	43.4	3.0
$BR4_2$	2.64	10.74	2.82	–	–	38.1	4.1
$BR4_1$	1.02	4.59	1.53	–	–	47.7	4.5
BR12	1.06	13.00	9.82	–	–	35.0	12.3

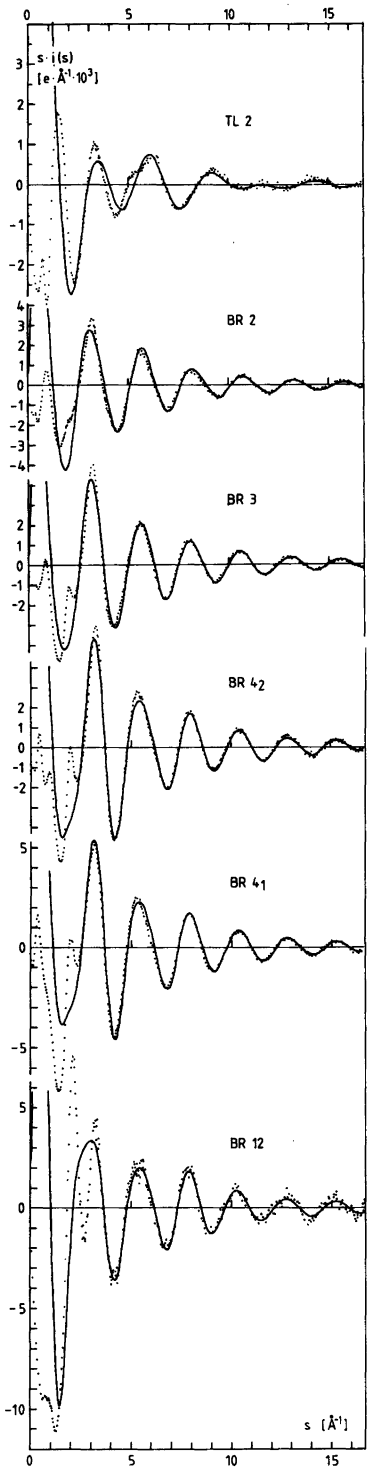

Fig. 2. Reduced intensity values, $si(s)$, for the solutions investigated. Experimental values are represented by dots. Full lines show the intensities calculated for the nearest neighbour interactions shown in Fig. 3. (Note that the scale on the y-axis for the TL2 solution is expanded for clarity.)

$$M(s) = \{([n_{Tl} f_{Tl}(0)]^2 + [n_{Tl}\Delta f''_{Tl}]^2)/([n_{Tl} f_{Tl}(s)]^2 + [n_{Tl}\Delta f''_{Tl}]^2)\} \exp(-0.007 s^2).$$

Contributions to the intensity curves from intramolecular interactions were calculated according to the expression

$$i_{calc}(s) = \sum_{\substack{p,q \\ p \neq q}} n_{pq}[f_p(s) f_q(s) + \Delta f''_p \Delta f''_q] \frac{\sin sr_{pq}}{sr_{pq}} \cdot \exp(-\tfrac{1}{2} l^2_{pq} s^2)$$

where the summation is over the atoms in the stoichiometric unit of volume and the scattering factors, $f(s)$, are corrected for the real part of the anomalous dispersion. Parameters characterizing intramolecular interactions, that is the distance, r_{pq}, the number of distances, n_{pq}, and the mean square variation, l^2_{pq}, were refined with a least-squares procedure, seeking the minimum for the function

$$U = \sum w(s)[i_{obs}(s) - i_{calc}(s)]^2.$$

The weighting function, $w(s) = I^{-2}(s)$, was chosen to give each point a weight approximately proportional to the inverse of the square of the estimated standard deviation in $i(s)$. In order to detect and to reduce the influence of systematic errors, the refinements were performed for different s ranges.

The $s \cdot i(s)$ values for the solutions investigated are shown in Figs. 2 and 4 and the $D(r) - 4\pi r^2 \rho_0$ functions in Figs. 3 and 4.

RESULTS AND DISCUSSION

A. The Structure of the Hydrated Thallium(III) Ion

Intramolecular interactions. Thallium(III) is not expected to form complexes with the perchlorate ion in aqueous solution.[1,19] Even in crystals of

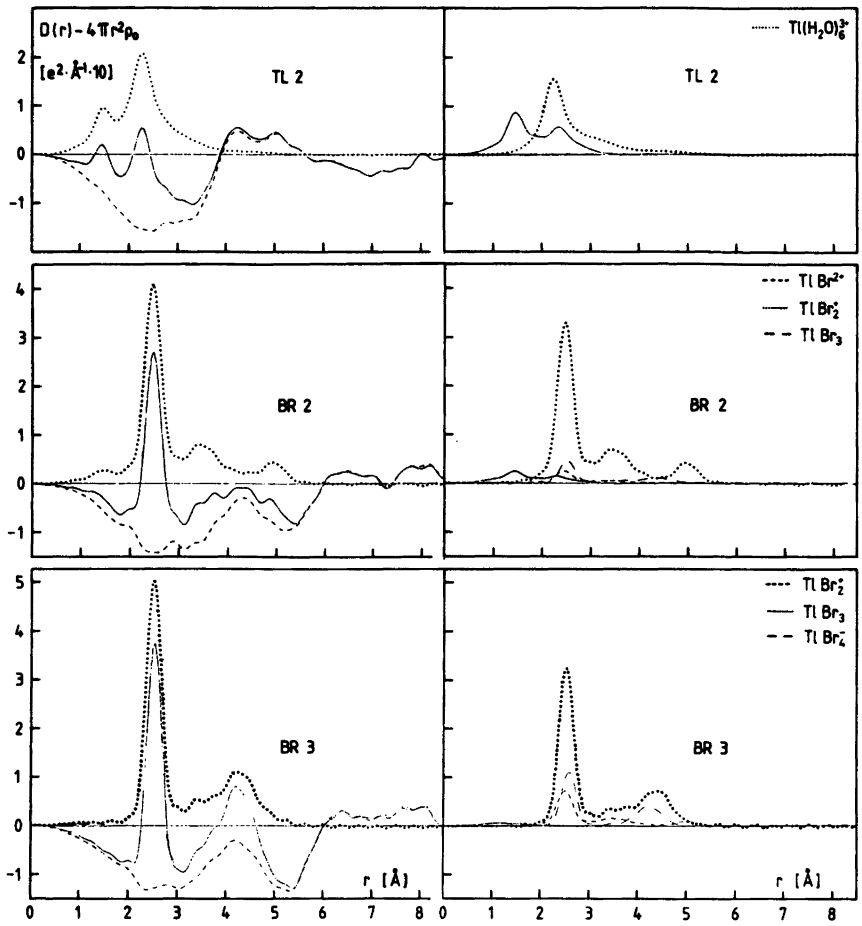

Fig. 3a. Comparison between the experimental radial distribution functions, $D(r)-4\pi r^2\rho_o$, and peak shapes, calculated for nearest neighbour interactions. The curves to the right show, for each solution, the sum of the peak shapes calculated for H_2O, ClO_4^- and $Li(H_2O)_4^+$ (−; parameter values given in Ref. 32 were used), the sum of the peak shapes for the interactions within the dominating Tl(III) complex(···) and the corresponding contributions from the minor Tl(III) species (---).

The curves to the left represent the experimental $D(r)-4\pi r^2\rho_o$ functions (−); the sum of the peak shapes shown to the right (···); and the difference between the experimental and the calculated curve (---).

$Tl(ClO_4)_3 \cdot 6H_2O$, the Tl^{3+} ion is coordinated only to water molecules, which form a regular octahedron with Tl−H_2O bond lengths of 2.23 Å.[20] Perchlorate was, therefore, chosen as the anion for the determination of the structure of the hydrated thallium(III) ion in solution. The radial distribution functions for two such solutions, 1 and 2 M respectively, are shown in Fig. 4a.

The first peak in each of the RDF's occurs at about 1.4 Å and originates from the Cl−O distances within the tetrahedral perchlorate groups.[21] The second peak, at about 2.3 Å, is close to the distance found for Tl−H_2O in the solid perchlorate.[20] Contributions to this peak should also come from the O−O distances of the perchlorate group, which are expected at about 2.3 Å. Water−water contact distances are indicated, particularly for the more dilute solution, at about 2.8 Å. The large peak between 4 and 5 Å appears differently for the two solutions and probably contains major contributions from distances between the Tl atom and molecules in its second coordination sphere.

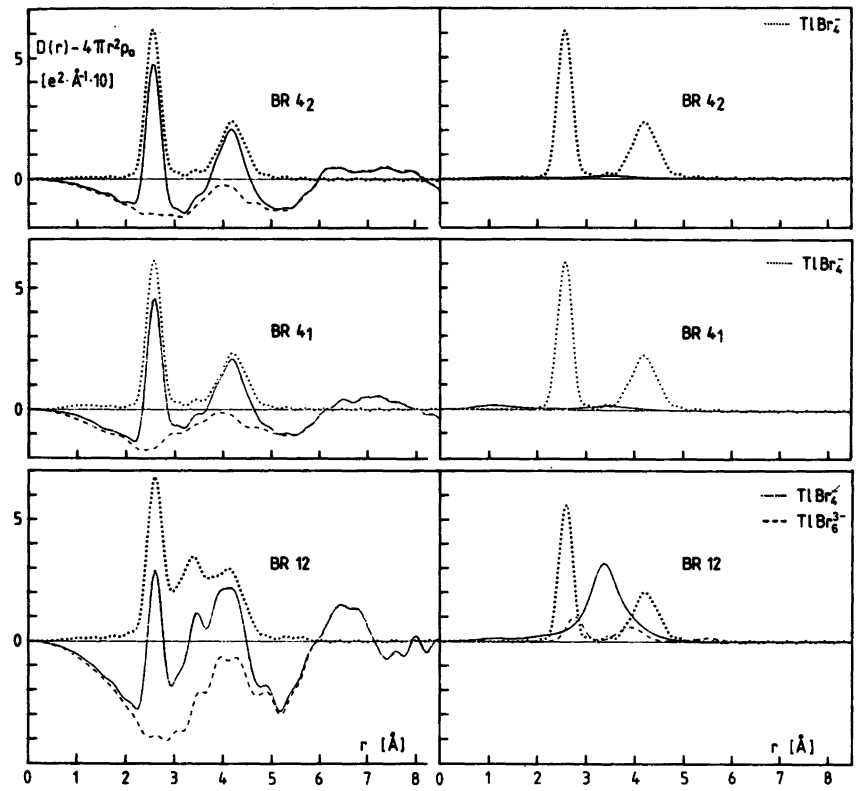

Fig. 3b. The same functions for the BR4 and the BR12 solutions as those shown for the other solutions in Fig. 3a. The vertical axes are shrunk by a factor 2 compared with those in Fig. 3a. Br–H_2O contact distances[32] are included in the calculated peak shapes for the BR12 solution.

The well-defined intramolecular interactions of the perchlorate group and the hydrated Tl^{3+} ion will give dominant contributions to the $i(s)$ values in the outermost parts of the intensity curves. These parts can be used, therefore, for a least-squares refinement of the parameters characterizing the interactions. The results of a number of refinements, performed for different regions of s, are given in Table *2a*. The Cl–O bond lengths are close to values found in crystal structures,[21] and the mean square variation, l^2_{Cl-O}, is of the same order of magnitude as the values obtained from spectroscopic measurements (0.0015 Å^2).[22] The difference between the Cl–O bond lengths in the dilute and the concentrated solution may be significant, since it could not be traced to any systematic errors in the data. The Tl–H_2O distances of 2.24 Å are identical with those found in the solid perchlorate, which indicates a similar octahedral coordination in the solution. The number of Tl–H_2O interactions per Tl atom, obtained in the least-squares refinements, is not sufficiently precise to differentiate between a fourfold and a sixfold coordination, (*cf.* Table *2a*). The RDF's, however, give clear support for an octahedral coordination. This is demonstrated for example in Fig. 4b in which calculated shape functions for a thallium atom coordinating four and six water molecules, respectively, are compared with a shape function derived from the experimental RDF for the 2 M solution. This function was derived as a difference between the RDF for TL2, from which the perchlorate interactions were subtracted, and the RDF for TL1, from which the interactions within the $Tl(H_2O)_n^{3+}$ (n=6) and the ClO_4^- units had been subtracted. The calculations were based on a stoichiometric unit of volume containing one thallium atom for the TL2 solution. For the TL1 solution, the stoichiometric volume was chosen to correspond

to the same amount of water as that for TL2. This procedure should to a large extent eliminate most of the contributions from the intermolecular interactions in the region of interest, that is around 2.3 Å.

Neither the values for the root mean square variation of the Tl−O distance obtained in the least-squares refinements nor the radial distribution curves give any support for the occurrence of non-equivalent Tl−H_2O bonds within the first coordination sphere of the Tl^{3+} ion. It seems reasonable to assume, therefore, that the coordination of the Tl^{3+} ion in aqueous solution is regularly octahedral, that is the same as is found in the crystals of $Tl(ClO_4)_3 \cdot 6H_2O$.[20]

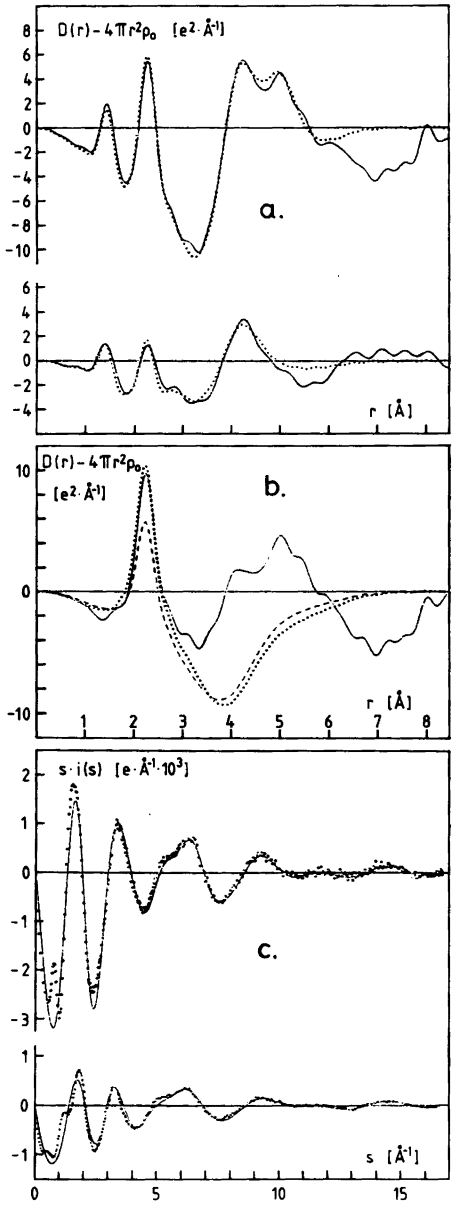

Intermolecular interactions. Hydrated metal ions are known to have a second coordination shell of water molecules, w_2, hydrogen bonded to the water molecules w_1 of the first sphere.[23] In several salt hydrates the orientation of the w_1 molecules can vary from mostly tetrahedral for M^+ ions (a lone pair of w_1 is directed towards the metal ion, while the other lone pair is accessible to accept a hydrogen bond) to usually trigonal for small M^{3+} ions (w_1 points the negative side of the dipole of the H_2O molecule toward the metal ion).

If the water molecules of the $Tl(H_2O)_6^{3+}$ ion are assumed to be hydrogen-bonded to surrounding water molecules the corresponding Tl−H_2O distances would be, assuming a w_1-w_2 distance of 2.75 Å, about 4.1 Å for a tetrahedral bonding, or about 4.3 Å for a trigonal arrangement. Peaks occur in the RDF's at about 4.1 Å for both the 1 M and the 2 M perchlorate solutions. In the 2 M solution, in which the number of water molecules per Tl atom is not sufficient to fill out a second coordination sphere, the 4.1 Å peak decreases and another peak occurs at 5.0 Å. This may originate from a Tl−Cl distance and may indicate an ordering of perchlorate groups within the second coordination

Fig 4a. The experimental (−) and the calculated (···) RDF's for the two Tl(III) perchlorate solutions. Intermolecular interactions have been approximated by assuming that the complexes $Tl(H_2O)_6^{3+}$, ClO_4^- and H_2O occupy spherical holes in an evenly distributed scattering density. The calculations are referred to stoichiometric units of volume containing the same number of water molecules for the two solutions. *b.* The shape function for the hydrated Tl^{3+} ion in the Tl2 solution (−) derived with the aid of the RDF for the TL1 solution. Calculated shape functions for a $Tl(H_2O)_6^{3+}$ complex (···) and a $Tl(H_2O)_4^{3+}$ complex (---) are given for comparison. *c.* Reduced intensity values, *si*(*s*), for the two perchlorate solutions, referred to the same stoichiometric volumes as those in Fig. 4a. Experimental values are represented by dots. Full lines show the intensities corresponding to the theoretical curves shown in Fig. 4a.

Table 2. Results of least-squares refinements (r is the distance, n the number of distances per Tl atom, and l^2 the mean-square variation of the distance). The estimated standard deviations are those obtained in the least-squares procedure but adjusted upwards to account for the variation in the parameters when different s-ranges were used in the refinements. Only the parameters for which standard deviations are given were refined.

Solution	$r_{Tl-(H_2O)}$	$l^2_{Tl-(H_2O)}$	$n_{Tl-(H_2O)}$	r_{Cl-O}	l^2_{Cl-O}		
a. Perchlorate solutions (in ClO_4: l^2_{O-O} was held constant at 0.003 Å^2)							
TL1	2.237(5)	0.010(2)	5(1)	1.412(3)	0.0018(4)		
TL2	2.235(5)	0.008(2)	5(1)	1.443(4)	0.0046(5)		
Solution	r_{Tl-Br}	l^2_{Tl-Br}	n_{Tl-Br}	r_{Br-Br}	l^2_{Br-Br}	n_{Br-Br}	r_{Br-Br}/r_{Tl-Br}
b. Tl–Br and Br–Br interactions only (no other complexes included)							
BR2	2.485(3)	0.002(2)	1.8(2)	–	–	–	–
BR3	2.521(4)	0.006(1)	3.1(1)	4.30(2)	0.05	3(1)	1.70
$BR4_2$	2.563(1)	0.0038(5)	3.8(1)	4.16(3)	0.05(2)	6(1)	1.62
$BR4_1$	2.565(1)	0.0054(5)	4.0(1)	4.18(3)	0.05(2)	8(2)	1.63
BR12	2.593(4)	0.004(2)	4.1(3)	4.16(2)	0.05	8(2)	1.60
c. Tl–Br and Br–Br interactions within the main complex (the minor Tl(III) complexes included with constant parameter values)							
BR2	2.481(2)	0.004(1)	2.0	4.94(4)	0.02(2)	1.0	1.99
BR3	2.512(2)	0.004(1)	2.7(2)	4.38(5)	0.05(2)	3.0	1.74
$BR4_2$	2.563(1)	0.0038(5)	3.8(1)	4.16(3)	0.05(2)	6(1)	1.62
$BR4_1$	2.565(1)	0.0054(5)	4.0(1)	4.18(3)	0.05(2)	8(2)	1.63
BR12	2.581(4)	0.002(2)	4.0(3)	4.22(5)	0.05	7(2)	1.64

sphere. Such an ordering is also indicated by Tl–NMR measurements on aqueous solutions of $Tl(ClO_4)_3$ in perchloric acid, where the chemical shift for the hydrated Tl^{3+} ion is clearly dependent on the concentration of the perchlorate ion.[24] Furthermore, in the crystal structure of $Tl(ClO_4)_3 \cdot 6H_2O$, the $Tl(H_2O)_6^{3+}$ unit is surrounded by fourteen ClO_4^- ions, eight of which have a Tl–Cl distance of 5.0 Å.[20]

A comparison between observed and calculated $s \cdot i(s)$ values and $D(r) - 4\pi r^2\rho_0$ functions for the TL1 and TL2 solutions are shown in Fig. 4. The calculated curves include contributions from intramolecular interactions of ClO_4^-, $Tl(H_2O)_6^{3+}$, and H_2O, and distances between Tl and molecules in an assumed second coordination sphere. Remaining intermolecular interactions are approximated by assuming that the complexes occupy spherical holes in an evenly distributed scattering density.

B. The Structures of the Bromide Complexes

Intramolecular interactions. In the presence of bromide in the solutions the most pronounced peak in the radial distribution curves appears at about 2.5 Å, which is close to Tl–Br bonding distances found in crystal structures.[25–27] The second most pronounced peak is found at about 4 Å, *i.e.* in a region where Br–Br contact distances would be expected.

The results of least-squares refinements using the high-angle parts of the intensity curves and including only the Tl–Br and the Br–Br interactions are given in Table 2b. There is a gradual increase in the Tl–Br bonding distances with the increasing Br:Tl ratio in the solutions from 2.485(3) Å in BR2 to 2.593(4) Å in BR12.

The number of Tl–Br interactions per Tl atom increases from 2 in the BR2 solution to 4 in the solutions containing the highest Br–Tl ratios, and thus follows the stoichiometric Br:Tl ratio except for the BR12 solution, which contains a large excess of bromide. In the two BR4 and the BR12 solutions, the ratio r_{Br-Br}/r_{Tl-Br} does not differ significantly from the theoretical value, 1.633, for a regular tetrahedral arrangement. In the solution BR3, this ratio has increased to 1.70, which indicates a larger Br–Tl–Br bonding angle in the complexes. In the solution BR2 only minor peaks appear in the region

where the Br – Br distances are expected and they were not, therefore, included in the least-squares refinement.

These results of the scattering measurements are consistent with the predictions made on the basis of the stability constants about the compositions and the distribution of the complexes in the solutions (Fig. 1). Since the stability constants were determined for the same solutions as those used for the diffraction measurements, we can, with some confidence, also use them as an estimate of the presence of minor species in each solution and introduce these as corrections in the calculations. This was done in least-squares calculations, where the Tl – Br and the Br – Br interactions within the dominating Tl(III) species in each solution were refined keeping the parameters of the minor species constant. The final results are given in Table 2c.

For the BR2 solution, the Br – Br peak is not very pronounced and other peaks, which could conceivably be taken as Br – Br intramolecular interactions, are also present (Fig. 3). The 4.94 Å peak was, however, the only one of these interactions that could be successfully refined (*cf.* Table 2c) and the most probable conclusion is, therefore, that the BR2 solution contains linear $TlBr_2^+$ complexes ($r_{Br-Br}/r_{Tl-Br}=2.0$). In the BR3 solution, the ratio found between the Br – Br and the Tl – Br distances is 1.74, which can be compared with the theoretical value of 1.732 for a planar – triangular complex. For the BR4 solutions, where the $TlBr_4^-$ complex constitutes 99.9 % of the total thallium content, according to the stability constants, the results are, of course, identical with those given in Table 2b. The BR12 solution will be discussed below.

Comparison with crystal structures and spectroscopic measurements. It is of interest to compare the structures of the complexes, derived from the solution scattering data, with those found in the solid state. Unfortunately, no crystals with a stoichiometric Br/Tl ratio of 2:1 are known and no $TlBr_2^+$ complexes have yet been found in any crystal structure. Crystals of $TlBr_3 \cdot 4H_2O$ contain almost planar triangular $TlBr_3$ complexes with Tl – Br bonding distances of 2.515(3) Å,[25] the same as those found for the solution BR3 (Table 2c). In the crystal structure, the Tl atom is also in contact with two water molecules at distances of 2.60(2) and 2.52(2) Å, respectively, thus forming a trigonally bipyramidal arrangement. In the radial distribution function for the BR3 solution no separate peaks corresponding to such Tl – H_2O distances can be distinguished but they have been assumed to be present for the calculation of the peak shapes (Fig. 3). The Tl – NMR chemical shift for the third complex in aqueous solution is close to the shift for the compound $TlBr_3 \cdot 4H_2O$.[8] This is in agreement with the assumption, that the essentially trigonal – bipyramidal $TlBr_3(H_2O)_2$ complex found in the solid is also present in the solution.

Tetrahedral $TlBr_4^-$ units occur in crystals of $KTlBr_4 \cdot 2H_2O$.[26b] The Tl – Br distances of 2.554(3) Å do not differ significantly from those found in the solution, 2.564(2) Å (Table 2c). Discrete $Tl_2Br_9^{3-}$ ions, consisting of two face-sharing $TlBr_6$ octahedra, probably occur in crystals of $Cs_3Tl_2Br_9$[8,12] and have been proposed to be the dominant species in concentrated aqueous solutions with high Br:Tl ratios.[7] The scattering data for the 2.6 M solution $BR4_2$ and the 1 M solutions $BR4_1$ and BR12 give no support for this assumption. Nor could any support be obtained from the Tl – NMR measurements.[8]

Preliminary results for a crystal structure determination of $Rb_3TlBr_6 \cdot \frac{13}{7} H_2O$ show that it contains octahedral $TlBr_6^{3-}$ units with Tl – Br distances of about 2.75 Å.[12] NMR measurements on aqueous solutions[8] have indicated that for very large Br:Tl ratios, higher complexes than $TlBr_4^-$ can form, probably $TlBr_6^{3-}$ (Fig. 1). With the stability constants derived from the NMR measurements, we can estimate that in the Br12 solution the concentration of the $TlBr_6^{3-}$ complex would amount to about 13 % of the total thallium content. The resulting change in the number of the Tl – Br interactions from that expected for $TlBr_4^-$ complexes alone would be below the significance level in our determinations (Table 2b). The expected change in the Tl – Br distance would, however, if estimated as a weighted average between the distances in the $TlBr_4^-$ and the $TlBr_6^{3-}$ complexes, be around 0.035 Å and should be observable. The least-squares refinements show an increase in the Tl – Br distance for the BR12 solution of 0.03 Å compared with that found for the $BR4_1$ solution (Table 2b), and this is probably a significant difference. It may support the assumption of the formation of a higher complex than $TlBr_4^-$, although other explanations of this difference are possible, especially when the rather drastic changes in composition between the BR4 and the BR12 solutions are considered (see below).

Results from Raman measurements are consistent with these conclusions as far as the higher complexes

are concerned. Spectra for the $BR4_1$ solution and for a 3.2 M solution with a Br/Tl ratio of 4.5 do not differ significantly and the frequencies observed (~200 sh, 187 vs, ~57 w) are in agreement with those for crystals containing tetrahedral $TlBr_4^-$ units (*e.g.* $KTlBr_4 \cdot 2H_2O$[28]) and for the, presumably, tetrahedral $TlBr_4^-$ complexes present in the noncoordinating solvents CH_3CN[29] and CH_2Cl_2.[11b] If $Tl_2Br_9^{3-}$ species were present in the solutions, much more complex spectra would be expected, as judged from the Raman spectrum of the compound $Cs_3Tl_2Br_9$ (206 m, 192 s, 186 vs, 159 vs, 139 w, 96 w, 69 m *etc.*).

The BR12 solution gives the same Raman spectrum as that for the $BR4_1$ solution except for a small but significant frequency shift of the Tl–Br symmetric stretching line from 185.7 cm^{-1} to 184.5 cm^{-1}. This indicates a weakening of the Tl–Br bonds and probably corresponds to a lengthening of these bonds. The Raman measurements of Jones, who investigated the dependence of the Hg–Cl frequencies on the Hg–Cl bond length,[30] would suggest that a drop of 1.2 cm^{-1} as observed here corresponds to a bond lengthening of about 0.005 Å. This cannot explain the difference of 0.03 Å between the Tl–Br distances obtained in the least-squares refinements for the $BR4_1$ and the BR12 solutions (Table 2b) and thus it supports the conclusion that this difference results from the formation of higher complexes, probably $TlBr_6^{3-}$. Raman lines for a $TlBr_6^{3-}$ complex are probably too weak to be observed in the BR12 solution. Their expected positions can be inferred from the Raman spectrum of the compound $[Co(NH_3)_6]TlBr_6$ containing octahedral $TlBr_6^{3-}$ units[27] (160 vs, 89 m, 72 w, 56 w, 39 m, 27 s).

Intermolecular interactions. A comparison of the observed $D(r)-4\pi r^2\rho_0$ functions with calculated peak shapes, based on the parameter values in Table 2c and the distribution of complexes according to Fig 1, is shown in Fig. 3. Subtraction of the calculated peaks leads, for all of the bromide solutions, to smooth background curves with remaining diffuse maxima primarily in the region between 3 and 5 Å, where H_2O-H_2O (2.8 Å), $Br-H_2O$ (3.3 Å) and distances between the Tl atom and molecules in its second coordination sphere are expected.

For the $BR4_1$ solution, which contains almost solely tetrahedral $TlBr_4^-$ complexes and Li^+ ions, probably as tetrahedral $Li(H_2O)_4^+$,[32] a simple model for the approximation of the intermolecular interactions was employed. A packing of water molecules around the $TlBr_4^-$ complex, as illustrated in Fig. 5 and previously used for solutions containing $HgBr_4^-$ complexes,[31] with a continuous electron distribution outside a sphere of radius 5 Å leads to a good agreement between observed and calculated *si*(*s*) values even in the low angle region of the intensity curve as shown in Fig. 6. In this figure, the *D*(*r*) function, calculated with the aid of this model, is also compared with the experimental function.

CONCLUSIONS

The results obtained with the different methods discussed above are all consistent and lead to the following overall picture of the complex formation between Tl(III) and Br^- in aqueous solution. In solutions of thallium(III) perchlorate, thallium is octahedrally surrounded by six equidistant water molecules with Tl–O bond lengths of 2.235(5) Å.

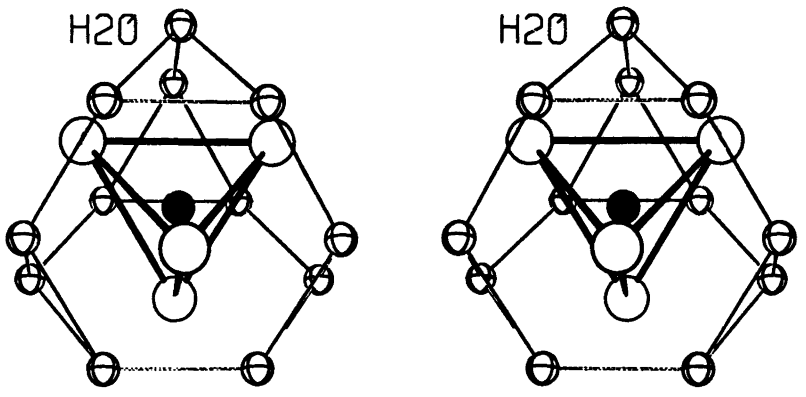

Fig. 5. The model used in the calculations for the packing of water molecules around the $TlBr_4^-$ complex.

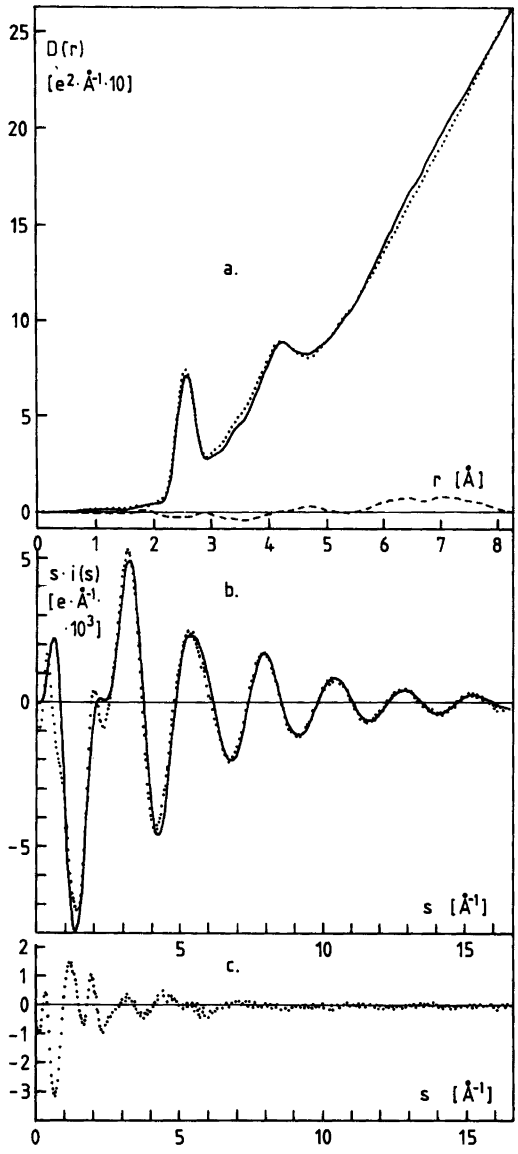

Fig. 6a. Comparison between the experimental RDF for the $BR4_1$ solution (−) and a calculated function including both intra- and intermolecular interactions (···). The difference between the experimental and the calculated curve is given by the broken line.

b. Comparison of the experimental *si*(*s*) curve (···) with the curve calculated for the model shown in Fig. 6a (−). *c.* The difference between the experimental and the calculated *si*(*s*) curves shown in Fig. 6b.

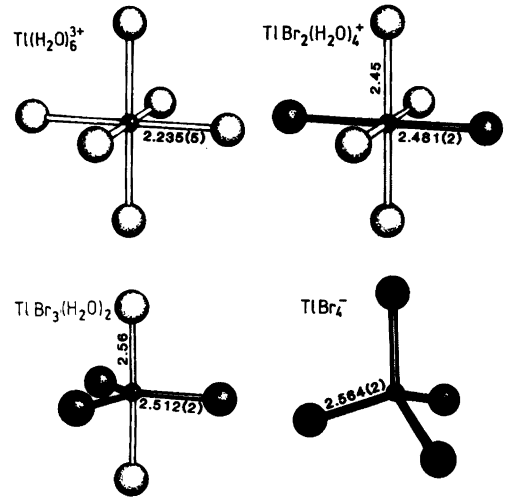

Fig. 7. Suggested structures for the $TlBr_n(H_2O)_m^{3-n}$ complexes in aqueous solution. Only the distances for which standard deviations are given have been determined. Dark spheres represent Br and light spheres H_2O.

When bromide is added, the octahedral symmetry is retained in the first two complexes formed, $TlBr^{2+}$ and $TlBr_2^+$, which results in a linear $TlBr_2^+$ complex with Tl−Br distances of 2.481(2) Å. When the third complex, $TlBr_3$, is formed, the coordination changes to trigonal – planar with Tl−Br distances of 2.512(2) Å. The fourth complex, $TlBr_4^-$, has as regular tetrahedral symmetry with Tl−Br bond lengths of 2.564(2) Å. For very large Br/Tl ratios small amounts of a higher complex form, probably an octahedral $TlBr_6^{3-}$ species. The structures of the complexes are illustrated in Fig. 7. A comparison between the calculated peak shapes and the experimental RDF's (Fig. 3), as well as the good agreement between calculated and experimental intensity values at high *s* ranges (Fig. 2) confirm the conclusions made on the structures of the complexes.

Acknowledgements. We thank Dr. Peter Goggin and Dr. Magnus Sandström for recording the Raman spectra and Mr. Ernst Hansen for skilful technical assistance.

The work has been supported by the Swedish Natural Science Research Council (NFR).

REFERENCES

1. a. Smith, R. M. and Martell, A. E. *Critical Stability Constants*, Plenum, New York 1977, Vol. 4; b. Sillén, L. G. and Martell, A. E. *Stability Constants*, The Chemical Society, London 1964.
2. Lee, A. G. *The Chemistry of Thallium*, Elsevier, Amsterdam 1971 and references therein.
3. Woods, M. J. M., Gallagher, P. K., Hugus, Z. Z. and King, E. L. *Inorg. Chem. 3* (1964) 1313.
4. a. Ahrland, S., Grenthe, I., Johansson, L. and Norén, B. *Acta Chem. Scand. 17* (1963) 1567; b. Ahrland, S. and Johansson, L. *Acta Chem. Scand. 18* (1964) 2125.
5. Yakovlev, Y. B., Kulba, F. Y. and Mironov, V. E. *Zh. Neorg. Khim. 12* (1967) 3283.
6. Leden, I. and Ryhl, T. *Acta Chem. Scand. 18* (1964) 1196.
7. Figgis, B. N. *Trans. Faraday Soc. 55* (1959) 1075.
8. Glaser, J. and Henriksson, U. *J. Am. Chem. Soc. 103* (1981) 6642.
9. Biedermann, G. and Spiro, T. G. *Chem. Scr. 1* (1971) 155.
10. Spiro, T. G. *Inorg. Chem. 4* (1965) 731.
11. a. Delwaulle, M. L. *C. R. Acad. Sci. Fr. 238* (1954) 2522; b. Andrews, S. P., Badger, P. E. R., Goggin, P. L., Hurst, N. W. and Rattray, A. J. M. *J. Chem. Res. (M)* (1978) 1401; c. Davies, E. D. and Long, D. A. *J. Chem. Soc. A* (1968) 2050.
12. Glaser, J. *Thesis*, Royal Institute of Technology, Stockholm 1981.
13. Johansson, G. *Acta Chem. Scand. 20* (1966) 553.
14. a. Norman, N. *Thesis* Na 219 (1954) Universitetets Fysiska Institutt, Oslo; *Acta Crystallogr. 10* (1957) 370; b. Krogh-Moe, J. *Acta Crystallogr. 9* (1956) 951.
15. *International Tables for X-Ray Crystallography*, Kynoch Press, Birmingham 1974, Vol. IV.
16. Narten, A. H. and Levy, H. A. *J. Chem. Phys. 55* (1971) 2263.
17. a. Cromer, D. T. and Mann, J. B. *J. Chem. Phys. 47* (1967) 1892; b. Cromer, D. T. *J. Chem. Phys. 50* (1969) 4857; c. Compton, A. H. and Allison, S. K. *X-Rays in Theory and Experiment*, Van Nostrand, New York 1935.
18. Johansson, G. and Sandström, M. *Chem. Scr. 4* (1973) 195.
19. Hester, R. E. *Inorg. Chem. 3* (1964) 769.
20. Glaser, J. and Johansson, G. *Acta Chem. Scand. A 35* (1981) 639.
21. Berglund, B., Thomas, J. O. and Tellgren, R. *Acta Crystallogr. B 31* (1975) 1842.
22. a. Nagarajan, G. *Indian J. Pure Appl. Phys. 2* (1964) 17; b. Müller, A. and Nagarajan, G. *Z. Naturforsch. Teil. B 21* (1966) 508.
23. Friedman, H. L. and Lewis, L. *J. Sol. Chem. 5* (1976) 445.
24. *Unpublished results* from this laboratory.
25. a. Zvonkova, Z. V. *Zh. Fiz. Khim. 30* (1956) 340; b. Glaser, J. *Acta Chem. Scand. A 33* (1979) 789.
26. a. Hazell, A. C. *J. Chem. Soc.* (1963) 3459; b. Glaser, J. *Acta Chem. Scand. A 34* (1980) 157.
27. Watanabe, T., Atoji, M. and Okazaki, Ch. *Acta Crystallogr. 3* (1950) 405.
28. Spiro, T. G. *Inorg. Chem. 6* (1967) 569.
29. Walton, R. A. *Coord. Chem. Rev. 6* (1971) 1.
30. Jones, T. *Thesis*, City Polytechnic, Sheffield 1979.
31. Sandström, M. and Johansson, G. *Acta Chem. Scand. A 31* (1977) 132.
32. a. Palinkas, G., Radnai, T. and Hajdu, F. *Z. Naturforsch. Teil. A 35* (1980) 107: b. Narten, A. H., Vaslov, F. and Levy, H. A. *J. Chem. Phys. 58* (1973) 5017.

Received May 22, 1981.

Acta Chemica Scandinavica A 36 (1982) 137–140

Preparation and Characterization of 2-Mercaptobenzoic Acid Complexes of Mercury – Lead and Mercury – Cadmium

BASIM M. ALSAADI

Department of Chemistry, College of Education, Wazeria, Baghdad, Iraq

Using bis(2-mercaptobenzoato)-*S*-mercury(II) as a starting ligand, the preparation of complexes of empirical formulae $Hg(C_{14}H_8O_4S_2)Pb.2H_2O$ and $Hg(C_{14}H_8O_4S_2)Cd.2H_2O$ is described. The infrared spectra, in the region 4000 – 200 cm^{-1}, and ^{199}Hg and ^1H NMR spectra of these complexes are dicussed. It has been concluded that the coordination of lead(II) and cadmium(II) occurs through oxygen while the sulfur mercury bonds are not altered appreciably.

The analytical applications of 2-mercaptobenzoic acid (TSA) are widely known.[1] Recently, it has been used as an extracting agent for chromium(III)[2] and as a quantitative precipitant for mercury between pH 2.5 and 5.5.[3] Its importance in pharmaceutical and biological applications stems from its uses (in the form of mono-complex of methylmercury) as a diuretic[4] and preservative in eye drops.[5] Also, it has been found to inhibit the activity of metal-dependant enzymes.[6] The inhibition of the activity of metalloenzymes is a result of its ability to bind a variety of metal ions, thus competing with the enzyme.

In a previous paper[7] we have reported the binding ability of TSA with divalent zinc, cadmium, lead and mercury. It has been shown that the coordination of TSA in the complexes of Zn(II), Cd(II) and Pb(II) occurs through both sulfur and oxygen atoms, while in the case of mercury it coordinates through sulfur only. Two complexes were described; the mono-complex, which contains a free carboxyl group and the bis-complex which contains two carboxyl groups. A molecular model of the bis(2-mercaptobenzoato)-*S*-mercury(II) (BTM) shows that the two carboxyl groups, in the *cis*-form, are near one another, hence the two groups may

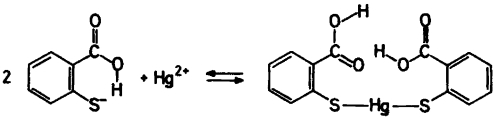

interact through hydrogen bonding. The binding constant (β_2), in 75 % dioxane-water mixture, for the reaction is of the order of 10^{27}.[7] Thus, in principle, the two carboxylate groups are available to form two coordinate bonds with metal ions of weak class b properties, without altering the Hg – S bonds appreciably. Metal ions which are candidates for such reaction include Pb(II), Cd(II), lanthanoids(III), *etc.* In this paper we shall attempt to prepare such mixed semplexes. The complexes include those of lead(II) and cadmium(II) ions.

EXPERIMENTAL

BTM was prepared as described earlier.[7] It has been found that its disodium salt tends to produce grey granules consisting of metallic mercury. The ammonium salt, yellow with absorption maximum at 290 nm, is stable. The 1:1 BTM:Pb (BTMPb) was prepared by dissolving 0.5 g of BTM (1 mmol) in 6 ml of 10 % NH_3 (7 mmol). The solution was added, while stirring, to 1 mmol of $Pb(NO_3)_2$ dissolved in 25 ml of water. The pH was adjusted to 6.0 with dilute hydrochloric acid. The precipitate, pale yellow, was filtered off, washed with water, hot ethanol and then dried under vacuum. Found: Pb 27.27; Hg 26.34; S 8.60; H 1.18 and C 23.60. Calc. for $Hg(C_{14}H_8O_4S_2)Pb.2H_2O$: Pb 27.79; Hg 26.90; S 8.58; H 1.61 and C 22.53.

The same above procedure is used to prepare the cadmium complex (BTMCd), pale green. Found: Cd 17.22; Hg 30.04; S 9.84; H 1.66 and C 26.94.

0302-4377/82/020137-04$02.50

Calc. for $Hg(C_{14}H_8O_4S_2)Cd.2H_2O$: Cd 17.27; Hg 30.82; S 9.83; H 1.84 and C 25.80.

All the above analyses were made by Alfred Berhardt Mikroanalytisches Laboratorium, West Germany.

Deuterated BTM was prepared by dissolution of BTM in warm dioxane – deuterium oxide mixture and evaporation at room temperature *in vacuo*.

RESULTS AND DISCUSSION

Mixed metal complexes of 2-mercaptobenzoic acid containing two metal ions per complex are prepared.The two complexes are bis(2-mercaptobenzoato)-*O*-lead(II)-*S*-mercury(II) (BTMPb) and bis(2-mercaptobenzoato)-*O*-cadmium(II)-*S*-mercury(II) (BTMCd). The complexes were characterized through elemental analysis, TGA, IR and ^{199}Hg and ^1H NMR spectroscopy. The complexes in dimethylsulfoxide and in the solid state are currently under investigation by X-ray diffraction.

TGA showed that the complexes are stable up to 230 °C but decompose readily around 250 °C. This analysis was carried out with the aim of investigating the nature of the two water molecules in these complexes, but unfortunately no distinct change in the thermal gravimetric curve corresponding to water molecules was detectable.

Infrared spectra of the complexes were recorded using a Perkin-Elmer 180-spectrometer, equipped with air-drier, in nujol mulls between CsI discs (in the range 500 – 200 cm^{-1}) and in KBr discs (in the range 4000 – 500 cm^{-1}). No change in the positions of different bands are detected on changing the medium. Detailed assignments of the bands cannot be made unambiguously, but nevertheless certain conclusions can be reached.

The spectrum of BTM in the region 3200 – 2500 cm^{-1} showed a broad absorption band with many submaxima. Such absorption is characteristic of OH-stretching vibration of dimeric carboxyl groups.[8] The investigation of the IR-spectra of a number of carboxylic acids has shown that the OH-stretching vibration frequency of a monomer carboxylic acid lies near 2550 cm^{-1} while that of dimeric species gives rise to a broad absorption region with many submaxima between 3000 – 2500 cm^{-1} (see Ref. 8 and references therein). In general, therefore, the broad band absorption in the BTM, and especially the absorption near 2700 cm^{-1}, is a strong indication of the presence of a hydrogen-bonded OH-group. This interpretation is supported by the fact that the spectrum of the deuterated BTM shows that part of the broad absorption band, centered at 2550 cm^{-1}, has shifted 270 cm^{-1} to lower frequency, *i.e.* appeared at 2280 cm^{-1}. Another medium broad band, centered at 925 cm^{-1} also shifted to lower frequency and appeared as a sharp strong band at 855 cm^{-1}. This band could be

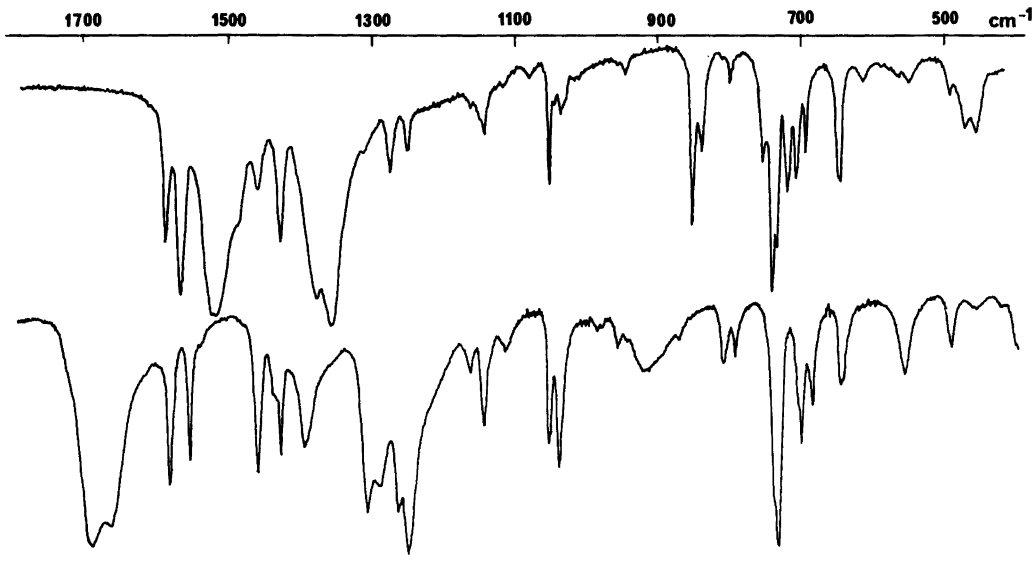

Fig. 1. Infrared spectra of BTM (lower) and BTMPb (upper) complexes in KBr discs.

assigned to the OH-out-of-plane deformation.[8] The isotopic ratio for the two bands is 1.10 ± 0.02. No other significant change was observed in the spectrum of BTM on deuterium substitution.

The spectrum of the BTMPb shows the complete disappearance of the broad OH-stretching frequency in the region 3200–2500 cm^{-1} leaving a weak broad band in the region 3550–3350 cm^{-1}. This band could be due to lattice water.[9] The spectrum also showed the disappearance of the band at 925 cm^{-1}, which was assigned to OH-out-of-plane deformation, Fig. 1. The three doublet bands of the carbonyl stretching frequencies at 1682, 1305 and 1269 cm^{-1} (average) in the BTM, have also disappeared, Fig. 1. The three bands did not show any appreciable shift on deuteration. The disappearance of the carbonyl stretching frequencies in the spectrum of BTMPb-complex is accompanied by the appearance of two doublet bands at 1522 and 1370 cm^{-1} arising from the carbonyl asymmetric and symmetric stretching frequencies, respectively. The above changes in the spectrum of BTM complex confirm the replacement of the protons of the hydrogen-bonded carboxyl groups by lead(II).

Metal–sulfur stretching vibration lies in the range 480–210 cm^{-1},[10] and the Hg–S stretching band, in the BTM-complex, was assigned near 298 cm^{-1}.[7] The general feature of the spectrum of BTMPb in this region is very much the same as that of the BTM-complex. A shift of a few cm^{-1} in all the bands is observed. The similarity between the spectra of BTM and BTMPb complexes in this region indicates that the Hg–S bonds are not altered appreciably.

The general feature of the IR-spectrum of BTMCd-complex is very much the same as that of BTMPb-complex, but the bands are slightly broader.

It should be emphasized, that although detailed assignment of the IR-bands has not been possible, the IR-spectral data of these complexes indicate that the coordination of the Pb(II) and Cd(II) ions occurs through oxygen while the Hg–S bonds are not altered appreciably.

^{199}Hg nuclear magnetic spectra were obtained in natural abudance in a 10 mm tube at 16.1 MHz, using a Bruker cxp-90 spectrometer, at 20 °C. The field was locked to the ^{2}H signal of an external capillary of D_2O. Saturated $Hg(NO_3)_2$ solution was used as external reference. Concentrations ranging from 0.2–0.5 M of these complexes were used to observe mercury signals. The ^{1}H NMR spectra were obtained on a Bruker wp-200 spectrometer, at 25 °C. Tetramethylsilane was used as an internal standard. The spectra of the complexes were resolved by simulating the theoretical spectra with the aid of an iterative program, PANIC, supplied by Bruker. Table 1 represents a summary of the chemical shifts of these complexes.

Table 1. ^{199}Hg and ^{1}H chemical shifts of 2-mercaptobenzoic acid complexes of mercury–lead and mercury–cadmium.

Compound	Hg[a] (ppm)	H3[b] (Hz)	H4 (Hz)	H5 (Hz)	H6 (Hz)
TSA	–	1511.1	1485.3	1447.0	1591.9
BTM	1235.0	1523.5	1458.4	1436.4	1525.1
BTMPb	1187.0	1497.4	1437.7	1432.0	1475.8
BTMCd	1328.5	1491.6	1428.7	1421.7	1454.0

[a] Shifts to low-field relative to saturated $Hg(NO_3)_2$ solution; mercury signal of saturated $Hg(NO_3)_2$ is at −2460 ppm from Me_2Hg. [b] Shifts to low-field relative to internal TMS.

It is to be noticed from Table 1 that for each complex studied only one mercury signal is observed. This indicates that only one conformation exists, in DMSO, for each of the complexes studied. Table 1 also shows that the mercury signal of BTM is shifted to a lower-field on complexing cadmium and to a higher-field on complexing lead. This could be explained by considering two factors influencing the chemical shift of mercury in these complexes. Firstly, the weaking of Hg–S bonds as a result of the presence of another cation, in this case a shift to low-field in the mercury signals should be observed,[11] secondly, the presence of another cation with its solvation sphere nearby. This will influence the dispositions of DMSO molecules around the mercury ion and consequently the coordination of mercury. The larger the cation the greater the effect. The chemical shift of mercury in various compounds is known to be sensitive to the coordination sphere.[11,12] Table 1 shows that the signals of various aromatic protons, except H3, of 2-mercaptobenzoic acid are shifted to a high-field upon complexing mercury. This is inconsistent with the breaking-down of the hydrogen bonding between 2-mercaptobenzoic acid and solvent molecules.[13,14] Further up-field shifts in all the signals are observed on further complexation of lead(II). On substituting a stronger binding ion, Cd(II), instead of Pb(II) ion,[7] the positions of the signals continue to move up-field. This is reflected clearly

in the chemical shifts of H6, which is the nearest proton to the carbonyl group, *i.e.* it is also influenced by the variation in the effect of the chemical shift anisotropy of the carbonyl group resulting from various orientations relative to the aromatic protons.[15,16] Table 1 shows that only one set of signals appeared for both aromatic rings. This clearly indicates that the two rings are experiencing the same chemical environments, *i.e.* symmetrically disposed around the two metal ions.

The coupling constants between these protons, in the free and bound TSA, are nearly the same irrespective of the type of interactions involved with the sulfhydryl and the carboxyl groups. The values of the coupling constants are, $J_{34}=7.95\pm 0.05$ $J_{35}=1.10\pm 0.04$, $J_{36}=0.40\pm 0.03$, $J_{45}7.43\pm 0.03$, $J_{46}=1.64\pm 0.04$ and $J_{56}=7.70\pm 0.05$. The results indicate that the above interactions cause weak or no perturbation in the ring moiety.

Acknowledgements. The author is on a 10-month visit to the Inorganic Chemistry Department, Royal Institute of Technology, Stockholm, supported by the International Seminar in Chemistry and Physics, University of Uppsala, Uppsala, Sweden; he wishes to thank Dr. H. Stymne for putting the IR-equipment at his disposal and Professors I. Grenthe and U. Henriksson for useful discussions.

REFERENCES

1. Lewicka, M. *Mat. Fiz. Chem. 1* (1976) 179.
2. Sebastian, D. G. and Hilderland, D. C. *Anal. Chem. 50* (1978) 488.
3. Kadhum, K. H. and Alsaadi, B. M. *To be published.*
4. McAuliffe, C. A. *The Chemistry of Mercury*, Macmillan, London 1977, p. 31.
5. Wozniak-Parnowska, W., Zenbrzusk, E. and Milewsk, E. *Farm. Pol. 35* (1979) 269.
6. Wagner, J., Vitali, P., Schoun, J. and Giroux, E. *Can. J. Chem. 55* (1977) 4028.
7. Alniaimi, N. S. and Alsaadi, B. M. *J. Inorg. Nucl. Chem. 36* (1974) 1617.
8. Bellamy, L. J. *The Infrared Spectra of Complex Molecules*, Wiley, New York 1958, Chapter 10.
9. Nakamoto, K. *Infrared Spectra of Inorganic and Coordination Compounds*, Wiley, New York 1970, Part III.
10. Adams, D. M. *Metal-Ligand and Related Vibrations*, Edward Arnold, London 1967.
11. Sens, M. A., Wilson, N. K., Ellis, P. D. and Odom, J. D. *J. Magn. Reson. 19* (1975) 323.
12. Kennedy, J. D. and McFarlane, W. *J. Chem. Soc. Faraday Trans. 2 72* (1976) 1653.
13. Ödberg, L. and Högfeldt, E. *Acta Chem. Scand. 23* (1969) 1330.
14. Kondo, M. *Bull. Chem. Soc. Jpn. 45* (1972) 2790.
15. Zanger, M., Simons, W. W. and Gennaro, A. R. *J. Org. Chem. 33* (1968) 3673.
16. Bartels-Keith, J. R. and Cieciuch, R. F. W. *Can. J. Chem. 46* (1968) 2593.

Received June 12, 1981.

Acta Chemica Scandinavica A 36 (1982) 141 – 157

Zero Surface Tension (ZST) Theory of Micellization

TORBEN SMITH SØRENSEN

Fysisk-Kemisk Institut, DTH 206, DK-2800 Lyngby, Denmark

A theory of micellization is proposed describing micelle formation as an interrupted droplet nucleation process. The aggregation stops when a surface tension of the micelle close to zero or negative is produced by the growing surface concentration of polar heads. The decrease in surface tension is caused by repulsive forces between head groups of steric or electrostatic origin.

From data on aggregation numbers of oligo-oxyethylene derivatives of n-alkanoles, the distance of displacement of the surface of tension from the surface of the hypothetical hydrocarbon core of the micelle is calculated. The surface of tension is positioned from 5 to 11 Å *inside* the hydrocarbon core. Those figures are somewhat higher than calculated by Tolman for liquids in equilibrium with vapor or by Nielsen and Sarig for droplet nucleation within a miscibility gap in a ternary liquid system. The reason is probably the large size of the head groups of the amphiphiles considered.

The zero surface tension model mostly coincides with the phase separation model with regard to data on critical micelle concentration (cmc). From such data the thermodynamics of transfer of the hydrophobic part of the amphihile can be calculated because of the small or vanishing contribution of surface free energy in a zero surface tension model.

The mean shape of micelles is assumed spherical rather than ellipsoidal. For large micelles a "central hole" is avoided by head group burial or water inclusion in the hydrophobic core. Because of the low surface tension, micelles are vigorously oscillating and dividing/coalescing predominantly according to a "peanut shape". Some observed anomalies in rheology and light scattering may be explained that way. The cloud point observed for nonionic micelles is possibly the temperature where the surface tension becomes exactly zero and long surfactant cylinders are formed by secondary aggregation of micelles.

The diffuse electric double layer lowers the surface tension more at low ionic strength than at high. Therefore, the aggregation number of ionic micelles increases sharply with increasing ionic strength and approaches a nonionic limit with bound counterions.

In the past decade, a number of important contributions to the theory of micelles has appeared from the point of view of phenomenological thermodynamics [1-4] and from the point of view of reaction kinetics (relaxation processes).[5-8] Nevertheless, the field of micelle research still appears to be confusing, and it is hard to make genuine predictions from the existing theories. As an example, take the theory of Tanford where we have two adjustable parameters: one correction for "surface roughness" and a coefficient of "opposing forces" of steric origin. The latter is not calculable from first principles, see the 1980 edition of Ref. 1, pp. 72 – 73.

It is the purpose of the present paper to propose a *simple* picture of micellization by using some of the features of the previous thermodynamic models and suggesting some modifications which seem inevitable. The most important modification made in the present paper is the introduction of a micellar surface tension which varies with the aggregation number of the micelle according to simple laws known from the surface chemistry of monolayers. The approximation made here is to regard the micelle interior as an oil phase and the polar heads at the oil-water interface as "surfactants" which lower the interfacial tension. Now, steric effects become calculable by means of an excluded area approach.

The surface concentration of heads increases with aggregation number, and the surface tension becomes lower. Finally, a situation is reached, where the surface tension becomes close to zero or even negative. Then, the micelle will be destabilized by

0302-4377/82/020141-17$02.50

Brownian motion or micro-Marangoni effects, and dissolution of the micelle occurs. Thus, the picture of micellization which is given here is one which might be described as an "interrupted nucleation process". The difference between classical theory of nucleation and the present theory of micellization is precisely the *variable surface tension* in the latter theory. The value zero of the surface tension provides an upper bound for the size of the micelle and prevents phase separation in any macroscopic sense taking place.

THEORY OF NONIONIC, SPHERICAL MICELLES

Free amphiphile molecules in aqueous solution (A) associate into a cluster of aggregation number m according to the equilibrium K_m being the association constant. Assuming ideality we have from the law of mass action eqn. (1), where X and X_m

$$mA \overset{K_m}{\rightleftharpoons} A_m$$

$$K_m = \frac{X_m}{X^m} = \exp\left[\frac{-\Delta G_m^{\ominus}}{kT}\right] \tag{1}$$

are the mol fractions of free amphiphile and m-mer, respectively. $\Delta G_m^{\ominus}$ is the standard free energy of formation of one m-cluster, k is Boltzmann's constant and T is the absolute temperature. For the standard free energy we have eqn. (2), $\mu_m^{\ominus}$ being the

$$\Delta G_m^{\ominus} = \mu_m^{\ominus} - \mu_A^{\ominus} m \tag{2}$$

standard chemical potential of the aggregate and $\mu_A^{\ominus}$ the standard chemical potential of the free amphiphile. The standard chemical potential of the aggregate can be divided into two parts, eqn. (3),

$$\mu_m^{\ominus} = m\mu_B^{\ominus} + \mu_m' \tag{3}$$

where $\mu_B^{\ominus}$ is the size-independent part (due to hydrophobicity) and μ_m' the size-dependent part [eqn. (4)].

$$\mu_m' = f(m) \tag{4}$$

Following Ruckenstein and Nagarajan[3] we introduce a rescaled mol fraction of free amphiphile, eqn. (5).

$$\xi \equiv X \exp\left[\frac{\mu_A^{\ominus} - \mu_B^{\ominus}}{kT}\right] \tag{5}$$

From the preceding equations we obtain eqn. (6).

$$X_m = \xi^m exp\left[\frac{-\mu_m'}{kT}\right] \tag{6}$$

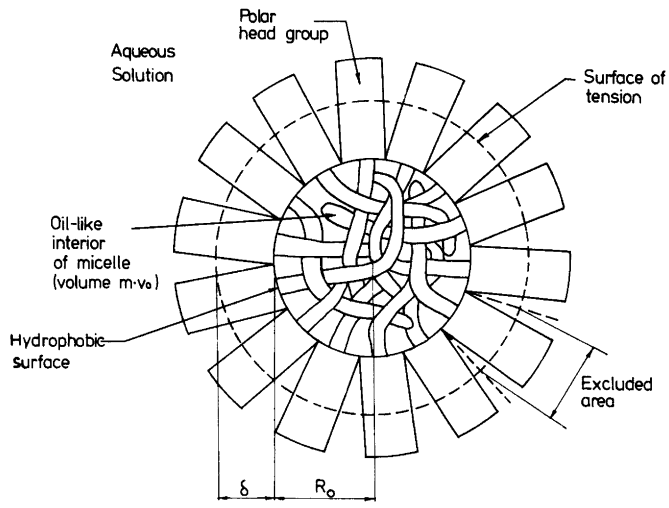

Fig. 1. Model of the micelle as a spherical oil-like droplet surrounded by polar heads. For simplicity, the surface of tension is situated outside the hydrophobic core as assumed by previous authors. In reality δ shows up to be negative. The polar heads are not in their state of closest packing, but in the state yielding zero surface tension, but the difference in area/head is not great.

Fixing the mol fraction of free amphiphile, the rescaled mol fraction ξ is fixed, and from any assumed functional dependence f(m) in eqn. (4), the size distribution of micelles can be calculated from eqn. (6).

The picture of the micelle is the one given schematically in Fig. 1. The hydrocarbon chains of the amphiphile molecules are assumed to form an "oil-like" hydrophobic core. The core is surrounded by polar head groups floating as "surfactants" at the oil – water interface. The volume of the hydrophobic core is simply given by mv_o, where v_o is the volume of a single hydrocarbon chain given by eqn. (7),[1,3] n_C being the number of carbon atoms in the hydrocarbon chain. Eqn. (7) is based on

$$v_o(\text{Å}^3/\text{amphiphile}) = 27.4 + n_C \cdot 26.9 \quad (T = 298.2\ \text{K}) \tag{7}$$

volume measurements of Reiss-Husson and Luzzati on pure alkanes.[9] Thus, the radius of the hydrophobic core is given as eqn. (8), with β given in eqn. (9).

$$R_o = \beta \cdot \sqrt[3]{m} \tag{8}$$

$$\beta \equiv \sqrt[3]{\frac{3v_o}{4\pi}} \tag{9}$$

The so-called *surface of tension* for small droplets is located in such a way that the overpressure in the droplet satisfies the Laplace equation, eqn. (10), with γ = surface tension.

$$\Delta p = \frac{2\gamma}{R_o + \delta} \tag{10}$$

For more details, the papers of Tolman[10] and Kondo[11] should be consulted.

The size-independent part of the standard free energy of transfer $(\mu_A^{\ominus} - \mu_B^{\ominus})$ is assumed to be a linear function of n_C as estimated from data of solubilities of hydrocarbons in water (Ref. 1, Chapter 2). We shall return to this later and confine ourselves here to the size-dependent part of the standard free energy of the micelle μ'_m, eqn. (11), where a is the area available for one polar head at the surface of tension, *viz.* eqn. (12).

$$\mu'_m = \gamma m a + \frac{2\gamma}{R_o + \delta}\left[\frac{4}{3}\pi(R_o + \delta)^3\right] \tag{11}$$

$$a = \frac{4\pi}{m}(R_o + \delta)^2 \tag{12}$$

The first term on the r.h.s. of eqn. (11) is the contribution from the surface free energy of the micelle. The second term is the contribution from the Laplace overpressure to the standard chemical potential of the micelle. Eqn. (11) may be rewritten as eqn. (13).

$$\mu'_m = \frac{44}{3}\pi\gamma[\beta \cdot \sqrt[3]{m} + \delta]^2 \tag{13}$$

It should be remembered, however, that the surface tension γ is a function of m. The relation between γ and the area per polar head will be assumed to be similar to the relation between those quantities at an oil-water interface with surfactants. We shall use the simplest possible relation, *viz.* the Szyszkowski isotherm, which is obtained by combination of the Langmuir adsorption isotherm with the Gibbs adsorption isotherm.[12,13] Thus, we have eqn. (14), where Π is the surface pressure, γ_o is the surface tension of the pure oil-water interface and a_{min} is the *excluded area* of a polar head group.

$$\Pi \equiv \gamma_o - \gamma = -\frac{kT}{a_{min}} \ln\left[1 - \frac{a_{min}}{a}\right] \tag{14}$$

Eqn. (14) is valid for plane interaces or for curved interfaces with large radii of curvature. Tolman[10] has shown that the surface tension has to be corrected for very small droplets, however, when the surface of tension is displaced from the surface of no superficial density of the drop material. Strictly speaking, Tolman's correction was derived for a droplet in equilibrium with its own vapor, but the experimental nucleation study of Nielsen and Sarig[14] of droplet formation within the miscibility gap of the ternary liquid system methanol – water – tribromomethane seems to indicate the correction to be approximately valid also for liquid – liquid interfaces. In the present case, the surface of no superficial density should be taken approximately to be the hydrophobic surface at R_o, and Tolman's correction would imply that the surface tension given by eqn. (14) should be divided by the factor $1 - 2\delta/(R_o + \delta)$. The final expression for the micellar surface tension is therefore eqn. (15), where γ_o^{∞} is the surface tension of a pure oil – water interface with an infinite radius of curvature.

$$\gamma = \left(\frac{R_o+\delta}{R_o-\delta}\right)\cdot\left(\gamma_o^{\infty} + \frac{kT}{a_{min}}\ln\left[1-\frac{a_{min}}{a}\right]\right) \qquad (15)$$

The machinery is now ready for the calculation of the distribution of aggregation numbers by means of eqns. (6), (13) and (15). For simplicity, we shall first assume $\delta = 0$ and only introduce δ as a correction to fit experimental data.

On Fig. 2 the calculations of surface tension and of the variable part of the standard free energy of the micelle are shown for $a_{min} = 60$ Å^2 and 8 carbon atoms in the hydrophobic chain ($n_C = 8$). The surface tension is seen to be a decreasing function of aggregation number m. If we consider for a moment m to be a continuous variable, we can calculated the aggregation number corresponding to zero surface tension from eqn. (15) with $\delta = 0$. The result is $m_o = 30.9$ which means that $m = 30$ is the last stable cluster size. The pure surface tension γ_o^{∞} has been put equal to 50 mN/m all over in the present paper as an average value for the surface tension between the higher alkanes and water at 298.2 K.

The mol fractions of clusters with $m = 2$, 5, 10, 29 and 30 have been calculated for several fixed values of $\ln\xi$ in Table 1. It has been assumed that $X_m = 0$ for $m = 31$, 32 *etc.* It is seen that the mol fraction of $m = 30$ becomes important above $\ln\xi$-values around 9.2. In a very narrow range of ξ-values X_{30} grows rapidly from negligible values to values above unity corresponding to unattainable ξ-values (unattainable concentrations of free amphiphile). This narrow ξ-range corresponds to the concentration range around the *critical micelle concentration* (cmc).

In comparison to X_{30} we have negligible amounts of clusters with $m = 29$ *around* ξ_{cmc}. It is also remarkable that X_2 is negligible although $\mu'_2/kT < \mu'_{30}/kT$, but the fluid sphere model is of course inappropriate for low aggregation numbers. It is seen that the cmc-behaviour as well as the appearance of a definite micelle size around and

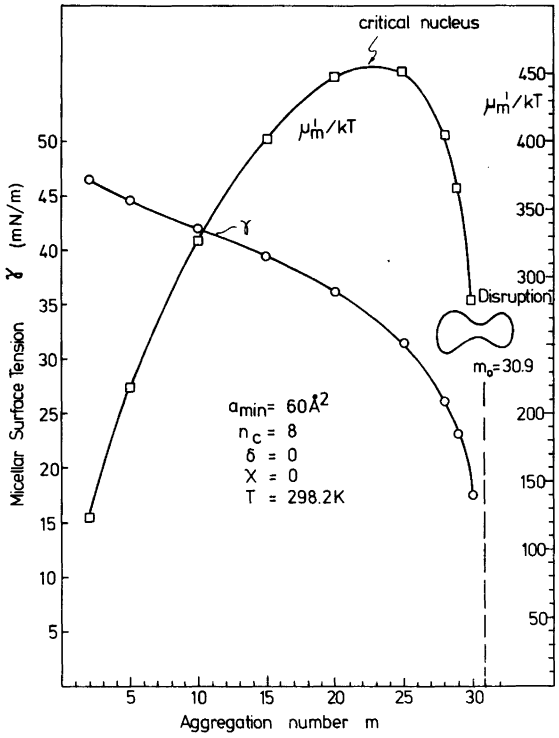

Fig. 2. Micellization described as a nucleation process with disruption at zero surface tension. Due to the large excluded area and the short hydrocarbon chains, the aggregation numbers have small values. The micellar surface tension and the micellar, variable free energy are shown as function of aggregation number.

Table 1. Mol fractions of aggregates of selected aggregation numbers as a function of ln ξ in the vicinity of ξ_{cmc}. Conditions as for Fig. 2.

m	ln ξ 5	8	9	9.2	9.3	9.4
2	4.2×10^{-50}	1.7×10^{-47}	1.2×10^{-46}	1.9×10^{-46}	2.3×10^{-46}	2.8×10^{-46}
5	8.3×10^{-85}	2.5×10^{-78}	4.0×10^{-76}	1.1×10^{-75}	1.8×10^{-75}	3.0×10^{-75}
10	1.5×10^{-120}	7.2×10^{-108}	1.6×10^{-103}	1.2×10^{-102}	3.2×10^{-102}	8.7×10^{-102}
29	1.9×10^{-96}	1.2×10^{-58}	4.6×10^{-46}	1.5×10^{-43}	2.7×10^{-42}	5.0×10^{-41}
30	1.4×10^{-58}	1.7×10^{-19}	1.85×10^{-6}	7.46×10^{-4}	1.50×10^{-2}	3.01×10^{-1}

above cmc is inherent in the present model. We shall go into details with other examples in the next sections.

HEAD GROUP BURIAL AND "OPPOSING FORCES"

Tanford (Ref. 1, Chapter 6) has given some arguments for the larger micelles being of an ellipsoidal rather than a spherical shape. Experimental evidence should be the high intrinsic viscosity and the high light scattering dissymmetry exhibited by such micellar solutions. A purely geometric consideration is the following: In the case of large aggregation numbers, the radius of an assumed spherical hydrophobic core becomes larger than the maximum length of a fully extended alkane chain of a single amphiphile. According to Tanford it is impossible to maintain the spherical shape of the micelle, since no micelle can have a hole in the middle.

In the opinion of the present author, many arguments *against* an ellipsoidal shape can be raised, however. Firstly, it is not possible to use viscosity models for rigid ellipsoids for fluid-like micelles with rapid exchange of amphiphiles with the surrounding solution (relaxation times around 10^{-4} s or greater [5,8]). Secondly, it is not possible to imagine an *equilibrium* shape of a fluid droplet which is not spherical. Either there will be pressure differences or surface tension gradients and Marangoni effects in an ellipsoidal droplet.

How do we then avoid the central hole in large micelles? I can here suggest two ways: (1) Inclusion of water pockets in the micelle as suggested by Menger,[15] (2) by the mechanism of *head group burial* in the hydrophobic core. Even in large micelles, a central hole may easily be filled out by pulling a small fraction of the head groups into the interior of the micelle. Both mechanisms will give rise to adverse energetic effects or "opposing forces" in the terminology of Tanford.

Thus, it is believed that the equilibrium shape of the micelle is always spherical. A micelle is a small thermodynamic system,[16] however, with vigorous fluctuations around the equilibrium state. Since micelles with low surface tensions will dominate according to the present theory, those micelles are easily deformable and will almost never be in the equilibrium spherical shape. In an appendix it is shown that the dominant mode of deformation due to Brownian motion and due to micro-Marangoni effects from thermal fluctuations is a *peanut shape* of the micelle. Since all the micelles are oscillating around the spherical shape, and since a snapshot of a solution of micelles would show a collection of randomly oriented peanuts, Tanford's concept of ellipsoidal micelles is quite precise, but the interpretation is more subtle. The light scattering data and the high intrinsic viscosities should be understood from this "fluctuating peanut" picture of a micellar solution.

We shall now discuss the influence of head group burial on the distribution of micellar aggregation numbers. The Szyszkowski isotherm [eqn. (14)] is linked to a Langmuir adsorption isotherm for the surfactant (here the polar heads), see Sheludko.[12] Therefore, we can write eqn. (16), where K is the

$$\frac{a_{min}}{a} = \frac{Kc}{1+Kc} \tag{16}$$

adsorption constant and c is the concentration of polar heads in the interior of the micelle. For c we have eqn. (17).

$$c = \frac{a_{min}/a}{K(1-a_{min}/a)} \tag{17}$$

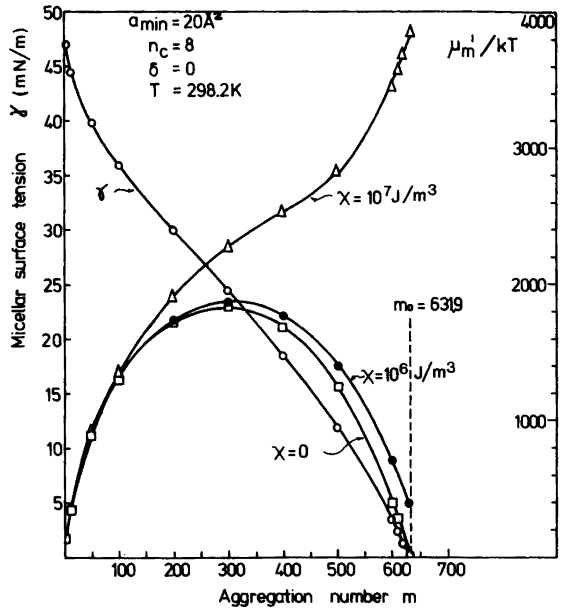

Fig. 3. Smaller excluded areas lead to higher aggregation numbers and a closer approximation to zero surface tension of the micelles. The energetic effects of head group burial (χ) is also shown. When χ-effects become dominating, the free energy becomes monotonously increasing, and a size distribution of micelles is produced above cmc.

It is reasonable to assume that the *free energy density* in the interior of the micelle is proportional to the concentration of buried head groups. The contribution to μ_m' from head group burial is therefore given by eqn. (18), where χ is a coefficient

$$\mu_m'(\text{burial}) = \chi \cdot \frac{a_{min}/a}{1 - \frac{a_{min}}{a}} \cdot m v_o \qquad (18)$$

characteristic for the type of head group. (The singularity at $a = a_{min}$ has no importance, since a reaches the area of zero surface tension a_o before it reaches a_{min} for growing size of the micelle). Instead of eqn. (13) we have now eqn. (19).

$$\mu_m' = \frac{44}{3}\pi\gamma[\beta\sqrt[3]{m} + \delta]^2 + \chi \cdot v_o \frac{a_{min} m^2}{4\pi(\beta\sqrt[3]{m} + \delta)^2 - a_{min} m} \qquad (19)$$

From eqn. (19) and eqns. (6) and (15) the aggregation number distribution can be calculated.

In Fig. 3 calculations for $a_{min} = 20$ Å^2, $\delta = 0$ and $n_c = 8$ are shown ($T = 298.2$ K). The aggregation "number" corresponding to zero surface tension is $m_o = 631.9$, and for $m_{max} = 631$, γ as well as μ_m'/kT come very close to zero in comparison to the case in Fig. 2. Free energy curves are also shown for $\chi = 10^6$ and 10^7 J/m^3. In the latter case the free energy maximum ("critical nucleus") disappears and μ_m'/kT

Table 2. Mol fractions of the two most frequent aggregation numbers in the case $n_c = 8$ and $a_{min} = 20$ Å^2. $\chi = 0$. See also Fig. 3.

	ln ξ				
m	0	0.005	0.010	0.015	0.018
630	6.6×10^{-12}	1.5×10^{-10}	3.6×10^{-9}	8.4×10^{-8}	5.6×10^{-7}
631	6.0×10^{-6}	1.39×10^{-4}	3.28×10^{-3}	7.69×10^{-2}	5.11×10^{-1}

Table 3. The influence of a_{min} and χ on micellar aggregation number and on cmc.

a_{min} (Å^2)	60	20	20	20	20
χ (J/m^3)	0	0	10^5	10^6	10^7
m_{max}	30	631	631	631	631
$m_{micelle}$	30	631	631	631	535 – 555
ξ_{cmc}	9.25×10^3	1.00447	1.0675	1.844	2.61×10^2

becomes monotonously increasing.

In Table 2 the mol fractions corresponding to the two most frequent aggregation numbers for $\chi = 0$ are shown. It appears that we have also in this case a practically monodisperse distribution of aggregates with aggregation number equal to $m_{max} = 631$ for ln ξ-values above around 0.005.

Table 3 summerizes the influence of a_{min} and χ on micellar aggregation numbers and on cmc. A lower value of the excluded area yields higher aggregation numbers and values of ξ_{cmc} closer to unity (for $\chi = 0$). For very high values of χ where the free energy maximum disappears, a *distribution* of molecular weights and aggregation numbers is introduced. The distribution is shown in Fig. 4 for two values of $\xi \gtrsim \xi_{cmc}$. It is seen that opposing forces caused by head group burial also increase ξ_{cmc} well above unity.

Different kinds of empirical or semi-empirical expressions for "opposing force" contributions to μ'_m have been considered by Tanford,[1,2] Ruckenstein and Nagarajan[3] and Israelachvili *et al.*[4] They all lead to a distribution of aggregation numbers as above. The "opposing force" contribution is claimed to be caused by steric or electrostatic reoulsion between head groups, however. The present author fundamentally disagrees with that position for the following reasons: The effect of increased steric repulsion (increased excluded area) is to *increase* the surface pressure. Thus, the surface tension and the variable free energy *decrease* because of repulsion between head groups. As we shall see later, the same can be said for electrostatic repulsion. Thus, to have an *increase* in surface free energy a Π-a-relationship including *attractive* forces between the head groups in the monolayer should be invoked, *e.g.* a Frumkin isotherm.[1,2]

In a certain sense, the position of the above-mentioned authors is correct, however. Repulsive forces between head groups lead to a faster decrease

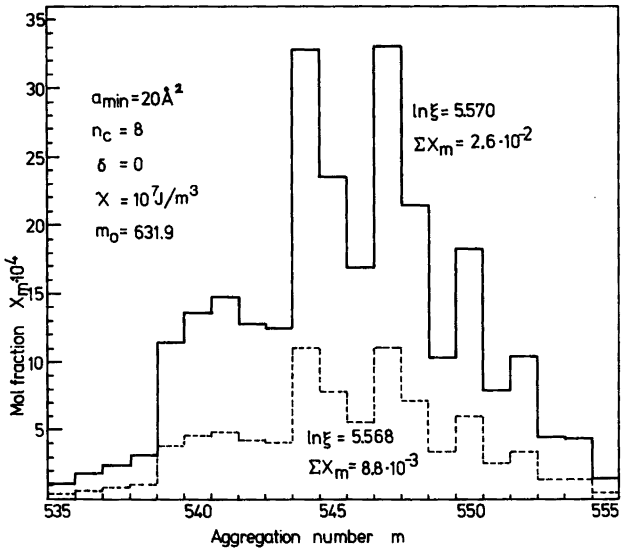

Fig. 4. Histograms showing the size distribution produced by large energetic effects in connection with head group burial ($\chi = 10^7$ J/m^3). Two different values of ln ξ have been taken, exhibiting the sharp increase in total micelle mol fraction (Σx_m) around ξ_{cmc}.

of surface tension with aggregation number. Therefore, the surface tension is brought to zero faster. From eqn. (6) and the fact that we assume $X_m = 0$ for all $m \geq m_0$ it appears that we assume an "opposing force" contribution which rises from zero to infinity at $m = m_0$. Therefore, the interpretation of the "principle of opposing forces" is indeed a subtle one (Ref. 1 pp. 70–77).

To summarize, I have assumed a "switch-on" opposing force of infinity above m_0. Apart from that, opposing forces are believed to originate in *attractive* forces between head groups or in head group burial or water inclusion in the hydrophobic core.

COMPARISON WITH EXPERIMENTAL RESULTS FOR NONIONIC MICELLES

In this section we shall test the ZST model of micellization on data for mean aggregation numbers for oligo-ethylene oxide derivatives of n-alkanoles. Such data have been reported earlier by Becher.[17] The amphiphiles are characterized by the number of carbon atoms in the alkane chain (n_C) and the number of ethylene oxide groups (n_{EO}).

If the micellar size distribution is assumed approximately monodisperse with aggregation number $\bar{m} = m_{max} \cong m_0$, we obtain from eqns. (8), (9), (12) and (15) with $\delta = 0$ and $\gamma = 0$ the relation (20).

$$\bar{m} \cong m_0 = \frac{36\pi v_0^2}{a_{min}^3}\left[1 - \exp\left(-\frac{\gamma_0^\infty a_{min}}{kT}\right)\right]^3 \qquad (20)$$

Isolating instead a_{min} and taking $\delta \neq 0$ we obtain eqn. (21).

$$\frac{a_{min}}{1 - \exp\left(-\frac{\gamma_0^\infty a_{min}}{kT}\right)} = \frac{\sqrt[3]{36\pi v_0^{2/3}}}{\sqrt[3]{\bar{m}}}\left(1 + \frac{\delta}{\beta\sqrt[3]{\bar{m}}}\right)^2 \qquad (21)$$

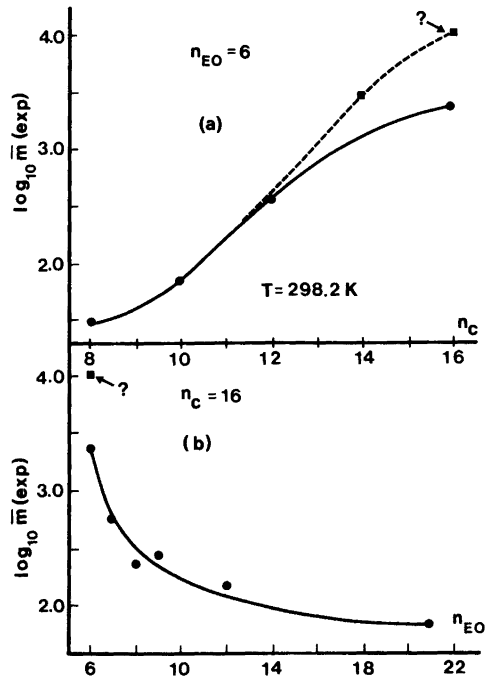

Fig. 5. (a) Experimental aggregation numbers of hexoxyethylene alkanol ether micelles as a function of the number of carbon atoms in alkane chain. Data from Becher.[17] Question mark indicates a probably erroneous value. (b) Influence of varying n_{EO} on experimental aggregation numbers of Becher. $n_C = 16$. Question mark corresponds to question mark on Fig. 5(a).

Since the volume v_0 of the hydrocarbon chain grows linearly with the number of carbon atoms, we see from eqn. (20) that we should expect a drastic increase in aggregation number for increasing length of the hydrocarbon chain. It is indeed observed that for $n_{EO} = 6$, the aggregation number

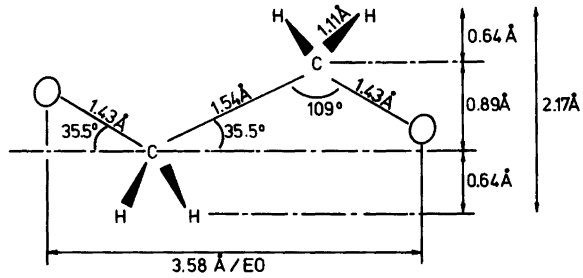

Fig. 6. Characteristic dimensions of a monomeric unit of an oligo-ethylene oxide chain.

Table 4. Influence of varying n_C on experimental aggregation numbers of hexa-ethylene oxide derivatives of n-alkanoles. $n_{EO}=6$. $T=298.2$ K.

n_C	$\bar{m}$(exp)[a]	$\bar{m}$(corr)[b]	v_o (Å^3)	R_o (Å)	δ (Å) for $a_{min}=15$ Å^2	δ for 20 Å^2
8	32	32	243	12.3	−5.5	−4.8
10	73	73	296	17.3	−7.1	−6.0
12	400	400	350	32.2	−8.3	−5.8
14	3100	–	404	66.9	(−0.33)	(+6.7)
14		1400	404	51.3	−6.7	−1.9
16	2430	2430	458	64.3	−5.5	+0.85
16	10500	–	458	104.7	(+17.6)	(+30.7)
Average and range of displacement of surface of tension					−6.6±1.7	−3.5±4.4

[a] Experimental data from Becher, Ref. 17. [b] Corrected data according to Fig. 5(a).

increases from 32 for $n_C=8$ to 2430 for $n_C=16$ (perhaps even higher aggregation numbers, see Fig. 5 and Table 4). In order to obtain quantitative agreement, one has to assume $\delta \neq 0$, however.

Fig. 6 shows the dimensions of a segment of a fully stretched poly-oxyethylene segment. When rotated around the longitudinal axis, the methylene hydrogen atoms describe a cylindrical surface with a cross sectional diameter equal to 2.17 Å. Adding twice the van der Waal radius for hydrogen (1.2 Å) we obtain an efficient diameter equal to 4.57 Å and a cross sectional area equal to 16.4 Å^2. The circumscribed quadrangle has an area equal to 20.9 Å^2. One could also imagine, however, that the excluded area were less than 16.4 Å^2 due to interpenetration of poly-oxyethylene chains. We shall therefore consider $a_{min}=15$ and 20 Å^2, respectively. From eqn. (21) we obtain eqn. (22), where the value 1.924 corresponds to $a_{min}=15$ Å^2 and the value 2.130 corresponds to $a_{min}=20$ Å^2. Values of δ have been calculated and the results are shown in Table 4 and Table 5.

$$\frac{\delta}{R_o} = \begin{Bmatrix} 1.924 \\ 2.130 \end{Bmatrix} \cdot \frac{\sqrt[6]{\bar{m}}}{[27.4+26.9n_C]^{1/3}} - 1 \qquad (22)$$

When n_{EO} is fixed and n_C varies one should not expect any great variation in δ. This is indeed the case in Table 4 for $a_{min}=15$ Å^2, but *not* for $a_{min}=20$ Å^2. Two of the experimental values of the aggregation numbers seem to be in error, however, see also Fig. 5. The average value of δ for $a_{min}=15$

Table 5. Influence of varying n_{EO} on aggregation numbers. $T=298.2$ K.

n_{EO}	$\bar{m}$(exp)[a]	$\bar{m}$(corr)[b]	R_o (Å)	δ (Å) for $a_{min}=15$ Å^2	δ for 20 Å^2
$n_C=13$					
8	71	–	18.6	−8.5	−7.4
10	61	–	17.6	−8.3	−7.3
12	55	–	17.0	−8.2	−7.2
$n_C=16$					
6	2430	2430	64.3	−5.5	+0.85
7	594	594	40.2	−11.1	−8.0
8	240	316	32.5	−11.3	−9.0
9	279	224	29.0	−11.2	−9.2
12	150	125	23.9	−10.6	−9.1
21	70	70	19.7	−9.7	−8.6

[a] Experimental data from Becher, Ref. 17. [b] Corrected data according to Fig. 5(b).

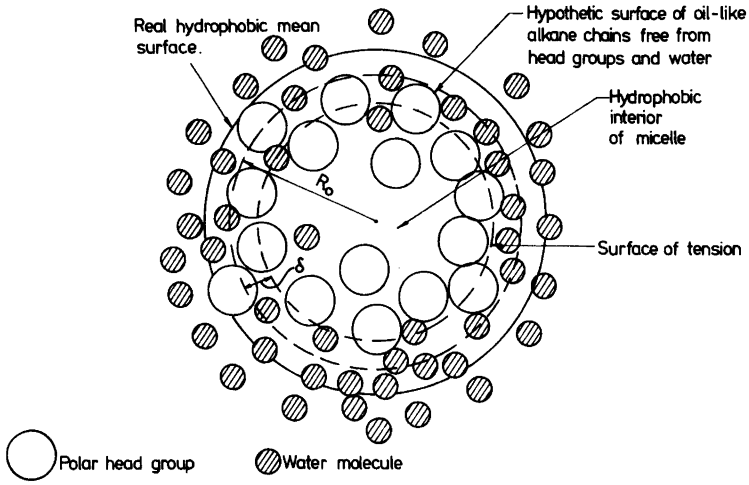

Fig. 7. Revised picture of a nonionic micelle. The surface of tension is displaced into the hydrophobic core due to water penetration and head group burial, and the distributions of molecules are statistical rather than regular as in Fig. 1.

Å^2 is -6.6 Å with a range equal to ± 1.7 Å. Thus, the surface of tension seems to be positioned *inside* the surface of the hydrophobic core. In comparison, for plane interfaces between liquids and their vapors, Tolman has found the surface of tension to be positioned around 1.0 – 3.5 Å inside the "surface of no superficial density of liquid". For very small spherical droplets (radii 14 – 32 Å) of tribromomethane in methanol – water mixtures, Nielsen and Sarig[14] have used Tolman's equation for the curvature correction of the interfacial tension in connection with the classical Volmer-Becker-Döring theory of homogeneous nucleation. A value of $-\delta$ equal to $+2.4$ Å was estimated for those critical nuclei. The larger values of $-\delta$ in Table 5 are not surprising in view of the bulky poly-oxyethylene groups present at the surface.

Fig. 5(b) and Table 5 show that also n_{EO} has an appreciable effect on aggregation numbers. The calculated values of $-\delta$ seem to be somewhat larger for longer poly-oxyethylene chains than $n_{EO}=6$ (Table 4), especially for the larger micelles with $n_C=16$. This may be seen as some evidence of increased water penetration into the micelle with increased poly-oxyethylene chain length and of increased head group burial for the larger micelles, although the data are far from conclusive.

The schematic picture of a micelle given in Fig. 1 should therefore be revised in the sense of Fig. 7 which shows the negative displacement of the surface of tension, the fluctuating head groups delving sometimes into the hydrophobic core and the water molecules penetrating quite far into the micelle.

THERMODYNAMICS OF TRANSFER

In addition to the aggregation number another important parameter is the *critical micelle concentration* (cmc). From Table 1 and Table 2 we see that the value of ξ_{cmc} jmay be estimated as the value yielding a molar fraction of $m=m_{max}$ equal to 10^{-4}, say. From eqn. (6) we have then eqn. (23).

$$\ln \xi_{cmc} \cong \frac{1}{m_{max}} \cdot \left[\frac{\mu'_{m_{max}}}{kT} - 9.21 \right] \tag{23}$$

For $m=m_{max}$ and $\chi=0$ (or at least not too great) we usually have $\mu'_m/kT \cong 0$ because of the low surface tension. Since m_{max} is mostly of the order of 100 or more, $\ln \xi_{cmc}$ will normally be quite close to zero and ξ_{cmc} quite close to unity. A very sharp transition takes place around this value for the molar fraction of $m=m_{max}$ because of the large power to which ξ is raised in eqn. (6).

With ξ_{cmc} close to unity we obtain from eqn. (5) the relation (24) between cmc and the free energy of transfer of the hydrocarbon part of the amphiphiles from water to the hydrophobic core of the micelle;

$$\ln X_{cmc} \cong \ln \frac{[cmc]}{55.5} \cong \frac{\mu_B^{\ominus} - \mu_A^{\ominus}}{kT} \quad (24)$$

[cmc] is in mol/dm^3 and 55.5 is the number of mol H_2O per dm^3 pure water. Thus, the ZST-theory yields the same basic result as the incorrect phase separation model as far as cmc is concerned. The reason is the very small contribution of the polar heads to the free energy of micellization. This fact serves as an explanation of why the phase separation model has maintained its popularity in thermodynamic studies of micellization based on cmc-measurements. Just to cite one recent example among numerous, see the paper by Kucharski.[18] However, the phase separation model can by its very nature give no idea whatsoever about aggregation numbers.

It should be remarked that ξ_{cmc} may *not* be close to unity for small micelles where m_{max} is small and μ_m'/kT may still be appreciable for $m = m_{max}$, see for example Fig. 2. The approximation may also break down for very large micelles if head group burial and water inclusion become energetically dominant.

If it is correct that cmc largely reflects the thermodynamics of transfer of the hydrocarbon chains, then cmc-data for oligo-oxyethylene derivatives of n-alkanoles should depend only on n_C, but not on n_{EO}. This is indeed the case as shown in Fig. 8 where data for ln([cmc]/55.5) *vs.* n_C for $n_{EO} = 3$, 6 and 9 are fitted by the same regression line. A comparison is made also with the regression lines for the transfer of n-alkanes from water to liquid alkane and for solubilization of n-alkanes from 0.1 mol/dm^3 NaCl solution into sodium dodecyl sulphate micelles. The latter regression lines are taken from Tanford [1] and correspond to $T = 298.2$ K.

It is remarkable that the standard free energy of transfer from water to micelles of the alkane chains is greater than the free energy of transfer of the corresponding n-alkane from aqueous solution to liquid alkane. Probably, this is due to the more restricted motion of alkane chains in the micelle. The smaller hypervolume occupied in the statistical mechanical phase space gives rise to a greater chemical potential in the micelle in comparison with bulk, liquid alkane. Also, the effect of buried head groups and water inclusion will tend to elevate the chemical potential. A great part of the micelles is rather to be described as a surface region than as a bulk fluid.

Alkanes solubilized in micelles seem to occupy an intermediary position from Fig. 8. The chemical potential is higher for an alkane solubilized in a

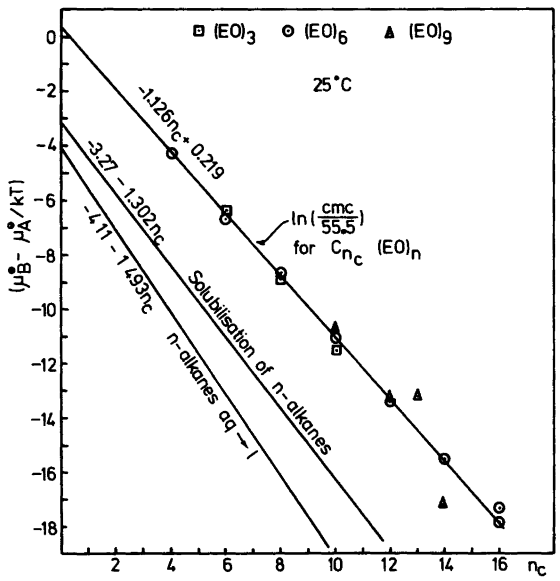

Fig. 8. Thermodynamics of transfer into nonionic micelles of the hydrophobic part of the amphiphiles as compared with the thermodynamics of solubilization of n-alkanes in SDS micelles and of n-alkanes from water into liquid n-alkanes as given by Tanford (1).

micelle than for an alkane dissolved in bulk alkane. However, the chemical potential of a solubilized alkane is lower than the chemical potential of the hydrocarbon chain of an amphiphile, since a solubilized alkane is more free to move in the interior of the micelle, being not restricted by a polar head group.

PRELIMINARY TREATMENT OF IONIC MICELLES

In order to be able to treat ionic micelles, it is necessary to know the influence of the electric forces on surface tension. The situation here is quite parallel to the situation arising in the thermodynamic description of microemulsions. Ruckenstein and Krishnan[19,20] have calculated equilibrium droplet radii of microemulsions formed with ionic surfactants and nonionic cosurfactants. In the case of ionic micelles, the charged heads are considered as "surfactants" and there are no cosurfactants. In that case the equation of Ruckenstein and Krishnan for the interfacial tension (Ref. 19, eqn. 36) reads as eqn. (25), where ψ_s

$$\gamma = \gamma_o - \frac{kT}{a_{min}} \ln[1 + K' c_A] - \int_0^{\psi_s} \sigma \mathrm{d}\psi_s' \tag{25}$$

is the surface potential and σ the surface charge density. The Langmuir adsorption constant K' has a contribution from the surface potential, *viz.* eqn. (26),

$$K' \equiv K \exp(-z_A \psi_s / kT) \tag{26}$$

z_A being the charge of the amphiphile. Now, the Langmuir isotherm yields for the surface concentration of occupied states eqn. (27) or eqn. (28).

$$\Gamma = \frac{1}{a} = \frac{1}{a_{min}} \cdot \frac{K' c_A}{1 + K' c_A} \tag{27}$$

$$1 + K' c_A = \left[1 - \frac{a_{min}}{a}\right]^{-1} \tag{28}$$

When eqn. (28) is introduced into eqn. (25) we obtain eqn. (29), which is simply a Szyszkowski isotherm

$$\gamma = \gamma_o + \frac{kT}{a_{min}} \ln\left[1 - \frac{a_{min}}{a}\right] - \int_0^{\psi_s} \sigma \mathrm{d}\psi_s' \tag{29}$$

with a contribution from surface charge. The last term represents the free energy of formation of the diffuse double layer. The interpretation of γ_o is still that of a pure oil–water interfacial tension, since the hypothetical "adsorption process" is carried out at constant micellar radius starting from a "micelle" with no head groups on the surface.

Strictly speaking, a Tolman correction for γ should be introduced. The correction drops out, however, for zero surface tension. Ruckenstein and Krishnan did not correct for curvature either, but they found also for microemulsions that the interfacial tension was zero to a good approximation. Microemulsions of the type studied by Ruckenstein and Krishnan may be described as highly oil-solubilized micelles formed with surfactants and cosurfactants, so those calculations support the zero surface tension theory of micellization proposed in the present paper.

If we neglect the radius of the counterions in comparison to the radius of the micelle, and if we take the surface charge as being located at the hydrophobic surface ($\delta = 0$), the surface potential according to simple Debye-Hückel theory (see for example Ref. 21) is given as eqn. (30), where m is the

$$\psi_s = \frac{mF}{4\pi N_o \varepsilon R_o} [1 + \kappa R_o]^{-1} \tag{30}$$

number of head groups, F the Faraday, N_o Avogadro's number, ε the absolute permittivity of water and κ the inverse Debye-Hückel length. The charge density on the surface is given by eqn. (31)

$$\sigma = \frac{mF}{4\pi R_o^2 N_o} \tag{31}$$

and m may be used as the integration variable remembering to leave R_o constant during the integration. With the integration performed and with $\delta = 0$, eqn. (29) can now be written as eqn. (32).

$$\gamma = \gamma_o + \frac{kT}{a_{min}}\left[1 - \frac{a_{min}\sqrt[3]{m}}{4\pi\beta^2}\right] - \frac{1}{2}\frac{F^2 m^2 (1 + \kappa\beta\sqrt[3]{m})^{-1}}{16\pi^2 \varepsilon N_o^2 \beta^3 m} \tag{32}$$

Note that we have (afterwards!) introduced the m-dependence of R_o. The aggregation number leading to zero surface tension can now be determined by eqn. (33). In practice, it is easier to determine κ as a function of m_o; eqn. (34).

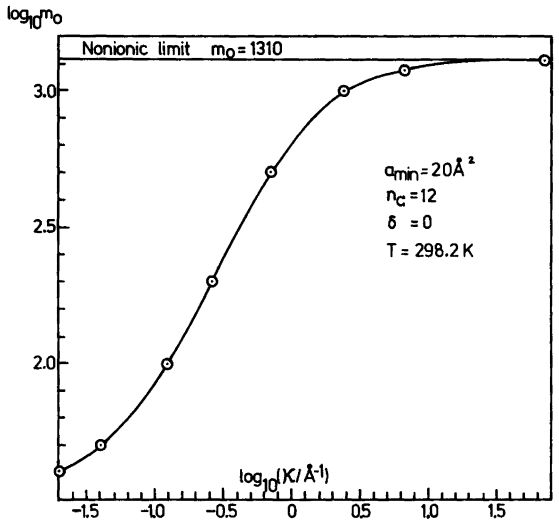

Fig. 9. The increase and saturation of aggregation numbers of ionic micelles with $n_C = 12$ with increase in the inverse thickness of the diffuse double layer.

$$(1+\kappa\beta\sqrt[3]{m_o})\left[\frac{\gamma_o a_{min}}{kT}+f_2(m_o)\right]=f_1(m_o) \tag{33}$$

$$\kappa\beta = m_o^{-1/3}\left[\frac{f_1(m_o)}{\frac{\gamma_o a_{min}}{kT}+f_2(m_o)}-1\right] \tag{34}$$

In eqns. (33) and (34) the functions (35) and (36) have

$$f_1(m_o)=\frac{a_{min}F^2 m_o}{32kT\pi^2 N_o^2 \varepsilon \beta^3} \tag{35}$$

$$f_2(m_o)=\ln\left[1-\frac{a_{min}\sqrt[3]{m_o}}{4\pi\beta^2}\right] \tag{36}$$

been introduced. As an example, we may take an amphiphile with $n_C = 12$, $\beta = 4.37$ Å and $a_{min} = 20$ Å^2. The temperature is 298.2 K, γ_o is 50 mN/m and $\varepsilon = 6.954 \times 10^{-10}$ A s/V m.

The aggregation number m_o is shown as a function of κ in Fig. 9. Values of m_o below about 40 yield negative values of κ as calculated from eqn. (34). Therefore, aggregation numbers below 40 cannot exist under any circumstances. At $\kappa \cong 0$, the aggregation number is around 40 corresponding to very small ionic strengths where electrostatic repulsion is very efficient in lowering the surface tension. At higher values of κ and the ionic strength, the aggregation number rises sharply to orders of magnitude 10^2 and 10^3.

Such a behaviour has indeed been found experimentally by Mazer, Benedek and Carey [22] in a light scattering study of micellar weights of (impure) sodium dodecyl sulphate (SDS) as a function of NaCl concentration. The behaviour has been confirmed for pure SDS samples using membrane osmometry by Birdi, Dalsager and Backlund.[23] Both studies were carried out at 40 °C, however. The latter authors found aggregation numbers rising from 103 at 0.1 mol/dm^3 to 700 at 0.8 mol/dm^3 of added NaCl.

In the case of cationic micelles, it should be mentioned that Dalsager [24] has also observed an increase in the aggregation number of TTAB-micelles (tetradecyl trimethyl ammonium bromide) with added KBr-koncentration from 126 (30 °C) or 148 (40 °C) at 0.1 mol/dm^3 KBr to 546 at 0.8 mol/dm^3 KBr and 30 °C or 345 at 0.7 mol/dm^3. In the simplified theory given here there should be no difference in that respect between anionic and cationic micelles, since the electrostatic term lowering the surface tension in eqn. (32) is proportional to the squared charge on the micelle.

None of the above-mentioned authors have observed the saturation effect shown in Fig. 9. It is seen that the aggregation number in the model example approaches 1310 at high ionic strengths.

That limit will be called the *nonionic limit*, since it is the aggregation number calculated from eqn. (20) without regard to electrostatic effects. The double layer is so narrow here that the counterions are best described as being bound to the ionic amphiphiles.

If the Debye-Hückel theory were strictly valid, κ^2 would be proportional to the ionic strength. It is well-known, however, that the Debye-Hückel approach yields only qualitatively correct results for higher ionic strengths than 0.01 mol/dm^3. I have used it here only for preliminary survey purposes. A better approach would be to invoke solutions of the non-linear Poisson-Boltzmann equation as done by Ruckenstein and Krishnan for microemulsions.[19,20] Furthermore, one would expect an asymmetry between anionic and cationic micelles. For small inorganic ions, activity and conductance data suggest that only the cations are hydrated and not the anions, see for example Sørensen.[25,26] For micelles one should then expect a more developed Stern layer of polarized water molecules around cationic micelles than around anionic micelles. Model refinements of that kind will be the object of a forthcoming paper.

DISCUSSION

The ZST model of micellization seems to be quite successful in explaining aggregation numbers and cmc-values in the case of nonionic micelles and probably also for ionic micelles. In contrast to earlier theories, the "opposing forces" in the surface layer of the micelles are assumed to lower the free energy of the micellar surface rather than to increase the free energy of the micelle. When the surface tension comes close to zero or becomes negative, the aggregates become destabilized. The aggregates then disintegrate predominantly into two (highly unstable) parts. The dominating stable aggregates have a quite low surface tensions and will tend to oscillate in a "peanut mode" around the equilibrium, spherical shape. Thus, high intrinsic viscosities and light scattering dissymetries may at least partially be explained that way instead of in terms of ellipsoid equilibrium shapes.

A simple model such as the ZST theory will necessarily have shortcomings, however. One of the most serious seems to be the prediction of monodispersity. Experimentally, one finds some dependence of molecular weights of micelles on concentration, and Hall and Pethica [27] have shown that such a dependence would be produced by a molecular weight distribution of micelles. Aniansson *et al.*[6] have demonstrated by chemical relaxation studies on sodium alkyl sulphates at 298.2 K that there is an aggregation number distribution width ranging from 6 to 16. The distribution has little or no effect on micelle polydispersity expressed as M_w/M_n, however. I would like to stress here that the prediction of monodispersity is not essential in the ZST-theory. It is very likely that the crude Szyszkowski isotherm exaggerates the decrease in surface tension in the neighbourhood of zero surface tension. A more "flat approach" produced by a more realistic adsorption isotherm would produce polydispersity in the ZST model too. As we have seen, a distribution of aggregation numbers is also produced by water inclusion, head group burial and attractive surface forces.

Another phenomenon which seems hard to explain by the ZST-model is the socalled "cloud point" of poly-oxyethylene surfactants. The size of the aggregates increases rapidly as the temperature is raised towards that cloud point.[28-31] Most authors have seen this as an increase in micellar aggregation numbers, but Tanford *et al.*[32] has suggested that what is observed is aggregation of micelles. An NMR-study by Staples and Tiddy seems to confirm that proposal.[33] From eqn. (21) only a slight temperature dependence of m_0 is predicted, since a_{min}, v_0 and β are expected to be only slightly dependent on temperature and since the exponential is small in comparison to unity. However, one could imagine a phase transition in the poly-oxyethylene surface layer or a change in water structure which altered a_{min} or changed the nature of the equation of surface tension. If the aggregation theory is correct, it may be taken as support for the ZST-theory. Long rods could form by aggregation of spherical micelles, but only at ultralow surface tensions. Any finite surface tension would lead to breakdown of a surfactant cylinder due to a kind of Rayleigh instability. Imagine then that the most stable micelles have a surface tension close to zero, but not exactly equal to zero at a given temperature. By raising the temperature, the surface tension decreases slightly and reaches zero at the cloud temperature where long rods form. Such lines of thought seem worthwhile to pursue in the future.

Acknowledgement. Prof. Eli Ruckenstein, Faculty of Engineering and Applied Sciences, State

University of New York at Buffalo, Buffalo, New York, is thanked for useful discussions during his visit to *Fysisk-Kemisk Institut* in 1981.

APPENDIX

Destabilization of droplets of low surface tension. The kinetic energy of a droplet in one spatial direction during Brownian motion is in the mean (root mean square) $kT/2$. The free energy increase in the process of formation of n equally sized droplets from one droplet of radius R is equal to

$$\left(\frac{20}{3}\right)\pi\gamma\cdot[\sqrt[3]{n}-1]R^2$$

where the "Kelvin effect" (increase in free energy due to increase in Laplace overpressure) has been included. Those two energies have to be comparable to each other to have a significant destabilization, *i.e.* eqn. (A1). It is seen that $n=2$ (peanut division)

$$\gamma_{\text{critical}}(n)=\frac{kT}{\frac{40}{3}\pi[\sqrt[3]{n}-1]R^2} \qquad \text{(A 1)}$$

becomes unstable before $n=3,4\ldots$ when the surface tension γ decreases. For a small micelle with $R=10$ Å, the critical surface tension is around 0.10 mN/m. For a large micelle with $R=70$ Å, $\gamma_{\text{critical}}\cong 2\times 10^{-3}$ mN/m. Both figures are indeed close to zero in comparison to the pure oil–water interfacial tension around 50 mN/m.

Sørensen and Hennenberg[34] and Sørensen[35] have considered the destabilizing effect of low surface tension during the diffusion of surfactants into droplets. A considerable decrease of the critical thresholds for Marangoni instability was predicted. By the analogy between heat and mass transfer, the results may immediately be transferred to heat conduction instabilities. A solution of micelles is of course an equilibrium system, but a single micelle may be far from equilibrium by, for example, thermal fluctuations. According to elementary statistical mechanics we have for the standard deviation of the temperature fluctuations of a small volume of heat capacity C_V immersed in a heat bath at temperature T, eqn. (A 2). If C_{sp} is the specific heat

$$\sigma(T)=T\sqrt{\frac{k}{C_v}} \qquad \text{(A 2)}$$

of fluid alkanes and ρ the density of fluid alkanes, we can write eqn. (A 3), where C_{sp} has been taken as

$$\frac{\sigma(T)}{T}\cong\sqrt{\frac{k}{C_{sp}mv_o\rho}}\cong\frac{3.14}{\sqrt{mv_o}} \qquad \text{(A 3)}$$

2090 J/kg deg and ρ as 700 kg/m^3. The value of v_o should be inserted in Å^3 as calculated from eqn. (7) for $T=298.2$ K. For simplicity, we assume in a given moment a parabolic temperature distribution in the micelle, eqn. (A 4), and the temperature T outside the

$$T_{\text{micelle}}=T_{\text{middle}}+\theta\left(\frac{r}{R}\right)^2 r\leq R \qquad \text{(A 4)}$$

micelle. Thermal fluctuations in surface tension are given by eqn. (A 5).

$$\delta\gamma=-\alpha\delta T_{\text{surface}} \qquad \text{(A 5)}$$

The thermal Marangoni number according to the theory of Sørensen and Hennenberg is defined as eqn. (A 6), where $l=2,3,4\ldots$ is the quantum number

$$Ma\equiv\frac{-2\theta\alpha R}{(2l-1)(2l-3)\left[\frac{l+1}{l}\kappa_2+\kappa_1\right]\eta_1} \qquad \text{(A 6)}$$

characterizing the considered spherical harmonics of surface deformation, κ_1 is the thermal diffusivity in the drop and κ_2 the thermal diffusivity outside. The dynamic viscosity in the drop is equal to η_1. For low surface tensions, the theory predicts a critical Marangoni number equal to eqn. (A 7), with a

$$Ma_{cr}=-\hat{\gamma}\hat{V} \qquad \text{(A 7)}$$

dimensionless surface tension number, eqn. (A 8), and a dimensionless viscosity number, eqn. (A 9)

$$\hat{\gamma}\equiv\frac{\gamma\cdot R}{\kappa_1\cdot\eta_1} \qquad \text{(A 8)}$$

$$\hat{V}\equiv\frac{(l+2)(l)(l-1)}{(2l-1)(2l-3)}\cdot\frac{1+\eta_2/\eta_1}{l-1+(l+2)\eta_2/\eta_1} \qquad \text{(A 9)}$$

(surface viscosity has been neglected). For positive surface tensions Ma_{cr} will be negative. Therefore, θ has to be positive and heat transfer from outside

and into the micelle to obtain instability. We derive that γ should be less than γ_{cr}; eqn. (A 10). The

$$\frac{\gamma_{cr}}{\theta\alpha} = \frac{2}{(l+2)l(l-1)} \cdot \frac{l-1+(l+2)\eta_2/\eta_1}{1+\eta_2/\eta_1} \cdot \frac{\kappa_1}{\frac{l+1}{l}\kappa_2+\kappa_1} \quad \text{(A 10)}$$

viscosity of water is $\eta_2 = 8.9 \times 10^{-4}$ kg/m s at 25 °C. At the same temperature, the viscosity of n-hexadecane is 30×10^{-4} kg/m s. However, Shinitsky *et al.*[36] have calculated the microviscosity in the interior of cationic micelles with n_C from 12 to 16 by measuring the fluorescence depolarization of aromatic hydrocarbon probes. Values as high as 170 to 320×10^{-4} kg/m s are found at 27 °C. The high values are probably reflecting the more restricted motion of the hydrocarbon chains in the micelles. We shall assume $\eta_1 = 250 \times 10^{-4}$ kg/m s. The thermal diffusivity in water at 25 °C is $\kappa_2 = 14.6 \times 10^{-8}$ m^2/s. In the micelle we use the value for transformer oil[37] $\kappa_1 = 7.4 \times 10^{-8}$ m^2/s. The following table can now be calculated from eqn. (A 10):

Critical surface tension for thermal Margangoni instability for micelles as a function of the spherical harmonic number.

l	$\gamma_{cr}/\theta\alpha$
2	0.0690
3	0.0383
4	0.0246
5	0.01724
7	0.00983
10	0.00527
15	0.00252
∞	$(2/3l^2)$

The size dependence of the critical surface tension enters only indirectly through the magnitude of the thermal fluctuations. We take approximately

$$\theta \cong \sigma(T) \cong \frac{3.14T}{\sqrt{mv_o}} \quad \text{(A 11)}$$

For α we take the value for a n-decane/water interface 0.05 mN/m deg.[38] For $n_C = 8$ and $m = 32$ we calculate a critical surface tension equal to 0.038 mN/m for the $l = 2$ normal mode (peanut). For $n_C = 16$ and $m = 10^4$ we obtain $\gamma_{cr} = 0.0017$ mN/m. We see that for both very small and very large micelles it is necessary with very low surface tensions to trigger instability. The critical surface tensions for thermal fluctuations are of the same order of magnitude as the critical surface tensions estimated for momentum fluctuations (Brownian motion). Again, the peanut mode is the mode triggered first when γ decreases.

REFERENCES

1. Tanford, C. *The Hydrophobic Effect. Formation of Micelles & Biological Membranes*, Wiley-Interscience, New York 1980. (1st edition 1973).
2. Tanford, C. *J. Phys. Chem. 78* (1974) 2469.
3. Ruckenstein, E. and Nagarajan, R. *J. Phys. Chem. 79* (1975) 2622.
4. Israelachvili, J. N., Mitchell, D. J. and Ninham, B. W. *J. Chem. Soc. Faraday Trans. 2, 72* (1976) 1525.
5. Aniansson, E. A. G., Wall, S. N., Almgren, M., Hoffmann, H., Kielmann, I., Ulbricht, W., Zana, R., Lang, J. and Tondre, C. *J. Phys. Chem. 80* (1976) 905.
6. Aniansson, E. A. G. *Ber. Bunsenges. Phys. Chem. 82* (1978) 981.
7. Sams, P. J., Wyn-Jones, E. and Rassing, J. *J. Chem. Soc. Faraday Trans. 2, 69* (1973) 180.
8. Rassing, J., Sams, P. J. and Wyn-Jones, E. *J. Chem. Soc. Faraday Trans. 2, 70* (1974) 1247.
9. Reiss-Husson, F. and Luzzati, V. *J. Phys. Chem. 68* (1964) 3504.
10. Tolman, R. C. *J. Chem. Phys. 17* (1949) 333.
11. Kondo, S. *J. Chem. Phys. 25* (1956) 662.
12. Sheludko, A. *Colloid Chemistry*, Elsevier, Amsterdam-London-New York 1966, pp. 114 – 119.
13. Szyszkowski *Z. Physik. Chem. 64* (1908) 385.
14. Nielsen, A. E. and Sarig, S. *J. Crystal Growth 8* (1971) 1.
15. Menger, F. M. *J. Phys. Chem. 83* (1979) 893.
16. Hill, T. L. *Thermodynamics of Small Systems*, Benjamin, New York 1963 (Part I), 1964 (Part II).
17. Becher, P. In Schick, M. J., Ed., *Nonionic Surfactants*, Dekker, New York 1967, Chapter 15.
18. Kucharski, S. *J. Colloid Interface Sci. 77* (1980) 488.
19. Ruckenstein, E. and Krishnan, R. *J. Colloid Interface Sci. 75* (1980) 476.
20. Ruckenstein, E. and Krishnan, R. *J. Colloid Interface Sci. 76* (1980) 188.
21. Tanford, C. *Physical Chemistry of Macromolecules*, Wiley, New York 1961, pp. 461 – 466.

22. Mazer, N. A., Benedek, G. B. and Carey, M. C. *J. Phys. Chem. 80* (1976) 1075.
23. Birdi, K. S., Dalsager, S. U. and Backlund, S. *J. Chem. Soc. Faraday Trans. 1, 76* (1980) 2035.
24. Dalsager, S. U. *Teoretisk og Eksperimentel Analyse af Micelledannelse*, Ph.D. Thesis, Technical University of Denmark, Lyngby 1980.
25. Sørensen, T. S. *Acta Chem. Scand. A 32* (1978) 571.
26. Sørensen, T. S. *Acta Chem. Scand. A 33* (1979) 583.
27. Hall, D. G. and Pethica, B. A. In Schick, M. J., Ed., *Nonionic Surfactants*, Dekker, New York 1967, Chapter 16.
28. Balmbra, R. R., Clunie, J. S., Corkill, J. M. and Goodman *Trans. Faraday Soc. 58* (1962) 1661.
29. Balmbra, R. R., Clunie, J. S., Corkill, J. M. and Goodman *Trans Faraday Soc. 60* (1964) 979.
30. Elworthy, P. H. and Macfarlane, C. B. *J. Chem. Soc.* (1963) 907.
31. Atwood, D. *J. Phys. Chem. 72* (1968) 339.
32. Tanford, C., Nozaki, Y. and Rohde, M. F. *J. Phys. Chem. 81* (1977) 1555.
33. Staples, E. J. and Tiddy, G. J. T. *J. Chem. Soc. Faraday Trans. 1, 74* (1978) 2530.
34. Sørensen, T. S. and Hennenberg, M. In Sørensen, T. S., Ed., *Dynamics and Instability of Fluid Interfaces, Lecture Notes in Physics No. 105*, Springer, Berlin-Heidelberg-New York 1979, pp. 276–315.
35. Sørensen, T. S. *J. Chem. Soc. Faraday Trans. 2,76* (1980) 1170.
36. Shinitsky, M., Dianoux, C., Gitler, C. and Weber, G. *Biochemistry 10* (1971) 2106.
37. Isachenko, V. P., Osipova, V. A. and Sukomel, A. S. *Heat Transfer*, MIR Publishers, Moscow 1977, Appendices, Tables 5 and 7, pp. 481–482.
38. Landolt-Börnstein, *Zahlenwerte und Funktionen, II. Band, 3. Teil*, Springer-Verlag, Berlin 1956, 6th Ed., p. 462, Tabelle 23, 1321.

Received June 5, 1981.

Acta Chemica Scandinavica A 36 (1982) 159 – 166

The Molecular Structures of Dimethyl-, Diethyl- and Dipropylzinc Determined by Gas Phase Electron Diffraction. Normal Coordinate Analysis and *ab initio* Molecular Orbital Calculations on Dimethylzinc

ARNE ALMENNINGEN, TRYGVE U. HELGAKER, ARNE HAALAND and SVEIN SAMDAL

Department of Chemistry, University of Oslo, Blindern, Oslo 3, Norway

Dimethyl-, diethyl- and dipropylzinc (Me_2Zn Et_2Zn and n-Pr_2Zn) have been investigated by gas phase electron diffraction. The Zn – C bond distance in Me_2Zn, 193.0(2) pm, is significantly smaller than in Et_2Zn and n-Pr_2Zn, 195.0(2) and 195.2(3) pm, respectively. The valence angle <ZnCC is 114.5(3)° in Et_2Zn and 114.5(5)° in n-Pr_2Zn. 74(4) % of the alkyl chains in n-Pr_2Zn are in a *synclinal* conformation suggesting the presence of a weak attraction between the Zn atom and the terminal methyl group. Least squares refinement of a relatively simple valence force field for Me_2Zn yielded force constants that reproduce the frequencies of the normal modes according to the latest assignment to the nearest cm^{-1}. The structure of Me_2Zn has been fully optimized by *ab initio* molecular orbital calculations with a *double zeta* basis. The optimal structure is in reasonable agreement with the experimental results, and the orbital energy sequence in agreement with the published PE spectrum. Population analysis indicates that the 3*d* electrons of Zn must be regarded as non-bonding and the Zn – C bond as a pure σ-bond.

When di-5-hexenylzinc is prepared from di-5-hexenylmercury by metal exchange: $[CH_2=CH-(CH_2)_4]_2Hg + Zn \rightarrow [CH_2=CH(CH_2)_4]_2Zn + Hg$, di-(cyclopentylmethyl)zinc is obtained as a biproduct.[1] If the reaction mixture is kept at 120 °C for 3½ days, di(cyclopentylmethyl)zinc is formed in approximately 90 % yield.[1] The cyclization reaction is thought to proceed through a four-center transition state:

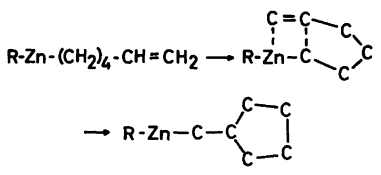

Di-4-pentenylzinc is found to be stable under the same conditions, probably because an analogous cyclization reaction would yield a strained cyclobutane ring.[1] The proton NMR spectrum of this compound shows an anomalous downfield shift of one of the vinyl H atoms relative to the parent hydrocarbon. This shift has been interpreted as evidence for weak intramolecular interaction between the metal atom and the double bonds.[1]

Recently we have investigated di-4-pentenylzinc by gas phase electron diffraction. The scattering pattern was found to be consistent with a molecular model in which both chains are coiled back to bring the CC double bonds close to the Zn atom, Zn – C ~ 220 pm.[2] In the hope that information about bond distances, valence angles, force fields and conformational preferences of simple dialkylzinc compounds would put this study on a firmer basis, we decided to investigate dimethylzinc, Me_2Zn, diethylzinc, Et_2Zn and dipropylzinc, n-Pr_2Zn.

Several studies of the vibrational spectrum of Me_2Zn have made it clear that the valence angle ∠CZnC is 180° and that the barrier to internal rotation is negligible.[3,4] The instantaneous sym-

0302-4377/82/020159-08$02.50

metry of the molecule is thus D_3. The moment of inertia obtained by rotational Raman spectroscopy yields a Zn–C bond distance of 192.9(4) pm.[5]

Normal coordinate analysis and calculation of spectroscopic parameters. Me_2Zn. Since the methyl groups undergo virtually free internal rotation, a classification of the normal modes must be made using the permutation–inversion double group G_{36}^{+} introduced by Hougen.[6] Moreover, the conventional *FG* formalism for rigid molecules is no longer appropriate, and an extension for dealing with molecules exhibiting nearly free internal rotation has been presented by Bunker.[7] Symmetry coordinates are chosen that render the *G* matrix rigorously independent of the torsional angle, the *F* matrix dependence is then expected to be small. Furthermore, the vibrational and torsional modes can be separated provided the torsional frequency is so low that the torsional angle remains essentially constant during the period of a genuine vibration. Proceeding as usual it is then possible to calculate 3N-7 normal coordinates and frequencies for some fixed value of the torsional angle. The resulting force field may be considered to be a reasonable approximation to the true, torsional dependent field.

The vibrational spectra of gaseous, liquid and solid Me_2Zn have recently been reinvestigated and partly reassigned by Butler and Newbury,[4] see Table 1. Using their results we have carried out a least squares refinement of the molecular force field for an eclipsed (D_{3h}) conformation employing a program written by G. O. Sørensen [8] and modified in our laboratory. The symmetry coordinates are listed in Table 2 and correspond to those given for dimethylacetylene [7] ($\gamma=0°$). Δr, ΔR, $\Delta\alpha$, $\Delta\beta$, $\Delta\phi$ refer to small displacements in the C–H, Zn–C bond lengths and ∠HCH, ∠ZnCH, ∠CZnC bond angles, respectively.

In order to keep the force field as simple as possible we first assumed a diagonal valence force field. It was found, however, that a satisfactory agreement required the inclusion of the interaction constants $f_{R\beta}$, and f_{rr} (within the methyl groups) and $f'_{\alpha\alpha}$ and $f'_{\beta\beta}$ (between the methyl groups). The last two small interactions will presumably show a strong torsional dependence, they are however essential for splitting of the otherwise nearly degenerate modes ν_9/ν_{13} and ν_{10}/ν_{14}. The final force field is listed in Table 3, and in Table 1 we list the calculated frequencies and the potential energy distributions for each mode. The agreement between this and earlier [9] force fields is reasonable.

Following Bunker and Hougen [10] we have calculated the torsional dependence of degenerate modes for several plausible force fields. Bunker and Hougen have shown that for dimethylacetylene close-lying pairs of modes can be either (E_{1d}, E_{2d}) or (E_{1s}, E_{2s}) depending on the γ-dependent terms in the force field. For Me_2Zn the situation is more clear-cut in that two of these pairs (ν_9, ν_{13}) and (ν_{10}, ν_{14}) are not found to be nearly degenerate. Force constants of type (6) in Bunker and Hougen's

Table 1. Observed and calculated frequencies for Me_2Zn (cm^{-1}).

Vibration number	Symmetry species	Obs. frequency [a]	Calc. frequency	Potential energy distribution
ν_1	a_{1s}	2916	2915	99r
ν_2	a_{1s}	1180	1180	$73\alpha+36\beta$
ν_3	a_{1s}	511	510	114R
ν_5 [b]	a_{4s}	2914	2915	99r
ν_6	a_{4s}	1183	1183	$72\alpha+35\beta$
ν_7	a_{4s}	613	613	114R
ν_8	e_{1d}/e_{1s}	2970	2970	99r
ν_9	e_{1d}/e_{1s}	1301	1301	96α
ν_{10}	e_{1d}/e_{1s}	704	704	95β
ν_{11}	e_{1d}	157 [c]	157	98ϕ
ν_{12}	e_{2d}/e_{2s}	2970 [c]	2970	99r
ν_{13}	e_{2d}/e_{2s}	1435 [c]	1435	97α
ν_{14}	e_{2d}/e_{2s}	611	611	98β

[a] Ref. 4. [b] Assuming free rotation of methyl groups, there is no methyl torsional mode. [c] These modes have not been observed in the gas phase. ν_{11} and ν_{13} are transferred from corresponding liquid data, ν_{12} is set equal to ν_8 gas phase frequency.

Table 2. Symmetry coordinates for Me_2Zn in eclipsed conformation.[a]

$a_{1s}(a_1')$

$$s_1 = \frac{1}{\sqrt{6}}(\Delta r_1+\Delta r_2+\Delta r_3+\Delta r_4+\Delta r_5+\Delta r_6)$$
$$s_2 = \frac{1}{\sqrt{6}}(\Delta\alpha_1+\Delta\alpha_2+\Delta\alpha_3+\Delta\alpha_4+\Delta\alpha_5+\Delta\alpha_6)$$
$$s_3 = \frac{1}{\sqrt{6}}(\Delta\beta_1+\Delta\beta_2+\Delta\beta_3+\Delta\beta_4+\Delta\beta_5+\Delta\beta_6)$$
$$s_4 = \frac{1}{\sqrt{2}}(\Delta R_1+\Delta R_2)$$

$a_{4s}(a_2'')$

$$s_5 = \frac{1}{\sqrt{6}}(\Delta r_1+\Delta r_2+\Delta r_3-\Delta r_4-\Delta r_5-\Delta r_6)$$
$$s_6 = \frac{1}{\sqrt{6}}(\Delta\alpha_1+\Delta\alpha_2+\Delta\alpha_3-\Delta\alpha_4-\Delta\alpha_5-\Delta\alpha_6)$$
$$s_7 = \frac{1}{\sqrt{6}}(\Delta\beta_1+\Delta\beta_2+\Delta\beta_3-\Delta\beta_4-\Delta\beta_5-\Delta\beta_6)$$
$$s_8 = \frac{1}{\sqrt{2}}(\Delta R_1-\Delta R_2)$$

$e_{1d}(e')$

$$s_{9a} = \frac{1}{\sqrt{12}}(2\Delta r_1-\Delta r_2-\Delta r_3+2\Delta r_4-\Delta r_5-\Delta r_6)$$
$$s_{9b} = \frac{1}{2}(\Delta r_2-\Delta r_3+\Delta r_5-\Delta r_6)$$
$$s_{10a} = \frac{1}{\sqrt{12}}(2\Delta\alpha_1-\Delta\alpha_2-\Delta\alpha_3+2\Delta\alpha_4-\Delta\alpha_5-\Delta\alpha_6)$$
$$s_{10b} = \frac{1}{2}(\Delta\alpha_2-\Delta\alpha_3+\Delta\alpha_5-\Delta\alpha_6)$$
$$s_{11a} = \frac{1}{\sqrt{12}}(2\Delta\beta_1-\Delta\beta_2-\Delta\beta_3+2\Delta\beta_4-\Delta\beta_5-\Delta\beta_6)$$
$$s_{11b} = \frac{1}{2}(\Delta\beta_2-\Delta\beta_3+\Delta\beta_5-\Delta\beta_6)$$
$$s_{12a} = \Delta\phi_x$$
$$s_{12b} = \Delta\phi_y$$

$e_{2d}(e'')$

$$s_{13a} = \frac{1}{2}(\Delta r_2-\Delta r_3-\Delta r_5+\Delta r_6)$$
$$s_{13b} = \frac{1}{\sqrt{12}}(2\Delta r_1-\Delta r_2-\Delta r_3-2\Delta r_4+\Delta r_5+\Delta r_6)$$
$$s_{14a} = \frac{1}{2}(\Delta\alpha_2-\Delta\alpha_3-\Delta\alpha_5+\Delta\alpha_6)$$
$$s_{14b} = \frac{1}{\sqrt{12}}(2\Delta\alpha_1-\Delta\alpha_2-\Delta\alpha_3-2\Delta\alpha_4+\Delta\alpha_5+\Delta\alpha_6)$$
$$s_{15a} = \frac{1}{2}(\Delta\beta_2-\Delta\beta_3-\Delta\beta_5+\Delta\beta_6)$$
$$s_{15b} = \frac{1}{\sqrt{12}}(2\Delta\beta_1-\Delta\beta_2-\Delta\beta_3-2\Delta\beta_4+\Delta\beta_5+\Delta\beta_6)$$

[a] Redundancies are removed by the program. Hydrogen atoms 1/4, 2/5 and 3/6 are eclipsed.

Table 3. F matrix and force constants for Me_2Zn.

a_{1s}	$F_{11}=f_r+2f_{rr}$	a_{4s}	$F_{55}=f_r+2f_{rr}$
	$F_{22}=f_\alpha$		$F_{66}=f_\alpha$
	$F_{33}=f_\beta$		$F_{77}=f_\beta$
	$F_{34}=\sqrt{3}\,f_{R\beta}$		$F_{78}=\sqrt{3}\,f_{R\beta}$
	$F_{44}=f_R$		$R_{88}=f_R$
e_{1d}	$F_{99}=f_r-f_{rr}$	e_{2d}	$F_{1313}=f_r-f_{rr}$
	$F_{1010}=f_\alpha+f'_{\alpha\alpha}$		$F_{1414}=f_\alpha-f'_{\alpha\alpha}$
	$F_{1111}=f_\beta+f'_{\beta\beta}$		$F_{1515}=f_\beta-f'_{\beta\beta}$
	$F_{1212}=f_\phi$		
f_r	476.4 N/m	f_α	0.517 aJ/rad^2
f_R	241 N/m	f_β	0.3057 aJ/rad^2
f_{rr}	4.9 N/m	f_ϕ	0.322 aJ/rad^2
		$f'_{\alpha\alpha}$	−0.054 aJ/rad^2
$f_{R\beta}$	3.20 nN/rad	$f'_{\beta\beta}$	0.0412 aJ/rad^2

paper are thus excluded in these cases, giving modes of species (E_{1s}, E_{2s}). For the close-lying pair (ν_8, ν_{12}) both fields (6) and (7) are plausible. However, due to lower degenerate modes this gives (E_{1s}, E_{2s}) in either case. It is important to realize that these arguments hold only if we assume that $\cos 6\gamma$-terms predominate over $\cos 12\gamma$- (and higher) terms – which seems physically reasonable. We thus arrive at the conclusion that (E_{1s}, E_{2s}) seems more probable than (E_{1d}, E_{2d}) for all modes except skeletal bending, contrary to what has previously been tacitly assumed by others.[4,11]

Root mean square vibrational amplitudes, *l*, and perpendicular amplitude correction coefficients, *K*, were calculated using the force constants given in Table 3.

Et_2Zn and n-Pr_2Zn. Approximate force fields for these molecules (Table 4) were constructed from the force field of Me_2Zn and the valence force constants of saturated alkanes.[12] The C–C stretching force constant of Et_2Zn was adjusted to reproduce the observed frequency at 922 cm^{-1}.[13] The value adopted for the ZnCC bending force constant yields bending frequencies around 270 cm^{-1}, in agreement with a recent normal coordinate calculation.[14] For torsional force constants we have used values estimated for 1-chloropropane.[15] Though reasonable, these values must be regarded as very uncertain. Calculations of vibrational amplitudes and correction coefficients were carried out with a program written by Hilderbrandt.[16]

Finally we calculated the vibrational partition functions (defined equal to unity at 0 Kelvin) for two conformers of n-Pr_2Zn: One with both chains

Table 4. Approximate valence force fields of Et_2Zn and n-Pr_2Zn.

Stretch (N/m)			
ZnC	242	C(1)H	455
C(1)C(2)	354	C(2)H	470[a]/455[b]
C(2)C(3)	439	C(3)H	470
Bend (aJ/rad^2)			
ZnCC	0.70	C(2)C(3)H	0.645
ZnCH	0.307	HC(1)H	0.550
CCC	1.13	HC(2)H	0.540[a]/0.550[b]
C(2)C(1)H	0.656	HC(3)H	0.540
C(1)C(2)H	0.645[a]/0.656[b]		
Torsion (aJ/rad^2)			
C(1)–C(2)	0.086[a]	C(1)–C(1')	0.01[b]
C(1)–C(2) (*sc*)	0.20[b]	C(2)–C(3)	0.086[b]
C(1)–C(2) (*ap*)	0.14[b]		
Linear bend (aJ/rad^2)			
CZnC	0.322		
Stretch-stretch (N/m)			
ZnC/CC	10	CC/CC	10
C(2)H/C(2)H	4.3[a]/0.0[b]	C(3)H/C(3)H	4.3
Stretch-bend (nN/rad)			
ZnC/ZnCC	4.2	CC/CCH	3.3
ZnC/ZnCH	3.2	CC/CCC	4.2[b]
Bend-bend (aJ/rad^2)			
C(i)C(j)H/C(j)C(i)H(*ap*)	0.127		

[a] Et_2Zn. [b] n-Pr_2Zn.

in the *antiperiplanar* conformation and one with both chains in a *synclinal* conformation. (For a more accurate description, see the section on electron diffraction.) We regard the square roots of these partition functions as the partition functions of a chain in the *ap* and *sc* conformations, respectively. The ratio $Q_{ap}/Q_{sc} = 1.25$ is greater than unity largely because the torsional force constant is assumed lower in the *ap* conformation.

Molecular orbital calculations. The molecular structure of Me_2Zn was fully optimized by *ab initio* molecular orbital calculations assuming D_{3h} (eclipsed) molecular symmetry. The optimization was carried out by Pulay's force relaxation method[17] using the program MOLFORCE written by S. Sæbø,[18] which is based on MOLECULE written by J. Almlöf.[19]

The basis consisted of four GTO *s*-functions on H contracted to $2s^{20}$ and (7*s*, 3*p*) functions for C contracted to $\langle 4s, 2p \rangle$.[21] For Zn we chose the (12*s* 6*p* 4*d*) basis of Roos *et al.*[22] augmented by two sets of diffuse 4*p* functions, contracted to $\langle 8s\ 6p\ 2d \rangle$. The total energy for the optimized model was −1856.09045 au.

ELECTRON DIFFRACTION

Experimental. The samples of Me_2Zn and Et_2Zn were gifts from J. Weidlein, Stuttgart, and the sample of n-Pr_2Zn from H. Lehmkuhl, Mülheim.

The electron scattering patterns were recorded on the Oslo electron diffraction unit[23] with nozzle temperatures of about 20 °C (Me_2Zn), 30 °C (Et_2Zn) and 60 °C (n-Pr_2Zn). Exposures were made with

nozzle-to-plate distances of about 48 and 20 cm for Me_2Zn, and 48 and 26 cm for Et_2Zn and n-Pr_2Zn. This study is based on two sets of six plates for Me_2Zn, six 48 cm and five 26 cm plates for Et_2Zn, and six 48 cm and three 26 cm plates for n-Pr_2Zn.

The data were processed by standard methods.[24] The complex atomic scattering factors, f'(s), were calculated from an analytical representation of the atomic potential[25] using a program written by Yates.[26] The molecular intensities were modified through multiplication with $s/|f'_C||f'_{Zn}|$. The average modified molecular intensities covered the ranges:

Me_2Zn: $s=13.75$ to $180.00\ nm^{-1}$ with $\Delta s=1.25\ nm^{-1}$
and $s=75.00$ to $325.00\ nm^{-1}$ with $\Delta s=2.50\ nm^{-1}$
Et_2Zn: $s=20.00$ to $197.50\ nm^{-1}$ with $\Delta s=1.25\ nm^{-1}$
and $s=65.00$ to $340.00\ nm^{-1}$ with $\Delta s=2.50\ nm^{-1}$.
n-Pr_2Zn: $s=40.00$ to $185.00\ nm^{-1}$ with $\Delta s=1.25\ nm^{-1}$
and $s=55.00$ to $270.00\ nm^{-1}$ with $\Delta s=2.50\ nm^{-1}$.

Structure refinement. In accordance with results of spectroscopic studies Me_2Zn was assumed to have D_3 symmetry with freely rotating (V=0) methyl groups. The molecular structure is then determined by the Zn−C and C−H bond distances and the valence angle ∠ZnCH.

It was likewise assumed that ∠CZnC=180° in both Et_2Zn and n-Pr_2Zn.

A molecular model of n-Pr_2Zn showing the numbering of the C atoms is shown in Fig. 1. A similar numbering scheme was adopted for Me_2Zn and Et_2Zn. Hence C(1) refers to the C_α atom in each of the three compounds, C(2) to the C_β and C(3) to the C_γ atom. The carbon atoms in the other chain are denoted C(1′), C(2′) and C(3′), respectively. The H atoms are numbered as the C atom to which they are bonded.

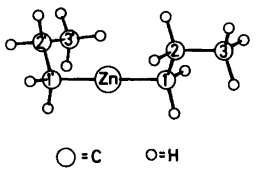

Fig. 1. Molecular model of n-Pr_2Zn. The right hand propyl chain is in the *antiperiplanar* (*ap*) conformation, the left hand chain in a *synclinal* (*sc*) conformation.

Initial refinements on Et_2Zn were carried out assuming a model of C_2 symmetry. It was further assumed that the $C-CH_3$ fragments have C_{3v} symmetry and that the methyl groups are oriented in such a way that one C(2)−H bond is *anti* the Zn−C(1) bond. The ∠HC(1)H angle of the methylene group was assumed equal to 106° and to be bisected by the ZnC(1)C(2) plane. Finally all C−H bond distances were assumed equal. The molecular structure is then determined by the Zn−C, C−C and C−H bond distances, by the valence angles ∠ZnCC, ∠ZnCH and ∠C(1)C(2)H and by the angle between the planes ZnC(1)C(2) and ZnC(1′)C(2′), ϕ[C(1)C(1′)]. The final refinements were carried out on a dynamic model with $V(\phi)=\frac{1}{2}V_0\cos\phi$. ϕ was defined as zero when C(2) and C(2′) are eclipsed. The refinement yielded $V_0=-1.5(16)$ kJ mol^{-1}, *i.e.* a value close to and not significantly different from zero. Introduction of the dynamic model yielded a slight improvement of the fit.

n-Pr_2Zn is present in the gas jet as a conformational mixture: The experimental radial distribution curve contains both a peak at about 440 pm corresponding to an *antiperiplanar* (*ap*) Zn−C(3) distance, and a shoulder at about 335 pm corresponding to a *synclinal* (*sc*) distance. Since conformation-dependent distances between atoms in different chains are greater than 475 pm and the experimental radial distribution curves show no perceptible structure in this range, we believe that for our purpose each chain may be regarded as independent of the other. We therefore assumed the mixture to consist of only two conformers, one with both chains in the *ap* conformation, and one with both chains in the *sc* conformation. Both conformers were assumed to have C_2 symmetry. The possible presence of other conformers, as for instance one containing one *ap* and one *sc* chain or one containing two *sc* chains but with molecular symmetry other than C_2, was thus disregarded.

The dihedral angle ϕ[C(1)C(1′)] was assumed equal in the two conformers, and was refined as an independent parameter. The resulting value, $\phi=77(25)°$, appears a reasonable average value for the permissible range, 0 to 180°.

In addition to the assumptions regarding molecular structure which had been made for Et_2Zn, it was assumed that the bond distances C(1)−C(2) and C(2)−C(3) are equal, and that the fragment $C(1)-C(2)H_2-C(3)$ has C_{2v} symmetry with ∠HC(2)H=106°. The valence angle ∠C(2)C(3)H was fixed at 110°.

The molecular structure of n-Pr_2Zn is then determined by eight independent parameters, the Zn−C, C−C and C−H bond distances, the valence angles ∠ZnCC, ∠ZnCH and ∠CCC, and by the mol fraction, χ_{sc} and dihedral angle ϕ(C(1)C(2)) of the *sc* conformer.

Table 5. Bond distances (r_a) and valence angles of Me_2Zn, Et_2Zn and n-Pr_2Zn. Dihedral angle (ϕ_{sc}) and mol fraction (χ_{sc}) of *synclinal* chains in n-Pr_2Zn. Estimated standard deviations in parentheses in units of the last digit.

	Me_2Zn	Et_2Zn	n-Pr_2Zn
Bond distances (pm)			
Zn–C	193.0(2)	195.0(2)	195.2(3)
C–C		154.0(3)	153.5(5)[a]
C–H	110.0(5)	110.5(4)[a]	109.7(4)[a]
Valence angles (deg)			
∠ZnCH	112.5(5)	107.9(8)	106.3(20)
∠ZnCC		114.5(3)	114.5(5)
∠CCH		114.0(13)[b]	[110][c]
∠CCC			113.6(16)
ϕ(C(1)–C(2))$_{sc}$ (deg)			60(4)
χ_{sc}			0.74(4)

[a] Average value. [b] ∠C(1)C(2)H. [c] ∠C(2)C(3)H, not refined.

The molecular structures of each of the three compounds were refined by least-squares calculations on the intensity data with a non-diagonal weight matrix[27,28] and under the constraints of geometrically consistent r_α structures. For Me_2Zn five root mean square vibrational amplitudes were included in the refinement, for Et_2Zn ten amplitudes were refined, and for n-Pr_2Zn eight. Those amplitudes that could not be refined, were fixed at the values calculated from the molecular force field. The resulting structure parameters and vibrational amplitudes are listed in Table 5 and Table 6, respectively.

Experimental radial distribution curves are compared to the theoretical curves calculated for the best models in Fig. 2. We consider the agreement satisfactory.

Table 6. Root mean square vibrational amplitudes, *l*, of Me_2Zn, Et_2Zn and n-Pr_2Zn, calculated from the molecular force fields (FF) and from least square refinements on the electron diffraction data (ED). All values in pm.

r_a	Me_2Zn *l*(FF)	*l*(ED)	Et_2Zn *l*(FF)	*l*(ED)	n-Pr_2Zn *l*(FF)	*l*(ED)
Zn–C	5.6	5.0(2)	5.6	5.2(3)	5.8	4.7(8)
C–C	–	–	5.5	5.1(3)	5.6	4.2(7)
C–H	7.8	8.4(5)	7.9	7.5(4)	7.9	6.5(7)
Zn···C(2)	–	–	8.5	10.0(4)	8.9	9.2(7)
Zn···C(3)$_{sc}$	–	–	–	–	17.4	23.7(23)
Zn···C(3)$_{ap}$	–	–	–	–	9.5	9.5[b]
Zn···H(1)	12.5	12.2(5)	12.5	11.2(12)	13.2	13.3(46)
C(1)···C(3)	–	–	–	–	7.3	7.3[b]
C(1)···C(1′)	7.6	7.8(9)	7.7	8.3(15)	8.0	7.1(21)
C(1)···C(2′)	–	–	12.8	17.4(17)	13.4	13.4[b]
C···H_{gem}	15.4	17.9(23)[a]	10.9	9.6(10)	11.1	10.9(14)

[a] C(1)···H(1′). [b] Not refined.

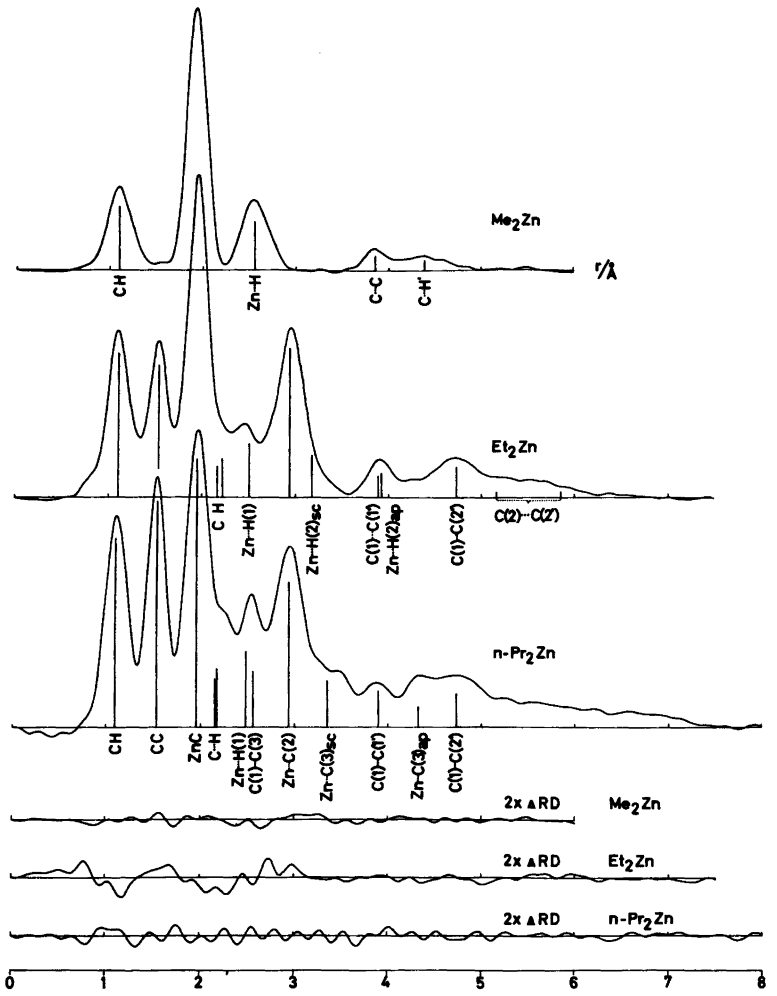

Fig. 2. Experimental radial distribution (RD) curves for Me_2Zn, Et_2Zn, and n-Pr_2Zn. Artificial damping constant $k=0.0025$ Å^2. Major interatomic distances are indicated by bars of height approximately proportional to the area under the corresponding peak. Below: Difference between experimental RD curves and theoretical curves calculated for the best models.

RESULTS AND DISCUSSION

The bond distances and valence angles of Me_2Zn, Et_2Zn and n-Pr_2Zn are listed in Table 5. It is seen that the Zn–C bond distance in Me_2Zn determined by gas phase electron diffraction is very close to the value obtained by rotational Raman spectroscopy, 192.9(4) pm.[5] It is significantly shorter than the Zn–C bond distances in Et_2Zn and n-Pr_2Zn.

The valence angle ∠ZnCC is about 114.5° in both Et_2Zn and n-Pr_2Zn and seems reasonable considering the size of the Zn atom.

Somewhat surprisingly 74(4) % of the alkyl chains in n-Pr_2Zn are found in the *synclinal* conformation, corresponding to a free energy difference $\Delta\bar{G}=\bar{G}_{ap}-\bar{G}_{sc}=-RT\ln(\chi_{ap}/\chi_{sc})=2.9(6)$ kJ mol^{-1}. Introduction of the ratio of the partition functions, Q_{ap}/Q_{sc}, allows calculation of the energy difference at zero K:

$\Delta\bar{E}^\circ = \bar{E}_{ap} - \bar{E}_{sc} = -RT\ln(\chi_{ap}/\chi_{sc}) + RT\ln(Q_{ap}/2Q_{sc})$.

If the ratio is equal to unity, $\Delta\bar{E}^\circ = 1.0(6)$ kJ mol^{-1}. If the ratio is greater than unity, $\Delta\bar{E}^\circ$ increases. The ratio calculated from the approximate molecular force field in Table 4, $Q_{ap}/Q_{sc} = 1.25$, yields $\Delta\bar{E}^\circ = 1.5$ kJ mol^{-1}. The present study therefore suggests that the *sc* conformer is stabilized by a weak interaction between the Zn atom and the terminal methyl group, $Zn-C(3)_{sc} = 335$ pm.

The molecular force field of Me_2Zn in Table 3 is simpler than those obtained in previous normal coordinate analyses [9] and reproduces the observed frequencies [4] to the nearest cm^{-1}. The interaction terms $f'_{\alpha\alpha}$ and $f'_{\beta\beta}$ are necessary to reproduce the observed splitting of CH_3 deformation frequencies ν_9/ν_{13} and rocking frequencies ν_{10}/ν_{14}.

The equilibrium geometry obtained by *ab initio* calculations on eclipsed Me_2Zn has $Zn-C = 197.7 \pm 3$ pm, $C-H = 108.5 \pm 2$ pm and $\angle ZnCH = 111.5 \pm 2°$, in reasonable agreement with the experimental results. Rigid rotation of the methyl groups into a staggered conformation changes the energy with less than 10^{-5} au (0.05 kJ mol^{-1}). Spectroscopic studies indicate that the barrier is negligible.[3]

The picture of the bonding emerging from the population analysis is similar to that obtained by others:[29-31] The 3*d* electrons are nonbonding, the orbital energies increasing in the order $\varepsilon_\delta < \varepsilon_\pi < \varepsilon_\sigma$ as expected from ligand field arguments and found by photoelectron spectroscopy.[30] The Zn–C bonds are pure σ-bonds (the $p\pi - p\pi$ overlap population being negligible) polarized towards the C atoms. The gross atomic populations correspond to net atomic charges of +0.92 on Zn, −0.99 on C and +0.18 on H.

Acknowledgements. We are grateful to Professors J. Weidlein (Stuttgart) and H. Lehmkuhl (Mülheim) for samples, to our colleagues in Oslo, Claus Nielsen and Jan Almlöf for helpful discussions and to The Norwegian Research Council for Science and the Humanities for financial support.

REFERENCES

1. Denis, J. S., Oliver, J. P., Dolzine, T. W. and Smart, J. B. *J. Organomet. Chem 71* (1974) 315.
2. Helgaker, T. U., Haaland, A., Samdal, S., Lehmkuhl, H. and Nehl, H. *Unpublished result.*
3. Boyd, D. R. J., Thompson, H. W. and Williams, R. L. *Discuss. Faraday Soc. 9* (1950) 154.
4. Butler, I. S. and Newbury, M. L. *Spectrochim. Acta A 33* (1977) 699 and references therein.
5. Rao, K. S., Stoicheff, B. P. and Turner, R. *Can. J. Phys. 38* (1960) 1516.
6. Hougen, J. T. *Can. J. Phys. 42* (1964) 1920.
7. Bunker, P. R. *J. Chem. Phys. 47* (1967) 718, Erratum: *J. Chem. Phys. 48* (1968) 2832.
8. Bjørklund, S., Augdahl, E., Christensen, D. H. and Sørensen, G. O. *Spectrochim. Acta A 32* (1976) 1021.
9. Gutowsky, H. S. *J. Chem. Phys. 17* (1949) 128; Walsh Bakke, A. M. *J. Mol. Spectrosc. 41* (1972) 1.
10. Bunker, P. R. and Hougen, J. T. *Can. J. Phys. 45* (1967) 3867.
11. Durig, J. R. and Brown, S. C. *J. Mol. Spectrosc. 45* (1973) 338.
12. Snyder, R. G. and Schachtschneider, J. H. *Spectrochim. Acta 21* (1965) 169.
13. Kaesz, H. D. and Stone, F. G. A. *Spectrochim. Acta 15* (1959) 360.
14. Nagel, B. and Brüser, W. *Z. Anorg. Allg. Chem. 468* (1980) 148.
15. Stølevik, R. *Acta Chem. Scand. A 31* (1977) 359.
16. Hilderbrandt, R. L. and Wieser, J. D. *J. Chem. Phys. 55* (1971) 4648.
17. Pulay, P. *Mol. Phys. 17* (1969) 197; *Ibid. 18* (1970) 473.
18. Sæbø, S. *MOLFORCE Program Manual*, Department of Chemistry, University of Oslo, Oslo 1979.
19. Almlöf, J. *USIP No. 74-29*, University of Stockholm, Stockholm 1974.
20. Dunning, T. H. *J. Chem. Phys. 53* (1970) 2823.
21. Roos, B. and Siegbahn, P. *Theor. Chim. Acta 17* (1970) 209.
22. Roos, B., Veillard, A. and Vinot, G. *Theor. Chim. Acta 20* (1971) 1.
23. Bastiansen, O., Hassel, O. and Risberg, E. *Acta Chem. Scand. 9* (1955) 232.
24. Andersen, B., Seip, H. M., Strand, T. G. and Stølevik, R. *Acta Chem. Scand. 23* (1969) 3224.
25. Strand, T. G. and Bonham, R. A. *J. Chem. Phys. 40* (1964) 1686.
26. Yates, A. C. *Comput. Phys. Commun. 2* (1971) 175.
27. Gundersen, G. and Samdal, S. *The Norwegian Electron Diffraction Group, Annual Report*, Oslo 1980.
28. Seip, H. M., Strand, T. G. and Stølevik, R. *Chem. Phys. Lett. 3* (1969) 617.
29. Guest, M. F., Hillier, I. H. and Saunders, V. R. *J. Organomet. Chem. 44* (1972) 59.
30. Bancroft, G. M., Creber, D. K., Ratner, M. A., Moskowitz, J. W. and Topiol, S. *Chem. Phys. Lett. 50* (1977) 233.
31. Serafini, A., Barthelat, J. C. and Durand, P. *Mol. Phys. 36* (1978) 1341.

Received June 12, 1981.

Acta Chemica Scandinavica A 36 (1982) 167 – 171

Structure of Schiff Bases Derived from Heptane-2,4,6-trione and Diamines as Obtained from UV Absorption and Circular Dichroism Spectra

HANS PETER JENSEN

Chemistry Department A, Building 207, The Technical University of Denmark, DK-2800 Lyngby, Denmark

Absorption and circular dichroism spectra of the $\pi^* \leftarrow \pi$ transitions in Schiff bases derived from heptane-2,4,6-trione and $(-)_D$-(*R*)-1,2-propanediamine, together with their mono- and dinuclear copper(II) inner sphere complexes, have been studied. The results are interpreted by means of exciton theory to give stereochemical information.

Over the years absorption and circular dichroism (CD) spectra of internal ligand $\pi^* \leftarrow \pi$ transitions in dimeric Schiff base derivatives of various β-diketones and diamines have been studied and interpreted to give information about stereochemistry by use of exciton theory.[1-5] Further, especially copper(II) complexes of these types of ligand have been studied and interpreted similarly.[5-8] The stereochemical results thus obtained have been checked by independent means both for the ligands[5] and for the complexes.[9]

Assignments of the ligand field CD spectra have been performed using simple LCAO – MO theory and the assumption that the $d-d$ transitions borrow electric dipole moment for production of rotatory strength from the nearest allowed transitions, the internal ligand $\pi^* \leftarrow \pi$ transitions.[6-8] It has, in the case of acetylacetone derivatives, been possible to check these assignments through determination of transition polarization directions from linear dichroism measurements.[10,11]

We thus, as demonstrated before,[1-8] have a method of providing stereochemical assignments in solution, which in this paper will be exploited to gain information about Schiff bases of heptane-2,4,6-trione (diacetylacetone) and diamines, the preparation and properties of which have been recently described.[12-20]

EXPERIMENTAL

Heptane-2,4,6-trione ($dacacH_2$) was prepared from dehydroacetic acid by the method of Bethell and Maitland,[21] a procedure analogous to the original one by Feist.[22]

Synthesis of the macrocyclic Schiff base between two mol of heptane-2,4,6-trione and two mol of $(-)_D$-(*R*)-1,2-propanediamine [(*R*)-$pn_2(dacacH_2)_2$] was accomplished by the method of Yano *et al.*[12] This type of macrocyclic Schiff base has been shown to undergo partial hydrolysis on reaction with copper(II) acetate in *e.g.* aqueous ethanol to give the copper(II) complex of the acyclic Schiff base: diamine$(dacacH_2)_2$[12-17] [*i.e.* in this case (*R*)-pn$(dacacH_2)_2$].

1,2-Propanediamine was resolved into enantiomers by established procedures.[2]

The identity of the compounds was verified by chemical analysis. A Cary 11 spectrophotometer, a Roussel-Jouan Dichrographe II and a Jobin-Yvon Dichrographe III were used for the measurements of optical spectra. The dimension of absorptivities is $M^{-1}\,cm^{-1}$.

RESULTS AND DISCUSSION

It is well-known that the absorption band of the acetylacetonate anion at 34.300 cm^{-1} is due to a $\pi^* \leftarrow \pi$ transition with the moment oriented along the oxygen – oxygen direction and with a dipole strength of $0.7 \times 10^{-19}\,cm^{-1}\,cm^3$.[1,23]

0302-4377/82/020167-05$02.50

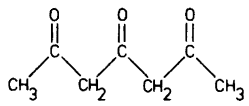

I

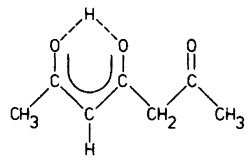

II

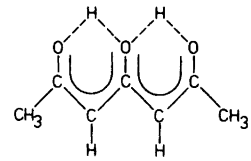

III

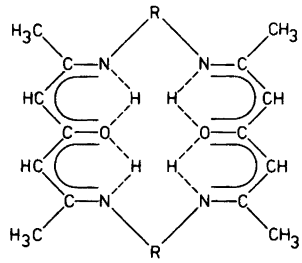

IV

With salts of heptane-2,4,6-trione (diacetylacetone), spectra with maxima at 33.900 cm^{-1} are obtained as in spectra of acetylacetone in alkali, suggesting a monoanionic form. A small shoulder on the low energy side of the absorption maxima, which in strong alkaline solutions develops into a maximum at 27.800 cm^{-1}, is attributable to a dianionic structure.[24,25]

In organic solvents, however, absorption spectra of heptane-2,4,6-trione are fairly uncharacteristic due to a solvent dependent distribution between the tautomers triketo (I), monoenol (II) and dienol (III) as has been demonstrated in a number of papers discussing assignments of ^1H NMR signals from heptane-2,4,6-trione.[26-29]

Heptane-2,4,6-trione may form 1:2 or 2:2 chelates with copper(II) ions.[30-32] From spectroscopic data it is concluded that the 1:2 chelate is analogous to the 1:2 chelate between copper(II) ions and acetylacetone and that also the 2:2 chelate exhibits a slight distortion from planar structure around coordinated copper(II) ions.

The above indicated facts justify that we may conveniently apply the exciton formalism, originally presented by Larsen for acetylacetone Schiff base derivatives,[1] in the present study on the molecular structure of heptane-2,4,6-trione Schiff base derivatives.

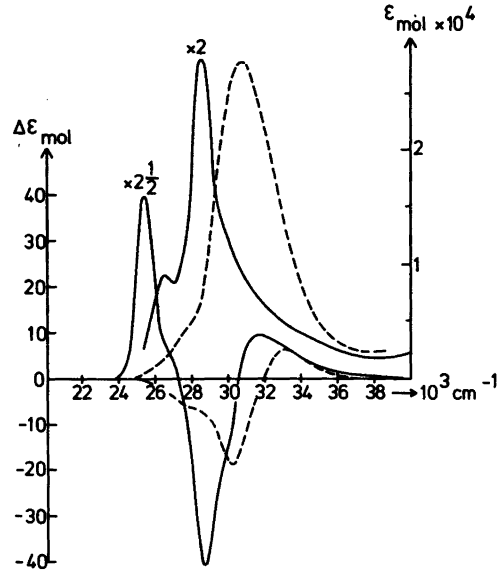

Fig. 1. Molar absorption and circular dichroism spectra of (*R*)-$pn_2(dacacH_2)_2$ dissolved in chloroform; —— initial spectra; - - - final spectra after a week of dissolution at room temperature. The intensities of the initial spectra are multiples of the indications according to the scale.

In Fig. 1 absorption and circular dichroism spectra of the macrocyclic Schiff base (*R*)-$pn_2(dacacH_2)_2$ dissolved in chloroform are reproduced. It is seen that the spectra observed several days after the macrocylic compound was dissolved in chloroform are quite analogous to the spectra of the Schiff base between (*R*)-1,2-propanediamine and acetylacetone [(*R*)-$pn(acacH)_2$], both with respect to dipole strength and with respect to envelope and magnitude of the circular dichroism. (*cf.* Fig. 2 of Ref. 1). Accordingly, it is obvious that an old solution in chloroform, of what was initially the macrocyclic species (*R*)-$pn_2(dacacH_2)_2$, contains a Schiff base derivative of two molecules of the monoenol form (II) of heptane-2,4,6-trione and one molecule of diamine the production of which is probably catalyzed by hydrochloric acid from the chloroform. Thus, exciton coupling between two essentially acetylacetone chromophores (as en-amines) brought into mutual position by a (*R*)-1,2-propanediamine bridge is the cause of the observed CD spectrum. This conclusion is also supported by the observation that when the macrocyclic Schiff base is dissolved in chloroform, with the purpose of preparing its copper(II) complex, an opening of the macrocycle is observed in combination with precipitation of a 1:1 chelate of the resultant Schiff base from one molecule of diamine and two molecules of the triketone.[12,13]

The initial spectra of (*R*)-$pn_2(dacacH_2)_2$ in chloroform are somewhat more complicated than the final ones, as may be seen from Fig. 1. First of all it is obvious that the initial dipole strength in the chloroform solution is almost twice the final dipole strength (3.1 against 1.9×10^{-19} cm^{-1} cm^3) which suggests the number of excited electrons in the macrocycle more likely to be four as compared with two in (*R*)-$pn(acacH)_2$ and (*R*)-$pn(dacacH_2)_2$. Furthermore, the absorption maximum is found at lower energy for the macrocycle in comparison with (*R*)-$pn(dacacH_2)_2$, as we observe the major peak at 28.500 cm^{-1} and the minor at 26.500 cm^{-1}. These two peaks are distributed in the same spectral region as the peak at 27.800 cm^{-1} found for heptane-2,4,6-trione in alkaline solution, assignable as mentioned above to a $\pi^* \leftarrow \pi$ transition in a dianionic structure derived from the dienol (III). From these observations it is deduced that the initial UV spectra are mainly caused by exciton coupling between two $\pi^* \leftarrow \pi$ transitions in the two conjugated parts of structure IV, where the

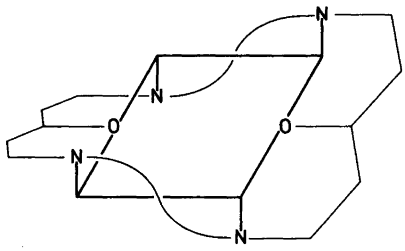

Fig. 2. (*R*)-$pn_2(dacacH_2)_2$. An indication of the structure and the absolute configuration of the chiral system formed by the conjugated ligand parts.

transitions for symmetry reasons have to be directed in the nitrogen – nitrogen direction of the same conjugated part. Thus the CD spectrum with a positive peak at low energy reflects, according to our adopted method,[1,33] a right-handed distribution (*i.e.* positive optical factor) of the two out-of-phase $\pi^* \leftarrow \pi$ transitions in the conjugated diacetylacetone backbones (Fig. 2). It is further clear that our assignment of the spectra as due to exciton coupling with a splitting between the excited states of 2.000 cm^{-1} gives molecular parameters of reasonable magnitude [*cf.* eqn. (6) of Ref. 1].

The structure of a conjugated macrocyclic Schiff base cannot be very flexible and thus the CD spectrum of (*R*)-$pn(dacacH_2)_2$ has appreciable magnitude in comparison with that of *e.g.* (*R*)-$pn(acacH)_2$.

From the initial CD spectrum and dipole strength it is further concluded that the macrocyclic molecules present in solution do not all take a structure as represented in Fig. 2. There is, as seen from Fig. 1, another pattern characteristic of exciton coupling around 31.000 cm^{-1} represented by the positive peak at 33.000 cm^{-1} and the negative shoulder at 30.000 cm^{-1}. The shape is the same as in the CD spectrum of (*R*)-$pn(acacH)_2$, and thus part of the macrocyclic molecules, when dissolved in chloroform, has the diacetylacetone backbone represented by the monoenolic structure (II). This part of the macromolecules are accordingly only capable of showing exciton coupling of transitions in acetylacetone chromophoric parts obviously distributed so as to give negative optical factor for the out-of-phase $\pi^* \leftarrow \pi$ couplet.[1,33] Again the rigidity of the macrocycle makes the CD peaks fairly intense.

From (*R*)-$pn_2(dacacH_2)_2$ the complex Cu(*R*)-$pn(dacacH)_2$ was prepared. The absorption and

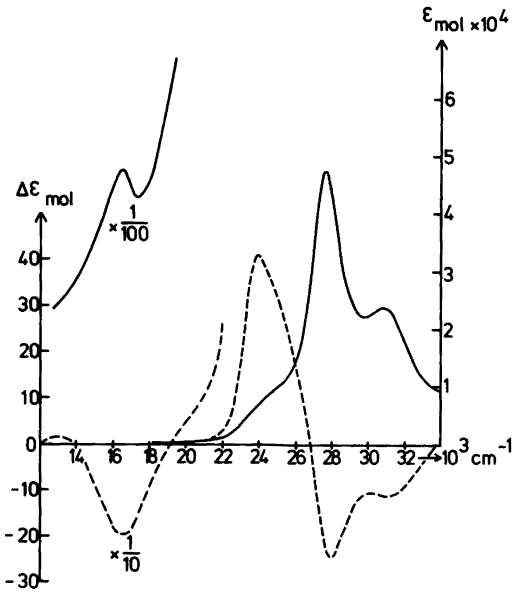

Fig. 3. Molar absorption (———) and circular dichroism spectra (– – –) of $Cu_2(R)$-pn(dacac)$_2$ dissolved in $(CH_3)_2SO$.

circular dichroism spectra of this complex are analogous to those of Cu(*R*)-pn(acac)$_2$ with respect to positions of maxima and magnitudes as well as to envelopes (Fig. 1 of Ref. 6). Accordingly the compound Cu(*R*)-pn(dacacH)$_2$ has an N_2O_2 tetracoordinated copper(II) ion, as also postulated by Yano *et al.*,[5] around which the distribution of the ligators are as shown in Fig. 2 of Ref. 6.

From the mononuclear compound the dinuclear species $Cu_2(R)$-pn(dacac)$_2$ was prepared according to methods of the literature.[14] The spectra of this compound is given in Fig. 3 and it is interesting to note that the exciton coupled internal ligand $\pi^* \leftarrow \pi$ transitions in this case are positioned around 26.000 cm^{-1}, *i.e.* in a spectral range which corresponds to conjugation in the two diacetylacetone backbones. The CD spectrum in this region is fairly intense since it corresponds to a four-electron transition. However, the ligator set N_2O_2 has to be twisted towards a fairly planar configuration in comparison with the mononuclear compound in order also to provide binding within an O_2O_2 ligator set (*cf.* Ref. 8).

A discussion of the Cotton effects of the $d-d$ transitions in the dinuclear complex is difficult since the rather intense internal ligand absorption hides two bands[6] and only the third, a negative band at 16.000 cm^{-1} probably assignable to the transition $(xy) \leftarrow (x^2-y^2)$, can be seen.

Acknowledgements. The author wishes to acknowledge the skilful technical assistance of Mrs. L. Penzien.

The dichrographs were provided by the Danish Natural Science Research Council.

REFERENCES

1. Larsen, E. *Acta Chem. Scand. 23* (1969) 2158.
2. Jensen, H. P. and Larsen, E. *Acta Chem. Scand. A 29* (1975) 157.
3. Jensen, H. P. and Larsen, E. *Gazz. Chim. Ital. 107* (1977) 143.
4. Jensen, H. P. *Acta Chem. Scand. A 32* (1978) 149.
5. Jensen, H. P., Kristensen, B. S., Mosbæk, H. and Søtofte, I. *Acta Chem. Scand. A 32* (1978) 141.
6. Jensen, H. P. and Larsen, E. *Acta Chem. Scand. 25* (1971) 1439.
7. Jensen, H. P. *Acta Chem. Scand. A 32* (1978) 895.
8. Jensen, H. P. *Acta Chem. Scand. A 34* (1980) 469.
9. Larsen, E., Larsen, S., Røen, S. and Watson, K. J. *Acta Chem. Scand. A 30* (1976) 125.
10. Jensen, H. P. *Acta Chem. Scand. A 30* (1976) 137.
11. Davidsson, Å., Jensen, H. P. and Nordén, B. *Chem. Scr. 11* (1977) 83.
12. Yano, T., Ushijima, T., Sasaki, M., Kobayashi, H. and Ueno, K. *Bull. Chem. Soc. Jpn. 45* (1972) 2452.
13. Vigato, P. A., Vidali, M., Casellato, U., Graziani, R. and Benetollo, F. *Inorg. Nucl. Chem. Lett. 11* (1975) 595.
14. Vidali, M., Casellato, U., Vigato, P. A. and Graziani, R. *J. Inorg. Nucl. Chem. 38* (1976) 1455.
15. Fenton, D. E. and Gayda, S. E. *Chem. Commun.* (1974) 960.
16. Fenton, D. E. and Gayda, S. E. *Inorg. Chem. Acta 14* (1975) L11.
17. Fenton, D. E., Gayda, S. E. and Kowalski, R. S. *Z. Transition Met. Chem. 1* (1976) 95.
18. Fenton, D. E. and Gayda, S. E. *J. Chem. Soc. Dalton Trans.* (1977) 2095.
19. Fenton, D. E. and Gayda, S. E. *J. Chem. Soc. Dalton Trans.* (1977) 2101.
20. Fenton, D. E. and Gayda, S. E. *J. Chem. Soc. Dalton Trans.* (1977) 2109.
21. Bethell, J. R. and Maitland, P. *J. Chem. Soc.* (1962) 3751.
22. Feist, F. and Belart, H. *Ber. Dtsch. Chem. Ges. 28* (1895) 1817.
23. Larsen, E., Mason, S. F. and Searle, G. H. *Acta Chem. Scand. 20* (1966) 191.
24. Schwarzenbach, G., Lutz, K. and Felder, E. *Helv. Chim. Acta 27* (1944) 576.

25. Birch, A. J., Fitton, P., Smith, D. C. C., Steere, D. E. and Stelfox, A. R. *J. Chem. Soc.* (1963) 2209.
26. Regitz, M. and Geelhaar, H. J. *Justus Liebigs Ann. Chem. 728* (1969) 108.
27. Dudley, C. W., Huckerby, T. N. and Oldham, C. *J. Chem. Soc. A* (1970) 2605.
28. Gelin, S. and Rouet, J. *Bull. Soc. Chim. Fr.* (1971) 1874.
29. Sagara, F., Kobayashi, H. and Ueno, K. *Bull. Chem. Soc. Jpn. 45* (1972) 900.
30. Baker, D., Dudley, C. W. and Oldham, C. *J. Chem. Soc. A* (1970) 2608.
31. Sagara, F., Kobayashi, H. and Ueno, K. *Bull. Chem. Soc. Jpn. 41* (1968) 266.
32. Sagara, F., Kobayashi, H. and Ueno, K. *Bull. Chem. Soc. Jpn. 45* (1972) 794.
33. Schellman, J. A. *Acc. Chem. Res. 1* (1968) 144.

Received June 12, 1981.

Acta Chemica Scandinavica A 36 (1982) 173 – 181

Microwave Spectrum, Intramolecular Hydrogen Bond, Dipole Moment and Centrifugal Distortion of 2-Fluoropropanol

OLE-ANDERS BRAATHEN, K.-M. MARSTOKK and HARALD MØLLENDAL

Department of Chemistry, The University of Oslo, P.O. Box 1033, Blindern, Oslo 3, Norway

The microwave spectra of 2-fluoropropanol, CH_3CHFCH_2OH, and one deuterated species, CH_3CHFCH_2OD, have been examined in the 17.9 – 32.5 GHz spectral region at about −30 °C. Only one conformation with an intramolecular hydrogen bond formed between the fluorine atom and the hydroxyl group hydrogen atom was assigned. This rotamer has the methyl and hydroxyl groups in *anti* positions to each other. The OCCF dihedral angle is 65(2)°, the HOCC dihedral angle is 65(3)° and the COH angle is 101(4)°. Further conformations, if they exist, are at least 3 kJ/mol less stable. Five vibrationally excited states belonging to four different normal modes were assigned and their frequencies determined by relative intensity measurements. Force field calculations were performed using the quartic centrifugal distortion constants allowing an independent determination to be made of the heavy-atom torsional frequency as 147(7) cm^{-1}; a considerable improvement as compared to relative intensity measurements which yielded 140(25) cm^{-1}. The barrier to internal rotation of the methyl group is *ca.* 16.1 kJ/mol. The dipole moment is $\mu_a = 1.41(1)$ D, $\mu_b = 1.19(2)$ D, $\mu_c = 0.1(3)$ D, and $\mu_{tot.} = 1.85(4)$ D. Extensive centrifugal distortion analyses were carried out for the ground and the first excited states of the heavy-atom torsional mode and accurate values were determined for the quartic constants.

In 1973 Hagen and Hedberg [1] showed that the *gauche* conformation of gaseous 2-fluoroethanol possessing an intramolecular hydrogen bond is at least 11.3 kJ/mol more stable than the *anti* conformation which does not of course have this stabilizing interaction. In the closely related molecule 2-fluoropropanol, CH_3CHFCH_2OH, the two hydrogen-bonded rotamers of Fig. 1 were therefore expected to be several kJ/mol more stable than further non-hydrogen-bonded conformations. The steric conditions are rather similar in both I and II. It was thought that II would be additionally stabilized as compared to I through an interaction between the methyl group and the hydroxyl group lone-pair electrons. It was thus expected that the microwave spectrum would reveal roughly equal amounts of both I and II. However, it was found that I predominates and is at least 3 kJ/mol more stable than conformation II for which no assignments could be made.

2-Fluoropropanol is the fifth of a series of related hydrogen-bonded molecules which have been investigated by microwave spectroscopy in recent years. In $CH_3CH(NH_2)CH_2OH$ [2] and $CH_3CH(OH)CH_2OH$ [3] conformations similar to both I and II of Fig. 1 were identified; in $CH_3CH(OH)CH_2NH_2$ [4] and $CH_3CH(OH)CH_2F$ [5] only one rotamer similar to I was assigned in each case. These investigations may give some indication of the forces responsible for delicate equilibria of the kind shown in Fig. 1. In particular, the fluorine atom seems to play a rather unique role as pointed out in the Discussion.

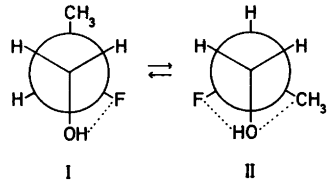

I II

Fig. 1. Possible hydrogen-bonded conformations of CH_3CHFCH_2OH viewed along the $HOCH_2-CHFCH_3$ bond. Dots indicate possible non-bonded stabilizing interactions.

0302-4377/82/020173-09$02.50

Table 1. Selected transitions for the ground vibrational state of conformation I of CH_3CHFCH_2OH.

Transition	Observed frequency[a] (MHz)	Obs. − calc. frequency (MHz)	Centrifugal distortion	
			Total (MHz)	Sextic (MHz)
a-type				
$2_{0,2} \rightarrow 3_{0,3}$	18774.65	0.02	−0.06	
$2_{2,1} \rightarrow 3_{2,2}$	19181.42	−0.02	−0.24	
$2_{2,0} \rightarrow 3_{2,1}$	19588.39	−0.01	−0.27	
$2_{1,1} \rightarrow 3_{1,2}$	20397.93	−0.08	−0.16	
$3_{1,3} \rightarrow 4_{1,4}$	23674.04	−0.04	−0.16	
$3_{0,3} \rightarrow 4_{0,4}$	24614.52	−0.01	−0.15	
$3_{2,1} \rightarrow 4_{2,2}$	26454.13	−0.03	−0.46	
$3_{3,0} \rightarrow 4_{3,1}$	25808.83	−0.07	−0.69	
$3_{1,2} \rightarrow 4_{1,3}$	27056.10	0.09	−0.31	
$4_{1,4} \rightarrow 5_{1,5}$	29445.25	−0.03	−0.29	
$12_{3,10} \rightarrow 12_{3,9}$	18642.68	−0.01	−4.54	
$16_{4,13} \rightarrow 16_{4,12}$	23414.91	−0.02	−10.02	0.01
$23_{6,18} \rightarrow 23_{6,17}$	25078.78	0.04	−23.67	0.06
$30_{8,23} \rightarrow 30_{8,22}$	24651.72	0.05	−42.36	0.24
$40_{11,30} \rightarrow 40_{11,29}$	18061.85	−0.02	−63.51	0.95
$49_{13,37} \rightarrow 49_{13,36}$	30883.85	−0.02	−151.36	3.72
b-type				
$6_{0,6} \rightarrow 6_{1,5}$	18218.67	−0.15	−0.93	
$8_{0,8} \rightarrow 8_{1,7}$	28044.26	0.07	−2.00	
$4_{1,4} \rightarrow 4_{2,3}$	20247.53	−0.04	−0.56	
$6_{1,6} \rightarrow 6_{2,5}$	25287.05	−0.08	−1.26	
$5_{2,3} \rightarrow 5_{3,2}$	24178.05	−0.02	−0.98	
$8_{2,6} \rightarrow 8_{3,5}$	20283.03	−0.01	−2.12	
$8_{2,7} \rightarrow 8_{3,6}$	30933.20	0.01	−3.07	
$10_{3,7} \rightarrow 10_{4,6}$	30384.44	0.03	−4.58	
$12_{3,9} \rightarrow 12_{4,8}$	26915.69	0.03	−6.13	
$14_{3,11} \rightarrow 14_{4,10}$	26558.71	−0.04	−8.63	
$1_{1,0} \rightarrow 2_{2,1}$	28153.28	−0.02	−0.18	
$3_{0,3} \rightarrow 4_{1,4}$	26816.31	0.01	−0.19	
$6_{3,4} \rightarrow 7_{2,5}$	25321.02	0.05	−0.46	
$9_{4,5} \rightarrow 10_{3,8}$	26336.24	0.03	1.07	
$14_{7,7} \rightarrow 15_{6,10}$	31012.90	−0.12	2.46	0.01
$21_{12,9} \rightarrow 22_{11,12}$	23108.87	0.04	12.84	0.02
$21_{12,10} \rightarrow 22_{11,11}$	23108.87	−0.04	12.84	0.02
$27_{15,12} \rightarrow 28_{14,15}$	30914.95	−0.05	26.15	0.07
$27_{15,13} \rightarrow 28_{14,14}$	30914.95	−0.05	26.15	0.07
$33_{19,14} \rightarrow 34_{18,17}$	27637.75	−0.02	51.61	0.15
$33_{19,15} \rightarrow 34_{18,16}$	27637.75	−0.02	51.61	0.15
$43_{25,18} \rightarrow 44_{24,21}$	29646.49	−0.03	116.47	0.44
$43_{25,19} \rightarrow 44_{24,20}$	29646.49	−0.03	116.47	0.44
$53_{31,22} \rightarrow 54_{30,25}$	31713.21	0.05	219.99	1.06
$53_{31,23} \rightarrow 54_{30,24}$	31713.21	0.05	219.99	1.06

[a] ±0.07 MHz.

EXPERIMENTAL

2-Fluoropropanol was synthesized using the procedure of Bergmann and Cohen.[6] The sample was purified by gas chromatography before use. CH_3CHFCH_2OD was produced by direct exchange with heavy water in the wave guide. Vapour pressures in the 20–60 micron range were employed during the spectral measurements. The temperature was about −30 °C. Lower temperature could not be used due to insufficient vapour pressure. Measurements were made in the 17.9 −32.5 GHz spectral region.

RESULTS

Microwave spectrum and assignment of the ground state of conformation I. Preliminary rotational constants of both conformation I and the hypothetical rotamer II of Fig. 1 were computed by combining structural parameters taken from related compounds. Bond moment calculations of the dipole moment and its components along the principal axes were then performed using the values of Ref. 7. The principal axes components of the dipole moment were predicted to be $\mu_a = 1.1$ D, $\mu_b = 0.9$ D and $\mu_c = 0.2$ D for conformation I and $\mu_a = 0.3$ D, $\mu_b = 0.0$ D and $\mu_c = 1.3$ D for the hypothetical rotamer II. Each rotamer was thus predicted to possess comparatively strong and rich spectra dominated by strong Q-branch transitions.

The observed spectrum was relatively strong with absorptions occurring every few megahertz. Assignments were readily made for low J a- and b-type transitions of conformation I; these were lying close to their predicted frequencies. The rotational constants were then determined and used to predict the positions of further transitions which were measured and included in the least-squares fit in which centrifugal distortion was also taken into account. This procedure was repeated several times, and ultimately 143 lines of the a- and b-type varieties were assigned. No c-type transitions were definitely identified because of the small μ_c being 0.1(0.3) D (see later section). These lines thus have insufficient intensities to allow their assignments. The highest J- and K_{-1}-transitions identified belonged to the coalescing pair of $53_{31,22} \rightarrow 54_{30,20}$ and $53_{31,23} \rightarrow 54_{30,24}$. Even higher J-transitions were searched for but not found, presumably because of insufficient intensities. A portion of the ground state spectrum is shown in Table 1.*

The derived spectroscopic constants are shown in Table 2. The rotational and quartic centrifugal distortion constants are accurately determined, while the two sextic constants included have standard deviations of about 10%. Inclusion of more sextic distortion constants resulted in only a marginal improvement of the fit, high correlations among the sextic constants and associated large

* The complete list of frequencies for the ground, the vibrationally excited states, and for the ground state of CH_3CHFCH_2OD is available from the authors upon request, or from the Microwave Data Center, Molecular Spectroscopy Section, National Bureau of Standards Bldn. 221, Washington D.C. 20234, U.S.A., where it has been deposited.

Table 2. Spectroscopic constants for the ground vibrational states of CH_3CHFCH_2OH and CH_3CHFCH_2OD.[a]

Species		CH_3CHFCH_2OH	CH_3CHFCH_2OD
Number of transitions		143	29
Root-mean-square dev. (MHz)		0.066	0.101
A_0	(MHz)	8461.7439(35)	8367.062(29)
B_0	(MHz)	3625.6374(14)	3538.610(17)
C_0	(MHz)	2768.2557(11)	2707.914(17)
Δ_J	(kHz)	0.8611(36)	0.21(38)
Δ_{JK}	(kHz)	6.007(23)	5.51(32)
Δ_K	(kHz)	2.1394(97)	1.1(22)
δ_J	(kHz)	0.1978(15)	0.196(17)
δ_K	(kHz)	3.537(40)	3.39(33)
H_J	(Hz)	0.000678(93)	−[b]
H_{JK}	(Hz)	−0.0166(17)	−[b]

[a] Uncertainties represent one standard deviation. [b] Not determined. Assumed to be zero in least-squares fit.

Table 3. Vibrationally excited states of CH_3CHFCH_2OH.[a]

Vibrational state		First ex. heavy-atom tors.	Second ex. heavy-atom tors.	Lowest bending	Highest bending	Methyl torsion
Number of transitions		68	26	33	6	19
Root-mean-square dev. (MHz)		0.102	0.083	0.093	0.641	0.098
A_v	(MHz)	8418.6679(86)	8383.176(24)	8487.792(22)	8413.5(40)	8445.116(36)
B_v	(MHz)	3620.0511(33)	3614.597(14)	3626.315(14)	3618.69(16)	3623.683(16)
C_v	(MHz)	2765.3234(27)	2762.158(14)	2765.197(14)	2762.51(19)	2766.553(17)
Δ_J	(kHz)	0.8458(97)	1.69(30)	1.27(32)	0.5(35)	0.63(40)
Δ_{JK}	(kHz)	5.98(13)	6.10(46)	5.59(27)	—[b]	0.29(56)
Δ_K	(kHz)	1.609(63)	−2.3(28)	6.3(18)	—[b]	11.9(35)
δ_J	(kHz)	0.209(10)	0.199(19)	0.160(14)	—[b]	0.237(26)
δ_K	(kHz)	3.02(21)	2.76(40)	4.69(30)	—[b]	2.80(50)
H_J	(Hz)	0.0090(40)	—[b]	—[b]	—[b]	—[b]
H_{JK}	(Hz)	−0.016(25)	—[b]	—[b]	—[b]	—[b]

[a] Uncertainties represent one standard deviation. [b] Not determined. Assumed to be zero in least-squares fit.

standard deviations. It was thus concluded that five quartic and two sextic constants give the best physical representation of the spectrum.

The quartic centrifugal distortion constants are quite similar to those previously determined for 1-fluoro-2-propanol.[5] This is indicative of similar force fields and mass distribution for the two related molecules, whose rotational constants are also fairly similar.

Vibrationally excited states. The ground vibrational state transitions were accompanied by a rich satellite spectrum. The strongest of these absorption lines were about 50% as intense as the corresponding ground state transitions. They are assigned as the first excited state of the heavy-atom (OC−CF) torsional mode. A total of 68 transitions were assigned for this mode. Maximum value of J was 40 of the $40_{11,30} \rightarrow 40_{11,29}$ transition. The spectroscopic constants are shown in Table 3. They are close to their ground-state counterparts as expected, with one exception, namely Δ_K which differs by about 30% between the two states. This is about ten times the standard deviation. The reason for this is not known.

Relative intensity measurements were made observing most of the precautions of Esbitt and Wilson.[8] The frequency was determined as 140(25) cm^{-1}. Using an alternative, completely independent force-field calculation as described below, this frequency was found as 147(7) cm^{-1} in good agreement with the relative-intensity determination. This frequency is not far from 109(10) cm^{-1} determined for the corresponding normal mode of 1-fluoro-2-propanol.[5]

The changes of the rotational constants upon excitation of this mode is close to what was found for the corresponding mode of 1-fluoro-2-propanol.[5] Attempts to reproduce these changes by opening up the OCCF dihedral angle by 2° met with some success. This indicates that the heavy-atom torsional mode of this molecule is not strongly coupled with other normal vibrations.

The second excited state of this mode was also assigned with the spectroscopic constants determined as shown in Table 3. The intensity of these transitions is roughly 25% of their ground state counterparts as expected. However, the changes of the rotational constants upon excitation from the first to the second excited state were $\Delta A = -35.5$ MHz, $\Delta B = -5.5$ MHz, and $\Delta C = -3.2$ MHz, respectively, as compared to $\Delta A = -43.1$ MHz, $\Delta B = -5.6$ MHz and $\Delta C = -2.9$ MHz obtained upon excitation of the ground state to first excited state of this heavy-atom torsional mode. Similar findings were made for 1-fluoro-2-propanol[5] indicating a very slight anharmonic contribution or interaction with other normal vibrations.

The third excited state transitions of this torsional mode should, in case of a near-harmonic vibration, have approximately 12% of the intensity of the ground state lines. They should thus clearly have sufficient intensities to allow definite assignments to be made. Moreover, their spectral positions should be possible to predict quite accurately since both the first and the second excited states were identified. The strongest third excited state transitions of the torsion were searched for thoroughly, but were not

found. Resonance with another normal mode is suggested as the reason for this.

The first excited state of what is assumed to be the lowest heavy-atom bending mode was assigned as shown in Table 3. The intensities of these transitions were about 30% of the corresponding groundstate lines. A frequency of 220(40) cm^{-1} was determined by relative-intensity measurements. The changes of the rotational constants upon excitation as well as the vibrational frequency of this mode is again found to correspond well with the findings for 1-fluoro-2-propanol.[5]

It is likely that the heavy-atom bending modes are strongly coupled. Despite this, attempts were made to see if this excited state could be located to either the CCC, FCC or OCC bending mode. Model calculations were made by opening up each of these angles by 0.5°. None of them reproduced the observed changes of the rotational constants very satisfactorily. However, the agreement for the CCC bending mode is much better than for the other two. We therefore believe that this mode is largely a CCC bending vibration.

Another low-frequency mode having about 15% intensity of the ground state was also assigned as shown in Table 3. The energy of this state was estimated to be roughly 320 cm^{-1} above the ground state. Again, the changes of the rotational constants closely resemble an excited state identified for 1-fluoro-2-propanol.[5] This excited state is tentatively assigned as another bending mode of the molecule. The changes of the rotational constants upon excitation in no way resemble what was calculated by opening up the three heavy-atom angles as described above. It is therefore concluded that complex coupling must exist for this presumed bending mode.

The first excited state of what is believed to be the methyl group torsional mode was identified with the spectroscopic constants displayed in Table 3. The changes of the rotational constants once more were found to agree closely with their counterparts of 1-fluoro-2-propanol.[5] Relative intensity measurements yielded 260(50) cm^{-1} for this mode.

No splittings due to internal rotation were observed for this mode or for any of the other of the excited states described above. It is believed that splittings would have been observed if they had exceeded 0.5 MHz. Computations using the computer programme MB10 described previously,[9] and assuming splittings not exceeding 0.5 MHz, makes it possible to estimate the barrier to be at least 14.2 kJ/mol. Using the approximation of a harmonic oscillator[10] with a torsional frequency of 260 cm^{-1} yields as a result that the barrier is roughly 16.1 kJ/mol. This is in keeping with values obtained for CH_3CH_2F[11] (14.1 kJ/mol) and CH_3CHFCH_3[12] (14.9 kJ/mol).

Determination of the heavy-atom torsional frequency from force-field calculations. Low-frequency torsional vibrations are generally difficult to observe experimentally by Raman or IR spectroscopy. Relative intensity measurements in the microwave range with Esbitt-Wilson's procedure[8] often give rather large uncertainties as exemplified above. An alternative method for their determination would be desirable as a supplement to these methods. Perhaps accurate centrifugal distortion constants could be used in many cases for this end.

The centrifugal distortion constants depend primarily on low-frequency normal vibrations, as the force constants enter inversely in their mathematical expressions.[13] Moreover, the torsional modes are often well isolated from other fundamentals as in the present case where 140(25) cm^{-1}, 220(40) cm^{-1}, 260(50) cm^{-1} and *ca.* 320 cm^{-1} are the lowest normal vibrations. Torsional modes thus often couple little with other frequencies as is assumed to be the case for the title compound.

A simple diagonal force field as shown in Table 4 was selected from related molecules. Only the torsional force constant of the heavy-atom torsion was allowed to vary in a least-squares fitting procedure of the centrifugal distortion constants. All the remaining force constants of the simple valency force field shown in this table were kept constant at the values reported there. The programme used was NCA written by Christen.[14]

Quite good agreement was obtained between the observed and calculated centrifugal distortion constants, as shown in Table 4, and the torsional frequency was found as 147 cm^{-1} in good agreement with the value obtained by relative-intensity measurements [140(25) cm^{-1}]. The uncertainty of this frequency (147 cm^{-1}) is difficult to estimate since several assumptions are involved in its derivation. However, it is felt that ± 7 cm^{-1} is a realistic error limit; a considerable improvement in comparison with the relative intensity method which yielded 140(25) cm^{-1}.

It is hoped that use of centrifugal distortion constants in this manner may have some merit as an independent way of determining the elusive torsional frequencies.

Table 4. Assumed force field, centrifugal distortion constants, and torsional frequency of CH_3CHFCH_2OH.

Force constants			
Stretching (m dyn Å^{-1})			
C(1)–C(2)	4.60	C(1)–H	4.81
C–F	5.15	C–O	4.90
C(2)–C(3)	4.42	O–H	7.48
C(2)–H	4.81	C(3)–H	4.70
Bending (m dyn Å rad^{-2})			
C–O–H	0.76	C–C–C	1.27
H–C–O	0.70	C(3)–C(2)–F	1.08
H–C(1)–H	0.51	C(3)–C(2)–H	0.72
C–C–O	1.18	C(2)–C(3)–H	0.66
C(2)–C(1)–H	0.71	H–C(3)–H	0.49
C(1)–C(2)–F	1.01	C(1)–C(2)–H	0.81
Torsion (m dyn Å rad^{-2})			
C(2)–C(3)	0.13	C–O	0.053
C(1)–C(2)	0.204[a]		
Centrifugal distortion constants			
	Obs.	Calc.	
Δ_J (kHz)	0.8611	0.9687	
Δ_{JK} (kHz)	6.0071	6.1973	
Δ_K (kHz)	2.1394	2.4715	
δ_J (kHz)	0.1978	0.2020	
δ_K (kHz)	3.5372	3.7146	
Heavy-atom torsional frequency (cm^{-1})			
	147[a]		

[a] Obtained from least-squares fit. $H_3C(3)-C(2)HF-C(1)H_2OH$.

Dipole moment. Stark coefficients of low J transitions were used to determine the dipole moment. A d.c. voltage was applied between the Stark septum and the cell with the modulating square wave voltage superimposed. The d.c. voltage was calibrated using the OCS $J=1\rightarrow2$ transition with $\mu_{OCS}=0.71521$ D.[15] Each second order coefficient shown in Table 5 was assigned a standard deviation. A least squares fit using a diagonal weight matrix was performed. The weights were chosen as the inverse squares of the standard deviations appearing in Table 5. This table also gives the total dipole moment and its components along the principal axes. It is seen that there is reasonable agreement between the observed dipole moment and that calculated by the bond-moment method as described above.

Table 5. Stark coefficients and dipole moment[a] of CH_3CHFCH_2OH.

Transition		$\Delta\nu/E^2$ (MHz V^{-1} cm^2) × 10^6	
		Obs.	Calc.
$2_{0,2}\rightarrow3_{0,3}$	|M|=2	16.24(6)	15.96
	|M|=1	2.12(1)	2.15
	M=0	−2.43(2)	−2.45
$2_{1,1}\rightarrow3_{1,2}$	|M|=2	−24.10(90)	−25.35
	|M|=1	−5.36(9)	−5.55
	M=0	1.04(1)	1.04
$3_{1,3}\rightarrow3_{2,2}$	|M|=3	−227(2)	−232

[a] $\mu_a=1.41(1)$ D; $\mu_b=1.19(2)$; $\mu_c=0.1(3)$ D; $\mu_{tot}=1.85(4)$.

Table 6. Plausible structural parameters[a] and observed and calculated rotational constants of CH_3CHFCH_2OH and CH_3CHFCH_2OD.

Assumed structural parameters			
H_3C-C (pm)	150.5	∠CCO (°)	112.0
HOH_2C-C (pm)	150.3	∠CCF (°)	109.7
C–O (pm)	141.1	∠CCC (°)	112.4
C–H (pm)	109.3	∠CCH (°)	111.0
O–H (pm)	96.6		
C–F (pm)	139.5		
Fitted structural parameters			
∠COH (°)	101(4)		
∠OCCF (°)	65(2) from *syn*		
∠HOCC (°)	65(3) from *syn*		
Kraitchman's coordinates for the hydroxyl hydrogen			
	|a|	|b|	|c|
Obs. (pm)	184.502(19)	83.090(44)	13.716(263)
Calc. (pm)	183.9	83.1	23.9
Hydrogen bond parameters			
H···F (pm)	248	∠O–H···F (°)	104
F···O (pm)	287	∠C–F···H (°)	76
		∠C–F, O–H (°)[b]	4
Sum of van der Waals radii[c]			
H···F (pm)	255	O···F (pm)	275
Rotational constants			
CH_3CHFCH_2OH			
	Obs.	Calc.	Diff. (%)
A_0 (MHz)	8461.74	8428.43	0.39
B_0 (MHz)	3625.64	3636.18	0.29
C_0 (MHz)	2768.26	2774.78	0.24
CH_3CHFCH_2OD			
	Obs.	Calc.	Diff. (%)
A_0 (MHz)	8367.06	8329.36	0.45
B_0 (MHz)	3538.61	3548.23	0.27
C_0 (MHz)	2707.91	2714.43	0.24

[a] See text. [b] Angle between C–F and O–H bonds. [c] See Ref. 20.

Deuterated species. The deuterated species CH_3CHFCH_2OD was studied mainly to determine accurately the position of the hydroxyl hydrogen. The spectrum was readily assigned and its spectroscopic constants are listed in Table 2. The position of the hydroxyl hydrogen atom was computed using Kraitchman's equations [16] with the result shown in Table 6.

Searches for further conformations. A total of 295 transitions were assigned for conformation I. This includes all the strongest lines, the majority of the medium intensity transitions as well as many weak ones. Careful Stark effect studies were made for all the unassigned lines of medium intensity. None of them displayed any splitting. Low J R-branch lines of the c-type variety were predicted to be among the

strongest of the hypothetical conformation II. Careful searches were made for several of these transitions, but none were found. In addition to these lines, medium and high J c-type Q-branch transitions were predicted to be relatively strong, numerous and form a distinct spectral pattern. This feature was not recognizable.

Moreover, the absolute intensities of the spectral lines depend on the fraction of the gas belonging to a specific conformation.[17] Absolute intensities are hard to determine accurately. This makes it somewhat difficult to use this property to determine exactly how large a fraction of a gaseous mixture belongs to a particular conformation. In spite of this difficulty, absolute intensity estimates were made. It was again found that conformation I predominates. No indications for the existence of further rotamers were obtained from the absolute intensity studies.

From these studies it is concluded that conformation I predominates. It is conservatively estimated that at least 80 % of the gas consists of this conformation at −30 °C. It is even likely that more than 90 % of the gas consists of I. This conformation is thus at least 3 kJ/mol more stable than II or any other non-hydrogen-bonded rotamer. A computer-drawn model of the identified rotamer I is shown in Fig. 2.

Structure. Only six moments of inertia were determined for conformation I. Consequently, a full molecular structure cannot be determined. Instead, we restricted ourselves to fitting the OCCF, HOCC dihedral angles, and the COH angle, because these parameters are sensitive to the experimental data at hand and because they are considered to be chemically interesting. The remaining bond lengths and angles were kept constant in the fit at the values shown in Table 6. These parameters were selected from recent, accurate studies of related compounds.

The OCCF dihedral angle was just fitted until a satisfactory agreement between the observed and calculated rotational constants was found. This occurred with 65(2)°. The dihedral angle ∠HOCC and the angle ∠COH were then fitted to Kraitchman's coordinates for the hydroxyl group hydrogen atom. ∠HOCC was found to be 65(3)°, and ∠COH to be 101(4)°.

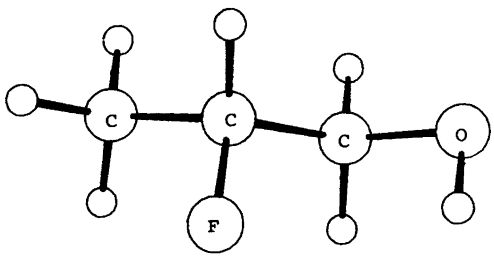

Fig. 2. Computer-drawn model of CH_3CHFCH_2OH.

Table 6 shows that good agreement exists between the observed and calculated rotational constants. Kraitchman's coordinates of the hydroxyl hydrogen atom are also well reproduced. The error limits of the three fitted parameters are assumed to encompass not only random errors but uncertainties of the assumed structural parameters as well.

The hydrogen bond parameters as shown in Table 6 are indicative of a strained hydrogen bond. This situation resembles very much what has previously been found for CH_2FCH_2OH,[1,18] CHF_2CH_2OH[19] and $CH_3CH(OH)CH_2F$.[5] The major stabilizing interaction is perhaps the near-ideal bond-dipole interaction between the O−H and C−F bonds which are almost parallel. Covalency is hardly of much significance for the hydrogen bond of this molecule as the non-bonded H···F distance is almost equal to the sum of the corresponding van der Waals radii.[20]

It is noteworthy that the OCCF dihedral angle takes a value of 65(2)°. This is 3 − 6° more than in the three above-mentioned compounds. No obvious explanation for this can be given.

DISCUSSION

The conformational behaviour of $CH_3CH(OH)CH_2NH_2$,[4] $CH_3CH(NH_2)CH_2OH$[2] and $CH_3CH(OH)CH_2OH$[3] can be understood at least qualitatively within the framework of existing theories of steric interaction, hydrogen bonding and dipole interaction. This is hardly the case for $CH_3CH(OH)CH_2F$[5] and the title compound, CH_3CHFCH_2OH. The fact that neither of these have conformations similar to II with energies roughly the same as for I cannot be explained using only the popular theories of steric, hydrogen bonding, or dipole interactions. Some additional effect must be operative for these two molecules containing the fluorine atom.

$CH_3CH(OH)CH_2F$ and CH_3CHFCH_2OH are not the only known examples of small alifatic molecules containing fluorine and also displaying unique conformational properties, *e.g.*, CH_2FCH_2F[21,22] takes the *gauche* conformation as

its preferred form. In CHF_2CH_2OH only one of the two possible hydrogen-bonded rotamers makes up more than 95 % of the gas. It appears that theoretical work is needed to explain the conformational behaviour of alifatic molecules containing the "troublesome" fluorine atom.

Acknowledgement. Cand.real. Arne Møller Naley is thanked for synthesizing the compound used in this work.

REFERENCES

1. Hagen, K. and Hedberg, K. *J. Am. Chem. Soc. 95* (1973) 8263.
2. Ellingsen, B.-H., Marstokk, K.-M. and Møllendal, H. *J. Mol. Struct. 48* (1978) 9.
3. Caminati, W. *J. Mol. Spectrosc. 86* (1981) 193.
4. Marstokk, K.-M. and Møllendal, H. *J. Mol. Struct. 35* (1976) 57.
5. Marstokk, K.-M. and Møllendal, H. *J. Mol. Struct. 40* (1977) 1.
6. Bergmann, E. D. and Cohen, S. *J. Chem. Soc.* (1958) 2259.
7. Smyth, C. P. *Dielectric Behavior and Structure*, McGraw-Hill, New York 1955, p. 244.
8. Esbitt, A. S. and Wilson, E. B. *Rev. Sci. Instrum. 34* (1963) 901.
9. Marstokk, K.-M. and Møllendal, H. *J. Mol. Struct. 32* (1976) 191.
10. Gordy, W. and Cook, R. L. *Microwave Molecular Spectra*, Wiley, New York 1970, p. 476.
11. Tuazon, E. C., Manocha, A. S. and Fately, W. G. *Chem. Phys. Lett. 23* (1973) 63.
12. Griffiths, J. H., Owen, N. L. and Sheridan, J. *J. Chem. Soc. Faraday Trans. 2 69* (1973) 1359.
13. Ref. 10, p. 212.
14. Christen, D. *J. Mol. Struct. 48* (1978) 101.
15. Muenter, J. S. *J. Chem. Phys. 48* (1968) 4544.
16. Kraitchman, J. *Am. J. Phys. 21* (1953) 17.
17. Marstokk, K.-M. and Møllendal, H. *J. Mol. Struct. 18* (1973) 247.
18. Buckton, K. S. and Azrak, R. G. *J. Chem. Phys. 52* (1970) 5652.
19. Marstokk, K.-M. and Møllendal, H. *Acta Chem. Scand. A 34* (1980) 765.
20. Pauling, L. *Nature of the Chemical Bond*, 3rd Ed., Cornell University Press, New York 1960, p. 260.
21. Fernholt, L. and Kveseth, K. *Acta Chem. Scand. A 34* (1980) 163.
22. Friesen, D. and Hedberg, K. *J. Am. Chem. Soc. 102* (1980) 3987.

Received June 9, 1981.

Acta Chemica Scandinavica A 36 (1982) 189–194

The Crystal Structure of Tetrakis [trifluoroacetato-μ-(2-diethylaminoethanolato)copper(II)]

KIMMO SMOLANDER

Department of Chemistry, University of Joensuu, SF-80100 Joensuu 10, Finland

The crystal structure of $Cu_4(Et_2NC_2H_4O)_4(F_3CCOO)_4$, $C_{32}H_{56}Cu_4N_4O_{12}F_{12}$ is tetragonal with space group $I4_1/a$ and $a=17.903(6)$ Å, $c=14.543(4)$ Å. The structure was solved with direct and Fourier methods to $R=0.051$ for 1451 reflections (3885 total).

The molecule has a cubane-type Cu_4O_4 core of boat conformation formed by bridging ethanolato oxygen atoms. The point group of the molecule is S_4. In the core there are four Cu···Cu distances of 3.206(1) Å and two of 3.714(1) Å.

The copper(II) ion has octahedral (4+2) environment. In the basal plane there are two bridging oxygen atoms Cu–O 1.933(4) and 1.947(4) Å a carboxylate oxygen atom Cu–O2 1.949(4) Å and a nitrogen atom Cu–N 2.100(5) Å.

In the fifth position is the ethanolato oxygen atom Cu–O1 2.721(4) Å and in the sixth position the carboxylato oxygen atom Cu–O3 2.756(5) Å. The angle O3–Cu–O1 is 143.1(1)°.

The trifluoroacetate is bridging asymmetrically in syn–syn configuration from an equatorial coordination site of one copper atom to an axial site of another.

The structures of many alkoxo-bridged copper(II) complexes with *N,N*-dialkylaminoethanols ($R_2NCH_2CH_2OH=R_2LOH$), as the second ligand have been reported. The structures have been shown to be dimeric,[1] trinuclear,[2] tetrameric[3–13] or hexanuclear.[14] Mergehem and Haase[3] have reported two different types of tetramers classified by the distortion of the idealized Cu_4O_4 cubane by stretching four edges. There are two extreme types, distinguished by the arrangement of the Cu–Cu and Cu–O distances. In the first type there are two short (~2.92 Å) and four long (~3.44 Å) and in the second type four short (~3.18 Å) and two long (~3.45 Å) intramolecular Cu–Cu distances.

In the haloacetate complexes[7–13] have been found two long Cu–Cu distances ranging from 3.609 to 4.024 Å and four short ones ranging from 3.094 to 3.372 Å, *i.e.* considerably longer than in the second type. The haloacetate complexes have the cubane tetramers in boat conformation. To have more information on the tetramers we have now prepared in the Et_2LOH series the first fluoroacetate complex of tetrakis[trifluoroacetato-μ-(2-diethylaminoetanolato)copper(II)].

EXPERIMENTAL

Copper(II) trifluoroacetate was prepared from basic copper(II) carbonate (Merck) and trifluoroacetic acid (Merck) by the method of Bateman and Conrad.[15] The salt was dissolved in methanol and an equimolar amount of 2-diethylaminoethanol (Fluka AG) was added. The solution was filtered and allowed to evaporate slowly at room temperature. After some weeks dark blue crystals were obtained. They were filtered off, washed and drained at ambient temperature.

Unit cell dimensions and the orientation matrix were determined by the least-squares method from 20 centered reflections measured at room temperature on a Syntex $P2_1$ four-circle diffractometer. The crystal used had approximate dimensions of 0.2 × 0.2 × 0.3 mm.

Intensities were collected ($2°<2\theta<47°$) with graphite monochromatized Mo$K\alpha$-radiation. The ω-scan technique was employed with a scan range of 1.0° and the scan speed varied from 2.50 to 29.30° min^{-1}, depending on the number of counts accumulated in a preliminary scan. Background measurements were taken at both ends of the scan with a displacement of 1.0° from the $K\alpha$-peak. Each background was measured for half the scan time. The intensities of two standard reflections were

0302-4377/82/030189-06$02.50

recorded after every 100 measurements and remained essentially constant. The intensities were corrected for Lorentz and polarization effects and for absorption from empirical ψ-scan data. Of the 3885 reflections collected, 1451 had $F_o > 4\sigma(F_o)$ and were used in subsequent calculations.

CRYSTAL DATA

$Cu_4(C_6H_{14}NO)_4(F_3C_2O_2)_4$, $FW = 1171.08$
Crystal system: Tetragonal
Space group: $I\,4_1/a$ (No. 88)
$a = 17.903(6)$, $c = 14.543(4)$ Å
$V = 4661.2$ Å^3, $Z = 4$, $F(000) = 2384$
$\mu(\text{Mo}K\alpha) = 19.8$ cm^{-1}, $\lambda(\text{Mo}K\alpha) = 0.71069$ Å
$D_m = 1.67$ g cm^{-3} (flotation technique)
$D_x = 1.67$ g cm^{-3}

STRUCTURE DETERMINATION

The crystal structure was solved by direct methods which gave the positions of copper and oxygen atoms. The remaining nonhydrogen atoms were found from a Fourier synthesis. The structure was refined by the blocked-cascade full-matrix least-squares method[16] with anisotropic temperature factors for nonhydrogen atoms.

The hydrogen atoms were included at the calculated positions (C – H = 0.96 Å). In the final refinement the positions of the hydrogen atoms were refined. The isotropic thermal parameters for hydrogen atoms were set at 1.2 times the equivalent isotropic value for the corresponding carbon atom.

The final value of R was 0.051 and the weighted discrepancy factor R_w was 0.051. The weighting scheme was $w^{-1} = \sigma^2(F_o) + 0.0002F_o^2$ and the $R_w = \sum||F_o| - |F_c||\sqrt{w}/\sum|F_o|\sqrt{w}$.[16] The neutral atom scattering factors have been taken from *International Tables for X-Ray Crystallography*.[17]

The calculations were performed on a Nicolet R3m diffractometer system with SHELXTL[16] software for minicomputer (Nova 3).

Thermal parameters with their standard deviations for non-hydrogen atoms are given in Table 1 and the coordinates and isotropic thermal parameters of hydrogen atoms in Table 2. Bond distances and angles are given in Table 3.

DISCUSSION

The crystal structure of tetrakis[trifluoroacetato-μ-(2-diethylaminoethanolato)copper(II)] consists of four discrete tetrameric $[Cu(Et_2LO)(F_3Ac)]_4$ molecules per unit cell. The structure of the molecule is shown in Figs. 1 and 2.

Each molecule has an eight-membered Cu_4O_4 core formed by four copper and four ethanolato oxygen atoms with Cu – Cu distances of 3.206(1) Å

Table 1. Fractional atomic coordinates ($\times 10^4$) and thermal parameters[a] ($\times 10^3$). Estimated standard deviations are in parentheses.

Atom	X	Y	Z	U_{11}	U_{22}	U_{33}	U_{23}	U_{13}	U_{12}
Cu	−1006(1)	2248(1)	618(1)	43(1)	46(1)	51(1)	−11(1)	−8(1)	7(1)
F1	−3189(3)	3790(5)	915(6)	84(4)	302(10)	202(8)	133(8)	62(5)	78(5)
F2	−2705(4)	4584(3)	134(6)	124(5)	92(4)	272(8)	60(5)	−44(5)	22(3)
F3	−2963(4)	3583(4)	−406(7)	165(6)	177(7)	241(9)	−98(6)	−138(6)	103(5)
O1	−82(2)	1690(2)	631(3)	45(2)	41(2)	45(2)	−5(2)	−7(2)	5(2)
O2	−1878(2)	2888(2)	465(3)	58(3)	64(3)	84(4)	−27(3)	−24(3)	24(2)
O3	−1450(3)	4017(2)	966(3)	63(3)	60(3)	80(4)	−5(3)	2(3)	1(2)
N	−1185(3)	1770(3)	−682(3)	43(3)	49(3)	54(3)	−6(3)	−11(3)	2(2)
C1	−101(4)	1109(4)	−41(5)	56(4)	50(4)	58(4)	−9(3)	−1(4)	8(3)
C2	−453(3)	1426(4)	−899(4)	54(4)	63(4)	49(4)	−19(3)	1(3)	−6(3)
C3	−1379(4)	2358(4)	−1381(5)	66(5)	70(5)	57(5)	7(4)	−10(4)	−6(4)
C4	−1391(6)	2126(5)	−2384(6)	131(8)	109(7)	60(5)	20(5)	−2(5)	31(6)
C5	−1767(4)	1168(4)	−685(5)	55(4)	61(4)	58(4)	−5(4)	−11(3)	−5(3)
C6	−2534(4)	1411(4)	−440(5)	61(4)	79(5)	81(6)	−4(4)	7(4)	−1(4)
C7	−1931(4)	3585(3)	618(5)	58(4)	52(4)	58(4)	−6(3)	6(4)	13(3)
C8	−2689(4)	3888(4)	313(6)	71(5)	55(5)	88(6)	−3(4)	1(5)	18(4)

[a] The anisotropic thermal parameters are of the form $\exp|-2\pi^2(h^2a^{*2}U_{11} + ... 2hka^*b^*U_{12} + ...)|$.

(4×) and 3.714(1) Å (2×), the O–O distances are 2.736(6) Å (4×) and 2.914(7) Å (2×). The arrangement of the oxygen atoms in the Cu_4O_4 core is nearly tetrahedral, Fig. 1.

The clusters are of the cubane type and have boat conformation with S_4 point group molecular symmetry as in $[Cu(Et_2LO)(ClAc)]_4$[7] and in $[Cu(Me_2LO)(ClAc)]_4$.[10] The molecular symmetry in $[Cu(Me_2LO)(F_3Ac)]_4$[12] is close to S_4. $[Cu(Et_2LO)(NCO)]_4$,[4] $[Cu(Et_2LO)Br]_4 \cdot 4CCl_4$[5] and $[Cu[Cu(Et_2LO)Cl]_4 \cdot 4CCl_4$[5] also have S_4 symmetry but not the boat conformation. Other nearly similar but distorted boat conformations have been reported. The molecular symmetries of $[Cu(Me_2LO)(Cl_2Ac)]_4$,[11] $[Cu(Et_2LO)(Cl_2Ac)]_4$,[8] $[Cu(Et_2LO)(Cl_3Ac)]_4$,[9] $[Cu(Bu_2LO)(Cl_2Ac)]_4$[13] are C_2, close to C_2, C_1 and C_1, respectively.

This lowering in the symmetry of the tetramers follows the differences between the longest and shortest intramolecular Cu–Cu and axial Cu–O distances. The differences increase with increasing

Table 2. Fractional atomic coordinates (×10³) and isotropic thermal parameters[a] (×10²) for hydrogen atoms.

Atom	*X*	*Y*	*Z*	*U*
H1(C1)	38(3)	97(3)	−8(4)	6
H2(C1)	−40(3)	69(3)	19(4)	6
H1(C2)	−53(3)	101(3)	−139(4)	7
H2(C2)	−9(3)	183(3)	−116(4)	7
H1(C3)	−181(4)	253(4)	−124(5)	8
H2(C3)	−101(3)	274(3)	−128(4)	8
H1(C4)	−148(5)	262(5)	−274(5)	12
H2(C4)	−179(5)	181(4)	−253(6)	12
H3(C4)	−91(5)	197(5)	−255(6)	12
H1(C5)	−162(3)	81(3)	−20(4)	7
H2(C5)	−176(3)	99(3)	−128(4)	7
H1(C6)	−289(4)	99(4)	−49(5)	9
H2(C6)	−273(3)	182(4)	−86(5)	9
H3(C6)	−253(4)	165(4)	16(5)	9

[a] The isotropic thermal parameters are set at 1.2 times the equivalent isotropic value for the corresponding carbon atom.

Table 3. Interatomic distances (Å) and angles (°) with estimated standard deviations in parentheses.[a]

The copper(II) environment					
Cu–O1	1.933(4)	O1–Cu–N	86.0(2)	$O1^{ii}$–Cu–$O1^{i}$	69.5(1)
Cu–O2	1.949(4)	O1–Cu–$O1^{i}$	89.7(2)	$O3^{iii}$–Cu–O1	82.0(1)
Cu–N	2.100(5)	N–Cu–O2	90.8(2)	$O3^{iii}$–Cu–N	93.1(2)
Cu–$O1^{i}$	1.947(4)	O2–Cu–$O1^{i}$	94.0(2)	$O3^{iii}$–Cu–O2	105.3(1)
Cu–$O1^{ii}$	2.721(4)	O1–Cu–O2	172.1(2)	$O3^{iii}$–Cu–$O1^{i}$	81.7(1)
Cu–$O3^{iii}$	2.756(5)	N–Cu–$O1^{i}$	173.7(2)	$O3^{iii}$–Cu–$O1^{ii}$	143.1(1)
Cu...Cu^{i}	3.206(1)	$O1^{ii}$–Cu–O1	75.4(1)		
Cu...Cu^{ii}	3.714(1)	$O1^{ii}$–Cu–N	113.6(2)		
Cu...Cu^{iii}	3.206(1)	$O1^{ii}$–Cu–O2	99.4(1)		
The 2-diethylaminoethanolato ligand					
O–C1	1.428(7)	Cu–N–C2	103.0(3)	N–C3–C4	117.6(6)
C1–C2	1.507(9)	Cu–N–C3	111.0(4)	N–C5–C6	115.5(5)
N–C2	1.483(8)	Cu–N–C5	113.7(4)	O–C1–C2	107.7(5)
N–C3	1.503(9)	C2–N–C3	110.6(5)	C1–O–Cu	110.4(3)
N–C5	1.499(8)	C2–N–C5	108.3(5)	C1–O–Cu^{iii}	121.1(3)
C3–C4	1.516(11)	C3–N–C5	110.0(5)	Cu–O–Cu^{iii}	111.4(2)
C5–C6	1.482(10)	N–C2–C1	110.5(5)		
The trifluoroacetate ligand					
O2–C7	1.271(7)	O2–C7–O3	131.0(6)	F1–C8–F2	105.2(8)
O3–C7	1.204(8)	O2–C7–C8	111.4(6)	F1–C8–F3	103.6(7)
C7–C8	1.527(10)	O3–C7–C8	117.7(6)	F2–C8–F3	104.0(8)
C8–F1	1.264(11)	C7–C8–F1	112.2(7)		
C8–F2	1.273(10)	C7–C8–F2	115.3(7)		
C8–F3	1.278(12)	C7–C8–F3	115.3(7)		

[a] i: $-1/4+y, 1/4-x, 1/4-z$; ii: $-x, 1/2-y, z$; iii: $1/4-y, 1/4+x, 1/4-z$.

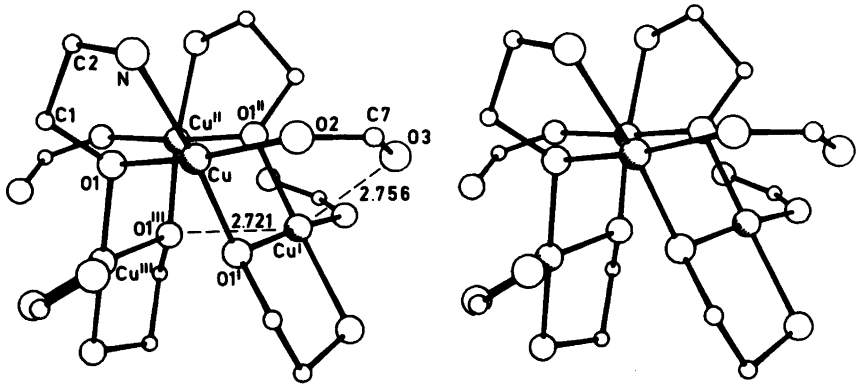

Fig. 1. Stereoview of the $Cu_4(NCCO)_4(COO)_4$ fragment.

number of chloro substituents. In the ethyl series they are 0.546 and 0.057 Å in $[Cu(Et_2LO)(ClAc)]_4$,[7] 0.848 and 0.67 Å in $[Cu(Et_2LO)(Cl_2Ac)]_4$.[8] In $[Cu(Et_2LO)(Cl_3Ac)]_4$[9] where the number of chloro substituents is three the Cu – Cu difference is 0.902 Å and one Cu – O (carboxylate) bond is presented by an ethyl group of the 2-diethylaminoethanolato ligand.

The situation is similar in the methyl series where the differences are 0.584 and 0.025 Å in $[Cu(Me_2LO)(ClAc)]_4$[10] and 0.811 and 0.546 Å in $[Cu(Me_2LO)(ClAc)]_4$.[11]

In the $[Cu(Bu_2LO)(Cl_2Ac)]_4$[13] complex the Cu – Cu difference is 0.686 Å and also here one Cu – O (carboxylate) bond is blocked by a butyl group.

In the $[Cu(Et_2LO)(F_3LO)]_4$ cluster the distances, the angles and the differences 0.508 and 0.035 Å are nearly similar to the ethyl[7] and methyl[10] monochloroacetate complexes.

In the chloro substituent series of the ethyl complexes the maximum distortion and lowest molecular symmetry is in the trichloroacetate complex. The difference between the trichloroacetate and trifluoroacetate complexes is considerable. When the chlorine atoms are replaced by fluorine atoms there is a change in the molecular symmetry from the lowest C_1 to the maximum S_4. This is apparently due to more favourable packing effects as the covalent radius decreases. When the ethyl groups replace the methyl groups the sym-

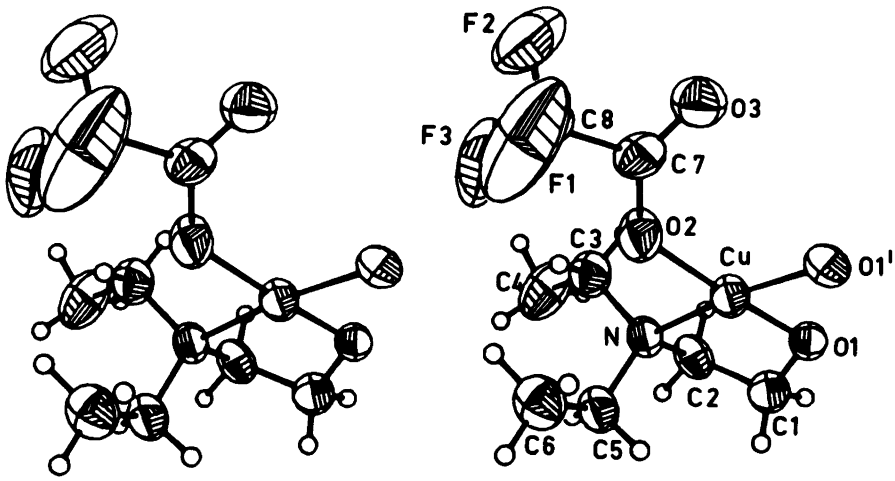

Fig. 2. Stereoview of the $Cu(Et_2NC_2H_4O)(F_3CCOO)O^i$ fragment with thermal ellipsoids at the 50 % probability level, hydrogen atom radii are set at 0.1 Å.

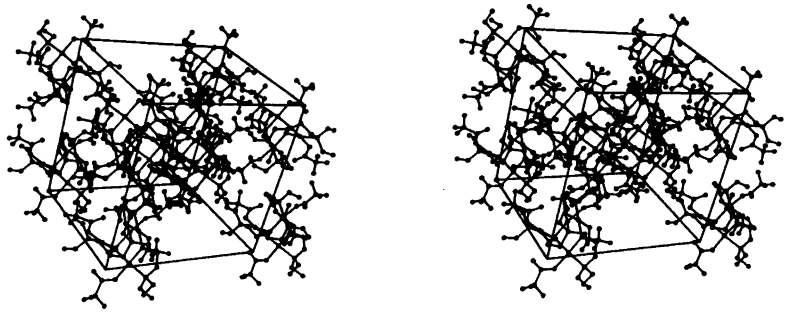

Fig. 3. Stereoview of the packing.

metry gets lower though it is still close to S_4. Here steric hindrance and packing effects may also have influence.

The copper(II) ion has a distorted octahedral (4+2) environment. In the basal plane there is an amino nitrogen atom, two bridging ethanolato oxygen atoms and a carboxylate oxygen atom at quite normal distances for coordination bonds.[1-14]

The O1 and O2 atoms lie 0.102 and 0.093 Å below and N and $O1^i$ ($-1/4+y$, 1/4-x, 1/4-z) 0.096 and 0.098 Å above the least-squares plane of atoms O1,O2,N,$O1^i$. The copper(II) ion is practically in the plane, only 0.02 Å above. There is some tetrahedral distortion which can also be seen from the dihedral angle of 8.3° between the Cu,O1,N and Cu,$O1^i$,O2 planes.

In fifth position there is an ethanolato oxygen atom $O1^{ii}$ ($-x$, $\frac{1}{2}$-y, z) and in sixth position a carboxylate oxygen atom $O3^{iii}$ (1/4-y, 1/4+x, 1/4-z). The Cu – O distances are nearly equal but the copper ethanolato oxygen length is slighty shorter (0.035 Å). In the other complexes with S_4 molecular symmetry the copper carboxylate distance is shorter than the copper ethanolato distance as in $|Cu(Me_2LO)(ClAc)|_4$[10] (2.712 and 2.737 Å) and in $|Cu(Et_2LO)(ClAc)|_4$[7] (2.663 and 2.720 Å). In $|Cu(Me_2LO)(F_3Ac)|_4$[12] where the symmetry is close to S_4 the copper ethanolato distances varied from 2.717 to 2.819 Å and the copper carboxylate distances from 2.663 to 2.847 Å.

In $|Cu(Me_2LO)(ClAc)|_4$[11] where the symmetry is C_2 one copper ethanolato distance is 2.633 Å

Tables 4. The shortest and longest interatomic Cu – Cu and axial Cu – O distances (Å), the differences (Å) between the longest and shortest distances and the point group molecular symmetry in cubane type molecules of haloacetate complexes.

Compound	Cu – Cu Long	Short	Δ	Cu – O LO	Ac	Δ	Symmetry	Ref.
$[Cu(Me_2LO)(ClAc)]_4$	3.766	3.182	0.584	2.737	2.712	0.025	S_4	10
$[Cu(Me_2LO)(Cl_2Ac)]_4$	3.609	3.124	0.811	2.633	2.517	0.546	C_2	11
	3.935	3.256		2.858	3.063			
$[Cu(Me_2LO)(F_3Ac)]_4$	3.713	3.154	0.659	2.717	2.663	0.184	close to S_4	12
	3.813	3.231		2.819	2.847			
$[Cu(Et_2LO)(ClAc)]_4$	3.746	3.200	0.546	2.720	2.663	0.057	S_4	7
$[Cu(Et_2LO)(Cl_2Ac)]_4$	3.658	3.176	0.848	2.71	2.59	0.67	close to C_2	8
	4.024	3.290		2.95	3.26			
$[Cu(Et_2LO)(Cl_3Ac)]_4$	3.672	3.094	0.902	2.52	2.44	[a]	C_1	9
	3.996	3.372		3.01	2.60			
$[Cu(Et_2LO)(F_3Ac)]_4$	3.714	3.206	0.508	2.721	2.756	0.035	S_4	This work
$[Cu(Bu_2LO)(Cl_2Ac)]_4$	3.619	3.134	0.686	2.60	2.43	[a]	C_1	13
	3.824	3.313		2.97	2.74			

[a] Ethyl or butyl group is blocking the carboxylate oxygen place of one copper(II).

and the other is elongated to 2.858 Å. Corresponding to this the copper carboxylate distances are 3.063 to 2.517 Å, respectively. In $|Cu(Et_2LO)(Cl_2LO)|_4$[8] where the symmetry is pseudo C_2 there are two copper ethanolato distances ~2.93 Å and two ~2.72 Å while two copper carboxylate distances are ~2.62 Å and one 2.90 Å. The fourth copper carboxylate distance is elongated to 3.26 Å.

In C_1 complexes $|Cu(Et_2LO)(Cl_3Ac)|_4$[9] and $|Cu(Bu_2LO)(Cl_2Ac)|_4$[13] the ethanolato Cu–O distances vary from 2.52 to 3.01 Å and the carboxylate distances from 2.43 to 2.74 Å. In both clusters one of the four copper atoms has square-pyramidal environment where the apical position is occupied by an ethanolato oxygen atom (2.52–2.60 Å). The sixth position is blocked by an ethyl or butyl substituent of the aminoethanolato ligand.

The bond lengths and angles of the 2-diethylaminoethanolato ligand are as expected. The mean value of the angles around the ethanolato oxygen atoms is 109.0° which indicates sp^3 hybridization. It is quite distorted, however because the angles vary from 85.0 to 121.4°. In the five-membered ethanolato ring the dihedral angle O,C1,C2,N is 53.5°.

The trifluoroacetate group is bridging two copper atoms asymmetrically in syn–syn configuration. One oxygen is coordinated equatorially and the other is in the axial coordination position of a copper atom. The C–O bond lengths are different, corresponding to the short and long Cu–O distances. The acetate group is planar with the largest deviation from the least-square plane defined by O2,C7,C8,O3 on the carbon atom C7 (0.008 Å). The mean value of the C–F bond lengths is 1.272 Å. These lengths and angles agree well with data from trifluoroacetate groups.[18–20]

The CF_3 group displays a relatively high degree of anisotropic thermal motion. This has also been observed in other structures containing CF_3 groups[19–21] and may be due to torsional motion and rotational disorder.

The molecules are held together by van der Waals forces. The shortest intermolecular distances are F2···C6^v 3.314 Å and F2···C5^v 3.383 Å ($x, \frac{1}{2}+y, -z$).

REFERENCES

1. Smolander, K. *Acta Chem. Scand. A 35* (1981) 815.
2. Muhonen, H., Pajunen, A. and Hämäläinen, R. *Acta Crystallogr. B 36* (1980) 2790.
3. Mergehenn, R. and Haase, W. *Acta Crystallogr. B 33* (1977) 1877.
4. Merz, L. and Haase, W. *J. Chem. Soc. Dalton Trans.* (1978) 1594.
5. Mergehenn, R., Metz, L. and Haase, W. *J. Chem. Soc. Dalton Trans.* (1980) 1703.
6. Merz, L. and Haase, W. *Acta Crystallogr. B 34* (1978) 2128.
7. Turpeinen, U., Hämäläinen, R., Ahlgrén, M. and Smolander, K. *Finn. Chem. Lett.* (1979) 108.
8. Smolander, K., Turpeinen, U. and Ahlgrén, M. *Finn. Chem. Lett.* (1978) 195.
9. Ahlgrén, M., Hämäläinen, R., Turpeinen, U. and Smolander, K. *Acta Crystallogr. B 35* (1979) 2870.
10. Turpeinen, U., Ahlgrén, M. and Hämäläinen, R. *Acta Chem. Scand. A 33* (1979) 593.
11. Turpeinen, U., Hämäläinen, R. and Ahlgrén, M. *Acta Crystallogr. B 36* (1980) 927.
12. Ahlgrén, M., Turpeinen, U. and Hämäläinrn, R. *Acta Crystallogr. B. In press.*
13. Turpeinen, U., Hämäläinen, R. and Ahlgrén, M. *Cryst. Struct. Commun. 10* (1981) 179.
14. Ahlgrén, M., Turpeinen, U. and Smolander, K. *Acta Crystallogr. B 36* (1980) 1091.
15. Bateman, W. G. and Conrad, D. B. *J. Am. Chem. Soc. 37* (1915) 2553.
16. *The SHELXTL 1980 System*, Nicolet XRD Corporation, 10061 Bubb Road, Cupertino, California 95014, USA.
17. *International Tables for X-Ray Crystallography*, Kynoch Press, Birmingham 1974, Vol. 4, p. 71.
18. Bullivant, D. P., Dove, M. F. A. and Haley, M. J. *J. Chem. Soc. Dalton, Trans.* (1979) 109.
19. Birchall, T. and Johnson, J. P. *J. Chem. Soc. Dalton Trans.* (1981) 69.
20. Pradilla, J., Chen, S. H. W., Koknat, F. W. and Fackler, J. P. *Inorg. Chem. 18* (1979) 3519.
21. Little, R. G., Moreland, J. A., Yawney, D. B. W. and Doedens, R. J. *J. Am. Chem. Soc. 96* (1974) 3834.
22. Bondi, A. *J. Phys. Chem. 68* (1964) 441.

Received June 12, 1981.

Acta Chemica Scandinavica A 36 (1982) 195–202

A True Square-planar Te(II) complex with Bidentate Ligands. The Preparation and Crystal Structure of Bis(imidotetraphenyldithiodiphosphino-*S*,*S*′)tellurium(II)

STURLE BJØRNEVÅG, STEINAR HUSEBYE and KNUT MAARTMANN-MOE

Department of Chemistry, University of Bergen, N-5014 Bergen, Norway

The preparation and structural characterization of bis(imidotetraphenyldithiodiphosphino-*S*,*S*′)tellurium(II), $[Te\{N(Ph_2PS)_2\}_2]$, is reported. The molecular structure has been determined by X-ray crystallographic methods. Unit cell dimensions are $a=10.187(1)$ Å, $b=12.929(5)$ Å, $c=18.282(3)$ Å, $\alpha=89.04(2)°$, $\beta=82.98(1)°$, $\gamma=77.40(2)°$ $Z=2$. Full-matrix least-squares refinement of 4456 observed reflections gave an *R*-value of 0.068. The crystals are triclinic and are built up of discrete, centrosymmetric, square-planar Te(II) complexes. The imidotetraphenyldithiodiphosphinato ligands are bidentate and the molecules have an approximate chair form. There are two crystallographically independent half molecules in the asymmetric unit with an average Te–S bond length of 2.685(13) Å. The average intra-ligand S–Te–S angle is 86.8(1.1)°.

Previous work on divalent sulfur, selenium and tellurium compounds with monodentate and bidentate sulfur-containing ligands, indicated that their structures could be divided into five classes.[1] With bidentate ligands having small bites, the resulting structures are trapezoid planar with greatly asymmetric central atoms to ligand bonds (Classes I and II). It was however predicted that with a bidentate ligand with a large bite, symmetric square planar complexes might be prepared.[1]

The imidotetraphenyldithiodiposphinate anion was chosen as a suitable ligand to test this hypothesis. It has a large S–S bite ranging from 3.67 to 4.03 Å,[2–4] a variation which demonstrates the flexibility of the ligand. The bite is also up to *ca.* 1 Å larger than that found in the dialkyldithiophosphates, phosphinates, -carbamates and alkylxanthates all of which give class I and II complexes of tellurium(II).

The imidotetraphenyldithiodiphosphinate anion is uninegative and has a delocalized S···S donor system like the class I and II ligands. This fact should minimize the effect of electronic differences upon the structure of the complexes.

EXPERIMENTAL

Preparation of the complex. The acid, $HN(Ph_2PS)_2$, and its ammonium salt were prepared by published procedures.[5,6] The tellurium complex, $[Te\{N(Ph_2PS)_2\}_2]$, was prepared by adding 0.47 g (1.0 mmol) of $NH_4\{N(Ph_2PS)_2\}$ dissolved in 80 ml methanol to 0.20 g (0.38 mmol) of $[Te(tu)_4Cl_2]\cdot 2H_2O$ (tu = thiourea) dissolved in 20 ml methanol and stirring. The yellow precipitate was filtered, washed with ethanol and dried. Yield, based on $[Te(tu)_4Cl_2]\cdot 2H_2O$, was 75 %. Crystals were formed by slow recrystallization from chloroform; m.p. 257 °C (dec.). Found C 55.9; H 3.9; N 2.8; S 12.2. Calc for $C_{48}H_{40}N_2P_4S_4Te$: C 56.27; H 3.94; N 2.73; S 12.52.

X-Ray data. Intensity data and data for measurement of unit cell parameters were obtained on an Enraf-Nonius CAD-4 diffractometer. The crystal used for data collection had approximate dimensions $0.06\times0.29\times0.15$ mm^3. Unit cell parameters were found from least-squares refinement of the setting angles of 25 high-angle reflections. They are $a=10.187(1)$ Å, $b=12.929(5)$ Å, $c=18.282(3)$ Å, $\alpha=89.04(2)°$, $\beta=82.98(1)°$, $\gamma=77.40(2)°$, $Z=2$, $D_m=D_x=1.46$ g cm^{-3}, $\mu(MoK\alpha)=10.1$ cm^{-1}. Space group $P\bar{1}$ (No. 1) or $P1$ (No. 2).

Reflection intensities were collected using an omega-scan with scan width $(1.00+0.35\ \mathrm{tg}\ \theta)°$, a graphite monochromator and Mo$K\alpha$ radiation. The

0302-4377/82/030195-08$02.50

scan rate varied from 3.3 to 0.5° min^{-1}; 4456 unique reflections of a total of 7298 with $2\theta \leqslant 48°$ had $I \geqslant 2\sigma(I)$ and were treated as observed. The intensities were corrected for absorption. (Transmission factor range 0.85–0.94.) For further details about data collection and computer programs used throughout this investigation, the reader is referred to a previous paper.[7]

IR spectrum. An IR spectrum was obtained, using a Perkin-Elmer 683 instrument and the KBr disc technique (Fig. 5).

STRUCTURE DETERMINATION

The structure was solved by means of conventional heavy atom techniques. It was refined by least-squares full-matrix methods assuming the centrosymmetric space group $P\bar{1}$. The asymmetric unit was found to contain two crystallographically independent half molecules, with the tellurium atoms at centers of symmetry (0,0,0 and 0,1/2,1/2). The successful refinement indicates that the correct space group had been chosen. In the final refinements, anisotropic temperature factors were used for the heavy atoms (Te, P and S). In addition, the hydrogen positions were computed (based on C–H bond lengths of 0.97 Å) and all hydrogen atoms were included with fixed positions and with a constant temperature factor, $B = 7.0$ Å^2. The final conventional R factor was 0.067, while R_w with $p = 0.02$[7] was 0.074. A difference map showed no peaks above 0.4 e/Å^3. Refined atomic coordinates are shown in Table 1. Tables of thermal parameters and observed and calculated structure factors are available from the author S. H. upon request.

RESULTS

Interatomic distances and angles are shown in Tables 3–4, while molecular planes and other structural data are shown in Table 5. Fig. 1 is a

Table 1. Atomic coordinates for the asymmetric unit in fractions of cell edges with standard deviations.

Molecule I	*x*	*y*	*z*
Te1	0	0	0
S1	−0.1690(3)	0.0948(2)	−0.0941(2)
S2	0.2008(4)	0.0396(3)	−0.0997(2)
P1	−0.1372(3)	0.2432(2)	−0.0878(2)
P2	0.1567(3)	0.1949(2)	−0.0709(2)
N1	0.0055(10)	0.2585(7)	−0.0674(5)
C111	−0.1679(11)	0.3042(8)	−0.1765(6)
C112	−0.1504(13)	0.2451(9)	−0.2392(7)
C113	−0.1712(14)	0.2947(10)	−0.3063(7)
C114	−0.2006(14)	0.4005(10)	−0.3100(7)
C115	−0.2161(15)	0.4599(10)	−0.2488(8)
C116	−0.2025(14)	0.4124(10)	−0.1803(7)
C121	−0.2604(12)	0.3188(9)	−0.0182(6)
C122	−0.2329(14)	0.4065(10)	0.0124(7)
C123	−0.3287(18)	0.4694(13)	0.0639(9)
C124	−0.4531(17)	0.4429(12)	0.0820(9)
C125	−0.4821(16)	0.3594(12)	0.0492(8)
C126	−0.3884(14)	0.2963(10)	−0.0032(7)
C211	0.2085(12)	0.2069(9)	0.0198(6)
C212	0.1378(15)	0.2873(11)	0.0684(8)
C213	0.1773(17)	0.2948(12)	0.1396(9)
C214	0.2804(17)	0.2227(12)	0.1571(9)
C215	0.3521(17)	0.1451(12)	0.1131(9)
C216	0.3160(15)	0.1352(10)	0.0436(8)
C221	0.2577(13)	0.2611(9)	−0.1351(7)
C222	0.2051(15)	0.3445(11)	−0.1734(8)
C223	0.2843(17)	0.3995(12)	−0.2241(9)
C224	0.4202(17)	0.3588(12)	−0.2294(9)
C225	0.4778(18)	0.2798(12)	−0.1952(9)
C226	0.4006(14)	0.2255(10)	−0.1462(7)

Molecule II			
Te2	0	1/2	1/2
S3	−0.1240(3)	0.4710(2)	0.3837(2)
S4	0.2234(3)	0.3694(2)	0.4330(2)
P3	−0.1253(3)	0.3156(2)	0.3981(2)
P4	0.1521(3)	0.2353(2)	0.4381(2)
N2	0.0147(9)	0.2346(7)	0.4046(5)
C311	−0.2513(11)	0.2982(8)	0.4740(6)
C312	−0.3426(12)	0.3813(9)	0.5092(6)
C313	−0.4447(15)	0.3623(11)	0.5643(8)
C314	−0.4470(15)	0.2579(11)	0.5830(8)
C315	−0.3570(14)	0.1751(10)	0.5482(7)
C316	−0.2560(13)	0.1935(9)	0.4948(7)
C321	−0.1883(11)	0.2751(8)	0.3191(6)
C322	−0.1024(15)	0.2246(10)	0.2613(8)
C323	−0.1486(16)	0.1962(12)	0.1965(8)
C324	−0.2829(17)	0.2207(12)	0.1933(9)
C325	−0.3749(18)	0.2752(12)	0.2459(9)
C326	−0.3276(16)	0.3015(11)	0.3118(8)
C411	0.2802(12)	0.1373(8)	0.3863(6)
C412	0.2528(13)	0.0775(9)	0.3314(7)
C413	0.3556(14)	0.0039(10)	0.2899(7)
C414	0.4885(15)	−0.0069(11)	0.3042(8)
C415	0.5137(18)	0.0520(13)	0.3578(9)
C416	0.4132(14)	0.1255(10)	0.4015(7)
C421	0.1425(11)	0.1864(8)	0.5313(6)
C422	0.0911(13)	0.0959(9)	0.5457(7)
C423	0.0903(14)	0.0511(10)	0.6156(7)
C424	0.1377(13)	0.0955(10)	0.6702(7)
C425	0.1878(14)	0.1836(10)	0.6569(7)
C426	0.1910(13)	0.2311(9)	0.5885(7)

drawing of the two crystallographically independent, but similar molecules in the cell. The average TeS_4 coordination is shown in Fig. 2. In Fig. 3, the molecules are viewed in such a way that their overall conformational differences are emphasized. The relative positions of the molecules in the unit

Table 2. Interatomic distances (Å) with standard deviations in the two crystallographically independent half molecules in the asymmetric unit.

Molecule I		Molecule II	
Te1 – S1	2.675(2)	Te2 – S3	2.673(2)
Te1 – S2	2.699(3)	Te2 – S4	2.691(2)
S1 – P1	2.022(3)	S3 – P3	2.025(3)
S2 – P2	2.023(3)	S4 – P4	2.018(3)
P1 – N1	1.597(7)	P3 – N2	1.590(6)
P2 – N1	1.574(7)	P4 – N2	1.597(7)
P1 – C111	1.821(8)	P3 – C311	1.818(8)
P1 – C121	1.807(9)	P3 – C321	1.781(8)
P2 – C211	1.819(9)	P4 – C411	1.795(8)
P2 – C221	1.796(9)	P4 – C421	1.807(8)
S1 – S2	3.667(4)	S3 – S4	3.711(3)
P1 – P2	2.975(3)	P3 – P4	2.966(3)
S1 – P2	3.835(3)	S3 – P4	3.877(3)
S2 – P1	3.886(3)	S4 – P3	3.893(3)

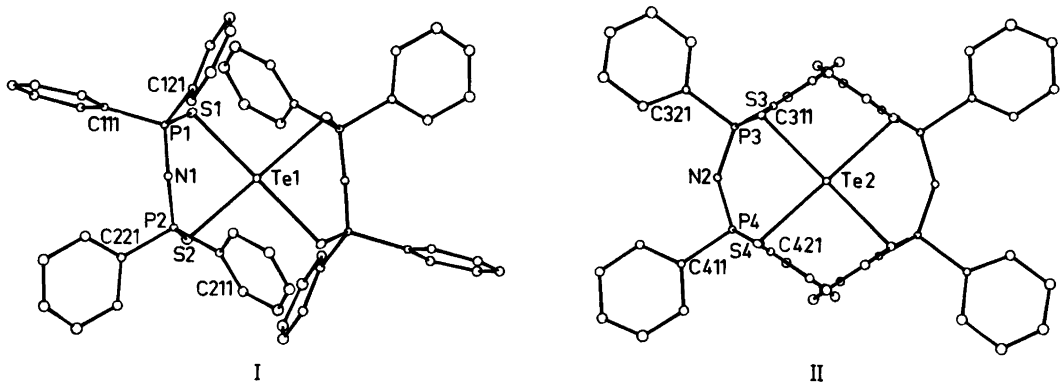

I II

Fig. 1. Molecules I and II seen along the normals to their TeS_4 planes.

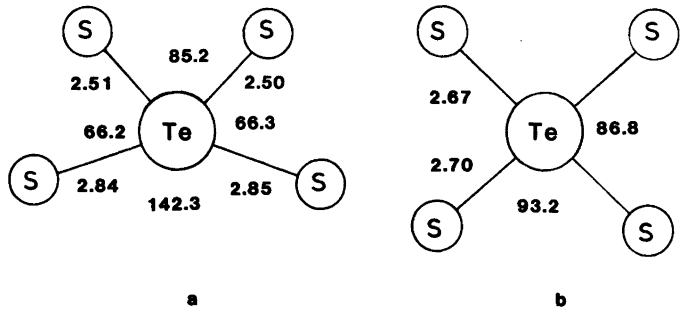

Fig. 2. The inner coordination sphere in a class I complex [a, dimethylxanthatotellurium(II)[1]] and in a class V complex (b, present investigation). The planar groups are seen along their normals; bond lengths and angles (average values in b) are in ångströms and degrees, respectively.

cell are shown in Fig. 4. From the figures, it is seen that the structure is built up of discrete bis(imido-tetraphenyldithiodiphosphino-*S*,*S*')tellurium(II) molecules. The tellurium atoms are located at centers of symmetry and are coordinated to the four sulfur atoms in the molecule in a square planar configuration.

DISCUSSION

The TeS_4 group. The group is centrosymmetric and thus planar in both molecules. There is a slight asymmetry in the Te–S bond lengths in both molecules. The long Te–S bonds are 2.699(3) and 2.691(3) Å, while the short ones are 2.675(2) and 2.673(2) Å for I and II, respectively. With intraligand angles of 86.05(8) and 87.54(7) for the two molecules, both are true square-planar complexes of divalent tellurium. These angles correspond to S–S bites of 3.667(4) and 3.771(3) Å, much larger than the value of 2.95 Å commonly found in corresponding dialkyldithiocarbamate and alkylxanthate complexes. The small bite forces the latter compounds to adopt a class I type trapezoid, planar structure, with greatly asymmetric Te–S bond lengths. However, with a larger bite, such as found in the present investigation, the tendency of Te(II) to form square planar complexes results in just such a structure belonging to class V in accordance with the previous prediction. Surprisingly, the corresponding Ni(II) complex with methyl groups replacing phenyl groups, is tetrahedral.[3] However the corresponding Pd(II) and Pt(II) complexes are probably planar,[8] but then these metals resemble tellurium in their stereochemistry.[9] Bonding in the linear, three-center S–Te–S systems is probably of the three-center four-electron type.

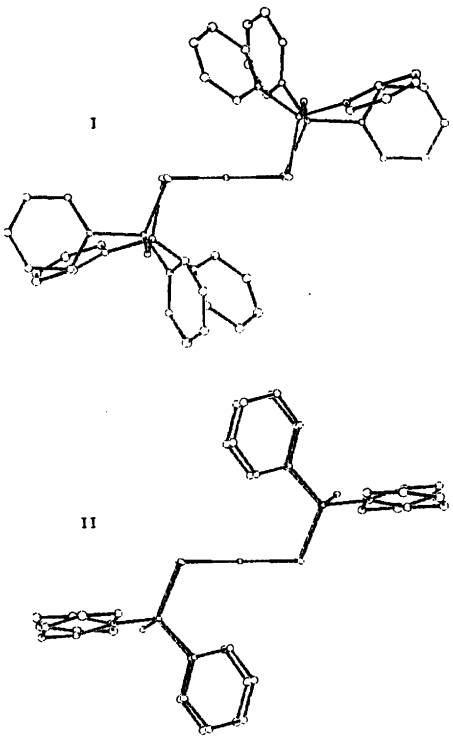

Fig. 3. Molecules I and II viewed along the bisector of the S1′–Te1–S2 and S3′–Te2–S4 angles, respectively.

The average Te–S bond length of 2.685(13) Å is typical for such bonding found in numerous Te(II) complexes with monodentate sulfur-containing ligands.[9] In these linear systems 5*p* orbitals on tellurium are overlapping with suitable σ orbitals on the sulfur atoms.

The imidotetraphenyldithiodiphosphinate ligands. Several coordination compounds containing the above or related ligands are known,[2-5,10-16] but few structures have been determined.[2-4,11,12] The average bond lengths (and angles) found here agree well with corresponding dimensions found in previous structure determinations (Table 4). Average S–P and P–N bond lengths of 2.022(3) and 1.590(11) Å indicate a considerable amount of double bond character in both bond types.[7,17] The chelate ring angles in Table 4 vary somewhat due to variation in size of central atom and overall structure. The large variation in the average P–N–P (10°) and M–S–P angles (8°) demon-

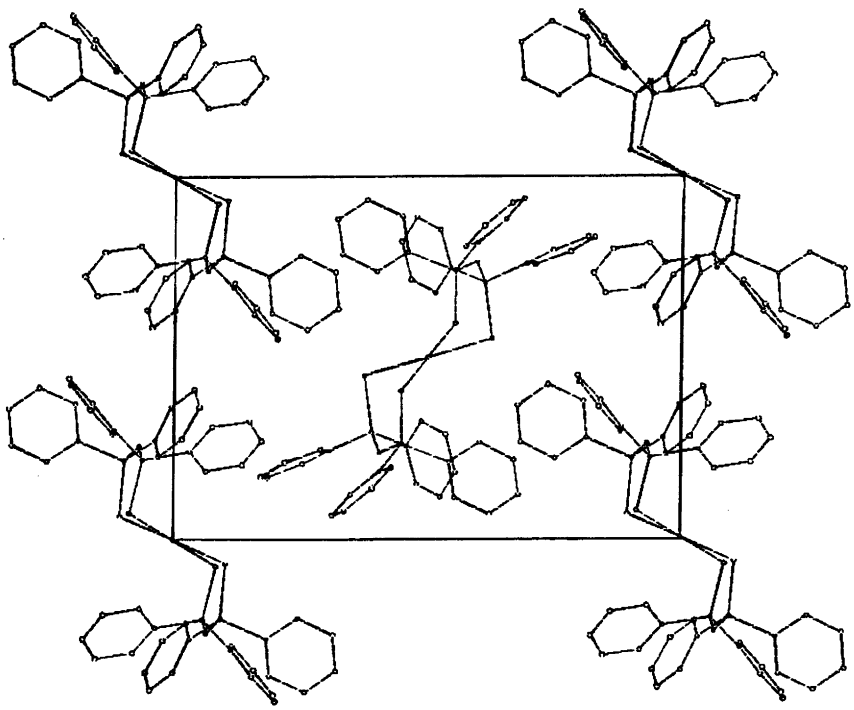

Fig. 4. The unit cell contents seen in projection along *a*.

Table 3. Bond angles (°) with standard deviations. Primed letters denote atoms in the other half of the molecules related to those in the first half (Table 1) by molecular centers of symmetry.

Molecule I		Molecule II	
S1 – Te1 – S2	86.05(8)	S3 – Te2 – S4	87.54(7)
S1 – Te1 – S2′	93.95(8)	S3 – Te2 – S4′	92.46(7)
Te1 – S1 – P1	98.69(10)	Te2 – S3 – P3	98.47(9)
Te1 – S2 – P2	91.76(11)	Te2 – S4 – P4	97.77(10)
S1 – P1 – N1	119.0(3)	S3 – P3 – N2	118.4(3)
S2 – P2 – N1	118.7(3)	S4 – P4 – N2	119.0(3)
P1 – N1 – P2	139.5(4)	P3 – N2 – P4	137.0(4)
S1 – P1 – C111	106.3(3)	S3 – P3 – C311	110.8(3)
S1 – P1 – C121	109.7(3)	S3 – P3 – C321	106.0(3)
N1 – P1 – C111	109.5(4)	N2 – P3 – C311	110.4(3)
N1 – P1 – C121	104.5(4)	N2 – P3 – C321	106.2(4)
C111 – P1 – C121	107.5(4)	C311 – P3 – C321	103.8(4)
S2 – P2 – C211	108.4(3)	S4 – P4 – C411	105.9(3)
S2 – P2 – C221	107.7(3)	S4 – P4 – C421	110.2(3)
N1 – P2 – C211	106.7(4)	N2 – P4 – C411	105.7(4)
N1 – P2 – C221	107.4(4)	N2 – P4 – C421	110.0(4)
C211 – P2 – C221	107.5(4)	C411 – P4 – C421	104.9(4)
P1 – C111 – C112	121.6(6)	P3 – C311 – C312	122.9(6)
P1 – C111 – C116	118.9(6)	P3 – C311 – C316	117.3(6)
P1 – C121 – C122	119.2(7)	P3 – C321 – C322	121.0(7)
P1 – C121 – C126	120.0(7)	P3 – C321 – C326	121.1(7)
P2 – C211 – C212	120.7(7)	P4 – C411 – C412	122.8(7)
P2 – C211 – C216	121.5(7)	P4 – C411 – C416	117.8(7)
P2 – C221 – C222	122.9(8)	P4 – C421 – C422	118.2(6)
P2 – C221 – C226	120.3(7)	P4 – C421 – C426	123.3(6)

strates the flexibility of the ligand and indicates that the S – S bite can be greater or smaller than the range indicated in the table. In the present investigation, three of the Te – S – P angles are close to 98° while the fourth, Te1 – S2 – P2, is 91.76(11)°. This is a highly significant difference, and it corresponds to an S1 – P2 intramolecular distance which is significantly smaller than the others (Table 2). An increased repulsion in the ligand of molecule I as compared to molecule II may then be lessened by the greater puckering in the chelate ring of the ligand in molecule I as compared to that of molecule II. Also the greater P – N – P angle in I as compared to II (139.5(4) and 137.0(4)° respectively) will lessen repulsion between the atoms of the chelate rings. The large P – N – P angle is, however, not unusual when compared to that found in the bis(triphenylphosphineiminium) cation where it is often above 140° and may even be 180°.[7]

In molecule I the N1 atom is 0.133 Å below the best plane for the S and P atoms while Te1 is 1.875 Å below it. Consequently the chelate ring may be

Table 4. Average interatomic distances and angles in some $[M\{N(R_2PS)_2\}_2]$ chelate rings. The three first structures are tetrahedral.

M	R	M – S	S – P	P – N	∠S – M – S	∠M – S – P	∠S – P – N	∠P – N – P	S---S bite
Ni(II)[3]	Me	2.282(12)	2.023(6)	1.580(7)	107.9(8)	104.6(14)	116.6(8)	128.4(9)	3.69(3)
Fe(II)[4]	Me	2.360(17)	2.020(8)	1.591(11)	111.3(16)	99.5(22)	116.7(13)	132.3(53)	3.90(4)
Mn(II)[2]	Ph	2.443(12)	2.013(5)	1.588(6)	111.9(3)	99.9(34)	118.7(4)	133.5(18)	4.05(3)
Te(II)	Ph	2.685(13)	2.022(3)	1.590(11)	86.8(11)	96.7(33)	118.8(3)	138.3(4)	3.69(3)

Table 5. Planes in the molecules.

No. of plane	Atoms included	Interplanar angles (°)			
1	Te1,S1,S2	1–2	66.2	7–8	66.8
2	Te1,S1,P1	1–3	65.0	7–9	70.2
3	S1,P1,N1	1–4	86.9	7–10	36.8
4	P1,N1,P2	1–5	79.3	7–11	70.8
5	S2,P2,N1	1–6	75.2	7–12	66.7
6	Te1,S2,P2	1–17	72.8	7–18	67.7
7	Te2,S3,S4	2–3	27.3	8–9	54.7
8	Te2,S3,P3	3–4	23.8	9–10	34.8
9	S3,P3,N2	3–13	92.9	9–15	90.2
10	P3,N2,P4	3–17	15.2	9–18	12.1
11	S4,P4,N2	4–5	8.0	10–15	35.5
12	Te2,S4,P4	4–17	14.7	10–18	30.7
13	C111,P1,C121	5–6	50.3	11–12	55.0
14	C211,P2,C221	5–14	90.5	11–16	90.0
15	C311,P3,C321	13–17	90.9	15–19	96.6
16	C411,P4,C421	14–17	86.7	16–18	83.8
17	S1,P1,P2,S2	13–14	82.8	15–16	99.0
18	S3,P3,P4,S4				

Atomic displacements from the two last planes (Å)

17 S1 −0.097(3); P1,0.119(3); P2, −0.119(3); S2, 0.096(4); Te1, −1.875(0); N1, −0.133(9); C111, 1.81; C121, −1.03; C211, −1.68; C221, 1.22.
18 S3; −0.003(3); P3, 0.004(3); P4, −0.004(3); S4, 0.003(3); Te2, −1.793(0); N2, 0.300(9); C311, −1.51; C321, 1.30; C411, 1.29; C421, −1.53.

considered to have a very distorted boat conformation, however the N1 atom is not more than 0.014 Å further from the best plane than P1 and P2. The S and P atoms of molecule II are almost coplanar with N2 0.300 Å above their least-squares plane and Te2 1.793 Å below. Thus the chelate ring has a distorted chair configuration. The conformations of the chelate rings may best be seen from Fig. 3. In the Mn(II) complex with the same ligand, the chelate rings are arranged in twisted boat conformations but with sulfur and phosphorus atoms at the apices instead of metal and nitrogen. Such a conformation is supposed to minimize phenyl–phenyl interactions.[2] There are, however, no especially short phenyl–phenyl contacts in the present structure.

The phosphorus atoms are essentially sp^3 hybridized and the P–C bonds to the phenyl groups are normal. In the phenyl groups, the bond lengths and angles have average values of 1.38(3) Å and 120.0 (2.2)° respectively. Individual standard deviations are close to 0.01 Å and 1.0°.

Overall structure of the molecules and molecular packing. As can be seen from Fig. 3, the molecules have an overall "chair" configuration. The two crystallographically independent molecules, I and II, have almost identical bond lengths. However, many bond angles are significantly different in the two. Larger differences are found in their overall structures as indicated by the interplanar angles. The angle $TeS_4-S_2P_2$ is 72.8° in I and 67.7° in II whereas the angle $S_2P_2-P_2N$ is 14.7 and 30.7°, respectively. The extra puckering in the chelate ring in I relative to II also results in differences in the orientation of the phenyl groups: Interplanar TeS_4–phenyl group angles are 97.8, 97.5, 119.2 and 24.7° in molecule I while they are 90.4, 11.5, 17.7 and 89.8° in molecule II. The phenyl groups above are listed in order of their phosphorus connected carbon atoms, *i.e.* C111, C121, C211, C221, C311, C321, C411 and C421 (See also Fig. 1).

The molecular packing is indicated in Fig. 4. There are no especially short intermolecular contacts, the closest van der Waals contacts are phenyl–phenyl with C–C distances from 3.63 Å and up (only seven below 3.8 Å).

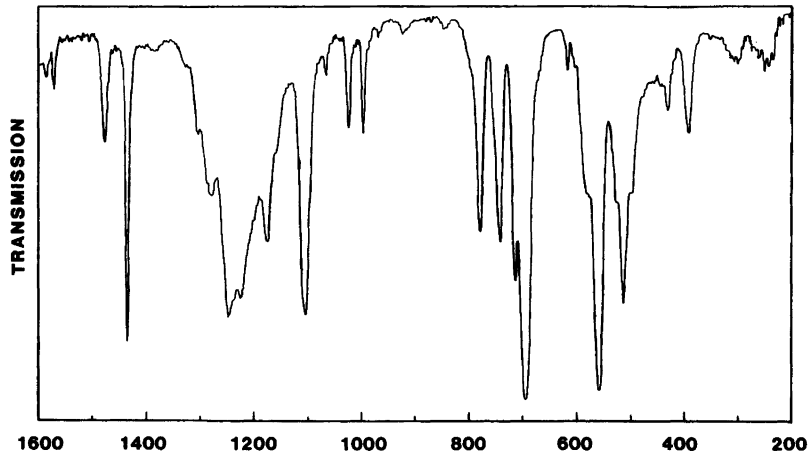

Fig. 5. IR spectrum of the compound. Frequency units are cm^{-1}.

The IR spectrum. The spectrum in the 1600 – 200 cm^{-1} region (Fig. 5) is similar to the spectra of corresponding divalent Fe,Co and Cu compounds.[13] Tentative assignments have been made by comparison with these and spectra of similar compounds[14-16] (frequencies in cm^{-1}): ν_{as}(PNP), 1175 ms; ν(PC), 713 ms and 696 vs; ν_s(PS), 580 ms(sh); ν_{as}(PS), 559 vs; δ(PNP), 527 w(sh); δ(NPS), 430 w-ms. Abbreviations are ms, medium strong; vs, very strong; w, weak and sh, shoulder. The above assignments agree with the partial double bonding found in the P–S and P–N bonds. The usual phenyl group bands, common for tetraphenylimidiphosphinates, were found with expected frequencies and relative band intensities.[16] (Absorption maxima near 1478 w, 1435 s, 1305 w, 1290 w, 1180 w, 1160 w, 1108 s, 1070 w, 1028 m, 998 m, 970 w, 845 w and 618 cm^{-1}w).

Some of the low lying absorption bands between 200 and 400 cm^{-1} may be due to the TeS_4 group. Absorptions observed here are 391 m, 305 w-ms, 245 w-ms.

REFERENCES

1. Brøndmo, N. J., Esperås, S. and Husebye, S. *Acta Chem. Scand. A 29* (1975) 93; Graver, H. and Husebye, S. *Acta Chem. Scand. A 29* (1975) 14.
2. Siiman, O. and Gray, H. B. *Inorg. Chem. 13* (1974) 1185.
3. Churchill, M. R., Cooke, J., Fennessey, J. P. and Wormald, J. *Inorg. Chem. 10* (1971) 1031.
4. Churchill, M. R. and Wormald, *J. Inorg. Chem. 10* (1971) 1778.
5. Bereman, R. D., Wang, F. T., Najdzionek, J. and Braitsch, D. M. *J. Am. Chem. Soc. 98* (1976) 7266.
6. Schmidpeter, A. and Groeger, H. *Z. Anorg. Allg. Chem. 345* (1966) 106.
7. Aaberg, A., Gramstad, T. and Husebye, S. *Acta Chem. Scand. A 34* (1980) 717 and references therein.
8. Davison, A. and Switkes, E. *Inorg. Chem. 10* (1971) 837.
9. Ault, H. K. and Husebye, S. *Acta Chem. Scand. A 32* (1978) 157.
10. Schmidpeter, A., Böhm, R. and Groeger, H. *Angew. Chem. 76* (1964) 860.
11. Williams, D. J. *Inorg. Nucl. Chem. Lett. 16* (1980) 189.
12. Ivamoto, T., Ebina, F., Nakazawa, H. and Nakatsuka, C. *Bull. Chem. Soc. Jpn. 52* (1979) 1857.
13. Czernuszewicz, R., Maslowsky, E., Jr. and Nakamoto, K. *Inorg. Chim. Acta 40* (1980) 199.
14. Ojima, I., Iwamoto, T., Onishi, T., Inamoto, N. and Tamaru, K. *Chem. Commun. (1969)* 1501.
15. Ziegler, A., Botha, U. P. and Haiduc, I. *Inorg. Chim. Acta 15* (1975) 123.
16. Siiman, O. and Vetuskey, J. *Inorg. Chem. 19* (1980) 1672.
17. Husebye, S. *Acta Chem. Scand. 20* (1966) 24.

Received June 16, 1981.

Acta Chemica Scandinavica A 36 (1982) 203–206

Structural Investigations on the Monoclinic Sigma Phase in the Cr—Fe—Ni—Mo System

INGER HJERTÉN,[a] BENGT-OLOV MARINDER,[a] ANDERS SALWÉN[b] and PER-ERIK WERNER[a]

[a] Departments of Structural and Inorganic Chemistry, Arrhenius Laboratory, University of Stockholm, S-106 91 Stockholm, Sweden and [b] Steel Research Center of Sandvik, S-811 00 Sandviken, Sweden

The crystal structure of a σ-phase with the approximate composition $Cr_{11}Fe_{13}Ni_3Mo_3$ has been determined and refined from single-crystal data to an *R*-value of 0.073 in space group *P*2 (No. 3). A monoclinic deviation from the generally assumed tetragonal symmetry *P*4/*mnm* for σ-phases was inferred from small splits in some of the powder diffraction lines. The monoclinic angle refined by least-squares profile analysis of Guinier-Hägg diffraction data is 90.15(1)°. The Mo atoms can be described as distributed within *one* of the two subsidiary layers situated between the pseudohexagonal main layers, causing a shift of the subsidiary layers of approximately 0.1 Å from a level halfway between the main layers.

The σ-phase with the approximate composition $Cr_{12}Fe_{13}Ni_3Mo_2$ has also been studied by single crystal diffraction. The result obtained confirms the general distribution scheme for the Mo atoms and the monoclinic space group as found for $Cr_{11}Fe_{13}Ni_3Mo_3$. No significant deviation from 90° is found for the monoclinic angle, however.

The effect of Mo on the lattice parameters and on the chemical composition of σ-phase and $M_{23}C_6$ carbide in austenitic 25Cr-20Ni steel has been investigated by Andersson and Lundberg.[1] In connection with these studies we decided to investigate the distribution of the Mo atoms in the σ-phases by X-ray diffraction techniques. We therefore made single crystal and powder diffraction studies on two samples with chemical compositions close to $Cr_{12}Fe_{13}Ni_3Mo_2$ and $Cr_{11}Fe_{13}Ni_3Mo_3$, named F and G by Andersson and Lundberg.[1]

EXPERIMENTAL

The concentrations of Cr, Fe, Ni and Mo in the F- and G-samples were determined on polished sections by electron-probe microanalysis using the procedure described by Andersson and Lundberg.[1] The analytical results, which should have relative errors less than 4 percent, are given in Table 1.

X-Ray powder diffraction patterns were obtained by a Guinier-Hägg focusing camera with $CrK\alpha_1$ radiation ($\lambda = 2.28970$ Å). Potassium chloride ($a = 6.2929$ Å)[2] was used as an internal theta-standard. The photographs were measured with a film scanner described by Johansson, Palm and Werner.[3] Small splits in some of the diffraction lines caused by a monoclinic deviation from tetragonal symmetry were observed for compound G (see Fig. 1).

Single crystals of the F- and G-samples were prepared by annealing in evacuated silica tubes for

Table 1. Chemical composition of σ-phase obtained by electron-probe microanalysis.

Sample	Cr	Fe	Ni	Mo	$Cr_xFe_yNi_zMo_t$
F Wt %	34.6	42.9	10.4	11.4	$Cr_{12}Fe_{13}Ni_3Mo_2$
At %	38.5	44.4	10.2	6.9	
G Wt %	32.7	41.3	10.9	15.5	$Cr_{11}Fe_{13}Ni_3Mo_3$
At %	36.7	43.1	10.8	9.4	

0302-4377/82/030203-04$02.50

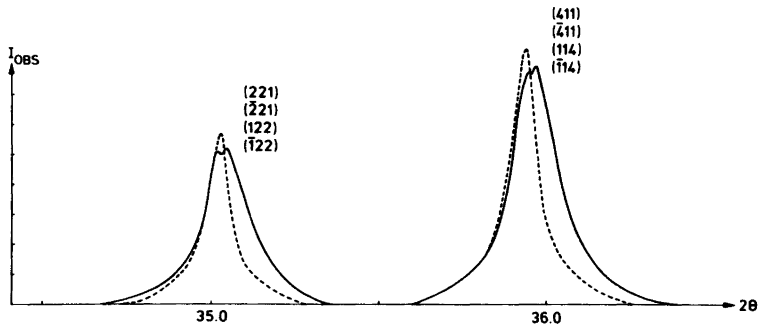

Fig. 1. Observed intensity curves, 34.5 – 36.5° in 2θ, for compound G (solid line) and compound F (dashed line). Small monoclinic splits are observed for G.

ten and six weeks, respectively, at 750 °C followed by quenching in water. X-Ray diffraction data were collected with a Philips diffractometer, PW 1100, using Mo$K\alpha$ radiation. Intensity data were recorded using the $\theta/2\theta$ scanning mode with a scan speed (2θ) of 0.9 – 1.8° min^{-1}. The upper limit of $(\sin\theta)/\lambda$ was 0.704 $Å^{-1}$ for the F- and 1.078 $Å^{-1}$ for the G-compound. Background counts were taken for 0.5 times the scan time at each end of the scan range, the latter being 1.8° and 1.4° for F and G, respectively. Reflexions with intensity greater than $2\sigma(I)$ were regarded as observed and used in the refinements. The number of observed independent reflexions was 846 for F and 1851 for G. The usual corrections were made for Lorentz and polarization effects as well as for absorption.

REFINEMENTS

The unit cell dimensions (*cf.* Table 2) used in the least-squares refinements of the single-crystal data were obtained from profile refinements of the powder diffraction data using the program described by Werner *et al.*[4] No significant deviations in cell parameters were found from profile refinements using preliminary or final positional coordinates obtained from single-crystal data. A monoclinic angle of 90.15(1)° was found for compound G.

The preliminary assumption was that the atoms Cr, Fe, Ni and Mo are distributed at random over the atomic sites of the structure. The scattering factor curve for Mn[5,6] was used for all metal atoms, and the distribution of the Mo atoms was determined from refinements of the formal occupancy factors. The Mn scattering factor was chosen as a weighted average of Cr, Fe and Ni, whose scattering powers are quite similar. Preliminary refinements showed that the occupancy factors for the four twofold positions derived from position III (*cf.* Table 3) were almost equal. In order to facilitate a comparison between the F- and G-compounds

Table 2. Crystal data.

Compound	F	G
Approximate composition	$Cr_{12}Fe_{13}Ni_3Mo_2$	$Cr_{11}Fe_{13}Ni_3Mo_3$
F.W.	1722.4[a]	1755.6[a]
a(Å)	8.8544(20)	8.8915(8)
b(Å)	4.5920(2)	4.6088(2)
c(Å)	8.8447(19)	8.8618(8)
β(°)	90.03(8)	90.15(1)
V(Å^3)	359.62(5)	363.15(5)
μ(Mo$K\alpha$)(cm^{-1})	272	273
D_x(g cm^{-3})	7.952	8.027
Space group	$P2$ (No. 3)	$P2$ (No. 3)

[a] Calculated from the compositions given in Table 1.

these "occupancy factors" were normalized to 1.0 in both refinements. The start parameters for the single crystal refinements were derived from the data published by Bergman and Shoemaker[7] for tetragonal σ-FeCr. The splitting of point positions from *P4/mnm* to *P2* is illustrated in Table 3, where the refined parameters for compound G are also listed. For compound F, only the refined occupation factors are reported in the table. The conventional *R*-values obtained for isotropic refinements were 0.120 and 0.073 for F and G, respectively.

DISCUSSION

As stated above, a monoclinic deviation from the generally assumed tetragonal symmetry for σ-phase is obviously present in G (*cf.* Fig. 1). This fact, however, could hardly have been detected from single crystal data alone as the small deviation of 0.15° from 90° in the β angle made it impossible to refine the unit cell parameters from single crystal data. Refinement of unit cell parameters by profile analysis of powder diffraction data was also facilitated by the longer wavelength used in the powder data collection.

The σ-phase structure can be described as built up of pseudo-hexagonal main layers perpendicular to the monoclinic *b* axis. Between them are subsidiary layers, whose atoms are located above and beneath holes in the main layers (Fig. 2). The atoms in the subsidiary layers have close interlayer contact with each other, leading to improved overall packing and to rather short distances along vertical rows in the structure.[7,8] This feature is also observed in the present study. Thus, in compound G, the shortest Me–Me distances 2.277(11), 2.297(11), 2.315(11) and 2.333(11) Å are the four vertical distances between the subsidiary layers. The corresponding atomic parameters are those originating from point position 8(j) in *P4/mnm* (*cf.* Table 3). As a comparison, the shortest distance between two atoms within a main layer, (1/2, 1/2, 1/2) to (0.5659, 0.5179, 0.7609) (see Table 3), is found to be 2.385(2) Å. The average Me–Me contact distance in G is 2.637 Å.

The most pronounced effect of the monoclinic deviation from tetragonal symmetry is that the two subsidiary layers are displaced about 0.1 Å along [010] in the same direction, thus keeping the interlayer distance constant.

It has been stated by Kasper and Waterstrat[9]

Table 3. Final atomic parameters (e.s.d.'s in parentheses).

Splitting of point positions			Compound G					Compound F
Position	*P4/m n m*	*P2*	*x*	*y*	*z*	*B*/Å²	"Occup. factors"	"Occup. factors"
I	2(a)	1(a)	0	0	0	0.29(3)	1.05(2)	1.07(2)
		1(d)	0.5	0.5	0.5	0.29(3)	1.05(2)	1.07(2)
II	4(f)	2(e)	0.3987(2)	0.0052(19)	0.3985(2)	0.37(3)	0.97(1)	0.96(2)
		2(e)	0.8987(2)	0.5059(19)	0.1015(2)	0.37(3)	0.97(1)	0.98(2)
III	8(i)	2(e)	0.4638(2)	0.0093(21)	0.1314(2)	0.38(2)	1.0[a]	1.0[a]
		2(e)	0.9636(2)	0.5039(18)	0.3684(2)	0.38(2)	1.0[a]	1.0[a]
		2(e)	0.1312(2)	0.0192(16)	0.4630(2)	0.38(2)	1.0[a]	1.0[a]
		2(e)	0.6314(2)	0.5132(21)	0.0366(2)	0.38(2)	1.0[a]	1.0[a]
IV	8(i)	2(e)	0.7390(2)	0.0053(19)	0.0664(2)	0.38(2)	1.06(1)	1.06(2)
		2(e)	0.2392(2)	0.5168(17)	0.4340(2)	0.38(2)	1.06(1)	1.07(2)
		2(e)	0.0656(2)	0.0158(19)	0.7389(2)	0.38(2)	1.06(1)	1.07(2)
		2(e)	0.5659(2)	0.5179(17)	0.7609(2)	0.38(2)	1.05(1)	1.08(2)
V	8(j)	2(e)	0.1833(5)	0.2709(18)	0.1797(6)	0.32(2)	0.86(3)	0.96(3)
		2(e)[b]	0.6789(4)	0.7665(16)	0.3166(4)	0.32(2)	1.15(3)	1.13(3)
		2(e)[b]	0.1821(4)	0.7648(15)	0.1853(5)	0.32(2)	1.09(3)	1.09(3)
		2(e)	0.6880(5)	0.2646(19)	0.3182(6)	0.32(2)	0.82(3)	0.90(3)

[a] Fixed parameter. [b] Preferably occupied by Mo atoms.

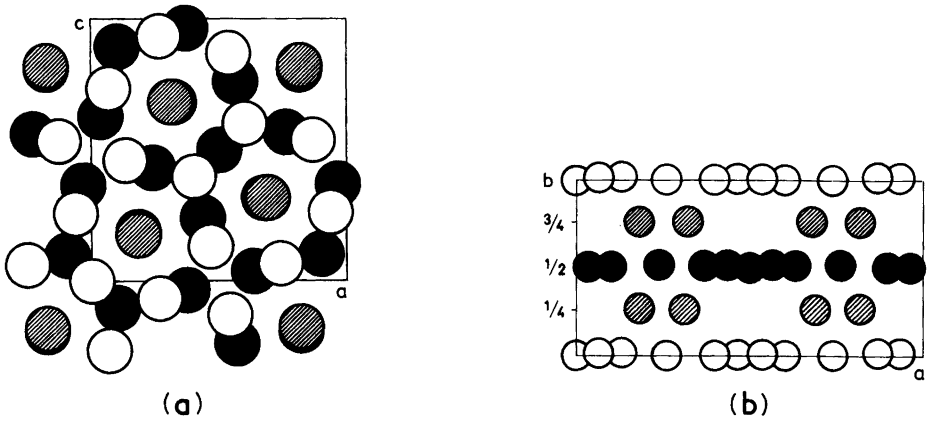

Fig. 2. The structure of the monoclinic σ-phase. (a) Projection along [010]. (b) Projection along [001]. Unfilled circles represent atoms in the main layers at $y=0$; filled circles, atoms in the main layers at $y=1/2$; and shaded circles, atoms in the subsidiary layers at $y\approx 1/4$ and $y\approx 3/4$ [almost coincident in (a)].

that the metals to the left of manganese in the periodic table (Cr, Mo) occupy the position of type II (see Table 3) and those to the right (Fe, Ni) occupy positions of type I and IV. The remaining positions, III and V, are termed mixed positions and they contain varying proportions of the component atoms. These statements were made for binary, tetragonal, σ-phases and may not be strictly valid for the present type of quaternary phases. No definite conclusions about the distribution of Cr, Fe and Ni can be drawn from the present study because of the small differences in scattering power these atoms exhibit. From the occupancy parameters reported in Table 3, however, it can be inferred that the Mo atoms are situated in the subsidiary layer at $y=0.76$. As can be seen from the table, the same type of Mo concentration is found from the occupancy parameters of the less molybdenum-rich F-compound. Thus, the Mo atoms are located in a "mixed" position of type V. The distribution of the relatively large Mo atoms in *one* of the subsidiary layers excludes short Mo – Mo contact in the [010] direction.

Acknowledgements. The interest and encouragement of Professors P. Kierkegaard and A. Magnéli are highly appreciated. The skilful technical assistance of Mr. L. Göthe is gratefully acknowledged.

This work has received financial support from the Swedish Natural Science Research Council.

REFERENCES

1. Andersson, T. and Lundberg, B. *Metall. Trans. A 8* (1977) 787.
2. Hambling, P. G. *Acta Crystallogr. 6* (1953) 98.
3. Johansson, K. E., Palm, T. and Werner, P.-E. *J. Phys. E 13* (1980) 1289.
4. Werner, P.-E., Salomé, S., Malmros, G. and Thomas, J. O. *J. Appl. Crystallogr. 12* (1979) 107.
5. Doyle, P. A. and Turner, P. S. *Acta Crystallogr. A 24* (1968) 390.
6. Cromer, D. T. and Liberman, D. *J. Chem. Phys. 53* (1970) 1891.
7. Bergman, G. and Shoemaker, D. P. *Acta Crystallogr. 7* (1954) 857.
8. Tucker, C. W. and Senio, P. *Acta Crystallogr. 6* (1953) 753.
9. Kasper, J. S. and Waterstrat, R. M. *Acta Crystallogr. 9* (1956) 289.

Received July 1, 1981.

Acta Chemica Scandinavica A 36 (1982) 207–217

Crystal Growth of Some Intermediate Titanium Oxide Phases γ-Ti_3O_5, β-Ti_3O_5, Ti_4O_7 and Ti_2O_3 by Chemical Transport Reactions

SAM-HYO HONG

Department of Inorganic Chemistry, Arrhenius Laboratory, University of Stockholm, S-106 91 Stockholm, Sweden

Chemical transport reactions of γ-Ti_3O_5, β-Ti_3O_5, Ti_4O_7 and Ti_2O_3 were performed in closed silica ampoules by using $TeCl_4$ as a transport medium. Especially, single crystals of γ-Ti_3O_5 were obtained for the first time. The previously unexplained sources of extra oxygen and oxidation introduced into the titanium oxides during transport reactions were discovered in an analysis of 53 experiments. A method is presented which predicts the oxidation state of a transported titanium oxide using empirical equations which take account of the amounts of $TeCl_4$, H_2O liberated from the wall of the silica ampoule, and the starting material with varied chemical compositions.

The temperature range of coexistence of the γ-Ti_3O_5 and β-Ti_3O_5 crystals was analysed. The twin crystal orientations of the β-Ti_3O_5 phase and an X-ray powder diffraction pattern yielding the refined unit cell parameters of γ-Ti_3O_5 are presented.

The polymorphism and phase transitions of Ti_3O_5 have been extensively studied by several researchers at this institute. In a phase analysis of the titanium-oxygen system it was found that the room temperature modification of a Ti_3O_5 sample prepared at 1150 °C has a monoclinic structure.[1] The crystal structure[2] which was later called β-Ti_3O_5 is quite different from the orthorhombic pseudobrookite-type of structure (anosovite) assigned to Ti_3O_5 some years earlier by Zhdanov and Rusakov.[3] The pseudobrookite structure was found to exist as a high-temperature modification in the binary titanium-oxygen system (α-Ti_3O_5). The rapid reversible α-$Ti_3O_5 \rightleftarrows \beta$-$Ti_3O_5$ reaction appearing at 150–160 °C in the strictly binary system could be depressed below room temperature in the presence of impurities, *e.g.* iron in the case of anosovite.

The existence of a new monoclinic modification of Ti_3O_5 (called γ-Ti_3O_5 for the room temperature phase which magnetically transformed to δ-Ti_3O_5 at *ca.* −23 °C) was reported by Åsbrink *et al.*[4] However, to date, single crystal growth of γ-Ti_3O_5 was unsuccessful; therefore the crystal structure, many physical properties and thermodynamical data still remain unknown.

In the course of the preparative work it was also possible to prepare crystals of β-Ti_3O_5, Ti_2O_3 and of Ti_4O_7, of which the latter is the first member of the homologous series[1] ($4 \leq n \leq 10$) Ti_nO_{2n-1}.

EXPERIMENTAL

Preparation of starting materials. As starting materials Ti_2O_3 and β-Ti_3O_5 powders were used, and these two compounds were carefully prepared in an argon atmosphere by arc-melting mixture of titanium powder (99.9 %, Ventron, USA) and titanium dioxide (99.97 %, J. T. Baker Chemical Co., USA). The titanium powder and the titanium dioxide were dried before use at 120 °C for *ca.* a week. The stoichiometrically mixed powders for making Ti_2O_3 and β-Ti_3O_5 were compacted at *ca.* 10 kbar to form pellets of 1.2 g each.

After arc-melting each pellet was finely ground in an agate mortar, and the composition was checked by means of X-ray ($CuK\alpha_1$) Guinier-Hägg powder photographs taken with a very long exposure time in order to reveal undesired phases. As starting material for further work only the

0302-4377/82/030207-11$02.50

thoroughly pure samples of Ti_2O_3 (*ca.* 25 g) and β-Ti_3O_5 (*ca.* 10 g), respectively, were retained.

Silica ampoule. Schäfer *et al.*[5] reported that H_2O from the wall of the silica ampoule had a decisive influence on the chemical transport rate of molybdenum and tungsten and of their dioxides and sulfides by means of iodine. According to their experience the water content in the transparent silica ampoule varied between 0.01 wt % for extremely water free silica and 0.10 wt % for ordinary grade silica.

Throughout the experiments ordinary grade transparent silica tubes (99.9 %, Thermal Syndicate Ltd., England) were used, of which the water content was estimated to be *ca.* 0.10 wt % after cleaning in liquid soap and distilled water and drying at *ca.* 120 °C for several days. Ordinary grade silica glass was used as its water solubility and diffusion rate[6] at high temperatures is known. At the same time it seemed to be very difficult to exclude traces of water even from the most water-free silica tube by heating at 900–1000 °C for a couple of days in vacuum.

Furnace. Fig. 1 shows a temperature profile of a horizontal furnace with length $l = 500$ mm (inner diameter ID = 29 mm, outer diameter OD = 250 mm). An effort was made to obtain a very smooth temperature profile and a small temperature gradient in order to make possible the use of long silica ampoules (up to 200 mm) with $\Delta T (= T_2 - T_1) \approx 20$ °C. A Kanthal A-1 helix was carefully wound closer near both ends rather than in the central part of the furnace to yield the small temperature gradient. Sometimes three ampoules as shown in Fig. 1 were inserted for transport reactions simultaneously. The transverse temperature difference was $\lesssim 2$ °C in the furnace.

A chromel-alumel thermocoax (stainless steel or high-melting steel sheath, OD = 1.5 mm, SODERN, France) was used with a proportional temperature regulator (Witronic II, Philips, Holland), which gave a temperature stability of *ca.* ±1 °C. At an early stage of the experiments a furnace with two Pt-Pt(Rh) thermocouples at separate temperature control points was used. It was later abandoned, however, because it did not easily yield a very smooth temperature profile.

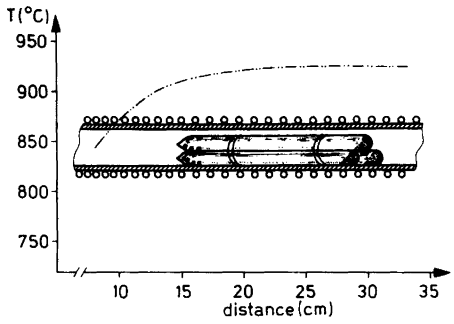

Fig. 1. Inner part of the horizontal furnace with temperature profile indicated (—···—). Sometimes three ampoules were simultaneously inserted.

RESULTS AND DISCUSSION

Parameters to control the oxidation state of the transported crystals.

(1) Amount of $TeCl_4$ and previous theories of the extra oxygen and oxidation sources. Niemysky *et al.*[7] showed that above 900 °C $TeCl_4$ is a more effective transport agent for the TiO_2 (rutile) preparation than other halides and halogens. After that work some other oxides[8-13] were also transported by using $TeCl_4$. Crystals of some intermediate vanadium oxides[14-19] between V_2O_3 and V_2O_5 were also grown by using $TeCl_4$. Analogously, Mercier and Lakkis[20] obtained the titanium oxides: β-Ti_3O_5, Ti_4O_7 and Ti_5O_9 (Mercier *et al.* only reported the composition Ti_3O_5 and the phase must be β-Ti_3O_5 according to the crystal shape and the temperatures used (*ca.* 1100 °C) for the chemical transport reaction).

Comparing the above two cases, of vanadium oxides and titanium oxides, there was an essential difference with regard to the compositions of the starting materials and the transported crystals. For the vanadium oxides one observed no composition changes between the starting material and the transported crystals. Even when composition changes were observed in some cases, they were usually small or within the range of homogeneity. However, for the titanium oxide transport reactions one always needed a starting material with a lower oxidation state than that of the grown crystals. In order to grow *e.g.* β-Ti_3O_5 one needed Ti_2O_3 as starting material; similarly, Ti_3O_5 and Ti_4O_7 were required for the growth of Ti_4O_7 and Ti_5O_9, respectively. This phenomenon was explained by a quasiequilibrium[20] in the reaction ampoule; it means that the oxygen partial pressures in the hotter zone (at T_2, *e.g.* Ti_3O_5 as a starting material with the lower oxidation state) and in the colder zone (at T_1, *e.g.* transported crystals of Ti_4O_7 with the higher oxidation state) are the same and are equal to the corresponding equilibrium pressures above the two solid oxides, at their respective temperatures.

According to the above explanation the used temperatures T_1 and T_2 are the most significant parameters, together with the oxidation state of the starting material, determining the oxygen partial pressures in the two zones, and therefore they determine the oxidation state of the transported crystals.

No satisfactory explanation has been published which accounts for the extra oxygen and oxidation sources in the chemical transport reactions of the titanium oxides, even though the chemical transport direction and main gas species ($TiCl_4$, $TeOCl_2$, $TeCl_4$, $TeCl_2$ and Cl_2) involved in the system TiO_2:$TeCl_4$ were established by matrix isolation infrared spectroscopy.[21]

Recently, Since *et al.*[22] offered a new hypothesis, stating that the extra oxygen source was probably water from the wall of the silica ampoule and the hygroscopic transport agent $TeCl_4$.

The experimental results from 53 careful runs (*cf.* Table 3), initially intended for the γ-Ti_3O_5 and β-Ti_3O_5 preparation by chemical transport reactions, showed that water could not be the sole oxidizing agent, and that a completely new explanation was required (*cf.* runs Nos. 29 in Table 1; 34, 36 and 52 in Table 2). Tables 1 and 2 show some typical experimental parameters: special attention was paid to water possibly adsorbed on the starting material and on the inside surface of the silica ampoule or to water in $TeCl_4$. The tellurium tetrachloride was stored, weighed and charged into the silica ampoule in a dry box. After charging, the hygroscopic $TeCl_4$ was carefully dried by gentle heating in vacuum ($10^{-6}-5\times10^{-5}$ Torr, $\geq$15 hours) just until sublimation of $TeCl_4$ occured. The transport reaction of each pair of runs: Nos. 28 and 29, 40 and 41 in Table 1 were performed simultaneously as shown in Fig. 1 in order to ensure identical temperature conditions.

When the concentration of $TeCl_4$ (99.99 %, Mitsuwa Chemicals, Japan) was 4.0 mg/ml or less, dark violet Ti_2O_3 crystals were transported to the colder zone, while run No. 28 yielded well-developed single phase crystals of γ-Ti_3O_5 with 7.2 mg/ml. For the two runs Nos. 28 and 29 possible H_2O amounts liberated from the wall of the silica ampoules should be exactly equal, because each pair of the ampoules used in runs Nos. 28 and 29, 40 and 41 was prepared from the same length of silica tube.

Analogously, a comparison between runs Nos. 40 and 41 and the results of further experiments with different silica ampoule volumes, but with the same concentration (mg/ml) of $TeCl_4$ showed that the oxidation state of the transported crystals was dependent on the input amount of $TeCl_4$, even though the higher concentration of $TeCl_4$ gives the larger amount of $TeCl_4$ with a similar ampoule volume (discussed later). The oxidation state of the transported titanium oxide crystals will increase with increasing amount of $TeCl_4$. This oxidizing effect of the transport agent $TeCl_4$ was also observed on the chemical transport of NbO_2 and $NbO_{2.417}$.[23]

(2) Amounts of H_2O and of starting materials. Table 2 shows the influence of the silica ampoule

Table 1. Influence of the amount of $TeCl_4$ on the oxidation state of the transported crystals. Each pair of runs Nos. 28 and 29, 40 and 41 was simultaneously performed, as shown in Fig. 1. The abbreviations *l*, ID and wt stand for length, inner diameter and weight, respectively. $T_2 \rightarrow T_1$ indicates the direction of the chemical transport.

Run No.	Starting material (g)		Ampoule			$TeCl_4$ (mg/ml)	Temp. (°C)		Transported crystals	Residue	Transport time (day)
			l (mm)	ID (mm)	wt (g)		$T_2\rightarrow$	T_1			
29	Ti_2O_3	0.30								Ti_2O_3	
	β-Ti_3O_5	0.10	130	10.0	12.7	4.0	900	880	Ti_2O_3	γ-Ti_3O_5	16
										β-Ti_3O_5	
28	Ti_2O_3	0.30								γ-Ti_3O_5	
	β-Ti_3O_5	0.10	130	10.0	12.7	7.2	900	880	γ-Ti_3O_5	β-Ti_3O_5	16
40	Ti_2O_3	0.30								γ-Ti_3O_5	
	β-Ti_3O_5	0.10	145	10.0	13.5	7.8	960	910	γ-Ti_3O_5	β-Ti_3O_5	24
41	Ti_2O_3	0.30							γ-Ti_3O_5	β-Ti_3O_5	
	β-Ti_3O_5	0.10	145	10.0	13.5	10.1	960	910	Ti_4O_7	Ti_4O_7	24

Table 2. Influence of the silica ampoule wt (H_2O content ≈ 0.001 wt) and the amount of starting material with a certain composition on the oxidation state of the transported crystals.

Run No.	Starting material (g)		Ampoule			$TeCl_4$ (mg/ml)	Temp. (°C)		Transported crystals	Residue	Transport time (day)
			l (mm)	ID (mm)	wt (g)		$T_2\rightarrow$	T_1			
36	Ti_2O_3	0.30							Ti_2O_3	Ti_2O_3	
	β-Ti_3O_5	0.10	95	10.3	7.5	7.0	940	910	β-Ti_3O_5	γ-Ti_3O_5	20
34	Ti_2O_3	0.60								Ti_2O_3	
	β-Ti_3O_5	0.20	120	10.2	9.3	6.0	935	910	Ti_2O_3	γ-Ti_3O_5	28
										β-Ti_3O_5	
35	Ti_2O_3	0.30								γ-Ti_3O_5	
	β-Ti_3O_5	0.10	130	10.2	10.1	8.0	930	908	γ-Ti_3O_5	β-Ti_3O_5	24
52	Ti_2O_3	0.50	140	10.0	10.7	6.6	1005	920	Ti_2O_3	Ti_2O_3 β-Ti_3O_5	9
32	Ti_2O_3	0.30								γ-Ti_3O_5	
	β-Ti_3O_5	0.10	140	10.3	11.0	6.0	955	925	γ-Ti_3O_5	β-Ti_3O_5	8
49	Ti_2O_3	0.40	165	10.0	12.6	7.6	985	900	γ-Ti_3O_5	γ-Ti_3O_5 β-Ti_3O_5	21
19	Ti_2O_3	0.30								γ-Ti_3O_5	
	β-Ti_3O_5	0.20	150	9.5	14.0	8.5	900	800	Ti_4O_7	β-Ti_3O_5 Ti_4O_7	7

dimensions on the oxidation state of the transported crystals. The length of the silica ampoules was varied; accordingly the weight (wt) of the silica ampoules was also varied, while the concentration of $TeCl_4$ was kept between 6.0–8.5 mg/ml. Under these conditions 18 successful runs of single phase γ-Ti_3O_5 growth were performed (*cf.* Table 3).

Comparing run No. 28 in Table 1 with run No. 36 in Table 2, the concentrations of $TeCl_4$ were almost equal to 7 mg/ml in both cases (which should give almost the same total pressure with similar temperatures), run No. 28 yielded high-quality γ-Ti_3O_5 crystals, whereas single phase Ti_2O_3 was obtained in run No. 36. One of the significant differences between the experimental parameters of the two runs was the length of the silica ampoules, which was generally expected to influence only the transport rate.[24] The total amounts of $TeCl_4$ for the two runs of Nos. 28 and 36 were 73 mg and 55 mg, respectively. This difference should also be significant, as discussed previously; and the decisive significance of the relation between the amounts of H_2O and $TeCl_4$ will be quantitatively discussed later.

Table 3. Specification of the 53 transport runs.

Transported crystals	Total No. of runs
γ-Ti_3O_5	18
β-Ti_3O_5	3
Ti_4O_7	11
Ti_2O_3	12
γ-Ti_3O_5 + Ti_4O_7	4
γ-Ti_3O_5 + Ti_2O_3	1
β-Ti_3O_5 + Ti_2O_3	4

Runs Nos. 32 and 34 in Table 2 were performed at similar temperatures and with the same concentration of $TeCl_4$, 6.0 mg/ml. Run No. 32 yielded single phase γ-Ti_3O_5, while No. 34 transported single phase Ti_2O_3 from twice the amount of starting material with the same composition.

The previous results and a further comparison between run No. 52 and run No. 49 clearly suggested that the oxidation state of the transported crystals was essentially dependent on the silica ampoule dimensions, the total amount of starting materials with a certain chemical composition and the input amount of $TeCl_4$, but not primarily dependent on the total pressure in the ampoule.

The oxidation state of the transported crystals was raised by increasing the input amount of $TeCl_4$ and the ampoule weight; the oxidation state was lowered by increasing the total amount of starting material.

In all 53 runs the ampoules, which had been quenched in water, emitted strongly concentrated white fumes of HCl upon breaking after the transport reaction. Addition of a water volume equal to that of the ampoule yielded a HCl solution with pH $\approx$ 1. However, in the chemical transport reactions of V_3O_5 (starting material = V_3O_5, T_1 = 950 °C and T_2 = 1050 °C) performed under the same experimental conditions, neither these white fumes of HCl nor Te metal (discussed below) was observed. The hydrogen source of HCl must be H_2O from the wall of the silica ampoule, because the starting materials and $TeCl_4$ were carefully dried before use, and especially the starting materials had no contact with hydrogen gas during the preparation. Exactly the same phenomenon was observed by Mercier *et al.*[20] in the chemical transport reactions of titanium oxides by using $TeCl_4$; however, they assumed the source of hydrogen to be their starting materials, which were obtained by reduction of TiO_2 by hydrogen gas.

A large amount of silvery white tellurium metal (b.p. = 989.8 ± 3.8 °C) was always observed in the silica ampoule after quenching in water. Concerning the observed liquid and solid components in the quenched ampoule, tellurium metal in the shapes of thin plates, spheres and crystals appeared in significant amounts besides the titanium oxides (including the starting materials and transported crystals). The major portion of the Te metal was found in the colder zone, which was raised 1 – 2 mm above the hotter zone in order to preclude contact between liquid Te and the growing titanium oxide crystals. When *ca.* 8 mg γ-Ti_3O_5 was transported with T_1 = 910 °C and T_2 = 955 °C, *ca.* 17 mg Te metal (*ca.* 41 % of the total input as $TeCl_4$) was observed in the colder zone. The transported Te metal was usually 40 – 50 % of the input amount. The material was not TeO_2 (m.p. = 733 °C, b.p. = 1245 °C), as earlier assumed in analogy with the rutile transport.[7]

One may now summarize the experimental results in the stoichiometric equation (1) for the γ-Ti_3O_5 and β-Ti_3O_5 transports using $TeCl_4$ as transport medium and a charge of Ti_2O_3 or a mixture of Ti_2O_3 and β-Ti_3O_5 powders as starting material.

$$3Ti_2O_3(s) + H_2O(g) + \tfrac{1}{2}TeCl_4(g) \rightleftarrows 2Ti_3O_5(s) + 2HCl(g) + \tfrac{1}{2}Te(l \text{ and } g) \quad (1)$$

Eqn. (1) is not intended to explain the whole transport system. It excludes many equilibrium reactions of carrier gases ($TiCl_4$, $TiCl_3$, $TeOCl_2$ and *etc.*)[21] and of thermal dissociation,[25] *e.g.*, $TeCl_4(g) \rightleftarrows TeCl_2(g) + Cl_2(g)$. However, the eqn. (1) is clearly able to explain the extra oxygen and oxidation sources and to quantitatively clarify the relationship between input and output in the closed transport system of a silica ampoule. Furthermore it is capable of predicting the oxidation state of the transported crystals (discussed later in detail); this capability is most important in order to obtain a desired phase in a strictly controlled way.

When one considers eqn. (1) as a *redox* reaction, one may formulate a *net redox* reaction, eqn. (2).

$$2Ti^{3+} + \tfrac{1}{2}Te^{4+} \rightleftarrows 2Ti^{4+} + \tfrac{1}{2}Te \quad (2)$$

Hereby one can clearly see Te^{4+} ($TeCl_4$) as an oxidizer, and one may understand the decisive importance of the total input amount of $TeCl_4$ for the oxidation state of the transported crystals, as discussed previously (*cf.* Table 1). However, it seems hardly believable that $TeCl_4$ should actively function as oxidizer without the coexistence of H_2O liberated from the wall of the silica ampoule as an extra oxygen source.

Coexistence of γ-Ti_3O_5 and α-Ti_3O_5 (β-Ti_3O_5). Single crystals of γ-Ti_3O_5 were obtained in a single phase transport to the colder zone whose temperature was varied within T_1 = 800 – 930 °C with ΔT = 15 – 100 °C. When one inspected the residue in the hotter zone (at T_2) after successful transport reactions, γ-Ti_3O_5 and α-Ti_3O_5 crystals were always found to have developed together in the temperature range 900 °C $\lesssim T_2 \leq$ 990 °C. The γ-Ti_3O_5 and β-Ti_3O_5 crystals could be easily distinguished since they have completely different shapes, as shown in Fig. 2. However, in the residue

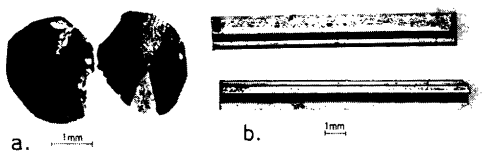

Fig. 2. Photograph of two modifications of the Ti_3O_5 crystals. a, γ-Ti_3O_5, black; b, β-Ti_3O_5, black.

the crystal quality of γ-Ti_3O_5 is always much higher than that of β-Ti_3O_5.

In run No. 49 in Table 2, with $T_2 = 985$ °C, the residue consisted mostly of β-Ti_3O_5 crystals; only 2–3 % was γ-Ti_3O_5 crystals, observable under the microscope, but hardly detectable by X-ray powder diffraction. The lower temperature limit of γ-Ti_3O_5 and α-Ti_3O_5 coexistence in the hotter zone seems to be slightly below 900 °C, because the β-Ti_3O_5 crystals were still observed at $T_2 = 900$ °C. No experiment was done at $T_2 < 900$ °C due to too slow water diffusion[6] into the reaction room of the ampoule. A consequence of the slow water diffusion, combined with a large transport rate ($\gtrsim 3$ mg/h), is a two-phase transport or varied oxygen content in the single phase transported crystals, as the transport system takes much longer time ($\gtrsim 2$ day) to reach a state of equilibrium. Meanwhile, a major part of the crystals would already be transported. On the other hand, at $T_2 = 990$ °C only β-Ti_3O_5 crystals were observed. One may draw a borderline at *ca.* 940 °C: at that temperature the amounts of γ-Ti_3O_5 and β-Ti_3O_5 crystals in the residue were equal.

The coexistence temperature range in the colder zone seemed to be very narrow, as no trace of β-Ti_3O_5 crystals was found below $T_1 = 930$ °C; and at that temperature well-formed crystals of γ-Ti_3O_5 appeared regularly. When the two phases γ-Ti_3O_5 and Ti_4O_7 were transported simultaneously as in run No. 41 in Table 1, the temperature range of coexistence was also narrow – no trace of γ-Ti_3O_5 was found in the hotter zone at $T_2 = 960$ °C.

Prediction of the yield. Table 3 shows the results of the 53 experimental runs, which thoroughly demonstrated the decisive influence of the amounts of $TeCl_4$ and H_2O liberated from the silica ampoules upon the oxidation state of the transported crystals. Table 4 lists quantitative comparisons between the input (in) amounts of H_2O and $TeCl_4$ and those calculated (calc) to fully oxidize the starting material to Ti_3O_5 according to the empirical equation (1). The input amount of H_2O for the transport system was taken to be 0.10 wt % of the used silica

Table 4. Different combinations of Q_1 and Q_2 for the single phase transports of Ti_2O_3, γ-Ti_3O_5, Ti_4O_7 or for the two-phase transports of γ-Ti_3O_5 and Ti_4O_7. See text for explanation of symbols Q_1, Q_2, H_2O(in), H_2O(calc), $TeCl_4$(in) and $TeCl_4$(calc).

Run No.	H_2O(in) (mg)	H_2O(calc) (mg)	Q_1	$TeCl_4$(in) (mg)	$TeCl_4$(calc) (mg)	Q_2
Ti_2O_3						
29	12.7	12.5	1.02	41	93.7	0.44
34	9.3	25.0	0.37	59	187.4	0.31
36	7.5	12.5	0.60	55	93.7	0.59
52	10.7	20.9	0.51	73	156.0	0.47
γ-Ti_3O_5						
11	9.6	10.2	0.94	66	76.2	0.87
28	12.7	12.5	1.02	73	93.7	0.78
30	13.7	12.5	1.10	77	93.7	0.82
32	11.0	12.5	0.88	70	93.7	0.75
35	10.1	12.5	0.81	85	93.7	0.91
40	13.5	12.5	1.08	89	93.7	0.95
43	11.0	14.2	0.77	92	106.2	0.87
45	10.3	15.9	0.65	90	118.7	0.76
49	12.6	16.7	0.75	99	125.0	0.79
γ-Ti_3O_5 + Ti_4O_7						
41	13.5	12.5	1.08	115	93.7	1.23
Ti_4O_7						
17	13.1	10.4(20.6)	1.26(0.64)	88	78.1(154.7)	1.13(0.57)
18	14.0	10.2(19.3)	1.37(0.73)	85	76.2(144.4)	1.12(0.59)
19	14.0	12.5(22.8)	1.12(0.61)	90	78.1(170.6)	1.15(0.53)

ampoule. Table 4 shows only runs with different combinations of the amounts of H_2O, $TeCl_4$ and starting materials of varied chemical compositions.

As starting material Ti_2O_3 or a mixture of Ti_2O_3 and β-Ti_3O_5 powders was used. As shown in Tables 1 and 2, single phase transport of the γ-Ti_3O_5 crystals only occurred when the residue was completely oxidized to Ti_3O_5.

Table 4 lists the two ratios $Q_1 = m_{H_2O(in)}/m_{H_2O(calc)}$ and $Q_2 = m_{TeCl_4(in)}/m_{TeCl_4(calc)}$, with the $m_{(calc)}$-values derived from eqn. (1). The average values $Q_1 = 0.80$ and $Q_2 = 0.80$ were calculated from 18 successful single phase transport reactions of γ-Ti_3O_5 crystals (*cf.* Table 3) with an average temperature of 926 °C. One can hereby predict the oxidation state of the transported crystals by combining these two empirical values of Q_1 and Q_2. When both Q_1 and Q_2 are within 0.80 ± 0.15, one should obtain single phase γ-Ti_3O_5 or β-Ti_3O_5, assuming optimal temperature control.

In runs Nos. 28, 30 and 40 in Table 4, yielding γ-Ti_3O_5, Q_1 was slightly larger than the upper limit 0.95. However, one could still obtain the single phase transport of γ-Ti_3O_5 as long as the other ratio was kept within the range 0.80 ± 0.15. It is quite reasonable to assume that the oxidation state of the transport system is determined by the smallest of the two values Q_1 and Q_2.

Twelve runs yielded single phase Ti_2O_3 (*cf.* Table 3) when one or both of Q_1 and Q_2 were smaller than the lower limit 0.65. The yield of single phase Ti_2O_3 from the starting material, Ti_2O_3 or a mixture of Ti_2O_3 and β-Ti_3O_5 (≤ 50 wt % of the charge), was completely unexpected judged from previous theories[20,22] about the extra oxygen and oxidation sources. However, the empirical values of Q_1 and Q_2 based on eqn. (1) quantitatively predicted the yield of Ti_2O_3 crystals when the average oxidation state of the transport system was lower than Ti_3O_5. Two phase transport of γ-Ti_3O_5 and Ti_2O_3 was especially rare. In only one of the 53 runs this happened (*cf.* Table 3), and then it was probably caused by the back transport step with a large $\Delta T > 200$ °C, a large temperature oscillation ($\gtrsim \pm 5$ °C) and an uneven temperature profile of the furnace. On the other hand, two phase transport of β-Ti_3O_5 and Ti_2O_3 was rather frequent (*cf.* Table 3). However, the β-Ti_3O_5 crystals always grew in the vicinity of the hotter zone and Ti_2O_3 in the colder zone, with $T_1 = 1060 - 1070$ °C, $\Delta T = 25 - 70$ °C and $TeCl_4(in) = 1.5 - 4$ mg/ml. When the amount of β-Ti_3O_5 (300 mg) was three times that of Ti_2O_3 (100 mg) or more in the starting material, only β-Ti_3O_5 crystals were transported to the hotter zone. This reverse transport was also observed by Westphal *et al.*[21] with similar mean temperatures ≥ 1080 °C and $TeCl_4(in) = 2$ mg/ml in the rutile transport reactions.

Analogously one can predict the yield of Ti_4O_7 crystals when both Q_1 and Q_2 are slightly larger than the upper limit 0.95, derived for the single phase transport of γ-Ti_3O_5. For the single phase transport of Ti_4O_7 the additional values of Q_1 and Q_2 within parentheses in Table 4 were calculated on the assumption that the whole starting material of Ti_2O_3 and β-Ti_3O_5 was oxidized to Ti_4O_7 according to eqns. (3) and (4).

$$4Ti_2O_3(s) + 2H_2O(g) + TeCl_4(g) \rightleftarrows 2Ti_4O_7(s) + 4HCl(g) + Te(l \text{ and } g) \quad (3)$$

$$4Ti_3O_5(s) + H_2O(g) + \tfrac{1}{2}TeCl_4(g) \rightleftarrows 3Ti_4O_7(s) + 2HCl(g) + \tfrac{1}{2}Te(l \text{ and } g) \quad (4)$$

After single phase transport of Ti_4O_7 as well as Ti_2O_3 one always observed a large quantity of γ-Ti_3O_5 and β-Ti_3O_5 crystals in the residue together with the phase of the transported oxide, as shown in Tables 1 and 2. Surprisingly, the single phase transport of Ti_2O_3 was possible with the residue consisting of up to 80–90 % Ti_3O_5 crystals. It was not possible to find a satisfactory explanation of the fact that the average oxidation state differed between transported crystals and residue in the Ti_2O_3 and Ti_4O_7 transport reactions, whereas the single phase transport of γ-Ti_3O_5 invariably required the residue to be pure Ti_3O_5. This sensitivity to the oxidation state in the transport system might be the reason why it was difficult to find optimal parameters by trial and error for the single phase transport of γ-Ti_3O_5 crystals, without a knowledge of the chemical equation (1) and the related values of Q_1 and Q_2.

Correcting the values of Q_1 and Q_2 for the Ti_2O_3 and Ti_4O_7 growth by taking account of the amount of Ti_3O_5 in the residue, one obtains new values within the limit 0.80 ± 0.15.

With TiO_2 (rutile), the highest oxidation state among the titanium oxides, one did not observe any difference in oxidation state between the starting material (TiO_2) and the transported crystals (TiO_2). However, the oxygen content of the transported crystals might be changed to the upper phase boundary within the homogeneity range, according to the oxidation mechanism provided by H_2O and $TeCl_4$.

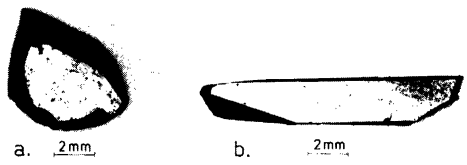

Fig. 3. Photograph of the transported crystals. a, Ti_2O_3, dark violet; b, Ti_4O_7, black.

After establishing eqn. (1) and the related values of Q_1 and Q_2 derived from the 53 runs, seventeen further test runs (not included in Table 3) of the γ-Ti_3O_5 transport were performed with varied amounts and composition of the starting materials, utilizing the presented method to predict the yield. High quality crystals of single phase γ-Ti_3O_5 were invariably transported when the amounts of H_2O and $TeCl_4$ were adjusted to place Q_1 and Q_2 within 0.80 ± 0.15. The concentration of $TeCl_4$ was kept within 6–9 mg/ml in order to produce a suitable transport rate and crystal quality.

Similar chemical equations and related values of Q_1 and Q_2 for the higher titanium oxides of the homologous series Ti_nO_{2n-1}[1] will surely serve to optimize the transport parameters, of which the combinations are otherwise numerous and often laborious to check. In such a manner it should be possible to obtain a desired phase, crystal quality and transport rate by choosing an adequate composition and amount of the starting material, dimensions of silica ampoule (not only *l* and ID but also masses are significant), total amount of $TeCl_4$ and temperature interval.

Description of the transported crystals. The typical crystals of γ-Ti_3O_5 and β-Ti_3O_5 are shown in Fig. 2, and the crystals of Ti_2O_3 and Ti_4O_7 are seen in Figs. 3a and 3b, respectively. The crystals of the γ-Ti_3O_5 and β-Ti_3O_5 and Ti_4O_7 phases are black. The crystals of Ti_2O_3 are dark violet. Further investigations of the hexagonal Ti_2O_3 or triclinic Ti_4O_7 crystals were not performed, because the primary interest was in the monoclinic γ-Ti_3O_5 and β-Ti_3O_5 phases.

The β-Ti_3O_5 crystals have the shape of well-developed rectangular plates with typical dimensions of *ca.* $0.5 \times 1.5 \times 10$ mm^3. The longest edge (*ca.* 10 mm) was always the unique monoclinic *b* axis. A Weissenberg zero-level film with *b* as the rotation axis revealed twin formation, although the pieces of material looked like beautiful single

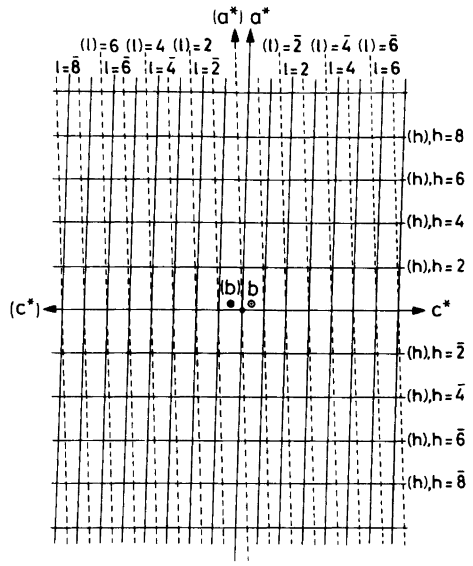

Fig. 4. Twin crystal orientations of the transported β-Ti_3O_5 crystals (*cf.* Fig. 2). One orientation of an $h\,0\,l$ lattice plane is drawn with solid lines (c^* a^* b) and the other is indicated with broken lines. The indices and the signs of the axes for the latter orientation are given within parentheses ((*c**) (*a**) (*b*)). ⊙ indicates that the positive direction of the unique monoclinic *b* axis is from the paper to the reader, and ⊗ denotes the opposite direction (right-handed system). The horizontal lines of *h* and (*h*) indices are identical with each other. The *b* and (*b*), c^* and (c^*) orientations are coincident, respectively; however the directions are opposite. $\beta^* = 88.45°$.

crystals. Fig. 4 shows the twin orientations in β-Ti_3O_5. The ratios of I ($h\,0\,l$) and I ($h\,0\,\bar{l}$) intensities were almost equal even for a small fragment broken from a large "crystal", indicating that the twin formation is of the intergrowth type.

A preliminary study of the structural transition to α-Ti_3O_5 (transition point (t_T) $\approx 150-160$ °C) was performed. When β-Ti_3O_5 was very slowly heated in a stream of hot nitrogen gas,[26] the twin crystals converted to a single crystal of α-Ti_3O_5. However, the crystals used to crack when cooled again through t_T. The reason for cracking could be either a too large change of the unit cell volume in the first-order transition, or twin formation, or both. Therefore efforts to transport single crystals of β-Ti_3O_5 are now in progress by sharply optimizing the transport conditions.

Table 5. X-Ray powder diffraction pattern for the γ-Ti_3O_5 phase at 24 °C. Cu$K\alpha_1$ ($\lambda = 1.540598$ Å),[28] Si ($a = 5.431065$ Å)[28] as an internal standard. $\Delta 2\theta = 2\theta_{obs} - 2\theta_{calc}$. Figure of merit $F_N(= \frac{1}{|\overline{\Delta 2\theta}|} \times \frac{N}{N_{poss}})$ was defined by Smith *et al.*[31] N_{poss} = number of possible reflexions up to Nth observed reflexion. The refined unit cell parameters are shown in Table 6.

d_{obs} (Å)	I_{obs}	$h\,k\,l$	$2\theta_{obs}$(°)	$\Delta 2\theta$	$F_N(\lvert\overline{\Delta 2\theta}\rvert, N_{poss})$
4.68459	33	2 0 0	18.9288	0.0159	63 (0.0159, 1)
4.46147	12	1 1 0	19.8845	0.0070	87 (0.0115, 2)
3.37590	66	0 0 2	26.3793	0.0076	59 (0.0102, 5)
3.32780	11	−2 0 2	26.7676	0.0055	74 (0.0090, 6)
2.93048	62	−1 1 2	30.4793	0.0013	96 (0.0075, 7)
2.66133	100	3 1 0	33.6489	−0.0001	108 (0.0062, 9)
2.53663	42	0 2 0	35.3562	0.0104	103 (0.0068, 10)
2.50509	11	1 1 2	35.8164	−0.0012	119 (0.0061, 11)
2.46533	58	−3 1 2	36.4140	0.0038	127 (0.0059, 12)
2.38284	6	2 0 2	37.7214	0.0009	143 (0.0054, 13)
2.23997	63	1 2 1	40.2278	−0.0048	122 (0.0053, 17)
2.23656		−4 1 1	40.2916	0.0113	115 (0.0058, 18)
2.14593	33	−2 1 3	42.0724	−0.0094	107 (0.0061, 20)
2.02852	24	0 2 2	44.6344	0.0002	112 (0.0057, 22)
1.75906	51	5 1 0	51.9401	0.0007	91 (0.0053, 31)
1.73705	56	2 2 2	52.6484	−0.0017	98 (0.0051, 32)
1.72160	12	4 2 0	53.1580	0.0081	94 (0.0053, 34)
1.67143	76	−1 1 4	54.8855	−0.0086	84 (0.0055, 39)
1.64795	28	−6 0 2	55.7346	−0.0114	75 (0.0058, 44)
1.53009	8	−1 3 2	60.4545	0.0040	69 (0.0057, 51)
1.48778	16	3 3 0	62.3625	−0.0049	68 (0.0057, 54)
1.45081	67	−3 3 2	64.1383	−0.0038	67 (0.0056, 59)
1.44009	10	2 0 4	64.6733	0.0051	67 (0.0056, 61)
1.41036	18	−6 0 4	66.2093	0.0049	70 (0.0055, 62)
1.39156	37	−4 2 4	67.2215	0.0026	69 (0.0054, 67)
1.38924		5 1 2	67.3490	−0.0024	72 (0.0053, 68)

Single crystals of γ-Ti_3O_5 were 1 − 3 mm in both length and width, and 0.5 − 1.5 mm in thickness after transport periods of 7 − 28 days. The two best developed crystal faces were (0 0 $\bar{1}$) and (1 0 0). Their intersection formed a very sharp edge parallel to the unique monoclinic b axis. The angle between the faces was easily confirmed under the microscope to be $\beta^* \approx 70.1°$.

Refinement of unit cell and stoichiometry control of γ-Ti_3O_5. Tables 5 shows the X-ray powder diffraction pattern for γ-Ti_3O_5 at 24 °C, of which the refined unit cell dimensions and space group are presented in Table 6 together with those of β-Ti_3O_5[2] and the high-temperature modification of V_3O_5 (high-V_3O_5).[27] By using a Guinier-Hägg focussing camera an optimally exposed powder film was obtained with Cu$K\alpha_1$ radiation ($\lambda = 1.540598$ Å,[28] quartz monochromator). A thin Al-foil was used to improve the S/N ratio of the powder film, which was measured on a SAAB automatic film scanner Mk II.[29] The measured powder diffraction pattern of γ-Ti_3O_5 was parabolically corrected[30] by five Si ($a = 5.431065$ Å[28]) internal standard lines ($\theta < 40°$).

The figure of merit, F_N, and N_{poss} in Table 5 were defined by Smith and Snyder.[31] N_{poss} means the number of possible reflexions up to the Nth observed reflexion. The powder pattern was indexed by careful comparison of the powder intensities with single crystal diffractometer data. The single crystal data were used to refine the structure[32] to a conventional R value of 0.0185 ($R_w = 0.0219$) with an overdetermination degree of *ca.* 40 (number of observed independent reflexions/refined parameters 1595/40), $\sigma_{Ti-Ti} = 0.0001 - 0.0003$ Å, $\sigma_{Ti-O} = 0.0003 - 0.0005$ Å and $\sigma_{O-O} = 0.0004 - 0.0009$ Å. The accuracy of the crystal structure determination and of the unit cell refinement ($\sigma(a_i)/a_i = 5 - 6 \times 10^{-5}$,

Table 6. Comparison of the unit cell parameters and space groups of γ-Ti_3O_5, β-Ti_3O_5 [2] and high-V_3O_5.[27]

	γ-Ti_3O_5 at 24 °C	β-Ti_3O_5 at 20 °C	high-V_3O_5 at 185 °C
a (Å)	9.9701(5)	9.752(1)	9.846(2)
b (Å)	5.0747(3)	3.8020(5)	5.0268(4)
c (Å)	7.1810(4)	9.442(1)	7.009(1)
β (°)	109.867(4)	91.55(1)	109.536(15)
V (Å^3)	341.70	349.95	326.93
Space group	I 2/c (No. 15)	C 2/m (No. 12)	I 2/c (No. 15)

cf. Table 6) also partly demonstrated the quality of the γ-Ti_3O_5 crystals obtained by chemical transport reactions.

Possible deviation from the stoichiometry of the γ-Ti_3O_5 crystals was carefully checked by refining the unit cell parameters for crystals transported with an extreme combination of the empirical values of Q_1 and Q_2. No changes of the unit cell parameters larger than the measurement errors ($\lesssim 2\sigma$) were observed even for the γ-Ti_3O_5 crystals which were transported simultaneously with the crystals of Ti_4O_7 or Ti_2O_3. Furthermore, no differences of the unit cell parameters were observed between the vapour transported and non-vapour-transported preparation.[4]

Reports on the crystal structures of γ-Ti_3O_5 [32] and δ-Ti_3O_5,[33] and of the results of electric conductivity measurements will shortly appear elsewhere.

Acknowledgements. I wish to express my sincere gratitude to Professor Arne Magnéli and Dr. Stig Åsbrink for their kind interest and valuable comments, and to Dr. Sven Westman for linguistic correction of the article.

I am also grateful for a grant from *Stiftelsen Bengt Lundqvists Minne.* This work has been supported by the Swedish Natural Science Research Council.

REFERENCES

1. Andersson, S., Collén, B., Kuylenstierna, U. and Magnéli, A. *Acta Chem. Scand. 11* (1957) 1641.
2. Åsbrink, S. and Magnéli, A. *Acta Crystallogr. 12* (1959) 575.
3. Zhdanov, G. S. and Rusakov, A. V. *Trudy Inst. Kristallogr. Akad. Nauk. SSSR 9* (1954) 165.
4. Åsbrink, G., Åsbrink, S., Magnéli, A., Okinaka, H., Kosuge, K. and Kachi, S. *Acta Chem. Scand. 25* (1971) 3889.
5. Schäfer, H., Grofe, T. and Trenkel, M. *J. Solid State Chem. 8* (1973) 14.
6. Moulson, A. J. and Roberts, J. P. *Trans. Faraday Soc. 57* (1961) 1208.
7. Niemyski, T. and Piekarczyk, W. *J. Cryst. Growth 1* (1967) 177.
8. Sakata, T., Sakata, K., Höfer, G. and Horiuchi, T. *J. Cryst. Growth 12* (1972) 88.
9. Wolf, E. and Oppermann, H. *Wisse. Ber. Zentralinst. Festkörperphysik und Werkstoffforschung 5* (1975) 30.
10. Davtyan, G. D. *Sov. Phys. Crystallogr. 21* (1976) 499.
11. Gerlach, U. and Oppermann, H. *Z. Anorg. Allg. Chem. 429* (1977) 25.
12. Gerlach, U. and Oppermann, H. *Z. Anorg. Allg. Chem. 432* (1977) 17.
13. Ritschel, M., Oppermann, H. and Mattern, N. *Krist. Tech. 13* (1978) 1421.
14. Bando, Y., Nagasawa, K., Kato, K. and Takada, T. *Jpn. J. Appl. Phys. 8* (1969) 633.
15. Nagasawa, K. *Mater. Res. Bull. 6* (1971) 853.
16. Saeki, M., Kimizuka, N., Ishii, M., Kawada, I., Nakano, M., Ichinose, A. and Nakahira, M. *J. Cryst. Growth 18* (1973) 101.
17. Oppermann, H., Stöver, G. and Wolf, E. *Z. Anorg. Allg. Chem. 410* (1974) 179.
18. Oppermann, H., Reichelt, W. and Wolf, E. *J. Cryst. Growth. 31* (1975) 49.
19. Oppermann, H., Reichelt, W., Krabbes, G. and Wolf, E. *Krist. Tech. 12* (1977) 919.
20. Mercier, J. and Lakkis, S. *J. Cryst. Growth 20* (1973) 195.
21. Westphal, G. H. and Rosenberger, F. *J. Cryst. Growth 49* (1980) 607.
22. Since, J., Ahmed, S. and Mercier, J. *J. Cryst. Growth 40* (1977) 301.
23. Ritschel, R. and Oppermann, H. *Krist. Tech. 13* (1978) 1035.
24. Schäfer, H. *Chemical Transport Reactions*, Academic, New York 1964.
25. Oppermann, H. *Z. Anorg. Allg. Chem. 434* (1977) 239.
26. Hong, S.-H. and Åsbrink, S. *J. Appl. Crystallogr. 14* (1981) 43.

27. Hong, S.-H. and Åsbrink, S. *4th European Crystallographic Meeting*, Oxford 1977, Abstracts B, p. 575; *Acta Crystallogr. B 38* (1982). *In press.*
28. Deslattes, R. D. and Henins, A. *Phys. Rev. Lett. 31* (1973) 972.
29. Abrahamsson, S. *J. Sci. Instrum. 43* (1966) 931.
30. Malmros, G. and Werner, P. E. *Acta Chem. Scand. 27* (1973) 493.
31. Smith, G. S. and Snyder, R. L. *J. Appl. Crystallogr. 12* (1979) 60.
32. Hong, S.-H. and Åsbrink, S. *Acta Crystallogr. To be published.*
33. Hong, S.-H. and Åsbrink, S. *Acta Crystallogr. To be published.*

Received June 16, 1981.

Acta Chemica Scandinavica A 36 (1982) 219–225

Dynamic NMR Studies of Lithium Cation Complexes of 1,5,9,13-Tetraoxacyclohexadecanes

KJELL M. AALMO and JOSTEIN KRANE

Kjemisk institutt, NLHT, Universitetet i Trondheim, N-7055 Dragvoll, Norway

The complexation of lithium ions with sixteen-membered cyclic oligoethers has been investigated by ^{1}H, ^{13}C and ^{7}Li nuclear magnetic resonance spectroscopy. For 1,5,9,13-tetraoxacyclohexadecane acting as ligand, a decomplexation barrier of $\simeq 54$ kJ mol^{-1} was determined and its 3,3,7,7,11,11,15,15-octamethyl derivative gave a decomplexation barrier of $\simeq 71$ kJ mol^{-1}. These barriers were obtained using ^{1}H and ^{13}C probes. A barrier of 79 kJ mol^{-1} has been measured for the decomplexation reaction of the latter using a ^{7}Li probe. Reasons for this difference are discussed. Conformational barriers in the ligands have been determined and variation in chemical shifts of free and complexed cyclic ethers are discussed on the basis of conformational shift effects.

Some years ago we communicated[1] on the ability of the 16-membered cyclic tetramers of oxetan (trimethylene oxide) (A) and 3,3-dimethyloxetan (B) to complex lithium salts. Several lithium complexes with crown ethers,[2-4] cyclic decapeptides[5] and cryptands[6] have been characterized. High selectivity towards lithium cation has been reported for 14-crown-4,[2,4] [2.1.1] cryptand[6] and 1,10-dioxa-4,7-diaza-11-phosphocycloundecane.[7] Simon and his co-workers[8] have synthesized acyclic ionophores capable of selectively binding lithium, notably the *N,N'*-diheptyl-*N,N'*,5,5-tetramethyl-3,7-dioxanonane diamide shows the highest selectivity. Quite recently Cram and co-workers[9] reported on some remarkably strong complexands for lithium; the spherands have for good reasons been characterized as scavengers.

Lithium complexing agents have been shown to alter the reactivity and stereochemistry in reduction reaction with $LiAlH_4$ and $LiBH_4$[10] and cause change in product composition in reaction with R_2CuLi.[11] The [2.1.1] cryptand has been shown to influence polymerization of styrene initiated by lithium.[12]

NMR techniques are very well-suited for the study of complexing interactions. Information about structural features of complexes and ligands can be obtained and kinetic and thermodynamic parameters can be gained from such measurements. In addition, direct information about stoichiometry of complexes is obtainable from NMR methods. Popov and coworkers have used the ^{7}Li NMR technique to study the complexation of lithium ion by cryptands [2.1.1], [2.2.1] and [2.2.2][13] and the kinetics of the [2.1.1] · Li^+ decomplexation reaction in various solvents.[14] Just recently Smetana and Popov reported their ^{7}Li NMR study of lithium complexes of 12-crown-4, 15-crown-5 and 18-crown-6 in various solvents.[15] Jagur-Grodzinski and co-workers[16] have studied the tetradentate amido ethers designed by Simon and his co-workers[8] by ^{1}H and ^{7}Li NMR methods in various solvents.

Results of ^{1}H, ^{13}C and ^{7}Li NMR investigations of ligands A and B and their complexes with lithium salts in various solvents are discussed in the present paper.

EXPERIMENTAL

Synthesis of oxetan.[17] 208 g of 1,3-propanediol (Fluka AG) dissolved in 111 ml sulfuric acid (98 %) was slowly added to 442 g of a 54.5 % boiling NaOH solution kept in a flask fitted with a mechanical stirrer and a reflux condenser. The cyclic ether was co-distilled with water. Two layers were formed and the organic phase was collected. The water phase was salted out and extracted with dichloromethane. The ether phase and the dichloromethane solution

0302-4377/82/030219-07$02.50

were dried over solid KOH and CaH_2 before distillation. The yield of cyclic ether was 35 ml of oxetan (16.5 %), b.p. 48 °C.

By using 2,2-dimethyl-1,3-propanediol (Fluka AG) as the starting material, 3,3-dimethyloxetan was synthesized after the same procedure in about the same yield, b.p. 78 – 82 °C.

Synthesis of the tetramers (Ligands A and B). These were synthesized after a modified procedure originally described by Rose.[18] The monomeric cyclic ether (15 ml) dissolved in benzene (200 ml) (Merck *p.a.*) was slowly added to a solution of boron-trifluoride ethyl etherate (2 ml) (Fluka AG) in benzene (300 ml) (Merck *p.a.*); the solution was kept in a flask equipped with a mechanical stirrer. The whole reaction was run under an inert atmosphere. The reaction mixture was kept at room temperature for 24 h. The mixture was then treated with powdered anhydrous $KHCO_3$ (2.5 g) for 24 h in order to neutralize the Lewis acid. The solvent was evaporated off on a rotavapour. A semi-solid material was obtained after removal of solvent. The tetramers were isolated by sublimation under vacuum at 50 – 60 °C. The yield was 0.7 g (6.4 %) for the octamethyl tetramer, m.p. 157 °C. The melting point for the parent tetramer was 70 °C and the yield was 10 %.

Preparation of LiSCN. Li_2SO_4 (Merck *p.a.*) and $Ba(SCN)_2$ (Merck *p.a.*) were separately dissolved in water in a 1:1 mol ratio. The solutions were mixed together and most of the water was evaporated before filtering off the $BaSO_4$. The rest of the water was removed on a rotavapour. Benzene was added by azeotropic distillation. The LiSCN was then dried in vacuum with P_2O_5 for 72 h.

$LiClO_4$, $LiBF_4$ and $LiPF_6$ (ALFA Chemicals) were used without further purification.

Deuterated solvents (Merck) were taken from sealed ampoules and used without further purification. 1,2-Dichloroethane (Merck) was freshly distilled before use. The samples were prepared in a glove box under a dry nitrogen atmosphere.

NMR Spectroscopy. The ^1H NMR spectra were recorded at 98 MHz on a Varian HA-100 spectrometer operating in the continuous sweep mode, and at 99.54 MHz on a Jeol FX-100 spectrometer operating in the Fourier transform mode equipped with a ^1H and ^{13}C dual probe. 5 mm o.d. sample tubes were used. The HA-100 spectrometer had a proton internal lock, and the deuterium signal in solvents served as internal lock for the FX-100 instrument. Me_4Si was used as an internal reference. The variable temperature units on the two spectrometers were calibrated with ethylene glycol and methanol. All temperatures were measured with a copper-constantan thermocouple situated in the probe a few centimeters below the sample.

The ^{13}C spectra were obtained with 5 mm o.d. tubes on the Jeol FX-100 spectrometer operating at 25 MHz and are Fourier transforms of accumulated free induction decays under the following conditions: 45° pulse angle, 8 K data points, 5000 Hz spectrum width and an exponential broadening function corresponding to 1 Hz broadening. The chemical shifts were referenced to internal Me_4Si.

^7Li NMR spectra at 38.66 MHz were measured on the Jeol FX-100 spectrometer equipped with a variable frequency probe using 10 mm o.d. sample tubes. CD_3NO_2 was used as a solvent. A 4.0 M solution of $LiClO_4$ in H_2O in a 1 mm o.d. melting point capillary inserted coaxially in the tube was used as an external standard. The observed chemical shifts were not corrected for the bulk diamagnetic susceptibility of the solvents. The temperature measurements were done in the same fashion as for the ^1H and ^{13}C dual probe. The spectra are Fourier transforms of free induction decays, and the following conditions were used: 10000 to 50000 transients, 4 K data points, 2000 Hz and 45° pulse angle.

RESULTS AND DISCUSSION

^1H and ^{13}C NMR studies. The ^1H and ^{13}C chemical shifts for ligand A (1,5,9,13-tetraoxacyclohexadecane) (Fig. 1A) are given in Table 1. The ^1H and ^{13}C chemical shifts of the 1:1 complex between ligand A and LiSCN are also included in Table 1. The ^1H chemical shift of ligand A changes

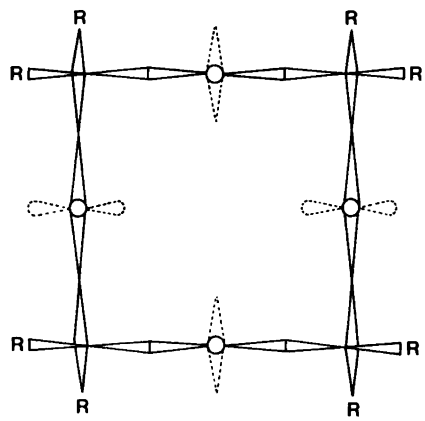

A: – R = – H

B: – R = – CH_3

Fig. 1. The [4444] conformation of ligands A and B.

Table 1. ^{1}H and ^{13}C chemical shifts in ppm from TMS for ligands A and B in uncomplexed state and complexed with lithium cation in $CDCl_3$ as a solvent.

Probe	Ligand				Lithium complex			
	$-CH_2-$	$-CH_2O-$	$-CH_3$	$-C-$	$-CH_2-$	$-CH_2O-$	$-CH_3$	$-C-$
Ligand A								
^{1}H	1.81[a]	3.55[b]	–	–	1.91[a]	3.64[b]	–	–
^{13}C	30.2	66.1	–	–	28.9	72.1	–	–
Ligand B								
^{1}H	–	3.07	0.83	–	–	3.33	0.87	–
^{13}C	–	75.6	22.6	36.3	–	82.1	22.4	36.3

[a] Center of a quintet. [b] Center of a triplet.

very little on complexing. The ^{13}C chemical shifts of the CH_2O carbon, however, are very much dependent on whether LiSCN is present or not.

We have investigated the ^{1}H and ^{13}C NMR spectra of both the free ligand A and its 1:1 $LiBF_4$ complex at variable temperature. The ligand A has a temperature-independent ^{13}C spectrum, and although the ^{1}H spectrum is temperature-dependent, no slow-exchange spectrum is reached down to $-140\,°C$ at 100 MHz. The 1:1 $LiBF_4$ complex also shows no ^{13}C temperature variable spectrum, but here a slow-exchange ^{1}H spectrum is obtained at $-130\,°C$. The spin-system, however, is too complicated for analysis at the magnetic field used.

When the ^{13}C NMR spectrum of the solution of a 1:1 mixture of ligand A and its 1:1 complex with LiSCN in $CDCl_3$ (*i.e.*, the stoichiometry is two parts in ligand A and one part in LiSCN) is recorded at ambient temperature, we observe single resonances for the various chemically different carbons, and the chemical shifts are mean averages of those in the free ligand and in the complexed form, respectively. By lowering the temperature, a dynamic NMR pehnomenon is observed, and the limiting low-temperature spectrum shows resonances equivalent to those observed in the uncomplexed and the complexed ligand, respectively, in 1:1 ratios. The interpretation of the variable temperature ^{13}C spectrum is that we observe a decomplexation process most simply described as eqn. (1), whose corresponding free energy of activa-

$$\mathrm{Li^+C\ Ligand\ A + Ligand\ A^* \rightleftharpoons Li^+C\ Ligand\ A^* + Ligand\ A} \quad (1)$$

tion is about 54 kJ mol^{-1} ($\Delta G^{\neq}$). The kinetic and thermodynamic parameters for the process described in eqn. (1) are given in Table 2.

The stoichiometry of the complex is solvent dependent and also varies with the anion present. The lithium salts LiBr, LiCl, LiI, $LiPF_6$, $LiBF_4$ all form 1:1 complexes in solvents tried: $CDCl_3$, CD_3NO_2 and CD_3CN. Also LiSCN gives 1:1 complexes in $CDCl_3$, but in $CHCl_2F$ (Freon 21) two equivalents of lithium salt are bound to ligand A. The ^{13}C chemical shifts in the 2:1 complex and in

Table 2. Kinetic and thermodynamic parameters for the decomplexation reaction of ligand A complexed with LiSCN in $CDCl_3$ as a solvent.

Group	Probe	$\Delta\nu$ Hz	T_c K	k^a s^{-1}	$\Delta G_{T_c}^{\neq\,b}$ kJ mol^{-1}
$-CH_2-$	^{13}C	34	259	76	54.0
$-CH_2O-$	^{13}C	149	273	331	53.6

[a] Calculated according to Ref. 23. [b] Calculated according to Ref. 24.

Table 3. Kinetic and thermodynamic parameters for the decomplexation reaction or ligand B complexed with LiSCN in 1,2-dichloroethane as a solvent.

Group	Probe	$\Delta\nu$ Hz	T_c K	k s^{-1}	$\Delta G_{T_c}^{\neq}$ kJ mol^{-1}
$-CH_3$	^1H	4	315	9	71.5
$-CH_3$	^{13}C	6	323	13	72.4

the 1:1 complex between LiSCN and ligand A are the same. It is easy to determine the stoichiometry because of the large ^{13}C chemical shift difference of ligand A in uncomplexed and complexed form. This has been done either by titration above coalescence temperature, or by integration of the ^{13}C resonances obtained in a non-nuclear Overhauser experiment in the slow-exchange spectrum, as a function of the Li^+ concentration.

Ligand B (3,3,7,7,11,11,15,15-octamethyl-1,5,9,13-tetraoxacyclohexadecane) (Fig. 1B) was investigated in the same way as described for ligand A above. The chemical shifts for the various chemically different protons and carbons for the free ligand B and its 1:1 complex with LiSCN in $CDCl_3$ as a solvent at ambient temperature are given in Table 1. Here again, the same trend as seen for ligand A is observed for ligand B; small differences in ^1H chemical shifts, large differences in the ^{13}C chemical shift of CH_2O-carbons on complexing.

The decomplexation process observed by dissolving two equivalents of ligand B and one equivalent of LiSCN in 1,2-dichloroethane (with a few drops of C_6D_6 added, to serve as an internal deuterium lock) has a higher barrier ($\Delta G^{\neq} \simeq 71$ kJ mol^{-1}) than for the ligand A ($\Delta G^{\neq} \simeq 54$ kJ mol^{-1}); an effect that must be due to the methyl groups. The kinetic and thermodynamic parameters for the decomplexation reaction as given by eqn. (1) using ligand B instead of ligand A are given in Table 3.

The solution of a 1:1 ratio of LiSCN and ligand B in $CHCl_2F$ as a solvent was investigated at low temperature. Both the ^1H and the ^{13}C spectra are temperature-dependent. The low-temperature ^1H spectrum is shown in Fig. 2. The methylene protons split into an AB-quartet ($J_{AB}=8.8$ Hz) and the methyl protons into a doublet. In the ^{13}C spectrum, only the methyl carbons show a coalescence phenomenon. The activation free energy is 36.8(8) kJ mol^{-1} for the process observable both by ^1H and ^{13}C spectroscopy. The kinetic and thermodynamic parameters pertinent to this experiment are given in Table 4.

We did not observe a 2:1 complex between LiSCN and ligand B in $CHCl_2F$ as a solvent, as was the case with ligand A.

^7Li NMR studies. As shown in Table 5, we observe different ^7Li chemical shifts as a result of variation in environment around the ^7Li nucleus. We also observe a broadening by about 2 Hz of the ^7Li resonance for Li^+ in the complex with ligand B compared to the resonance of $LiClO_4$ in CD_3NO_2.

The Gibbs free activation energy associated with the process (eqn. 2) may not represent the $\Delta G^{\neq}$

$$Li^+ \subset (\text{ligand A or B}) + {}^*Li^+ \rightleftharpoons {}^*Li^+ \subset (\text{ligand A or B}) + Li^+ \qquad (2)$$

associated with the forward reaction in eqn. (1). $\Delta G^{\neq}$ for the forward reaction in eqn. (2) might be dependent on the amount of free Li^+ in solution, and intermediate complexes of the type $Li^+ . {}^*Li^+ \subset$

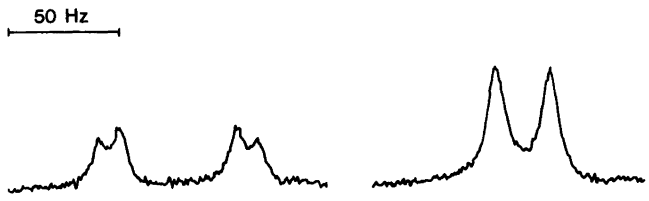

Fig. 2. The low-temperature ^1H spectrum at -110 °C of the solution of a 1:1 ratio of LiSCN and ligand B in $CHCl_2F$ as a solvent.

Table 4. Kinetic and thermodynamic parameters for conformational changes in ligand B in the 1:1 complex with LiSCN in $CHCl_2F$ as a solvent.

Group	Probe	$\Delta\nu$ Hz	T_c K	k s^{-1}	$\Delta G_{T_c}^{\neq}$ kJ mol^{-1}
$-CH_2O-$	^1H	61	183	137[a]	36.4
$-CH_3$	^{13}C	28	178	62	36.8
$-CH_3$	^1H	23	178	51	36.8

[a] A J-coupling constant of 8.8 Hz has been taken into consideration in calculation of k.

Table 5. ^7Li chemical shifts in ppm.

Compound	$^7Li^{a,b}$
4 M $LiClO_4$ in H_2O	0
$LiClO_4$ in CD_3NO_2[c]	−1.36
$LiClO_4$ complexed with ligand A	−1.66
$LiClO_4$ complexed with ligand B	−1.84

[a] No correction for bulk diamagnetic susceptibility has been made. [b] All ^7Li chemical shifts are reference to an external solution of 4 M $LiClO_4$ contained in a 1 mm melting point capillary and centered in a 10 mm NMR tube and upfield shifts are given as negative. [c] Concentration of 0.13 M $LiClO_4$.

(ligand A or B) might exist. At ambient temperature we observe separate resonances for Li^+ in complexed and uncomplexed state for ligand B. By choosing a composition of two equivalents of $LiClO_4$ and one equivalent of ligand B in CD_3NO_2 as a solvent, we observe a coalescence phenomenon at $\simeq 100\,°C$ with a corresponding activation free energy of 79 kJ mol^{-1} ($\Delta G^{\neq}$) which is about 8 kJ mol^{-1} above what we determined for the process according to eqn. (1). Unfortunately, the solubility of $LiClO_4$ in CD_3NO_2 below 0 °C is very limited, and therefore we were not able to do a similar experiment for ligand A because the coalescense temperature is below 0 °C.

From the experiments described above one can conclude: The decomplexation barriers excede by far any conformational barriers in the ligands and the $\Delta G^{\neq}$'s associated with the forward reaction in eqns. (1) and (2) are not necessarily the same.

Conformations. The crystal structure of ligand A has been determined by Groth[19] and the molecule has the "square" diamond lattice [4444] ring conformation with a D_{2d} symmetry. The IR-spectra in solid state and solution, respectively, of both ligand A and B show that these compounds are conformationally homogeneous. The *gem*-dimethyl groups in ligand B must necessarily occupy the corner positions, and therefore ligand B no doubt also occupies the same "square" ring conformation. In the conformation under discussion, two contributions to the ^{13}C NMR shifts should be of importance, namely the γ and the *vicinal-gauche* (V_g) effect.[20] The γ effect results in an upfield shift of about 5 ppm for the terminal carbons in a *gauche* butane fragment. The effect of heteroatoms in such a fragment is not clear, but for the sake of argument we do not differentiate between oxygen atom and methylene group in this respect. A third effect, V_t, occurs for the central carbons in an *anti* butane fragment, but its magnitude (0.8 ppm upfield) is very much smaller than that of either the γ or the V_g effect. For the carbon in the CH_2O groups in the [4444] conformation shown in Fig. 1 we count $\gamma + V_g + V_t$ chemical shift effects (the effect of the *gem*-dimethyl groups has been left out).

The ^1H and ^{13}C low-temperature spectra of 1:1 complex between ligand B and LiSCN are such that a conformation as shown in Fig. 3 would satisfy the observed spectra. We refer to this particular conformation as [16], which indicates a non-

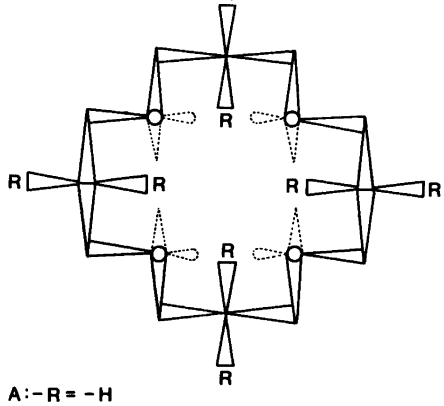

A:- R = - H

B:- R = - CH_3

Fig. 3. The [16] ring conformation of ligands A and B.

corner conformation with a D_{2d} symmetry element. By comparing the changes in ^{13}C chemical shifts for both ligands A and B, in free and complexed state (Table 1), it is fair to conclude that both ligands have the same ring conformation when complexed. In addition, the particular changes in chemical shifts also support the [16] ring conformation for the ligands when complexed. In the [16] form the carbon in the CH_2O groups has lost the $\gamma + V_t$ chemical shift effects, which amounts to $\simeq 6$ ppm. That is exactly what we observe, downfield shifts for CH_2O carbons of 6.0 and 6.5 ppm for the complexed ligands A and B, respectively, compared to the free cyclic ethers.

Raymond *et al.*[21] have determined the crystal structure of the tetraaza analogue of ligand A, namely the 1,5,9,13-tetraazacyclohexadecane, which has a ring conformation identical with the one depicted in Fig. 3. By using structural data from their X-ray analysis, the cavity in our oxygen analogues ought to have a radius of about 0.7 Å. Here we have used an O---O edge distance of 2.9 Å and a van der Waals radius for oxygen of 1.40 Å. The lithium ion, whose radius is reported in the range of 0.60 – 0.78 Å, will fit very well into the cavity. A subsequent X-ray analysis of the LiSCN · ligand A complex confirms the proposed conformation[22] based on NMR results. The open [4444] form (Fig. 1), has a larger cavity, and the oxygen lone-pairs are directed in such a way that they do not give good interactions with a cation in the middle of the ring. The cavity of the open form can easily accomodate a sodium ion.

We have here an example of a situation where the guest (Li^+) organizes the host (ligand A and B) in order to get thermodynamically more stable complexes.

The variation in stoichiometry for the LiSCN complex of ligand A with the solvents used might be explained on the basis of the solvation of ion pairs. In chloroform the complex probably exists as a loose ion pair, while in $CHCl_2F$ we are dealing with a tighter ion pair, and we envision a structure as shown in Fig. 4 for the 2:1 complex between LiSCN and ligand A in $CHCl_2F$. The two Li^+ ions are displaced from the mean plane of the oxygens. As ahown in Fig. 3, a total of eight oxygen lone-pair electrons are pointing out from the mean plane of the oxygens, four on each side, and these lone-pair electrons give reasonable support for a 2:1 complex. For ligand B, however, such a complex is hard to envision, due to the steric hindrance of the methyl groups.

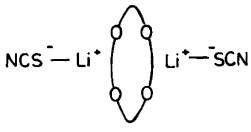

Fig. 4. Suggested structure for the tight ion pair 2:1 complex between LiSCN and ligand A in $CHCl_2F$.

REFERENCES

1. Dale, J. and Krane, J. *J. Chem. Soc. Chem. Commun.* (1972) 1012.
2. Christensen, J. J., Eatough, D. J. and Izatt, R. M. *Chem. Rev. 74* (1974) 351.
3. Anet, F. A. L., Krane, J., Dale, J., Daasvatn, K. and Kristiansen, P. O. *Acta Chem. Scand. 27* (1973) 3395.
4. Pedersen, C. J. *Fed. Proc. Fed. Am. Soc. Exp. Biol. 27* (1968) 1305.
5. Karle, I. L. *J. Am. Chem. Soc. 96* (1974) 4000.
6. Lehn, J.-M. and Sauvage, J.-P. *J. Chem. Soc. Chem. Commun.* (1971) 440; *J. Am. Chem. Soc. 97* (1975) 6700.
7. Grandjean, J., Laszlo, P., Picaret, J. P. and Sliwa, H. *Tetrahedron Lett.* (1978) 1861.
8. Ammann, D., Bissig, R., Guggi, M., Pretsch, E., Simon, W., Borowitz, I. J. and Weiss, L. *Helv. Chim. Acta 58* (1975) 1535.
9. Cram, D. J., Kaneda, T., Helgeson, R. C. and Lein, G. M. *J. Chem. Soc. Chem. Commun.* (1979) 948; *J. Am. Chem. Soc. 101* (1979) 6752.
10. Pierre, J. L. and Handel, H. *Tetrahedron Lett.* (1974) 2317.
11. Ouannes, C., Dressaire, G. and Langlois, T. *Tetrahedron Lett.* (1977) 815.
12. Boileau, S., Kaempf, B., Lehn, J.-M. and Schué, F. *J. Polym. Sci. Part B, Polym. Lett. Ed. 12* (1974) 203.
13. Cahen, Y. M., Dye, J. L. and Popov, A. I. *J. Phys. Chem. 79* (1975) 1289.
14. Cahen, Y. M., Dye, J. L. and Popov, A. I. *J. Phys. Chem. 79* (1975) 1292.
15. Smetana, A. J. and Popov, A. I. *J. Solution Chem. 9* (1980) 183.
16. Olsher, U., Elgavish, G. A. and Jagur-Grodzinski, J. *J. Am. Chem. Soc. 102* (1980) 3338.
17. Schmoyer, L. F. and Case, L. C. *Nature 187* (1960) 592.
18. Rose, J. B. *J. Chem. Soc.* (1956) 542.
19. Groth, P. *Acta Chem. Scand. 25* (1971) 725.
20. Stothers, J. B. *Carbon-13* NMR Spectroscopy, Academic, New York 1972; Dalling, D. K. and Grant, D. M. *J. Am. Chem. Soc. 89* (1967) 6612;

Ibid. *94* (1972) 5319; *Ibid.* *96* (1974) 1827; Dalling, D. K., Grant, D. M. and Paul, E. G. *Ibid.* *95* (1973) 3718.
21. Smith, W. L., Ekstrand, J. D. and Raymond, K. N. *J. Am. Chem. Soc.* *100* (1978) 3539.
22. Groth, P. *Acta Chem. Scand. A* *35* (1981) 460.
23. Glasstone, S., Laidler, K. J. and Eyring, H., *The Theory of Rate Processes*, McGraw-Hill, New York 1941.
24. Anet, F. A. L. and Anet, R. In Nachod, F. C. and Zuckerman, J. J., Eds., *Determination of Organic Structures by Physical Methods*, Academic, New York 1971, Vol. 3, p. 343.

Received June 16, 1981.

Acta Chemica Scandinavica A 36 (1982) 227–234

1,5,9,13-Tetraoxacyclohexadecane and Its 3,3,7,7,11,11,15,15-Octamethyl Derivative as Neutral Carriers for Lithium Ion through Artificial Membranes

KJELL M. AALMO and JOSTEIN KRANE

Kjemisk institutt, NLHT, Universitetet i Trondheim, N-7055 Dragvoll, Norway

1,5,9,13-Tetraoxacyclohexadecane and its 3,3,7,7,-11,11,15,15-octamethyl derivative have been synthesized and used as neutral carriers in membrane electrodes, the membrane consisting of the cyclic polyethers in tris(2-ethylhexyl)phosphate as plasticizer in a PVC matrix. Selectivities, working range and pH dependence have been studied. Lithium ion activities can be measured in the range 1 M to approximately 10^{-5} M, and the selectivities of lithium over ammonium, sodium, potassium, rubidium, cesium, magnesium, calcium, strontium and barium go from about 3 to 800.

The conformational behaviour of the carriers in the membrane is discussed. The title compounds have different ring conformations depending on whether they are transporting Li^+ or not.

During the last decade much attention has been focused on the use of neutral carrier species as membrane components, having the capability to selectively extract ions from aqueous solution into a hydrophobic membrane phase and to transport these ions across such a barrier by carrier translocation. Different polyesters,[1] antibiotics[2,3] and cyclic polyethers[3–5] (crown ethers) have been investigated as neutral carriers. Some of them have shown to be quite useful together with different plasticizers as membrane components in ion selective membrane electrodes, especially for alkaline and alkaline earth ions.

Recently, Güggi *et al.*[6] reported on the characteristics of a lithium ion selective electrode based on the neutral carrier *N,N'*-diheptyl-*N,N'*,5,5-tetramethyl-3,7-dioxanonane diamide in tris(2-ethylhexyl)phosphate as membrane components in a polyvinyl chloride (PVC) matrix.

We have investigated the complexing ability between Li^+ and the crown ether 1,5,9,13-tetraoxacyclohexadecane (*A*) (Fig. 1) and its 3,3,7,7,11,-11,15,15-octamethyl derivative (*B*) (Fig. 1) both by ^1H, ^{13}C and ^7Li NMR spectroscopy.[7] It was of interest to determine if these crown ethers could act as neutral carriers in membranes. We here report on the characteristics of these neutral carriers for Li^+ in PVC membrane electrodes.

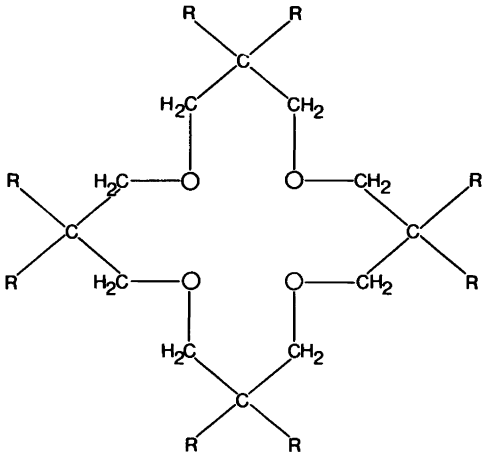

A: - R = - H

B: - R = - CH_3

Fig. 1. Structure of the neutral carriers investigated.

0302-4377/82/030227-08$02.50

$$Hg; Hg_2Cl_2, KCl_{sat} \,|NH_4NO_3(10^{-1}\ M)||\text{sample solution}||\text{membrane}||LiCl(10^{-3}\ M), AgCl; Ag. \quad (1)$$

EXPERIMENTAL

Synthesis of neutral carriers. (A) and (B) were synthesized after a modified procedure[7] originally described by Rose.[8]

Membrane preparation. The membranes were prepared according to Mascini and Pallozzi[3] with the following composition: 180 mg PVC (Norvinyl PVC, S 2–70, Norsk Hydro A/S, Norway). 8.5 mg neutral carrier. 350 mg tris-(2-ethylhexyl)-phosphate (Merck).

Disks of 9 mm diameter and approx. 0.2 mm thickness were cut with a cork-borer and conditioned for 24 h in 1 M lithium chloride solution.

Electrode system. The membranes were incorporated into an Orion 93-19 electrode module with a silver–silver chloride internal reference electrode. The measurements were performed at 25 °C on a cell of the type given in eqn. (1).

The ammonium nitrate solution was connected to the sample solution *via* an ammonium nitrate agar bridge (Bacto-agar, Difco Laboratories, Detroit, Michigan) to minimize the liquid junction potentials.[9] The sample solutions were unbuffered.

Selectivity coefficients and activity coefficients. In the same way as by Güggi *et al.*[6] selectivity coefficients were determined by the separate solution technique on 10^{-1} M aqueous solutions of the chlorides using the relationship (2), where R; gas

$$\log k_{LiM} = \frac{(E_2 - E_1)F}{2.303RT} - \log a_{M^{z+}}^{1/z} + \log a_{Li^+} \quad (2)$$

constant; a; ion activities; T; absolute temperature; z; charge of the interfering ion; F; Faraday constant; E_1; EMF of the cell assembly, the sample being a LiCl solution of analytical concentration 10^{-1} M; E_2; EMF of the cell assembly, the sample being a 10^{-1} M solution of the chloride of the interfering cation.

The activity coefficients for sodium and calcium were calculated from eqns. (3) and (4),[6,10] where I is the ionic strength. For all other cations the

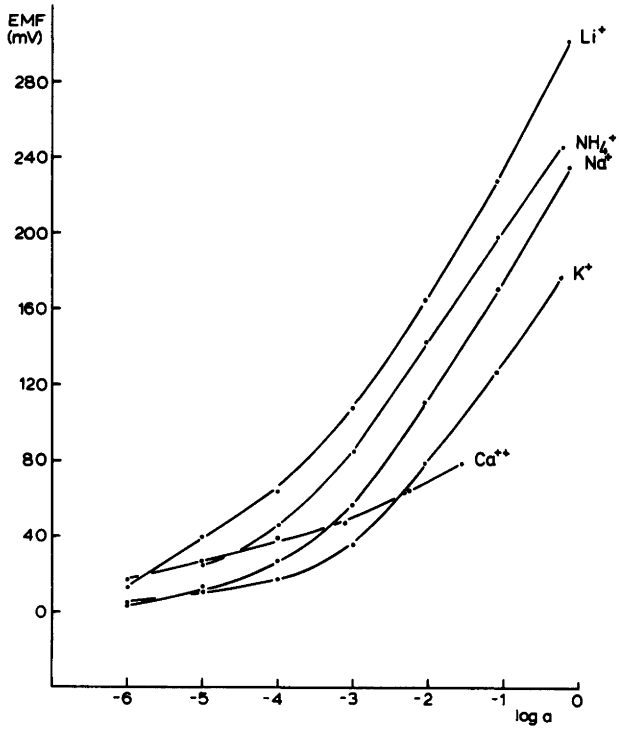

Fig. 2. EMF response of cell (1) to aqueous solutions of the chlorides of Li^+, NH_4^+, Na^+, K^+ and Ca^{++} using neutral carrier A (Fig. 1) as a membrane component.

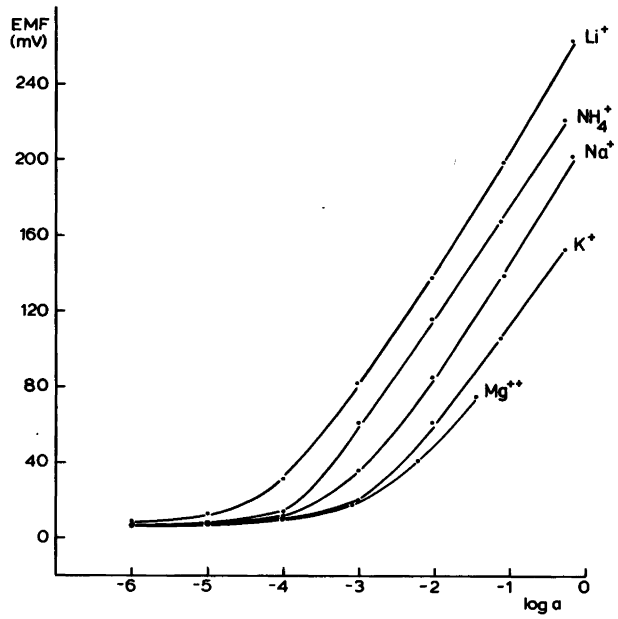

Fig. 3. EMF response of cell (1) to aqueous solutions of the chlorides of Li^+, NH_4^+, Na^+, K^+ and Mg^{++} using neutral carrier B (Fig. 1) as a membrane component.

$$\log \gamma_{Na} = \frac{-0.51 I^{\frac{1}{2}}}{1+1.30 I^{\frac{1}{2}}} + 0.06I \quad (3)$$

$$\log \gamma_{Ca} = \frac{-2.04 I^{\frac{1}{2}}}{1+1.55 I^{\frac{1}{2}}} + 0.2I \quad (4)$$

activity coefficients were calculated according to the form (5) of Debye-Huckel equation[11]

$$-\log \gamma_i = Az^2 \frac{I^{\frac{1}{2}}}{1+Bb\, I^{\frac{1}{2}}} \quad (5)$$

A and B were taken to be 0.509 and 0.328, respectively, and b denotes the effective size of the hydrated ion.[11]

Reagents. De-ionized water and chemicals from Merck (*pro analysis*) were used throughout the investigation.

Table 1. Electrode selectivity coefficients, k_{LiM}, determined by the separate solution technique on 10^{-1} M aqueous solutions of the chlorides.

	Carrier (A)		Carrier (B)	
	k_{LiM}	$1/k_{LiM}$	k_{LiM}	$1/k_{LiM}$
Li^+	1.0	1.0	1.0	1.0
H^+	4.7	0.2	3.5	0.3
NH_4^+	3.4×10^{-1}	3	3.2×10^{-1}	3
Na^+	1.0×10^{-1}	10	9.9×10^{-1}	10
K^+	2.0×10^{-2}	50	2.9×10^{-2}	35
Rb^+	1.4×10^{-2}	72	1.5×10^{-2}	67
Cs^+	1.3×10^{-2}	77	1.4×10^{-2}	71
Mg^{++}	1.7×10^{-3}	590	3.5×10^{-3}	286
Ca^{++}	1.4×10^{-3}	715	9.5×10^{-3}	105
Sr^{++}	1.2×10^{-3}	830	1.4×10^{-3}	715
Ba^{++}	1.2×10^{-3}	830	1.6×10^{-3}	625

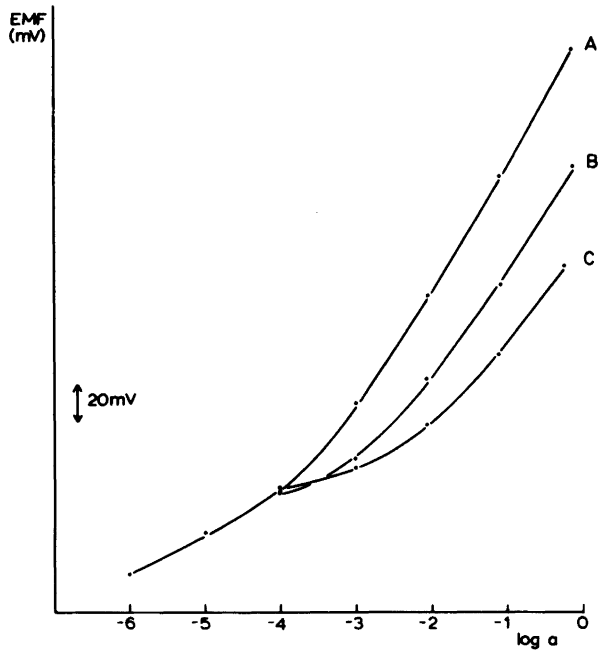

Fig. 4. EMF response of cell (1) to aqueous solutions of the chlorides of: A, Li^+ only; B, Na^+ with $[Li^+]=10^{-4}$ M as background; C, K^+ with $[Li^+]=10^{-4}$ M as background. Neutral carrier A (Fig. 1) used as membrane component.

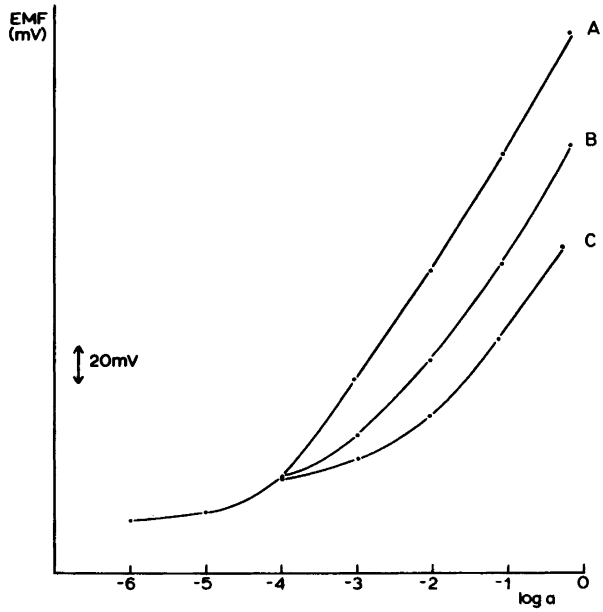

Fig. 5. EMF response of cell (1) to aqueous solutions of the chlorides of: A, Li^+ only; B, Na^+ with $[Li^+]=10^{-4}$ M as background; C, K^+ with $[Li^+]=10^{-4}$ M as background. Neutral carrier B (Fig. 1) used as membrane component.

RESULTS

The response of cell (1) to Li^+, NH_4^+, Na^+, K^+ and Ca^{++} using (A) as the neutral carrier is shown in Fig. 2. The response of the same cell to Li^+, NH_4^+, Na^+, K^+ and Mg^{++} using (B) as the neutral carrier is shown in Fig. 3. The EMF readings are not corrected for changes in the liquid junction potential by Henderson's equation.[12,13] The uncertainties in the EMF readings should be comparable to those estimated by others using the same kind of experimental setup.[3,4]

As shown in Figs. 2 and 3, the response is linear over the activity range 10^{-4} to 1 M for both (A) and (B), with nearly Nearnstian slopes of 59 mV per activity decade for a monovalent ion at 25 °C. The membranes can also be used at lower concentrations. The electrodes also react in a near Nernstian fashion in different concentration regions for NH_4^+, K^+ and Na^+. This indicates that the electrodes can change from lithium ion response to an interfering ion response depending upon the relative concentrations. This is illustrated in Figs. 4 and 5 where EMF readings for NaCl and KCl solutions in the concentration region 10^{-4} to 1 M with a constant background of 10^{-4} M LiCl are shown together with the readings for pure LiCl solution. The electrodes change rapidly, and reproducibly, from a lithium ion response to an interfering ion response during a single experiment and indicate a high rate of ion-replacement in both carriers. The same kind of behaviour has been found for other PVC membrane electrodes using crown ethers as neutral carriers.[3]

Selectivity coefficients obtained by the separate solution technique on 10^{-1} M solutions of the chlorides are indicated in Fig. 6 together with results from a glass electrode[14] and investigations by Güggi *et al.*[6] on their neutral carrier PVC membrane electrode. The selectivity coefficients are listed in Table 1. The present electrodes based on the neutral carriers (A) and (B) give better selectivity for lithium

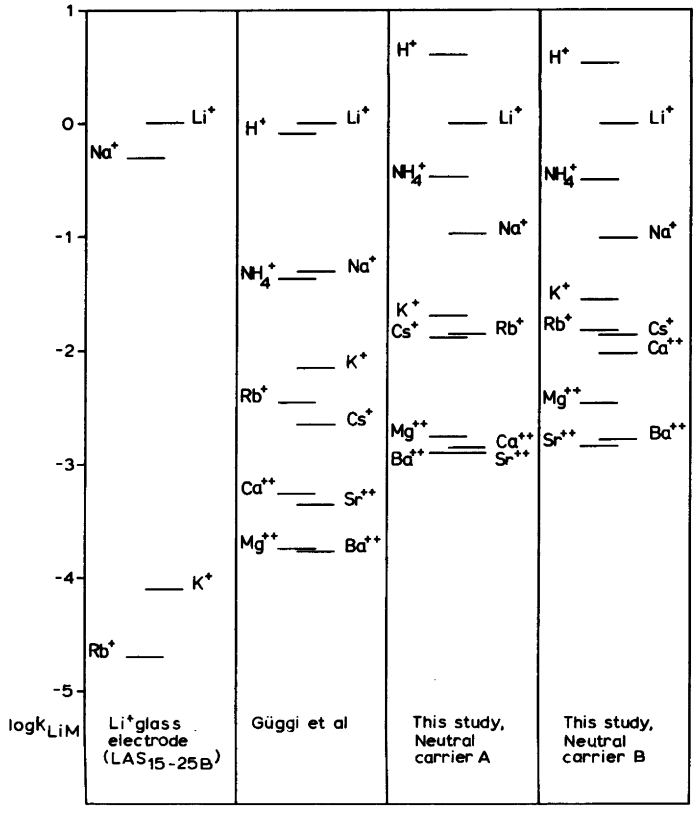

Fig. 6. Selectivity coefficients obtained by the separate solution technique on 10^{-1} M solutions of the chlorides. (See Refs. 6 and 14).

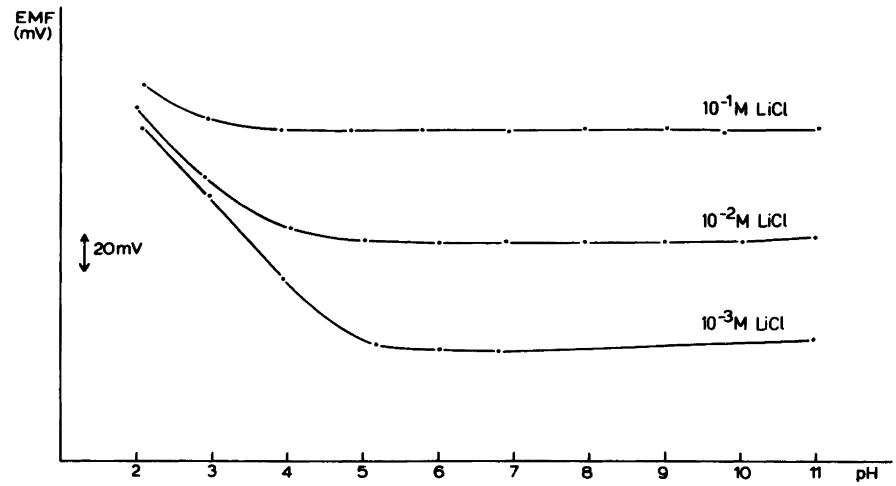

Fig. 7. EMF response of cell (1) for different LiCl concentrations as a function of pH. Neutral carrier A (Fig. 1) used as membrane component, HCl and KOH used to change the pH value.

to sodium than can be obtained with the glass electrode, but the selectivities are not as good as those found by Güggi *et al.*[6] using the neutral carrier *N,N'*-diheptyl-*N,N'*,5,5-tetramethyl-3,7-dioxanonane diamide.

Attempts were made to prepare membranes with plasticizers other than tris(2-ethylhexyl)phosphate, especially because the octamethyl derivative carrier was rather sparingly soluble in this medium, and sometimes the carrier crystallized in the PVC matrix. Plasticizers such as tributylphosphate, dibuthylphthalate, diphenylether, nitrobenzene and didecylphthalate were investigated, but did not give good results. We think that further attempts should be made to find a more suitable plasticizer for the neutral carrier (B), *i.e.* a more hydrophobic plasticizer where solubility and mobility of the carrier would be enhanced.

Figs. 7 and 8 show the EMF readings for different lithium chloride solutions as a function of pH. The readings are constant in a wide region of the pH scale, but at low pH values there is serious inter-

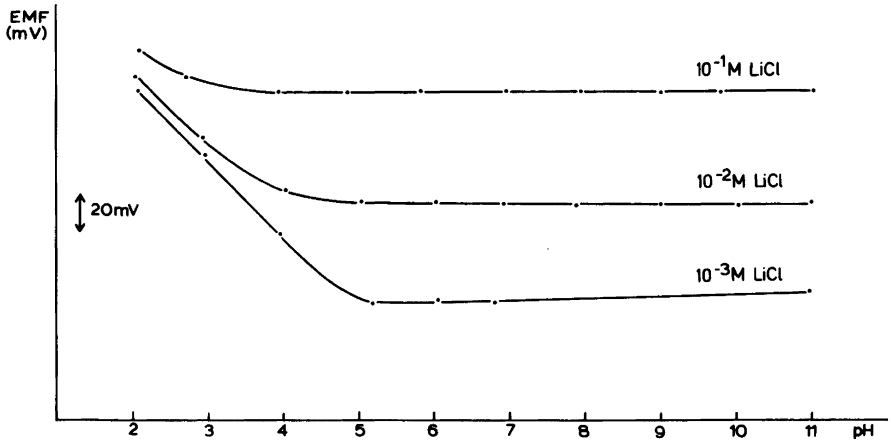

Fig. 8. EMF response of cell (1) for different LiCl concentrations as a function of pH. Neutral carrier B (Fig. 1) used as membrane component, HCl and KOH used to change the pH value.

ference with H^+ ions. This is to be expected according to the selectivity coefficients measured in 10^{-1} M solutions (Fig. 6 and Table 1).

Güggi *et al.*[6] pointed out that an anion interference of 5 mV was observed for SCN^- compared to Cl^- in 10^{-1} M solutions. The same kind of behaviour is observed in the two membranes investigated in this work. The response time for both electrodes is in the order of a few seconds both in concentrated and dilute solutions, and the lifetime of the membranes is substantial, as is found for other PVC membranes. The uncertainty in the EMF readings is ± 0.15 mV. Stirring the solutions has very little effect upon the EMF readings.

DISCUSSION

The interactions between ligand binding sites and cations are normally analyzed into several energy contributions, mostly in electrostatic terms. An excellent review article by Lehn[15] deals with the various factors influencing complexation. A number of factors influence cation selectivity. For inorganic cations the following factors are important: charge, size, electronic structure and associated ions or counterions. The most important factors for the ligand are cavity size, donor atom type and number, ring conformation and ring substituents. Some data also indicate that the type of polymer used may change the selectivity drastically.[16]

Winkler[17] has pointed out that in the case of lithium, which has a very high field density at the surface, the energy required to strip off the inner hydration shell of four water molecules is 510 kJ mol^{-1} (122 Kcal mol^{-1}) and that the interaction of any acceptor ligand with the cation must be very favourable to compete with this hydration energy. However, individual water molecules in this shell have a very high rate of substitution by ligands and Winkler suggests that the optimal acceptor would be one which substitutes water molecules in a step-wise fashion and was itself flexible enough to change conformation sequentially to a more compact structure. We think we have two such compounds at hand.

The conformational situation for ligands (A) and (B) has been discussed in the preceeding article[7] both with and without Li^+ present. We believe that the following situation exists when (A) and (B) are transporting Li^+ through the so-called solid-liquid membrane: the ring conformation of (A) and (B) in the membrane without Li^+ present is as depicted in Fig. 1 in the preceeding article.[7] On the membrane surface the carriers (A) and (B) substitute one of the four inner water molecules around Li^+ with an ether oxygen. The closed unoccupied oxygens in the ring are facing away from the incoming Li^+, now with three water molecules. A successive inward rotation of oxygens can now substitute one water molecule after the other, and the final ring conformation of the ligand is as depicted in Fig. 3 in the preceeding article.[7] The activation energies for these conformational changes are also discussed in detail in that article.[7] The complex can now diffuse across the membrane. The ligands in the complexed form have a much more hydrophobic exterior than the uncomplexed square form. The release action of Li^+ at the opposite boundary on the membrane is likely to be the reverse of what has been described above.

If the description as given above is correct, then the compounds (A) and (B) meet the criteria set forth by Winkler for good carriers.[17]

Acknowledgements. We are grateful to Mrs. K. Tanem for help in making up solutions and carrying out some of the EMF measurements. Financial support from the Norwegian Research Council for Science and Humanities is gratefully acknowledged.

REFERENCES

1. Scholer, R. P. and Simon, W. *Chimia 24* (1970) 372.
2. Pioda, L. A. R., Stankova, V. and Simon, W. *Anal. Lett. 2* (1969) 665.
3. Mascini, M. and Pallozzi, F. *Anal. Chim. Acta 73* (1974) 375.
4. Rechnitz, G. A. and Eyal, E. *Anal. Chem. 44* (1972) 370.
5. Pedersen, C. J. *J. Am. Chem. Soc. 89* (1967) 7017.
6. Guggi, M., Fiedler, U., Pretsch, E. and Simon, W. *Anal. Lett. 8* (1975) 857.
7. Aalmo, K. M. and Krane, J. *Acta Chem. Scand. A 36* (1982) 219.
8. Rose, J. B. *J. Chem. Soc.* (1956) 542.
9. Lakshminarayanaiah, N. *Membrane Electrodes*, Academic, New York, San Francisco and London 1976, pp. 61–62.
10. Bates, R. G. and Alfenaar, M. *Natl. Bur. Stand. (U.S.) Spec. Publ. 314* (1969).
11. Butler, J. N. *Ionic Equilibrium, A Mathematical Approach*, Addison-Wesley Reading, Palo Alto, London 1964, pp. 432–434.

12. Henderson, P. *Z Phys. Chem. 59* (1907) 118.
13. Henderson, P. *Z. Phys. Chem.* 63 (1908) 325.
14. Eisenman, G. In Reilly, C. N., Ed., *Advances in Analytical Chemistry and Instrumentation*, Wiley, New York 1965, Vol. 4, p. 213.
15. Lehn, J.-M. *Struct. Bonding Berlin 16* (1974) 1.
16. Fiedler, V. and Ruzička, J. *Anal. Chim. Acta 67* (1973) 179.
17. Winkler, R. *Neurosci. Res. Program. Bull. 14* (1976) 139.

Received June 16, 1981.

Acta Chemica Scandinavica A 36 (1982) 235–238

Spin-Lattice Relaxation Measurements Used in an Attempt at Detecting Complex Formation between Noradrenaline and Lithium in Aqueous Solution at Physiological pH and Temperature

DAVID S. B. GRACE and JOSTEIN KRANE

Kjemisk institutt, NLHT, Universitetet i Trondheim, N-7055 Dragvoll, Norway

The longitudinal relaxation times of ^{7}Li and ^{13}C have been measured in aqueous solutions of D,L-noradrenaline and lithium chloride by the FIRFT method with correction for the effect of inhomogeneities in the RF field. The results indicate negligible complex-formation between Li^+ and noradrenaline at physiological pH and temperature.

Lithium salts have for long been one of the main agents used in the treatment of mania but the biochemical basis of its therapeutic effect remains undetermined. One way in which lithium may affect the nervous system is by influencing the release or uptake of noradrenaline *1*.[1] It would be of interest, therefore, to determine whether or not there is complex-formation between lithium ions and noradrenaline in aqueous solution at physiological pH and temperature.

As pointed out by James and Noggle[2] the longitudinal relaxation-rate of quadrupolar nuclei such as ^{23}Na is very sensitive to the electronic environment around and hence complexation of the ion. This is because relaxation is due predominantly to the interaction of the quadrupole moment of the nucleus with the electric field-gradiant at the nucleus and the size of the latter depends heavily on the symmetry of the complex. The quadrupolar relaxation-rate is also directly proportional to the correlation-time of the nucleus and this is likely to be increased on complexation of the ion with a larger molecule. Thus, Forsén *et al.*[3] used ^{23}Na T_1 measurements to study the weak complexation of sodium ions by sugars in aqueous solution. Relaxation of ^{7}Li is not always dominated by quadrupolar relaxation, but relaxation seems nevertheless to be quite sensitive to complexation. Jagur-Grodzinski *et al.*[4] measured a formation constant of 1.1 M^{-1} for complexation of Li^+ with *N,N*-diheptyl-*N,N'*-tetramethyl-3,7-dioxanonanediamide (NDA) in pyridine solution, and Plaush *et al.*[5] have studied the complexation of nucleosides, nucleic acid bases and ribose in DMSO solution using this method. Yokono *et al.*[6] have studied the interaction of $^{7}Li^+$ with nucleotides in aqueous solution and reported significant increase in the relaxation rate of $^{7}Li^+$.

Quadrupolar relaxation is responsible for about 44 % of the relaxation rate of $^{7}Li^+$ in aqueous solution at ambient temperature, the other 56 % being due to dipole – dipole relaxation.[7] The electric field-gradient at the Li^+ nucleus in dilute solution is expected to be small because of the tetrahedral arrangement of the solvating water molecules.[8] Complexation *via*, for example, the catechol hydroxyl groups of noradrenaline with displacement of water molecules from the inner coordination-shell of Li^+ would greatly decrease the symmetry around the ion and one could anticipate a correspondingly increased relaxation rate. If the coordination was, on the other hand, outer-sphere, the electric field-gradient might not be greatly enhanced, but the relaxation rate would nevertheless be expected to increase due to an increase in the correlation-time.

In the latter case one might also expect to observe some increase in the relaxation rate of the ^{13}C nuclei of noradrenaline, especially if a 2:1 complex (noradrenaline:Li^+) was formed.

Preparation of solutions. All glassware was freed from possible contamination by paramagnetic ions by being soaked overnight in basic EDTA solution followed by being extensively washed with deionised water. Solutions containing the desired concentrations of lithium chloride (Merck, *p.a.*) and D,L-

0302-4377/82/030235-04$02.50

noradrenaline hydrochloride (Fluka, *purum*) were prepared in a nitrogen atmosphere, using nitrogen-degassed solvents and solutions, and sealed under nitrogen into the sample tubes. The pH of the solutions were measured using a pH-meter with a combined glass-calomel electrode, pD = 7 was approximated by adjusting to a pH-meter reading of 6.6.[9] Adjustments were made by the addition of small quantities of LiOH solution in the case of H_2O solutions and of NaOD solution in the case of D_2O solutions. The final $[Na^+]$ of the latter solutions did not exceed 0.01 M compared with an $[Li^+]$ of 2 M.

Measurement and calculation of T_1. T_1 measurements were made using a JEOL FX-100 spectrometer operating at a frequency of 25.05 MHz with proton noise-decoupling for ^{13}C and at a frequency of 38.71 MHz for ^7Li. Measurements on ^{13}C were performed on D_2O solutions using 5 mm tubes filled to a depth of 2.6 cm. Measurements on ^7Li were performed in H_2O solution. In the latter case, the samples were contained in spherical cells of approximately 6 mm diameter inserted into 10 mm tubes containing a few mls of D_2O as lock-substance, see Fig. 1.

The Fast Inversion-Recovery Fourier Transform (FIRFT) technique,[10] which uses the pulse-sequence $(-180°-t_i-90°-\text{Acquire}-\text{Pulse-delay}-)_n$, was used for measuring T_1. The FIRFT experiment is optimally efficient when the waiting time (W = Pulse-delay + Acquisition-time) is made to be $2T_B$ where T_B is the longest T_1 to be measured in a given experiment.[11] This optimal value of T_B was used in all of the ^7Li measurements; however, $W = 2.5T_B$ and $W = T_B$ were used in the two ^{13}C experiments. T_1 was calculated by a non-linear least-squares fit[12] of the data to eqn. (1): $M_{t_i} = M_0[1-\{1+I[1-\exp(-W/T_1)]\}\cdot\exp(-t_i/T_1)]$.[13] (1) In this equation I is a B_1-inhomogeneity parameter whose input value is calculated as described in Ref. 13 from relative peak-intensities obtained after the application of 90 and 270° pulses. M_0 and T_1 were treated as variable- and I and W as fixed-parameters in the fitting procedure. At least eight different values of t_i were used in each determination and the resulting T_1 values given in Tables 1 and 2 are the result of at least one determination on at least two separately-prepared samples. Inaccuracies in the measured T_1 values caused by inhomogeneities in the radio-frequency field (B_1) become more serious as W is decreased.[13] This problem could be decreased in the case of ^7Li measurements by using a small spherical sample placed centrally in the receiver coil (Fig. 1). However, the use of small samples for the ^{13}C measurements would have necessitated much longer experimental times due to the low concentrations of noradrenaline achievable. The use of eqn. (1) takes into account the B_1-inhomogeneity by the application of an inhomogeneity parameter I which can be measured experimentally. We have tested the use of eqn. (1) to calculate T_1 on data obtained from normal-sized (2.6 cm depth in 5 mm tubes) samples in our NMR instrument. Undegassed samples containing (by volume) 80 % cyclohexanol and 20 % C_6D_6 were used. Data for the calculation of the ^{13}C T_1's of cyclohexanol were obtained using the FIRFT sequence with various values of W. T_1 values were then calculated using a non-linear least-squares fit to eqn. (1) at

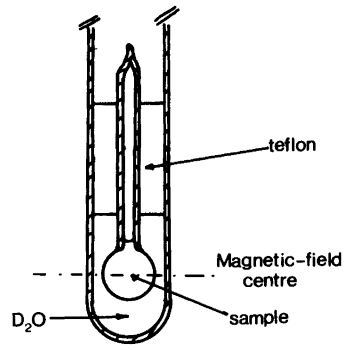

Fig. 1. Sample-arrangement for T_1 measurements on ^7Li.

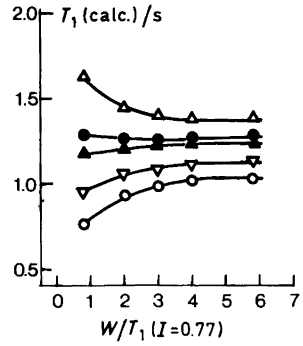

Fig. 2. Plot of calculated T_1 values from eqn. (1) against waiting-time W using different input values of inhomogeneity parameter I. △, $I = 0.7$; ●, $I = 0.77$; ▲, $I = 0.8$; ▽, $I = 0.9$; ○, $I = 1.0$. Experimental data are from C-3,5 in cyclohexanol.

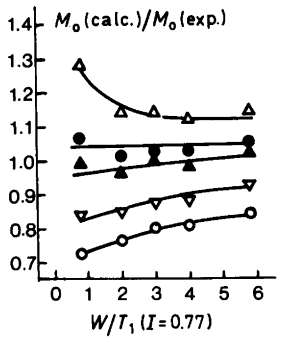

Fig. 3. Plot of $M_{o(calc.)}/M_{o(exp.)}$ against waiting-time W using different input values of the inhomogeneity parameter I. △, $I=0.7$; ●, $I=0.77$; ▲, $I=0.8$; ▽, $I=0.9$; ○, $I=1.0$. Experimental data are from C-3,5 in cyclohexanol.

various input values of the inhomogeneity parameter I. The inhomogeneity parameter was also measured experimentally. Results for the C-3,5 in cyclohexanol are plotted in Fig. 2. As can be seen, the calculated T_1 values are relatively constant with change in W when the input I lies between 0.77 and 0.80 agreeing well with the measured value of I which was 0.79 (0.02). Larger and smaller values of I cause increasing dependency of $T_{1(calculated)}$ on W. Special attention is drawn to the large variation in $T_{1(calculated)}$ when I is given the value of 1, corresponding to the situation when results are calculated without taking into account B_1-inhomogeneity. It is also worth noting that even when $W=5T_1$ (Inversion-Recovery conditions), the T_1 values calculated without taking B_1-inhomogeneity into account are about 17 % lower than those calculated taking it into account. That the results obtained when B_1-inhomogeneity is taken into account are more correct, is supported by the data in Fig. 3, which is a plot of M_0 determined experimentally, divided by M_0 calculated from eqn. (1), against W. $M_{0(experimental)}$ was obtained by including a pulse-interval (t_i) of approximately $5T_1$ in the experiments. The M_0 (calc.) values are closest to M_0 (exp.) when I is the experimentally measured value.

Measurement of I on each of the noradrenaline-containing samples was impractical due to the very long experimental times which would have been required. Instead a value of $I=0.80$ (0.02) measured on a 2.6 cm deep sample of 0.6 M sucrose in D_2O was used in the calculation of T_1 from noradrenaline ^{13}C data. I was also measured on a 0.6 M sucrose solution containing 2 M LiCl to ensure that the high salt-concentration did not alter I. The result was the same within experimental error. B_1-inhomogeneity was also taken into account in calculating ^{7}Li data, but here, I was measured on the relevant sample.

The probe-temperature was controlled by a JEOL temperature-control unit at 38 °C (calibration after every experiment by the use of methanol and ethylene glycol samples) and at least 20 min were allowed for thermal equilibration of the samples before measurements were begun. In order to avoid variations in temperature between pairs of samples (*e.g.* ^{7}Li T_1 measured with and without noradrenaline) due to possible inaccuracies in resetting the temperature-control unit, the second of a pair was always run directly after the first without readjustment of the temperature.

Discussion. Our suggestion that noradrenaline (*1*) might be complexed by lithium ions, stems from the observation that this catecholamine contains four potential ligand groups. As the predominant form of noradrenaline at pH 7 is likely to be the cation (*2*),[14,15] complex formation at the side-chain might be disfavoured, but this still leaves the possibility of complexation by the two aromatic hydroxyl groups. Complexation could result in either the 1:1 species (*3*) or the 2:1 species (*4*). The formation of (*3*) would be reflected in a powerful decrease in the ^{7}Li T_1 due to both an increase in correlation time and an increase in the electric field-gradient at the metal nucleus. Formation of (*4*) would result in a decreased ^{7}Li T_1 due to the increase in correlation-time of the complex over that of the free ion; furthermore, there should be a decrease in the ^{13}C T_1 due to an increased correlation time of a 2:1 complex over that of the uncomplexed molecule. By consideration of the results of Jagur-Grodzinski *et al.*[4] we estimate that the formation of complexes with formation constants of around 10^{-1} M or

Table 1. ^{7}Li longitudinal relaxation times. $[Li^+]=$ 0.02 M, H_2O solution pH7, 38 °C.

[Noradrenaline]/M	T_1/s[a]
0.0	23.6
0.2	22.3

[a] ±10%.

Table 2. ^{13}C longitudinal relaxation times. [Noradrenaline] = 0.2 M, D_2O solution pD7, 38 °C.

Carbon No.[a]	T_1/s[b]		$T_1(-Li^+)/T_1(+Li^+)$
	$Li^+ = 0.0$ M	$Li^+ = 2.0$ M	
2	1.5	1.1	1.4
5	1.5	1.1	1.4
6	1.4	1.2	1.2
7	1.8	1.5	1.2
8	0.9	0.7	1.3

[a] Assignments according to Ref. 14. [b] ±12%.

less should be possible by application of T_1 measurements to this system.

The results of our studies are given in Tables 1 and 2. Our observation that there is no significant decrease in T_1 either for ^7Li, in the presence of a 10-fold molar excess of noradrenaline, or for ^{13}C of noradrenaline in the presence of a 10-fold molar excess of lithium ions, means that the formation of either (*3*) or (*4*) does not occur to any significant extent in aqueous solution at physiological temperature and pH. The ratio of T_1 in the absence of Li^+ to T_1 in the presence of Li^+ of approximately 1 for all measured carbons, is no more than expected from the difference in viscosity of these two solutions (η 2MLiCl/η H_2O at 25° = 1.2). Our results would also seem to rule out the possibility of complex-formation between lithium and the other neurochemically important catecholamines dopamine and adrenaline as these have similar or worse complexing possibilities than noradrenaline.

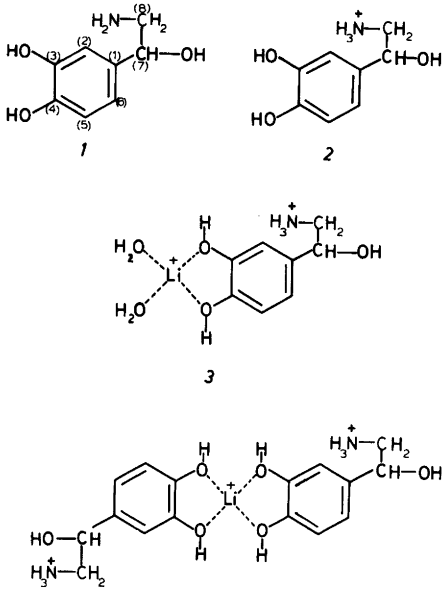

REFERENCES

1. Cooper, J. R., Bloom, F. E. and Roth, R. H. *The Biochemical Basis of Neuropharmacology*, Oxford Univ. Press, New York 1978, p. 190.
2. James, T. L. and Noggle, J. H. *Anal. Biochem. 49* (1972) 208.
3. Andrasko, J. and Forsén, S. *Biochem. Biophys. Res. Commun. 52* (1973) 233.
4. Olsher, U., Elgavish, G. A. and Jagur-Grodzinski, J. *J. Am. Chem. Soc. 102* (1980) 3338.
5. Plaush, A. C. and Sharp, R. R. *J. Am. Chem. Soc. 98* (1976) 7973.
6. Yokono, T., Shimokawa, S. and Sohma, J. *Mem. Fac. Eng., Hokkaido Univ. 14* (1977) 57.
7. Harris, R. K. and Mann, B. E. *NMR and the Periodic Table*, Academic, New York 1978, p. 134.
8. Hertz, H. G., Holz, M., Keller, G., Versmold, H. and Yoon, C. *Ber. Bunsenges. Phys. Chem. 78* (1974) 493.
9. Borzo, M., Detellier, C., Laszlo, P. and Paris, A. *J. Am. Chem. Soc. 102* (1975) 1124.
10. Levy, G. C. and Peat, I. R. *J. Magn. Reson. 18* (1975) 500.
11. Becker, E. D., Ferretti, J. A., Gupta, R. K. and Weiss, G. H. *J. Magn. Reson. 37* (1980) 381.
12. Enwall, E. L. *Non-Linear Least-Squares Programme*, adapted for us by Christian, S., Oklahoma State University.
13. Hanssum, H., Maurer, W. and Rüterjans, H. *J. Magn. Reson. 31* (1978) 231.
14. Haran, R., Nepveu-Juras, F. and Laurent, J.-P. *Org. Magn. Reson. 12* (1979 153.
15. Granot, J. *FEBS Lett. 67* (1976) 271.

Received June 16, 1981.

Acta Chemica Scandinavica A 36 (1982) 239–249

Calcium Phosphate Crystallization. III. Overall Growth Kinetics of Tetracalcium Monohydrogen Phosphate

H. E. LUNDAGER MADSEN

Chemistry Department, Royal Veterinary and Agricultural University, Thorvaldsensvej 40, DK-1871 Copenhagen V, Denmark

The growth kinetics of OCP crystals (OCP = $Ca_4H(PO_4)_3 \cdot 2.5H_2O$) in brushite ($CaHPO_4 \cdot 2H_2O$) suspensions has been investigated by pH-static titration with calcium hydroxide solution. At high supersaturation growth takes place mainly by surface nucleation, whereas at lower supersaturation the growth rate is proportional to $(\beta-1) \ln \beta$, where β is the ratio between the ionic product and the solubility product of OCP, which indicates a spiral growth mechanism. On the basis of the values of the kinetic parameters for spiral growth, including the activation energy, and the edge free energy determined from the rate of surface nucleation, it is shown that the spiral growth follows a BCF surface diffusion mechanism with the rate of incorporation of growth units as the rate-determining step.

In the first paper in this series[1] a study of the kinetics of crystallization of tetracalcium monohydrogen phosphate [$Ca_4H(PO_4)_3 \cdot 2.5H_2O$, "octacalcium phosphate", in the following abbreviated OCP] in suspensions of brushite ($CaHPO_4 \cdot 2H_2O$) under conditions of freely varying pH was reported. The initial supersaturation was very high ($6.4 < \ln\beta < 10.8$, where β is the saturation ratio defined as the ionic product of the substance divided by its solubility product) and it was found that the time lag of crystallization does not follow the classical (Becker-Döring-Volmer) scheme of surface nucleation, but is proportional to $[PO_4^{3-}]^{-2}$, *i.e.* nucleation is a second-order process for an ionic species occurring in very low concentration (of the order of 10^{-8} M). The method suffers from two disadvantages, however: (1) the course of the reaction is very difficult to analyze since the degree of supersaturation is not constant, and (2) we cannot separate the individual contributions from nucleation and from crystal growth to the overall rate of precipitation. It would be desirable to determine the growth kinetics of OCP by measurements on single crystals, but these are very difficult to obtain in good quality, as the substance normally crystallizes in spherulites, and furthermore, the growth rate would be expected to be so low that it could be measured only with difficulty and at very high supersaturation. Instead the overall growth rate of a well-defined, though unknown, number of crystals has been measured; the total surface area may eventually be determined by an adsorption method.

When growth of OCP crystals takes place in a brushite suspension under vigorous agitation it may be assumed that the rate of dissolution of brushite is so much faster than the rate of growth of the OCP crystals that the solution is constantly saturated with respect to brushite. Even if heterogeneous nucleation on the brushite crystals should take place simultaneously with growth of the added OCP seeds, there should be no risk of blocking the surface of the brushite crystals, as shown in previous investigations.[1] We are then dealing with equilibrium in a 2-phase, 3-component system if no foreign component is added, whence, according to the phase rule, there are 3 degrees of freedom. Temperature and pressure are constant, and pH is kept constant by pH-static titration with calcium hydroxide solution. As $Ca(OH)_2$ is one of the components, the system is invariant, and if the amount of OCP is allowed to increase by only a small fraction, *in casu* about 10 %, we should expect an essentially constant rate of precipitation during an experiment. The overall reaction is, omitting water of crystallization

0302-4377/82/030239-11$02.50

$$3CaHPO_4 + Ca(OH)_2 \rightarrow Ca_4H(PO_4)_3 + 2H_2O$$

from which it is seen that apart from the effect of volume increase of the solution, the number of mol of $Ca(OH)_2$ added is equal to the number of mol of $Ca_4H(PO_4)_3$ formed.

The precision of the results reported here is limited by a number of factors. Firstly, there is the amount of substance available for a single series of experiments: The OCP is prepared by hydrolysis of brushite in dilute phosphoric acid, and by this method only a few grams at a time are obtained, permitting not more than about 20 experiments. The product obtained is not sufficiently reproducible with respect to size, defect concentration, and surface properties of the individual crystals to permit pooling of results for different preparations. Another source of uncertainty is the variation in pH which takes place at each addition of $Ca(OH)_2$ as a result of "nonvanishing" mixing time. This variation, though probably not exceeding 0.05 pH units, leads to an uncertainty in β which may amount to as much as 20 %. The results, however, seem to indicate that the uncertainty is substantially lower, but it was preferred not to carry out series of experiments with pH increments of less than 0.1 between successive experiments.

EXPERIMENTAL

Apparatus. The pH-static titrations were carried out with Radiometer equipment comprising an SBR 2 syringe burette recorder, an ABU 11 autoburette unit equipped with a 2.5 cm^2 syringe burette, and either a TTT 1 titrator or a TTT 60 titrator in conjunction with a PHM 64 digital pH-meter. Standard phthalate buffer (pH 4) and standard equimolar phosphate buffer were used for pH calibration.

The temperature of the thermostatted titration vessel was constant within 0.05 K or less.

Materials. Water of adequate purity was obtained by passing ordinary demineralized water first through an activated carbon filter, then through a Silex-1 mixed-bed ion-exchange column. The outflow was monitored with a conductivity meter which indicated a resistivity well above 10^5 ohm m; the resistivity of pure water is 1.8×10^5 ohm m.

Brushite was prepared as described by Tovborg Jensen and Rathlev.[3] The product was sieved, and the fraction passing the 90 μm sieve was used.

OCP was prepared by addition of 16 g brushite (in one case 32 g) to 4 dm^3 10^{-4} or 2×10^{-4} M phosphoric acid at 37 °C under constant stirring. The solution was renewed twice when pH had fallen below 6. At the third run pH stabilized near 6, indicating complete hydrolysis, and calculations showed that the Ca/P molar ratio of the solid phase should now be equal to 1.33. The crystals were filtered off, washed with ethanol, and dried at ambient temperature. The use of dilute phosphoric acid for the hydrolysis ensures a product free from apatite, and X-ray powder diffractometry showed only reflections due to OCP; in any case, the presence of minute amounts of brushite would be of no consequence. Individual crystals of OCP thus obtained were typically 0.01 mm long.

Saturated calcium hydroxide solution used for pH-static titrations was standardized by titration against standardized dilute hydrochloric acid. The calcium hydroxide concentration was about 0.02 M.

Determination of the solubility product of OCP. To 25 cm^3 10^{-4} M H_3PO_4 in a thermostatted vessel were added 0.25 g brushite and 0.25 g OCP. After 3 days of vigorous agitation pH became constant within <0.01. The solubility product of OCP was then calculated from this equilibrium pH value and the known solubility product of brushite[4] ($pK_{sp} = 6.59$).

Determination of growth rate of OCP. To 25 cm^3 phosphoric acid of suitable concentration in a thermostatted vessel was added 0.25 g brushite. The suspension was stirred so rapidly that no solid rested on the bottom, and pH was adjusted to the desired value by dropwise addition of 0.01 M H_3PO_4. When, after a few minutes, equilibrium had been attained, 0.25 g OCP was added and the pH-stat recording was started immediately. After each experiment the vessel, electrodes, stirrer and delivery tube from the burette were rinsed carefully, first with dilute hydrochloric acid to remove all crystal seeds and then with water.

RESULTS

For the sake of consistency, Bjerrum's and Unmack's values[5] for the dissociation constants of phosphoric acid were used together with Bjerrum's values[4] of the solubility products in all the calculations. Activity coefficients were calculated from the Debye-Hückel formula using Kielland's values for the ionic radii.[2]

Bjerrum used the definition (1) of the solubility product of OCP. The measurement of solubility

$$K_{sp} = a(Ca^{2+})^4 a(HPO_4^{2-})^3 / a(H^+)^2 \quad (1)$$

at 25 °C yielded pH = 5.879 for the three-phase equilibrium. This leads to

$pK_{sp} = 10.84$

for OCP at 25 °C with the above definition of K_{sp}.

Values of the equilibrium constants at other temperatures than those at which they have been measured were calculated from the van't Hoff-equation, assuming ΔH^{θ} constant.

Kinetic experiments were carried out at pH values ranging from 5.7 to 7.5, corresponding to $7 < \beta < 10^4$.

The recorded growth curves were perfectly straight lines at high supersaturation, but showed a steadily decreasing slope at low supersaturation. For this reason the initial slope was chosen as representative of the growth rate. All results have been calculated as mol $Ca(OH)_2$ per mol OCP per second.

Fig. 1 shows the results at 37 °C for two different preparations of OCP, one using 10^{-4} M H_3PO_4, the other using 2×10^{-4} M H_3PO_4 yielding larger crystals. Fig. 2 shows the results obtained at four different temperatures using OCP from a third preparation.

DISCUSSION

We see from Fig. 1 that as the level of supersaturation becomes high, there is a tendency for growth rate to level off or even decrease, at least for the larger crystals. This behaviour sets in at somewhat lower supersaturation levels as temperature decreases (Fig. 2).

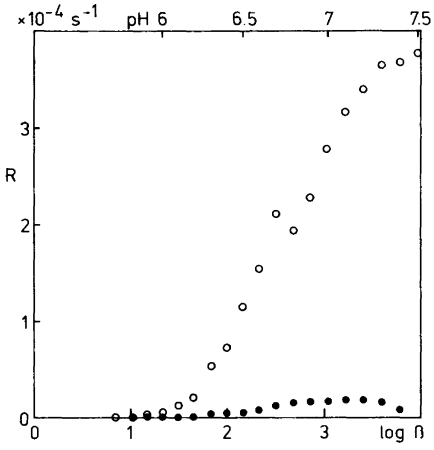

Fig. 1. Growth rate of OCP at 37 °C as a function of supersaturation for two different preparations. Open circles: preparation I, fine crystals. Filled circles: preparation II, coarse crystals.

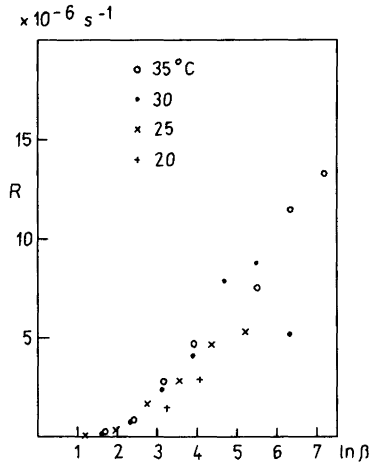

Fig. 2. Growth rate as a function of supersaturation at four different temperatures.

The shape of the curves of R against $\ln \beta$ at lower supersaturations suggests a surface-nucleation mechanism. Assuming a "polynuclear" mechanism and square nuclei, R is given by[6,7] eqn. (2), where λ

$$R = f\{c_i\} \exp(-4\lambda^2 \bar{s}/3k^2T^2 \ln \beta) \quad (2)$$

is the edge free energy, $\bar{s}$ is the surface area of one formula unit, and $f\{c_i\}$ is a function of the concentrations of the different ionic species present. Several expressions for this function are to be found in the literature, but only rather simple systems have been considered, and the approximations used are often valid only for relatively low supersaturations.

At very high supersaturation the exponential tends to 1, and the growth rate then becomes limited by the supply of growth units, *i.e.* calcium and phosphate ions. All phosphate species will probably contribute, because the deprotonation is so fast that it can hardly be rate-determining. We thus postulate that the rate-determining step in the absence of a nucleation barrier is the bimolecular reaction between a calcium and a phosphate ion, which leads to the expression (2a) for R, where [P]

$$R = k_2[Ca^{2+}][P]\exp(-4\lambda^2 \bar{s}/3k^2T^2 \ln \beta) \quad (2a)$$

is the total phosphate concentration in solution. Eqn. (2a) predicts a decrease in growth rate at very high supersaturation due to the decreasing solubility

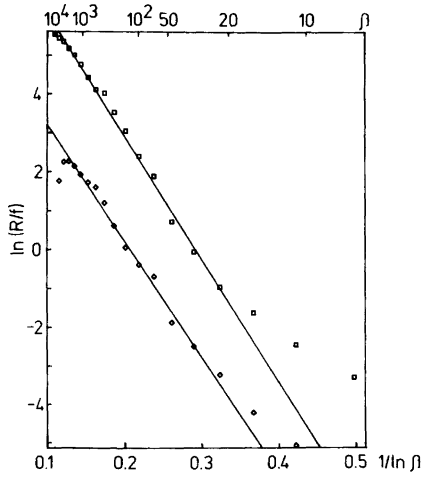

Fig. 3. Test of surface nucleation for preparations I (upper curve) and II (lower curve). $f=[Ca^{2+}][P]$.

of brushite with increasing pH, in good agreement with experiment. If our hypothesis is valid, a plot of $\ln(R/[Ca^{2+}][P])$ against $1/\ln\beta$ should yield a straight line with slope $-4\lambda^2\bar{s}/3k^2T^2$. Fig. 3 shows the result.

Since two parallel lines are obtained for $\ln\beta>3$, the hypothesis is confirmed. The following parameters are found by linear regression:

Upper curve: $\lambda\sqrt{\bar{s}} = 12.6\pm0.1$ kJ/mol
$k_2 = 10\,000\pm2000$ dm^6 mol^{-2} s^{-1}
Lower curve: $\lambda\sqrt{\bar{s}} = 12.2\pm0.2$ kJ/mol
$k_2 = 500\pm100$ dm^6 mol^{-2} s^{-1}
Mean value: $\lambda\sqrt{\bar{s}} = 12.5\pm0.1$ kJ/mol

Putting $\sqrt{\bar{s}}=6.79\times10^{-10}$ m, the cubic root of the molar volume of OCP calculated from unit cell parameters,[8] we find

$$\lambda=3.06\times10^{-11}\ \text{J/m}$$

This is the order of magnitude to be expected for an ionic crystal in aqueous solution. The number of formula units in the critical nucleus is given by eqn. (3), which in the actual range, $3<\ln\beta<9$,

$$N^*=4\lambda^2\bar{s}/(kT\ln\beta)^2 \tag{3}$$

yields values between 1 and 10.

However, the growth rate does not tend to zero with decreasing supersaturation as fast as it should if surface nucleation were the only mechanism, so we must try a BCF mechanism[9,10] as well. The general expression for the surface-diffusion mechanism is eqn. (4), where D_s is the surface-diffusion

$$R=2\frac{D_s\alpha C_o n_{so}\Omega}{x_s y_o}(\beta-1)\tanh(y_o/2x_s) \tag{4}$$

coefficient, n_{so} is the equilibrium surface concentration of growth units, Ω is the volume of a growth unit in the crystal, x_s is the mean distance travelled by a growth unit on the surface, y_o is the distance between steps in the growth spiral, and α and C_o are special correction factors. α is related to the rate of incorporation of growth units into the step and is given by eqn. (5), where τ_k is the time constant for

$$\alpha=\left[1+\frac{D_s C_o\tau_k}{x_s a}\tanh(y_o/2x_s)\right]^{-1} \tag{5}$$

incorporation of growth units, and $a(=\sqrt{\bar{s}})$ is the distance between growth units in the crystal. If τ_k is large, we have $\alpha\ll1$ and, from (4) and (5), eqn. (6),

$$R=2\frac{n_{so}\Omega a}{\tau_k y_o}(\beta-1) \tag{6}$$

which is known as the secondary law due to $\alpha\ll1$. C_o is related to the roughness of the steps and is in general a complicated function of x_o, the distance between kinks, and x_s. If the step is rough, so that $x_o\ll x_s$, then $C_o=1$, but if the step is smooth, the situation depends on how much diffusion along the step contributes to the transport of growth units along the kinks. If $x_s\sim a$, we have[9] eqn. (7) with b

$$C_o=\{1+2b\tanh(y_o/2x_s)[\ln(4bx_s/a[1+(1+b^2)^{\frac{1}{2}}])+(2x_s/y_o)\arctan b]\}^{-1} \tag{7}$$

defined in eqn. (8).

$$b=x_o/2\pi x_s \tag{8}$$

Eqn. (7) is interesting only if $C_o\ll1$ which yields, when inserted into (4) (C_o cancels out if α is not $\simeq1$) eqn. (9).

$$R=2\pi\frac{D_s n_{so}\Omega}{x_o y_o}(\beta-1)\{\ln(4bx_s/a[1+(1+b^2)^{\frac{1}{2}}])+(2x_s/y_o)\arctan b\}^{-1} \tag{9}$$

If $b\gg1$ the first term in braces may be simplified to $\ln(4x_s/a)$, and if $x_s\ll y_o$, the second term may be neglected, and we then obtain eqn. (10), whereas

$$R=2\pi\frac{D_s n_{so}\Omega}{x_o y_o\ln(4x_s/a)}(\beta-1) \tag{10}$$

$x_s \gg y_o$ yields eqn. (11).

$$R = \pi \frac{D_s n_{so} \Omega}{x_s x_o \arctan(x_o/2\pi x_s)} (\beta - 1) \quad (11)$$

In (11) $x_o \gg x_s$ yields $\arctan(x_o/2\pi x_s) \simeq \frac{\pi}{2}$ whence

$$R = 2 \frac{D_s n_{so} \Omega}{x_o x_s} (\beta - 1) \quad (12)$$

whereas $x_o \ll x_s$ yields $\arctan(x_o/2\pi x_s) \simeq x_o/2\pi x_s$ and

$$R = 2\pi^2 \frac{D_s n_{so} \Omega}{x_o^2} (\beta - 1) \quad (13)$$

Let us now return to (4) with $\alpha = C_o = 1$. There are two cases to consider: $x_s \ll y_o$, which leads to $\tanh(y_o/2x_s) \simeq 1$, and $x_s \gg y_o$, which leads to $\tanh(y_o/2x_s) \simeq y_o/2x_s$. The former yields eqn. (14), the so-called

$$R = 2 \frac{D_s n_{so} \Omega}{x_s y_o} (\beta - 1) \quad (14)$$

primary law, and the latter yields eqn. (15).

$$R = \frac{D_s n_{so} \Omega}{x_s^2} (\beta - 1) \quad (15)$$

All the above expressions are based on the assumption of surface diffusion. If this is unimportant, we must consider volume diffusion[9] or direct integration.[10] The former mechanism yields eqn.

$$R = \frac{D N_o \Omega a}{x_o y_o} (\beta(x_o) - 1) \quad (16)$$

(16), where D is the volume-diffusion coefficient, and N_o is the volume concentration of growth units at equilibrium. $\beta(x_o)$, the saturation ratio at the distance x_o from a kink, is given by eqn. (17),

$$\frac{\beta(x_o) - 1}{\beta - 1} = \left[1 + \frac{2\pi a(\delta - y_o)}{x_o y_o} + \frac{2a}{x_o} \ln \frac{y_o}{x_o}\right]^{-1} \quad (17)$$

where δ is the thickness of the diffusion layer. The direct-integration mechanism yields eqn. (18), where

$$R = \frac{l^2 N_o \Omega}{\tau_k' y_o} (\beta - 1) \quad (18)$$

τ_k' is the time constant for the incorporation of growth units, and l has been designated[10] as the mean free path of growth units in solution; however, it should rather be considered a molecular jump distance.[14]

Since $y_o = 19r^*$[11,12], where r^*, the radius of the critical nucleus, is given by the two-dimensional Gibbs-Kelvin equation, eqn. (19), the equations

$$kT \ln \beta = 2\lambda \bar{s}/r^* \quad (19)$$

(6, 10, 14, 16, 18) yield an expression of the

$$R = b(\beta - 1) \ln \beta \quad (20)$$

form (20) whereas (11 – 13, 15) and in some cases (16) yield eqn. (21).

$$R = b(\beta - 1) \quad (21)$$

Figs. 4 and 5 show that (20) accounts well for the growth rate at low supersaturations, but (21) does not. We thus have the following possibilities: (1) a primary law with $x_s \ll y_o$ [eqn. (14)], (2) a secondary law with slow integration [eqn. (6)], (3) a secondary law with widely spaced kinks [eqn. (10)], (4) one of the cases of volume diffusion [eqn. (16)], and (5) direct integration [eqn. (18)].

An important parameter to be considered when choosing a mechanism is the overall activation energy E_a, eqn. (22).

$$E_a = -R \frac{\partial \ln b}{\partial (1/T)} \quad (22)$$

If we plot the results given in Fig. 2 as a function of $(\beta - 1) \ln \beta$, we find b for the different temperatures, and an Arrhenius plot then yields

$$E_a = 33 \pm 3 \text{ kJ/mol}$$

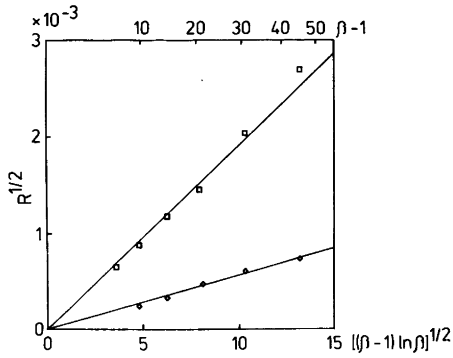

Fig. 4. Test of spiral growth for preparations I (upper curve) and II (lower curve).

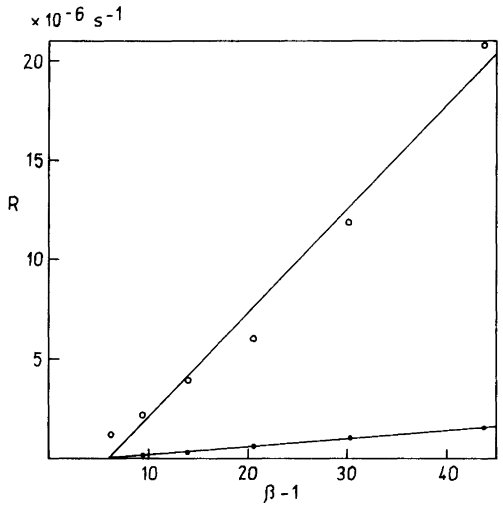

Fig. 5. Test of a linear growth law. The regression lines are drawn in order to show the deviation from linearity more clearly.

Before drawing any conclusions on the basis of this value, we should make clear what is meant by a growth unit in the present case, as the surface or volume concentration of growth units enters into all the expressions to be considered. This question is trivial for non-electrolytes or for congruent solutions of electrolytes, but not for incongruent solutions. Since no really satisfactory discussion of this problem appears to be found in literature, we shall use an *ad hoc* definition based on the following considerations:

It is desirable to define the growth unit in such a way that the formalism developed for simple systems of one solvent and one solute may be applied. This is possible in the present case because, apart from temperature and pressure, the system has only one degree of freedom; as a matter of fact, the system behaves as if we were dealing with the crystallization of calcium hydroxide from solution. The ionic product of OCP, defined in accordance with (1), is given by eqn. (23), where K_B is the solubility

$$Q = a(Ca^{2+})^4 a(HPO_4^{2-})^3/a(H^+)^2 = (K_B^3/K_W^2)a(Ca^{2+})a(OH^-)^2 \quad (23)$$

product of brushite, and K_W is the dissociation constant of water. With the values of the constants inserted, we find at saturation with respect to OCP at 37 °C

$$a(Ca^{2+})a(OH^-)^2 = 3.29 \times 10^{-20}$$

which is, of course, much lower than the actual solubility product of calcium hydroxide.

The standard enthalpy of solution ΔH_d^θ of calcium hydroxide in our system may now be calculated from the temperature coefficients of the constants K_{sp} for OCP, K_B, and K_W. We find

K_{sp}(OCP): $\Delta H_d^\theta = -186$ kJ/mol
K_B : $\Delta H_d^\theta = -4.5$ kJ/mol
K_W : $\Delta H_d^\theta = 56$ kJ/mol

which yields

$$\Delta H_d^\theta = -60.5 \text{ kJ/mol}$$

for calcium hydroxide in our system. This quantity contributes to the overall activation energy calculated from (16) and (18). The total contribution from all the other temperature-dependent factors would then amount to $33-(-60.5)=93.5$ kJ/mol.

In (16), the temperature-dependent factors are N_o, D, x_o, and y_o. The activation energy for volume diffusion may be calculated from the variation of the equivalent conductivity of calcium hydroxide with temperature.[13] We find

$$E_{a,diff} = 11.0 \text{ kJ/mol}$$

In order to calculate the temperature dependence of x_o and y_o, we make use of a set of equations derived by Burton, Cabrera, and Frank.[9] The edge free energy is given by eqn. (24), where ϕ_1 is the

$$\lambda a = \phi_1/2 - kT \ln q \quad (24)$$

nearest-neighbour interaction energy, and q is the partition function per interstice, given by eqn. (25).

$$q = \coth(\phi_1/4kT) \quad (25)$$

The (total) edge energy per interstice is given by

$$U_\lambda = \tfrac{1}{2}\phi_1(1+s) \quad (26)$$

eqn. (26), where s is the roughness, given by eqn. (27).

$$s = 1/\sinh(\phi_1/2kT) \quad (27)$$

If $s \ll 1$, then x_o is approximately equal to a/s.

These equations are strictly valid only for a crystal-vapour system where second-nearest neigh-

bour interaction is negligible. For a crystal-solution system ϕ_1 is somewhat ambiguous; however, if we define it from eqns. (24) and (25), we may consider it as a characteristic parameter of the system and use it in calculating U_λ and s from (26) and (27). The values thus obtained should then be at least approximately correct.

We find accordingly

$\phi_1 = 25.1$ kJ/mol
$s = 0.0155$
$U_\lambda = 12.7$ kJ/mol

As $s \ll 1$, we have

$x_o = a/s = 65a = 438$ Å

This ensures $\beta(x_o) = \beta$ according to (17). We further have

$$\frac{\partial \ln x_o}{\partial (1/T)} = \frac{\phi_1}{2k} \coth\left(\frac{\phi_1}{2kT}\right) \tag{28}$$

which yields the contribution

$E_{a,rough} = 12.5$ kJ/mol

Finally, as

$$y_o = \frac{38\,\lambda \bar{s}}{kT \ln \beta} \tag{29}$$

we obtain a contribution to E_a from eqn. (30), where

$$\frac{\partial \ln y_o}{\partial (1/T)} = \frac{\partial \ln (\lambda/T)}{\partial (1/T)} = \frac{TU_\lambda}{\lambda a} \tag{30}$$

we have made use of the Gibbs-Helmholtz equation. The corresponding contribution to E_a is

$E_{a,spiral} = 2.63$ kJ/mol

The resultant activation energy is

$E_a = \Delta H_d^\theta + E_{a,diff} + E_{a,rough} + E_{a,spiral} = -34$ kJ/mol

This is far below the experimental value, whence we must exclude the BCF volume-diffusion mechanism.

In the expression (18) for the direct-integration mechanism we may probably neglect the temperature-dependence of l, and there are then three factors to consider: N_o, τ_k, and y_o. The expression for the activation energy becomes eqn. (31), where

$$E_a = \Delta H_d^\theta + E_{a,k} + E_{a,spiral} \tag{31}$$

$E_{a,k}$ is the activation energy for the integration process. We cannot calculate this quantity theoretically, but insertion of the other values yields

$E_{a,k} = 91$ kJ/mol

All that can be said for the moment is that this value is acceptable.

In all the expressions for a surface-diffusion mechanism we find the factor n_{so}, the temperature dependence of which is given for a dilute adlayer by[14] eqn. (32), where Γ_1^o is the interface excess of

$$\frac{\partial \ln n_{so}}{\partial (1/T)} = -\frac{\Gamma_1^o a_2^* \Delta H_{1des}^o + \Delta H_{ks}^*}{k} \tag{32}$$

water, a_2^* is the partial molar area of adsorbed growth units, ΔH_{1des}^o is the desorption enthalpy of water, and ΔH_{ks}^* is the enthalpy increment for transfer of growth units from crystal to adlayer (kink→surface). ΔH_{1des}^o and ΔH_{ks}^* are very difficult to calculate for an aqueous electrolyte system, whence we shall not try to exclude any of the remaining possibilities by considering the activation energy.

We may easily show, by considering the conditions for the primary law, that this mechanism is not possible. The conditions are (1) $x_s \ll y_o$ and (2) $C_o \simeq 1$, which is equivalent to $x_s \gg x_o$. We have already calculated x_o. Using (29) we obtain

$$y_o = \frac{184\,a}{\ln \beta}$$

We found that R is proportional to $(\beta - 1) \ln \beta$ up to $\ln \beta = 3.5$, which corresponds to $y_o = 53a$. Comparison of this value with the value of $x_o = 65a$ shows that the two conditions cannot be met simultaneously.

We are thus left with three possible mechanisms: (1) the secondary law due to $\alpha \ll 1$, (2) the secondary law due to $C_o \ll 1$, and (3) the direct integration, and we cannot proceed any further without knowing at least the order of magnitude of the absolute growth rate, which means that we must know the specific surface of the substance. The straightforward way of determining this quantity is by nitrogen adsorption, using the BET isotherm. Unfortunately,

it was impossible to degas the sample sufficiently without losing some of the water of crystallization, and this certainly has some effect on the surface area. However, this result is probably not too far from the true value.

It was found that 4 g of OCP from preparation III (used for activation energy determinations) adsorbed 16.3 cm^3 N_2 at STP. This corresponds to an area of 8750 m^2/mol; the mean linear dimensions of the crystals should then be equal to 0.13 μm, which agrees fairly well with microscopic observations. We may then calculate the absolute value of b in eqn. (20); the result at 37 °C is

$$b = 9.47 \times 10^{-16} \text{ m/s}$$

We have the following expressions for b:

(1) $\alpha \ll 1$:

$$b = \frac{n_{so}\Omega a k T}{19\lambda\bar{s}\tau_k} \tag{33}$$

(2) $C_o \ll 1$:

$$b = \frac{D_s n_{so}\Omega k T}{19\lambda\bar{s}x_o \ln(4x_s/a)} \tag{34}$$

(3) direct integration:

$$b = \frac{l^2 N_o \Omega k T}{38\lambda\bar{s}\tau_k'} \tag{35}$$

We start with case (2): $C_o \ll 1$ means $x_s \ll x_o$ and hence $\ln(4x_s/a)$ must lie between 1 and 5; let us take $\ln(4x_s/a) = 3$. Insertion of the known values leads to

$$D_s n_{so} = 0.0249 \text{ s}^{-1}$$

The minimum value of n_{so} is found if we assume that the concentration in the adlayer is the same as in solution. Assuming further that the effective thickness of the adlayer is equal to a, which is also a lower bound, we find, with a volume concentration of growth units equal to 4×10^{-4} M:

$$n_{so} \geq 1.7 \times 10^{14} \text{ m}^{-2}$$

which yields

$$D_s \leq 1.5 \times 10^{-16} \text{ m}^2 \text{ s}^{-1}$$

As the volume-diffusion coefficient, calculated from conductivity data,[13] is about 8×10^{-9} $m^2 s^{-1}$ for $Ca(OH)_2$ at 37 °C, it is evident that the product $D_s n_{so}$ is too low for surface diffusion to contribute significantly to the transport of growth units to the kinks, whence the secondary law due to $C_o \ll 1$ must be excluded.

In case 3 we assume $l \simeq a$ and find, with $N_o = 4 \times 10^{-4}$ M $= 2.4 \times 10^{23}$ m^{-3}

$$\tau_k' = 0.3 \text{ s}$$

According to the Arrhenius equation we have

$$1/\tau_k' = A \exp(-E_{a,k}/kT) \tag{36}$$

which, with the value of $E_{a,k}$ previously found, yields

$$A = 7 \times 10^{15} \text{ s}^{-1}$$

In order to see whether this value is possible, we make use of collision theory which, although derived for a solid-gas interface, should yield reasonable results also for the solid-solution interface.[15] The collision frequency of growth units is

$$Z = N_o \sqrt{kT/2\pi m} \tag{37}$$

where m is the mass of a growth unit. The number of growth units arriving at a growth site per unit time is A, whence

$$A = Z\bar{s} \tag{38}$$

Insertion of the known values yields

$$A = 8 \times 10^6 \text{ s}^{-1}$$

Comparison of the two values of A shows that the direct-integration mechanism is not possible; growth must be assisted by surface diffusion, and the only possibility remaining is the secondary law due to $a \ll 1$.

We now have

$$n_{so}/\tau_k = 2.79 \times 10^{14} \text{ m}^{-2} \text{ s}^{-1}$$

and as $n_{so} \geq 1.7 \times 10^{14}$ as above, we find

$$\tau_k \geq 0.6 \text{ s}$$

which is a plausible value. The condition $\alpha \ll 1$, with α given by (5), leads to

$$\frac{D_s C_o \tau_k}{x_s a} \tanh\left(\frac{y_o}{2x_s}\right) \gg 1$$

There are two subcases to consider: (1a) $x_s \ll y_o$, which also means $x_s \ll x_o$ and hence

$$\tanh(y_o/2x_s) \simeq 1$$

as well as, from (7)

$$C_o \simeq \frac{\pi x_s}{x_o \ln(4x_s/a)} \ll 1$$

and (1b) $x_s \gg y_o$, which means $x_s \gg x_o$ and hence

$$\tanh(y_o/2x_s) \simeq y_o/2x_s$$

as well as

$$C_o \simeq 1$$

1a yields

$$\frac{\pi D_s \tau_k}{a x_o \ln(4x_s/a)} \gg 1$$

or, with $\ln(4x_s/s) \simeq 3$ as above

$$D_s \tau_k \gg 2.8 \times 10^{-17}\ \mathrm{m}^2$$

An upper bound for τ_k is found by taking $n_{so} = n_o$, the total number of adsorption sites on the surface. We have $n_o = \bar{s}^{-1} = 2.18 \times 10^{18}\ \mathrm{m}^{-2}$ and find, with the above value of n_{so}/τ_k

$$\tau_k \leq 8 \times 10^3\ \mathrm{s}$$

and thus

$$D_s \gg 3.6 \times 10^{-21}\ \mathrm{m}^2\ \mathrm{s}^{-1}$$

There should be no difficulty in fulfilling this condition. On the other hand, 1b yields

$$\frac{\tau_k y_o}{2\tau_{des} a} \gg 1$$

with the substitution $x_s^2 = D_s\, \tau_{des}$, τ_{des} being the time constant for desorption of growth units. We then find

$$\tau_k/\tau_{des} \gg 0.0109 \ln \beta$$

or, as $\ln \beta$ may be at least 3.5

$$\tau_k/\tau_{des} \gg 0.04$$

With the same upper bound for τ_k as above, we have

$$\tau_{des} \ll 2 \times 10^5\ \mathrm{s}$$

which is also easily fulfilled.

From transition-state theory we have[10]

$$\tau_k = (h/kT) \exp(\Delta G_k^{\neq}/kT) \qquad (39)$$

With the limits we have found for τ_k, this yields

$$75 < \Delta G_k^{\neq} < 100\ \mathrm{kJ/mol}$$

We cannot know much about the activation entropy for incorporation; if the adsorbed growth units were unhydrated, we should expect a negative $\Delta S_k^{\neq}$, but the adsorbed calcium ions are probably highly hydrated, and the dehydration prior to incorporation leads to an entropy increase. If we assume $\Delta S_k^{\neq} = 0$, we have $75 < \Delta H_k^{\neq} < 100$ kJ/mol.

Calculating E_a from (6) in the same manner as we did for the other mechanisms yields eqn. (40),

$$E_a = \Gamma_1^{\circ} a_2^* \Delta H_{1des}^{\circ} + \Delta H_{ks}^* + E_{a,spiral} + E_{a,k} \qquad (40)$$

and we find with $E_{a,k} = \Delta H_k^{\neq}$

$$-60 < \Gamma_1^{\circ} a_2^* \Delta H_{1des}^{\circ} + \Delta H_{ks}^* < -45\ \mathrm{kJ/mol}$$

which means that the enthalpy increment for transfer of growth units from the kink to the surface plus the enthalpy increment for desorption of the amount of water occupying the same area as a growth unit is somewhat less negative than the enthalpy of solution, which is to be expected. ΔH_{ks}^* is probably the dominating term and comprises the enthalpy of hydration of calcium ions in the adlayer; we may expect it to be approximately equal to $-\Delta H_k^{\neq}$, which requires a small, positive value of ΔH_{1des}° and a moderately negative value of $\Delta S_k^{\neq}$. This appears reasonable.

Finally we should verify that the kinetic constants of the upper and the lower parts of the curve of R *versus* β agree with each other. At low supersaturation, crystals from preparation I consume calcium

hydroxide 2.2 times as fast as do crystals from preparation III. We therefore assume that the specific area of I is 2.2 times as large as that of III, or 19000 m^2/mol, and we may now recalculate the rate constant k_2 for surface nucleation into absolute growth rate; the result is

$$k_2 = 0.526 \text{ mol m}^{-2} \text{ s}^{-1} \text{ M}^{-2}$$

Under the given conditions, β is an increasing function of pH, and for increasing supersaturation, the right-hand side of (2a) tends to eqn. (41).

$$R_{max} = k_2[Ca^{2+}][HPO_4^{2-}] \quad (41)$$

From the solubility product of brushite we find

$$R_{max} = 3.68 \times 10^{-11} \text{ m/s}$$

The growth rate resulting from the polynuclear mechanism is[6,7]

$$R = d(\frac{\pi}{3} J n_o v^2)^{1/3} \quad (42)$$

where d is the thickness of a crystal layer ($=a$), J is the rate of nucleation at a site, and v is the rate of advancement of a step; the nuclei are assumed to be circular. Inserting known parameters yields for the limiting rate of nucleation

$$J_{max} v^2_{max} = 7.01 \times 10^{-23} \text{ m}^2 \text{ s}^{-3}$$

where v_{max} is the limiting rate of advancement of a step. The number of growth units being incorporated per unit length of step and per unit time is given by[10]

$$J_{step} = 2\frac{a n_{so}}{\tau_k}(1-\alpha)(\beta-1) \quad (43)$$

In the present case we have $\alpha \ll 1$, and the limiting value of J_{step} is found by substituting n_o for n_{so} $(\beta-1)$, taking into account the non-ideality of a concentrated adlayer.[16] Further, the rate of advancement of a step is related to J_{step} by

$$v = J_{step}\bar{s} \quad (44)$$

whence, as $n_o = \bar{s}^{-1}$

$$v_{max} = 2a/\tau_k \quad (45)$$

which yields, with the limits of τ_k found above,

$$1.7 \times 10^{-13} < v < 2.3 \times 10^{-9} \text{ m/s}$$

and then

$$1.38 \times 10^{-5} < J_{max} < 2400 \text{ s}^{-1}$$

J_{max} is presumably approximately equal to $1/\tau_k$; we should then have

$$\tau_k = 30 \text{ s}$$

and

$$J_{max} = 0.03 \text{ s}^{-1}$$

As both τ_k and J_{max} are found within the permitted limits, we have now seen that the kinetic constants of spiral growth and of surface nucleation agree well with each other

CONCLUSION

The analysis of the crystal growth kinetics of OCP has been performed along the same lines as those followed previously for paraffin crystals.[17] An aqueous electrolyte system is, however, less suited for detailed theoretical calculations than nonpolar crystals in a nonpolar solvent. In spite of this, it has been possible to demonstrate that at low supersaturation growth takes place according to a surface-diffusion (BCF) mechanism in which the rate-determining step is the incorporation of growth units into the kinks. It is reasonable to assume that the adsorbed calcium ions are highly hydrated, though probably less so than in solution, and that the dehydration which must take place prior to incorporation into the growth site is a slow process in comparison with surface diffusion. This assumption is borne out by numerous examples of the rule that anhydrous salts crystallize much more slowly than their hydrated counterparts.[18]

Two observations have not been discussed: the decrease of growth rate with time at low supersaturation, and the sudden transition from spiral growth to surface nucleation at a certain supersaturation, as compared to the mixed kinetics of hexatriacontane in light petroleum.[17] Both are probably morphological phenomena like habit change during growth and cooperation of growth spirals. A growth pyramid which is not a spiral may

even originate from repetitive nucleation at the same point,[19] *i.e.* without the intervention of a screw dislocation, and such a pyramid may eventually disappear. These hypotheses are, however, very difficult, if not impossible, to test experimentally.

Acknowledgements. This work was supported financially by NATO Research Grant No. 1438 and by a grant from the Carlsberg Foundation's Legacy for the Royal Veterinary and Agricultural University. The author wishes to thank Mrs. L. Klein for technical assistance.

REFERENCES

1. Madsen, H. E. L. *Acta Chem. Scand. 24* (1970) 1677.
2. Kielland, J. *J. Am. Chem. Soc. 59* (1937) 1675.
3. Jensen, A. T. and Rathlev, J. *Inorg. Syn. 4* (1953) 20.
4. Bjerrum, N. *Nordiska (19. skandinaviska) Naturforskarmötet*, Helsingfors 1936, p. 344.
5. Bjerrum, N. and Unmack, A. *K. Dan. Vidensk. Selsk. Mat.-Fys. Medd. 9* (1929) No. 1.
6. Cahn, J. W., Hillig, W. B. and Sears, G. W. *Acta Metall. 12* (1964) 1421.
7. Hillig, W. B. *Acta Metall. 14* (1966) 1868.
8. Brown, W. E. *Nature 196* (1962) 1048.
9. Burton, W. K., Cabrera, N. and Frank, F. C. *Philos. Trans. R. Soc. London 243* (1951) 299.
10. Bennema, P. and Gilmer, G. H. *Kinetics of Crystal Growth;* In Hartman, P., Ed., *Crystal Growth, An Introduction*, North-Holland, Amsterdam 1973, p. 263.
11. Cabrera, N. and Levine, M. M. *Philos. Mag. 1* (1956) 450.
12. Budevski, E., Staikov, G. and Bostanov, V. *J. Cryst. Growth 29* (1975) 316.
13. Robinson, R. A. and Stokes, R. H. *Electrolyte Solution*, Butterworth, London 1955.
14. Madsen, H. E. L. *J. Cryst. Growth 39* (1977) 250.
15. van Leeuwen, C. and Blomen, L. J. M. J. *J. Cryst. Growth 46* (1979) 96.
16. Madsen, H. E. L. *J. Cryst. Growth 46* (1979) 495.
17. Madsen, H. E. L. and Boistelle, R. *J. Cryst. Growth 46* (1979) 681.
18. Jensen, A. T. *Ark. Kemi 30* (Hägg-festskrift) (1968) 165.
19. Frank, F. C. *Personal communication.*

Received June 19, 1981.

Acta Chemica Scandinavica A 36 (1982) 251–258

Crystal Structure and Topological Interpretation of the β-Modification of Silver(I) Diethyldithiocarbamate

HELGA ANACKER-EICKHOFF, ROLF HESSE, PER JENNISCHE and ANDERS WAHLBERG

Institute of Chemistry, University of Uppsala, Box 531, S-751 21 Uppsala, Sweden

The crystal structure of the β-modification of silver(I) diethyldithiocarbamate, $AgS_2CN(C_2H_5)_2$, has been determined by X-ray diffraction. The crystals are monoclinic. Space group $C2/c$; $a=18.406(3)$, $b=9.726(2)$, $c=14.305(4)$ Å, $\beta=104.79(3)°$, $Z=12$. The silver atoms and the ligands are linked in chains running along c. The silver atoms are four coordinated with Ag–S in the range 2.5 to 3.0 Å. The structure is compared to the less regular α-modification using a new type of topological maps which reveal similarities also with a large number of other sterically restricted coordination compounds.

The dialkyldithiocarbamates of the univalent coinage metals, copper, silver and gold, belong to a class of compounds where sterical restrictions strongly influence the crystal structures. Successful metal coordination requires that the ligands are arranged closely around the metal atom but the large and bulky ligands are not easily arranged in such a manner. This conflict may be solved by the formation of low polymers or chain or layer polymers. These complex structures, of which a large number have been determined at this Institute, may be difficult to grasp and to analyze. We present here, along with the crystal structure of the β-modification of silver(I) diethyldithiocarbamate, some topological tools for the interpretation and understanding of these structures.

The crystal structure of silver(I) diethyldithiocarbamate, was studied by Hesse.[1] By X-ray powder diffraction he discovered that the compound crystallized in two forms when prepared according to Åkerström.[2] However, crystals suitable for structure determination were found for only one of the forms. The structure determined by Hesse for this α-modification has been verified by Yamaguchi *et al.*[3] and again by us. There are no significant differences between the three determinations. Suitable crystals of the other form, the β-modification have now been prepared.

EXPERIMENTAL

Silver(I) diethyldithiocarbamate was obtained on mixing aqueous solutions of silver nitrate and sodium diethyldithiocarbamate trihydrate. A saturated solution of the dry precipitate in carbon disulfide was cooled to −40 °C. Crystals were obtained after three h. The pale yellow crystals appeared as six-sided plates. The cell parameters were based on 34 lines from a Guinier-Hägg powder photograph with $CrK\alpha_1$ radiation ($\lambda=2.28962$ Å) and silicon ($a=5.43054$ Å) as an internal standard. The density was measured by flotation using an aqueous solution of K_2HgI_4.

Crystal data. $AgS_2CN(C_2H_5)_2$. Monoclinic. Unit cell parameters: $a=18.406(3)$, $b=9.726(2)$, $c=14.305(4)$ Å, $\beta=104.79(3)°$. $Z=12$, $D_m=2.051$ g cm^{-3}, $D_x=2.062$ g cm^{-3}, $\mu(MoK\alpha)=27.8$ cm^{-1}. Systematic absences: hkl for $h+k=2n+1$ and $h0l$ for $l=2n+1$. Possible space groups: Cc (No. 9) and $C2/c$ (No. 15).

The intensity data were collected on a Stoe-Philips four-circle PDP 8/I computer-controlled diffractometer with graphite monochromatized $MoK\alpha$ radiation ($\lambda=0.71069$ Å) and with the $\omega-2\theta$ scan technique. The faces of the crystal were (001), (100), (110) and ($\bar{1}10$), and the corresponding approximate inter-planar distances were 0.03, 0.20, 0.15 and 0.17 mm. The count rate was reduced by a factor 2^n, $0\leq n\leq 3$ (scan time and one filter). The longest scan time was 141 s, and the background intensities were measured for 20 s on each side of a peak. Reflexions within $-21\leq h\leq 21$,

0302-4377/82/030251-08$02.50

$-11 \leq k \leq 0$, $0 \leq l \leq 17$ and $\sin\theta/\lambda \leq 0.60$ Å^{-1} were recorded. The intensities of three standard reflexions, 040, $\bar{1}0$ 0 4 and 006, measured at intervals of 40 reflexions, varied by less than ± 3.4 %. Correction were made for background, Lorentz, polarization and absorption effects. A total of 2501 intensities were reduced to 2181 independent structure amplitudes. Of these 1737 having $|F_m| \geq 2\sigma(F)$, $|F_m|/|F_c| \leq 2.0$ and $\sin\theta/\lambda > 0.060$ Å^{-1} were used in the final refinement.

The approximate positions of the silver atoms were obtained from the three-dimensional Patterson function. The sulfur, nitrogen and carbon atoms were located in difference syntheses assuming the non-centrosymmetric space group *Cc*. No attempt was made to locate the hydrogen atoms. The scale factor, the coordinates and the thermal parameters (anisotropic for silver and sulfur, isotropic for nitrogen and carbon) were refined by full-matrix least squares. The expression minimized was $\Sigma w(|F_m| - |F_c|)^2$, where $w^{-1} = \sigma^2(F) = \sigma^2_{count}(F) + (0.05|F_m|)^2$. As the structure turned out to possess center of symmetry the refinement was terminated using the space group *C*2/*c* with one of the silver, carbon and nitrogen atoms placed in the special position (e): 0 *y* 1/4, 0 $\bar{y}$ 3/4. The refinement converged at $R(F) = 0.065$ and $R_w(F) = 0.103$. The final shifts were all smaller than 0.10 of the estimated standard deviations. The fractional coordinates and the thermal parameters are presented in Tables 1 and 2. Lists of structure factors may be obtained on request from the authors. For Ag, S, N and C the scattering factors and the f' and f'' anomalous dispersion corrections were taken from *International Tables for X-Ray Crystallography*.[4] Lundgren[5] has described the computer programs. The calculations were performed on the IBM 370/155–158 and IBM 1800 computers in Uppsala.

DESCRIPTION AND DISCUSSION

General Features. The silver atoms and the diethyldithiocarbamate ligands are linked together by Ag–S bonds to form unlimited chains parallel to *c*. The only contacts between different chains are of the van der Waals type. Fig. 1 shows a part of a

Table 1. Fractional coordinates and isotropic thermal parameters B (Å^2) defined from $\exp\{-B[(\sin\theta)/\lambda]^2\}$.

	x	*y*	*z*	*B*
Ag1	0.0	−0.0552(1)	0.2500	
Ag2	−0.01838(5)	0.1253(1)	0.44914(7)	
S1	0.0749(1)	0.1802(3)	0.2259(2)	
S2	−0.1220(1)	−0.0852(3)	0.4888(2)	
S3	−0.0760(1)	0.1773(2)	0.5980(2)	
N1	0.0	0.4029(11)	0.2500	2.9(2)
N2	−0.2066(4)	0.0472(8)	0.5833(5)	2.9(1)
C1	0.0	0.2714(14)	0.2500	2.9(2)
C2	0.0631(6)	0.4882(11)	0.2319(7)	3.7(2)
C3	0.0450(6)	0.5174(12)	0.1209(8)	4.2(2)
C4	−0.1402(5)	0.0439(9)	0.5606(6)	2.8(2)
C5	−0.2603(6)	−0.0677(11)	0.5594(7)	3.6(2)
C6	−0.3159(6)	−0.0472(12)	0.4624(8)	4.0(2)
C7	−0.2343(7)	0.1704(13)	0.6276(9)	4.8(2)
C8	−0.2116(9)	0.1495(19)	0.7392(12)	7.0(4)

Table 2. Anisotropic thermal parameters b_{ij} defined from $\exp(-b_{11}h^2 - \cdots - 2b_{23}kl)$.

	b_{11}	b_{22}	b_{33}	b_{12}	b_{13}	b_{23}
Ag1	0.00339(5)	0.0091(1)	0.00643(9)	0.0	−0.00007(5)	0.0
Ag2	0.00406(4)	0.0133(1)	0.00744(7)	0.00169(5)	0.00315(4)	0.00388(7)
S1	0.00293(9)	0.0088(3)	0.0059(2)	0.0005(1)	0.00164(9)	−0.0003(2)
S2	0.00294(9)	0.0101(3)	0.0051(2)	−0.0006(1)	0.00163(9)	−0.0027(2)
S3	0.00260(8)	0.0067(3)	0.0051(1)	−0.0004(1)	0.00121(9)	−0.0004(2)

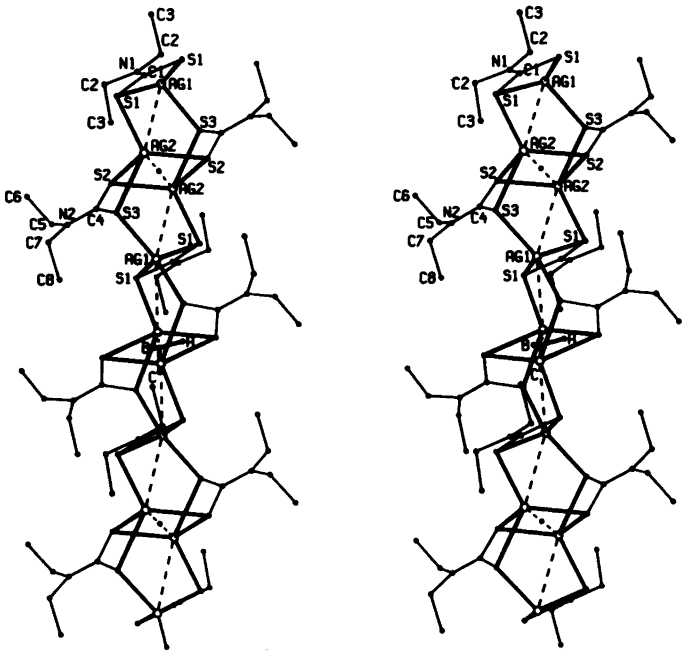

Fig. 1. The chain structure in the β-modification of silver(I) diethyldithiocarbamate.

chain which can be described as built of *monomers* of the metal-ligand unit with twofold rotational symmetry alternating with centrosymmetric *dimers* with their centres at 0,0,0 and 0,0,1/2. The silver atoms Ag1 belong to the monomers and Ag2 to the dimers. In the monomers the silver, central carbon and nitrogen atoms are situated on the twofold axes, $0,y,1/4$ and $0,\bar{y},3/4$, the carbon–nitrogen vectors pointing alternately in the $+b$ and $-b$ directions. The silver atoms form a zig-zag chain close to the plane $x=0$. One short and two long Ag···Ag distances are repeated periodically along the chain. The short distances, 2.83 Å, occur within the dimers and the long distances, 3.44 Å, between the dimers. The angles in the silver chain are 118.5° at Ag1 and 85.7° at Ag2.

The bond distances and angles of the ligands (Table 3) have usual values, and the C_2NCS_2

Table 3. Distances (Å) and angles (°) in the diethyldithiocarbamate ligands.

S1–C1	1.746(7)	S1–C1–S1	118.9(8)
C1–N1	1.278(18)	S1–C1–N1	120.6(4)
N1–C2	1.503(12)	C1–N1–C2	123.5(5)
C2–C3	1.564(15)	C2–N1–C2	113.0(11)
S2–C4	1.709(9)	N1–C2–C3	107.5(7)
S3–C4	1.744(9)	S2–C4–S3	120.6(5)
C4–N2	1.342(11)	S2–C4–N2	119.5(7)
N2–C5	1.474(13)	S3–C4–N2	119.7(7)
N2–C7	1.504(15)	C4–N2–C5	121.7(8)
C5–C6	1.512(15)	C4–N2–C7	123.3(8)
C7–C8	1.557(21)	C5–N2–C7	114.9(8)
		N2–C5–C6	111.7(9)
		N2–C7–C8	107.3(11)

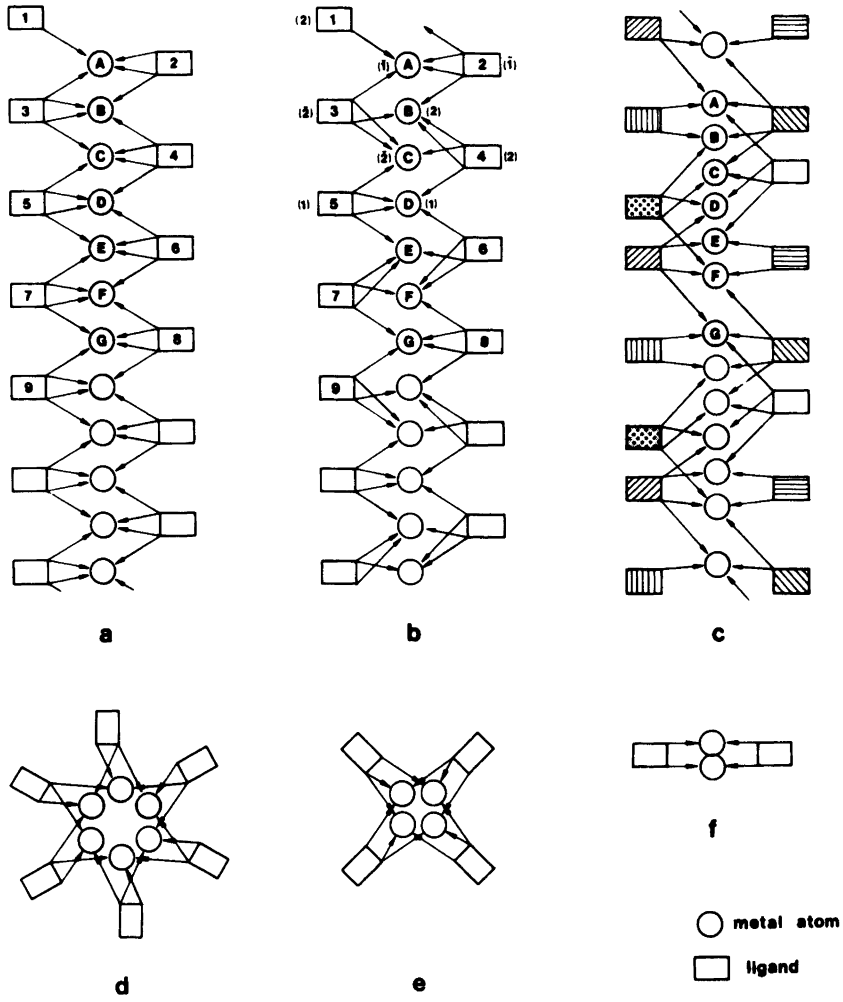

Fig. 2. Schematic representations of AX structures. The ligands are labelled 1, 2, 3, ... and the metal atoms are given alphabetical notations. In Fig. 2b the extra notations (1), ($\bar{1}$) correspond to the monomers and (2), ($\bar{2}$) to the dimers discussed in the text.

fractions of the ligand molecules are almost planar. The outer carbon atoms are in *trans*-position which is the usual case. As a contrast, two of the ligands of a hexamer in the α-modification[3] occur in *cis*-position which may be a consequence of the complicated linkage in that structure.

Coordination and geometrical dependencies. The coordination net formed by the linkage between the metal atoms and the ligands is schematically illustrated in Fig. 2b. The silver atoms are four-coordinated and the sulfur atoms two-coordinated. Each silver atom is coordinated by three ligands, one of which by chelate formation.

The silver coordination polyhedra are distorted tetrahedra. The distances of coordination vary from 2.51 to 2.95 Å (Table 4). The smallest S–Ag–S angles, 64.4 and 66.6°, are found in the chelate rings. The remaining larger angles, 102.5 to 127.6°, illustrate a tendency of the silver atoms to maintain a regular coordination environment despite the restrictions imposed by the chelate rings. The coordination angles are, however, also influenced

Table 4. Some distances (Å) and angles (°) in the chain structure.

Ag2···Ag2^i	2.831(2)	Ag1···Ag2···Ag2^i	85.7(1)
Ag1···Ag2	3.436(1)	Ag2···Ag1···Ag2^i	118.5(1)
Ag1 – S1	2.739(3)	Ag1 – S1 – Ag2	81.6(1)
Ag1 – S3	2.558(3)	Ag2 – S2 – Ag2^i	61.5(1)
Ag2 – S1	2.511(3)	Ag1 – S3 – Ag2	110.4(1)
Ag2 – S2	2.540(3)		
Ag2 – S3	2.658(3)	S1 – Ag1 – S1^i	66.6(1)
Ag2 – S2^i	2.951(3)	S1 – Ag1 – S3	117.7(1)
		S1 – Ag1 – S3^i	108.1(1)
Ag1 – S1 – C1	87.3(4)	S3 – Ag1 – S3^i	124.7(1)
Ag1 – S3 – C4	95.5(3)	S1 – Ag2 – S2	120.4(1)
Ag2 – S1 – C1	99.1(1)	S1 – Ag2 – S3	127.6(1)
Ag2 – S2 – C4	103.9(3)	S1 – Ag2 – S2^i	102.5(1)
Ag2 – S3 – C4	89.5(3)	S2 – Ag2 – S3	109.1(1)
Ag2 – S2^i – C4	80.9(3)	S2 – Ag2 – S2^i	118.5(1)
		S3 – Ag2 – S2^i	64.4(1)

by other geometrical details of the structure, *e.g.* the Ag – S – Ag and the Ag – S – C angles.

The Ag – S – Ag angles are between 61.5 and 110.4° (Table 4). The lowest angle is found in the S2 – Ag2 – $\overline{S2}$ – $\overline{Ag2}$ parallelogram of the dimer. Since the metal – sulfur – metal angles show similar strong variations in a number of other dithiocarbamates there seems to be no pronounced restrictions in these angles.

The metal – sulfur – carbon angles have a remarkable stability in a number of sulfur complexes of copper, silver and gold. In unchelated compounds their values are usually in the range 100 – 110° as pointed out by Jennische.[6] In the present compound the Ag – S – C angles have low values in the chelate rings, 80.9 – 89.5° as can be expected, whereas the unchelated angles are in the range of 95.5 – 103.9°. These angles are of considerable importance as they may influence the geometry of the coordination net by imposing sterical restrictions. They are also related to the orientations of the ligands and accordingly to the packing possibilities.

Interdepencies of the angles and distances in molecular and crystal structures have been given explicit attention by Hesse in a degree of freedom rule.[7] Consider the parallelogram S2 – Ag2 – $\overline{S2}$ – $\overline{Ag2}$ as an example. The small Ag2 – S2 – $\overline{Ag2}$ angles, 61.5°, can be considered as the geometrical consequence of the angles S2 – Ag2 – $\overline{S2}$ which have a value, 118.5°, close to the average of 116°, for the non-chelated S – Ag – S angles. The short Ag2 – $\overline{Ag2}$ distance, 2.83 Å, and the long Ag2 – S2 distance, 2.95 Å, which occur in the same parallelogram may also be interpreted by the interdependencies. A long silver – sulfur distance (Ag2 – S3, 3.57 Å), which is considered to be outside the range of coordination, may be interpreted analogously.

A more complicated coordination net is found in the α-modification of silver(I) diethyldithiocarbamate[3] (Fig. 2c) which represents a border case between high and low polymers. Irregular hexamers may be discerned and they are linked in chains by weak bonds only, Ag – S = 2.99 Å. Two of the six silver atoms have fourfold coordination, the others threefold. Two ligands coordinate to only two metal atoms, the others to four. Five short metal – metal distances occur in each of the hexamers. In the present structure, the β-modification, which is a true high polymer, all the silver atoms have fourfold coordination and all the ligands are linked to three metal atoms. There are only two short metal – metal distances per six silver atoms.

The hypothetical structure of Fig. 2a represents the most regular coordination net obtainable in a chain with chelated four-coordinated metal atoms. All the metal atoms are engaged in two double bridges and each double bridge tetragon has two edges in common with adjacent chelate rings. As in the β-modification one would then expect high silver coordination angles in the bridging tetragons and thus short metal – metal distances. In this case, however, all the metal – metal distances would be short.

Regular networks are also found in the low polymers of some coinage metal dithiocarbamates

and thiocarbamates. Hexamers (Fig. 2d) are found in copper(I) dipropylthiocarbamate,[8] silver(I) dipropylthiocarbamate[9] and silver(I) dipropyldithiocarbamate,[10] and tetramers (Fig. 2e) in copper(I) diethyldithiocarbamate.[7] Dimers (Fig. 2f) are formed in the dipropyldithiocarbamate[11] and the dibutyldithiocarbamate[12] of gold(I).

The formation of polymers in these compounds is the obvious result of the tendency of the metal atoms to obtain as high coordination numbers as possible. It is worth noticing that dimers are found only for the compounds of gold(I) which has a marked tendency for twofold linear coordination. For the copper and silver compounds the coordination number increases as the bulk of the ligand decreases. Threefold coordination is found in the tetramers and hexamers. The formation of chains or layers to attain higher coordination is probably prevented by the large size of the ligands as compared to the distances of coordination.

Fourfold coordination is found in the two modifications of the present compound and is likely to be found in the lowest homologues of the series, the dimethyldithiocarbamates of silver and copper. The structures of these compounds have not yet been determined but their high melting points and low solubilities indicate the presence of high polymers. A similar pronounced trend for the metal atom to obtain a higher coordination number in lower dialkyldithiocarbamate homologues has been found in a systematic study of the dithiocarbamates of thallium(I).[6]

Topological maps. The topological map representations given in Fig. 3 have been found to be powerful tools for recognition of linkage patterns, deriving alternatives, comparing common features and excluding sterically unreasonable networks. They have been in use for many years and were briefly mentioned by Hesse at the Sixth International Conference of Coordination Chemistry in 1961 but are published here for the first time.

Let the bonding interaction between a metal atom and a ligand be represented by a *link*. The link then corresponds to a line in an adjacency graph. There is just *one* link between the metal atom and the ligand even if there may be two or several bonds between them. In the topological map a particular link is represented by a square element of a mosaic pattern.

The networks depicted in Fig. 2 are represented by the maps of Figs. 3a–e. Since *links* are considered, the nets 2a and 2b have the same map

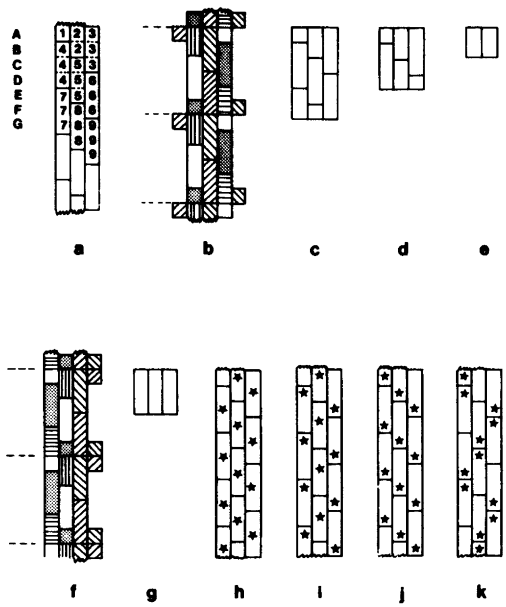

Fig. 3. Topological maps.

representation 3a. The pattern transformations from Fig. 2 to Fig. 3 can easily be followed by the letters, numbers and "colours" given in 2abc and 3 ab. Each horizontal row in Fig. 3 corresponds to a metal atom (A,B,C,,,). Each square element in a row corresponds to a link between the metal atom and a particular ligand. The ligands are labelled 1,2,3... in 3a and "coloured" in 3b as in 2abc.

Since the ligand notations are irrelevant they may be permuted arbitrarily. For the same reason the rows representing the metal atoms can be permuted at will. The order of the elements within a row can also be changed at will. Since the elements represent *links* an element with a given "colour" can only occur once in a row.

Using these permutation rules the elements can be rearranged to form easily recognizable patterns. The links belonging to the same ligand are, for instance, usually ordered to a vertical field as seen in Fig. 3a. In this way geometrically meaningful graphs can be found from the maps.

Relationships between different structures can be seen by comparing motifs in the corresponding topological maps. The structures $(LiCH_3)_4$[13,14] and $[CuS_2CN(C_2H_5)_2]_4$[7] are both represented by the map 3d which is the only way of obtaining threefold linkage of the metal atoms and ligands in a tetramer. As a starting point for bond dis-

cussions one must then ask the question: In which *other* way can the metal atoms and ligands be combined?

The hexamer, 3c, the tetramer, 3d, and the dimer, 3e, represent three possibilities of regular linkage among the low polymers. Fig. 3 shows that they may be cut from the unlimited topological chain, 3a, which is the most regular type of chain with threefold linkage in a compound with the composition AX.

By permutation of columns in 3b (the α-modification) the map 3f is obtained, still representing the same linkage pattern. On comparison of the repeat motif in 3f and 3a (the β-modification) striking similarities are seen which have been used for the construction of the graphs to be discussed in the next section.

The maps may also facilitate the exclusion of topologically possible combinations on sterical grounds. An example of a linkage scheme which is extremely unlikely to be realized in a chemical system is 3g. Three metal atoms would have to coordinate the same three ligands. A map which can be made to contain a section such as that of 3g by a series of allowed permutations must thus be discarded.

The coordination nets of the hypothetical chain, 2a, and the β-modification, 2b, are distinguished by the pattern of the chelate rings. The two structures are thus *chelate isomers*. These chelate isomers are represented by the maps 3h and 3i, where the chelate links are marked by asterisks. Two other isomers which will be discussed are given in the map 3j and 3k.

Topological maps of the type presented here define the combinatorial possibilities and restrictions of the metal–ligand linkage. The maps have been used for the derivation of a large number of theoretically possible networks for low polymers and chains in AX compounds. They can also be used for studies of AX nets in compounds with the composition A_pX_qR. The maps contain only essential information and obviate the large number of zeroes occurring in the combinatorial adjacency or bond order matrices commonly used in graph theory.[15]

The realization in space of topological schemes. Graphs corresponding to the topological maps are readily drawn. Fig. 4a shows the simple graph corresponding to the topological map of the unlimited chain, 3a. Again the notation is that of Fig. 2. The broken line illustrates the metal–metal chain.

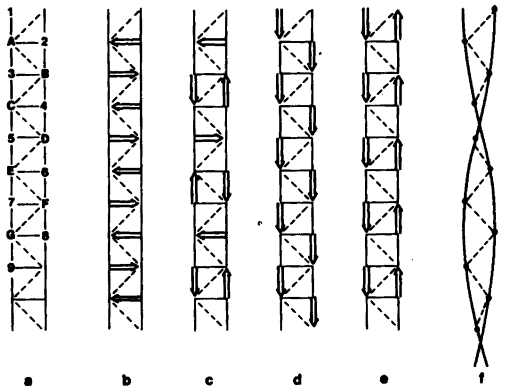

Fig. 4. Alternative chain structures.

Figs. 4b–e show the graphs of the set of chelate isomers 3h–k. The chelate links are denoted by arrows.

The distribution of arrows in Fig. 4 follows certain rules which are evident from the figure. A horizontal arrow as in 4b must be followed either by a horizontal arrow in the opposite direction, 4b, or by a pair of antiparallel vertical arrows, 4c. A vertical arrow, must be followed by a parallel arrow, 4d, or be accompanied by an antiparallel arrow, 4e. It is interesting to note that the pattern of 4d cannot be broken once it has been started. The monomers of 4b and the dimers of 4e may, however, be combined in an infinite number of sequential patterns, the pattern with the shortest repeat distance being that of 4c.

The graph 4c shows that the alternating directions of the monomers in the structure of the β-modification (Fig. 1) is a consequence of the linkage.

Despite its attractive simplicity the linkage scheme of 4b must be discarded for silver(I) diethyldithiocarbamate. Model studies indicate clearly that it cannot be realized in a planar fashion because of collisions between the ligands. If the linkage scheme is to be maintained, a twist must then be introduced so that a helix is formed, 4f. This helix is very likely to be an *irrational helix*, where the rotational repeat angle $h \times 360°$ has a value of h equal to an irrational number. Such irrational helices are not crystallizable. Theoretical aspects of rational and irrational helices and packing will be given in a separate paper.

Planar realizations are unlikely also for the linkage schemes 4d and e. The short repeat distance

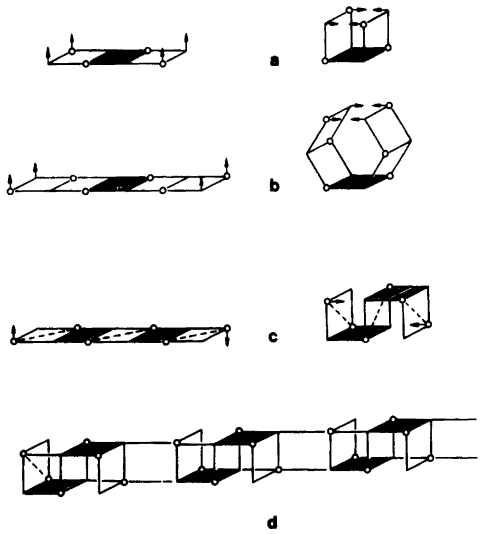

Fig. 5. Folding procedures of chain fragments (Fig. 4a) giving low polymers and the structure of the α-modification of silver(I) diethyldithiocarbamate.

make ligand–ligand collisions unavoidable. The β-modification is represented by 4c. In this scheme the repeat distance is three times as long as in the other three (4b,d,e) making it possible to form the almost planar metal–metal chain.

Instead of twisting the entire chain, which likely would produce an irrational helix, the ligand collisions may be avoided by folding sections of the chain. This is done in the low polymers and in the α-modification.

The simple foldings required to produce the tetramer and hexamer are illustrated in Figs. 5a,b. In this way it is also possible to produce even number polymers of higher polymerity. The metal atoms will always be arranged as antiprisms: linear, trigonal, tetragonal *etc.* Odd number polymers are topologically possible but very unlikely sterically as they will be realized as Möbius strips.

The irregular hexameric units of the α-modification are produced by the more complicated folding shown in Fig. 5c. The linking of the units to produce chains is shown in 5d.

This analysis makes it clear that the two apparently very different modifications of silver(I) diethyldithiocarbamate, as well as the low polymers of other coinage metals dithiocarbamates and thiocarbamates, are sterical realizations of very similar topological patterns.

REFERENCES

1. Hesse, R. In Kirschner, S., Ed., *Advances in the Chemistry of the Coordination Compounds*, Macmillan, New York 1961, p. 314.
2. Åkerström, S. *Ark. Kemi 14* (1965) 387.
3. Yamaguchi, H., Kido, A., Uechi, T. and Yasukouchi, K. *Bull. Chem. Soc. Jpn. 49* (1976) 1271.
4. *International Tables for X-Ray Crystallography*, Kynoch Press, Birmingham 1974, Vol. 4.
5. Lundgren, J.-O. *Crystallographic Computer Programs*, Report UUIC-B13-4-03. Institute of Chemistry, University of Uppsala, Uppsala 1976.
6. Jennische, P. *Acta Univ. Ups. Abst. Ups. Diss. Fac. Sci. 353* (1975) 3.
7. Hesse, R. *Ark. Kemi 20* (1963) 481.
8. Hesse, R. and Aava, U. *Acta Chem. Scand. 24* (1970) 1355.
9. Jennische, P. and Hesse, R. *Acta Chem. Scand. 25* (1971) 423.
10. Hesse, R. and Nilson, L. *Acta Chem. Scand. 23* (1969) 825.
11. Hesse, R. and Jennische, P. *Acta Chem. Scand. 26* (1972) 3855.
12. Jennische, P. *The Crystal Structure of Gold(I) Dibutyldithiocarbamate*, Report UUIC-B20-02. Institute of Chemistry, University of Uppsala, Uppsala 1975.
13. Weiss, E. and Lucken, E. A. C. *J. Organomet. Chem. 2* (1964) 197.
14. Weiss, E. and Hencken, G. *J. Organomet. Chem. 21* (1970) 265.
15. Balaban, A. T. *Chemical Applications of Graph Theory*, Academic, London 1976.

Received July 23, 1981.

Acta Chemica Scandinavica A 36 (1982) 259–266

Poly(vinyl alcohol) Polymers with a Low Degree of Hydrolysis. I. Formation and Dissociation of Multimers in Aqueous Solution

IVAN ALADJOFF, HOLGER NILSSON, CHRISTER SILVEGREN and BERTIL TÖRNELL

Department of Chemical Technology, The Lund Institute of Technology, Chemical Center, P.O.Box 740, S-220 07 Lund, Sweden

In aqueous solution poly(vinyl alcohol) polymers with a relatively high content of residual acetate groups were found to form associates of a micellar-like type. The associates dissociated on addition of ammonium laurate and reformed on removal of the tenside. The associating tendency and the tendency to form red complexes with iodine increased rapidly with an increase in the amount of residual acetate groups, suggesting that these phenomena were caused by the presence in the polymer molecules of poly(vinyl acetate) blocks. The results indicated that the hydrophobic blocks were unevenly distributed over the molecules. The cloud point temperature of aqueous solutions of these blocky polymers decreased on addition of vinyl chloride and increased on addition of ammonium laurate. This most likely was caused by interactions between these substances and the hydrophobic blocks of the polymer molecules.

Water soluble polymers obtained by partial or complete hydrolysis of poly(vinyl acetate) are commonly referred to as poly(vinyl alcohols), PVAL. Such polymers with a rather low degree of hydrolysis (a relatively high content of residual acetate groups) have recently attracted a growing interest as suspension stabilizers in the manufacture of poly (vinyl chloride), PVC, by the suspension process.[1] In the manufacture of suspension PVC resins, the choice of the suspension stabilizing system is rather important as it determines the product properties which are related to the size, shape and morphology of the resin particles. In practice, this makes the stabilizing system the single most important process variable.

The suspension stabilizing systems used in PVC production usually contain a water soluble polymer as the main component. This is often combined with small amounts of a low molecular weight surfactant. The present knowledge of the mechanisms by which the suspension stabilizers control the resin properties is very sparse and mainly empirical.

The present work was carried out as part of a larger study aiming at a better understanding of the role of the suspension stabilizing system in PVC production. The PVAL polymers of primary interest in this work are soluble in cold water and their aqueous solutions tend to turn turbid on heating. This occurs with polymers having a degree of hydrolysis lower than about 75 mol % (75 % of the monomer units in the polymer have been converted to vinyl alcohol residues). PVAL polymers of this type have been the subject of very few studies as compared to those with a higher degree of hydrolysis, *e.g.* 85 %, which give stable solutions in cold as well as in hot water or to the almost fully hydrolyzed polymers (=about 99 %), which give stable solutions in hot water only.[2]

The present paper will deal with the phenomenon of self-association or multimerization[3] of a number of commercial PVAL products. The effect of ammonium laurate, AL, and vinyl chloride, VCM, on this phenomenon will also be discussed. In a subsequent paper, a report will be given about the complexation of the same set of PVAL polymers with ammonium laurate and sodium lauryl sulfate.[4] In a forthcoming paper the effect of PVAL with a low degree of hydrolysis on the interfacial tension at the VCM/water interface and on the stability of emulsions of VCM in water will be reported and compared with a cellulose derivative.[5]

0302-4377/82/030259-08$02.50

Table 1. Commercial PVAL polymers used in the present study.

Trade name	Degree of hydrolysis %	Producer
Rhodoviol 5/270	71.5	Rhone-Poulenc
Mowiol LP 5.72	70.5	Hoechst AG
Polyviol M 05/290	74.7	Wacker Chemie
Alcotex 72.5 L	71.7	Revertex Ltd.
Alcotex 75 L	72.2	Revertex Ltd.
Elvanol 51–05	87.5	Du Pont
Elvanol 70–05	98.9	Du Pont

EXPERIMENTAL

Polymers. The commercial polymers used in this work are presented in Table 1. The values given for the degree of hydrolysis were determined by a method described by Finch.[2] Most of the experiments were carried out using Rhodoviol as an example of the PVAL's with a low degree of hydrolysis. In most cases the polymers were used without previous purification. Reference experiments with Rhodoviol purified by reprecipitation (water–acetone) or by ultrafiltration indicated that this could be done without introducing any errors in the self association studies.

Chemicals. AL was prepared by dissolution of lauric acid, LA, (BDH, specially pure) in dilute ammonia. Vinyl chloride was obtained from Kema-Nobel, Sweden. It was distilled from the steel cylinder prior to use. All aqueous solutions were prepared using distilled and then deionized water.

Gel permeation chromatography (GPC) experiments. The GPC or gel filtration experiments were carried out using thermostatted columns of the type provided by Pharmacia. Except where otherwise stated, the GPC experiments were carried out at 23 °C. The samples were added using a sampling valve. A peristaltic pump, a motor driven syringe or a reciprocating chromatography pump (Altex, model 110) were used for pumping the eluant. A differential refractometer was used as detector (Optilab Multiref 901 or LDC). In most cases a pre-column was used to eliminate pressure variations in the detector. The columns were calibrated using Dextran solutions with a broad molecular weight distribution, MWD, prepared by mixing fractions of Dextran T obtained from Pharmacia. The calibration was made according to the method developed by Abdel-Alim and Hamielec.[6]

Solubilization of vinyl chloride. The ability of PVAL polymers and AL to solubilize VCM was determined by vapour pressure measurements on aqueous solutions containing weighed amounts of VCM. The experimental arrangement used has been described in a previous paper.[7]

RESULTS AND DISCUSSION

Formation and dissociation of polymer associates. Preliminary ultracentrifugation runs on aqueous solutions of Rhodoviol 5/270 (Table 1) had indicated that this polymer contained two components; one with a high and one with a low sedimentation coefficient. In agreement with this observation the GPC results reproduced in Fig. 1 also indicated that this polymer contained two fractions; one with a high molecular weight (I), which was not fully resolved on the column used, and one with a much lower molecular weight (II). When fractions I and II, collected from a series of experiments were rerun on the same columns, the results shown in Fig. 2 were obtained. The fact that the two fractions gave quite different chromatograms, supported the indication that the MWD of the sample was bimodal. It had been observed, however, that the cloud point temperature of dilute solutions of this polymer

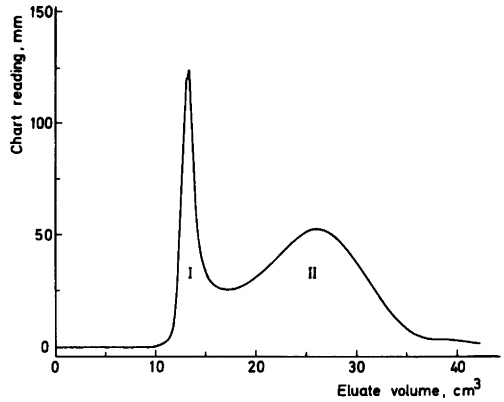

Fig. 1. GPC of Rhodoviol 5/270 (0.3 cm^3 of a 1 % solution) on Sepharose Cl-6B. Column: 15 × 220 mm. Elution: Water, 044 cm^3/min.

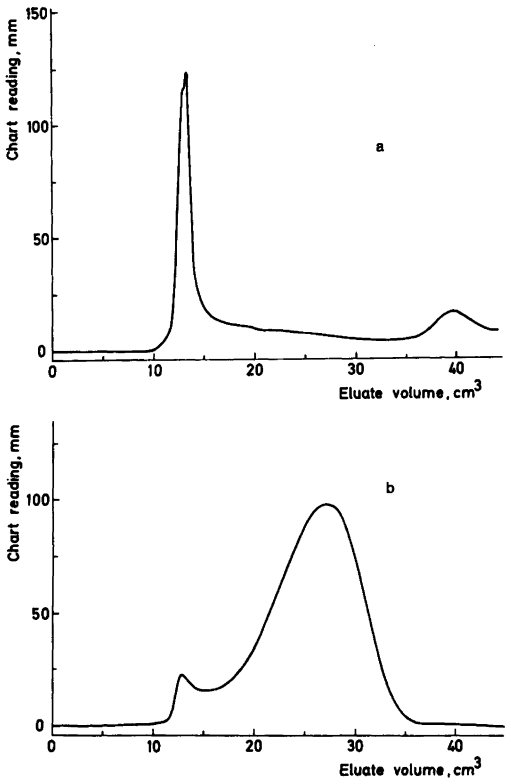

Fig. 2. GPC of fraction I (a) and II (b) from Rhodoviol 5/270 on Sepharose Cl-6B. Column: 15 x 220 mm. Elution: Water, 0.44 cm^3/min.

increased (in these systems the cloud point is reached by heating from room temperature) rapidly on addition of AL. This initiated GPC experiments in which dilute solutions of AL were used as an eluant instead of pure water. Results from such an experiment are given in Fig. 3. The peak at 40 cm^3 in this figure corresponds to the excess amount of AL in the sample solution and has no relation to the polymer. As can be seen, in the presence of AL the high molecular weight fraction seems to have disappeared. As will be shown below, this effect of AL was reversible. This means that the difference between results in Figs. 1 and 3 cannot be ascribed to a hydrolysis of the polymer in the weakly alkaline laurate solution. Instead, the difference must be interpreted to show that in pure aqueous solution this polymer to a large extent associates and forms multimers with a high apparent molecular weight. These associates dissociate on addition of a small amount of AL.

The results in Fig. 4 were obtained using 0.1 M NaCl as an eluant instead of water. Although the shape of the chromatogram was affected by the presence of salt, the multimers did not dissociate. This means that the dissociative effect of AL on the PVAL associates was due to a selective interaction between the soap and the polymer and not the result of nonspecific electrolyte interactions. The influence of NaCl on the shape of the chromatogram will not be discussed here. It should be pointed out, however, that the total effect of NaCl includes that on the separation properties of the Sepharose gel.

The question could be raised whether the association of the polymer as observed in pure aqueous solution was an equilibrium property of the solution or not. To test this, the following experiments were made. To an aqueous solution of Rhodoviol was added AL. The mixture was then placed in an ultra filtration cell and the laurate was washed out

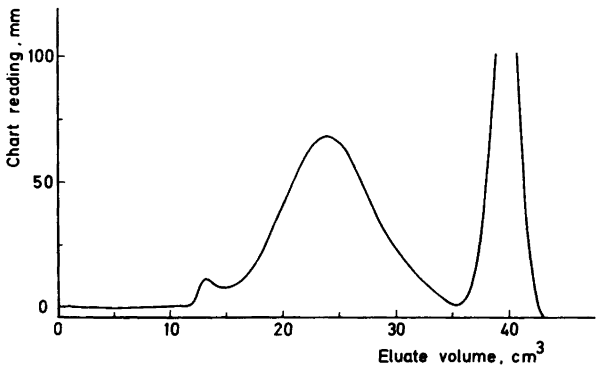

Fig. 3. GPC of Rhodoviol 5/270 (0.3 cm^3 of a 1 % solution containing 0.5 % AL) on Sepharose Cl-6B. Column: 15 x 220 mm. Elution: 0.1 % AL, 0.44 cm^3/min.

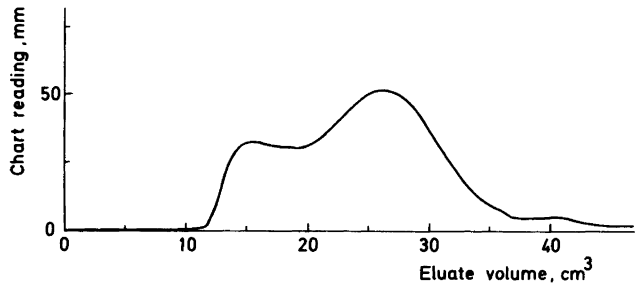

Fig. 4. GPC of Rhodoviol 5/270 (0.2 cm^3 of a 1 % solution containing 0.1 M NaCl) on Sepharose Cl-6B. Column: 15 × 220 mm. Elution: 0.1 M NaCl, 0.44 cm^3/min.

with water. Results from a GPC run on the resulting polymer solution (Fig. 5) showed that reassociation had occurred on removal of the laurate. The association observed in pure water thus must be an equilibrium property of the polymer solution.

Association of commercial products with different degrees of hydrolysis. Fig. 6 is based on results from GPC studies on a set of commercial PVAL products. In this case 0.01 M NaCl was used as eluant in order to suppress the possible effect of charged groups on the polymers (*i.e.* initiator fragments). In preparing this figure the area under peak I was measured as the total area up to the eluate volume corresponding to the minimum between the two fractions. The diagram shows that the relative amount of associated molecules increased rapidly with a decrease in the degree of hydrolysis. No tendency to form aggregates was observed for sample 6 (degree of hydrolysis 87.5 %). The results for sample 7 (degree of hydrolysis 99.8 %) was obtained in an experiment in which the sample solution was heated before the run in order to dissociate the molecular aggregates which form when solutions of highly hydrolyzed PVAL polymers are kept at room temperature (*cf.* Ref. 2). These types of aggregates were observed in GPC runs on old solutions of sample 7.

Structural requirements for association. The results in Fig. 6 strongly suggest that the observed aggregation of PVAL polymers with a low degree of hydrolysis depends on association between polymer segments having a high content of residual acetate groups. This in combination with the fact that fraction I of Rhodoviol could be isolated and rechromatographed without the appearence of a

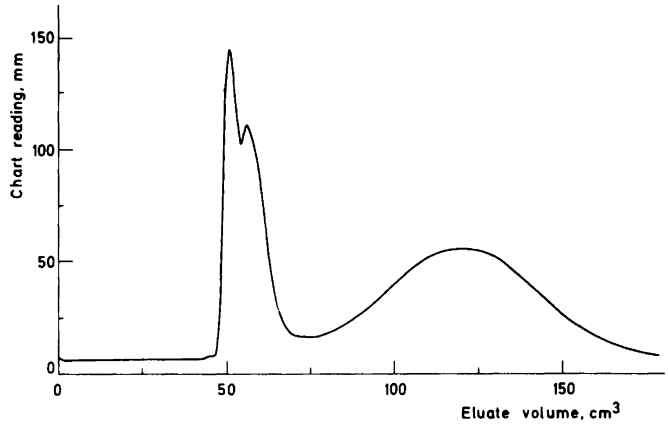

Fig. 5. GPC on Sepharose Cl-6B of a solution obtained by washing with water, pH 9.3, in a membrane filter cell a solution containing 1 % Rhodoviol 5/270 and 0.1 % AL. Column: 25 × 400 mm. Elution: Water, 1.33 cm^3/min.

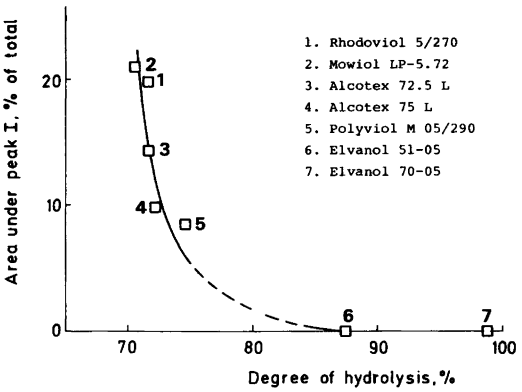

Fig. 6. Relative size of fraction I as determined by GPC experiments with commercial PVAL polymers on Sepharose Cl-6B. Column: 15 × 230 mm. Elution: 0.01 M NaCl, 1.3 cm^3/min.

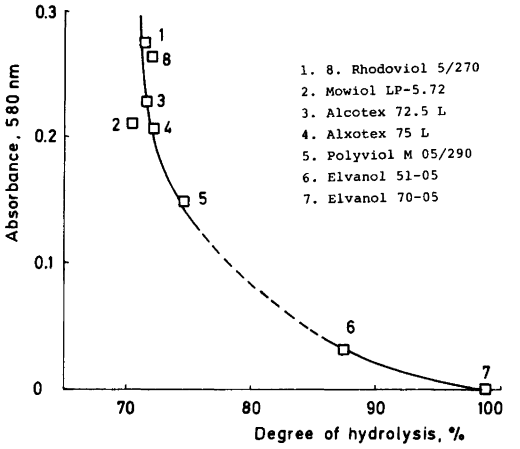

Fig. 7. Absorbance at 580 nm of solutions containing 100 ppm of PVAL polymers and 50 ppm of I added as the $I_2 - KI$ complex.

a large fraction of dissociated molecules (*cf.* Fig. 2), a fact which could not be expected if the association were governed by the law of mass action, indicated that fractions I and II differed in their chemical constitution. Direct analysis of fractions I and II collected from a number of runs with Rhodoviol confirmed this. The average degree of hydrolysis of fraction I was 65 % and that of fraction II 73 %. This difference in the composition of the fractions was parallelled by a difference in cloud point. At a concentration of 0.3 %, a solution of fraction I on heating became turbid at 30 °C and then clear again at 90 °C, whereas a solution of fraction II became turbid at 45 °C and was not cleared on further heating to the boiling point. Fractions I and II also differed in their tendencies to form complexes with iodine. In the presence of borate, with fraction II, the well-known blue complex[8] often used for the determination of poly(vinyl alcohol) dominated, whereas with fraction I a large contribution from the red colour ascribed to a complex between iodine and acetate groups[9] was evident.

Fig. 7 shows that for the PVAL polymers studied, the absorbance of the red iodine complex (in this case borate was not present) increased as the degree of hydrolysis decreased. The increase in the absorbance was much faster than in proportion to the concentration of acetate groups. This indicated that the formation of the iodine complex required the presence of blocks of vinyl acetate residues in the polymer. This has recently been confirmed by Pritchard and Ahmed by measurements on poly(vinyl acetate-*co*-vinyl alcohol) polymers prepared by different routes.[10] The shapes of the curves in Figs. 6 and 7 were rather similar. This strongly suggested that the tendencies to self-associate and to form red complexes with iodine were due to the same factor. It can thus be concluded that the self-association of PVAL polymers observed in this work was due to interactions between polymer segments containing blocks of residual acetate groups. The tendency of these hydrophobic blocks to associate was dramatically reduced by selective binding of AL.[4] With reference to the results in Fig. 2, the vinyl acetate blocks responsible for association were unevenly distributed over the polymer molecules. This, of course might be a consequence of the occurrence of a two-phase system during the hydrolysis of the parent poly(vinyl acetate). Because of such a phase separation different conditions during the hydrolysis may give rise to large differences in the properties of the partly hydrolyzed products.

The size of the polymer aggregates. To learn more about self-association of PVAL with a low degree of hydrolysis, GPC experiments were carried out on Rhodoviol at various temperatures using a Sepharose Cl 4B column. This column had a higher exclusion limit than for those previously used. It was calibrated with Dextran T fractions. The chromatograms were resolved into two fractions as shown in Fig. 8, assuming fraction II to be

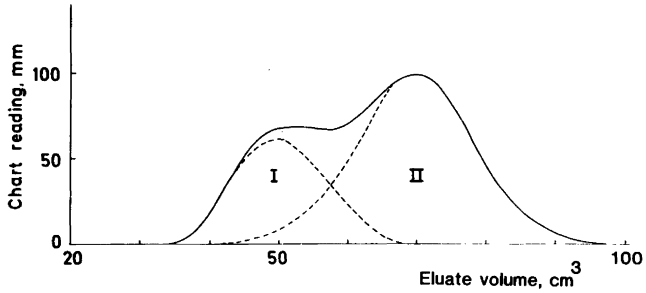

Fig. 8. Resolution of a GPC chromatogram obtained by running Rhodoviol 5/270 on Sepharose Cl-4B at 24.8 °C. Column: 15 × 500 mm. Elution: 0.01 M NaCl, 0.8 cm^3/min.

symmetrical and the results are given in Table 2. As can be seen, the relative amount of fraction I increased with an increase in temperature. There was also a slight increase in the relative amount of fraction I when the concentration of the sample solution was increased. The MWD found for fraction II agreed well with that for the whole polymer as determined after complete hydrolysis. This justifies the method used for resolution of the chromatograms. With the fully hydrolyzed sample the following data were obtained: $\bar{M}_n = 18 \times 10^3$ g/mol, $\bar{M}_w = 45 \times 10^3$ g/mol, and $\bar{M}_w/\bar{M}_n = 2.5$. As can be seen, the apparent molecular weight and the heterogeneity index ($\bar{M}_w/\bar{M}_n$) for fraction I seemed to be almost independent of the conditions. The results suggested that, on the average, the multimers contained about ten polymer molecules. The value for $\bar{M}_w/\bar{M}_n$ for fraction I was close to the value expected on the assumption that all aggregates contained an equal number of polymer molecules.[3] Assuming the MWD of fraction II to be representative for that of the unassociated molecules, this would give 1.2 instead of 1.3 as actually found. These results suggest a micellization type of association. The possibility of such a type of association in solutions of polymers having both hydrophilic and hydrophobic groups has been discussed previously (*cf. e.g.* Ref. 11).

Influence of VCM and AL on the solution behaviour of PVAL. As mentioned previously, small amounts of AL were found to produce a large increase in the cloud point temperature of aqueous solutions of Rhodoviol. Thus, the addition of 0.05 % AL to a 0.5 % solution gave an increase in the cloud point from 35 to 75 °C. Experiments with VCM showed that this substance had the opposite effect. In Fig. 9 the cloud point is given as a function of the relative pressure of VCM over the solution, P/P_0 where P_0 is the saturation pressure. Considering the fact that the solubility of VCM in

Table 2. Influence of temperature and sample solution concentration on the relative amount of fraction I (the associated molecules) and on the MWD for fractions I and II from Rhodoviol 5/270 as determined in GPC experiments (conditions as given in the text to Figure 8).

Temp. °C	Conc. of PVAL in sample %	Size of fraction I % of total	$\bar{M}_w$(I) $\times 10^{-3}$ g/mol	$\bar{M}_n$(II) $\times 10^{-3}$ g/mol	$(\bar{M}_w/\bar{M}_n)_I$	$(\bar{M}_w/\bar{M}_n)_{II}$
4.8	1	11.8	180	19	1.3	2.6
10.2	1	15.4	180	21	1.4	2.4
14.0	1	23.0	160	16	1.4	2.7
20.2	1	28.1	180	18	1.3	2.6
24.8	1	32.3	210	22	1.3	2.5
20	0.50	26.4	170	18	1.3	2.8
20	1.0	28.0	150	14	1.3	2.8
20	2.0	32.0	150	14	1.4	2.7
20	3.0	34.6	130	13	1.5	2.7

Table 3. Solubilization of VCM by PVAL polymers as determined on aqueous solutions at 35 °C and at a relative VCM pressure of 0.9.

Polymer	Degree of hydrolysis	VCM solubilized (mg/g polymer)
Rhodoviol 5/270	71.5	86
Elvanol 51–05	87.5	25
Elvanol 70–05	98.9	1

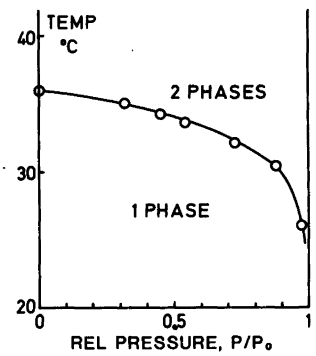

Fig. 9. The influence of VCM on the cloud point temperature of a 0.5 % solution of Rhodoviol 5/270.

water is less than 1 %,[7] the large decrease in the cloud point temperature as the saturation limit was approached indicated a highly specific interaction. As seen from the data in Table 3, small amounts of VCM were solubilized by PVAL polymers with a low degree of hydrolysis. Experiments with Rhodoviol at different temperatures showed that the solubilization was weakly exothermic ($\Delta H = -13$ kJ/mol).

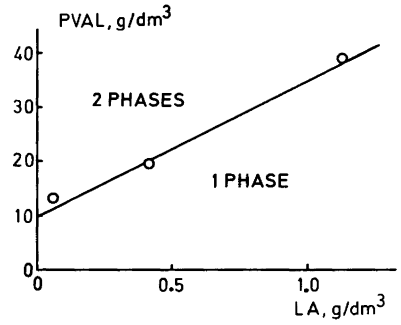

Fig. 10. Influence of AL on the phase separation at 35 °C in solutions of Rhodoviol 5/270 almost saturated with VCM ($P/P_0 = 0.99$). Concentrations in % by weight.

The phase separation in Rhodoviol solutions induced by VCM could be prevented by adding fairly small amounts of AL. Fig. 10 shows that the amount of laurate required increased with the concentration of Rhodoviol. In these experiments the partial pressure of VCM was kept just slightly below the saturation pressure. Obviously, AL had a stronger tendency to bind to the hydrophobic segments of the polymer than had VCM. Although it was found that VCM could be solubilized in AL micelles (0.34 g/g at $P/P_0 = 0.9$), very little extra VCM was solubilized in a Rhodoviol solution containing AL if the concentration of the latter was lower than the critical micelle concentration. The results obtained in these experiments with VCM and AL point out the high complexity of the practical systems in which the PVAL polymers are used.

Acknowledgement. This work was supported by The Swedish Board for Technical Development.

REFERENCES

1. a. Shiraishi, M. and Toyoshima, K. *Br. Polym. J. 5* (1973) 419; b. Anon. *Gohsenol*, Product information from Nippon Gohsei, Japan; c. Bjerke, O. and Pettersson, S. *Private communication* (1978).
2. Finch, C. A. *Polyvinyl Alcohol Properties and Applications*, Wiley, New York 1973.
3. Elias, H. G. In Solc, K., Ed., *Order in Polymer Solutions, Midland Macromol Monographs*, 1976, Vol. 2, p. 209.
4. Aladjoff, I., Nilsson, H., Silvegren, C. and Törnell, B. *Acta Chem. Scand. A 36* (1982) 267.
5. Nilsson, H., Norviit, T., Silvegren, C. and Törnell, B. *In preparation.*
6. Abdel-Alim, A. H. and Hamielec, A. E. *J. Appl. Polym. Sci. 18* (1974) 297.
7. Nilsson, H., Silvegren, C. and Törnell, B. *Eur. Polym. J. 14* (1978) 737.

8. Pritchard, J. G. and Akintola, D. A. *Talanta 19* (1971) 877.
9. Pritchard, J. G. and Akintola, D. A. *Talanta* (1972) 897.
10. Pritchard, J. G. and Ahmed, I. *Polymer 20* (1979) 1492.
11. Kunieda, H. and Shinoda, K. In Mittal, K. L., Ed., *Am. Chem. Soc. Symp. Ser. 9* (1975) 278.

Received June 30, 1981.

Acta Chemica Scandinavica A 36 (1982) 267–272

Poly(vinyl alcohol) Polymers with a Low Degree of Hydrolysis. II.* Complex Formation with Ammonium Laurate and Sodium Lauryl Sulfate

IVAN ALADJOFF, HOLGER NILSSON, CHRISTER SILVEGREN and BERTIL TÖRNELL

Department of Chemical Technology, The Lund Institute of Technology, Chemical Center, P.O. Box 740, S-220 07 Lund, Sweden

The binding of tensides (sodium laurate, SL, ammonium laurate, AL, and sodium layryl sulfate, SLS) to a number of commercial PVAL polymers of different degrees of hydrolysis have been studied at tenside concentrations below the critical micelle concentration using membrane and gel filtration techniques. The results showed that SLS binds much more readily to the polymer than SL or AL. The tendency to bind tensides increased rapidly as the degree of hydrolysis of the polymer became lower. Binding of laurate seems to require the presence of acetate groups on the polymer, whereas SLS was found to bind also to a fully hydrolyzed polymer. In all cases studied, binding became more favourable at higher tenside concentrations. Attempts to study the enthalpy of binding using flow micro calorimetry indicated that complex formation with the polymer was energetically slightly more favourable than micellization.

As discussed in the previous paper in this series, poly(vinyl alcohol) polymers with a rather low degree of hydrolysis are of interest as suspension stabilizers in the manufacture of suspension PVC.[1] In aqueous solution and at room temperature, polymers of this type were found to associate. The relative amount of associated molecules increased rapidly with a decrease in the degree of hydrolysis. The results indicated that the phenomenon was caused by interactions between hydrophobic poly(vinyl acetate) blocks remaining in the polymers. It was also found that the associated molecules dissociated on addition of ammonium laurate. It was suggested that this was due to binding of laurate to the hydrophobic parts of the polymer molecules. These observations and the fact that in suspension polymerization of vinyl chloride the polymeric stabilizer often is used in combination with tensides, initiated the present study on complex formation between tensides and a set of commercial poly(vinyl alcohol) polymers. The study refers to concentrations of tensides below their critical micelle concentration, c.m.c. A lot of work has been done on complex formation between tensides and poly(vinyl alcohol)[2] but no previous studies have been made involving the composition of complexes between tensides and the type of polymers used here.

EXPERIMENTAL

Poly(vinyl alcohol) polymers, PVAL. The commercial PVAL polymers used in this study are presented in Table 1. The values given for the degree of hydrolysis [the relative number of the acetate groups in the parent poly(vinyl acetate) converted to hydroxyl groups] were determined by a method described by Finch.[3] The polymers were used as received except for in the experiments with Rhodoviol. In this case the polymer was purified either by reprecipitation from acetone–water or by ultrafiltration in a stirred membrane filter cell fitted with an Amicon PM 10 membrane, in order to eliminate the small error caused by the presence of low molecular weight impurities (see below).

Tensides. Ammonium laurate, AL, and sodium laurate, SL, were prepared by dissolution of lauric acid, LA (BDH, specially pure) in dilute ammonia or

*Part I, see Ref. 1.

0302-4377/82/030267-06$02.50

Table 1. Commercial PVAL polymers used in the present study.

Trade name	Degree of hydrolysis %	Producer
Rhodoviol 5/270	71.5	Rhone-Poulenc
Mowiol LP 5.72	70.5	Hoechst AG
Polyviol M 05/290	74.7	Wacker Chemie
Alcotex 72.5 L	71.7	Revertex Ltd.
Alcotex 75 L	72.2	Revertex Ltd.
Elvanol 51-05	87.5	Du Pont
Elvanol 70-05	98.9	Du Pont

sodium hydroxide. The pH of the AL solutions used was between 9.6 and 9.8 and that of SL between 9.2 and 9.3. Sodium lauryl sulfate, SLS (BDH, specially pure) was used as received. Deionized and then distilled water was used for preparing all aqueous solutions.

Binding studies. Two techniques, one based on membrane filtration and the other on gel filtration, were used, With the membrane filtration technique, the sample (300 ml) containing known total amounts of polymer and tenside was placed in a membrane filter cell fitted with stirrer and Amicon PM 10 or PM 30 membranes. The first 10 ml of the filtrate was discarded and the next 5 – 10 ml was analyzed for tenside. The concentration found was assumed to represent that of the free tenside. Laurate was determined by potentiometric titration with 0.1 M HCl after adding a small amount of SLS to the solution to ensure that a sharp end point was obtained in the titration of the excess amount of base.[4] SLS in the filtrates was determined colorimetrically as its methylene blue complex.[5]

The gel filtration method used for determination of bound tensides has been described by Hummel and Dreyer[6] and is outlined in Fig. 1. The column is saturated with a tenside solution of concentration

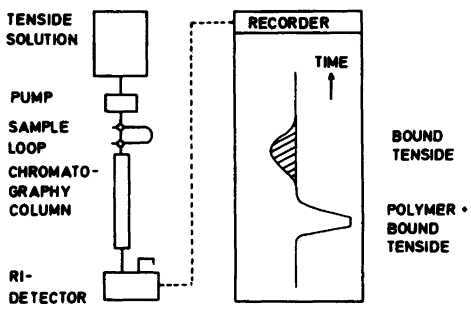

Fig. 1. Determination of the binding of tensides to polymers by gel chromatography.

C. A sample of the polymer dissolved in the tenside solution is then applied *via* a sampling valve. If the polymer binds the tenside, two peaks will appear. The first is positive and contains the polymer, the second is negative and corresponds to a deficiency in tenside. The area of the negative peak gives the amount of bound tenside. The column can be calibrated in experiments with water samples of various volumes. The method requires that the positive and negative peaks are separated by a horizontal base line. This is a guarantee that the polymer peak contains free tenside of concentration *C*. The determination of a binding isotherm requires experiments at a set of various concentrations of tenside. Impurities in the polymer with a low molar mass might interfere with the negative peak and give low values for bound tenside.

The binding studies with AL were carried out using Sephadex G10 (35 × 400 mm). With SLS it was necessary to use a more porous gel, Sephadex G25-SF (16 × 600 mm). In this case it was also found necessary to keep the tenside solution reservoir flask at a temperature slightly above room temperature to avoid problems caused by association of the tenside. The columns were jacketed and all experiments carried out at 25 °C. The columns were fed by a peristaltic pump. The flow rate was about 0.8 (Sephadex G10) and 0.5 ml/min (Sephadex G25-SF) and was determined in each of the experiments. The effluent was analyzed by a refractive index (RI) detector (Optilab Multiref 901).

Enthalpy of binding. The enthalpy of binding SLS and AL to Rhodoviol (Table 1) was evaluated from the heat effects observed on mixing solutions of the tenside with solutions of the polymer, or by diluting a polymer – tenside mixture by water. The experiments were carried out in a flow microcalorimeter.[7] Corrections were applied for the heat of dilution of the component solutions. The same technique was used for estimating the enthalpy of micellization of AL and SLS. The extent of reaction was calculated from the binding isotherms and values for the c.m.c. of the tensides, respectively.

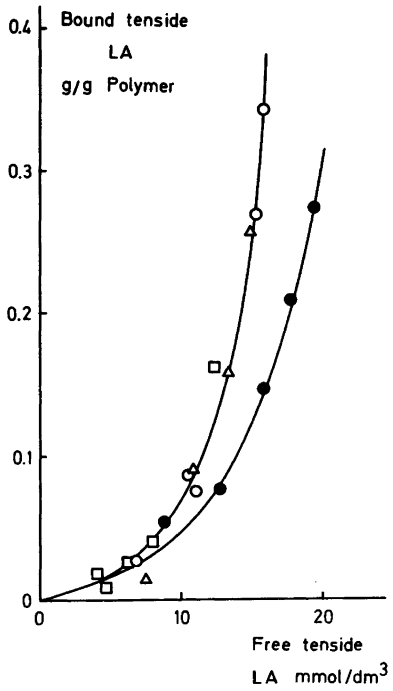

Fig. 2. Binding isotherms for ammonium laurate, AL, and sodium laurate, SL, to Rhodoviol 5/270 as determined by membrane filtration at room temperature. □, AL, PM 10; ○, AL, PM 30, △, AL, – (Data from Table 2); ●, SL, PM 30.

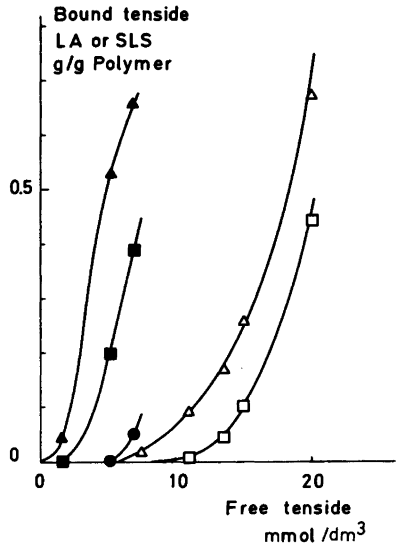

Fig. 3. Binding isotherms for sodium lauryl sulfate, SLS, and ammonium laurate, AL, to some commercial poly(vinyl alcohol) polymers. Open symbols, AL; filled symbols, SLS. △, ▲, Rhodoviol 5/270, 71% hydrolysis; □, ■, Elvanol 51-05, 88% hydrolysis; ●, Elvanol 70-05, 99% hydrolysis.

RESULTS

Most of the binding studies were carried out using the gel chromatography technique. The results obtained are given in Tables 2 and 3. Results obtained with the alternative method, membrane filtration, are presented in Fig. 2. These refer to experiments with laurate and one of the polymers, Rhodoviol, only. Gel chromatography results for this system from Table 2 have been included in Fig. 2 in order to permit a direct comparison between the two methods. A comparison of SLS and AL in terms of binding isotherms with some of the polymers is given in Fig. 3. Fig. 4 shows the effect of SLS and AL on the specific viscosity of Rhodoviol. Values for the apparent enthalpy of binding are given in Table 4.

Table 2. Binding of ammonium laurate, AL, at 25 °C to some commercial poly(vinyl alcohol) polymers expressed as g lauric acid, LA, per g of polymer.

AL[a] % by weight	Rhodoviol	Mowiol	Polyviol	Alcotex 72.5	Alcotex 75	Elvanol 51-05
0.15	0.014	0.016	0.016	0.016	0.016	–
0.22	0.092	0.080	0.076	0.093	0.082	0.009
0.27	0.17	0.16	0.14	0.17	0.16	0.048
0.30	0.26	0.30	0.25	0.27	0.26	0.10
0.40	0.68		0.77			0.45
0.44	1.36					

[a] Conc. of free AL in the solution calculated as LA.

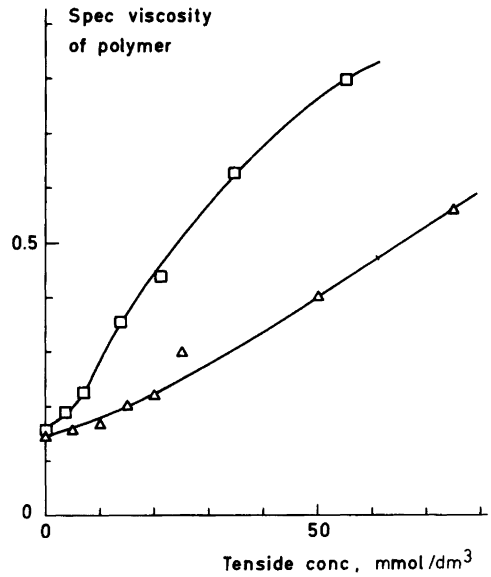

Fig. 4. Specific viscosity at 25 °C for Rhodoviol 5/270 as determined at a polymer concentration of 0.5 % by wt. and in the presence of various amounts of sodium lauryl sulfate (□) or ammonium laurate (△).

DISCUSSION

Methods. As seen from Fig. 2, the agreement between the results obtained with the gel chromatography and the membrane filtration methods was very good. In the gel filtration experiments with Rhodoviol, no systematic differences were observed between polymer samples purified by membrane filtration or by precipitation. The low value obtained with the gel chromatography technique at the lowest concentration can be explained by the difficulty in evaluating the true area under the tails of a low and fairly wide chromatography peak. The difference between SL and AL in Fig. 2 most likely reveals a direct counter-ion effect. The differences in electrolyte concentration between the SL and AL solutions were very small.

Table 4. Apparent enthalpy of binding of sodium lauryl sulfate, SLS, and ammonium laurate, AL, to Rhodoviol 5/270 at 25 °C.

Tenside	Increase in[a] tenside binding g/g polymer	ΔH_b kJ/mol
SLS	0–0.31	−4.8
	0–0.45	−4.8
	0–0.60	−5.0
	0.49–0.72	−3.9
AL	0–0.31	3.3
	0–0.41	3.3
	0–0.64	2.7
	0.27–0.70	5.2

[a] For AL in g lauric acid/g polymer.

Attempts were made to use the membrane filtration method also for the determination of binding isotherms with SLS but were unsuccessful. In experiments with pure SLS solutions the filtrates contained much less SLS than did the parent solutions. The reason for this probably was that the experiments were carried out at room temperature, that is at a temperature slightly lower than 24 °C, which according to recent data seems to be the minimum temperature at which clear solutions of pure SLS can be obtained.[8] This was not understood at the time and experiments with the membrane filtration technique were not carried out at higher temperatures. However, also with the gel chromatography technique difficulties were encountered in experiments with SLS until provisions were made for keeping all parts of the chromatography system at 25 °C.

Binding isotherms. As can be seen from Fig. 3 and Tables 2 and 3, SLS and AL gave binding isotherms

Table 3. Binding of sodium lauryl sulfate, SLS, at 25 °C to some commercial poly(vinyl alcohol) polymers in g per g of polymer.

SLS[a] % by weight	Rhodoviol	Mowiol	Polyviol	Elvanol 51-05	Elvanol 70-05
0.05	0.061	0.046	0.033	0	0
0.15	0.48	0.50	0.47	0.23	0
0.20	0.74	0.79	0.68	0.39	0.05

[a] Conc. of free SLS in the solution.

of the same general shape. In all cases studied, binding became more favourable at higher concentrations. This is a behaviour quite different from that observed for the adsorption of tensides of hydrophobic colloids, which normally can be fairly well described by Langmuir isotherms.

It can be seen that the tendency to bind SLS and AL decreases with an increase in the degree of hydrolysis. It is also seen that SLS binds much more readily to the polymer than does AL. Thus, with SLS a significant extent of binding was observed even in the experiments with the fully hydrolyzed polymer, in which case no detectable binding of AL could be observed. The higher complex ability of SLS was reflected also in a much stronger viscosity effect than that produced by AL (Fig. 4). These differences between SLS and AL are in agreement with previous information.[9] An analysis of the data in Fig. 4 using the binding isotherms in Fig. 3 showed that also when compared at the same amount of bound tenside (g/g polymer), the specific viscosity of the SLS polymer complex was higher than that of the AL polymer complex.* Within the concentration range covered by the isotherms, the difference between SLS and AL in its effect on the specific viscosity seemed to increase with an increase in the amount of bound tenside.

In the previous paper, it was shown that the cloud point temperature (which in these systems is reached by heating from room temperature) of a 0.5 % solution of Rhodoviol increased from 35 to 75 °C on addition of 5 mmol/dm^3 of AL.[1] From Fig. 2 it can be calculated that this effect was produced by the binding of 0.015 g lauric acid per g polymer, which would correspond to only about 1 molecule of lauric acid per 240 monomer residues or about 1 molecule of lauric acid per 70 vinyl acetate residues. It is likely that the large effect on the cloud point temperature observed in this case was due to a selective binding of the tenside to polymer molecules with a higher than average content of acetate groups. The acetate groups in partly hydrolyzed poly(vinyl acetate) are unevenly distributed over and along the molecules in a manner which depends on the conditions used during hydrolysis (*cf. e.g.* Refs. 1, 10). This makes a closer discussion of the binding isotherms very complicated.

* The data in Fig. 4 include the viscosity effect of the free tenside. The contribution of this effect to the specific viscosities would be rather small and would not even at the highest tenside concentration exceed 10 %.

The methods used for the binding studies were based on separation of the free tenside from the tenside polymer complex. Because of the size of tenside micelles, studies were not possible at tenside concentrations above the c.m.c. As can be seen from Table 2, AL concentrations approaching the c.m.c value (0.44 % by weight LA as determined by conductometry) the polymer bound more than its own weight of LA. The highest concentration observed corresponded to a binding of about 1.3 molecules of lauric acid per vinyl acetate residue. This result suggests that the polymer acted more or less as a catalyst for the association of the tenside.

Enthalpy of binding. The results in Table 4 suggest that the binding of SLS to Rhodoviol was exothermic and that of AL endothermic. The difference, however, compares rather well with the difference in enthalpy of micellization. The enthalpies of micellization were estimated as 7.3 kJ/mol for AL and about zero for SLS. This means that with both tensides, complex formation with the polymer was energetically slightly more favourable than micellization. The experimental material is not large enough to permit a full discussion of the results. However, the following comments can be made. The values for the apparent enthalpy of binding obtained in the experiments based on mixing polymer and tenside solutions contained a contribution from the enthalpy of dissociation of the associated polymer molecules. Such a contribution would not be present in the values obtained in the dilution experiments in which the polymer-tenside complexes were partly dissociated. A comparison of the results from these different types of experiments indicates that the formation of polymer associates is an endothermic process. This is in agreement with the fact that the aqueous polymer solution turns turbid on heating.

Acknowledgements. The authors are indebted to Mr. Simon Burg for his very careful and skilled experimental assistance and to Prof. Ingemar Wadsö who put a flow microcalorimeter at our disposal. The work has been supported by the Swedish Board for Technical Development.

REFERENCES

1. Aladjoff, I., Nilsson, H., Silvegren, C. and Törnell, B. *Acta Chem. Scand. A 36* (1982) 259.
2. a. Saito, S. *Kolloid Z. 137* (1954) 98; b. Saito, S. *Kolloid Z. 154* (1957) 19; c. Lewis, K. E. and Robinson, C. P. *J. Colloid Interface Sci. 32* (1970) 539.

3. Finch, C. A. *Polyvinyl Alcohol Properties and Applications*, Wiley, New York 1973.
4. Hassander, H., Nilsson, H., Silvegren, C. and Törnell, B. In Fitch, R. M., Ed., *Polymer Colloids II*, Plenum, London, New York 1980, p. 511.
5. Jones, J. H. *J. Assoc. Off. Agric. Chem. 28* (1945) 398.
6. Hummel, J. P. and Dryer, W. J. *Biochim. Biophys Acta 63* (1962) 530.
7. Monk, P. and Wadsö, I. *Acta Chem. Scand. 22* (1968) 1842.
8. Fontell, K. *Mol. Cryst. Liq. Cryst. 63* (1981) 59.
9. Isemure, T. and Imanischi, A. *J. Polym. Sci 33* (1958) 337.
10. Pritchard, J. G. and Ahmed, I. *Polymer 20* (1979) 1492.

Received June 30, 1981.

Acta Chemica Scandinavica A 36 (1982) 273–276

The Complex Formation of Dibenzyl Sulfoxide with Various Proton Donors

P. RUOSTESUO and J. KARJALAINEN

Department of Chemistry, University of Oulu, SF-90570 Oulu 57, Finland

The complex formation of dibenzyl sulfoxide with phenol, 1-naphthol, 2-naphthol, 2,2,2-trifluoroethanol, 2,2,2-trichloroethanol, 2,2,2-tribromoethanol, pyrrole, indole and carbazole has been studied by near infrared spectrophotometry in carbon tetrachloride at 288.15, 298.15, 308.15 and 318.15 K.

The results show the proton-accepting ability of dibenzyl sulfoxide to be smaller than that of dimethyl sulfoxide and greater than that of diphenyl sulfoxide toward all the OH and NH proton donors studied.

This paper is a part of our attempt to clarify systematically the complex formation ability of sulfonyl and sulfinyl compounds. The earlier results suggest a close similarity in the proton accepting behaviours of sulfones and sulfonamides and, correspondingly, of sulfoxides and sulfinamides. On the other hand, the complex formation ability of dimethyl sulfoxide is known to be relatively strong and that of diphenyl sulfoxide has been found to be half as great, as measured by the K values.[1,2] We have now extended our studies to the complex formation of dibenzyl sulfoxide with various OH and NH proton donors in carbon tetrachloride.

EXPERIMENTAL

Dibenzyl sulfoxide (a *purum* reagent from Fluka AG) was crystallized several times from absolute ethanol. Carbon tetrachloride for IR-spectroscopy (Fluka AG, Buchs, Switzerland) was dried and preserved above Union Carbide molecular sieves, Type 4 A, from Fluka AG.

The proton donors were commercial products, purified as described earlier.[1-6]

All spectra were recorded with a Beckman ACTA MIV spectrophotometer at 288.15, 298.15, 308.15 and 318.15 K in carbon tetrachloride solution. A quartz cell of 10-mm path length was used. The temperature of the measuring and reference cells was kept constant to within ± 0.2 °C. The concentration of the proton donors was between 0.002 and 0.004 mol dm^{-3} and the dibenzylsulfoxide was used in various amounts of excess depending on the proton donor. The cell in the reference beam contained the base in carbon tetrachloride at the same initial concentration as in the sample cell. Details of the apparatus and the methods have been reported previously.[1]

RESULTS

The equilibrium constants at different temperatures for the complex formation of dibenzyl sulfoxide with various proton donors are presented in Table 1. The K values were calculated from the absorbance values of the free OH/NH group stretching band of the proton donor observed before ($A°$) and after (A) the complex formation, using eqn. (1), where

$$K_{11} = \frac{1 - A/A°}{A/A°[C_B° - C_A°(1 - A/A°)]} \quad (1)$$

$C_B°$ and $C_A°$ are the initial concentrations of proton acceptor and proton donor, respectively. The K values, as well as the ΔH values and other quantities presented in Table 2, are mean values of 3–5 independent measurements. The standard error of the mean values is also given in Tables 1 and 2. The ΔH values were obtained from the temperature dependence of the K values and other thermodynamic quantities according to the normal thermodynamic relations.

For comparison Tables 3 and 4 contain the equilibrium constants (K) at 298.15 K, the complexation enthalpies (ΔH), and the wavenumber shifts ($\Delta\bar{\nu}_{OH}/\Delta\bar{\nu}_{NH}$) for the complexes of dimethyl sulfoxide

0302-4377/82/030273-04$02.50

Table 1. Values of $K_{11}/dm^3\ mol^{-1}$ for the complex formation of dibenzyl sulfoxide with various proton donors in carbon tetrachloride at different temperatures.

Proton donor	288.15 K	298.15 K	308.15 K	318.15 K
Phenol	205 ±15	145 ±12	106 ±8	78.7 ±5.5
1-Naphthol	272 ±20	190 ±16	135 ±10	97.1 ±6.0
2-Naphthol	307 ±16	213 ±13	151 ±10	110 ±7
2,2,2-Tribromoethanol	53.9±4.2	41.3±3.3	33.4 ±2.7	26.1 ±1.9
2,2,2-Trichloroethanol	63.4±5.2	46.9±4.0	35.3 ±3.1	25.9 ±2.2
2,2,2-Trifluoroethanol	141 ±12	104 ±9	77.0 ±7.0	59.1 ±5.6
Pyrrole	12.7±1.0	10.5±0.9	8.76±0.80	7.17±0.62
Indole	21.3±2.0	17.2±1.7	14.1 ±1.3	12.1±1.1
Carbazole	30.9±2.3	24.8±1.9	19.8 ±1.4	16.3 ±1.2

Table 2. Values of thermodynamic quantities ΔH, $\Delta G°$ and $\Delta S°$ and the wavenumber shifts $\Delta\bar{\nu}_{OH}/\Delta\bar{\nu}_{NH}$ for the complex formation between dibenzyl sulfoxide and various proton donors in carbon tetrachloride.

Proton donor	$-\Delta H$ / kJ mol^{-1}	$-\Delta G°$ / kJ mol^{-1}	$-\Delta S°$ / J mol^{-1} K^{-1}	$\Delta\bar{\nu}_{OH}/\Delta\bar{\nu}_{NH}$ / cm^{-1}
Phenol	24.3±1.9	12.34±0.20	42.0±5.2	342±2
1-Naphthol	26.2±1.2	13.00±0.21	44.3±4.8	369±2
2-Naphthol	26.1±1.3	13.29±0.15	43.0±5.0	359±2
2,2,2-Tribromoethanol	18.1±0.9	9.22±0.11	29.9±3.3	277±2
2,2,2-Trichloroethanol	22.6±0.8	9.54±0.20	43.8±3.4	283±2
2,2,2-Trifluoroethanol	23.2±0.7	11.50±0.25	39.2±3.3	285±2
Pyrrole	14.4±0.9	5.82±0.21	28.7±3.8	167±2
Indole	14.5±0.8	7.05±0.26	24.9±3.6	186±2
Carbazole	16.4±1.2	7.96±0.18	28.2±4.6	190±2

Table 3. Values of K^{298}, ΔH and $\bar{\nu}_{OH}/\Delta\bar{\nu}_{NH}$ for the complex formation of dimethyl sulfoxide with various proton donors in carbon tetrachloride.

Proton donor	K^{298} / dm^3 mol^{-1}	$-\Delta H$ / kJ mol^{-1}	$\Delta\bar{\nu}_{OH}/\Delta\bar{\nu}_{NH}$ / cm^{-1}	Ref.
Phenol	220	24.3	362	1
1-Naphthol	254	27.1	389	3
2-Naphthol	288	27.1	376	4
2,2,2-Tribromoethanol	48.1	21.3	296	7
2,2,2-Trichloroethanol	68.4	21.3	301	7
2,2,2-Trifluoroethanol	148	23.1	306	5
Pyrrole	16.5	15.6	185	6
Indole	21.9	16.9	203	6
Carbazole	31.2	17.4	210	6

with the same proton donors.[1-7] The complex formation of dibenzyl sulfoxide with napthols has earlier been studied under quite different conditions[8] and some isolated values have been published for phenol[9] and indole.[10]

DISCUSSION

It is well known that sulfoxides act as electron donors in hydrogen bond formation and that their electron donating ability is much greater than that of sulfones.[3,4,11-13] Among sulfoxides, the

Table 4. Values of K^{298}, ΔH and $\Delta\bar{\nu}_{OH}/\Delta\bar{\nu}_{NH}$ for the complex formation of diphenyl sulfoxide with various proton donors in carbon tetrachloride.

Proton donor	K^{298} / dm^3 mol^{-1}	$-\Delta H$ / kJ mol^{-1}	$\Delta\bar{\nu}_{OH}/\Delta\bar{\nu}_{NH}$ / cm^{-1}	Ref.
Phenol	61.4	20.3	298	2
1-Naphthol	77.9	23.1	321	3
2-Naphthol	89.8	23.4	315	4
2,2,2-Tribromoethanol	17.6	18.8	243	7
2,2,2-Trichloroethanol	22.1	18.8	247	7
2,2,2-Trifluoroethanol	48.6	21.0	250	5
Pyrrole	9.05	13.5	153	6
Indole	11.6	14.8	172	6
Carbazole	15.8	13.5	174	6

complex formation of dimethyl sulfoxide[14,15] with various proton donors has been extensively studied, and to a lesser extent the complex formation of diphenyl sulfoxide.[16-18] These studies have shown that the complex formation ability of dimethyl sulfoxide is greater than that of diphenyl sulfoxide, as do the results gathered from our earlier studies collected in Tables 3 and 4.

The results obtained here for the complex formation of dibenzyl sulfoxide with various proton donors seem to be in agreement with those reported earlier in the literature,[9,10] *i.e.* the tendency of dibenzyl sulfoxide to form hydrogen-bonded complexes is a little smaller than that of dimethyl sulfoxide (Table 3). This finding is consistent with the tendency of the phenyl group to withdraw electrons, in contrast to the methyl group in dimethyl sulfoxide. Steric factors may further help to lower the ability of dibenzyl sulfoxide to form hydrogen-bonded complexes. Taken together the results presented in Tables 1–4 show the relative basicities of the sulfoxides to be as follows:

diphenyl sulfoxide < dibenzyl sulfoxide < dimethyl sulfoxide

It may also be noted that there is no possibility of direct interaction between the phenyl ring and the sulfur atom in dibenzyl sulfoxide, a fact which is consistent with the sequence of the proton accepting ability found for diphenyl sulfoxide $[(C_6H_5)_2SO]$ and dibenzyl sulfoxide $[(C_6H_5-CH_2)_2SO]$.

As the experimental data in Tables 1 and 2 show, the proton donor ability of various proton donors towards dibenzyl sulfoxide, as displayed in the K and $-\Delta H$ values, decreases in the order:

2-naphthol > 1-naphthol > phenol > 2,2,2-trifluoroethanol > 2,2,2-trichloroethanol > 2,2,2-tribromoethanol > carbazole > indole > pyrrole

The $\Delta\bar{\nu}_{OH}$ and $\Delta\bar{\nu}_{NH}$ values also follow this same sequence, except in naphthols, where the $\Delta\bar{\nu}_{OH}$ is greater (369 cm^{-1}) for the 1-naphthol–dibenzyl sulfoxide complex than for the 2-naphthol–dibenzyl sulfoxide complex (359 cm^{-1}). It is unnecessary therefore to consider the possibility of specific interactions between dibenzyl sulfoxide and the various proton donors studied.

The presented complex formation ability of phenol, 1-naphthol and 2-naphthol towards sulfur–oxygen electron donors follows the acidity order of the proton donors and that of 2,2,2-trifluoroethanol follows the proton donor ability of phenol.[4,5,19] Among NH proton donors the proton donor ability is also in agreement with the acidity order between pyrrole and indole expressed as pK_a values determined in water.[6,20]

Finally, the recent studies by us and earlier studies by other investigators suggest that the complex formation ability of sulfoxides resembles that of sulfinamides.[1-7,21] The complex formation ability of sulfinamides is, in turn, of about the same order of magnitude as that of carboxamides. The K values are 145 dm^3 mol^{-1} for *N,N*-dimethylacetamide–phenol and 155 dm^3 mol^{-1} for *N,N*-dimethylmethanesulfinamide–phenol complexes at 298.15 K in carbon tetrachloride.[21,22] The sulfoxides are widely used as solvents, as well as extraction agents in liquid–liquid extraction or in extraction chromatography.[23] It may also be worth noticing that aromatic sulfoxides like dibenzyl sulfoxide seem to be more suitable than aliphatic sulfoxides

for the extraction of *e.g.* inorganic compounds due to their lower ability to form complexes as also the results presented in this paper clearly demonstrate.[23,24]

Acknowledgement. The financial support by the Magnus Ehrnrooth Foundation (to P.R.), by the Finnish Academy of Science and the Research Foundation of Medica (to J.K.) is gratefully acknowledged.

REFERENCES

1. Ruostesuo, P. *Finn. Chem. Lett.* (1979) 202.
2. Ruostesuo, P. *Finn. Chem. Lett.* (1979) 206.
3. Ruostesuo, P. and Karjalainen, J. *Finn. Chem. Lett.* (1979) 210.
4. Ruostesuo, P. and Karjalainen, J. *Acta Chem. Scand. A 33* (1979) 765.
5. Karjalainen, J. and Ruostesuo, P. *Finn. Chem. Lett.* (1980) 169.
6. Karjalainen, J. and Ruostesuo, P. *Acta Chem. Scand. A 34* (1980) 573.
7. Ruostesuo, P. and Karjalainen, J. *Spectrochim. Acta A 37* (1981) 535.
8. Saffioti, W., Nazario, G. and Gullo, I. M. de L. *Ecletica Quim. 1* (1976) 59.
9. Gramstad, T. *Spectrochim. Acta 19* (1963) 829.
10. Hadzi, D., Klofutar, C. and Oblak, S. *J. Chem. Soc. A* (1968) 905.
11. Barnard, D., Fabian, J. M. and Koch, H. P. *J. Chem. Soc.* (1949) 2442.
12. Cairns, T., Eglinton, G. and Gibson, D. T. *Spectrochim. Acta 20* (1964) 31.
13. Biscarini, P., Galloni, G. and Ghersetti, S. *Spectrochim. Acta 20* (1964) 267.
14. Augdahl, E. and Klæboe, P. *Acta Chem. Scand. 18* (1964) 18.
15. Drago, R. S., Wayland, B. and Carlson, R. L. *J. Am. Chem. Soc. 85* (1963) 3125.
16. Figueroa, R. H., Roig, E. and Szmant, H. H. *Spectrochim. Acta 22* (1966) 1107.
17. Kivinen, A., Murto, J. and Silvennoinen, B. *Acta Chem. Scand. A 28* (1974) 697.
18. Kivinen, A., Murto, J., Liljequist, S. and Vaara, S. *Acta Chem. Scand. A 29* (1975) 911.
19. Bhowmik, B. B. and Basu, S. *Trans. Faraday Soc. 59* (1963) 813.
20. Yagil, G. *Tetrahedron 23* (1967) 2855.
21. Møllendal, H., Grundnes, J. and Klæboe, P. *Spectrochim. A 24* (1968) 1669.
22. Nakano, H., Nakano, N. I. and Higuchi, T. *J. Phys. Chem. 71* (1967) 3954.
23. Vlacil, F. and Adamcova, E. *Collect. Czech. Chem. Commun. 43* (1978) 1606.
24. Vlacil, F. and Khanh, H. D. *Collect. Czech. Chem. Commun. 44* (1979) 1918.

Received July 1, 1981.

Acta Chemica Scandinavica A 36 (1982) 277–282

Short Communications

Some Medium Effects on the Nitration of 2-Iodo-1,3,5-trineopentylbenzene and 2-Iodo-1,3,5-triisopropylbenzene

INGEGÄRD JOHANSSON

Department of Organic Chemistry, University of Göteborg and Chalmers University of Technology, S-412 96 Göteborg, Sweden

In the nitration of 2-iodo-1,3,5-trialkylbenzenes two main products are formed, 2-nitro-1,3,5-trialkylbenzene and 2-iodo-4-nitro-1,3,5-trialkylbenzene from nitrodeiodination and nitrodeprotonation, respectively.[1-4] The rate-constant ratios for these two reactions of a series of 2-iodo-1,3,5-trialkylbenzenes in a nitric acid-nitromethane medium have been reported previously.[4] For sterically crowded substrates, branching in the α-position favours deiodination, while β-branching favours deprotonation. A rather large difference is found *e.g.* between 2-iodo-1,3,5-triisopropylbenzene, *1*, and 2-iodo-1,3,5-trineopentylbenzene, *2*, with deiodination – deprotonation rate ratios of 3.75 and 0.57, respectively. An explanation of the last-mentioned low ratio was sought in the interactions between the neopentyl substituents in 1,3,5-trineopentylbenzene derivatives found by Carter *et al.*[5] to give rise to two types of rotamer, A and B (see Fig. 1). Assuming preferential attack of the nitronium ion on the unsheltered side of rotamer A, expulsion of the iodonium ion would be hindered by the interacting alkyl branches (provided that such interaction in the transition state is similar to that occurring in the ground state). Thus, the nitrodeprotonation reaction would be favoured despite the resulting increase of steric strain in the product. The present communication reports an attempt to shed some light on this problem.

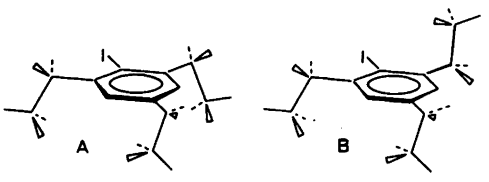

Fig. 1. Two possible rotamers of 2-iodo-1,3,5-trineopentylbenzene.

In order to vary the extent of intramolecular interaction and find out the effect on the deiodination – deprotonation ratio, two methods were used – changing the solvent and changing the temperature. Both substrates *1* and *2* were investigated to see if the solvent effects are fundamentally different for these two rather different molecules.

Results and discussion. Four nitroalkanes, nitromethane, *a*, nitroethane, *b*, 1-nitropropane, *c*, and 2-nitropropane, *d*, were examined as solvents with the idea that the alkyl branches of these molecules would interact with the neopentyl branches of substrate *2* and thus change the intramolecular interaction possibilities. The reactions were run in organic solvent – nitric acid media with the same acid concentration and similar substrate concentrations. The kinetics show a similar pattern for all the nitroalkanes, *i.e.*, changing from zeroth to first order during the course of the reaction. Initial rates and initial nitrodeiodination – nitrodeprotonation product ratios (=rate constant ratios[3]) are given in Table 1. The nitrodeiodination reaction is sometimes followed by an iodination process (only with *1* in this examination) which complicates the kinetics. This secondary reaction has been examined thoroughly in previous investigations.[3,4] Here, only the initial product ratios are given and hence the iodination is of no significance. The kinetics of the nitration will be discussed below. As can be seen, the product ratios for *1* are the same within the error limits (*cf.* 3.75 ± 0.11 as reported earlier[4]). The differences found with substrate *2* are also very small but a vague trend might be seen in the direction that the ratio is smaller when the solvent nitroalkane has a longer alkyl chain. This could be interpreted in terms of the above-mentioned interaction with the neopentyl branches (in this case causing a further decrease of the deiodination).

Next, one aromatic solvent, *p*-fluoronitrobenzene, *e*, was chosen to show the effect of a possible $\pi-\pi$ interaction between the solvent and the solute.

0302-4377/82/030277-03$02.50

Table 1. Nitrodeiodination–nitrodeprotonation product ratios (adjusted for the number of available positions) and initial rates for the nitrations of 2-iodo-1,3,5-triisopropylbenzene, *1*, and 2-iodo-1,3,5-trineopentylbenzene, *2*, in the solvents *a*–*f*. Conditions: 4.94 M nitric acid, 1.32 M water in solvents *a*–*e*, respectively, at 0 °C. In solvent *f* the same amounts of acid and water were added leading to a heterogenous reaction.

Substrate	Concentration of substrate (M)	Solvent	Nitrodeiodination–nitrodeprotonation product ratio	$\frac{d[ArHI]}{dt}$ (10^{-6} M s^{-1})	Reaction order in the aromatic substrate
1	0.00463	*a*	3.8	0.21	0–1
1	0.00468	*b*	3.6	0.12	0–1
1	0.00466	*c*	3.7	0.18	0–1
1	0.00465	*d*	3.7	0.11	0–1
1	0.00487	*e*	3.3	1.7	1
1	0.00594	*f*	4.3		
2	0.00221	*a*	0.57	0.50	0–1
2	0.00250	*b*	0.56	0.17	0–1
2	0.00268	*c*	0.50	0.22	0–1
2	0.00321	*d*	0.52	0.18	0–1
2	0.00274	*e*	0.50	2.9	1
2	0.00263	*f*	0.64		

Using hexafluorobenzene as solvent, Carter *et al.*[5] found a different rotamer population ratio in 2,4-dibromo-1,3,5-trineopentyl-6-nitrobenzene as a consequence of the $\pi-\pi$ interaction. The nitrodeiodination – nitrodeprotonation ratio measured in solvent *e* with the same acid concentration and in the same way as above is found to be somewhat smaller for both substrates *1* and *2* (product ratio in *e* relative to that in *a* is 0.85 for *1* and 0.875 for *2*), showing no fundamental difference in this case. The product ratios and the initial rates are accounted for in Table 1. Inspection of CPK models of the Wheland intermediates for nitrodeiodination and nitrodeprotonation reveals that that of the first-mentioned reaction is the most sterically demanding one. This would mean that if a certain solvent interacts more closely (*e.g.* by $\pi-\pi$ interaction) with the solute, the nitrodeiodination would be more hindered than the nitrodeprotonation. The increased hindrance as depicted by the models is especially obvious with substrate *2*, in which a rotation of an adjacent alkyl substituent seems necessary during the rehybridization process.

A complementary study was made with carbon tetrachloride, *f*, representing a system with less interaction with the solute. The same acid concentration was used, which resulted in a heterogenous mixture. Aliquots were nevertheless taken from the reaction mixture to make sure that the product ratio was the same during the reaction. Under these conditions the deiodination – deprotonation ratio is only somewhat larger for both substrates (product ratio in *f* relative to that in *a* is 1.13 for both, see Table 1). This may show that *f*, because it interacts very slightly with the solute, hinders the expulsion of the iodonium ion to a somewhat less extent than the other solvents do.

Investigations were also made in nitromethane with substrate *2* at two different temperatures; −28 °C (6 M acid) and 40 °C (2 M acid) to see if the different populations of the energy levels caused by the temperature increase would affect the deiodination – deprotonation ratio. This ratio was found to be 0.55 and 0.59, respectively, which, within the error limits, corresponds to what can be expected from the temperature difference according to transition state theory, assuming that there is no difference in entropy of activation between the two reactions.

Conclusion. The fact that the product ratio varies very little with the solvent indicates that the interaction between the solvent and the product-determining transition states is weak or, maybe more probable, that the interactions with the different solvents affect the nitrodeiodination and nitrodeprotonation reactions in the same way. The latter suggestion would mean that the product-determining transition states are rather similar. This is not self-evident in view of the differences in the electronegativity and polarizability of the two leaving substituents in question. However, as the reactions are very fast, the product-determining transition states may occur relatively early on the reaction path and thus resemble the preceeding

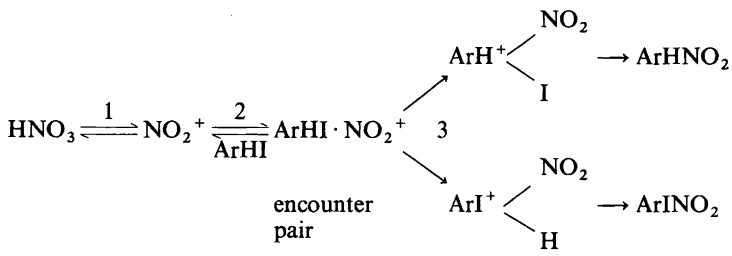

Scheme 1.

encounter pair and not differ too much among themselves.

Kinetics. The most widely accepted mechanism for the nitration reaction is described in Scheme 1. The kinetics are of zeroth order in the aromatic substrate when step 1 is rate-determining and first order when 2 or 3 is rate-determining.[6] In this investigation, the reaction order is found to be close to first order in solvent *e* and to change from zeroth to first order during the reaction in solvents *a*–*d*.

Inspection of the initial rates given in Table 1 reveals that in *p*-fluoronitrobenzene, *e*, the nitration is faster than in nitromethane, *a*, and that *a* is the "best" solvent for nitration compared to the other nitroalkanes, *b*, *c* and *d*. The relative order of *b* and *c* is also somewhat unexpected. When the reactions are close to zeroth order in the aromatic substrates, the initial rates are a measure of the rate of the nitronium ion production (step 1 in Scheme 1). The initial rate values should thus depend on the polarity of the solvent. Physical constants change in a monotonous way when the alkane chain is elongated [7] and thus the initial rate should change in the same way. However, as has been pointed out by Reichardt,[8] "no single macroscopic physical parameter could possibly account for the multitude of solute–solvent interactions on the molecular –microscopic level".

Experimental. The substrates have been synthesized for earlier investigations.[3,4] The equipment and methods used have been described.[3,4] The solvents used were commercial. Purity was tested by GLC and NMR and found to be: nitromethane (Aldrich Chem. Company, spectrophotometric grade) 95% with 2% nitroethane and 3% 2-nitropropane; nitroethane (Fluka) 97% with 2.5% 2-nitropropane and 0.5% nitromethane; 1-nitropropane (Fluka) 96% with 4% 2-nitropropane; 2-nitropropane (Fluka) 98% with 2% 1-nitropropane; *p*-fluoronitrobenzene (Fluka) 99.5%. All the measurements have been made at 0 °C unless otherwise stated. As the melting point of *e* is 21 °C the substrate solution was kept at room temperature and added to the acid solution at 0 °C. The reaction mixture was then cooled down to 0 °C before the measurements started, which meant that an extrapolation to the starting point had to be made.

Acknowledgements. I wish to thank Professor Lars Melander for all his valuable and constructive criticism during the preparation of this manuscript. Financial support from the Swedish Natural Science Research Council is gratefully acknowledged.

1. Olsson, K. *Acta Chem. Scand. B 28* (1974) 322.
2. Olsson, K. and Martinsson, P. *Acta Chem. Scand. 26* (1972) 3549.
3. Johansson, I. and Olsson, T. *Acta Chem. Scand. A 35* (1981) 481.
4. Johansson, I. *Acta Chem. Scand. B 35* (1981) 723.
5. Carter, R. E., Nilsson, B. and Olsson, K. *J. Am. Chem. Soc. 97* (1975) 6155.
6. Ridd, J. H. *Adv. Phys. Org. Chem. 16* (1978) 1.
7. Riddick, J. A. and Bunger, W. B. *Organic Solvents*, Wiley-Interscience, New York 1970.
8. Reichardt, C. *Solvent Effects in Organic Chemistry*, Verlag Chem., Weinheim–New York 1979, p. 225.

Received November 24, 1981.

Magnetic Properties of the Dimeric Complex Di-μ-chloro-bis[bis-(benzotriazole)chlorocopper(II)] Monohydrate

DEREK J. HODGSON* and
ERIK PEDERSEN

Chemistry Department I, Inorganic Chemistry, H. C. Ørsted Institute, University of Copenhagen, Universitetsparken 5, DK-2100 Copenhagen Ø, Denmark

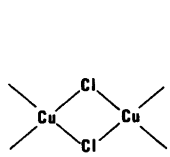

1

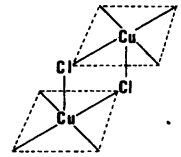

2

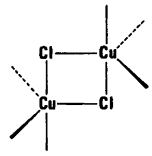

3

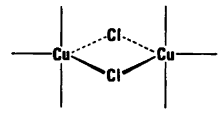

4

The structural and magnetic properties of dimeric copper(II) complexes have been the subjects of intense recent research activity. For the case of planar complexes with two hydroxo bridges, $[CuL(OH)]_2^{n+}$ where L is a bidentate ligand, a linear correlation between the isotropic magnetic exchange parameter, J, and the bridging Cu–O–Cu angle, ϕ, has been demonstrated,[1,2] but distortions from square planar geometry[3] or from bridge planarity[4] give rise to complexes which do not follow this simple relationship between J and ϕ. A similar relationship apparently does obtain[5] for the analogous, in-plane chloro-bridged dimers $[CuL(Cl)]_2^{n+}$ (*1*), but this geometry is relatively uncommon for halogen-bridged copper(II) dimers which evidently prefer to form apical–basal bridges with either square pyramidal (*2*) or (less commonly) trigonal bipyramidal (*3*) geometry at copper.[1] We have been searching for a structural–magnetic correlation for complexes of types *2* and *3*, but while we have made some progress in identifying the Cu–Cu′ distance (R) and the Cu–Cl–Cu′ angle (ϕ) as the principal structural parameters[6] no entirely satisfying model has yet emerged.

We were, therefore, particularly interested to learn of the structure of the title complex, $[Cu(BTAH)_2Cl_2]_2 \cdot H_2O$, (where BTAH = $C_6H_5N_3$) which was recently determined by Søtofte and Nielsen.[7] This complex crystallizes with two independent dimeric units in the cell, both of which can be viewed as the hitherto unreported equatorial–equatorial trigonal bipyramidal dimer (*4*) or alternatively as highly distorted dimers of type *2*. In the idealized case of *4*, the magnetic orbital at each copper center is d_{z^2} and the axial systems at the two centers are parallel. The d_{z^2} orbitals transform as a_g in either the idealized D_{2h} symmetry (where the axial ligands are assumed to be identical) or the observed[7] C_i symmetry, and the overlap integral $\langle a_g|a_g\rangle$ between these magnetic orbitals is a function of the bridging angle ϕ. For most bridging angles, this overlap is expected to be very weak, and there will be some value of ϕ near 90° where it vanishes. Since we can write the magnetic exchange parameter J as the sum of ferromagnetic (J_F) and antiferromagnetic (J_{AF}) components[8] where the antiferromagnetic contribution to J is a function of this overlap $\langle a_g|a_g\rangle$, and since ϕ is observed to be near 90° in both independent molecules,[7] it is apparent that we expect $|J_{AF}|$ to be very small. The ferromagnetic term J_F is a function of the internuclear Cu–Cu′ separation in the dimer and has been described[9] as

$$J_F = K\langle\psi_A(1)\psi_B(2)|R^{-1}|\psi_A(2)\psi_B(1)\rangle$$

where A and B are the two metal centers. Since R here is[7] approximately 3.5 Å rather than the value of approximately 3.0 Å observed[2] in the dihydroxo-bridged dimers, J_F is expected to be small also. Hence, on this qualitative basis, we anticipate that for the present dimer $|J|$ should be small and that J should be positive. In order to test these ideas, we have examined the magnetic susceptibility of the complex $[Cu(BTAH)_2Cl_2]_2 \cdot H_2O$.

The magnetic susceptibility of a powdered sample (the generous gift of I. Søtofte) was measured by the Faraday method at a field strength of 12,000 Oe in the temperature range 4–240 K; a description of the instrumentation has been provided previously.[10,11] Since it was apparent from the data that the isotropic exchange parameter, J, is small in magnitude and that consequently the application of the usual Bleaney-Bowers expression[12] is

*Permanent address: Department of Chemistry, University of North Carolina, Chapel Hill, NC 27514, U.S.A.

0302-4377/82/030281-02$02.50

inappropriate since the necessary condition $|J| \gg g\mu_B H$ would not be satisfied, the data were fitted to the magnetization expression [13] [eqn. (1)],

$$M = \frac{Ng\mu_B \sinh(g\mu_B H/kT)}{1+\exp(-2J/kT)+2\cosh(g\mu_B H/kT)} \quad (1)$$

$$H_{ex} = -2J\vec{S}_1 \cdot \vec{S}_2 + g\mu_B H\vec{S} \quad (2)$$

where the exchange Hamiltonian is given by eqn. (2) and $\vec{S}$ is the total spin (*i.e.* $\vec{S} = \vec{S}_1 + \vec{S}_2$). Inter-dimer interactions, which are not included in these expressions, can be estimated from a molecular field approximation, eqn. (3), where H_{eff} is the effective magnetic field. The susceptibility data were fitted to

$$H_{eff} = H + \gamma M \quad (3)$$

$$\chi = M/H \quad (4)$$

expression (1), where the magnetization M is defined by eqn. (4) with the parameters g and J as variables, using a non-linear least-squares procedure. This process resulted in the values $g = 2.055 \pm 0.006$ and $J = +0.90 \pm 0.09$ cm^{-1}; the mean fractional deviation (MFD) for this fit was 0.026. It should be noted that with J defined as in expression (2) the single – triplet separation is $|2J|$ and positive values of J correspond to triplet ground states. Attempts to fit the data with non-zero values of γ [see expression (3)] were unsuccessful, presumably because for these data the parameters J and γ are more than 99% correlated.

An alternate model for the susceptibility of a dimer using a molecular field approach to inter-dimer interactions has recently been developed by van Santen, van Duyneveldt and Carlin [SDC],[14] who derive an expression which can be written as eqn. (5), where J' represents the inter-dimer

$$\chi = Ng^2\mu_B{}^2/3k\{T[1+1/3\ \exp(-2J/kT)] - 32\ J'/k\} \quad (5)$$

exchange interaction and positive values of J and/or J' again imply ferromagentic interactions. Ths use of this model is particularly appropriate when expressions involving only a single exchange parameter indicate large ferromagnetic interactions, and it was hoped that it would provide valuable insights in the present case also. The data fit reasonably well to expression (5) with J' fixed as zero and g and J as variables, which is equivalent to the Bleaney-Bowers expression,[12] and gave values of $g = 2.045 \pm 0.003$ and $J = +1.1 \pm 0.2$ cm^{-1}. This fit, which has MFD = 0.030, is not as good as that described above for expression (1), but it is encouraging to note that these values for g and J are not significantly different from those obtained above. Attempts at varying J' in addition to g and J were unsuccessful, and the fit with a variety of fixed values of J' (both positive and negative) was far inferior to that obtained with $J' = 0$. It may be that data at much lower temperatures would be required in the present case in order to abstract meaningful values of J' or, alternatively, of γ.

We can, however, conclude that the complex exhibits a weakly ferromagnetic interaction indicative of a triplet ground state lying 1.8 ± 0.2 cm^{-1} below the singlet excited state. This result, of course, is entirely consistent with our expectations based on the observed [7] structure of the dimer.

Acknowledgements. We are very grateful to Dr. Inger Søtofte for providing the sample used in this analysis and for giving us a copy of her manuscript prior to its publication. We are also grateful to her and to Dr. Kurt Nielsen for stimulating conversations. DJH is grateful to Chemistry Department I, H. C. Ørsted Institute, for hospitality and support as Visiting Professor. Acknowledgement is made to the Petroleum Research Found, administered by the American Chemical Society, for support of this research through grant No. 12128-AC3,6 (to DJH) and to the Danish National Science Research Council through grants Nos. 511 – 742, 511 – 3993, and 511 – 10516 (to E.P.).

1. Hodgson, D. J. *Prog. Inorg. Chem. 19* (1975) 173.
2. Crawford, V. H., Richardson, H. W., Wasson, J. R., Hodgson, D. J. and Hatfield, W. E. *Inorg. Chem. 15* (1976) 2107.
3. Countryman, R. M., Robinson, W. T. and Sinn, E. *Inorg. Chem. 13* (1974) 2013.
4. Charlot, M. F., Kahn, O., Jeannin, S. and Jeannin, Y. *Inorg. Chem. 19* (1980) 1410.
5. Roundhill, S. G. N., Roundhill, D. M., Bloomquist, D. R., Landee, C., Willett, R. D., Dooley, D. M. and Gray, H. B. *Inorg. Chem. 18* (1979) 831.
6. See, for example, Marsh, W. E., Hatfield, W. E. and Hodgson, D. J. *Inorg. Chem. In press.*
7. Søtofte, I. and Nielsen, K. *Acta Chem. Scand. A 35* (1981) 733.
8. Kahn, O., Tola, P., Galy, J. and Coudanne, H. *J. Am. Chem. Soc. 100* (1978) 3931.
9. Tola, P., Kahn, O., Chauvel, C. and Coudanne, H. *Nouv. J. Chim. 1* (1977) 467.
10. Pedersen, E. *Acta Chem. Scand. 26* (1972) 333.
11. Josephsen, J. and Pedersen, E. *Inorg. Chem. 16* (1977) 2523.
12. Bleaney, B. and Bowers, K. D. *Proc. R. Soc. London, Ser. A 214* (1952) 451.
13. Meyers, B. E., Berger, L. and Friedberg, S. A. *J. Appl. Phys. 40* (1969) 1149.
14. van Santen, J. A., van Duyneveldt, A. J. and Carlin, R. L. *Inorg. Chem. 19* (1980) 2152.

Received November 19, 1981.

Acta Chemica Scandinavica A 36 (1982) 283–295

The Molecular Structure of Gaseous 5-Methyl-1,3,4-oxathiazole-2-one, $CH_3C{=}N{-}S{-}CO{-}O$

BØRGE BAK,[a] OLE NIELSEN,[a] HENRIK SVANHOLT,[a] ARNE ALMENNINGEN,[b] OTTO BASTIANSEN,[b] GEIR BRAATHEN,[b] LIV FERNHOLT,[b] GRETE GUNDERSEN,[b] CLAUS J. NIELSEN,[b] BJØRG N. CYVIN[c] and SVEN J. CYVIN[c]

[a] Chemical Laboratory V, The H. C. Ørsted Institute, University of Copenhagen, DK-2100 Copenhagen, Denmark, [b] Department of Chemistry, University of Oslo, Oslo 3, Norway and [c] Division of Physical Chemistry, University of Trondheim, N-7034 Trondheim-NTH, Norway

The title compound has been studied by microwave, infrared and Raman spectroscopy and by electron diffraction from the vapour. The spectral data have been interpreted in terms of C_s-symmetry, and a normal coordinate analysis has been carried out. The final structural refinement was based upon electron-diffraction intensities in combination with the microwave rotational constants. The vibrational amplitude parameters applied were derived from force field calculations, which were also used to calculate shrinkage corrections and to make the electron-diffraction and spectroscopic rotational constants compatible. As compared with the structure of 1,3,4-oxathiazol-2-one, the results suggest that methyl substitution has caused only minor changes in the ring geometry. The C(ring)–C (sp^3) bond (r_a) was found to be 1.487(3) Å and the three fold rotational barrier for the methyl group as determined from the microwave data was 5.98 kJ/mol. Due to some inconsistencies in the force-field calculations for the title compound and the parent molecule a recalculation for the latter was included. A new set of amplitude quantities was used in the structural reanalysis, but significant changes in the geometrical parameters were not encountered.

The results of spectroscopic and electron-diffraction studies of 1,3,4-oxathiazol-2-one (I) have recently been published.[1] The investigation was carried out in order to provide a basis for a future theoretical treatment of its facile pyrolysis. The methyl derivative, 5-methyl-1,3,4-oxathiazol-2-one (II), starts to break down at about 600K on a quartz surface under low pressure[2] and thus exhibits similar pyrolysis properties as the parent molecule (I). Comparable structural information was wanted for I and II, and this paper reports results for II as obtained by microwave, infrared and Raman spectroscopy and by electron-diffraction.

EXPERIMENTAL

(a) Sample. 5-Methyl-1,3,4-oxathiazole-2-one was prepared as described elsewhere.[3] None of the recorded infrared, Raman or microwave spectra indicated the presence of impurities.

(b) Microwave. Microwave spectra were recorded at 10–50 mTorr and at room temperature in the 12.5–40 GHz regions using a Hewlett-Packard 8460 MRR instrument. Stark voltages in the range 25–2000 V/cm were applied.

(c) Infrared and Raman. Infrared spectra of the vapour (pathlength 1 m), the CCl_4 and CS_2 solutions, the pure liquid and of the unannealed and annealed solid at liquid nitrogen temperature were recorded on a Perkin-Elmer Model 225 spectrometer and with a fast scan Bruker Model 114C interferometer. Far infrared spectra of cyclohexane solutions were obtained with the Bruker interferometer over the region 400–50 cm^{-1}.

Raman spectra were obtained on a modified[4] Cary Model 81 Raman spectrometer using the 5145 Å line from an argon ion laser for excitation. The liquid sample was studied in a sealed glass tube and polarization data were obtained.

(d) Electron diffraction. The electron-diffraction data were recorded in the Oslo Apparatus[5] for nozzle-to-plate distances of 479.30 and 199.30 mm, using Kodac Electron Image plates and a nozzle-tip temperature of 62 °C. The electron wavelength was 0.06469 Å as calibrated against diffraction patterns

0302-4377/82/040283-13$02.50

of gaseous benzene. The estimated standard deviation in the determination of the electron wavelength is 0.1 %. Three, respectively, four plates for the long (48 cm) and the short (20 cm) camera distances were selected for the structure analysis. The plates were densitometered while oscillating the plates and the obtained densities were processed[6] using a blackness correction of $1+0.03D+0.09D^2+0.03D^3$. A modification function $s/|f'_C|\cdot|f'_S|$ was applied and a computer program, essentially equal to that described by L. Hedberg,[7] was used to subtract the background on the modified form employing polynomia of 9th degree. The various atomic scattering amplitudes and phases[6] were calculated as described for the parent molecule.[1]

ANALYSIS OF MICROWAVE DATA

Rotational and distortion constants. A total of 81 *R*-type μ_a-lines ($3<J<13$) and 3 *Q*-type lines:

$11_{1.11}\rightarrow 11_{1.10}$ at 28340.19 MHz

$14_{3.12}\rightarrow 14_{3.11}$ at 27605.09 MHz

$16_{4.13}\rightarrow 16_{4.12}$ at 27464.76 MHz

were assigned to the ground state by their relative intensities and observed Stark patterns. The three *Q*-type transitions above are reported to introduce as a *sine qua non* that rotational and distortion constants (Table 1) of a molecule should never be published without some experimental frequencies which may be used to identify compounds by searching for authentic transitions. All experimental frequencies are available upon request. The 84 observed lines were fitted by the least squares method (r.m.s. deviation 0.07 MHz). One of the distortion constants, Δ_K, had virtually no influence on the frequencies. It was hence constrained to 1.025 kHz as calculated from a force field. This approach affected the determination of the remaining distortion constants and was necessary to give agreement with values obtained in force field calculations.

Line splittings due to the quadrupole moment of nitrogen or to CH_3 tunnelling (*A*,*E*) splitting for the ground state were not observed. The established $ID=I_c-I_b-I_a=3.0987$ uÅ^2 is consistent with a planar heavy atom structure.

Table 1. Rotational ground state parameters for 5-methyl-1,3,4-oxathiazole-2-one. Rotational constants (A_o, B_o, C_o) in MHz. Quartic distortion constants (Δ_J,Δ_{JK},Δ_K,δ_J,δ_{JK}) in kHz. Inertial defect (ID) in uÅ^2 and the asymmetry parameter (κ) dimensionless.[a]

A_o	4239.844 (18)[a]
B_o	2113.2295(28)
C_o	1422.6055(20
κ	−0.5097
ID	−3.0987
Δ_J	0.1161(77)
Δ_{JK}	0.110 (31)
Δ_K	1.025 −[b]
δ_J	0.0224(52)
δ_{JK}	0.218 (84)

[a] Values in parentheses represent one standard deviation. [b] Constrained to value calculated from a force field.

Table 2. Observed transitions (MHz) associated with the first torsionally excited level of 5-methyl-1,3,4-oxathiazole-2-one (ν_A, ν_E) and the corresponding observed and calculated line splittings ($\nu_A-\nu_E$); with the ground vibrational state values ($\nu^\circ_{A,E}$) in square brackets; and the calculated CH_3-torsion hindering barrier, V_3 in cm^{-1}.

Transition	ν_A	ν_E	$\nu_A-\nu_E$		V_3[a]
			Obs.	Calc.	
$4_{2.2}-5_{2.3}$	19245.3	19229.5	15.8	15.3	498.6
	[19257.73]		–	[0.01]	
$5_{2.4}-6_{2.5}$	20581.4	20589.4	−8.0	−7.8	498.7
	[20591.34]		–	[0.05]	
$6_{1.5}-7_{1.6}$	24545.6	24550.8	−5.2	−5.4	501.3
	[24556.37]		–	[0.15]	
$7_{2.5}-8_{2.6}$	30285.2	30289.0	−3.8	−4.0	502.3
	[30302.34]		–	[0.14]	

[a] $V_3=500.2$ cm^{-1} corresponds to a CH_3 torsional frequency of 143 cm^{-1}.

Table 3. Infrared and Raman spectral data[a] for 5-methyl-1,3,4-oxathiazole-2-one.

Infrared						Raman			Assignment
Vapour		Solution	Liquid	Amorphous solid −180°	Polycryst. solid −180°	Liquid	Amorphous solid −180°	Polycryst. solid −180°	
~3570	vw,?	3505 w[b]	3495 w	3490 w,bd	3460 w 3442 w				$2\times\nu_3$
		3235 w	3230 vw	3240 vw	3260 vw				$2\times\nu_4$
		3022 vw	3020 vw	3028 w		3025 m	3025 m 2999 m,sh	3016 m 3001 m	$\nu_4+\nu_5$
		2980 w	2980 vw	2985 w	2984 w	2984 m,D	2982 s	2982 s	ν_{17}
		2936 w	2935 w	2933 w	2930 w	2934 vs,P	2933 vs	2929 vs	ν_1
		2848 w	2850 vw	2850 w	2851 w 2846 w	2847 w,P	2842 w	2843 w	ν_2
		2809 vw	2810 vw		2803 vw				$\nu_5+\nu_6$
		2744 vw	2740 vw		2735 vw	2745 w,P	2739 w	2739 w	$2\times\nu_6$
1945	w,?	1955 w	1959 w	1970 w	1968 m				comb.[c]
1898	m,?	1907 w	1914 w	1925 m	1919 m				comb.
1833 1820	vs,AB	1820 s	1825 m	1836 m,bd	1836 m	1825 w	1833 w,bd	1833 w	ν_3, FR
1775 1766	s,AB	1766 vs	1762 vs	1756 s	1763 s	1755 m,P	1756 m	1753 m	$2\times\nu_{10}$, FR
		1740 s	1743 s	1734 s	1743 s	1741 m,sh,P	1738 m	1744 m 1726 s	$\nu_9+\nu_{11}$, FR
			1719 w,sh	1718 m			1716 w	1716 m	$\nu_8+\nu_{12}$
		1698 w	1698 w	1700 w	1695 w	1697 w	1698 w	1694 w	$\nu_7+\nu_{15}$
		1646 w	1649 w	1655 w	1658 w 1637 w	1648 w,sh	1650 w	1656 w	comb.
1636 1625	s,AB	1623 s	1624 s	1626 s	1632 s	1622 s,P	1624 s	1632 s	ν_4
				1616 w	1619 m 1611 w				
		1600 vw,sh	1603 w,sh		1604 w 1589 m			1587 w	comb.
		1562 w 1482 vw	1562 w 1483 vw	1567 w	1577 w	1561 w			$2\times\nu_{11}$ $\nu_{10}+\nu_{13}$
			1440 m,sh	1439 m,sh	1444 s		1440 w,sh	1440 w	ν_{18}
1450 1443 1437	m,AB	1433 m	1431 m	1430 m	1432 s	1431 m,P	1426 m	1426 s	ν_5

		1389 m	1390 m	1393 w,sh	1427 s 1401 w	1392 w,sh	1403 w,sh		comb., FR
1398 1392 1387	m,AB	1381 m	1380 m	1381 m	1379 m 1376 s	1381 m,P	1379 m	1378 m	ν_6, FR
		1355 vw	1357 vw,sh						$\nu_{11}+\nu_{21}$
1348 1340 1331	w,AB	1340 vw	1339 vw			1338 vw			$\nu_{10}+\nu_{15}$
		1302 w	1304 w	1308 w	1319 w 1311 w	1303 w			$2\times\nu_{21}$, FR
1274 1270 1263	s,AB	1261 s	1259 s	1261 s	1262 s	1259 w	1260 w		ν_7, FR
1244	w,?	1248 m	1248 m	1250 m,sh	1253 s 1249 m	1248 w	1247 w	1251 w	comb., FR
		1231 w,sh	1225w,sh	1230 w,sh	1228 w				
1180	vw,?	1210 vw,sh	1211 vw		1215 w 1207 w				
		1199 vw,sh			1200 vw	1198 w			comb.
		1161 vw	1159 vw						
1118	vw,?	1138 vw 1112 vw 1087 vw	1137 vw 1109 vw	1146 vw	1151 vw				
1048 1044 1038	m,AB	1041 s	1044 s	1050 s 1039 m,sh	1050 s 1045 s 1041 s	1043 m,P	1048 m	1049 m	ν_8, ν_{19}
1002 995 990	m,AB	993 m	997 m	999 s	1000 s 998 s	997 w	997 w	997 w	ν_9
911 905 900	s,AB	912 s	920 s,bd	930 vs,bd	923 vs	919 w,bd	926 w,bd	919 m	ν_{10}
		881 vw 861 vvw,sh 840 vvw 822 vvw	882 vw 864 vvw,sh 846 vvw 818 vvw	862 vvw	900 vw 855 vvw				comb.
791 786 780	w,AB	783 m	785 m	787 s	803 s 796 m	784 m,P	786 m	803 s	ν_{11}
		766 vvw,sh 745 vvw	766 vvw,sh 744 vw	765 vvw 737 vw	765 vw 733 vw				$\nu_{21}+\nu_{23}$ $\nu_{21}+\nu_{24}$

704 691	w,AB	699 w	700 w	702 m	700 m	699vs,P	701 vs	699 vs	ν_{12}
661 652 639	w,C	651 m	651 m	651 s	658 s	650 w,D	652 w	656 w	ν_{20}
		639 vw,sh	638 vw,sh	638 vw	641 vw				
606 603 600	vw,AB	606 w	605 w	607 m	604 m	605 vs,P	608 vs	609 vs	ν_{13}
596		598 w	598 w	596 w	600 m	597 w,sh	597 w,sh	598 w	ν_{21}
562 556 550	w,AB	557 m	555 m	556 m	563 s 550 s	555 s,P	556 vs	561 s 549 s	ν_{14}
		549 vw,sh	547 vw,sh	548 vw,sh	546 m,sh				$\nu_{16}+\nu_{22}$
442 438 432	w,AB	439 m	440 m	443 m	448 m	440 s,P	444 s	448 s	ν_{15}
		302 w	305 w	310 w	312 m 289 m	305 m,D	308 m	312 m 283 w	ν_{22}
		255 m	258 m	272 m	280 s 271 m	258 w	269 w	270 w	ν_{16}
		180 vw				187 w,D			ν_{23}
143[d]									ν_{24}

[a] Bands in the regions 5000 – 3500 and 2700 – 2000 cm^{-1} were omitted. [b] Abbreviations; s, strong; m, medium; w, weak; v, very; bd, broad; P, polarized; D, depolarized; FR, Fermi resonance; A, B and C denote vapour contours. [c] Combination or overtone, used when several possibilities present. [d] From microwave investigation, see text.

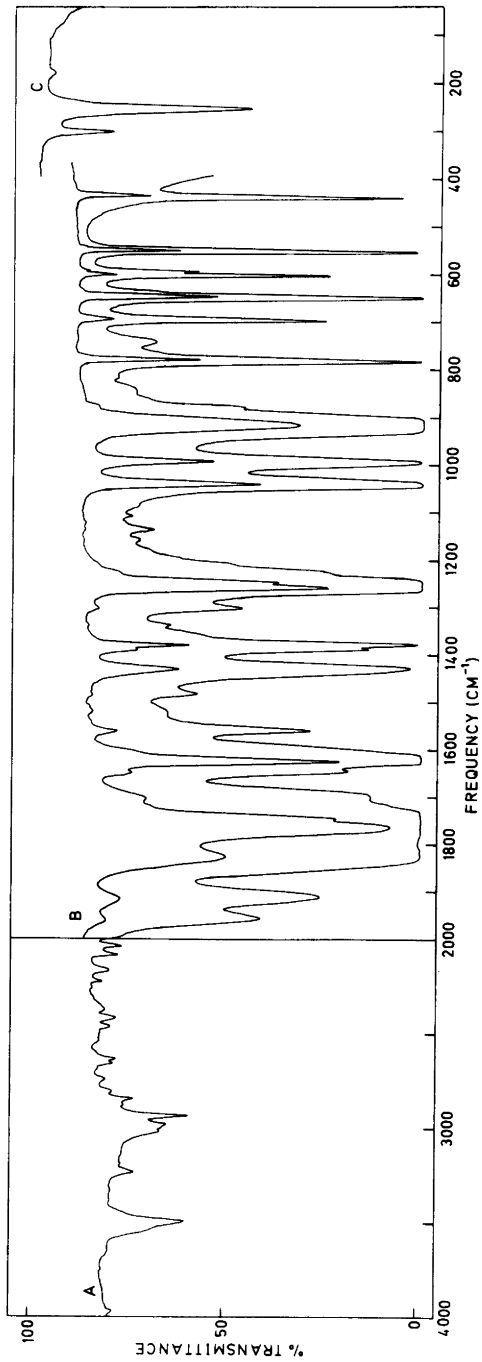

Fig. 1. Infrared spectrum of 5-methyl-1,3,4-oxathiazole-2-one in the liquid phase, (A) 0.025 mm cell and (B) thin film and in cyclohexane solution (C).

Rotational barrier. Transitions associated with the first torsionally excited level are reported in Table 2. Neglecting interference from other vibrational modes, Coriolis coupling *etc.*, and assuming a torsion hindering potential of 3-fold symmetry, $V_3 = 500.2 \pm 1.4$ cm^{-1} (1.43 kcal/mol; 5.98 kJ/mol) reproduces the observed *A,E* splittings within 0.2–0.5 MHz (Table 2). In agreement with our observations for the vibrational ground state, the corresponding calculated $\nu_A^\circ - \nu_E^\circ$ values are too small to be observed with our instrumentation.

VIBRATIONAL SPECTRA

The wavenumbers of the observed bands are listed in Table 3 and the infrared (IR) and Raman spectra of the liquid are shown in Figs. 1 and 2, respectively. The spectra have been interpreted in terms of C_s-symmetry. The 24 fundamental vibrations, divided into 16 *A′* and 8*A″* modes, are all active in both IR and Raman. The A′ modes polarized and have *A,B* hybrid contours, while the *A″* modes exhibit *C*-type contours. The *PR* separations calculated from the rotational constants determined from the rotational spectra[8] were 14, 10 and 21 cm^{-1} for the *A*, *B* and *C* bands, respectively. This is distinctly different from the values of the parent molecule (I).[1]

As apparent from Table 3, the assignment is, with few exceptions, straightforward. Several intense bands are observed in the carbonyl stretching region. The relative intensity of the two strongest infrared bands are reversed going from the vapour phase to the liquid state. Similar effects were observed for the parent molecule,[1] and this behaviour is assumed to be caused by Fermi resonance between ν_3 and a number of combination and overtone bands (Table 3). Except for the lowest *A′* mode, ν_{16}, the remaining *A′* fundamentals have been assigned on basis of the vapour phase contours and the polarization data. The in-plane bending of the methyl group (ν_{16}) has been assigned to an IR band around 255 cm^{-1} for which no vapour phase band contours nor polarization data are available.

Only four of the eight *A″* fundamentals (ν_{17}, ν_{20}, ν_{22} and ν_{23}, Table 3) can readily be assigned on basis of vapour phase band and polarization data. The CH_3 deformation modes, ν_{18} and ν_{19}, were in analogy with 2-methyl-furane[9] assigned to the bands around 1440 and 1041 cm^{-1} with the latter coinciding with ν_8. The weak band at 598 cm^{-1} observed both in IR and Raman was assigned to

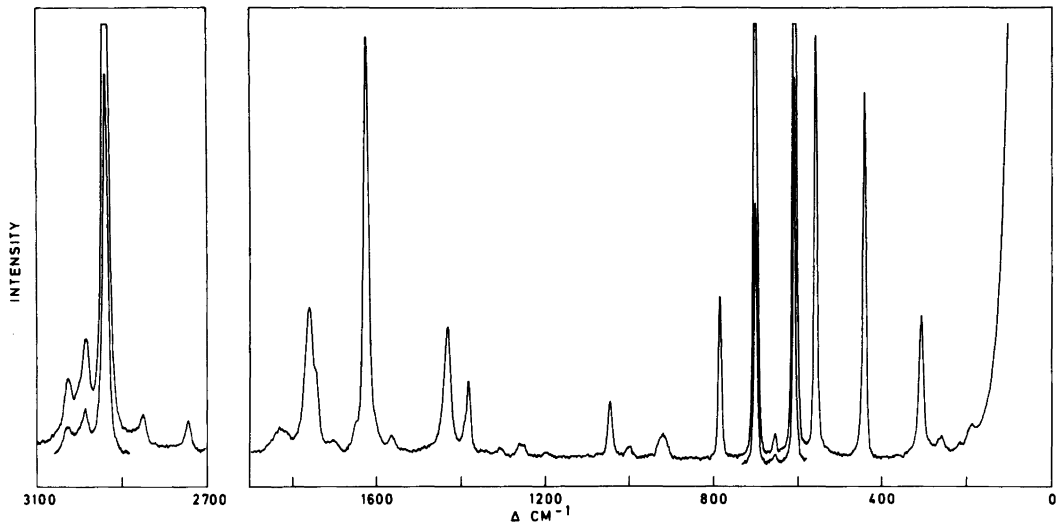

Fig. 2. Raman spectrum of 5-methyl-1,3,4-oxatiazole-2-one in the liquid phase.

the ring deformation, ν_{21}. For the lowest A'' fundamental, the methyl torsional mode, the value of 143 cm^{-1} proposed by the microwave investigation (Table 2), but not observed in the vibrational spectra has been adopted.

FORCE FIELD CALCULATIONS

As for the parent molecule, a force field based on the vibrational spectra data was derived in order to provide possibilities for calculations of vibrational quantities needed in the further structural analysis. A set of initial force constants was based on an estimated force field used for I, augmented with appropriate coordinates for the methyl group accounting for some expected effects from methyl substitution. It was necessary to introduce five additional coordinates in species A' and four in A''. For this purpose the symmetry-adapted combinations of stretchings and bondings were applied, *viz.* $2a_1+3e$, pertaining to local C_{3v} symmetry.[10] In addition one methyl torsion coordinate was introduced. The methyl force constants were thus assumed to be part of a local diagonal F-matrix. The correlations with the symmetry species of C_s, which is the symmetry of the whole molecule, are very simple, *viz.* $5A'(2a_1+3e_a)+4A''(3e_b+c)$. Here c is the ring-methyl coupling, and it is covered by the torsional coordinate. The approximate force field including redundancies, gave calculated frequencies in fair agreement with the observed ones. A set of independent symmetry coordinates was constructed. The secular equation of molecular vibrations was solved in terms of these coordinates. The symmetry force constants were adjusted to fit accurately the experimentally assigned frequencies. This last piece of the analysis was achieved by a method of maintaining the normal-coordinate transformation matrix (L) from the approximate computation.

The final force field was used to calculate root-mean square and perpendicular amplitudes of vibration (u and K-values). The results are given in Table 4 for temperatures of 0 K and 335 K (subscripts O and T, respectively) using atomic coordinates transferred from the parent molecule and describing the methyl group by $\angle OCC=114.5°$ $r(CC)=1.50$ Å, $\angle CCH=109.7°$, $r(CH)=1.09$ Å and $\theta(HCC=N)=0°$. Using the calculated u- and K-values the corrections from r_a to r_α and r_a° were computed as described for I.[1] The force field was also used to compute the vibrational correction terms to the rotational constants (δB_{vib}), and the B_o values were converted to the B_z counterparts neglecting the centrifugal and electronic corrections. The r_z representatives of the rotational constants are given in Table 5, and their standard deviations, σ_z, given in parentheses, are estimated to be 30 % of the calculated δB_{vib} values.

Table 4. Vibrational amplitude quantities in Å for 5-methyl-1,3,4-oxathiazol-2-one calculated from a force field as described in the text at temperatures of 335 and 0 K (subscripts T and 0, respectively).

	u_T	K_T	u_0	K_0
O1–C2	0.0477	0.00425	0.0466	0.00263
O1–C5	0.0478	0.00363	0.0466	0.00250
S3–C2	0.0453	0.00170	0.0436	0.00132
S3–N4	0.0460	0.00321	0.0445	0.00202
N4=C5	0.0458	0.00293	0.0450	0.00246
O6=C2	0.0397	0.00591	0.0392	0.00377
C5–C7	0.0486	0.00730	0.0475	0.00378
C7–H8	0.0790	0.06746	0.0790	0.02901
C7–H9	0.0787	0.07275	0.0787	0.03060
C7–H10	0.0787	0.07275	0.0787	0.03060
S3···O1	0.0489	0.00250	0.0464	0.00116
N4···C2	0.0540	0.00216	0.0517	0.00151
S3···C5	0.0496	0.00182	0.0468	0.00115
O1···N4	0.0549	0.00298	0.0530	0.00175
C2···C5	0.0531	0.00204	0.0509	0.00159
O1···O6	0.0618	0.00591	0.0564	0.00260
S3···O6	0.0580	0.00195	0.0521	0.00101
O1···C7	0.0768	0.00616	0.0642	0.00266
N4···C7	0.0729	0.00415	0.0629	0.00216
O6···N4	0.0588	0.00178	0.0553	0.00088
O6···C5	0.0603	0.00210	0.0558	0.00109
S3···C7	0.0615	0.00107	0.0552	0.00054
C2···C7	0.0694	0.00177	0.0608	0.00101
O6...C7	0.0840	0.00069	0.0681	0.00045
C5···H8	0.1121	0.04089	0.1106	0.01664
C5···H9	0.1118	0.04229	0.1102	0.01729
C5···H10	0.1118	0.04229	0.1102	0.01729
O1···H8	0.1099	0.02891	0.1050	0.01127
O1···H9	0.1974	0.03027	0.1515	0.01217
O1···H10	0.1974	0.03027	0.1515	0.01217
C2···H8	0.1167	0.01817	0.1134	0.00726
C2···H9	0.1716	0.01927	0.1425	0.00766
C2···H10	0.1716	0.01927	0.1425	0.00766
S3···H8	0.1453	0.01875	0.1338	0.00701
S3···H9	0.1406	0.01684	0.1265	0.00662
S3···H10	0.1406	0.01684	0.1265	0.00662
N4···H8	0.1532	0.03292	0.1399	0.01273
N4···H9	0.1617	0.02567	0.1289	0.01063
N4···H10	0.1617	0.02567	0.1289	0.01063
O6···H8	0.1175	0.01230	0.1122	0.00519
O6···H9	0.2131	0.01432	0.1600	0.00564
O6···H10	0.2131	0.01432	0.1600	0.00564
H8···H9	0.1297	0.11626	0.1293	0.04329
H9···H10	0.1297	0.11626	0.1293	0.04329
H8···H10	0.1305	0.12166	0.1302	0.04471

STRUCTURE DETERMINATION

The electron-diffraction intensity data and the corresponding experimental radial distribution curve are shown in Figs. 3 and 4, respectively. The latter figure contains a molecular model with the numbering of the atoms. The geometry is described by the fourteen independent parameters defined in Table 5. In accordance with the results for I and the

Table 5. Structural results[a] for 5-methyl-1,3,4-oxathiazol-2-one obtained in refinements based on electron-diffraction intensities (Fig. 3 and Table 6) in combination with microwave rotational constants[b] (A_z, B_z, C_z) using calculated vibrational parameters (Table 4).

Distances (r_a, Å)	
1. r (O1 – C2)	1.391(6)
2 r (O1 – C5)	1.367(9)
3 r (S3 – C2)	1.768(2)
4 r (S3 – N4)	1.685(2)
5 r (N4 = C5)	1.289(4)
6 r (C2 = O6)	1.198(2)
7 r (C5 – C7)	1.487(3)
8 r (C – H)	1.102(30)
Angles ($\angle_\alpha$, θ_α, degrees)	
9 ∠C5O1C2	111.8(3)
10 ∠O1C2O6	123.6(4)
11 ∠C2S3N4	93.5(2)
12 ∠O1C5C7	115.3(4)
13 ∠CCH	109.6(5)
14 θ(N4C5C7H8)	0. (fixed)
∠O1C2S3	106.4(3)
∠O1C5N4	119.3(2)
∠C5N4S3	109.2(3)
Rotational constants (MHz)[b]	
A [4240.45(18)]	4240.40(18)
B [2112.75(14)]	2112.82(11)
C [1422.53(2)]	1422.55(2)

[a] The independent geometrical parameters are numbered. The correlation coefficients $|\rho(i,j)| > 60\%$ are, $\rho(2,1) = -95$, $\rho(5,1) = +68$, $\rho(5,2) = -75$, $\rho(7,1) = -63$, $\rho(9,2) = -64$, $\rho(12,10) = -77$. Uncertainty in the s-scale (0.1 and 0.2 %, respectively, for r and A, B, C-values) are not included in the estimated standard deviations given in parentheses. [b] Experimental r_z-values in square brackets and r_α°-counterparts are given. Ground state rotational constants in Table 1.

interpretation of the spectral data, the heavy atom skeleton was assumed to be planar. Local C_{3v} symmetry was introduced for the methyl group. The chosen model represented the data well and the constraints were not relaxed.

The vibrational parameters (u-values) were fixed at the calculated values (Table 4), and the geometrical parameters were refined by the least-squares method based on the intensity data using data ranges and diagonal weighting as given in Table 6. The obtained standard deviations were, however, augmented as indicated by comparative refinements using the given diagonal weight matrices and nondiagonal ones with standard values for the off diagonal elements.[11] Shrinkage corrections were implemented by the use of an r_α-model which gave the geometrically inconsistent set of r_a-distances. As for the parent molecule this resulted in insignificant shifts in the refined parameter values. The calculations of the r_α-coordinates were always parallelled by computations of r_α°-coordinates which were simultaneously used to compute the r_α°-representatives of the rotational constants (A_α°, B_α°, C_α°). Thus the structural results obtained from the refinement based on the electron-diffraction data could always be checked against the A_z, B_z and C_z counterparts obtained from the spectroscopic data (Table 5). Such comparisons did not reveal any serious scale problems the A_α°, B_α° and C_α° being 4226(12), 2110(5) and 1420(2) MHz. The final refinement was based on the electron-fiffraction intensities in combination with the experimental rotational constants (A_z, B_z, and C_z) as described previously. The combined approach made it possible to refine the parameter ∠CCH which was previously constrained to 110°. The fitting of the rotational constants is in general accompanied by a poorer fit to the electron-diffraction intensities, which, however, in the present case was insignificant as the pertinent agreement factor changed only from 6.62 to 6.79 %. Consequently, the structural results for the latter refinement (presented in Table 5) are not significantly different from those obtained from the electron-diffraction data alone. The quality of the fit to the electron-diffraction data is also demonstrated by comparisons of calculated intensity and radial distribution curves with the experimental counterparts shown in Figs. 3 and 4, respectively.

As seen from Table 5, the parameter for the conformational orientation of the methyl group, θ(H8C7C5N4) was assigned to 0°. The second conformation ($\theta = 180°$) which gives overall C_s symmetry for the molecule did not give significantly better agreement to the data, the R-factor ratio [$R(180)/R(0)$] being 0.99. Several intermediate orientations were tested, and it was shown that the least-squares fit as well as the remaining geometrical parameters were practically invariant to assumptions regarding this parameter. Therefore, it was not found worthwile to pursue the analysis by including large amplitude treatment for the internal rotor, shown by the interpretation of the microwave data to have a barrier height of 5.98 kJ mol^{-1}.

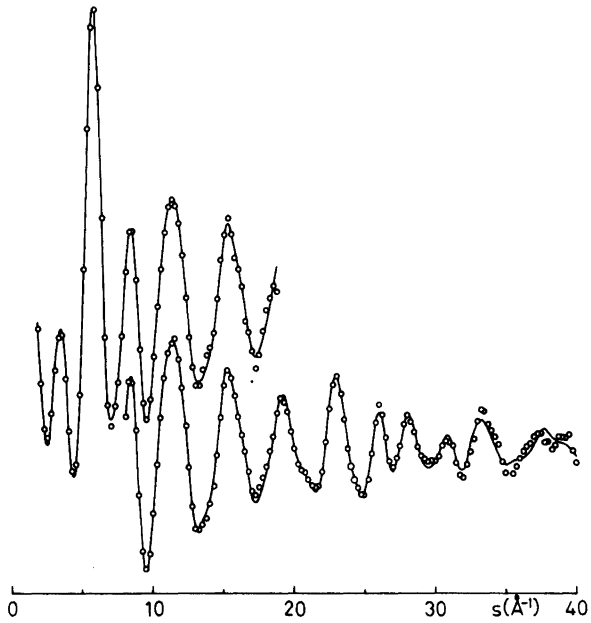

Fig. 3. Observed molecular electron-diffraction intensities (○) 5-methyl-1,3,4-oxathiazole-2-one compared to calculated counterparts (full lines) from parameter values given in Table 5.

DISCUSSION

Comparison of the geometrical parameters of II (Table 5) with those obtained for the parent molecule (I),[1] seems to demonstrate that the effect of the methyl substitution is small, the error limits taken into consideration. On the other hand, there appeared to be some unacceptable deviations in some of the u-values. For example, the u_T-values for the three distances S_3-C_2, S_3-N_4, and $N_4=C_5$ of I were from spectroscopical calculations (third, and final set)[1] found to be 0.0502, 0.0541 and 0.0417 Å, respectively, while the corresponding values for II (Table 4) were 0.0453, 0.0460 and 0.0458 Å. The discrepancies, particularly for the bonds containing sulfur, were too large to be easily rationalized. The close similarity in corresponding geometrical parameter values for I and II probably corroborates the previous conclusion[1] that the molecular geometry is not too sensitive to changes in the u-values, even in these rather difficult cases with severe distance overlap. However, the mentioned discrepancy led to a thorough checking of the normal coordinate calculations for both molecules. Care was taken to base the force fields on transferred force constants from one molecule to the other in the initial set, and to use the same method to adjust the force constants to fit accurately the experimentally assigned frequencies.

For compound II the new vibrational amplitude

Table 6. Data ranges and constants of the weighting schemes[a] used for the electron-diffraction in the structure refinements.

(Camera dist.)	s_{min}	s_{max}	Δs	s_1	s_2	w_1	w_2
48 cm	1.75	18.75	0.125	2.00	18.00	0.1	0.03
20 cm	8.00	40.00	0.250	8.00	40.00	1.0	0.02

[a] See Ref. 6 for definitions of the symbols.

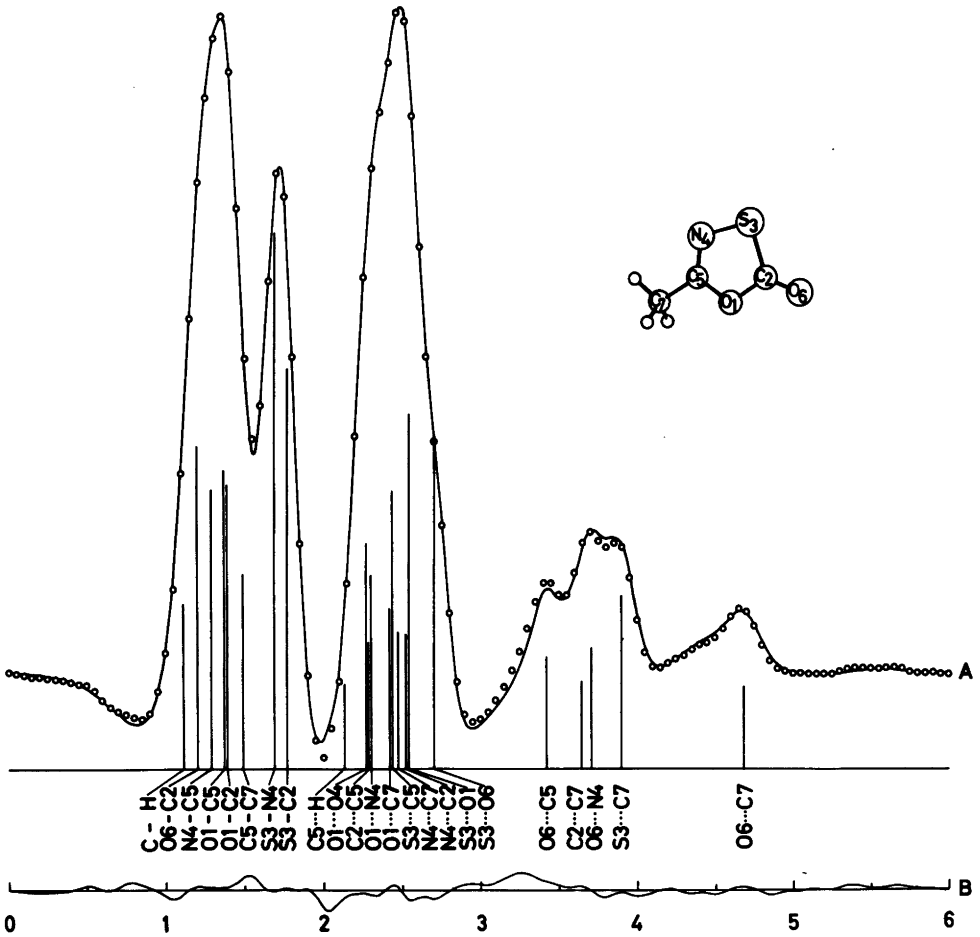

Fig. 4. Experimental radial distribution curve (○) for 5-methyl-1,3,4-oxathiazole-2-one calculated from the intensity data in Fig. 3 using appropriate theoretical intensity values for $s < 1.75$ Å and an artificial damping constant of $k = 0.0020$ Å^2, the calculated counterpart (full line), and the corresponding difference curve. The vertical lines indicate the positions of the interatomic distances, and the numbering of the atoms are given on the inserted model of the molecule.

quantities showed only small deviations from the values given in Table 4. In spite of this the electron-diffraction refinements and the combined electron-diffraction microwave refinements were repeated. None of the new geometrical parameters thus obtained deviate as much as one standard deviation from the data presented in Table 5. A possible influence on the torsion of the methyl group was also tested with no significant changes.

For the parent substance the new set of u-values deviates from that earlier used in the final structural refinement.[1] The new and the old set of u_T-values are presented in Table 7. All the refinements carried out earlier with the old set[1] have been repeated using the new set. The earlier and the new set of final geometrical parameters are also included in Table 7. The difference in distances and angles can hardly be characterized as significant. As one would have expected, the difference between the two bond distances containing a sulfur atom has increased slightly as a result of the decrease in the corresponding u-values.

In compound II as in the parent molecule (I) $r(O1-C5) < r(O1-C2)$, but the difference appears

Table 7. Amplitudes and molecular geometry[a] for 1,3,4-oxathiazol-2-one as previously published in columns I, and in columns I′ u-values calculated from a new force field (see text) and geometry obtained when using the new set of amplitude quantities in the refinements.

Force field calculations			Electron diffraction		
	I (Ref. 1)	I′ (this work)		I (Ref. 1)	I′ (this work)[b]
u(O1 – C2)	0.0471	0.0471	1 r(O1 – C2)	1.402(3)	1.398(3)
u(O1 – C5)	0.0473	0.0475	2 r(O1 – C5)	1.356(3)	1.355(3)
u(S3 – C2)	0.0502	0.0446	3 r(S3 – C2)	1.767(2)	1.773(2)
u(S3 – N4)	0.0541	0.0468	4 r(S3 – N4)	1.690(2)	1.687(2)
u(N4 = C5)	0.0417	0.0457	5 r(N4 = C5)	1.286(2)	1.283(2)
u(O6 = C2)	0.0377	0.0398	6 r(O6 = C2)	1.192(2)	1.193(2)
u(C5 – H7)	0.0767	0.0768	7 r(C5 – H7)	1.102(19)	1.107(20)
u(S3···O1)	0.0561	0.0482			
u(N4···C2)	0.0606	0.0548	8 ∠C5O1C2	110.8(2)	110.9(2)
u(S3···C5)	0.0564	0.0509	9 ∠O1C2O6	122.6(3)	123.4(3)
u(O1···N4)	0.0532	0.0536	10 ∠C2S3N4	93.8(1)	93.7(1)
u(C2···C5)	0.0576	0.0534	11 ∠O1C5H7	114.5(31)	114.8(31)
u(O1···O6)	0.0582	0.0610			
u(S3···O6)	0.0612	0.0590	∠O1C2S3	106.3	106.2(2)
u(O1)···H7)	0.0999	0.1052	∠O1C5N4	121.1	121.2(2)
u(N4···H7)	0.0972	0.1046	∠C5N4S3	107.9	108.1(2)
u(O6···N4)	0.0638	0.0601			
u(O6···C5)	0.0615	0.0607	A[c]	5582.6(13)	5583.3(6)
u(S3···H7)	0.0940	0.0920	B	3643.8(4)	3643.3(3)
u(C2···H7)	0.0957	0.0958	C	2204.7(2)	2204.8(1)
u(O6···H7)	0.1031	0.1063			
			R(%)	9.91	9.35

[a] Distances (r) and amplitudes (u) in Å; angles (∠) in degrees; and rotational constants (A, B, C) in MHz. [b] The independent geometrical parameters are numbered. The correlation coefficients $|\rho(i,j)| > 60\%$ are $\rho(1,2) = -78$ and $\rho(10,11) = -66$. [c] The r_z representatives for the rotational constants are for column I 5582.0(16), 3643.5(7) and 2204.8(2) MHz; and for column II 5582.8(18), 3643.5(8), 2204.9(2) MHz, respectively.

Table 8. Per mille changes of ring parameters (S) and of combinations of type [O1 – C2, ∠O1C2S3, C2 – S3] *etc.* as taken counter clockwise (Fig. 4) when H of compound I is substituted by CH_3, producing II. Distances in Å angles in degrees.

	I	II	S[a]	Combination[b]
O1 – C2	1.398	1.391	5.0	
O1 – C2 – S3	106.2	106.4	1.9	9.7
C2 – S3	1.773	1.768	2.8	
C2 – S3 – N4	93.7	93.5	2.1	6.1
S3 – N4	1.687	1.685	1.2	
S3 – N4 = C5	108.2	109.2	9.2	15.1[d]
N4 = C5	1.283	1.289	4.7	
N4 = C5 – O1	121.2	119.3	15.9	29.4[c]
C5 – O1	1.355	1.367	8.8	
C5 – O1 – C2	110.9	111.8	8.1	21.9[d]
O1 – C2	1.398	1.391	5.0	

[a] Single parameter. [b] Appropriate combination. [c] Maximum change at atom C5 where CH_3 substitution occurs. [d] Changes at atoms neighbouring C5.

to be less pronounced in II [0.024(6) Å] than in I [0.044(6) Å], whereas the averages of the O–C bonds in the two compounds are rather similar [1.379(4) and 1.377(4) Å, respectively]. Inspection of the structural results for the two compounds does not suggest drastic changes in the ring geometry due to methyl substitution. The larger changes occur at C5 and its two neighbouring atoms. In fact, the ring angle (∠O1C5N4) decreases by about 2° at the site of methyl substitution and there is indicative evidence for corresponding bond elongations (*i.e.* O1–C5 and C5=N4). This is consistent with effects of methyl substitution in benzene[12,13] where a corresponding decrease in the ring angle has been related to different spatial requirements for the C–C *vs.* C–H σ-bonding electron pairs in the valence shell of the *ipso* carbon.[12] Also, the molecular structure of *p*-benzoquinone[14] in the solid state as compared to those of various methyl derivatives of *p*-benzoquinone[15] suggests the presence of similar effects of methyl substitution.

The C5–C7 bond length of 1.487(3) Å appears to be slightly shorter than the values of 1.50–1.52 Å most often found for $C(sp^3)-C(sp^2)$ bonds, as for example on the before-mentioned methyl derivatives of benzene[13] and *p*-benzoquinone.[15] However, it compares favourably with the C–C bond length of 1.484(4) Å found in $CH_3HC=N-N=CHCH_3$.[16]

The barrier to internal rotation for methyl groups attached to sp^2 type carbons in heterocyclic five-membered ring molecules has been shown to be strongly dependent on the ring type and the different positions in the rings.[17] For II the rotational barrier of 5.98 kJ mol^{-1} (1.43 kcal mol^{-1}) is, for example, larger than that of 2-methylfuran, $CH_3-C=CH-CH=CH-O$, reported to be 1.19 kcal mol^{-1}.[18]

Acknowledgements. N. W. Larsen, Th. Pedersen and G. O. Sørensen, all of Chem. Lab. V, Copenhagen, are gratefully acknowledged for providing important computer programs for our calculations (SEM, ROTFIT and STARK); and H. V. Volden for densitometering the electron-diffraction photographic plates. This work has been supported by The Danish Research Council for Natural Sciences and the Norwegian Research Council for Science and the Humanities.

REFERENCES

1. Bak, B., Nielsen, O., Svanholt, H., Almenningen, A., Bastiansen, O., Fernholt, L., Gundersen, G., Nielsen, C. J., Cyvin, B. N. and Cyvin, S. J. *Acta Chem. Scand. A 32* (1978) 1005.
2. Bak, B., Nielsen, O. and Svanholt, H. *Unpublished results. Details on request.*
3. *Brit. Pat.* 1079 348 (1967); *Chem. Abstract 68* 6900w (1968).
4. Gilbert, B. and Duyckaerts, G. *Spectrochim. Acta A 26* (1970) 2197.
5. Bastiansen, O., Hassel, O. and Risberg, E. *Acta Chem. Scand. 9* (1955) 232.
6. Andersen, B., Seip, H. M., Strand, T. G. and Stølevik, R. *Acta Chem. Scand. 23* (1969) 3224.
7. Hedberg, J. *5th Austin Symposium on Gas Phase Molecular Structure*, Austin, Texas 1974, p. 37.
8. Seth-Paul, W. A. and Demeyer, H. *J. Mol. Struct. 3* (1969) 403.
9. Sénéchal, M. and Saumagne, P. *J. Chim. Phys. 69* (1972) 1246.
10. Cyvin, S. J. and Lyham, L. *J. Mol. Struct. 25* (1975) 151; Andreassen, R., Cyvin, S. J. and Lyham, L. *J. Mol. Struct. 25* (1975) 155; Cyvin, S. J. *J. Mol. Struct. 30* (1976) 311.
11. Seip, H. M., Strand, T. G. and Stølevik, R. *Chem. Phys. Lett. 3* (1969) 617.
12. Domenicano, A., Mazzeo, P. and Vaciago, A. *Tetrahedron Lett.* (1976) 1029 and references therein.
13. a. Seip, R., Schultz, Gy., Hargittai, I. and Szabó, Z. G. *Z. Naturforsch. Teil A 32* (1977) 1178; b. Domenicano, A., Schultz, Gy., Kolonits, M. and Hargittai, I. *J. Mol. Struct. 53* (1979) 197.
14. Trotter, J. *Acta Crystallogr. 13* (1960) 86.
15. Rabinovich, D., Schmidt, G. M. and Ubell, E. *J. Chem. Soc. B* (1967) 131 and references therein.
16. Hargittai, I., Schultz, G., Naumov, V. A. and Kitaev, Yu. P. *Acta Chim. Acad. Sci. Hung. 90* (1976) 165.
17. Mjøberg, P. J., Ralowski, W. M. and Ljunggren, S. O. *Z. Naturforsch. Teil A 30* (1975) 1279.
18. Ogata, T. and Kozima, K. *Bull. Chem. Soc. Jpn. 44* (1971) 2344.

Received July 8, 1981.

Acta Chemica Scandinavica A 36 (1982) 297 – 301

High-resolution Variable-temperature ^1H and ^{13}C NMR of a 1,8-Bis-*gem*-substituted Cyclotetradecane

JOSTEIN KRANE

Kjemisk institutt, NLHT, Universitetet i Trondheim, N-7000 Trondheim, Norway

Cyclotetradecane-1,8-dione-bis(ethylene ketal) has been investigated by variable temperature ^1H and ^{13}C NMR spectroscopy. The ^1H NMR spectra reveal two conformational processes with corresponding activation free energies of 38.3 (0.8) kJ mol^{-1} and 31 kJ mol^{-1}, respectively. The low energy process is also visible in the ^{13}C NMR spectra; the free energy barrier is found to be 31.6 (0.8) kJ mol^{-1} at $-103°$. Based on observed lineshape changes and chemical shift arguments we conclude that the title compound exists in a diamond lattice [3434] conformation with the *gem*-dioxa substituents on corner positions. Conformational interconversion modes are discussed.

Cyclotetradecane belongs to the family of "large-membered" rings in which transannular nonbonded repulsions are absent.[1] Cyclotetradecane is thought to be conformationally homogeneous and have the rectangular diamond lattice conformation.[2] An examination of the conformation of this hydrocarbon using ordinary molecular models (*e.g.* Dreiding models) is not very fruitful, and the molecule appears to be exceedingly flexible, even if non-bonded atoms are kept reasonably far apart. A semiquantitative strain-energy calculation carried out by Dale,[3] however, suggests that the diamond lattice or [3434] conformation is distinctly lower in energy than any other conformation.

Cyclotetradecane has been investigated by variable temperature ^{13}C NMR.[4] In the first attempt,[4a] the spectrum at low temperature (-132 °C) of the natural abundant ^{13}C compound contains peaks of an approximately 4:1:2 intensity ratio. In the second attempt,[4b] four well-resolved lines in the ratio of 2:2:2:1 are observed for (1-^{13}C)cyclotetradecane. These results are consistent with a [3434] conformation. A successful interpretation of the lineshape changes requires that the low-temperature spectrum must be assigned correctly, which is difficult in the present case, because two low-field lines are separated by only 0.6 ppm.

We now report a study of the temperature dependence of ^1H and ^{13}C NMR spectra of cyclotetradecane-1,8-dione-bis(ethylene ketal) (I).

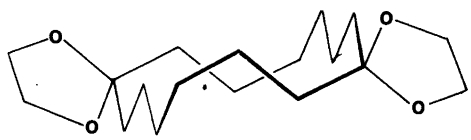

I

This compound has many features similar to the parent hydrocarbon. It is a 1,1,8,8-tetrasubstituted cyclotetradecane and only one conformer is possible on the lowest energy [3434] ring conformation, since the geminal substituents are restricted to corner positions.

EXPERIMENTAL

Cyclotetradecane-1,8-dione-bis(ethylene ketal) was prepared by azeotropic distillation from a mixture of the diketone and ethylene glycol in benzene containing a little p-toluene-sulfonic acid, in the same way as described for other ketones by Hartley.[5] Cyclotetradecane-1,8-dione was prepared from suberic acid by ketene cyclization.[6]

0302-4377/82/040297-05$02.50

NMR Spectra. NMR spectra were obtained on a superconducting solenoid spectrometer operating at 59 kG.[7] The proton spectra were obtained with standard 5-mm sample tubes in a frequency-sweep mode. The ^{13}C spectra are Fourier transforms of accumulated free-induction decays and were obtained with 10-mm tubes with the magnetic field locked on a ^{19}F peak of the solvent. A 1:1 mixture of $CHCl_2F$ and $CHClF_2$ was used as solvent. All temperatures were measured with a copper-constantan thermocouple situated in the probe a few centimeters below the sample and connected to a Newport Laboratories digital thermometer reading to 0.1 °C and accurate to 0.2 °C. The variable temperature unit was calibrated with methanol, and for very low temperatures with a thermocouple situated inside the spinning sample tube. The chemical shifts are referenced to internal tetramethylsilane.

Free energies of activation were calculated from rate constants by the absolute rate theory with a transmission coefficient of 1. The rate constants were obtained at the coalescence temperatures of the separated peaks in the ^1H NMR spectra by the expression $k = \Pi\Delta\nu/\sqrt{2}$.* The erros given in the text are our best estimates of 90 % confidence limits and include possible systematic errors and the effects of couplings and natural line widths. As a result of high power (*ca.* 10W) used for decoupling protons in the ^{13}C spectra, the temperature measurements associated with these spectra are of lower accuracy (±3 °C) than those of the ^1H spectra (±1 °C). The accuracy (0.8 kJ mol^{-1}) of the free-energy barriers obtained from the ^{13}C spectra was entirely adequate for determining a correspondence with one of the two barriers obtained in the ^1H spectra.

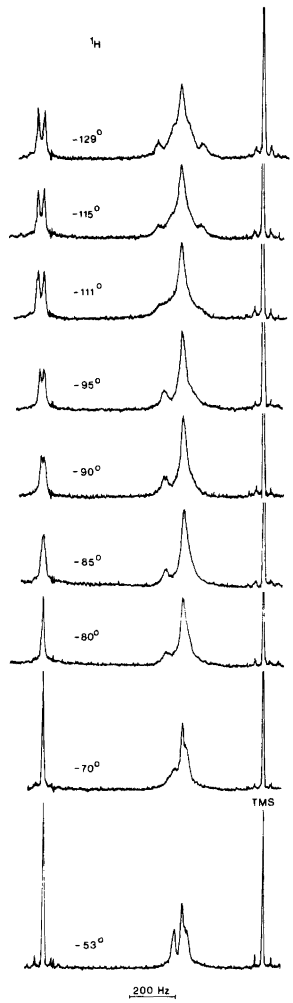

Fig. 1. The 251 MHz ^1H NMR spectra of I (3.5 % in a 1:1 mixture of $CHCl_2F$ and $CHClF_2$) at various temperatures.

RESULTS AND DISCUSSION

The ^1H NMR spectra of I at various temperatures are given in Fig. 1. The spectrum above −53 °C consists of a resonance for ethylene ketal bridge protons at 3.83 ppm, ring protons α to the ketal groups at 1.55 ppm and the rest of fourteen-membered ring protons in the range of 1.47 to 1.24 ppm. Below −75 °C, the α protons split into two resonances, ($\Delta\nu = 120$ Hz; the high field portion is hidden), with a corresponding activation free energy ($\Delta G^{\ddagger}_{-75°C}$) of 38.3 (0.8) kJ mol^{-1}. The same process is visible in the ethylene ketal bridges with a coalescence temperature of −84 °C; the $\Delta G^{\ddagger}_{-85°C}$ is 38.8 (0.8) kJ mol^{-1}. Below −95 °C, a second process is visible. The most reasonable interpretation is that the band at $\delta = 1.73$ splits into two resonances with a separation of 34 Hz (where the high field portion is hidden). The lower energy

*This expression is strictly valid for an exchange process between two equally populated sites and where exchange is the only broadening effect; errors resulting from coupling and natural line-width effects are least when the chemical shift difference is greatest. The experimental data available are not suitable for obtained meaningful values of $\Delta H^{\ddagger}$ and $\Delta S^{\ddagger}$, even though the errors in $\Delta G^{\ddagger}$ are not large. (Anet, F. A. L. and Anet, R., *Dynamic Nuclear Magnetic Resonance Spectroscopy*, In Cotton, F. A. and Jackman, L. M., Eds., Academic, New York 1975, p. 543).

Table 1. Dynamic NMR data.

Nucleus	Probe	T_c K	$\Delta\nu$ Hz	$\Delta G^{\neq}$ kJ mol^{-1}
^{1}H	protons α to ketal bridge	198	120	38.3(0.8)
^{1}H	ethylene glycol units	189	27	38.8(0.8)
^{1}H	protons α to ketal bridge	162	~34	~31
^{13}C	α carbons	170	260	31.6(0.8)

process is calculated to have a $\Delta G^{\neq}$ of about 31 kJ mol^{-1} at −111 °C. The changes in the rest of the spectrum are too complex for analysis. The ^{1}H NMR data are listed in Table 1.

The ^{13}C NMR spectra of I are shown in Fig. 2. The spectrum at ambient temperature contains the following resonances: at 63.5 ppm for the carbons in the ethylene ketal bridges; at 34.9 ppm for carbons α to the quaternary carbons; at 27.2 and 22.5 ppm for the carbons β and γ to the quaternary carbons. The assignment of which resonances correspond to the β and γ carbons is not straightforward, as will be discussed later. The quaternary carbons which resonate at 110.8 ppm are not shown. The spectrum at −143 °C shows that there are two types of α, β and γ carbons. The resonance from the quaternary carbons remains a single line. The chemical shifts for the carious resonances are listed in Table 2. The activation free energy fro the ^{13}C visible process is 31.6 (0.8) kJ mol^{-1} at −103 °C calculated from a separation of 260 Hz for the α carbons. The ^{13}C NMR data are included in Table 1.

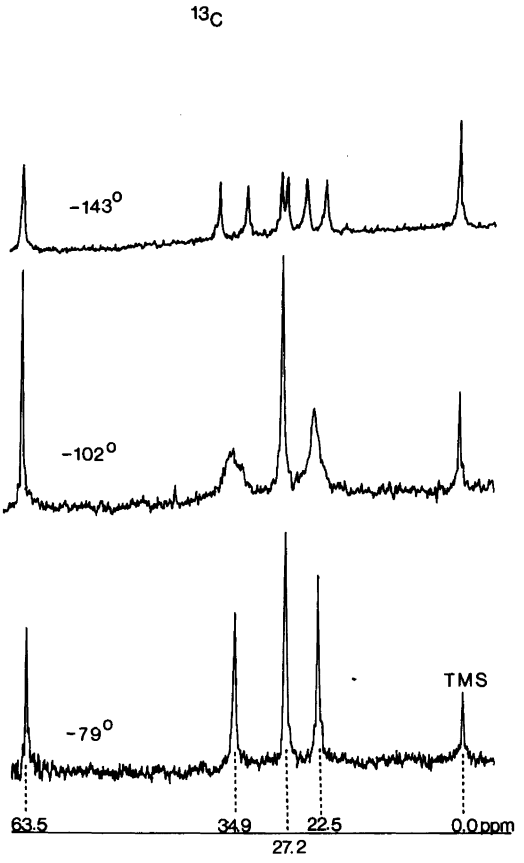

Fig. 2. The 63.1 MHz ^{13}C NMR spectra of I at various temperatures, with the protons noise decoupled.

Table 2. ^{13}C chemical shifts and effects.

Conformational sites[a]	Observed chemical shifts[b] −79 °C	−143 °C	Observed splitting	Chemical shift effects[c]	Predicted splitting
quaternary	110.7	110.8		$2V_g$	
α	34.9	36.1	4.3	$\gamma+V_g+2V_t$	$\gamma-V_t=4.2$
α′		31.8		$2\gamma+V_g+V_t$	
γ′	27.2	27.4	0.5	$2V_g$	$\gamma-V_g+V_t=2.3$
γ		26.9		$\gamma+V_g+V_t$	
β	22.5	23.8	3.0	$3\gamma+2V_t$	$V_g-V_t=2.7$
β′		20.8		$3\gamma+V_g+V_t$	

[a] As given in Fig. 3. [b] In parts per million downfield from Me_4Si. [c] Includes the effect from the *gem*-dioxa substituents, $\gamma=5$ ppm, $V_g=3.5$ ppm, $V_t=0.8$ ppm.

The observation derived from the ^{1}H NMR data is supported by the ^{13}C NMR spectra. As expected, only the lower energy process is observed with both probes.

^{13}C chemical shifts in saturated hydrocarbons show regular features that are relatively well understood,[8] at least from an empirical point of view. In the conformation of the compound under discussion, two contributions to the ^{13}C NMR shifts should be of importance, namely the γ and the "*vicinal – gauche*" (V_g) effect. The γ effect results in an upfield shift of about 5 ppm for the terminal carbons in a *gauche* butane fragment. The V_g effect occurs for the two central carbons in the same fragment, and results in an upfield shift, but is somewhat smaller (3.5 ppm) than the γ effect. A third effect, V_t, has also been postulated, and occurs for the central carbons in an *anti* butane fragment, but its magnitude (*ca.* 0.8 ppm upfield) is much smaller than that of either the γ or the V_g effect. Still another complication is to what extent the oxygen atoms will contribute differently to the γ-, V_g- and V_t-effects compared to methyl or methylene groups. We have not tried to differentiate between oxygen atoms and methylene groups in this respect. It has been found that the γ effect varies considerably in magnitude and depends on the precise structure of the compound examined.

Despite the uncertainties enumerated above, we have found it quite useful to compare the observed chemical shifts in I with those calculated from chemical-shift effects present in an appropriate conformation, namely the [3434] conformation as shown in Fig. 3. The results are given in Table 2. With arguments using chemical-shift effects we find that

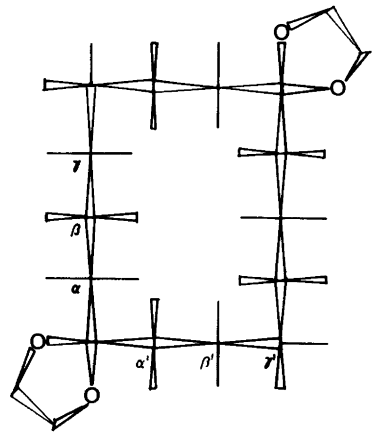

Fig. 3. Wedge representation[3] of the [3434] conformation of I. The letters α, α', β, β', γ and γ' refer to carbon sites.

the β carbons are more shielded than the γ carbons.* The agreement between observed and predicted splitting of the resonances is excellent for the α- and the β-carbons, but not so good for the γ-carbons. The chemical shift for the quaternary carbons in I (100.8 ppm) agrees well with the shift for C-2 in 2,2-dimethyl-1,3-dioxolane (108.5 ppm).[9]

The available results preclude detailed com-

*This is consistent with the situation in cyclotetradecane itself. The middle carbon on the 4-side in the [3434] conformation has a relative intensity of 1 and can therefore be assigned (δ 23.1). The resonance at δ 21.4 probably belongs to the carbons on the 3-side, see Ref. 4a.

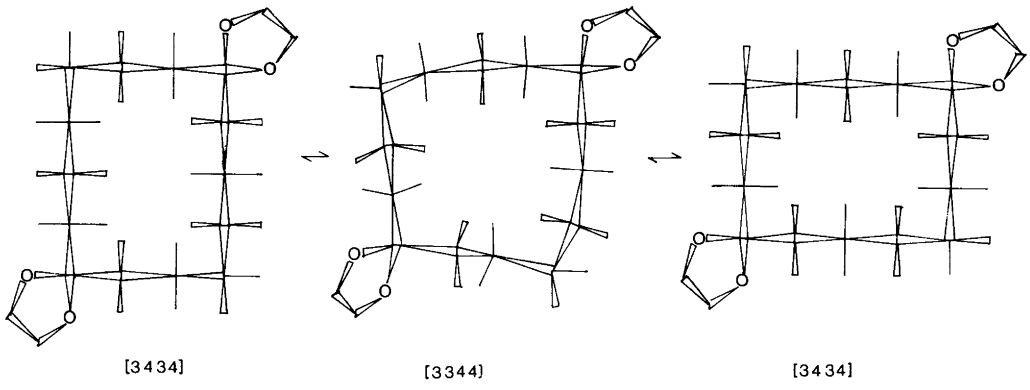

Fig. 4. Partial pseudorotation itinerary for the [3434] conformation of I which averages carbon sites and leaves geminal hydrogens non-equivalent.

parisons, and a larger body of data is needed for determination of γ-, V_g- and V_t-values in large ring compounds. Nevertheless, the assignments made in Table 2 show reasonable agreement with the [3434] conformation having substituents at corner positions.*

Finally, we may consider the line-shape changes in both the ^1H and the ^{13}C NMR spectra at intermediate temperature. The lowest energy pseudorotation mechanism for the [3434] conformation with 1,8-bis-*gem*-substituents, involves, according to Dale's semiquantitative calculations,[3] the following itinerary: [3434]→[3434]→[3434] as shown in Fig. 4. This leads to exchange of the carbon atom sites, but the methylene hydrogens remain geminally non-equivalent. It is worth noticing that the barrier calculated from the ^{13}C spectrum agrees very well with the low-temperature process in the ^1H spectrum. To achieve site exchange so as to reach the high-temperature spectrum requires passage over barriers with higher energies, because the *gem*-dioxa substituents can no longer remain at relatively unhindered corner positions. The present analysis leads to a free energy of activation for the overall high energy process of 38.3 (0.8) kJ mol^{-1} at -57 °C. The precise nature of the barriers involved in the high-energy process is difficult to predict at this stage and will be the topic of future empirical force-field calculations. However, it suffices to state that the difference between the high- and low-energy process of only 7.1 kJ mol^{-1}, indicates that *gem*-dioxa substituents require much less space than *gem*-dimethyl groups.**

Acknowledgements. I am grateful to Professor F. A. L. Anet for the use of his NMR equipment at University of California, Low Angeles, where this research was done; and to *Norges Teknisk-Naturvitenskapelige Forskningsråd* for a Fellowship support. I thank Professor J. Dale for stimulating discussions.

* Infrared spectroscopy and dipole moment studies also suggest that this conformation is the exclusive one in solution. Alvik, T., Borgen, G. and Dale, J. *Acta Chem. Scand. 26* (1972) 1805.

** A discussion of the effect of placing *gem*-dimethyl groups on conformational energies and barrier heights has been done by Dale (*Acta Chem. Scand. 27* (1973) 1149) and by Anet and Anet, Ref. 4b, p. 562.

REFERENCES

1. Eliel, E. L., Allinger, N. L., Angyal, S. J. and Morrison, G. A. *Conformational Analysis*, Wiley-Interscience, New York 1965.
2. Borgen, G. and Dale, J. *J. Chem. Soc. Chem. Commun.* (1970) 1340.
3. Dale, J. *Acta Chem. Scand. 27* (1973) 1115.
4. a. Anet, F. A. L., Cheng, A. K. and Wagner, J. J. *J. Am. Chem. Soc. 94* (1972) 9250; b. Anet, F. A. L. and Anet, R. In Jackman, L. M. and Cotton, F. A., Eds. *Dynamic Nuclear Magnetic Resonance Spectroscopy*, Academic, New York 1975, p. 561.
5. Hartley, D. *J. Chem. Soc.* (1962) 4722.
6. Grob, C. A. and Schiess, P. W. *Helv. Chim. Acta 43* (1960) 1546.
7. Anet, F. A. L., Basus, V. J., Bradley, C. H. and Cheng, A. K. *Paper presented at the 12th Experimental NMR Conference*, Gainesville, Fla., Feb. 1971.
8. a. Stothers, J. B. *Carbon-13 NMR Spectroscopy*, Academic, New York 1972; b. Dalling, D. K. and Grant, D. M. *J. Am. Chem. Soc. 89* (1967) 6612; *94* (1972) 5319; *96* (1974) 1827; c. Dalling, D. K., Grant, D. M. and Paul, E. G. *Ibid. 95* (1973) 3718.
9. Eliel, E. L., Rao, V. A. and Pietrusiewicz, K. M. *Org. Magn. Reson. 12* (1979) 461.

Received July 13, 1981.

Acta Chemica Scandinavica A 36 (1982) 303 – 308

Deuteration of Crystalline Hydroxides. Hydrogen Bonds of γ-AlOO(H,D) and γ-FeOO(H,D)

A. NØRLUND CHRISTENSEN,[a] M. S. LEHMANN[b] and P. CONVERT[b]

[a] Department of Inorganic Chemistry, Aarhus University, DK – 8000 Aarhus C, Denmark and [b] Institut Max von Laue – Paul Langevin, F-38042 Grenoble Cedex, France

The hydrogen deuterium exchange between D_2O and the crystalline hydroxides α-CrOOH, γ-AlOOH, γ-FeOOH, $In(OH)_3$ and $Y(OH)_3$ was studied in the temperature range 20 – 120 °C by neutron diffraction. Only the compounds γ-AlOOH and γ-FeOOH showed a measurable H – D exchange.

The hydrogen bonds of γ-$AlOO(H_{0.33}D_{0.67})$ with the unit cell parameters $a = 2.876(3)$, $b = 12.24(1)$, $c = 3.709(3)$ Å and γ-$FeOO(H_{0.04}D_{0.96})$ with the unit cell parameters $a = 3.070(2)$, $b = 12.53(2)$, $c = 3.876(3)$ Å were measured from neutron diffraction powder patterns using the space group *Cmcm*, No. 63. The hydrogen bond distances are 2.73(2) Å for γ-$AlOO(H_{0.33}D_{0.67})$ and 2.65(2) Å for γ-$FeOO(H_{0.04}D_{0.96})$.

In investigations of structures containing hydroxy groups, water molecules or other hydrogen-containing groups by neutron diffraction it is preferable to have deuterated specimens instead of hydrogen-containing specimens, as these yield high scattering backgrounds in contrast to deuterated compounds. For the cases of hydroxides or oxide hydroxides of the transition metals or the group III elements such deuterated compounds have been made by hydrothermal synthesis where all solutions were made with D_2O and where NaOD for the precipitation of the hydroxides was made by reaction of sodium with D_2O.[1,2]

The rate of crystallization of amorphous iron(III) hydroxide to α-Fe_2O_3 and α-FeOOD was recently investigated at hydrothermal conditions by measurements of neutron powder diffraction diagrams simultaneously with the hydrothermal crystallization treatment of the specimens.[3] It was found that the crystallizations of amorphous iron(III) hydroxide in D_2O to α-Fe_2O_3 and α-FeOOD were fast processes that in the temperature range 100 – 180 °C were complete within 1 – 4 h. The hydrothermal deuteration of crystalline hydroxides may also be a relatively fast process that may be dependent upon reaction temperature, crystallite size of specimen, structure and hydrogen bonding of the compounds. If this was the case, such deuterated compounds could be made by hydrothermal deuteration of the crystalline hydroxides instead of by the rather tedious method of preparation described above. The reaction kinetics of such hydrothermal deuterations of crystalline hydroxides have not been investigated previously, and five compounds, α-CrOOH, γ-AlOOH, γ-FeOOH, $In(OH)_3$ and $Y(OH)_3$ with different structures and degrees of hydrogen bonding were selected for this investigation.

EXPERIMENTAL

Sample preparation and characterization. The compounds α-CrOOH,[1] γ-AlOOH,[4] $In(OH)_3$ [5] and $Y(OH)_3$,[6] were all made by hydrothermal synthesis as described previously. In addition, two samples of γ-AlOOH were obtained from *Haldor Topsøe A/S* and the sample of γ-FeOOH was obtained from Minnesota Mining and Manufacturing Company. X-Ray powder patterns of all specimens were measured on a Philips powder diffractometer. Some of the patterns showed a broadening of the powder lines. The instrumental broadening of the powder lines was estimated from powder patterns taken of Si and NaCl and used in a calculation of the apparent crystal size of the hydroxides and oxide hydroxides using the methods described by

0302-4377/82/040303-06$02.50

Table 1. Average crystallite size (Å) of compounds investigated.

γ-AlOOH	500	$In(OH)_3$	700
γ-AlOOH	500[a]	$Y(OH)_3$	1000
γ-AlOOH	1650[a]	γ-FeOOH	200
α-CrOOH	500		

[a] Suppliers values.

Drenck,[7] and by Lipson and Steeple.[8] The results of these investigations are listed in Table 1.

Determination of the H – D exchange rate by on-line neutron diffraction. In a typical experiment 1.00 g of the crystalline compound was mixed with 3.0 ml D_2O in an 11 mm diameter vanadium container. The container was closed, so that no D_2O was lost during the experiment. The neutron diffraction powder pattern of the container was measured using a 400 cell multidetector covering 80° in 2θ at the powder diffractometer D1B at the Laue-Langevin Institute. The container was placed in a thermostated vanadium oven with a temperature stability of ±1.0 °C.[3] Each experiment was started by a fast heating of the container in hot water. The container was then transferred to the oven at the spectrometer table when it had reached the same temperature as that of the oven or 100 °C in the case when the temperature of the oven was greater than 100 °C. The neutron diffraction powder patterns were recorded repeatedly and were extracted at 6, 12 and 18 min intervals dependent upon the H – D exchange rate. The specimens of γ-AlOOH were investigated in the temperature range 31 – 110 °C and showed a measurable H – D exchange rate. The specimen of γ-FeOOH was measured at room temperature and at 100 °C. The exchange rate was so fast that the H – D exchange was complete within 6 min. The specimens of α-CrOOH, $In(OH)_3$ and $Y(OH)_3$ were measured at the temperatures 120, 130 and 130 °C, respectively. At these temperatures none of the compounds showed a measurable H – D exchange rate over a 1 – 2 h period.

Neutron diffraction powder pattern of γ-AlOO(H,D). A sample of crystalline γ-AlOOH (crystallite size 500 Å) was partly deuterated by treatment with D_2O. Approximately 5 g γ-AlOOH was kept at 100 °C with 30 ml D_2O for 6 h. After this treatment the product was dried in air and used for the neutron diffraction experiments.

A neutron diffraction powder pattern of γ-AlOO(H,D) was measured at 4.7 K at the D1A spectrometer at the Laue-Langevin Institute in Grenoble, using neutrons of wave length $\lambda = 1.9145$ Å. The diagram was measured in the 2θ interval 10.0 to 145.95° in steps of 0.05°.

Neutron diffraction powder pattern of γ-FeOO(H,D). A sample of crystalline γ-FeOOH was deuterated by treatment with D_2O. The powder was so fine that it was difficult to wet it with D_2O. 10 g γ-FeOOH was treated with 30 ml D_2O and 5 drops of a liquid detergent that reduces the surface tension of D_2O so much that γ-FeOOH was wetted by the liquid. The suspension was kept at room temperature for 24 h. The product was then dried at 95 °C and used for the neutron diffraction experiment. The neutron diffraction powder pattern of γ-FeOO(H,D) was measured at room temperature at the spectrometer TAS5 at Risø, using 1.82 Å neutrons over the 2θ interval 11.0 to 90.8° in steps of 0.2°. The powder was housed in a 15 mm diameter vanadium container.

RESULTS AND DISCUSSIONS

Deuteration of γ-AlOOH. In the structure of γ-AlOO(H,D) the structure factor F_{020} is very sensitive to the H – D ratio of the specimen. Fig. 1 shows the variation in I_{020} with the H – D ratio normalized to 100 for I_{020} of γ-AlOOH and calculated using the Rietveld programme[9] and the structure data obtained for γ-AlOO(H,D), see below. The rate of exchange of hydrogen with deuterium in γ-AlOOH was followed by the variation of the intensity of the 020 reflection. For each recorded powder pattern I_{020} was measured by fitting the 020 peak to a Gaussian function.[10] For each series of measurements I_{020} for $t=0$ was found by extrapolation and all intensities of the 020 reflections were normalized after the value $I_{020,t=0} = 100$. The normalized intensities of a series showed decreasing values with time and using Fig. 1 the variation of hydrogen contents (% H = 100 for γ-AlOOH) was found. Figs. 2, 3 and 4 show the variation of the hydrogen contents in γ-AlOO(H,D) with the square root of time. It is characteristic that

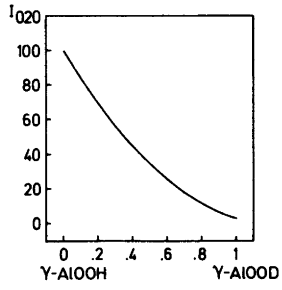

Fig. 1. The intensity of the 020 reflection of γ-AlOO(H,D) *vs.* the H – D ratio.

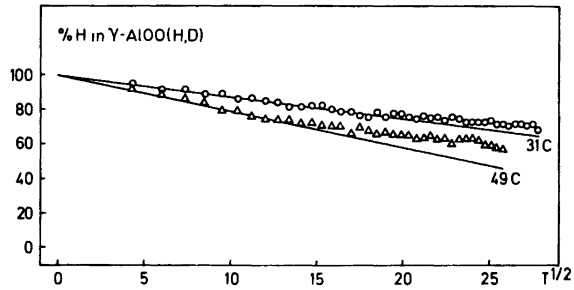

Fig. 2. The hydrogen contents in γ-AlOO(H,D) *vs.* the square root of time in minutes. 1650 Å particle size of γ-AlOOH.

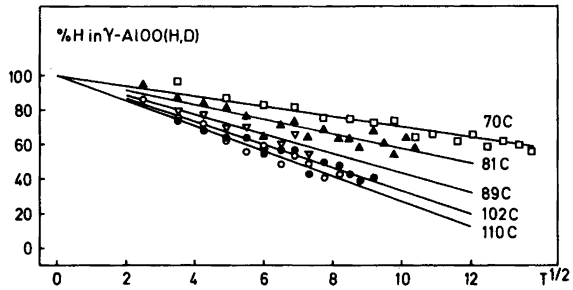

Fig. 3. The hydrogen contents in γ-AlOO(H,D) *vs.* the square root of time in minutes. 1650 Å particle size of γ-AlOOH.

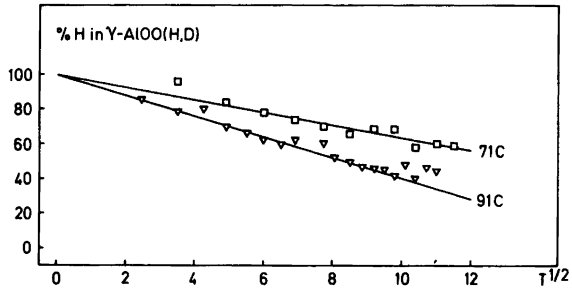

Fig. 4. The hydrogen contents in γ-AlOO(H,D) *vs.* the square root of time in minutes. 500 Å particle size of γ-AlOOH.

this variation over a long period of time is linear, indicating that the rate determining step for H−D exchange is diffusion.[11,12] This explains also that the exchange rate for γ-AlOOH with 500 Å crystallites is greater than the specimen for the same compound with 1650 Å crystallites. The investigation shows also that the exchange rate increases with temperature, and Table 2 lists the time necessary to exchange 25% of H in γ-AlOOH with D. The rates of exchange for γ-AlOOH at the crystallite sizes used are thus relatively high.

Deuteration of γ-FeOOH, α-CrOOH, In(OH)$_3$ and Y(OH)$_3$. The rate of deuteration of γ-FeOOH was extremely high. As γ-FeOOH and γ-AlOOH have the same structure and the specimen of γ-FeOOH has a very small crystallite size, the origin of the high rate of deuteration is assumed to be the small crystallite size of the specimen. The other three

Table 2. Time in min necessary to exchange 25 % of H in γ-AlOOH with D using 1 g of solid and 3 ml of D_2O. Uncertainty in parentheses.

γ-AlOOH particle size 1650 Å		500 Å	
Temp. °C	Time min	Temp. °C	Time min
31	400(40)		
49	145(15)		
70	72(10)	71	50(8)
81	35(7)		
89	20(4)	91	18(5)
102	14(2)		
110	12(2)		

compounds showed no measurable H – D exchange rate. They all have crystallite sizes comparable to those of the γ-AlOOH samples.

The investigation thus shows that the rate determining step in the first part of the H – D exchange between crystalline hydroxides and D_2O is diffusion, and that the rate depends upon the crystallite size of the solid and on the temperature. The investigation does not give a clear picture concerning a relation between the length of the hydrogen bonds in the solids and the rate of H – D exchange of the solid with D_2O. α-CrOOH[1] has short hydrogen bonds of 2.47 Å, γ-AlOOH has hydrogen bonds of 2.73 Å (this work), $In(OH)_3$[5] has hydrogen bonds of 2.733 and 2.892 Å, and $Y(OH)_3$[6] has no hydrogen bonds.

Hydrogen bonds in γ-AlOO(H,D). The structure was refined and the degree of deuteration was determined by least-squares refinements using the Rietveld refinement programme for powder intensities[9] and the scattering lengths (in 10^{-12} cm units): $b_{Al}=0.345$, $b_O=0.580$, $b_D=0.667$ and $b_H=-0.374$.[13] The structure was refined in the space groups *Cmcm* (No. 63) and $Cmc2_1$ (No. 36). Farmer[14] has suggested, based on interpretation of Raman and infrared spectra of γ-AlOOH, that the structure could be described in the space groups *Pnma* (No. 62) and $P2_1/c$ (No. 14). With the special positions of the atoms in the structure with $x=0$ and 1/2, and $z=1/4$ and 3/4, the coordinates arrived at in No. 62 are identical with the coordinates from No. 63. For the space group $P2_1/c$ the hydrogen atoms are described with two sets of coordinates instead of one set for the space group *Cmcm*. When the structure is refined in the space group $P2_1/c$ the coordinates arrived at are not significantly different from the coordinates found when the structure is refined in the space group *Cmcm*. In this space group the hydrogen atoms are placed in site 8*f* with 1/2 H atom in the site, and thus on each side of the centre of symmetry of the hydrogen bond. In the noncentrosymmetric space group $Cmc2_1$ the hydrogen atom is placed in site 4*a*. Slade and Halstead[15] have suggested, from interpretation of NMR absorption spectra, a centrosymmetric hydrogen bond in γ-AlOOH in space group *Cmcm* with four 1/4 H atoms in the bond. When such a model is refined including refinement of the occupancy of the hydrogen atoms one set of the 1/4 H atoms gets an occupancy close to zero and the other set gets an occupancy close to 0.5. This model can thus be ruled out.

The results of the refinement of the structure of γ-

Table 3. Results of refinement of the structure of γ-AlOO(H,D). $a=2.876(3)$, $b=12.24(1)$, $c=3.709(3)$ Å.

Atom	*x*	*y*	*z*	B(Å^2)	Occupancy
Space group *Cmcm*, $R=11.55$ %, 52 reflections					
Al	0	−0.3172(4)	1/4	0.14(4)	1
O1	0	0.2902(2)	1/4	0.14(4)	1
O2	0	0.0820(2)	1/4	0.14(4)	1
H,D[a]	0.5	0.5186(11)	0.3924(24)	0.14(4)	0.246(6)[b]
Space group $Cmc2_1$, $R=11.46$ %, 52 reflections					
Al	0	−0.3166(4)	1/4	0.16(4)	1
O1	0	0.2901(2)	0.2313(40)	0.16(4)	1
O2	0	0.0818(2)	0.2344(39)	0.16(4)	1
H,D[a]	0.5	0.5202(11)	0.3804(36)	0.16(4)	0.242(7)[b]

[a] 67.4 % D, 32.6 % H. [b] for a D-atom.

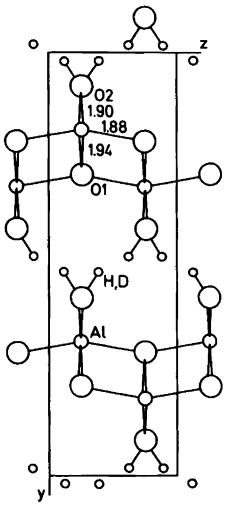

Fig. 5. Projection of the structure of γ-AlOO(H,D) along the 100-direction. Interatomic distances are in Å with standard deviations 0.01 Å.

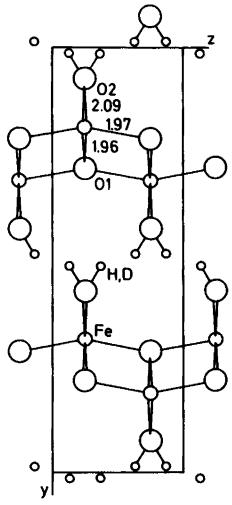

Fig. 6. Projection of the structure of γ-FeOO(H,D) along the 100-direction. Interatomic distances are in Å with standard deviations 0.02 Å.

AlOO(H,D) in space group *Cmcm* and $Cmc2_1$ are listed in Table 3. The *R*-value obtained in space group $Cmc2_1$ is not significantly better than that obtained in space group *Cmcm*, that is chosen as the space group for describing the structure of γ-AlOO(H,D). From the occupancy value listed in Table 3 the degree of deuteration is calculated to be 67.4%. Fig. 5 is a projection of the structure of γ-AlOO(H,D) along the 100-direction. The hydrogen atom is placed approximately 0.14 Å off the line connecting the oxygen atoms in the hydrogen bond. The distances found in the hydrogen bond are: O−H,D···O: 2.73(2) Å, and O−H,D: 0.94(2) Å, in agreement with the O−H···O distance 2.71(1) Å found in γ-AlOOH.[4]

Hydrogen bonds in γ-FeOO(H,D). The structure was refined in the space groups *Cmcm* and $Cmc2_1$ using the same programme and scattering lengths for O, H, and D as described above. In addition, the scattering length $b_{Fe} = 0.951$ (10^{-12} cm units)[13] was used. The coordinates arrived at are listed in Table 4. The hypothesis that the *R*-value 8.21% obtained in the space group $Cmc2_1$ is better than the *R*-value 9.99% obtained in the space group *Cmcm* can only

Table 4. Results of the refinement of the structure of γ-FeOO(H,D). $a = 3.070(2)$, $b = 12.53(2)$, $c = 3.876(3)$ Å.

Atom	*x*	*y*	*z*	B(Å^2)	Occupancy
Space group *Cmcm*, $R = 9.99\%$, 27 reflections					
Fe	0	−0.3137(9)	1/4	0.67(14)	1
O1	0	0.2842(12)	1/4	0.67(14)	1
O2	0	0.0724(13)	1/4	0.67(14)	1
H,D[a]	0.5	0.5143(32)	0.3663(63)	0.67(14)	0.471(27)[b]
Space group $Cmc2_1$, $R = 8.21\%$, 27 reflections					
Fe	0	−0.3140(10)	1/4	0.49(16)	1
O1	0	0.2852(13)	0.2926(101)	0.49(16)	1
O2	0	0.0738(14)	0.2902(87)	0.49(16)	1
H,D[a]	0.5	0.5186(32)	0.3850(67)	0.49(16)	0.472(26)[b]

[a] 96.4% D, 3.6% H. [b] for a D-atom.

be accepted on a 20% confidence level.[16] It is preferred to describe the structure in the centrosymmetrical space group instead of in the non-centrosymmetrical space group.[17] The structure of γ-FeOO(H,D) projected along the 100-direction is shown in Fig. 6. The distances found in the hydrogen bond are: O – H,D···O: 2.65(2) Å, and O – H,D: 0.86(2) Å, and the hydrogen atom is placed approximately 0.22 Å off the line connecting the oxygen atoms in the hydrogen bond. For γ-FeOOH the corresponding distances are 2.68(2) and 0.83(2) Å, respectively.[17]

A list of observed and calculated neutron intensities for γ-AlOO(H,D) and γ-FeOO(H,D) can be obtained from one of us (ANC).

Acknowledgements. We are indebted to Mr. J. Villadsen for specimens of γ-AlOOH and to Dr. D. L. Janes for the specimen of γ-FeOOH. The Danish Natural Science Research Council is acknowledged for financial support and for use of the X-ray powder diffractometer.

REFERENCES

1. Christensen, A. N., Hansen, P. and Lehmann, M. S. *J. Solid State Chem. 21* (1977) 325.
2. Christensen, A. N., Hansen, P. and Lehmann, M. S. *J. Solid State Chem. 19* (1976) 299.
3. Christensen, A. N., Convert, P. and Lehmann, M. S. *Acta Chem. Scand. A 34* (1980) 771.
4. Christoph, G. C., Corbato, E. E., Hofmann, D. A. and Tettenhorst, R. T. *Clays Clay Miner. 27* (1979) 81.
5. Christensen, A. N., Broch, N. C., von Heidenstam, O. and Nilsson, Å. *Acta Chem. Scand. 21* (1967) 1046.
6. Christensen, A. N., Hazell, R. G. and Nilsson, Å. *Acta Chem. Scand. 21* (1967) 481.
7. Drenck, K. *X-Ray Particle Size Determination and its Application to Flint*, Diss., Pennsylvania State University, University Park, Pa. 1959.
8. Lipson, H. and Steeple, H. *Interpretation of X-Ray Diffraction Patterns*, Macmillan, London 1968.
9. Rietveld, H. M. *Program F418 – Fortran IV Version*, Reactor Centrum Nederland, Petten (N.H.), The Netherlands.
10. Wolfers, P. *Programs for Treatment of Powder Profiles* (1975). *Private communication.*
11. Le Claire, A. D. In Hannay, N. B., Ed., *Treatise on Solid State Chemistry*, Plenum, New York 1976, Vol. 4, pp. 1 – 60.
12. Ward, A. F. H. *Proc. R. Soc. London A 133* (1931) 506.
13. Bacon, G. E. *Acta Crystallogr. A 28* (1972) 357.
14. Farmer, V. C. *Spectrochim. Acta A 36* (1979) 585.
15. Slade, R. C. T. and Halstead, T. K. *Solid State Chem. 32* (1979) 119.
16. Hamilton, W. C. *Statistics in Physical Science*, The Ronals Press Company, New York 1964.
17. Christensen, H. and Christensen, A. N. *Acta Chem. Scand. A 32* (1978) 87.

Received July 5, 1981.

Acta Chemica Scandinavica A 36 (1982) 309 – 311

The Crystal Structure of $Ba_2SnO_2(OH)_4 \cdot 10H_2O$

SIV GRIMVALL

Department of Inorganic Chemistry, University of Göteborg and Chalmers University of Technology, S-412 96 Göteborg, Sweden

The crystal structure of $Ba_2SnO_2(OH)_4 \cdot 10H_2O$ has been determined from three-dimensional X-ray diffractometer data. The symmetry is triclinic, space group $P\bar{1}$, with $a=8.771(3)$ Å, $b=8.816(4)$ Å, $c=6.175(2)$ Å, $\alpha=91.33(3)°$, $\beta=67.70(3)°$, $\gamma=116.16(3)°$ and $Z=1$. Full-matrix least-squares refinement based on 3069 non-zero reflections yielded a final R value of 4.9 %.

The tin atom is octahedrally coordinated to six oxygen atoms. The barium atoms are nine-coordinated. The tin oxygen octahedra and the barium atoms together with eight of the nine coordinated oxygen atoms form layers, while the remaining oxygen atoms lie in interposed layers. The different types of layer are held together by Ba – O and O···H – O bonds. Within the layers of oxygen atoms there are hydrogen bonds only. The Sn – O (or – OH) bond distances range from 2.041(4) to 2.068(5) Å while the Ba – O bond distances range from 2.756(5) to 2.912(5) Å.

In order to study the effect of the lone pair of electrons in Sn(II), a number of crystal structures[1-3] have been determined. It is, however, also of interest to study the same element without the lone pair *i.e.* Sn (IV) but with the same type of environment. An investigation of the crystal structure of $Ba_2SnO_2(OH)_4 \cdot 10H_2O$ was therefore undertaken.

EXPERIMENTAL

The barium stannate(IV) crystals were prepared together with barium stannate(II) crystals according to Ref. 4. No special precautions were taken to prevent oxidation of Sn(II) to Sn(IV). Stannate crystals containing both Sn(II) and Sn(IV) were obtained. At least two different compounds with approximately the same crystal form have been identified. A prism-shaped crystal with dimensions 0.18 mm × 0.04 mm × 0.32 mm was selected.

0302-4377/82/040309-03$02.50

Three-dimensional X-ray data were collected with a SYNTEX single crystal diffractometer (Mo$K\alpha$ radiation). No separate measurement of background was made during the data collection. A profile analysis based on the Larsen-Lehmann method[5] was instead applied to the 96-step profile collected for each reflection. 3069 independent reflections with $F_o^2 > 3\sigma(F_o^2)$ were considered observed and were used in the subsequent calculations.

One set of Weissenberg equi-inclination photographs was also taken, together with a rotation photograph around [001], using Cu$K\alpha$ radiation.

UNIT CELL AND SPACE GROUP

The crystals of $Ba_2SnO_2(OH)_4 \cdot 10H_2O$ are triclinic. The cell parameter calculations were based on sin $^2\theta$ values for twelve reflections and gave the following results:

$a=8.771(3)$ Å, $b=8.816(4)$ Å, $c=6.175(2)$ Å, $\alpha=91.33(3)°$, $\beta=67.70(3)°$, $\gamma=116.16(3)°$, $V=390.5(3)$ Å^3, $\mu_{MoK\alpha}=68.0$ cm^{-1}.

There were no systematically absent reflections which supports the triclinic system and the space group $P\bar{1}$ (No. 2).[6] The small standard deviations and the low R-value show that the symmetry ought not be lowered to the space group $P1$ (No. 1). (No. 1). For $Z=1$ a calculated density of 2.86 g/cm^3 is obtained.

STRUCTURE DETERMINATION

The intensity values were corrected for Lorentz and polarization effects (SYN).[7] A correction for absorption effects (DATAPH)[7] was performed when an approximate structure had been derived.

Table 1. Fractional coordinates and isotropic thermal parameters (standard deviations within parentheses).

Atom	x	Y	z	U(Å^2)
Ba	0.3040(1)	0.0378(1)	0.3470(1)	
Sn	0.0000	0.0000	0.0000	
O1	0.7358(6)	0.8332(6)	0.0265(8)	0.0195(7)
O2	0.8927(6)	0.1465(5)	0.1971(8)	0.0168(7)
O3	0.9528(6)	0.8754(6)	0.3151(8)	0.0175(7)
O4	0.6746(7)	0.1770(6)	0.0035(9)	0.0222(8)
O5	0.4660(10)	0.4094(9)	0.2847(13)	0.0388(13)
O6	0.4466(7)	0.8150(7)	0.4148(9)	0.0248(8)
O7	0.1965(9)	0.4772(8)	0.1163(12)	0.0366(13)
O8	0.8661(9)	0.5098(9)	0.3043(12)	0.0355(12)

Table 2. Anisotropic thermal parameters (standard deviations within parantheses). The temperature coefficient is exp $[-2\pi^2(U_{11}h^2a^{*2}+\cdots+2U_{23}klb^*c^*)]$.

Atom	U_{11}	U_{22}	U_{33}	U_{12}	U_{13}	U_{23}
Ba	0.0126(2)	0.0219(2)	0.0111(2)	0.0095(1)	−0.0046(1)	−0.0030(1)
Sn	0.0111(2)	0.0162(2)	0.0100(2)	0.0076(2)	−0.0039(1)	−0.0028(1)

The barium and tin parameters were evaluated from a Patterson synthesis (DRF).[7] Subsequent electron density calculations (DRF)[7] and successive cycles of block-diagonal least-squares refinement (BLOCK)[7] revealed the oxygen atoms. Atomic scattering factors for Ba, Sn and O were taken from Ref. 8. A correction for extinction was included (LINUS).[7] The final value of the isotropic extinction parameter was $g=0.29(3)\times10^4$. Anisotropic thermal parameters for the barium and tin atoms were also included. The R value converged to 4.9 % and R_w to 7.3 %. A weighting scheme according to Cruickshank[9] was used in the refinement ($w=(30.0+F_o+0.01F_o^2+0.00F_o^3)^{-1}$). No attempts were made to locate the hydrogen atoms.

A three-dimensional F_o-F_c Fourier synthesis calculated after the refinement showed some spurious maxima and minima in the vicinity of the heavy atoms. These peaks can probably be attributed to termination effects. Final positional parameters and temperature factors are given with

Table 3. Selected interatomic distances (Å) and angles (°) with their standard deviations in parentheses. Atoms in the unit cell above or below, in the z direction, are marked with an asterisk.

Ba−O1*	2.795(5)	Ba−O4*	2.850(5)
Ba−O2	2.756(5)	Ba−O5	2.905(7)
Ba−O3*	2.809(4)	Ba−O6	2.863(5)
Ba−O3	2.853(5)	Ba−O6′	2.912(5)
Ba−O4	2.818(5)		
Sn−O1	2.068(5)	O1−Sn−O1*	180.0
Sn−O2	2.041(4)	O1−Sn−O2	88.7(2)
Sn−O3	2.061(4)	O1−Sn−O3*	87.8(2)
		O2−Sn−O3	87.2(2)

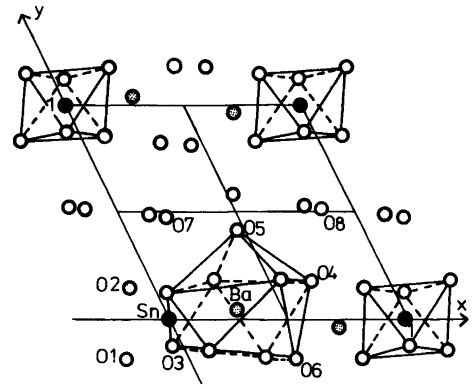

Fig. 1. Projection of the structure of $Ba_2SnO_2(OH)_4\cdot10H_2O$ on the xy plane. Coordination polyhedra for the Ba and Sn atoms are indicated. Dot-filled circles represent barium. Filled circles correspond to tin atoms and unfilled circles to oxygen.

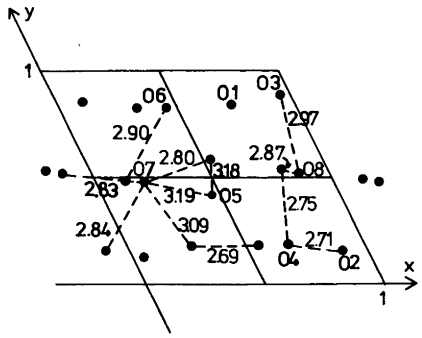

Fig. 2. Projection of the oxygen atoms in the structure of $Ba_2SnO_2(OH)_4 \cdot 10H_2O$ on the xy plane. Short O – O distances are indicated.

their standard deviations in Tables 1 and 2. Selected interatomic distances and angles and their standard deviations were calculated (DISTAN)[7] and the results are given in Table 3. A list of F_o and F_c is available on request.

DESCRIPTION AND DISCUSSION OF THE STRUCTURE

The structure contains two different types of layer parallel to [001] (see Fig. 1). One type consists of Sn and Ba atoms and 10 oxygen atoms coordinated to these. The other type is composed of the remaining water oxygen atoms. The atoms O1, O2 and O3 are bonded to both Sn and Ba. The other oxygen atoms are water oxygen atoms, one formula unit thus containing 10 H_2O. The Sn atoms are sixfold coordinated which means that the initial ion was $Sn(OH)_6^{2-}$. The correct formula must be $Ba_2SnO_2(OH)_4 \cdot 10H_2O$. From Table 3 it is seen that the O2 atoms are most strongly bonded to both Sn and Ba. Probably the O2 atom therefore corresponds to an O^{2-} ion. The $SnO_2(OH)_4^{4-}$ group has a somewhat distorted octahedral configuration (see Fig. 1), the distortion of angles being within limits known from other structures.[10] The remaining Sn – O (or – OH) distances are 2.06 – 2.07 Å, which are normal[11,12] for Sn(IV) – O.

The Ba^{2+} ions are ninefold coordinated. Eight of the oxygen atoms form a square antiprism which is distorted through the ninth oxygen atom (O5 outside one of the square faces (see Fig. 1). The Ba – O distances vary from 2.76 to 2.91 Å which is in good agreement with values published earlier.[13]

According to the formula of the compound there are 24 hydrogen atoms in the unit cell. Examination of short O – O distances shows that the different layers are held together by hydrogen bonds as well as Ba – O5 bonds. Within the oxygen layers there are no other bonding possibilities than these hydrogen bonds. As in indicated in Fig. 2, there are several hydrogen bond distances[14] between oxygen atoms.

Acknowledgements. The author wishes to thank Professor Georg Lundgren for encouraging and valuable discussions. Many thanks are also due to Dr. Evert Ljungström for manipulating the diffractometer, to Dr. Ove Lindgren for help concerning the computer programmes and to Dr. Susan Jagner for revising the English of this article. Financial support has been provided by the Swedish Natural Science Research Council (Contract No. 2318).

REFERENCES

1. Wernfors, G. *Acta Chem. Scand. 15* (1961) 1007.
2. Grimvall, S. *Acta Chem. Scand. A 29* (1975) 590.
3. Grimvall, S. *Acta Chem. Scand. A 36* (1982) 361.
4. Brauer, G. *Handbuch der Präparativen Anorganischen Chemie*, Ferdinand Enke Verlag, Stuttgart 1962, Teil 2.
5. Lehman, M. S. and Larsen, F. K. *Acta Crystallogr. A 30* (1974) 580.
6. *International Tables for X-Ray Crystallography*, 2nd Ed., Kynoch Press, Birmingham 1952, Vol. 1.
7. The Programme Library of the Dept. of Inorg. Chem., Göteborg.
8. Cromer, D. T. and Waber, J. T. *Acta Crystallogr. 18* (1965) 104.
9. Cruickshank, D. W. J. *The Equations of Structure Refinements*, Glasgow 1964.
10. Lindqvist, O. *The Oxygen Coordination of Tellurium(IV) and Tellurium(VI)*, Diss., University of Gothenburg, Göteborg 1973.
11. Larsen, F. K., Christensen, A. N. and Rasmussen, S. E. *Acta Chem. Scand. 21* (1967) 1281.
12. Christensen, A. N. and Hazell, R. G. *Acta Chem. Scand. 23* (1969) 1219.
13. *International Tables for X-Ray Crystallography*, Kynoch Press, Birmingham 1962, Vol. 3.
14. Hamilton, W. C. and Ibers, J. A. *Hydrogen Bonding in Solids*, Benjamin, New York 1968.

Received July 1, 1981.

Acta Chemica Scandinavica A 36 (1982) 313–322

Equilibria between Monohydroxo and Dihydroxo-bridged Binuclear Ethylenediamine Rhodium(III) Complexes

MARTIN HANCOCK, BENTE NIELSEN and JOHAN SPRINGBORG

Chemistry Department, Royal Veterinary and Agricultural University, Thorvaldsensvej 40, DK-1871 Copenhagen V, Denmark

The binuclear ion Δ,Λ-$[(en)_2Rh(OH)_2Rh(en)_2]^{4+}$ (diol) equilibrates in acid solution according to Scheme 1 (amine ligands omitted).

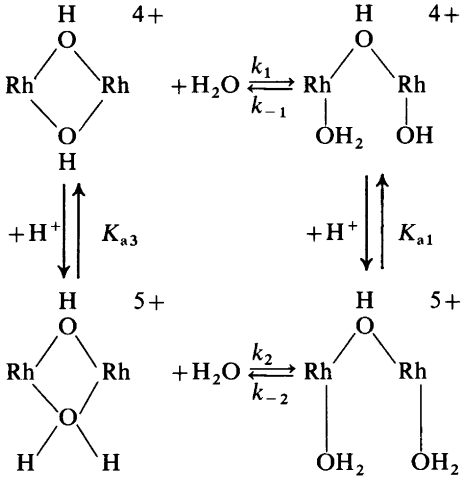

Scheme 1.

The kinetics and equilibria have been studied in 1 M $(Na,H)ClO_4$ in the temperature range 25–40 °C and the hydrogen ion concentration range 10^{-5}–0.1 M. The results were:
k_1 (25 °C) $= 4.6(1) \times 10^{-4}$ s^{-1};
$\Delta H^{\neq} = 86(3)$ kJ mol^{-1}.
k_{-1} (25 °C) $= 4.1(1) \times 10^{-5}$ s^{-1};
$\Delta H^{\neq} = 101(3)$ kJ mol^{-1}.
k_{-2} (25 °C) $= 5.1(1) \times 10^{-5}$ s^{-1};
$\Delta H^{\neq} = 100(2)$ kJ mol^{-1}.
k_2/K_{a3} (25 °C) $= 0.134(3)$ s^{-1} M^{-1};
$\Delta H^{\neq}(k_2) - \Delta H^{\circ}(K_{a3}) = 58(2)$ kJ mol^{-1}.
K_1 (25 °C) $= k_1/k_{-1} = 11.2(5)$;
$\Delta H^{\circ} = -14(3)$ kJ/mol^{-1}.

The acid dissociation constants for the diaqua monool, Δ,Λ-$[(H_2O)(en)_2Rh(OH)Rh(en)_2(H_2O)]^{5+}$, were found to be pK_{a1} (25 °C) $= 2.372(7)$ ($\Delta H^{\circ} = 28(4)$ kJ mol^{-1} and $\Delta S^{\circ} = 49(13)$ J mol^{-1} K^{-1}) pK_{a2} (25 °C) $= 9.128(7)$.

Additional kinetic data at ionic strength 0.1 M and at 25 °C support the proposed mechanism. From kinetic data in the basic pH region it was established that base catalysis is unimportant for pH ≤ 9.5. At higher pH base catalysis does occur, and in 0.01 M NaOH 0.99 M $NaClO_4$ cleavage of diol to dihydroxo monool is fast, k_{obs} (25 °C) $= 2.10(2) \times 10^{-3}$ s^{-1}.

The aquahydroxo monool was isolated as a solid salt, Δ,Λ-$[(H_2O)(en)_2Rh(OH)Rh(en)_2(OH)](ClO_4)_4 \cdot H_2O$.

A revised synthesis for the preparation of *cis*-$[Rh(en)_2(OH)(H_2O)]S_2O_6$ is given and the acid dissociation constants for *cis*-$[Rh(en)_2(H_2O)_2]^{3+}$ were determined to be pK_{a1} (25 °C) $= 6.338(2)$ and pK_{a2} (25 °C) $= 8.244(2)$ in 1 M $NaClO_4$.

A considerable amount of work has been done on the kinetics and thermodynamics of the bridge cleavage reactions of polynuclear hydroxo-bridged complexes of Co(III) and Cr(III) in aqueous solution.[1–19] In our own laboratory attention has centered on the so-called '*diol*' complexes of Cr(III), *i.e.* binuclear dihydroxo-bridged species of the type $[(en)_2Cr(OH)_2Co(en)_2]^{4+}$ and $[L_4Cr(OH)_2CrL_4]^{4+}$ ($L = NH_3, \frac{1}{2}en$), for which the kinetics and thermodynamics of the hydroxo bridge cleavage reaction in acidic solution to give monohydroxo-bridged species, '*monool*', have been investigated in detail.[14–19]

In these systems the monool species have been isolated as crystalline salts and are well-char-

0302-4377/82/040313-10$02.50

acterized,[20] and studies of the equilibration between monool and diol can be made without complications due to loss of ammine or amine ligands or further hydrolysis to give monomeric complexes. In the case of Co(III) diols, in none of the systems examined have the monool species been isolated or characterized definitively, so that an unequivocal interpretation of the kinetic data is not possible.[3,4]

Very little is known about the corresponding Rh(III) reactions.[21] Following the synthesis[22] of the rhodium(III) diols with ammonia and ethylenediamine it was, therefore, natural to extend the previous investigations to include the latter complexes, and the present work describes our results for the Rh(III) ethylenediamine system. Work on the Rh(III) ammonia system is in progress and will be reported later.

RESULTS

Synthesis and properties of the complexes. The rhodium diol was synthesized recently from *cis*-$[Rh(en)_2(OH)(H_2O)]S_2O_6$, which on heating to 120 °C for 24 h gives Δ,Λ-$[(en)_2Rh(OH)_2Rh(en)_2](S_2O_6)_2$ quantitatively.[22] This salt, which is rather insoluble in water, is converted to the more soluble bromide salt by treatment with ammonium bromide and purified by reprecipitation. However, with the latter procedure there exists the possibility of contamination of the sample with monohydroxo-bridged species, monools, formed by the fairly rapid equilibration reaction between diol and monool (*vide infra*). In order to avoid this complication the reprecipitation of the diol bromide salt has to be carried out as quickly as possible and in the cold, as described in a modified procedure given in this work. The diol perchlorate salt which has been used in the present study was obtained from the bromide salt using standard procedures.[23]

A slightly revised procedure for the synthesis of *cis*-$[Rh(en)_2(OH)(H_2O)]S_2O_6$ and a procedure for reprecipitation of this salt is given. In this connection it should be mentioned that the *cis*-dichloro complex, which is used for the synthesis of the *cis*-aquahydroxo salt, was previously[24] formulated incorrectly as a chloride salt and that the correct formulation is *cis*-$[Rh(en)_2Cl_2](Cl)_{\frac{1}{2}}(ClO_4)_{\frac{1}{2}}$.

The acid dissociation constants for *cis*-$[Rh(en)_2(H_2O)_2]^{3+}$ were determined by glass-electrode measurements using *cis*-$[Rh(en)_2(OH)(H_2O)]S_2O_6$ and the values $pK_{a1}=6.338(2)$ and $pK_{a2}=8.244(2)$ were obtained for unit ionic strength ($NaClO_4$) at 25 °C. These values are close to those previously[25] reported for ionic strength 0.5 M (6.09 and 8.08) and for ionic strength 0.01 M (5.82 and 7.98) at 25 °C.

In the following the synthesis of a monohydroxo-bridged species from diol is described. The diol is very robust in acid solution with respect to hydrolysis of the amine ligands, but cleavage of one hydroxo bridge occurs fairly rapidly as can be seen in eqn. (1).

$$\Delta,\Lambda\text{-}[(en)_2Rh(OH)_2Rh(en)_2]^{4+} + H_2O \underset{k_{-1}}{\overset{K_1 k_1}{\rightleftharpoons}} \Delta,\Lambda\text{-}[(H_2O)(en)_2Rh(OH)Rh(en)_2(OH)]^{4+} \quad (1)$$

Further acid hydrolysis of the monools, such as bridge cleavage to give the monomeric species, *cis*-$[Rh(en)_2(H_2O)_2]^{3+}$, is much slower. The equilibrium above lies very much to the right, and when a suspension of Δ,Λ-$[(en)_2Rh(OH)_2Rh(en)_2](ClO_4)_4$ in water is heated to 55 °C for a few minutes the resulting solution contains essentially aquahydroxo monool, which can be precipitated as its perchlorate salt, Δ,Λ-$[(H_2O)(en)_2Rh(OH)Rh(en)_2(OH)](ClO_4)_4 \cdot H_2O$. This crude product, which is slightly contaminated with diol, is then dissolved in 1 M perchloric acid, whereupon the aquahydroxo salt is converted completely into the much more soluble diaqua salt. Under the acidic conditions the small residual amount of diol is rapidly hydrolyzed to monool, and the resulting solution contains pure diaquamonool. From the data presented later in this work it can easily be calculated that an equilibrium solution with $[H^+]=1.0$ M (25 °C) contains 99.5 % monool. Subsequent addition of the appropriate amount of base leads to precipitation of pure Δ,Λ-$[(H_2O)(en)_2Rh(OH)Rh(en)_2(OH)](ClO_4)_4 \cdot H_2O$. The purity of this compound, which is very crucial for the accuracy of the spectrophotometric determination of the equilibrium constant K_1 in eqn. (1) (*vide supra*), was checked by observing that the absorption spectrum measured in 1 M $NaClO_4$ (for the entire region 350 – 240 nm) did not change upon further reprecipitations.

Solid Δ,Λ-$[(H_2O)(en)_2Rh(OH)Rh(en)_2(OH)](ClO_4)_4 \cdot H_2O$ is stable at room temperature for days, but at elevated temperatures it is converted into diol. For example, heating of solid monool salt for two hours at 100 °C resulted in almost quantitative conversion into diol.

The absorption spectra of aqueous solutions of Δ,Λ-$[(en)_2Rh(OH)_2Rh(en)_2](ClO_4)_4$ changed with time due to the monool–diol equilibration reaction, and linear extrapolation back to the time of dissolution had therefore to be made. Such extrapolations can be made linearly only if based on measurements taken within a period after the time of dissolution which is short relative to the time-scale of the equilibration reaction. This could be done at 25 °C for weakly acidic solutions where the equilibration takes hours. In strongly acidic solutions the reaction is very fast, and additional measurements have therefore been made at 0 °C. The observation that identical spectra have been obtained for $[H^+]$ varying from 0.1 M to $\sim 10^{-12}$ M (Table 1) confirms the absence of a terminal non-bridging hydroxo group. The result further implies that protonation of the diol to give μ-aqua-μ-hydroxo species must be negligible for solutions with $[H^+] \leq 0.1$ M. The observation that the spectrum is unchanged even in 0.01 M NaOH, 0.99 M $NaClO_4$ implies that the acid-base equilibrium between diol and an oxo-bridged species must have $pK_a \geq 14$.

Spectra of the monool salt were measured in the entire $[H^+]$ region $1.0 \geq [H^+] \geq 10^{-13}$ M. All the spectral measurements could be interpreted in terms of the two consecutive acid-base equilibria given in eqns. (2) and (3).

$$\Delta,\Lambda\text{-}[(H_2O)(en)_2Rh(OH)Rh(en)_2(H_2O)]^{5+} \overset{K_{a1}}{\rightleftharpoons} \Delta,\Lambda\text{-}[(H_2O)(en)_2Rh(OH)Rh(en)_2(OH)]^{4+} + H^+ \quad (2)$$

$$\Delta,\Lambda\text{-}[(H_2O)(en)_2Rh(OH)Rh(en)_2(OH)]^{4+} \overset{K_{a2}}{\rightleftharpoons} \Delta,\Lambda\text{-}[(OH)(en)_2Rh(OH)Rh(en)_2(OH)]^{3+} + H^+ \quad (3)$$

Spectral data for the three monool cations are presented in Table 1. The result further shows that deprotonation of the hydroxo bridge to form an oxo-bridged species is unimportant for $pH \leq 13$.

The proposed hydroxo-bridged structure of the monool species follows from the acid-base properties, which clearly establish the presence of two terminal (non-bridging) hydroxo groups (*vide infra*). Strong evidence for the proposed structure is also provided by the observation that solid Δ,Λ-$[(H_2O)(en)_2Rh(OH)Rh(en)_2(OH)](ClO_4)_4 \cdot H_2O$ readily forms diol on heating. The structure assignment is also in agreement with the thermodynamic and kinetic results discussed below. The assignment of the configuration as Δ,Λ is based on the configura-

Table 1. Ligand-field spectra extrapolated to the time of dissolution at 25 °C.

Compound	Medium[a]	$(\varepsilon,\lambda)_{max}$	$(\varepsilon,\lambda)_{max}$	$(\varepsilon,\lambda)_{min}$
Δ,Λ-$[(en)_2Rh(OH)_2Rh(en)_2](ClO_4)_4$	0.125 M $HClO_4$[b]	(532,331)		(370,301)
	0.001 M $HClO_4$	(535,331)		(375,301)
	Buffer pH = 9.5[c]	(528,331)		(367,301)
	0.01 M NaOH	(531,331)		(377,301)
	0.001 M $HClO_4$	(526,331)		(368,301)
Δ,Λ-$[(en)_2Rh(OH)_2Rh(en)_2]Br_4 \cdot 2H_2O$	1 M $HClO_4$	(590,329)	(553,273)	(445,299)
Δ,Λ-$[(H_2O)(en)_2Rh(OH)Rh(en)_2(OH)](ClO_4)_4 \cdot H_2O$	0.1 M $HClO_4$	(597,329)	(559,273)	(448,299)
	0.05 M NaOH	(519,327)	(635,278)	(487,309)
	Buffer pH = 10.5[c]	(520,327)	(638,278)	(488,309)
	1 M $NaClO_4$	(514,330)	(553,270)$_{sh}$	(391,302)
	Buffer pH = 5.2[d]	(516,330)	—[e]	(391,302)

[a] Unit ionic strength maintained with $NaClO_4$. The concentration of complex was always $\sim 10^{-3}$ M. [b] Measured at 0.8 °C. [c] 0.01 M NH_4ClO_4, 0.01 M NH_3, 0.99 M $NaClO_4$ (pH = 9.5) and 0.01 M NH_4ClO_4, 0.1 M NH_3, 0.99 M $NaClO_4$ (pH = 10.5).[35] [d] 0.1 M py H_2ClO_4, 0.1 M py, 0.9 M $NaClO_4$ (py = pyridine).[35] [e] Obscured by absorption band of pyridine.

Table 2. Thermodynamic data for monools and diol at 25 °C and unit ionic strength, (Na,H)ClO_4.[a]

pK-values		$\Delta H°$ (kJ mol^{-1})	$\Delta S°$ (J mol^{-1} deg^{-1})
pK_{a1}	2.372(7)	28(4)	49(13)
pK_{a2}	9.128(7)	–	–
K_1	11.2(5)	−14(3)	−28(8)

[a] K_1, K_{a1} and K_{a2} are defined by eqns. (1), (2) and (3), respectively.

tion of the parent diol and the well-known tendency of Rh(III) to undergo substitution reactions without isomerization.

Determination of the acid dissociation constants for the monools. The two acid dissociation constants K_{a1} and K_{a2} for the diaqua monool were determined by glass-electrode measurements. Owing to the equilibration reaction between the monool and diol a normal titration could not be made. Each pH measurement was therefore made on a freshly prepared solution, and pH was then extrapolated back to the time of dissolution. At higher temperatures this method becomes difficult since equilibration is then fast relative to the response of the glass electrode. The determination of pK_{a1} at 35.0 °C was therefore made using equilibrium conditions (see experimental section). The results are quoted in Table 2.

Measurement of the kinetics and thermodynamics of the equilibrium between monool and diol. The kinetics and thermodynamics of the equilibrium between monool and diol were studied spectrophotometrically in the $[H^+]$ region $0.1 \geq [H^+] \geq 10^{-5}$ M. The rate of equilibration is very pH-dependent, as is also that of the subsequent hydrolysis of the monools to monomeric *cis*-$[Rh(en)_2(H_2O)_2]^{3+}$. However, at a given $[H^+]$ the latter reaction is always much slower, by a factor of at least 100, than the former reaction.

The spectra of solutions initially containing diol and monool, respectively, changed with time and became constant within a period varying from minutes to hours at 25 °C, depending on pH. The spectral changes were always attended by well-defined isosbestic points, and for a given $[H^+]$ the final spectra were identical for solutions initially containing monool and diol, respectively. The final spectra are thus those of equilibrium mixtures of monool (diaqua and aquahydroxo) and diol, and the stoichiometry of the solutions can therefore be expressed by eqns. (1), (2) and (3).

The equilibrium constant K_1 was determined spectrophotometrically from measurements in solutions with $[HClO_4] = 10^{-3}$, 5×10^{-4} and 10^{-4} M, respectively (see also experimental section). From measurements at the two temperatures 25.0 and 40.6 °C the parameters quoted in Table 2 were calculated.

Kinetic data were obtained from spectrophotometric measurements, and pseudo first-order rate constants, k_{obs}, for solutions initially containing pure diol or pure monool were calculated using non-linear regression analysis. Most of the kinetic measurements were made on solutions initially containing diol, and $[H^+]$ was varied from 0.1 to 10^{-5} M.

Kinetic measurements on solutions initially containing monool were made only for $[H^+] = 10^{-3}$ and 10^{-4} M. At higher $[H^+]$ and in the basic region there is practically no change of absorbance with time for solutions initially containing monool.

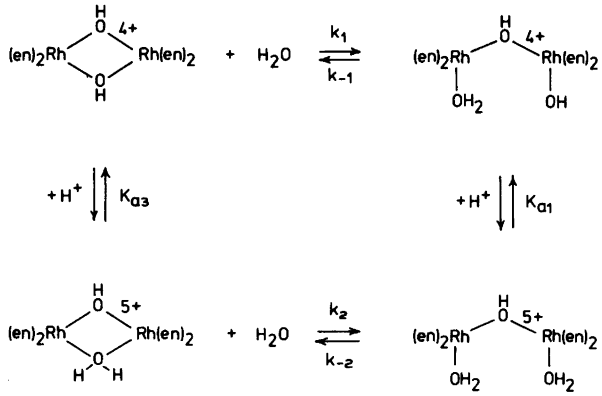

Scheme 2.

All kinetic measurements were made under pseudo first-order conditions, *i.e.* the change in the hydrogen-ion concentration during an experiment was typically less than 3 %.

As established above, the stoichiometry of the equilibrium mixture can be described by the equilibrium between diol and aquahydroxo monool [eqn. (1)], and the acid-base equilibrium between the diaqua- and aquahydroxo monools [eqn. (2)]. However, the rate-expression derived from these equilibria alone is insufficient for an interpretation of the kinetic data and an additional, acid-catalyzed reaction path must be included as shown in Scheme 2. From this reaction scheme the following rate-expression is derived assuming that $K_{a3} \geq [H^+]$, *i.e.* that protonation of the diol is stoichiometrically negligible as can be concluded from the spectral data for diol in strongly acidic media, and using the relations $K_{a3}/K_2 = K_{a1}/K_1$, $K_1 = k_1/k_{-1}$ and $K_2 = k_2/k_{-2}$; eqn. (4). Two of the parameters, K_1

$$k_{calc} = k_1 + \frac{[H^+]K_1 k_{-2}}{K_{a1}} + \frac{K_{a1}K_1^{-1}k_1 + [H^+]k_{-2}}{K_{a1} + [H^+]} \quad (4)$$

and K_{a1}, in this equation have been determined in separate experiments as described above. Using these values, the two rate constants, k_1 and k_{-2}, were determined by the method of non-linear regression analysis (Fig. 1) and gave the parameter values shown in Table 3.

Additional kinetic measurements made at ionic strength 0.1 M (Na,H)ClO_4 and 25 °C showed a linear relationship between k_{obs} and $[H^+]$. From the calculations above it is seen that this linear relationship is accidental and is due to the fact that the values of k_{-1} and k_{-2} are almost equal. This reduces eqn. (4) to the approximate relationship (5). Assuming that this approximate equation can be applied to the data for $I = 0.1$ M, the values $k_2/K_{a3} = 5.2(1) \times 10^{-2}$ s^{-1} M^{-1} and $k_1 + k_{-1} = 4.83(10) \times 10^{-4}$ s^{-1} were then calculated (Table 4). Since K_1 and K_{a1} were not determined at $I = 0.1$ M, any further interpretation of the kinetic data was not possible.

$$k_{calc} = k_1 + k_{-1} + \frac{[H^+]k_2}{K_{a3}} \quad (5)$$

A few kinetic measurements were made in the basic region (at 25 °C and ionic strength 1.0 M). At pH = 9.5 (0.01 M NH_3, 0.01 M NH_4ClO_4, 0.99 M $NaClO_4$), the value for k_{obs} of $4.68(10) \times 10^{-4}$ s^{-1} is in good agreement with the value $4.57(11) \times$

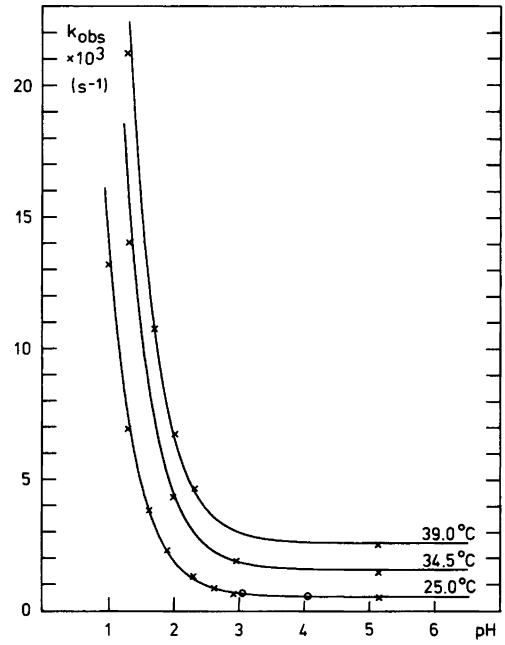

Fig. 1. The observed pseudo first-order rate constants, k_{obs}, for the equilibration reaction between monool and diol as a function of pH = log$[H^+]$ at three different temperatures and at unit ionic strength. The k_{obs} values have been obtained for solutions initially containing diol (×) or monool (○). The solid lines represent calculated values of k_{obs} [eqn. (4)] with parameters as quoted in Tables 2 and 3.

Table 3. Kinetic data for the equilibration reactions between monools and diol at 25 °C and ionic strength 1.0 M (Na,H)ClO_4.

Reaction	$10^5 \times k$ s^{-1}	$\Delta H^{\neq}$ kJ mol^{-1}	$\Delta S^{\neq}$ J mol^{-1} deg^{-1}
k_1	45.6(11)	86(3)	−19(8)
k_{-1}	4.07(10)	101(3)	9(9)
k_{-2}	5.10(12)	100(2)	9(7)
Reaction	k s^{-1} M^{-1}	$\Delta H^{\neq} - \Delta H^{\circ}$ kJ mol^{-1}	$\Delta S^{\neq} - \Delta S^{\circ}$ J mol^{-1} deg^{-1}
k_2/K_{a3}	0.134(3)	57.8(20)	−68(7)

Table 4. Observed and calculated rate constants for the equilibrium between the monools and the diol at ionic strength 0.1 M (Na,H)ClO_4 and at 25 °C. k_{calc} from eqn. (5).

$[H^+]$ mol/l	$10^4 \times k_{obs}$ s^{-1}	$10^4 \times k_{calc}$ s^{-1}
0.1	55.8	56.8
0.05	31.0	30.8
0.01	10.3	10.0
0.002	5.92	5.87
5×10^{-6} [a]	4.77	4.83

[a] 0.01 M pyH,ClO_4, 0.01 M py, 0.09 M $NaClO_4$ (py = pyridine).[35]

10^{-4} s^{-1} calculated according to the reaction scheme above, but including the acid-base equilibrium in eqn. (3). Base-catalysis can therefore be ignored for pH ≤ 9.5.

At higher pH base-catalysis does occur: The reaction of diol in 0.01 M NaOH, 0.99 M $NaClO_4$ was investigated spectrophotometrically at 25 °C and was shown to give dihydroxo monool quantitatively. The change of absorbance with time obeyed first-order kinetics and gave $k_{obs} = 2.10(2) \times 10^{-3}$ s^{-1} [which is 5 times faster than the uncatalyzed reaction (k_1)].

DISCUSSION

The equilibration between the monools and the diol in the present Rh(III) system occurs *via* an acid-catalyzed and an uncatalyzed reaction path, and a similar reaction scheme was recently observed for the first bridge cleavage of the ammonia Cr(III) diol, $[(NH_3)_4Cr(OH)_2(NH_3)_4]^{4+}$.[18,19] This similarity between Rh(III) and Cr(III), however, is no longer apparent if one compares with other bridged Cr(III) complexes; the first bridge cleavage of the two isomers (Δ,Δ-Λ,Λ and Δ,Λ) of $[(en)_2Cr(OH)_2Cr(en)_2]^{4+}$ and of the mixed compound Δ,Λ-$[(en)_2Co(OH)_2Cr(en)_2]^{4+}$ occurs only *via* an uncatalyzed reaction path.[14-16] Similarly, no acid catalysis has been observed for the bridge-cleavage of the *cis*-aquaerythro cation, $[(NH_3)_5Cr(OH)Cr(NH_3)_4(OH_2)]^{5+}$, and for the related anionoerythro complexes.[11-13]

The analogous Co(III) complexes exhibit pronounced acid-catalysis.[1-8] Bridge cleavage of the Co(III) complex $[(NH_3)_5Co(OH)Co(NH_3)_5]^{5+}$ has been reported to proceed *via* two reaction paths, an acid-catalyzed and an uncatalyzed.[1,2] Acid-catalysis has also been reported for the first bridge cleavage of several trihydroxo-bridged complexes of Co(III), and in fact in these systems an uncatalyzed path was not observed.[5] Cleavage of the cobalt(III) diols $[(NH_3)_4Co(OH)_2Co(NH_3)_4]^{4+}$ and Δ,Λ-$[(en)_2Co(OH)_2Co(en)_2]^{4+}$ is acid-catalyzed, although in none of these cases has it been possible to establish with certainty whether the acid-catalyzed path is associated with the first or the second bridge-cleavage, or both.[3,4]

By analogy with the above-mentioned studies on Co(III) and Cr(III) the acid-catalyzed reaction path in the present Rh(III) system is proposed to involve protonation of one hydroxo bridge to give a labile aqua-bridged intermediate. In the Rh(III), Cr(III) and Co(III) systems the aqua-bridged intermediates are very strong acids with acid dissociation constants much greater than unity, and only the ratio k_2/K_{a3} has been determined. The activation parameters given for the acid-catalyzed path are therefore composite terms, $[\Delta H^{\neq}(k_2) - \Delta H^{\circ}(K_{a3})]$ and $[\Delta S^{\neq}(k_2) - \Delta S^{\circ}(K_{a3})]$. Since $\Delta H^{\circ}(K_{a3})$, referring to a very strong acid, is undoubtedly negative[26] we obtain as an upper-limit estimate for the Rh(III) system that $\Delta H^{\neq}(k_2) < 58$ kJ mol^{-1}. This reflects, as anticipated, that water is a poor bridging group, and similar low $\Delta H^{\neq}$ values have been observed for the Cr(III) and Co(III) complexes.[5,18,19]

The values for k_{-1} and k_{-2} in the rhodium(III) system are similar, and the corresponding $\Delta H^{\neq}$ values are nearly identical. The values for $\Delta S^{\neq}$ are also similar. These results suggest that the k_{-1} and k_{-2} paths involve the same mechanism. Both reactions involve replacement of coordinated water, but since coordinated water is a much poorer nucleophile than coordinated hydroxide an essentially associative mechanism would require very different $\Delta H^{\neq}$ values, which clearly is not the case.

We therefore propose that the k_{-1} and k_{-2} reactions are both essentially dissociative in character. In both reactions a rate-determining Rh-OH_2 bond-rupture is then assumed to give a transition state in which both coordinated OH (k_{-1}) and coordinated H_2O (k_{-2}) are captured by intramolecular reactions, faster than intermolecular capture of solvent water. Accordingly, we expect k_{-1} and k_{-2} to be similar to k_{ex} for the water-exchange reactions of related hydroxo-bridged complexes (*i.e.* complexes for which intramolecular reactions do not compete with the solvent exchange reaction). However, no such data have been

reported, and we are therefore restricted to data for monomeric complexes.

For water exchange[27,28] in the pentaammine complex, $[Rh(NH_3)_5(H_2O)]^{3+}$, we have $k_{ex}=1.0\times 10^{-5}$ s^{-1} (25 °C, $I=0.5$ M), which is a factor of five less than k_{-1} and k_{-2}. The $\Delta H^{\neq}$ values for all three processes are similar ($\Delta H^{\neq}$ (exchange)$=101$ kJ mol^{-1}). The result seems to support an essentially dissociative mechanism in the case of the bridged complexes. In contrast to this the water exchange of the pentaammine complex is assigned an I_a mechanism.[27-31]

Relevant to this discussion is the corresponding chromium(III) ammine system (*i.e.* $[(NH_3)_4Cr(OH)_2Cr(NH_3)_4]^{4+}$). In the chromium(III) system, ring closure of the monools (k_{-1} and k_{-2}) has been assigned an essentially associative mechanism and the different nucleophilic properties of coordinated OH^- and OH_2 were clearly demonstrated by a large difference between the $\Delta H^{\neq}$ values (80.6 and 123 kJ/mol^{-1}, respectively).[18,19] This difference in associative behaviour of the hydroxo-bridged complexes of Cr(III) and Rh(III) corresponds qualitatively to the observation that for pentaammine complexes the degree of association increases along the series $Co(NH_3)_5X<Ir(NH_3)_5X<Rh(NH_3)_5X<Cr(NH_3)_5X$ (X is a singly charged anion or water).[29-32]

The influence of ionic strength on the rate constants supports the proposed reaction scheme. For the composite term k_1+k_{-1} there is no significant change on going from ionic strength 1.0 to 0.1 M. This is a reasonable result since k_1 is associated with a reaction between a cation and a neutral molecule and k_{-1} is associated with an intramolecular reaction. According to conventional reaction rate theory, both reactions should be influenced to a very small extent by the ionic strength.[33]

For the composite term k_2/K_{a3} there is a decrease by a factor of 3 on going from ionic strength 1.0 to 0.1 M. Since k_2 is associated with a reaction between a cation and a neutral molecule, its ionic-strength dependency is probably negligible and the change is consequently essentially caused by a change in K_{a3}. This requires that K_{a3} increases by a factor of *ca.* 3 when the ionic strength is decreased from 1.0 to 0.1 M, which is qualitatively in agreement with the behaviour predicted theoretically for a cationic acid.

The difference between the two pK_a values for the diaqua monool is nearly 7 units. As discussed below, this large difference reflects a simultaneous decrease in pK_{a1} and increase in pK_{a2} relative to what would be expected on the basis of semi-quantitative charge considerations.

From charge considerations alone we expect the acid strength of Δ,Λ-$[(H_2O)(en)_2Rh(OH)Rh(en)_2(OH_2)]^{5+}$ to be greater than that of *cis*-$[Rh(en)_2(H_2O)_2]^{3+}$. On the basis of the pK_a values for *cis*-$[(Cr(NH_3)_4(H_2O)_2]^{3+}$ (4.96)[34] and for *cis*-$[(NH_3)_5Cr(OH)Cr(NH_3)_4(H_2O)]^{5+}$ (3.5)[35] we estimate, allowing for a statistical factor of two (0.3 pK_a units), that the rhodium diaqua monool should be a stronger acid than the monomeric diaqua ion by approximately 1.8 pK_a units. From the pK_a values (6.34 and 8.24) of *cis*-$[Rh(en)_2(H_2O)_2]^{3+}$ we therefore estimate that the rhodium diaqua monool should have p$K_{a1}\approx 4.5$ and p$K_{a2}\approx 6.4$ (upper limit). The observed pK_a values (2.4 and 9.1) are clearly significantly different from these predicted values and we note that the deviation applies to both pK_{a1} and pK_{a2}.

A similar increased stability of the aquahydroxo form relative to its acid and base form has also been observed in the corresponding chromium(III) ethylenediamine and ammine systems.[14-19] Following a recent discussion[18] in connection with the chromium(III) systems we propose that the Rh(III) aquahydroxo monool, by analogy with the chromium(III) monools, is stabilized relative to the diaqua and dihydroxo monools by internal hydrogen-bond formation between coordinated water and hydroxide, as shown in Fig. 2. A similar internal hydrogen-bond stabilization might also occur in the diaqua and in the dihydroxo complexes, but the very symmetrical conformation in the aquahydroxo monool, with H_2O donating hydrogen to OH, is likely to be more stable than those of the latter. This hydrogen-bond stabilization can therefore account for the decrease in pK_{a1} and the increase in pK_{a2} relative to the values expected purely on the basis of charge considerations.

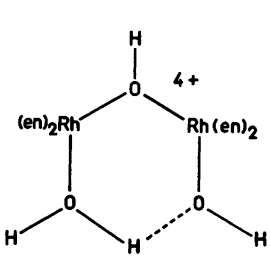

Fig. 2. The proposed hydrogen-bond stabilized structure of the aquahydroxo monool.

EXPERIMENTAL

Materials. The complex *cis*-$[Rh(en)_2Cl_2]Cl_{\frac{1}{2}}(ClO_4)_{\frac{1}{2}}$ was prepared as described previously.[24] All chemicals were of analytical grade.

Instruments. A Zeiss DMR 21 spectrophotometer was used for all spectrophotometric measurements in the visible region. Data are given with the molar decadic absorption coefficient ε in 1 mol^{-1} cm^{-1} and the wavelength λ in nm. The molarity of solutions of the binuclear complexes is in all cases defined in terms of the number of mol of complex rather than the number of mol of rhodium(III) per litre of solution.

The pH measurements were made with a Radiometer GK 2301 C combined glass and calomel electrode in conjunction with a Radiometer PHM 61 digital pH-meter.

Analyses. C, H, N, Br and Cl analyses were performed by the microanalytical laboratory at the H. C. Ørsted Institute, Copenhagen.

Potentiometric measurements. The pH measurements at 25 °C were made as described previously in connection with the corresponding chromium(III) systems,[14-19] and the definition $pH = -\log[H^+]$ was employed throughout. The determination of pK_{a1} of the diaqua monool at 35.0 °C was made using equilibrium conditions as described in the following.

Partly neutralized solutions of the aquahydroxo monool salt were kept at 35.0 °C and pH was monitored. The pH initially decreased with time due to the formation of diol and became constant after 15 min, showing that equilibrium had been attained. From the $[H^+]$ measured at equilibrium, pK_{a1} can be calculated using standard procedures if corrections are made for the small content (~ 10 %) of diol. Such corrections can be made if K_1 is known. However, the spectrophotometric determination of K_1 requires a knowledge of K_{a1}, and the calculations of K_{a1} and of K_1 were therefore made simultaneously using iteration. Only one iteration was necessary.

Spectra and treatment of spectral data. Spectra of monool and of diol salts in different media, extrapolated to the time of dissolution and at equilibrium, were obtained as described recently.[19] Pseudo first-order rate constants, k_{obs}, and activation parameters were calculated as described previously.[19] The k_{obs} values were calculated from absorbances measured at two or three of the wavelengths $\lambda = 330$, 300 and 280 nm (for solutions initially containing diol) or $\lambda = 254$, 250, 246, and 242 nm (for solutions initially containing monool). All kinetic runs were performed in duplicate.

In all kinetic runs the hydrogen ion concentration changed slightly. These changes were generally about 1–3 %, although in experiments with low $[H^+]$, changes of up to 8 % were calculated [eqns. (1) and (2)]. However, the error introduced by this variation is very small, since at low $[H^+]$ the dependence of k_{obs} on $[H^+]$ is small. For each experiment the hydrogen ion concentrations at t_o, $[H^+]_o$, and at equilibrium, $[H^+]_\infty$, were calculated and the values $[H^+] = \frac{1}{2}([H^+]_o + [H^+]_\infty)$, were then used in the subsequent calculations.

The calculations of K_1 were based on absorbances of solutions of pure diol, ε_D, pure monool, ε_M, and the equilibrium solution, ε_∞, measured at $\lambda = 254$, 250, 246 and 242 nm and using eqn. (6).

$$K_1 = \frac{(\varepsilon_D - \varepsilon_\infty)}{(\varepsilon_\infty - \varepsilon_M)} \frac{K_{a1}}{[H^+] + K_{a1}} \qquad (6)$$

The ratio $(\varepsilon_D - \varepsilon_\infty)/(\varepsilon_\infty - \varepsilon_M)$ is experimentally difficult to measure since the equilibrium is shifted very much toward monool and accordingly the relative difference between ε_∞ and ε_M is very small. This difference is greatest in weakly acid solution, for which the ratio is approximately equal to K_1 and the measurements were therefore made in solutions with $[HClO_4] = 10^{-3}$, 5×10^{-4} and 10^{-4} M, respectively.

The value of K_1 at 25 °C was then calculated using the value for K_{a1} determined as above. As discussed above, the calculations of K_1 and K_{a1} at the higher temperatures were made simultaneously, using iteration.

Preparations

1. cis-*Aquabis(ethylenediamine)hydroxorhodium(III) dithionate*, *cis*-$[Rh(en)_2(OH)(H_2O)]S_2O_6$. *cis*-$[Rh(en)_2Cl_2]Cl_{\frac{1}{2}}(ClO_4)_{\frac{1}{2}}$ (6.0 g; 16.60 mmol) and $AgNO_3$ (8.57 g; 50.45 mmol) were heated under reflux for 3 h in water (50 ml) in the dark. The reaction mixture was allowed to stand overnight. 1.00 M HCl (11.0 ml) was added, and after standing for *ca.* 10 min the solution was filtered. The flask and funnel were rinsed with boiling water (3×10 ml) and the filtered washings added to the bulk filtrate. Finely powdered $Na_2S_2O_6 \cdot 2H_2O$ (6.0 g) was added and dissolved by stirring at room temperature. Then 1.00 M NaOH (24 ml) was added and a finely-divided pale-yellow precipitate was formed. After leaving the mixture to stand for *ca.* 1 h at room temperature and then in an ice-bath for *ca.* 20 min, the product was isolated by filtration, washed with ice-cold water, then 96 % ethanol and ether and air-dried. Yield 5.32 g (77 %).

The pure product was obtained by reprecipitation. Crude aquahydroxo dithionate (2.0 g; 4.78 mmol) and finely powdered $Na_2S_2O_6 \cdot 2H_2O$ (2.4 g)

were stirred together in 0.50 M HCl (12.0 ml) until all was dissolved. 1.0 M NaOH was then added dropwise to the stirred, filtered solution to give pH = 7, when a pale-yellow precipitate formed rapidly. After stirring at room temperature for *ca.* 15 min the mixture was kept in an ice-bath for 45 min and then filtered. Washing and drying were performed as before. Yield 1.88 g (94 %). The product reprecipitated twice in this manner showed no changes in the UV-visible absorption spectrum on further reprecipitation. Anal. $[Rh(en)_2(OH)(H_2O)]S_2O_6$: C, H, N. Spectral data (0.1 M $HClO_4$, 0.9 M $NaClO_4$; 25 °C) $(\varepsilon,\lambda)_{max}$: (175,317), (137,271). $(\varepsilon,\lambda)_{min}$: (117,289), (32,236).

2. *Δ,Λ-Di-μ-hydroxobis[bis(ethylenediamine)rhodium(III)]bromide dihydrate*, Δ,Λ-$[(en)_2Rh(OH)_2Rh(en)_2]Br_4 \cdot 2H_2O$. Crude diol dithionate (4.81 g; 6.01 mmol) was stirred vigorously in saturated NH_4Br solution (55 ml) at room temperature for 1 h. The resulting crude bromide salt was then isolated by suction filtration on a fine-porosity sintered glass funnel and washed with ice-cold 1:1 aqueous ethanol. The product was extracted on the filter with water (temp. 20 °C) in portions within a total of 20 min (total extraction volume *ca.* 200 ml) and the portions of solution were filtered immediately into an ice-cooled 500 ml conical flask containing stirred NH_4Br solution (80 ml, saturated at room temp.). A dense pale-yellow precipitate was immediately formed, and after cooling with stirring for a further 20 min the product was isolated by filtration, washed with ice-cold 1:1 aqueous ethanol, then 96 % ethanol and finally ether, and air-dried. Yield 3.85 g (77 %). Anal. $[Rh_2(en)_4(OH)_2]Br_4 \cdot 2H_2O$: C, H, N, Br.

3. *Δ,Λ-Di-μ-hydroxobis[bis(ethylenediamine)rhodium(III)]perchlorate*, Δ,Λ-$[(en)_2Rh(OH)_2Rh(en)_2](ClO_4)_4$. Δ,Λ-$[(en)_2Rh(OH)_2Rh(en)_2]Br_4 \cdot 2H_2O$ (3.85 g) was stirred vigorously with a mixture of saturated $NaClO_4$ (20 ml) and water (20 ml) at *ca.* 16 °C for 1 h. The precipitate was filtered off by suction on a fine-porosity sintered glass funnel, washed with 96 % ethanol and sucked almost dry. The product was then extracted on the filter with water (*ca.* 16 °C) in small portions within a total of 7 min (total volume *ca.* 70 ml) and the portions filtered immediately into an ice-cooled flask containing stirred $NaClO_4$ solution (50 ml, saturated at room temp.). After cooling and stirring for a further 15 min the product was isolated by filtration, washed with 96 % ethanol and then ether, and air-dried. Yield. 3.70 g (91 %). Anal. $[Rh_2(en)_4(OH)_2](ClO_4)_4$: C, H, N, Cl. The spectral data (Table 1) for this salt are identical with those for the bromide dihydrate, which is strong evidence for the purity of the products.

4. *Δ,Λ-Aquatetrakis(ethylenediamine)-μ-hydroxohydroxo dirhodium(III) perchlorate*, Δ,Λ-$[(H_2O)(en)_2Rh(OH)Rh(en)_2(OH)](ClO_4)_4 \cdot H_2O$. Δ,Λ-$[(en)_2Rh(OH)_2Rh(en)_2](ClO_4)_4$ (3.0 g, 3.42 mmol) was added to water (9.0 ml) at 55.0 ± 0.5 °C and the stirred mixture was kept at that temperature for 20 min. All the complex dissolved within the first 3 min. The solution was then cooled in ice and a saturated (at 20 °C) solution of sodium perchlorate (9 ml) was added. After 20 min the precipitate was filtered off and washed thoroughly with 96 % ethanol. Drying in air gave 2.80 g of crude aquahydroxo monool salt. The crude perchlorate salt (2.8 g) was dissolved in 1.000 M perchloric acid (10.00 ml) at 25.0 ± 0.1 °C within 30 s. After a further 120 s the filtered solution was cooled in ice and a saturated solution of sodium perchlorate (15 ml) added. After a further *ca.* 10 min the almost colourless solution was filtered and then 2.00 M sodium hydroxide (5.00 ml) was added. The aquahydroxo monool salt precipitated within a few minutes and was isolated as above. Yield 2.50 g (80 %) of a pure salt. Further reprecipitation did not change the absorption spectrum in the region 350 – 240 nm. Anal. $[Rh_2(en)_4(H_2O)(OH)_2](ClO_4)_4 \cdot H_2O$: C, H, N, Cl.

Acknowledgements. The authors wish to thank Finn Christensson for determining the acid dissociation constants for *cis*-$[Rh(en)_2(H_2O)_2]^{3+}$, and Ole Mønsted and Finn Christensson for critical reading of the manuscript.

REFERENCES

1. Wharton, R. K. and Sykes, A. G. *J. Chem. Soc. Dalton Trans.* (1973) 439.
2. Buckingham, D. A., Marty, W. and Sargeson, A. M. *Inorg. Chem. 13* (1974) 2165.
3. Ellis, J. D., Scott, K. L., Wharton, R. K. and Sykes, A. G. *Inorg. Chem. 11* (1972) 2565.
4. Meloon, D. R. and Harris, G. M. *Inorg. Chem. 16* (1977) 434 and references therein.
5. Wieghardt, K., Schmidt, W., Nuber, B. and Weiss, J. *Chem. Ber. 112* (1979) 2220 and references therein.
6. Laier, T. and Springborg, J. *Acta Chem. Scand. A 35* (1981) 145.
7. Sykes, A. G. and Weil, J. A. *Prog. Inorg. Chem. 13* (1970) 1.
8. Taylor, R. S. and Sykes, A. G. *Inorg. Chem. 13* (1974) 2824.
9. Thompson, G. Report UCRL-11410, Lawrence Radiation Laboratory, Berkeley 1964.
10. Wolcott, D. and Hunt, J. B. *Inorg. Chem. 7* (1968) 755.
11. Hoppenjans, D. W. and Hunt, J. B. *Inorg. Chem. 8* (1969) 505.

12. Po, H. N. and Enomoto, H. *J. Inorg. Nucl. Chem. 35* (1973) 2581.
13. Po, H. N., Chung, Y. H. and Davis, S. R. *J. Inorg. Nucl. Chem. 35* (1973) 2849.
14. Springborg, J. and Toftlund, H. *Acta Chem. Scand. A 30* (1976) 171.
15. Christensson, F., Springborg, J. and Toftlund, H. *Acta Chem. Scand. A 34* (1980) 317.
16. Springborg, J. and Schäffer, C. E. *Inorg. Chem. 15* (1976) 1744.
17. Springborg, J. and Schäffer, C. E. *Acta Chem. Scand. A 30* (1976) 787.
18. Christensson, F. and Springborg, J. *Poster, XXI ICCC*, Toulouse, 7–11th July, 1980. Proceedings 217.
19. Christensson, F. and Springborg, J. *Acta Chem. Scand. A 36* (1982) 21.
20. Kaas, K. *Acta Crystallogr. B 35* (1979) 1603.
21. Wieghardt, K., Schmidt, W., Eldik, R., Nuber, B. and Weiss, J. *Inorg. Chem. 19* (1980) 2922.
22. Hancock, M. P. *Acta Chem. Scand. A 33* (1979) 499.
23. Springborg, J. and Schäffer, C. E. *Inorg. Synth. 18* (1978) 75.
24. Hancock, M. P. *Acta Chem. Scand. A 33* (1979) 15.
25. Palmer, D. A., Eldik, R., Kelm, H. and Harris, G. M. *Inorg. Chem. 19* (1980) 1009.
26. Bell, P. P. *The Proton in Chemistry*, Chapman and Hall, London 1973, 2nd Ed.
27. Monacelli, F. and Viel, E. *Inorg. Chim. Acta 1* (1967) 467.
28. Bott, H. L., Poë, A. J. and Shaw, K. *J. Chem. Soc. A* (1970) 1745.
29. Swaddle, T. W. and Stranks, D. R. *J. Am. Chem. Soc. 94* (1972) 8357.
30. Gattegno, D. and Monacelli, F. *Inorg. Chim. Acta 7* (1973) 370.
31. Tong, S. B. and Swaddle, T. W. *Inorg. Chem. 13* (1974) 1538.
32. Mønsted, L. *Acta Chem. Scand. A 32* (1978) 377.
33. Frost, A. A. and Pearson, R. G. *Kinetics and Mechanism*, Wiley, New York 1961, 2nd Ed.
34. Mønsted, L. and Mønsted, O. *Acta Chem. Scand. A 30* (1976) 202.
35. Bjerrum, J., Schwarzenbach, G. and Sillén, L. G. *Stability Constants of Metal-Ion Complexes.* The Chemical Society, 2nd Ed., London 1964, 3rd. Ed., London 1971.

Received July 23, 1981.

Acta Chemica Scandinavica A 36 (1982) 323–327

Conformation and Anomer Ratio of D-Glucopyranose in Different Potential Energy Functions

KJELD RASMUSSEN

Chemistry Department A, The Technical University of Denmark, Building 207, DK-2800 Lyngby

For low-energy conformers of α- and β-D-glucopyranose, a two-parameter Lennard-Jones function is just as adequate as a three-parameter Buckingham exp-6 function in representing the non-bonded interactions.

When Coulomb interactions based on the monopole approximation are included, it makes essentially no difference whether the anomeric carbon atom is given its proper charge or is treated as any other carbon atom.

These results imply that it is sensible to employ much fewer parameters in consistent potential energy functions than indicated by theoretical considerations.

In the course of the development of a new potential energy function (PEF) to postdict and predict structures, vibrational spectra, dipole moments and thermodynamic properties of several classes of molecules it is of paramount interest to keep down the number of parameters in the PEF.

The present investigation was initiated to answer two questions. (1) In some applications, Coulomb interactions are not necessary. Then non-bonded interactions are usually represented by Buckingham 6-exp functions. Will Lennard-Jones functions, with two rather than three parameters per interaction, give comparable results? (2) When Coulomb terms are necessary, the most sensible approach to initial choice of parameters is to reproduce charges calculated by Mulliken population analysis of *ab initio* results found with reasonably large basis sets. If more than one type of the same atom, say carbon, are present, what are the consequences of neglecting this distinction?

For a test case, D-glucopyranose (Glc) was selected, as rather elaborate calculations on this compound are already available.

The structures of α and β anomers of Glc have been calculated by energy minimisation with full relaxation of all coordinates, using three different PEF's, PEF3,[1] PEF300[2] and PEF400.[3] From calculated free enthalpy differences, equilibrium ratios were calculated. All calculated data fitted well to experimentally observed values, with the single exception of the short anomeric C1–O1 bond.

PEF300 is just a slight correction to PEF3, as the torsional (Pitzer) terms were removed, but PEF400 is a completely different set of functions, incorporating Coulomb interactions into the non-bonding part, and with different sets of bond and angle deformation parameters.

In the present work more conformers are studied than in the earlier papers. They all have the same ring conformation, 4C1, but differ in exocyclic torsions. Altogether six conformers are now minimised in PEF300 and PEF400 and in two variants of these, PEF301 and PEF422.

In PEF301, the Buckingham 6-exp functions for non-bonded interactions of PEF300 are substituted by Lennard-Jones 12-6 functions, with ε and r* fitted to reproduce the minima of the original functions. This is done in order to see whether these two-parameter functions give as good a representation as the three-parameter functions.

In PEF422, the anomeric carbon atom C1 is given a charge parameter different from the other carbon atoms. The change has implications for all atomic charges; but all other parameters are left unchanged. This is done in order to see whether a better fit to results of Mulliken population analysis of *ab initio* calculations[4] with IBMOL-6 would cause significant changes.

0302-4377/82/040323-05$02.50

Table 1. Non-bonded functions of PEF301. $E_{n-b} = \varepsilon(r/r^*)^{12} - 2\varepsilon(r/r^*)^6$

	ε/kJ mol^{-1}	r^*/Å
O---O	0.4152	3.260
O---C	0.4153	3.373
O---H	0.2943	3.023
C---C	0.4101	3.498
C---H	0.2817	3.152
H---H	0.1486	2.979

Table 2. Atomic charges.

Parameters	PEF400	PEF422	
O.	−0.400	−0.400	
K.	−0.050	+0.300	
C.	−0.050	+0.050	
H.	+0.125	+0.200	
Assignments	PEF400	PEF422	ab initio[4]
O(KOC)	−0.407	−0.465	−0.422
O(OH)	−0.407	−0.465	−0.531
K[a]	−0.057	+0.235	+0.203
C(CHOH)	−0.057	−0.015	−0.007
C(CH2)	−0.057	−0.015	−0.180
H(O)	+0.393	+0.335	+0.360
H(C)	+0.118	+0.135	+0.185
Dipole moment α	2.24	1.62	2.74
β	3.27	2.41	4.64

[a] K is the anomeric carbon atom C1.

CALCULATIONS

The program. The Consistent Force Field system[5] was used, with later additions for thermodynamics[6] and changes for charge handling.[7]

Potential energy functions. PEF300 is described[2] as a modification to PEF3;[1] it is also listed separately.[8] PEF400 is also available in the literature.[3,7,9] The non-bonded functions of PEF301 are presented in Table 1, and the charge parameters of PEF400 and PEF422 in Table 2, together with atomic charges assigned by the program for PEF400 and PEF422, and calculated by Mulliken population analysis of results from IBMOL-6.[4]

Initial conformations. Two conformers of the α and two of the β anomers as found with PEF400[9,10] were used, the global minima having O6 *gauche* to O5 and *anti* to C4, two others, with O6 *minus-gauche* to O5 and *gauche* to C4. In addition, the global minima of α and β in PEF300[2] were used; they have O6 *gauche* to O5 and *anti* to C4 and differ from the former in the exocyclic torsions around C2−O2, C3−O3 and C4−O4.

Minimisation. 20 steepest-descent plus 10−15 modified Newton iterations sufficed to minimise all conformations which were not already in minimum (2 in PEF300[2] and 4 in PEF400[9,10]).

Thermodynamics. The free enthalpy was calculated at 298K. Statistical summation over translations and rotations was left out, as the calculated equilibrium ratios are compared with values measured in aqueous solution.

Table 3. Conformational details for D-glucopyranose. Angles in degrees, energy terms in kJ mol^{-1}.

	α-Anomer			β-Anomer		
PEF300						
O5−C1−O1	110.7	110.6	110.8	109.1	109.1	108.9
C5−O5−C1	113.4	113.4	113.4	112.5	112.5	112.5
O5−C1−O1−H	60.7	61.0	60.1	52.0	52.0	−64.4
C1−C2−O2−H	−67.8	−67.9	72.9	81.8	81.8	160.6
C2−C3−O3−H	−81.0	−81.1	−159.4	−79.5	−80.0	−159.1
C3−C4−O4−H	81.4	81.8	−62.0	81.2	81.6	−62.4
C4−C5−C6−O6	−173.5	59.4	−179.6	−174.2	59.1	−179.8
O5−C5−C6−O6	65.4	−62.5	59.6	65.1	−62.3	59.7
C5−C6−O6−H	−77.3	75.2	72.6	−77.6	75.0	73.0
E	5.602	6.016	5.410	3.783	4.115	4.127
G	477.021	478.030	476.829	473.995	474.925	474.830
ΔE	1.819	2.233	1.627	0.000	0.332	0.344
ΔG	3.026	4.035	2.834	0.000	0.930	0.835
n_i	0.092	0.061	0.099	0.311	0.214	0.222

Table 3. Continued.

	α-Anomer			β-Anomer		
PEF301						
O5–C1–O1	110.8	110.8	111.0	109.1	109.1	108.9
C5–O5–C1	113.8	113.8	113.8	113.8	113.3	113.2
O5–C1–O1–H	55.3	55.3	54.6	52.6	52.6	−57.4
C1–C2–O2–H	−66.3	−66.6	64.7	70.8	70.7	170.3
C2–C3–O3–H	−70.2	−70.3	−169.9	−69.4	−69.5	−169.6
C3–C4–O4–H	70.5	70.3	−61.9	70.7	70.5	−62.3
C4–C5–C6–O6	−172.2	58.7	178.8	−172.9	58.3	178.6
O5–C5–C6–O6	66.6	−63.3	58.0	66.3	−63.2	58.1
C5–C6–O6–H	−68.3	67.2	66.3	−68.6	67.1	66.5
E	13.006	13.512	12.595	11.769	12.160	11.818
G	495.338	496.612	494.945	493.233	494.378	493.628
ΔE	1.237	1.743	0.826	0.000	0.391	0.049
ΔG	2.105	3.379	1.712	0.000	1.145	0.395
n_i	0.117	0.070	0.137	0.273	0.172	0.233
PEF400						
O5–C1–O1	111.6	111.5	112.0	109.0	109.0	109.4
C5–O5–C1	113.5	113.6	113.6	113.7	113.8	113.7
O5–C1–O1–H	45.2	45.1	43.9	38.3	37.8	−33.0
C1–C2–O2–H	−54.1	−54.2	46.9	47.6	47.6	−178.9
C2–C3–O3–H	−48.6	−48.5	172.4	−52.4	−52.4	168.8
C3–C4–O4–H	52.9	53.9	−64.0	52.7	53.9	−66.3
C4–C5–C6–O6	−168.2	59.4	−169.7	168.7	58.6	−169.4
O5–C5–C6–O6	69.7	−63.2	69.9	70.2	−63.0	70.6
C5–C6–O6–H	−51.0	49.7	−52.1	−48.7	51.0	−51.1
E	−49.017	−48.686	−40.202	−48.479	−47.427	−41.273
G	438.122	440.069	445.755	436.489	439.038	442.740
ΔE	0.000	0.331	8.815	0.538	1.590	7.744
ΔG	1.633	3.580	9.266	0.000	2.549	6.251
n_i	0.234	0.107	0.011	0.451	0.161	0.035
PEF422						
O5–C1–O1	111.5	111.4	111.5	109.0	108.9	108.8
C5–O5–C1	113.4	113.6	113.5	113.7	113.9	113.9
O5–C1–O1–H	46.6	46.8	45.8	39.2	39.8	−35.9
C1–C2–O2–H	−58.5	−58.7	53.5	53.1	53.5	−179.5
C2–C3–O3–H	−52.4	−51.9	174.9	−54.4	−54.1	171.8
C3–C4–O4–H	52.7	54.4	−61.5	53.1	55.0	−63.7
C4–C5–C6–O6	−166.4	59.3	−167.5	−167.3	58.5	−167.9
O5–C5–C6–O6	71.3	−63.6	71.9	71.5	−63.2	72.1
C5–C6–O6–H	−51.9	51.6	−52.8	−51.4	52.7	−53.4
E	3.891	5.319	14.190	5.945	7.245	10.648
G	490.712	493.669	500.077	490.398	493.281	494.588
ΔE	0.000	1.428	10.299	2.054	3.354	6.757
ΔG	0.314	3.271	9.679	0.000	2.883	4.190
n_i	0.331	0.100	0.008	0.375	0.117	0.069

RESULTS

Table 3 shows conformational and thermodynamic details of the six conformers in all four potential energy functions.

The overall anomer ratios are, for PEF300, PEF301, PEF400 and PEF422: $\alpha:\beta = 0.25:0.75$, 0.32:0.68, 0.35:0.65 and 0.44:0.56. The experimental value, measured by different techniques,[11-15] is 0.36:0.64.

The rotamer ratios for the hydroxymethyl group, ga:g'g, counting both anomers, are for PEF300, PEF301, PEF400 and PEF422: 0.72:0.28, 0.76:0.24, 0.73:0.27 and 0.78:0.22. A compilation[16] for the glucose moiety for about 60 crystal structures gave ga:g'g = 0.40:0.60.

DISCUSSION

Geometric details. Bond lengths, valence angles, endocyclic and hybrid torsional angles show the same deviations from experimental values as in the previous work.[1,2,9]

Two particular angles involving the anomeric carbon atom C1 may be of interest as indicatrices: C5–O5–C1, which is 113.8° in the α[17] and 112.7° in the β[18] anomer, and O5–C1–O1, which is 111.6° in α[17] and 107.0° in β.[18] All four PEF's give a good reproduction of C5–O5–C1 for α, but for β, PEF300 is obviously best, followed by PEF301. For O5–C1–O1, all PEF's give the right trend, but PEF400 and PEF422 the better fit.

As to the exocyclic torsions, at O1, O2, O3 and O4, none changes character (*g*, *g'*, *a*) from one PEF to another. At O6, the simulated hydrogen bond to O5 in PEF400 and PEF422 induces a change from PEF300 and PEF301 in one α and one β conformer.

Thermodynamics. As pointed out before,[3,8,9] it is imperative to sum over internal degrees of freedom when energy differences are as small as here. This point is well illustrated by the ΔE and ΔG data in Table 3.

It may be noted that both α and β are much more homoconformational in the two PEF's with Coulomb terms than in the two without.

The anomeric ratio. The values presented in the previous section were calculated by summation over all six conformers. Therefore they differ, for PEF300 and PEF400, from what was published before,[1-3,9] when only two conformers were considered for PEF300 and four for PEF400. In this respect, now PEF301 gives a significantly better result than PEF300, PEF400 gives still the correct value, and PEF422 overestimates the α anomer to the same extent as PEF300 underestimates it.

Vibrational spectra. Although the results are not shown here, it may be mentioned that the calculated normal modes are very similar in PEF400 and PEF422. The similarity includes even the infrared intensities in the C–H stretching region, in spite of the different charges on C1. This reflects, of course, that no normal coordinate is exclusively localised to any one particular C–H bond.

CONCLUSIONS

The questions asked in the first section can now be answered: (1) The two-parameter Lennard-Jones functions for non-bonded interactions give just as good results as the (theoretically more justified) three-parameter Buckingham exp-6 functions. In the present case, PEF301 with L-J even gives better results in thermodynamic calculations than PEF300 with exp-6.

It is perhaps more surprising that the different charge characteristics of C1 in PEF400 and PEF422 are not reflected in the conformational changes to any significant extent. This result is particularly welcome in the development of PEF's including more types of atoms than those treated here, as one might hope to obtain a reasonably good consistent parameter set with a smaller number of parameters than what would be expected from a theoretical point of view.

Acknowledgements. The work was begun when the author was a guest at Chemical Physics Department, The Weizmann Institute of Science, Israel, supported by an *EMBO* grant. Most of the computations were paid through a grant from the Danish Natural Science Research Council.

REFERENCES

1. Kildeby, K., Melberg, S. and Rasmussen, K. *Acta Chem. Scand. A 31* (1977) 1.
2. Melberg, S. and Rasmussen, K. *Acta Chem. Scand. A 32* (1978) 187.
3. Melberg, S. and Rasmussen, K. *Carbohydr. Res. 78* (1980) 215.
4. Melberg, S., Rasmussen, K., Scordamaglia, R. and Tosi, C. *Carbohydr. Res. 76* (1979) 23.

5. Niketić, S. R. and Rasmussen, K. *The Consistent Force Field: A Documentation, Lecture Notes in Chemistry*, Springer, Heidelberg 1977, Vol. 3.
6. Rasmussen, K. and Woldbye, F. In Banerjea, D., Ed., *Coordination Chemistry 20*, Pergamon, Oxford 1980, p. 219.
7. Melberg, S. and Rasmussen, K. *J. Mol. Struct. 57* (1980) 215.
8. Melberg, S. and Rasmussen, K. *Carbohydr. Res. 69* (1979) 27.
9. Rasmussen, K. In Balaban, M., Ed., *Molecular Structure and Dynamics*, Balaban, Jerusalem 1980, p. 171.
10. Melberg, S. *Thesis*, The Technical University of Denmark, Lyngby 1979.
11. Isbell, H. S. and Pigman, W. W. *J. Res. Natl. Bur. Stand. 18* (1937) 141.
12. Rudrum, M. and Shaw, D. F. *J. Chem. Soc.* (1965) 52.
13. Lemieux, R. U. and Stevens, J. D. *Can, J. Chem. 44* (1966) 249.
14. Williams, C. and Allerhand, A. *Carbohydr. Res. 56* (1977) 173.
15. Kjær, A. M., Sørensen, P. E. and Ulstrup, J. *J. Chem. Soc. Perkin Trans. 2* (1978) 51.
16. Lemieux, R. U. and Brewer, J. T. *Adv. Chem. Ser. 117* (1973) 121.
17. Brown, G. M. and Levy, H. A. *Science 147* (1965) 1038.
18. Chu, S. S. C. and Jeffrey, G. A. *Acta Crystallogr. B 24* (1968) 830.

Received June 30, 1981.

Acta Chemica Scandinavica A 36 (1982) 329 – 344

Activities and Phase Diagram Data of $NaF - AlF_3 - Al_2O_3$ Mixtures Derived from Electromotive Force and Cryoscopic Measurements. Standard Thermodynamic Data of β-Al_2O_3(s), Na_3AlF_6(s), $Na_5Al_3F_{14}$(s) and $NaAlF_4$(l)

ÅSMUND STERTEN, KJELL HAMBERG and INGE MÆLAND

Institutt for teknisk elektrokjemi, NTH, Univ. i Trondheim, N-7034 Trondheim-NTH, Norway

Activity data of NaF and AlF_3 were derived from electromotive force (emf) measurements of various types of galvanic cells containing $NaF - AlF_3$ melts saturated with alumina. The transport number of Na^+ increases with increasing content of AlF_3 and approaches unity for melts more acidic than the cryolite $3NaF \cdot AlF_3$ composition. Phase diagram data obtained in conjunction with the emf measurements were in excellent agreement with corresponding cryoscopic data. The standard Gibbs energy change associated with the reaction

$$3NaF(l) + AlF_3(s) = Na_3AlF_6(s)$$

was derived as $\Delta G^\circ = -151.745(\pm 0.550) + 0.0290\ (\pm 0.0005)T$ kJ (998 K $< T <$ 1237 K) with a standard deviation of ± 0.250 kJ. Corresponding data for the formation of chiolite ($Na_5Al_3F_{14}$) according to

$$5NaF(l) + 3AlF_3(s) = Na_5Al_3F_{14}(s)$$

was found to be $\Delta G^\circ = -229.890(\pm 1.290) + 0.00647\ (\pm 0.00013)T$ kJ (956 K $< T <$ 998 K) with a standard deviation of ± 0.043 kJ. For the reaction

$$NaF(l) + AlF_3(s) = NaAlF_4(l)$$

the following expression was obtained, $\Delta G^\circ = 27.167 - 0.07283T$ kJ (956 K $< T <$ 1300 K) with an estimated uncertainty of ± 4 kJ. The equilibrium between α-Al_2O_3 and β-Al_2O_3 ($Na_2O \cdot xAl_2O_3$) can be expressed by

$$2NaF(l) + \frac{3x+1}{3}\,\alpha\text{-}Al_2O_3(s) = Na_2O \cdot xAl_2O_3(s)$$

for which the standard Gibbs energy, enthalpy and entropy changes at 1300 K were determined as $\Delta G^\circ = 47.250$ kJ, $\Delta H^\circ = -11.460$ kJ and $\Delta S^\circ = -45.162$ J/degree. The enthalpy and entropy changes of this reaction decrease with decreasing temperature. A discussion of the interaction between aluminium and the melt is also given.

$$6NaF + Al_2O_3 = 2AlF_3 + 3Na_2O \qquad (1)$$

The ternary reciprocal system, eqn. (1), is important from a technical point of view since it constitutes the basic electrolyte in the Hall-Heroult process for the electrolytic production of aluminium. Thermodynamic data for the greater part of the system have not yet been established.[1] The present work was undertaken in order to determine activity data for $NaF - AlF_3$ melts saturated with alumina. Such data are most conveniently derived from emf measurements. In a previous study[2] it was demonstrated that the Pt/O_2 electrode behaves reversibly in such melts.

The three cells given in Scheme 1 were applied in the present study. The melt compositions were varied in the right hand side compartments of the concentration cells [I] and [II]. The melts in these cells were always saturated with α-Al_2O_3, while the $NaF - AlF_3$ melts in cell [III] were saturated with β-Al_2O_3. The lines separating the stability ranges of α-Al_2O_3 and β-Al_2O_3 are illustrated in Fig. 1. Yoshida and Dewing[3] and Thonstad and Rolseth[4] obtained emf data by replacing the oxygen electrodes in cell [II] with aluminium electrodes. This cell was also

0302-4377/82/040329-16$02.50

$(Pt)O_2$ (1 atm)	Na_3AlF_6(l) α-Al_2O_3(s)	α-Al_2O_3 diaphragm	NaF(l) AlF_3(diss) α-Al_2O_3(s)	$(Pt)O_2$ (1 atm)	[I]
Pb – Na	Na_3AlF_6(l) α-Al_2O_3(s)	α-Al_2O_3 diaphragm	NaF(l) AlF_3(diss) α-Al_2O_3(s)	Pb – Na	[II]
Pb – Na	NaF(l), AlF_3(diss), β-Al_2O_3(s)			$(Pt)O_2$ (1 atm)	[III]

Scheme 1.

used in a single run of the present study. The results of these authors[3,4] are discussed in terms of corresponding data from the present work. Some phase diagram data for the ternary reciprocal system (1) are reported and compared with data from the literature. Standard Gibbs energy of formation of β-Al_2O_3(s), Na_3AlF_6(s), $Na_5Al_3F_{14}$(s) and $NaAlF_4$(l) together with enthalpy and entropy values are also derived. Finally, vapour pressures of Na(g) and AlF(g) are calculated as a function of composition for melts in equilibrium with aluminium metal.

The conditions required for the existence of concentration gradients in the diffusion layer on the electrolytic side of the metal – melt interface are discussed.

THEORY

Unless specified otherwise, the ternary reciprocal system (1) is taken to be constituted of the components NaF, AlF_3 and Al_2O_3.

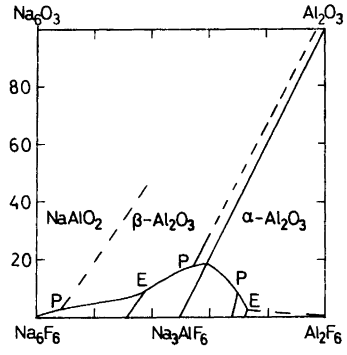

Fig. 1. Schematic diagram of the ternary reciprocal system $Na_6F_6 - Al_2F_6 - Al_2O_3 - Na_6O_3$. Some eutectic (E) and peritectic (P) points are indicated together with the corresponding crystallization fields. The diagram is based on data from Foster,[17,18] Holm[19] and the present work.

The α-Al_2O_3 diaphragm in cells [I] and [II] acts as a semipermeable membrane in cryolite melts saturated with alumina.[2,3] The emf of cell [I] generated between two identical oxygen electrodes is denoted E_1 while the emf of cell [II] with corresponding melt composition is denoted E_2. The corresponding cell reactions contain transport numbers which need not be known in the present case. Subtracting cell reaction [II] from cell reaction [I] cancels these transport numbers. The resulting reaction is given in eqn. (2). The components in the

$$6NaF(1) + 2\,AlF_3 + Al_2O_3(1) = 6\,NaF + 2\,AlF(1) + Al_2O_3 \quad (2)$$

reference compartments on the left hand side of the cells [I] and [II] are denoted (1). The emf corresponding to reaction (2), is as given in eqn. (3),

$$E = E_1 - E_2 = \frac{RT}{F}\ln\left[\frac{a_{NaF(1)}}{a_{NaF}}\right] + \frac{RT}{3F}\ln\left[\frac{a_{AlF_3}}{a_{AlF_3(1)}}\right] \quad (3)$$

keeping in mind that the melts in both cells are saturated with α-Al_2O_3, the standard state of the activity. This means also that the Gibbs-Duhem equation can be written as eqn. (4), where r is the mol

$$d\ln a_{AlF_3} = -r\,d\ln a_{NaF} \quad (4)$$

ratio $n_{NaF} - n_{AlF_3}$. Derivation of eqn. (3) and combining with eqn. (4) yields eqn. (5) or alternatively eqn. (6).

$$d\ln a_{AlF_3} = \frac{3Fr\,dE}{RT(r+3)} \quad (5)$$

$$d \ln a_{NaF} = -\frac{3F\,dE}{RT(r+3)} \quad (6)$$

Graphical integration of eqn. (5) is straightforward since emf measurements are available for melts saturated with AlF_3, the standard state of the activity. For the melt compositions applied we do not have an absolute value for the activity of NaF. The only ions of importance in the basic part of the pure NaF – Na_3AlF_6 melts are F^- and AlF_6^{3-} with the common cation Na^+. It has been shown [5] that the Temkin model [6] is roughly valid in such melts. Thus, the activity of NaF is readily calculated as 0.92 for $r = 15$ ($x_{AlF_3} = 0.0625$). Adding alumina to this melt the temperature of first crystallization decreases slightly,[5] which also means a minor decrease of the activity of NaF. The numerical value of the activity is taken to be 0.90 when the melt becomes saturated with alumina. The error involved in applying this activity value of liquid NaF should be quite small.

The α-Al_2O_3 diaphragm breaks down rapidly if it is used in basic melts where β-Al_2O_3 is the stable solid compound. Therefore, cell [III] was applied for melt compositions in the stability range of β-Al_2O_3. The cell reaction is given in eqn. (7), with the

$$2Na_{(in\ Pb)} + \tfrac{1}{2}O_2(g, 1\ atm) = Na_2O(l) \quad (7)$$

$$E_3 = E_3^\circ - \frac{RT}{2F} \ln \left[a_{Na_2O} / a_{Na}^2 \right] \quad (8)$$

$$E_3 = E' - \frac{RT}{3F} \ln \left[a_{NaF}^3 / a_{AlF_3} \right] \quad (9)$$

corresponding emf E_3, eqn. (8). Oxygen at 1 atm. pressure was chosen as the standard state. Eqn. (8) is combined with the equation for the equilibrium constant for reaction (1) which gives eqn. (9), where E' is assumed to be a constant for a given temperature and a fixed activity of sodium. This is not strictly correct, since the activity of Al_2O_3 decreases slightly with increasing basicity in the stability range of β-Al_2O_3. However, the error in the final activity data caused by this simplified treatment is believed to be negligible.

Derivation of eqn. (9) and combining with eqn. (4) give equations identical with those derived for the cells [I] and [II]. Eqns. (5) and (6) combined with emf data from cell [III] are then used to derive activities in the stability field of β-Al_2O_3.

EXPERIMENTAL

The melts in the compartments on the right-hand side of cells [I] and [II] were contained in alumina tubes serving as diaphragms between the electrode compartments. The main cell crusible was also made of α-Al_2O_3.

The oxygen electrode in cell [III] was located inside an open ended α-Al_2O_3 tube. The electrode and the tube were lowered into the melt only during the emf measurements. The time of immersion was made as short as possible in order to minimize the transformation reaction of α-Al_2O_3 to β-Al_2O_3 and to protect the oxygen electrode against possible attack by dissolved metal.[2]

The weighing and the preparation of sodium electrodes were carried out in a dry box. A freshly prepared piece of sodium metal was wrapped in lead foil and placed in a small alumina container. This container was then transferred to the main cell which was a graphite crucible. Electrical contact to the electrode was established by means of a tantalum wire of 1 mm diameter shielded by an alumina tube.

The cryoscopic measurements were carried out by using a mechanical stirrer in a graphite crucible. The Pt – Pt 10Rh thermocouple applied was calibrated several times against the melting point of silver, 1235.1 K. Other details of the cells with accessories are described elsewhere.[2]

The chemicals used were sublimed AlF_3, handpicked Greenland cryolite, and reagent grade NaF supplied by Merck.

RESULTS AND DISCUSSION

Emf data. Fig. 2 shows that the emf of cell [II] as a function of r can be fitted to a linear relationship within the limits of experimental uncertainty. It was not possible to obtain reliable emf readings for $r < 2$,

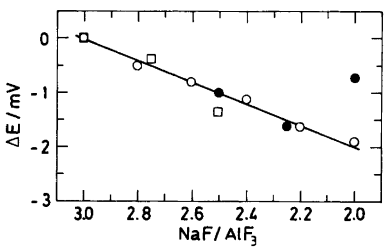

Fig. 2. The variation of the emf of cell [II] with the mol ratio NaF – AlF_3 in melts saturated with α-Al_2O_3 at 1278 K. One symbol for each series of experiments.

probably because a separate aluminium phase was formed according to the reaction (10).

$$3Na_{(in\ Pb)} + AlF_3(diss) = 3NaF(l) + Al(l) \qquad (10)$$

The sodium content of the Na – Pb alloy electrode was in the range 0.5 to 1.0 weight %. As long as the reaction is displaced to the left ($r < 2$) the alloy electrode will contain only minor amounts of aluminium.[8-11]

The variation of only 2 mV in the emf over the compositional range shown in Fig. 2 means that the transport number of Na^+ is close to unity as discussed below. This means also that the Na – Pb alloy acts as a reliable sodium electrode. The variation of the emf with time was usually within ±0.1 mV/h but occasionally it increased to ±0.5 mV/h.

Fig. 3 shows emf data of cell [I] as a function of temperature and composition. Within the experimental uncertainties the emf does not change with the temperature in the range of composition shown in the figure. All the points given represent average values from several runs carried out under identical conditions. A reference melt with $r = 1.15$ was also used in several runs in order to establish emf data along the boundary lines shown in the figure. The data plotted along these univariant curves are based on the assumption of a temperature independent emf for $r = 1.15$ as shown by the solid line in Fig. 3. Accurate and reproducible emf data were obtained with this reference melt when the other cell compartment contained melts in equilibrium with solid AlF_3 and solid α-Al_2O_3. The cooling rate of the cell was never allowed to exceed 1 degree/min during these measurements. However, the temperature of the cell had to be stabilized applying the same reference melt ($r = 1.15$) and melt compositions in the other compartment corresponding to the $Na_3AlF_6(s)$, $Al_2O_3(s)/Al_2O_3(s)$ univariant line, shown in Fig. 3. Phase diagram data to be discussed below show that the emf is independent of temperature for all acidic melt compositions studied in the present work. The single point in Fig. 3, obtained with cell [I] using two aluminium electrodes, is in general agreement with the other data given in the figure. This point is discussed below.

Fig. 4 shows emf data of cell [III] as a function of r at 1278 K. The emf of the reference melt, cryolite saturated with alumina, is taken to be zero. For melt compositions corresponding to $r > 17$ it was not possible to obtain reliable readings since the emf was unstable. Actually, the emf of cell [III] was less

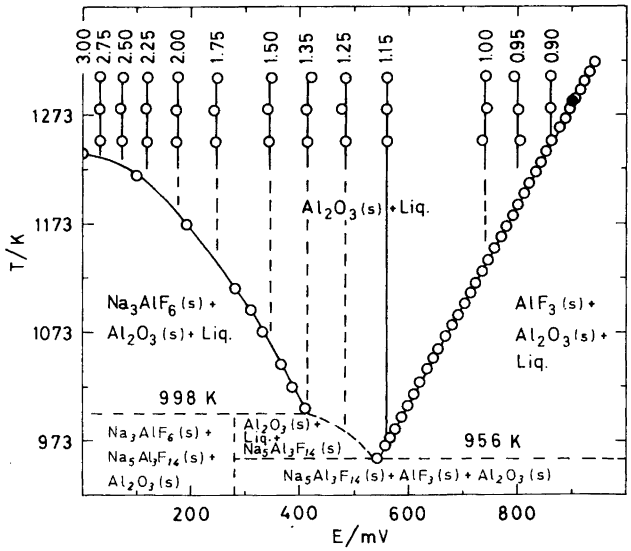

Fig. 3. The relationship between temperature and emf of cell [I] for various $NaF - AlF_3$ mol ratios as indicated on the top of each vertical line. Corresponding primary crystallization fields and univariant curves in the acidic part of the $NaF - AlF_3$ system saturated with alumina are given. ●, Emf of cell [I] obtained by using two aluminium electrodes.

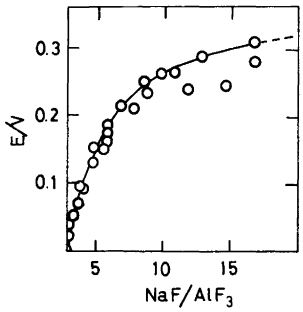

Fig. 4. The emf of cell [III] as a function of the mol ratio $NaF-AlF_3$ at 1278 K. The reference melt is Na_3AlF_6 saturated with alumina for which the emf is set equal to zero.

stable than the emf of the cells [I] and [II]. The cell voltage also decreased slightly with time. Such a drift in the cell voltage can be explained by the fact that the α-Al_2O_3 tube containing the oxygen electrode reacted gradually to β-Al_2O_3 ($Na_2O{\cdot}xAl_2O_3$) according to the reaction scheme, eqn. (11).

$$2NaF(l)+\frac{(3x+1)}{3}\alpha\text{-}Al_2O_3(s) = Na_2O{\cdot}xAl_2O_3(s)+\tfrac{2}{3}AlF_3(diss) \qquad (11)$$

The numerical value of x is discussed below. This reaction reduced gradually the r-value of the melt and a drift in the emf must occur. Therefore, it seems reasonable to draw the curve in Fig. 4 in such a way that it fits the highest emf values obtained. Since it was difficult to obtain accurate emf data, no attempt was made to establish the relationship between cell voltage and temperature in basic melts.

Activity data. The emf of cell [I] can be expressed by the empirical eqns. (12) and (13).

$r<1.24$

$$E_1(V)=3.63\ln\left(\frac{0.3}{r}+0.9\right)-0.3r+0.372 \qquad (12)$$

$3>r>1.24$

$$E_1(V)=3.63\ln\left(\frac{0.3}{r}+0.9\right) \qquad (13)$$

The standard deviation is ± 11.2 mV taking into account all experimental emf values. Using the average emf data shown in Fig. 3 the standard deviations is ± 4.3 mV. An error of this magnitude corresponds to a very small compositional uncertainty as can be deduced from Fig. 3. When deriving the activity data, the emf of cell [II] shown in Fig. 2 was neglected since the values involved are low and less than the standard deviation of E_1.

It turns out that the emf of cell [III] can be described by an expression identical to eqn. (13), *i.e.* eqn. (14).

$r>3$

$$E_3(V)=3.63\ln\left(\frac{0.3}{r}+0.9\right) \qquad (14)$$

The curve in Fig. 4 is in fact drawn in agreement with eqn. (14). Since E_1 does not change with temperature it is in a first approximation assumed that E_3 also is independent of the temperature. This point is further discussed below.

Derivation of eqns. (12), (13) and (14) and combination with eqns. (5) and (6) followed by integration give empirical eqns. (15)–(18) for the natural logarithm of the activities, where r^* is the NaF/AlF_3 mol ratio of a melt saturated with both AlF_3 and Al_2O_3. The relationship between r^* and temperature is derived in eqn. (20). The last term in eqn. (16) is the natural logarithm of the activity at $r=1.24$ to be computed from eqn. (15) for the temperature in question.

$r^*<r<1.24$

$$\ln a_{AlF_3}=\frac{F}{RT}\left[1.361\ln\frac{(3+r)(0.3+0.9r^*)}{(3+r^*)(0.3+0.9r)}+0.9r^*-0.9r+2.7\ln\frac{(3+r)}{(3+r^*)}\right] \qquad (15)$$

$1.24<r<15$

$$\ln a_{AlF_3}=\frac{F}{RT}\left[1.361\ln\frac{(3+r)}{(0.3+0.9r)}-1.493\right]+\ln a_{AlF_3}\quad (r=1.24) \qquad (16)$$

$15>r>1.24$

$$\ln a_{NaF}=\frac{F}{RT}\left[3.63\ln r+0.454\ln(3+r)-4.084\ln(0.3+0.9r)-0.423\right]-0.106 \quad (17)$$

$1.24>r>r^*$

$$\ln a_{NaF}=\frac{F}{RT}\left[3.63\ln r+1.354\ln(3+r)-4.084\ln(0.3+0.9r)-1.724\right]-0.106 \quad (18)$$

These equations are valuable in conjunction with computer calculations and have been applied in connection with the development of an ionic structure model for cryolitic melts containing alumina.[12]

The temperature dependence of the emf of cell [I] corresponding to melts saturated with both AlF_3 and Al_2O_3 shown in Fig. 3 is well described by the empirical eqn. (19). The standard deviation is ± 4 mV. Combining eqns. (12) and (19) gives eqn. (20), which represents the relationship between temperature and composition of melts in equilibrium with solid AlF_3 and solid Al_2O_3. The numerical value of r^* for a given temperature can be estimated from Fig. 3 and determined more accurately from eqn. (20) by trial and error.

$$E_1(\mathrm{V})=1.106\times10^{-3}T-0.514 \quad (19)$$

$$T(\mathrm{K})=3282\ln\left[\frac{0.3}{r^*}+0.9\right]-271.2r^*+801 \quad (20)$$

Activity data for NaF have also been fitted to equations of the type (21). Table 1 shows the results.

Table 1. Calculated values for A in the equation, $\ln a_{NaF}=(A/T)-0.106$, where $\ln a_{NaF}$ is the natural logarithm of the activity of NaF in $NaF-AlF_3$ melts saturated with alumina at $T<1300$ K. The standard state is liquid NaF, while the composition given by the mol ratio $NaF-AlF_3$ is denoted r.

r	A	r	A	r	A
0.90	−8000	2.20	−2080	3.70	−880
1.00	−6860	2.40	−1810	4.9	−770
1.20	−5040	2.60	−1600	5.0	−500
1.40	−4010	2.80	−1410	6.0	−350
1.60	−3330	3.00	−1260	8.0	−180
1.80	−2810	3.20	−1130	10	− 90
2.00	−2400	3.40	−1020	15	0

$$\ln a_{NaF}=A/T+B \quad (21)$$

The temperature dependence of the activity of AlF_3 cannot be described by such a simple equation as eqn. (21). Therefore, some activity data for AlF_3 at two different temperatures are shown in Table 2.

A comparison of activity data from various sources is made in Table 3. Yoshida and Dewing[3] derived activity data from the emf of cell [I] with two aluminium electrodes and from the sodium content of aluminium assumed to be in equilibrium with the melt. Kvande[13] estimated the activity data shown in

Table 2. The natural logarithm of the activity of AlF_3 in $NaF-AlF_3$ melts saturated with alumina ($-\ln a$). The $NaF-AlF_3$ mol ratio is denoted r. The standard state is solid AlF_3.

r	1237 K	1300 K	r	1237 K	1300 K
0.90	0.000	0.367	2.80	7.532	7.591
1.00	0.816	1.200	3.00	7.890	7.931
1.20	2.430	2.736	3.20	8.215	8.240
1.40	3.500	3.753	3.70	8.915	8.906
1.60	4.326	4.540	4.0	9.272	9.246
1.80	5.040	5.219	5.0	10.218	10.146
2.00	5.663	5.812	6.0	10.909	10.803
2.20	6.212	6.335	8.0	11.851	11.699
2.40	6.701	6.800	10.0	12.465	12.283
2.60	7.138	7.216	15.0	13.346	13.127

Table 3. Activity data of NaF and AlF_3 in Na_3AlF_6 melts saturated with α-Al_2O_3. The standard states are liquid NaF and solid AlF_3.

Authors	T/K	a_{NaF}	a_{AlF_3}
Yoshida and Dewing[3]	1273	0.31	5.8×10^{-4}
Kvande[13]	1300	0.30	5×10^{-4}
This work	1273	0.334	3.64×10^{-4}
This work	1300	0.341	3.60×10^{-4}

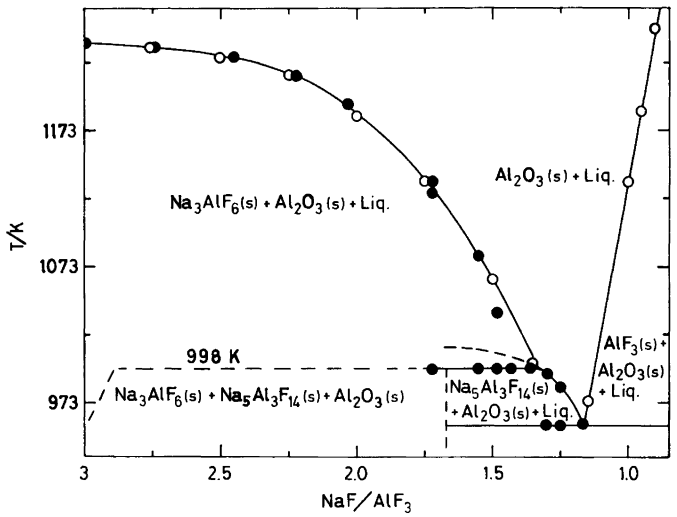

Fig. 5. Primary crystallization fields in the acidic part of the $NaF-AlF_3$ system saturated with alumina. $NaF-AlF_3$ denotes the mol ratio. ● Cryoscopic data. ○, Emf–temperature–composition points from the data given in Fig. 3.

Table 3 from the total vapour pressure and the average molar mass of the vapour. The discrepancies between the literature values and the present data cannot be explained exclusively by the experimental uncertainties in the emf values of the present work. It should be emphasized that the variations of the activities with temperature and composition in acidic melts are quite well described by the present data. The accuracy of the data in the basic range is discussed below.

Phase diagram data. The constant emf values corresponding to the given melt compositions shown in Fig. 3 are extrapolated linearly (dashed lines) to the univariant curves. Melt compositions and temperatures corresponding to these univariant curves are replotted in Fig. 5 together with phase diagram data obtained from cryoscopic measurements. As may be seen from the figure the two sets of data are in very good agreement, which means that the emf values given in Fig. 3 are fairly accurate. The previous assumption that the emf of cell [I] is independent of temperature is justified for a given melt composition in the acidic range.

Ternary eutectic and peritectic data from various sources[7,14–17] are given in Table 4. The composition of the ternary eutectic point represented by the *r*-value, seems to be well defined. The eutectic and peritectic temperatures de-

Table 4. Ternary eutectic and peritectic data for the system $Na_3AlF_6-AlF_3-Al_2O_3$. The $NaF-AlF_3$ mol ratio is denoted *r*.

Authors	Ref.	Eutectic data		Peritectic data	
		T/K	*r*	*T*/K	*r*
Philips *et al.*	7	938	1.16		1.44
Fuseya *et al.*	14	938	1.16	980	1.46
Fenerty *et al.*	15				1.44
Rolin	16	945	1.18	983	1.43
Foster	17	957	1.17	996	1.45
Present work		956	1.17	998	1.33
		±2	±.01	±2	±.02

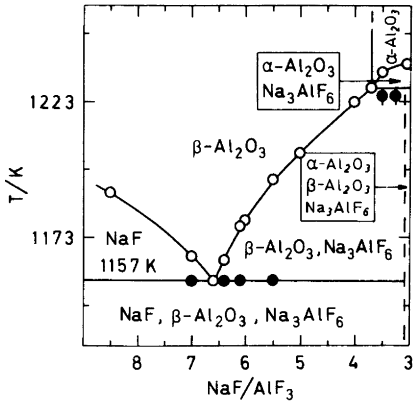

Fig. 6. Cryoscopic data in the basic part of the NaF $-AlF_3$ system saturated with either α-Al_2O_3 or β-Al_2O_3. The liquid phase present above the solidus (1157 K) is not denoted on the figure. NaF $-AlF_3$ indicates the mol ratio.

termined by Fuseya *et al.*[14] and Rolin[16] are obviously too low presumably due to supercooling. The peritectic melt composition resulting from the present work corresponding to $r=1.33\pm0.02$, differs considerably from the literature data given in Table 4. In the present work it was not possible to obtain reliable liquidus temperatures by cryoscopy in the range $1.50>r>1.33$. However, a well-defined and constant solidus temperature of 998 ± 2 K was established in this range, which means that the peritectic composition $r=1.33$ cannot be much in error.

Fig. 6 shows stability fields close to the cryolite corner of the $Na_3AlF_6-NaF-Al_2O_3$ system. The cryoscopic data in the range $3<r<4$ were determined for melt compositions containing 12 wt % Al_2O_3. This concentration is only slightly higher than the saturation limit corresponding to the univariant line. The eutectic temperature in the binary system $Na_3AlF_6-Al_2O_3$ was found to be 1237 ± 1 K which is in agreement with or slightly higher than most of the literature data cited by Grjotheim *et al.*[1]

The peritectic point where the solid phases α-Al_2O_3, β-Al_2O_3 and β-Na_3AlF_6 coexist in equilibrium with the melt is located at $r=3.7\pm0.1$ and at 1228 ± 2 K. The peritectic reaction is given in eqn. (22). For melt compositions in the range

$$12NaF(l)+(3x+1)\alpha\text{-}Al_2O_3(s)=3Na_2O\cdot xAl_2O_3(s)+2Na_3AlF_6(s) \quad (22)$$

$3.0<r<3.7$ and alumina concentrations corresponding to the univariant curve, α-Al_2O_3 and β-Na_3AlF_6 will precipitate until the peritectic point is reached. At the peritectic temperature reaction (22) proceeds to the complete consumption of either the melt (NaF) or of solid α-Al_2O_3.

By use of reaction (22) and an alumina (Al_2O_3) solubility of 18 mol per cent it is calculated that the final compounds of crystallization are α-Al_2O_3, β-Al_2O_3* and Na_3AlF_6 for melt compositions in the range $3.00<r<3.10$. It should be emphasized that the upper limit of the range depends on the amount of alumina present initially. The final products of crystallization in the neighbouring field are NaF, Na_3AlF_6 and β-Al_2O_3 as indicated in Fig. 6.

Foster[18] found that the boundary line separating the primary crystallization field of α-Al_2O_3 and β-Al_2O_3 varied slightly with the NaF content of the melt in the temperature range $1229-1330$ K. The location of the peritectic point was found to be $r=3.40$ at 1229 K, a temperature in agreement with the present study. The melt composition given by Foster for the peritectic point is then slightly different from $r=3.7\pm0.1$ found in the present work. However, taking the average composition data defining the α-Al_2O_3, β-Al_2O_3 univariant line in the range $1229-1330$ K from the work of Foster,[18] one finds $r=3.7\pm0.3$ in agreement with the present study. It is believed that this interpretation of the data is correct. The line is indicated in Figs. 1 and 6.

The ternary eutectic point shown in Fig. 6 located at $r=6.6\pm0.1$ and $T=1157\pm2$ K is in fair agreement with data given by Foster[18] and Holm.[19]

Activities of liquid NaF are calculated at temperatures corresponding to the points defining the NaF/β-Al_2O_3 univariant curve shown in Fig. 6. The calculations are based on standard Gibbs energies from the JANAF tables[21] for reaction (23)

$$NaF(s)=NaF(l) \quad (23)$$

and the assumption of no solid solubility. The activities calculated in this way are compared with corresponding data from the present work as shown in Table 5. The maximum deviation between these

*If the stoichiometric formula is taken to be $Na_2O\cdot9Al_2O_3$ the range will be $3.00<r<3.10$. If the formula is taken to be $Na_2O\cdot11Al_2O_3$ the range will be $3.00<r<3.08$. In these calculations the system is taken to be constituted of the compounds NaF, Na_3AlF_6 and Al_2O_3.

Table 5. Comparison of activities of liquid NaF at various temperatures and melt compositions expressed by the mol ratio $NaF-AlF_3$ denoted *r*.

T/K	r	a_{NaF} [a]	a_{NaF} [b]
1157	6.60	0.736	0.706
1166	7.00	0.755	0.729
1189	8.50	0.809	0.793

[a] From JANAF tables. [b] Present work.

two sets of data is at the ternary eutectic point and amounts to 4.2%.

The activities obtained using the JANAF data will be lowered and brought into better agreement with the present data if some solid solubility is assumed in the stability field of solid NaF. However, it is possible that there is a minor error in the temperature dependence of the activities in the basic range of the present work. Nevertheless, the results given in Table 5 show that eqns. (16) and (17) can be used to calculate activities as a function of temperature with reasonable accuracy also in basic melts. It is believed that the error in the present activity data will not exceed 5% of the absolute values given in eqns. (15)–(18) for melts saturated with alumina and for $T<1300$ K.

Thermodynamic data for formation of β-Al_2O_3. The value of *x* in $Na_2O\cdot xAl_2O_3$ (β-Al_2O_3) coexisting with α-Al_2O_3 is not accuractely known.[20] It is, however, generally accepted that the numerical value is in the range $9\leq x\leq 11$. The corresponding equilibrium is conveniently expressed by reaction (11). The standard Gibbs energy change of this reaction is then calculated from the present activity data for $r=3.7$, keeping in mind that the activities of α-Al_2O_3 and β-Al_2O_3 are equal to unity. The results are tabulated for various temperatures in Table 6 together with standard enthalpy and entropy data for the reaction. The enthalpy data given are derived from the slope obtained by plotting $\Delta G^\circ/T$ *versus* $1/T$. The data given in Table 6 combined with standard thermodynamic data for NaF(l),[21]

Table 6. Standard thermodynamic properties of the reaction $2\,NaF(l)+\frac{(3x+1)}{3}\,\alpha\text{-}Al_2O_3(s)=Na_2O\cdot xAl_2O_3(s)+\frac{3}{3}AlF_3(s)$.

T/K	ΔG°/kJ	ΔH°/kJ	ΔS°/(J/degree)
1180	41.539[a]		
1200	42.526[a]	−16.300	−49.022
1220	43.522[a]		
1228	43.873		
1240	44.468		
1260	45.426		
1280	46.334		
1300	47.250	−11.460	−45.162
1320	48.175[a]		
1350	49.480[a]		
1400	51.643[a]	− 7.690	−42.381
1500	55.798[a]		

[a] Extrapolated values.

$AlF_3(s)$[21] and α-$Al_2O_3(s)$[22] give the standard formation properties of $Na_2O\cdot xAl_2O_3$ shown in Table 7. The uncertainty in the Gibbs energies is estimated to be $\pm x$ kJ. The only other thermodynamic data for β-Al_2O_3 known to the authors are from a work of Weber described by Kummer,[20] for a solid state electrolyte cell reaction proposed to be as given in eqn. (24).

$$2NaAlO_2(s)+(x-1)\,\alpha\text{-}Al_2O_3(s)=Na_2O\cdot xAl_2O_3(s) \quad (24)$$

Thermodynamic properties of this reaction calculated from the emf values of Weber and shown in Table 8 do not compare favourably with corresponding data from the present work for β-Al_2O_3 (Table 7) and data for $NaAlO_2(s)$[21] and α-$Al_2O_3(s)$[22] from the JANAF tables. For a solid state reaction of the type described by reaction (24) the entropy change is expected to be rather small. The data for β-Al_2O_3 resulting from the present work are in agreement with this principle while those derived by Weber from emf measurements are not.

Table 7. Standard formation data of $Na_2O\cdot xAl_2O_3$ (β-Al_2O_3) in equilibrium with α-Al_2O_3.

T/K	ΔG_f° kJ/mol	ΔH_f° kJ/mol	ΔS_f° (J/mol, degree)
1200	$-1295.103x-485.100$	$-1691.662x-844.950$	$-330.466x-299.875$
1300	$-1262.099x-455.512$	$-1690.482x-834.608$	$-329.525x-291.612$
1400	$-1229.188x-426.689$	$-1689.215x-825.532$	$-328.591x-284.888$

Table 8. Thermodynamic data calculated from the emf values of Weber described by Kummer[20] for the reaction $2NaAlO_2(s)+(x-1)\ \alpha\text{-}Al_2O_3(s)=Na_2O\cdot xAl_2O_3(s)$ and corresponding data from the present work (β-Al_2O_3) and from the JANAF tables ($NaAlO_2$,[21] α-Al_2O_3[22]).

T/K	$\Delta G°$/kJ	$\Delta H°$/kJ	$\Delta S°$/(J/degree)
1200	−34.340	17.260	43.0
1300	−38.640	17.260	43.0
1400	−42.940	17.260	43.0
1200[a]	−48.346	−59.994	−9.707
1300[a]	−47.643	−52.631	−3.837
1400[a]	−47.472	−46.739	0.523

[a] From JANAF tables.

Without discussing details it should be emphasized that the overall cell reaction (24) proposed by Kummer[20] is not completely correct, which means that some deviations from the present data are to be expected.

Another set of interesting data are obtained when properties for solid and liquid NaF from the JANAF tables[21] are combined with data in Table 6 for reaction (11). The results for the solid state reaction given in Table 9 show reasonable values for the entropy change.

The stability of β-Al_2O_3 may be illustrated by reaction (25). The data given in Table 10 show that β-

$$Na_2O(s)+x\alpha\text{-}Al_2O_3(s)=Na_2O\cdot xAl_2O_3(s) \qquad (25)$$

Al_2O_3 is a fairly stable compound. As expected the entropy change of the reaction turns out to be small.

Thermodynamic data for solid Na_3AlF_6. The standard Gibbs energy change associated with

Table 9. Thermodynamic properties of the solid state reaction $2NaF(s)+\frac{(3x+1)}{3}\ \alpha\text{-}Al_2O_3(s)=Na_2O\cdot xAl_2O_3(s)+\frac{2}{3}AlF_3(s)$. Data is from the present work (Table 6) and from the JANAF tables for NaF.

T/K	$\Delta G°$/kJ	$\Delta H°$/kJ	$\Delta S°$/(J/degree)
1200	46.133	49.647	2.929
1300	45.618	55.413	7.535
1400	44.723	59.446	10.517

Table 10. Thermodynamic properties of the reaction $Na_2O(s)+x\alpha\text{-}Al_2O_3(s)=Na_2O\cdot xAl_2O_3(s)$. Data for β-Al_2O_3 are from the present work (Table 7) while data for α-Al_2O_3 and Na_2O are from the JANAF tables.[22,21]

T/K	$\Delta G°$/kJ	$\Delta H°$/kJ	$\Delta S°$/(J/degree)
1200	−234.764	−240.153	−4.489
1300	−234.019	−245.567	−8.883
1400	−233.317	−240.463	−5.104

$$3NaF(l)+AlF_3(s)=Na_3AlF_6(s) \qquad (26)$$

$$\Delta G°(26)=RT\ln a^3_{NaF}a_{AlF_3} \qquad (27)$$

reaction (26) can be expressed by eqn. (27) if Na_3AlF_6 is in its standard state. For melt compositions along the univariant line shown in Fig. 5, the requirement of unit activity of Na_3AlF_6 is fulfilled in the temperature range 998 K $< T <$ 1237 K provided that there is no solid solubility. The Gibbs energy is then readily calculated from the activity data described above. It should be remembered that the standard states of the activities are liquid NaF and solid AlF_3. Fig. 7 shows the results of the calculations. Three points calculated from the work of Dewing,[23] obtained with solid state electrochemical cells, have been included after appropriate adjustment of standard states. These points, which are outside the temperature range of the present work, seem to give a nice overall fit. The data shown in Fig. 7 with the exception of those derived from basic melts, are fitted to a straight line,

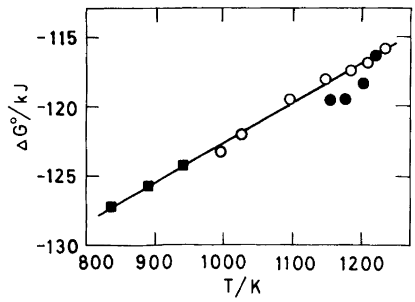

Fig. 7. The standard Gibbs energy of the reaction $3NaF(l)+AlF_3(s)=Na_3AlF_6(s)$ as a function of temperature. ■, From the work of Dewing.[23] ○, ●, Present data corresponding to the univariant curves on the acidic and the basic side of the cryolite composition, respectively.

eqn. (28). The standard deviation in the Gibbs energy is ±0.25 kJ.

$$\Delta G°(26) = -151.745(\pm 0.550) + 0.0290(\pm 0.0005)T \text{ (kJ)} \quad (28)$$

The derivation of the activity data in the basic range ($r > 3$) was based on the assumption of a temperature independent emf of cell [III], eqn. (14). The activity data derived and based on this assumption are used to determine the variation in the Gibbs energy of reaction (26) for temperatures and melt compositions defining the univariant curve in Fig. 6, where solid Na_3AlF_6 is in equilibrium with the melt. As shown in Fig. 7 these data deviate slightly from the corresponding values obtained on the acidic side of the cryolite composition. However, the deviation is small and within the experimental uncertainty of the activity data discussed above.

From a study of the cryolite liquidus curve of the binary $NaF-AlF_3$ system and from electrical resistivity measurements, Dewing[24,25] concluded that cryolite is a non-stoichiometric compound containing AlF_3 in solid solution at temperatures above 838 K. The present data do not directly support this hypothesis, although a minor solid solubility within the limits of experimental uncertainty is to be expected.

The free energy function $(\Delta G° - \Delta H°_{298})/T$ of reaction (26) can be calculated for any temperature by linear interpolation of the data in the JANAF tables.[21] $\Delta H°_{298}$ is then calculated for all the $\Delta G°$ and T values obtained on the acidic side of the system and shown in Fig. 7. Corresponding $\Delta H°_{298}$ and T values are plotted in Fig. 8. The apparent variation of $H°_{298}$ with temperature can hardly be explained only by errors in the present activity data. This means that the free energy function of reaction (26) from the JANAF tables[21] is not strictly correct and a minor revision is needed. The shape of the curve in Fig. 8 may indicate that a constant value for $\Delta H°_{298}$ is approached with decreasing temperature. It is believed that the major part of the discrepancy can be related to the data for solid Na_3AlF_6 given in the JANAF tables.[21]

Table 11. Standard Gibbs energy of formation of solid Na_3AlF_6. The differences between $\Delta G°$ from the present work and from the JANAF tables[21] are denoted $\Delta(\Delta G°)$.

T/K	$\Delta G°_f$/kJ	$\Delta(\Delta G°_f)$/kJ
800	−2871.333[a]	−6.360
900	−2818.715	−7.117
1000	−2766.101	−7.661
1100	−2714.060	−8.619
1200	−2657.032	−9.820
1300	−2581.766[a]	−10.770

[a] Extrapolated values.

The standard Gibbs energy of formation of solid Na_3AlF_6 is calculated from eqns. (26) and (28) and Gibbs energy data for NaF(l) and AlF_3(s) from the JANAF tables.[21] The values are shown in Table 11 together with the difference in $\Delta G°$ resulting from the present work and from the JANAF tables.[21] The discrepancies between the two sets of data decrease rapidly with decreasing temperature.

Thermodynamic data for solid $Na_5Al_3F_{14}$. The standard Gibbs energy change of reaction (29) was determined from the present activity data and the points defining the univariant curve shown in Fig. 5

$$Na_5Al_3F_{14}(s) = 5NaF(l) + 3AlF_3(s) \quad (29)$$

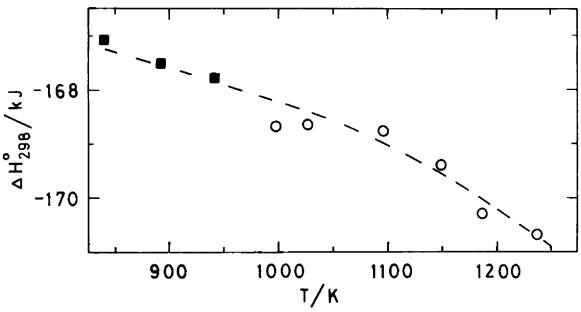

Fig. 8. Apparent temperature variation of $\Delta H°_{298}$ for the reaction $3NaF(l) + AlF_3(s) = Na_3AlF_6(s)$. ■, Calculated from the work of Dewing.[23] ○, Present work.

Table 12. Standard Gibbs energy change of the reaction $Na_5Al_3F_{14}(s) = 5NaF(l) + 3AlF_3(s)$.

T/K	$\Delta G°$/kJ	T/K	$\Delta G°$/kJ
998	223.421	985	223.480
994	223.505	956	223.714

where solid chiolite ($Na_5Al_3F_{14}$) is in equilibrium with the melt. The results are shown in Table 12. A second-law treatment of the data gives eqn. (30). The

$$\Delta G°(29) = 229.890 - 0.00647T \text{ (kJ)} \quad (30)$$

standard errors in the enthalpy and entropy terms are ± 1.29 kJ and ± 0.00013 kJ/degree, respectively. The standard deviation of $\Delta G°$ is ± 0.043 kJ. The real uncertainties are considerably larger than these statistical values, since there may be some solid solubility of AlF_3 in chiolite.[25] It should be recalled that the standard states of the activities are liquid NaF, solid AlF_3 and solid $Na_5Al_3F_{14}$.

Eqn. (30) combined with thermodynamic data for NaF(l) and AlF_3(s) gives the standard Gibbs energy of formation of chiolite, eqn. (31), strictly valid only in the range $956 < T < 998$ K.

$$\Delta G_f° = -7474.911 + 1.17919T\text{(kJ)} \quad (31)$$

Thermochemical data for solid $Na_5Al_3F_{14}$ obtained in the present study are compared with previously published values (partly updated) in Table 13. Grjotheim *et al.*[26] derived the standard Gibbs energy change of reaction (32) at temperatures around 900 K to be as given in eqn. (33).

$$5/3\ Na_3AlF_6(s) + 4/3\ AlF_3(s) = Na_5Al_3F_{14}(s) \quad (32)$$

$$\Delta G° = 12.55 - 0.0251T\ (kT) \quad (33)$$

Thermodynamic data for solid $Na_5Al_3F_{14}$ are then derived from these equations using data for solid Na_3AlF_6 from the present work, while data for liquid NaF and solid AlF_3 are from the JANAF tables.[21] The results are given in Table 13. Cantor *et al.*[27] studied the equilibrium vapour pressure of BF_3(g) according to reaction (34). Cantor *et al.*[27]

$$4/3\ NaBF_4(l) + 1/3\ Na_5Al_3F_{14}(s) = Na_3AlF_6(s) + 4/3\ BF_3(g) \quad (34)$$

used the standard Gibbs energy of solid Na_3AlF_6 from the work of Dewing,[23] shown to be in excellent agreement with the present data, when deriving the thermodynamical data for chiolite shown in Table 13. The results of Dewing included in the table are based on emf measurements of solid electrolyte galvanic cells corresponding to reaction (35) and of

$$5NaF(s) + 3AlF_3(s) = Na_5Al_3F_{14}(s) \quad (35)$$

thermodynamic data for NaF(s) and AlF_3(s) from the JANAF tables.[21]

The good agreement between the Gibbs energy data from the different sources shown in Table 13 should be noted.

Thermodynamic data for liquid $NaAlF_4$. The equilibrium constant of reaction (36) was derived to

$$NaF(l) + AlF_3(s) = NaAlF_4(l) \quad (36)$$

be 476 at 1285 K in a previous paper.[12] The derivation was based on the assumption of an ideal Temkin activity of $NaAlF_4$ and on liquid NaF and solid AlF_3 as standard states. It can be estimated that the ideal Temkin activity in a pure $NaAlF_4$ melt is 0.95 ± 0.05 at 1285 K. Defining the activity of pure $NaAlF_4$(l) as equal to one results in an equilibrium constant of 476/0.95 at 1285 K.

The next step is to derive a reasonable value for

Table 13. Standard Gibbs energy, enthalpy and entropy of formation of solid $Na_5Al_3F_{14}$ at 900 K.

Source	$\Delta G_f°$/kJ	$\Delta H_f°$/kJ	$\Delta S_f°$/(J/degree)
Dewing[23]	−6423.322	−7539.878	−1240.62
Grjotheim *et al.*[26]	−6408.908	−7472.984	−1182.306
Cantor *et al.*[27]	−6425.118	−7488.523	−1181.562
This work[a]	−6413.618	−7462.515	−1165.441

[a] Extrapolated from eqn. (30) and combined with data from the JANAF tables.

the equilibrium constant for eqn. (36) from activities corresponding to the ternary eutectic point $r=1.17$ and $T=956$ K. The activity of AlF_3 is unity, while that of NaF is found from eqn. (18) to be 3.59×10^{-3}. The activity of $NaAlF_4$ must be estimated. In a pure $NaF-AlF_3$ melt with $r=1.17$ the anion fraction of AlF_4^- is approximately 0.85. Adding the relatively small amount of Al_2O_3 needed to reach the ternary eutectic point[17] the anion fraction of AlF_4^- is reduced to 0.70–0.75. The thermodynamic activity of $NaAlF_4$ corresponding to the ternary eutectic is then expected to be 0.75 ± 0.10. A second-law calculation then gives eqn. (37) for the standard

$$\Delta G^\circ(36)=27.167-0.07283T\ (\mathrm{kJ}) \qquad (37)$$

Gibbs energy change of reaction (36). The standard Gibbs energy of formation of $NaAlF_4$ is then derived by use of data for NaF(l) and AlF_3(s) from the JANAF tables,[21] eqn. (38). The entropy of formation

$$\Delta G_f^\circ,\ NaAlF_4(l)=-2024.930+0.2648T\ (\mathrm{kJ}) \qquad (38)$$

of $NaAlCl_4$(l) in the corresponding chloride system was recently derived[28] to be −0.2639 kJ/(mol,degree) which compares favourably with the entropy term in eqn. (38). From the data given, the activity of $NaAlF_4$ is readily calculated for whatever temperature and composition within the validity range of the activity data of NaF and AlF_3.

Transport numbers. It is assumed that the only uncomplexed ions, Na^+ and F^-, are responsible for the transport of all current in the system. In order to assess the variation of the transport numbers with composition, the emf of cell [II] is conveniently

$$E_2(\mathrm{V})=0.019a_{NaF}^2-0.0021 \qquad (39)$$

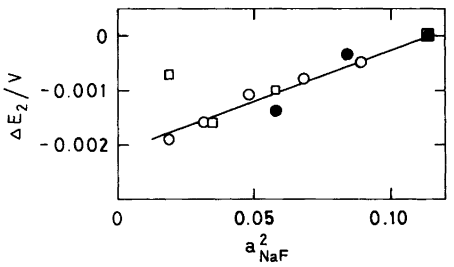

Fig. 9. The emf of cell [II] as a function of the square of the sodium fluoride activity in $NaF-AlF_3$ melts saturated with alumina at 1278 K. One symbol for each series of experiments.

$$dE_2=0.038a_{NaF}da_{NaF} \qquad (40)$$

expressed by the empirical eqn. (39), which may be written as eqn. (40). The fit to the experimental data is satisfactory as illustrated by the straight line in Fig. 9.

The differential form of the emf of cell [II], eqn. (41), combined with eqn. (40) gives eqn. (42) for the

$$dE_2=\frac{RT}{F}(1-t_{Na^+})d\ \ln a_{NaF} \qquad (41)$$

$$t_{Na^+}=1-0.038\frac{F}{RT}a_{NaF}^2 \qquad (42)$$

transport number of Na^+. The transport number plotted in Fig. 10 indicates clearly, as one may expect, that the current carried by F^- $(1-t_{Na^+})$ is increasingly important as the basicity of the melt increases. The transport number of Na^+ derived agrees reasonably well with the results of Frank and Foster[29] who investigated transport phenomena in the $Na_3AlF_6-Al_2O_3$ system by means of radioactive tracers. The present data are also in general agreement with the work reported by Tual and Rolin.[30] These authors found the transference number of Na^+ to be slightly less than unity and that F^- carried the rest of the current.

It should be emphasized that eqn. (42) is strictly valid only in the range $2<r<3$. However, extrapolation outside this range gives reasonable results. For pure NaF at 1285 K eqn. (42) gives $t_{Na^+}=0.66$ in agreement with $t_{Na^+}=0.64\pm0.05$ determined experimentally by Grjotheim *et al.*[31]

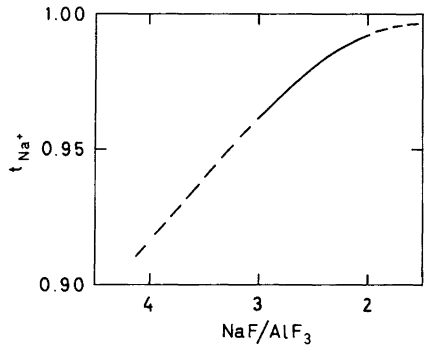

Fig. 10. The transport number of Na^+ as a function of the $NaF-AlF_3$ mol ratio in $NaF-AlF_3$ melts saturated with alumina at 1278 K.

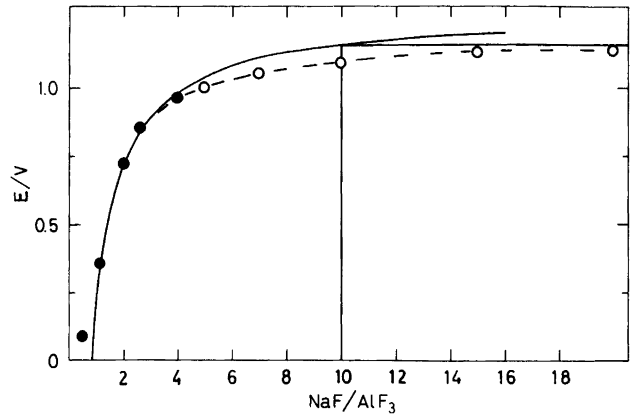

Fig. 11. Emf as a function of the $NaF-AlF_3$ mol ratio in melts saturated with alumina. The fully drawn curve corresponds to eqns. (12)–(14) while ● and ○ are data points replotted from Yoshida and Dewing [3] and Thonstad and Rolseth,[4] respectively (see text). Temperature: 1273 to 1295 K.

The activity data in the acidic range ($r<3$) was derived by setting E_2 equal to zero. The error introduced by doing this can be shown to be only of minor importance.

The $NaF-AlF_3-Al_2O_3$ system in presence of liquid aluminium. The emf expressed by eqns. (12)–(14) is shown in Fig. 11 (fully drawn line) together with corresponding data of a cell with two aluminium electrodes [3,4,32] (broken line). The present work revealed that the emf of the cell with aluminium electrodes was in agreement with that of the corresponding cell using oxygen electrodes in the acidic range of the system. Thus, it is convenient to choose a melt saturated with AlF_3 and Al_2O_3 as the reference for the emf as indicated in Fig. 11. The present data for acidic melts agree quite well with the data of Yoshida *et al.*[3] except for their data concerning the reference melt which obviously are in error.

As shown in Fig. 11 there is an increasing discrepancy in the two sets of data with increasing basicity. Only a minor part of this discrepancy can be explained by the fact that the transport number of Na^+ decreases with increasing NaF content of the melt. The possible contribution of electronic conductivity is believed to be of minor importance. A rational discussion of the discrepancies between the two sets of emf data shown in Fig. 11 should be based on the equilibria (43)–(45). The apparent

$$2Al(l)+AlF_3(diss)=3AlF(g) \quad (43)$$

$$Al(l)+3NaF(l)=AlF_3(diss)+3Na(g) \quad (44)$$

$$Al(l)+3NaF(l)=AlF_3(diss)+3Na(diss) \quad (45)$$

equilibrium vapor pressures of AlF(g) and Na(g) as a function of the composition are shown in Fig. 12. The vapour pressures on the acidic side of the system are so small that they do not effect the emf to any extent. However, on the basic side the vapour pressure of sodium reaches one atmosphere at $r=10$. The emf corresponding to this composition is shown as a straight horizontal line in Fig. 11. If the

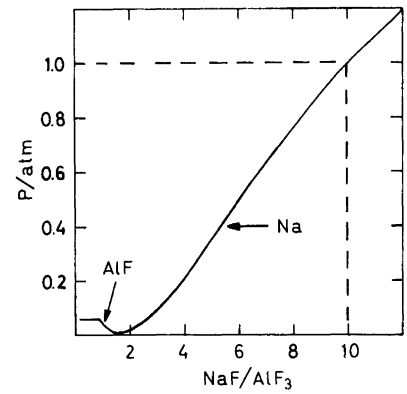

Fig. 12. Apparent equilibrium vapour pressures of Na(g) and AlF(g) as a function of the mol ratio $NaF-AlF_3$ in $NaF-AlF_3$ melts saturated with alumina at 1285 K. The calculations are based on equilibrium constants for eqns. (43) and (44) obtained from the JANAF tables [21] and activity data from the present work.

concentration cell with aluminium electrodes constitutes an open system one will expect the cell potential to approach this horizontal line in Fig. 11 as the basicity of the melt increases. The results shown indicate clearly that the melt in contact with the aluminium surface approaches the composition $r=10$ at increasingly high NaF content of the melt. This means that there is a steady state equilibrium on the metal–melt interface [eqn. (45)], with compositional variations in the adjacent diffusion layer on the electrolytic side of the interface. When the vapour pressure of sodium is less than one atmosphere at the interface the relationship (46)

$$J_{NaF} = -3J_{AlF_3} = -J_{Na(diss)} \quad (46)$$

between the mass fluxes may be valid. From the results given in Fig. 11 and eqn. (46) one expects these fluxes and the corresponding concentration gradients to become increasingly important with increasing basicity if the experimental set-up corresponds to an open system. It follows that the equilibrium concentration of dissolved metal [Na(diss)] must be relatively high in basic melts.

A rough estimate of the metal solubility of a melt with an original composition of $r=10$ from the work of Thonstad,[33] yields a value of 0.6 when the solubility is expressed as weight per cent aluminium. It is readily calculated that an original r-value of 10 will be lowered to 8.6, if the metal solubility reaction is correctly described by eqn. (45). In an open system the immediate lowering of the r-value in the bulk of the melt is not so large, since the bulk phase is not in equilibrium with the aluminium metal. In this case, however, a gradual decrease in the r-value of the bulk phase must occur, even to values below 8.6, since sodium continuously escapes to the surroundings.

In a previous work [2] it was found that the cell [IV] should be decribed by the emf eqn. (47), where

$$Al|Na_3AlF_6(l), Al_2O_3(s)||Na_3AlF_6(l), Al_2O_3(s)|(Pt), O_2\ (1\ atm) \quad [IV]$$

$$E_{IV} = E^{\circ}_{Al_2O_3} - \frac{RT}{F}\ln\frac{a_{NaF}}{a_{NaF(l)}} + \frac{RT}{3F}\ln\frac{a_{AlF_3}}{a_{AlF_3(l)}} \quad (47)$$

$E^{\circ}_{Al_2O_3}$ is the standard emf for the formation of α-Al_2O_3 and (I) denotes activities in the left-hand side compartment. The experimental results [2] showed that the activities of NaF and AlF_3 in the left-hand side compartment were not equal to those in the other compartment, in spite of the fact that the original compositions were identical. The activity terms of eqn. (47) corresponded to approximately 12 mV which is equivalent to a shift in the melt composition from $r=3.00$ to $r=2.90$. A metal solubility of 0.10 weight % aluminium [1,33] combined with eqn. (45) gives an apparent change in the r-value from 3.00 to 2.95. Thus, the metal solubility reaction explains, at least partly, the observed change in the r-value. However, also in this case it is suggested that the main reason for the change of the r-value can be related to concentration gradients in the diffusion layer on the electrolytic side of the metal–melt interface. This interpretation means that an aluminium electrode in the basic part of an open system behaves reversibly as regards the melt on its surface, but not with respect to the bulk properties. Another important conclusion to be drawn is that the metal dissolution reaction in basic melts should be studied in a closed system, where sodium is not allowed to escape to the surroundings. This conclusion is supported by a recent study of Rolseth [34,35] concerning the reoxidation reaction in aluminium electrolysis.

Acknowledgement. Financial support from the Royal Norwegian Council for Scientific and Industrial Research is gratefully acknowledged.

REFERENCES

1. Grjotheim, K., Krohn, C., Malinovsky, M., Matiasovsky, K. and Thonstad, J. *Aluminium Electrolysis*, Aluminium Verlag, Düsseldorf 1977.
2. Sterten, Å., Haugen, S. and Hamberg, K. *Electrochim. Acta 21* (1976) 589.
3. Yoshida, K. and Dewing, E. W. *Met. Trans. 3* (1972) 683.
4. Thonstad, J. and Rolseth, S. *Proc. ICSOBA 3rd Int. Meeting*, Nice 1973, 657.
5. Ratkje, S. K. *Complex Formations in Alkali –Aluminium Fluoride Melts*, Diss., Univ. of Trondheim, NTH, Trondheim, Norway 1974.
6. Temkin, M. *Acta Physicochim. URSS 20* (1945) 411.
7. Phillips, N. W. F., Singleton, R. H. and Hollingshead, E. A. *J. Electrochem. Soc. 102* (1955) 690.
8. Pearson, T. G. and Waddington, J. *Discuss. Faraday Soc. 1* (1947) 307.

9. Feinleib, M. and Porter, B. *J. Electrochem. Soc. 103* (1956) 231.
10. Mitchell, J. C. and Samis, C. S. *Trans. Metall. Soc. AIME 245* (1969) 122.
11. Wilkening, S. and Ginsberg, H. *Metall 27* (1973) 787.
12. Sterten, Å. *Electrochim. Acta 25* (1980) 1673.
13. Kvande, H. *Thermodynamics of the System NaF $-AlF_3-Al_2O_3-Al$*, Diss., Univ. of Trondheim, NTH, Trondheim, Norway 1979.
14. Fuseya, G. and Takeda, B. *J. Electrochem. Soc. Jpn. 27* (1959) 339.
15. Fenerty, A. and Hollingshead, E. A. *J. Electrochem. Soc. 107* (1960) 993.
16. Rolin, M. *Bull. Soc. Chim. Fr.* (1961) 1112.
17. Foster, P. A. *J. Am. Ceram. Soc. 58* (1975) 288.
18. Foster, P. A. *J. Chem. Eng. Data 9* (1964) 200.
19. Holm, J. L. *Thermodynamic Properties of Molten Cryolite and Other Fluoride Mixtures*, Diss., Univ. of Trondheim, NTH, Trondheim, Norway 1971.
20. Kummer, J. T. *Prog. Solid State Chem. 7* (1972) 141.
21. Stull, D. R. and Prophet, H. *JANAF Thermochemical Tables*, 2nd Ed., NSRDS-NBS 37, Washington 1971.
22. Chase, M. W., Curnett, J. L., McDonald, R. A. and Syverud, A. N. *JANAF Thermochemical Tables, Suppl.* 1978.
23. Dewing, E. W. *Metall. Trans. 1* (1970) 2211.
24. Dewing, E. W. *Metall. Trans. 3* (1972) 2699.
25. Dewing, E. W. *Metall. Trans. 9B* (1978) 687.
26. Grjotheim, K., Motzfeldt, K. and Rao, D. B. In Edgeworth, T. G., Ed., *Light Metals*, Proc. AIME Meeting, New York 1971, Vol. 1, p. 223.
27. Cantor, S., Hitch, B. F. and Heatherly, D. E. In Pemsler, J. P., Braunstein, J. and Nobe, K., Eds., *Molten Salts*, Proc. Int. Symp., Electrochem. Soc., Princeton, N.J. 1976, p. 417.
28. Bjørgum, A., Sterten, Å., Thonstad, J. and Tunold, R. *Electrochim. Acta. 26* (1981) 491.
29. Frank, W. B. and Foster, L. M. *J. Phys. Chem. 61* (1957) 1531.
30. Tual, A. and Rolin, M. *Electrochim. Acta 17* (1972) 2277.
31. Grjotheim, K., Matiasovsky, K., Myhre-Andersen, S. and Øye, H. A. *Electrochim. Acta 13* (1968) 91.
32. Thonstad, J. and Rolseth, S. Ref. 1, p. 186.
33. Thonstad, J. *Can. J. Chem. 43* (1965) 3429.
34. Rolseth, S. *Tilbakereaksjonen i aluminiumelektrolysen*, Diss., Univ. of Trondheim, NTH, Trondheim, Norway 1980.
35. Rolseth, S. and Thonstad, J. In Bell, G. M., Ed., *Light Metals*, Proc. AIME Meeting, Chicago 1981, p. 289.

Received July 20, 1981.

Acta Chemica Scandinavica A 36 (1982) 345–351

The Structures of two Binuclear Copper(II) Complexes with μ-Oxamido-bridges; $[Cu_2(C_2H_2N_2O_2)(C_{10}H_9N_3)_2(NO_3)_2]$ and $[Cu_2(C_2H_2N_2O_2)(C_{10}H_8N_2)_2(NO_3)_2]\cdot 3H_2O$

JORUNN SLETTEN

Department of Chemistry, University of Bergen, N-5014 Bergen, Norway

The structures of (μ-oxamido-bis-2,2′-dipyridylamine dinitrate) dicopper(II), compound I, and (μ-oxamido-bis-2,2′-bipyridyl dinitrate) dicopper(II) trihydrate, compound II, have been determined by X-ray crystallographic methods. The crystals are monoclinic, space group $P2_1/n$, $a=8.136(2)$, $b=8.889(1)$, $c=17.296(2)$ Å, $\beta=92.19(1)°$; and triclinic, space group $P\bar{1}$, $a=7.426(1)$, $b=9.353(2)$, $c=9.979(2)$ Å, $\alpha=83.49(2)$, $\beta=87.61(2)$, $\gamma=83.94(2)°$, for I and II, respectively.

In both compounds the oxamido group in *trans* conformation is bridging two copper ions, forming five-membered chelate rings. The coordination in II is distorted square pyramidal with oxamide and pyridyl in the equatorial plane and a nitrate in apex position. In I the distortion from the square pyramide is appreciable; the geometry being better described as intermediate between square pyramidal and trigonal bipyramidal.

Oxamide (oxalic acid diamide, A) acts as a bidentate ligand and may coordinate to the metal ion through both nitrogen atoms, both oxygen atoms, or one nitrogen and one oxygen atom. Based on IR-studies it has been concluded that monomeric bis-oxamido complexes of Cu and Ni have a square planar diimido structure, with the oxamide in *cis* conformation and coordinating through both nitrogen atoms.[1]

The oxamido ion would be expected to bridge metal ions to form binuclear complexes analogous to those formed by oxalate.[2] In such a dimer the oxamide bridge is expected to be in the *trans* conformation rather than in the *cis* conformation proposed for the monomer.

Recently a report on the syntheses of a series of binuclear copper complexes with μ-oxamido and μ-oxamato bridges appeared.[3] These complexes have subnormal magnetic moments at room temperature, suggesting the presence of magnetic interaction between copper ions. The magnetic exchange interaction is supposed to be propagated by the μ-oxamido and μ-oxamato groups in the same way as proposed for μ-oxalato complexes.[4] The magnetic moment data indicate that for analogous complexes the magnetic interaction between copper atoms decreases in the order μ-oxamido > μ-oxamato > μ-oxalato.[3]

In this paper the results of structure determinations of two μ-oxamido Cu(II) complexes are reported. Investigations of corresponding oxamato and oxalato compounds are in progress.

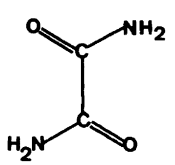

A
oxamide

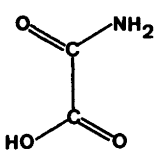

B
oxamic acid

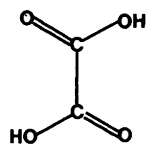

C
oxalic acid

0302-4377/82/040345-07$02.50

EXPERIMENTAL

Both compounds were synthesized according to the procedure described by Nonoyama *et al.*[3] Of compound I tiny, light blue needles grown from water were not found suitable for X-ray investigation. From a methanol solution a mixture of two different crystal modifications were obtained, one with the same appearance as those grown from water, and a second one crystallizing as bright green needles. The latter type were used in the X-ray work. From a water solution crystals of II grew as dark turquoise plates which fractured easily to platelets of minute thickness. The crystals selected for data collection had dimensions $0.25 \times 0.07 \times 0.06$ mm and $0.18 \times 0.64 \times 0.10$ mm for I and II, respectively. Data were recorded on an Enraf-Nonius CAD-4 diffractometer using monochromatized Mo$K\alpha$ radiation. For I preliminary scans and $\Delta\theta/\Delta\omega$ plots indicated that the $\theta-2\theta$ scan technique should be used, with scan widths $\Delta\theta = 0.70+0.35 \tan\theta$. The scan speeds varied between 0.6 and 4° min^{-1} depending on peak intensity. Crystals of II had poor quality and fractured easily along (001). For the crystal selected the ω-scan technique were found most appropriate. Due to the high mosaic spread rather wide scan angles had to be used; $\Delta\omega = 2.9+0.35 \tan\theta$. Scan speeds were selected at 2° min^{-1}. In both cases data were recorded up to $2\theta = 50°$. Fluctuations in intensities during data collections were monitored remeasuring three reference reflections at regular intervals; variations of ± 3 % were observed and the data were adjusted accordingly. The error in the intensity of any one reflection was estimated as $\sigma_I = [\sigma_c^2 + (0.02N_{net})^2]^{1/2}$. Of the 2205 independent reflections recorded for compound I, 1331 had $I > 1.5\ \sigma_I$ and were used in the structure analysis. For compound II, out of the 2225 reflections recorded, 1907 with $I > 2.0\sigma_I$ were retained. The intensities were corrected for Lorentz and polarization effects, and for absorption; the maximum and minimum transmission factors being 0.92 and 0.87 for I, and 0.85 and 0.78 for II.

CRYSTAL DATA

I. (μ-Oxamido-bis-2,2′-dipyridylamine dinitrate)-dicopper(II), $Cu_2C_{22}H_{20}N_{10}O_8$. Monoclinic, $P2_1/n$ (No. 14),
$a = 8.136(2)$, $b = 8.889(1)$, $c = 17.296(2)$ Å,
$\beta = 92.19(1)°$, $V = 1249.9(7)$ Å^3, $M = 679.55$, $Z = 2$,
$D_m = 1.80$ gcm^{-3}, $D_x = 1.806$ gcm^{-3},
μ(Mo$K\alpha$) = 18.43 cm^{-1}.

II. (μ-Oxamido-bis-2,2′-bipyridyl dinitrate)dicopper(II)trihydrate, $Cu_2C_{22}H_{24}N_8O_{11}$. Triclinic, $P\bar{1}$ (No. 2),
$a = 7.426(1)$, $b = 9.353(2)$, $c = 9.979(2)$ Å,
$\alpha = 83.49(2)$, $\beta = 87.61(2)$, $\gamma = 83.94(2)°$,
$V = 684.5(4)$ Å^3, $M = 703.56$, $Z = 1$, $D_m = 1.71$ gcm^{-3},
$D_x = 1.707$ gcm^{-3}, μ(Mo$K\alpha$) = 16.93 cm^{-1}.

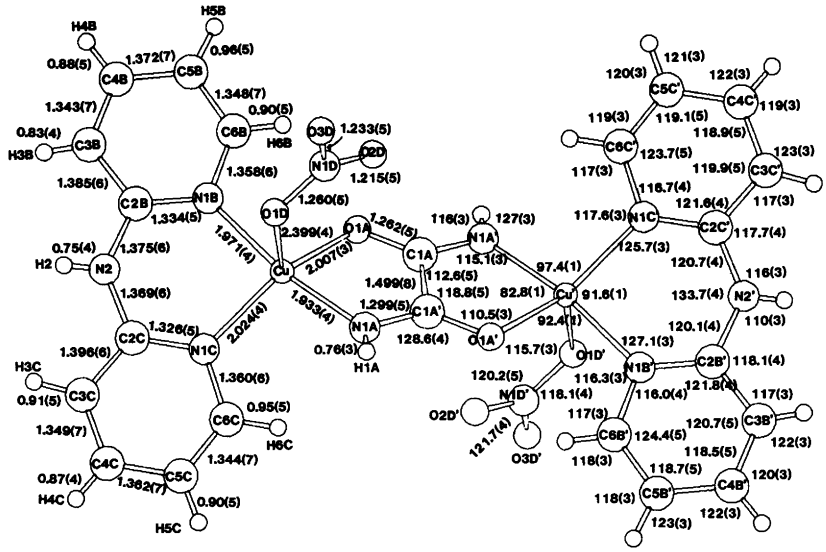

Fig. 1. The dimeric unit of compound I. Bond distances and angles are shown with their corresponding standard deviations, as obtained from the least squares matrix, in parentheses.

STRUCTURE DETERMINATIONS

The structures were both solved by the heavy atom method, and refined by least squares. In compound II one of the water molecules in the dimer is disordered. An attempt was made to refine an ordered model in the non-centrosymmetric space group $P1$, without success; hence the refinement was continued in $P\bar{1}$. It was not possible, however, to find a well-defined location for the last water molecule, which was thus left out of the calculations. In the difference Fourier map a channel of

Table 1. Final atomic parameters of non-hydrogen atoms with estimated standard deviations in parentheses. Anisotropic temperature factor: $\exp[-2\pi^2(U_{11}h^2a^{*2}+\cdots+2U_{23}klb^*c^*)]$.

Atom	x	y	z	$U(1,1)$	$U(2,2)$	$U(3,3)$	$U(1,2)$	$U(1,3)$	$U(2,3)$
Compound I									
Cu	0.17821(7)	0.24601(8)	0.51368(3)	0.0479(3)	0.0361(3)	0.0384(2)	−0.0134(4)	−0.0143(2)	0.0061(4)
O1A	−0.0319(4)	0.1788(3)	0.4597(2)	0.042(2)	0.029(2)	0.042(2)	−0.004(2)	−0.010(2)	0.004(2)
O1D	0.4254(5)	0.1863(4)	0.4489(2)	0.074(2)	0.057(2)	0.047(2)	−0.028(2)	0.013(2)	−0.017(2)
O2D	0.2728(5)	0.0517(5)	0.3722(2)	0.062(2)	0.096(3)	0.068(2)	−0.027(2)	−0.009(2)	−0.015(2)
O3D	0.5299(4)	0.0739(5)	0.3531(2)	0.055(2)	0.112(3)	0.050(2)	0.022(2)	−0.004(2)	−0.014(2)
N1A	0.1772(4)	0.0432(4)	0.5540(2)	0.035(2)	0.042(2)	0.044(2)	−0.004(2)	−0.019(2)	0.009(2)
N1B	0.1820(5)	0.4352(4)	0.4543(2)	0.049(2)	0.042(2)	0.037(2)	−0.011(2)	−0.013(2)	0.009(2)
N1C	0.2872(5)	0.3461(4)	0.6074(2)	0.052(2)	0.034(2)	0.031(2)	−0.009(2)	−0.011(2)	0.004(2)
N2	0.3390(5)	0.5747(4)	0.5455(2)	0.061(2)	0.030(2)	0.038(2)	−0.013(2)	−0.007(2)	0.001(2)
N1D	0.4080(5)	0.1008(4)	0.3910(2)	0.057(2)	0.035(2)	0.040(2)	−0.005(2)	−0.005(2)	0.003(2)
C1A	−0.0579(5)	0.0413(5)	0.4728(2)	0.028(2)	0.031(2)	0.033(2)	−0.002(2)	0.001(2)	−0.000(2)
C2B	0.2634(5)	0.5609(5)	0.4734(3)	0.035(2)	0.035(3)	0.043(3)	0.003(2)	0.004(2)	0.003(2)
C3B	0.2732(6)	0.6808(6)	0.4226(3)	0.058(3)	0.030(2)	0.050(3)	−0.003(3)	0.003(3)	0.005(3)
C4B	0.2021(7)	0.6733(6)	0.3514(3)	0.069(4)	0.052(3)	0.042(3)	0.003(3)	0.003(3)	0.020(3)
C5B	0.1200(7)	0.5440(7)	0.3300(3)	0.071(4)	0.073(4)	0.050(3)	−0.020(3)	−0.023(3)	0.022(3)
C6B	0.1134(7)	0.4306(7)	0.3815(3)	0.086(4)	0.063(4)	0.051(3)	−0.031(3)	−0.028(3)	0.020(3)
C2C	0.3480(5)	0.4845(5)	0.6097(3)	0.032(2)	0.030(2)	0.037(2)	0.000(2)	−0.002(2)	−0.002(2)
C3C	0.4244(6)	0.5429(6)	0.6768(3)	0.059(3)	0.042(3)	0.039(3)	−0.013(3)	−0.001(3)	−0.008(3)
C4C	0.4344(7)	0.4589(6)	0.7418(3)	0.063(3)	0.057(3)	0.043(3)	−0.004(3)	−0.014(3)	−0.015(3)
C5C	0.3672(7)	0.3185(6)	0.7407(3)	0.082(4)	0.055(3)	0.034(3)	−0.000(3)	−0.014(3)	0.007(3)
C6C	0.2949(7)	0.2670(6)	0.6748(3)	0.094(4)	0.039(3)	0.045(3)	−0.016(3)	−0.017(3)	0.010(3)
Compound II									
Cu	0.3334(1)	0.2691(1)	0.4987(1)	0.0451(5)	0.0264(4)	0.0507(6)	−0.0151(4)	−0.0004(4)	−0.0047(4)
O1A	0.3810(8)	0.4391(6)	0.3733(6)	0.062(3)	0.043(3)	0.049(4)	−0.023(2)	−0.010(3)	−0.002(3)
O1D	0.0471(9)	0.3607(7)	0.5703(8)	0.066(4)	0.050(3)	0.087(5)	−0.007(3)	0.008(4)	−0.027(3)
O2D	0.0678(25)	0.5227(14)	0.7203(24)	0.22(2)	0.101(8)	0.48(3)	−0.036(9)	0.01(2)	−0.11(1)
O3D	0.0252(25)	0.3218(14)	0.8174(16)	0.35(2)	0.128(8)	0.19(1)	−0.112(9)	−0.08(1)	0.081(8)
O1W	0.5566(24)	0.3116(16)	0.9211(11)	0.38(2)	0.21(1)	0.084(6)	−0.10(1)	−0.113(8)	0.079(7)
N1A	0.4737(9)	0.3546(7)	0.6203(7)	0.056(4)	0.034(3)	0.031(4)	−0.018(3)	−0.011(3)	0.006(3)
N1B	0.2467(8)	0.1627(7)	0.3565(7)	0.035(3)	0.032(3)	0.058(4)	−0.010(3)	0.002(3)	−0.007(3)
N1C	0.3153(8)	0.0788(7)	0.6078(7)	0.036(3)	0.031(3)	0.046(4)	−0.007(3)	0.001(3)	−0.004(3)
N1D	0.0539(22)	0.3977(14)	0.6944(31)	0.13(1)	0.060(7)	0.60(4)	−0.024(8)	0.05(2)	−0.07(1)
C1A	0.527(1)	0.4762(8)	0.5702(8)	0.038(4)	0.029(4)	0.041(4)	−0.006(3)	−0.002(4)	−0.005(3)
C2B	0.222(1)	0.0218(8)	0.3977(9)	0.028(4)	0.032(4)	0.050(5)	−0.006(3)	0.002(3)	−0.005(3)
C3B	0.170(1)	−0.0665(8)	0.3072(9)	0.047(4)	0.034(4)	0.062(6)	−0.010(3)	−0.006(4)	−0.013(4)
C4B	0.145(1)	−0.0127(10)	0.1747(10)	0.048(5)	0.059(5)	0.066(6)	−0.012(4)	−0.007(4)	−0.025(4)
C5B	0.169(1)	0.1322(11)	0.1344(10)	0.053(5)	0.068(6)	0.046(5)	−0.010(4)	−0.008(4)	−0.005(5)
C6B	0.222(1)	0.2139(10)	0.2266(10)	0.046(5)	0.055(5)	0.048(5)	−0.011(4)	−0.003(4)	0.003(4)
C2C	0.256(1)	−0.0228(8)	0.5394(9)	0.028(4)	0.030(4)	0.059(5)	−0.006(3)	0.007(4)	−0.010(4)
C3C	0.234(1)	−0.1600(8)	0.6015(10)	0.044(4)	0.030(4)	0.065(6)	−0.005(3)	0.006(4)	−0.004(4)
C4C	0.275(1)	−0.1906(9)	0.7384(11)	0.052(5)	0.037(4)	0.077(7)	−0.004(4)	0.013(5)	0.009(5)
C5C	0.334(1)	−0.0863(10)	0.8082(10)	0.048(5)	0.053(5)	0.051(5)	−0.004(4)	0.005(4)	0.003(4)
C6C	0.351(1)	0.0480(9)	0.7381(10)	0.039(4)	0.046(4)	0.066(6)	−0.012(4)	0.003(4)	−0.008(4)

Table 2. Atomic parameters of hydrogen atoms. Isotropic temperature factor: $\exp[-B \sin^2\theta/\lambda^2]$.

Atom	x	y	z	B
Compound I				
H1A	0.246(4)	0.004(4)	0.577(2)	0.7(7)
H2	0.383(4)	0.648(4)	0.549(2)	1.9(8)
H3B	0.321(4)	0.758(4)	0.439(2)	1.4(7)
H4B	0.213(5)	0.748(5)	0.319(2)	3.6(9)
H5B	0.068(6)	0.530(6)	0.280(3)	6.4(14)
H6B	0.069(5)	0.343(5)	0.366(2)	4.0(11)
H3C	0.474(5)	0.634(5)	0.672(2)	3.8(10)
H4C	0.480(5)	0.497(5)	0.784(2)	3.9(11)
H5C	0.359(6)	0.266(5)	0.785(3)	5.2(12)
H6C	0.255(6)	0.167(5)	0.673(3)	5.0(12)
Compound II				
H1A	0.492(7)	0.348(6)	0.677(6)	0(1)
H3B	0.156(9)	−0.162(8)	0.328(7)	3(2)
H4B	0.104(9)	−0.068(7)	0.115(7)	2(1)
H5B	0.159(11)	0.157(9)	0.043(8)	4(2)
H6B	0.240(14)	0.326(11)	0.201(10)	7(3)
H3C	0.184(13)	−0.223(10)	0.541(10)	6(2)
H4C	0.260(11)	−0.274(9)	0.783(8)	4(2)
H5C	0.378(16)	−0.058(13)	0.913(12)	10(3)
H6C	0.411(15)	0.132(12)	0.748(11)	8(3)

electron density, was found running parallel to the a-axis and close to $y=0.5$, $z=0.0$.

In both structures hydrogen atoms, except those on water in II, were localized by difference Fourier synthesis, and were refined isotropically. For the non-hydrogen atoms anisotropic thermal parameters were used. The weight assigned to each reflection in the refinement is $w=1/\sigma_F^2$, where $\sigma_F=\sigma_I(I\cdot Lp)^{-1/2}$. Final R values are 0.040 and 0.071 for I and II, respectively, weighted R 0.036 and 0.101. Standard deviation of an observation of unit weight 1.30 and 9.30, respectively. The high disagreement factors for II reflect the poor quality of the crystal and the deficiency in the model as described above.

Table 3. Copper-coordination bond angles (°) for compounds I and II.

	Compound I	Compound II
O1D−Cu−O1A	115.5(1)	96.0(1)
O1D−Cu−N1A	88.7(2)	98.3(2)
O1D−Cu−N1B	85.1(2)	95.5(1)
O1D−Cu−N1C	97.0(1)	92.7(1)
O1A−Cu−N1A	82.8(1)	84.0(1)
O1A−Cu−N1B	92.4(1)	94.1(1)
O1A−Cu−N1C	147.4(1)	170.6(1)
N1A−Cu−N1B	169.7(2)	166.2(2)
N1A−Cu−N1C	97.4(1)	98.3(2)
N1B−Cu−N1C	91.6(1)	81.4(1)

Atomic scattering factors used were those of Cromer and Waber.[5] All calculations were carried out on a PDP 11/55 computer using the Enraf-Nonius Structure Determination Programs (SDP).[6]

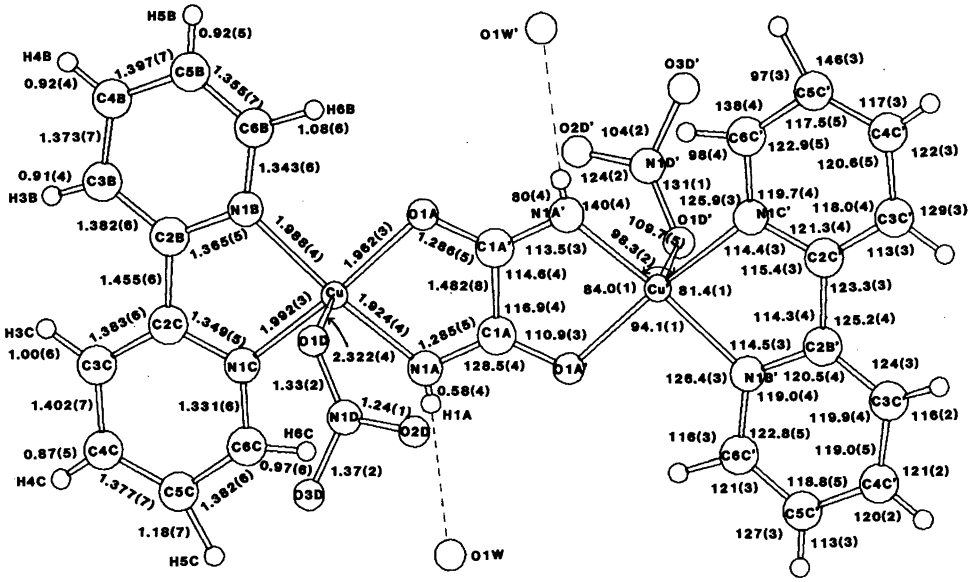

Fig. 2. The dimeric unit of compound II with bond distances and angles.

Final atomic parameters are listed in Tables 1 and 2. ORTEP drawings of the two molecules including atomic numbering scheme, bond lengths and bond angles are shown in Figs. 1 and 2. Bond angles around copper are listed in Table 3.

Lists of structure factors may be obtained from the author.

RESULTS AND DISCUSSION

The coordination geometry. In compound I the coordination geometry is intermediate between square pyramidal and trigonal bipyramidal. If regarding the complex as distorted square pyramidal the oxamido oxygen and nitrogen atoms occupy two equatorial positions and the nitrogen atoms of the pyridyl rings the two remaining equatorial positions. An oxygen atom of the nitrate group. O1D, occupies the apex position at a distance of 2.399 Å. Opposite to O1D the sixth position is blocked by the proximity of a pyrididyl group of a symmetry related molecule, the closest neighbour being C3B^{ii} ($-x$, $1-y$, $1-z$) at a distance of 3.93 Å. A least squares plane through the four equatorial ligands shows the following displacements in I: -0.37, 0.36, 0.33, -0.32 Å for O1A, N1A, N1B, N1C, respectively; and with Cu displaced 0.22 Å out of this plane towards the apical ligand. As seen from this description and the bond angles in the coordination sphere, listed in Table 3, the distortion from square pyramidal geometry is appreciable, and is approaching a trigonal bipyramide. When regarding the geometry as distorted trigonal bipyramidal, O1A, O1D and N1C constitute the equatorial ligands, while N1A and N1B are occupying the axial positions. Geometries intermediate between square pyramidal and trigonal bipyramidal have also been observed in the structures of a chloroanilate bridged dimer of Cu[7] and in an azide bridged compound.[8]

In compound II the distortion from square pyramidal geometry is only minor, with O1A, N1A, N1B, N1C constituting the equatorial plane with deviations of 0.04, -0.04, 0.04, -0.04 Å, respectively, from the best least squares plane. The Cu ion is displaced 0.19 Å out of this plane towards the apical nitrate ligand, Cu–O1D being 2.322 Å. In this case as well, the sixth position opposite to O1D is blocked by pyridyl, Cu···C3C^{ii} ($1-x$, $-y$, $1-z$) = 3.41 Å. It is to be noted that in both compounds nitrate is found to be weakly coordinated; this contradicts previous assumptions based on IR and electronic spectra, that nitrate is coordinated in I, but not in II.[3]

The distortion of I towards trigonal bipyramidal geometry is reflected in the bond distances around Cu. The two Cu–N(pyridyl) bonds are significantly different; Cu–N1C, which is equatorial in the trigonal bipyramide, being longer than the axial Cu–N1B bond (2.024(4) Å *vs.* 1.971(4) Å). This observation is in good agreement with previous findings that the ratio r_a/r_e in d^8 and d^9 complexes of trigonal bipyramidal geometry tends to be slightly less than unity.[9,10] Equatorial bonds in trigonal bipyramids tend to be longer than corresponding equatorial bonds in square pyramides. This trend is also observed in the present structures where Cu–O1A and Cu–N1C both are significantly longer in I than in II.

The oxamido ion. In each compound the complex is dimeric with the oxamido group acting as a bridge between two metal centres. The bridge is essentially planar with copper displaced 0.10 and 0.04 Å from this plane in I and II, respectively. The oxamido ion is in the *trans* conformation, situated on a crystallographic centre of symmetry, and is forming five-membered chelate rings with each of the copper ions. Oxalate ions have been found to form similar bridged structures in binuclear Cu(II) oxalato complexes,[4,11] as well as in a polynuclear Cu(II) oxalato-ammine complex.[12]

The C–C bonds in neutral oxamide (1.5340(5) Å)[13] and in oxalic acid [1.538(2) Å][14] are found to be appreciably longer than expected for a C_{sp^2}–C_{sp^2} bond. In Cu–oxalate complexes the C–C bond remains long (1.53–1.56 Å),[4,7,11] while in the present oxamido complexes a significant shortening is observed. This difference between oxalato and oxamido complexes is difficult to rationalize.

The molecular structures of I and II are such that magnetic exchange may be propagated through the oxamido bridge. Mechanisms for such an exchange have been suggested for square pyramidal geometry with the bridging ligand in the equatorial plane,[15] as well as for trigonal bipyramidal geometry with one equatorial and one axial position occupied by the bridging group.[4] The Cu···Cu distances in the dimers are 5.259 Å and 5.202 Å, for I and II, respectively.

Nitrate ions. The nitrate ion in I shows the expected geometry, with a slight elongation of the N–O bond involved in coordination. In II the refinement revealed that N1D, O2D, O3D either

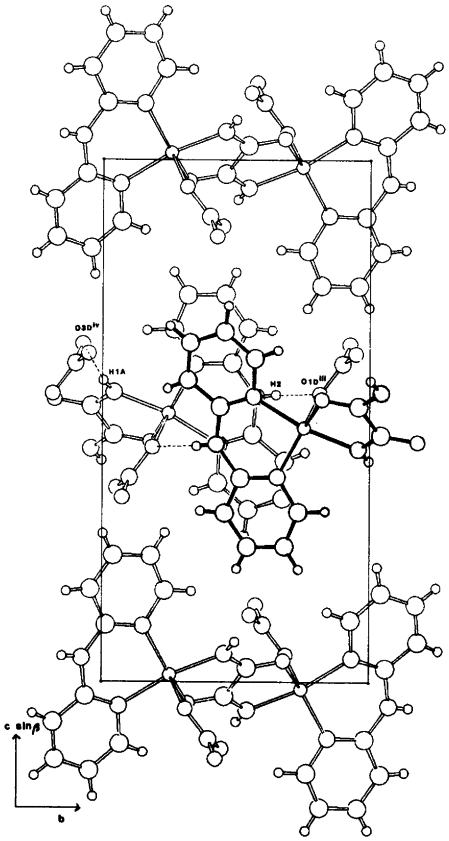

Fig. 3. Crystal packing of I as viewed down the *a*-axis.

had large thermal motion or were disordered. A well-defined disordered model was not obtained.

Hydrogen bonding and molecular packing. The molecular packing of compound I is illustrated in Fig. 3. There is one hydrogen bond between N2 and O1D^{iii} $(1-x, 1-y, 1-z)$, N2···O1D^{iii} = 2.860(6) Å, $<$N2−H2−O1D^{iii} = 162(4)°; linking dimeric units along the *ab* diagonal. An additional hydrogen bond between N1A and O3D^{iv} $(1-x, -y, 1-z)$, N1A···O3D^{iv} = 3.009(5) Å, ∠N1A−H1A···O3D^{iv} = 170(4)°, links together the dimeric units stacked along *a*.

In Fig. 4 the packing of compound II is shown. Hydrogen bonding occurs between N1A and O1W, N1A···O1W = 3.063(7) Å, ∠N1A−H1A···O1W = 177(3)°. The disordered water molecule which could not be properly located may give a very weak link along *c* between dimers.

REFERENCES

1. Armendarez, P. X. and Nakamoto, K. *Inorg. Chem. 5* (1966) 796.
2. Nakamoto, K. *Infrared and Raman Spectra of Inorganic and Coordination Compounds*, 3rd Ed., Wiley, New York 1978, p. 233.
3. Nonoyama, K., Ojima, H., Ohki, K. and Nonoyama, M. *Inorg. Chim. Acta 41* (1980) 155.
4. Felthouse, T. R., Laskowski, E. J. and Hendrickson, D. N. *Inorg. Chem. 16* (1977) 1077.
5. Cromer, D. T. and Waber, J. T. *International Tables for X-Ray Crystallography*, Kynoch

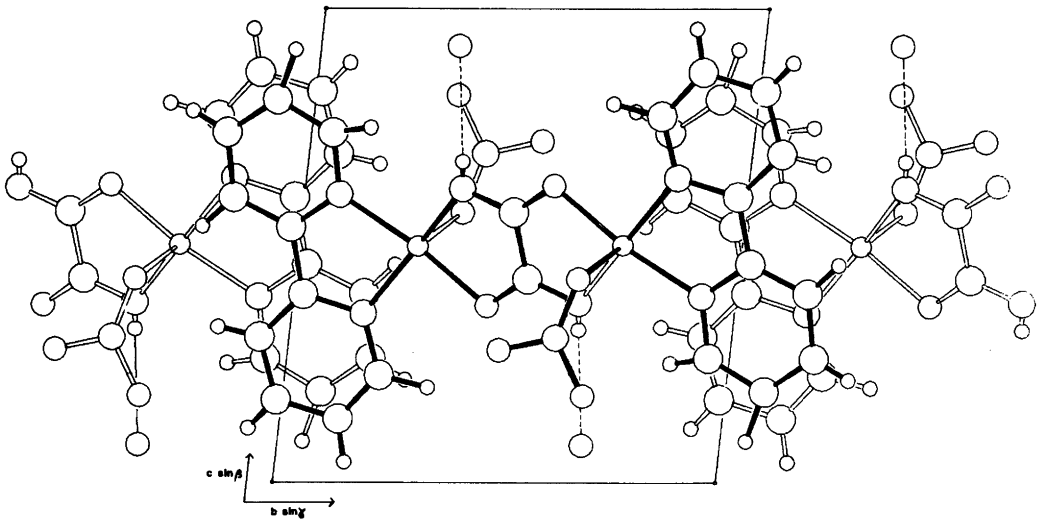

Fig. 4. Crystal packing of II as viewed down the *a*-axis.

Press, Birmingham 1974, Vol. IV, p. 99 (Table 2.2B).
6. Frez, B. *The SDP User's Guide*, Enraf-Nonius, Delft, The Netherlands 1979.
7. Pierpont, C. G., Francesconi, L. C. and Hendrickson, D. N. *Inorg. Chem. 16* (1977) 2367.
8. Felthouse, T. R., Laskowski, E. J., Bieksza, D. S. and Hendrickson, D. N. *J. Chem. Soc. Chem. Comm.* (1976) 777.
9. Muetterties, E. L. and Guggenberger, L. J. *J. Am. Chem. Soc. 96* (1974) 1748.
10. Wood, J. S. *Prog. Inorg. Chem. 16* (1972) 227.
11. Curtis, N. F., Mc Cormick, I. R. N. and Waters, T. N. *J. Chem. Soc. Dalton Trans.* (1973) 1537.
12. Cavalca, L., Chiesi Villa, A., Gaetani Manfredotti, A., Mangia, A. and Thomlinson, A. A. G. *J. Chem. Soc. Dalton Trans.* (1972) 391.
13. de With, G. and Harkema, S. *Acta Crystallogr. B 33* (1977) 2367.
14. Delaplane, R. G. and Ibers, J. A. *Acta Crystallogr. B 25* (1969) 2423.
15. Girerd, J. J., Jeannin, S., Jeannin, Y. and Kahn, O. *Inorg. Chem. 17* (1978) 3034.

Received June 16, 1981.

Acta Chemica Scandinavica A 36 (1982) 353–359

Chromium(III) Complexes of Macrocyclic Ligands. I. Crystal Structure of *trans*-Bis(*O*-carbamato)(1,4,8,11-tetraazacyclotetradecane)chromium(III) Perchlorate Sesquihydrate

E. BANG and O. MØNSTED

Department I, Inorganic Chemistry, H. C. Ørsted Institute, University of Copenhagen, Universitetsparken 5, DK-2100 Copenhagen Ø, Denmark

trans-$[Cr(cyclam)(OCONH_2)_2]ClO_4.1\frac{1}{2}H_2O$ crystallizes in the $C2/c$ space group with $a=15.174(6)$ Å, $b=17.257(10)$ Å, $c=16.964(8)$ Å, $\beta=109.05(3)°$. The structure contains two independent centrosymmetrical complex ions which are almost identical except for the orientation of the carbamate ligands. The macrocyclic tetraamine ligand has the 5-membered ring in the *gauche* and the 6-membered ring in the *chair* conformation. The perchlorate ion is disordered. The final R-values were $R\sim0.047$ and $R_w\sim0.053$ (4817 refl.).

The cyclic tetraamine 1,4,8,11-tetraazacyclotetradecane (cyclam) forms complexes with most transition metal ions but until recently only compounds with the ligand in the *cis* configuration were readily obtained for chromium(III).[1,2] During preparative work on the *trans* series of complexes an orange compound, present as an impurity in crude *trans*-$[Cr(cyclam)(NH_3)_2]Cl_3$ prepared from *trans*-$[Cr(cyclam)Cl_2]Cl$ and $NH_3(l)$, was isolated. Various types of evidence suggested that coordinated carbamate could be present, a situation so far not encountered in chromium(III) chemistry. To settle this question, and also to determine the cyclam ligand conformation, which could possibly explain both the increased robustness of *trans*-'cyclam' complexes compared to other *trans*-tetraamine chromium(III) complexes, and also the unusually high spectrochemical Δ-value for the cyclam ligand, this structural investigation was undertaken.

EXPERIMENTAL

Suitable crystals of *trans*-$[Cr(cyclam)(OCONH_2)_2]ClO_4.1\frac{1}{2}H_2O$ for the crystallographic work were obtained by slowly cooling a saturated aqueous solution from 50 to 0 °C. The yield is low, probably due to decomposition reactions. The identity between this recrystallized product and the analyzed starting material was established through Hägg-Guinier powder diagrams. The monoclinic orange crystals are strongly pleochroitic and of different habitus with well-developed faces, where a prism after [010] and plates with the well-developed form {010} often occur.

The crystals could be assigned to the space group Cc or $C2/c$ through Weissenberg and precession photographs. Intensity data for a $0.28\times0.18\times0.18$ mm^3 large crystal were collected on a Picker FACS-1 diffractometer with graphite monochromated Mo$K\alpha$ radiation and 4817 independent reflections including 1008 classified as 'less thans' $[I<3\sigma(I)]$ were measured. The data were corrected for crystal decay, but not for absorption.

Crystal data. trans-$[Cr(C_{10}H_{24}N_4)(OCONH_2)_2]ClO_4.1\frac{1}{2}H_2O$. Monoclinic $C2/c$ (Cc). $a=15.174(6)$ Å, $b=17.257(10)$ Å and $c=16.964(8)$ Å; $\beta=109.05(3)$. $Z=8$. μ(Mo$K\alpha$)$=7.63$ cm^{-1}. $D_m=1.564$, $D_x=1.579$ g cm^{-3}. $V=4199$ Å^3. $M=498.9$ g mol^{-1}. $F(000)=2096$.

Structure determination and refinement. The structure was solved by conventional methods. Possible positions of Cr and Cl atoms were indicated in the Patterson function, and a subsequent Fourier synthesis carried out in the space group Cc revealed the positions of all C, N and O atoms. Least squares refinement with anisotropic temperature factors for all these atoms gave an agreement factor of $R=0.073$. The result of this calculation suggested

0302-4377/82/040353-07$02.50

that the cations were centrosymmetrical and the space group possibly $C2/c$. A difference electron density synthesis clearly showed the hydrogen atoms at reasonable positions. Weighted least squares refinement in the space group $C2/c$ including hydrogen atoms with isotropic temperature factors and with weights derived from counting statistics but modified to downweigh the most intense reflections, *i.e.*:

$$1/w \sim \sigma^2(F_{obs}) + 0.005F_{obs} + 0.00003F_{obs}^2$$

gave agreement factors $R = 0.054$ and $R_w = 0.061$. Large temperature factors of the perchlorate oxygen atoms indicated a static or dynamic disorder of this anion, in agreement with parameters for two rather different perchlorate ions in the initial Cc space group refinements. Further calculations were therefore carried out with two perchlorate ions, each of

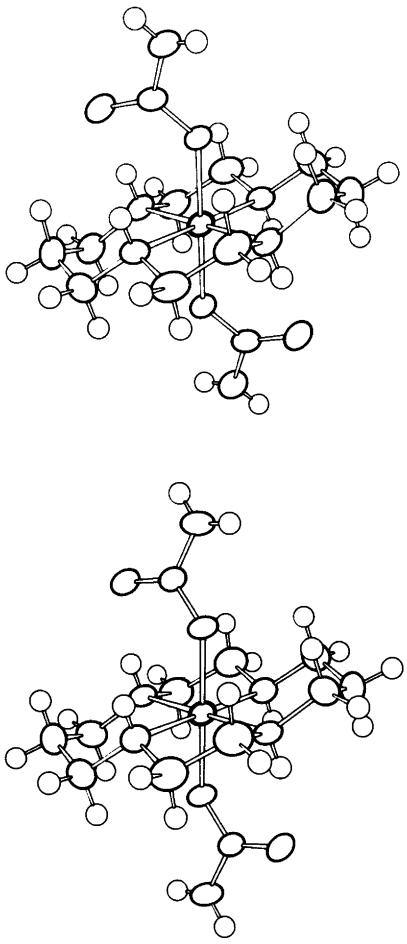

Fig. 1. The two different complex cations. Upper drawing: Cr1-complex, lower drawing: Cr2-complex. Cr-, O-, N- and C-atoms are drawn as 50% probability ellipsoids, H-atoms as spheres with a radius of 0.15 Å.

Table 1. Fractional coordinates for *trans*-$[Cr(cyclam)(OCONH_2)_2]ClO_4.1\frac{1}{2}H_2O$.

Atom	X	Y	Z
Cr1	.25000	.25000	.50000
N101	.12568(15)	.19091(13)	.45412(13)
N102	.25910(15)	.27423(13)	.38402(13)
N103	.07261(19)	.43664(15)	.47577(19)
O101	.18324(11)	.34652(10)	.50346(10)
O102	.09373(13)	.36748(11)	.37123(11)
C101	.11414(21)	.14213(17)	.37969(19)
C102	.12759(21)	.18742(20)	.30800(18)
C103	.22730(21)	.21190(18)	.32075(17)
C104	.35636(20)	.29904(18)	.39889(19)
C105	.38445(20)	.35193(17)	.47381(20)
C106	.11668(16)	.38155(13)	.44749(16)
H101N	.0860 (18)	.2245 (15)	.4416 (15)
H102N	.2240 (21)	.3125 (18)	.3663 (19)
H103M	.0257 (25)	.4565 (21)	.4436 (22)
H103N	.0803 (21)	.4377 (17)	.5238 (20)
H101A	.1594 (20)	.0985 (17)	.3959 (17)
H101B	.0515 (22)	.1202 (17)	.3630 (18)
H102A	.1068 (24)	.1571 (21)	.2602 (23)
H102B	.0902 (22)	.2359 (18)	.2956 (19)
H103A	.2709 (19)	.1687 (16)	.3407 (17)
H103B	.2327 (20)	.2315 (17)	.2664 (19)
H104A	.3930 (21)	.2508 (17)	.4085 (18)
H104B	.3609 (21)	.3251 (18)	.3529 (20)
H105A	.4503 (23)	.3712 (18)	.4871 (18)
H105B	.3458 (20)	.3960 (17)	.4651 (17)
Cr2	.75000	.25000	.50000
N201	.73479(16)	.13890(13)	.45301(15)
N202	.88179(14)	.23125(13)	.58232(14)
N203	.88402(20)	.33755(17)	.34217(16)
O201	.79575(11)	.28499(11)	.41061(10)
O202	.94716(13)	.25555(12)	.44765(13)
C201	.77411(22)	.07604(17)	.51431(21)
C202	.87609(22)	.08820(19)	.56125(24)
C203	.89981(21)	.15456(19)	.62311(20)
C204	.90274(22)	.29709(19)	.64091(17)
C205	.86591(21)	.37124(19)	.59398(20)
C206	.87771(17)	.29038(14)	.40293(15)
H201N	.7602 (22)	.1403 (19)	.4202 (20)
H202N	.9141 (19)	.2340 (16)	.5534 (17)
H203M	.9389 (24)	.3444 (18)	.3415 (20)
H203N	.8404 (22)	.3598 (17)	.3182 (18)
H201A	.7378 (20)	.0726 (18)	.5522 (19)
H201B	.7645 (24)	.0270 (22)	.4840 (22)
H202A	.9002 (23)	.0406 (20)	.5889 (20)
H202B	.9082 (22)	.0922 (19)	.5231 (20)
H203A	.8655 (21)	.1517 (17)	.6615 (19)
H203B	.9682 (23)	.1517 (18)	.6593 (19)
H204A	.8767 (22)	.2857 (18)	.6830 (20)
H204B	.9680 (22)	.3021 (18)	.6704 (19)
H205A	.8761 (19)	.4152 (18)	.6318 (17)
H205B	.8949 (19)	.3822 (16)	.5523 (18)
Cl1	.6903 (4)	.4975 (6)	.2115 (7)
O11	.7551 (11)	.4532 (12)	.1875 (11)
O12	.7209 (6)	.5111 (6)	.2981 (6)
O13	.6789 (7)	.5697 (7)	.1683 (6)
O14	.6009 (6)	.4621 (5)	.1918 (6)
Cl2	.3121 (6)	.5021 (7)	.2952 (8)
O21	.2522 (10)	.4404 (13)	.3063 (10)
O22	.3075 (14)	.4958 (9)	.2125 (9)
O23	.2720 (6)	.5755 (6)	.2991 (6)
O24	.3965 (7)	.4945 (7)	.3550 (8)
O1	.41779(25)	.05982(24)	.34304(20)
H101W	.3680 (42)	.0498 (35)	.3309 (36)
H102W	.4402 (35)	.0319 (29)	.3119 (31)
O2	.0	.47101(18)	.25000
H201W	.0344 (21)	.4437 (17)	.2844 (18)

a population of ½ in $C2/c$. This gave the final agreement factors $R \sim 0.047$ and $R_w \sim 0.053$ without significant changes of the remaining parameters. The scattering factors for Cr(0) and the corrections for anomalous dispersion for Cr and Cl were taken from Ref. 3. The scattering factors for the other atoms, *i.e.* Cl(0), O(0), N(0), C(0) and H(0), were those of the XRAY system,[4] which was used for the calculations. The determined positional parameters are given in Table 1. Lists of observed and calculated structure factors as well as temperature factors are available from the authors.

RESULTS AND DISCUSSION

Two chromium atoms are placed at two non-equivalent centres of symmetry. This gives two independent complex cations in which, however, bond lengths and angles in both the cyclam and carbamate ligand sets are almost identical. This is shown in Figs. 1 and 2, and Table 2.

The macrocyclic ligand has a conformation in which the five-membered ring has the *gauche*, and the six-membered ring the *chair* conformation, respectively. It has a crystallographic symmetry centre and is close to having a mirror plane orthogonal to the CrN_4-plane and containing the symmetry centre and the middle carbon atom of the six-membered ring. This conformation is predicted by semi-empirical calculations to have the lowest energy[5] and is also found in a number of other compounds including $(cyclamH_2)(ClO_4)_2$,[6] *trans*-$[Ni(cyclam)Cl_2]$,[7] $[Co(cyclam)](ClO_4)_2$[8] and $[Cu(cyclam)](ClO_4)_2$.[9]

The bond lengths in the present complex and in the uncoordinated diprotonated ligand are almost identical, *cf.* Table 3. The average value for the Cr – N bond length of 2.059 Å is very close to both the value of 2.07 Å calculated semiempirically to be the "ideal" metal – nitrogen bond length in *trans*-'cyclam' complexes[5] and also to the experimentally found chromium – nitrogen bond lengths in a number of complexes containing ammonia, 1,2-ethanediamine (en) and 1,3-propanediamine (tn), *cf.* Table 4. The data of Table 4 do not support a correlation between bond lengths and spectrochemical Δ-values, and the high Δ-value of *trans*-'cyclam' complexes of chromium(III) cannot therefore reasonably be ascribed to a statically strained metal – nitrogen bond, but is more likely the result of a dynamically very rigid ligand.

The N – Cr – N angles deviate from the average values found in a number of chelate diamine complexes, *cf.* Table 4, but accord with a greater flexibility of 6-membered chelate rings *vs.* 5-membered.

In solution the axial ligands in *trans*-'cyclam' complexes show an increased substitution inertness compared to that of most other tetraamine chromium(III) complexes.[10] Both the pentaamine- and pentaaquachromium(III) series of complexes are known to react by an associative interchange mechanism,[11] but plausible transition state structures[12] for *trans*-'cyclam' complexes reacting by

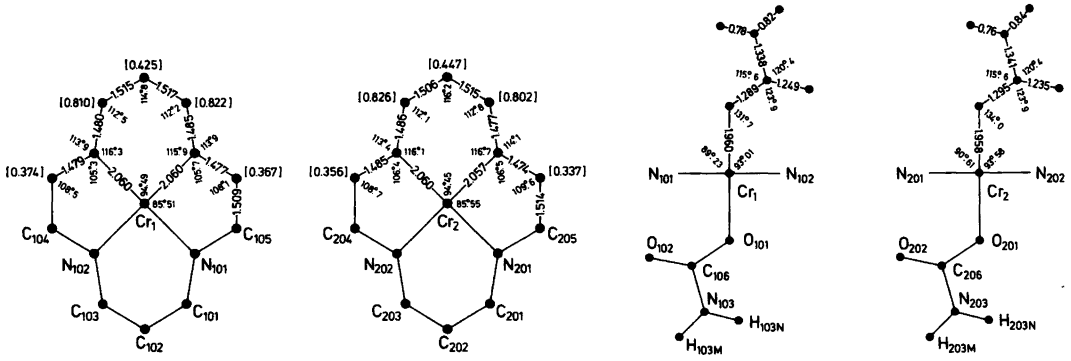

Fig. 2. Numbering scheme and bond lengths and angles for left: The two macrocyclic tetraamine rings, with carbon atom distances from the CrN_4-plane shown in square brackets, and right: The two carbamate ligands for which the O – Cr – N angles are to those two nitrogen atoms of the macrocyclic tetraamine ligand which are closest to the uncoordinated carbamate oxygen atom, and are donor atoms of a 6-membered chelate ring, *cf.* Fig. 1. Standard deviations are almost constant for each bond and angle type and are: $\sigma(Cr-X) \sim 0.002$ Å (X = N,O); $\sigma(C-X) \sim 0.004$ Å (X = C,N,O); $\sigma(X-Cr-Y) \sim 0.09°$ (X,Y = N,O); and $\sigma(X-Y-Z) \sim 0.2°$ (X,Y,Z = C,N,O).

Table 2. Summary of C – H, N – H, O – H and Cl – O bond lengths, [Å], and angles [°] in *trans*-[Cr(cyclam)-$(OCONH_2)_2$]ClO_4.$1\frac{1}{2}H_2O$.

	No. of indep. determinations.	Average (Std.dev.)	Range
d (C – H)	20	0.970(7)	0.92 – 1.02
∠(H – C – H)	10	106.6(9)	101.6 – 110.9
∠(H – C – N)	12	108.1(5)	105.4 – 111.1
∠(H – C – C)	28	110.2(4)	105.2 – 113.6
d (N – H)	8	0.803(12)	0.76 – 0.84
∠(Cr – N – H)	4	104.2(11)	103.2 – 105.6
∠(C – N – H)	8	108.0(7)	106.5 – 110.2
d (O – H)	3	0.800(24)	0.74 – 0.86
∠(H – O – H)	2	107.1(23)	105.7 – 107.4
d (Cl – O)	8	1.409(6)	1.355 – 1.452
∠(O – Cl – O)	12	109.4(3)	103.7 – 118.3

Table 3. Comparison of bond lengths [Å] in *trans*-[Cr(cyclam)$(OCONH_2)_2$]$^+$ with literature data for [cyclamH_2]$^{2+}$.

	No. of indep. determinations.	Average	Range	Ref.
C – N	8	1.480(2)	1.474 – 1.486	This work
	4	1.482(3)	1.464 – 1.504	6
C – C	6	1.513(2)	1.506 – 1.517	This work
	3	1.509(4)	1.503 – 1.520	6
$\bar{1}$ – N	4	2.059(2)	2.057 – 2.060	This work
	2	2.045	1.98 and 2.11	6

such a mechanism are seen to be sterically hindered, particularly by the axial hydrogen atoms of two of the carbon atoms in the 6-membered rings, *cf.* Fig. 1. The increased robustness of *one* of the axial ligands in *trans*-difluorido-(1,4,8,11-tetraazaundecane)-chromium(III), which is similarly shielded by the hydrogen atoms of the equatorial amine ligand[13] supports this explanation.

The two independent carbamate ligands are planar within the estimated uncertainties and close to being congruent, but their orientations towards the cyclam ligand are different and seem to be dominated by differences in the hydrogen bonds, primarily to the uncoordinated oxygen atom as described in Table 5. The distances from the coordinated oxygens to chromium are the same, *cf.* Fig. 2 B, and the average value, 1.959 Å, is close to the values found for a number of other chromium oxygen bond lengths, *i.e.* Cr-OH_2 ~ 2.00_7 Å, Cr-OH

Table 4. Comparison with selected average literature values for Cr – N bond lengths, N – Cr – N angles and spectrochemical Δ-values of chromium(III) complexes containing ammonia and 5- and 6-membered chelate diamine ligand rings.

Amine	*d*(Cr – N) [Å]	∠(N – Cr – N) [°]		Δ [μm^{-1}]
cyclam	2.059	85.53	94.47	~2.44
a[a]	2.06_8	–	–	2.111[d]
en[b]	2.07_7	82.4	–	2.166[e]
tn[c]	2.08_9	–	89.5	2.164[e]

[a] a = ammonia. Data for [Cra_6][$CuCl_5$],[17] [Cra_6][$CuBr_5$][18] and [Cra_6][$Ni(CN)_5$].$2H_2O$.[19] [b] en = 1,2-ethanediamine. Data for [$Cren_3$]I_3.H_2O (118 K),[20] [$Cren_3$]$(SCN)_3$.$\frac{3}{4}H_2O$,[21] $(+)_D$-[$Cren_3$]-Cl_3.$2H_2O$ (123 K),[22] $(-)_D$-[$Cren_3$]$(SCN)_3$,[23] [$Cren_2tn$]Br_3.H_2O[24] and [$Crentn_2$]I_3.H_2O.[24] [c] tn = 1,3-propanediamine. Data from Ref. 24 and for [$Crtn_3$][$Ni(CN)_5$].$2H_2O$.[19] [d] Ref. 25. [e] Ref. 26.

Table 5. Selected intermolecular hydrogen bonds with d(H···B) less than 2.75 Å in *trans*-[Cr(cyclam)-$(OCONH_2)_2$]$ClO_4.1\frac{1}{2}H_2O$, *cf.* Fig. 3.

A–H···B	d(A–H) [Å]	d(H···B) [Å]	d(A···B) [Å]
N101–H101N···O202	0.81(3)	2.21(3)	2.898(3)
N102–H102N···O21	0.84(3)	2.53(4)	3.143(21)
···O11	0.84(3)	2.65(4)	3.298(21)
N103–H103M···O1	0.82(3)	2.64(3)	3.414(5)
–H103N···O1	0.78(4)	2.25(4)	3.030(5)
N201–H201N···O23	0.77(4)	2.40(4)	3.048(11)
···O13	0.77(4)	2.35(4)	3.023(13)
N202–H202N···O202[a]	0.80(3)	2.05(3)	2.803(4)
N203–H203M···O102	0.84(4)	2.27(4)	3.100(4)
–H203N···O11	0.76(3)	2.71(3)	3.367(18)
···O21	0.76(3)	2.54(3)	3.219(17)
O1–H101W···O12	0.74(6)	2.22(6)	2.954(9)
···O22	0.74(6)	2.69(7)	3.418(20)
···O23	0.74(6)	2.55(5)	3.106(9)
–H102W···O2	0.86(6)	1.91(6)	2.771(5)
O2–H201W···O102	0.80(3)	1.96(3)	2.745(3)

[a] This hydrogen bond is intramolecular.

(bridge)$\sim 1.95_3$ Å and Cr-O (oxalat)$\sim 1.97_4$ Å.*

In Table 6 selected bond lengths in the coordinated carbamate are compared with the analogous distances in the carbamate ion of ammonium-carbamate[14] and in ethylcarbamate.[15] In all three cases a planar carbamate group is found and the present carbamate ligand is seen to show intermediate bond lengths between the free anion and the organic derivative.

The variation in C–H, N–H and O–H bond lengths is as expected, and since it has been shown in accurate studies as *e.g.* that of urea[16] that bond lengths involving hydrogen are highly dependent on the model used to interprete the data, the results in Table 2 will not be discussed further.

The present perchlorate salt contains only one independent perchlorate anion in the space group $C2/c$. The data were, however, as stated above, better represented using two anions, each with a population of ½, for which the average results are given in Table 2. The temperature factors of the oxygen atoms were rather large, but primarily in directions perpendicular to the Cl–O bond, in

* Data for: *trans*-$[Cr(OH_2)_4Cl_2]Cl.2H_2O$,[27,28] $[Cr(chel)(OH_2)OH]_2.4H_2O$,[29] $[Cr(Cl\text{-}dipic)(OH_2)OH]_2.2H_2O$,[29] $Na_4[Crox_2OH]_2.6H_2O$,[30] K[Cr en ox_2].KI.$2H_2O$[31] and K_3[Cr ox_3].$3H_2O$.[32]

Table 6. Comparison with average literature values for bond lengths [Å] in carbamate type derivatives.

	d(C–O′)	d(C–O″)	d(C–N)	Ref.
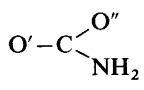	1.28_4	1.28_4	1.36_1	14
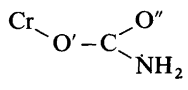	1.29_2	1.24_2	1.34_0	This work
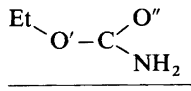	1.33_8	1.22_1	1.34_5	15

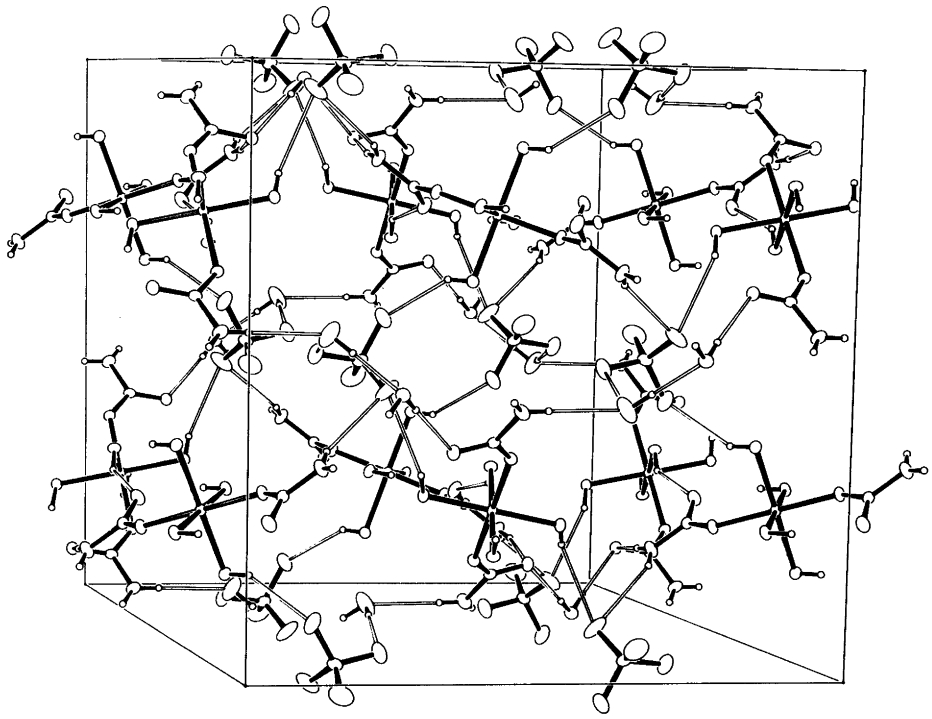

Fig. 3. Packing of the unit cell, *b*-axis vertical, showing the hydrogen bonds between the complex ions, the perchlorate ions and the water molecules, *cf.* Table 5. CH_2-groups of the 'cyclam' ligands are omitted and only the Cl1-perchlorate ion has been included. H-atoms are drawn as spheres with a radius of 0.10 Å, and all other atoms as 35% probability ellipsoids.

agreement with a statically or dynamically disordered anion.

The rather complicated net of hydrogen bonds between complex ions, perchlorate ions and water molecules is shown in Fig. 3. The corresponding distances are given in Table 5.

All hydrogen atoms bound to nitrogen or oxygen are seen to be involved in hydrogen bonding to various types of oxygen atoms. Rather short bonds are formed to both water and carbamate oxygens, whereas the bond to the disordered perchlorate oxygens are somewhat longer.

Acknowledgements. Our thanks are due to F. Hansen for collection of the diffractometer data and to J. Eriksen for assistance with the preparative work.

REFERENCES

1. Ferguson, J. and Tobe, M. *Inorg. Chim. Acta* 4 (1970) 109.
2. Poon, C. K. and Pun, K. C. *Inorg. Chem. 19* (1980) 568.
3. *International Tables for X-Ray Crystallography*, Kynoch Press, Birmingham 1974, Vol. 4.
4. Stewart, J. M., Machin, P. A., Dickinson, C., Ammon, H. L. and Flack, H. *The X-Ray System, Version of 1976*, Technical Report TR-446, Computer Science Center, University of Maryland, College Park 1976.
5. Martin, L. Y., DeHayes, L. J., Zompa, L. J. and Busch, D. H. *J. Am. Chem. Soc. 96* (1974) 4046.
6. Nave, C. and Truter, M. R. *J. Chem. Soc. Dalton Trans.* (1974) 2351.
7. Bosnich, B., Mason, R., Pauling, P. J., Robertson, G. B. and Tobe, M. L. *Chem. Commun.* (1965) 97.
8. Endicott, J. F., Lilie, J., Kuszaj, J. M., Ramaswamy, B. S., Schmonsees, W. G., Simic, M. G., Glick, M. D. and Rillema, D. P. *J. Am. Chem. Soc. 99* (1977) 429.

9. Tasker, P. A. and Sklar, L. *J. Cryst. Mol. Struct. 5* (1975) 329.
10. Campi, E., Ferguson, F. and Tobe, M. L. *Inorg. Chem. 9* (1970) 1781.
11. Mønsted, L. *Acta Chem. Scand. A 32* (1978) 377 and references therein.
12. Mønsted, O. *Acta Chem. Scand. A 32* (1978) 297.
13. Bang, E. and Pedersen, E. *Acta Chem. Scand. A 32* (1978) 833.
14. Adams, J. M. and Small, R. W. H. *Acta Crystallogr. B 29* (1973) 2317.
15. Bracher, B. H. and Small, R. W. H. *Acta Crystallogr. 23* (1967) 410.
16. Mullen, D. and Hellner, E. *Acta Crystallogr. B 34* (1978) 1624.
17. Raymond, K. N., Meek, D. W. and Ibers, J. A. *Inorg. Chem. 7* (1968) 1111.
18. Goldfield, S. A. and Raymond, K. N. *Inorg. Chem. 10* (1971) 2604.
19. Jurnak, F. A. and Raymond, K. N. *Inorg. Chem. 13* (1974) 2387.
20. Alcock, N. W., deMeester, P. and Kemp, T. J. *Acta Crystallogr. B 34* (1978) 3367.
21. Brouty, C., Spinat, P., Whuler, A. and Herpin, P. *Acta Crystallogr. B 33* (1977) 1913.
22. Whuler, A., Spinat, P. and Brouty, C. *Acta Crystallogr. B 34* (1978) 793.
23. Brouty, C., Spinat, P. and Whuler, A. *Acta Crystallogr. B 33* (1977) 3453.
24. Duesler, E. N. and Raymond, K. N. *Inorg. Chim. Acta 30* (1978) 87.
25. Glerup, J., Mønsted, O. and Schäffer, C. E. *Inorg. Chem. 15* (1976) 1399.
26. Glerup, J., Mønsted, O. and Schäffer, C. E. *Inorg. Chem. 19* (1980) 2855.
27. Freeman, H. C. and Dance, I. G. *Inorg. Chem. 4* (1965) 1555.
28. Morosin, B. *Acta Crystallogr. 21* (1966) 280.
29. Cline, S. J., Kallesøe, S., Pedersen, E. and Hodgson, D. J. *Inorg. Chem. 18* (1979) 796.
30. Scaringe, R. P., Hatfield, W. E. and Hodgson, D. J. *Inorg. Chim. Acta 22* (1977) 175.
31. Glasser, L. S. D. and Lethbridge, J. W. *J. Chem. Soc. Dalton Trans.* (1976) 2065.
32. Taylor, D. *Aust. J. Chem. 31* (1978) 1455.

Received August 18, 1981.

Acta Chemica Scandinavica A 36 (1982) 361–364

The Crystal Structure of $Sn_7(OH)_{12}(SO_4)_2$

SIV GRIMVALL

Department of Inorganic Chemistry, University of Göteborg and Chalmers University of Technology, S-412 96 Göteborg, Sweden

The crystal structure of $Sn_7(OH)_{12}(SO_4)_2$ has been determined from Weissenberg film data taken with Cu$K\alpha$ radiation. The symmetry is orthorhombic, space group *Pbca* with $a = 12.472(1)$ Å, $b = 12.649(3)$ Å, $c = 12.676(2)$ Å and $Z = 4$. The structure was refined by the block-diagonal least-squares method to a final R value of 8.9 %.

The Sn(II) atoms are three- or fourfold coordinated by oxygen atoms while Sn(IV) is sixfold coordinated. The tin and oxygen atoms form a three-dimensional network strengthened by sulfate groups and hydrogen bonds. The Sn(II) – O bond distances range from 2.05 to 2.56 Å and the Sn(IV) – O values vary between 1.89 and 2.06 Å.

The crystal structures[1–4] of some compounds of divalent tin have been determined in order to investigate tin(II)-oxygen coordination. The present work provides information on configurations around Sn(II) and Sn(IV). A compound containing the same element in two oxidation states has been included in order to examine the differences arising from the lone pair of electrons in Sn(II). The results from the crystal structure determination of $Sn_7(OH)_{12}(SO_4)_2$ are reported below.

EXPERIMENTAL

Crystals of $Sn_7(OH)_{12}(SO_4)_2$ were prepared together with $Sn_3O(OH)_2SO_4$ according to Ref. 5 but with air access in order to permit oxidation of tin(II) to tin(IV) by atmospheric oxygen. A prism shaped crystal with dimensions 0.20 mm × 0.10 mm × 0.03 mm was selected.

Rotation and Weissenberg photographs ($0kl$–$7kl$) were registered with Ni-filtered Cu radiation. 277 independent reflections were measured with an Optronics rotating-drum microdensitometer. Accurate cell parameters were obtained from a Guinier photograph.

Thermogravimetric (TG) and differential thermal analysis (DTA) in argon atmosphere were carried out to determine the water and sulfur (as SO_2) contents. A Mettler Recording Thermoanalyzer was used with Al_2O_3 as reference. The different values of weight loss gave 8.8 % SO_2 and 7.8 % H_2O as compared with the calculated values 10.4 % SO_2 and 8.8 % H_2O. These deviations are to be expected since the gas was not completely free from oxygen, which caused oxidation of Sn(II) to Sn(IV) thus concealing part of the weight loss (*cf.* Ref. 3).

UNIT CELL AND SPACE GROUP

From rotation and Weissenberg photographs $Sn_7(OH)_{12}(SO_4)_2$ was seen to crystallize in the orthorhombic system. Systematically absent reflections are:

$0\,k\,l$ with $k = 2n+1$
$h\,0\,l$ with $l = 2n+1$
$h\,k\,0$ with $h = 2n+1$

which indicates that the crystals belong to space group *Pbca* (No. 61).[6]

A Guinier photograph calibrated with KCl was taken using Cu$K\alpha_1$ radiation. 33 lines were indexed and unit cell dimensions were refined by means of the programme POWDER.[7] The refined cell parameters (at 21 °C) are:

$a = 12.472(1)$ Å
$b = 12.649(3)$ Å
$c = 12.676(2)$ Å
$V = 1999.6(6)$ Å^3

A list of observed and calculated $\sin^2\theta$ values is available on request. For $Z = 4$ a calculated density of 4.07 g/cm^3 is obtained.

0302-4377/82/040361-04$02.50

Table 1. Fractional coordinates and isotropic thermal parameters (estimated standard deviations within paranthesis).

Atom	x	y	z	B(Å^2)
Sn1	0.2489(7)	0.3361(5)	0.0807(5)	0.09(10)
Sn2	0.1649(9)	0.0808(5)	0.2525(6)	0.07(10)
Sn3	−0.0816(7)	0.2526(5)	0.1632(5)	0.02(10)
Sn4	0.0	0.0	0.5	−0.33(15)
S	0.138(2)	0.365(2)	0.364(2)	−0.3(4)
O1	0.068(5)	0.423(3)	0.433(3)	−1.4(8)
O2	0.256(6)	0.366(4)	0.386(5)	0.3(13)
O3	0.106(5)	0.253(5)	0.369(4)	−0.9(11)
O4	0.127(7)	0.397(4)	0.253(7)	0.4(13)
O5	0.149(8)	0.475(5)	0.021(6)	1.2(16)
O6	0.060(5)	0.147(3)	0.143(4)	−1.1(8)
O7	0.358(5)	0.449(4)	0.154(4)	−0.7(11)
O8	0.475(5)	0.344(4)	0.460(4)	−1.1(10)
O9	0.335(8)	0.135(5)	0.446(6)	1.6(16)
O10	0.029(8)	0.023(7)	0.356(7)	2.2(24)

STRUCTURE DETERMINATION

Lorentz and polarization corrections (DATAP2)[7] and approximate interlevel scale factors based on exposure times were applied. No correction for absorption could be carried out owing to optical reflections from the mounted crystal ($\mu_{CuK\alpha}$=736.9 cm^{-1}).

The structure was determined using Patterson and Fourier (DRF)[7] techniques first in two and later in three dimensions. All refinement was carried out with the block-diagonal least-squares method (BLOCK).[7] Scattering factors according to Cromer and Waber,[8] and Cruickshank's[9] weighting scheme $w=(a+F_o+cF_o^2+dF_o^3)^{-1}$ with a= 80.0, c=0.02 and d=0 were used. The R-value converged to 8.9 %. A difference synthesis calculated after the final cycle of refinement showed no significant peaks apart from some fluctuations in the vicinity of the tin atoms.

Final positional parameters with their standard deviations and temperature factors with their estimated standard deviations are given in Table 1. Selected interatomic distances and angles and their standard deviations (DISTAN)[7] are given in Table 2. A list of observed and calculated structure factors can be obtained on request.

DESCRIPTION AND DISCUSSION OF THE STRUCTURE

The structure can be described as a three-dimensional network of tin and oxygen atoms strengthened by the sulphate groups. No discrete Sn(II)−Sn(II) triangles can be observed (*cf.* Fig. 1) as in $Sn_3O(OH)_2SO_4$[3] but the longer chain-builing Sn−Sn distances found in the latter structure are frequent. The shortest Sn(II)−Sn(II) distances are 3.9−4.0 Å while the shortest Sn(II)−Sn(IV) distances are less then 3.9 Å, owing to enchanced electrostatic attrac-

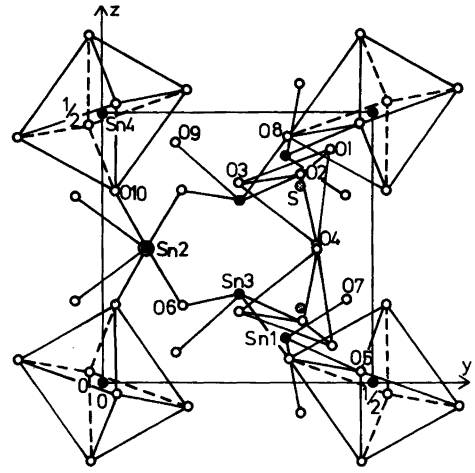

Fig. 1. Projection of the structure of $Sn_7(OH)_{12}(SO_5)_2$ on the *yz* plane. Coordination polyhedra are indicated for tin(IV) and sulphur atoms; bonding distances are indicated for tin(II) atoms. Filled circles represent tin, a ring around a filled circle means two tin atoms at different heights. Dot-filled circles correspond to sulphur atoms and unfilled circles to oxygen.

Table 2. Selected interatomic distances (Å) and angles (°) with their estimated standard deviations in parentheses.

Within the Sn1 coordination polyhedron			
Sn1 – O5	2.28(8)	O5 – Sn1 – O7	88.6(2.6)
Sn1 – O7	2.17(6)	O5 – Sn1 – O9	82.7(3.1)
Sn1 – O9	2.05(8)	O7 – Sn1 – O9	85.2(2.7)
[Sn1 – O4	2.77(9)]		
Within the Sn2 coordination polyhedron			
Sn2 – O6	2.08(5)	O6 – Sn2 – O7	80.8(2.0)
Sn2 – O7	2.11(5)	O6 – Sn2 – O10	92.9(2.8)
Sn2 – O10	2.26(10)	O7 – Sn2 – O10	89.3(2.9)
[Sn2 – O3	2.73(6)]		
Within the Sn3 coordination polyhedron			
Sn3 – O2	2.56(7)	O2 – Sn3 – O6	159.1(1.9)
Sn3 – O6	2.23(5)	O2 – Sn3 – O8	77.0(2.2)
Sn3 – O8	2.07(5)	O2 – Sn3 – O9	81.5(2.5)
Sn3 – O9	2.28(8)	O6 – Sn3 – O8	88.5(2.0)
		O6 – Sn3 – O9	84.6(2.6)
		O8 – Sn – O9	93.7(2.3)
Within the Sn4 coordination polyhedron			
Sn4 – 2 × 05	1.91(10)	O5 – Sn4 – O5	179.9(0)
Sn4 – 2 × 08	2.06(5)	O5 – Sn4 – O8	92.6(2.6)
Sn4 – 2 × O10	1.89(9)		87.4(2.6)
		O5 – Sn4 – O10	94.6(3.7)
			85.4(3.7)
		O8 – Sn4 – O10	96.9(3.1)
			83.1(3.1)
Within the sulfate group			
S – O1	1.43(6)	O1 – S – O2	119.3(3.5)
S – O2	1.49(8)	O1 – S – O3	107.5(3.3)
S – O3	1.48(7)	O1 – S – O4	112.7(3.8)
S – O4	1.48(8)	O2 – S – O3	105.2(3.4)
		O2 – S – O4	105.6(4.4)
		O3 – S – O4	105.6(3.4)

tion to interposed oxygen atoms. The three tin(II) atoms have similar coordination. However, Sn1 and Sn2 have three neighbours at short distances and a fourth more remote (*cf.* Table 2). As in Ref. 3 these two tin atoms can be described as being threefold coordinated. Sn3 has a fourth neighbour somewhat closer and can thus be described as being three- or fourfold coordinated. The Sn(II) – O distances are in good agreement with values[3,10] obtained previously. The O – Sn(II) – O angles (see Table 2) for Sn1 and Sn2 are rather small for threefold coordination[10] and mark a tendency towards fourfold coordination which is also indicated by the position of the fourth oxygen neighbour.

The tetravalent tin atoms denoted Sn4 are sixfold coordinated by a slightly distorted octahedron of oxygen atoms. The Sn(IV) – O distances, which range from 1.89 to 2.06 Å, are within known limits,[11,12] which is also true for the octahedral angles.[13] Short O – O distances outside the coordination groups indicate hydrogen bonding (see Fig. 2). From Fig. 2 it is seen that the basic structural element for Sn(IV) is the $Sn(OH)_6^{2-}$ ion which also is suggested by writing the formula of the compound $[Sn(OH)]_6Sn(OH)_6(SO_4)_2$. No such discrete ion can, however, be observed in the structure.

Outside the Sn(II) coordination groups on the

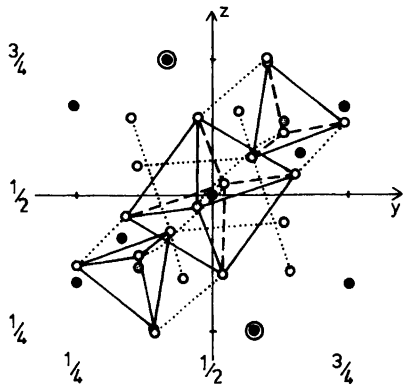

Fig. 2. Projection of the structure of $Sn_7(OH)_{12}(SO_4)_2$ on the *yz* plane. Dotted lines denote short O–O distances (<3 Å) available for hydrogen bonds. The atoms are marked as in Fig. 1.

side away from the oxygen atoms the distances to neighbouring atoms are large. This is a result of the positions of the space-requiring lone pair of electrons.[14] No corresponding effect is found for Sn(IV) (Sn4) because its outer electronic configuration is an inert gas shell.

The sulfate groups are distorted tetrahedra, due to several bonding forces. The O1 oxygen atom is influenced by Sn2 giving the latter atom a feature of more than threefold coordination. Equivalent conditions occur for the O4 atom in relation to Sn1. Sn2 includes the oxygen atom O2 in its coordination polyhedron. At the same time all the sulfate oxygen atoms have short distances to other oxygen atoms outside the coordination polyhedron which indicates participation in hydrogen bonds.

The similarity in the unit cell parameters indicates cubic pseudosymmetry as do the values of the fractional coordinates (*cf.* Table 1). If ½ is added to all *y* coordinates, the positions of atoms Sn1, Sn2, and Sn3 correspond to a twenty-fourfold position in the cubic space group *Pa*3 (No. 205). The atoms O2, O3 and O4 conform to another twenty-fourfold position as do O5, O8, O10 and O6, O7, O9, respectively. Sn4 can be assigned a fourfold position. The fractional coordinates for S can be denoted $(\frac{1}{2}+x, \frac{1}{2}-x, \bar{x})$ and for O1 $(\frac{1}{2}-x, \frac{1}{2}+x, x)$, thus also confirming cubic pseudosymmetry.

Acknowledgements. The author is most grateful to Professor Georg Lundgren for encouraging and valuable discussions concerning this work. She also wishes to thank Professor Bengt Aurivillius for helpful criticism, Dr. Over Lindgren for help with the computer programmes and Dr. Susan Jagner for revising the English text. This work has been supported financially by the Swedish Natural Science Research Council (Contract No. 2318).

REFERENCES

1. Wernfors, G. *Acta Chem. Scand. 15* (1961) 1007.
2. Jelen, A. and Lindqvist, O. *Acta Chem. Scand. 23* (1969) 3071.
3. Grimvall, S. *Acta Chem. Scand. A 29* (1975) 590.
4. Grimvall, S. *Acta Chem. Scand. A 36* (1982) 309.
5. Davies, C. G. and Donaldson, I. D. *J. Chem. Soc. A* (1967) 1790.
6. *International Tables for X-Ray Crystallography*, 2nd Ed., Kynoch Press, Birmingham 1952, Vol. 1.
7. The Programme Library of the Dept. of Inorg. Chem., Göteborg.
8. Cromer, D. T. and Waber, J. T. *Acta Crystallogr. 18* (1965) 104.
9. Cruickshank, D. W. J. *The Equations of Structure Refinements*, Glasgow 1964.
10. Donaldson, J. D. *Prog. Inorg. Chem. 8* (1967) 287.
11. Tournoux, M. *Ann. Chim. Paris (13) 9* (1964) 579.
12. *International Tables for X-Ray Crystallography*, 2nd Ed., Kynoch Press, Birmingham 1962, Vol. 3.
13. Lindqvist, O. *The Oxygen Coordination of Tellurium(IV) and Tellurium(VI)*, Diss., University of Gothenburg, Göteborg 1973.
14. Åström, A. *Det ensamma elektronparets stereokemiska effekt i vissa fasta oxider, oxidflourider och flourider*, Thesis, Institute of Inorganic Chemistry 2, Chemical Centre, Lund 1972.

Received July 1, 1981.

Acta Chemica Scandinavica A 36 (1982) 365–370

Reaction Rate Studies of the Acid Hydrolysis of Some Chromium(III) Complexes. XII. Water Exchange of *cis*-Diamminetetraaquachromium(III) in Aqueous Perchloric Acid

L. MØNSTED[a] and O. MØNSTED[b]

[a] Royal Veterinary and Agricultural University, Thorvaldsensvej 40, DK-1871 Copenhagen V, Denmark and [b] Chemistry Department I, Inorganic Chemistry, H. C. Ørsted Institute, University of Copenhagen, Universitetsparken 5, DK-2100 Copenhagen Ø, Denmark

The rate of water exchange of *cis*-diamminetetraaquachromium(III) in an acid 1 M perchlorate medium has been investigated. The kinetics of this system is characterized by two first order processes, for which the rate constants at 25 °C and activation energies are:

1: $(4.94 \pm 0.37) \times 10^{-5}\ s^{-1}$, $103.4 \pm 2.8\ kJ\ mol^{-1}$;
2: $(1.024 \pm 0.087) \times 10^{-5}\ s^{-1}$, $107.8 \pm 4.2\ kJ\ mol^{-1}$.

Different methods of oxygen-18 labelling have allowed the estimation that the exchange process of both water ligand sites is largely stereoretentive, with the rate constant for the process which moves water ligands between the two sites less than $(0.09 \pm 0.04) \times 10^{-5}\ s^{-1}$ at 25 °C. In less acid solution this latter type of isomerization is detectable and plays a significantly greater role.

Water exchange reactions of all ammineaquachromium(III) ions with equivalently coordinated water ligands, *i.e.* pentaammineaqua-, *cis*- and *trans*-tetraamminediaqua-, *fac*-triamminetriaqua-, *trans*-diamminetetraaqua- and hexaaquachromium(III) have earlier been investigated.[1] The kinetics of water exchange in aquaions with water ligands in different environments are more difficult to interpret in detail, and kinetic experiments have so far been limited to only the pentaaquachlorido-, bromido-, iodido-, and -isothiocyanatochromium(III) cations.[2,3] The present work describes water exchange experiments with the *cis*-diamminetetraaquachromium(III) ion labelled with oxygen-18 at the two different water ligand sites.

0302-4377/82/040365-06$02.50

EXPERIMENTAL

Chemicals. *cis*-$[Cr(NH_3)_2(OH_2)_2Cl_2]Cl$ was prepared according to Andersen and Berg.[4] The sources of other chemicals have been described previously.[1]

Preparation of oxygen-18 labelled cis-*diamminetetraaquachromium(III).* This cation was labelled with oxygen-18 enriched water either by removal of the chloride ligands or by equilibration of the water ligands in *cis*-diammine-*cis*-diaqua-*trans*-dichloridochromium(III), or by a combination of these two methods. The experimental approach follows closely that used previously by us,[1] and the three different methods which were tried are schematically outlined in Fig. 1 and described in detail for some typical experiments below.

Method A. 70 mg *cis*-$[Cr(NH_3)_2(OH_2)_2Cl_2]Cl$ +300 mg Ag(tos)* was reacted in 1.0 ml O^{18}-enriched water, I. P. ~95 %, at 40 °C for 40 min. Excess water was removed by sublimation and the remaining solid dissolved in 0.01 M $HClO_4$. Excess Ag(I) was precipitated by adding excess NaBr-solution, and the resulting *cis*-$[Cr(NH_3)_2(OH_2)_4]^{3+}$-solution was purified by cation exchange chromatography essentially as described in Ref. 1.

Method B. 90 mg *cis*-$[Cr(NH_3)_2(OH_2)_2Cl_2]Cl$ +350 mg Ag(tos) was reacted at 25 °C in 1.0 ml O^{18}-enriched water, I. P. ~95 %, which had been acidified, pH ~1, by the addition of solid *p*-toluenesulfonic acid. This accelerated removal of the chloride ligands turned out, however, to be a rather slow process, and it was therefore stopped after 20 min when about 90 % of the chromium was present as the monochlorido complex. Excess

* tos ≡ *p*-toluenesulfonate ≡ *p*-$CH_3C_6H_4SO_3^-$.

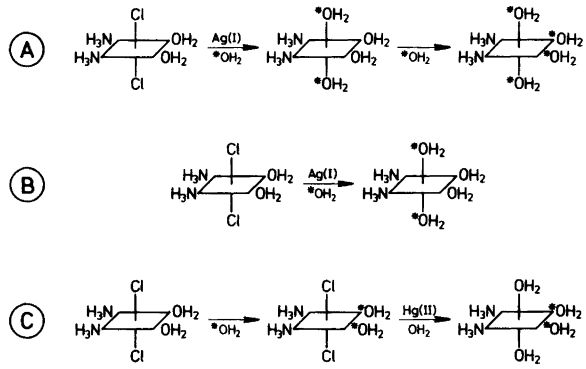

Fig. 1. Schematic drawing of different methods for oxygen-18 labelling *cis*-diammine̲tetraaquachromium(III). *Cf.* the experimental section.

O^{18}-water and Ag(I) was removed as described at method A, and the monochlorido complex was isolated by cation exchange chromatography by using a 15 cm × 2 cm Sephadex SP-C-25 filled column: The band of dipositive cations, *i.e.* the monochlorido- and small amounts of monotosylate complex, could be separated from other chromium species by elution with 0.4 M $NaClO_4$-solution at pH ~ 2. The eluate, about 25 ml, containing the monochlorido complex was reacted with Hg(II) at pH ~ 1. The production of the *cis*-diamminetetraaquachromium(III) ion was followed spectrophotometrically, and was essentially quantitative within 5 min. Excess Hg(II)-aqua ions were complexed with Br^- and the resulting *cis*-diamminetetraaquachromium(III) solution purified as described at method A.

Method C. 100 mg *cis*-$[Cr(NH_3)_2(OH_2)_2Cl_2]Cl$ was aged in 1.0 ml of ^{18}O-enriched water, I.P. ~95 %, at pH ~1 for 2 h at 25 °C. Under these conditions the half-life for release of the first chloride ligand is about 3.2 h.[8] Excess water was removed by sublimation and *cis*-$[Cr(NH_3)_2(OH_2)_2Cl_2]^+$ which is the only monopositive chromium(III) species in the reaction product was obtained free of other chromium species by cation exchange chromatography as described at method B. 0.2 M $NaClO_4$-solution at pH ~2 was used as eluent. Production and purification of *cis*-diamminetetraaquachromium(III) from this eluate followed closely method B, *i.e.* reaction with Hg(II) followed by cation exchange chromatography.

In most C-type experiments attempts were made to accelerate the water exchange using CO_2/HCO_3^- which is known to be an effective catalyst for oxygen exchange in the pentaammineaquachromium(III) ion.[5] The amount of oxygen-18 introduced was, however, not reproducible (experiments C1 and C3 – C6 in Table 1), and was also significantly smaller than that of the uncatalyzed reaction (experiment C2 in Table 1).

All manipulations of oxygen-18 enriched complexes including the ion exchange separations were carried out in the dark and at temperatures below 5 °C in order to minimize water exchange prior to the kinetic runs. *cis*-Diamminetetraaquachromium-(III) prepared by all three methods had spectral characteristics in complete agreement with those of this cation prepared by other methods.[6]

Kinetic measurements, methods of analyses, spectrophotometric measurements and *mass spectrometric measurements* were performed essentially as described previously.[1]

Method of calculation. The measured δ-values were corrected for isotope fractionation during sublimation by the empirical function earlier established.[1] The corrected δ-values as function of time, $\delta_{corr,t}$, were approximated by a curve calculated from:

$$\delta_t = \delta_0 + \delta_1[1 - \exp(-k_1 t)] + \delta_2[1 - \exp(-k_2 t)]$$

with the two rate constants k_1 and k_2 and the three measures of oxygen-18 concentrations δ_0, δ_1 and δ_2, *cf.* Appendix and Ref. 1, estimated by minimization of:

$$\sum_t (\delta_{corr,t} - \delta_t)^2 / \sigma^2(\delta_{corr,t})$$

by non-linear regression analysis. $\sigma^2(\delta_{corr,t})$ is the variance of $\delta_{corr,t}$. Some examples of the agreement between calculated curves and experimental data are shown in Fig. 2. The further calculations to yield activation parameters were carried out as described previously.[7] It should be noted that the mathematical form of eqn. (1), with k_1 not very

Table 1. Summary of kinetic data for water exchange in *cis*-$[Cr(NH_3)_2(OH_2)_4]^{3+}$ in 0.50 M $HClO_4$ + 0.50 M $NaClO_4$.

Exp.[a]	Temp. [°C]	[Cr(III)] [mM]	δ'_1 [^{18}O/Cr]	δ'_2 [^{18}O/Cr]	$\delta'_1+\delta'_2$ [^{18}O/Cr]
A1	15.1	1.52	1.48±0.24	1.34±0.19	2.82±0.06
A2	24.9	1.04	1.49±0.14	1.81±0.13	3.30±0.04
A3	35.1	1.20	1.31±0.15	1.73±0.14	3.04±0.04
B1	25.2	2.22	0.53±0.06	0.76±0.05	1.29±0.03
B2	25.2	1.84	0.50±0.07	0.76±0.05	1.26±0.03
C1	15.2	2.39	0.38±0.06	0.25±0.05	0.66±0.02
C2	25.0	1.80	0.84±0.06	0.36±0.06	1.20±0.02
C3	25.2	2.29	0.47±0.06	0.22±0.09	0.69±0.04
C4	25.2	1.61	0.41±0.05	0.10±0.05	0.51±0.02
C5	25.2	2.38	0.39±0.04	0.10±0.04	0.49±0.02
C6	35.1	3.05	0.50±0.04	0.27±0.04	0.77±0.01

k_1 (25 °C) ~ (4.94±0.37) × 10^{-5} s^{-1}; $\Delta H_1^{\ddagger}$ ~ 100.9±2.8 kJ mol^{-1}; $\Delta S_1^{\ddagger}$ ~ +11±9 J K^{-1} mol^{-1}
k_2 (25 °C) ~ (1.024±0.087) × 10^{-5} s^{-1}; $\Delta H_2^{\ddagger}$ ~ 105.3±4.2 kJ mol^{-1}; $\Delta S_2^{\ddagger}$ ~ +13±14 J K^{-1} mol^{-1}
$\rho(k_1,k_2)^b$ ~ 0.741; $\rho(\Delta H_1^{\ddagger},\Delta H_2^{\ddagger})^b$ ~ 0.873

[a] Prefixes A, B and C refer to the method of preparation of *cis*-$[Cr(NH_3)_2(OH_2)_4]^{3+}$ as described in the experimental section. [b] Correlation coefficients.

different from k_2, seriously limits the accuracy of the kinetic parameters for this system compared to systems in which only *one* exchange process takes place. Therefore the uncertainties of rate constants and activation energies for the *cis*-diamminetetraaquachromium(III) ion are significantly larger, but strongly positively correlated, *cf.* the correlation coefficients, ρ, of Table 1, than those earlier determined by us, using the same experimental approach, for aqua complexes with only one type of water ligands present.

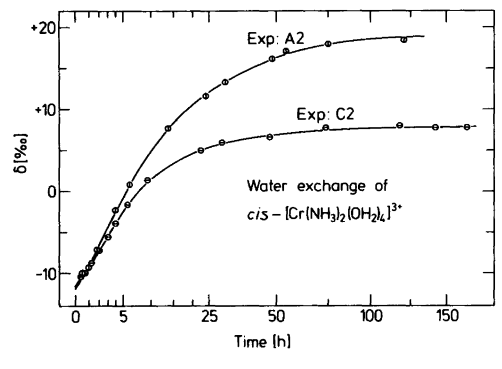

Fig. 2. Reaction kinetic experiments for water exchange in *cis*-diamminetetraaquachromium(III). The solid curves have been calculated from the parameters of Table 1.

RESULTS AND DISCUSSION

Exchange of oxygen-18 labelled water from *cis*-diamminetetraaquachromium(III) equilibrated in this solvent takes place with retention of the ammine configuration. The exchange follows a sum of two exponential functions and this is illustrated by exp. A2 in Fig. 2. Two rate constants can be determined from such an experiment, and as they differ by only a factor of about 5, *cf.* Table 1, the kinetic parameters cannot be very accurately determined, *cf.* the experimental section. From the experiments A1, A2 and A3 of Table 1 it seems, however, that the preexponential factor to the term containing the larger rate constant, *i.e.* δ'_1, is smaller than δ'_2 and an average ratio $\delta'_1/\delta'_2 \sim 0.82 \pm 0.09$ is obtained from these three experiments. If the water exchange takes place with retention of configuration of not only the ammonia ligands which is observed experimentally but also of the unsubstituted water ligands, δ'_1 and δ'_2 are: $\delta'_1 = \varkappa_N$ and $\delta'_2 = \varkappa_O$, *cf.* Appendix, and $\delta'_1/\delta'_2 = 1$ should therefore be expected for these experiments. A value smaller than 1 could point towards a larger extent of exchange during the purification steps of the 'fast' water ligand site than of the 'slow' site, but it could also be that the smaller ratio is the result of a non-stereoretentive water exchange reaction of the type

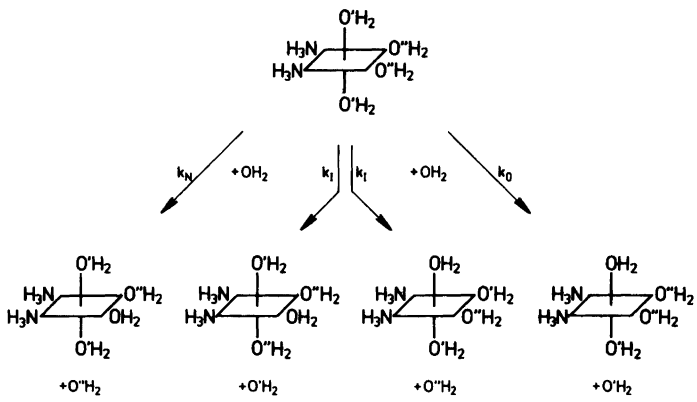

Fig. 3. Water exchange in *cis*-diamminetetraaquachromium(III) by stereoretentive processes, k_N and k_O, and by processes accompanied by isomerization, k_I.

labelled with k_I in Fig. 3. The mathematics of this latter suggestion is analyzed in Appendix, and will give δ-ratios smaller than 1.*

To differentiate between the two possibilities outlined above it was attempted to label the *cis*-diamminetetraaquachromium(III) ion stereospecifically with oxygen-18 by induced silver(I) or mercury(II) aquations as schematically outlined in Fig. 1. Such induced aquations normally proceed with retention of configuration, and this observation was the basis for the two attempted preparative routes B and C in Fig. 1.

Silver(I) accelerated removal of the chloride ligands in oxygen-18 enriched water, from a complex with the water ligands *trans* to the ammonia ligands of normal isotopic distribution, was first tried. This method, B, however, turned out to be less successful as the rate of water exchange in the chloride ligand containing species was apparently fast enough to label significant amounts of water ligands already present in the complex by solvent exchange. Thus, even if the accelerated chloride ligand removal was stopped at the formation of monochloridocomplex, the generated *cis*-diamminetetraaqua-ion contained about 1.28 ^{18}O/Cr, which based on a 95 % oxygen-18 content of the reactant water, means that at least $1.28-0.95\sim0.33$ ^{18}O/Cr are introduced by a solvent exchange path. It is significant, however, that the average δ-ratio for this type of experiment: $\delta_1'/\delta_2' \sim 0.76\pm0.09$ is comparable to but slightly smaller than that observed for the kinetic experiments based upon *cis*-diammine ion labelled by method A.

The faster water exchange in the dichlorido ion of the starting material observed by the B-type experiments provided the basis for some more successful attempts to label the water ligands *trans* to the ammonia ligands by method C of Fig. 1. For this type of experiment δ_1' was invariably found greater than δ_2', the average ratio being $\delta_1'/\delta_2' \sim 2.0\pm0.3$.

The presence of two differently coordinated types of water ligands in *cis*-diamminetetraaquachromium(III) provides an opportunity, not present in complexes with only equivalently coordinated water ligands, to investigate the relative importance of *cis*, k_N- and k_O-paths of Fig. 3, *vs.* *trans* attack, k_I-paths of Fig. 3, of the entering water ligand by the water exchange reactions. Kinetic schemes composed of these types of reactions may be analyzed as shown in Appendix.

*Three types of *trans* attack reactions have not been included in Fig. 3.

One of these is the reaction which isomerizes the *cis*-diammine to the *trans*-diammine. This reaction is not observed experimentally but at 70 °C it is estimated to have a rate constant which is smaller than 0.06×10^{-5} s^{-1}.[6]

The other reaction shifts one of the water ligands between the two equivalent positions *trans* to ammonia simultaneously with exchange of the other water ligand of this type. Contributions from such a process will therefore be described by the k_N-path.

Finally the third reaction type is that which moves an ammonia ligand but maintains the *cis*- diammine configuration. It can be shown that contributions from this type of process will be described by both the k_O and k_I rate constants. Ammine isomerization processes are, however, at least a thousandfold slower than the present water exchange reactions, and contributions from this latter type of process are therefore very unlikely.

The variation in δ_1'/δ_2' ratios as function of the mode of preparation of the *cis*-diammine ion and the known configuration of the diamminediaquadichloridochromium(III) ion of the starting material[8] unequivocally assigns the greater rate constant primarily to the reactivity of the water ligands *trans* to the ammonia ligands, the k_N-path.

Since k_N, k_O and k_I are all positive or zero, eqn. Ap 1 and the experimental data in Table 1 limit k_I to values smaller than 0.275×10^{-5} s^{-1} at 25 °C. For this range of k_I-values $16k_I^2 \ll (k_N - k_O)^2$ and eqn. Ap 1 may be reduced to

$$k_1 \sim k_N + 4k_I$$
$$k_2 \sim k_O + 4k_I \quad (1)$$

The validity of these approximations may be tested by noting that they give:

$$k_I \lesssim (0.26 \pm 0.02) \times 10^{-5} \text{ s}^{-1}$$

in good agreement with the maximum value of 0.275×10^{-5} s^{-1} derived from the exact equations.

A more detailed analysis of the δ'-values can further significantly reduce this value. Eqn. Ap. 2 in the Appendix may be reduced by applying eqn. 1 to give:

$$\varkappa_N \sim \delta_1' + \frac{2k_I(\delta_1' + \delta_2')}{k_1 - k_2}$$
and (2)
$$\varkappa_O \sim \delta_2' - \frac{2k_I(\delta_1' + \delta_2')}{k_1 - k_2}$$

Solvent exchange prior to the kinetic run will most likely make $\varkappa_N$ smaller than $\varkappa_O$. Assuming $\varkappa_N \lesssim \varkappa_O$ allows the much more restrictive estimate on k_I at 25 °C:

$$k_I \lesssim (0.09 \pm 0.04) \times 10^{-5} \text{ s}^{-1} \quad (3)$$

to be made using eqn. 2 and averaged δ'-data for experiments A1, A2 and A3. In combination with eqn. 1 this allows estimation of k_N and k_O at 25 °C as:

$$(4.6 \pm 0.4) \times 10^{-5} \text{ s}^{-1} \lesssim k_N \lesssim (4.9 \pm 0.4) \times 10^{-5} \text{ s}^{-1}$$

and

$$(0.66 \pm 0.18) \times 10^{-5} \text{ s}^{-1} \lesssim k_O \lesssim (1.02 \pm 0.09) \times 10^{-5} \text{ s}^{-1}$$

i.e. the exchange of both types of water ligands is largely stereoretentive in 0.5 M acid solution.

At higher pH-values the water exchange is less stereoretentive, and this may be demonstrated by analyzing the C-type experiments using the upper limit for k_I given by eqn. 3. For exp. C2 it may thus be calculated from eqns. 2 and 3:

$$0.84 \pm 0.06 \lesssim \varkappa_N \lesssim 0.90 \pm 0.07$$
and (4)
$$0.36 \pm 0.06 \gtrsim \varkappa_O \gtrsim 0.30 \pm 0.07$$

The non-zero value for $\varkappa_O$ is particularly significant as this means that some isomerization of the water ligands must have taken place prior to the kinetic runs. This isomerization may occur either at the generation of the ammineaqua ion from the dichlorido complex, or, more likely, during the process of purification either by reaction through a base-catalyzed path at pH ~ 2 where the separations are carried out or catalyzed by the ion exchange resin. In this context it is noteworthy that the prepared aqua ions contain less oxygen-18 than estimated on the basis of the purity of the reactant oxygen-18 water, and the rate constants for water exchange in more acid solution. k_1 of Table 1 extrapolated to 0 °C, the temperature at which the separations are carried out, indicates $t_{1/2} \sim 180$ h for this process, to be compared with the time for purification of less than 1 h. Therefore base catalysis does probably operate although resin accelerated reactions are also known to occur for some similar complex ions.[9]

The contribution from an isomerization process to the base- or resin-catalyzed reaction can also be seen to be significantly greater than that observed for the kinetic experiments in strongly acid solution. Thus if it is assumed that the mercury(II) treatment of the dichlorido-complex generates the cis-diamminetetraaquachromium(III) ion with $\varkappa_O \sim 0.00$ and $\varkappa_N \lesssim 1.90$, the upper limit for k_1: $k_1 \lesssim 0.09 \times 10^{-5}$ s^{-1} will give $\varkappa_N \gtrsim 1.11$ and $\varkappa_O \lesssim 0.09$, for exp. C2 with $\varkappa_N + \varkappa_O = 1.20$, to be compared with the estimated values in eqn. 4 above.

In conclusion the water exchange reactions of *cis*-diamminetetraaquachromium(III) proceeds mainly by the k_N and k_O paths, and although both these paths may contain contributions from a nonstereoretentive process the small value for k_I makes it likely that the well-established stereoretentivity of thermal aquations of chromium(III)

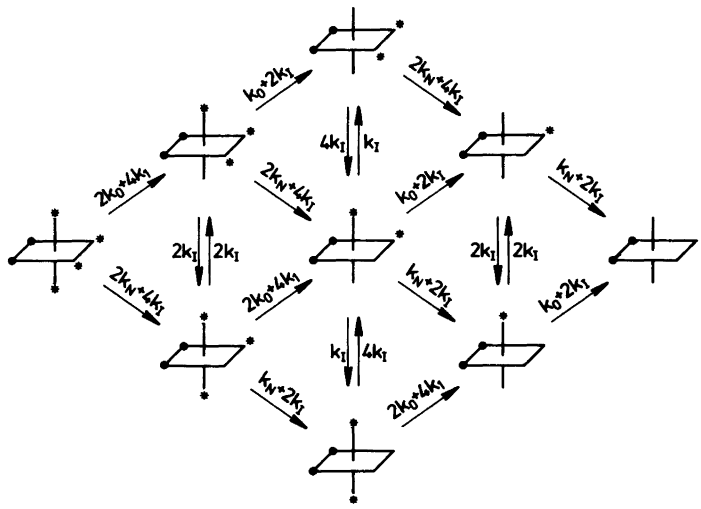

Fig. 4. Complete reaction scheme for irreversible oxygen-18 aquation in *cis*-diamminetetraaquachromium(III) by k_N, k_O and k_I paths of Fig. 3. ● $=NH_3$; * $=^{18}OH_2$.

complexes is also observed for the present water exchange reactions in acid solution. However, significant water ligand isomerization does take place during the preparation of the *cis*-diamminetetraaquachromium(III) ion *via* a base- or ion exchange resin-catalyzed path.

A further discussion of the kinetic data reported here will be given when current investigations on the water exchange reactions of *mer*-triamminetriaqua- and amminepentaaquachromium(III) have been concluded.

Acknowledgement. The authors wish to thank the Geophysical Isotope Laboratory at the University of Copenhagen, particularly Dr. Niels Gundestrup, for carrying out the mass spectrometric analyses.

APPENDIX

The complete reaction scheme for water exchange in *cis*-diamminetetraaquachromium(III) by the elementary reactions shown in Fig. 3 is given in Fig. 4. This scheme has been analyzed in detail, and it can be shown that the concentration of oxygen-18 in the solvent, $[^{18}O]$, as function of time, t, is given by

$$[^{18}O]=[^{18}O]_{t=0}+[Cr]\times[\delta_1'(1-\exp(-k_1t))+\delta_2'(1-\exp(-k_2t))]$$

with

$$(k_1,k_2)=\tfrac{1}{2}(k_N+k_O+8k_I\pm\sqrt{(k_N-k_O)^2+16k_I^2}) \quad \text{(Ap. 1)}$$

$$\delta_1'=\frac{(k_O+6k_I-k_1)(\varkappa_N(k_N+4k_I-k_2)-2\varkappa_Ok_I)}{(k_N+4k_I-k_2)(k_O+4k_I-k_1)-4k_I^2}$$

and (Ap. 2)

$$\delta_2'=\frac{(k_N+6k_I-k_2)(\varkappa_O(k_O+4k_I-k_1)-2\varkappa_Nk_I)}{(k_N+4k_I-k_2)(k_O+4k_I-k_1)-4k_I^2}$$

where $\varkappa_N$ and $\varkappa_O$ are the average number of oxygen-18 labelled water molecules *trans* to ammonia and water, respectively, at the start of the kinetic experiment.

REFERENCES

1. Mønsted, L. and Mønsted, O. *Acta Chem. Scand. A 34* (1980) 259 and references therein.
2. Moore, P., Basolo, F. and Pearson, R. G. *Inorg. Chem. 5* (1966) 223.
3. Bracken, D. E. and Baldwin, H. W. *Inorg. Chem. 13* (1974) 1325.
4. Andersen, P. and Berg, T. *To be published.*
5. Alexander, W. and Early, J. *J. Am. Chem. Soc. 92* (1970) 2299.
6. Mønsted, L. and Mønsted, O. *Acta Chem. Scand. 27* (1973) 2121.
7. Mønsted, L. and Mønsted, O. *Acta Chem. Scand. A 32* (1978) 19.
8. Mønsted, L. and Mønsted, O. *Acta Chem. Scand. A 32* (1978) 917.
9. Mønsted, L. and Mønsted, O. *Acta Chem. Scand. A 28* (1974) 1040.

Received August 21, 1981.

Acta Chemica Scandinavica A 36 (1982) 371–376

Acid-catalyzed Hydrolyses of Bridged Bi- and Tricyclic Compounds. XX. The Location of the Transition State in the Hydration of Norbornenes and Nortricyclanes

MARTTI LAJUNEN and ARJA ANDERSSON

Department of Chemistry and Biochemistry, University of Turku, SF-20500 Turku 50, Finland

The isotopic Brönsted α_i values have been measured for the $A\text{-}S_E2$ hydration of 2-methyl-*endo*-5-hydroxy-2-norbornene (*1*, 0.73 ± 0.03 at 298.2 K), 5-methylene-2-methyl-*endo*-2-hydroxynorbornane (*2*, 0.91 ± 0.03 at 318.2 K) and 1,6-dimethyl-3-hydroxynortricyclane (*3*, 0.65 ± 0.02 at 328.2 K). They are similar to those measured earlier for less reactive norbornenes and nortricyclanes with the product-like transition states and do not clearly indicate earlier transition states for the faster proton transfer reactions. The large experimental scattering of the α_i values and the rather narrow rate scale, however, make it difficult to draw conclusions. A comparison of the α_i values with the ordinary Brönsted α values measured earlier in carboxylic acid buffers for the $A\text{-}S_E2$ hydration of several unsaturated compounds indicates that the Hammond postulate is probably valid: α or $\alpha_i = -(0.020\pm0.006)\log(k_{H^+}/\mathrm{dm^3\ mol^{-1}\ s^{-1}}) + (0.67\pm0.02)$, if $0.5 \leq \alpha$ or $\alpha_i \leq 1$.

The generally accepted mechanism for the acid-catalyzed hydration of the carbon–carbon double bond and the three-membered carbon ring is the rate-determining proton transfer from a catalytic acid to a substrate followed by the fast water attack on the carbocation ($A\text{-}S_E2$ mechanism).[1-3] The reaction is subject to general acid catalysis, whose observation is usually easy in dilute buffer solutions if the reaction rate is quite great (*e.g.* vinyl ethers).[1-2] The Brönsted relation (1) indicates the correlation between the second-order rate constant

$$k_{HA}/p = G(K_{HA}q/p)^{\alpha} \qquad (1)$$

k_{HA} and the dissociation constant of the catalytic acid K_{HA} in different buffer solutions. The constants q and p are statistical factors and α and G are parameters, which depend on the nature of the reaction and on the conditions but not on the acid used. The exponent of the Brönsted relation, the so-called Brönsted α, is believed to characterize the degree of proton transfer in the transition state ($0 \leq \alpha \leq 1$).[1-2]

If the reaction is rather slow (*e.g.* simple alkenes and cyclopropanes), the detection of general acid catalysis in buffer solutions is difficult.[1,2,4,5] In this case measurements can be made in acidic light water–heavy water mixtures, where the kinetic solvent deuterium isotope effect obeys eqn. (2),[1,2,6,7] when the proton transfer occurs from the lyonium ion L_3O^+ (L = H or D) to a substrate S [eqn. (3)].

$$\frac{k_x}{k_H} = \frac{(1-x+x\phi_1)(1-x+x\phi_2)^2}{(1-x+xl)^3}\,F(x) \qquad (2)$$

$$S + L_3O^+ \overset{l}{\rightleftharpoons} \{S\cdots L\cdots OL_2\}^+ \overset{\phi_1\ \ \phi_2}{\rightarrow} SL^+ + OL_2 \qquad (3)$$

The parameters l, ϕ_1 and ϕ_2 are isotopic fractionation factors for the lyonium ion, the transferring hydrogen and the remaining hydrogens in the transition state, and F(x) is a correction factor (mostly assumed to be unity), which takes into account the transfer energies of the substrate, the lyonium ion and the transition state from H_2O to a H_2O-D_2O mixture of deuterium atom fraction x. The fractionation factor ϕ_2 depends on l according to the exponential eqn. (4),[6] where α_i (isotopic Brönsted α) characterizes the degree of proton

$$\phi_2 = l^{1-\alpha_i} \qquad (4)$$

0302-4377/82/040371-06$02.50

transfer in the transition state ($0 \leq \alpha_i \leq 1$).

In many reactions both the ordinary Brönsted α and the isotopic α_i have been determined and no systematic deviations have been observed between them although single values often differ by 0.1 or even more,[1,2] possibly at least partly due to an experimental error. In reality α depends to some extent on the character of the catalytic acid (charged or uncharged)[8] and α_i is very sensitive to experimental scattering.[2] However, anomalous values have been found for α and explanations have been given to them.[2,9,10]

Isotopic technique has been used to detect a general acid catalysis in the hydration of substituted norbornenes and nortricyclanes,[11-14] since the observations in buffer solutions were uncertain.[5] The following α_i values were measured: from 0.77 to 0.94 (av. 0.85) for 5-hydroxy-2-norbornenes,[11] from (0.49?) 0.59 to 0.79 (av. 0.72) for 5-hydroxymethyl-2-norbornenes,[14] and from 0.67 to 0.96 (av. 0.83) for 3-hydroxynortricyclanes[12] (possible methyl substituents have not been mentioned, *cf.* Table 2). The values (0.5?, $0.6 \leq \alpha_i \leq 1$) indicate that the transition state is mostly product-like.

The displacement of a 2- or 3-hydrogen atom by a methyl group increases the hydration rate of 5-hydroxy-2-norbornenes by a factor of 10^4 to 10^5.[15,16] Surprisingly, the activation entropies also change in many cases from slightly negative to slightly positive values but the solvent deuterium isotope effects remain normal (k_D/k_H 0.5 to 0.6). In order to see if the hydration mechanism possibly changes from the slow proton transfer (*A*-S_E2 mechanism) to a fast pre-equilibrium protonation of the substrate (*A*-1 or *A*-2 mechanism) or the location of the transition state of the *A*-S_E2 mechanism moves toward the initial state (according to the Hammond postulate),[17] the α_i values are determined in this work for 2-methyl-*endo*-5-hydroxy-2-norbornene (*1*) and 5-methylene-2-methyl-*endo*-2-hydroxynorbornane (*2*) in H_2O-D_2O mixtures.

The displacement of 1- or 1- and 6-hydrogen(s) by methyl increases the reaction rate by a small factor of 5 to 6 (1-methyl) and 17 (1,6-dimethyl) in the hydration of 3-hydroxynortricyclane.[12,18] The mean value of α_i does not change markedly due to the 1-methyl substitution [0.85 (1-H)→0.82 (1-Me)]. The effect of the 1,6-dimethyl substitution is studied in this work by measuring α_i for the hydration of 1,6-dimethyl-3-hydroxynortricyclane(*3*).

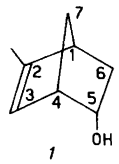

1

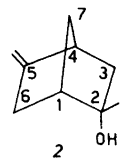

2

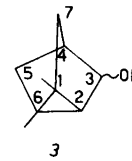

3

EXPERIMENTAL

The syntheses of the substrates (*1*-*3*) have been described.[15,18]

The kinetic measurements were made in 0.1 mol dm^{-3} $LClO_4$ (L_2O) solutions by following the disappearance of the substrate by taking samples after proper intervals during 2.5 half-lives, neutralizing them with 1.3 mol dm^{-3} ammonia and analyzing by GLC with cyclohexanol or norcamphor as inert internal standard. First-order kinetics was always observed. The measurements were repeated at least once, often twice or more times. In the cases of *1* and *2* a little isomerization (*e.g.* 2-methyl-5-hydroxy-2-norbornene to 5-methylene-2-hydroxynorbornane) occurred in the gas chromatograph, which decreased the accuracy of the measurements. Isomerization due to the acid-catalyzed dehydration of the alcoholic substrates [$R^1OH + H^+ \rightleftharpoons (R^1)^+ + H_2O \rightleftharpoons (R^2)^+ + H_2O \rightleftharpoons R^2OH + H^+$] was not observed (*cf.* Ref. 15).

RESULTS AND DISCUSSION

The observed solvent deuterium isotope effects for the hydration of the substrates in 0.1 mol dm^{-3} perchloric acid of varying deuterium atom fraction (x) are listed in Table 1. The isotope effects k_D/k_H ($k_x = k_H$ when $x=0$ and $k_x = k_D$ when $x=1$) for the bicyclic substrates *1* and *2* are fairly similar to those measured earlier for the same compounds: 0.543 (this work at 298.2 K) and 0.507 (at 293.2 K)[15] for *1* and 0.618 (this work at 318.2 K) and 0.587 (at 303.2 K)[15] for *2*. They, as well as the value for *3* (0.513 at 328.2 K), are typical of the rate-determining proton transfer from the lyonium ion to the carbon–carbon double bond or the three-membered carbon ring.[11-14]

Eqn. (2) fitted the experimental data fairly well. The values 0.69 at 298.2 K and 0.71 at 318.2 and 328.2 K were used for the fractionation factor of the lyonium ion (*l*).[19] The fractionation factor of the hydroxylic hydrogen of the substrates was assumed to remain unchanged in the initial and transition states. $F(x)$ was approximated to unity. The computed fractionation factors ϕ_1 and ϕ_2 (see eqn. (3)) and the isotopic α_i values [from eqn. (4)]

Table 1. Observed and calculated [eqn. (2)] solvent deuterium isotope effects in the hydration of 2-methyl-*endo*-5-hydroxy-2-norbornene (*1*), 5-methylene-2-methyl-*endo*-2-hydroxynorbornane (*2*) and 1,6-dimethyl-3-hydroxynortricyclane (*3*) in 0.1 mol dm^{-3} $LClO_4$ (L=H or D) of deuterium atom fraction x. Isotopic fractionation factors ϕ_1 and ϕ_2 [see eqn. (3)] and isotopic α_i values have been calculated from eqns. (2) and (4).

Substrate (Temp.)	x	k_x/k_H(obs.)	k_x/k_H(calc.)	ϕ_1, ϕ_2 and α_i
1	0	1.000	1.000	
(298.2 K)	0.2	0.958	0.986	
	0.4	0.932	0.951	
	0.5	0.923	0.922	$\phi_1=0.225(6)$
	0.6	0.869	0.883	$\phi_2=0.906(8)$
	0.7	0.849	0.832	$\alpha_i=0.73(3)$
	0.8	0.788	0.764	
	0.9	0.686	0.676	
	1.0	0.543	0.563	
2	0	1.000	1.000	
(318.2 K)	0.2	0.958	1.002	
	0.4	0.964	0.983	
	0.5	0.962	0.962	$\phi_1=0.240(6)$
	0.6	0.950	0.930	$\phi_2=0.969(8)$
	0.7	0.883	0.885	$\alpha_i=0.91(3)$
	0.8	0.844	0.823	
	0.9	0.737	0.739	
	1.0	0.618	0.629	
3	0	1.000	1.000	
(328.2 K)	0.2	0.964	0.968	
	0.4	0.923	0.917	$\phi_1=0.235(4)$
	0.6	0.819	0.835	$\phi^2=0.888(5)$
	0.7	0.787	0.779	$\alpha_i=0.65(2)$
	0.8	0.717	0.710	
	0.9	0.626	0.624	
	1.0	0.513	0.518	

are also given in Table 1 together with the k_x/k_H values calculated from them. The values of ϕ_1 (0.23 to 0.24), ϕ_2 (0.89 to 0.97) and α_i (0.65 to 0.91) are similar to those measured earlier for the hydration of norbornenes and nortricyclanes.[11,12,14]

The comparison of the α_i values for the substrates *1* and *2* (0.73 and 0.91) with the mean values for much less reactive compounds, 5-hydroxy-2-norbornenes (0.85) and 5-hydroxymethyl-2-norbornenes (0.72), and the comparison of the α_i value for *3* (0.65) with the mean value of the slightly less reactive 3-hydroxynortricyclanes (0.83) do not indicate clearly the movement of the transition state toward the initial state as the Hammond postulate predicts.[17] This may, however, be due to the large experimental error of the α_i values (it is more probable that the error limits are 0.1 or even more, rather than 0.01−0.05 as calculated by the computer) and to the narrow rate scale. The values of ϕ_1 (0.2) and α_i (<1), however, eliminate other possible reaction mechanisms than $A\text{-}S_E2$ (see above).

It is of interest to compare α_i values presented by us for norbornenes and nortricyclanes, including a similar value measured for the hydration of isobutene (*ca.* 0.9 by Gold and Kessick or 0.84 as recalculated by Williams and Kreevoy),[1,20] with the Brönsted α values measured for the rate-determining protonation ($A\text{-}S_E2$ mechanism) of more reactive unsaturated compounds (vinyl ethers, a vinyl thioether, a bridgehead olefin, azulenes, halomercuro olefins and keten acetals) in carboxylic acid buffers.[21-28] This comparison is made in Table 2 and Fig. 1 and it more than doubles the rate scale (from 4.8 to 10.6 powers of ten). The interpretation of the data is, however, not easy.

Table 2. Values of ordinary Brönsted α in carboxylic acid buffers and of isotopic α_i in 0.1 mol dm^{-3} $LClO_4$ (L = H or D), and rate constants (k_{H^+}) in 1.0 mol dm^{-3} aqueous perchloric acid at 298.2 K (unless otherwise marked) for rate-determining proton transfer reactions.

Substrate	No.	α	α_i	k_{H^+}/dm^3 mol^{-1} s^{-1}	Ref.
2-Methyl-*endo*-5-hydroxy-2-norbornene	*1*		0.73(3)	2.6×10^{-2}	15, this work
5-Methylene-2-methyl-*endo*-2-hydroxynorbornane	*2*		0.91(3)[a]	4.1×10^{-3}	15, this work
1,6-Dimethyl-3-hydroxynortricyclane	*3*		0.65(2)[b]	4.7×10^{-5}	18, this work
exo-5-Hydroxy-2-norbornene	*4*		0.77(5)[c]	4.3×10^{-7}	11, 30
endo-5-Hydroxy-2-norbornene	*5*		0.94(1)[c]	9.9×10^{-7}	11, 30
exo-5-Hydroxymethyl-2-norbornene	*6*		0.59(2)[c]	8.9×10^{-6}	14
endo-5-Hydroxymethyl-2-norbornene	*7*		0.79(2)[c]	1.23×10^{-5}	14
5-Methyl-*exo*-5-hydroxymethyl-2-norbornene	*8*		0.79(1)[c]	8.5×10^{-6}	14
5-Methyl-*endo*-5-hydroxymethyl-2-norbornene	*9*		0.49(1)?[c]	1.07×10^{-5}	14
3-Hydroxynortricyclane	*10*		0.85(2)[c]	2.8×10^{-6}	12, 30
1-Methyl-*cis*-3-hydroxynortricyclane	*11*		0.96(3)[c]	1.27×10^{-5}	12
1-Methyl-*trans*-3-hydroxynortricyclane	*12*		0.67(3)[c]	1.67×10^{-5}	12
Isobutene	*13*		0.84[d]	6.4×10^{-4}[e]	1, 20
Phenyl vinyl ether	*14*	0.84(5)		7.2×10^{-3}[e]	21
Ethyl vinyl ether	*15*	0.70(3)		3.9[e]	21
Phenyl isopropenyl ether	*16*	0.61(3)		13.2[e]	21
Methyl cyclohexenyl ether	*17*	0.66(3)		93[e]	21
Ethyl cyclohexenyl ether	*18*	0.58(3)		176[e]	21
Ethyl cyclopentenyl ether	*19*	0.63(3)		1.00×10^3[e]	21
Ethyl isopropenyl ether	*20*	0.64(4)		1.27×10^3[e]	21
Methyl-α-cyclopropyl vinyl ether	*21*	0.67(3)		1.65×10^4[e]	22
β-Methoxy-*trans*-β-methyl styrene	*22*	0.70(3)		3.7[e]	23
3-Methoxyindene	*23*	0.64(5)		127[e]	24
Bicyclo[3.3.1]non-1-ene	*24*	0.67(5)		69[e]	25
Methyl vinyl sulfide	*25*	0.73[f]		4.6×10^{-2}[e,g]	26, 27
Azulene	*26*	0.61(7)		0.40[e,g]	28
Quaiazulene	*27*	0.54(3)		13.4[e,g]	28
Allyl mercuric iodide	*28*	0.67(2)		3.1×10^{-2}[e]	1, 9
Isobutenyl mercuric bromide	*29*	0.69(4)		5.3×10^{-2}[e]	1, 9
2,2-Dichloromethylene-1,3-dioxolan	*30*	0.49		230[e]	1, 9
Cyanoketen dimethyl acetal	*31*	0.62		53[e]	1, 9

[a] 318.2 K. [b] 328.2 K. [c] 348.2 K. [d] In 0.442 mol dm^{-3} $LClO_4$. [e] An H_0 correction has been made, *i.e.* the second-order rate constants in dilute acid ($[H^+] \leq 0.1$ mol dm^{-3}) have been multiplied by 2.2. [f] 323.2 K. [g] In aq. HCl.

Kresge[21] concluded from the values for the vinyl ethers *14*–*20* (numbering in Table 2) that the α values depend, although slightly, on the rates of the reactions: the slope for α *vs.* log $[k_{HA}/(\text{dm}^3\ \text{mol}^{-1}\ \text{s}^{-1})$ at $pK_{HA} = 4]$ is -0.036 ± 0.010. However, if an exceptional point for less reactive phenyl vinyl ether (*14*) is omitted, the slope is reduced to -0.013 ± 0.016. Very recently Johnson interpreted the same data together with some others (*14* to *27* excluding *24*) so that the slope is really zero and he used this result as evidence against the reactivity–selectivity principle.[29]

If we use the α values for the reactive substrates *14* to *31* in Table 2, we get eqn. (5) (the broken line in

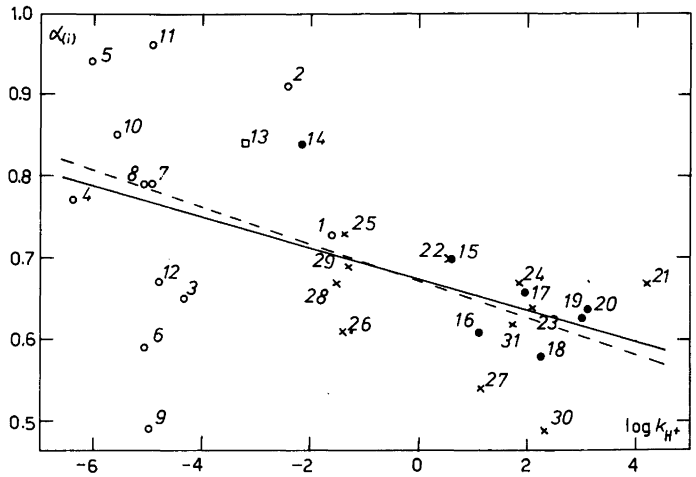

Fig. 1. Values of Brönsted α in carboxylic acid buffers and of isotopic α_i in 0.1 mol dm^{-3} $LClO_4$ *vs.* log ($k_{H^+}/dm^3\ mol^{-1}\ s^{-1}$) ($k_{H^+}$ in 1 mol dm^{-3} mineral acid at 298.2 K) for rate-determining proton transfer reactions. (The numbering, see Table 2. Symbols: ○, norbornenes and nortricyclanes; □, isobutene; ●, original values for vinyl ethers by Kresge; ×, other values for vinyl ethers, a vinyl thioether, a bridgehead olefin, azulenes, halomercuro olefins and keten acetals. ——, compounds *1* to *31*; – – –, compounds *14* to *31*.)

$$\alpha = -(0.023 \pm 0.009) \log (k_{H^+}/dm^3\ mol^{-1}\ s^{-1}) + (0.67 \pm 0.02) \quad (5)$$

Fig. 1), and if we use the α and α_i values for all the substrates in Table 2, we get equation (6) (the full line in Fig. 1). The rate constant k_{H^+} in eqns. (5) and (6) refers to the value in 1 mol dm^{-3} aqueous

$$\alpha \text{ or } \alpha_i = -(0.020 \pm 0.006) \log (k_{H^+}/dm^3\ mol^{-1}\ s^{-1}) + (0.67 \pm 0.02) \quad (6)$$

mineral acid at 298.2 K. The equations are very similar and indicate, in our opinion, a slight but probably significant dependence of α or α_i on the rate of the slow proton transfer when $0.5 \leq \alpha$ or $\alpha_i \leq 1$. (Perhaps a slightly nonlinear relationship between the α or α_i values and the log k_{H^+} values would be more truthful but it has not been applied owing to the large experimental scattering of the data.)

The calculated difference between the α_i value of the most reactive norbornene [*1*, α_i (calc.)=0.70 (obs. 0.73)] and the least reactive norbornene [*4*, α_i(calc.)=0.80 (obs. 0.77)] is hardly larger than the experimental error, but the difference between the mean values of the less reactive compounds *1* to *13* ($\bar{\alpha}_i = 0.77 \pm 0.04$; 0.75 ± 0.05 for the bicyclic compounds and 0.78 ± 0.07 for the tricyclic compounds) and the more reactive compounds *14* to *31* ($\bar{\alpha} = 0.65 \pm 0.02$) is evident, if we take into account the great number of the data. This result agrees with the Hammond postulate.[17]

According to Bell[2] and Kresge[21] there might be a difference (0.1 or even more) between the α values measured in carboxylic acid buffers and the α_i values determined in strong mineral acids. The two equations [(5) and (6)], however, imply that the difference is not significant, which is in agreement with the opinion of Williams and Kreevoy.[1]

Acknowledgment. The authors wish to thank Mr. Reijo Ollikka for his assistance in the kinetic measurements.

REFERENCES

1. Williams, J. M. and Kreevoy, M. M. *Adv. Phys. Org. Chem. 6* (1968) 63.
2. Bell, R. P. *The Proton in Chemistry*, 2nd Ed., Chapman, London 1973, Chapters 10–12.
3. DePuy, C. H. *Fortschr. Chem. Forsch. 40* (1973) 73.
4. Kresge, A. J., Chiang, Y., Fitzgerald, P. H., McDonald, R. S. and Schmid, G. H. *J. Am. Chem. Soc. 93* (1971) 4907.

5. Lajunen, M. and Wallin, M. *Finn. Chem. Lett.* (1974) 251.
6. Kresge, A. J. *Pure Appl. Chem. 8* (1964) 243.
7. Salomaa, P. *Acta Chem. Scand. A 23* (1969) 2095.
8. Chwang, W. K., Eliason, R. and Kresge, A. J. *J. Am. Chem. Soc. 99* (1977) 805.
9. Kresge, A. J. *Chem. Soc. Rev. 2* (1973) 473.
10. Murdoch, J. R. *J. Am. Chem. Soc. 102* (1980) 71.
11. Lajunen, M. and Wallin, M. *Finn. Chem. Lett.* (1975) 18.
12. Lajunen, M. and Lyytikäinen, H. *Finn. Chem. Lett.* (1975) 97.
13. Lajunen, M. and Lyytikäinen, H. *Acta Chem. Scand. A 30* (1976) 63.
14. Lajunen, M. and Peuravuori, J. *Finn. Chem. Lett.* (1976) 99.
15. Lajunen, M. and Lyytikäinen, H. *Acta Chem. Scand. A 35* (1981) 131.
16. Lajunen, M. and Lyytikäinen, H. *Acta Chem. Scand. A 35* (1981) 139.
17. Hammond, G. S. *J. Am. Chem. Soc. 77* (1955) 334.
18. Lajunen, M. and Ollikka, R. *Finn. Chem. Lett.* (1978) 272.
19. Salomaa, P. and Aalto, V. *Acta Chem. Scand. 20* (1966) 2035.
20. Gold, V. and Kessick, M. A. *J. Chem. Soc.* (1965) 6718.
21. Kresge, A. J., Chen, H. L., Chiang, Y., Murrill, E., Payne, M. A. and Sagatys, D. S. *J. Am. Chem. Soc. 93* (1971) 413.
22. Kresge, A. J. and Chwang, W. K. *J. Am. Chem. Soc. 100* (1978) 1249.
23. Kresge, A. J. and Chen, H. J. *J. Am. Chem. Soc. 94* (1978) 2818.
24. Chiang, Y., Chwang, W. K., Kresge, A. J., Robinson, L. H., Sagatys, D. S. and Young, C. I. *Can. J. Chem. 56* (1978) 456.
25. Chiang, Y., Kresge, A. J. and Wiseman, J. R. *J. Am. Chem. Soc. 98* (1976) 1564.
26. McClelland, R. A. *Can. J. Chem. 55* (1977) 548.
27. Okuyama, T., Nakada, M. and Fueno, T. *Tetrahedron 32* (1976) 2249.
28. Thomas, R. J. and Long, F. A. *J. Am. Chem. Soc. 86* (1964) 4770.
29. Johnson, C. D. *Tetrahedron 36* (1980) 3461.
30. Lajunen, M. and Hirvonen, P. *Finn. Chem. Lett.* (1974) 245.

Received August 26, 1981.

Acta Chemica Scandinavica A 36 (1982) 377–389

The Structures of Sulfate, Sulfite and Disulfite Ions in Aqueous Solution Determined by X-Ray Diffraction

TOSHIO YAMAGUCHI and OLIVER LINDQVIST

Department of Inorganic Chemistry, Chalmers University of Technology and the University of Göteborg, S-412 96 Göteborg, Sweden

X-Ray scattering measurements were carried out at 25 °C for concentrated aqueous solutions of ammonium sulfate (pH = 4.8), ammonium sulfite (pH = 8.3) and ammonium disulfite (pH = 5.5 and 5.1). Intensity data were analyzed in terms of the radial distribution functions and reduced intensities. The sulfate ion has a tetrahedral structure with an S–O distance of 1.481(3) Å, while the sulfite ion has a pyramidal C_{3v} structure. The S–O distance within SO_3^{2-} is 1.529(4) Å; the lone-pair of electrons of S(IV) is stereochemically active in solution. The $S_2O_5^{2-}$ ion has an S–S bridge with a bond length of 2.221(11) Å. The S–O distances of the thionite and thionate groups could not be distinguished, but the average S–O distance is 1.498(2) Å. Plausible hydration models of the ions are discussed.

The equilibrium species resulting when dissolving sulfur dioxide in water have been extensively studied by spectroscopic techniques. The interest in this system arises not only from a theoretical point of view but also from the needs in practical fields, i.e. research on SO_2-induced atmospheric corrosion [1] and catalytic oxidation of SO_2 in polluted air.[2]

The sulfite ion, SO_3^{2-}, the hydrogen sulfite ion, HSO_3^-, and the disulfite ion, $S_2O_5^{2-}$, occur in equilibrium in aqueous solution, the equilibrium constants being reported by Bourne *et al.*[3] Raman spectra of an Na_2SO_3 aqueous solution have indicated that the sulfite ion has a pyramidal C_{3v} structure.[4] However, much controversy has persisted for more than 100 years regarding the structures of the HSO_3^- and $S_2O_5^{2-}$ ions. The structure of the hydrogen sulfite ion was first proposed by Simon *et al.*[5] to have pyramidal C_{3v} structure containing an H–S bond. Their result was based on the Raman spectra of cesium hydrogen sulfite. Recently, this structure was confirmed both by isotopic Raman spectroscopic measurements of $CsHSO_3$,[6] where all six fundamentals of the bisulfite ion were observed and assigned, and by X-ray and neutron crystal structure determinations of $CsHSO_3$.[7] The existence of both $HOSO_2^-$ and HSO_3^- ions in solution has been suggested [9] but the equilibrium distribution is not known. Concerning the disulfite ion, Simon *et al.*[8] originally proposed a symmetrical $O_2SOSO_2^{2-}$ structure from Raman spectra of potassium salts in the solid state and in solution. However, he later changed his assignments of the bands, accepting the S–S bridge giving an $O_3SSO_2^{2-}$ structure with C_s symmetry,[5] later confirmed in other investigations.[4,6,9] X-Ray structural analyses of $K_2S_2O_5$ [10] and $(NH_4)_2S_2O_5$ [11] confirmed the C_s symmetry containing the S–S bond in the solid state.

Tautomeric structures of both hydrogen sulfite and disulfite ions may occur in solution since the assignement of Raman bands of such solutions is incomplete.[6] In the present investigation, the X-ray diffraction method was applied to determine the structures of sulfite and disulfite ions in aqueous solution. The ammonium ion was chosen as cation, since it fits well into the bulk water structure. Thus, the structure of anion hydration will not be seriously disturbed by that of cation hydration. Besides, ammonium sulfite and ammonium disulfite are more soluble in water than other salts,[12] which makes the data analyses more accurate. In order to discuss the S–O bond distances and the hydration of the SO_3^{2-} and $S_2O_5^{2-}$ ions in solution, it was considered profitable to make comparisons with an SO_4^{2-} solution. Recently, Caminiti *et al.*[13] investigated a concentrated ammonium sulfate solution with X-ray diffraction techniques. In their

0302-4377/82/050377-13$02.50

Table 1. Compositions of the solutions (mol dm^{-3}). V is the stoichiometric volume ($Å^3$) per sulfur atom, μ the linear absorption coefficient (cm^{-1}) and d the density (g cm^{-3}).

	$(NH_4)_2SO_4$	$(NH_4)_2SO_3$	$(NH_4)_2S_2O_5$	$(NH_4)_2S_2O_5$
S	3.900	3.711	8.314	10.92
O	55.59	52.94	50.60	51.31
N	7.800	7.542	11.20	11.35
H	111.2	113.8	101.5	92.99
pH	4.8	8.3	5.3	5.1
V	425.8	440.4	199.7	152.1
μ	2.50	2.40	3.79	4.60
d	1.236	1.191	1.335	1.424

analysis, however, the S–O interaction within the SO_4^{2-} ion was subtracted as a known parameter. Therefore, but also to study the hydration of the sulfate ion, we decided to include a reinvestigation of an ammonium sulfate solution in the present work. Raman spectral measurements have also been carried out to identify the main species in the solutions used in the X-ray experiments.

EXPERIMENTAL

Preparation and analysis of sample solutions

Since the equilibrium, $2HSO_3^- \rightleftarrows S_2O_5^{2-} + H_2O$, inclines to the right-hand side with increasing concentration,[3] it is not possible to prepare an HSO_3^- solution suitable for the X-ray analysis.

Solutions of ammonium sulfite (pH = 8.3) and ammonium disulfite (pH = 5.3 and 5.1) were prepared under nitrogen atmosphere by dissolving gaseous SO_2 in a cold solution (*ca.* 0 °C). which had previously been saturated with ammonia, until the required pH was obtained. pH determinations were made by means of a Radiometer Model 29 pH-meter, calibrated with a buffer solution (Merck, pH = 4.0).

A saturated solution of ammonium sulfate was prepared by dissolving ammonium sulfate (Merck, pro analysi), without further purification, into distilled water.

The concentrations of the sulfite and the disulfite solutions were determined by oxidation to sulfate with hydrogen peroxide. The sulfate was analyzed gravimetrically as $BaSO_4$. The content of ammonium was determined by the Kjeldahl method.[14] The solution densities were measured with pycnometers. The compositions of the sample solutions are given in Table 1.

X-Ray measurements

X-Ray scattering measurements were carried out at 25 °C by a $\theta - \theta$ diffractometer of the same type as described elsewhere[15] with a bent LiF monochromator in the diffracted beam. Mo$K\alpha$ radiation ($\lambda = 0.7107$ Å) was used, a 2 kW fine focus X-ray tube being employed. The sample solution, contained in a flat teflon tray (inner diameter 40 mm and depth 10 mm) was enclosed in an airtight shield with a cylindrical Be window for X-rays. During the measurements of sulfite and disulfite solutions, the inside of the container was filled with nitrogen gas to prevent oxidation. The scattered intensities were collected by a step scanning mode at dicrete points over the range of scattering angle (2θ) from 2 to 130°, corresponding to the range $0.3 \leqq s \leqq 16.0$ $Å^{-1}$ ($s = 4\pi \sin\theta/\lambda$). The intervals of 0.1 and 0.25° were used, respectively, for the range of $1 \leqq \theta \leqq 20$ and $20 \leqq \theta \leqq 65°$. Measurements were repeated until total counts at each data point amounted to 80000 ($1 \leqq \theta \leqq 10°$) and 120000 ($10 \leqq \theta \leqq 65°$). Pairs of divergent and scattering slits of 1/12 – 1/2°, 1/6 – 1/2° and 1 – 1° were used for the ranges $1° \leqq \theta \leqq 8°$, $3° \leqq \theta \leqq 12°$ and $8° \leqq \theta \leqq 65°$, respectively.

Data analysis

Experimental intensities, corrected for background,[16] absorption,[17] double scattering,[18] polarization[19] and Compton radiation,[20] were scaled to absolute units by comparison of measured intensities with the total independent theoretical scattering in a high angle region ($s \geqq 13.5$ $Å^{-1}$). The scaling factor thus obtained agreed within 2 % with that calculated by the Krogh-Moe[21] and the Norman[22] methods. The scattering factors for neutral atoms were taken from the International Tables for X-Ray Crystallography,[23] except H_2O for which molecular form factors proposed by Hajdu[24] were used. The values for incoherent scattering factors were taken

from those given by Cromer and Mann[25] for N, by Cromer[26] for O and S, by Compton and Allison[27] for H, and by Hajdu[24] for H_2O. The incoherent scattering factors were corrected for the Breit-Dirac effect.[28,29] The values for anomalous dispersion were taken from the International Tables for X-Ray Crystallography.[23] The reduced intensities, $i(s)$, were derived from eqn. (1), where $I(s)_{obs}$ is the

$$i(s)_{obs} = I(s)_{obs} - \Sigma n_i\{(f_i(s)+\Delta f_i')^2 + (\Delta f_i'')^2\} \quad (1)$$

scaled measured intensities, n_i the number of atom "i" in a stoichiometric volume V containing one S atom, f_i, $\Delta f_i'$ and $\Delta f_i''$ the scattering factor, the real and imaginary parts of anomalous dispersion of atom "i", respectively. The electronic radial distribution function, $D(r)$, was then obtained by Fourier inversion (2). Here ρ_0 represents the average

$$D(r) = 4\pi r^2\rho_0 + \frac{2r}{\pi}\sum_0^{s_{max}} s \cdot i(s)M(s)\sin(rs)\Delta s \quad (2)$$

scattering density $\{[\Sigma n_i f_i(0)+\Delta f_i']^2 + (\Sigma n_i \Delta f_i''^2\}/V$, the modification function $M(s)$ is $\{(f_S(0)+\Delta f_S')^2 + (\Delta f_S'')^2\}/\{(f_S(s)+\Delta f_S')^2 + (\Delta f_S'')^2\}\exp(-0.01s^2)$ and s_{max} the maximum value of s available in each experiment. Spurious ripples observed in a hard-core region of the $D(r)$ function were removed in the usual manner.[19]

Theoretical reduced intensities based on models were calculated by eqn. (3), where r_{ij}, b_{ij} and n_{ij}

$$i(s)_{calc} = \Sigma\Sigma n_{ij}\{(f_i(s)+\Delta f_i')(f_j(s)+\Delta f_j') + (\Delta f_i'')(\Delta f_j'')\}\frac{\sin(rs)}{rs}\exp(-b_{ij}s^2) \quad (3)$$

denote the distance, the temperature factor and the frequency factor of a pair of atoms, "i–j". The corresponding peak shapes were obtained by Fourier transformation [eqn. (2)]. These calculations were carried out by means of the KURVLR program.[30]

For a quantitative analysis, the least-squares method was applied to the reduced intensities, the function $\sum_{s_{min}}^{s_{max}} w(s)\{i(s)_{obs} - i(s)_{calc}\}^2$ being minimized by means of the NLPLSQ program.[31] The weighting function $w(s)$ was proportional to $I_{obs}^2 \cos\theta$. Lower and upper values s_{min} and s_{max} were set for adequate model fitting.

Raman measurements

Raman spectra were recorded with a Cary 82 laser Raman spectrophotometer using the 4880 Å excited line of an argon laser. The solutions were contained in glass tubes of 1 mm diameter.

RESULTS AND DISCUSSION

1. Solution of ammonium sulfate (pH = 4.8)

Fig. 1A shows the radial distribution curve, $D(r)-4\pi r^2\rho_0$, for the $(NH_4)_2SO_4$ solution. The general features of the distribution curve are similar to those obtained by Caminiti *et al.*,[13] except for the S–O peak at 1.5 Å subtracted from their data. The O–O interaction within the sulfate ion contributes to a shoulder around 2.40 Å. The 2.90 Å peak is typical for aqueous solution, attributed to the first neighbor H_2O-H_2O (or $H_2O-NH_4^+$) interaction in the bulk structure.[32] The peak around 3.80 Å can be ascribed to the interaction between the S atom in the sulfate ion and hydration water molecules, as Caminiti *et al.* suggested.[13] The shoulder at 4.80 Å and the broad peak observable at 6.0–7.2 Å reflect long-range interactions which are difficult to interpret in detail.

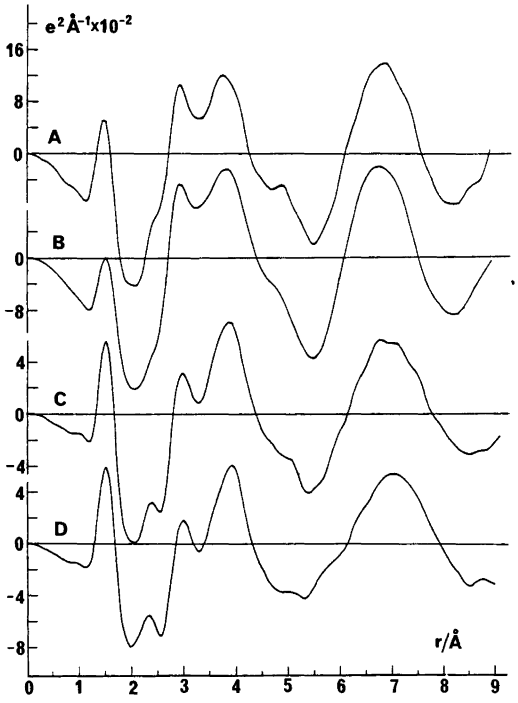

Fig. 1. Experimental radial distribution curves, $D(r)-4\pi r^2\rho_0$, of the solutions investigated. (A) $(NH_4)_2SO_4$ (pH = 4.8), (B) $(NH_4)_2SO_3$ (pH = 8.3), (C) $(NH_4)_2S_2O_5$ (pH = 5.3), (D) $(NH_4)_2S_2O_5$ (pH = 5.1).

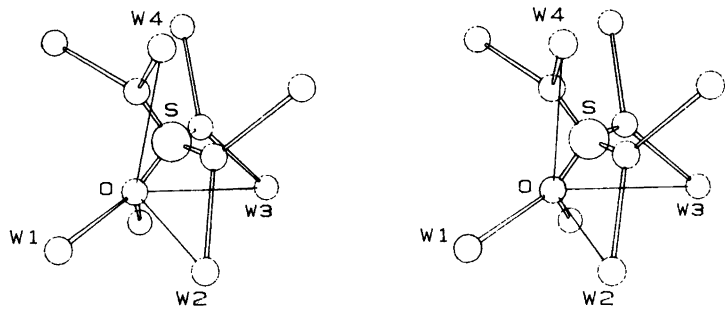

Fig. 2. A symmetric hydration model of the sulfate ion (stereoview).

From the dissociation constant[33] of the HSO_4^- ion and the measured pH value of 4.8 in the sample solution, it can be calculated that the SO_4^{2-} ion should dominate completely. Thus, the model adopted for the analysis had the following characteristics.

(a) A tetrahedral sulfate ion described by parameters r_{S-O}, b_{S-O} and b_{O-O}.

(b) Hydration of the SO_4^{2-} with $S-H_2O$ interactions described by three parameters r_{S-W}, b_{S-W} and n_{S-W}. Interactions between sulfate oxygen atoms and hydration water molecules were also taken into account.

(c) The bulk structure was treated as that of pure water and calculated by using Narten's original data (*cf.* Ref. 32).

In a first step of refinement, parameter n_{S-W} was refined independently to estimate the number of

Table 2. Results of least-squares refinements A, B and C (see text) for the $(NH_4)_2SO_4$ solution obtained in the range $2.0 \leqq s \leqq 15.0$ Å^{-1}. Standard deviations are given in parentheses.

		A	B	C
S–O	*r*	1.464(5)	1.481(2)	1.480[c]
	b	0.0008(4)	0.0011(2)	0.0005(4)
	n	4	4	4
O–O	*r*	2.391[a]	2.418[a]	2.417
	b	0.059(6)	0.0036(7)	0.0016
	n	6	6	6
S–W	*r*	3.45(4)	3.70(1)	3.64[c]
	b	0.06(2)	0.020(1)	0.064(7)
	n	8	8	8
O–W(1)	*r*	2.48[b]	2.86(1)	2.66[c]
	b	0.023(4)	0.004(1)	0.039(7)
	n	8	8	8
O–W(2)	*r*	3.28[b]	3.17(2)	3.20[c]
	b	0.08(2)	0.009(1)	0.008(6)
	n	4	4	4
O–W(3)	*r*	3.70[b]	4.05(3)	4.06[c]
	b	0.045(12)	0.009(2)	0.086(16)
	n	8	8	8
O–W(4)	*r*	4.43[b]	4.67(5)	4.53[c]
	b	0.045(20)	0.034(3)	0.42(9)
	n	8	8	8
R-factor[d]		0.340	0.114	0.317

[a] Fixed to the value ($=\sqrt{8/3} \times r_{S-O}$). [b] Estimated from the geometry shown in Fig. 2. [c] Average distances found in the crystal structure.[34] [d] $R = \{\Sigma s^2 \Delta i(s)^2 / \Sigma s^2 i(s)^2_{obs}\}^{\frac{1}{2}}$ with $\Delta i(s) = i(s)_{obs} - i(s)_{calc}$.

water molecules bonded to the sulfate ion. In agreement with the result obtained by Caminiti *et al.*,[13] $n_{S-W} = \sim 8$ was obtained. The construction of a complete hydration model of the SO_4^{2-} ion seemed difficult since the distribution curve does not give any clear indication about the hydration geometry. Crystal structures are sometimes comparable with the geometry in solution. Kjällman and Olovsson[34] have determined the crystal structure of $H_2SO_4 \cdot 4H_2O$, in which two water molecules are hydrogen bonded to each sulfate oxygen atom. Based on this structure, we built up a symmetric hydration model with W–O–W angles of 120° and minimun W–W repulsion as shown in Fig. 2. Least-squares calculations were carried out in various ways as summarized in Table 2.

In refinement A, the distances of the S–O and the S–W interactions were refined, while other distances were fixed to the values based on the geometry of the symmetric model. The temperature factors of all interactions were allowed to vary independently. In refinement B, only the assumption of the tetrahedral SO_4^{2-} structure hydrated by eight water molecules was retained, while all the other parameters of the model were allowed to vary. As a comparison, refinement C was also carried out using distances reported in the actual crystal[34] with all the temperature factors as adjustable parameters.

The S–O distance obtained in refinement B was in good agreement with the average value in the solid state, while that in refinement A is somewhat shorter but still falls in the range of S–O distances reported for sulfate salts.[35] Also other interaction distances obtained in refinement B were consistent with the corresponding distances in the crystal, except the O–W(1) distance. The refinement was carried out, however, based on a simple assumption concerning the bulk structure, which may affect the O–W(1) interaction.

The distances of the S–W and O–W(3) interactions obtained in refinement A are significantly

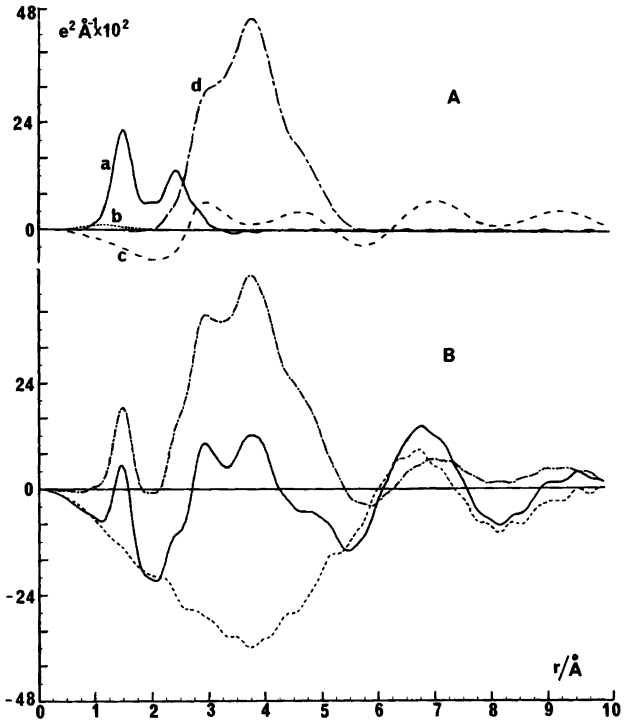

Fig. 3. (A) Peak shapes calculated for (a) the SO_4^{2-} ion, (b) the NH_4^+ ion, (c) the bulk structure and (d) the hydration structure of the SO_4^{2-} ion (S–W, O–W(1), O–W(2), O–W(3) and O–W(4)). (B) Experimental (–) and theoretical (-·-) radial distribution curves with their difference (---) for the $(NH_4)_2SO_4$ solution.

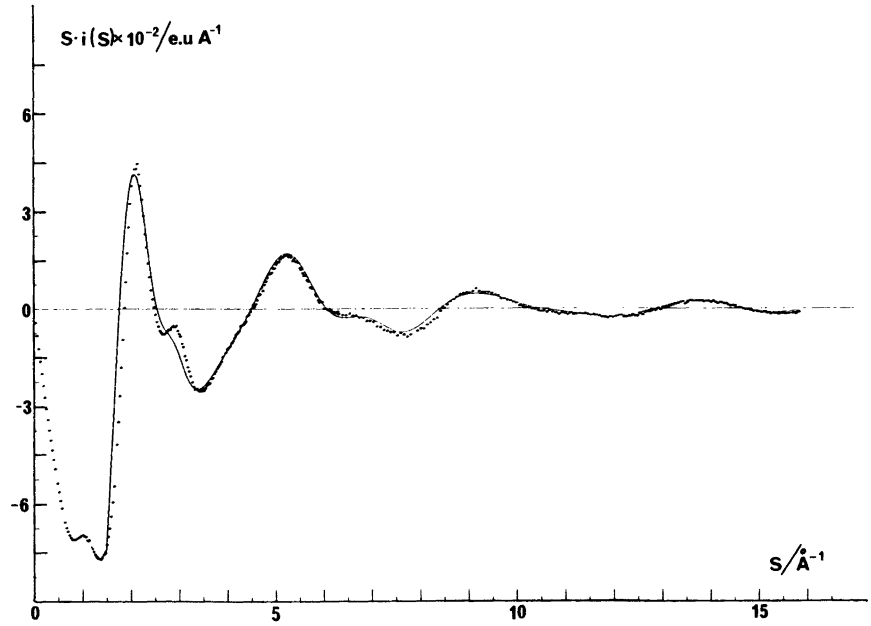

Fig. 4. Observed (dots) and calculated (solid line) $s \cdot i(s)$ values for the $(NH_4)_2SO_4$ solution.

shorter than those in refinements B and C. It is therefore reasonable to assume that the water molecules are not as rigidly hydrogen bonded to the SO_4^{2-} ion as suggested in the symmetric model in Fig. 2. The basic results of refinement B as a time average, *i.e.* a hydration sphere containing eight water molecules at ~3.7 Å from the center of the SO_4^{2-} ion, having hydrogen bond distances [O–W(1)] of ~2.85 Å, are thus strongly supported by the experimental data. The distances O–W(2), O–W(3) and O–W(4) probably include long-range interactions.

Fig. 3 A shows the individual theoretical contributions to the radial distribution curve from (1) the SO_4^{2-} ion, (2) the hydration of the SO_4^{2-} ion and (3) the bulk structure according to model B. Fig. 3 B shows the experimental distribution curve and theoretical peak shape with their difference.

Fig. 4 shows observed $s \cdot i(s)$ values compared to the values calculated from model B.

2. Solution of ammonium sulfite (pH = 8.3)

Fig. 1 B represents the radial distribution curve of the ammonium sulfite solution. The 1.5 Å peak can be ascribed to the S–O bonds within the sulfite ion, being in agreement with the results of crystal structure determination.[36-41] The area under the peak corresponds to approximately three S–O bonds within the sulfite ion. The shoulder around 2.4 Å may be due to the O–O bonds within the SO_3^{2-} ion. The peak centered at 2.9 Å can be attributed to the bulk structure.[32] The interaction between sulfite oxygen atoms and hydration water molecules may also contribute partly to this peak. The peak observed at 3.8 Å may indicate the hydration of the SO_3^{2-} ion as found in the sulfate solution.

The structure of the ammonium sulfite solution was analyzed by means of least-squares calculations in the following way.

(a) The structure of the sulfite ion was first described by distances (r_{S-O} and r_{O-O}) and temperature factors (b_{S-O} and b_{O-O}) of the S–O and O–O bonds since the O–S–O bond angle cannot be postulated in the sulfite ion. In some preliminary refinements, however, the O–O distance converged to unreasonable values, probably because of its small contribution to the intensity data. Therefore, the O–O distance was fixed to the value estimated from the radial distribution curve, also being in accordance with the results of crystal structure determinations.[36-41] This restriction is relevant, since the O–O distance in the sulfite ion does not

Table 3. Results of least-squares refinements A, B and C (see text) for the $(NH_4)_2SO_3$ solution obtained in the range $2.0 \leqq s \leqq 15.0$ Å^{-1}. Standard deviations are given in parentheses.

		A	B	C
S–O	*r*	1.529(4)	1.524[b]	1.517(8)
	b	0.0021(3)	0.0017(4)	0.0033(7)
	n	3	3	3
O–O	*r*	2.42[a]	2.414[b]	2.85(11)
	b	0.005(2)	0.002	0.014(7)
	n	3	3	3
S–W	*r*	3.79(2)	3.80[b]	3.73(4)
	b	0.022(1)	0.064	0.050(3)
	n	8	9	12
O–W(1)	*r*	2.81(3)	2.82[b]	2.85(3)
	b	0.020(3)	0.005(1)	0.005(2)
	n	6	9	9
O–W(2)	*r*	3.23(4)	3.60[b]	3.01(23)
	b	0.024(3)	0.015(8)	0.11(3)
	n	7	5	9
O–W(3)	*r*	4.22(7)	4.21[b]	4.30(9)
	b	0.013(4)	0.10(5)	0.015(4)
	n	6	4	9
O–W(4)	*r*	4.59(7)	4.75[b]	4.71(12)
	b	0.009(3)	0.011(5)	0.011(6)
	n	6	5	9
R-factor		0.119	0.311	0.253

[a] The value estimated from the distribution curve, in accordance with the crystal structures.[36–41] [b] Average distances found in the crystal structures.

change significantly with the S–O distance as discussed by Kierkegaard *et al.*[42]

(b) The interactions between the sulfite ion and hydration water molecules are described by the S–W (r_{S-W}, b_{S-W} and n_{S-W}) and O–W (r_{O-W}, b_{O-W} and n_{O-W}) parameters obtained from different models.

(c) The contribution from the bulk structure was calculated in a manner similar to that described in the previous section.

Table 3 summarizes the results of the least-squares refinements. Refinement A is based on a hydration model (Fig. 5 A), in which two water molecules are bonded to each sulfite oxygen atom as found for the sulfate ion. In addition, there are two more water molecules located toward the lone-pair of electrons of S(IV). Model B (Fig. 5 B) was constructed from the crystal structure of $(NH_4)_2SO_3.H_2O$.[36,37] A third refinement was based on the $MgSO_3.6H_2O$[38] structure (Fig. 5 C). In this structure each sulfite oxygen is hydrogen bonded to three water molecules at distances 2.66–2.72 Å and three more water molecules lie on the lone-pair side of the S atom.

The refinement results of hydration models A and B are rather comparable, except for the O–W(2) distance which may be affected by the bulk structure. Hydration model C was refined in two ways, *i.e.* (1) restricted to the geometry found in the $MgSO_3.6H_2O$ crystal (R = 0.63) and (2) unrestricted as shown in Table 3 C ($R = 0.25$). From the results given in Table 3, it can be concluded that the sulfite ion is surrounded by 8–9 water molecules at an S–W distance of ~3.8 Å, according to model A. The O–W(1) hydrogen bond distance is of the same order of magnitude as in the sulfate solution, *i.e.* ~2.8 Å. The O–W(2), O–W(3) and O–W(4) interactions are influenced by the bulk structure, and may be regarded as model fitting parameters.

The S–O bond length in the sulfite ion was found to be 1.529(4) Å, which agrees well with those found in hydrogen bonded sulfite ions in crystals, *e.g.* 1.536 Å ($NiSO_3.6H_2O$[41]), 1.517 Å[37] and 1.529 Å[36] ($(NH_4)_2SO_3.H_2O$), 1.533 Å (α-$FeSO_3.3H_2O$[39]), 1.536 Å (β-$FeSO_3.3H_2O$[40]) and 1.526 Å ($MgSO_3.6H_2O$[38]).

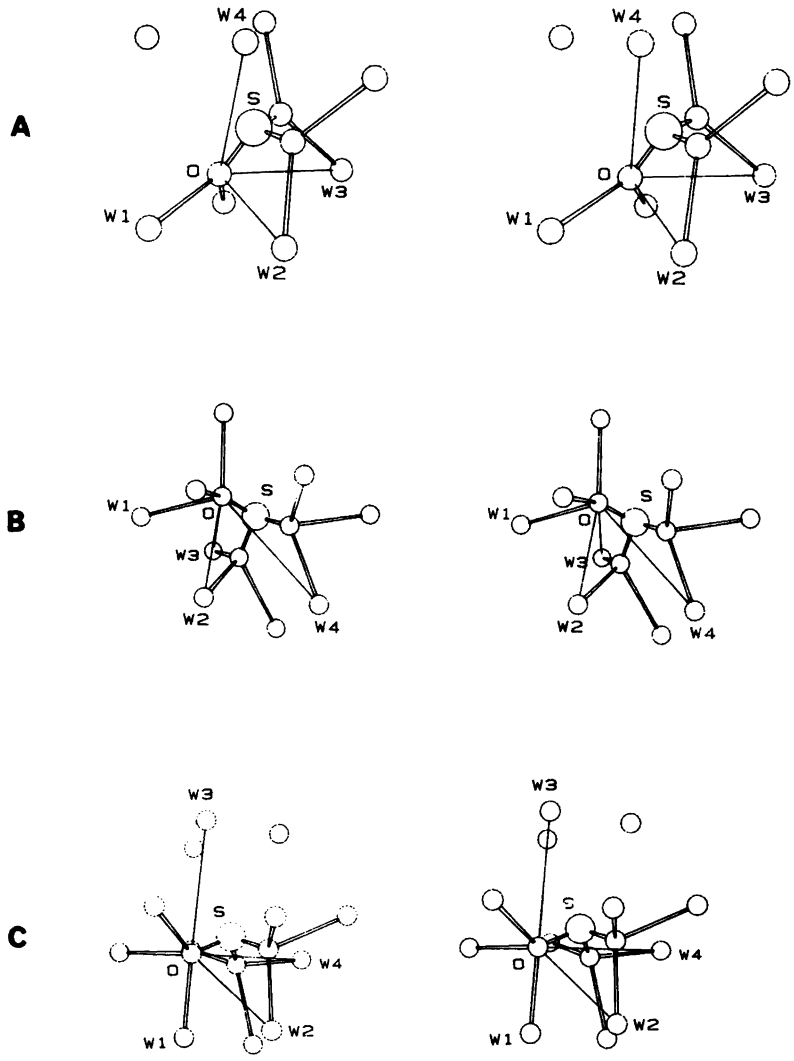

Fig. 5. Several hydration models of the sulfite ion (stereoview).

Fig. 6 B shows the experimental and theoretical radial distribution curves. Individual peak shapes (Fig. 6 A) have been calculated from the parameter values in Table 3 A. Fig. 7 represents the corresponding $s \cdot i(s)$ values.

As apparent from the residual curve in Fig. 6 B, there is no other significant peak less than 5 Å, though small ripples are still left, probably due to experimental uncertainties in the observed data. This indicates that the lone-pair of electrons of S(IV) is stereochemically active in solution in a similar way as found in the solid state.[36-41]

3. Solution of ammonium disulfite (pH = 5.1 and 5.3)

Before data analyses, the mol fractions of the hydrogen sulfite and the disulfite ions were estimated by the equilibrium constant given by Bourne *et al.*[3] at an ionic strength of 2.0. The result indicated that the disulfite ion should be present predominantly, *i.e.* 80–90 %, in the two measured solutions (*cf.* Table 1). In order to investigate if this distribution holds in our concentrated solutions, their Raman spectra were measured. The results were negative

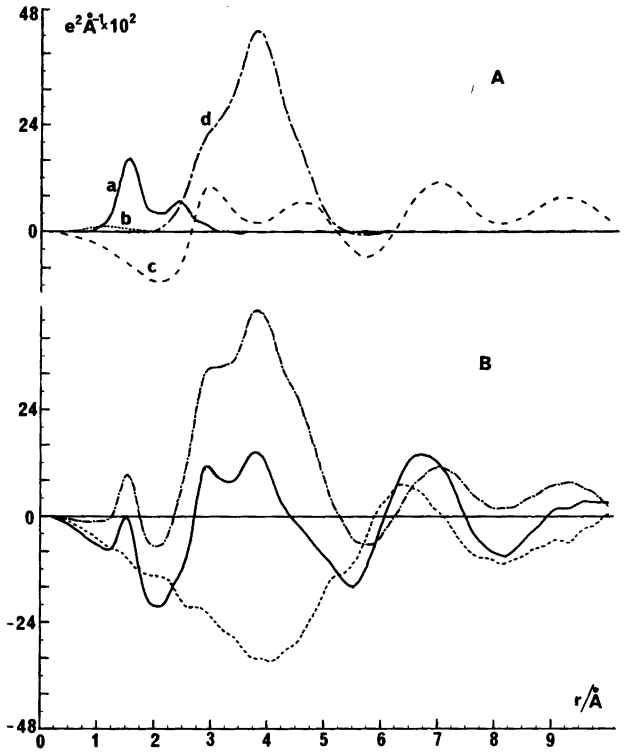

Fig. 6. (A) Peak shapes calculated for (a) the SO_3^{2-} ion, (b) the NH_4^+ ion, (c) the bulk structure and (d) the hydration structure of the SO_3^{2-} ion (S – W, O – W(1), O – W(2), O – W(3) and O – W(4)). (B) Experimental (—) and theoretical (---) radial distribution curves with their difference (----) for the $(NH_4)_2SO_3$ solution.

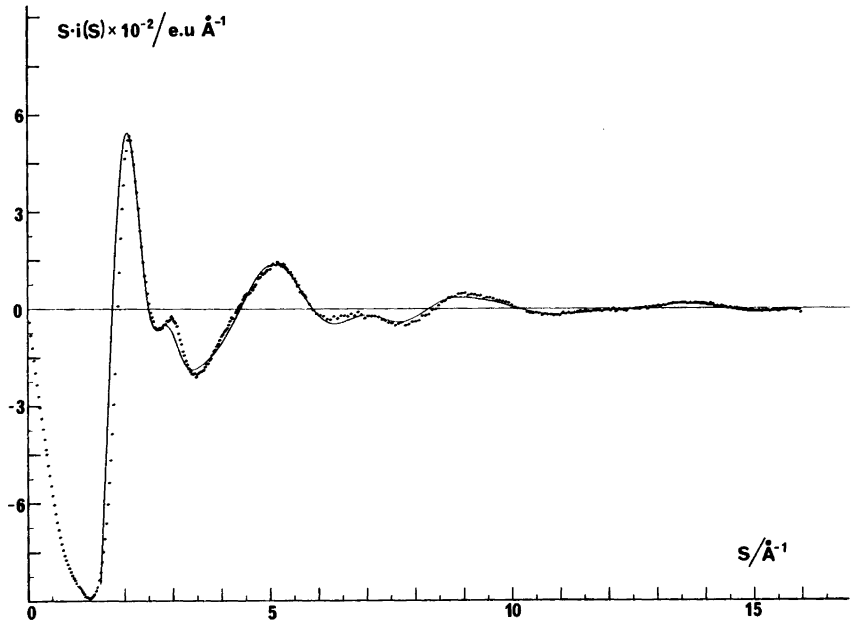

Fig. 7. Observed (dots) and calculated (solid line) $s \cdot i(s)$ values for the $(NH_4)_2SO_3$ solution.

for presence of the HSO_3^- ion (*cf.* Section 4). Therefore, the analysis of the diffraction data was made assuming presence of the disulfite ion only.

The radial distribution curves of the two ammonium disulfite solutions are shown in Figs. 1 C and D. The peak at 1.5 Å is due to the S–O interaction within the disulfite ion, in agreement with crystal structure determinations.[43,44] The number of the S–O bonds of about five was preliminarily obtained from analysis of the peak area. This result prefers C_s symmetry for the structure of the $S_2O_5^{2-}$ ion, since C_{2v} symmetry structure containing an S–O–S bridge would require six S–O bonds. Another piece of evidence supporting the C_s symmetry structure is the peak centered at 2.35 Å which may correspond to four nearest neighbor O–O interactions within the $S_2O_5^{2-}$ ion. However, the position of the peak appears at a shorter distance than expected for the O–O interactions (2.42–2.47 Å[43,44]) and the area under the peak could not be explained only by four O–O bonds (C_s symmetry) or six O–O bonds (C_s symmetry) within the $S_2O_5^{2-}$ ion. When the theoretical peaks calculated for five S–O and four nearest neighbor O–O bonds within the $S_2O_5^{2-}$ ion, parameter values of which were estimated from the distribution curves and the crystal structures,[43,44] were subtracted from the original curve, a very significant difference peak appeared at around 2.20 Å (Fig. 9 C). The value agrees well with the S–S bond distance within the $S_2O_5^{2-}$ ion found in the crystal structures.[44,45] The area under the peak is also in agreement with one S–S interaction. Thus, it is clearly evidenced that the $S_2O_5^{2-}$ ion has C_s symmetry containing an S–S bond in solution as has also been found in the crystal structures investigated so far.

The 3.8 Å peak may be attributed to the S–H_2O interaction as found in the sulfate and sulfite solutions.

The refinement of the structure of the S_2O_5 solution was performed in the following manner.

(a) The structure of the $S_2O_5^{2-}$ ion was described by two different S–O interactions, S–O(1) and S–O(2), an S–S bond, and nearest neighbor O–O interaction within each group (Fig. 8). The interactions between oxygen atoms within different groups were not included because of their small contribution to the reduced intensities.

(b) The interactions between the $S_2O_5^{2-}$ ion and nearest water molecules (or NH_4^+ ion) were taken into consideration by assuming n water molecules hydrogen bonded to disulfite oxygen atoms.

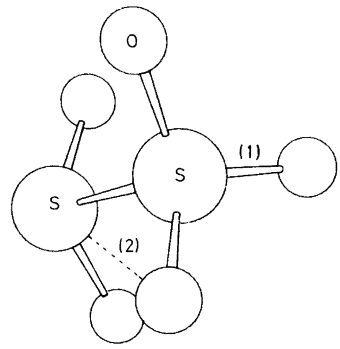

Fig. 8. The C_s symmetry structure of the disulfite ion.

The results of the refinements are given in Table 4. In refinement A, parameter $n_{S-O(1)}$ was allowed to vary in order to check the distribution of the HSO_3^- and the $S_2O_5^{2-}$ ions predicted from the thermodynamic data, and to confirm C_s symmetry structure of the $S_2O_5^{2-}$ ion. The relatively large temperature factor b_{S-S} may indicate the existence

Table 4. The results of the least-squares refinements for A and B (see text) for the $(NH_4)_2S_2O_5$ solution (pH = 5.1) obtained in the range $3.0 < s < 15.0$ Å^{-1}. Standard deviations are given in parentheses.

		A	B
S–O(1)	r	1.498(2)	1.498(2)
	b	0.0025(2)	0.0030(2)
	n	4.80(4)	5
O–O	r	2.45(2)	2.42(2)
	b	0.003(1)	0.0011(9)
	n	4	4
S–S	r	2.236(11)	2.221(11)
	b	0.0051(7)	0.0052(7)
	n	1	1
S–O(2)	r	2.960[a]	2.947[a]
	b	0.015(1)	0.016(1)
	n	5	5
S–W	r	3.76(2)	3.77(2)
(per $S_2O_5^{2-}$	b	0.031(1)	0.030(1)
	n	9.2(2)	8.9(2)
O–W	r	2.98(2)	2.98(2)
(per $S_2O_5^{2-}$)	b	0.017(2)	0.018(2)
	n	9.2[b]	8.9[b]
R-factor		0.101	0.104

[a] Fixed to the value estimated from the geometry. [b] Assumed that $n_{S-W} = n_{O-W}$.

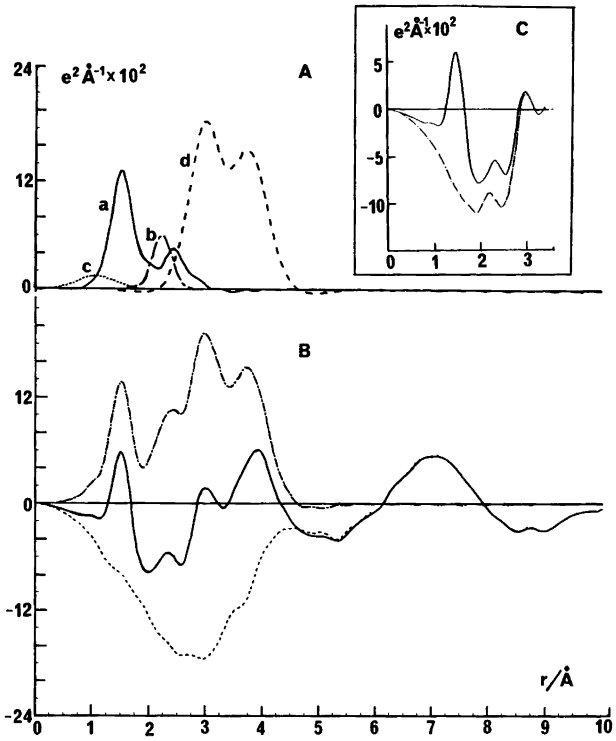

Fig. 9. (A) Peak shapes calculated for (a) S–O(1) and O–O bonds (b) the S–S bond and (c) N–H and O–H bonds within NH_4^+ and H_2O, respectively. (B) Experimental (–) and theoretical (-·-) radial distribution curves and their difference (---) of the $(NH_4)_2S_2O_5$ solution (pH = 5.1). (C) The residual distribution curve (chain line) obtained by subtracting 5 × S–O(1) and 4 × O–O interactions within the $S_2O_5^{2-}$ ion from the experimental distribution curve (solid line).

of a small fraction of HSO_3^- which is in accordance with the result from the equilibrium constant. The temperature factor of the S–O(1) bond is larger than those obtained for the S–O bonds in the sulfate and sulfite solutions (*cf.* Tables 2 and 3). This indicates the overlap of peaks due to different S–O bonds within the thionite and thionate groups. Attempts to refine their distances failed, however. The average S–O distance of 1.498(2) Å is in reasonable agreement with the weighted average S–O distance in the two groups found in the solid state (thionite: 1.431–1.472 Å, thionate: 1.495 and 1.499 Å).[43,44]

The S–S bond distance has been found to be 2.221(11) Å, consistent with the crystal data (2.209 Å[43] and 2.170 Å[44]).

The difference between experimental and theoretical radial distribution curves is shown in Fig. 9, and the observed and calculated $s \cdot i(s)$ values in Fig. 10.

The value of n_{S-W} of about nine (*cf.* Table 4) implies that some water molecules or NH_4^+ ions are shared between neighboring $S_2O_5^{2-}$ ions since the content of water molecules and NH_4^+ is not sufficient for hydration of the $S_2O_5^{2-}$ ion. It is not possible to suggest any detailed hydration model of the disulfite ion in solution. However, the refinement results indicate that approximately nine water molecules are attached to the $S_2O_5^{2-}$ ion with an S–H_2O distance of ~3.8 Å.

4. Raman spectra of the solutions

The Raman spectrum of the $(NH_4)_2SO_4$ solution showed four bands at 451(ν_2), 620 (ν_4), 983(ν_1) and 1108(ν_3) cm^{-1}, characteristic for a tetrahedral

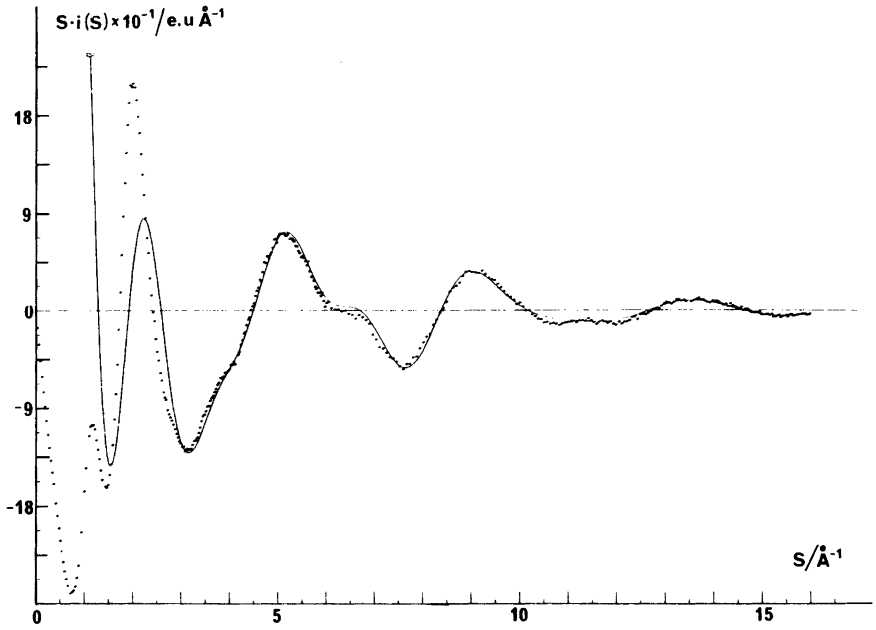

Fig. 10. Observed (dots) and calculated (solid line) $s \cdot i(s)$ values of the $(NH_4)_2S_2O_5$ solution (pH = 5.1).

SO_4^{2-} ion, while in the $(NH_4)_2SO_3$ solution three Raman bands appeared at 470(ν_4), 615(ν_2) and 960(ν_1 and ν_3), belonging to the sulfite ion.[4] No other bands due to different species were observed.

Raman spectra of the $(NH_4)_2S_2O_5$ solutions were carefully measured in order to examine the formation of the hydrogen sulfite ion. In the two disulfite solutions, Raman bands appeared at 230, 430, 655 and 1050 cm^{-1}, all of which belong to the $S_2O_5^{2-}$ ion.[6] Bands characteristic for the HSO_3^- ion should appear at 467, 1021, 1128 and 2533 cm^{-1},[6] none of which could be observed for our solutions. It seems therefore reasonable to assume that the HSO_3^- ion is present only to a small extent in the concentrated solutions, probably less than suggested by the equilibrium study.[3] Previous Raman spectra, measured for less concentrated solutions (1 – 2 M), have given bands corresponding to the HSO_3^- ion.[6]

Acknowledgements. The authors thank Professor Georg Lundgren for his kind interest in this study and Professor Kåre Larsson for making the Raman spectrophotometer available. The Swedish Natural Science Research Council is gratefully acknowledged for financial aid.

REFERENCES

1. Johansson, L.-G. and Vannerberg, N.-G. *Corros. Sci.* (1981). *In press.*
2. Brosset, C. *Kem. Tidskr. 11* (1975) 92.
3. Bourne, D. W. A., Higuchi, T. and Pitman, I. H. *J. Pharm. Sci. 63* (1974) 865.
4. Davis, A. R. and Chatterjee, R. M. *J. Solution Chem. 4* (1975) 399.
5. Simon, A. and Schmidt, W. *Z. Electrochem. 64* (1960) 737.
6. Meyer, B., Peter, L. and Shaskey-Rosenlund, C. *Spectrochim. Acta A 35* (1979) 345.
7. Johansson, L.-G., Lindqvist, O. and Vannerberg, N.-G. *Acta Crystallogr. B 36* (1980) 2523.
8. Simon, A., Waldmann, K. and Steger, E. *Z. Anorg. Allg. Chem.* 288 (1956) 131.
9. Herlinger, A. W. and Long, T. V. *Inorg. Chem. 8* (1969) 2661.
10. Lindqvist, I. and Mörtsell, M. *Acta Crystallogr. 10* (1957) 406.
11. Baggio, S. *Acta Crystallogr. B 27* (1971) 517.
12. Linke, W. F. and Seidell, A., Eds., *Solubilities of Inorganic and Metal Organic Compounds*, 4th Ed., Am. Chem. Soc. 1965, Vol. 2, pp. 747 – 755.
13. Caminiti, R., Paschina, G., Pinna, G. and Magini, M. *Chem. Phys. Lett. 64* (1979) 391.
14. Kolthoff, I. M., Sandell, E. B., Meehan, E. J. and Bruckenstein, S. *Quantitative Chemical Analysis*, 4th Ed., Macmillian, London 1971.

15. Johansson, G. *Acta Chem. Scand. 20* (1966) 553.
16. Ohtaki, H., Maeda, M. and Ito, S. *Bull. Chem. Soc. Jpn. 47* (1974) 2217.
17. Milberg, M. E. *J. Appl. Phys. 29* (1958) 64.
18. Warren, B. E. and Mozzi, R. L. *Acta Crystallogr. 21* (1966) 459.
19. Levy, H. A., Danford, M. D. and Narten, A. H. *Data Collection and Evaluation with an X-Ray Diffractometer Designed for the Study of Liquid Structure*, Report ORNL-3960, Oak Ridge National Laboratory, Oak Ridge 1966.
20. Sandström, M., Persson, I. and Ahrland, S. *Acta Chem. Scand. A 32* (1978) 607.
21. Krogh-Moe, J. *Acta Crystallogr. 9* (1956) 951.
22. Norman, N. *Acta Crystallogr. 10* (1957) 951.
23. *International Tables for X-Ray Crystallography*, Kynoch Press, Birmingham 1974, Vol. 4.
24. Hajdu, F. *Acta Crystallogr. A 28* (1972) 250.
25. Cromer, D. T. and Mann, J. B. *J. Chem. Phys. 47* (1967) 1892.
26. Cromer, D. T. *J. Chem. Phys. 50* (1969) 4857.
27. Compton, A. H. and Allison, S. K. *X-Rays in Theory and Experiment*, Van Nostrand-Reinhold, New York 1935.
28. Breit, G. *Phys. Rev. 27* (1926) 362.
29. Dirac, P. A. M. *Proc. R. Soc. London A 111* (1926) 405.
30. Johansson, G. and Sandström, M. *Chem. Scr. 4* (1973) 195.
31. Ohtaki, H., Yamaguchi, T. and Maeda, M. *Bull. Chem. Soc. Jpn. 49* (1976) 701.
32. Narten, A. H. *X-Ray Diffraction Data on Liquid Water in the Temperature Range 4 °C–200 °C*, Report ORNL-4578, Oak Ridge National Laboratory, Oak Ridge 1970.
33. Sillén, L. G. and Martell, A. E. *Stability Constants of Metal Ion Complexes, Special Publ. No. 25*, 1971.
34. Kjällman, T. and Olovsson, I. *Acta Crystallogr. B 28* (1972) 1692.
35. Schlemper, E. O. and Hamilton, W. C. *J. Chem. Phys. 44* (1966) 4498.
36. Battelle, L. F. and Trueblood, K. N. *Acta Crystallogr. 19* (1965) 531.
37. Durand, P. J., Galigne, J. L. and Cot, L. *Acta Crystallogr. B 33* (1977) 1414.
38. Flack, P. H. *Acta Crystallogr. B 29* (1973) 656.
39. Johansson, L.-G. and Lindqvist, O. *Acta Crystallogr. B 35* (1979) 1017.
40. Johansson, L.-G. and Ljungström, E. *Acta Crystallogr. B 35* (1979) 2683.
41. Baggio, S. and Becka, L. N. *Acta Crystallogr. B 25* (1969) 1150.
42. Kierkegaard, P., Larsson, L. O. and Nyberg, B. *Acta Chem. Scand. 26* (1972) 218.
43. Lindqvist, I. and Mörtsell, M. *Acta Crystallogr. 10* (1957) 406.
44. Baggio, S. *Acta Crystallogr. B 27* (1971) 517.

Received September 18, 1981.

Acta Chemica Scandinavica A 36 (1982) 391 – 397

A Mechanism Involving Two Photoinduced Transients for the Photocyanation of Phenanthrene in the Presence of Oxygen and Potassium Cyanide-18-crown-6 Ether in Anhydrous Acetonitrile

H. LEMMETYINEN,[a] J. KOSKIKALLIO,[a] M. LINDBLAD[a] and M. G. KUZMIN[b]

[a] Physical Chemistry Laboratory, University of Helsinki, SF-00170 Helsinki 17, Finland and [b] Laboratory of Photochemistry, Faculty of Chemistry, Lomonosov Moscow State University, 11234 Moscow, USSR

The dependence of the quantum yield, of the photocyanation of phenanthrene by potassium cyanide-18-crown ether, on the exciting light intensity, and the concentrations of the reagents was studied in the presence of oxygen in anhydrous acetonitrile. The proposed mechanism involves two transients. The first transient is formed by interaction of triplet phenanthrene with a cyanide anion and transformed into the second transient by second order reaction. The latter is oxidized by molecular oxygen into the reaction product 9-cyanophenanthrene. The rate constants of the reactions are estimated from the concentration dependences.

Photochemically-induced nucleophilic reactions, among them the cyanation of aromatic hydrocarbons, have been studied extensively during the last decade.[1]

Nilsson[2] and Lok and Havinga[3] found that the methoxy group activates nucleophilic hydrogen atom photosubstitution of an aromatic compound. Mizuno[4] reported photocyanation of phenanthrene and naphthalene in the presence of 1,4-dicyanobenzene.

Photocyanation is usually carried out in a mixture of organic solvent and a small amount of water in which cyanide salts are dissolved. Beugelmans[5] found that the photosubstitution is more efficient in aprotic organic solvents than in protic solvents when the reaction takes place in the presence of cyclic polyether, 18-crown-6. Recently it has been shown[6] that photocyanation of anisole is also enhanced when crown ether is replaced by polyethylene glycol. Polyethylene glycol and crown ether both activate anions in non-polar aprotic solvents by increasing the ion-dissociation. On the other hand, anions are strongly solvated by protic solvents[7] and by small amounts of water, which retards the nucleophilic reactivity.

Den Heijer[8] showed that the presence of an oxidizing agent is essential for hydrogen atom substitution reaction. Oxygen, nitrous oxide and ammonium persulfate can be used for this purpose.

Cornelisse[1] suggested that photoionization of the hydrocarbon is the primary step in nucleophilic photosubstitution of an aromatic hydrocarbon activated by an electron donating group. The radical cation formed then reacts with a nucleophile to form the product. Bunnett and his group[9] have shown that the primary step in many nucleophilic photosubstitutions is formation of a radical anion, which then reacts with a nucleophile.

We have investigated photocyanation of phenanthrene in anhydrous acetonitrile in the presence of potassium cyanide-18-crown-6 ether and oxygen at 25 °C. Variations in the intensity of the exciting radiation and the concentrations of cyanide anion and oxygen are found to influence the rate of product formation in a complex way. A simplified mechanism is proposed which explains the experimental results.

EXPERIMENTAL

Materials. Acetonitrile was purified by stirring it with calcium hydride, decanting, distilling with

0302-4377/82/050391-07$02.50

phosphorous pentoxide, refluxing with calcium hydride and distilling. It was protected against moisture and stored under nitrogen. Phenanthrene was recrystallized several times. Potassium cyanide-18-crown-6 complex was prepared by dissolving equivalent amounts of 18-crown-6 ether and KCN in dry methanol, refluxing the solution 30 min and removing the solvent at reduced pressure. The resulting complex was dissolved under nitrogen in dry acetonitrile by stirring the solution in the dark. The undissolved complex was removed from the solvent by centrifugation. The concentration of cyanide anion was determined by titration.[7] By this method a 4.2×10^{-2} mol dm^{-3} solution of the cyanide was obtained.

Methods. The reaction mixture was prepared in a 3.0 cm^3 quartz cuvette, with optical path of 1.0 cm, from known amounts of phenanthrene and cyanide solutions. Air was removed from the solution by repeated freezing and pumping to about 5×10^{-6} Torr. Oxygen of a known pressure (10–150 Torr) was added to the reaction vessel containing the frozen reaction solution. The gas volume in the reaction vessel was 12 cm^3. Equilibrium between the gas and liquid phases was established by stirring the solution in the dark. The solubility of oxygen in the reaction mixture (5.0×10^{-3} mol dm^{-3} of both KCN-crown ether complex and phenanthrene) was determined separately by measuring the drop in pressure when oxygen was dissolved in 100 cm^3 of reaction mixture. The solubility of oxygen is $(1.2 \pm 0.1) \times 10^{-3}$ mol dm^{-3} at 25 °C when the partial pressure of oxygen is 150 Torr, and this corresponds to an oxygen concentration of 8×10^{-5} mol dm^{-3} at an oxygen pressure of 10 Torr.

The intensities of the exciting radiation and quantum yields of photosubstitution were measured with a potassium ferrioxalate actinometer, using the method of Calvert and Pitts.[10] As light sources we used a 100 W high pressure Hg lamp (254 nm and 313 nm) from Illumination Ind. Inc. and a 450 W Xe lamp (270 nm, 330 nm and 346 nm) from Osram GmbH in combination with an MDR-2 High Intensity Monochromator. The linear dispersion of the monochromator was 6 nm. The intensities of the exciting radiation varied, depending on the wavelength, between (1.0 and 17.0) $\times 10^{-8}$ einsteins dm^{-2} s^{-1}. The intensities were measured during each experiment. The yield of the product, 9-cyanophenanthrene, was determined by liquid chromatography with a Perkin-Elmer Series 1 chromatograph and Model LC-15 UV–detector attached to a HC-ODS Sil-x-1 column. A 60 % CH_3OH–water eluent was used. As internal standard we used toluene, which was added to the reaction mixture after irradiation. The time of irradiation was selected to yield about 1–5 % of product. Two unidentified products, less than 10 % the amount of the main product, 9-cyanophenanthrene, were also obtained. The ratio of the three products was constant in all experiments.

RESULTS AND DISCUSSION

Our investigations showed that the rate of nucleophilic photosubstitution of phenanthrene to 9-cyanophenanthrene in dry acetonitrile depends on the concentrations of both cyanide anion and oxygen (Tables 1 and 2) and is proportional to the square of the intensity of the absorbed radiation

Table 1. Dependence of the rate of photocyanation of phenanthrene on potassium cyanide concentration at phenanthrene concentration 5.0×10^{-5} mol dm^{-3} in acetonitrile at 25 °C.

$(CN^-) \times 10^3$ / mol dm^{-3}	Rate[a] $\times 10^{11}$ / mol dm^{-3} s^{-1}	$\alpha^b \times 10^{-2}$ / mol^{-1} dm^3 s	$\sqrt{(O_2)(CN^-)^2/\alpha} \times 10^8$ / mol^2 dm^{-6} s$^{-1/2}$
0.1	5.9	1.70	6.9
0.2	13.4	3.84	9.2
0.3	14.9	4.27	13.1
0.4	14.4	4.12	17.7
1.0	23.8	6.54	35.0
2.0	31.0	8.92	59.8
3.0	28.4	8.15	94.1
4.0	28.8	8.29	124.2

[a] Measured rate. [b] Calculated using eqn. (3). $(O_2) = 8 \times 10^{-5}$ mol dm^{-3}, $\lambda_{ex} = 254$ nm, $I_o = 4.18 \times 10^{-8}$ ein dm^{-2} s^{-1}, $I_a = 4.06 \times 10^{-7}$ ein dm^{-3} s^{-1}, $I_t = 0.075 \times 10^{-8}$ ein dm^{-2} s^{-1}, $\log (I_o/I_t) = 1.74$.

Table 2. Dependence of the rate of photocyanation of phenanthrene on oxygen concentration at phenanthrene concentration 5.0×10^{-5} mol dm^{-3} in acetonitrile at 25 °C.

$(O_2) \times 10^3$ / mol dm^{-3}	Rate[a] $\times 10^{11}$ / mol dm^{-3} s^{-1}	$\alpha^b \times 10^{-2}$ / mol^{-1} dm^3 s	$\sqrt{(O_2)(CN^-)^2/\alpha} \times 10^8$ / mol^2 dm^{-6} s$^{-1/2}$
0.01	4.0	1.13	21.4
0.02	18.7	5.37	17.0
0.08	20.8	5.97	29.2
0.16	21.3	6.12	40.9
0.32	13.9	3.99	71.8
0.75	8.3	2.36	142.4
1.20	6.4	1.85	203.8

[a] Measured rate. [b] Calculated using eqn. (3). $(CN^-) = 8.0 \times 10^{-4}$ mol dm^{-3}, $\lambda_{ex} = 254$ nm, $I_0 = 4.18 \times 10^{-8}$ ein dm^{-2} s^{-1}, $I_a = 4.06 \times 10^{-7}$ ein dm^{-3} s^{-1}, $I_t = 0.075 \times 10^{-8}$ ein dm^{-2} s^{-1}, $\log (I_0/I_t) = 1.74$.

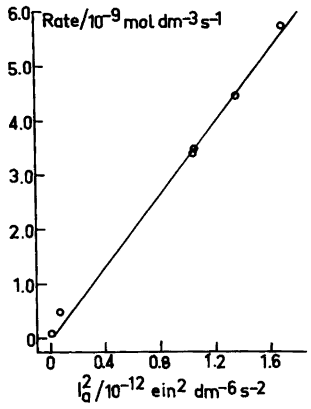

Fig. 1. Dependence of the rate of photocyanation on the square of the intensity of the absorbed radiation at phenanthrene concentration 5.0×10^{-3} mol dm^{-3}.

(Table 3 and Fig. 1). Two transients were observed [11] by flash photolysis. One of the transients decayed by second order kinetics in the absence of oxygen, and the optical density of the absorption of the another transient was proportional to the square of the intensity of the exciting light.

Eqn. (1) gives the dependence of the total reaction rate, w_R, on the square of the absorbed light intensity,

$$w_R = \alpha w_o^2 = \alpha(I\varepsilon c)^2, \quad (1)$$

where α is a parameter similar to quantum yield and a function of the concentrations of cyanide anion and oxygen, w_o is the rate of the excitation, ε is the molar absorption coefficient, c is the concentration of the absorber and I is the light intensity at any point in the system. Along the pathway the light intensity decreases exponentially, $I = I_0 \exp(-\varepsilon cl \ln 10)$, where I_0 is the incident light intensity

Table 3. Dependence of the rate of photocyanation of phenanthrene on the exciting radiation at phenanthrene concentration 5.0×10^{-3} mol dm^{-3} in acetonitrile at 25 °C.

Rate[a] $\times 10^9$ / mol dm^{-3} s^{-1}	$I_a \times 10^7$ / ein dm^{-3} s^{-1}	$I_a^2 \times 10^{12}$ / ein^2 dm^{-6} s^{-2}	λ_{ex} / nm
0.10	0.6	0.004	313[b]
0.53	2.7	0.073	313[c]
3.47	10.2	1.04	313
3.47	10.2	1.04	330
4.47	11.6	1.35	313
5.73	13.0	1.68	346

$(CN^-) = 2.0 \times 10^{-3}$ mol dm^{-3}, $(O_2) = 8 \times 10^{-5}$ mol dm^{-3}. [a] Measured rate. [b] Pyrex filter 2.0 mm. [c] Pyrex filter 1.0 mm.

and l is the distance from the front of the reaction cell. Thus the rate of the reaction decreases along the reaction cell. The average rate of the reaction is given in eqn. (2), where d is the optical path of the

$$\bar{w}_R = \alpha \frac{(I_o \varepsilon c \ln 10)^2}{d} \int_0^d \exp(-2\varepsilon c l \ln 10)\, dl$$

$$= \alpha \frac{I_o^2 \ln 10}{2d^2} D(1 - 10^{-2D})$$

$$= 1.15 \frac{\alpha}{d^2}(I_o - I_t)(I_o + I_t)D, \qquad (2)$$

reaction cell, $D = \varepsilon cd$ is the optical density of the system and I_t is the transmitted light intensity. Eqn. (2) can be rewritten to eqn. (3).

$$\frac{0.87 \bar{w}_R d^2}{(I_o^2 - I_t^2)} = \alpha D \qquad (3)$$

The linear dependence of the reaction rate on the optical density according to equation (2) explains the observed dependence of the rate on phenanthrene concentration (Fig. 2, Table 4) and it confirms the dependence of the substitution reaction on the square of the absorbed light intensity.

The squared dependence of the reaction rate on the absorbed light intensity indicates either that the formation of the reaction intermediate is a two-photon process or that the product is formed in the reaction between teo transients, both formed by monophotonic processes. The flash photolysis experiments support the latter mechanism.

We propose a mechanism (Scheme 1) involving the formation of a transient X in the primary step,

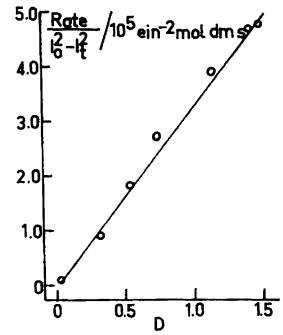

Fig. 2. Dependence of the rate of photocyanation on the optical density.

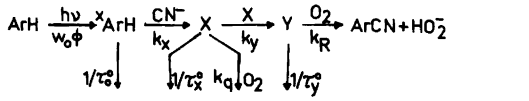

Scheme 1.

followed by its transformation into another transient Y by a second order process. The transient Y reacts with oxygen and yields the final reaction product 9-cyanophenanthrene.

The fluorescence of phenanthrene is not quenched by cyanide anion at the concentrations used in our experiments ($<10^{-2}$ mol dm^{-3}). Obviously the triplet state of phenanthrene reacts with cyanide anion. The transient X is probably a triplet exciplex or a radical anion formed from phenanthrene and a cyanide radical. Its nature will

Table 4. Dependence of the rate of photocyanation of phenanthrene on the optical density in acetonitrile at 25 °C.

(ArH)[a] × 10³	Rate[b] × 10⁹	$I_o \times 10^8$	$I_t \times 10^8$	$I_a \times 10^7$	D
mol dm^{-3}	mol dm^{-3} s^{-1}	ein dm^{-2} s^{-1}		ein dm^{-3} s^{-1}	
1.0	0.03	13.5	12.3	1.2	0.04
2.0	1.29	13.6	6.5	7.1	0.32
3.3	2.78	13.5	3.9	9.6	0.54
5.0	4.52	13.5	2.5	11.0	0.73
10.0	8.76	15.0	1.1	13.9	1.14
16.7	10.48	15.0	0.6	14.4	1.40
20.0	10.65	15.0	0.5	14.5	1.48

[a] Concentration of phenanthrene. [b] Measured rate. $(CN^-) = 2.5 \times 10^{-3}$ mol dm^{-3}, $(O_2) = 0.11 \times 10^{-3}$ mol dm^{-3}, $\lambda_{ex} = 346$ nm.

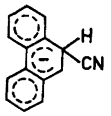

Scheme 2.

be discussed in greater detail in the next paper.[11] The transient Y is assumed to be a σ-complex (Scheme 2). This σ-complex can be formed due to a recombination of the phenanthrene radical anion and the cyanide radical or through an interaction of two triplet exciplexes. Oxidation of the σ-complex by molecular oxygen yields 9-cyanophenathrene and the peroxide anion HO_2^-.

The rates of the formation of transients X and Y are given in eqn. (4), where ϕ is the quantum yield for

$$w_x = w_o k_x \phi(CN^-)\tau_o$$
$$w_y = k_y w_x^2 \tau_x^2 \quad (4)$$

the formation of reactive excited state of phenathrene, τ_o is its lifetime and τ_x is the mean real lifetime of the transient X. w_x and w_y are the rates of the formation of transients X and Y, and k_x and k_y are the rate constants of these reactions. The local rate of the final product formation is given by eqn. (5). Here τ_y is the real lifetime of the transient Y and

$$w_R = k_R(O_2)(Y) = k_R(O_2)w_y\tau_y$$
$$= k_R k_y \tau_y (O_2)[w_o \phi \tau_o \tau_x k_x (CN^-)]^2 \quad (5)$$

k_R is the reaction rate constant. The real lifetime of the excited phenanthrene, in the presence of cyanide anion, is determined by the Stern-Volmer relation in eqn. (6), where $K_x = k_x\tau_o^o$. If the real lifetime of the

$$\tau_o = \tau_o^o/[1+K_x(CN^-)], \quad (6)$$

transient X is determined mainly by first order processes (the unimolecular decay and the quenching by oxygen) then $k_y(X) \ll [1/\tau_x^o + k_q(O_2)]$, where k_q is the quenching rate constant of X by oxygen. Furthermore, if the rate of oxidation of the σ-complex is smaller than the rate of its decomposition into phenanthrene and cyanide anion, eqn. (7), then we have eqns. (8) and (9), where $K_q = k_q\tau_x^o$.

$$k_R(O_2) \ll 1/\tau_y^o, \quad (7)$$

$$\tau_x \approx \tau_x^o/[1+K_q(O_2)], \quad (8)$$

$$\tau_y \approx \tau_y^o \quad (9)$$

Thus eqn. (5) can be written in the form (10).

Applying eqn. (1) we obtain eqns. (11) or (12).

$$w_o(CN^-)\sqrt{\frac{(O_2)}{w_R}} = \frac{[1+K_x(CN^-)][1+K_q(O_2)]}{\phi\tau_o^o k_x \tau_x^o (k_y \tau_y^o k_R)^{1/2}} \quad (10)$$

$$\sqrt{\frac{(CN^-)^2(O_2)}{\alpha}} = (\phi^2 k_R k_x^2 k_y \tau_x^{o2} \tau_o^{o2} \tau_y^o)^{-\frac{1}{2}} \cdot [1+K_x(CN^-)][1+K_q(O_2)] \quad (11)$$

$$\sqrt{\frac{(CN^-)^2(O_2)}{\alpha}} = a[1+K_x(CN^-)] = b[1+K_q(O_2)] \quad (12)$$

Thus the inverse of the square root of the rate can be presented as a function of substrates (CN^-) and (O_2). Applying eqn. (12) to the experimental results in Tables 1 and 2 we get straight lines for the functions of both cyanide anion and oxygen concentrations at phenanthrene concentration 5.0×10^{-5} mol dm^{-3} (Figs. 3 and 4).

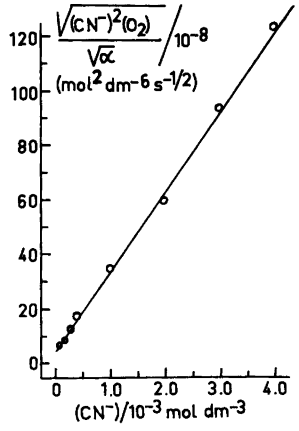

Fig. 3. Dependence of the rate of photocyanation on cyanide concentration according to eqn. (12) at phenanthrene concentration 5.0×10^{-5} mol dm^{-3}.

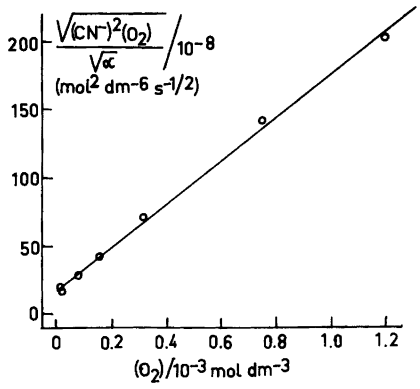

Fig. 4. Dependence of the rate of photocyanation on oxygen concentration according to eqn. (12) at phenanthrene concentration 5.0×10^{-5} mol dm^{-3}.

The values obtained for the coefficients are given in Table 5. The values of $(\phi^2\tau_o^{o2}k_x^2\tau_x^{o2}k_y\tau_y^ok_R)$ obtained from the dependence of the quantum yield on both cyanide anion and oxygen concentrations are quite close to each other. This confirms the proposed kinetic scheme. Similar linear relationships were obtained at phenathrene concentration 5.0×10^{-3} mol dm^{-3} (Tables 6 and 7) with some different values of the coefficients (Table 5). This is probably due to the observed increase of the rate of the cyanation reaction when some reaction products are formed or to some more complex mechanism at higher concentration of phenanthrene.

Also at cyanide concentration higher than 10×10^{-3} mol dm^{-3}, the dependence on the cyanide concentration begins to deviate from linearity (Table 6). This may be due to an additional

Table 5. Values of the coefficients in eqns. (11) and (12) obtained at phenanthrene concentrations 5.0×10^{-5} mol dm^{-3} and 5.0×10^{-3} mol dm^{-3}.[a]

(ArH)	mol dm^{-3}	5.0×10^{-5}	5.0×10^{-3}
a	mol^2 dm^{-6} s$^{-1/2}$	4.0×10^{-8}	9.5×10^{-8}
K_x	mol^{-1} dm^3	7.4×10^3	1.6×10^3
$(\phi\tau_o^ok_x\tau_x^o)^2k_y\tau_y^ok_R$	mol^{-4} dm^{12} s	1.8×10^{15}	0.5×10^{15}
b	mol^2 dm^{-6} s$^{-1/2}$	1.8×10^{-7}	4.0×10^{-7}
K_q	mol^{-1} dm^3	9.0×10^3	13.0×10^3
$(\phi\tau_o^ok_x\tau_x^o)^2k_y\tau_y^ok_R$	mol^{-4} dm^{12} s	1.5×10^{15}	0.5×10^{15}

[a] At phenanthrene concentration 5.0×10^{-5} mol dm^{-3} the concentrations of oxygen and cyanide anion were 8×10^{-5} mol dm^{-3} and 8.0×10^{-4} mol dm^{-3} and at phenanthrene concentration 5.0×10^{-3} mol dm^{-3} they were 8×10^{-5} mol dm^{-3} and 5.0×10^{-3} mol dm^{-3}, respectively.

Table 6. Dependence of the rate of photocyanation of phenanthrene on potassium cyanide concentration at phenanthrene concentration 5.0×10^{-3} mol dm^{-3} in acetonitrile at 25 °C.

$(CN^-) \times 10^3$ / mol dm^{-3}	Rate[a] $\times 10^9$ / mol dm^{-3} s^{-1}	$\alpha^b \times 10^{-2}$ / mol^{-1} dm^3 s	$\sqrt{(O_2)(CN^-)^2/\alpha} \times 10^8$ / mol^2 dm^{-6} s$^{-1/2}$
0.5	1.90	6.9	17
1.0	4.37	15.9	22
2.0	4.90	17.9	42
2.0	5.03	18.4	42
3.5	6.88	25.1	63
5.0	7.50	27.4	86
7.1	7.94	28.9	118
14.1	6.75	24.6	254
21.4	5.29	19.3	436

[a] Measured rate. [b] Calculated using eqn. (3). $(O_2) = 8 \times 10^{-5}$ mol dm^{-3}, $\lambda_{ex} = 313$ nm, $I_o = 12.52 \times 10^{-8}$ ein dm^{-2} s^{-1}, $I_a = 12.14 \times 10^{-7}$ ein dm^{-3} s^{-1}, $I_t = 0.37 \times 10^{-8}$ ein dm^{-2} s^{-1}, log $(I_o/I_t) = 1.52$.

Table 7. Dependence of the rate of photocyanation of phenanthrene on oxygen concentration at phenanthrene concentration 5.0×10^{-3} mol dm^{-3} in acetonitrile at 25 °C.

$(O_2) \times 10^3$ / mol dm^{-3}	Rate[a] $\times 10^9$ / mol dm^{-3} s^{-1}	$\alpha^b \times 10^{-2}$ / mol^{-1} dm^{-3} s	$\sqrt{(O_2)(CN^-)^2/\alpha} \times 10^8$ / mol^2 dm^{-6} s$^{-1/2}$
0.08	5.71	26.5	86
0.16	4.94	23.1	131
0.25	4.13	19.3	180
0.36	2.72	12.6	266
0.56	2.02	9.4	385
0.80	1.11	5.2	688
1.60	0.60	2.8	1195

[a] Measured rate. [b] Calculated using eqn. (3). $(CN^-) = 5.0 \times 10^{-3}$ mol dm^{-3}, $\lambda_{ex} = 313$ nm, $I_o = 10.88 \times 10^{-8}$ ein dm^{-2} s^{-1}, $I_a = 10.60 \times 10^{-7}$ ein dm^{-3} s^{-1}, $I_t = 0.28 \times 10^{-8}$ ein dm^{-2} s^{-1}, log $(I_o/I_t) = 1.58$.

quenching of some excited state by the cyanide anion.

It is possible to evaluate $(\phi\tau_x^o)^2 k_y$ from the value obtained for $(\phi\tau_o^o k_x \tau_x^o)^2 k_y \tau_y^o k_R = 1.7 \times 10^{15}$ mol^{-4} dm^{12} s. Using the approximation (7) and the obtained value of $K_x = k_x\tau_o^o$ (Table 5)

$$\phi^2\tau_x^{o2}k_y = \frac{1.7 \times 10^{15} \text{ mol}^{-4} \text{ dm}^{12} \text{ s}}{(k_x\tau_o^o)^2 k_R \tau_y^o}$$

$$> 3.1 \times 10^7 (O_2) \text{ mol}^{-2} \text{ dm}^6 \text{ s}.$$

Because $k_y \leq 1 \times 10^{10}$ dm^3 mol^{-1} s^{-1}, $(O_2) > 0.08 \times 10^{-3}$ mol dm^{-3} and $\phi \leq 1$, $\tau_x^o > 5 \times 10^{-4}$ s. Furthermore, because $K_q = k_q\tau_x^o = 9.0 = 10^3$ mol^{-1} dm^3, $k_q < 2 \times 10^7$ dm^3 mol^{-1} s^{-1}.

Acknowledgement. This work has been done within the framework of the scientific collaboration between the University of Helsinki and Lomonosov Moscow State University.

REFERENCES

1. Cornelisse, J., Lodder, G. and Havinga, E. *Rev. Chem. Intermed. 2 (3)* (1979) 231.
2. Nilsson, S. *Acta Chem. Scand. 27* (1973) 329.
3. Lok, C. M. and Havinga, E. *Proc. K. Ned. Akad. Wet. B 77* (1974) 15.
4. Mizuno, K., Pac, C. and Sakurai, H. *J. Chem. Soc. Chem. Commun.*. (1975) 553.
5. Beugelmans, R., Le Goff, M.-T., Pusset, J. and Roussi, G. *J. Chem. Soc. Chem. Commun.* (1976) 377.
6. Suzuki, N., Shimazu, K., Ito, T. and Izawa, Y. *J. Chem. Soc. Chem. Commun.* (1980) 1253.
7. Lemmetyinen, H., Lehtinen, L. and Koskikallio, J. *Finn. Chem. Lett.* (1979) 72.
8. Den Heijer, J., Shadid, O. B., Cornelisse, J. and Havinga, E. *Tetrahedron 33* (1977) 779.
9. Kim, J. K. and Bunnett, J. F. *J. Am. Chem. Soc. 92* (1970) 7463.
10. Calvert, J. G. and Pitts, J. N., Jr. *Photochemistry*, Wiley, New York 1966, p. 780.
11. Lemmetyinen, H., Ivanov, V. L., Kuzmin, M. G. and Koskikallio, J. *To be published.*

Received August 26, 1981.

Acta Chemica Scandinavica A 36 (1982) 399–405

Structural Studies on the Sulfur—Nitrogen Bond. I. The Crystal Structure of Bis(morpholino)sulfide

CHRISTIAN RØMMING,[a] GUNNAR O. NEVSTAD[b] and JON SONGSTAD[b]

[a] Department of Chemistry, University of Oslo, Oslo 3, Norway and [b] Department of Chemistry, University of Bergen, N-5014 Bergen-Univ., Norway

The structure of the title compound, $[O(CH_2CH_2)_2N]_2S$, has been determined by X-ray crystallographic methods. Fullmatrix least-squares refinement led to a conventional *R*-value of 0.050 for 2373 reflections.

The crystals are monoclinic, space group $P2_1/c$. There are two fairly similar molecules per asymmetric unit. Cell dimensions (at −150 °C) are: $a = 11.207(2)$ Å; $b = 15.658(3)$ Å; $c = 11.574(2)$ Å; $\beta = 90.19(2)°$. The molecule possesses a pseudo two-fold axis with the morpholino rings in the chair conformation and linked equatorially to the central sulfur atom. The NSN bond angle is 113.2° and the average S–N bond length is 1.680 Å. The sum of the bond angles at the nitrogen atoms is close to 350.0° and the direction of the nitrogen lone pairs is cisoidal to the sulfur lone pairs. The two morpholino groups of a molecule are slightly twisted; the torsion angles NSNC being about −67 and +74° for each morpholino ring.

Although being known for close to a century,[1] bis(dialkylamino)sulfides, $(R_2N)_2S$, is a class of compounds which has only been the subject of limited studies. Their simple preparation was described by Blake[2] some 40 years ago and the compounds are known to be most stable toward both hydrolysis and thermal degradation. With the exception of $(Et_2N)_2S$, bis(dialkylamino)sulfides are generally crystalline and colourless materials at room temperature.[3]

Bis(dialkylamino)sulfides are apparently quite unreactive species and only very powerful electrophilic species seem to be attacked by this class of compounds. Strongly alkylating agents such as R_3O^+-salts form *S*-alkylsulfonium salts[4–6] while the hard Lewis acid BF_3 forms a fairly stable 1:2 adduct with $(Me_2N)_2S$ through N–B bonds.[7] Bis(dialkylamino)sulfides are thus in principle ambident but very weakly nucleophilic species;[8] the potential ambident nature but not the limited reactivity resembles that of $(R_2N)_3P$ and $(R_2N)_3As$.[9,10] Contrary to the latter compounds $(R_2N)_2S$ exhibits none or only weak reactivity toward protic species and alcohols are convenient crystallization agents.

In order to improve our knowledge of the chemistry of $(R_2N)_2S$ it appears necessary to obtain more information with regard to both the electronic distribution within the N–S–N part of the molecules and also to the preferred conformation. The various studies published so far including mass

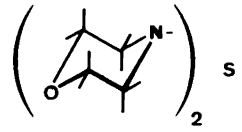

1

spectral studies,[11,12] NMR studies[13,14] and UV studies,[15] do not allow any definite conclusions to be made. X-Ray crystallographic examination appears to be a useful approach and in the present study we want to report on the crystal structure of bis(morpholino)sulfide, Mor_2S (*1*). By choosing morpholino groups as substituents, a nicely crystalline material was obtained and a comparison with the structure of $(MorS-)_2$,[16] $(MorS_2-)_2$,[17] Mor_3P[9] and Mor_3As[10] could be made. X-Ray studies of S_7NSNMe_2 and of $((C_6H_{11})_2N)_2S$[18] and an electron diffraction study of $(Me_2N)_2S$[19] have recently been published.

0302-4377/82/050399-07$02.50

EXPERIMENTAL

Material. Bis(morpholino)sulfide, Mor_2S, was made as described in Ref. 2 from sulfur dichloride, SCl_2, freshly distilled from 2% phosphorus trichloride, PCl_3, to remove traces of S_2Cl_2.[20] The compound was first purified by sublimation; subsequent crystallization from ethanol yielded crystals suitable for the X-ray experiments. M.p. 124 −125 °C (125 °C [2]); NMR (CH_2Cl_2): [δ 3.23−3.37 (m, 8, NCH_2), 3.56−3.70 (m, 8, OCH_2)]; IR (KBr-disc): 685 cm^{-1} (S−N).

X-Ray data. Data for the measurements of cell dimensions and intensity data were collected on a SYNTEX $P\bar{1}$ diffractometer using graphite crystal monochromated Mo$K\alpha$ radiation (λ=0.71069 Å). The temperature at the crystal site was −150 °C, crystal size 0.1 × 0.4 × 0.4 mm. Cell parameters were determined by a least squares fit to the diffractometer settings of 15 general reflections with $2\theta > 35°$. Intensities were measured with the θ-2θ scan technique, scan speed 2−4° min^{-1} depending on the peak intensity, scan width ±1.0° up to a sin θ/λ value of 0.60 $Å^{-1}$. Background counts were taken for 0.35 times the scan time at each of the scan limits. Out of the 3618 unique reflections recorded, 2373 with $I > 2.5\sigma(I)$ were retained for the structure analysis. The standard deviations for the intensities were calculated as $\sigma(I) = [C_T + (0.02\ C_N)^2]^{\frac{1}{2}}$, where C_T is the total number of counts and C_N is the scan count minus background count. The intensities were corrected for Lorentz and polarization effects but not for absorption.

A description of the computer programs used for the structure determination is given in Ref. 21. Atomic form factors were those of Doyle and Turner [22] for the heavy atoms and of Stewart, Davidson and Simpson [23] for the hydrogen atoms.

CRYSTAL DATA

Bis(morpholino)sulfide, $C_8H_{16}N_2O_2S$, m.p. 124−125 °C. Monoclinic, a=11.207(2) Å; b=15.658(3) Å; c=11.574(2) Å; β=90.19(2)°; V=2031.0(7) $Å^3$; (t=−150 °C); M=204.29; Z=8; $F(000)$=880; μ(Mo$K\alpha$) =2.9 cm^{-1}; D_x=1.336 g cm^{-3}. Absent reflections: ($h0l$) for l odd, ($0k0$) for k odd. Space group $P2_1/c$ (No. 14).

STRUCTURE DETERMINATION

The structure was determined by direct methods [24] and refined in the way described in Ref. 9. There are two molecules per asymmetric unit. The refinement converged to a conventional R-value of 0.050, R_w=0.052 and a goodness of fit, $[\Sigma w\Delta F^2/(m-n)]^{\frac{1}{2}}$, of 2.11.

Final atomic parameters are listed in Table 1. Tables of observed and calculated structure factors with standard deviations are available from the authors.

RESULTS AND DISCUSSION

The geometry of the two molecules of the asymmetric unit is nearly identical; no chemically significant differences in bond lengths and bond angles nor in S−N torsion angles are apparent.

A drawing of a molecule is shown in Fig. 1, where the numbering of the atoms is also indicated. In Table 2 bond lengths, bond angles, torsion angles and various other structural data are given. Estimated standard deviations are calculated from the variance−covariance matrix. In Fig. 2 the Newman projection of the S−N bond in the average molecule is shown; the broken lines indicate approximate directions of the sulfur and nitrogen lone pairs. In Table 3 a comparison is made between the most relevant structural parameters (average values) in Mor_2S, determined in the present study, in $(MorS-)_2$ and in $(MorS_2-)_2$ from Refs. 16 and 17, respectively, in $((C_6H_{11})_2N)_2S$ [18] and in $(Me_2N)_2S$.[19]

Conformational considerations. In the case of bis(dialkylamino)sulfides the preferential conformation seems to be a compromise between the operation of essentially two competing factors; the tendency of the sulfur and the nitrogen lone pairs to avoid each other and the opposing tendency to maximize dative $p-d$ π bonding.[25,26] This is apparently a quite common phenomenon in compounds with lone pairs on adjacent atoms, particularly for atoms from the upper part of the periodic system with lone pairs exhibiting some directional properties.[27] For a relevant comparison,

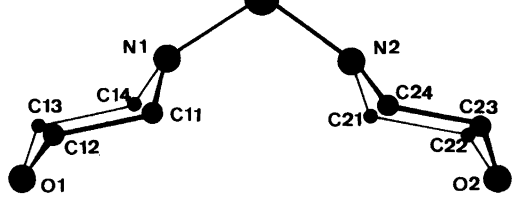

Fig. 1. Bis(morpholino)sulfide as seen normal to the NSN plane.

Table 1. Fractional atomic coordinates and thermal parameters with estimated standard deviations. The anisotropic temperature factor is given by $\exp[-2\pi^2(U11a^{*2}h^2+\ldots+2U12a^*b^*hk+\ldots)]$.

Atom	*x*	*y*	*z*	*U*11	*U*22	*U*33	*U*12	*U*13	*U*23
S1	0.10677(10)	0.26755(5)	0.63365(9)	0.0270(5)	0.0144(4)	0.0226(4)	−0.0010(5)	0.0092(4)	−0.0019(5)
S2	0.60145(10)	0.26104(5)	0.13867(9)	0.0223(5)	0.0160(4)	0.0289(5)	−0.0008(5)	0.0037(4)	0.0015(5)
O1	0.3079(3)	0.4437(2)	0.3963(3)	0.0372(17)	0.0242(15)	0.0357(16)	−0.0054(14)	0.0147(13)	0.0018(13)
O2	−0.0931(3)	0.4429(2)	0.8728(3)	0.0271(16)	0.0237(13)	0.0304(15)	0.0036(14)	0.0074(12)	−0.0024(14)
O3	0.3656(2)	0.4365(2)	−0.0697(2)	0.0284(16)	0.0238(15)	0.0339(17)	0.0014(12)	0.0000(13)	0.0028(13)
O4	0.8536(2)	0.4333(2)	0.3338(2)	0.0245(15)	0.0218(15)	0.0345(17)	−0.0001(11)	0.0058(12)	−0.0042(12)
N1	0.1854(3)	0.3279(2)	0.5413(3)	0.0232(17)	0.0215(17)	0.0210(16)	0.0010(14)	0.0081(14)	0.0025(13)
N2	0.0279(3)	0.3256(2)	0.7290(3)	0.0221(17)	0.0208(17)	0.0210(16)	0.0024(14)	0.0075(14)	−0.0012(13)
N3	0.5081(3)	0.3192(2)	0.0574(3)	0.0220(17)	0.0205(18)	0.0272(18)	0.0012(14)	0.0062(14)	0.0011(14)
N4	0.6989(3)	0.3203(2)	0.2139(3)	0.0182(16)	0.0252(19)	0.0249(17)	−0.0019(14)	0.0073(14)	−0.0028(14)
C11	0.1210(4)	0.3793(3)	0.4558(3)	0.0286(23)	0.0282(23)	0.0239(21)	−0.0003(19)	0.0063(18)	0.0045(18)
C12	0.2047(4)	0.3993(3)	0.3569(3)	0.0409(26)	0.0299(24)	0.0216(21)	0.0015(20)	0.0103(20)	0.0021(17)
C13	0.3705(4)	0.3925(3)	0.4778(4)	0.0249(22)	0.0298(24)	0.0402(25)	−0.0025(18)	0.0130(20)	−0.0026(19)
C14	0.2943(3)	0.3706(3)	0.5831(3)	0.0184(20)	0.0259(22)	0.0319(23)	−0.0027(17)	0.0074(18)	−0.0016(17)
C21	0.0936(4)	0.3746(3)	0.8166(3)	0.0251(21)	0.0236(21)	0.0218(20)	0.0008(17)	0.0052(17)	−0.0057(17)
C22	0.0091(4)	0.3972(3)	0.9137(4)	0.0356(25)	0.0316(25)	0.0255(22)	0.0100(20)	0.0054(20)	−0.0032(18)
C23	−0.1563(4)	0.3915(3)	0.7917(4)	0.0239(22)	0.0247(23)	0.0339(23)	0.0000(18)	0.0093(19)	−0.0003(18)
C24	−0.0790(3)	0.3700(3)	0.6885(3)	0.0231(21)	0.0261(22)	0.0264(21)	−0.0012(18)	0.0062(18)	−0.0004(17)
C31	0.4222(3)	0.3757(3)	0.1166(3)	0.0199(21)	0.0278(23)	0.0297(22)	−0.0024(18)	0.0076(18)	−0.0011(17)
C32	0.3220(4)	0.3966(3)	0.0331(4)	0.0212(21)	0.0295(23)	0.0361(24)	0.0029(17)	0.0029(19)	0.0039(18)
C33	0.4495(4)	0.3808(3)	−0.1258(3)	0.0339(22)	0.0245(22)	0.0277(22)	−0.0011(18)	0.0053(19)	0.0006(17)
C34	0.5532(4)	0.3599(3)	−0.0484(3)	0.0255(21)	0.0210(21)	0.0230(20)	−0.0022(17)	0.0073(17)	−0.0002(16)
C41	0.7919(3)	0.3689(3)	0.1519(3)	0.0209(20)	0.0213(21)	0.0263(21)	−0.0006(16)	0.0086(17)	0.0001(16)
C42	0.8935(3)	0.3868(3)	0.2348(4)	0.0202(20)	0.0231(22)	0.0330(22)	0.0008(16)	0.0079(18)	−0.0054(17)
C43	0.7640(4)	0.3852(3)	0.3935(3)	0.0298(22)	0.0207(21)	0.0272(21)	−0.0009(17)	0.0055(19)	−0.0015(16)
C44	0.6589(4)	0.3679(3)	0.3166(3)	0.0224(21)	0.0239(22)	0.0239(22)	0.0006(18)	0.0072(17)	−0.0015(17)

Atom	*x*	*y*	*z*	*B*	Atom	*x*	*y*	*z*	*B*
H111	0.096	0.432	0.493	2.2	H112	0.050	0.344	0.432	2.2
H121	0.162	0.434	0.300	2.2	H122	0.226	0.344	0.313	2.2
H131	0.444	0.423	0.050	2.2	H132	0.395	0.338	0.441	2.2
H141	0.276	0.429	0.625	2.2	H142	0.340	0.331	0.633	2.2
H211	0.124	0.431	0.783	2.2	H212	0.164	0.338	0.844	2.2
H221	0.051	0.433	0.969	2.2	H222	−0.018	0.339	0.952	2.2
H231	−0.226	0.426	0.766	2.2	H232	−0.177	0.338	0.832	2.2
H241	−0.060	0.424	0.649	2.2	H242	−0.119	0.336	0.632	2.2
H311	0.461	0.428	0.137	2.2	H312	0.389	0.348	0.183	2.2
H321	0.266	0.439	0.070	2.2	H322	0.279	0.340	0.012	2.2
H331	0.471	0.411	−0.201	2.2	H332	0.407	0.328	−0.148	2.2
H341	0.598	0.416	−0.026	2.2	H342	0.604	0.319	−0.088	2.2
H411	0.754	0.423	0.122	2.2	H412	0.820	0.335	0.090	2.2
H421	0.959	0.425	0.198	2.2	H422	0.925	0.326	0.258	2.2
H431	0.745	0.421	0.461	2.2	H432	0.796	0.328	0.424	2.2
H441	0.617	0.421	0.292	2.2	H442	0.604	0.331	0.360	2.2

cf. the structure of tris(dialkylamino)phosphines and arsines.[9,10]

In $(R_2N)_2S$ several conformations are in principle possible, the three most conceivable ones having both the nitrogen lone pairs transoidal, one being transoidal and one cisoidal, and finally both being cisoidal to the sulfur lone pairs.[19] Conformations based upon the direction of the lone pairs being perpendicular to the NSN plane seem to be highly sterically hindered. In all compounds of the general

Table 2. Structural data.

		Mol. A	Mol. B
Bond lengths (Å)			
S1	N1	1.679(3)	1.674(3)
S1	N2	1.683(3)	1.675(3)
N1	C11	1.463(5)	1.478(5)
C11	C12	1.515(6)	1.515(6)
C12	O1	1.424(5)	1.431(5)
O1	C13	1.421(6)	1.439(5)
C13	C14	1.529(6)	1.501(6)
C14	N1	1.472(5)	1.472(5)
N2	C21	1.468(5)	1.478(5)
C21	C22	1.514(6)	1.513(6)
C22	O2	1.429(5)	1.431(5)
O2	C23	1.423(5)	1.435(5)
C23	C24	1.516(6)	1.499(6)
C24	N2	1.462(5)	1.473(5)

Bond angles (°)						Mol. A	Mol. B
N1	S1	N2				113.0(1)	113.3(1)
S1	N1	C11				118.8(3)	118.2(3)
S1	N1	C14				118.9(3)	119.2(3)
N1	C11	C12				108.6(3)	108.4(3)
C11	C12	O1				111.3(3)	111.7(3)
C12	O1	C13				109.6(3)	109.6(3)
O1	C13	C14				112.3(3)	111.6(3)
C13	C14	N1				107.7(3)	108.9(3)
C14	N1	C11				112.3(3)	110.6(3)
S1	N2	C21				118.2(2)	119.5(3)
S1	N2	C24				118.6(3)	120.0(2)
N2	C21	C22				108.8(3)	108.5(3)
C21	C22	O2				111.9(3)	111.4(3)
C22	O2	C23				109.4(3)	109.9(3)
O2	C23	C24				111.1(3)	111.0(3)
C23	C24	N2				108.8(3)	109.3(3)
C24	N2	C21				112.4(3)	110.4(3)
Various averaged data							
$\overline{S-N}$	(Å)	1.678(4)					
$\overline{N-C}$	(Å)	1.470(6)					
$\overline{C-C}$	(Å)	1.512(9)					
$\overline{C-O}$	(Å)	1.429(6)					
$\angle\overline{NSN}$	(°)	113.2(2)					
$\angle\overline{SNC}$	(°)	118.8(4)					
$\angle\overline{CNC}$	(°)	111.4(10)					
$\angle\overline{NCC}$	(°)	108.6(5)					
$\angle\overline{CCO}$	(°)	111.5(4)					
$\angle\overline{COC}$	(°)	109.6(2)					
Torsion angles (°)							
N2	S1	N1	C11			−68.1(3)	−65.6(3)
N2	S1	N1	C14			74.7(3)	73.7(3)
N1	S1	N2	C21			−68.1(3)	−67.4(3)
N1	S1	N2	C24			73.6(3)	74.6(3)

Average sum of nitrogen bond angles: 349.5(5)°
Average deviation of N from plane SCC: 0.29(1) Å
Average torsion angle N−S−N−Lone pair N: −176.6(6)°

type $(R_2N)_2S$ only the cisoidal conformation has so far been observed in the solid state; in the gas phase $(Me_2N)_2S$ may contain some of the two other conformers.[19] A similar conformation has also been observed for $(Me_2N)_2SO$[28] and for $(Me_2N)_2SO_2$.[29] Apparently, the determining factor is the tendency of the nitrogen lone pairs to be as far apart as possible and at the same time avoid the sulfur lone pairs in the divalent species and the oxygen atoms in the corresponding sulfoxides and sulfones.

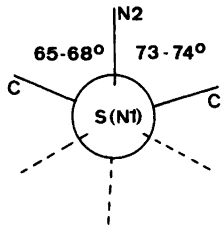

Fig. 2. Newman diagram of the S−N bond in bis-(morpholino)sulfide.

As long as the cisoidal conformation is preferred, an ideal C_{2v} symmetry would favour a maximum overlap between a single sulfur *d*-orbital and the nitrogen *p*-orbitals since the axes of the nitrogen *p*-orbitals thus would be parallel. As a result, the four carbon atoms linked to the two nitrogen atoms would be coplanar as observed in $[(C_6H_{11})_2N]_2S$.[18] In Mor_2S, however, the two morpholino groups are twisted, and in opposite directions, some 10° away

Table 3. Comparison of some average structural parameters in Mor_2S_2, $(MorS-)_2$ $(MorS-)_2$, $((C_6H_{11})_2N)_2S$ and $(Me_2N)_2S$.

	Mor_2S	$(MorS-)_2$	$(MorS_2-)_2$	$((C_6H_{11})_2N)_2S$	$(Me_2N)_2S$
S–N	1.678(4)	1.685(4)	1.668(2)	1.657(4)	1.688(6)
$\Sigma\angle N°$	349.5(5)	343–344	344–345	358–359	351(2)
$\angle NSN°(\angle NSS°)$	113.2(2)	(112)	[109.1(2)]	110.7(2)	114.5(16)
$\angle CNS°$	118.8(4)	116(1)	116(1)	120(1)	117.9(6)
$\angle CNC$	111.4(10)	111(1)	112.1(3)	117.9(4)	116.5(16)
N–C	1.470(6)	1.47	1.462(6)	1.467	1.473(6)
Method	X-ray	X-ray	X-ray	X-ray	El.-diff.
Reference	This study	16	17	18	19

from the conformation of highest possible symmetry. Presumably, this twisting is caused by the hydrogen atoms on the carbon atoms linked to the nitrogen atoms. In the twisted form as observed in the present study four intramolecular H–H distances are in the range 2.45–2.52 Å.

The N–S–N bond angle. The N–S–N bond angle in Mor_2S and in comparable compounds, *cf.* Table 3, is slightly but significantly larger than the tetrahedral angle and considerably larger than the C–S–C bond angle in R_2S for which bond angles close to 100° are generally observed.[30] It has been suggested that the N–S–N angle is large because of repulsion between the partial double bonds between the central sulfur atom and the nitrogen atoms.[18] However, the spatial demands of a dialkylamino group will be better satisfied the larger the N–S–N bond angle is.

Bond angles around the nitrogen atoms. The sum of the bond angles around the nitrogen atoms, $\Sigma\angle N$, is 349.5(5)° in Mor_2S; the given sum being the average of the four independent determinations, two for each of the two molecules in the asymmetric unit. The coordination of the nitrogen atoms is thus pyramidal, but the hybridization is closer to sp^2 than to sp^3. The average distance from the nitrogen atoms to the plane through the three adjacent atoms is 0.29(1) Å.

In $(Me_2N)_2S$[19] and in $(Me_2N)_2SO_2$[29] a fairly similar hybridization of the nitrogen atoms is observed while in $(Mor_2S-)_2$,[16] in $(Mor_2S_2-)_2$[17] and in $(Me_2N)_2SF_2$[26] the nitrogen atoms have significantly more *p*-character, $\Sigma\angle N$ being in the 343–345° range. In $((C_6H_{11})_2N)_2S$ and in S_7NSNMe_2[17] the nitrogen atoms are essentially sp^2 hybridized, $\Sigma\angle N$ being from 355°to 359°. The near planar geometry of the nitrogen atoms in $[(C_6H_{11})_2N]_2S$ is apparently caused by the large CNC bond angle, 117.9(4)°, *cf.* Table 3, which presumably has its origin in the steric demands of the two cyclohexyl groups linked to the same nitrogen atom.

The sulfur nitrogen bond length. A number of X-ray, electron diffraction and microwave studies on compounds with S–N bonds have appeared in recent years. In non-charged species the S–N bond length is presently known to cover a larger range, from 1.446 Å in F_3SN[31] to 1.90 Å for the axial bond in a spirocyclic sulfurane.[32] For surveys of S–N bond lengths, *cf.* Refs. 33 and 34. The exceptional large range for the S–N bond length observed may suggest that this bond length is even more sensitive to the oxidation state of the central atom and of the hybridization of the nitrogen atom than is the P–N bond in phosphorus–nitrogen compounds.[9,35]

According to the Stevenson-Schomaker equation[36] the S–N single bond is 1.735 Å, which is the same length as the P–N single bond.[37] In Mor_2S, as observed in the present study, the average S–N bond length is 1.678(4) Å indicating a bond order of approximately 1.1.[38] It is notable that the S–N bond lengths in Mor_2S are as in several other compounds, *cf.* Table 3, but are significantly longer than in $[(C_6H_{11})_2N]_2S$, 1.657(4) Å.[18] Presumably, this difference is due to the difference in the hybridization of the nitrogen atoms in Mor_2S and in $[(C_6H_{11})_2N]_2S$ combined with the lack of C_{2v} symmetry in Mor_2S. Since the four carbon atoms linked to the two nitrogen atoms are not coplanar the nitrogen *p*-orbitals will not have the ideal direction for maximum overlap with a sulfur *d*-orbital. As a result, the delocalization of the nitrogen lone pairs onto the sulfur atom is limited and causing the nitrogen atoms to retain much of their

sp^3 hybridization. The S – N bond length is thus only slightly shorter than the S – N single bond length.

Intramolecular contacts. The shortest distances between the hydrogen atoms are in the range 2.45 – 2.52 Å. There is little doubt that these contacts are of importance both for the magnitude of the N – S – N angle and for the torsion angles about the S – N bonds. As may be seen from Table 2 the torsion angles about the four non-equivalent S – N bonds are nearly equal; this is also depicted in the Newman diagram in Fig. 2.

The structure of the substituents. The morpholino substituents are in the expected chair conformation and linked equatorially to the central sulfur atom. The bond lengths and the bond angles listed in Table 2 are all of the expected magnitude.

CONCLUSIONS

Bis(dialkylamino)sulfides, $(R_2N)_2S$, seem to prefer a conformation by which the nitrogen lone pair are cisoidal to the sulfur lone pairs. For substituents of sufficiently small steric demands the molecules may attain a C_{2v} symmetry whereby the nitrogen *p*-orbitals are parallel and well suited for interaction with a sulfur *d*-orbital through $d_\pi - p_\pi$ overlap. In less symmetrical compounds, as in Mor_2S, the $d_\pi - p_\pi$ overlap is not maximized, resulting in longer S – N bonds and more pyramidal nitrogen atoms. The reactivity pattern of bis(dialkylamino)sulfides may thus be significantly dependent upon the steric demands of the substituents linked to the nitrogen atoms.

The weak nucleophilicity of the sulfur atom in $(R_2N)_2S$ has its probable background in the large N – S – N bond angle, ~113°. The presence of nitrogen atoms of some sp^3 character is in agreement with the observation that this class of compounds may act as nitrogen donors toward certain Lewis acids. The weak nucleophilicity of the central sulfur atom combined with its ability to undergo insertion reactions with CS_2 and other species[39] suggests that chemically $(R_2N)_2S$ resembles $(R_2N)_3As$[10] far more than $(R_2N)_3P$.[9] It is presently not known whether $(R_2N)_2S$ acts as biphilic species toward CS_2 or if the insertion product is formed through a multistep mechanism. However, the fairly low torsional barrier about the S – N bond in $(R_2N)_2S$[14] may allow these compounds to easily adapt to any necessary conformation in solution, especially at elevated temperatures.

REFERENCES

1. Schenk, R. *Justus Liebigs Ann. Chem. 290* (1896) 171.
2. Blake, E. S. *J. Am. Chem. Soc. 65* (1943) 1267.
3. Levschenko, E. S., Sheinkman, I. E. and Kirsanov, A. V. *Zh. Obshch. Khim. 33* (1963) 3068.
4. Richards, J. L. and Tarbell, D. S. *J. Org. Chem. 35* (1970) 2079.
5. Minato, H., Okuma, K. and Kobayashi, M. *J. Org. Chem. 43* (1978) 652.
6. *Unpublished results.*
7. Burg, H. B. and Woodrow, H. W. *J. Am. Chem. Soc. 76* (1954) 219.
8. Epschtein, L. M., Zdanova, A. N., Khazanova, Y. A., Feldshtein, M. S. and Kazitsyna, L. A. *Izv. Akad. Nauk SSSR Ser. Khim.* (1974) 87.
9. Rømming, C. and Songstad, J. *Acta Chem. Scand. A 32* (1978) 689.
10. Rømming, C. and Songstad, J. *Acta Chem. Scand. A 34* (1980) 365.
11. Harpp, D. N., Back, T. G. and Snyder, J. P. *Phosphorus Sulfur 1* (1976) 143.
12. Raban, M., Noyd, D. and Bermann, L. *Phosphorus Sulfur 1* (1976) 153.
13. Hu, V. W., Gilje, J. W. and Bopp, T. T. *Inorg. Chem. 12* (1973) 955.
14. Raban, M. and Cho, T.- m. *Int. J. Sulfur Chem. A 1* (1971) 269.
15. Fehér, F. and Münzner, H. *Chem. Ber. 98* (1963) 1131.
16. Nyburg, S. C. and Pickard, F. H. *J. Cryst. Mol. Struct. 3* (1973) 343.
17. Foss, O. and Janickis, V. *J. Chem. Soc. Dalton Trans.* (1980) 632.
18. Bruce, R. B., Gillespie, R. J. and Slim, D. R. *Can. J. Chem. 56* (1978) 2927.
19. Hargittai, I. and Hargittai, M. *Acta Chim. Acad. Sci. Hung. 75* (1973) 129.
20. Brauer, G. *Handbuch der Präparativen Anorganischen Chemie*, Ferdinand Enke Verlag, Stuttgart 1954, p. 288.
21. Groth, P. *Acta Chem. Scand. 27* (1973) 1837.
22. Doyle, P. A. and Turner, P. S. *Acta Crystallogr. A 24* (1968) 390.
23. Stewart, R. F., Davidson, E. R. and Simpson, W. T. *J. Chem. Phys. 42* (1965) 3175.
24. Germain, G., Main, P. and Woolfson, M. M. *Acta Crystallogr. A 27* (1971) 368.
25. Chen, M. M. L. and Hoffmann, R. *J. Am. Chem. Soc. 98* (1976) 1647.
26. Cowley, A. H., Riley, P. E., Szobota, J. S. and Walker, M. L. *J. Am. Chem. Soc, 101* (1979) 5620.
27. Gillespie, R. J. *Molecular Geometry*, Van Nostrand-Reinhold, London 1972, p. 109.
28. Hargittai, I. and Vilkov, L. V. *Acta Chim. Acad. Sci. Hung. 63* (1970) 143.

29. Jordan, T., Smith, H. H., Lohr, L. L., Jr. and Lipscomb, W. N. *J. Am. Chem. Soc. 85* (1963) 846.
30. Pierce, L. and Hayashi, M. *J. Chem. Phys. 35* (1961) 479.
31. Kirckhoff, W. H. and Wilson, E. B. *J. Am. Chem. Soc. 85* (1963) 1726.
32. Adzima, L. J., Chiang, C. C., Paul, I. C. and Martin, J. C. *J. Am. Chem. Soc. 100* (1978) 953.
33. Roesky, H. W. In Senning, A., Ed., *Sulfur in Organic and Inorganic Chemistry*, Dekker, New York 1971, Chapter 3, p. 13.
34. Shaw, R. A. *Phosphorus Sulfur 4* (1978) 101.
35. Rømming, C. and Songstad, J. *Acta Chem. Scand. A 33* (1979) 187.
36. Stevenson, D. P. and Schomaker, V. *J. Am. Chem. Soc. 62* (1940) 1913.
37. Faucher, J.-P., van de Grampel, J. C., Labarre, J.-F., Nabi, S. N., de Ruiter, B. and Shaw, R. A. *J. Chem. Res.* (1977) *S* 112, *M* 1257.
38. Gillespie, R. J., Ireland, P. R. and Vekris, J. E. *Can. J. Chem. 53* (1975) 21.
39. Dunbar, J. E. and Rogers, J. H. *J. Org. Chem. 35* (1970) 279.

Received August 27, 1981.

Acta Chemica Scandinavica A 36 (1982) 407–415

Structural Studies on the Sulfur—Nitrogen Bond. II. The Crystal Structure of Tris(morpholino)sulfonium Tetraphenylborate. A Comparison with the Structure of Tris(morpholino)phosphine

CHRISTIAN RØMMING,[a] GUNNAR O. NEVSTAD[b] and JON SONGSTAD[b]

[a] Department of Chemistry, University of Oslo, Oslo 3, Norway and [b] Department of Chemistry, University of Bergen, 5014 Bergen-Univ., Norway

The structure of the title compound, $[O(CH_2CH_2)_2N]_3S^+ (C_6H_5)_4B^-$, has been determined by X-ray diffraction techniques. The compound is monoclinic, space group $P2_1/c$, with (at −150 °C): $a=9.483(2)$ Å; $b=19.890(3)$ Å; $c=17.350(2)$ Å; $\beta=90.29(1)°$, $Z=4$. Full-matrix least-squares refinement led to a final R-value of 0.054 for 3991 high order reflections ($\sin\theta/\lambda > 0.45$ Å^{-1}).

The cation, Mor_3S^+, is highly asymmetric and its structure is in principle quite analogous to that of tris(morpholino)phosphine, Mor_3P: (*i*) Two smaller N–S–N bond angles of 99.0 and 97.3°, respectively, and one larger angle of 117.4°; (*i i*) two shorter S–N bond lengths of 1.620(3) and 1.636(2) Å while the third is significantly longer, 1.683(3) Å; (*i i i*) the nitrogen atom linked to the surfur atom through the long S–N bond is essentially sp^3 hybridized and its lone pair is *anti* with respect to the sulfur lone pair; (*i v*) the remaining two nitrogen atoms are essentially sp^2 hybridized and their lone pair directions are roughly normal to that of the sulfur atom and to each other; (*v*) the two morpholino groups linked through short bonds to the central atom are twisted in opposite directions with torsion angles of ±71.4° about the S–N bond.

The anion, Ph_4B^-, is close to tetrahedral with regard to the BC_4 moiety. The average B–C bond length is 1.645(4) Å. The phenyl groups are significantly distorted from hexagonal symmetry, the internal angles at the carbon atoms linked to the central boron atom being only 115.6(3)°.

In recent studies from these laboratories the crystal and molecular structure of tris(dialkylamino)phosphines, $(R_2N)_3P$, arsines, $(R_2N)_3As$, and phosphine chalcogenides, $(R_2N)_3PSe$ and $(R_2N)_3PTe$, have been described. For a review of references, *cf.* Ref. 1. It was shown that none of these compounds possesses C_3 local symmetry but are highly asymmetric species. The P–X bond in $(R_2N)_3PX$ and the rather diffuse lone pair of the larger arsenic atom in $(R_2N)_3As$ apparently exert the same conformational influence as does the lone pair of the phosphorus atom in $(R_2N)_3P$. It was therefore concluded that the orthogonalization of the nitrogen lone pairs relative to each other is the determining factor with regard to the structure of these compounds.[2]

In an attempt to test the generality of this suggestion we have turned to tris(dialkylamino)-sulfonium salts, $(R_2N)_3S^+X^-$, a class of compounds which only recently has become available.[3–7] Tris(dialkylamino)sulfonium cations are isoelectronic with $(R_2N)_3P$ and some knowledge to their structure and preferred conformation might shed further light upon the factors determining the asymmetric structure of the compounds from the fifth main group. $(R_2N)_3S^+$ cations, contrary to $(R_2N)_3P$, are known to be most stable towards strong nucleophiles and protic solvents.[5] Triazasulfonium cations containing one primary amine, however, are unstable species.[8]

In the present study we want to report on the crystal and molecular structure of tris(morpholino)-

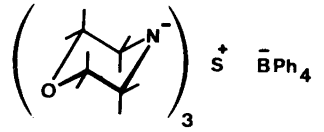

Scheme 1.

0302-4377/82/050407-09$02.50

sulfonium tetraphenylborate, $Mor_3S^+Ph_4B^-$ (Scheme 1). This cation was chosen since previous structural studies of Mor_3P,[9] Mor_3As[2] and Mor_2S[10] allowed a direct comparison to be made. By using the tetraphenylborate anion as counter ion a nicely crystalline and non-hygroscopic salt was obtained.

During its preparation it was noted that tris(dialkylamino)sulfonium bromides may easily be prepared from $(R_2N)_2S$ and a secondary amine in the presence of bromine in dichloromethane,[11] eqn. (1).

$$(R_2N)_2S + 2R_2NH + Br_2 \xrightarrow{CH_2Cl_2} (R_2N)_3SBr + R_2NH \cdot HBr \quad (1)$$

The two products are fairly easily separated from each other owing to their greatly different solubility in dry acetone. The sulfonium bromides are converted into their corresponding tetraphenylborates in nearly quantitative yield with a slight excess of $NaBPh_4$ in aqueous solution.

EXPERIMENTAL

Material. A dichloromethane solution of freshly prepared bis(morpholino)sulfide, Mor_2S[10] (1M), dry morpholine (2M) and bromine (1M) was stirred for 48 h at room temperature. The solvent together with traces of unreacted morpholine and bromine were removed in vacuum while unreacted Mor_2S was removed with diethyl ether. Tris(morpholino)-sulfonium bromide, $Mor_3S^+Br^-$, was then extracted from the remaining solid with cold acetone in which the other product, morpholinium hydrobromide, is rather insoluble. In order to remove traces of the latter compound the acetone solution was twice evaporated to dryness, the residue treated with acetone and the least soluble part discarded. The very soluble sulfonium bromide was finally precipitated with a large volume of diethyl ether.

Since suitable crystals of the apparently hygroscopic bromide could not be obtained, the corresponding tetraphenylborate, $Mor_3S\ BPh_4$, was prepared by precipitation in aqueous solution with $NaBPh_4$. After azeotropic drying from an acetonitrile–benzene solution the product was crystallized from an acetone–diethyl ether mixture from which satisfactory crystals for the X-ray study were obtained.

M.p.215–217 °C (210–211 °C[5]); NMR (CH_2Cl_2): [δ 2.78–2.96 (m,12,NCH_2), 3.50–3.67 (m,12,OCH_2), 6.80–7.40 (m,20,BPh_4)]; IR (KBr-disc):710 cm^{-1} (S–N).

Table 1. Atomic coordinates for non-hydrogen atoms.

Atom	*x*	*y*	*z*
S	.22569(7)	.59362(3)	.78075(3)
O1	−.0835(3)	.4675(1)	.9104(2)
O2	.1456(4)	.7977(1)	.7357(2)
O3	.1742(3)	.5267(1)	.5393(1)
N1	.0895(3)	.5522(1)	.8201(1)
N2	.1818(3)	.6696(1)	.8043(1)
N3	.1978(2)	.5705(1)	.6914(1)
C11	.0948(4)	.4780(1)	.8108(2)
C12	−.0496(5)	.4509(2)	.8327(2)
C13	−.0816(4)	.5384(2)	.9210(2)
C14	.0619(3)	.5678(1)	.9025(1)
C21	.0402(3)	.6994(1)	.7957(2)
C22	.0363(4)	.7492(2)	.7289(2)
C23	.2794(5)	.7655(2)	.7347(2)
C24	.2970(3)	.7196(2)	.8041(2)
C31	.3185(3)	.5780(2)	.6390(2)
C32	.3060(3)	.5227(2)	.5786(2)
C33	.0605(4)	.5181(2)	.5919(2)
C34	.0603(3)	.5735(2)	.6523(2)
C41	.6079(3)	.7096(1)	1.0138(2)
C42	.5037(3)	.6934(1)	1.0676(2)
C43	.4264(3)	.6335(2)	1.0645(2)
C44	.4498(3)	.5875(2)	1.0062(2)
C45	.5520(4)	.6021(2)	.9515(2)
C46	.6289(3)	.6616(2)	.9551(2)
C51	.6326(3)	.8221(1)	.9366(1)
C52	.4989(3)	.8518(1)	.9407(2)
C53	.4368(4)	.8858(2)	.8784(2)
C54	.5082(4)	.8906(2)	.8091(2)
C55	.6399(4)	.8600(2)	.8018(2)
C56	.7005(4)	.8264(1)	.8649(2)
C61	.8671(3)	.7678(1)	1.0053(1)
C62	.9579(3)	.8200(1)	.9823(2)
C63	1.1040(3)	.8130(2)	.9811(2)
C64	1.1659(3)	.7528(2)	1.0043(2)
C65	1.0793(3)	.7005(1)	1.0289(2)
C66	.9328(3)	.7081(1)	1.0284(2)
C71	.6829(3)	.8258(1)	1.0904(1)
C72	.6855(3)	.8964(1)	1.0895(2)
C73	.6867(3)	.9347(2)	1.1576(2)
C74	.6818(3)	.9035(2)	1.2295(2)
C75	.6805(4)	.8337(2)	1.2323(2)
C76	.6836(4)	.7962(2)	1.1649(2)
B	.6966(3)	.7807(1)	1.0114(2)

X-Ray data. Data for the measurement of cell dimensions and intensity data were collected on a SYNTEX $P\bar{1}$ diffractometer using graphite crystal monochromated Mo$K\alpha$ radiation ($\lambda = 0.71069$ Å). The temperature at the crystal site was -150 °C, crystal dimensions were approximately $0.4 \times 0.4 \times 0.4$ mm. Cell parameters were determined by a least-squares fit to the diffractometer settings of 15 general reflections with $2\theta > 35°$. The θ-2θ scan technique was used for the collection of intensity data with a scan speed of $3-6°$ min^{-1} and a scan range of $\pm 1°$. The background counts were taken for 0.35 times the scan time at each of the scan limits. Out of the 6959 unique reflections recorded within $\sin\theta/\lambda = 0.7$ Å^{-1}, 6188 with $I > 2.5\sigma(I)$ were retained for the structure analysis. The standard deviations for the intensities were calculated as $\sigma(I) = [C_T + (0.02\ C_N)^2]^{\frac{1}{2}}$, where C_T is the total number of counts and C_N is the scan count minus background count. The intensities were corrected for Lorentz and polarization effects but not for absorption.

For description of computer programs and references to atomic form factors, *cf.* Ref. 10.

CRYSTAL DATA

Tris(morpholino)sulfonium tetraphenylborate, $C_{36}H_{44}BN_3O_3S$, m.p. 216–217 °C. Monoclinic, $a = 9.483(2)$ Å; $b = 19.890(3)$ Å; $c = 17.350(2)$ Å; $\beta = 90.29(1)°$; $V = 3272.5(8)$ Å^3; ($t = -150$ °C); $M = 609.63$; $Z = 4$; $F(000) = 1304$; $D_x = 1.237$ g cm^{-3}. Absent reflections: ($h0l$) for l odd, ($0k0$) for k odd. Space group $P2_1/c$ (No. 14).

STRUCTURE DETERMINATION

The structure was determined by direct methods and refined in the way described in Ref. 9. In order to avoid the influence of bonding electrons, the final cycles of least-squares refinement were performed with only high angle data included ($\sin\theta/\lambda > 0.45$ Å^{-1}, 3991 reflections). The refinements converged to the following figures of merit: R (All data, 6188 reflections): 0.069; R (high angle data, 3991 reflections): 0.054; $R_w = 0.068$; $S = 2.13$.

Final positional parameters for non-hydrogen atoms are listed in Table 1. Thermal parameters, hydrogen atomic parameters and tables of observed and calculated structure factors are available from the authors.

ORTEP drawings of the ions are shown in Fig. 1 where the numbering of the atoms is also indicated.

RESULTS AND DISCUSSION

In Table 2 are summarized the various structural data determined in the present study. Estimated standard deviations in bond lengths and angles are calculated from the variance–covariance matrix.

The compound consists of discrete cations and anions in the crystal lattice with no exceptionally short contacts. Between, as well as within the ions, the contacts are of the van der Waals' type, mainly between hydrogen atoms.

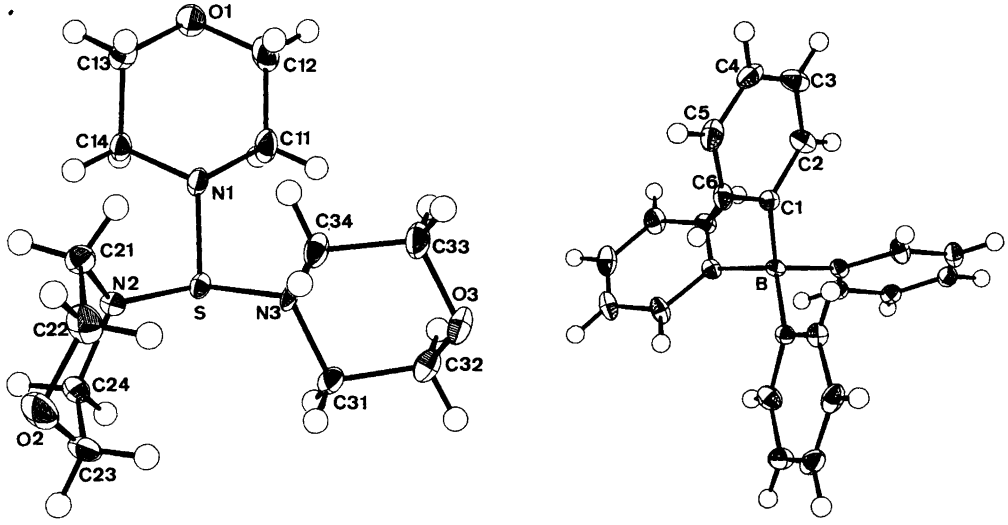

Fig. 1. ORTEP plots of the tris(morpholino)sulfonium ion and the tetraphenylborate ion.

Table 2. Structural data.

Bond lengths (Å)

S	N1	1.680(3)
S	N2	1.620(3)
S	N3	1.636(2)
N1	C11	1.486(4)
C11	C12	1.522(6)
C12	O1	1.426(4)
O1	C13	1.423(4)
C13	C14	1.516(4)
C14	N1	1.488(3)
N2	C21	1.472(4)
C21	C22	1.526(4)
C22	O2	1.421(5)
O2	C23	1.421(6)
C23	C24	1.520(5)
C24	N2	1.477(4)
N3	C31	1.473(3)
C31	C32	1.524(4)
C32	O3	1.423(4)
O3	C33	1.426(4)
C33	C34	1.521(4)
C34	N3	1.469(3)
B	C41	1.647(4)
B	C51	1.649(4)
B	C61	1.640(4)
B	C71	1.645(4)

Bond angles (°)

N1	S	N2	99.0(1)
N2	S	N3	117.4(1)
N1	S	N3	97.3(1)
S	N1	C11	114.7(2)
S	N1	C14	115.3(2)
S	N2	C21	125.8(2)
S	N2	C24	115.9(2)
S	N3	C31	115.8(2)
S	N3	C34	124.4(2)
N1	C11	C12	107.1(3)
C11	C12	O1	111.2(3)
C12	O1	C13	110.5(2)
O1	C13	C14	111.5(3)
C13	C14	N1	106.6(2)
C14	N1	C11	108.5(2)
N2	C21	C22	110.9(3)
C21	C22	O2	111.2(3)
C22	O2	C23	110.1(3)
O2	C23	C24	110.9(3)
C23	C24	N2	109.1(3)
C24	N2	C21	113.7(3)
N3	C31	C32	107.1(2)
C31	C32	O3	110.8(2)
C32	O3	C33	110.6(2)
O3	C33	C34	111.0(3)
C33	C23	N3	106.6(3)
C34	N3	C31	113.6(2)
C41	B	C51	105.2(2)
C41	B	C61	111.8(2)
C41	B	C71	113.9(2)
C51	B	C61	112.7(2)
C51	B	C71	110.7(2)
C61	B	C71	102.8(2)

Torsion angles (°)

N3	S	N1	C11	61.6(2)
N3	S	N1	C14	−171.3(2)
N3	S	N2	C21	56.9(3)
N3	S	N2	C24	−97.4(3)
N2	S	N3	C31	94.5(2)
N2	S	N3	C34	−56.0(3)
N1	S	N3	C31	−161.4(2)
N1	S	N3	C34	48.1(2)

Various averaged and derived data

N_x	N1	N2	N3
$\overline{N-C}$ (Å)	1.487	1.475	1.471
$\overline{C-C}$ (Å)	1.519	1.523	1.523
$\overline{C-O}$	1.425	1.421	1.425
Sum of N bond angles (°)	338.5	355.4	353.8
Torsion angle about $S-N_x$	−175.2	−71.8	71.3

Tetraphenylborate ion

$\overline{B-C1}$ (Å)	1.645(4)	$\overline{C6-C1-C2}$ (°)	115.6(3)
$\overline{C1-C2}$ (Å)	1.406(8)	$\overline{C1-C2-C3}$ (°)	122.5(3)
$\overline{C2-C3}$ (Å)	1.398(6)	$\overline{C2-C3-C4}$ (°)	120.4(4)
$\overline{C3-C4}$ (Å)	1.394(6)	$\overline{C3-C4-C5}$ (°)	118.4(4)

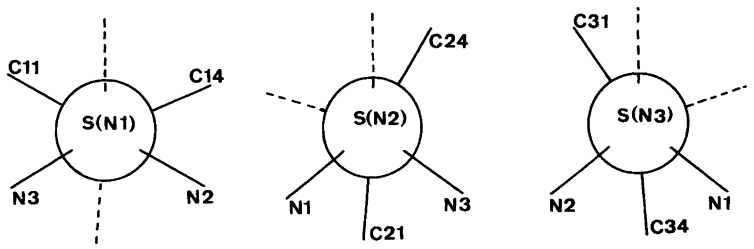

Fig. 2. Newman diagram of the S–N bonds. Broken lines indicate lone pair directions.

The tris(morpholino)sulfonium cation. In the cation there are two short S–N bonds, 1.620(3) and 1.636(2) Å, the third bond being significantly longer, 1.680(3) Å. The nitrogen atom linked to the central sulfur atom through a long bond is essentially sp^3 hybridized, the bond angle sum, $\Sigma\angle$N, being 338.5°. The lone pair of this nitrogen atom is *anti* to the sulfur atom lone pair, the torsion angle about the S–N bond is 175.2°. The two other nitrogen atoms are mainly sp^2 hybridized and their lone pair directions are nearly orthogonal to the sulfur lone pair and to each other. For these atoms $\Sigma\angle$N is 353.8 and 355.4°, the morpholino groups being twisted in opposite directions with torsion angles about the S–N bonds of 71.3 and −71.8°, respectively. In Fig. 2 are shown the Newman projections of the S–N bonds; the torsion angles are defined as outlined in Ref. 9.

The cation is highly asymmetric with regard to the N–S–N bond angles; two of these bond angles are fairly small, 97.3(1) and 99.0(1)°, while the third, the one between bonds to sp^2 hybridized nitrogen atoms, is 117.4°. The sum of the N–S–N angles is 313.7°.

The morpholino groups are all in the expected chair conformation. The N–S bond directions correspond approximately to that of an equatorial bond of the morpholino rings. In the morpholino groups the bond lengths and the bond angles are, with one possible exception, of the expected magnitude; the N–C bond length in the morpholino group linked to the central sulfur atom through an sp^3 hybridized nitrogen atom, and thus a long S–N bond, is 1.487 Å which is about 3 times the e.s.d. longer than the average N–C bond lengths in the two remaining morpholino groups.

Fundamentally, the structure of Mor_3S^+ in $Mor_3S\ BPh_4$ is most similar to that of the

Table 3. Comparison of some structural parameters in the tris(morpholino)sulfonium cation, in bis(morpholino)sulfid and in tris(morpholino)phosphine.

	[a]	Mor_3S^+		Mor_2S[b]		[a]	Mor_3P[c]	
∠NSN°, ∠NPN°	117.4	97.3	99.0	113.2		110.7	97.7	98.0
Σ∠NSN°, Σ∠NPN°		313.7					306.6	
Σ∠N°	338.5	355.4	353.8	349.5		337.6	353.2	350.5
S–N, P–N (Å)	1.680	1.620	1.636	1.680		1.726	1.691	1.696
$S^+-N_{sp^3}$, $P^{III}-N_{sp^3}$ (Å)		1.71[d]					1.74[d]	
$S^+-N_{sp^2}$, $P^{III}-N_{sp^2}$ (Å)		1.61[d]					1.68[d]	
∠SNC°, ∠PNC°	114.7	124.4	125.8	118.5	118.9	114.4	125.9	124.3
	115.3	115.8	115.9	119.1	119.3	115.0	116.7	115.6
S–N, P–N								
torsion angles (°)[e]	−175.2	−71.8	71.3			170.6	−70.9	73.2
N–C (Å)	1.487	1.475	1.471	1.470		1.470	1.463	1.460
C–C (Å)	1.519	1.523	1.523	1.512		1.498	1.497	1.505
C–O (Å)	1.425	1.421	1.425	1.429		1.421	1.423	1.417

[a] The nitrogen atom with its lone pair *anti* to the lone pair of the hetero atom. [b] From Ref. 10, average values. [c] Ref. 9. [d] Extrapolated values, *cf.* Fig. 3. [e] Torsion angles as defined in Ref. 9.

isoelectronic species Mor_3P.[9] In Table 3 a comparison is made between the most important structural parameters in the sulfonium cation and in the aminophosphine. Also are included some relevant structural parameters of bis-(morpholino)sulfide obtained in a recent structural study.[10] From Table 3 it is apparent that the only parameter significantly different in Mor_3S^+ and in Mor_3P, apart from the S–N and P–N bond lengths, is the one N–X–N bond angle between bonds to sp^2 hybridized nitrogen atoms. In the sulfonium cation this bond angle is 117.4° as compared to 110.7° in the aminophosphine. As a result, the sum of the N–S–N bond angles is greater than the sum of the N–P–N angles, 313.7 and 306.6°, respectively.

The introduction of a third morpholino group around the sulfur atom forming Mor_3S^+ from Mor_2S results in only minor structural and conformational changes in two of the substituents. The torsion angles remain essentially unaltered while the N–S–N bond angle is increased from 113.0 to 117.4°. A slight increase of the *s*-character of the nitrogen atoms is also observed; the sum of the nitrogen bond angles being 353.8 and 355.4° in Mor_3S^+ while being 350° in Mor_2S. The S–N bond lengths, however, are different; 1.680(3) Å in the sulfide while only 1.620(3) and 1.636(3) Å in the sulfonium cation. The third morpholino group being linked through an essentially sp^3 hybridized nitrogen atom to the central sulfur atom is bonded with an S–N bond of 1.680(3) Å, which is comparable to that in the parent sulfide. As in Mor_3P[9] the lone pair of this third nitrogen atom is essentially *anti* to the hetero atom lone pair.

In Fig. 3 is plotted the sum of the nitrogen bond angles *vs.* the corresponding S–N bond lengths in Mor_3S^+, and, similarly, the P–N bond lengths in Mor_3P from Ref. 9. A fairly linear dependence is apparent and the least-squares straight lines are indicated. By extrapolation $S^{II+}-N_{sp^2}$ and $S^{II+}-N_{sp^3}$ bond lengths of 1.61(1) and 1.71(1) Å, respectively, are obtained compared with $P^{III}-N_{sp^2}$ and $P^{III}-N_{sp^3}$ bond lengths of 1.68(1) and 1.74(1) Å, respectively.[9] As may be seen from Fig. 3 the slope of the two least-squares lines are quite different; the S^+-N bond length being apparently more dependent upon the hybridization of the nitrogen atom than is the $P^{III}-N$ bond lengths. As a result, the difference between the two extrapolated S^+-N bond lengths is 0.10 Å as compared to 0.06 Å for the corresponding P–N bond lengths. This observation may suggest that the orbitals at the sulfur atom are better suited for overlap with the nitrogen orbitals than are the phosphorus orbitals, especially when some positive charge is residing on the central atoms. The S–N bond length in uncharged species is known to range from 1.416 to 1.90 Å [10,13] while in the $|NS|^+$-cation the S^+-N bond length is estimated to be as short as 1.25 Å.[14] A similar extensive range for P–N bond lengths has so far not been observed.[9,13,15,16]

In Fig. 3 are also indicated the S–N bond length in bis(morpholino)sulfide[10] and the P–N bond length in 4-nitrobenzyl tris(morpholino)phosphonium perchlorate, abbreviated Mor_3P^+R.[15] (In these compounds only one S–N and one P–N bond length together with essentially only one type of nitrogen hybridization are observed.[10,15]) From Fig. 3 it is apparent that the positive charge causes a decrease of the S–N bond length of about 0.04 Å and of the P–N bond length of about 0.05 Å when the hybridization on the nitrogen atom is retained as viewed by the sum of the nitrogen bond angles. If

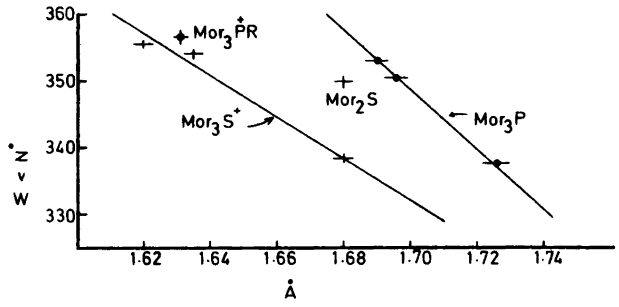

Fig. 3. Plot of the sum of nitrogen bond angles *vs.* the corresponding S–N bond lengths in Mor_3S^+ and Mor_2S and the P–N bond lengths in Mor_3P and Mor_3P^+R.

one assumes a similar dependence of the S–N bond length in uncharged species upon the hybridization of the nitrogen atom as observed for the S^+–N bond length in the sulfonium cation, *cf.* Fig. 3, one obtains an $S^{II}-N_{sp^3}$ bond length of about 1.75 Å. The extrapolated value is in excellent agreement with the Schomaker-Stevenson estimate, 1.74 Å.[17] In comparison, the Schomaker-Stevenson value for the P^{III}–N single bond is 1.76 Å[17] and it has been suggested that the S–N and P–N single bonds are of comparable length.[18]

However, the present and admittedly fairly crude estimate of 1.75 Å for an $S^{II}-N_{sp^3}$ single bond may be hard to verify experimentally. Actually, owing to the apparent facility by which the sulfur and nitrogen orbitals on adjacent atoms interact, *cf.* Ref. 10, causing a decrease in both the S–N bond length and the *p*-character of the nitrogen atom, it is highly doubtful whether uncharged sulfur–nitrogen compounds with sulfur in oxidation state II and with sp^3 hybridized nitrogen atoms exist. An interesting comparison may be made with the S–N bond length of 1.76 Å as observed in sulfamic acid, $^-O_3SNH_3^+$.[19] This compound is known to exist in the crystalline state as the zwitterion and thus leaving no electrons on the nitrogen atom available for π bonding. The S–N bond in this compound should thus be a classical single bond. However, the single bond in sulfamic acid is an $S^{IV}-N_{sp^3}$ single bond. From previous structural studies on phosphorus–nitrogen compounds it is well known that when discussing bond lengths in this class of compounds it is necessary to consider not only the hybridization of the nitrogen atom but also the oxidation state of the central atom.[1,2] For bond lengths in S–N compounds the same care should apparently also be exercised. Fortunately, since S^{II}–N and S^{VI}–N single bonds appear to be of comparable length,[20,21] the excellent agreement between our extrapolated value for an $S^{II}-N_{sp^3}$ single bond length and the $S^{VI}-N_{sp^3}$ single bond length as observed in sulfamic acid[19] may be more than fortutious.

The preference of S–N bonds to attain a bond order slightly but significantly greater than unity[10,22] is reflected by the considerable rotational energy for rotation about the S–N bond as observed in numerous sulfur–nitrogen compounds.[23] In the case of an aminosulfonium cation, $(Me_2N)_3S^+$, the barrier to S–N rotation is 61.4 kJ mol^{-1},[6] even though one of the nitrogen atoms in this cation is presumably sp^3 hybridized as observed in Mor_3S^+ in the present study. In comparison, the P–N rotational barrier for the isoelectronic tris(dialkylamino)phosphines, $(R_2N)_3P$, is usually too small to be detected by the NMR technique. With bulky substituents the P–N torsional barrier in this class of compounds may be raised to 35–40 kJ mol^{-1}.[24] Presumably, the positive charge on the sulfur atom in the triazasulfonium ion causes a contraction of the sulfur *d*-orbitals which make these orbitals more suitable for overlap with the lone pair on the nitrogen atoms. In sulfur compounds in which the atoms linked to the central sulfur atom have no lone pairs, the charge on the sulfur atom is of negligible influence upon the S–X bond lengths, *cf.* Refs. 25 and 26 for S–C bond lengths in Me_2S and in Me_3S^+.

The tetraphenylborate ion, Ph_4B^-. In Table 2 are listed the average values of bond lengths and angles; the standard deviations from the mean (in parenthesis) are small and indicate the similarity in the structural parameters in the four phenyl groups and the B–C bond lengths.

The six C–B–C bond angles in the anion are less similar and range from 102.8(3)° to 113.9(2)°. The boron atom is thus in principle tetrahedrally surrounded by the *ipso* carbon atoms which has also been observed in numerous structural studies on various tetraphenylborates, *cf.* Refs. 27–32. The average B–C bond length of 1.645(4) Å is as observed in previous studies; *cf.* Ref. 33 for a survey of B–C bond lengths and their dependence upon the refinement procedure. In Ph_3B and in $[(Ph_3B)_2CN]^-$ the B–C bonds are significantly shorter, ranging from 1.571(3) Å to 1.589(5) Å in Ph_3B[34] and being 1.603(11) Å in the anion.[35]

As is apparent from the data in Table 2 significant deviations from perfect D_{6h} symmetry in the phenyl rings occur in the tetraphenylborate anion which also has been encountered in previous structural studies.[36] The internal C–C–C bond angles at the *ipso* carbon atom are only 115.6(3)° while the bond angles at the neighbouring carbon atom are significantly larger than 120°, the average value being 122.5(3)°. The bond angle at the *ipso* carbon atom is known to range from 115 to 125° depending upon the electronegativity of the substituent linked to the phenyl group, Ph_3B^- and $N\equiv N^+$ causing the extreme values.[36] For substituents of low electronegativity 117.5–118° is the expected bond angle and not 120° as observed in tetraphenylmetane,[37] and in tri-,[38] tetra-[39] and pentaphenylethane.[40]

It has been argued that significantly smaller C–C–C bond angles at the *ipso* carbon atom in substituted phenyl compounds than about 118° is due to the small X–C bond length and are thus sterically induced.[28,31] However, the significantly larger C–C–C bond angle in Ph_4C[37] than in Ph_4B^-, the former being even more crowded owing to the shorter $C-C_{ipso}$ bond, points against an explanation based upon steric crowding. Sheldrick[41] several years ago from a structural study on Ph_4Si suggested that the distortion of the phenyl rings could not be rationalized by short contacts involving *ortho* carbon and hydrogen atoms. Furthermore, small C–C–C bond angles are observed in several transition metal aryls in which the metal–carbon bond lengths are significantly longer than the B–C bond length in Ph_4B^-.[42]

It thus seems conceivable that the cause for the distortion in the phenyl rings in Ph_4B^- has its origin in the inherently low electronegativity of boron which is further lowered by the negative charge of the anion. Even in $PhBX_2$, X being electronegative halides, is the BX_2 substituent an electron donor to the phenyl groups.[43] The central part of the anion may thus be formulated as $B^{\delta+}-C^{\delta-}$, indicating that some negative charge is residing on the *ipso* carbon atoms, a suggestion for which there is some chemical evidence. The carbanionic nature of the carbon atoms linked to the boron atom in Ph_4B^- is the probable cause for the instability of this anion in the presence of mineral acids forming Ph_3B and benzene.[44] Furthermore, salts of Ph_4B^- appear to have some synthetic potential as arylating agents toward powerful Lewis acids; *cf.* the facile formation of $Ph_3Te^+Ph_4B^-$ from $TeCl_4$ and $NaBPh_4$ and related reactions.[45]

CONCLUSIONS

The tris(dialkylamino)sulfonium cations are not symmetrical and are structurally most similar to the isoelectronic species tris(dialkylamino)phosphine. The cause for the asymmetric structure of these compounds may thus be of the same origin, presumably the desire of the nitrogen lone pairs to be orthogonal. For a recent review of references, *cf.* Ref. 46.

The similarity in the structures of $(R_2N)_3S^+$ and $(R_2N)_3P$ offers a possible explanation for the exceptional chemical stability of triazasulfonium ions.[5] $(R_2N)_3P$ are known to be very poor electrophilic species and their chemistry is nearly entirely governed by the nucleophilicity of the phosphorus atom and, in some few instances, the nitrogen atoms.[9,47] The positive charge on the central sulfur atom in $(R_2N)_3S^+$ will obviously subdue any nucleophilicity of the sulfur atom and presumably also of the neighbouring nitrogen atoms, even though one of these atoms is essentially sp^3 hybridized. However, strong mineral acids may interact with this latter nitrogen atom and initiate decomposition of the cation.

The available structural data on S–N compounds suggest that great care should be exercised when comparing S–N bond lengths without taking into account both the oxidation state and the charge of the sulfur atom as well as the hybridization of the nitrogen atom.

REFERENCES

1. Rømming, C., Iversen, A. J. and Songstad, J. *Acta Chem. Scand. A 34* (1980) 333.
2. Rømming, C. and Songstad, J. *Acta Chem. Scand. A 34* (1980) 365.
3. Minato, H., Okuma, K. and Kobayashi, M. *J. Chem. Soc. Commun.* (1975) 868.
4. Minato, H., Okuma, K. and Kobayashi, M. *Bull. Chem. Soc. Jpn. 49* (1976) 3601.
5. Minato, H., Okuma, K. and Kobayashi, M. *J. Org. Chem. 43* (1978) 652.
6. Cowley, A. H., Pagel, D. J. and Walker, M. L. *J. Am. Chem. Soc. 100* (1978) 7065.
7. Levchenko, E. S., Sheinkman, J. E. and Kirsanov, A. V. *Zh. Obshch. Khim. 33* (1963) 3068.
8. Dawson, A. D. and Swern, D. *J. Org. Chem. 42* (1977) 592.
9. Rømming, C. and Songstad, J. *Acta Chem. Scand. A 32* (1978) 689.
10. Rømming, C., Nevstad, G. O. and Songstad, J. *Acta Chem. Scand. A 36* (1982) 399.
11. *Unpublished results.*
12. Germain, G., Main, P. and Woolfson, M. M. *Acta Crystallogr. A 27* (1971) 368.
13. Shaw, R. A. *Phosphorus Sulfur 4* (1978) 101.
14. *Tables for Interatomic Distances and Configurations in Molecules and Ions,* The Chemical Society Spec. Publ. No. 11, 1958.
15. Rømming, C. and Songstad, J. *Acta Chem. Scand. A 34* (1980) 631.
16. Clardy, J. C., Kolpa, R. L. and Verkade, J. G. *Phosphorus 4* (1974) 133.
17. Stevenson, D. P. and Schomaker, V. *J. Am. Chem. Soc. 62* (1940) 1913.

18. Faucher, J.-P., van de Grampel, J. C., Labarre, J.-F., Nabi, S. N., de Ruiter, B. and Shaw, R. A. *J. Chem. Res.* (1977) *S* 112, *M* 1257.
19. Sass, R. L. *Acta Crystallogr. 13* (1960) 320.
20. Truter, M. R. *J. Chem. Soc.* (1962) 3400.
21. Hargittai, I. and Hargittai, M. *Acta Chim. Acad. Sci. Hung. 75* (1973) 129.
22. Bruce, R. B., Gillespie, R. J. and Slim, D. R. *Can. J. Chem. 56* (1978) 2927.
23. Raban, M. and Cho, T.-m. *Int. J. Sulfur Chem. A 1* (1971) 269.
24. Cowley, A. H., Dewar, M. J. S., Jackson, W. R. and Jennings, W. B. *J. Am. Chem. Soc. 92* (1970) 5206.
25. Pierce, L. and Hayashi, M. *J. Chem. Phys. 35* (1961) 479.
26. Zuccaro, D. E. and McCullough, J. D. *Z. Kristallogr. 112* (1959) 401.
27. Hoffmann, K. and Weiss, E. *J. Organomet. Chem. 67* (1974) 221.
28. Di Vaira, M. and Orlandini, A. B. *J. Chem. Soc. Dalton Trans.* (1972) 1704.
29. Segal, B. G. and Lippard, S. J. *Inorg. Chem. 16* (1977) 1623.
30. Duggan, D. M. and Hendrichson, D. N. *Inorg. Chem. 13* (1974) 1911, 2056.
31. Ziolo, R. F. and Troup, J. M. *Inorg. Chem. 18* (1979) 2271.
32. Domenicano, A. and Vaciago, A. *Acta Crystallogr. B 31* (1975) 2553.
33. Domenicano, A., Vaciago, A. and Coulson, C. A. *Acta Crystallogr. B 31* (1975) 1630.
34. Zettler, F., Hausen, H. D. and Hess, H. *J. Organomet. Chem. 72* (1974) 157.
35. Giandomenico, C. M., Dewan, J. C. and Lippard, S. J. *J. Am. Chem. Soc. 103* (1981) 1407.
36. Domenicano, A., Mazzeo, P. and Vaciago, A. *Tetrahedron Lett.* (1976) 1029.
37. Robbins, A., Jeffrey, G. A., Chesick, J. P., Donohue, J., Cotton, F. A., Frenz, B. A. and Murillo, C. A. *Acta Crystallogr. B 31* (1975) 2395.
38. Destro, R., Pilati, T. and Simonetta, M. *Acta Crystallogr. B 36* (1980) 2495.
39. Destro, R., Pilati, T. and Simonetta, M. *Acta Crystallogr. B 36* (1980) 2497.
40. Destro, R., Pilati, T. and Simonetta, M. *J. Am. Chem. Soc. 100* (1978) 6507.
41. Glidewell, C. and Sheldrick, G. M. *J. Chem. Soc. A* (1971) 3127.
42. Churchill, M. R. and O'Brien, T. A. *J. Chem. Soc. A* (1969) 266.
43. Ramsey, B. G. and Longmuir, K. *J. Org. Chem. 45* (1980) 1322.
44. Meisters, M., Vandeberg, J. T., Cassaretto, F. P., Posvic, H. and Moore, C. E. *Anal. Chim. Acta 49* (1970) 481.
45. Ziolo, R. F., Thornton, C. J., Smith, A. C., Titus, D. D., Smith, C. S. and Bueno, N., Jr. *J. Organomet. Chem. 190* (1980) C 64.
46. Gonbeau, D., Sanchez, M. and Pfister-Guillouzo, G. *Inorg. Chem. 20* (1981) 1966.
47. Amonoo-Neizer, E. H., Ray, S. K., Shaw, R. A. and Smith, B. C. *J. Chem. Soc.* (1965) 4296.

Received September 4, 1981.

Acta Chemica Scandinavica A 36 (1982) 417–422

The Hydrolysis Kinetics of Glucono-δ-lactone in Solutions without Anion Catalysis and a Systematical Error in Weakly Buffered pH-static Kinetics

E. M. SKOU[a] and T. JACOBSEN[b]

[a] Department of Chemistry, Odense University, Campusvej 55, DK-5230 Odense M, Denmark and [b] Fysisk-Kemisk Institut, The Technical University of Denmark, DK-2800 Lyngby, Denmark

The hydrolysis of glucono-δ-lactone has been investigated by a pH-static method in the pH-range from 4.5 to 8.5. Kinetic measurements have been made in pure water or in very dilute buffer solutions to avoid anion catalysis. The rate constants for water and hydroxide ion catalysis have been determined to $k_{H_2O}=4.59\times10^{-5}$ s^{-1} and $k_{OH^-}=2.76\times10^{3}$ s^{-1} l mol^{-1}, at 25 °C.

The temperature dependency has been investigated, and the activation energies of the water and hydroxide ion catalyzed reactions have been determined to $E_{H_2O}/R=7360$ K^{-1} and $E_{OH^-}/R=8880$ K^{-1}.

In solutions with very low buffer capacity too high initial rates were observed. These are shown to be caused by pH-gradients in the solution due to insufficient stirring. A model describing the effect has been set up, and correct reaction rates are shown to be obtained after sufficient time. Furthermore, it is shown that the mixing time for the added base must be several orders of magnitude lower than the half-life of the reaction, thus introducing uncertainties in kinetic constants determined from initial slopes in weakly buffered solutions.

In the electrochemical oxidation of glucose on Pt, the δ-lactone of gluconic acid has been shown to be a primary reaction product.[1,2]

To investigate the role of the lactone and gluconic acid as possible inhibitors of the glucose oxidation or as sources of further oxidation steps, a detailed knowledge of the kinetics of the hydrolysis of glucono-δ-lactone in different ionic media is necessary.

Several authors have investigated the hydrolysis of the lactone[3–7] and have shown the reaction scheme to be as given in eqn. (1).

$$\text{D-Glucono-}\delta\text{-lactone} + H_2O \underset{k^-}{\overset{k^+}{\rightleftharpoons}} \text{Gluconic acid} \overset{K_a}{\rightleftharpoons} \text{Gluconate ion} + H^+ \quad (1)$$

Mitchell and Duke[5] have shown the interconversion of the δ-lactone to the γ-lactone to be insignificant in the pH-range investigated in the present work.

The kinetics of the hydrolysis has been investigated by polarimetric[3,5,6] colorimetric[4] and pH-static methods[3] and the results obtained show large discrepancies. An explanation of most of the discrepancies was given by Pocker and Green[6] who carefully investigated the role of the buffer system used. They showed the reaction to be general acid-base catalyzed, an effect previous workers did not take into account, and determined the catalytic constants for a variety of acid-base pairs. The constants for H_3O^+, H_2O and OH^- were determined by measuring the rate constants at a constant ionic strength of 0.5 mol l^{-1} with different buffer concentrations and then extrapolated to zero buffer concentration.

An inherent drawback of this method is that the activity coefficients of H_3O^+ and OH^- are needed in order to determine the actual concentrations.

At present no appropriate theoretical method to do this is known except for very dilute solutions.

One way of avoiding the influence of the buffer system is to determine the kinetic constants pH-

0302-4377/82/050417-06$02.50

statically in pure water or in an inert supporting electrolyte.

In the present work the hydrolysis constants for glucono-δ-lactone have been determined by a pH-static method in pure water or with very low buffer concentrations (4×10^{-3} M) in the pH range from 4.5 to 8.5, which has allowed the catalytic constants for water and OH^- to be determined. Special care has been taken to avoid the influence from the low buffering capacity.

The activation energy. In spite of its biological importance most of the measurements of the hydrolysis of the lactone have been made at ambient temperature and very few attempts have been made to determine the activation energy. Sawyer and Bagger[3] have determined the activation energy at pH = 4 in the temperature range from 20 to 25 °C and Pocker and Green[6] have determined it at pH = 4.4 in the range from 20 to 45 °C using data extrapolated to zero buffer concentration.

In the present work rate constants determined pH-statically in the temperature range from 25 to 37 °C at different pH values have been used to determine the activation energy of both the water catalyzed and the hydroxide ion catalyzed hydrolysis of glucono-δ-lactone.

THEORY

In the pH-static experiment the total amount of base used to neutralize the protons formed in the overall reaction:

δ-lactone → gluconic acid → gluconate ion + H^+

or: $\delta \rightarrow HGH_4 \rightarrow GH_4^- + H^+$

is measured.

Reversible first order kinetics of reaction (1) leads to

$$\ln \frac{c_\delta - c_{\delta,\infty}}{c_\delta^\circ - c_{\delta,\infty}} = (k_+ + k_-)t$$

The amount of hydroxide ions added per liter at the time t is

$$[OH^-]_t = c_{GH_4^-}$$

The mass balance

$$c_\delta^\circ - c_\delta = c_{GH_4^-} + c_{HGH_4}$$

gives by the use of

$$c_{HGH_4} = \frac{a_{H^+}}{K_a} \cdot \gamma_- c_{GH_4^-} = A[OH^-]_t$$

$$c_\delta^\circ - c_\delta = (1 + A)[OH^-]_t$$

and

$$\frac{c_\delta - c_{\delta,\infty}}{c_\delta^\circ - c_{\delta,\infty}} = \frac{[OH^-]_\infty - [OH^-]_t}{[OH^-]_\infty} \qquad (2)$$

which leads to the final integrated rate expression (3), where

$$\ln([OH^-]\infty - [OH^-]_t) = -k't + \ln[OH^-]\infty \qquad (3)$$

$$k' = (k_{H^+} c_{H^+} + k_{OH^-} c_{OH^-} + k_{H_2O})[1 + K_\delta^{-1}/(1 + K_a/c_{H^+})]$$

THE TEMPERATURE DEPENDENCY

In the pH-range where only water and hydroxyl ion catalysis takes place the rate constant is

$$k' = k_{H_2O} + k_{OH^-} c_{OH^-} = k_1 + k_2$$

In a temperature range which is small compared to the absolute temperature the following approximation can be used:[8]

$$\ln k' \cong \ln (k_\infty^\circ + k_2^\circ) + \frac{k_1^\circ \cdot \frac{E_1^*}{R} + k_2^\circ \cdot \frac{E_2^*}{R}}{k_1^\circ + k_2^\circ} \cdot \Delta\frac{1}{T}$$

This shows that the energy of activation E^*/R found by a plot of $\ln k'$ *vs.* T^{-1} is a mean value of the activation energies of the two parallel reactions

$$\frac{E^*}{R} = \frac{k_1^\circ \frac{E_1^*}{R} + k_2^\circ \frac{E_2^*}{R}}{k_1^\circ + k_2^\circ} \qquad (4)$$

EXPERIMENTAL

In the experiments a RADIOMETER pH-stat (TTT2 + ABU13 + REA300), was used, and the thermostated (150 ml) reaction vessel was deaerated with nitrogen. To avoid leakage from the burette tip in the long time runs (up to 900 min) the glass tip of the burette was drawn to a capillary and bent so the tip ended just above the surface of the solution.

The D-glucono-δ-lactone obtained from Merck, Darmstadt, melted at 151–153 °C and was used without further purification. All other chemicals were analytical grade, also from Merck.

To keep the volume changes negligible the lactone concentration was *ca.* 2×10^{-2} mol l^{-1} and 1 mol l^{-1} NaOH was used as titrant. In the initial runs the $[OH^-]_t$ *vs.* time curve showed steps due to pH changes caused by the addition of base [the base is not added continuously but in small portions (10^{-2} ml)]. To diminish this effect a small amount of phosphate buffer (4×10^{-3} M) was added to the solution. This buffer concentration is so low that the influence on the rate constant is insignificant at pH ≥ 7 and less than 5 % at pH = 6.25.

After addition of buffer the $[OH^-]_t$ *vs.* time curves became smooth, but a slight curvature of the log $([OH^-]_t - [OH^-]_\infty)$ *vs.* time curve remained as can be seen in Fig. 1. This curvature is due to a difference in the mean pH of the solution and the pH measured by the glass electrode and is caused by an insufficient dilution and mixing of the added base. This effect is treated in detail in the appendix, where the correct slope is shown to be obtained after sufficient time. Increased stirring did remove the curvature and thus shows the effect to be solely caused by the inhomogeneity of the solution. At these high stirring rates however, excessive splashing took place. A little lower stirring rate was therefore used and the rate constants were determined from the straight portion of the curve.

At pH = 4.5 and 4.75 the rate constant is so low that even the small amount of buffer, which was used at the higher pH values would cause significant error. Fortunately, at these pH values the buffer capacity of water and the gluconic acid – gluconate pair is sufficient to give reasonably straight lines as can be seen in Fig. 1b.

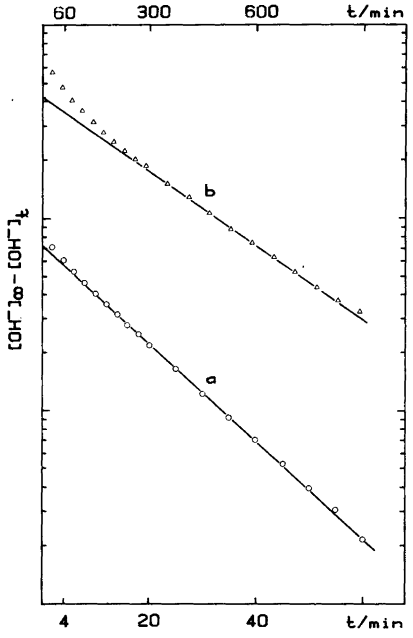

Fig. 1. Plot of $\log([OH^-]_\infty - [OH^-]_t)$ *vs.* time. a: 0.0117 M lactone in 0.004 M phosphate buffer, pH = 7.5, t = 25 °C. b: 0.0147 M lactone in pure water, pH = 4.5, t = 25 °C.

RESULTS AND DISCUSSION

Rate constants determined in the pH-range from 4.5 to 8.5 at 25 °C are shown in Fig. 2.

Eqn. 3 in the form

$$k' = (k_{H_2O} + k_{OH^-} \times 10^{pH-14})[1 + K_\delta^{-1}/(1 + K_a/10^{-pH})]$$

is fitted to the experimental points with $K_\delta = 3.68$* and $K_a = 2.40 \times 10^{-4}$ l mol^{-1} [7] and substituting activities with concentrations in those very diluted solutions ($\gamma_\pm \approx 0.998$).

The best values found are

$k_{H_2O} = 4.59 \times 10^{-5}$ s^{-1} and $k_{OH^-} = 2.76 \times 10^3$ s^{-1} l mol^{-1}

* To determine the value of $K_\delta = a_{HGH_4}/a_\delta$, we have used the value of $K_L = a_{HGH_4}/(a_\delta + a_\gamma) = 1.53$ determined by Skibsted and Kilde [7] and the value of $K_{\delta,\gamma} = a_\delta/a_\gamma = 0.712$ determined by Mitchell and Duke.[5]

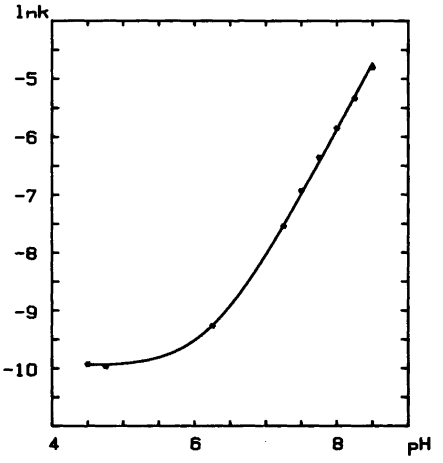

Fig. 2. Hydrolysis of glucono-δ-lactone. pH-dependence of the rate constant. *, experimental values; -, values computed with $k_{H_2O} = 4.59 \times 10^{-5}$ s^{-1} and $k_{OH^-} = 2.76 \times 10^3$ s^{-1} l mol^{-1}.

and the k' *vs.* pH curve calculated from these values is also shown in Fig. 2.

The value of $k_{H_2O} = 4.59 \times 10^{-5}\ s^{-1}$ is very close to the value of $k_{H_2O} = 4.3 \times 10^{-5}\ s^{-1}$ determined by Pocker and Green and lower than the values determined by other workers in cases where anion catalysis or pH-stat errors might have influenced the results. The value of $k_{OH^-} = 2.76 \times 10^3\ s^{-1}\ l\ mol^{-1}$, however, differs from the value of $k_{OH^-} = 1.9 \times 10^3\ s^{-1}\ l\ mol^{-1}$ determined by Pocker and Green, and the difference is larger than the experimental uncertainties of the constants presented in this paper. One reason for this discrepancy might be that the values determined by Pocker and Green are obtained by extrapolation to infinite dilution from ionic strengths where the theoretical expressions used for activity coefficients are inadequate.

The values determined by Jermyn[4] and Mitchell and Duke[5] ($4 \times 10^3\ s^{-1}\ l\ mol^{-1}$) may be expected to be larger than the values presented here as they are determined in buffers, where anion catalysis is present.

At pH = 6.25, 7.24 and 7.75 the rate constants were determined as function of temperature in the range from 25 °C to 37 °C, and the results are shown in Fig. 3.

The plots of log k *vs.* T^{-1} are seen to give straight lines and the apparent activation energies are found to be $E^*/R = 7360$, 8500 and 8840 K^{-1} at pH = 6.25, 7.25, and 7.75. The use of eqn. (4) then gives the following activation energies of the water catalyzed and the hydroxide ion catalyzed reactions:

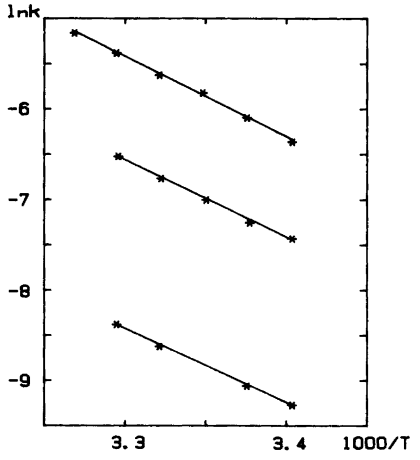

Fig. 3. Temperature dependence of the rate constants at pH = 6.25 (upper curve), pH = 7.25 and pH = 7.75 (lower curve).

$E^*_{H_2O}/R = 7360$ and $E^*_{OH^-}/R = 8880\ K^{-1}$.

The $E^*_{H_2O} = 61.1$ kJ mol^{-1} (= 14.6 kcal mol^{-1}) value is in fair agreement with activation energies of 15.3 kcal mol^{-1} determined by Sawyer and Bagger[3] at pH = 4.0 and 14 kcal mol^{-1} determined by Pocker and Green[6] at pH = 4.44.

APPENDIX

A systematical error in weakly buffered pH static kinetics. As many reactions studied by pH static technique are general acid-base catalyzed it is often necessary to work in slightly buffered medium to prevent the catalytic effect of the buffer system. To avoid an appreciable dilution the solution added to maintain pH at the preset value normally has a pH far from that of the reaction medium. Therefore, gradients in pH will be present at the burette outlet and the reaction will be accellerated in this region. In the following the influence of the finite mixing time on the observed overall reaction rate will be analyzed and it will be shown that this effect explains the deviations from a linear log c *versus* t relationship observed in the present work.

Consider the reaction

$$\delta + OH^- \rightarrow GH_4^-$$

with the rate expression

$$\frac{dc_\delta}{dt} = -k_{H_2O}c_\delta - k_{OH^-}c_{OH^-}c_\delta$$

in a volume V_o of a solution with the preset OH^- concentration $\bar{c}_{OH^-}$ containing a buffer system HA/A^- with concentrations c°_{HA} and $c^\circ_{A^-}$.

Let ΔV_j be the volume of NaOH solution, with concentration $c^\circ_{OH^-}$, added from the pH stat burette in the time interval $t_j/t_j + \Delta t_j$ to compensate for the OH^- consumption of the reaction. After the addition this volume will be diluted with bulk solution and to the time t it will be contained in the volume V_j. Initially when the OH^- concentration is large compared to the buffer concentration the mixing is a simple dilution process and c_{OH^-} is determined by:

$$c_{OH^-} = \frac{c^\circ_{OH^-}\Delta V_j - c^\circ_{HA}(V_j - \Delta V_j)}{V_j}$$

$$\simeq c^\circ_{OH^-}\frac{\Delta V_j}{V_j} \qquad \text{(A1)}$$

After a certain time τ the base added is neutralized by the buffer and the concentration drops rapidly to the preset value, $\bar{c}_{OH^-}$. As c_{OH^-} is large compared to c_{OH^-} during the mixing period, the increased rate of the base catalyzed hydrolysis of glucono-lactone in the volume element V_j is given by

$$\frac{dn_{\delta,j}}{dt} = -V_j k_{OH^-} c_{OH^-} c_\delta \quad \text{(A2)}$$

or combined with eqn. (A1)

$$\frac{dn_{\delta,j}}{dt} = -k_{OH^-} c^\circ_{OH^-} c_\delta \Delta V_j \quad \text{(A3)}$$

This rate is independent of details in the mixing process, and the overall rate increase due to gradients in pH is only depending on the amount of base added in the mixing period τ. As τ must be small compared to the half time of the reaction, the overall reaction rate can be considered constant and the volume added in the time period τ is

$$V_\varepsilon = -\tau \frac{V_o}{c^\circ_{OH^-}} \frac{dc_\delta}{dt} \quad \text{(A4)}$$

where V_o is the total reaction volume. The overall rate increase can therefore be written as:

$$\frac{dn_\delta}{dt} = -k_{OH^-} V_o \tau \frac{d\bar{c}_\delta}{dt} \quad \text{(A5)}$$

and the reaction rate observed is:

$$\frac{d\bar{c}_\delta}{dt} = -k'\bar{c}_\delta + k_{OH^-}\tau \frac{d\bar{c}_\delta}{dt} \quad \text{(A6)}$$

where $k'\bar{c}_\delta$ is the ideal contribution. Integrating (A6) yields the observed concentration *vs.* time relation.

$$\ln \frac{\bar{c}_\delta}{c^\circ_\delta} + k_{OH^-}\tau(c^\circ_\delta - \bar{c}_\delta) = -k't \quad \text{(A7)}$$

where the term linear in $\bar{c}_\delta$ is the deviation from ideal behavior caused by the finite mixing time.

In Fig. 4 eqn. (A 7) is compared to an experimental curve. Reasonable agreement is obtained although the linear behaviour is observed somewhat earlier than predicted by the model. This is probably due to a decrease in mixing time caused by an increase in buffer capacity when gluconic acid is formed, which reduces the volume necessary to neutralize the base added. It is noted that a mixing time of only 0.02 s being six orders of magnitude smaller than the half time of the reaction may cause an appreciable deviation from linear behaviour. Therefore, great attention should be paid to the mixing efficiency and rate constants should not be determined from initial slopes in this kind of work.

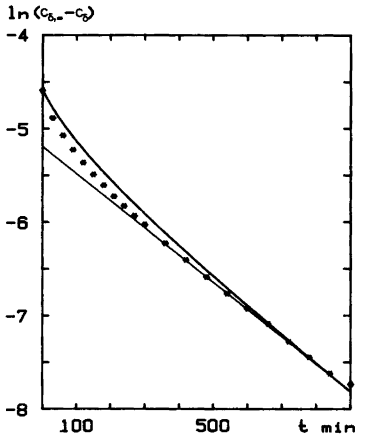

Fig. 4. Deviations from first order kinetics introduced by insufficient stirring. *, experimental values determined at pH = 4.5 and $t = 25\,^\circ C$; -, values calculated from eqn. (A7) with $k_{OH^-}\tau = 59$, $k_{H_2O} + k_{OH^-} c_{OH^-} = 4.91 \times 10^{-5}$ and $\Delta^\circ_\delta = 0.0102$ M.

$$t_{\frac{1}{2}} \gg \frac{k_{OH^-}\tau(c^\circ_\delta - \bar{c}_\delta)}{k'} \sim \frac{k_{OH^-}\tau c^\circ_\delta}{k'} \quad \text{(A8)}$$

may be of value in the planning of experiments and in the control of experimental results.

REFERENCES

1. a. Skou, E. M. *Electrochim. Acta 22* (1977) 313; b. Skou, E. M. *27th ISE Meeting*, Zürich 1976, extended abstracts No. 279.
2. Ernst, S., Heitbaum, J. and Hamann, C. H. *Ber. Bunsenges. Phys. Chem. 84* (1980) 50.
3. Sawyer, D. T. and Bagger, J. B. *J. Am. Chem. Soc. 81* (1959) 5302.

4. Jermyn, M. A. *Biochim. Biophys. Acta 37* (1960) 78.
5. Mitchell, R. E. and Duke, F. R. *Ann. N. Y. Acad. Sci. 172* (1970) 129.
6. Pocker, Y. and Green, E. *J. Am. Chem. Soc. 95* (1973) 113.
7. Skibsted, L. H. and Kilde, G. *Dan. Tidsskr. Farm 45* (1971) 320.
8. Bell, R. P. *Acid-base Catalysis*, Oxford Univ. Press, London, New York 1941, p. 179.

Received August 11, 1981.

Acta Chemica Scandinavica A 36 (1982) 423 – 427

The Crystal Structure of Tripotassium Pentafluoroperoxotantalate(V) Hydrogendifluoride, $K_3[HF_2][TaF_5(O_2)]$. A Redetermination at 290 and 170 K

ROLF STOMBERG

Department of Inorganic Chemistry CTH/GU, Chalmers Tekniska Högskola, S-412 96 Göteborg, Sweden

Crystals of $K_3[HF_2][TaF_5(O_2)]$ are orthorhombic, space group *Pnam* (No. 62), with $a = 6.976(4)$ Å, $b = 13.82(1)$ Å, $c = 9.072(4)$ Å at 290 K and $a = 6.957(3)$ Å, $b = 13.61(1)$ Å, $c = 9.082(7)$ Å at 170 K. $Z = 4$. Reflexion intensities were registered with an automatic single crystal X-ray diffractometer using Mo$K\alpha$ radiation. Least-squares refinement of structural and thermal parameters yielded a final R-value of 0.049 for 1203 observed reflexions at 290 K and of 0.073 for 1429 observed reflexions at 170 K, using different crystals.

The structure was originally solved by Ružić-Toroš *et al.* using 517 independent reflexions collected by the Weissenberg film technique. The space group $Pna2_1$ was selected. The present reinvestigation has shown, however, that the structure can be refined in space group *Pnam*. The principal features of the coordination geometry and the packing of the ions arrived at by Ružić-Toroš *et al.* are correct, however.

The present investigation has shown that the structure of $K_3[HF_2][TaF_5(O_2)]$ is the same at 290 K and 170 K, the largest discrepancy between bond distances being less than 2.3σ. It is not isomorphous with that of $Na_3[HF_2][NbF_5(O_2)]$.

Peroxo oxygen bond distances are normally 1.49 Å or somewhat shorter in transition metal peroxo compounds.[2-6] Rare exceptions among peroxofluorometallates, a class of compounds being studied at this department, are the dinuclear complex in $K_6[TaF_5(O_2)][O\{TaF_4(O_2)\}_2] \cdot H_2O$,[7] and, possibly, $[TaF_5(O_2)]^{2-}$ in $K_3[HF_2][TaF_5(O_2)]$.[1] O – O distances of 1.69(3) and 1.75(3) Å in the former and of 1.64(16) Å in the latter were observed. In view of the large e.s.d.'s in $K_3[HF_2][TaF_5(O_2)]$, it was thought worthwhile to perform a reinvestigation using diffractometer data.

Ružić-Toroš *et al.*[1] mention that their recorded films were of poor quality due to the decomposition of the crystal. Therefore, it seemed profitable to collect the intensity data at low temperature and, for comparison, at room temperature as well.

EXPERIMENTAL

Preparation. Tantalum(V) oxide was dissolved in an excess of boiling 38 % hydrofluoric acid. The stoichiometric amount of potassium in the form of the hydroxide and an excess of hydrogen peroxide were added. By evaporation of the solvent at room temperature, well-developed, transparent prismatic crystals were obtained. They were crystallographically identified as $K_3[HF_2][TaF_5(O_2)]$.[1]

Data collection. Complete sets of intensities were recorded at 290 K and at 170 K, for different crystals (crystal size $0.09 \times 0.11 \times 0.14$ mm and $0.13 \times 0.14 \times 0.39$ mm, respectively), with a SYNTEX $P2_1$ automatic four-circle single crystal X-ray diffractometer using graphite-monochromatized Mo$K\alpha$ radiation. The crystals were coated with a thin layer of epoxy resin. The $\omega - 2\theta$ scan method was used, and the 2θ scan speed was allowed to vary between $3 - 20°$/min, depending on the intensity of the measured reflexion. Data were collected for $2\theta \leqslant 65°$. Three test reflexions, measured after each fiftieth reflexion, showed no significant difference in intensity during the data collection at 170 K. At 290 K, the intensities of the test reflexions decreased linearly with time, however. The intensity data were corrected for this. Weissenberg photographs, taken as a check measure before and after the data collection, also showed the slight decrease in intensity. These photographs were of rather good quality, unlike those described by Ružić-Toroš *et al.* A profile analysis based on the Lehmann-Larsen method[8] was applied to the

0302-4377/82/050423-05$02.50

96-step profile collected for each reflexion. Those reflexions having $I_o \geqslant 3\sigma(I_o)$ (1203 reflexions at 290 K and 1429 at 170 K) were regarded as being observed and were used in the subsequent calculations. The intensities were corrected for Lorentz, polarization and absorption effects.

The unit cell parameters were determined from a least-squares fit of refined diffractometer setting angles for 15 reflexions.

CRYSTAL DATA

Tripotassium pentafluoroperoxotantalate(V) hydrogendifluoride, $K_3[HF_2][TaF_5(O_2)]$. F.W.= 464.24. Space group *Pnam* (No. 62; non-standard setting). General positions: $\pm(x,y,z)$; $\pm(\bar{x},\bar{y},\frac{1}{2}+z)$; $\pm(\frac{1}{2}-x,\frac{1}{2}+y,\frac{1}{2}+z)$; $\pm(\frac{1}{2}+x,\frac{1}{2}-y,z)$. At 290 K: $a=6.976(4)$ Å, $b=13.82(1)$ Å, $c=9.072(4)$ Å, $V=874.4(9)$ Å^3, $Z=4$, $D_c=3.53$ g cm^{-3}. At 170 K: $a=6.957(3)$ Å, $b=13.61(1)$ Å, $c=9.082(7)$ Å, $V=859.9(9)$ Å^3, $Z=4$, $D_c=3.59$ g cm^{-3}. μ(Mo$K\alpha$)=14.7 mm^{-1}, λ(Mo$K\alpha$)=0.71069 Å.

Lists of structure factors and thermal parameters are available from the author upon request.

STRUCTURE REFINEMENT

Block-diagonal least-squares refinement of positional and isotropic thermal parameters, starting with those given by Ružić-Toroš *et al.*, led to an *R*-value of 0.089. Further refinement, introducing anisotropic thermal parameters, reduced the *R*-value to 0.069. F(2) and O(2) showed large anisotropy, however, and the peroxo oxygen bond distance was unacceptably short (1.20 Å). Further refinement along these lines did not seem profitable. A closer examination of the atomic positions at this point showed, however, that the symmetry was almost that of space group *Pnam*, the average discrepancy being 0.09 Å ($=3\sigma$), and the largest 0.25 Å. The latter value applied to O(2), probably due to strong coupling to O(1). The arguments put forward by Ružić-Toroš *et al.* for choosing space group $Pna2_1$ – the number of molecules in the unit cell and the Patterson map – do not seem convincing. Further refinement was, therefore, performed according to space group *Pnam*, which turned out to lead to an acceptable structure proposal.

Full-matrix least-squares refinement of overall scale factors and positional and anisotropic thermal parameters for all non-hydrogen atoms yielded *R*-values of 0.049 and 0.073 for 1203 observed reflexions at 290 K and 1429 at 170 K, respectively. The weighting scheme used was that of Cruickshank:[9] $w=(a+|F_o|+c|F_o|^2+d|F_o|^3)^{-1}$ with $a=50$, $c=0.006$ and $d=0.0003$ for the data collected at 290 K and $a=30$, $c=0.004$ and $d=0.0001$ for those at 170 K. The scattering factors for Ta, K^+, F and O were taken from the *International Tables for X-Ray Crystallography, Vol. IV* (1974), as were the dispersion corrections.

The highest peaks in the difference syntheses calculated after the last refinement cycles, 6 and 7 e/Å^3 at 290 and 170 K, respectively, appeared at less than 1.1 Å from Ta, while the peaks at larger distances than 1.1 Å from Ta or K were smaller than 3.5 e/Å^3.

Calculations were carried out on an IBM 3033 computer using the crystallographic programmes described by Lindgren.[10]

Table 1. Atomic coordinates for $K_3[HF_2][TaF_5(O_2)]$ at 290 and 170 K. Space group *Pnam*. $U_{eq}=\frac{1}{3}(U_{11}+U_{22}+U_{33})$.

		290 K				170 K			
Atom	Site	x	y	z	U_{eq}/Å^2	x	y	z	U_{eq}/Å^2
Ta	4*c*	0.26481(7)	0.07050(4)	$\frac{1}{4}$	0.025	0.26473(10)	0.07003(5)	$\frac{1}{4}$	0.022
K(1)	4*c*	0.2288(4)	0.5983(2)	$\frac{1}{4}$	0.031	0.2293(5)	0.5986(2)	$\frac{1}{4}$	0.016
K(2)	8*d*	0.2328(3)	0.3481(2)	0.0234(2)	0.038	0.2261(4)	0.3488(2)	0.0217(2)	0.022
F(1)	4*c*	0.5522(12)	0.0780(6)	$\frac{1}{4}$	0.035	0.5532(13)	0.0796(7)	$\frac{1}{4}$	0.019
F(2)	4*c*	0.2664(18)	0.2070(7)	$\frac{1}{4}$	0.067	0.2653(22)	0.2077(7)	$\frac{1}{4}$	0.041
F(3)	8*d*	0.3181(14)	0.0691(7)	0.0382(7)	0.062	0.3208(15)	0.0691(6)	0.0391(6)	0.033
F(4)	4*c*	0.3226(15)	−0.0671(6)	$\frac{1}{4}$	0.041	0.3246(15)	−0.0698(6)	$\frac{1}{4}$	0.019
F(5)	8*d*	0.0000(9)	0.2362(5)	0.6264(8)	0.051	−0.0042(12)	0.2340(5)	0.6271(9)	0.027
O	8*d*	0.0119(13)	0.0464(8)	0.1734(13)	0.068	0.0102(14)	0.0478(8)	0.1706(12)	0.033

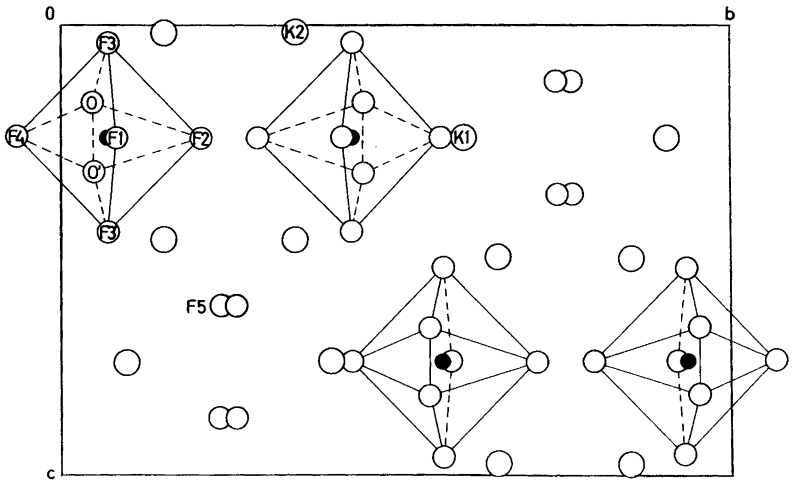

Fig. 1. The crystal structure of $K_3[HF_2][TaF_5(O_2)]$ viewed along the *a*-direction. Full circles represent tantalum atoms.

Table 2. Bond distances and angles in $K_3[HF_2]$-$[TaF_5(O_2)]$ at 290 and 170 K.

	Distance/Å at 290 K	170 K
Ta–F(1)	2.007(8)	2.011(9)
Ta–F(2)	1.886(10)	1.873(10)
Ta–F(3)	1.957(6)	1.955(7)
Ta–F(4)	1.943(9)	1.948(8)
Ta–O	1.925(10)	1.936(10)
O–O′	1.389(24)	1.443(22)
F(5)···F(5)′	2.242(15)	2.233(16)
	Angle/° at 290 K	**170 K**
F(1)–Ta–F(2)	86.7(5)	86.2(5)
F(1)–Ta–F(3)	79.1(3)	78.5(3)
F(1)–Ta–F(4)	81.0(4)	81.4(4)
F(1)–Ta–O	157.5(4)	157.4(3)
F(2)–Ta–F(3)	90.5(3)	90.3(3)
F(2)–Ta–F(4)	167.7(5)	167.5(6)
F(2)–Ta–O	100.2(5)	99.1(5)
F(3)–Ta–F(3)′	158.0(6)	157.0(6)
F(3)–Ta–F(4)	87.2(3)	87.2(3)
F(3)–Ta–O	79.5(4)	79.4(4)
F(3)–Ta–O′	121.8(4)	123.1(4)
F(4)–Ta–O	91.2(4)	92.5(4)
O–Ta–O′	42.3(7)	43.7(6)

RESULTS AND DISCUSSION

The positional parameters as well as U_{eq} are given in Tables 1. The unit cell content projected on (100) is shown in Fig. 1 and the anion in Fig. 2. Bond distances and angles are given in Table 2 and coordination distances to the potassium ions in Table 3.

The crystals of tripotassium pentafluoroperoxotantalate(V) hydrogendifluoride consist of potassium ions, pentafluoroperoxotantalate(V) ions and hydrogendifluoride ions held together by ionic forces. K(1) and K(2) are surrounded by ten and eight nearest fluorine and oxygen atoms at distances ranging from 2.666(6) to 3.006(7) Å and from 2.584(7) to 3.124(10) Å, respectively, at 290 K and from 2.678(7) to 2.981(8) Å and from 2.572(8) to 3.066(9) Å, respectively, at 170 K. These distances may be compared with the radii sum of 2.7 Å. $K_3[HF_2]$-$[TaF_5(O_2)]$ is not isomorphous with $Na_3[HF_2]$-$[NbF_5(O_2)]$.[4]

$[TaF_5(O_2)]^{2-}$ has a pentagonal bipyramidal arrangement of ligands, a configuration met with in several transition metal peroxo complexes (see, *e.g.*, Refs. 2–7, 11–14). In Table 4 are listed the lengths of the edges of the coordination polyhedron. These agree well with the corresponding ones in other pentafluoroperoxometallates.[5] The distances from the equatorial plane, defined by F(1), F(3), F(3)′, O and O′, to these atoms and to Ta, F(2) and F(4) are given in Table 5. This plane is perpendicular

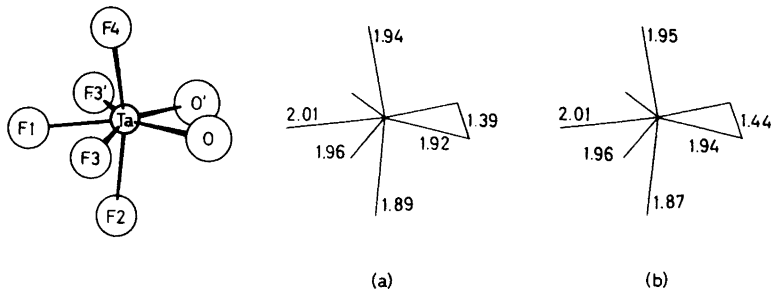

Fig. 2. The ion $[TaF_5(O_2)]^{2-}$. Bond distances at (a) 290 K and (b) 170 K.

to the crystallographic mirror plane through F(1), F(2), F(4) and the midpoint between O and O'. Besides, the angles F(1)–Ta–F(2) and F(1)–Ta–F(4) are approximately equal. The equatorial plane is, therefore, almost a mirror plane. Hence, the point symmetry of $[TaF_5(O_2)]^{2-}$ is almost C_{2v}.

The $Ta-F_{equatorial}$ bond distances, 1.957–2.007 Å at 290 K and 1.955–2.011 Å at 170 K are somewhat longer than the $Ta-F_{apical}$ bond distances, 1.886–1.943 Å and 1.873–1.948 Å, respectively. This compares well with the corresponding distances in a number of pentafluoroperoxoniobates[3-6,14] as well as in $K_6[TaF_5(O_2)][O\{TaF_4(O_2)\}_2]\cdot H_2O$.[7]

The Ta–O distances 1.925 and 1.936 Å, respectively, are normal Ta–O single bond distances, observed ones in $K_6[TaF_5(O_2)][O\{TaF_4(O_2)\}_2]\cdot H_2O$ being 1.86–1.99 Å.[7]

Table 3. Coordination distances to the potassium ions in $K_3[HF_2][TaF_5(O_2)]$.

	Distance/Å at 290 K	170 K
$K(1)\cdots F(3)^{i,ii}$	2.666(6) ×2	2.678(7) ×2
$K(1)\cdots F(1)^{iii}$	2.729(9)	2.717(10)
$K(1)\cdots F(4)^{iii}$	2.867(11)	2.842(11)
$K(1)\cdots O^{iv,v}$	2.894(11) ×2	2.882(11) ×2
$K(1)\cdots F(5)^{vi,vii}$	2.910(7) ×2	2.881(8) ×2
$K(1)\cdots F(5)^{viii,ix}$	3.006(7) ×2	2.981(8) ×2
$K(2)\cdots F(5)^{v}$	2.584(7)	2.572(8)
$K(2)\cdots F(1)^{iii}$	2.619(6)	2.587(6)
$K(2)\cdots F(5)^{x}$	2.622(7)	2.614(8)
$K(2)\cdots F(4)^{ii}$	2.770(5)	2.728(4)
$K(2)\cdots O^{iv}$	2.786(11)	2.777(11)
K(2)···F(2)	2.843(7)	2.839(7)
$K(2)\cdots F(3)^{iii}$	3.114(10)	3.037(10)
$K(2)\cdots F(3)^{ii}$	3.124(10)	3.066(9)

Symmetry codes

i	$\frac{1}{2}-x,\frac{1}{2}+y,1+z$	vi	$\frac{1}{2}-x,\frac{1}{2}+y,-\frac{1}{2}+z$
ii	$\frac{1}{2}-x,\frac{1}{2}+y,-z$	vii	$\frac{1}{2}-x,\frac{1}{2}+y,1-z$
iii	$-\frac{1}{2}+x,\frac{1}{2}-y,z$	viii	$-x,1-y,-\frac{1}{2}+z$
iv	$\frac{1}{2}+x,\frac{1}{2}-y,z$	ix	$-x,1-y,1-z$
v	$\frac{1}{2}+x,\frac{1}{2}-y,\frac{1}{2}-z$	x	$x,y,\frac{1}{2}-z$

Table 4. The lengths of the edges of the pentagonal bipyramidal coordination polyhedron in $K_3[HF_2]$-$[TaF_5(O_2)]$. The designation of the edges conforms to Fig. 3 in Ref. 5. Compare with Table 5 in Refs. 5 and 6.

Edge		Distance/Å at 290 K	170 K
a, b	F(1)···F(3)	2.524(10)	2.511(10)
c, e	F(3)···O	2.483(13)	2.486(14)
d	O···O'	1.389(24)	1.443(22)
f, h	F(2)···F(3)	2.730(11)	2.716(11)
g	F(2)···F(1)	2.675(14)	2.655(16)
i, j	F(2)···O	2.926(15)	2.899(16)
k, m	F(4)···F(3)	2.689(10)	2.692(9)
l	F(4)···F(1)	2.565(13)	2.582(13)
n, o	F(4)···O	2.764(14)	2.805(14)

Table 5. Displacements of the atoms from the least-squares equatorial plane in $[TaF_5(O_2)]^{2-}$. Defining atoms are F(1), F(3), F(3)', O and O'.

Atom	Distance/Å at 290 K	170 K
F(1)	0.040	0.026
F(2)	−1.970	−1.941
F(3), F(3)'	−0.035	−0.023
F(4)	1.837	1.857
O, O'	0.019	0.010
Ta	−0.099	−0.082

The peroxo oxygen bond distance is 1.389(24) Å at 290 K and 1.443(16) Å at 170 K and does not deviate significantly from other observations,[2-6,12] although the distance obtained at 290 K seems a bit short. In fact, it is the author's experience that such short distances are often observed when, as in this case, the substance disintegrates during the collection of the data.

The tantalum atom is displaced about 0.1 Å from the equatorial plane. Such small displacements have been observed for other pentafluoroperoxometallates as well as for other transition metal compounds, when, as in this case, the apical positions are occupied by identical ligands.

The F···H···F distance, 2.242 Å at 290 K and 2.233 Å at 170 K, does not differ significantly from the observed values of 2.283 and 2.292 Å in $Na_3[HF_2][NbF_5(O_2)]$[4] or 2.294 Å found in KHF_2 by the neutron diffraction method.[15,16]

Acknowledgement. I wish to express my gratitude to Mrs. Solveig Olson for technical assistance.

REFERENCES

1. Ružić-Toroš, Ž., Kojić-Prodić, B. and Šljukić, M. *Acta Crystallogr. B 32* (1976) 1096.
2. Svensson, I.-B. and Stomberg, R. *Acta Chem. Scand. 25* (1971) 898.
3. Stomberg, R. *Acta Chem. Scand. A 34* (1980) 193.
4. Stomberg, R. *Acta Chem. Scand. A 35* (1981) 389.
5. Stomberg, R. *Acta Chem. Scand. A 35* (1981) 489.
6. Stomberg, R. *Acta Chem. Scand. A 36* (1982) 101.
7. Massa, W. and Pausewang, G. *Z. Anorg. Allg. Chem. 456* (1979) 169.
8. Lehmann, M. S. and Larsen, F. K. *Acta Crystallogr. A 30* (1974) 580.
9. Cruickshank, D. W. J. In *Crystallographic Computing*, Munksgaard, Copenhagen 1970, p. 195.
10. Lindgren, O. *Thesis*, University of Göteborg and Chalmers University of Technology, Göteborg 1977.
11. Larking, I. and Stomberg, R. *Acta Chem. Scand. 24* (1970) 2043.
12. Larking, I. and Stomberg, R. *Acta Chem. Scand. 26* (1972) 3708.
13. Ružić-Toroš, Ž., Kojić-Prodić, B., Gabela, F. and Šljukič, M. *Acta Crystallogr. B 33* (1977) 692.
14. Stomberg, R. *Acta Chem. Scand. To be published.*
15. Peterson, S. W. and Levy, H. A. *J. Chem. Phys. 20* (1951) 704.
16. Carrell, H. L. and Donohue, J. *Israel J. Chem. 10* (1972) 195.

Received August 27, 1981.

Acta Chemica Scandinavica A 36 (1982) 429–433

The Crystal Structure of Tin(II) Dithionite, $Sn_2(S_2O_4)_2$

ASTRID MAGNUSSON and LARS-GUNNAR JOHANSSON

Department of Inorganic Chemistry, Chalmers University of Technology and the University of Göteborg, S-41296 Göteborg, Sweden

The title compound crystallizes in the monoclinic space group $P2_1/c$ with $a=7.015(1)$, $b=7.480(1)$, $c=12.652(1)$ Å, $\beta=133.59(1)$ Å, $Z=2$. $R=0.037$ for 1264 reflections. In the cage-like $Sn_2(S_2O_4)_2$ complex Sn^{2+} is coordinated to four oxygens from two $S_2O_4^{2-}$ ions in a slightly distorted square pyramidal configuration with Sn–O distances ranging from 2.237(2) to 2.323(3) Å. The dithionite ion has a slightly distorted C_{2v} configuration with an S–S distance of 2.350(1) Å and S–O distances from 1.503(3) to 1.517(3) Å. The smallest distance separating two $Sn_2(S_2O_4)_2$ complexes is 3.013(3) Å.

Due to the inherent instability of the dithionite ion only a few solid dithionites have been characterized so far. Among these, two of the more stable compounds, $Na_2S_2O_4$[1] and $ZnS_2O_4 \cdot$ pyridine,[2] have been investigated by X-ray single crystal methods. The present investigation was made in connection with studies on the reactions between metal surfaces and sulfur dioxide in the presence of water at ambient temperatures. It was found that when tin metal corroded in liquid sulfur dioxide containing some H_2O crystalline tin(II) dithionite was formed. Tin(II) dithionite was first prepared in an impure microcrystalline state by Brunck.[3] Later Cooke[4] reported a crystalline compound which had formed in tin piping used for liquid and gaseous sulfur dioxide. An elemental analysis for tin and sulfur indicated the empirical formula SnS_2O_4. He does not seem to have made any conclusive tests, however, as to whether dithionite was indeed present. Apparently the compound synthesized by us is identical with the one reported by Cooke.

EXPERIMENTAL

0.1 g of p.a. tin powder was placed in a sealed glass ampoule together with 3.0 g of liquid sulfur dioxide and 0.02 g water. No precautions were undertaken to exclude oxygen. The ampoule was then kept at *ca.* 278 K. After one week colourless, platelike crystals of sufficient size for single-crystal work had formed. In the absence of water no reaction takes place. If the synthesis is carried out at a temperature much higher than *ca.* 278 K the product decomposes. Decomposition also takes place if enough water is present to form two liquid phases. The tin powder must be oxide-free otherwise sulfate is produced rather than dithionite.

The IR spectrum was recorded on a Nicolet MX-1 spectrometer using the KBr-disc technique: 1045(s), 991(s), 878(s), 532(w), 460(w), 431(m), 412(vw) cm^{-1}. The spectrum showed no traces of sulfur–oxygen species other than dithionite.

Tin(II) dithionite is insoluble in water. It precipitates silver from an aqueous solution of silver nitrate, although only after heating. The compound is stable in dry air at room temperature but decomposes in presence of moisture. A thermal analysis made in air showed that $Sn_2(S_2O_4)_2$ decomposes exothermally between 398 and 438 K evolving SO_2, producing among other things elemental sulfur. 56 reflections were measured on a Guinier focussed powder photograph using Si as internal standard ($a_{Si}=5.43054$ Å at 298 K[5]). Determination of cell parameters was carried out with the program *TREOR*.[6] Powder data can be obtained from the authors on request.

CRYSTAL DATA

$Sn_2(S_2O_4)_2$, $M=493.62$, space group $P2_1/c$ (No. 14), $a=7.015(1)$ Å, $b=7.480(1)$ Å, $c=12.652(1)$ Å, $\beta=133.59(1)°$, $Z=2$, $D_c=3.41$ g cm^{-3}, $\mu(MoK\alpha)=6.06$ mm^{-1}.

0302-4377/82/050429-05$02.50

STRUCTURE DETERMINATION

Intensities from a crystal of size $0.10 \times 0.08 \times 0.05$ mm were measured on a Syntex $P2_1$ diffractometer by the $\omega - 2\theta$ scan technique with scan speeds of $2-14°$ min^{-1}. Graphite monochromated Mo$K\alpha$ radiation was used and data were collected with a maximum 2θ angle of 70°. 2223 reflections with $h \geq 0$ and $k \geq 0$ were measured. Of these 1264 had $I \geq 3\sigma(I)$ and were used in subsequent calculations. The crystal was stable during the data collection, as indicated by the measurement of a standard reflection ($\bar{1}\bar{2}2$; $I = 121\,000 \pm 4220$) at intervals of 50 reflections. The systematic absences $k = 2n+1$ for $0k0$ and $l = 2n+1$ for $h0l$ indicated space group $P2_1/c$. Intensities were calculated after the data collection from the 96 point intensity profile obtained for each reflection.[7,8] Correction was made for Lorentz and polarization effects but not for absorption or extinction. A ψ-scan of the $\bar{1}\bar{2}2$ reflection showed that the intensity decreased 20 % when the crystal was rotated from the least to the most absorbing position. The Sn atomic position was determined from a Patterson synthesis, and the S and O atoms were located from subsequent electron density summations.[9] The positional parameters, given in Table 1, and the anisotropic thermal parameters were refined to an R of 0.037, ($R = 0.077$ including unobserved reflections), using the program BLOCK.[10] Structure factors and anisotropic thermal parameters can be obtained from the authors on request. The structure factors were weighted according to $w = (\sigma^2(F_o) + 0.0006F_o^2)^{-1}$, $\sigma(F_o)$ being based on counting statistics. Scattering factors for Sn°, S° and O° were used.[12]

Table 1. Fractional coordinates and equivalent isotropic temperature factors (Å^2) with e.s.d.'s in parentheses. $B_{eq} = \frac{4}{3} \sum_{ij} b_{ij}(a_i a_j)$.[11]

	x	y	z	B_{eq}
Sn	0.22353(5)	0.74818(3)	0.91168(3)	2.20(1)
S(1)	0.7994(2)	0.8161(1)	0.9898(1)	1.86(3)
S(2)	0.4531(2)	0.9793(1)	0.7811(1)	1.96(3)
O(1)	0.6306(6)	0.7083(4)	1.0003(3)	2.5(1)
O(2)	0.2377(5)	0.8955(3)	0.7634(3)	2.4(1)
O(3)	0.9258(5)	0.9708(3)	1.0951(3)	2.6(1)
O(4)	0.5233(6)	1.1597(4)	0.8547(3)	2.6(1)

DISCUSSION

The structure of tin(II) dithionite is shown in Figs. 1 and 2. In Tables 2 and 3 some interatomic

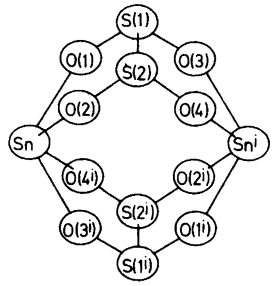

Fig. 1. The dimeric complex.

Table 2. Some distances (Å) and angles (°) with the e.s.d.'s in parentheses. Symmetry codes (i) $1-x$, $2-y$, $2-z$, (ii) $x-1$, $\frac{3}{2}-y$, $z-\frac{1}{2}$, (iii) $1-x$, $1-y$, $2-z$, (iv) $-x$, $y-\frac{1}{2}$, $\frac{3}{2}-z$, (v) $x-1$, y, z.

The Sn – O coordination			
Sn – O(1)	2.255(3)	Sn – O(3^i)	2.323(3)
Sn – O(2)	2.237(3)	Sn – O(4^i)	2.264(3)
O(1) – Sn – O(2)	73.1(3)	O(1) – Sn – O(3^i)	121.5(3)
O(3^i) – Sn – O(4^i)	72.6(3)	O(2) – Sn – O(4^i)	119.8(3)
O(1) – Sn – O(4^i)	78.9(1)		
O(2) – Sn – O(3^i)	78.6(1)		
Shortest intermolecular contacts			
Sn – O(3^{ii})	3.399(3)		
Sn – O(1^{iii})	3.518(3)		
Sn – O(2^{iv})	3.528(3)		
Sn – S(1^v)	3.761(1)		

Table 3. Bond lengths (Å), short non-bonded distances (Å) and angles (°) of the dithionite ion.

	$Sn_2(S_2O_4)_2$	$ZnS_2O_4 \cdot pyr^2$	$Na_2S_2O_4{}^1$
S(1)–S(2)	2.350(1)	2.386(2)	2.389
S(1)–O(1)	1.513(3)	1.517(3)	1.515
S(1)–O(3)	1.507(3)	1.511(3)	1.496
S(2)–O(2)	1.503(3)		
S(2)–O(4)	1.517(3)		
S(2)–S(1)–O(1)	96.3(3)	96.89(12)	99.4
S(2)–S(1)–O(3)	96.7(3)	96.61(12)	98.0
S(1)–S(2)–O(2)	96.0(3)		
S(1)–S(2)–O(4)	97.2(3)		
O(1)–S(1)–O(3)	110.5(3)	110.37(17)	108.3
O(2)–S(2)–O(4)	109.2(4)		
O(1)–S(1)–S(2)–O(4)	110.7(5)	111.5	110.0
O(2)–S(1)–S(2)–O(3)	111.2(5)		
S(1)–S(2)∠O(1)–S(1)–O(3)	101.2	101.8	105.3
S(1)–S(2)∠O(2)–S(2)–O(4)	101.8		

distances and angles are listed. The structure is seen to result from the stacking of a neutral cage-like dimer. The crystallographically equivalent tin atoms are at the apex of a slightly distorted square pyramid with oxygen atoms in the corners of the basal plane. The oxygen atoms belong to two dithionite ions which each contribute two to each tin atom, thus acting as four-dentate ligands. There are six lone pairs projecting from the dimer, one from each tin atom and one from every sulfur atom. The cage has C_i symmetry, but is quite close to D_{2h} symmetry.

The minimum distances separating two dimers are 3.013(3) and 3.044(3) Å. These, being S–O contacts, are shorter than would be expected from the sum of the van der Waals radii given by Pauling.[13] These are 1.40 and 1.85 Å for O and S, respectively.

As shown in Fig. 1 the eight oxygens form a distorted cube in the middle of the dimer. The edges of the oxygen polyhedron fall between 2.462(4) and 2.890(4) Å while the average value of the space-diagonals is 4.655(2) Å. With an ionic radius of oxygen of 1.40 Å[13] this would leave room in the centre of the complex for a particle with a radius somewhat less than 1 Å. Thus it hardly seems possible to trap an atom or a molecule inside the cage.

The dithionite ion has a slightly distorted C_{2v} structure. Bond distances and angles within the

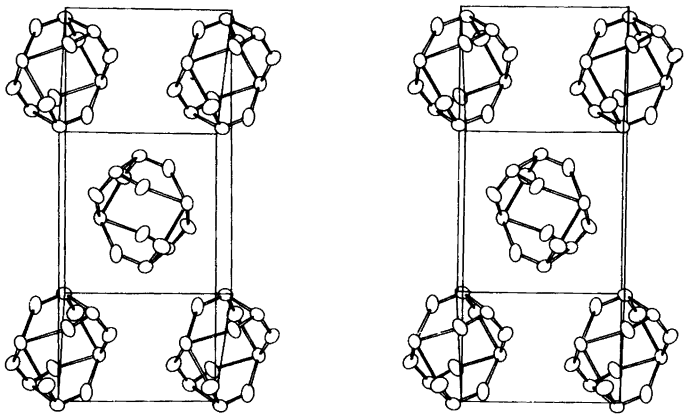

Fig. 2. A stereoscopic view of the unit cell. *b* and *c* are parallel to the picture plane.

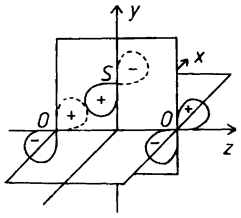

Fig. 3. A schematic view of the antibonding $3b_1$ orbital of SO_2^-.

dithionite group are similar to the values found for the two earlier reported structures. One exception is a small but significant shortening of the distance between the two "eclipsed" SO_2 units. This shortening is seen in the S–S bond. However, the S–S bond distance in tin(II) dithionite is much longer than is normally the case for disulfide links, indicating a weak S–S bond. As suggested by Dunitz[1] the dithionite ion may be regarded as two SO_2^--radicals weakly linked together. In solution the dithionite ion is known to be in equilibrium with the radical ion SO_2^-.[14] Thus a consideration of the electronic structure of the radical ion may be a starting point for a discussion of the structure of the dithionite ion.

According to Dacre and Elder[15] the least stable occupied orbital in the ground state of SO_2^- is the antibonding $3b_1$ orbital, *c.f.* Fig. 3. This orbital is built from *p* orbitals from all three atoms, overlapping out of phase. It may also have some sulfur 3*d* character. While it is S–O antibonding it is slightly O–O bonding. Being an antibonding orbital most of the electron density will be concentrated around the sulfur atom. If two such radical ions, each having one electron in a $3b_1$ orbital, approach each other in such a way that the $3b_1$ orbitals give an in-phase overlap, dimerization will occur. Most of the overlap will occur between the sulfur atoms. It is however probable, as put forward by Kiers and Vos,[2] that some bonding exists between the oxygens in the two SO_2 groups, thus explaining the eclipsed configuration of the ion.

The coordination of divalent tin in most compounds may be described as either a trigonal pyramidal configuration, *i.e.* $Sr[Sn(CH_2ClCO_2)_3]_2$[16] or as a square pyramidal configuration, *i.e.* $Na_2Sn(C_2O_4)_2$.[17] In both cases the tin atom occupies the apex of the pyramid. These coordination figures are thought to result from the stereochemical activity of the lone pair on tin, the lone pair being pictured as projecting from the apex of the pyramid, away from the ligands. The only tin(II) compound with a completely regular square pyramidal coordination is SnO,[18] in all other cases the ideally square pyramid is more or less distorted. The nature of this distortion is normally such that two of the four ligands are considerably closer to the tin than the other two[17] (*c.f.* Table 4). As seen in Table 4 this type of distortion is not present in $Sn_2(S_2O_4)_2$. This probably results from the constraints forced upon the tin environment by the configuration of the dimeric complex with the dithionite ion acting as a four-dentate ligand. The average Sn–O distance in tin(II) dithionite of 2.270(2) Å is typical for compounds belonging to this class, *c.f.* Table 4.

The somewhat simplified picture of the coordination of divalent tin given above disregards the existence of weak tin–ligand interactions in the directions not occupied by the three or four closest neighbours. Such interactions, increasing the coordination of tin to six or more, are a conspicious

Table 4. Sn–O distances (Å) in some compounds containing four-coordinated divalent tin.

Compound	Ref.	Four closest Sn–O contacts	Average	Fifth closest Sn–O contact
$Sn_2(S_2O_4)_2$	This work	2.237(2), 2.255(3), 2.264(3), 2.323(3)	2.270(2)	3.399(3)
SnO	18	2.21(1) × 4	2.21	4.15(1)
$SnC_4H_2O_4 \cdot H_2O$	19	2.176(7), 2.196(3), 2.312(9), 2.440(6)	2.281	2.817(5)
$Sn(H_2PO_4)_2$	20	2.209(2) × 2, 2.466(2) × 2	2.338	2.913(3)
SnC_2O_4	21	2.23 × 2, 2.39 × 2	2.31	2.88
$K_2Sn(C_2O_4)_2 \cdot H_2O$	21	2.13, 2.14, 2.31, 2.36	2.24	3.00
$Na_2Sn(C_2O_4)_2$	17	2.25(1) × 2, 2.36(2) × 2	2.30	2.91(2)
$Sn_3O(OH)_2 \cdot SO_4$	22	2.094(8), 2.144(9), 2.394(8), 2.467(7)	2.275	3.331(9)
		2.062(7), 2.161(8), 2.384(8), 2.485(11)	2.273	3.225(9)

feature of the crystal chemistry of divalent tin.[23] However, in $Sn_2(S_2O_4)_2$ the closest Sn contacts outside the complex, *i.e.* one oxygen belonging to another dimer at 3.399(3) Å which is too far for the oxygen to be bonded to tin.

Acknowledgements. The authors wish to thank Mr. Erland Andersson for determining the cell constants and Professor Nils-Gösta Vannerberg for valuable discussions.

REFERENCES

1. Dunitz, J. D. *Acta Crystallogr. 9* (1956) 579.
2. Kiers, C. T. and Vos, A. *Acta Crystallogr. B 34* (1978) 1499.
3. Brunck, O. *Justus Liebigs Ann. Chem. 336* (1904) 281.
4. Cooke, W. T. *Aust. Chem. Inst. J. Proc. 6* (1939) 58.
5. *International Tables for X-Ray Crystallography*, Kynoch Press, Birmingham 1962, Vol. 3.
6. Werner, P. E. *Z. Kristallogr. 120* (1964) 375.
7. Lindqvist, O. and Ljungström, E. *J. Appl. Crystallogr. 12* (1979) 134.
8. Lehmann, M. S. and Larsen, F. K. *Acta Crystallogr. A 30* (1974) 580.
9. *XTL Operations Manual*, Syntex Analytical Instruments, Cupertino, California 1973.
10. Lindgren, O. *On the Oxygen Coordination of Cerium in Some Sulfates and Chromates*, Diss., University of Göteborg, Göteborg 1977.
11. Hamilton, W. C. *Acta Crystallogr. 12* (1959) 609.
12. *International Tables for X-Ray Crystallography*, Kynoch Press, Birmingham 1974, Vol. 4.
13. Pauling, L. *The Nature of the Chemical Bond*, Cornell University Press, New York 1960.
14. Rinker, R. G., Gordon, T. P., Mason, D. M. and Corcoran, W. H. *J. Phys. Chem. 63* (1959) 302.
15. Dacre, P. D. and Elder, M. *Theor. Chim. Acta 25* (1972) 254.
16. Dewan, J. C. *Acta Crystallogr. B 36* (1980) 1935.
17. Donaldson, J. D., Donoghue, M. T. and Smith, C. H. *Acta Crystallogr. B 32* (1976) 2098.
18. Moore, W. and Pauling, L. J. *J. Am. Chem. Soc. 63* (1941) 1392.
19. Dewan, J. C., Silver, J., Andrews, R. H., Donaldson, J. D. and Laughlin, D. R. *J. Chem. Soc. Dalton Trans.* (1977) 368.
20. Herak, R., Preslesnik, B., Curic, M. and Vasic, P. *J. Chem. Soc. Dalton Trans.* (1978) 566.
21. Christine, A. D., Howie, R. A. and Moser, W. *Inorg. Chim. Acta 36* (1979) 447.
22. Davies, C. G., Donaldson, J. D., Laughlin, D. R., Howie, R. A. and Beddoes, R. *J. Chem. Soc. Dalton Trans.* (1975) 2241.
23. Zubieta, J. A. and Zuckermann, J. J. *Prog. Inorg. Chem. 24* (1978) 251.

Received September 2, 1981.

Acta Chemica Scandinavica A 36 (1982) 435–438

The Hydroalumination of Ethylene. A Self-consistent Field Molecular Orbital Study

ODD GROPEN [a] and ARNE HAALAND [b]

[a] Department of Chemistry, Institute of Mathematical and Physical Sciences, University of Tromsø, N-9001 Tromsø, Norway and [b] Department of Chemistry, University of Oslo, Blindern, Oslo 3, Norway

Self-consistent field molecular orbital calculations have been performed on the reactants and product of the model reaction $H_2AlH^* + H_2C=CH_2 \rightarrow H_2Al-CH_2-CH_2H^*$, on a symmetric π-complex formed from the reactants, and on the system at various points along the reaction path.

The reaction is best described as one in which bonds are broken and formed in a concerted manner, proceeding through a four center (Al,H*,C,C) transition state. A symmetric π-complex represents a possible intermediate in the reaction.

The calculated energy of formation of the π-complex, $\Delta E = -36$ kJ, and the calculated energy of the reaction, $\Delta E = -123$ kJ, are in good agreement with experimental estimates, but the calculated energy of activation, $E^* = 50$ kJ is considerably higher than the experimental estimate, which is about 5 kJ.

The hydroalumination of an α-olefin, eqn. (1), is of great industrial importance as the first step in

$$R'_2AlH^* + H_2C=CHR \rightarrow R'_2Al-CH_2-C(R)HH^*, \quad (1)$$

Ziegler-catalyzed polymerization of ethylene (R = H, R′ = ethyl), and in the dimerization of propene (R = methyl, R′ = n-propyl).[1] The terminal step in the catalytic cycles of both processes consists of the reverse reaction, the β-elimination of an olefin from a trialkylaluminium compound,[1] eqn. (2). The

$$R'_2Al-CH_2-C(R'')(R''')H^* \rightarrow R'_2AlH^* + H_2C=C(R'')R'''. \quad (2)$$

kinetics of both reactions *in the gas phase* have been extensively studied by Egger and coworkers [2] who conclude that both reactions proceed through a four center transition state as indicated in Fig. 1c.

As part of their investigations Eggers and coworkers have determined the activation energies, E_2^*, for the elimination of ethylene from triethylaluminium,[3] for the elimination of 1-butene from dimethylbutylaluminium,[4] and for the elimination of isobutene from triisobutylaluminium:[5]

	E_2^*(kJ)	ΔH_2(kJ)
Et_3Al	126(1)	122
Me_2n-BuAl	116(2)	111
i-Bu_3Al	111(3)	103

The enthalpies of the corresponding reactions, ΔH_2, have been estimated by Smith.[6] It appears, therefore, that the corresponding hydroalumination reactions (1) are exothermic, $\Delta H_1 = -\Delta H_2$, and proceed with a small activation energy, $E_1^* = E_2^* - \Delta H_2 \sim 5$ kJ.

We have investigated the model reactions

$$H_2AlH^* + H_2C=CH_2 \underset{(2')}{\overset{(1')}{\rightleftarrows}} H_2Al-CH_2-CH_2H^*$$

by *ab initio* molecular orbital calculations in the hope of obtaining more information about the nature of the reaction and geometry and bonding in the transition state. A similar study of the hydroalumination of acetylene has already been published.[7]

COMPUTATIONS

The calculations were performed under the LCAO – MO – SCF approximation using program

0302-4377/82/050435-04$02.50

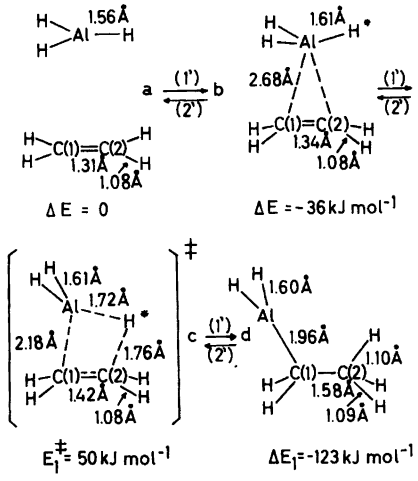

Fig. 1. Bond distances and relative energies of the reactants, products and activated complex of reactions (1') and (2'). The symmetric π-complex represents a possible intermediate.

MOLPRO written by Pulay and Meyer. The basis set consisted of (10,6) GTO functions on Al contracted to $\langle 5,3\rangle$, (7,3) GTO functions on C contracted to $\langle 3,2\rangle$[8] and four GTO functions on H contracted to $\langle 2\rangle$.[9] This set was augmented by a set of d-functions on Al.[7]

The geometries of the two reactants and product of (1'), of a π-complex formed from the reactants, and of intermediate species with fixed reaction coordinate, were optimized using the force relaxation method of Pulay.[10]

RESULTS AND DISCUSSION

Reactants and product. The optimal bond distances and valence angles of reactants and product are listed in Table 2. The optimal Al–H and Al–C bond distances are in good agreement with the experimental values for $H_3AlN(CH_3)_3$[11] and monomeric $(CH_3)_3Al$,[12] 1.56(1) and 1.957(3) Å, respectively. The CC and CH bond distances and valence angles are in reasonable agreement with standard values. The energy of reaction (1') calculated from the electronic energies of reactants and product, $\Delta E_1 = -123$ kJ, agrees very well with Smith's estimated enthalpies of reaction listed above. We conclude, therefore, that our calculations are reasonably successful in reproducing both the geometries and the relative energies of reactants and product.

The π-complex. A symmetric π-complex (Fig. 1b) is found to represent a local *minimum* on the potential energy surface. The calculated energy of formation of the complex is $\Delta E = -36$ kJ. As in the case of the reaction of H_3Al with acetylene,[7] this π-complex represents a possible intermediate, and not the transition state of the reaction.

Dolzine and Oliver[13] have found that while the average degree of association of tripentylaluminium in freezing cyclohexane is $n = 1.80$, the analogous terminal trialkenyl compound, $[H_2C=CH(CH_2)_3]_3Al$, is monomeric ($n = 0.99$) under the same conditions. They suggest that the alkenyl compound achieves valence saturation through intramolecular coordination of one C=C bond to the metal. Since the enthalpy of dissociation of the tripentynaluminium dimer is about 62 kJ mol^{-1},[14] the Al···C=C interaction energy must be at least −31 kJ, in good agreement with our theoretical estimate.

The reaction coordinate. As in our study of the hydroalumination of acetylene, we selected the perpendicular distance from H* to the CC bond axis as the reaction coordinate.[7] This distance was denoted by z^* and varied in steps from its value in the π-complex, 2.88 Å, to its value in the product, 1.04 Å. After each step all other structure parameters were reoptimized. The resulting energies are listed in Table 1 and the optimal structure parameters for each step on the way are

Table 1. SCF energies (in atomic units) and energy differences relative to reactants (in kJ mol^{-1}) along the reaction path of (1'). The reaction coordinate, z^*, is defined as the perpendicular distance from H* to the CC bond axis.

	z^* (Å)	E_{SCF}	ΔE_{SCF}
Reactants	∞	−321.2059	0
π-complex	2.88	−321.2194	−36
	2.00	−321.2058	0
	1.80	−321.1936	+32
	1.70	−321.1861	+52
Activated complex	1.66	−321.1867	+50
	1.60	−321.1887	+45
	1.50	−321.1952	+28
	1.40	−321.2032	+7
	1.20	−321.2374	−83
Product	1.04	−321.2527	−123

Table 2. Selected bond distances (in Å) and valence angles (in degrees) at different points along the reaction path of (1').

z^*	∞ Reactants	2.88 π-complex	2.00	1.80	1.70	1.66 Activated complex	1.60	1.50	1.40	1.20	1.04 Product
Al–H	1.56	1.61	1.61	1.61	1.61	1.61	1.61	1.61	1.61	1.61	1.60
Al–H*	1.56	1.63	1.61	1.62	1.76	1.72	1.90	1.93	1.96	–	–
Al–C(1)	–	2.68	2.68	2.47	2.17	2.18	2.06	2.06	2.06	1.95	1.96
C(1)–C(2)	1.31	1.34	1.34	1.34	1.42	1.42	1.48	1.50	1.50	1.56	1.58
C(2)–H*	–	3.02	2.16	1.94	1.80	1.76	1.70	1.60	1.50	1.31	1.10
C(2)–H	1.08	1.08	1.08	1.08	1.08	1.08	1.08	1.07	1.07	1.08	1.09
∠HAlH	120	117	117	117	125	125	120	120	120	120	125
∠AlC(1)C(2)	–	75	75	77	82	81	84	84	84	92	122
∠C(1)C(2)H*	–	108	112	112	108	109	109	110	112	113	109
∠HC(1)H	117	116	116	116	118	118	118	118	118	110	109
δ^a	0	0	0	0	20	20	30	30	30	45	50

[a] δ is the angle between the CC bond and the CH_2planes.

listed in Table 2. The highest energies were obtained for $z^* = 1.7$ and 1.6 Å, and a series of calculations involving more careful structure optimization located the saddle point on the potential energy surface, corresponding to the activated complex, at $z^* = 1.66$ Å.

Inspection of Table 2 shows that the bond distances Al–H*, Al–C and C–H* change rapidly near the saddle point. The reaction may therefore be described as one in which these bonds are broken and formed in a concerted manner.

The activated complex. A sketch of the activated complex is shown in Fig. 1C. The magnitude of the Al–H*, Al–C, C–C and C–H bond distances confirms Eggers suggestion that the reaction proceeds *via* a four center transition state. This description is also consistent with the overlap populations listed in Table 3. The structure of the activated complex is similar to the structure of the activated complex in the reaction of H_3Al with HC≡CH, and – considering the different sizes of Al and B – to the activated complex in the reaction of BH_3 with $H_2C{=}CH_2$.[15]

The calculated activation energy, $E_1^{\ddagger} = 50$ kJ, is considerably higher than the experimental value, which is about 5 kJ. It is not clear whether the

Table 3. Selected overlap populations and gross atomic populations.

	Reactants	π-complex	Activated complex	Product
Overlap populations				
Al–H*	0.80	0.79	0.49	−0.02
Al–C(1)	–	0.09	0.34	0.70
C(1)–C(2)	1.20	1.02	0.60	0.52
C(2)–H*	–	−0.02	0.25	0.80
Gross atomic populations				
Al	12.50	12.60	12.47	12.22
C(1)	6.31	6.37	6.72	6.87
C(2)	6.31	6.36	6.27	6.40
H*	1.17	1.19	1.16	0.87
H(Al)	1.17	1.18	1.13	1.14
H(C(1))	0.84	0.78	0.76	0.82
H(C(2))	0.84	0.78	0.79	0.85

difference is due to an inadequate basis or to the neglect of correlation effects.

The gross atomic populations listed in Table 3 indicate that the atomic charges in the activated complex are intermediate between the atomic charges in reactants and product.

We wish to return to a discussion of the regiospecificity of the reaction after having made calculations on methyl derivatives of H_3Al and ethylene.

REFERENCES

1. Coates, G. E. and Wade, K. *Organometallic Compounds*, Menthuen, London 1967, Vol. 1, p. 319.
2. Egger, K. W. *Helv. Chim. Acta 55* (1972) 1502 and references therein.
3. Cocks, A. T. and Egger, K. W. *J. Chem. Soc. Faraday Trans. 1, 68* (1972) 423.
4. Egger, K. W. and Cocks, A. T. *Trans. Faraday Soc. 67* (1971) 2629.
5. Egger, K. W. *J. Am. Chem. Soc. 91* (1969) 2867.
6. Smith, M. B. *J. Organomet. Chem. 76* (1974) 171.
7. Gropen, O. and Haaland, A. *Acta Chem. Scand. A 35* (1981) 305.
8. Huzinaga, S. *International report.*
9. Huzinaga, S. *J. Chem. Phys. 42* (1965) 1293.
10. Pulay, P. *Mol. Phys. 17* (1969) 197; *18* (1970) 473.
11. Almenningen, A., Gundersen, G., Haugen, T. and Haaland, A. *Acta Chem. Scand. 26* (1972) 3928.
12. Almenningen, A., Halvorsen, S. and Haaland, A. *Acta Chem. Scand. 25* (1971) 1937.
13. Dolzine, T. W. and Oliver, J. P. *J. Am. Chem. Soc. 96* (1974) 1737.
14. Smith, M. B. *J. Organomet. Chem. 70* (1974) 13.
15. Nagase, S., Ray, K. N. and Morokuma, K. *J. Am. Chem. Soc. 102* (1980) 4536.

Received September 4, 1981.

Acta Chemica Scandinavica A 36 (1982) 439–444

The Preparation and Characterization of Some Chloro(1,2-ethanediamine)iridium(III) Species

FRODE GALSBØL and BIRGITTE S. RASMUSSEN

Chemistry Department I, Inorganic Chemistry, H. C. Ørsted Institute, University of Copenhagen, Universitetsparken 5, DK-2100 Copenhagen Ø, Denmark

An investigation of a published procedure for the preparation of *cis*- and *trans*-$[Ir(en)_2Cl_2]Cl$ (en = 1,2-ethanediamine) revealed that besides these species also $[Ir(en)Cl_4]^-$ and the hitherto unknown *mer*-$[Ir(en)(enH)Cl_3]^+$ (enH^+ = 2-aminoethylammonium ion) are formed. The latter is assigned as the meridional geometrical isomer by comparison of the absorption spectrum with that calculated using the angular overlap model. A modified procedure for the isolation of the *cis*- and *trans*-isomers in a yield of *ca.* 40 % for each is given. The slightly soluble *trans*-$[Ir(en)_2Cl_2]_3[IrCl_6].H_2O$ has also been prepared. In addition to chemical analysis the compounds have been characterized by thermogravimetry and by their electronic spectra. The concentration acidity constant of *mer*-$[Ir(en)(enH)Cl_3]^+$ is estimated to be $10^{-9.12\pm0.04}$ mol/l (25 °C, 1 M $NaClO_4$).

A survey of the published methods[1–4] for the preparation of *cis*- and *trans*-dichlorobis(1,2-ethanediamine)iridium(III) shows that the preparations are cumbersome and/or give low yields. We considered that the procedure published by Baranovskii *et al.*[2] was the most promising and tried to reproduce it. However, both the *cis*- and *trans*-isomers isolated by this method were contaminated with red by-products which were very difficult to remove by crystallization. We therefore examined the products of the reaction by chromatography on a cation exchanger. In addition to *cis*- and *trans*-$[Ir(en)_2Cl_2]^+$ (en = 1,2-ethanediamine) the mixture contained $[Ir(en)Cl_4]^-$ and also the hitherto unknown *mer*-$[Ir(en)(enH)Cl_3]^+$ (enH^+ = 2-aminoethylammonium ion). A procedure is given for the isolation of these compounds.

Furthermore, an alternative method has been developed for the isolation of pure *cis*- and *trans*-$[Ir(en)_2Cl_2]Cl$ in a yield of *ca.* 40 % for each and the slightly soluble olive green *trans*-$[Ir(en)_2Cl_2]_3[IrCl_6].H_2O$ has been prepared by metathesis. The compounds were identified by chemical analysis, by their electronic spectra and by thermogravimetry.

EXPERIMENTAL

Materials. Iridium(III) chloride hydrate (*ca.* 6.6 mol H_2O/mol Ir) was obtained from Johnson, Matthey and Co. and 1,2-ethanediamine ("*puriss. p.a.*") from Fluka. All other chemicals were of analytical or reagent grade and were used without further purification.

Instrumentation. Absorption spectra were recorded on a Cary 118C spectrophotometer. Thermogravimetric measurements were performed on the thermobalance described by Pedersen.[5]

Synthetic Procedures

1. cis- *and* trans-$[Ir(en)_2Cl_2]^+$, mer-$[Ir(en)(enH)Cl_3]^+$ *and* $[Ir(en)Cl_4]^-$. A 6.40 g sample of $IrCl_3.6.6H_2O$ (15.3 mmol) is dissolved in 50 ml of water by heating to boiling in a 250 ml flask fitted with a condenser. Then a mixture of 2.6 ml of 1,2-ethanediamine (39 mmol) and 4.4 ml of acetic acid (77 mmol) diluted to 50 ml with water is added with reflux over a period of *ca.* 10 min. The refluxing is continued for a further 10 h after which the reddish brown reaction mixture is filtered, and the filter washed thoroughly with water. The filtrate and washings are evaporated to dryness on a rotating vacuum evaporator, RVE, (final bath temperature 50 °C), and the residue is dissolved in 20 ml of boiling water. 25 ml of 12 M HCl are added to the hot

0302-4377/82/050439-06$02.50

solution (if the solution is boiled an olive green precipitate of the slightly soluble *trans*-$[Ir(en)_2Cl_2]_3[IrCl_6].H_2O$ is formed) and the solution is again evaporated to dryness on an RVE (final bath temperature 90 °C).

The orange residue is dissolved in 10 ml of boiling water. The solution is allowed to stand for crystallization, first at room temperature, then in the refrigerator overnight, and is finally cooled in ice. The orange crystals are filtered and washed, first with two 1 ml portions of ice-cold water, then with ethanol, finally with ether, and dried in air (product A). The filtrate and washings are evaporated to dryness on an RVE (final bath temperature 50 °C). The residue is boiled with 5 ml of water, and 7.5 ml of 12 M HCl are added. The solution is allowed to stand for crystallization, first at room temperature, then in the refrigerator overnight, and is finally cooled in ice. The crystals are filtered and washed, first with two 1 ml portions of ice-cold 6 M HCl, then with ethanol, finally with ether, and dried in air (product B).

The products A and B (*ca.* 6 g) are mixed and dissolved in 500 ml of water and 12 M HCl is added until pH = *ca.* 2 (*ca.* 0.4 ml). The solution is filtered and the filtrate is applied on a column of 30 g of SP-Sephadex C-25 cation exchanger (Li^+-form, *ca.* 60 cm long and *ca.* 2 cm diameter) which is then washed with water until the eluate which contains the red $[Ir(en)Cl_4]^-$, fraction I, is colourless. The column is then eluted with 0.02 M LiOH, which will neutralize $[Ir(en)(enH)Cl_3]^+$ (usually more than 500 ml are necessary) and the golden coloured fraction II containing $[Ir(en)(en^*)Cl_3]$ (en* = unidentate 1,2-ethanediamine) is collected. The column is then washed with 200 ml of water and finally the yellow band, containing *cis*- and *trans*-$[Ir(en)_2Cl_2]^+$, is eluted with 0.25 M LiCl. The yellow fraction III is collected.

Fraction I is acidified with 2 ml of 12 M HCl, before it is evaporated to a volume of *ca.* 10 ml.* Then 3 ml of 2 M KOH are added and the solution is evaporated to dryness on an RVE (final bath temperature 50 °C). LiCl and HCl are extracted by boiling with 20 ml of absolute ethanol followed by filtration and washing with absolute ethanol. The residue is dissolved in the minimum volume (*ca.* 5 ml) of boiling 0.1 M HCl and the solution is allowed to stand overnight for crystallization. The precipitate is filtered and washed, first with two 0.5 ml portions of ice-cold water, then with ethanol, finally ether, and dried in air. Yield 0.7 g (10%) of reddish orange $K[Ir(en)Cl_4].2H_2O$. (Found: C 5.17; H 2.47; N 5.88; Cl 30.45; K 8.29. Calc. for $KIrC_2H_{12}N_2Cl_4O_2$: C 5.12; H 2.58; N 5.97; Cl 30.22; K 8.33). Thermogravimetry: loss of weight 81.0 mg/g sample, *i.e.* 38.2 g/mol.

Fraction II is acidified with HCl and evaporated to dryness on an RVE (final bath temperature 50 °C). LiCl is extracted by boiling with 20 ml of absolute ethanol followed by filtration and washing with absolute ethanol. The residue is dissolved in the minimum volume (*ca.* 3 ml) of boiling water and the solution is allowed to stand overnight for crystallization. The precipitate is filtered, washed with two 1 ml portions of ice-cold water, and dried in air. Yield 1.5 g (21%) of orange *mer*-$[Ir(en)(enH)Cl_3]Cl.H_2O$. (Found: C 10.17; H 3.86; N 11.94; Cl(tot.) 29.18; Cl(ion.) 7.55. Calc. for $IrC_4H_{19}N_4Cl_4O$: C 10.15; H 4.05; N 11.84; Cl(tot.) 29.97; Cl(ion.) 7.49). Thermogravimetry: loss of weight 39.0 mg/g sample, *i.e.* 18.5 g/mol.

Fraction III is acidified with HCl and evaporated to dryness on an RVE (final bath temperature 50 °C). LiCl is extracted by boiling with 30 ml of absolute ethanol followed by cooling, filtration, and washing with absolute ethanol. The residue is dissolved in the minimum volume (*ca.* 4 ml) of boiling water and the solution is allowed to stand overnight for crystallization. The precipitate is filtered, washed with 1 ml of ice-cold water, and dried in air. Yield 1.5 g (22%) of pale yellow *cis*-$[Ir(en)_2Cl_2]Cl.H_2O$. (Found: C 11.04; H 4.25; N 12.79; Cl(tot.) 24.60; Cl(ion.) 8.16. Calc. for $IrC_4H_{18}N_4Cl_3O$: C 11.00; H 4.15; N 12.83; Cl(tot.) 24.35; Cl(ion.) 8.12). Thermogravimetry: loss of weight 48.4 mg/g sample, *i.e.* 21.3 g/mol.

The filtrate and washings are heated to boiling and 1.5 volumes of 12 M HCl are added. The solution is allowed to stand at room temperature for crystallization, and is finally cooled in ice. The precipitate (*trans*-$[Ir(en)_2Cl_2]Cl.HCl.2H_2O$) is filtered and washed, first with two 0.5 ml portions of 6 M HCl, then with ethanol, finally with ether, and dried at 135 °C. Yield 0.8 g (12%) of yellow *trans*-$[Ir(en)_2Cl_2]Cl$. (Found: C 11.51; H 3.92; N 13.39; Cl(tot.) 25.35; Cl(ion.) 8.51. Calc. for $IrC_4H_{16}N_4Cl_3$: C 11.47; H 3.85; N 13.38; Cl(tot.) 25.40; Cl(ion.) 8.47). By recrystallization from water (*ca.* 0.6 ml/g) the monohydrate is obtained. Anal. $IrC_4H_{18}N_4Cl_3O$: C, H, N, Cl(tot.), Cl(ion.). Thermogravimetry: loss of weight 42.7 mg/g sample, *i.e.* 18.7 g/mol.

2. Dichlorobis(1,2-ethanediamine)iridium(III) chlorides. A 6.40 g sample of $IrCl_3.6H_2O$ (15.3 mmol) is dissolved in a mixture of 0.9 ml of acetic acid (16 mmol) and 17 ml of water by heating to boiling in a 50 ml flask fitted with a condenser. Then 3.1 ml of 1,2-ethanediamine (46 mmol), diluted to 6 ml with water, are added with reflux: first 1 ml then 0.5 ml

*If the solution is not acidic the pink compound $(Ir(en)Cl_3)_x$ is precipitated.[11] This compound can be reconverted to $[Ir(en)Cl_4]^-$ by boiling with 2 M HCl. In the analytical data for $(Ir(en)Cl_3)_x$ given in Ref. 11 it seems likely that the values found for C and N have been interchanged.

every half hour. After the last addition the solution is refluxed for further 5 h and then evaporated to dryness on an RVE (final bath temperature 90 °C). The solid brown residue is heated to 170 °C for 24 h and is then dissolved in 20 ml of boiling water. The solution is filtered, flask and filter are washed with two 10 ml portions of boiling water, and the filtrate and washings are evaporated to dryness on an RVE. The residue is dissolved in 10 ml of boiling water and the solution is allowed to stand for crystallization, first 2 h at room temperature then in the refrigerator overnight. The crystal cake is then broken up and the mixture is cooled in ice-water for 3 h before the crystals are filtered, washed with two 1 ml portions of ice-cold water, and dried in air. Yield 2.5 g (37 %) of *cis*-$[Ir(en)_2Cl_2]Cl.H_2O$.* Anal. $IrC_4H_{18}N_4Cl_3O$: C, H, N, Cl(tot.), Cl(ion.).

The combined filtrate and washings are heated to boiling, 20 ml of 12 M HCl are added, and the mixture is allowed to stand at room temperature for 1 h before it is cooled in ice for 2 h. The crystals are filtered and washed, first with two 3 ml portions of ice-cold 6 M HCl,** then with ethanol, finally with ether. The yellow product is dried at 135 °C. Yield 2.5 g (39 %) of *trans*-$[Ir(en)_2Cl_2]Cl$. Anal. $IrC_4H_{16}N_4Cl_3$: C, H, N, Cl.

3. trans-Dichlorobis(1,2-ethanediamine)iridium(III) hexachloroiridate(III), monohydrate. 10 ml of 12 M HCl are added to a solution of 0.25 g of $IrCl_3.6.6H_2O$ (0.60 mmol) in 5 ml of boiling water. The mixture is heated to boiling and a hot solution of 0.75 g of *trans*-$[Ir(en)_2Cl_2]Cl$ (1.8 mmol) in 5 ml of water is added. The solution is heated to boiling and then allowed to stand overnight for crystallization. The olive green precipitate is then filtered, washed thoroughly with water, and dried in air. Yield 0.82 g (87 %) of *trans*-$[Ir(en)_2Cl_2]_3[IrCl_6].H_2O$. (Found: C 9.16; H 3.28; N 10.71; Cl 27.38. Calc. for $Ir_4C_{12}H_{50}N_{12}Cl_{12}O$: C 9.16; H 3.20; N 10.69; Cl 27.05). Thermogravimetry: loss of weight 15.0 mg/g sample, *i.e.* 23.6 g/mol.

RESULTS AND DISCUSSION

The content of water (and HCl) of crystallization was determined by thermogravimetry. Fig. 1 shows the results for *trans*-$[Ir(en)_2Cl_2]Cl.HCl.2H_2O$ and

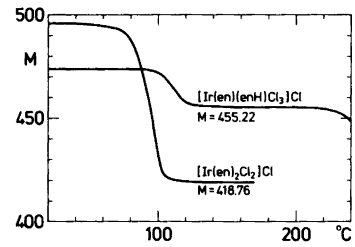

Fig. 1. Thermogravimetric analysis of *trans*-$[Ir(en)_2Cl_2]Cl.HCl.2H_2O$ and *mer*-$[Ir(en)(enH)Cl_3]$-$Cl.H_2O$ in air. Heating rate 2 °C/min. The ordinate gives a number which is proportional to the sample weight, so that the value at the plateau to the right equals the molecular weight of the material without water (and HCl) of crystallization.

mer-$[Ir(en)(enH)Cl_3]Cl.H_2O$. The curves for the other three compounds are similar in shape. The compounds start to loose water of crystallization at the following approximate temperatures: K-$[Ir(en)Cl_4].2H_2O$: 50 °C, *cis*- and *trans*-$[Ir(en)_2Cl_2]$-$Cl.H_2O$: 60 °C, and *trans*-$[Ir(en)_2Cl_2]_3[IrCl_6].H_2O$: 45 °C.

The absorption spectra of *cis*- and *trans*-$[Ir(en)_2Cl_2]Cl.H_2O$ are shown in Fig. 2. They are in good agreement with earlier published results.[1,4,6-10] Fig. 3 shows the absorption spectra of $K[Ir(en)Cl_4].2H_2O$ and *mer*-$[Ir(en)(enH)Cl_3]$-$Cl.H_2O$. Baranovskii *et al.*[11] reports maxima at 320, 369 and 498 nm for the former. The latter compound is assigned as the meridional geometrical isomer by comparison of the absorp-

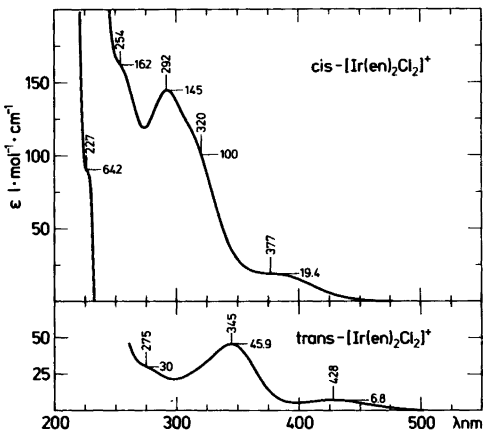

Fig. 2. The absorption spectra of *cis*- and *trans*-$[Ir(en)_2Cl_2]Cl.H_2O$.

*Both (+)-α-bromocamphor-π-sulfonic acid and $(+)^{RD}_{546}$-ethylenediaminetetraacetatocobaltate(III) have been reported[4,9] as resolving agents for *cis*-$[Ir(en)_2Cl_2]^+$.

**If the washing with ethanol and ether is omitted and the product is dried in air, *trans*-$[Ir(en)_2Cl_2]Cl.HCl.2H_2O$ is obtained. Yield 2.6 g (39 %). (Found: C 9.65; H 4.23; N 11.43; Cl(tot.) 28.62; Cl(ion.) 14.44; H^+ 2.037 mmol/g. Calc. for $IrC_4H_{21}N_4Cl_4O_2$: C 9.78; H 4.31; N 11.41; Cl(tot.) 28.87; Cl(ion.) 14.43; H^+ 2.036 mmol/g). Thermogravimetry: loss of weight 155 mg/g sample, *i.e.* 76.7 g/mol.

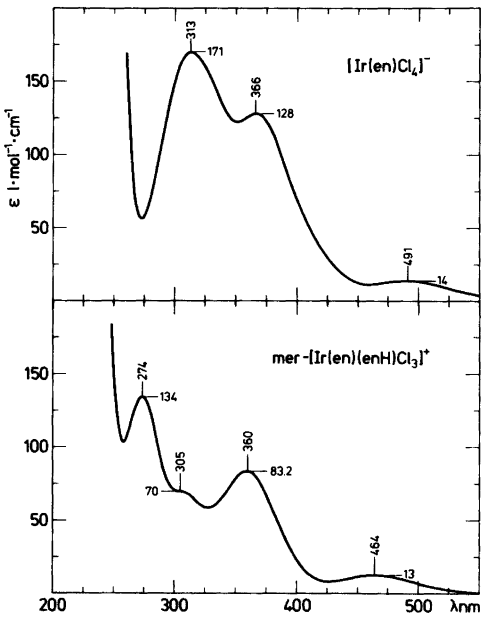

Fig. 3. The absorption spectra of $K[Ir(en)Cl_4].2H_2O$ and *mer*-$[Ir(en)(enH)Cl_3]Cl.H_2O$.

tion spectrum with the transitions calculated using the angular overlap model (Fig. 4). The calculations of the transition energies are based on the expanded radial function model[12] for the d^6 system, where the energy level $^1A_{1g}$ (O_h) is assigned the t_{2g}^6 configuration and both $^1T_{1g}$ (O_h) and $^1T_{2g}$ (O_h) the t_2^5e configuration. The center of gravity rule is lost, because of the non-diagonal elements between $^1T_{1g}$ (O_h) and $^1T_{2g}$ (O_h), which have been taken into account in this model. The connecting lines show the cubic parentage of the energy levels. The holohedric symmetry D_{4h} for *cis*-N_4Cl_2 and *cis*-N_2Cl_4 and O_h for *fac*-N_3Cl_3 accounts for the degeneracies of the energy levels. As seen from Fig. 4, there is a reasonably good agreement between the calculated and the observed transition energies. It should be noted that in the *cis*-N_2Cl_4 case, the calculations show an absorption band at 36.7×10^3 cm^{-1} (272 nm), where the spectrum (Fig. 3) shows a very narrow minimum; however, only 1000 cm^{-1} uncertainty in the calculations would change the calculated value to 37 700 cm^{-1} (265 nm) or 35 700 cm^{-1} (280 nm) and at both these places the experimental spectrum could accommodate a band

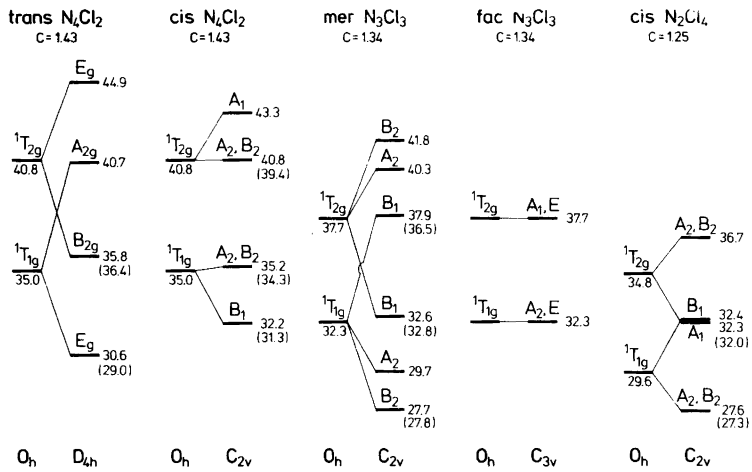

Fig. 4. Comparison of calculated and experimental (in parentheses) transition energies for some $[IrN_xCl_{6-x}]^{x-3}$ species. All energies in the figure are given in 1000 cm^{-1} units. The calculated values were obtained by using the angular overlap model matrices published by Schäffer and Jørgensen,[12] the relations $\Delta = \sigma + C = \Delta_\sigma - \Delta_\pi$, $C = 4B$, $\Delta_\sigma = 3e'_\sigma$, and $\Delta_\pi = 4e'_\pi$ and the following parameters $\sigma_{Cl_6} = 24.1 \times 10^3$ cm^{-1} (Ref. 14), $B_{Cl_6} = 265\ cm^{-1}$, and $\Delta_{\pi Cl} = 1 \times 10^3\ cm^{-1}$ *i.e.* $\Delta_{\sigma Cl} = 26.2 \times 10^3\ cm^{-1}$, and $\sigma_{N_6} = 40.5 \times 10^3\ cm^{-1}$ (Ref. 15), $B_{N_6} = 405\ cm^{-1}$, and $\Delta_{\pi N} = 0$ *i.e.* $\Delta_{\sigma N} = 42.1 \times 10^3\ cm^{-1}$. The $C_{N_xCl_{6-x}}$-values have been calculated by linear interpolation between the $C_{Cl_6}-$ and $C_{N_6}-$values.

Table 1. Concentration acidity constants of the 1,2-ethanediammonium ion and of various complexes containing the 2-aminoethylammonium moiety.

Acid	pK_a	Medium	Ref.
enH^+	10.17	1 M KNO_3	18
	10.06	1 M KCl	19
	10.16	1 M NaCl	20
	10.03	I=0.1 M	21
enH_2^{2+}	7.49	1 M KNO_3	18
	7.44	1 M KCl	19
	7.52	1 M NaCl	20
	7.22	I=0.1 M	21
$Ag(enH)^{2+}$	8.98	I=0.1 M	21
$Hg(enH)^{3+}$	8.2	1 M KNO_3	18
$(NH_3)_5CrOCr(NH_3)_4(enH)^{5+}$	8.42	0.1 M KCl	22
$(NH_3)PtCl_2(enH)^+$	*ca.* 7	1 M KCl	23
$Cr(en)_2(OH)(enH)^{3+}$	8.8	0.25 M NH_4Cl	20
mer-$Ir(en)Cl_3(enH)^+$	9.12	1 M $NaClO_4$	This work

component. The B values were estimated from the complete d^6 matrices for O_h-symmetry,[13] assuming $C=4B$ and using the first ($^1A_{1g}\rightarrow{}^1T_{1g}$) and second ($^1A_{1g}\rightarrow{}^1T_{2g}$) transition energies 24.1×10^3 cm^{-1} and 28.1×10^3 cm^{-1} (Ref. 14) for $[IrCl_6]^{3-}$ and 40.5×10^3 cm^{-1} (Ref. 15) for $[Ir(en)_3]^{3+}$ and 46.7×10^3 cm^{-1} (Ref. 16) for $[Ir(NH_3)_6]^{3+}$. We have used the energy of the second spin allowed transition band for $[Ir(NH_3)_6]^{3+}$, firstly, because the $^1A_{1g}\rightarrow{}^1T_{2g}$ transition for $[Ir(en)_3]^{3+}$ only appears as a shoulder in the spectrum,[15] secondly, because in both the analogous CoN_6 and RhN_6 chromophores of d^6 configuration the $^1A_{1g}\rightarrow{}^1T_{2g}$ transition is observed at the same energy.

An X-ray crystal structure analysis of $[Ir(en)(enH)Cl_3]Cl.H_2O$ is presently being made.

The concentration acidity constant of *mer*-$[Ir(en)(enH)Cl_3]^+$ (1.0 M $NaClO_4$, 25.0 °C) was estimated to be $10^{-9.12\pm0.04}$ mol/l by regression analysis of the titration data as described by Mønsted and Mønsted.[17] A comparison with relevant literature data is shown in Table 1.

Acknowledgements. The authors wish to thank Dr. Ole Mønsted for borrowing his regression analysis computer program and Prof. Claus Schäffer for many valuable discussions of the spectral data. We also thank Johnson, Matthey & Co. for a loan of the iridium chloride used in these studies.

REFERENCES

1. Kida, S. *Bull. Chem. Soc. Jpn. 39* (1966) 2415.
2. Baranovskii, I. B., Kovalenko, G. S. and Babaeva, A. V. *Russ. J. Inorg. Chem. 13* (1968) 1708.
3. Bauer, R. A. and Basolo, F. *Chem. Commun.* (1968) 458.
4. Bauer, R. A. and Basolo, F. *Inorg. Chem. 8* (1969) 2231.
5. Pedersen, E. *J. Sci. Instrum. 1* (1968) 1013.
6. Baranovskii, I. B., Kovalenko, G. S. and Babaeva, A. V. *Russ. J. Inorg. Chem. 14* (1969) 1478.
7. DeArmond, M. K. and Hillis, J. E. *J. Chem. Phys. 54* (1971) 2247.
8. Blanchard, W. D. and Mason, W. R. *Inorg. Chim. Acta 28* (1978) 159.
9. Ogino, H. and Bailar, J. C., Jr. *Inorg. Chem. 17* (1978) 1118.
10. Telebinasab-Sarvari, M. and Ford, P. C. *Inorg. Chem. 19* (1980) 2640.
11. Baranovskii, I. B., Sevast'yanova, R. E., Mazo, G. Y. and Nefedov, V. I. *Russ. J. Inorg. Chem. 19* (1974) 1535.
12. Schäffer, C. E. and Jørgensen, C. K. *K. Dan. Vidensk. Selsk., Mat.-Fys. Medd. 34* (1965) No. 13.
13. Tanabe, Y. and Sugano, S. *J. Phys. Soc. Jpn. 9* (1954) 753.
14. Jørgensen, C. K. *Acta Chem. Scand. 10* (1956) 500.
15. Galsbøl, F. and Rasmussen, B. S. *Acta Chem. Scand. A 36* (1982) 83.
16. Schmidtke, H.-H. *J. Mol. Spectrosc. 11* (1963) 483.
17. Mønsted, L. and Mønsted, O. *Acta Chem. Scand. A 30* (1976) 203.

18. Bjerrum, J. and Larsen, E. In Schneider, W., Anderegg, G. and Gut, R., Eds., *Essays in Coordination Chemistry Dedicated to Gerold Schwarzenbach, Exper. Suppl. IX*, Birkhäuser Verlag, Basel 1964, 39.
19. Pecsok, R. L. and Bjerrum, J. *Acta Chem. Scand. 11* (1957) 1419.
20. Andersen, P., Berg, T. and Jacobsen, J. *Acta Chem. Scand. A 29* (1975) 381.
21. Schwarzenbach, G. *Helv. Chim. Acta 36* (1953) 23.
22. Schwarzenbach, G. and Magyar, B. *Helv. Chim. Acta 45* (1962) 1454.
23. Mønsted, O. and Bjerrum, J. *Proceedings of the XIth. ICCC*, Elsevier, Amsterdam 1968, 103.

Received September 1, 1981.

Acta Chemica Scandinavica A 36 (1982) 445–449

The Crystal and Molecular Structure of 2-Diisopropylamino-4-methyl-3,4-diaza-1,6,6a-trithiapentalenylium-5-thiolate, $C_{10}H_{17}N_3S_4$

LARS K. HANSEN

Department of Chemistry, Institute of Mathematical and Physical Sciences, University of Tromsø, Box 953, N-9001 Tromsø, Norway

The crystal and molecular structure of the title compound has been determined by X-ray methods. The compound crystallizes in the triclinic space group $P\bar{1}$ with unit cell dimensions, $a=5.946(2)$, $b=9.021(2)$, $c=13.900(3)$ Å, $\alpha=91.06(2)$, $\beta=99.81(2)$, and $\gamma=98.02(2)°$. There are two molecules in the unit cell. The structure was solved by the heavy-atom method and refined full matrix least squares to an R-value of 0.040 for 1948 observed reflections.

The two five-membered rings of the central ring system deviate a little from planarity, and the angle between the least squares planes of the rings is 9.9°. Bond lengths in the central part of the molecule are: S(1)–S(6a)=2.554(2) and S(6a)–S(6)=2.190(2) Å with the angle S(1)–S(6a)–S(6)=172.99(6)°, S(1)–C(2)=1.693(3), S(6a)–C(3a)=1.755(3), S(6)–C(5)=1.706(4), C(2)–N(3)=1.378(5), N(3)–C(3a)=1.297(5), C(3a)–N(4)=1.389(4), and N(4)–C(5)=1.378(5) Å. The bond lengths have been corrected for libration. In the crystal structure there is a short intermolecular S···S contact of 3.48(2) Å.

It has been shown in two earlier papers[1,2] that the =N–Ph (Ia) as well as the =N–Me group (Ib) in 6-position of 1,6a-dithiapentalene derivatives (I) perturbs the bonding in the linear S–S–N sequences of these molecules, although to slightly different degrees. Thus, in Ia the S–S and S–N bonds are 2.447(1) and 1.863(2) Å, respectively, while they are 2.494(1) and 1.814(2) Å in Ib. It has further been shown that different heteroatoms such as S, Se, O and N–Ph (IIa-d) in 6-position of 1,6a-dithiapentalene analogues (II) have different effects on the S(1)–S(6a) bonding.[3–6] The S(1)–S(6a) bond length is found to vary from 2.106(3) Å in IIc (X=O)[5] to 2.499(3) Å in IIa(X=S).[3] For IId (X=N-Ph)[6] and IIb (X=Se)[4] the values are 2.396(12) and 2.492(3) Å, respectively. The present structure analysis has been carried out in order to find the length of the S(1)–S(6a) bond in Ic where the 6-position in I is occupied by a sulfur atom. The results may then be compared with the S(1)–S(6a) bond lengths as found in Ia and Ib.

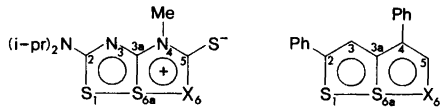

(I)

X_6 = N–Ph (Ia)
X_6 = N–Me (Ib)
X_6 = S (Ic)

(II)

X_6 = S (IIa)
X_6 = Se (IIb)
X_6 = O (IIc)
X_6 = N–Ph (IId)

STRUCTURE ANALYSIS

The title compound was synthesized by Dr. J. Goerdeler, University of Bonn.[7] The crystals were bright yellow prisms and a crystal of dimensions 0.40 × 0.25 × 0.20 mm was used for all X-ray measurements.

Crystal data

$C_{10}H_{17}N_3S_4$; M.W. = 307.52
Space group $P\bar{1}$ with $Z=2$
$a=5.946(2)$ Å, $b=9.021(2)$ Å, $c=13.900(3)$ Å

0302-4377/82/050445-05$02.50

$\alpha = 91.06(2)°$, $\beta = 99.81(2)°$, $\gamma = 98.02(2)°$
$V = 726.8(9)$ Å^3
$D_x = 1.405$ g/cm^3, $D_m = 1.39$ g/cm^3
$\mu(\mathrm{Mo}K\alpha) = 6.14$ cm^{-1}, $F_{000} = 324$

The X-ray measurements were made on an Enraf-Nonius CAD4 diffractometer using graphite monochromator and Mo$K\alpha$ radiation ($\lambda = 0.71069$ Å). The unit cell dimensions were calculated from the setting angles of 24 reflections with $2\theta > 32°$. Three dimensional intensity data for 3484 independent reflections within $2\theta < 56°$ were measured at 20 °C by the $\omega - 2\theta$ scan technique and a scan width of $\Delta\omega = 0.75° + 0.35° \tan\theta$. After data reduction including Lp-correction but no absorption correction 1948 reflections with net intensity I greater than $2\sigma(I)$ were regarded as observed; σ(I) was based on counting statistics.

The structure was solved by the heavy atom (S) method from a sharpened Patterson map. The four

Table 1. Atomic coordinates and temperature parameters U_{ij} (Å)^2 for the sulfur, nitrogen and carbon atoms. The temperature factor is $\exp(-2\pi^2(h^2a^{*2}U_{11} + \ldots 2hka^*b^*U_{12} + \ldots))$. The U_{ij}'s are multiplied by 10^4.

Atom	x	y	z	U_{11}	U_{22}	U_{33}	U_{12}	U_{13}	U_{23}
S(1)	.69730(20)	.26995(11)	.06155(7)	823(9)	541(6)	314(5)	359(6)	64(5)	42(4)
S(6a)	.43435(19)	.44592(11)	.11281(7)	652(7)	449(6)	334(5)	261(5)	35(5)	56(4)
S(6)	.22548(21)	.59090(12)	.17518(7)	688(8)	565(7)	517(6)	363(6)	52(6)	38(5)
S(7)	.32449(21)	.71946(11)	.37535(8)	779(9)	499(6)	551(6)	255(6)	256(6)	-3(5)
C(2)	.78379(62	.24219(37)	.18117(23)	426(23)	391(20)	345(19)	109(17)	43(16	29(15)
N(3)	.74475(49)	.33900(29)	.25206(19)	441(19)	358(16)	321(15)	120(14)	55(14)	29(13)
C(3a)	.59811(60)	.43138(34)	.22852(23)	441(24)	315(19)	335(18)	76(17)	94(17)	45(15)
N(4)	.56535(51)	.52660(30)	.30274(20)	463(20)	349(16)	359(16)	106(14)	110(14)	24(13)
C(5)	.38605(65)	.60968(37)	.28945(26)	507(26)	330(19)	486(22)	95(18)	177(19)	72(16)
C(8)	.71939(102)	.52995(71)	.39739(34)	752(39)	711(35)	357(23)	258(30)	40(24)	-82(25)
N(9)	.89417(53)	.12882(30)	.21428(20)	572(21)	382(17)	374(16)	216(16)	28(15)	8(13)
C(10)	.97454(66)	.10539(41)	.31970(25)	422(24)	415(21)	392(20)	119(19)	-12(18)	68(16)
C(11)	1.16651(84)	.22615(53)	.36499(35)	521(30)	594(29)	528(27)	104(24)	-52(23)	-11(22)
C(12)	.77963(92)	.07819(62)	.37781(38)	580(34)	699(34)	584(30)	118(28)	139(26)	235(26)
C(13)	.93776(86)	.01344(46)	.14353(29)	904(37)	539(27)	418(23)	415(26)	-26(23)	-67(20)
C(14)	1.19240(102)	.00935(59	.15120(41)	910(44)	591(32)	714(36)	282(30)	379(33)	17(27)
C(15)	.80357(97)	-.13813(60)	.15779(55)	526(35)	630(34)	1355(58)	138(28)	-118(36)	-456(37)

Table 2. Atomic coordinates and isotropic thermal parameters U (Å)^2 for the hydrogen atoms. The temperature factor is $\exp\{-8\pi^2 U(\sin^2\theta/\lambda^2)\}$. The U's are multiplied by 10^3.

Atom	x	y	z	U	Atom	x	y	z	U
H(81)	.6813(96)	.4690(56)	.4268(36)	103(25)	H(123)	.6595(78)	.0154(48)	.3446(31)	89(18)
H(82)	.6828(87)	.6106(54)	.4306(36)	119(20)	H(13)	.8939(62)	.0530(38)	.0784(25)	63(12)
H(83)	.9016(103)	.5638(59)	.3733(38)	172(25)	H(141)	1.2938(78)	.1107(50)	.1410(32)	101(18)
H(10)	1.0507(58)	.0195(36)	.3192(23)	49(10)	H(142)	1.2670(75)	-.0245(46)	.2106(30)	82(16)
H(111)	1.2264(73)	.1953(44)	.4290(29)	81(15)	H(143)	1.2129(66)	-.0639(41)	.1042(27)	67(13)
H(112)	1.1066(77)	.3209(48)	.3682(31)	99(17)	H(151)	.8266(78)	-.1928(49)	.1053(31)	87(17)
H(113)	1.3120(85)	.2290(48)	.3270(32)	118(19)	H(152)	.8759(90)	-.1773(52)	.2256(35)	117(21)
H(121)	.7171(84)	.1820(52)	.3918(32)	115(18)	H(153)	.6318(79)	-.1293(47)	.1427(31)	93(16)
H(122)	.8528(77)	.0495(48)	.4448(32)	105(17)					

sulfur atoms were located, and a subsequent Fourier map revealed the remaining non-hydrogen atoms. The hydrogen atoms were found from difference maps and the atomic parameters were refined by full matrix least squares to an R factor of 0.040. The weighted R_w was 0.029. The average shift was less than 0.05σ and the shifts in all parameters were less than 0.2σ.

The atomic scattering factors used for sulfur, nitrogen and carbon were those of Doyle and Turner,[8] and for hydrogen those of Stewart *et al.*[9] Final atomic coordinates and temperature parameters for the non-hydrogen atoms are listed in Table 1; those of the hydrogen atoms are listed in Table 2. The final structure factor list is available from the author on request.

Rigid body analysis (RBM) has been carried out according to the method of Schomaker and Trueblood.[10] The system treated as a rigid body was the central ring system plus the atoms S(7), C(8), N(9), C(10) and C(13).

All calculations were carried out on the UNIVAC 1110 computer at the University of Bergen. The programs used were mainly those of the X-RAY 76 program system except for the data reduction and RBM-analysis programs which were adopted for the UNIVAC 1110 computer by L.K. Hansen and L. J. Sæthre, this University.

DISCUSSION

An ORTEP[12] drawing showing the structure of the title compound and the numbering of atoms is given in Fig. 1. The rings A and B deviate both slightly from planarity. The equations for the least squares planes through rings A and B are:

Plane A:

$$3.92969\,x + 5.80658\,y - 3.43527\,z = 3.99363$$

Plane B:

$$3.37000\,x + 6.31804\,y - 5.13653\,z = 3.64117$$

with x, y and z as fractional coordinates.

The largest deviations from the planes are -0.13 Å for atom C(2) in plane A and -0.07 Å for atom

Table 3. Bond lengths (l) in 2-diisopropylamino-4-methyl-3,4-diaza-1,6,6a-trithiapentalenylium-5-thiolate. Standard deviations in parentheses. The $l^{\parallel}$ values have been corrected for libration.

Bond	l(Å)	$l^{\parallel}$(Å)
S(1)–S(6a)	2.550(2)	2.554
S(6a)–S(6)	2.187(2)	2.190
S(1)–C(2)	1.689(3)	1.693
S(6a)–C(3a)	1.750(3)	1.755
S(6)–C(5)	1.701(4)	1.706
C(2)–N(3)	1.375(5)	1.378
N(3)–C(3a)	1.295(5)	1.297
C(3a)–N(4)	1.387(4)	1.389
N(4)–C(5)	1.376(5)	1.378
C(5)–S(7)	1.657(4)	1.661
N(4)–C(8)	1.467(5)	1.471
C(2)–N(9)	1.338(5)	1.340
N(9)–C(10)	1.491(4)	1.495
N(9)–C(13)	1.497(5)	1.500
C(10)–C(11)	1.506(6)	
C(10)–C(12)	1.517(7)	
C(13)–C(14)	1.505(8)	
C(13)–C(15)	1.518(7)	

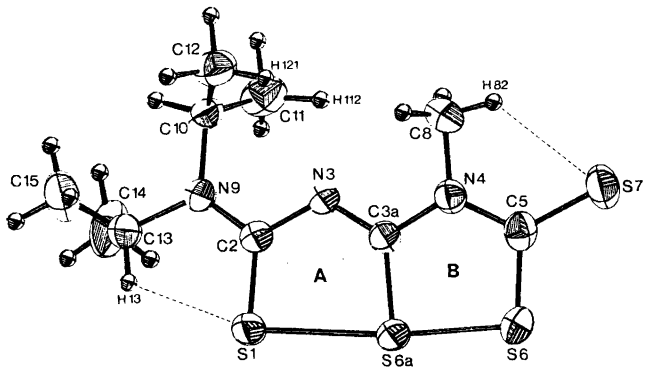

Fig. 1. ORTEP[12] drawing of the title compound with numbering of atoms. Thermal ellipsoids for the non-hydrogen atoms are drawn at the 50% probability level.

Table 4. Bond angles ∠(*ijk*) in 2-diisopropylamino-4-methyl-3,4-diaza-1,6,6a-triapentalenylium-5-thiolate. The standard deviations in parentheses.

i	*j*	*k*	∠(*ijk*)°
C(2)	S(1)	S(6a)	88.0(1)
S(1)	S(6a)	S(6)	172.99(6)
S(1)	S(6a)	C(3a)	82.7(1)
C(3a)	S(6a)	S(6)	90.4(1)
S(6a)	S(6)	C(5)	96.5(1)
S(6)	C(5)	S(7)	121.3(2)
S(6)	C(5)	N(4)	114.3(3)
S(7)	C(5)	N(4)	124.4(3)
C(5)	N(4)	C(8)	121.0(4)
C(5)	N(4)	C(3a)	120.9(3)
C(8)	N(4)	C(3a)	118.1(4)
N(4)	C(3a)	S(6a)	116.9(3)
N(4)	C(3a)	N(3)	116.7(3)
S(6a)	C(3a)	N(3)	126.4(3)
C(3a)	N(3)	C(2)	119.0(3)
N(3)	C(2)	N(9)	115.3(3)
C(1)	C(2)	N(3)	120.7(3)
S(1)	C(2)	N(9)	124.0(3)
C(2)	N(9)	C(10)	124.2(3)
C(2)	N(9)	C(13)	119.8(3)
N(9)	C(10)	C(11)	111.9(3)
N(9)	C(10)	C(12)	113.4(3)
N(9)	C(13)	C(14)	110.7(3)
N(9)	C(13)	C(15)	110.4(4)
C(11)	C(10)	C(12)	113.5(4)
C(10)	N(9)	C(13)	116.1(3)
C(14)	C(13)	C(15)	112.8(4)

C(3a) in plane *B*. The angle between the planes is 9.9°. The atoms of the diisopropylamino group, N(9), C(10) and C(13) lie out of plane *A*, by −0.47, −0.65 and −0.72 Å, respectively, while the substituent atoms S(7) and C(8) lie 0.07 and 0.09 Å, respectively, out of plane *B*.

Bond lengths and angles for the non-hydrogen atoms are listed in Tables 3 and 4. The bond lengths between non-hydrogen atoms, with the exceptions of the C−C bonds in the isopropyl-groups, have been corrected for libration, *cf.* Table 3. The l^1 values are corrected according to Cruickshank's[13] method. The maximum angle of libration is 3.7°, and the corrections range from 0.002 to 0.005 Å.

The S(1)−S(6a) bond length of the present structure is 2.554(2) Å and the S(6a)−S(6) bond length 2.190(2) Å; the S(1)−S(6a)−S(6) angle is 173.0(1)°. A comparison with the S(1)−S(6a) bond lengths in Ia and Ib, respectively, shows that those are 0.107 and 0.060 Å shorter than those of the present structure. Thus, by replacing the N−R group in I with sulfur the S(1)−S(6a) bond becomes significantly longer. This observation is in good agreement with results from structural studies on trithiapentalene derivatives.[3,6] Thus, in IId[6] the S(1)−S(6a) bond length is 2.396(12) Å while that in IIa[3] is 2.499(3) Å. The increase in the S(1)−S(6a) bond length is 0.103 Å as compared with the difference of 0.107 Å between the S(1)−S(6a) bond lengths in Ic and Ia. A comparison of the lengths of other bonds in Ic with those of equivalent bonds in Ia and Ib shows insignificant differences.

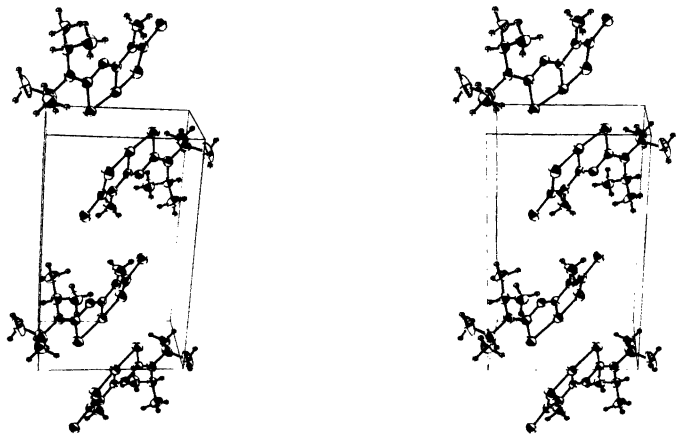

Fig. 2. A stereoscopic view of the arrangement of molecules in the unit cell.

The C–H bond lengths have a mean value of 0.98(10) Å. The bond angles involving hydrogen atoms have a mean value of 109(6)°.

As in Ia and Ib there are also a few short intramolecular S···H and N···H contacts in Ic. These are, S(1)···H(13)=2.41(4) Å, S(7)···H(82)=2.48(5) Å, N(3)···H(121)=2.44(4) Å and N(3)···H(112)=2.49(4) Å, *cf.* Fig. 1. Especially the S···H distances are rather short compared to the corresponding van der Waals distance of 3.05 Å.[14] There is also a short intermolecular distance S(6a)···S(6a)=3.48(2) Å across a symmetry center. A stereoscopic view of the arrangements of molecules in the unit cell is given in Fig. 2.[12]

Acknowledgement. The author wishes to thank Dr. J. Goerdeler, University of Bonn, for supplying a crystalline sample of the compound.

REFERENCES

1. Hansen, L. K. *Acta Chem. Scand. A 31* (1977) 855.
2. Hansen, L. K. *Acta Chem. Scand. A 35* (1981) 61.
3. Hordvik, A., Sletten, E. and Sletten, J. *Acta Chem. Scand. 23* (1969) 1852.
4. Van den Hende, J. H. and Klingsberg, E. *J. Am. Chem. Soc. 88* (1966) 5045.
5. Hordvik, A., Sletten, E. and Sletten, J. *Acta Chem. Scand. 23* (1969) 1377.
6. Leung, F. and Nyburg, S. C. *Can. J. Chem. 50* (1972) 324.
7. Goerdeler, J., Büchler, R. and Sólyom, S. *Chem. Ber. 110* (1977) 285.
8. Doyle, P. A. and Turner, P. S. *Acta Crystallogr. A 24* (1968) 390.
9. Stewart, R. F., Davidson, E. R. and Simpson, W. T. *J. Chem. Phys. 42* (1965) 3175.
10. Schomaker, V. and Trueblood, K. N. *Acta Crystallogr. B 24* (1968) 63.
11. Stewart, J. M., Ed., *The X-Ray System, Version of 1976*, Technical Report TR-446, Computer Science Center, University of Maryland, College Park 1976.
12. Johnson, C. K. *ORTEP-II: A Fortran Thermal-Ellipsoid Plot Program For Crystal Structure Illustrations*, Report ORNL-3794, Oak Ridge National Laboratory, Oak Ridge 1971.
13. Cruickshank, D. W. J. *Acta Crystallogr. 9* (1956) 757.
14. Pauling, L. *The Nature of the Chemical Bond*, 3rd Ed., Cornell University Press, New York 1960.

Received September 28, 1981.

Acta Chemica Scandinavica A 36 (1982) 451–458

On the Structures of the Thallium(III) Chloride Complexes in Solution. I. Evidence for Tetrahedral $TlCl_4^-$ and Octahedral $TlCl_6^{3-}$ Species in Aqueous Solution

JULIUS GLASER

Department of Inorganic Chemistry, Royal Institute of Technology, S-100 44 Stockholm 70, Sweden

The structures of the $TlCl_4^-$ and the $TlCl_6^{3-}$ complexes have been determined from X-ray diffraction measurements on concentrated aqueous solutions of thallium(III) (0.9 M – 2.7 M) and chloride (6.2 M – 12.3 M). The TlCl complex is tetrahedral with a Tl–Cl distance of 2.43(1) Å and a Cl–Cl distance of 3.96(3) Å. The $TlCl_6^{3-}$ complex is octahedral with a Tl–Cl distance of 2.59(1) Å and a Cl–Cl distance of 3.69(6) Å. There is no evidence that polynuclear species are present in the investigated solutions. These results are in agreement with Raman spectra for solutions and for solids containing discrete thallium(III) chloride complexes.

The complexes formed between Tl^{3+} and Cl^- in aqueous solution are among the strongest metal ion-chloride complexes known.[1] They have been the subject of several studies,[2] and some of their properties have been elucidated. The stability constants[3–5] and the enthalpies of formation[3,6] can be explained assuming the $TlCl_n^{3-n}$ species (n=0,1,2,3,4) to be present in dilute aqueous solutions. The existence of higher complexes ($n>4$) has, however, for a long time been a matter of controversy.[2] Ultraviolet spectra[7] indicate the existence of the fifth complex, $TlCl_5^{2-}$, with the formation constant $K_5=[TlCl_5^{2-}]/[TlCl_4^-][Cl^-])=0.8(2)\ M^{-1}$. Extraction measurements have also been interpreted in terms of weak bonding of the fifth chloride ligand ($K_5=0.3\ M^{-1}$),[8] although other workers using the same method found no evidence for complexes higher than $TlCl_4^-$.[9]

In concentrated aqueous solutions clear evidence for at least one higher species, possibly octahedral $TlCl_6^{3-}$, was found by Spiro[10] and Davies[11] from Raman spectra. Tl NMR spectra also indicate the formation of complexes with more than four chlorides per thallium.[12,13] Figgis[12] claimed that the most stable species at higher chloride concentrations is $Tl_2Cl_9^{3-}$, a structural unit previously found to be present in the crystal structure of $Cs_3Tl_2Cl_9$.[14] Very little is known about the structures of the Tl^{3+} halide complexes formed in aqueous solution. The only information existing on this subject is inferred from vibrational spectra, where the interpretation of the data is difficult and ambiguous, particularly when two or three complexes coexist.[2,10,15]

In the solid state, several discrete thallium(III) chloride species have been found. In $TlCl_3 \cdot 4H_2O$,[16] as well as in $TlCl_3(C_6H_4N_2O)_2$,[17] a trigonal bipyramidal complex, $TlCl_3O_2$, exists, with the thallium atom 0.072(3) Å off the plane of the three chlorides. In tetrachlorothallates(III), the only discrete T(III) unit found is the $TlCl_4^-$ tetrahedron.[18–21] The existence of the higher complexes, $TlCl_5^{2-}$ and $TlCl_6^{3-}$, in the solid state is also evident.[22–24,24–28] The $TlCl_5^{2-}$ unit has a distorted square-pyramidal geometry in $[N(C_2H_5)_4]_2TlCl_5$,[29] but in salts obtained from aqueous solutions, such as $Cs_2TlCl_5(H_2O)$ or $Rb_2TlCl_5 \cdot H_2O$, a water molecule coordinates to $TlCl_5^{2-}$ and thus completes the octahedral geometry.[22–24] In hexachlorothallates, octahedral $TlCl_6^{3-}$ units have been found.[24–28] Polynuclear complexes have also been found in the solid state.[14,24] $Tl_2Cl_9^{3-}$ (see above) is composed of two $TlCl_6$ octahedra sharing one face,[14] and $Tl_2Cl_{10}^{4-}$ contains two octahedra sharing one edge.[24]

In order to elucidate the structures of the thallium(III) halide complexes in solution, a series of

0302-4377/82/050451-08$02.50

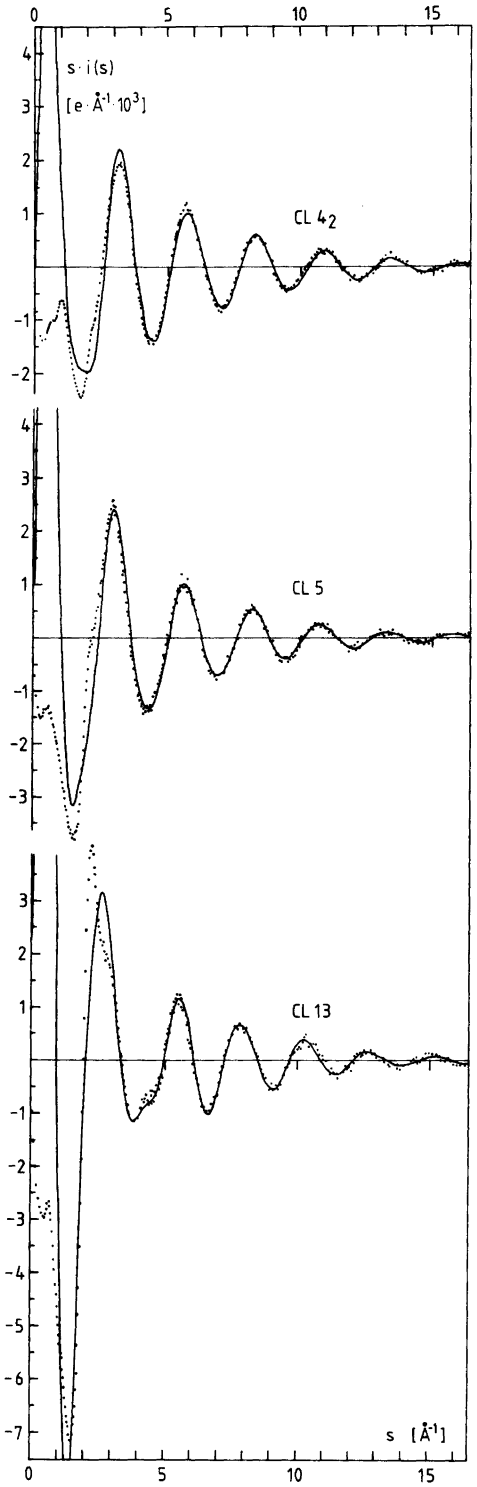

investigations has been started. The distribution of Tl(III) among the different TlX_n^{3-n} species (X= Cl,Br) in dilute and concentrated aqueous solutions have been determined by the ^{205}Tl NMR method.[30] The highest ligand number is proved to be six for the Tl(III) chloride system and is probably the same for the $TlBr_n^{3-n}$ complexes, but the stability constant is much lower in the latter case.

Accurate bond lengths within the different $TlX_n(H_2O)_m^{3-n}$ complexes have been derived from crystal structures, *e.g.* Refs. 16b, 21, 27. These give plausible models for the complexes existing in solution. Finally, X-ray diffraction measurements and Raman spectra have been recorded for concentrated aqueous solutions. The first part, dealing with thallium(III) aqua- and bromide complexes, was presented in the preceding paper.[31] In the present article, the structures of the $TlCl_4^-$ and $TlCl_6^{3-}$ complexes are elucidated.

EXPERIMENTAL

The solutions were prepared and analyzed as described previously.[32] The compositions of the solutions investigated by X-ray diffraction are given in Table 1. The $\theta-\theta$ diffractometer was used in the same way as previously.[33] The scattered radiation ($\lambda_{MoK\alpha}=0.7107$ Å) was monochromatized by a focusing LiF crystal and measured by a scintillation counter as a function of the scattering angle. The intensities were collected at discrete points at intervals of 0.1° for $1.5°<\theta<20°$ and of 0.25° for $20°<\theta<70°$, which corresponds to 0.3 $Å^{-1}<s=(4\pi \sin\theta)/\lambda<16.7$ $Å^{-1}$. Typically, 10^5 counts were collected for each point. A complete data collection was performed twice for each solution in order to eliminate any long-term experimental drift. Raman spectra were collected on a Cary 82 and a Coderg T800 laser source spectrophotometer.

DATA TREATMENT AND RESULTS

The data processing was performed as described in the preceding paper.[31] The curves were calculated for a stoichiometric unit of volume containing one Tl atom.

Fig. 1. The experimental reduced intensity curves, multiplied by *s*, for the investigated solutions (···). The *solid lines* are calculated for the interactions shown in Fig. 2, including the $Cl-(H_2O)$ and the long $Tl-(H_2O)$ contributions.

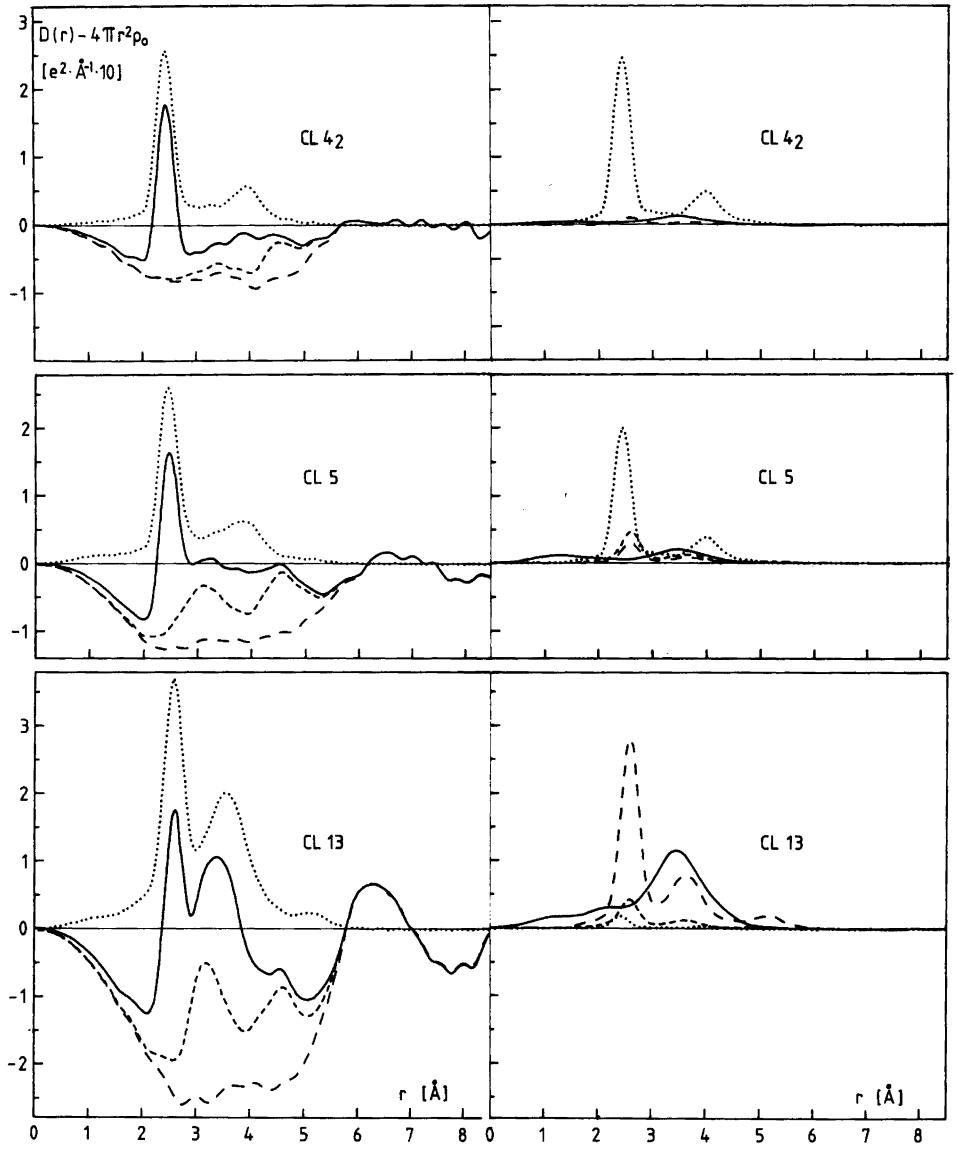

Fig. 2. Comparison between the experimental radial distribution functions, $D(r) - 4\pi r^2 \rho_o$, and the peak shapes calculated for the nearest neighbour interactions. The curves to the right show the peak shapes calculated for the following interactions: –, sums of the "background" contacts O–H and $Li(H_2O)_4^+$; ···, the tetrahedral $TlCl_4^-$ complex; ---, the octahedral $TlCl_5(H_2O)^{2-}$ complex; – – –, the octahedral $TlCl_6^{3-}$ complex. The curves to the left represent: –, the experimental $D(r) - 4\pi r^2 \rho_o$ functions; ···, the sums of the peak shapes shown in the figures to the right; ---, the differences between the experimental and the calculated curves; – – –, the differences between the experimental and the calculated curves when also the Cl–H_2O and the long Tl–H_2O interactions are taken into account.

Table 1. Compositions (in mol/l) of the solutions investigated by X-ray diffraction. The concentrations of the $TlCl_n^{3-n}$ complexes have been calculated using the stability constants in Ref. 30, determined for similar total Tl concentrations.

Solution	Tl	Cl	Li	H_2O	Ratio Cl/Tl	$TlCl_4^-$	$TlCl_5^{2-}$	$TlCl_6^{3-}$
CL5	1.29	6.23	2.36	48	4.8	0.99	0.20	0.10
CL13	0.92	12.3	9.54	42	13.4	0.06	0.13	0.73
$CL4_2$	2.65	10.87	2.92	41	4.1	2.57	–	0.08

The experimental reduced intensity values, multiplied by s, for the investigated solutions, are given in Fig. 1. The radial distribution functions (RDF's) $D(r)-4\pi r^2\rho_o$, (ρ_o is the average scattering power per stoichiometric volume[34]) obtained through Fourier inversion of the reduced experimental intensities, [34] are shown in Fig. 2.

Parameters for intramolecular interactions were obtained by a least-squares refinement procedure,[34] using different ranges of s in order to reduce the influence of systematic errors in different parts of the intensity curves. The refined parameters were: the distance, r, the mean-square variation in the distance, l^2, and the number of distances per Tl atom, n. The refinements were performed in different ways: (I) At first, only the Tl – Cl interactions (r_{Tl-Cl}, l^2_{Tl-Cl} and n_{Tl-Cl}) were refined, without any assumptions about the existing complexes, using the high angle region of the intensity curves. The results are given in Table 2a. (II) Next, the minor $TlCl_n^{3-n}$ complexes were included with distances found in the appropriate crystal structures.[21,22,27] The concentrations were calculated using the stability constants from Ref. 30 (*c.f.* Table 1) and the Tl – Cl contributions within the major species were refined. Finally, the Cl – Cl interactions were also refined.

The results from all the calculations under point (II) are given in Table 2b. For the solution CL5, the Cl – Cl interactions contribute too little to the intensity curve and consequently could not be refined.

Raman frequencies for some aqueous solutions of Tl(III) and Cl^-, as well as for several solid compounds containing discrete $TlCl_n^{3-n}$ complexes, are presented in Table 3.

Table 2. Results of least-squares refinements (r_{pq} is the distance in Ångström units between atoms "p" and "q"; n is the number of distances per Tl atom; and l^2 the mean-square variation of the distance, in $Å^2$). Only the parameters for which the estimated standard deviations are given were refined. The standard deviations are those obtained in the least-squares procedure, but they were increased in order to account for the variation of the parameters when different s-ranges were used in the refinements.

a. Tl – Cl interactions only (no other complexes included).

Solution	r_{Tl-Cl}	l^2_{Tl-Cl}	n_{Tl-Cl}
CL5	2.458(3)	0.011(2)	4.2(5)
CL13	2.568(3)	0.011(2)	5(1)
CL4	2.436(2)	0.009(1)	4.2(5)

b. Tl – Cl and Cl – Cl interactions within the dominating complex (the minor Tl(III) complexes included with constant parameter values).

Solution	The dominating complex	r_{Tl-Cl}	l^2_{Tl-Cl}	n_{Tl-Cl}	r_{Cl-Cl}	l^2_{Cl-Cl}	n_{Cl-Cl}	r_{Cl-Cl}/r_{Tl-Cl}
CL5	$TlCl_4^-$	2.446(2)	0.010(1)	4.6(6)	–	–	–	–
CL13	$TlCl_6^{3-}$	2.590(3)	0.009(2)	5.5(7)	3.69(6)	0.04	13(2)	1.42
$CL4_2$	$TlCl_4^-$	2.433(1)	0.009(1)	4.2(3)	3.96(3)	0.04	5(1)	1.63

Table 3. Raman band frequencies for aqueous solutions of Tl(III) and Cl^-. (1 M $TlCl_{4.1}$ means [Tl(III)] = 1 M; $[Cl^-]_{tot}/[Tl(III)] = 4.1$). The concentrations of the dominating Tl(III) species are given in percent of the total thallium content according to the stability constants in Ref. 30. Data for some solid compounds with known structures, containing discrete Tl(III)–Cl^- complexes, are given for comparison (the weakest peaks are omitted). The following abbreviations are used: s = strong, m = medium, w = weak, sh = shoulder, br = broad.

	Dominating complex	Frequencies in cm^{-1}	Ref.
Solutions			
A. 1 M $TlCl_{4.1}$	97 % $TlCl_4^-$	305 s, ~81 w, br	10
B. 2.7 M $TlCl_{4.1}$ ("$CL4_2$")	97 % $TlCl_4^-$	303 s, ~78 w, br	This work
C. 1.3 M $TlCl_{4.8}$ ("CL5")	77 % $TlCl_4^-$	302 s, 260–285 sh, ~120 sh, ~90 w, br	"
D. 2.7 M $TlCl_{4.8}$	72 % $TlCl_4^-$	303 s, 260–290 sh, ~120 sh, ~85 w, br	"
E. 2.5 M $TlCl_{6.4}$	79 % $TlCl_6^{3-}$	275 s, ~110 w, br	"
F. 0.9 M $TlCl_{13.4}$ ("CL13")	79 % $TlCl_6^{3-}$	270 s, ~120 m, br	"
Solid			
$[As(C_6H_5)_4]TlCl_4$		312 s, 296 w, 78, 60	10
$MTCl_4$ (M = K,Rb,Tl(I),NH_4)		300(±3) s, 289(±5) w, 125(±7) m, 96(±1) m	24 This work
$Rb_2TlCl_5(H_2O)$		294 s, ~249 w, ~143 m	24
$(NH_4)_2TlCl_5(H_2O)$		286 s, ~194 m, ~169 m	"
$Cs_2TlCl_5(H_2O)$		264 s, 152 m, 131 m	This work
$M_3TlCl_6 \cdot nH_2O$ (M = Na,Tl(I),$Co(NH_3)_6$,NH_4)		270(±7) s, 116(±24) m	24,39 This work
$Cs_3Tl_2Cl_9$		285 s, 260 w, 229 w, 155 w, 130 m, 108 m	40 This work

DISCUSSION

Intramolecular interactions. For all the investigated solutions the first prominent peak in the RDF's occurs at about 2.5 Å, a value close to the Tl–Cl distance found in several crystal structures.[17–28] Thus, it can be identified as representing the Tl–Cl interactions within the different thallium(III) chloride species. The Tl–Cl distances, refined without any assumptions concerning the complexes present in the solutions (Table 2a), increase noticeably from 2.436(2) Å for the $CL4_2$ solution to 2.568(3) Å for CL13 solution. The number of such distances per Tl atom could not be determined very precisely because of the low scattering power of the Cl atoms. Nevertheless, these results of the X-ray scattering measurements given in Table 2a are consistent with the formation of higher $TlCl_n^{3-n}$ ($n > 4$) complexes predicted by the stability constants determined for the same concentrations using Tl–NMR.[30] Thus, it seemed reasonable to include the minor $TlCl_n^{3-n}$ species (*cf.* Table 1) when refining the parameters of the dominant complex (Table 2b). The results for the CL4 solution provide the structure of the $TlCl_4^-$ complex: the ratio r_{Cl-Cl}/r_{Tl-Cl} is equal to 1.63, to be compared with the theoretical value for a tetrahedron, $\sqrt{2}/(\sqrt{3}/2) = 1.633$. The numbers of the Tl–Cl and the Cl–Cl interactions, 4 and 6, respectively, are also consistent with those expected for a tetrahedron.

The parameters determined for the Cl13 solution are in agreement with an octahedral $TlCl_6^{3-}$ complex: the ratio $r_{Cl-Cl}/r_{Tl-Cl}=1.42$ can be compared with the theoretical value, $\sqrt{2}=1.414$, and the frequencies, n_{Tl-Cl} and n_{Cl-Cl}, are not significantly different from the expected ones, 6 and 12, respectively. A comparison of the peak shapes, calculated on the basis of the parameter values in Table 2b for the $TlCl_n^{3-n}$ complexes and of the previously reported values for the "background" interactions (O–H and $Li(H_2O)_4^+$),[35] with the observed $D(r)-4\pi r^2\rho_o$ functions is given in Fig. 2. Raman spectra reported by Spiro,[10] Davies[11] and in the present work (see Table 3) are consistent with the conclusion reached on the basis of the X-ray diffraction and the NMR[30] results. For the solutions where the $TlCl_4^-$ complex dominates ($TlCl_{4.1}$ and $TlCl_{4.8}$ in Table 3) the major peak is observed at about 303 cm^{-1} (ν_1) and a minor, broad band occurs at 80–90 cm^{-1} (ν_4), in agreement with the Raman spectra of seversl solid tetrahalothallates containing discrete tetrahedral $TlCl_4^-$ units.[15,24] Similar ν_1 and ν_4 frequencies were observed for solutions of $[NBu_4]$-$TlCl_4$ in several non-coordinating solvents,[36] where, presumably, a tetrahedral $TlCl_4^-$ complex is present. Furthermore, infrared spectra for the $CL4_2$ solution and for a 0.2 M solution of $[NBu_4]TlCl_4$ in CH_2Br_2 are very similar to each other, with the dominating peak at 293 cm^{-1} (ν_3) and a minor, broader peak at about 100 cm^{-1} (ν_4),[37] *i.e.* essentially the same as the IR spectrum for the solid $KTlCl_4$(s), containing tetrahedral $TlCl_4^-$ units.[21]

When the ratio $R_{Cl}=[Cl^-]_{tot}/[Tl(III)]$ increases above 4.1, the major peak becomes broader and its centre moves towards lower frequencies. For $[Tl(III)]\approx 1$ M, it reaches the frequency of ~270 cm^{-1} at $R_{Cl}\approx 9$ and does not shift upon further addition of chloride up to $R_{Cl}\approx 13$,[11] whereas the intensity of the peak increases continuously.[10] For the CL13 solution, in addition, a very broad peak centered at ~120 cm^{-1} arises. Thus, the spectrum of the CL13 solution shows the same major frequencies as those observed in the Raman spectra of several crystalline hexachlorothallates containing octahedral $TlCl_6^{3-}$ species (*cf.* Table 3). Such changes in the spectra for the solutions with $R_{Cl}>4$ are nicely explained by the distribution of the complexes according to the stability constants for 1 M solutions.[30] For R_{Cl} values between 4 and 6 the concentration of the $TlCl_4^-$ complex decreases, whereas the concentrations of the higher species increase. For $6<R_{Cl}<8$ the concentrations of the $TlCl_4^-$, $TlCl_5^{2-}$ and $TlCl_6^{3-}$ complexes are all of the same order of magnitude and no species dominates. Finally, for $R_{Cl}\approx 9$, about 60 % of the total thallium is present as $TlCl_6^{3-}$ and the concentration of this complex increases upon further addition of chloride, reaching about 80 % of the total thallium for $R_{Cl}\approx 14$, where the solubility limit is reached.

The spectra for the solutions C and D are very similar to each other (see Table 3). The same is true for the solutions E and F. This gives no support for the assumption of Figgis[12] that $Tl_2Cl_9^{3-}$ dominates for $R_{Cl}>4.5$, since formation of polynuclear complexes should be more pronounced for the more concentrated solutions and thus alter the spectral patterns.

It is of interest to compare the distances determined for the $TlCl_4^-$ and the $TlCl_6^{3-}$ units in solution with the accurate values obtained for the same complexes in the solid state. The Tl–Cl distance of 2.433(1) Å and the Cl–Cl distance of 3.96(3) Å calculated for the $CL4_2$ solution (Table 2b) can be compared with the values 2.433(3) Å and 3.98 Å (average), respectively, determined for the tetrahedral $TlCl_4^-$ in the crystal structure of $KTlCl_4$.[21,*] For the CL5 solution the Tl–Cl distance is about 0.01 Å longer, but this slight increase may not be significant. Because of the high relative and absolute concentrations of the $TlCl_4^-$ complex in the $CL4_2$ solution as compared with that in CL5 (*cf.* Table 1), the value of 2.433 Å is more reliable.

The distances $r_{Tl-Cl}=2.590(3)$ Å and $r_{Cl-Cl}=3.69(6)$ Å found for the $TlCl_6^{3-}$ complex in solution are not significantly different from the values 2.593(3) Å and 3.68 Å, respectively, for the crystal structure of $Na_3TlCl_6\cdot 12H_2O$.[27,*]

Finally, it may be noted that the results in Table 2a are not consistent with the dominance of the $Tl_2Cl_9^{3-}$ complex[12] (see above) in the solutions investigated. The high scattering power of the thallium atoms would result, if the $Tl_2Cl_9^{3-}$ complex reached any considerable concentration, in a dominating Tl–Tl peak at ~3.6 Å[14] in the RDF's. For the $CL4_2$ and CL5 solutions, there are no peaks at this distance. For the CL13 solution, the broad peak centered at 3.4 Å can be satisfactorily explained by

*The distances in the crystal structures have been corrected for thermal motion,[38] assuming "riding" motion for the Tl–Cl distances and independent motion for the Cl–Cl distances. Note that an uncorrected distance for the atoms "p" and "q", r_{pq}, is obtained as $|\langle \mathbf{r}_q\rangle - \langle \mathbf{r}_p\rangle|$ in a crystal structure, but as $|\langle \mathbf{r}_q - \mathbf{r}_p\rangle|$ in a solution ($\mathbf{r}$ denotes a vector and the brackets mean values.

the Cl–Cl interactions in the $TlCl_6^{3-}$ complex and the generally accepted[35] "background" interactions (tetrahedral $Li(H_2O)_4^+$ species and Cl–H_2O distances). Moreover, in this type of complexes, $M_2Cl_9^{3-}$, the M–Cl distances are ~0.2 Å shorter for the terminal chlorine atoms than for the bridging ones, at least in the solid state.[14,24] If this property is retained in solution, as may be expected, it would lead to a significant increase of the mean-square variation of the Tl–Cl distance, l^2, in Table 2a. Such an increase in l^2 would also be expected if, for instance, two of the Tl–Cl bonds in $TlCl_6^{2-}$ were appreciably shorter than the remaining ones. Apparently, the $TlCl_6^{3-}$ octahedron is regular.

Intermolecular interactions. In the difference curves (Fig. 2, left side, short dashes) between the experimental RDF's and the peak shapes calculated for the intramolecular interactions, as described above, there remain broad maxima centered at ~3.2 and ~4.6 Å. In this region, several types of intermolecular interactions can be expected, *e.g.* H_2O-H_2O (~2.8 Å), Cl–H_2O (3.2 Å)[35] and distances between the Tl atom and the molecules in its second coordination sphere.

Close-packing of water molecules around the $TlCl_n^{3-n}$ complexes, as assumed in the preceding paper for the $TlBr_4^-$ complex,[31] is less probable in the present case because of the higher tendency of the chloride ions to participate in hydrogen bonds. Such a model would lead to Tl–H_2O distances slightly shorter than 4.0 Å, which are not present in the difference curves (Fig. 2).

In the crystal structure of the water-rich compound, $Na_3TlCl_6 \cdot 12H_2O$, three water molecules are hydrogen bonded to each of the chlorines within the $TlCl_6^{3-}$ octahedra, leading to 12 Tl–H_2O distances between 4.47 and 4.79 Å.[27] Similarly, it was assumed that in solution water molecules are arranged around the $TlCl_n^{3-n}$ complexes at the Tl–H_2O distances of ~4.55 Å, which also leads to several Cl–H_2O distances at ~3.2 Å. In addition to the generally accepted tetrahedral $Li(H_2O)_4^+$ unit,[35] already included in the calculated peak shapes (see above), the free chloride ions were also assumed to be in contact with water molecules (~3.2 Å).[35] The difference curves between the experimental RDF's and the peak shapes, where the Tl–H_2O and Cl–H_2O intermolecular interactions (described above) were also included in the calculations, are shown in Fig. 2 (long dashes). The agreement in the high angle region between experimental $s \cdot i(s)$ values and the theoretical curves calculated for the same model (Fig. 1) finally confirms the conclusions drawn above concerning the structures of the complexes.

Acknowledgements. The author is greatly indebted to Dr. G. Johansson for his continuous interest in the work and for many valuable suggestions. Thanks are due to Dr. P. L. Goggin and Dr. M. Sandström for recording several Raman spectra and to Mr. E. Hansen for skilful technical assistance. This work has been supported by the Swedish Natural Science Research Council (NFR).

REFERENCES

1. Smith, R. M. and Martell, A. E. *Critical Stability Constants*, Plenum, New York 1977, Vol. 4.
2. Lee, A. G. *The Chemistry of Thallium*, Elsevier, Amsterdam 1971 and references therein.
3. Woods, M. J. M., Gallagher, P. K., Hugus, Z. Z. and King, E. L. *Inorg. Chem. 3* (1964) 1313.
4. a. Ahrland, S., Grenthe, I., Johansson, L. and Norén, B. *Acta Chem. Scand. 17* (1963) 1567; b. Ahrland, S. and Johansson, L. *Acta Chem. Scand. 18* (1964) 212.
5. Biedermann, G. and Spiro, T. G. *Chem. Scr. 1* (1971) 155.
6. Leden, I. and Ryhl, T. *Acta Chem. Scand. 18* (1964) 1196.
7. Schmidt, K. J. *J. Inorg. Nucl. Chem. 32* (1970) 3549.
8. Horrocks, D. L. and Voigt, A. F. *J. Am. Chem. Soc. 79* (1957) 2440.
9. Nord, G. and Ulstrup, J. *Acta Chem. Scand. 18* (1964) 307.
10. Spiro, T. G. *Inorg. Chem. 4* (1965) 731.
11. Davies, E. D. and Long, D. A. *J. Chem. Soc. A* (1968) 2050.
12. Figgis, B. N. *Trans. Faraday Soc. 55* (1959) 1075.
13. Freeman, R., Gasser, R. P. H. and Richards, R. E. *Mol. Phys. 2* (1959) 301.
14. a. Powell, H. M. and Wells, A. F. *J. Chem. Soc.* (1935) 1008; b. Hoard, J. L. and Goldstein, L. *J. Chem. Phys. 3* (1935) 199.
15. a. Spiro, T. G. *Inorg. Chem. 4* (1965) 1290; b. *Ibid. 6* (1967) 569.
16. a. Zvonkova, Z. V. *Zh. Fiz. Khim. 30* (1956) 340; b. Glaser, J. *Acta Chem. Scand. A 33* (1979) 789.
17. Gutiérrez-Puebla, E., Vegas, A. and Garcia-Blanco, S. *Acta Crystallogr. B 36* (1980) 145.
18. Hazell, A. C. *J. Chem. Soc.* (1963) 3459.
19. Thiele, G. *Z. Naturforsch. Teil B 34* (1979) 1512.
20. Brodersen, K., Rath, J. and Thiele, G. *Z. Anorg. Allg. Chem. 394* (1972) 13.
21. Glaser, J. *Acta Chem. Scand. A 34* (1980) 75.

22. Rath, H. J. *Thesis*, Univ. Erlangen-Nürnberg, Erlangen 1972.
23. Watanabe, T. and Atoji, M. *J. Am. Chem. Soc. 72* (1950) 3819.
24. Grunwald, B. *Thesis*, Univ. Erlangen-Nürnberg, Erlangen 1977.
25. Linhard, M., Manthey, W. and Plieth, K. *Z. Electrochem. 57* (1953) 862.
26. Watanabe, T., Atoji, M. and Okazaki, Ch. *Acta Crystallogr. 3* (1950) 405.
27. Glaser, J. *Acta Chem. Scand. A 34* (1980) 141.
28. Böhme, R., Rath, J., Grunwald, B. and Thiele, G. *Z. Naturforsch. Teil B 35* (1980) 1366.
29. Joy, G., Gaughan, A. P., Wharf, I., Shriver, D. F. and Dougherty, J. P. *Inorg. Chem. 14* (1975) 1795.
30. Glaser, J. and Henriksson, U. *J. Am. Chem. Soc. 103* (1981) 6642.
31. Glaser, J. and Johansson, G. *Acta Chem. Scand. A 36* (1982) 125.
32. Glaser, J. *Thesis*, Royal Institute of Technology, Stockholm 1981.
33. Johansson, G. *Acta Chem. Scand. 20* (1966) 553.
34. Johansson, G. and Sandström, M. *Chem. Scr. 4* (1973) 195.
35. a. Palinkas, G., Radnai, T. and Hajdu, F. *Z. Naturforsch. Teil A 35* (1980) 107; b. Narten, A. H. Vaslov, F. and Levy, H. A. *J. Chem. Phys. 58* (1973) 5017.
36. Andrews, P. S., Badger, P. E. R., Goggin, P. L., Hurst, N. W. and Rattray, A. J. M. *J. Chem. Research.* (M) (1978) 1401.
37. Goggin, P. L. *et al. To be published.*
38. a. Busing, W. R. and Levy, H. A. *Acta Crystallogr. 17* (1964) 142; b. Busing, W. R., Martin, K. O. and Levy, M. A. *Function and Error Program*, Report ORNL-TM-306, Oak Ridge National Laboratory, Oak Ridge 1965.
39. Barrowcliffe, T., Beattie, I. R., Day, P. and Livingstone, K. *J. Chem. Soc. A* (1967) 1810.
40. Beattie, I. R., Gilson, T. R. and Ozin, G. A. *J. Chem. Soc. A* (1968) 2765.

Received September 14, 1981.

Acta Chemica Scandinavica A 36 (1982) 459–464

Metal Ammine Formation in Solution. XXII. The Nickel(II) Triethanolamine System

BADRI VISHAL AGARWALA* and JANNIK BJERRUM

Chemistry Department I, Inorganic Chemistry, H. C. Ørsted Institute, University of Copenhagen, DK-2100 Copenhagen Ø, Denmark

The present paper reports a potentiometric and spectrophotometric study of the nickel(II)–triethanolamine system. The formation curves ($\bar{n}$, p[L]) at different triethanolammonium concentrations are analyzed and constants determined for the for the formation of $Ni(tea)^{2+}$, $Ni(tea)_2^{2+}$ and of a hydrolysis product shown to be $Ni_2(tea)_2(OH)_2^{2+}$ [tea = $N(C_2H_4OH)_3$]. In 2 M tea$HClO_4$ hydrolysis is suppressed and the first two consecutive formation constants for pure amine complex formation determined at 25 °C to be: $K_1 = 10^{3.42\pm0.02}$ l mol^{-1} and $K_2 = 10^{0.87\pm0.03}$ l mol^{-1}. In 0.5 M (tea H,Na)ClO_4 values of $K_1 = 10^{2.85\pm0.01}$ l mol^{-1} and $K_2 = 10^{0.14\pm0.03}$ l mol^{-1} were determined. The hydrolysis constant $\beta^*_{2,2} = [Ni_2(tea)_2(OH)_2^{2+}][H^+]^2/[Ni(tea)^{2+}]^2$ was estimated to have the value $10^{-14.8\pm0.4}$ mol l^{-1}. The absorption curves in the visible region were analyzed, and spectra for $Ni(tea)^{2+}$, $Ni(tea)_2^{2+}$ and "$Ni_2tea_2(OH)_2^{2+}$" were obtained.

Complex formation between triethanolamine and nickel(II) ions in solution has been studied by several authors.[1–4] Calorimetric and pH-measurements have been made by Sychow *et al.*[1] and pH-titrations and spectrophotometric measurements by Bhat *et al.*[3] Both of these authors demonstrated the existence of $Ni(tea)^{2+}$ and $Ni(tea)_2^{2+}$ and determined values for their formation constants, but only Bhat *et al.*[3] mention the disturbance caused by the presence of polynuclear hydroxo complexes. Cadiot-Smith[4] studied the system by base titrations and reports the successive formation of $Ni(tea)^{2+}$, $Ni_2(tea)_2(OH)_2^{2+}$ and $Ni_4(tea)_4(OH)_6^{2-}$ by increasing pH. The formation of polymeric hydroxo complexes explain the fact that the authors concerned[1,3] obtain values for the second formation constant which are too high. Sklenskaya *et al.*[2] claim to have demonstrated the existence of $Ni(tea)_3^{2+}$, but their experimental results are undoubtedly attributable to the formation of hydroxo complexes. Triethanolamine nickel(II) salts of the composition $Ni(tea)_2X_2$ have been prepared[5] and Rasmussen and coworkers[6] have determined the crystal structure of $Ni(tea)_2(NO_3)_2$. It was found to have an octahedral configuration in which each of the triethanolamine ligands is tridentate and facially coordinated by the nitrogen atom and two of the oxygen atoms. The oxygen atom on the third branch of the ligand is, as expected, not coordinated to nickel.

The present paper supplements the literature data with improved values for the formation constants K_1 and K_2 and with an estimated value for the hydrolysis constant of $Ni(tea)^{2+}$. Furthermore, the absorption spectra of the complexes and of the hydrolysis product have been estimated.

EXPERIMENTAL

Reagents and solutions. All reagents were of analytical grade. The triethanolamine (tea) used was Merck *pro analysi* containing less than 1 % diethanolamine. The various solutions were prepared in volumetric flasks by weighing or pipetting from stock solutions. A 2.50 M stock solution of tea$HClO_4$ was prepared by neutralizing 5.00 M $HClO_4$ with the pure amine and diluting to the double volume. Complete equivalence between amine and perchloric acid was ensured as described earlier.[7]

* On leave from Department of Chemistry, University of Allahabad, Allahabad 211002, India.

0302-4377/82/050459-06$02.50

Table 1. Glass electrode measurements on nickel(II)triethanolamine solutions in 2 M teaHClO$_4$ at 25 °C. pH + p[tea] = 8.12 ± 0.01.[8] Estimation of log K_1 and log K_2.

No.	C_{Ni}	C_{tea}	p[tea]	pH	$\bar{n}$	log K_1[a]	log K_2[a]
1	0.02085	0.00663	3.743	4.377	0.311	3.397	
2	0.02092	0.01046	3.442	4.678	0.484	3.415	
3	0.02094	0.01625	3.026	5.094	0.731	3.460	
6[c]	0.06291	0.1187	1.395	6.725	1.246		0.909
9[d]	0.06274	0.1597	1.123	6.997	1.344		0.843
						Av. 3.42 ± 0.03[a]	0.87 ± 0.03[b]

[a] $K_1 \cong \bar{n}/\{(1-\bar{n})[\text{tea}]\}$. Mean of solutions 1–3. [b] $K_2 \cong (\bar{n}-1)/\{(2-\bar{n})[\text{tea}]\}$. Mean of 5 solutions with $1.2 \lesssim \bar{n} \lesssim 1.4$. [c] Calc. $\alpha_0 = 0.0072$, $\alpha_1 = 0.765$, $\alpha_2 = 0.228$. [d] Calc. $\alpha_0 = 0.00322$, $\alpha_1 = 0.640$, $\alpha_2 = 0.357$.

The stock solution of nickel(II)perchlorate (0.523 mol/l) and 0.476 mol/kg) was analyzed by electrolytic deposition of nickel in ammoniacal solution. pH was adjusted to ~5.8.

Spectrophotometric measurements (UV and Vis) were made with a Cary 118 spectrophotometer at room temperature (22–23 °C). Cells of pathlength 0.1 to 2 cm were used, the reference cells being filled with a corresponding nickel-free solution.

pH = $-\log[H^+]$ was determined by glass electrode measurements at 25 °C as described previously.[8]

Estimation of stability constants. Table 1 shows some data for the complex formation between Ni(II) ions and triethanolamine (tea) in 2 M teaHClO$_4$ at 25 °C. C_X denotes stoichiometric concentrations and [X] the molar concentrations of the individual species. p[tea] and pH were calculated using the previously determined value[8] for K_{teaH^+} and the ligand number was calculated from the relationship (1), where $[\text{tea}]' = [\text{tea}] + [H^+] - [OH^-]$. As a consequence on the steric hindrance to the uptake of the second amine molecule,

$$\bar{n} = (C_{tea} - [\text{tea}]')/C_{Ni} \quad (1)$$

$$K_1 = [\text{Nitea}^{2+}]/([Ni^{2+}][\text{tea}]) \quad (2)$$

$$K_2 = [\text{Ni(tea)}_2^{2+}]/([\text{Nitea}^{2+}][\text{tea}]) \quad (3)$$

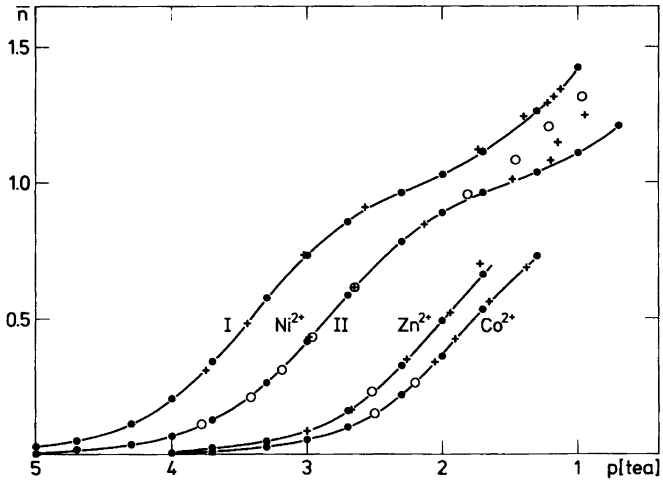

Fig. 1. Formation curves $\bar{n}$ *versus* p[tea]. Curve I for nickel(II) in solutions with $C_{tea^+} = 2.00$ M (+, exp; ●, calc); curve II for nickel(II) with $C_{teaH^+} = 0.50$ M (+) and with $C_{teaH^+} \cong 0.10$ M, $C_{Na^+} = 0.40$ M (○). The full curves are calculated by use of the estimated constants for pure amine complex formation neglecting hydrolysis. For comparison purposes the formation curves for zinc(II) and cobalt(II) in 0.5 M (teaH,K)NO$_3$ $C_{tea^+} = 0.40$ M (+), $C_{teaH^+} = 0.10$ M (○) drawn on the basis of earlier measurements[14,15] are shown.

Table 2a. Glass electrode measurements on nickel(II) triethanolamine solutions at 25 °C. $C_{teaHClO_4} + C_{NaClO_4} = 0.50$ M. $pK_{teaH^+} = 7.90 \pm 0.01$.[8]

No.	C_{teaH^+}	C_{Ni}	C_{tea}	p[tea]	pH	$\bar{n}$	log K_1	log "K_2"[a]
13	0.100	0.02094	0.01005	2.964	6.039	0.428	2.838	
14	0.500	0.02093	0.01000	2.980	5.283	0.428	2.853	
21	0.500	0.02097	0.08591	1.199	7.064	1.081		0.144
23	0.500	0.06280	0.1908	0.949	7.314	1.247		0.465
25	0.100	0.02095	0.08593	1.217	7.786	1.206		0.631
26[b]	0.115	0.06285	0.1906	0.971	7.972	1.329		0.661
27[b]	0.080	0.06267	0.2002	0.986	8.114	1.546		1.061
Mean of 8 solutions with $0.1 \lesssim \bar{n} \lesssim 0.8$						Av. 2.85 ± 0.01		

[a] $K_2" = (\bar{n}-1)/\{(2-\bar{n})[tea]\}$. [b] Calc. with $C_{teaH^+} = C^{\circ}_{teaH^+} + C''_{Ni}$.

Table 2b. Calculation of hydrolysis constants with log $K_1 = 2.85$ and log $K_2 = 0.144$.

No.	[tea]	$[Ni^{2+}]$	$[Ni(tea)^{2+}]$	$[Ni(tea)_2^{2+}]$	C''_{Ni}	$p\beta^*_{1,1}$	$p\beta^*_{2,2}$	$p\beta^*_{4,4}$
21	0.06324	0.000419	0.01843	0.001632	0.000488	8.64	14.27	25.23
23	0.1125	0.000582	0.04614	0.00726	0.00882	8.03	14.31	26.57
25	0.06067	0.0003715	0.01590	0.001351	0.00333	8.46	14.75	27.03
26	0.1070	0.000545	0.0411	0.00616	0.0150	8.41	15.29	28.76
27[a]	0.1033	0.000388	0.02826	0.00408	0.0299	8.09	14.95	28.39
Mean of 9 solutions with $0.0003 < C''_{Ni} < 0.03$.						Av. 8.49 ± 0.16	14.63 ± 0.34	26.63 ± 1.27

[a] Solution 27 deposited a blue crystalline precipitate after a few hours.

K_1 and K_2 can be calculated independently of each other as shown in the table; eqns. (2) and (3). The calculated values of both K_1 ($=10^{3.42}$) and K_2 ($=10^{0.87}$) are seen to be relatively good constants. Similar calculations are given in Table 2a for solutions with lower concentrations of $teaH^+$, in which $C_{teaHClO_4} + C_{NaClO_4} = 0.5$ M. The value obtained for K_1 ($=10^{2.85}$) in this medium is well-defined although lower than for 2 M $teaHClO_4$. However, the values for $K_2 = (\bar{n}-1)/\{2-\bar{n})[tea]\}$ show no constancy, and the drift in "K_2" is due to hydrolysis. The influence of this drift can also be seen in Fig. 1, in which the formation curves for 2 M $teaHClO_4$ (curve I) and for the 0.5 M salt medium (curve II) are plotted on the basis of data for all the measured solutions (Nos. 1–27). The full curves are calculated with the estimated constants. A tentative value for K_2 in the 0.5 M medium of $10^{0.144}$ (obtained for the solution with the lowest pH (No. 21 in Table 2a) was used. For curve I the calculated curve fits the experimental points up to the highest measured $\bar{n}$-values. The same is not the case for curve II for $\bar{n} \gtrsim 1$, and the deviations from the calculated curve are as expected especially pronounced for the ○-points corresponding to the lowest triethanolammonium concentrations. The midpoint relationship $\log(K_1K_2) = 2p[tea]^-_{\bar{n}=1}$ is found to be valid for curve I where $\log(K_1K_2) = 3.42 + 0.87 = 4.29$ and $p[tea]_{\bar{n}=1}$ is read from the curve to be 2.13. Applied to curve II with $p[tea]_{\bar{n}=1} = 1.50$ we obtained for log K_2: $2 \times 1.50 - 2.85 = 0.15$, in agreement with the tentatively chosen value 0.144. The uncertainty in log K_2 is probably not higher than 0.03. It should also be observed that the ratio between the constants (log $K_1/K_2 = 2.55$ in 2 M $teaHClO_4$ and 2.70 in the 0.5 M medium) are of the order and has as it could be expected the highest value in the medium in which the complexes have the lowest stability.

Analysis of a basic salt. One of the solutions (solution 27 in Table 2a) deposited after a few hours a blue crystalline precipitate which was analyzed to have the composition: $(Nitea)_2(OH)_3ClO_4,3H_2O$. The crystal water was lost on drying and the anhydrous salt was analyzed. Calc. for $(Nitea)_2(OH)_3ClO_4$: Ni 20.73, N 4.94, C 25.4, H 5.8, Cl 6.3. Found: Ni 20.87, N 4.93, C 25.0, H 5.5, Cl 6.4. The weight loss on drying the salt to constant weight at 80 °C

was found to be 16.0 %, and for another preparation 16.4 %. The average weight loss 16.2 % corresponds to 3.03 mol water.

Discussion of the hydrolysis. The dominating hydrolysis product of the aqua nickel(II) ion is, according to several investigators,[9-11] the species $Ni_4(OH_4^{4+}$. The cubane-like structure of $Ni_4(OH)_4^{4+}$ has been shown to exist in the complex salt $Ni_4(OH)_4tach_4(NO_3)_4.7H_2O$,[12] in which tach = 1,3,5-triamine(aaa)-cyclohexane acts as a stereospecific ligand according to Schwarzenbach.[12] By analogy the hydrolysis product of the Ni(tea)-$(H_2O)^{2+}$ complex should be $Ni_4(OH)_4tea_4^{4+}$. However, both our own measurements and those of Cadiot-Smith[4] are in better agreement with the assumption that the dominating hydrolysis product is the diol complex $[Ni(tea)]_2(OH)_2^{2+}$ as in the corresponding copper(II) system.[13] This is not unreasonable considering that $N(CH_2CH_2OH)_3$ can occupy 4 sites in the octahedron leaving only two water molecules in *cis*-position free for hydrolysis.

The data in Table 2 enables us to distinguish between the two possibilities as follows: The stoichiometric concentrations of nickel(II) and triethanolamine can be expressed as eqns. (4) and (5),

$$C_{Ni} = [Ni^{2+}] + [Nitea^{2+}] + [Ni(tea)_2^{2+}] + v[(Ni(tea)OH^+)_v] \quad (4)$$

$$C_{tea} - [tea]' = [Nitea^{2+}] + 2[Ni(tea)_2^{2+}] + 2v[(Ni(tea)OH^+)_v] \quad (5)$$

where v is either 2 or 4 and $[tea]'$ is defined in eqn. (1). By eliminating eqn. (6) from eqns. (4) and (5) by subraction and employing eqn. (2) we obtain eqn. (7).

$$C'_{Ni} = [Ni(tea)_2^{2+}] + v[(Ni(tea)OH^+)_v] \quad (6)$$

$$[Ni^{2+}] = \{2C_{Ni} - (C_{tea} - [tea]')\}/(2 + K_1[tea]). \quad (7)$$

$[Ni(tea)^{2+}]$ and $[Ni(tea)_2^{2+}]$ can now be calculated by eqns. (2) and (3) and the concentration of the hydrolysis product $C''_{Ni} = v[(Ni(tea)OH^+)_v]$ by means of eqn. (6).

Table 2b tabulates data for some of the measured solutions with pH > 7 which are used for calculating eqns. (8)–(10).

$$\beta^*_{1,1} = (C''_{Ni}[H^+])/[Ni(tea)^{2+}] \quad (8)$$

$$\beta^*_{2,2} = (0.5\, C''_{Ni}[H^+]^2)/[Ni(tea)^{2+}]^2 \quad (9)$$

$$\beta^*_{4,4} = (0.25\, C''_{Ni}[H^+]^4)/[Ni(tea)^{2+}]^4. \quad (10)$$

The values of C''_{Ni} are especially high for solutions 26 and 27, and for these solutions it has been necessary before the final calculation to introduce a correction for the change in the initial concentration of C°_{teaH+} caused by the hydrolysis (*cf.* the preceeding paper[13]). It will be seen from Table 2b that $\beta^*_{1,1}$ and $\beta^*_{2,2}$ are much better defined than $\beta^*_{4,4}$. A total of nine solutions with different pH and nickel concentration was examined. The mean error on the average values of the $p\beta^*$-constants is calculated in the usual manner as $\sqrt{\Sigma\Delta^2/(n-1)}$, where n is the number of determinations and Δ are the deviations from the average values of the constants. For comparison the mean errors on the $p\beta^*$-constants have to be divided with the degree of polymerization. Paying attention to this fact $\beta^*_{1,1}$ and $\beta^*_{2,2}$ have about the same uncertainty. The degree of polymerization is therefore lower than two and the value given for $p\beta^*_{2,2}$ in Table 2b for this reason somewhat too low. Tentatively we assume it to have the value 14.8 ± 0.4.

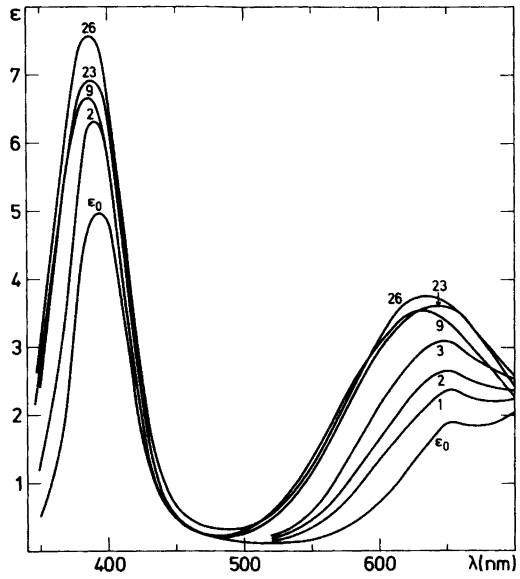

Fig. 2. Spectra (ε, λ) of nickel(II) – triethanolamine perchlorate solutions. The numbers on the curves refer to the corresponding solutions in Tables 1 and 2, and ε_0 to the data for the nickel(II) aqua-ion solutions in Table 3.

From base titrations at room temperature Cadiot-Smith[4] has estimated the constant

$$\beta_{2,2,2} = [Ni^{2+}]^2[tea]^2[OH^-]^2/[Ni_2(tea)_2(OH)_2^{2+}]$$

to be $10^{-18.2}$. Employing $[Ni(tea)^{2+}]$ and $[H^+]$ values calculated assuming $K_1 = 10^{2.85}$ and $K_W = 10^{-13.73}$ in 0.5 M $NaClO_4$,[15] respectively, our value for $\beta^*_{2,2} = 10^{-14.8}$ can be used to calculate for $\beta_{2,2,2}$. The value $10^{-18.4}$ thus obtained is in good agreement with Cadiot-Smith's value.

Table 3. Spectra of $Ni(aq)^{2+}(\varepsilon_0)$, $Ni(tea)^{2+}(\varepsilon_1)$, $Ni(tea)_2^{2+}$ and "$Ni_2tea_2(OH)_2^{2+}$"(ε_x) in the visible region calculated on basis of the spectra of the following solutions in Tables 1 and 2, Nos. 1, 2, 3, 6, 9 ($C_{teaH^+}=2.00$), 14, 23 ($C_{teaH^+}=0.50$), 13, 26 ($C_{teaH^+}=0.10$, $C_{Na^+}=0.40$).

No.		540	560	580	600	620	640	660	680	700 nm
	ε_0 [a]	0.15	0.22	0.41	0.74	1.18	1.68	1.86	1.87	2.03
1	ε_1	0.55	1.06	1.86	2.67	3.31	3.44	3.38	2.99	2.73
2	ε_1	0.54	1.05	1.84	2.60	3.26	3.53	3.37	3.02	2.73
3	ε_1	0.55	1.05	1.85	2.65	3.27	3.53	3.38	3.04	2.71
6	ε_2	1.93	2.84	3.50	3.92	3.90	3.70	3.07	2.30	1.58
9	ε_2	1.93	2.99	3.61	3.86	3.81	3.56	2.86	2.21	1.51
	ε_0 [b]	0.15	0.21	0.40	0.71	1.15	1.64	1.81	1.84	2.01
14	ε_1	0.47	0.98	1.71	2.66	3.36	3.55	3.34	2.99	2.69
13	ε_1	0.46	0.94	1.74	2.70	3.38	3.61	3.47	3.05	2.75
23	ε_x	2.07	2.94	3.72	4.10	3.47	3.55	3.29	2.68	2.04
26	ε_x	1.86	2.81	3.66	4.15	4.47	4.25	3.93	3.28	2.79

[a] Molar extinction coefficients of solution with $C_{Ni(ClO_4)_2}=0.0629$, $C_{HClO_4}=0.02$, $C_{teaHClO_4}=2.00$. [b] Molar extinction coefficients of solution with $C_{Ni(ClO_4)_2}=0.0524$, $C_{HClO_4}=0.02$, $C_{teaHClO_4}=0.50$.

The absorption spectra. The absorption curves (ε versus λ) for some of the solutions examined and for the aqua nickel(II) ion are shown in Fig. 2. On the basis of these data for a series of wavelengths (some of which are tabulated in Table 3) the molar extinction coefficients for $Ni(tea)^{2+}$ (ε_1), $Ni(tea)_2^{2+}$ (ε_2) and for the polymer (ε_x) were calculated by means of the general expression for the measured extinction coefficient:

$$\varepsilon=\alpha_0\varepsilon_0+\alpha_1\varepsilon_1+\alpha_2\varepsilon_2+\alpha_x\varepsilon_x$$

in which α_0, α_1, α_2 and $\alpha_x=c''_{Ni}/c_{Ni}$ are the fractions of the individual species. The extinction coefficients for $Ni(tea)^{2+}$ are obtained directly from the expression:

$$\varepsilon_1=(\varepsilon-\alpha_0\varepsilon_0/\alpha_1\approx(\varepsilon-(1-\bar{n})\varepsilon_0)/\bar{n}$$

for $\bar{n}$ values that are not too large. ε_2 is calculated by use of the values obtained for ε_1 and the α_n-values calculated for solutions 6 and 9 in Table 1. Finally ε_x is calculated from the C'_{Ni}-values and the concentrations of Ni^{2+}, $Ni(tea)^{2+}$ and $Ni(tea)_2^{2+}$ given in Table 2b. The values obtained for ε_1 and ε_2 are well-defined and it will be seen from Table 3 that the values obtained for ε_1 in 0.5 and 2 M $teaHClO_4$ are practically identical. The values obtained for the polymer are not so well-defined, and it is the value for solution 26 which is plotted in Fig. 3. This figure gives the estimated spectra of Ni^{2+}, $Ni(tea)^{2+}$,

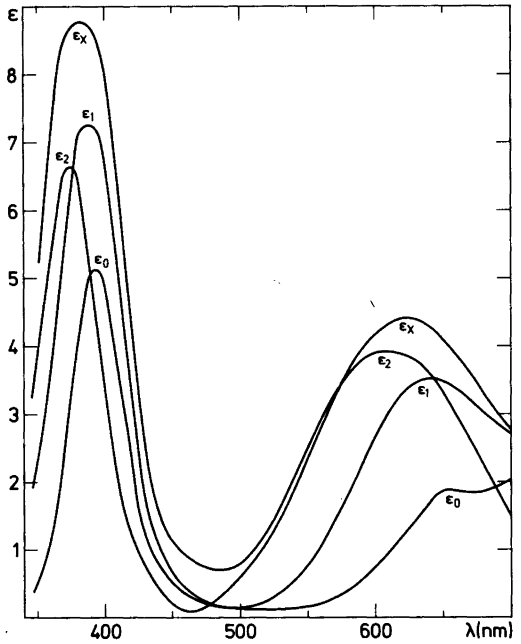

Fig. 3. Spectra (ε, λ) of $Ni(aq)_6^{2+}$ (ε_0), $Ni(tea)^{2+}$ (ε_1), $Ni(tea)_2^{2+}$ (ε_2) and "$Ni_2tea_2(OH)_2^{2+}$" (ε_x) drawn on the basis of the data given in Table 3. The curve for ε_x reproduces the data given for solution 26.

$Ni(tea)_2^{2+}$ and "$Ni_2tea_2(OH)_2^{2+}$" in the whole wavelength range from 350 to 700 nm.

Acknowledgement. The authors thank Dr. Martin Hancock for correcting the English manuscript.

REFERENCES

1. Sychow, A. Ya., Gerbeleu, A. P. and Migal, P. K. *Russ. J. Inorg. Chem. 8* (1963) 1081.
2. Sklenskaya, E. V. and Karapet'-yants, M. Kh. *Russ. J. Inorg. Chem. 11* (1966) 1478.
3. Bhat, G. A. and Subrahmanya, R. S. *Inorg. Chem. Acta* (1972) 403.
4. Cadiot-Smith, M. *J. Chim. Phys. 60* (1963) 976.
5. Hughes, M. N. and Rutt, K. J. *J. Chem. Soc. A* (1968) 2788.
6. Nielsen, K., Grønbæk Hazell, R. and Rasmussen, S. E. *Acta Chem. Scand. 26* (1972) 889.
7. Ilcheva, L. and Bjerrum, J. *Acta Chem. Scand. A 30* (1976) 343.
8. Bjerrum, J. and Agarwala, B. V. *Acta Chem. Scand. A 34* (1980) 475.
9. Burkov, K. A., Lilić, L. S. and Sillen, L. G. *Acta Chem. Scand. 19* (1965) 14.
10. Kolski, G. B., Kildahl, N. K. and Margerum, D. W. *Inorg. Chem. 8* (1969) 1211.
11. Milic, N. B., Bugarcic, Z. D. and Vasic, M. V. *Glas. Hem. Drus. Beograd 45* (1980) 349.
12. Aurivillius, B. *Acta Chem. Scand. A 31* (1977) 501.
13. Bjerrum, J., Agarwala, B. V. and Refn, S. *Acta Chem. Scand. A 35* (1981).
14. Bjerrum, J. and Refn, S. *6. Nordiska Kemistmötet*, Lund 1947, p. 227.
15. *Stability Constants of Metal-ion Complexes, Special Publ. 17*, The Chemical Society, London 1964.

Received September 30, 1981.

Acta Chemica Scandinavica A 36 (1982) 465–470

The Crystal and Molecular Structures of Two Hydrates of Ammonium Diaquapentanitratolanthanate(III)

BIRGITTA ERIKSSON,[a] LARS OLOF LARSSON†[a] and LAURI NIINISTÖ[b]

[a] Department of Structural Chemistry, Arrhenius Laboratory, University of Stockholm, Fack, S-106 91 Stockholm, Sweden and [b] Department of Chemistry, Helsinki University of Technology, Otaniemi, SF-02150 Espoo 15, Finland

The crystal structures of ammonium diaquapentanitratolanthanate(III) dihydrate $(NH_4)_2[La(NO_3)_5(H_2O)_2]\cdot 2H_2O$ (*1*) and ammonium diaquapentanitratolanthanate(III) monohydrate $(NH_4)_2[La(NO_3)_5(H_2O)_2]\cdot H_2O$ (*2*) have been determined from single crystal X-ray diffraction data. The compounds crystallize in the monoclinic space group *C*2/*c* (No. 15) with four formula units in the cell of dimensions $a=11.152(5)$, $b=8.966(4)$ $c=17.881(6)$ Å, $\beta=101.6(4)°$ and $a=10.969(10)$, $b=9.012(5)$, $c=17.439(10)$ Å, $\beta=100.1(1)°$ for *1* and *2*, respectively. Least-squares refinement with anisotropic thermal parameters for all nonhydrogen atoms yielded the final *R*-values of 0.065 and 0.041 for *1* and *2*, respectively. The number of reflections used in the refinements was 2389 (*1*) and 1866 (*2*). The surroundings of the lanthanum atom are identical in the two compounds; there are five symmetrically bonded nitrate groups and two water molecules forming a distorted icosahedron. The La–O(nitrate) distances range from 2.66 to 2.73 in *1* and from 2.68 to 2.72 Å in *2* while the corresponding La–O(water) distances are 2.59 and 2.54 Å. The only significant structural difference between the two complexes is in the three-dimensional framework where one water molecule is lacking in compound *2*.

In contrast to the well–characterized dodecanitrato hydrates, *eg.* $Mg_3Ce_2(NO_3)_{12}\cdot 24H_2O$,[1] the structural information on solid lanthanoid pentanitrato hydrates is scarce. Only very recently was a representative of the latter series, *viz.* $K_2La(NO_3)_5\cdot 2H_2O$, studied by X-ray single crystal methods.[2] There are, however, several examples of anhydrous pentanitrato species whose structures are known.[3–7] The coordination numbers are generally high, as in the case of simple nitrate hydrates, being twelve for $K_2[La(NO_3)_5]\cdot 2H_2O$ and ten for the other structures with the exception of scandium.[2–7]

In continuation of our investigation into the structures of inorganic nitrato complexes of the lanthanoids,[2,8] we are now reporting the structures of two closely related lanthanum pentanitrato complexes $(NH_4)_2[La(NO_3)_5(H_2O)_2]\cdot nH_2O$ where n is 1 and 2.

EXPERIMENTAL

Preparation. The compounds were crystallized at room temperature from an aqueous solution containing lanthanum and ammonium ions in molar ratio 1:2 and a slight excess of nitric acid. According to chemical analyses the predominant product under these conditions was $(NH_4)_2\cdot La(NO_3)_5\cdot 4H_2O$. The crystals with lower water content, *i.e.* 3 mol of water, obviously crystallize under nearly the same conditions as some of them were detected among the tetrahydrate crystals when carrying out unit cell determinations by single crystal diffractometry.

Data collection. The unit cell dimensions were obtained by least-squares refinements of setting angles for 25 reflections measured with an automated four-circle diffractometer. Several crystals were measured but the unit cell data given in Table 1 refer to crystals used in the intensity data collection with the same diffractometer. The monoclinic space group *C*2/*c* (No. 15) was chosen for both of the compounds on the basis of the systematic absences in the intensity data and corroborated by the structure determination. Net intensities were corrected for Lorentz and polarization effects but no absorption correction was applied.

Structure determination and refinement. A three-dimensional Patterson synthesis using the data for

† Deceased.

0302-4377/82/050465-06$02.50

Table 1. Details of the data collection.

	1	*2*
(a) Crystal data		
Crystal system	monoclinic	monoclinic
Space group	$C2/c$	$C2/c$
a, Å	11.152(5)	10.969(10)
b, Å	8.966(4)	9.012(5)
c, Å	17.881(6)	17.439(10)
β, deg	101.6(4)	100.1(9)
V	1751.4	1697.1
Z	4	4
Molwt	556.9	538.9
D_x(calc, g cm^{-3}	2.10	2.11
μ(MoK_α), cm^{-1}	25.4	26.3
(b) Intensity measurements		
Radiation	MoK_α	MoK_α
Monochromator	Highly oriented graphite	Highly oriented graphite
Reflections measured	$\pm h, +k, +l$ with $h+k=2n$	$\pm h, +k, +l$ with $h+k=2n$
No. of collected data	2782	2028
2θ range, deg	5–60	5–55
Scan speed, deg min^{-1}	3	2
Scan range, deg	$(2\theta$Mo$K_\alpha-0.75)-(2\theta$Mo$K_\alpha+0.75)$	$(2\theta$Mo$K_\alpha-1)-(2\theta$Mo$K_\alpha+1)$
Background measurement	At beginning and end of the 2θ, each for one half of the total scan time.	
Standards	3 reflections after each batch of 43 data; no decrease of the intensity was observed	
No. observed unique data with $\sigma(I_{net})/I_{net} \leq 0.33$	2389	1866

compound *2* showed the La atoms of the unit cell in the special position 4*e* of the space group $C2/c$. The coordinate of the La atom was refined to an *R*-value of 0.27 ($R=\Sigma||F_o|-|F_c||/\Sigma|F_o|$). The subsequent electron density maps gave the positions of all remaining nonhydrogen atoms in the unit cell. Full-matrix least-squares refinement with an overall scale factor and isotropic thermal factors gave an R-value of 0.084; anisotropic thermal parameters were then introduced whereupon the *R*-value dropped to 0.041.

The unit cell of compound *1* is 54 Å^3 larger by volume than that of compound *2*. This corresponds very closely to the space needed for one water molecule per formula unit. The coordinates from compound *2* were refined using data for compound *1*; an isotropic refinement resulted in an *R*-value of 0.122. With anisotropic thermal parameters the *R*-value dropped to 0.0651. Unit weights were used in all calculations and the largest shift to standard deviation in coordinates was 0.3 in the last cycle for both structures.

In an attempt to locate the hydrogen atoms, difference Fourier syntheses were calculated but the maps only had peaks up to 2.0 Å around the La atoms. The final coordinates and thermal parameters are listed in Table 2. The programs used in the structural analysis were SHELX and PLUTO. The analytical scattering factors of Cromer and Mann for the neutral atoms were used.[9] The listings of the structure factors are available request from B. Eriksson.

DESCRIPTION AND DISCUSSION OF THE STRUCTURES

In both compounds the lanthanum ion is twelve-coordinated by five bidentate nitrate groups and two water molecules thus forming the diaqua-pentanitratolanthanate(III) anion $[La(NO_3)_5$-

Table 2. Final positional and thermal[a] parameters ($\times 10^4$) with estimated standard deviations in parentheses.

Atom	x	y	z	U_{11}	U_{22}	U_{33}	U_{23}	U_{13}	U_{12}
Compound *1*, $(NH_4)_2[La(NO_3)_5(H_2O_2)] \cdot 2H_2O$									
La	0	0.0567(1)	0.25	145(3)	191(3)	327(3)	0	88(2)	0
O(11)	0.0925(6)	−0.2222(8)	0.2401(5)	241(30)	292(33)	784(56)	18(35)	241(33)	25(26)
O(12)	0	−0.4296(14)	0.25	979(109)	259(59)	2356(215)	0	1169(134)	0
O(21)	−0.0791(6)	0.2519(8)	0.1395(5)	260(31)	400(38)	590(49)	−87(34)	22(31)	112(28)
O(22)	0.1075(6)	0.2925(8)	0.1957(4)	275(31)	381(38)	530(45)	108(33)	−30(29)	−57(28)
O(23)	0.0272(9)	0.4213(12)	0.0961(6)	589(55)	778(69)	816(69)	442(58)	−56(49)	−272(51)
O(31)	0.0991(7)	−0.0017(11)	0.1277(5)	357(38)	737(58)	529(47)	−57(43)	217(35)	−62(39)
O(32)	−0.0852(6)	−0.0864(9)	0.1174(4)	315(33)	520(45)	501(43)	−127(36)	165(31)	−51(32)
O(33)	0.0235(11)	−0.1495(18)	0.0350(7)	873(8)	1801(144)	941(87)	871(94)	455(72)	−24(88)
N(1)	0	−0.2959(12)	0.25	266(48)	413(48)	267(50)	0	139(44)	0
N(2)	0.0186(7)	0.3244(10)	0.1426(5)	312(38)	348(42)	536(53)	100(40)	34(36)	−99(34)
N(3)	0.0144(9)	−0.0781(14)	0.0912(5)	384(46)	840(79)	423(49)	219(53)	178(39)	−51(50)
O(1)	0.2364(5)	0.0542(7)	0.2914(4)	176(25)	337(32)	481(37)	60(30)	102(24)	−4(24)
O(2)	0.2962(9)	−0.1157(14)	−0.0306(7)	555(57)	852(79)	992(86)	254(68)	−42(55)	−100(56)
NH_4	0.2757(11)	0.1431(18)	0.0573(8)	772(76)	1661(139)	1014(93)	−308(94)	485(71)	−585(87)
Compound *2*, $(NH_4)_2[La(NO_3)_5(H_2O)_2] \cdot H_2O$									
La	0	0.0572(1)	0.25	174(2)	175(2)	309(2)	0	44(2)	0
O(11)	0.0947(4)	−0.2195(5)	0.2413(3)	265(20)	261(21)	625(30)	−4(20)	169(20)	1(17)
O(12)	0	−0.4261(8)	0.25	827(63)	170(34)	2023(121)	0	828(74)	0
O(21)	−0.0789(4)	0.2518(5)	0.1362(3)	258(20)	372(24)	507(27)	−51(21)	1(18)	74(18)
O(22)	0.1067(4)	0.2935(5)	0.1945(3)	332(22)	291(22)	524(27)	110(20)	−75(19)	−55(18)
O(23)	0.0310(5)	0.4220(6)	0.0921(3)	597(33)	522(33)	570(32)	255(27)	−16(26)	−157(27)
O(31)	0.1106(5)	0.0053(6)	0.1264(3)	528(30)	491(30)	532(30)	39(25)	188(24)	−6(25)
O(32)	−0.0728(5)	−0.0861(6)	0.1131(3)	476(27)	444(29)	500(28)	−55(23)	119(23)	14(22)
O(33)	0.0466(7)	−0.1514(7)	0.0330(3)	1147(55)	715(42)	485(33)	150(31)	310(35)	−236(39)
N(1)	0	−0.2899(8)	0.25	272(33)	226(33)	467(42)	0	103(30)	0
N(2)	0.0190(5)	0.3246(6)	0.1398(3)	327(25)	265(25)	417(29)	41(22)	20(21)	−39(21)
N(3)	0.0287(6)	−0.0789(7)	0.0891(3)	636(39)	383(32)	361(29)	−20(25)	164(27)	−149(29)
O(1)	0.2342(4)	0.0546(5)	0.2902(3)	241(19)	206(19)	676(30)	54(20)	129(19)	−1(16)
O(2)	0.2842(10)	−0.0984(14)	−0.0213(7)	623(69)	884(90)	908(88)	176(67)	−55(55)	−11(59)
NH_4	0.2924(9)	0.1423(15)	0.0566(6)	772(61)	1838(121)	1080(78)	621(81)	−144(54)	−656(73)

[a] The form of the anisotropic thermal factor is $\exp[-2\pi^2(U_{11}h^2a^{*2} \cdots 2U_{23}klb^*c^*)]$.

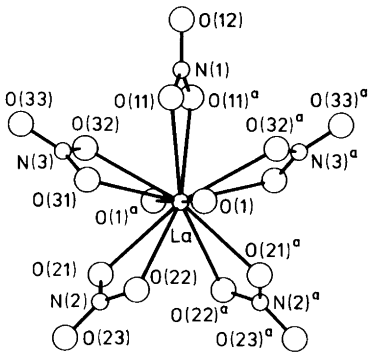

Fig. 1. A perspective view of the $[La(NO_3)_5(H_2O)_2]^{2-}$ complex with the atomic numbering system. The letter *a* refers to the symmetry operation $-x, y, \frac{1}{2}-z$.

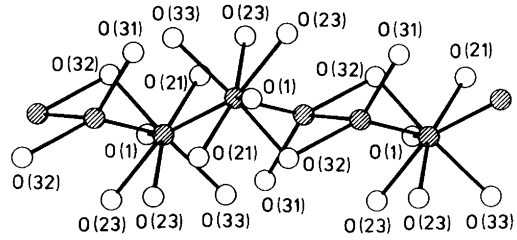

Fig. 2. A chain formed by ammonium ions and noncoordinated water molecules along the *y*-axis in compound *1*. The solid lines indicate possible hydrogen bonds within the chain and to coordinated oxygen atoms (numbered ones).

$(H_2O)_2]^{2-}$. A perspective view of the complex, which has very similar geometry in both compounds, is depicted in Fig. 1 which also gives the numbering system.

As well as the ammonium ions two water molecules remain outside the coordination sphere of lanthanum in $(NH_4)_2$ $[La(NO_3)_5(H_2O)_2] \cdot 2H_2O$ (*1*) and one water molecule in $(NH_4)_2[La(NO_3)_5$-$(H_2O)_2] \cdot H_2O$ (2). The ammonium ions and noncoordinated water molecules are connected by hydrogen bonds in a chain-like structure along the *y*-axis. As the electron densities of an ammonium ion and a water molecule are very similar it is impossible to distinguish between them on the basis of electron density maps. However, the thermal parameters for these atoms in compound *1* indicate the given locations for the ammonium ion and the water molecule. Furthermore, a refinement of the occupancy factors for both sites in compound *2* resulted in half occupancy for the water molecule (O(2)) and full occupancy for the ammonium site. Fig. 2 shows possible hydrogen bonds within the chain. Space group symmetry restricts the ammonium ions and water molecules to lie in the order $H_2O-H_2O-NH_4-NH_4$. It would be more favourable to place them in an alternating order: $H_2O-NH_4-H_2O-NH_4$, but the data is insufficient to prefer the later sequence. A stereoview showing the packing of the complexes in the unit cell of compound *1* is presented in Fig. 3.

In the dodecacoordinated lanthanoid nitrate structures $Mg_3La_2(NO_3)_{12} \cdot 24H_2O$ [1] and $K_2[La$-$(NO_3)_5(H_2O)_2]$ and in the present compounds La – O(nitrato) separations are similar. In both the ammonium compounds it is 2.70(2) Å while the corresponding distances for the magnesium and potassium compounds are 2.67(3) and 2.68(7) Å, respectively. The water oxygens may be at different distances, however, depending on the compound and

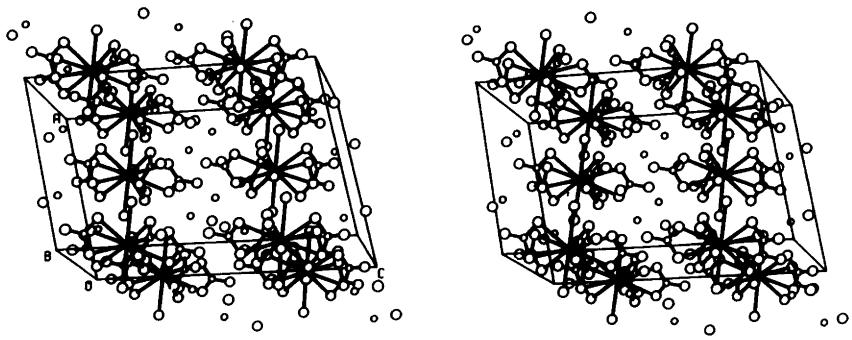

Fig. 3. A stereoview of the structure of $(NH_4)_2[La(NO_3)_5(H_2O)_2] \cdot 2H_2O$ (compound *1*) showing the unit cell packing.

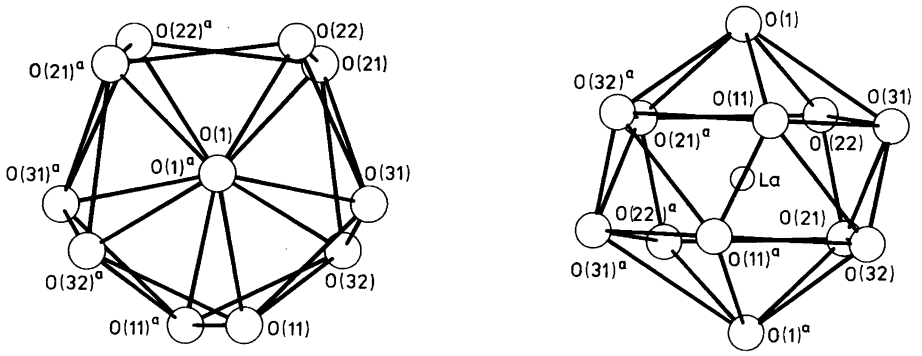

Fig. 4. Coordination polyhedron around the lanthanum atom. (a) A view along the "capping atoms" O(1) and O(1)^a. (b) A view perpendicular to that in (a). The letter *a* refers to the symmetry operation $-x, y, \frac{1}{2}-z$.

its hydrogen bonding network. Thus, the La–O (water) distances are 2.59(1) and 2.54(1) Å in ammonium compounds *1* and *2* while in the potassium compound, which is also a pentanitrato complex, the corresponding distance is 2.70(1) Å.

The coordination polyhedron around the La atom can be described in both compounds as a slightly distorted icosahedron. This was also the case for the magnesium and potassium compounds. The pattern of the coordinated nitrate groups is, however, different from the potassium compound. In both cases the water molecules occupy *trans* positions of the capping atoms in the icosahedron. In the present complexes each of the five nitrate groups contributes one oxygen atom to each of the two five-membered rings in the icosahedron while in the potassium compound one of the nitrate groups belongs entirely to one of the rings. Fig. 4 shows the coordination polyhedron; distances and angles involved are listed in Tables 3 and 4.

The geometry of nitrate groups shows the expected trends.[2,8,10] Thus, the N–O distances range

Table 3. Selected interatomic distances (Å) and angles (°).

	1	*2*
Environment of lanthanum		
La–O(11)^b (×2)	2.731(7)	2.716(6)
La–O(21)^b (×2)	2.663(8)	2.675(5)
La–O(22)^b (×2)	2.713(8)	2.690(6)
La–O(31)^b (×2)	2.703(8)	2.693(6)
La–O(32)^b (×2)	2.705(8)	2.709(6)
La–O(1)^b (×2)	2.594(6)	2.542(6)
O(11)–La–O(11)^a	46.7(3)	46.7(2)
O(11)–La–O(31)	63.0(3)	64.2(2)
O(11)–La–O(32)	63.2(3)	63.6(2)
O(11)–La–O(32)^a	65.0(3)	64.5(2)
O(11)–La–O(1)	68.6(2)	68.2(2)
O(21)–La–O(22)	47.3(3)	47.1(2)
O(21)–La–O(22)^a	69.4(3)	69.1(2)
O(21)–La–O(31)	69.6(3)	69.7(2)
O(21)–La–O(32)	69.7(3)	69.7(2)
O(21)–La–O(1)^a	68.1(2)	67.8(2)
O(22)–La–O(22)^a	77.2(3)	75.3(3)
O(22)–La–O(31)	65.0(3)	64.2(2)
O(22)–La–O(1)	67.1(3)	67.9(2)
O(31)–La–O(32)	47.2(3)	46.9(2)
O(31)–La–O(1)	70.8(3)	69.1(2)
O(32)–La–O(1)	65.5(3)	68.0(2)

Symmetry code

None	x, y, z
(*a*)	$-x, y, \frac{1}{2}-z$
(*b*)	x, y, z and $-x, y, \frac{1}{2}-z$

Table 4. Least-squares plane. Atoms involved: O(32)^a–O(11)–O(31)–O(22)–O(21).^{a}

	1	*2*
Angle between the planes (°)	1.1(12)^b	1.3(5)
Distances from the plane (Å)		
O(32)	0.045(4)	−0.003(3)
O(11)	0.002(4)	0.014(3)
O(31)	−0.051(5)	−0.019(3)
O(22)	0.076(3)	0.017(3)
O(21)	−0.072(4)	−0.008(3)

^{a}Symmetry code $-x, y, \frac{1}{2}-z$. ^{b}Estimated standard deviations are given in parentheses.

Table 5. Selected interatomic distances (Å) and angles (°) involving the nitrato groups.

	1	*2*
N(1)–O(11)[b] (×2)	1.269(9)	1.249(6)
N(1)–O(12) (×2)	1.202(17)	1.228(10)
O(11)–N(1)–O(11)[a]	117.1(10)	118.9(7)
O(11)–N(1)–O(12)	121.5(5)	120.5(4)
N(2)–O(21)	1.262(11)	1.251(7)
N(2)–O(22)	1.264(11)	1.262(7)
N(2)–O(23)	1.225(14)	1.233(8)
O(21)–N(2)–O(22)	117.2(9)	117.1(5)
O(21)–N(2)–O(23)	121.5(9)	122.2(5)
O(22)–N(2)–O(23)	121.3(9)	120.7(5)
N(3)–O(31)	1.243(13)	1.265(8)
N(3)–O(32)	1.295(12)	1.258(8)
N(3)–O(33)	1.219(17)	1.222(4)
O(31)–N(3)–O(32)	117.3(10)	116.8(6)
O(31)–N(3)–O(33)	123.2(10)	122.2(7)
O(32)–N(3)–O(33)	119.4(10)	121.0(7)

[a,b] For symmetry code, see Table 3.

from 1.202 to 1.295 Å; the lowest values belonging to terminal bonds while the bonds involving chelating oxygens are lengthened relative to the regular nonbonded nitrate group. Likewise, the O–N–O interbond angles deviate as expected from 120° when the oxygen atoms are involved in bonding, *cf.* Table 5.

The investigated structures have different compositions but exhibit nevertheless a close structural relationship. The central lanthanum ion is in both cases coordinated similarly by five nitrato groups and two water molecules. The coordination geometry of the complex anion and crystal symmetry do not deviate from one structure to another. The only significant change is the contraction of the unit cell when there is one water molecule less. In both compounds the $[La(NO_3)_5(H_2O)_2]^{2-}$ complexes are joined by hydrogen bonds involving the coordinated water molecules in the *xy*-plane and this is in agreement with the unit cell contraction in the *z*-direction. Whether or not the removal of water is reversible and can be brought about by heating is currently under study by thermoanalytical methods.

REFERENCES

1. Zalkin, A., Forrester, J. D. and Templeton, D. H. *J. Chem. Phys. 39* (1963) 2881; Anderson, M. R., Jenkin, G. T. and White, J. W. *Acta Crystallogr. B 33* (1977) 3933.
2. Eriksson, B., Larsson, L. O., Niinistö, L. and Valkonen, J. *Acta Chem. Scand. A 34* (1980) 567.
3. Karaghouli, A. R. and Wood, J. S., *J. Chem. Soc. Dalton Trans.* (1973) 2318.
4. Toogood, G. E. and Chieh, C. *Can. J. Chem. 53* (1975) 831.
5. Addison, C. C., Greenwood, A. J., Haley, M. J. and Logan, N. *J. Chem. Soc. Chem. Commun.* (1978) 580.
6. Sherry, E. G. *J. Inorg. Nucl. Chem. 40* (1978) 257.
7. Bünzli, J.-C. G., Klein, B., Chapuis, G. and Schenk, K. J. *J. Inorg. Nucl. Chem. 42* (1980) 1307.
8. Eriksson, B., Larsson, L. O. and Niinistö, L. *J. Chem. Soc. Chem. Commun.* (1978) 1616; Eriksson, B., Larsson, L. O., Niinistö, L. and Valkonen, J. *Inorg. Chem. 19* (1980) 1207.
9. *International Tables for X-Ray Crystallography*, Kynoch Press, Birmingham 1974, Vol. 4, pp. 99–101.
10. Addison, C. C., Logan, N., Wallwork, S. C. and Garner, C. D. *Q. Rev. Chem. Soc. 25* (1971) 289.

Received October 5, 1981.

Acta Chemica Scandinavica A 36 (1982) 471–484

Conformational Analysis. XVI. The Structure of 1,3-Difluoropropane $(CH_2F)_2CH_2$ as Determined by Electron Diffraction and Vibrational Spectroscopy and Compared with Molecular Mechanics Calculations

PETER KLÆBOE,[a] DAVID L. POWELL,[a] REIDAR STØLEVIK [b] and ØYVIND VORREN [b]

[a] Department of Chemistry, Univerrsity of Oslo, Oslo 3, Norway and [b] Department of Chemistry, University of Trondheim, NLHT, Rosenborg, N-7000 Trondheim, Norway

Gaseous 1,3-difluoropropane was studied at a nozzle temperature of 20 °C. Infrared spectra were obtained of the vapour, of a solution, and of the unannealed and annealed solid from 4000 to 30 cm^{-1}. Raman spectra of the liquid, including polarization measurements, of the sample in solvents of different polarity, and of the unannealed and annealed solid were recorded.

The compound is shown to exist with the following ratio of conformational abundance in the vapour phase: *GG*(63), *AG*(27), *GG*″(10). These values are compared with those calculated by molecular mechanics. The dominant *GG* conformer is also shown to be the one which persists in the crystalline state.

A complete vibrational assignment for the *GG* conformer and a partial one for the *AG* conformer are proposed, backed by a simple normal coordinate analysis. A comparison is made between the torsional modes observed in the infrared spectra and those predicted from the normal coordinate calculations.

Although 1,3-difluoropropane (DFP) was first prepared more than 30 years ago,[1] only three previous articles dealing in any way with its structure have appeared. Assuming that only staggered conformations are possible, four spectroscopically distinguishable forms are possible: *AA*, *AG*, *GG* and *GG*″; these are shown in Fig. 4 of Ref. 2.

In the only experimental work done previously, Lere-Porte, Petrissans and Gromb, in a study of the infrared spectra of some polyhalogenopropanes in the region 1400–1500 cm^{-1}, assigned two CH_2 scissoring modes, one to the *AG* and the other to the *GG* conformer.[3]

Meyer, using molecular mechanics calculations, predicted populations in CCl_4 solution as follows: *GG* (31%), *AG* (45%), *GG*″ (17%) and *AA* (7%).[4]

Lere-Porte and Petrissans also performed CNDO/2 and PCILO calculations from which they concluded that the conformational energies of *GG*, *AG* and *AA* are approximately equal while *GG*″ is about 1 kcal/mol higher in energy.[5,*] Essentially the same order of energies was obtained from Meyer's molecular mechanics calculations.[4]

In these laboratories we have long been involved in the study of the conformational behaviour of halogenated propanes. This work follows most closely our earlier studies of other 1,3-dihalogenated propanes. By electron diffraction, conformer *GG* was shown to be favoured in the vapour phase in both 1,3-dichloro-[6] and 1,3-dibromopropane:[7]

$E(AG) - E(GG) \simeq 1.0$ kcal/mol
$E(AA) - E(GG) \simeq 1.5$ kcal/mol
$E(GG'') - E(GG) \simeq 3.0$ kcal/mol

Following earlier studies by Sheppard and coworkers,[8] 1,3-dichloro-, 1,3-bromochloro-, 1,3-dibromo-, and 1,3-diiodopropane were shown to crystallize at low temperature exclusively in the *GG*

*1 kcal = 4.184 kJ.

0302-4377/82/060471-14$02.50

conformation by the use of infrared and Raman spectroscopy.[2] In this work it was also shown that the dibromo compound crystallized at high pressure as a *GG* conformer, but that the diiodo compound crystallized in the *AA* conformation.

Another compound in which the same conformational possibilities exist is 1,1,3,3-tetrachloropropane. This compound not only crystallizes in the *GG* conformation, but no detectable amounts of any other conformer were found in the vapour or liquid states.[9]

Relevant also to this study is our earlier work on 1,2,3-trichloro- and 1,2,3-tribromopropane. In both of these compounds the dominant form in the vapour phase was a conformer analogous to that dominant in the 1,3-dihalopropanes;[10,11] this form persisted in the crystalline solid in both cases.[12]

EXPERIMENTAL

The sample used for electron diffraction (ED) was provided by W. Lüttke and J. Zeitzling of the University of Göttingen and had a purity of *ca.* 99 %. That used for the spectroscopic measurements was prepared in the laboratories in Oslo, purified by gas chromatography, and had a purity in excess of 99 %.

ED-diagrams were recorded with the Balzers apparatus[13,14] at a nozzle temperature of 20 °C. Two sets of plates were obtained: *Set 1* (5 plates, electron wavelength 0.05858 Å, nozzle-to-plate distance 500.12 mm) and *set 2* (6 plates, 0.05858 Å, 250.12 mm). The electron wavelength was determined by calibration against TlCl and benzene.[15] The data were treated in the usual way[16] to yield an intensity curve for each plate. Average curves for each set of distances were formed. A composite curve was then made by connecting the two average curves after scaling. The final experimental intensity curve is shown in Fig. 1. The intensities have been modified by $s\{|f'_F||f'_C|\}^{-1}$. Scattering amplitudes (f') were calculated by the partial-wave method[17] using Hartree-Fock atomic potentials.[18] The radial distribution (RD) curves[16] are shown in Fig. 2.

The infrared spectra were recorded with a Perkin-Elmer model 225 spectrometer (4000 – 200 cm^{-1}) and with a Bruker fast scan Fourier transform spectrometer model 114 C (4000 – 30 cm^{-1}). Beamsplitters of germanium on KBr and of Mylar (3.5, 6, 12 and 24 μ thickness) were employed in the mid- and far infrared regions, respectively.

Vapour cells of 10 cm (CsI windows) and 20 cm path lengths (polyethylene windows) were used with pressures ranging from 6 to 130 Torr. Conventional sealed cells with KBr windows were used for the carbon tetrachloride solution of the sample, while vacuum tight cells with polyethylene windows were employed below 600 cm^{-1}. Spectra of the unannealed and annealed solid were recorded with cryostats cooled with liquid nitrogen which had windows of CsI and polyethylene. Attempts to form a crystal in a diamond anvil cell at a pressure of *ca.* 25 kbar were not successful.

Raman spectra were recorded with a modified[19] Cary 81 spectrometer excited by a CRL model 52 G argon ion laser, using the 5145 and the 4880 Å lines. Spectra were taken of the pure liquid contained in a sealed ampoule (including semi-quantitative polarization measurements), of CCl_4 and CH_3OH

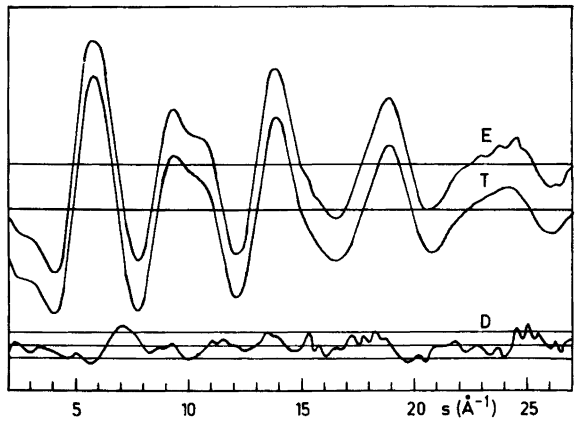

Fig. 1. Experimental (E) and theoretical (T) intensity curves for 1,3-difluoropropane and $D = 2(E - T)$ corresponding to the final least-squares parameters. The straight lines show the experimental uncertainties (± 3 times the experimental standard deviations).

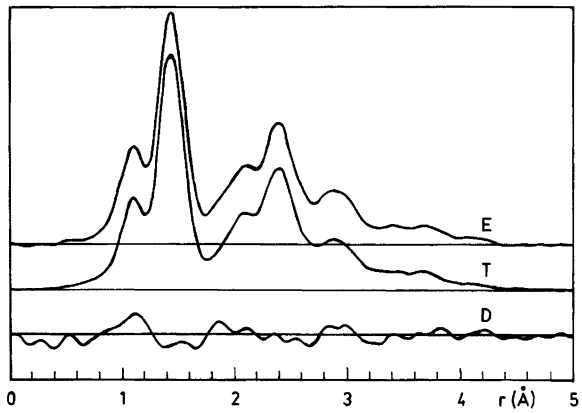

Fig. 2. Experimental (E) and theoretical (T) radial distribution curves for 1,3-difluoropropane and $D = 3(E - T)$. The artificial damping constant was 0.002 Å^2.

solutions, and of the unannealed and annealed solid deposited on a copper block cooled by liquid N_2.

CALCULATIONS

Calculations of conformational energies and torsional barriers. Molecular-mechanics calculations of conformational energies and barriers were performed using non-bonded potential functions in the Morse formulation.[20] The potential parameters[20,21] are found in Table 1, and the diagonal force constants of Crowder and Mao were used.[22] Potential parameters of the F···C interaction type were adjusted to fit the energy difference $\Delta E = E(\text{anti}) - E(\text{gauche}) = 0.47$ kcal/mol observed in 1-fluoropropane.[23] The charges on the atoms were calculated as suggested by Sanderson,[24] but were reduced by a factor of two.[25]

Calculated results are given in Table 2. Each energy value has been obtained by adjusting bond lengths (r) and bond angles (θ), and at the energy minima the values of the torsional angles (ϕ) were also adjusted. All energies, expressed in kcal/mol, are relative to the energy of the *GG* form. Energy minima are represented by the values 0 (*GG*), 0.3 (*GG''*), 1.2 (*AG*) and 2.4 (*AA*). Each energy minimum, represented by the central number in each block of Table 2, is surrounded by torsional barriers, represented by the remaining eight numbers in each block, corresponding to forms with one or both terminal groups eclipsing the central CH_2 group. The horizontal variation in energy values corresponds to a change of *ca.* 60° in the torsional angle ϕ_{1-2}, while the vertical variation corresponds to a change of *ca.* 60° in ϕ_{2-3}. Clearly, *AG*, *GG''* and *GG* have nearly staggered conformations, while *AA* is exactly staggered. The geometry of each conformer corresponds to well-defined minima.

The lowest barrier (2.9) is found for the transition *GG''*(0.3)→(3.2)→*GG*(0). In 1-fluoropropane[23] the barrier *G*→*A* is 4.2±1.5 kcal/mol in good

Table 1. Potential parameter values.[a]

Type	r_0 (Å)	r_{min} (Å)	ε(kcal/mol)	Ref.
F···F	1.97	2.64	3.60	21
F···H	2.37	2.90	0.29	21
F···C	2.74	3.26	0.61	This work
C···H	2.90	3.30	0.043	20
H···H	2.76	3.15	0.023	20

[a] The electrostatic terms of the potential have been calculated with the following charges (q) on the atoms: $q(F) = -0.175$e, $q(C_1) = q(C_3) = +0.027$e, $q(C_2) = 0.001$e, $q(H_1) = q(H_3) = 0.059$e, $q(H_2) = 0.030$e.

Table 2. Conformational energies for 1,3-difluoropropane obtained by molecular-mechanics calculations.

Type of conformer and (symmetry) $C_1C_2C_3$		Energies in kcal/mol Horizontal $\phi(1-2)$ Vertical $\phi(2-3)$			Deviations from staggered form ($C_1C_2C_3$) $\Delta\phi(1-2)°$	$\Delta\phi(2-3)°$
	HHH	10.0	6.5	9.9	0 [b]	0 [b]
AA (C_{2v})	FCCCF	6.5	2.4	6.5		
	HHH	9.9	6.5	10.0		
	HHH	9.9	4.6	9.0		
AG (C_1)	HCCCF	6.5	1.2	4.9	0.5	1.0
	FHH	10.0	4.9	9.0		
	HHH	9.0	3.2	9.8		
GG″ (C_s)	HCCCH	4.6	0.3	3.2	−2.1	+2.1
	FHF	9.9	4.6	9.0		
	HHF	10.0	4.9	9.0		
GG (C_2)	HCCCH	4.9	0 [a]	3.2	+1.5	+1.5
	FHH	9.0	3.2	9.8		

[a] Energies relative to this value. [b] Exactly staggered form.

agreement with 4.1 for the transition $AG \rightarrow AA$ as calculated here. The calculated energies suggest that *GG* will be the predominant conformer in the gas phase at 20 °C. The high-energy form is *AA*, not *GG″* as suggested by earlier calculations.[4,5] We consider the present energy values superior to our earlier calculations [21] mainly because of the new and better F···C potential parameters. The conformational differences between parameter values of bond angles were small. The largest value was found for $\theta = \angle CCC$ with $\theta(GG'') - \theta(AA) = 0.5°$ and $\theta(GG) - \theta(AG) = 0.1°$.

CALCULATION OF VIBRATIONAL QUANTITIES

One of the most fruitful areas of interplay between electron diffraction and vibrational spectroscopy is that concerned with the torsional vibrations. For example, we have recently exploited this connection in our comparison of the low frequency vibrations of 1,3-dichloro-, 1,3-dibromo-, 1,2,3-trichloro-, and 1,2,3-tribromopropane found experimentally [26] with those calculated earlier;[6,7] in this case the agreement between calculation and experiment was very satisfying.

Leading up to this comparison, a normal-coordinate analysis was carried out for each conformer,[27] and mean amplitudes of vibration (*u*-values) were computed.[28] The force constants, except for the torsional ones, were transferred from 1-fluoropropane.[22] The torsional force constants were estimated by adjusting two values to fit the experimental torsional frequencies observed for 1-fluoropropane.[23] The final values are F_ϕ(gauche) $= 0.142$ and F_ϕ(anti) $= 0.039$ in units of mdyn Å(rad)$^{-2}$. From the formula in Ref. 29 and partial force constants F_g^*(HH), F_g^*(CH), F_g^*(FC) and F_g^*(FH) equal to 0.013, 0.017, 0.065 and 0.021 mdyn Å(rad)$^{-2}$, the estimates became F_ϕ(anti) $= 0.102$ and F_ϕ(gauche) equal to the value 0.142 above. Molecular-mechanics estimates are F (anti) $= 0.10 - 0.11$ and F (gauche) $= 0.12 - 0.13$ depending on which conformer is considered.

All estimates agree in predicting F_ϕ(gauche) $> F_\phi$(anti) as intuitively expected. The values used in calculating the *u*-values were F_ϕ(anti) $= 0.039$ and F_ϕ(gauche) $= 0.142$ mdyn Å (rad)$^{-2}$. The calculated mean amplitudes of vibration are found in Table 3 and the torsional frequencies in Table 4, while the calculated fundamental frequencies are compared with the experimental values in Table 8.

In these tables, the assumption, which will be discussed later, is made that the *GG* conformer persists in the crystalline phase. As in our earlier work, it can be seen that here also the agreement between the experimental torsional frequencies and those calculated is very good.

Table 3. Calculated mean amplitudes of vibration (u). The range of u-values and corresponding internuclear distances (r) are given including values for the conformers *AA*, *AG*, *GG*, *GG″*. $T=293$ K.

Type of dist.	r (Å)	u (Å)
C–F	1.391	0.047
C–C	1.513	0.050
C–H	1.094	0.078
C···F	2.39	0.069
C···H	2.15	0.107–0.108
C···C	2.51	0.068
F···H	2.04	0.105
H···H	1.78	0.127–0.129
F···H(a)	3.32	0.103
F···H(g)	2.61–2.66	0.156–0.198
H···H(g)	2.44–2.52	0.204–0.172
H···H(a)	3.06	0.130
C···F(g)	2.91–2.96	0.139–0.140
C···F(a)	3.69	0.069
C···H(g)	2.72–2.74	0.158–0.204
C···H(a)	3.46	0.105
F···F(gg)	3.54	0.235
F···F(aa)	4.70	0.085
F···F(ag)	4.15	0.166
F···F(gg″)	2.71	0.225
F···H(gg)	2.59	0.227–0.268
F···H(ga)	3.89	0.152–0.162
F···H(ag)	4.02	0.181–0.196
F···H(gg)	3.25–3.30	0.320–0.241
F···H(aa)	4.53	0.118
H···H(gg)	2.99–3.11	0.247–0.368
H···H(ga)	3.69–3.75	0.195–0.170
H···H(aa)	4.29	0.144
H···H(gg″)	2.43–2.52	0.230–0.305

Table 4. Calculated values of the torsional frequencies in cm^{-1}. F_ϕ values in mdyn Å$(rad)^{-2}$.

F_ϕ(gauche)	0.114	0.142	0.170
GG	81	90	97
	158	173	186
GG″	104	112	119
	104	115	126
AG[a]	69	69	69
	126	138	148
AG[b]	108	108	108
	126	138	148

[a] F_ϕ(anti)=0.039. [b] F_ϕ(anti)=0.102.

The torsional frequency variation with the various values employed for F_ϕ(gauche) and F_ϕ(anti) is shown in Table 4.

RESULTS AND DISCUSSION

Structure and composition in the gas phase. RD-curves for the four possible conformers and the final experimental curve are shown in Fig. 3. Clearly the conformers *GG* and *AG* are present and *GG* is the most abundant conformer. The percentage of *AA* has to be very small. The fact that *GG″* is present in detectable concentration is not so easily seen directly from the curves in Fig. 3. According to the energy values in Table 2 *AG* and *AA* are less stable than *GG″*, corresponding approximately to the percentages 55 (*GG*), 30 (*GG″*), and 15 (*AG*) with less than one percent of *AA* at 20 °C. The composition parameters $\alpha(AG)$ and $\alpha(GG)$ were refined with the restrictions $\alpha(AA)=0$ and $\alpha(GG'')=100-\alpha(AG)-\alpha(GG)$.

It was assumed that the $C-CH_2F$ groups are equivalent and possess C_s symmetry, the $C-CH_2-C$ group possesses C_{2v} symmetry, and thus the conformers have identical structures except for the values of the torsional angles ϕ_{1-2} and ϕ_{2-3} which define the rotations around the C_1-C_2 and C_2-C_3 bonds.

The torsion angles were not all refined independently. A relationship between a deviation

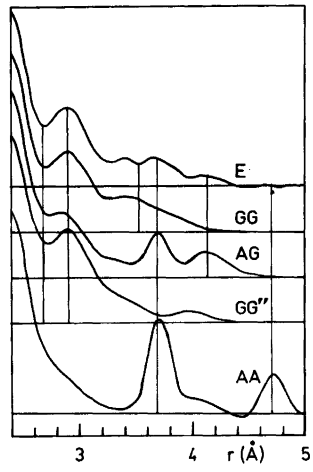

Fig. 3. Radial distribution curves for conformers of 1,3-difluoropropane. Calculated curves for the conformers *AA*, *AG*, *GG* and *GG″* are shown together with the final experimental curve.

Table 5. Structural parameters and conformational composition for 1,3-difluoropropane. Standard deviations (σ) apply to the last digit given.

Bond lengths (r_a) in Å and bond angles ($\angle\alpha$) in deg.			
C–H	1.094(5)	∠CCC	112.9(0.8)
C–C	1.513(3)	∠CCF	110.1(0.3)
C–F	1.391(2)	$\angle CC_1H$	112.1(1.4)
∠FCH	107.8(0.8)[b]	$\angle HC_2H$	108.5[a]
$\angle HC_1H$	105.9(1.5)[b]	$\angle(HC_1H)^*$	119.5[a]
$\angle CC_2H$	108.5(1.2)[b]		

Torsional angle deviations from staggered forms			
Conformer[c] ($C_1-C_2-C_3$)	*GG*	*AG*	*GG″*
$\Delta\phi_{1-2}$(deg.)	−4.0(2.0)	−2.0(2.0)	+4.0(2.0)
$\Delta\phi_{2-3}$(deg.)	−4.0(2.0)	−2.0(2.0)	−4.0(2.0)
Composition (%)	63(4)	27(2)	10(5)

[a] Assumed values. [b] Dependent angles. [c] See also Table 2.

parameter (ϕ_0) and the torsion angles was introduced as suggested by the molecular-mechanics results of Table 2. For the *GG* conformer it was assumed that $\phi_{1-2}=120°+\phi_0=\phi_{2-3}$, and for *GG″* $\phi_{1-2}=120°-\phi_0=-\phi_{2-3}$. For *AG* $\phi_{1-2}=120°+0.5\phi_0$ and $\phi_{2-3}=0.5\phi_0$, while *AA* has $\phi_{1-2}=\phi_{2-3}=0°$. The value $\phi_0=0°$ corresponds to exact staggered conformations, and the results in Table 2 suggest a value of ϕ_0 close to +2°, while −4° was found by least-squares refinement with $\sigma=2°$.

The parameters ϕ_0, r(C–H), r(C–C), r(C–F), ∠CCC, ∠CCF and $\angle CC_1H$ were refined simultaneously while $\angle HC_2H$ and $\angle(HC_1H)^*$, which is the projection of the HC_1H angle on a plane perpendicular to the C_1-C_2 axis, were kept at fixed values as shown in Table 5. Parameters from the final least-squares refinements and standard deviations (σ) corrected for correlation[30] are also given in Table 5. The uncertainty in the *s*-scale (0.14%) has been included in the standard deviations for the bond lengths. Non-bonded distances were computed as dependent parameters, restricted under the constraints of r_α parameters.[31,32]

Calculated mean amplitudes of vibration (u) were included in the least-squares analysis as fixed parameters (Table 3), except for the following values: u(C–H)=0.066(4), u(C–F)=0.052(5) and u(C···F/gauche)=0.121(6) Å found by refinement.

Table 6. Experimental ED-results for three 1,3-dihalopropanes. Standard deviations are shown in parentheses (σ).

$XCH_2-CH_2-CH_2X$	X=F This work	X=Cl Ref. 6	X=Br Ref. 7
Bond length			
r_g(C–C) in Å	1.515(3)	1.531(4)	1.529(5)
Bond angles ($\angle_\alpha$) in deg.			
∠CCC	112.9(0.8)	112.9(0.5)	111.4(1.6)
∠CCX	110.1(0.3)	111.6(0.1)	112.0(0.3)
Torsional angle deviations from staggered form in the conformer *GG*			
$\Delta\phi(GG)$	−4.0(2.0)	−5.8(1.0)	−6.6(2.0)
Percentages of conformers			
GG	63(4)	73(2)	67(2)
AG	27(2)	24(2)	30(2)
AA	0(−)[a]	3(3)	3(2)
GG″	10(5)	0(−)[a]	0(−)[a]
Temp. (°C)	20	38	65

[a] Experimentally not detected.

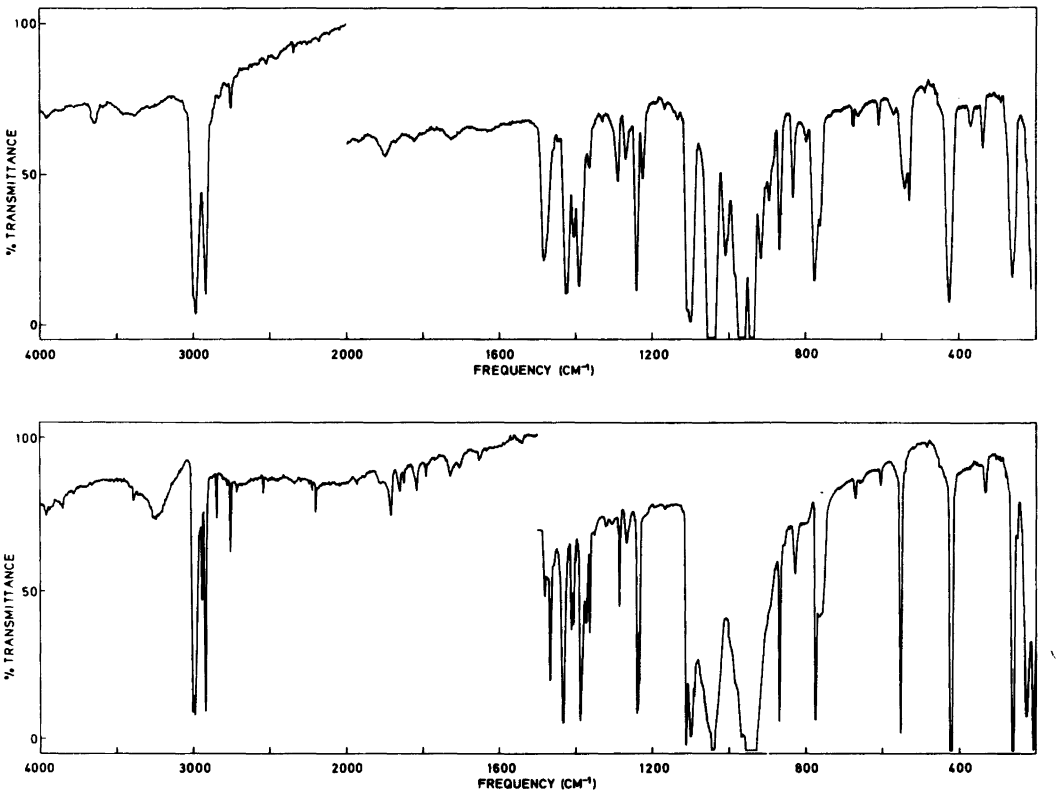

Fig. 4. Infrared spectra of 1,3-difluoropropane as an unannealed solid (upper curve) and as an annealed crystalline solid (lower curve) at *ca.* −180 °C.

The following correlation coefficients (ρ) had absolute values greater than 0.4: $\rho(1,2) = -0.42$, $\rho(3,4) = -0.69$, $\rho(3,5) = +0.43$ and $\rho(5,6) = -0.43$. The numbering of the parameters was 1, 2, 3, 4, 5 and 6 for r(C−C), ∠CCF, ∠CCC, ϕ_0, $\alpha(AG)$ and $\alpha(GG)$, respectively.

Assuming equal vibrational and rotational partition functions for the conformers, the values of the conformational energies calculated from the percentages in Table 5 are $\Delta E(AG) = E(AG) - E(GG) = 0.9$ and $\Delta E(GG'') = F(GG'') - E(GG) = 1.1$ in kcal/mol. However, using values for the vibrational partition functions corresponding to the calculated frequencies, the ΔE values become $\Delta E(AG) = 1.5$ and $\Delta E(GG'') = 1.2$. With $F_\phi(\text{anti}) = 0.102$ mdyn Å(rad)$^{-2}$ one gets $\Delta E(AG) = 1.1$. Including error limits the value 1.1 ± 0.4 is suggested for $\Delta E(AG)$ in agreement with the value 1.2 in Table 2. For $\Delta E(GG'')$ the lower limit of about 0.5 was estimated. However, the calculated value of 0.3 for ΔE (GG'') is too small compared to the best value of about 1.2 estimated above. The calculated value 2.4 for $\Delta E(AA)$ is consistent with the fact that AA was not present in detectable concentration.

Electron diffraction results for three 1,3-dihalopropanes have been compared in Table 6.

Spectral interpretations. We present in Table 7 the IR and Raman frequencies in the regions where fundamentals may appear. In Figs. 4 and 5 are given the IR spectra of the unannealed and annealed crystals in the mid and far IR. In Fig. 6 the Raman spectra of the liquid and of the annealed crystal are shown.

The most important problem we faced in our interpretation of the spectra was that of which conformer persists in the low temperature crystal. In our earlier work on the other 1,3-dihalopropanes,[2] not only could the evidence from the vapour phase compositions as determined from electron diffraction be employed, but also use could be made

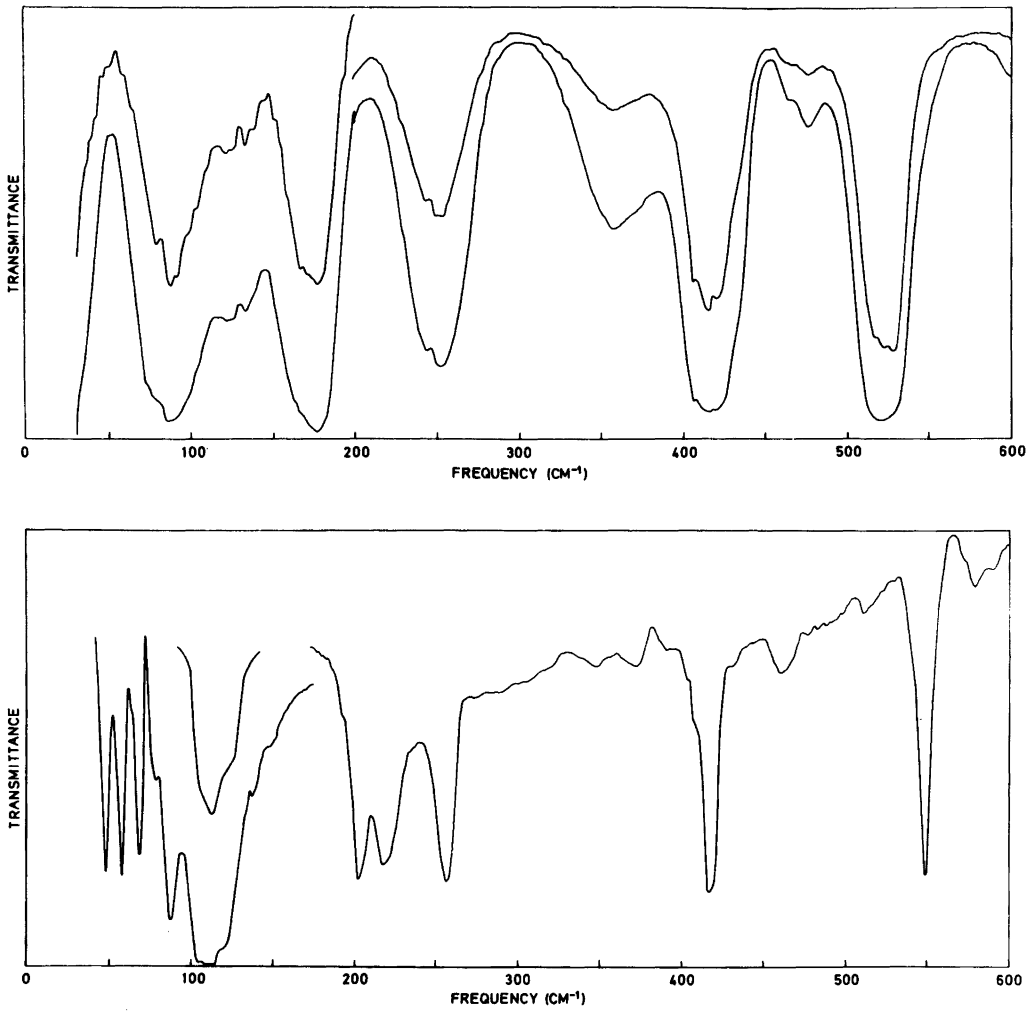

Fig. 5. Far infrared spectra of 1,3-difluoropropane as a vapour (upper curve) and as an annealed crystalline solid at *ca.* −180 °C (lower curve).

of the various empirical rules for the dependence of the C−X stretching modes on conformation.[33] Unfortunately, in the case of the fluoroalkanes, such rules do not exist because of the highly mixed character of the modes involving C−F stretching (*cf. e.g.* Ref. 34).

We now are certain that the conformer which persists in the crystal is the *GG*, but since this assignment is not completely straightforward we feel obligated to explain our reasoning.

On the basis of our experience with the other 1,3-dihalopropanes we would expect the *GG* form to persist in the crystal. Further, since it is the *GG* which is the dominant form in the gas phase at room temperature, it would be most likely that form would be the one which "takes over" in the crystal.

Our normal coordinate calculations are admittedly crude, and it can be easily seen that plausible assignments can be made assuming either that *GG* or that *AG* is the stable form in the crystal once one ascends past the first 4 fundamentals. However, for those lowest 4 fundamentals the more convincing assignment occurs with *GG* taken as the form in the crystal.

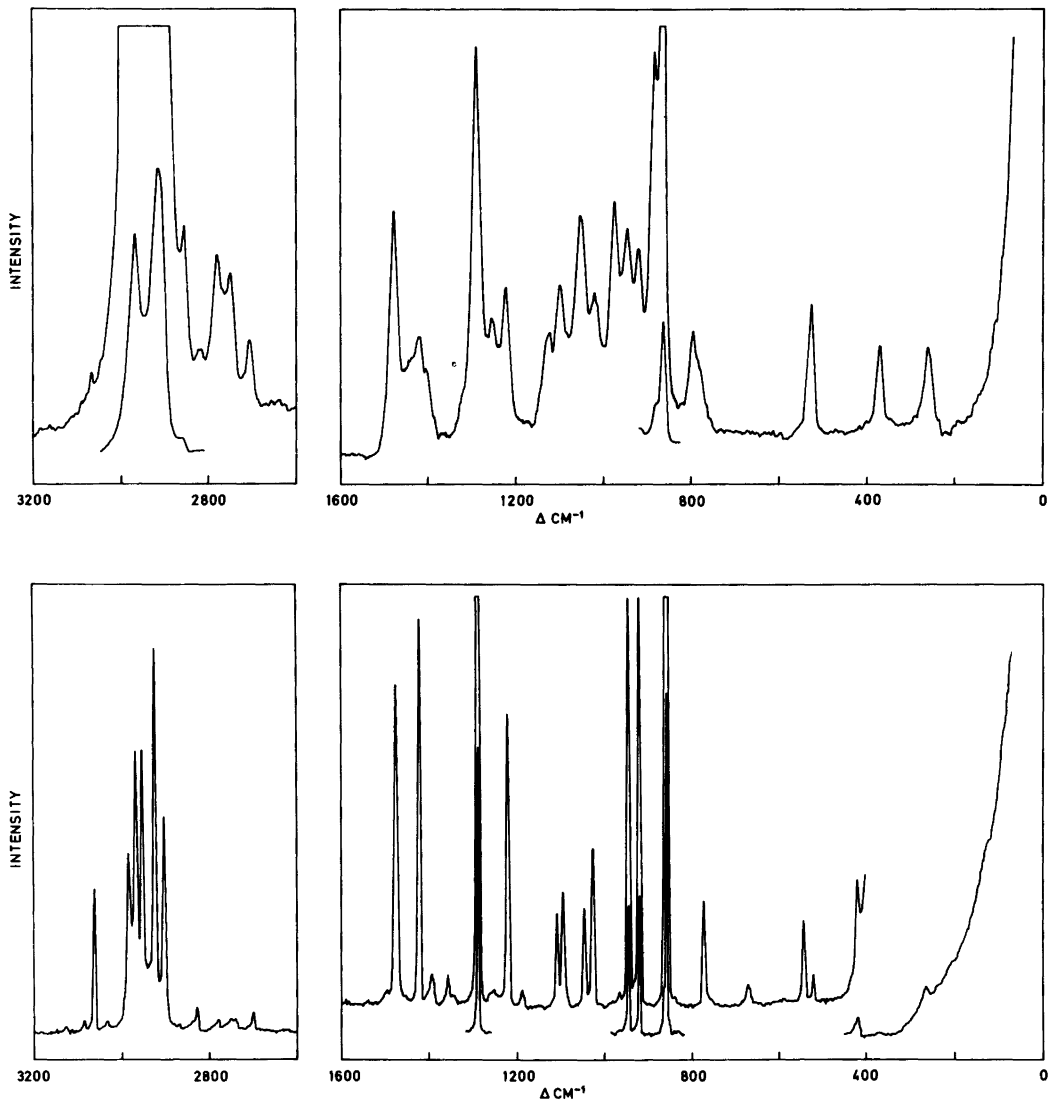

Fig. 6. Raman spectra of 1,3-difluoropropane as a liquid at room temperature (upper curve) and as an annealed crystalline solid at *ca.* −180 °C (lower curve).

A portion of this can be made even more convincing. Our calculations of the torsional frequencies (*cf.* Table 4) which can be made almost independently of the force field employed for the rest of the molecule agree much better with the experimental results when one assumes that the *GG* form is the one which crystallizes.

The infrared data, which provide the only complete link between the known composition of the gas phase and the crystal, strongly support this argument. There are no unexpected intensity variations as we proceed from vapour to solution to unannealed and annealed crystals; that is, it is in general the weaker bands in the spectra which disappear upon crystallization.

The Raman data, however, tell an inconsistent story. Lending support to the hypothesis given are the polarization data. Almost all the bands which

disappear upon crystallization are clearly polarized. This is the behaviour which would be expected if an unsymmetrical species was being destroyed. The *AG* conformer has no symmetry; hence all its bands should be polarized. On the other hand, 13 of the 27 fundamental bands for the *GG* conformer should be depolarized. The obvious conclusion to be drawn is that it is an unsymmetrical conformer which is being removed. It must be pointed out, though, that in the Raman spectra several of the more prominent bands disappear upon crystallization, notably those at 366, 520, 792, 884 and 977 cm^{-1} (*cf.* Fig. 6).

Dealing only with the evidence from the Raman data, we are inclined to give more credence to the polarization data. Arguments based on it rely only on symmetry with no intervening assumptions. By contrast, arguments based on intensities seem much shakier to us. Lacking both heavy atoms and multiple bonds, DFP lacks also the very intense Raman bands connected with the C–F stretches which could serve as the sort of undeniable landmarks which characterize the spectra of the chloro-, bromo-, and iodoalkanes (as shown, *e.g.*, in Refs. 2 and 12).

Finally, when we consider the weight of all the evidence at once, we return firmly to our initial statement, the assertion that the crystal is made up of conformers in the *GG* form. With this decision made, we can proceed to our consideration of the spectra.

Somewhat as we expected, the dipole moments of the two major individual conformers must be nearly the same inasmuch as we could observe almost no change in relative intensities of the bands in going from the Raman spectrum of the CCl_4 solution through that of the pure liquid to that of the CH_3OH solution, a series in which the dielectric constant of the medium increases greatly. The lone exception to this, a weak band at 363 cm^{-1} which does increase through these three spectra and which disappears upon crystallization, is the only band which we assign to the *GG″* conformer. The *GG″* conformer, since in it the 2 C–F bonds are nearly parallel, should have a much higher dipole moment than the *GG* and *AG* conformers and should be highly favoured in media of higher dielectric constant. Thus, even though from our electron diffraction work we obtain the result that the third most abundant conformer, the *GG″*, is present in 10% abundance at 20 °C in the vapour, the failure of this conformer to make its presence known to a greater extent in the more polar media suggests that this 10% value must be regarded as an extreme upper limit and that the abundance is probably considerably lower.

Of aid to us in our assignments were the infrared band contours, the Raman polarization data, and the normal coordinate calculations. For the *GG* conformer, the 14 fundamentals of species *a* should have type *B* band contours and should be polarized; the 13 fundamentals of species b should have *A/C* hybrid band contours and should be depolarized. With the aid of these pieces of information, we present the assignments shown in Tables 7 and 8. The agreement between calculated and observed frequencies seems to us quite good in view of the fact that the frequencies were in no way refined.

On the whole, in our assignments we have been able to find agreement both with the calculated frequencies and also with the spectral evidence. We note below only those cases where all the pieces of evidence do not agree.

In the C–H stretching region 4 of the 6 C–H stretches are ascribed to polarized Raman bands rather than the 3 which we expect. In this region, where there should be nearly complete correspondence between the fundamentals of the various conformers, each band should have components from the different conformers. Since all bands of the *AG* conformer will be polarized, nearly all bands in this region should appear polarized. Except for this, assignment in this region is reasonably straightforward and agrees well, for example, with the values reported by Harris *et al.* for 1,2-difluoroethane.[35]

Assignment of the 3 CH_2 scissoring modes between 1400 and 1500 cm^{-1} posed no difficulty.

Thirteen fundamentals are expected to lie between 600 and 1400 cm^{-1}. It is easy to pick out some of these, with their great intensity in the infrared, in which C–F stretching is playing a large role. However, with the highly mixed character of these modes, we prefer not to identify individual bands as being the C–F stretches. Our assignment for ν_7 is to a type *A* band whose Raman counterpart, though, is polarized. We reversed the numerical order of the normal coordinate results for ν_{10} and ν_{24} so as to satisfy the spectral evidence.

Below 600 cm^{-1} lie 5 fundamentals. The band at 416 cm^{-1} appears depolarized in the Raman; it does have the expected type *B* contour though. More serious is the problem of the band at 252 cm^{-1} which, against expectations, appears polarized in the Raman. We have no explanation for this once we

Table 7. Infrared and Raman spectral data[a] for 1,3-difluoropropane.

Infrared			Raman		Assignments
Vapour	Solution	Solid(90K)	Liquid	Solid(90K)	
3087w[b]					
3062w					
		3027vw			
		3004s		3005ms	ν_1, *GG*
		2999s			ν_{15}, *GG*
2985vs		2989s		2986s	
2979vs	2975vs	2972m,sh	2979vs,p	2973s	ν_2, *GG*
2973vs					
			2963m,dp	2956w	
		2945m		2945vs	ν_{16}, *GG*
			2927vs,p		
2925s					
2919s	2915s	2924s	2922vs,p	2924s	ν_{17}, *GG*
2912s					
		2877vw			
2850w		2866vw	2867w,p		ν_3, *GG*
		2847w		2844w	
2828w	2821w,sh		2828w,p		
1486m		1480w	1479m,dp	1484s 1481w,sh	ν_4, *GG*
1475m	1476m	*	1470w,sh	*	ν_7, *AG*
1465w					
	1456w	1465m			
	1440w		1444w,dp	*	ν_8, *AG*
1435m		1430s		1430s	ν_{18}, *GG*
		1409m			
1424m,sh	1419m	1403m	1421w,dp		ν_5, *GG*
1415m,sh					
1407m,sh	1400m	*	1404vw	*	ν_9, *AG*
1394s					
				1401w	*GG* comb?
				1397w	
1385s C	1382m	1386s			ν_{19}, *GG*
		1371vw			
1371w	1363w	1362w	1365vw	1363w	ν_6, *GG*
		1348vw			
	1325w	*	1325w	*	ν_{12}, *AG*
1307vw					
		1287vw			
1280w	1289w	1284w	1291s,dp(?)	1295vs	ν_{20}, *GG*
1272m					
	1250w	1265w	1255w,p	*	ν_{13}, *AG*
1258w					
		1238w			
1245m A	1235m	1235s	1225m,p	1227s	ν_7, *GG*
		1231s			
1238m					
1229m	1218w	*			
			1191vw	1193w	ν_{21}, *GG*
		1164vw			
1135w	1126w		1129w,p	1113m	ν_8, *GG*

Table 7. Continued.

1113s 1107s } C 1099s	1100vs	1110s } 1097s }	1100m,dp	1099s	ν_{22}, *GG*
			1085vw,sh		
1074vs 1067vs } A 1057vs	1052vs	1049vs 1034vs	1051s,dp	1050s	ν_{23}, *GG*
			1019m,dp	1030m	ν_{9}, *GG*
1045s } 1038s }	1021vs	*			ν_{18}, *AG*
994s } 987s } B	977s	977w } 966w } *	973s,dp	969w *	ν_{19}, *AG*
980s,sh					
958s 952s } C 942s	943s	958vs	944m,dp	948s	ν_{10}, *GG*
		935s		935vw	
928s 923s } 916s 910s,sh	917m	932s	917mw,p	921s	ν_{24}, *GG*
		892m,sh			
891m	881w	878w,sh(?)	884m,p	*	ν_{20}, *AG*
872w } 860w }	863w	868s	864vs,p	867w,sh 861vs } 856w,sh	ν_{11}, *GG*
		854vw			
821w	824w[c]	826w	827vw	*	ν_{21}, *AG*
	791w[c]	*	792m,p	*	ν_{22}, *AG*
784w,sh } B 773m }	778m[c]	773s	777w,dp	774m	ν_{25}, *GG*
		763w } 746w }	755vw(?)	758vw	
	660w[c]	668w			
		654vw			
606vw					
		570vw			
548w	536vw	549s		542m	ν_{12}, *GG*
526m 522m } A 514m	520m	*	520m,p	*	ν_{23}, *AG*
472vw	471w	*	470vvw?		$\nu_{24}+\nu_{27}$, *AG*
433w,sh					
419m 415m 413m } B 406m	416m	418s	419w,dp	419w	ν_{13}, *GG*
	397vvw(?)	*	396w,p	*	ν_{24}, *AG*
375w	363m	*	366m,p	*	ν_{14}, *GG″*
357w					
	333w	330w	325vw(?)		$\nu_{14}+\nu_{26}$, *GG*
302w } 289vw }	301vw				ν_{25}, *AG*

Table 7. Continued.

253w 248w 243w	252m	258s 255s	254m,p	263w	ν_{26}, *GG*
	205w[d]	216m			
178m 166m B	182m[d]	202s	184vw	205w	ν_{27}, *GG*
		172vw			
		154vw			
133w 126w	135vw[d]	*			ν_{26}, *AG*
93w 87w 82w	94w[d]	112s 87s	100vw	120w	ν_{14}, *GG*
		68m			
		58m			lattice modes
35vw	41w[d]	48m			

[a] The spectra are reported only for the regions 3100 to 2800 cm^{-1} and below 1500 cm^{-1}. [b] s, strong; m, medium; w, weak; v, very; sh, shoulder; A,B,C, vapour contours; p, polarized; dp, depolarized; asterisks (*) indicate bands which vanish in the crystalline solid. [c] Determined in CS_2 solution. [d] Determined in cyclohexane solution.

Table 8. Observed[a] and calculated normal frequencies for 1,3-difluoropropane.

GG		*AG*		*GG″*		*AA*
Obs.	Calc.	Obs.	Calc.	Obs.	Calc.	Calc.
3004	3002(a)[b]		3001		3002(a′)[b]	3001(b_1)[b]
2999	2999(b)		3000		2999(a″)	3000(a_2)
2975	2943(a)		2942		2943(a′)	2942(a_1)
2945	2942(b)		2942		2942(a″)	2941(b_2)
2915	2918(b)		2917		2917(a′)	2917(b_1)
2867	2857(a)		2857		2858(a′)	2857(a_1)
1479	1526(a)	1476	1520		1525(a′)	1513(a_1)
1435	1510(b)	1440	1500		1512(a″)	1487(b_2)
1419	1457(a)	1400	1442		1454(a′)	1426(a_1)
1382	1397(b)		1389		1397(a″)	1383(a_1)
1363	1390(a)		1366		1391(a′)	1354(b_2)
1289	1346(b)	1325	1350		1347(a″)	1342(b_2)
1235	1262(a)	1250	1256		1262(a″)	1249(a_2)
1191	1150(b)		1136		1145(a″)	1146(b_1)
1126	1121(a)		1128		1135(a′)	1094(a_2)
1100	1104(b)		1085		1091(a″)	1056(b_1)
1052	1050(b)		1043		1058(a′)	1038(a_1)
1019	1036(a)	1021	1028		1034(a′)	1027(a_1)
917	981(a)	977	1017		953(a″)	1024(b_1)
943	966(b)	881	934		928(a″)	981(b_2)
863	835(a)	824	890		919(a′)	915(a_2)
778	823(b)	791	808		809(a′)	779(b_1)
536	553(a)	520	528		552(a′)	485(b_2)
416	435(a)	397	358		367(a″)	383(a_1)
252	275(b)	301	301	363	360(a′)	232(a_1)
182	173(b)	135	138		115(a″)	87(a_2)
94	90(a)		69		112(a′)	71(b_1)

[a] When possible, frequency values taken from the liquid spectra are given. [b] a and b represent symmetry species for C_2, a′ and a″ for C_s and a_1, a_2, b_1, b_2 for point group C_{2v}.

rule out the tempting supposition that it possesses a contribution from another conformer. The *AG* fundamentals in this region seem well accounted for otherwise. Finally, the band at 182 cm^{-1} seems to be type *B*; however, we still confidently assign it as ν_{27}.

Numerically, the fundamentals which we assign to the *AG* conformer show even closer agreement between calculated and observed values than they do for the *GG*. It must be kept in mind, though, that polarization data and band contours were of no use here and that the assignments were done only by the numbers.

In all the spectra perhaps the most interesting feature were the two (for each conformer) torsional modes to be found in the far IR. For the dominant conformer we identify these as the two bands found at 87 and 172 cm^{-1} in the vapour and shifting to 112 and 202 cm^{-1} in the infrared spectrum of the crystal. Both have Raman counterparts. It will be seen in Table 4 that the agreement with the calculated values is quite satisfying no matter which value is taken for F_ϕ. One of the torsions for the disappearing conformer must be identified with the band at 135 cm^{-1}; for the other we have no direct evidence. We do, however, note the band at 417 cm^{-1} which disappears upon crystallization. If we restrict ourselves to first overtones and binary combinations of conformer *AG*, this can only be the combination $\nu_{24}+\nu_{27}$ which leads to a value of about 75 cm^{-1} for the lower torsion. If true, this value is also in excellent agreement with that calculated. The series of medium to strong bands which appear between 45 and 90 cm^{-1} upon crystallization are obviously lattice modes.

Acknowledgements. We are grateful to Prof. W. Lüttke and Dr. J. Zeitzling, Göttingen, for providing us with a sample of the compound. We wish also to thank siv.ing. R. Seip for recording the electron diffraction data and ing. A. Horn for recording some of the spectra. Financial support from *Norges Almenviteskapelige Forskningsråd* is acknowledged.

REFERENCES

1. Hoffmann, F. W. *J. Org. Chem. 14* (1949) 105.
2. Thorbjørnsrud, J., Ellestad, O. H., Klæboe, P. and Torgrimsen, T. *J. Mol. Struct. 15* (1973) 61.
3. Lere-Porte, J. P., Petrissans, J. and Gromb, S. *J. Mol. Struct. 40* (1977) 159.
4. Meyer, A. Y. *J. Mol. Struct. 49* (1978) 383.
5. Lere-Porte, J. P. and Petrissans, J. *J. Mol. Struct. 48* (1978) 289.
6. Grindheim, S. and Stølevik, R. *Acta Chem. Scand. A 30* (1976) 625.
7. Farup, P. E. and Stølevik, R. *Acta Chem. Scand. A 28* (1974) 680.
8. Brown, J. K. and Sheppard, N. *Proc. R. Soc. London A 231* (1955) 555; Dempster, A. B., Price, K. and Sheppard, N. *Spectrochim. Acta A 25* (1969) 1381.
9. Braathen, M., Christensen, D. H., Klæboe, P., Seip, R. and Stølevik, R. *Acta Chem. Scand. A 33* (1979) 437.
10. Stølevik, R. *Acta Chem. Scand. A 28* (1974) 299.
11. Farup, P. E. and Stølevik, R. *Acta Chem. Scand. A 28* (1974) 871.
12. Thorbjørnsrud, J., Ellestad, O. H., Klæboe, P., Torgrimsen, T. and Christensen, D. H. *J. Mol. Struct. 17* (1973) 5.
13. Zeil, W., Haase, J. and Wegmann, L. Z. *Instrumentenkd. 74* (1969) 84.
14. Bastiansen, O., Graber, R. and Wegmann, L. *Balzers High Vacuum Report 25* (1969) 1.
15. Tamagawa, K., Iijima, T. and Kimura, M. *J. Mol. Struct. 30* (1976) 243.
16. Andersen, B., Seip, H. M., Strand, T. G. and Stølevik, R. *Acta Chem. Scand. 23* (1969) 3224.
17. Yates, A. C. *Comput. Phys. Commun. 2* (1971) 175.
18. Strand, T. G. and Bonham, R. A. *J. Chem. Phys. 40* (1964) 1686.
19. Gilbert, B. and Duyckaerts, G. *Spectrochim. Acta A 26* (1970) 2197.
20. Abraham, R. J. and Stølevik, R. *Chem. Phys. Lett. 58* (1978) 622.
21. Abraham, R. J. and Stølevik, R. *Chem. Phys. Lett. 77* (1981) 181.
22. Crowder, G. A. and Mao, H. K. *J. Mol. Struct. 18* (1973) 33.
23. Hirota, E. *J. Chem. Phys. 37* (1962) 283.
24. Sanderson, R. T. *Chemical Bonds and Bond Energy*, Academic, New York and London 1976.
25. Rydland, T. *Thesis*, University of Trondheim, Trondheim 1981, p. 20.
26. Gustavsen, J. E., Klæboe, P. and Stølevik, R. *J. Mol. Struct. 50* (1978) 285.
27. Gwinn, W. D. *J. Chem. Phys. 55* (1971) 477.
28. Stølevik, R., Seip, H. M. and Cyvin, S. J. *Chem. Phys. Lett. 15* (1972) 263.
29. Stølevik, R. *Acta Chem. Scand. A 31* (1977) 359.
30. Seip, H. M. and Stølevik, R. In Cyvin, S. J., Ed., *Molecular Structures and Vibrations*, Elsevier, Amsterdam 1972.
31. Morino, Y., Kuchitsu, K. and Oka, T. *J. Chem. Phys. 36* (1962) 1108.
32. Kuchitsu, K. *J. Chem. Phys. 49* (1968) 4456.
33. Altona, C. *Tetrahedron Lett. 19* (1968) 2325.
34. Crowder, G. A. and Mao, H. K. *J. Mol. Struct. 16* (1973) 165.
35. Harris, W. C., Holtzclaw, J. R. and Kalasinsky, V. F. *J. Chem. Phys. 67* (1977) 3330.

Received October 20, 1981.

Acta Chemica Scandinavica A 36 (1982) 485–488

The Influence of Various Monovalent Counterions on the Thermodynamics of Proton Dissociation of Polyacrylic Acid

GERD OLOFSSON and KONSTANTIN VLASENKO *

Thermochemistry Laboratory, Chemical Center, University of Lund, P.O. Box 740, S-220 07 Lund, Sweden

Differential enthalpies of proton dissociation of polyacrylic acid have been determined calorimetrically as a function of the degree of dissociation α in the presence of K^+, Cs^+, NH_4^+ and $(CH_3)_4N^+$ at 298.15 K. The apparent dissociation constant at various α was determined from potentiometric measurements and the Gibbs free energy and the entropy changes were calculated.

Up to α about 0.4 the enthalpy and entropy changes in the presence of the four ions in this study as well as Na^+ (previously reported) are about the same and decrease in a similar manner. At higher α, ΔH_a for Na^+, K^+ and Cs^+ are close together and vary only slightly with α but showing a trend towards less negative values above $\alpha = 0.75$. The entropy changes for the alkali metal ions are the same above $\alpha = 0.5$. The enthalpy and entropy changes become significantly less negative for NH_4^+ and significantly more negative for $(CH_3)_4N^+$ compared to the alkali metal ions at higher degrees of dissociation.

A comparison of the experimental values of ΔH_a for Na^+, K^+ and Cs^+ with theoretical values derived from a solution of the Poisson-Boltzmann equation shows a qualitative agreement except at the highest α. The differences at higher α between the theoretical and experimental curves for ΔH_a may for NH_4^+ and the alkali metal ions be due to complex formation between the cations and the polyanion while the point charge approximation in the theoretical model may be the reason for the discrepancy for $(CH_3)_4N^+$.

In a previous paper the enthalpy of proton dissociation ΔH_a of polyacrylic acid in sodium chloride solution as function of degree of dissociation α at three different temperatures was reported.[1] The experimental values were compared with a theoretical calculation of ΔH_a based on a solution of the Poisson-Boltzmann equation. The calculated ΔH_a is of the right order of magnitude and shows a correct α-dependence. The calculated decrease in ΔH_a is about -2 kJ mol^{-1} when α changes from 0 to 1. However, the observed enthalpy changes are more exothermic. The predicted temperature dependence of ΔH_a does not agree with experimental findings. Thus, although the electrostatic model provides an important insight into the behaviour of polyacrylic acid dissociation it can only partly describe interactions in the system. The size and nature of the counterions can be expected to influence the dissociation thermodynamics. Selective interaction between monovalent counterions and other polycarboxylates has been observed.[2] To study the influence of variation of counterion, ΔH_a of polyacrylic acid has been determined from calorimateric measurements at 298.15 K in the presence of K^+, Cs^+, NH_4^+ and $(CH_3)_4N^+$. Some additional experiments at higher α were made with Na^+ as counterion. Values of the apparent dissociation constant were derived from pH-measurements.

EXPERIMENTAL

Solid poly(acrylic acid) $[-CH_2CH(COOH)-]_n$ (Aldriche-Europe) with an average molecular weight of 250 000 was used without further treatment. The purity was checked by pH titration and was better than 97.0 ± 0.5 wt%. The polyacrylate + polyacrylic acid solutions (MePA + PAH, Me $= (CH_3)_4N^+$, Cs^+, K^+, Na^+ and NH_4^+) were

*On leave from Moscow Chemical-Technological Institute named after D. J. Mendeleev, Miusskaya pl. 9, SU-125047 Moscow A-47, USSR.

0302-4377/82/060485-04$02.50

Table 1. Differential enthalpies of dissociation ΔH_a of polyacrylic acid at various degrees of dissociation $\bar{\alpha}$ and total PAH concentration of 0.05 monomol kg^{-1} and Me^+ counterion concentration of 0.05 mol kg^{-1} ($Me^+ = Na^+, K^+, Cs^+, NH_4^+, (CH_3)_4N^+$) at 298.15 K.

$\bar{\alpha}$	ΔH_a/kJ mol^{-1} Na^+	K^+	Cs^+	NH_4^+	$(CH_3)_4N^+$
0.07	−0.86[a]	−1.67	−1.89	−0.92	−0.51
0.16	−2.19[a]	−2.23	−2.60	−1.92	−1.51
0.21	–	–	−2.81	–	–
0.26	−3.29[a]	−3.35	−3.48	−2.82	−2.67
0.36	−3.91[a]	−3.71	−3.96	−3.21	−3.41
0.46	–	−4.19	−4.17	−3.34	−4.03
0.56	−4.37[a]	−4.30	−4.47	−3.22	−4.71
0.66	–	−4.27	–	−2.92	−5.58
0.76	−4.64[a]	−4.15	−4.49	−2.49	−6.83
0.86	−4.36	−4.02	–	−1.51	−8.08
0.91	−4.02	–	–	–	–

[a] From Ref. 1.

prepared by neutralizing a stock solution of PAH with aqueous MeOH to the desired degree of neutralization α. Solid MeCl and water were then added to give solutions containing 0.05 mol kg^{-1} of Me^+ and 0.05 monomol kg^{-1} of ($PAH + PA^-$). The CsOH solution was freed from carbonate by running it through an ion-change column of Amberlite IRA 400. The samples of MeCl (of analytical grade) were dried before use. The molality of the HCl solution used in the calorimetric experiments was found from pH titration to be 0.5053 ± 0.0003 mol kg^{-1}.

The calorimetric measurements were made using an LKB-8721 reaction-solution calorimeter with a 100 cm^3 glass reaction vessel. The experiments were performed and evaluated as described in Ref. 3. The pH-measurements were made using a Radiometer GK 2401C combination electrode.

RESULTS

In the calorimetric measurements 0.4×10^{-3} mol HCl (0.8 g of a 0.5 mol kg^{-1} solution) was added to 100 cm^3 of solution containing 0.05α mol kg^{-1} MePA + 0.05(1-α) mol kg^{-1} PAH + 0.05(1-α) mol kg^{-1} MeCl. Three to four experiments were made at each α. The pH of the initial and final solutions was

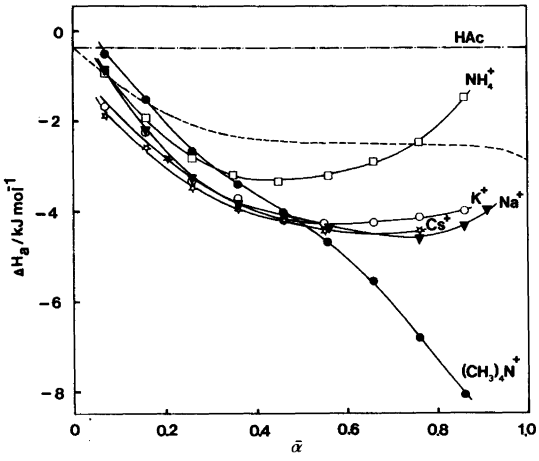

Fig. 1. ΔH_a of polyacrylic acid at various degrees of ionization α in the presence of various counterions. – – –, Theoretical curve (Ref. 1).

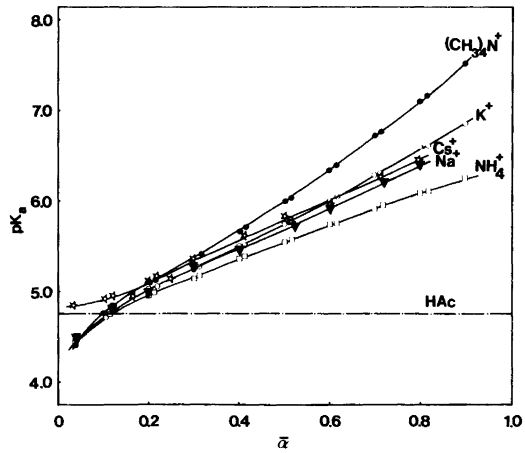

Fig. 2. Apparent pK_a of polyacryclic acid at various α in the presence of various counterions.

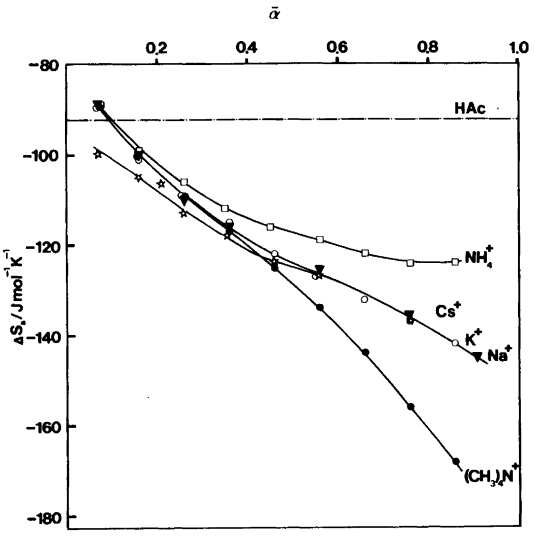

Fig. 3. ΔS_a of polyacrylic acid at various degrees of ionization in the presence of various counterions.

measured and the amount of HCl not reacting with the polyacrylate ion was estimated. The change in the degree of dissociation was 0.08 except at $\alpha = 0.10$ where it was 0.06. The observed enthalpy changes ΔH_{obs} are the sum of the enthalpy of protonation of polyacrylate ion and the enthalpy of dilution of HCl. The enthalpy of proton dissociation ΔH_a was calculated from

$$\Delta H_a = -\Delta H_{obs} + \Delta H_{diln}(HCl)$$

where $\Delta H_{diln}(HCl)$ denotes the enthalpy change for the infinite dilution of 0.51 mol kg^{-1} HCl. At 298.15 K, $\Delta H_{diln}(HCl)$ is -1.176 kJ mol^{-1}.[4] A more detailed description of the evaluation of ΔH_a is given in Ref. 1. Values of ΔH_a found in the present study are given in Table 1. Previously reported values in the presence of Na^+ are included. The mean degree of dissociation $\bar{\alpha}$ is shown in the first column and the found values of ΔH_a in the presence of the indicated cation are shown in the following columns. The estimated uncertainty expressed as twice the overall standard deviation of the mean is 0.10 kJ mol^{-1}. To illustrate the α-dependence for the various counterions, values of ΔH_a are plotted against $\bar{\alpha}$ in Fig. 1. Included in the figure is a curve representing the theoretical values of ΔH_a for polyacrylic acid as function of α calculated from a solution of the Poisson-Boltzmann equation.[1] The enthalpy of dissociation of acetic acid is assumed to equal the enthalpy of proton dissociation of an isolated carboxyl group.

Values of the apparent dissociation constant were calculated from the results of the pH measurements: $pK_a = pH + {}^{10}\log(1-\alpha)/\alpha$. The found values are summarized in Fig. 2. Estimates of the entropy change ΔS were calculated from

$$\Delta S_a = \Delta H_a/T - R \ln 10 pK_a$$

Fig. 3. shows a plot of ΔS_a as function of $\bar{\alpha}$ for the various counterions, ΔS_a for acetic acid is included in the figure.

DISCUSSION

The entropy changes ΔS_a are strongly negative and dominate the proton dissociation equilibrium of polyacrylic acid. Although the enthalpy changes ΔH_a become more exothermic with increasing α, ΔS_a decreases more rapidly leading to increasing values of pK_a. Up to α of 0.4 there are only minor differences in ΔH_a and ΔS_a between the various counterions. There is, however, a small but significant spread at the lowest α which may indicate specific interaction between Cs^+ and the undissociated polyacid. At the higher α the curves representing ΔH_a and ΔS_a continue to lie close together for the three alkali metal ions. There is a qualitative agreement between the theoretical curve calculated for ΔH_a and the experimental curves except at the highest α where the experimental curves indicate a trend towards less exothermic values. The differences between the Na^+, K^+ and Cs^+ ions are apparently too small to have any significant influence on the measured properties of the ionization of polyacrylic acid.

It sppears that the NH_4^+ is more effective and the large $(CH_3)_4N^+$ less efficient than the alkali metal ions in screening the carboxylate groups and thus reducing the effective charge density of the polyion. In the theoretical calculation of ΔH_a the counterions are treated as point charges. This approximation can be expected to give significant errors for systems with large ions and this is probably the main reason for the divergence of the experimental curve for $(CH_3)_4N^+$ from the calculated curve in Fig. 1. A plot of ΔH_a against ΔS_a gives for $(CH_3)_4N^+$ an approximately straight line over the whole α-range with a slope of about -100 K. The curves for the

smaller ions are linear and parallel to the line for $(CH_3)_4N^+$ up to α about 0.5. At higher α the curve for NH_4^+ turns sharply upwards while the curves for the alkali metal ions bend away from the $(CH_3)_4N^+$ line to become almost parallel to the ΔS_a-axis. Alkali metal ions are known to form complexes with ions of di- and tricarboxylic acids [5,6] and it seems likely that complex formation will also occur in polyacrylate solutions. The NH_4^+ ion has the possibility to form hydrogen bonds which could lead to more extensive complex formation and accordingly more effective screening than the alkali metal ions. The tendency for $(CH_3)_4N^+$ to interact specifically with the polyacrylate ion should be small and non-specific interactions can be expected to dominate. The differences between the theoretical and experimental curves for ΔH_a (Fig. 1) may therefore for the smaller ions be due to specific interactions between the cations and the polyanion while for $(CH_3)_4N^+$ it may be due to the point charge approximation in the theoretical model.

Acknowledgement. This work was supported by grants from the Swedish Natural Science Research Council.

REFERENCES

1. Gunnarsson, G., Wennerström, H., Olofsson, G. and Zacharov, A. *J. Chem. Soc. Faraday Trans. 1 76* (1980) 1287.
2. Quadrifoglio, F., Crescenzi, V. and Delben, F. *Macromolecules 6* (1973) 301.
3. Olofsson, G. and Olofsson, I. *J. Chem. Thermodyn. 9* (1977) 65.
4. Parker, V. D. *Thermal Properties of Aqueous Uni-Univalent Electrolytes*, NSRDS NBS, U.S. Gov. Print. Off., Washington 1965.
5. Daniele, P. G., Rigano, C. and Sammartano, S. *Ann. Chim. (Rome) 70* (1980) 119.
6. Arena, G., Cali, R., Grasso, M., Musumeci, S. and Sammartano, S. *Thermochim. Acta 36* (1980) 329.

Received September 24, 1981.

Acta Chemica Scandinavica A 36 (1982) 489–494

Carbon-13 Nuclear Magnetic Resonance Studies on Platinum(II) Complexes of Alicyclic 1,2-Diamines

TRILLE LIND and HANS TOFTLUND

Department of Chemistry, University of Odense, DK-5230 Odense M, Denmark

A series of new *cis*-diammino(diamine)platinum(II) chlorides, where the diamines are seven different 1,2-cycloaliphatic diamines, have been prepared, and the ^{13}C NMR spectra have been obtained. ^{13}C chemical shifts resemble those of the diamine dihydrochlorides with a *ca.* 10 ppm downfield shift of C(a) due to the platinum binding.

$^{2}J_{PtNC}$ in the chelate rings varies from 0 to 13.5 Hz, increasing with the strain in the chelate ring. $^{3}J_{PtNCC}$ values of 0 to 53.7 Hz were obtained. From these data and the relevant X-ray crystal data a Karplus-type dependence was found for $^{3}J_{PtNCC} = 54 \cos^2\phi$ where ϕ is the dihedral angle Pt–N–C–C.

The fact that the three-bond coupling constants $^{3}J_{PtNCC}$ normally are easily determined in the proton-decoupled carbon-13 NMR spectra of platinum(II) diamine complexes has resulted in several investigations on the conformational behavior of diamine and amino acid complexes of platinum(II).[1-5] The data have been interpreted by assuming a Karplus-type angular dependence with the dihedral angles in the four atom fragments Pt–N–C–C. It has been suggested that the variation of $^{3}J_{PtNCC}$ fits the simple relationship:

$$^{3}J_{PtNCC} = k \cos^2 \phi$$

ϕ being the dihedral angle between the planes Pt–N–C and N–C–C[2-4] and k being a constant. As most of the investigated complexes undergo rapid conformational inversion on the NMR time scale, the reported coupling constants represent average values of at least two conformers. In order to explore the true dihedral angle dependence of $^{3}J_{PtNCC}$ we have examined the ^{13}C NMR spectra of several new square–planar platinum(II) complexes with cyclic aliphatic 1,2-diamines. For these complexes, the range of possible geometries are restricted even in solution. Using reported X-ray crystal structural data it has been possible to find the relevant dihedral angles and check the reliability of the Karplus relationship for this kind of system.

Stereochemistry. As for the alicyclic condensed ring systems (hydrindanes and pentalanes) the systems obtained by fusing a five-membered chelate ring to an aliphatic ring give two strainless modifications differing in the type of locking (*cis*- or *trans*-) at the bridge. Cyclic *cis*-1,2-diamines lead to *cis*-fused systems and *trans*-1,2-diamines to *trans*-fused systems. In the fused ring systems several constrains are put on the involved angles. Especially the range of dihedral angles are far more restricted than for single ring systems. For the *cis*-fused systems the chelate ring will be least puckered when the alicyclic ring is nearly planar, whereas for the *trans*-fused systems the opposite trend will be seen. The *trans*-1,2-diamines are chiral and will only be able to coordinate with both the amino–groups in equatorial positions. For a given chirality of the 1,2-diamine the conformation (δ or λ) of the chelate ring is defined and no conformational inversions are possible in the complex. The *cis*-1,2-diamines are *meso* ligands with one amino-group axial and the other equatorial, the complexes will be *enantiotopic*, and in a *symmetrical* environment the potential energy of the δ and λ conformations of the chelate ring will be equal and the inversions are expected to occur easily.

0302-4377/82/060489-06$02.50

RESULTS AND DISCUSSION

Preparations. The dihydrochlorides of the cyclic 1,2-diamines were prepared according to methods reported in the literature,[6-8] except for the two isomers of *trans*-trimethyl-1,2-cyclohexanediamine (3,5,5-tmchxn and 3,3,5-tmchxn), which were separated from a commercial isomer mixture of "isophoronediamines".[9]

To ensure high solubility of all the samples used in the NMR experiments and to avoid complications due to steric or chemical interactions from other ligands, we have chosen a homologous series of *cis*-diammino(1,2-diamine)platinum(II) chlorides in our investigation. These salts were prepared in two steps. First the slightly soluble *cis*-dichloro(1,2-diamine)platinum(II) compounds were prepared by neutralization of a 70 °C warm aqueous solution of equimolar amounts of 1,2-diamine dihydrochloride and potassium tetrachloroplatinate(II) with sodium hydroxide (1 M). The *cis*-diammino(1,2-diamine)-platinum(II) chlorides were prepared by suspending the *cis*-dichloro(1,2-diamine)platinum(II) compounds in a 60 °C warm ammonia solution (2 M) until a complete dissolution was achieved. The *cis*-dichloro-*trans*(trimethyl-1,2-cyclohexanediamine)-platinum(II) compounds turned out to be too insoluble for this procedure to be usefull, so in these cases we reacted *cis*-dichlorodiamminoplatinum(II) with the pertinent diamines. For the two 1,2-cyclohexanediamines (chxn) the bis(chxn)platinum-(II) complexes were also prepared. Using optically pure *trans*-*R*,*R*-chxn only one isomer is possible.[11] For the bis(*cis*-*R*,*S*-chxn)platinum(II) complex two isomers exist, distinguished by the spatial arrangement (*cis* or *trans*) of the optical centers. Only one of these isomers, probably the "*trans*" isomer, was isolated. *trans*-$[Pt(RR\text{-}chxn)_2Cl_2]Cl_2$ was obtained by chlorination of the corresponding platinum(II) salt, as described earlier.[11]

The elemental analyses (Pt,C,H,N,Cl) were all

Table 1. ^{13}C NMR chemical shifts for cyclic 1,2-diammonium chlorides.

Compound	ppm C(a)	C(b)	C(c)	CH_3
(*c*-cbnH_2)$^{2+}$	48.49	23.45		
(*t*-cbnH_2)$^{2+}$	49.38	21.73		
(*c*-cptnH_2)$^{2+}$	53.75	28.07	20.01	
(*t*-cptnH_2)$^{2+}$	56.10	30.68	22.62	
(*c*-chxnH_2)$^{2+}$	50.96	26.77	21.25	
(*t*-chxnH_2)$^{2+}$	53.18	30.31	23.80	
(3,3,5-tmchxnH_2)$^{2+}$	61.09	38.85	47.76	26.15
	51.04	35.70	28.88	21.57
				19.91
(3,5,5-tmchxnH_2)$^{2+}$	59.33	42.74	45.86	31.89
	50.92	31.89	31.17	24.81
				18.58

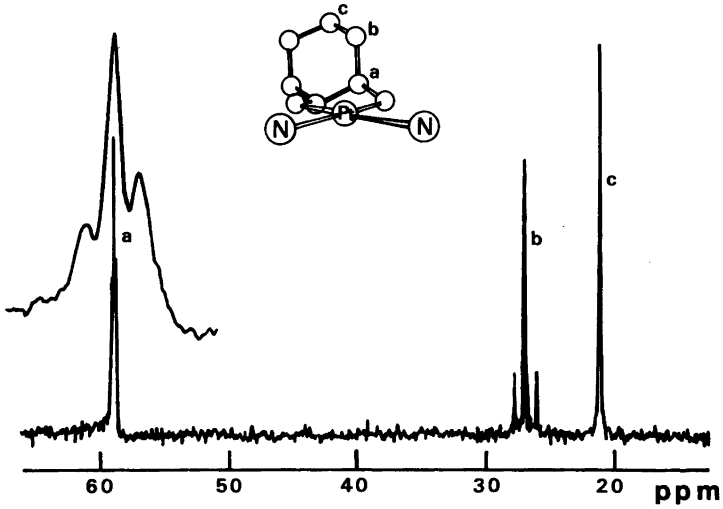

Fig. 1. The proton-decoupled 15.03 MHz ^{13}C NMR spectrum of *cis*-diammino-*cis*-1,2-cyclohexanediamine platinum(II) chloride in D_2O (0.5 M).

Table 2. ^{13}C NMR chemical shifts (ppm) and coupling constants (^{195}Pt – ^{13}C; Hz) for [Pt(1,2-diamine)$(NH_3)_2$]$^{2+}$ complexes.

Compound	C(a)	C(b)	C(c)	CH_3	$^{2,3}J_{PtC}$	$^{3}J_{PtC}$
[Pt(*c*-cbn)$(NH_3)_2$]$^{2+}$	59.50	24.20				<2
[Pt(*c*-cptn)$(NH_3)_2$]$^{2+}$	64.31	29.18	20.97			22.6
[Pt(*t*-cptn)$(NH_3)_2$]$^{2+}$	68.16	23.96	26.31		13.4	37.2
[Pt(*c*-chxn)$(NH_3)_2$]$^{2+}$	58.87	26.92	21.25		3.9	24.7
[Pt(*c*-chxn)$_2$]$^{2+}$	58.26	26.99	21.34		4	24.9
[Pt(*t*-chxn)$(NH_3)_2$]$^{2+}$	62.57	33.15	24.93		7.1	52.6
[Pt(*t*-chxn)$_2$]$^{2+}$	62.20	33.17	24.97			50.8
[Pt(*t*-chxn)$_2$Cl$_2$]$^{2+}$	62.76	32.51	24.51			29.9
[Pt(3,3,5-tmchxn)$(NH_3)_2$]$^{2+}$	70.54	41.81	48.53	27.77		50.0
	58.89	36.02	28.90	21.41		44.6
				19.51		
[Pt(3,5,5-tmchxn)$(NH_3)_2$]$^{2+}$	68.93	45.57	46.91	31.81		53.7
	59.98	31.84	32.46	25.50		46.4
				18.21		

satisfactory except for the *trans*-1,2-cyclobutanediamine (*trans*-cbn) complex, which contained an excess of nitrogen and chloride. In this case the product probably is polynuclear, due to the inability of *trans*-cbn to function as a bidentate ligand.

^{13}C NMR spectra. Typical features of the proton decoupled 15.03 MHz ^{13}C NMR spectra of these compounds are illustrated by the spectrum of [Pt(*cis*-chxn)$(NH_3)_2$]Cl_2 (0.5 M in D_2O), Fig. 1. The fact that only three resonances are seen confirm the bidentate nature of the ligand and shows that the conformational inversion is rapid on the NMR time scale. The data for all the ligands and the platinum complexes are given in Tables 1 and 2. Generally the resonances were assigned through the well-established rule that the C atoms next to the electronegative nitrogen C(a) are shifted more downfield than the other C atoms. These assignments were confirmed by the off-resonance spectra, showing a doublet for C(a) and triplets for the other C atoms. The coupling to ^{195}Pt ($I=\frac{1}{2}$, 33 % abundance) is expected to give rise to two satellite peaks of 17 % intensity, one on each side of the main peak, as indeed is seen in many cases.

^{13}C chemical shifts. The ^{13}C chemical shifts of the dihydrochlorides of the 1,2-diamine ligands are characteristic compared to other known diammonium salts.[1-5] On complexation to platinum(II) a downfield shift of about 10 ppm for the C(a) and a few ppm for the other C atoms is seen. The effect on the C atoms neighbour to nitrogen arises in part from electron withdrawal from the N atoms on the covalent binding to platinum(II). Only in the case of the *trans*-1,2-cyclopentanediamine (*trans*-cptn) platinum(II) complex is a marked deviation from this pattern observed. Most remarkable is the large upfield shift of C(b) (6.7 ppm) causing it to appear at higher field than the C(c). The same trend is observed for the [Co(*trans*-cptn)$_3$]Cl_3 salt.[10] It is difficult to rationalize this result within the present knowledge of ^{13}C NMR chemical shifts, but no doubt the effect is connected to the strain introduced in the cyclopentane ring on coordination. It is remarkable that the δ value for C(b) in [Pt(*cis*-cbn)$(NH_3)_3$] also is unusually small, here reflecting the strain in the cyclobutane ring. The change of the oxidation state of the platinum from II to IV has practically no influence on the ^{13}C NMR chemical shifts.

$^{195}Pt-^{13}C$ Coupling constants. The $^{2}J_{PtNC}$ coupling constants for the five-membered chelate diamine rings are given in Table 2. They are usually

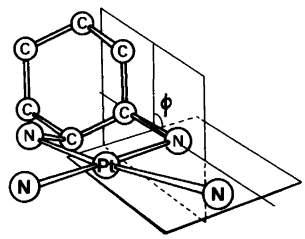

Fig. 2. The *cis*-diammino-(*cis*-1,2-cyclohexanediamine) platinum(II) ion, where one of the two Pt –N–C–C dihedral angles ϕ are outlined.

small or zero, which can be explained by a multipath coupling mechanism, as suggested by Erickson *et al.*[2] The coupling is regarded as the sum of couplings *via* a two-bond and a three-bond path through the chelate ring, where the ^2J and ^3J are assumed to have similar magnitude, but opposite signs. It is remarkable that the largest observed $^{2,3}J_{PtNC}$ coupling constant (13.4 Hz) is seen for [Pt(*trans*-cptn)$(NH_3)_2$]$^{2+}$, where the chelate ring is expected to be more puckered than usual, due to strain from the nearly planar cyclopentane ring. Among the platinum(II) complexes with cyclic *cis*-1,2-diamines, only the most strained one, *cis*-chxn, shows a $^{2,3}J$ coupling (3.5 Hz). In Fig. 3 the observed $^{2,3}J_{PtNC}$ coupling constants are plotted as a function of $\cos^2\alpha$, where α is the dihedral angle of the chelate ring, N−C(a)−C(a)′−N′ as found in the respective X-ray analysis[11,12,15] (for *cis*-cbn and *cis*-cptn, however, only estimated from models). Due to the strain in five-membered chelate rings α will be proportional to the Pt−N−C(a)−C(a)′ dihedral angle ϕ, which is expected to determine the $^3J_{PtNCC}$ coupling *via* a Karplus relation of the type $J = k\cos^2\phi$.* The points define a straight line with a slope of −50 Hz. The intercept on the $^{2,3}J$ axis of 24 Hz, corresponding to no contribution from the ^3J path, should reflect the ^2J and this value is actually in good agreement with values found for platinum(II) complexes of aliphatic monamines (appr. 25 Hz).[2,4] Thus the useful relation (1) seems to work. It is remarkable that the relation also holds for aromatic ligands as bipyridine, where $\alpha = 0$ gives $J = -26$ Hz in agreement with the value found by Erickson.[4] (28 −32 Hz.)

$$^{2,3}J_{PtNC} = {}^2J_{PtNC} - {}^3J_{PtNCC} = 24 - 50\cos^2\alpha \qquad (1)$$

The $^3J_{PtNCC}$ coupling constants to C(b) show the largest variation through the series (0 to 53.7 Hz). The coupling constants are smallest for the *cis*

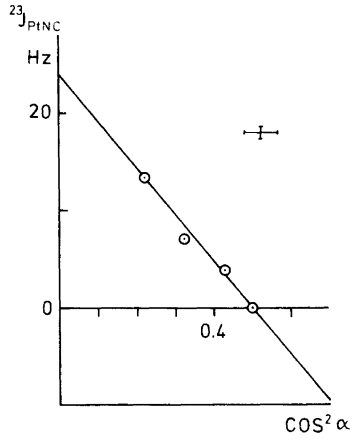

Fig. 3. A plot of the coupling constant $^{2,3}J_{PtNC}$ for the chelate ring as a function of $\cos^2\alpha$, where α is the dihedral angle $N_1-C_1-C_2-N_2$. The bars indicate the uncertainties.

complexes. Because of the rapid conformational inversion of the chelate ring in these complexes an averaged coupling to the methylene groups, spending equal times in equatorial and axial orientations, are seen. The unsymmetrical structure of a coordinated *cis*-chxn has recently been demonstrated through the X-ray crystal structure of [Pt(*cis*-chxn)Cl_2].[15] The geometry is shown in Fig. 2 for the corresponding *cis*-diammino complex and the dihedral angle ϕ for the axial methylene is depicted. From the data a value of 98° for the axial and 160° for the equatorial methylene group were calculated. Similar data were found from the crystal analysis of the *fac*-Δ-[Co(*cis*-chxn)$_3$]Cl_3, by Bernal.[14] Assuming a rapid conformational interchange in solution a time-averaged environment between the two conformers yields an average ϕ of 129°. We tried to estimate the rate of the conformational interchange by recording the ^{13}C NMR spectrum of [Pt(*cis*-chxn)$(NH_3)_2$]$(CF_3COO)_2$ in methanol at −100 °C. Apart from some broadening of the lines, no changes were observed in the spectrum compared to that at room temperature. As a separation of about 100 Hz between the resonances of an equatorial and an axial carbon atom is expected we see that even at −100 °C the rate is very high. In chelated *trans*-cptn, *trans*-chxn, *trans*-3,3,5-tmchxn and *trans*-3,5,5-tmchxn the conformational changes are locked and the C(b) are necessarily equatorial all the time. The

*The structure of a five-membered ring is completely specified by 9 independent parameters, so if just 5 distances and 3 angles (*e.g.* 2 interatomic angles and one dihedral angle) are specified, the remaining angles are interdependent. If it is assumed that the interatomic distances and angles are fixed the conformational changes of the ring can be described with a single dihedral angle and an interdependence will exist between this and the other dihedral angles. With data from the 1,2-diamineplatinum(II) structures,[11,15] the following relation is found for the five-membered chelate ring: $\cos\phi = 0.28 + 0.78\cos\alpha$. The relation is only defined for α larger than 23° ($\phi = 0$), excluding strain-free planar chelate rings.

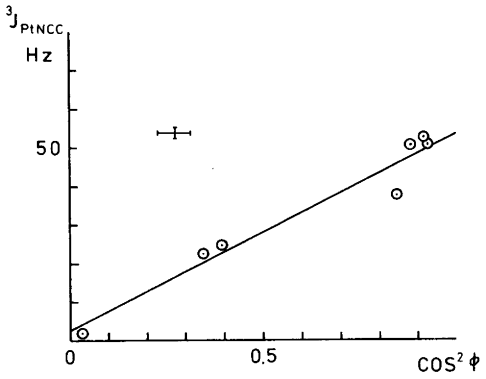

Fig. 4. A plot of the coupling constant $^3J_{PtNCC}$ as a function of $\cos^2\phi$, where ϕ is the angle defined in Fig. 2. The bars indicate the uncertainties.

$^3J_{PtNCC}$ values fall in the range 37.2 to 53.7 Hz. Because of the very stiff nature of the fused ring systems crystallographic data should give quite reliable data for the dihedral angle. Using data reported for $\Lambda(\delta\delta\delta)(lel)_3[Co(S,S\text{-cptn})_3]Cl_3$,[12] $\Delta(\delta\delta\delta)(lel)_3[Co(RR\text{-chxn})_3]Cl_3 5H_2O$ [13] and [Pt-(*R*,*R*-chxn)$_2$Cl]Cl$_2$,[11] we calculated ϕ values of 157, 162 and 164°, respectively (suggesting an uncertainty of +3° in the values). No structural data for coordinated *cis*-cbn are available, but by using data for 1,2-*cis*-cyclobutanedicarboxylic acid [17] and again assuming rapid conformational change, an average ϕ value very close to 90° is predicted. An average value for *cis*-cptn of 126° was estimated from molecular models. The validity of the Karplus relationship for the $^3J_{PtNCC}$ of the cyclic 1,2-diamine platinum(II) complexes is demonstrated by the plot of $^3J_{PtNCC}$ as a function of $\cos^2\phi$ in Fig. 4. It is seen that the best straight line through the points passes the origo, showing that no constant term is needed in the expression (2). That the point for *trans*-cptn is significantly below the line, might be due to the considerable strain in this system, weakening the Pt–N bond.

$$^3J_{PtNCC} = 54\cos^2\phi \qquad (2)$$

Expressions (1) and (2) might have useful applications in the determination of the conformation of amine platinum(II) complexes, however, the coupling constants show some variation with substitution at the involved atoms.[4] The corrections for methyl substitution at carbon can be obtained from the isomeric trimethyl-*trans*-1,2-cyclohexanediamine platinum(II) salts. Assuming that the substitution does not lead to large changes in the cyclohexanering geometry, the correction for one CH_3 substitution at C(b) will be a 12% reduction in $^3J_{PtNCC}$ corresponding to (2'). Substitution of two hydrogens for two CH_3 at the same carbon atom will lead to a 15% reduction of $^3J_{PtNCC}$ corresponding to (2'').

$$^3J_{PtNCC} = 47\cos^2\phi \qquad (2')$$

$$^3J_{PtNCC} = 46\cos^2\phi \qquad (2'')$$

Similar expressions are expected to work for the *J* values of methyl-substituted chelate rings. For substitution at a single carbon, eqn. (1') and for dimethyl substitution at one carbon atom, eqn. (1''). The predicted $^{2,3}J_{PtNC}$ for the 1,2-propylenediamine and isobutanediamine platinum(II) complexes (assuming $\alpha = 51°$ as in the crystal structure of [Pt(*R*-pn)$_2$]Cl$_2$ [19]) are then 7 and 8 Hz respectively, in agreement with the experimental values of 6 and 8 Hz.[4]

$$^{2,3}J_{PtNC} = 24 - 44\cos^2\alpha \qquad (1')$$

$$^{2,3}J_{PtNC} = 24 - 42\cos^2\alpha \qquad (1'')$$

By oxidation of [Pt(*trans*-chxn)$_2$]$^{2+}$ to [Pt(*trans*-chxn)$_2$Cl$_2$]$^{2+}$ the $^3J_{PtNCC}$ is nearly halved. This is understandable if it is assumed that the *s*-character on Pt is shared equally by all ligands. Then a change from square–planar to octahedral coordination should reduce the *s*-character in the Pt–N bonds with a factor of 0.67, not far from the 0.57 found.

EXPERIMENTAL

1. *Preparation of the 1,2-diamines.* cis *and* trans-*1,2-cyclobutanediamine* (*cis* and *trans*-cbn) were prepared from the 1,2-cyclobutanedicarboxylic acids by double Curtius degradations of the azides according to Buchman.[6] Yields as the dihydrochlorides: 20% (Anal. $C_4H_{12}N_2Cl_2$: C, H, N, Cl).

cis *and* trans-*1,2-cyclopentanediamine* (*cis* and *trans*-cptn) were prepared according to Toftlund [7] by reduction of 1,2-cyclopentanedionedioxime. Yields as the dihydrochlorides: 20% (Anal. $C_5H_{16}N_2Cl_2$: C, H, N, Cl).

cis- *and* trans-*1,2-cyclohexanediamine* (*cis* and *trans*-chxn) were prepared according to Toftlund [8]

and Galsbøl.[16] Yields as the dihydrochlorides: 10 and 60%. (Anal. $C_6H_{16}N_2Cl_2$: C, H, N, Cl).

trans-*3,3,5-Trimethyl-1,2-cyclohexanediamine* (3,3,5-tmchxn) and trans-*3,5,5-trimethyl-1,2-cyclohexanediamine* (3,5,5-tmchxn) were separated from a crude product of "isophoronediamine" purchased from VEBA-Chemie. The work-up was done *via* the nickel(II) complex chlorides as described elsewhere.[9] Yields as the dihydrochlorides: 8 % (Anal. $C_9H_{22}N_2Cl_2$: C, H, N, Cl).

2. *Preparation of the* cis-*diammino(diamine)platinum(II) chlorides.* The yellow *cis*-dichloro(diamine)-platinum(II) compounds were prepared in accordance with the procedure for the corresponding ethylenediamine complex.[18]

The colourless *cis*-diammino(diamine)platinum-(II) chlorides were obtained by stirring the corresponding *cis*-dichloro(diamine)platinum(II) compounds with ammonia solutions (2 M) at 70 °C for several hours. The resulting solutions were evaporated *in vacuo* and the salts were precipitated with ethanol (96 %). Yield: *cis*-$[Pt(cis\text{-cbn})(NH_3)_2]Cl_2$ 33 %. (Anal. $[Pt(C_4H_{10}N_2)(NH_3)_2]Cl$: Pt, C, H, N, Cl), *cis*-$[Pt(cis\text{-cptn})(NH_3)_2]Cl_2$ 50 % (Anal. $[Pt(C_5H_{12}N_2)(NH_3)_2]Cl_2$: Pt, C, H, N, Cl), *cis*-$[Pt(trans\text{-cptn})(NH_3)_2]Cl_2$ 60 % (Anal. $[Pt(C_5H_{12}N_2)(NH_3)_2]Cl_2$: Pt, C, H, N, Cl), *cis*-$[Pt(cis\text{-chxn})(NH_3)_2]Cl_2$: 70 % (Anal. $[Pt(C_6H_{14}N_2)(NH_3)_2]Cl_2$: Pt, C, H, N, Cl), *cis*-$[Pt(trans\text{-chxn})(NH_3)_2]Cl_2$: 70 % (Anal. $[Pt(C_6H_{14}N_2)(NH_3)_2]Cl_2$: Pt, C, H, N, Cl).

The platinum complex obtained starting from the *trans*-1,2-cyclobutanediamine was not pure and probably polymeric, as it shows broad ^{13}C NMR lines. Yield: 33 % (Anal. Found: C 12.4: H 4.0: N 10.3: Cl 16.5: Pt 48.6, Calc. for $[Pt(C_4H_{10}N_2)(NH_3)_2]Cl_2$: C 12.4: H 4.14: N 14.5: Cl 18.4: Pt 50.5).

In the case of the two *trans*-trimethyl-1,2-cyclohexanediamines the *cis*-dichloro(diamine)platinum-(II) compounds were not dissolvable in ammonia solutions, even after stirring for several days at 90 °C. Instead the two *cis*-diamine salts were obtained by reacting a suspension of *cis*-dichlorodiamminoplatinum(II) with the *trans*-trimethyl-1,2-cyclohexanediammonium chlorides and slowly neutralizing the solutions with sodium hydroxide at 70 °C. When *cis*-dichloro-diamminoplatinum(II) was dissolved, the solutions were evaporated *in vacuo* and the products were precipitated with ethanol (96 %). Yield of *cis*-$[Pt(3,3,5\text{-tmchxn})(NH_3)_2]Cl_2$: 58 % (Anal. $[Pt(C_9H_{20}N_2)(NH_3)_2]Cl_2$: Pt, C, H, N, Cl). Yield of *cis*-$[Pt(3,5,5\text{-tmchxn})(NH_3)_2]Cl_2$: 57 % (Anal. $[Pt(C_9H_{20}N_2)(NH_3)_2]Cl_2$: Pt, C, H, N, Cl).

3. *Bis*[(−)*1*R,*2*R-*cyclohexanediamine*]*platinum(II) chloride.* This salt was obtained as described by Toftlund.[11] Yield: 84 % (Anal. $[Pt(C_6H_{14}N_2)_2]Cl_2$: Pt, C, H, N, Cl).

Bis[cis-*1,2-cyclohexanediamine*]*platinum(II) chloride.* Was prepared analogous to the above compound. Yield: 80 % (Anal. $[Pt(C_6H_{14}N_2)_2]Cl_2$: Pt, C, H, N, Cl).

4. trans-*Dichloro-bis*[(−)-*1*R,*2*R-*cyclohexanediamine*]*platinum(IV) chloride*, was prepared as described by Toftlund.[11] Yield: 75 % (Anal. $[Pt(C_6H_{14}N_2)_2Cl_2]Cl_2$: Pt, C, H, N, Cl).

5. *Measurements.* All the ^{13}C NMR spectra were recorded on a 15.03 MHz JEOL FX-60 NMR spectrometer. The solvent was in every case D_2O (approx. 0.5 M) with a little methanol as reference.

Acknowledgement. The authors are greatly indebted to Dr. J. P. Jacobsen for many helpful discussions.

REFERENCES

1. Bagger, S. *Acta Chem. Scand. A 28* (1974) 467.
2. Erickson, L. E., Sarneski, J. E. and Reilley, C. N. *Inorg. Chem. 14* (1975) 3007.
3. Pregosin, P. S. and Sze, S. N. *Helv. Chim. Acta 60* (1977) 2514.
4. Erickson, L. E., Sarneski, J. E. and Reilley, C. N. *Inorg. Chem. 17* (1978) 1701.
5. Yano, S., Tukada, T., Saburi, M. and Yoshikawa, S. *Inorg. Chem. 17* (1978) 2520.
6. Buchmanm, E. R., Reims, A. O., Skei, T. and Schlatter, M. J. *J. Am. Chem. Soc. 64* (1942) 2696.
7. Toftlund, H. and Pedersen, E. *Acta Chem. Scand. 26* (1972) 4019.
8. Toftlund, H. and Laier, T. *Acta Chem. Scand. A 31* (1977) 651.
9. Toftlund, H. *To be published.*
10. Kunimatsu, M., Kanno, H., Kojima, M., Kashiwabara, K. and Fujta, J. *Bull. Chem. Soc. Jpn. 53* (1980) 1517.
11. Larsen, K. P. and Toftlund, H. *Acta Chem. Scand. A 31* (1977) 182.
12. Ito, M., Marumo, F. and Saito, Y. *Acta Crystallogr. B 27* (1971) 2187.
13. Marumo, F., Utsumi, Y. and Saito, Y. *Acta Crystallogr. B 26* (1970) 1492.
14. Bernal, I., Toftlund, H. and Laier, T. *Acta Chem. Scand. Submitted for publication.*
15. Lock, C. J. L. and Pilon, P. *Acta Crystallogr. B 37* (1981) 45.
16. Galsbøl, F., Steenbøl, P. and Sørensen, B. S. *Acta Chem. Scand. 26* (1972) 3605.
17. Van der Helm, D., Hsu, I-Nan and Sims, J. M. *Acta Crystallogr. B 28* (1972) 3109.
18. Johnson, G. L. and Michelfeld, T. A. *Inogr. Synth. 8* (1966) 242.
19. Maeda, C., Matsumoto, K. and Ooi, S. *Bull. Chem. Soc. Jpn. 53* (1980) 1755.

Received October 5, 1981.

Acta Chemica Scandinavica A 36 (1982) 495–499

The Molecular Structures of Trimethylindium and Trimethylthallium Determined by Gas Electron Diffraction

TORGNY FJELDBERG,[a] ARNE HAALAND,[b,*] RAGNHILD SEIP,[b] QUANG SHEN[c] and JOHAN WEIDLEIN[d]

[a] Department of Chemistry, University of Trondheim NLHT, Trondheim, Norway, [b] Department of Chemistry, University of Oslo, Blindern, Oslo 3, Norway, [c] Department of Chemistry, Colgate University, Hamilton, New York 13346, U.S.A. and [d] Institut für Anorganische Chemie der Universität Stuttgart, D-7 Stuttgart 80, Germany

The gas electron diffraction patterns of trimethylindium and trimethylthallium have been recorded with nozzle temperatures of 50 to 60 °C and 30 to 45 °C, respectively. The diffraction patterns are consistent with molecular models with planar MC_3 skeletons and freely rotating methyl groups. The M–C bond distances (r_a) are In–C = 2.161(3) Å and Tl–C = 2.206(3) Å. The variation of M–C bond distances among methyl derivatives of group IIA, IIB and IIIB elements is discussed.

Trimethylindium and trimethylthallium are monomeric in the gas phase and in hydrocarbon solution.[1] A relatively recent (1974) gas electron diffraction (GED) study of $(CH_3)_3In$ yielded an In–C bond distance of 2.093(6) Å.[2] As pointed out by the authors,[2] this value is significantly smaller than that obtained in an early (1941) GED study,[3] 2.16 ± 0.04 Å. It is also considerably smaller than the values obtained for single In–C bond distances by X-ray studies of several organoindium compounds.[2] We have recently completed a GED study of dimeric dimethyl(propynyl)indium where the terminal In–C (methyl) bond distance was found to be 2.18(2) Å.[4] We suggested, therefore, that the 1974 GED study of $(CH_3)_3In$ is marred by a scale error, and that the correct value for the In–C bond distance in this compound is around 2.16 Å.[4]

The molecular structures of $(CH_3)_3B$,[5] $(CH_3)_3Al$[6] and $(CH_3)_3Ga$[7] have all been determined by GED. And in the article describing their study of $(CH_3)_3Ga$, Beagley and coworkers[7] refer to an unpublished GED study of $(CH_3)_3Tl$ (Beagley, Robiette and Sheldrick, 1967) yielding a Tl–C bond distance of 2.218(3) Å.

In this paper we report the results of reinvestigations of trimethyl-indium and -thallium by GED.

EXPERIMENTAL

The electron scattering patterns of $(CH_3)_3In$ and $(CH_3)_3Tl$ were recorded on Balzers Eldigraph KDG-2 with nozzle temperatures of 50–60 °C (In) and 30–45 °C (Tl). Exposures were made with nozzle-to-photographic plate distances of 50 and 25 cm. This study is based on four 50 cm and three 25 cm plates for In and four 50 cm and four 25 cm plates for Tl. The data were processed by standard methods.[8]

The complex atomic scattering factors, $f'(s) = |f'(s)| \exp i\eta(s)$, were calculated from analytical representations of the atomic potentials[9] using a program written by Yates.[10] The molecular intensities were modified through multiplication with $s/|f'_M(s)||f'_C(s)|$ where M = In or Tl. The molecular intensity curves obtained for each nozzle-to-plate distance were averaged and connected. The final molecular intensity curves extended from $s = 2.00$ Å^{-1} to 19.75 Å^{-1} for M = In and from $s = 2.00$ Å^{-1} to 25.50 Å^{-1} for M = Tl. For M = In the "beat out", corresponding to $\Delta\eta_{MC}(s) = \eta_M(s) - \eta_C(s) = \pi/2$ occurs between $s = 19$ and 20 Å^{-1}. The factor cos $[\Delta\eta_{MC}(s)]$ clearly increases too slowly to allow the diffraction pattern to be detected at larger angles. For M = Tl the MC "beat out" occurs at about $s = 14$ Å^{-1} and the interference pattern could be detected out to 25 Å^{-1}.

* To whom correspondence should be addressed.

0302-4377/82/060495-05$02.50

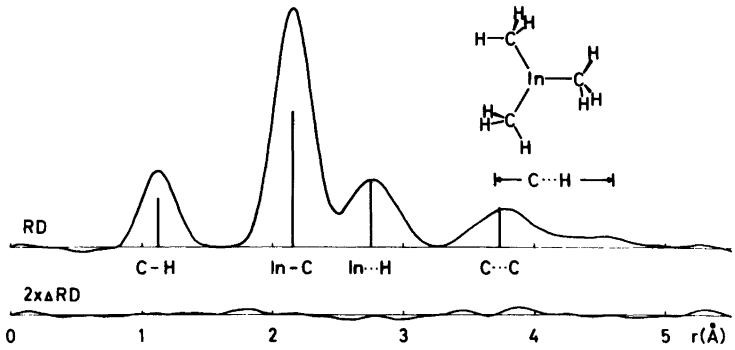

Fig. 1. Above: Experimental radial distribution curve for $(CH_3)_3In$. Artificial damping constant $k = 0.003$ Å^2. Major interatomic distances are indicated by bars of height proportional to the area under the corresponding peak. *Below:* Difference between the experimental curve and the theoretical curve calculated for the best model.

STRUCTURE ANALYSIS

Both $(CH_3)_3In$ and $(CH_3)_3Tl$ were assumed to have planar MC_3 skeletons with all $\angle CMC = 120°$. The methyl groups were assumed to have C_{3v} symmetry with the threefold axes coinciding with the M–C bonds. The methyl groups are expected to undergo virtually non-hindered internal rotation about the M–C axes, but the structure refinements were carried out on models of overall symmetry C_3 in which one C–H bond in each methyl group is lying in the MC_3 plane as indicated in Figs. 1 and 2. The molecular structure of each compound is then determined by only three parameters, the M–C and C–H bond distances and the valence angle $\angle MCH$.

Simple valence force fields of the two molecules were adjusted[11] to reproduce the vibrational frequencies assigned for the two molecules.[12] Since the out-of-plane MC_3 deformation frequency of $(CH_3)_3Tl$ has not been assigned, the corresponding force constant was transferred from $(CH_3)_3In$. Root mean square vibrational amplitudes, l, and perpendicular amplitude correction coefficients, K, were calculated using a program written by Hilderbrandt.[11]

The molecular structures were refined by least squares calculations with diagonal weight matrices under the constraints of geometrically consistent r_α structures.[13] Those vibrational amplitudes which could not be refined were fixed at their calculated values. The refinements converged to yield the structure parameters listed in Table 1. The estimated standard deviations have been multiplied by a factor

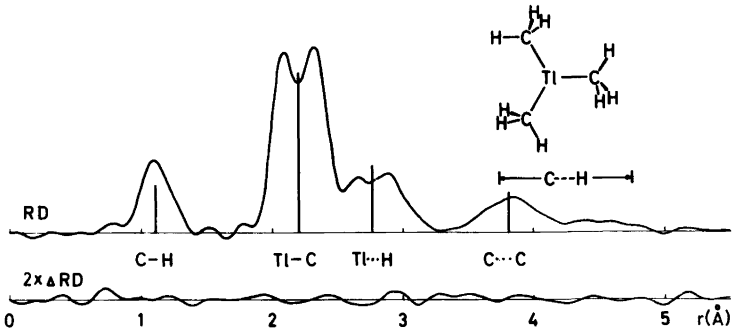

Fig. 2. Above: Experimental radial distribution curve for $(CH_3)_3Tl$. Artificial damping constant $k = 0.002$ Å^2. Major interatomic distances are indicated by bars of height proportional to the area under the corresponding (double) peak. *Below:* Difference between the experimental curve and the theoretical curve calculated for the best model.

Table 1. Internuclear distances (r_a), valence angles and root mean square vibrational amplitudes (l) of $(CH_3)_3In$ and $(CH_3)_3Tl$ obtained by least square refinement on gas electron diffraction (GED) data. (Estimated standard deviations in parentheses in units of the last digit.) Root mean square vibrational amplitudes and perpendicular amplitude correction coefficients (K) calculated from a molecular force field (FF).

	r_a (Å)	l (Å) (GED)	l (Å) (FF)	K (Å) (FF)
$(CH_3)_3In$				
In–C	2.161(3)	0.056(4)	0.058	0.005
C–H	1.124(4)	0.080(5)	0.078	0.060
In---H	2.755(6)	0.136(6)	0.133	0.060
C---C	3.735(2)	0.153(13)	0.102	0.001
C---H	3.69 to 4.61	0.22 to 0.13	0.22 to 0.13	
∠CInC (°)	120 (ass)			
∠InCH (°)	109.8(4)			
$(CH_3)_3Tl$				
Tl–C	2.206(3)	0.053(3)	0.059	0.005
C–H	1.108(7)	0.066(5)	0.078	0.059
Tl---H	2.767(9)	0.150(10)	0.133	0.060
C---C	3.815(4)	0.162(21)	0.103	0.001
C---H	3.78 to 4.76	0.22 to 0.13	0.22 to 0.13	
∠CTlC (°)	120 (ass)			
∠TlCH (°)	107.5(9)			

of two to compensate for the error introduced by the connection of intensity curves and the neglect of data correlation and expanded to include an estimated scale uncertainty of 0.1 %.

Experimental radial distribution curves calculated by Fourier inversion of experimental modified molecular intensity curves, are shown in Figs. 1 and 2 along with the difference between the experimental RD curves and their theoretical counterparts calculated for the best models. We consider the agreement satisfactory.

DISCUSSION

The experimental radial distribution curve of $(CH_3)_3In$ shown in Fig. 1 has the normal appearance: each internuclear distance, R_{ij}, in the molecule is represented by an approximately Gaussian peak centered around $r=R_{ij}$. The area under each peak is roughly proportional to $n_{ij}Z_iZ_j/R_{ij}$ where Z_i and Z_j are the atomic numbers and n_{ij} the number of times the distance occurs in the molecule, *e.g.* $n=3$ for the M–C bond distance; $Z_{In}=49$. Because of the high atomic number of Tl ($Z_{Tl}=81$), the factor in the intensity expression depending on the phase shift,[8] $\cos[\eta_{Tl}(s)-\eta_i(s)]$, varies greatly with s for i=C and H, and the Tl–C and Tl–H distances are consequently represented in the RD-curve (Fig. 2) by double peaks centered around the average value.

The close agreement between experimental and calculated RD curves in the ranges containing the C–C distance peaks, confirms the assumption that ∠CMC = 120° in both compounds. The appearance of the experimental RD curves in the ranges containing the nonbonded C–H distances suggests that the methyl groups undergo virtually nonhindered internal rotation. A molecular model as shown in Fig. 1 and 2 is clearly able to simulate this internal rotation if the C–H vibrational amplitudes are sufficiently large, $l=0.13$ to 0.22 Å.

The value obtained for the Tl–C bond distance in the present study is not significantly smaller than that obtained in the unpublished study by Beagley, Robiette and Sheldrick.[7]

The value obtained for the In–C bond distance is, however, significantly larger than that obtained in the 1974 study[2] and in better agreement with the values obtained for single In–C bond distances in other molecules. The 1974 study was based on three plates obtained with *one* nozzle to plate distance. Since our study is based on two independent sets of plates, the probability of a systematic scale error is greatly reduced, and we believe that our value should be regarded as more reliable. In the solid

Table 2. M – C bond distances in methyl derivatives of Group IIA, IIB and IIIB metals (M) determined by gas-electron diffraction (GED) or rotational Raman spectroscopy (RR).

Group IIA $(CH_3)_2M$	Group IIB $(CH_3)_2M$	Group IIIB $(CH_3)_3M$
$n=2$		
Be – C		B – C
1.698(2) GED [16]		1.578(1) GED [5]
$n=3$		
Mg – C [a]		Al – C
2.126(6) GED [17]		1.957(3) GED [6]
$n=4$		
Ca – C	Zn – C	Ga – C
	1.930(2) GED [18]	1.967(2) GED [7]
	1.929(4) RR [19]	
$n=5$		
Sr – C	Cd – C	In – C
	2.112(4) RR [19]	2.160(3) GED [b]
$n=6$		
Ba – C	Hg – C	Tl – C
	2.083(5) GED [20]	2.206(3) GED [b]
	2.094(5) RR [19]	

[a] In bisneopentylmagnesium. [b] This work.

state $(CH_3)_3In$ and $(CH_3)_3Tl$ are associated through the formation of very asymmetric $M-CH_3-M$ bridges.[14,15]

In Table 2 we compare M – C bond distances in monomeric di- or trimethyl derivatives of group IIA, IIB and IIIB metals. The radius of a hydrogen atom or hydrogen-like ion increases with the principal quantum number n of the filled atomic orbital and decreases with increasing nuclear charge Z. In accordance with this, the covalent radii, or the ionic radii of ions carrying the same net charge, are generally found to increase with increasing principal quantum number of the valence electrons down a group of *s*- or *p*-block elements in the periodic Table. Similarly, the decrease in the covalent radii with increasing atomic number generally found within the same period (n), has been explained as the effect of an increasing effective nuclear charge, Z_{eff}. The data collected in Table 2, however, show three apparent anomalies. Firstly, even though the covalent radii are expected to increase with n within the group, the Hg – C bond distance is significantly shorter than the Cd – C distance. The smaller covalent radius of Hg is probably a relativistic effect: Pyykkö and Desclaux [21] have shown that introduction of relativistic terms in the Schrödinger equation leads to a contraction of the atomic orbitals. The relativistic contraction shows a general increase with Z, but the increase is not monotonic; it appears to be particularly large for Au and the neighbouring elements Pt and Hg. Thus non-relativistic *ab initio* calculations on CdH_2 and HgH_2 predict that the Cd – H is shorter than the Hg – H bond distance, while relativistic calculations reverse the trend.[22]

Secondly the Ga – C is only 0.01 Å longer than the Al – C bond distance. This anomaly is probably due to the increase of the effective nuclear charge accompanying the filling in of ten 3*d* electrons between Ca and Zn.[7]

Finally, in each of the periods $n=4$, 5 and 6 the M(IIB) – C bond distance is *smaller* than the M(IIIB) – C bond distance. This difference might be rationalized as a hybridization effect. But since no such difference is visible between the M(IIA) – C and M(IIIB) – C bond distances in the $n=2$ and 3 series, we prefer to rationalize the larger covalent radii of Ga, In and Tl as an effect of the contracting $(n-1)d$ electron shells: In Group IB these electrons are valence electrons, but as we move to the right along the period they sink into the atomic core and thus become increasingly effective in shielding the nucleus.

Acknowledgement. We are grateful to the Norwegian Research Council for Science and the Humanities for financial support.

REFERENCES

1. Coates, G. E., Green, M. L. H. and Wade, K. *Organometallic Compounds*, Menthuen, London 1967, Vol. 1.
2. Barbe, G., Hencher, J. L., Shen, Q. and Tuck, D. G. *Can. J. Chem. 52* (1974) 3936.
3. Pauling, L. and Laubengayer, A. W. *J. Am. Chem. Soc. 63* (1941) 480.
4. Fjeldberg, T., Haaland, A., Seip, R. and Weidlein, J. *Acta Chem. Scand. A 35* (1981) 437.
5. Bartell, L. S., Kohl, D. A., Carroll, B. L. and Gavin, R. M. *J. Chem. Phys. 42* (1965) 3079.
6. Almenningen, A., Halvorsen, S. and Haaland, A. *Acta Chem. Scand. 25* (1971) 1937.
7. Beagley, B., Schmidling, D. G. and Steer, I. A. *J. Mol. Struct. 21* (1974) 437.
8. Andersen, B., Seip, H. M., Strand, T. G. and Stølevik, R. *Acta Chem. Scand. 23* (1969) 23.
9. Strand, T. G. and Bonham, R. A. *J. Chem. Phys. 40* (1964) 1686.
10. Yates, A. C. *Comput. Phys. Commun. 2* (1971) 175.
11. Hilderbrandt, R. L. and Wieser, J. D. *J. Chem. Phys. 55* (1971) 4648.
12. Karschin, J. *Zulassungsschrift*, Universität Stuttgart, Stuttgart 1979.
13. Seip, H. M., Strand, T. G. and Stølevik, R. *Chem. Phys. Lett. 3* (1969) 617; Gundersen, G. *Annual Report of the Norwegian Electron Diffraction Group*, Oslo 1977.
14. Amma, E. L. and Rundle, R. E. *J. Am. Chem. Soc. 80* (1958) 4141.
15. Sheldrick, G. M. and Sheldrick, W. S. *J. Chem. Soc. A* (1970) 28.
16. Almenningen, A., Haaland, A. and Morgan, G. L. *Acta Chem. Scand. 23* (1969) 2921.
17. Ashby, E. C., Fernholt, L., Haaland, A., Seip, R. and Smith, R. S. *Acta Chem. Scand. A 34* (1980) 213.
18. Almenningen, A., Helgaker, T. U., Haaland, A. and Samdal, S. *Acta Chem. Scand. A 36* (1982) *In press.*
19. Rao, K. S., Stoicheff, B. P. and Turner, R. *Can. J. Phys. 38* (1960) 1516.
20. Kashiwabara, K., Konaka, S., Iijima, T. and Kimura, M. *Bull. Chem. Soc. Jpn. 46* (1973) 407.
21. Pyykkö, P. and Desclaux, J.-P. *Acc. Chem. Res. 12* (1979) 276.
22. Pyykkö, P. *J. Chem. Soc. Faraday Trans. 2, 75* (1979) 1256.

Received October 27, 1981.

Acta Chemica Scandinavica A 36 (1982) 501 – 507

Solubility of Silver Tungstate in Aqueous Sodium Nitrate Solutions with Different pH Values at 25 °C. Evaluation of a Solubility *vs.* Ionic Strength Relation Valid for Ionic Strength up to 1.0 mol dm^{-3}

JØRGEN BIRGER JENSEN and JASPER S. R. BUCH

Fysisk-Kemisk Institut, DTH 206, DK-2800 Lyngby, Denmark

The solubility of stable silver tungstate has been measured in aqueous sodium nitrate solutions at $I = 0.1$ and $I = 0.5$ mol dm^{-3} and $4 < pH < 10$. The pH-dependence of the solubility is used to test a previously outlined theory. The ionic strength dependence of the solubility is used to outline the relation:

$$\ln s = \ln s_0 + 1.94 I^{\frac{1}{2}}(1 + I^{\frac{1}{2}})^{-1}$$

valid for $0 \leqq I \leqq 1.0$. Equilibrium constants for the following two equilibria

$$6WO_4^{2-} + 7H^+ \rightleftarrows HW_6O_{21}^{5-} + 3H_2O$$

and

$$6Ag_2WO_4(s) + 7H^+ \rightleftarrows 12Ag^+ + HW_6O_{21}^{5-} + 3H_2O$$

are found at different ionic strengths covering the interval $0 \leqq I \leqq 1.0$. The ionic strength dependences on these equilibria are found to be in accordance with theories outlined by Debye-Hückel and Brønsted.

Regarding the solubility of silver tungstate, much confusion and great discrepancies are found among the reported values.[1-5] At this institute the solubility of silver tungstate has been investigated in aqueous sodium nitrate solutions at various ionic strengths, pH and temperatures. Results representing measurements on dilute electrolyte solutions (c_{NaNO_3} below approximate 3×10^{-2} mol dm^{-3}) and measurements on 1.0 mol dm^{-3} sodium nitrate solutions have previously been reported in this journal.[6]

In the present paper results from solubility measurements on 0.1 mol dm^{-3} and 0.5 mol dm^{-3} will be presented. The presentation is initiated for two main reasons:

(1) The results give support to the theories outlined earlier,

(2) the new results together with those reported earlier create the basis of establishing a relationship between the solubility of silver tungstate and the concentration of sodium nitrate in aqueous solutions up to $c_{NaNO_3} = 1.0$ mol dm^{-3}.

In addition, some protolytic constants are calculated at different ionic strengths and the ionic strength dependences are discussed.

EXPERIMENTAL

The descriptions of chemicals, of preparing saturated solutions of thermodynamic stable silver tungstate, and of solubility determinations are reported earlier.[6] Only a few additional remarks shall be given to the procedure of preparing thermodynamic stable silver tungstate.

Freshly precipitated silver tungstate prepared by adding excess of aqueous sodium tungstate to well-stirred aqueous solution of silver nitrate is not stable, but undergoes chemical reactions, in which also protons are involved.[6] Therefore, the silver tungstate precipitate was allowed to equilibrate at least one year with the aqueous solution, (further equilibration was found to be unnecessary, shorter equilibration time has not been tried), whereupon it was rinsed in distilled and de-ionized water until the specific conductivity of a saturated solution in this water at 25 °C was below 20×10^{-6} ohm^{-1} cm^{-1}. Due to scattering in the reported values of molar conductivity of the tungstate ion it is impossible to

0302-4377/82/060501-07$02.50

give an exact value of the specific conductance of a saturated aqueous solution of silver tungstate at 25 °C. Two examples shall illustrate this: Landolt-Börnstein [7] gives the value 138.8 $ohm^{-1}\ cm^2\ mol^{-1}$ for the molar conductance of WO_4^{2-} at 25 °C. This, together with the value 62.2 $ohm^{-1}\ cm^2\ mol^{-1}$ for the molar conductance of Ag^+ gives the specific conductivity for a saturated solution of silver tungstate to 15.0×10^{-6} $ohm^{-1}\ cm^{-1}$ when the value 5.7×10^{-5} mol dm^{-3} is used for the solubility.[6] From the data of Watkins and Jones [8] the molar conductivity of WO_4^{2-}-ion can be calculated to 223 $ohm^{-1}\ cm^2\ mol^{-1}$ at 25 °C. This gives a specific conductivity of a saturated Ag_2WO_4-solution of 19.8×10^{-6} $ohm^{-1}\ cm^{-1}$.

Therefore, we decided that the ultimate test of the cleanness of our silver tungstate product should be that the specific conductance of a saturated aqueous solution was below 20×10^{-6} $ohm^{-1}\ cm^{-1}$.

The saturated solution was then filtered after which the silver tungstate was dried at 50 °C and used to prepare saturated aqueous sodium nitrate solutions as described earlier.[6]

RESULTS AND DISCUSSION

The pH-dependence of the solubility of stable silver tungstate has been investigated at two

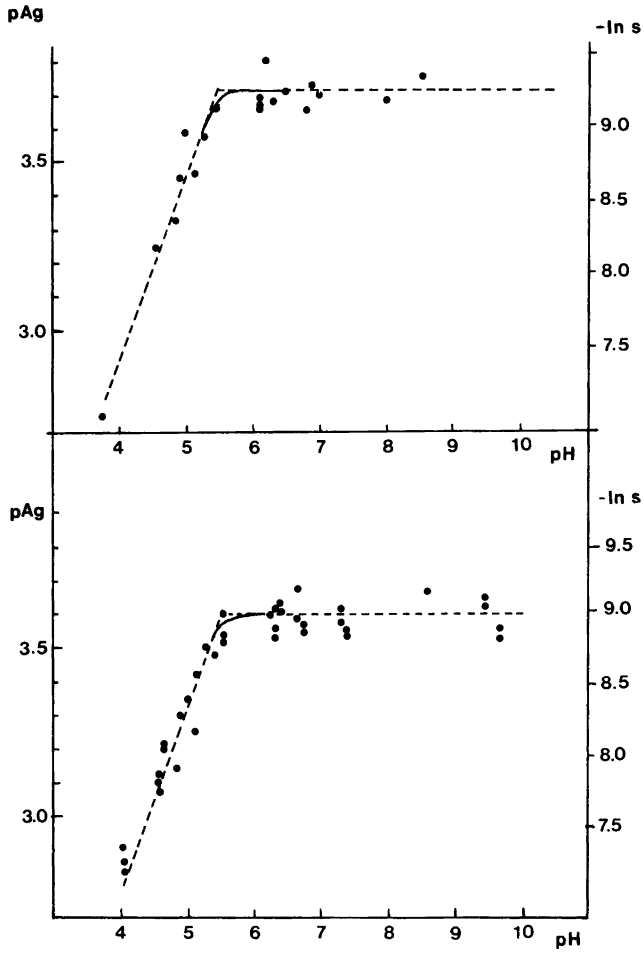

Fig. 1. Solubility of stable silver tungstate in aqueous sodium nitrate solutions as a function of pH. Upper curve: $C_{NaNO_3} = 0.1$ mol dm^{-3}. Lower curve: $C_{NaNO_3} = 0.5$ mol dm^{-3}. The two horizontal dotted lines are drawn through the mean value of experimental data corresponding to pH > 6.0. The two other dotted straight lines are drawn with a slope 7/13 through the intercept with the horizontal lines. The intercepts are calculated by means of eqn. (6).

different ionic strengths, *i.e.* $I=0.1$ and 0.5, respectively. The ionic strength was kept constant by means of sodium nitrate and the investigation was performed by titrimetric determination of silver ions in saturated aqueous solutions at 25 °C. The results are shown in Fig. 1.

Great similarities are observed between these results and the results previously reported for the solubility of stable silver tungstate in 1.0 mol dm^{-3} aqueous sodium nitrate solutions.[6] As an example: By regarding Fig. 1 it seems most likely that, also in the present case, some protolytic reactions are involved in the solubility process in weak acidic medium, whereas pAg obviously can be regarded as constant for pH > 6. Due to the uniformity – at first glance almost identity – among previously reported values and those reported in Fig. 1, we found it permissible to assume that the solubility of silver tungstate in both cases is governed by the same reactions. This means that the present results (Fig. 1) can be used as an independent test in order to support – or reject – the theories outlined earlier. The main features on the theories shall shortly be mentioned: According to Arnek and Sasaki[9] the first step in the acidification of WO_4^{2-}-ion can be expressed by eqn. (1), with the equilibrium constant

$$6WO_4^{2-} + 7H^+ \rightleftarrows HW_6O_{21}^{5-} + 3H_2O \qquad (1)$$

β_1. This equation, together with the saturation equilibrium, gives eqn. (2). Eqn. (2) together with the

$$C_{Ag^+} = 2(C_{WO_4^{2-}} + 6C_{HW_6O_{21}^{5-}}) \qquad (2)$$

expression for the solubility product, eqn. (3), and eqn. (1) gives eqn. (4), where $\beta'_1 = \beta_1/(C_{H_2O})^3$. Eqn. (4)

$$(C_{Ag^+})^2 C_{WO_4^{2-}} = K_c \qquad (3)$$

$$(C_{Ag^+})^{13} - 2K_c(C_{Ag^+})^{10} - 12\beta'_1 K_c^6 (C_{H^+})^7 = 0 \qquad (4)$$

expresses the concentration of silver-ions in saturated solutions of silver tungstate as a function of pH. This dependence can be calculated from knowledge of the two constants, K_c and β'_1. On the other hand, if the pH-dependence of the solubility is determined experimentally, the two constants can be calculated as has been done in 1.0 mol dm^{-3} sodium nitrate solutions. For pH > 6.5 it was assumed that the term $12\beta'_1 K_c^6 (H_{H^+})^7$ vanishes so that eqn. (4) was reduced to $C_{Ag^+} = (2K_c)^{1/3}$ and K_c determined from the mean C_{Ag^+}-value to 1.63×10^{-11} mol^3 dm^{-9}, corresponding to a solubility of 1.6×10^{-4} mol dm^{-3}. For pH-values below 5.5 it was assumed that the term $2K_c(C_{Ag^+})^{10}$ vanishes and eqn. (4) was then reduced to eqn. (5), *i.e.* a straight

$$pAg = \frac{7}{13} pH - \frac{1}{13} \log(12\beta'_1 K_c^6) \qquad (5)$$

line with the slope 7/13 from which log β'_1 can be calculated to be 57.34.

If eqns. (1)–(5) can be assumed to have general validity in aqueous sodium nitrate solution, the pH-dependence of the solubility can be determined by means of two straight lines:

(1) One horizontal line, valid in neutral media. The position of the line is determined from the mean C_{Ag^+}-value from saturated solutions in these media. From this line the solubility product can be calculated.

(2) One line with a slope 7/13 valid in slightly acidic media. The position of this line is governed by the point of intercept between this line and the horizontal one. This point can be calculated from eqn. (6) if β'_1 and K_c are known.

$$pH = \frac{1}{7} \log(12\beta'_1 K_c^6) - \frac{13}{21} \log(2K_c) \qquad (6)$$

By applying eqn. (4), the intervening part of the curve between the two straight lines can now be calculated.

In Fig. 1 the two horizontal dotted lines represent the two mean values of C_{Ag^+}, calculated from experimental data of C_{Ag^+} in media with pH > 6. Following values were obtained:

(a) For $I=0.1$; pAg = 3.715 ± 0.015, corresponding to a solubility $s = (9.65 \pm 0.35) \times 10^{-5}$ mol dm^{-3} and a solubility product $K_c = (3.6 \pm 0.4) \times 10^{-12}$ mol^3 dm^{-9}.

(b) For $I=0.5$; pAg = 3.592 ± 0.009, corresponding to $s = (1.28 \pm 0.04) \times 10^{-4}$ and a solubility product $K_c = (8.4 \pm 0.4) \times 10^{-12}$ mol^3 dm^{-9}.

Previously reported values[6] for $I=1.0$; pAg = 3.496 ± 0.007 corresponding to $s = (1.60 \pm 0.03) \times 10^{-4}$ mol dm^{-3} and solubility product $K_c = (1.63 \pm 0.08) \times 10^{-11}$ mol^3 dm^{-9}.

Furthermore in Ref. 6 it is shown that the ionic strength dependence of the solubility of silver tungstate in dilute sodium nitrate solutions ($I \leqq 0.03$) can be expressed by the Güntelberg equation, eqn. (7), and $\ln s_o$ was determined to be -9.77 ± 0.04.

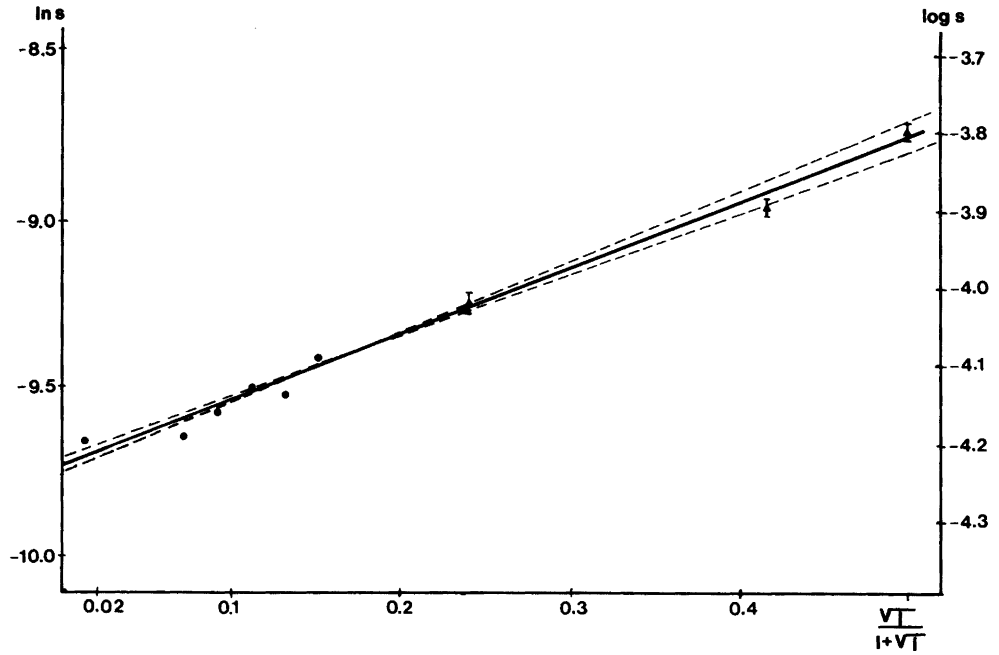

Fig. 2. Güntelberg plot [eqn. (13)] for experimental data of solubility of stable silver tungstate. Data marked as ● are previously reported. The fully drawn line indicates the best straight line through the data. The two dotted lines indicate the 67 % uncertainty limit for the straight line.

$$\ln s = \ln s_o + kI^{\frac{1}{2}}(1+I^{\frac{1}{2}})^{-1} \quad (7)$$

The validity of eqn. (7) in more concentrated solutions can be tested by applying the solubility data from dilute ionic media together with those reported above and carrying out a Güntelberg plot. This is done in Fig. 2.

A straight line is fitted through the points with a correlation coefficient =0.987. The slope is calculated to be 1.94 ± 0.08 and $\ln s_o$ is determined to be -9.74 ± 0.02, *i.e.* very close to the value obtained, when only dilute solutions were used in the plot.*

Clearly the Güntelberg equation very nicely describes the ionic strength dependence of ionic equilibria in sodium nitrate solutions up to $C_{NaNO_3} = 1.0$ mol dm^{-3}, provided(1) that the concentration of the ionic species in the equilibrium can be neglected, compared with the concentrations of sodium and nitrate ions and

(2) that the constant k is determined and valid for any arbitrary ionic species taking part in the equilibrium. This can be done by regarding the solubility product of silver tungstate. The relation (8) holds, where K_o is the solubility product at zero ionic strength, a is the activity, and y the activity coefficient of the ions. Since $C_{Ag^+} = 2s = 2C_{WO_4^{2-}}$, eqn. (8) can be written as eqn. (9), where s_o is the

$$K_o = (a_{Ag^+})^2 a_{WO_4^{2-}} = (C_{Ag^+} + y_{Ag^+})^2 C_{WO_4^{2-}} y_{WO_4^{2-}} \quad (8)$$

$$4s_o^3 = 4s^3 y_\pm^3 \quad (9)$$

solubility at zero ionic strength and $y_\pm$ is the mean activity coefficient defined from the equation

$$y_\pm^3 = y_{Ag^+}^2 y_{WO_4^{2-}}.$$

From the Güntelberg modified Debye-Hückel theory we have eqns. (10)–(12), where A is the

$$-\ln y_{Ag^+} = AI^{\frac{1}{2}}(1+I^{\frac{1}{2}})^{-1} \quad (10)$$

$$-\ln y_{WO_4^{2-}} = 4AI^{\frac{1}{2}}(1+I^{\frac{1}{2}})^{-1} \quad (11)$$

$$-\ln y_\pm = 2AI^{\frac{1}{2}}(1+I^{\frac{1}{2}})^{-1} \quad (12)$$

*This linearity strongly indicates that no possible complex formation between the present ions is substantial enough to be drawn into the calculations.

Debye-Hückel constant and I is the ionic strength. Substituting (12) in (9) we have eqn. (13). Comparing (13) with (7), the Debye-Hückel constant is found for aqueous sodium bitrate solutions at 25 °C; eqn. (14),

$$\ln s = \ln s_o + 2AI^{\frac{1}{2}}(1+I^{\frac{1}{2}})^{-1} \quad (13)$$

$$A = k/2 = 0.97 \quad (14)$$

compared with the theoretical value[10] 1.17. However, the theoretical value is calculated for an arbitrary ionic species in aqueous solution without taking into account special ion individualities, and is therefore supposed to be valid only in dilute ionic solutions. For further calculations, the value 0.97 will be used.

According to eqn. (4), β'_1 must be known in order to give a full description of the pH-dependence of solubility of stable silver tungstate. That means that in order to completely test the results shown in Fig. 1, the value of β'_1 must be known in 0.1 and 0.5 mol dm^{-3} sodium nitrate solutions. The expression for β'_1 at a given ionic strength is given by eqn. (15).

$$\beta'_1 = \frac{C_{HW_6O_{21}^{5-}}}{(C_{H^+})^7 \cdot (C_{WO_4^{2-}})^6} \quad (15)$$

The value of β'_1 at ionic strength $=0$ can be expressed as eqn. (16) or eqn. (17).

$$\beta'_1(I=0) = \frac{a_{HW_6O_{21}^{5-}}}{(a_{H^+})^7(a_{WO_4^{2-}})^6} = \frac{C_{HW_6O_{21}^{5-}}}{(C_{H^+})^7(a_{WO_4^{2-}})^6} \cdot \frac{y_{HW_6O_{21}^{5-}}}{(y_{H^+})^7(y_{WO_4^{2-}})^6} \quad (16)$$

$$\ln \beta'_1(I=0) = \ln \beta'_1(I=I) + \ln \frac{y_{HW_6O_{21}^{5-}}}{(y_{H^+})^7(y_{WO_4^{2-}})^6} \quad (17)$$

Due to the fact that all the concentrations in (15) are very small, the treatment outlined in eqns. (10)–(13) can be applied on the last term in eqn. (17) with eqn. (18) as a result. Eqn. (18) is substituted into eqn. (17) which then gives ($A=0.97$) eqn. (19). Utilizing the value $\log \beta'_1(I=1.0) = 57.34$ in eqn. (19) we get eqn. (20) and β'_1 can be calculated at $I=0.5$ and $I=0.1$ to $\log \beta'_1(I=0.5) = 57.56$ and $\log \beta'_1(I=0.1) = 58.00$.

$$\ln \frac{y_{HW_6O_{21}^{5-}}}{(y_{H^+})^7(y_{WO_4^{2-}})^6} = 6A \frac{I^{\frac{1}{2}}}{1+I^{\frac{1}{2}}} \quad (18)$$

$$\ln \beta'_1(I=0) = \ln \beta'_1(I=I) + 5.82 \cdot \frac{I^{\frac{1}{2}}}{1+I^{\frac{1}{2}}} \quad (19)$$

$$\log \beta'_1(I=I) = 58.60 - 2.53 \frac{I^{\frac{1}{2}}}{1+I^{\frac{1}{2}}} \quad (20)$$

By means of eqn. (6) pH can now be calculated at the point of intercept between the two straight lines in order to establish the position of the second straight line with the slope 7/13. The following pH-values were obtained: At $I=0.5$: pH (intercept) $=5.56$; $I=0.1$: pH (intercept) $=5.53$. Extrapolated values to zero ionic strength are: $\log \beta'_1(I=0) = 58.60$, corresponding to pH intercept $=5.45$. Through the two pH intercept-values two straight lines with the slope 7/13 are drawn (shown as dotted lines on Fig. 1). As can be seen, these lines fit the experimental data so nicely that we, on the basis of this fine agreement, feel it justified to make the following three conclusions:

(1) The results shown in Fig. 1 highly support the previously developed theory of the pH-dependence of stable silver tungstate. The theory is shortly outlined in eqns. (1)–(5).

(2) The nice fit in Fig. 1 seems to establish the validity of eqn. (20).

(3) By means of experimental data presented here and a theory previously outlined, it is possible to calculate the solubility of stable silver tungstate in aqueous sodium nitrate solutions with ionic strengths <1.0 and at any pH-value in the interval $4<\text{pH}<10$. Fig. 3 shows four calculated curves corresponding to four different ionic strength values.

Now regarding the equilibrium (21) with the equilibrium constant (22). This equilibrium constant can also be written as eqn. (23). The ionic strength

$$6Ag_2WO_4(s) + 7H^+(aq) \rightleftarrows 12Ag^+(aq) + HW_6O_{21}^{5-}(aq) + 3H_2O \quad (21)$$

$$\beta_{21} = \frac{(C_{Ag^+})^{12} C_{HW_6O_{21}^{5-}} (C_{H_2O})^3}{(C_{H^+})^7} \quad (22)$$

$$\beta_{21} = K_c^6 \beta_1 = K^6 \beta'_1 (C_{H_2O})^3 \quad (23)$$

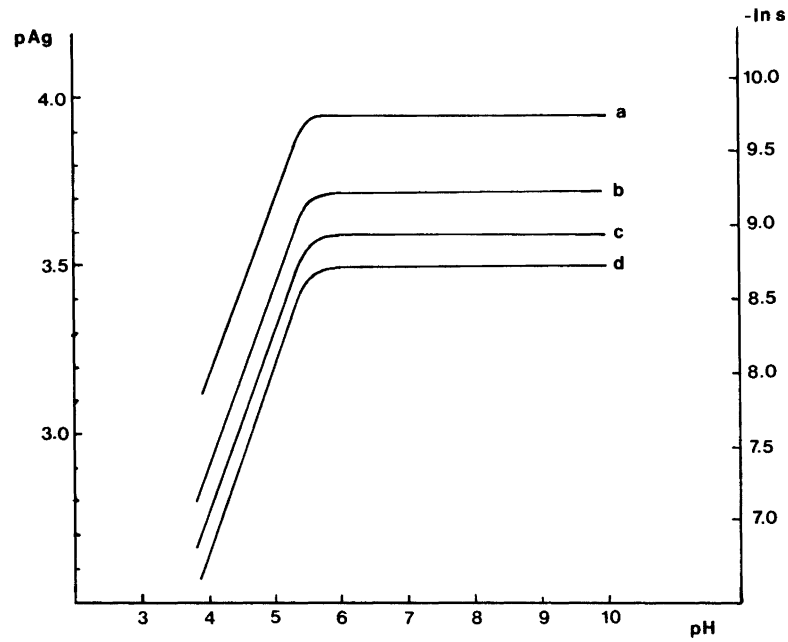

Fig. 3. Calculated solubilities of stable silver tungstate in different aqueous sodium nitrate solutions as a function of pH. Curve a: $I=0$; curve b: $I=0.1$; curve c: $I=0.5$; curve d: $I=1.0$. (Units for I: mol dm^{-3}.)

dependence of K_c and β'_1 in aqueous sodium nitrate solutions is evaluated in eqns. (13) and (20), and the proper value of the water concentrations at different ionic strengths can easily be found.[11] So, by means of eqn. (23), the constant β_{21} can be calculated. The values are collected in Table 1, together with the corresponding values of β_1.

Besides illustrating a general ionic strength dependence of ionic equilibria, the results in Table 1 agree with the theories in two decisive ways:

(1) The ionic strength dependence is much more pronounced in β_{21} than in β_1, which is in accordance with the Debye-Hückel theory.

(2) It is noticed that β_1 decreases and β_{21} increases with increasing ionic strength. This is in accordance with the theory of Brønsted[12-15] which predicts a negative secondary salt effect on (1) and a positive secondary salt effect on (21).

Table 1. Calculated values of β_1 [equilibrium (1)] and β_{21} [equilibrium (21)] at different ionic strengths in aqueous sodium nitrate solutions.

	$I=0$	$I=0.1$	$I=0.5$	$I=1.0$
β_1	6.8×10^{63}	1.7×10^{63}	5.9×10^{62}	3.4×10^{62}
β_{21}	1.8×10^{-9}	3.7×10^{-6}	2.1×10^{-4}	6.4×10^{-3}

Acknowledgements. Thanks are due to Lise Sørensen and Morten V. Kristiansen for skilled technical assistance and to our colleagues at *Fysisk-Kemisk Institut* for encouraging discussions and advice.

REFERENCES

1. Britton, H. T. S. and German, W. L. *J. Chem. Soc. Part II* (1934) 1156.
2. Buchholz, E. *Z. Anorg. Allg. Chem. 244* (1940) 149.
3. Pan, K. *J. Chin. Chem. Soc. (Teipei) 1* (1954) 1.
4. Saxena, R. S. and Gupta, C. M. *J. Ind. Chem. Soc. 35* (1958) 830.
5. Weiner, R. and Boriss, P. *Z. Anal. Chem. 168* (1959) 195.
6. Jensen, J. B. and Buch, J. S. R. *Acta Chem. Scand. A 34* (1980) 99.
7. Landolt-Börnstein, *Zahlenwerte und Funktionen*, 6. Auflage, II. Band, 7. Teil, p. 259.
8. Watkins, C. and Jones, H. C. *J. Am. Chem. Soc. 37* (1915) 2626.

9. Arnek, R. and Sasaki, Y. *Acta Chem. Scand. A 28* (1974) 20.
10. Robinson, R. A. and Stokes, R. H. *Electrolyte Solutions*, Butterworth, London 1955, p. 491.
11. *Handbook of Chemistry and Physics*, The Chemical Rubber Co., Cleveland 1977/78, 58th Ed., pp. D 256–257.
12. Brønsted, J. N. *J. Chem. Soc. 119* (1921) 574.
13. Brønsted, J. N. *J. Am. Chem. Soc. 42* (1920) 761.
14. Brønsted, J. N. *J. Am. Chem. Soc. 47* (1925) 2523.
15. Brønsted, J. N. *Om Syre- og Basekatalyse, Københavns Universitets Festskrift*, København 1926. *(In Danish).*

Received October 8, 1981.

Acta Chemica Scandinavica A 36 (1982) 509–512

Crystal and Molecular Structure of Bis(2-mercaptobenzoato-*S*)mercury(II) Monodioxane

BASIM M. ALSAADI * and MAGNUS SANDSTRÖM

The Department of Inorganic Chemistry, Royal Institute of Technology, S-100 44 Stockholm, Sweden

The structure of $Hg(C_7H_5O_2S)_2 \cdot C_4H_8O_2$ has been determined from three-dimensional single-crystal X-ray diffraction data and refined to $R = 0.047$ for 703 counter intensities. The crystals are monoclinic, space group $P2_1/a$, with $a = 21.86(2)$, $b = 4.117(4)$, $c = 11.42(1)$ Å, $\beta = 111.04(5)°$ and $Z = 2$. The Hg atom, at a centre of symmetry, is linearly coordinated to the S atoms of two thiosalicylic acid molecules with the Hg–S distance 2.361(7) Å. The O atoms of the centrosymmetric dioxane molecule are hydrogen-bonded to the carboxyl groups of two bis(2-mercaptobenzoato-*S*)mercury(II) complexes, forming endless zig-zag chains.

Ortho-mercaptobenzoic (= thiosalicylic) acid forms chelate complexes with a variety of metal ions.[1] Both the carboxyl and the sulfhydryl groups usually participate in the binding.[2] With mercury(II), however, it behaves differently. Two compounds have been described; with one or two molecules thiosalicylic acid per mercury atom. Infrared spectra of the solid compounds and potentiometric studies of the complex formation in solution indicated that the carboxyl groups do not coordinate to mercury.[2] Moreover, the bis(2-mercaptobenzoato-*S*)mercury(II) complex, BTM, can bind further metal atoms, such as Zn^{2+}, Cd^{2+} or Pb^{2+}.[3] In order to investigate the surroundings of mercury and to elucidate the coordination properties of the BTM compound, the crystal structure of the BTM dioxane solvate was determined.

* Permanent address: Chemistry Department, College of Education, University of Baghdad, Wazeria, Baghdad, Iraq.

0302-4377/82/060509-04$02.50

EXPERIMENTAL

Preparation. The BTM-compound was prepared as described previously[2] and recrystallized from a water–dioxane mixture. Thin colourless needles were obtained when the solution was evaporated under vacuum at room temperature. The ^1H NMR spectrum of the crystals dissolved in deuterated dimethylsulfoxide-d_6 (Merck, 99.8% D) showed an additional sharp signal at 3.58 ppm at low field relative to TMS. Its area corresponded to eight protons per BTM complex. Addition of dioxane to the solution increased the area of this signal, confirming the assignment of one dioxane molecule per BTM.

Data collection. A prismatic crystal of approximate dimensions $0.04 \times 0.33 \times 0.12$ mm was chosen for the data collection and enclosed in a capillary. The cell parameters were obtained by film methods and refined by least-squares methods using 14 selected reflexions, centered on the automatic Syntex $P2_1$ diffractometer.

The intensities of 946 unique reflexions with $3° < 2\theta < 41°$ were measured using the ω scan technique with different scan speeds, from 0.5° min^{-1} upwards. Of these, 709 reflexions with $I > 2\sigma(I)$ were used in the calculations and were corrected for Lorentz and polarization effects. Two check reflexions were measured at regular intervals. Their intensities decreased about 39% with a constant rate during the 120 h of data collection. A linear correction was applied to compensate for the decrease. A semiempirical absorption correction was applied.[4] The measured maximum transmission ratio was 1:0.54.

All calculations were carried out by means of the Syntex XTL Crystallographic Program System.[5]

Crystal data. $C_{18}H_{18}O_6S_2Hg$, $M = 595.06$, monoclinic, $a = 21.86(2)$, $b = 4.117(4)$, $c = 11.42(1)$ Å, $\beta = 111.04(5)°$, $V = 959(1)$ Å^3, $D_m = ca.\ 2$ g/cm^{-3}, $Z = 2$, $D_x = 2.06$ g/cm^{-3}, $F(000)$ 572, space group $P2_1/a$:

Table 1. Final fractional atomic positional parameters and isotropic mean square amplitudes U in Å^2. Estimated standard deviations are given in parentheses.

	x	y	z	U
Hg	0	0	0	
S	0.0848(3)	−0.320(2)	−0.0226(6)	
O1	0.0579(7)	−0.504(6)	0.2142(14)	
O2	0.1401(8)	−0.588(4)	0.3865(15)	
O3	−0.0504(8)	0.111(4)	0.5390(17)	
C1	0.1646(9)	−0.284(5)	0.2370(17)	0.020(5)
C2	0.1539(10)	−0.199(6)	0.1073(19)	0.033(5)
C3	0.2042(10)	−0.014(8)	0.0842(19)	0.043(5)
C4	0.2628(11)	0.057(7)	0.1849(22)	0.048(7)
C5	0.2713(11)	−0.042(7)	0.3100(21)	0.048(6)
C6	0.2234(10)	−0.213(6)	0.3279(18)	0.027(5)
C7	0.1162(11)	−0.461(7)	0.2749(21)	0.037(6)
C8	−0.103(13)	−0.016(9)	0.3724(21)	
C9	−0.0652(12)	0.045(8)	0.3211(26)	

non-standard setting of No. 14 with general positions $\pm(x,y,z)$, $\pm(\frac{1}{2}-x,\frac{1}{2}+y,\bar{z})$, MoKα x-radiation (graphite-monochromator), $\lambda = 0.71069$ Å, $\mu(\text{MoK}\alpha) = 84.2$ cm^{-1}.

STRUCTURE DETERMINATION AND REFINEMENT

Weissenberg photographs showed the systematic extinctions $h0l$: $h=2n+1$ and $0k0$: $k=2n+1$ consistent with the space group $P2_1/a$.[6] From a listing of Patterson vectors, initial values of the Hg and S positions were deduced and refined by least-squares methods. Subsequent difference Fourier maps and full-matrix least-squares refinements revealed the positions of all non-hydrogen atoms. The function minimized was $\Sigma w_i||F_o|-|F_c||^2$ with the weighting function $w_i = 1/\{\sigma^2(F_o)+(0.04\,F_o)^2\}$.

The scattering factors used were obtained from analytical expressions for the neutral atoms, including anomalous dispersion corrections for Hg and S.[6]

With isotropic temperature factors for all atoms, the agreement factors $R=\Sigma||F_o|-|F_c||/\Sigma|F_o| = 0.085$, $R_w=(\Sigma w_i||F_o|-|F_c||^2/\Sigma w_i|F_o|^2)^{1/2}=0.11$, were obtained. Anisotropic temperature factors could be introduced for all atoms except the carbon atoms of the aromatic ring. No definitive hydrogen atom positions could be found from the difference Fourier maps. They were therefore introduced at calculated positions with a C−H distance of 0.96 Å (omitting the proton of the carboxyl group) taking the usual underestimation of about 0.13 Å in X-ray studies into account.[7]

The final agreement factors were $R=0.047$, $R_w = 0.060$, with a largest shift of 0.01 σ in the parameter values in the last refinement cycle. The highest peaks, 0.9 e Å^{-3}, in a subsequent difference Fourier map were close to the mercury position. The final parameter values are given in Tables 1 and 2.

DESCRIPTION AND DISCUSSION OF THE STRUCTURE

The structure contains centrosymmetric molecular BTM complexes, formed by a linear S−Hg−S bond between two thiosalicylic acid molecules. The carboxyl groups of two adjacent BTM complexes are hydrogen-bonded to the oxygen atoms of the centrosymmetric dioxane molecules, forming zig-zag chains running through the crystal, Fig. 1.

These chains of molecules are stacked on top of each other along the b axis with a perpendicular distance of 4.12 Å. Two long Hg−S distances at 3.420(7) Å between adjacent S−Hg−S groups, and four Hg−O1 distances at 3.08(2) and 3.11(2) Å,

Table 2. Final anisotropic thermal parameters in Å^2 with estimated standard deviations in parentheses. The temperature factor expression used is $\exp[-2\pi^2(U_{11}h^2a^{*2}+...+2\,U_{12}hka^*b^*+...)]$

	U_{11}	U_{22}	U_{33}	U_{12}	U_{13}	U_{23}
Hg	0.0339(8)	0.0489(9)	0.0309(8)	0.0046(13)	0.0014(5)	−0.0009(11)
S	0.041(4)	0.042(4)	0.033(3)	−0.008(4)	0.005(3)	−0.006(4)
O1	0.039(9)	0.131(17)	0.048(9)	−0.036(16)	0.013(8)	−0.002(16)
O2	0.038(9)	0.062(17)	0.053(11)	−0.006(9)	0.002(8)	0.032(10)
O3	0.056(12)	0.057(15)	0.064(12)	−0.013(9)	0.033(11)	0.007(10)
C8	0.069(18)	0.073(18)	0.037(13)	−0.004(25)	0.021(14)	−0.009(21)
C9	0.049(15)	0.076(25)	0.065(18)	−0.010(19)	0.023(14)	0.013(20)

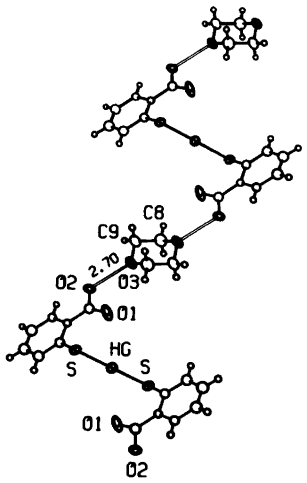

Fig. 1. The zig-zag chain of centrosymmetric BTM complexes and dioxane molecules. The hydrogen bond between O2 and O3 is indicated by the double line. The hydrogen atoms are shown in calculated positions (except for the hydrogen bond).

complete a distorted cube around each mercury atom, Fig. 2. These distances are, however, all in excess of the sum of the corresponding van der Waals radii (Hg: 1.50 Å,[7] S: 1.85 Å and O: 1.40 Å)[8] and represent therefore no significant interactions between the atoms. The length of the short Hg–S bonds, 2.361(7) Å, is typical for linearly coordinated mercury.[9] Selected interatomic distances and angles are given in Table 3.

Table 3. Selected interatomic distances (Å) and angles (°) with estimated standard deviations in parentheses. Symmetry codes:
$i = -x,1-y,-z$; $ii = -(x,y,z)$;
$iii = -x,-y,1-z$; $iv = -x,-y-1,1-z$

Within the BTM molecule			
Hg–S	2.361(7)	S–Hg–S^{ii}	180
S–C2	1.76(2)	Hg–S–C2	119.4(8)
C1–C7	1.47(3)	C1–C7–O1	128(2)
C7–O1	1.22(3)	C1–C7–O2	114(2)
C7–O2	1.30(3)	O1–C7–O2	118(2)
Within the dioxane molecule			
C8–O3	1.45(3)	O3^{iii}–C8–C9	109(2)
C9–O3	1.42(3)	C8^{iii}–O3–C9	110(2)
C8–C9	1.51(4)	C8–C9–O3	110(2)
Intermolecular distances and angles			
Hg–S^{i}	3.420(7)	S–Hg–S^{i}	88.9(2)
Hg–O1	3.11(2)	O1–Hg–O1^{i}	96.6(5)
Hg–O1^{i}	3.08(2)	C7–O2...O3^{iv}	114.3(15)
O2...O3^{iv}	2.70(3)	C8–O3^{iv}...O2	112.3(16)
		C9–O3^{iv}...O2	124.2(16)

The oxygen atoms O1 och O2 of the carboxyl group are twisted 0.30(2) and −0.24(2) Å, respectively, out of the plane of the benzene ring. The twist angle of 14° is probably a result of the relatively strong hydrogen bond, 2.70(3) Å, between the carboxyl oxygen O2 atom and the dioxane oxygen O3 atom, Fig. 1.

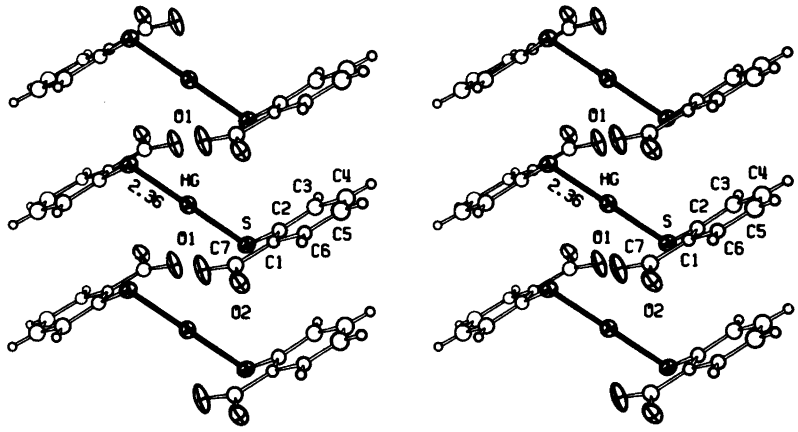

Fig. 2. BTM complexes stacked on top of each other along the monoclinic *b* axis of the unit cell. The short linear S–Hg–S bonds in the BTM complex are drawn with solid lines. The thermal ellipsoids are drawn to enclose 30% probability.

None of the carbon–carbon and carbon–oxygen distances and angles within the aromatic ring and the dioxane molecule are significantly different from their expected values.[6]

In view of the BTM dioxane structure discussed above, it seems probable that, in the mixed metal complexes formed by the ability of BTM to take up various metal ions, these additional metal ions can replace the dioxane molecule and be held between the carboxyl groups of neighbouring BTM complexes in solid state. In solution, however, intramolecular chelate bonding between the two carboxyl groups of a BTM molecule, might occur. The mode of coordination in solution will be the subject of a further study.

Acknowledgements. The authors wish to thank the Swedish National Science Research Council and the International Seminar for financial support. Professor Ingmar Grenthe is acknowledged for stimulating discussions.

REFERENCES

1. Lewicha, M. *Mat. Fiz. Chem. 1* (1976) 179.
2. Alniami, N. S. and Alsaadi, B. M. *J. Inorg. Nucl. Chem. 36* (1974) 1617.
3. Alsaadi, B. M. *To be published.*
4. Kopfmann, G. and Huber, R. *Acta Crystallogr. A 24* (1968) 348; North, A. C. T., Phillips, D. C. and Scott Mathews, F. *Ibid*, 351.
5. Nicolet XRD, 10060 Bubb Road, Cupertino, California 95014, U.S.A.
6. *International Tables for X-Ray Crystallography*, Kynoch Press, Birmingham 1969 and 1974, Vols. 1, 3 and 4.
7. Grdenic, D. *Q. Rev. Chem. Soc. 19* (1965) 303.
8. Pauling, L. *The Nature of the Chemical Bond*, 3rd Ed., Cornell University Press, New York 1960, p. 189.
9. Perchard, C., Zuppiroli, G., Gouzerti, P., Jeannin, Y. and Robert, F. *J. Mol. Struct. 72* (1981) 119.

Received November 10, 1981.

Acta Chemica Scandinavica A 36 (1982) 513–515

Equilibrium Geometry and Conformational Preference of Tricyclo[3.1.0.0^{2,4}]hexane

PER N. SKANCKE

Department of Chemistry, Institute for Mathematical and Physical Sciences, University of Tromsø, P.O. Box 953, N-9001 Tromsø, Norway

A complete geometry optimization of the chair and the boat form of tricyclo[3.1.0.0^{2,4}]hexane has been performed using the gradient technique of Pulay. The structural differences between the two molecular forms are consistent with severe strain in the boat form which is 20.7 kcal/mol less stable than the observed chair form.*

In a previous paper[1] we have carried through *ab initio* calculations on bicyclic hydrocarbons of the type [*n*.1.0] with $n=1$, 2 and 3. The purpose of those calculations was to obtain a detailed knowledge of the molecular ground state structures of these molecules using a complete geometry relaxation. In the discussion of the bonding characteristics of these systems special attention was paid to the properties of the transannular bonds of the rings.

The present paper is a natural extension of the work referred to above.[1] The molecule tricyclo-[3.1.0.0^{2,4}]hexane (TCH) has two intraannular bonds and is expected to have more ring strain than the corresponding bicyclic system. The nature of the intraannular bonds in this molecule as compared to the one in bicyclohexane is of interest in the present context.

The ground state structure of TCH has been examined in an electron diffraction investigation by Geise *et al.*.[2] Their work also included *ab initio* calculations using an STO-3G basis. The analysis of the diffraction data was based on an assumed chair form of the molecule. Due to near degeneracy of bond distances which always complicates experimental structure analyses of this kind, only average values of C–C and C–H bond distances were determined.

In a very recent paper that appeared after the initiation of the present study a complete geometry relaxation of the chair form of TCH has been given.[3] We decided to complete the present study for two reasons.

Firstly our basis, 4–31G, is slightly different from the 4–21 basis used in that paper. However, more important is the fact that we have also included in our study a complete relaxation of the boat form of the molecule. To our knowledge this form of the molecule has not been observed. This has been done in order to get information on possible structural differences between the two molecular forms, and also to obtain an estimate of their relative energies.

COMPUTATIONAL METHOD

The geometry optimizations were performed by means of the program TEXAS written by Pulay.[4] This program uses a force-relaxation method in the optimizations.[5]

The basis set applied was the 4–31G basis of Pople *et al.*[6] As demonstrated previously this basis is particularly suitable for the prediction of differences between related bond distances.[1] However, predicted absolute values using this basis have to be corrected in order to bring them in accordance with experimental values.[7]

The end points in the geometry variations were defined by changes less than 0.002 Å in bond distances and less than 0.5° in valence angles when reasonable values of the appropriate force constants were used.

*1 kcal = 4.184 kJ.

0302-4377/82/060513-03$02.50

Table 1. Optimized geometries of the chair and boat forms of tricyclo[3.1.0.0^{2,4}]hexane. The structural parameters are defined with reference to the labelling of atoms given in Fig. 1. Distances in Å, angles in degrees.

Parameter	Chair			Boat
	This work	Ref. 2	Ref. 3	This work
R(C1–C2)	1.515		1.520	1.557
R(C2–C3)	1.505	1.508	1.516	1.507
R(C1–C5)	1.543		1.550	1.520
R(C1–H7)	1.075		1.069	1.074
R(C3–H9)	1.079	1.080	1.073	1.080
R(C3–H10)	1.080		1.072	1.074
A(C1C2C3)	110.1	109.9	109.6	113.8
A(C3C2C4)	59.2	60.0	59.2	59.7
A(C5C1H7)	128.6	127.8		129.3
A(C2C1H7)	125.3	128.8		122.3
A(C2C3H9)	119.9			114.2
A(C2C3H10)	116.0	120.0		123.0
A(H9C3H10)	113.8	110.0		112.5

RESULTS AND DISCUSSION

Predicted molecular structures for the chair form and the boat form of the molecule are given in Table 1. Experimental results[2] and previously obtained theoretical results[3] for the chair form are included for comparison.

In the refinement of the geometries we assumed C_{2h} symmetry for the chair and C_{2v} symmetry for the boat. This implies that the 4-membered ring is constrained to be planar in both isomers. This assumption is in accordance with experimental findings for the chair form.[2]

The labelling of atoms and definition of structural parameters are presented in Fig. 1.

From the data in Table 1 the redundant parameters α and τ defined in Fig. 1 can be evaluated. For the chair form we find $\alpha = 66.3°$ whereas $\alpha = 62.1°$ for the boat form. The CH_2 groups do not exhibit local C_{2v} symmetry. In the chair form the rocking angle τ has a value of 2.4°. In the boat form this angle has increased to 5.4°. An increase in both the α- and the τ-value is to be expected in going from the chair to the boat form due to the steric contact between atoms H10 and H13. Even at the equilibrium geometry of the boat form this distance is only 1.02 Å.

A more interesting structural deviation between the two molecular forms is represented by the differences in the carbon–carbon bond distances

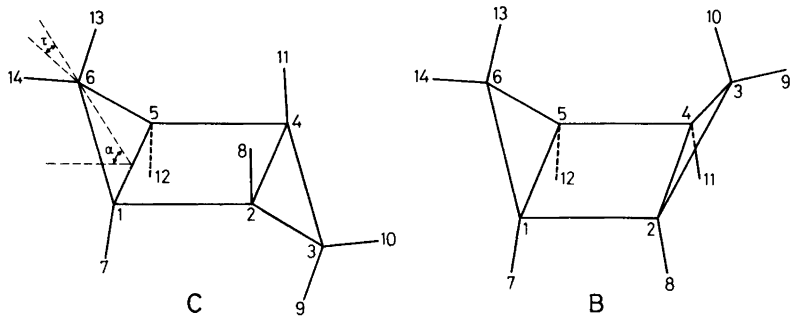

Fig. 1. Atomic arrangements and labelling in the chair (C) and boat (B) form of tricyclo[3.1.0.0^{2,4}]-hexane.

C1 – C2 and C1 – C5. The latter being a transannular bond is significantly shortened in the boat form as compared to the chair form. This shortening is coupled to an even more pronounced lengthening of the C1 – C2 bond. These structural features are compatible with a high energy model consisting of two cyclopropene units that interact more weakly than in the ground state chair form. The energy difference between the two forms is predicted to be 20.7 kcal/mol.

REFERENCES

1. Skancke, P. N. *Theochem. 86* (1982) 255.
2. Van den Enden, L., Geise, H. J., Figeys, H. P., Geerlings, P. and van Alsenoy, C. *J. Mol. Struct. 33* (1976) 69.
3. Scarsdale, J. N., van Alsenoy, C., Schäfer, L., van den Enden, L. and Geise, H. J. *Tetrahedron Lett. 22* (1981) 147.
4. Pulay, P. *Theor. Chim. Acta 50* (1979) 299.
5. Pulay, P. *Mol. Phys. 17* (1969) 197.
6. Ditchfield, R., Hehre, W. H. and Pople, J. A. *J. Chem. Phys. 54* (1971) 724.
7. Pulay, P., Fogarasi, G., Pang, F. and Boggs, J. E. *J. Am. Chem. Soc. 101* (1979) 2550.
8. Boys, S. E. In Löwdin, P. O., Ed., *Quantum Theory of Atoms, Molecules and the Solid State*, Academic, New York 1966, p. 253.

Received October 23, 1981.

Acta Chemica Scandinavica A 36 (1982) 517–533

Microwave Spectrum, Conformational Equilibria, Intramolecular Hydrogen Bonding, Dipole Moments, ^{14}N Nuclear Quadrupole Coupling Constants and Centrifugal Distortion Constants of 2,2-Difluoroethylamine

K.-M. MARSTOKK and HARALD MØLLENDAL

Department of Chemistry, The University of Oslo, P.O. Box 1033, Blindern, Oslo 3, Norway

The microwave spectrum of 2.2-difluoroethylamine, $CHF_2CH_2NH_2$, has been investigated in the 17.9 – 28.5 GHz spectral range. The three conformations denoted I, II and III and shown in Fig. 1 were assigned. Conformations I and II are stabilized by one and III by two weak intramolecular hydrogen bonds. The enthalpy difference between I and III is 1.0(7) kJ/mol with III as the more stable. III is also more stable than II by 1.5(7) kJ/mol. The two hypothetical rotamers IV and V (Fig. 1) are at least 2 kJ/mol less stable than any one of the three assigned conformations.

The FCCN dihedral angle of the hydrogen bond is 60.0(10)° in both I and II. The CCN angle has a "normal" value of 109.0(10)° in I, while this angle opens up to 114.0(10)° in both II and III.

Two vibrationally excited states were assigned for I and III, while one such excited state was identified for II. The vibrational frequencies of these excited states were determined by relative intensity measurements. Force field calculations using the centrifugal distortion constants were made as an independent method of determining the C–C torsional frequencies. The values found by this method were 107(10) cm^{-1} for I, 119(10) cm^{-1} for II, and 127(10) cm^{-1} for III, respectively.

The dipole moments are $\mu_a = 2.042(15)$ D, $\mu_b = 1.101(29)$ D, $\mu_c \sim 0$ D, and $\mu_{tot.} = 2.320(27)$ D, for I, $\mu_a = 1.073(14)$ D, $\mu_b = 0.22(23)$ D, $\mu_c = 1.483(26)$ D, and $\mu_{tot.} = 1.844(57)$ D for II, and $\mu_a = 0.090(28)$ D, $\mu_b = 0$ D (for symmetry reasons), $\mu_c = 1.427(28)$ D, and $\mu_{tot.} = 1.430(30)$ D for III, respectively.

^{14}N quadrupole coupling constants of conformation I are $\chi_{aa} = 3.1(10)$ MHz, and $\chi_{bb} = 2.5(6)$ MHz. No determination of these constants was made for II, whereas $\chi_{aa} = -3.77(17)$ MHz, and $\chi_{bb} = 2.78(17)$ MHz were found for III.

Extensive centrifugal distortion analyses were carried out for both the ground and excited states of all three rotamers and accurate values were found for the centrifugal distortion constants of the ground states of all the three rotamers assigned in this work.

Several amines with weak intramolecular hydrogen bonds have been studied by microwave spectroscopy in recent years. These studies include $CF_3CH_2NH_2$,[1] $CH_2NH_2CH_2NH_2$,[2] $CH_3OCH_2CH_2NH_2$[3] and $CH_2FCH_2NH_2$.[4] Amines may use both amino group hydrogen atoms for forming hydrogen bonds. More than one hydrogen-bonded conformation is thus possible in most cases. Two hydrogen-bonded rotamers have been assigned for $CH_2NH_2CH_2NH_2$[2] and for $CH_2FCH_2NH_2$,[4] while only one conformation has been found for each of $CF_3CH_2NH_2$[1] and $CH_3OCH_2CH_2NH_2$.[3]

2,2-Difluoroethylamine, $CHF_2CH_2NH_2$, may possess four weakly hydrogen-bonded rotamers as shown in Fig. 1. Conformations I, II, and IV each have one hydrogen bond, whereas III has two such bonds. Only one conformation having no hydrogen bonds is possible for $CHF_2CH_2NH_2$, *viz.* V. It is believed to be less stable than hydrogen-bonded conformations because it lacks this stabilizing interaction.

The object of this work has been to study the role of hydrogen bonding and other forces for the conformational preferences of $CHF_2CH_2NH_2$. Three rotamers, namely I, II, and III of Fig. 1 were

0302-4377/82/060517-17$02.50

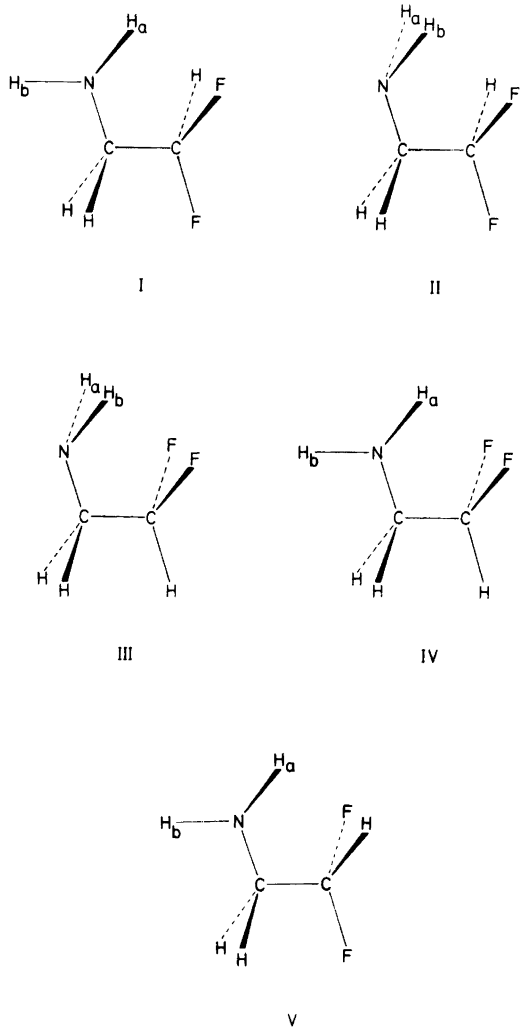

Fig. 1. Possible conformations of $CHF_2CH_2NH_2$ with all-staggered atomic arrangements. All but V contain hydrogen bonds. I, II, and III were assigned and each found to be at least 2 kJ/mol more stable than IV and/or V.

assigned, while no assignments could be made for IV and V which are presumed to be at least 2 kJ/mol less stable than any one of these three identified rotamers.

EXPERIMENTAL

The hydrochloride of 2,2-difluoroethylamine was donated by Professor R.W. Taft of the University of California at Irvine. This compound was mixed with solid powdered sodium hydroxide, heated gently and distilled. The pure amine was then obtained by gas chromatography of the water-containing distillate.

The microwave spectrum was recorded in the 17.9 – 28.5 GHz spectral region using a conventional microwave spectrometer equipped with free-running klystrons. With this equipment, quadrupole fine-structure splittings larger than about 0.6 MHz were resolved. The spectrum was recorded at pressures of about 1.3 Pa. Nearly all spectral measurements were made at −65(5) °C. A few recordings of relative intensities were also made at room temperature.

RESULTS

Microwave spectrum and assignment of the ground vibrational state of conformation I. The microwave spectrum of $CHF_2CH_2NH_2$ is dense with absorptions occurring practically everywhere. The most intense lines are of moderate strengths. The peak absorption coefficients of the strongest transitions observed were roughly 3×10^{-7} cm^{-1} at about -65 °C.

The dipole moment components along the principal axes were predicted to be $\mu_a = 2.1$ D, $\mu_b = 0.4$ D, and $\mu_c = 0$ D, respectively, for conformation I using the bond-moment method.[5] A comparatively simple spectrum dominated by strong *a*-type *R*-branch transitions was thus predicted for this rotamer. The $J = 2 \rightarrow 3$ *a*-type *R*-branch transitions were consequently searched for and readily assigned by their spectral positions, strengths, well-resolved Stark effects and rigid-rotor fit. The preliminary rotational constants thus obtained were used to predict the spectral positions of further *a*-type *R*-branch lines as well as the relatively strong *b*- and *c*-type *Q*-branch series. The *b*-type *Q*-branch series and additional *R*-branch *a*-type lines were found with ease. No *c*-type absorptions were seen. This is in keeping with the small μ_c being very close to zero as shown in a later section.

In addition to low J *a*- and *b*-type *R*-branch and low and medium J *b*-type *Q*-branch lines, the spectrum of conformation I also contains medium and high J *a*-type *Q*-branch transitions of considerable strengths since μ_a is 2.042(15) D (see below) in addition to moderate or low intensity medium and high J *P*- and *R*-branch *b*-type absorptions. These strong *Q*-branch lines have unresolved, comparatively slow Stark effects, whereas the *b*-type *P*- and *R*-branch lines in question have very rapid Stark effects because of the μ_a-connection between the coalescing K_{-1}-doublet energy levels.

The preliminary centrifugal distortion constants obtained from the strong low and medium J transitions were not very accurate. The spectral positions of the high J transitions could therefore not be predicted very precisely. The initial searches for these lines were, therefore, not conclusive because several alternatives were found in most cases in this dense spectrum. Their definite assignments were first made after the completion of the assignments of the ground vibrational states of conformations II and III which reduced the number of possibilities very much. The maximum J transitions identified were the coalescing pair of $35_{22} \rightarrow 34_{23}$ for the *P*-branch, the $65_{17,49} \rightarrow 65_{17,48}$ transition for the *Q*-branch and the coalescing K_{-1} energy level doublets $38_{21} \rightarrow 39_{20}$ for the *R*-branch transitions. Even higher J transitions were searched for but no identifications could be made presumably because of insufficient intensities of these lines.

A total of about 90 transitions were assigned for the ground vibrational state of conformation I. A portion of the spectrum * is shown in Table 1. The spectroscopic constants shown in Table 2 were derived using 78 well-resolved transitions. Fairly accurate quartic centrifugal distortion constants were obtained, while the two sextic distortion constants are of a rather poor quality. However, their inclusion was necessary in order to get a good fit.

Some of the transitions were split by quadrupole coupling between the nitrogen nucleus and the overall rotation. These lines were included in the final fit after allowance had been made for this effect in the manner to be described in the section on quadrupole coupling.

Vibrationally excited states of I. The ground state transitions were accompanied by a satellite spectrum presumably belonging to vibrationally excited states of conformation I. The strongest of these satellites had about 35 % of the intensity of the ground state at $-65(5)$ °C. Relative intensity measurements performed largely as prescribed by Esbitt and Wilson[6] yielded 141(30) cm^{-1} for this vibration. Force-field calculations as described below yielded 107(10) cm^{-1}; a considerable improvement of accuracy in comparison with the relative intensity method. The vibrational frequency is close to 124(10) cm^{-1} determined for the corresponding mode of the closely related molecule CHF_2CH_2OH.[7] The rotational constants as well as their variations upon excitation are close to their counterparts of CHF_2CH_2OH[7] which has a conformation and mass distribution quite similar to conformation I of $CHF_2CH_2NH_2$.

The transitions assigned for this excited state were the low J *a*-type *R*-branch lines, through which the initial identifications were made; and the high J *a*-type *Q*-branch lines with a maximum value of J of

* The complete microwave spectrum of all three rotamers assigned as well as their vibrationally excited states is available from the authors upon request or from Molecular Spectra Data Center, Bldg. 221, Room B 265, National Bureau of Standards, Washington D.C. 20234, U.S.A. where it has been deposited.

Table 1. Selected transitions for the ground vibrational state of conformation I of $CHF_2CH_2NH_2$.

Transition	Observed frequency[a] (MHz)	Obs. − calc. frequency (MHz)	Centrifugal distortion Total (MHz)	Sextic (MHz)
a-type				
$2_{1,2}\rightarrow 3_{1,3}$	18221.07	−0.10	−0.08	
$2_{0,2}\rightarrow 3_{0,3}$	19198.49	−0.11	−0.07	
$2_{2,1}\rightarrow 3_{2,2}$	19586.18	0.06	−0.28	
$2_{2,0}\rightarrow 3_{2,1}$	19973.84	0.02	−0.31	
$2_{1,1}\rightarrow 3_{1,2}$	20826.83	−0.04	−0.18	
$3_{1,3}\rightarrow 4_{1,4}$	24194.65	0.01	−0.17	
$3_{3,1}\rightarrow 4_{3,2}$	26292.85	−0.01	−0.81	
$3_{1,2}\rightarrow 4_{1,3}$	27636.17	0.00	−0.34	
$10_{2,9}\rightarrow 10_{2,8}$	24365.69	0.07	−3.91	
$19_{5,15}\rightarrow 19_{5,14}$	18790.03	0.07	−14.61	0.01
$27_{7,21}\rightarrow 27_{7,20}$	24156.87	0.03	−38.44	0.06
$46_{12,35}\rightarrow 46_{12,34}$	25928.75	0.07	−137.38	1.13
$57_{15,43}\rightarrow 57_{15,42}$	21524.99	0.07	−195.39	3.05
$65_{17,49}\rightarrow 65_{17,48}$	23305.61	0.16	−239.04	6.51
b-type				
$2_{0,2}\rightarrow 3_{1,3}$	22736.47	−0.09	−0.10	
$3_{1,3}\rightarrow 4_{0,4}$	21655.81	0.11	−0.12	
$4_{1,4}\rightarrow 5_{0,5}$	28421.56	−0.05	−0.24	
$8_{4,4}\rightarrow 9_{3,7}$	19017.72	−0.06	0.99	
$14_{7,7}\rightarrow 15_{6,10}$	26925.96	0.05	2.77	
$6_{0,6}\rightarrow 6_{1,5}$	18759.30	0.06	−1.07	
$7_{0,7}\rightarrow 7_{1,6}$	23634.51	−0.11	−1.58	
$6_{1,6}\rightarrow 6_{2,5}$	26794.50	0.09	−1.46	
$10_{1,9}\rightarrow 10_{2,8}$	26594.24	−0.08	−4.34	
$5_{2,3}\rightarrow 5_{3,2}$	26526.33	0.10	−1.09	
$8_{2,6}\rightarrow 8_{3,5}$	22343.96	−0.07	−2.51	
$12_{2,10}\rightarrow 12_{3,9}$	25463.56	0.04	−6.81	
Coalescing lines[b]				
$35_{22}\rightarrow 34_{23}$	25338.17	0.01	−25.71	0.99
$24_{13}\rightarrow 25_{12}$	24298.88	0.06	14.69	−0.15
$28_{15}\rightarrow 29_{14}$	28176.35	−0.06	22.96	−0.32
$33_{18}\rightarrow 34_{17}$	26988.42	−0.06	36.93	−0.72
$38_{21}\rightarrow 39_{20}$	25834.56	0.03	55.07	−1.45

[a] ±0.10 MHz. Transitions with resolved quadrupole splittings have been corrected for this effect. [b] The K_{-1}-energy doublets coalesce for high values of K_{-1}. Subscripts of J-quantum number refer only to K_{-1}.

49 belonging to the $49_{13,37}\rightarrow 49_{13,36}$ transition. In addition, the low J R- and Q-branch b-type lines were assigned. The high J P- and R-branch b-type lines were too weak to be assigned. A total of 41 transitions were identified for this mode and the spectroscopic constants shown in Table 2 were derived.

The second excited state lines of this normal mode should have about 10% of the intensities of the corresponding ground state transitions. These lines should thus have sufficient intensities to be observed. A search was made for them and tentative assignments were made for 7 a-type R-branch lines yielding $A = 8928.9(26)$ MHz, $B = 3687.84(13)$ MHz and $C = 2823.89(12)$ MHz (not included in Table 2).

The first excited state of what is assumed to be the lowest heavy-atom bending mode was also assigned with the spectroscopic constants displayed in Table 2. The types of transitions assigned were the same as for the first excited heavy-atom torsional mode.

Table 2. Spectroscopic constants for conformation I of $CHF_2CH_2NH_2$.[a]

Vibrational state	Ground	First ex. C−C tors.	First ex. lowest bending mode
Number of transitions	78	41	22
rms (MHz)	0.068	0.095	0.138
A_v (MHz)	8987.2718(51)	8947.288(15)	8987.217(50)
B_v (MHz)	3699.8821(19)	3692.383(11)	3692.988(21)
C_v (MHz)	2828.9179(18)	2826.230(11)	2823.580(21)
Δ_J (kHz)	0.9455(49)	−0.04(35)	1.47(60)
Δ_{JK} (kHz)	7.294(15)	6.28(21)	7.86(67)
Δ_K (kHz)	0.838(14)	1.4(13)	−25.8(43)
δ_J (kHz)	0.2089(16)	0.1779(68)	0.332(37)
δ_K (kHz)	4.793(61)	4.58(19)	4.29(75)
H_J (Hz)	−0.00258(58)	−[b]	−[b]
H_{JK}	−0.0092(10)	−0.0127(53)	−[b]

[a] Uncertainties represent one standard deviation. rms is the root-mean-square deviation. Further sextic centrifugal distortion constants were kept at zero in least-squares fit. [b] Kept at zero in least-squares fit.

Maximum J was 19 for the $19_{5,15}\rightarrow 19_{5,14}$ transition.

The intensities of the lines of this mode are about 20% of the corresponding ground state transitions. A frequency of 228(40) cm^{-1} was determined for this normal mode by relative intensity measurements. This corresponds well with 243(20) cm^{-1} found for the lowest bending mode of CHF_2CH_2OH.[7] However, the changes of the rotational constants upon excitation of this mode are not very similar in the two molecules. The reason for this dissimilarity is perhaps that somewhat different coupling schemes exist for the heavy-atom bending modes in each of the two molecules.

In the case of CHF_2CH_2OH [7] the second lowest bending mode having a frequency of 309(40) cm^{-1} was also assigned. A similar frequency for the corresponding mode of conformation I of $CHF_2CH_2NH_2$ should yield excited state transitions with about 10% of the intensities of their ground-state counterparts. Searches were made for such an excited state, but an assignment was not reached possibly because of the richness – and frequent overlaps – occurring in the spectrum of $CHF_2CH_2NH_2$.

Dipole moment of I. Stark coefficients of low J transitions were used to determine the dipole moment. Comparatively large Stark splittings were measured in order to minimize possible quadrupole coupling effects. A d.c. voltage was applied between the Stark septrum and the cell with the modulating square wave voltage superimposed. The d.c. field strength was calibrated using the OCS $J=1\rightarrow 2$ transition with $\mu_{OCS}=0.71521$ D.[8] Each second order coefficient shown in Table 3 was assigned a standard deviation presumed to take into account

Table 3. Stark coefficients[a] and dipole moment of conformation I of $CHF_2CH_2NH_2$.

Transition		$\Delta\nu/E^2$ (MHz V^{-2} cm^2) × 10^5 Obs.	Calc.
$2_{0,2}\rightarrow 3_{0,3}$	M = 0	−0.464(5)	−0.463
	|M| = 2	1.74(2)	1.73
$2_{2,1}\rightarrow 3_{2,2}$	M = 0	0.781(9)	0.766
	|M| = 1	105(2)	112.6
$2_{1,1}\rightarrow 3_{1,2}$	|M| = 1	−1.00(1)	−0.981
	|M| = 2	−3.98(4)	−4.05

[a] Uncertainties represent one standard deviation. [b] $\mu_a=2.042(15)$ D; $\mu_b=1.101(29)$ D; $\mu_c=0.0$ D[c]; $\mu_{tot}=2.320(27)$ D. [c] Assumed, see text.

the additional uncertainty arising from quadrupole coupling. A least squares fit using a diagonal weight matrix was performed. The weights were chosen as the inverse squares of the standard deviations of the Stark coefficients appearing in Table 3. An imaginary and small value of the c-axis dipole moment component was found when all three dipole moment components were varied in the least-squares fit. In the final fit, μ_c was assumed to be zero. The results thus obtained are shown in Table 3. From the dependency of the Stark coefficients of this table on μ_c, it is estimated that this dipole moment component is definitely less than 0.2 D.

There is reasonably good agreement between the observed dipole moment components and those predicted by the bond moment method as seen above. This is independent evidence for the fact that the assigned rotamer is indeed conformation I.

The total dipole moment was calculated to be 2.1 D by the bond moment method. The experimental value of 2.320(27) D may perhaps indicate some enhancement of the dipole moment as a result of hydrogen bonding, but this is quite uncertain because of the rather rough approximation used in the bond-moment method.

^{14}N quadrupole coupling constants of I. Several low and medium J b-type transitions were split due to quadrupole coupling of the ^{14}N nucleus with the molecular rotation. In order to determine the two independent quadrupole coupling constants χ_{aa} and χ_{bb} the following procedure was employed: Only lines with no resolved quadrupole fine structure were used in a least squares fit to predict the hypothetical unsplit frequencies of the relatively few remaining transitions exhibiting a resolved quadrupole fine structure. The splittings from these hypothetical unperturbed frequencies were then least squares fitted using eqn. (1). The symbols of this equation are defined in Ref. 9.

$$E_q = [2f(I,J,F)]/J(J+1)\sum_g \chi_{gg}\langle P_g^2\rangle \qquad (1)$$

The quadrupole splittings are relatively small for a nitrogen-containing molecule and normally overlap each other to lesser or greater extent. The data to be fitted to eqn. (1) are thus correlated and a symmetrical weight matrix applies to such cases. Application of this kind of weight matrix is not easy and the simpler method using diagonal weight matrix was chosen. This choice is not expected to have influenced the final results in any significant manner. The weights of the diagonal matrix were taken as the inverse squares of the standard deviations of the observed splittings, E_q, shown in Table 4. The entries of this table are the best resolved quadrupole components found for this molecule and consist basically of only one quadrupole component. Inclusion of lines consisting of basically two quadrupole components in the least-squares fit was attempted but yielded somewhat less accurate values for χ_{aa} and χ_{bb} than those reported in Table 4.

After this least-squares determination of the quadrupole coupling constants had been performed, the split lines were corrected for quadrupole effects and used in the final determination of the spectroscopic constants shown in Table 2.

Assignments of the ground vibrational state of conformation II. Many strong lines remained in the spectrum after the initial assignments had been made for the ground and the vibrationally excited states of conformation I. These so-far unidentified transitions were too numerous and too strong to be attributed to unassigned vibrationally excited states

Table 4. ^{14}N quadrupole splittings and diagonal elements of the quadrupole coupling tensor of conformation I of $CHF_2CH_2NH_2$.[a]

Transition	$F \rightarrow F'$	E_q (obs.)[b,c] (MHz)	E_q (obs.) − E_q (calc.) (MHz)
$6_{0,6} \rightarrow 6_{1,5}$	6→6	−1.63(3)	0.06
$7_{0,7} \rightarrow 7_{1,6}$	7→7	−1.67(3)	−0.04
$6_{0,6} \rightarrow 6_{2,5}$	6→6	−1.20(3)	−0.11
$5_{1,5} \rightarrow 5_{2,4}$	5→5	−1.24(3)	0.08
$8_{1,7} \rightarrow 8_{2,6}$	8→8	−0.85(3)	−0.02
$10_{1,9} \rightarrow 10_{2,8}$	10→10	−1.12(3)	−0.04
$12_{2,10} \rightarrow 12_{3,9}$	12→12	−0.48(4)	0.09

[a] χ_{aa} = 3.1(10) MHz; χ_{bb} = 2.5(6) MHz. [b] Uncertainties represent one standard deviation. [c] See text.

Table 5. Selected transitions for the ground vibrational state of conformation II of $CHF_2CH_2NH_2$.

Transition	Observed frequency[a] (MHz)	Obs. − calc. frequency (MHz)	Centrifugal distortion Total (MHz)	Sextic (MHz)
a-type				
$2_{1,2}\rightarrow 3_{1,3}$	18049.15	−0.04	−0.08	
$2_{0,2}\rightarrow 3_{0,3}$	18999.64	0.11	−0.06	
$2_{2,0}\rightarrow 3_{2,1}$	19726.55	−0.06	−0.28	
$2_{2,1}\rightarrow 3_{2,2}$	19363.10	0.11	−0.25	
$3_{1,3}\rightarrow 4_{1,4}$	23971.38	0.07	−0.15	
$3_{0,3}\rightarrow 4_{0,4}$	24951.10	−0.09	−0.14	
$3_{3,0}\rightarrow 4_{3,1}$	26023.01	0.04	−0.73	
$16_{4,13}\rightarrow 16_{4,12}$	20184.56	−0.07	−9.44	0.01
$24_{6,19}\rightarrow 24_{6,18}$	26083.65	0.01	−28.30	0.05
$27_{7,21}\rightarrow 27_{7,20}$	21255.12	−0.16	−32.12	0.10
$38_{10,29}\rightarrow 38_{10,28}$	18847.36	−0.11	−64.48	0.56
c-type				
$1_{0,1}\rightarrow 2_{1,1}$	19841.20	−0.03	−0.10	
$2_{0,2}\rightarrow 3_{1,2}$	27585.67	0.07	−0.24	
$5_{1,4}\rightarrow 6_{0,6}$	22136.17	−0.08	0.14	
$8_{1,7}\rightarrow 9_{0,9}$	24891.80	0.03	0.53	
$10_{5,6}\rightarrow 11_{4,8}$	21935.80	0.11	1.03	
$12_{1,11}\rightarrow 13_{0,13}$	26865.62	−0.03	1.54	
$12_{6,6}\rightarrow 13_{5,8}$	24968.40	−0.07	1.00	
$16_{8,9}\rightarrow 17_{7,11}$	28126.76	−0.01	3.48	
$3_{1,3}\rightarrow 3_{2,1}$	20049.69	0.02	−0.37	
$5_{2,3}\rightarrow 5_{3,3}$	26216.44	−0.09	−0.94	
$8_{2,6}\rightarrow 8_{3,6}$	19718.30	−0.04	−1.65	
$14_{3,11}\rightarrow 14_{4,11}$	18351.47	−0.06	−4.62	−0.01
$18_{4,14}\rightarrow 18_{5,14}$	23007.89	0.16	−9.48	−0.02
$27_{6,21}\rightarrow 27_{7,21}$	26285.76	−0.06	−23.73	−0.15
$32_{7,25}\rightarrow 32_{8,25}$	23874.02	−0.05	−29.92	−0.34
$45_{10,35}\rightarrow 45_{11,35}$	27123.64	0.01	−63.56	−2.04
$50_{11,39}\rightarrow 50_{12,39}$	22935.77	−0.09	−65.94	−3.09
$55_{12,43}\rightarrow 55_{13,43}$	18922.49	0.08	−66.08	−4.33
$63_{14,49}\rightarrow 63_{15,49}$	23667.06	−0.05	−103.53	−10.05
$68_{15,53}\rightarrow 68_{16,53}$	19144.58	0.05	−99.03	−12.51
Coalescing lines[b]				
$18_{12}\rightarrow 17_{13}$	24072.98	−0.09	−2.37	0.01
$26_{17}\rightarrow 25_{18}$	28371.20	0.05	−9.11	0.04
$30_{19}-29_{20}$	24731.83	−0.08	−16.60	0.06
$36_{22}\rightarrow 35_{23}$	19238.94	0.06	−32.66	0.09
$22_{12}\rightarrow 23_{11}$	21538.75	−0.04	10.19	0.02
$28_{15}-29_{14}$	27139.65	−0.05	20.63	0.06
$35_{19}-36_{18}$	27714.84	−0.03	40.02	0.16
$40_{22}\rightarrow 41_{21}$	26451.75	0.07	59.27	0.27
$48_{27}-49_{26}$	22108.50	−0.04	100.34	0.51

[a] ±0.10 MHz. [b] Comments as for Table 1.

of this conformation. Several of these transitions even displayed resolved Stark splittings, while others were suspected to be split by quadrupole coupling. The intensity patterns of the lines perturbed by presumed quadrupole interaction could in no way be predicted from χ_{aa} and χ_{bb} determined for conformation I.

In our work on 2-fluoroethylamine[4] it was found

that a rotamer similar to conformation II of Fig. 1 was almost as stable as the conformation corresponding to rotamer I of this figure. Assignment of conformation II of Fig. 1 thus became the next goal.

The dipole moment components of II were predicted as $\mu_a = 1.1$ D, $\mu_b = 0.2$ D, and $\mu_c = 1.6$ D, respectively, using the bond-moment method. A spectrum dominated by strong and numerous *c*-type *Q*-branch transitions and some few relatively intense *a*-type *R*-branch lines was expected for this rotamer. The existence of a μ_a-dipole moment component produces very rapid Stark effects for the low *J* *c*-type *Q*-branch lines. This property was exploited to achieve the initial assignment of the *Q*-branch series. The *a*-type *R*-branch lines were then easily found. Extension of the assignment to high *J* *Q*-branch transitions was not difficult, since the *c*-type *Q*-branch series are relatively strong and numerous. No *b*-type lines were definitely assigned although their frequencies could be predicted very accurately. This is in agreement with the fact that $\mu_b = 0.23(23)$ D as shown below. The *b*-type lines thus have insufficient intensities to be definitely identified. Finally, the medium and high *J* *R*-branch *c*-type lines were found by a trial and error procedure amongst medium-intensity lines with very rapid Stark effects produced by the μ_a-connection between the K_{-1}-doublets.

A total of about 130 transitions were assigned for the ground vibrational state of conformation II. 40 selected lines are shown in Table 5. The derived spectroscopic constants using 114 transitions are shown in Table 6. Very accurate values were derived for the quartic centrifugal distortion constants while the sextic constants hardly have much physical significance. Their inclusion was necessary, however, in order to produce a good fit. In this case, the highest *J* value assigned was the *c*-type $68_{15,53} \rightarrow 68_{16,53}$ *Q*-branch transition. Maximum *J* *P*- and *R*-branch lines were the $30_{19} \rightarrow 29_{20}$ and $48_{27} \rightarrow 49_{26}$ transitions, respectively.

Low *J* lines were scrutinized for quadrupole splittings. Some transitions were definitely broader by this effect while the shape of others deviated from the usual Lorentzian form. However, no obvious splittings were observed. It is therefore assumed that χ_{aa} and χ_{bb} in this case take values which do not produce splittings larger than about 0.6 MHz for intense components.

Vibrationally excited states of II. A strong satellite spectrum having about 1/3 of the intensity of the ground state spectrum was assigned as the first excited state of the C–C torsional mode. Relative intensity measurements yielded 160(30) cm^{-1} for this fundamental frequency. A value of 119(10) cm^{-1} is found by the force-field calculations described below. This is similar to the values determined for I, as one would expect. The changes of the rotational constants upon excitation also closely resemble the findings for I as expected.

The spectroscopic constants for this excited state are reported in Table 6. They were derived from 45 selected transitions. *c*-Type *Q*-branch lines up to the $58_{13,45} \rightarrow 58_{14,45}$ transition and *R*-branch lines with a maximum *J* value of 31 for the $31_{17} \rightarrow 32_{16}$ coalescing K_{-1}-doublets were identified for this excited state. No assignments could be made for the

Table 6. Spectroscopic constants for conformation II of $CHF_2CH_2NH_2$.[a]

Vibrational state	Ground	First ex. C–C tors.
Number of transitions	114	45
rms (MHz)	0.072	0.087
A_v (MHz)	8900.8048(46)	8863.8060(95)
B_v (MHz)	3646.8396(18)	3641.9421(36)
C_v (MHz)	2807.5735(13)	2806.0888(29)
Δ_J (kHz)	0.8440(10)	0.738(26)
Δ_{JK} (kHz)	6.576(11)	6.409(68)
Δ_K (kHz)	0.8284(37)	0.122(84)
δ_J (kHz)	0.19209(68)	0.2039(37)
δ_K (kHz)	3.979(15)	2.18(29)
H_J (Hz)	0.00042(14)	0.0092(23)
H_{JK} (Hz)	−0.01393(37)	0.0047(33)

[a] Comments as for Table 2.

Table 7. Stark coefficients[a] and dipole moment of conformation II of $CHF_2CH_2NH_2$.[b]

		$\Delta\nu/E^2$ (MHzV^{-2} cm^2) $\times 10^6$ Obs.	Calc.
$3_{2,2}\rightarrow 4_{2,3}$	$\lvert M\rvert=1$	15.0(1)	14.5
	$\lvert M\rvert=2$	60.9(7)	60.4
$2_{1,2}\rightarrow 3_{1,3}$	$\lvert M\rvert=1$	−23.0(2)	−22.9
$1_{0,1}\rightarrow 2_{1,1}$	$\lvert M\rvert=1$	36.8(3)	37.8
$3_{1,3}\rightarrow 3_{2,1}$	$\lvert M\rvert=2$	61.1(6)	56.8
	$\lvert M\rvert=3$	89.2(7)	95.3
$2_{1,1}\rightarrow 3_{1,2}$	$\lvert M\rvert=1$	−0.785(10)	−0.766

[a] Uncertainties represent one standard deviation. [b] $\mu_a=1.073(14)$ D; $\mu_b=0.22(23)$ D; $\mu_c=1.483(26)$ D; $\mu_{tot.}=1.844(57)$ D.

second excited state of this normal mode, despite intensive searching.

Tentative assignments (not reported in Table 6) were made for 13 medium J and high J Q-branch transitions of what might be the first exited state of the lowest bending mode. $A-C$ was found to be 6100.66(76) MHz and Ray's asymmetry parameter[10] κ was determined as −0.723982. The intensities of these tentatively assigned transitions were about 20% of their presumed ground state counterparts.

Dipole moment of II. The dipole moment of this rotamer was determined in the same manner as described for I. The results are seen in Table 7. There is good agreement between the above-mentioned bond-moment computations and the experimental findings. This is independent evidence for the fact that the identified conformation is indeed rotamer II.

Assignment of the ground vibrational state of conformation III. After the assignments of conformations I and II had been made, many strong lines remained in the spectrum. Two intense so-far unassigned transitions, at 24940.94 and 28465.82 MHz, respectively, had well-resolved Stark effects. Intensity patterns of the Stark components indicated that they had to be a $J=1\rightarrow 2$ and a $J=2\rightarrow 3$ transition, respectively. Moreover, several of the strong hitherto unassigned lines displayed partially resolved Stark effects typical for Q-branch transitions. In addition, lines with presumed quadrupole splittings remained unidentified. It was thus obvious that conformations I and II could not account for the entire microwave spectrum of $CHF_2CH_2NH_2$.

The existence of conformation III seemed quite probable since the related molecule $CF_3CH_2NH_2$ is known to possess a conformation similar to III as its most stable rotamer.[1] This is a conformation with two weak hydrogen bonds. The dipole moment components for III were predicted to be $\mu_a=0.10$ D and $\mu_c=0.82$ D. μ_b is zero for this conformation since the $a-c$-principal axes plane is also its symmetry plane. Conformation III was thus predicted to have a moderately strong c-type spectrum and a very weak a-type spectrum.

It was then assumed that the line at 24940.94 MHz was either the $1_{1,0}\rightarrow 2_{2,0}$ (which turned out to be correct) or the $1_{1,1}\rightarrow 2_{2,1}$ transition, while the absorption at 28465.82 MHz had to be the $2_{0,2}\rightarrow 3_{1,2}$ transition since this was predicted from the rotational constants found using a probable molecular model. The initial assignments were readily made using the two above-mentioned lines together with lines presumed to be medium J c-type Q-branch transitions as judged by their Stark effects. The assignments of the c-type Q-branch lines were easily extended up to the $64_{18,46}\rightarrow 64_{19,46}$ transition. Only the low J c-type R-branch lines were identified. The high J, P and R-branch lines were not sufficiently strong to be assigned. No a-type transitions were seen although their hypothetical frequencies could be very exactly predicted. This was expected since μ_a is 0.090(28) D (see below). About 50 transitions were assigned for this conformation. Some of them were resolvably split by quadrupole effects while others were distorted from the ordinary Lorentzian shape. The split lines were "corrected" for quadrupole coupling effects in the same manner as described for conformation I. (See also later section.) The 47 lines shown in Table 8 were used to derive the spectroscopic constants shown in Table 9.

For molecules possessing an $a-c$-axes symmetry plane the following relation exists for the principle moments of inertia, *viz.* $I_a+I_c-I_b=\Sigma m_i b_i^2+\Delta$

Table 8. Microwave spectrum of the ground vibrational state of conformation III of $CHF_2CH_2NH_2$.

Transition	Observed frequency[a] (MHz)	Obs. – calc. frequency (MHz)	Centrifugal distortion Total (MHz)	Sextic (MHz)
$6_{2,5}\rightarrow6_{3,3}$	19448.76	0.03	−1.60	
$7_{2,6}\rightarrow7_{3,4}$	22038.31	0.05	−2.39	
$8_{2,7}\rightarrow8_{3,5}$	25848.05	−0.04	−3.38	
$5_{3,2}\rightarrow5_{4,2}$	22608.17	−0.02	−0.61	
$6_{3,3}\rightarrow6_{4,3}$	21994.55	−0.04	−1.33	
$7_{3,4}\rightarrow7_{4,4}$	20899.46	−0.06	−2.14	
$8_{3,5}\rightarrow8_{4,5}$	19229.33	−0.04	−3.00	
$5_{3,3}\rightarrow5_{4,1}$	22970.71	0.09	−0.64	
$6_{3,4}\rightarrow6_{4,2}$	23039.98	−0.11	−1.42	
$7_{3,5}\rightarrow7_{4,3}$	23336.97	−0.12	−2.34	
$8_{3,6}\rightarrow8_{4,4}$	24067.68	−0.06	−3.40	
$9_{3,7}\rightarrow9_{4,5}$	25507.10	−0.08	−4.60	
$10_{3,8}\rightarrow10_{4,6}$	27960.88	0.12	−5.95	
$9_{4,5}\rightarrow9_{5,5}$	27855.29	0.05	−4.53	
$10_{4,6}\rightarrow10_{5,6}$	26514.70	−0.01	−6.06	
$11_{4,7}\rightarrow11_{5,7}$	24535.51	0.07	−7.65	
$12_{4,8}\rightarrow12_{5,8}$	21917.98	−0.01	−9.17	−0.01
$13_{4,9}\rightarrow13_{5,9}$	18793.05	0.08	−10.45	−0.01
$15_{5,10}\rightarrow15_{6,10}$	27006.08	0.05	−18.19	−0.02
$16_{5,11}\rightarrow16_{6,11}$	23463.79	−0.09	−20.32	−0.03
$19_{6,13}\rightarrow19_{7,13}$	28384.94	0.15	−35.35	−0.07
$20_{6,14}\rightarrow20_{7,14}$	23993.83	0.01	−37.66	−0.08
$21_{6,15}\rightarrow21_{7,15}$	19376.06	0.08	−38.42	−0.10
$24_{7,17}\rightarrow24_{8,17}$	23642.30	−0.04	−62.02	−0.21
$25_{7,18}\rightarrow25_{8,18}$	18521.94	−0.06	−60.73	−0.23
$27_{8,19}\rightarrow27_{9,19}$	28237.28	−0.01	−94.54	−0.41
$28_{8,20}\rightarrow28_{9,20}$	22558.72	−0.07	−93.50	−0.45
$31_{9,22}\rightarrow31_{10,22}$	26950.71	0.01	−137.49	−0.82
$32_{9,22}\rightarrow32_{10,23}$	20907.51	−0.02	−131.18	−0.86
$35_{10,25}\rightarrow35_{11,25}$	25052.15	0.07	−188.21	−1.48
$36_{10,26}\rightarrow36_{11,26}$	18862.64	0.03	−172.96	−1.48
$39_{11,28}\rightarrow39_{12,28}$	22710.35	−0.03	−244.16	−2.47
$42_{12,30}\rightarrow42_{13,30}$	26937.29	−0.12	−334.68	−3.92
$43_{12,31}\rightarrow43_{13,31}$	20101.48	0.06	−301.44	−3.79
$46_{13,33}\rightarrow46_{14,33}$	23995.64	0.00	−410.12	−5.91
$49_{14,35}\rightarrow49_{15,35}$	28273.52	−0.02	−544.78	−8.91
$53_{15,38}\rightarrow53_{16,38}$	24814.13	0.01	−638.48	−12.46
$57_{16,41}\rightarrow57_{17,41}$	21328.66	0.05	−720.18	−16.48
$60_{17,43}\rightarrow60_{18,43}$	25208.92	0.03	−936.88	−23.74
$61_{17,44}\rightarrow61_{18,44}$	17973.24	−0.02	−782.68	−20.72
$64_{18,46}\rightarrow64_{19,46}$	21401.19	−0.03	−1021.39	−29.76
$1_{0,1}\rightarrow2_{1,1}$	19682.70	−0.05	−0.09	
$1_{1,0}\rightarrow2_{2,0}$	24940.94	−0.06	−0.12	
$1_{1,1}\rightarrow2_{2,1}$	25561.31	0.03	−0.12	
$2_{0,2}\rightarrow3_{1,2}$	28465.82	0.09	−0.25	
$3_{1,2}\rightarrow4_{0,4}$	23367.84	−0.01	−0.05	
$3_{2,1}\rightarrow4_{1,3}$	23318.57	−0.02	−0.18	

[a] ±0.10 MHz. Transitions with resolved quadrupole splittings have been corrected for this effect.

Table 9. Spectroscopic constants for conformation III of $CHF_2CH_2NH_2$.[a]

Vibrational state	Ground	First ex. C−C tors.	First ex. lowest bending mode
Number of transitions	47	34	22
rms (MHz)	0.069	0.090	0.147
A_v (MHz)	7125.170(12)	7142.150(26)	7158.743(31)
B_v (MHz)	4185.890(13)	4179.324(27)	4184.917(28)
C_v (MHz)	3441.172(13)	3429.070(27)	3435.758(45)
Δ_J (kHz)	1.0(5)	−1.5(20)	−[b]
Δ_{JK} (kHz)	8.34(10)	9.32(15)	8.76(84)
Δ_K (kHz)	−6.59(36)	−7.87(55)	−7.7(29)
δ_J (kHz)	0.2420(58)	0.2521(94)	0.232(37)
δ_K (kHz)	1.53(15)	1.56(25)	0.39(68)
H_{JK} (Hz)	−0.02252(49)	−0.0200(16)	−[b]

[a,b] Comments as for Table 2.

where b_i is the b-principle axis coordinate of the out-of-plane atoms. The m_i's are their masses and Δ is the inertial defect. In the case of conformation III of $CHF_2CH_2NH_2$ $I_a+I_c-I_b$ is found to be 97.05663(68) uÅ^2. In the identified conformation of $CF_3CH_2NH_2$ the corresponding value was found as 96.9(3) uÅ^2. The close resemblance of the two values of $I_a+I_c-I_b$ is expected because each of the two conformations of the two molecules possesses two out-of-plane fluorine atoms, two methylene group hydrogen atoms, and two amino group hydrogen atoms.

Vibrationally excited states of III. Two vibrationally excited states were assigned for conformation III as indicated in Table 9. The strongest of these two excited state spectra had about 40 % of the intensity of the ground state spectrum. This state is assigned as the first excited state of the C−C torsional mode both because of its strength and because $I_a+I_c-I_b$ increases [11] upon excitation to 97.2166(14) uÅ^2. This is expected for an out-of- plane torsional mode. Low J c-type R-branch transitions and Q-branch lines with a maximum J value of 54 (for the $54_{15,39}\rightarrow 54_{16,39}$ transition) were assigned for this excited state. The frequency of this torsional mode was determined as 141(30) cm^{-1} by relative intensity measurements. A value of 127(10) cm^{-1} was found by the force-field calculations described below.

The second excited state which was identified for this conformation had about 20 % of the intensity of the ground state. Relative intensity measurements yielded 234(40) cm^{-1} for this normal vibration which is presumed to be the lowest heavy-atom bending mode. $I_a+I_b-I_c$ takes the value of 96.9274(21) uÅ^2 which is smaller than the corresponding ground state value. A reduction of $I_a+I_b-I_c$ upon excitation is predicted [11] for a bending mode of an A' vibrational species fundamental in agreement with the present finding.

The spectroscopic constants for this excited state (Table 9) were derived from 22 transitions with a maximum value of $J=43$ for the $43_{12,13}\rightarrow 43_{13,31}$ transition.

Table 10. Stark coefficients[a] and dipole moment of conformation III of $CHF_2CH_2NH_2$.[b]

Transition		$\Delta\nu/E^2$(MHzV^{-2} cm^2) × 10^6 Obs.	Calc.
$1_{1,0}\rightarrow 2_{2,0}$	M = 0	−6.79(7)	−7.48
	|M| = 1	7.30(7)	7.32
$2_{0,2}\rightarrow 3_{1,2}$	M = 0	1.26(2)	1.37
	|M| = 1	19.0(1)	17.9
	|M| = 2	74.5(7)	78.2

[a] Uncertainties represent one standard deviation. [b] $\mu_a=0.090(28)$ D; $\mu_c=1.427(28)$ D; $\mu_{tot.}=1.430(30)$ D.

Table 11. ^{14}N quadrupole splittings and diagonal elements of the quadrupole coupling tensor of conformation III of $CHF_2CH_2NH_2$.[a]

Transition	$F \rightarrow F'$	E_q(obs.)[b,c] (MHz)	E_q(obs.) − E_q(calc.) (MHz)
$1_{1,1} \rightarrow 2_{2,1}$	2→3	−0.17(3)	−0.04
	0→1	0.48(5)	0.03
$3_{2,1} \rightarrow 4_{1,3}$	4→5	0.34(3)	0.04
	3→4	−0.87(5)	−0.07
$5_{3,3} \rightarrow 5_{4,1}$	6→6	−0.19(4)	0.07
	5→5	0.73(3)	0.06
$5_{3,2} \rightarrow 5_{4,2}$	6→6	−0.30(4)	−0.02
	5→5	0.65(3)	−0.08
$6_{3,3} \rightarrow 6_{4,3}$	7→7	−0.14(4)	0.09
	6→6	0.58(3)	0.00

[a] $\chi_{aa} = -3.77(17)$ MHz; $\chi_{bb} = 2.78(17)$ MHz. [b,c] Comments as for Table 4.

Dipole moment of III. The dipole moment of III was determined in the same manner as described above for the two other rotamers. The results are shown in Table 10. The total dipole moment is 1.430(30) D as compared to 0.83 D calculated by the bond-moment method. The relatively large difference of 0.6 D may indicate that an enhancement of the dipole moment actually occurs in this conformation which has two contributing hydrogen bonds.

^{14}N quadrupole coupling constants of III. Several low J transitions were split by quadrupole coupling. The lines found to have a resolved quadrupole fine structure are shown in Table 11. χ_{aa} and χ_{bb} shown in this table were determined in the same manner as described for conformation I. Inclusion of lines consisting of more than one quadrupole component was made for conformation III. The standard deviations of E_q for such components were judiciously increased as compared with a line consisting of only one quadrupole component.

Searches for conformations IV and V. The assignments made as described above include about 430 transitions. Approximately 30 more lines were tentatively assigned. Every strong line of the spectrum has been identified. The great majority of intermediate intensity and many weak transitions have also been accounted for. Careful Stark effect studies have been made for the majority of the remaining unassigned lines of intermediate intensities. In none of these cases was a well-resolved Stark pattern seen.

Simulation of the spectra of conformations IV and V were made. These two hypothetical rotamers are the only two additional conformations with all-staggered atomic arrangements possible for $CHF_2CH_2NH_2$. The rotational constants of IV were predicted to be roughly $A = 7.2$ GHz $B = 4.2$ GHz, and $C = 3.4$ GHz. The principal axes dipole moment components were computed as $\mu_a = 1.6$ D, $\mu_b = 1.2$ D, and $\mu_c = 2.0$ D, using the bond-moment method. The corresponding molecular constants for V were computed as: $A = 9.0$ GHz, $B = 3.6$ GHz, $C = 2.8$ GHz, $\mu_a = 2.3$ D, $\mu_b = 1.7$ D, and $\mu_c = 1.7$ D. IV and V are thus each predicted to possess dipole moment components of about 2 D. They would then have as strong spectra as the identified forms provided they were present in the same amounts.

Typically, the most intense unassigned lines had roughly 15% of the intensities of the strongest (and identified) lines of the spectrum. If these unidentified transitions were indeed the spectra of IV and/or V they could not for intensity reasons be present in concentrations exceeding about 15% of each of I, II or III. It is thus concluded that conformations I, II and III each are at least 2 kJ/mol more stable than IV or V.

Furthermore, it is believed that the unidentified lines of medium strengths are high J transitions as judged by their Stark effects. More probably, they are weakly populated vibrationally excited state transitions of one or more of the three identified rotamers.

Force-field determination of the C−C torsional frequency of the three conformations. Accurate centrifugal distortion constants were determined for all the three rotamers. As shown in Table 12, these molecular constants may be used to determine the torsional frequency. The reasons for using

Table 12. Assumed force field, centrifugal distortion constants and torsional frequencies for conformations I, II, and III of $CHF_2CH_2NH_2$.[a]

Force constants common for I, II and III

Stretching (10^{-2} N m^{-1})			
C–C	4.2	C–H	4.7
C–N	5.1	N–H	6.4
C–F	4.9		
Bending (aJ rad^{-2})			
C–C–N	1.3	N–C–H	0.90
C–C–F	1.5	H–C–H	0.50
C–C–H	0.65	C–N–H	0.85
F–C–F	1.7	H–N–H	0.47
F–C–H	0.70		
Torsion (aJ rad^{-2})			
C–N	0.25		
C–C	0.0987 (conformation I)[b]		
C–C	0.1228 (conformation II)[b]		
C–C	0.1786 (conformation III)[b]		

Centrifugal distortion constants (kHz)

Conformation	I		II		III	
	Obs.	Calc.	Obs.	Calc.	Obs.	Calc.
Δ_J	0.9455(49)	1.06	0.8440(10)	0.992	1.0(5)	2.07
Δ_{JK}	7.294(15)	7.54	6.576(11)	6.92	8.34(10)	8.23
Δ_K	0.838(14)	1.00	0.8284(37)	1.25	−6.59(36)	−6.68
δ_J	0.2089(16)	0.245	0.19209(68)	0.220	0.2420(58)	0.239
δ_K	4.793(61)	4.56	3.979(15)	3.99	1.53(15)	1.06

C–C torsional frequency (cm^{-1})

Conformation	I	II	III
Force-field calculations[b]	107(10)	119(10)	127(10)
Relative intensity[a]	141(30)	160(30)	141(30)

[a] See text. [b] Obtained from least-squares fit.

centrifugal distortion constants for this purpose have been given previously.[12]

The simple diagonal force field shown in Table 12 was partly selected from related molecules or partly estimated. The centrifugal distortion constants depend primarily on the C–C torsional force constant. The C–C–F, C–C–N, and F–C–F bending force constants were also seen to contribute considerably to the centrifugal distortion constants. Only the C–C torsional force constant was varied in the least-squares fit. The remaining force constants were kept at the values shown in Table 12. Unit weights were given to the centrifugal distortion constants in the fitting procedure. The programme used was NCA written by Christen.[13]

The torsional frequencies were found to be 107 cm^{-1} for I, 119 cm^{-1} for II and 127 cm^{-1} for III. The uncertainties of these frequencies are difficult to estimate since several assumptions are involved in their derivation. However, it is felt that ± 10 cm^{-1} is a realistic error limit. The torsional frequencies obtained by this method are considerably more accurate than those obtained by the completely independent relative intensity method as shown in Table 12. The two methods yield results which agree within their estimated uncertainty limits.

It is satisfactory to note that the C–C torsional frequency of III obtained by the force-field method [127(10) cm^{-1}] is higher than those of I [107(10) cm^{-1}] and II [119(10) cm^{-1}], respectively. This is

expected since two hydrogen bonds exist in III. They would tend to make the torsional motion more rigid than in I or II where only one such bond exists.

Energy differences between the three conformers. Relative intensity measurements were made at −65(5) °C and room temperature to determine Gibbs free energy difference between the three conformers. The peak intensities were taken by slowly scanning the spectral lines. The carefully selected lines were strong and, hopefully, not seriously perturbed by overlapping lines or Stark components. Lines with unresolved quadrupole fine structure were used in order to avoid complications from this effect. In some cases high J lines with coalescing K_{-1}-doublet energy levels were utilized. The peak intensities of these lines were assumed to be equal to the sum of the intensities of the individual transitions of which these lines were composed. The equilibrium constant K for the II⇄I conformational equilibrium was calculated from[4,14] eqn. (2). The symbols of eqn. (2) have been

$$K = \frac{[\mathrm{I}]}{[\mathrm{II}]} = \frac{\alpha_{\mathrm{I}}}{\alpha_{\mathrm{II}}}\left(\frac{\nu_{\mathrm{II}}}{\nu_{\mathrm{I}}}\right)^2\left(\frac{A_{\mathrm{II}}B_{\mathrm{II}}C_{\mathrm{II}}}{A_{\mathrm{I}}B_{\mathrm{I}}C_{\mathrm{I}}}\right)^{\frac{1}{2}} \times \frac{\sum_g(\lambda_{\mathrm{II}}\mu_{g\mathrm{II}}\exp(-E^J_{r\mathrm{II}})/kT)}{\sum_g(\lambda_{\mathrm{I}}\mu_{g\mathrm{I}}\exp(-E^J_{r\mathrm{I}})/kT)} \quad (2)$$

defined previously.[4,14] This equation is based on many assumptions discussed elsewhere.[4,14] There are also many sources of errors in the measurements of peak absorption coefficients as discussed in Ref. 6. However, by using a rather large number of intensity observations as shown in Table 13, it was hoped that accurate values might be obtained for the thermodynamic parameters. The relatively small standard deviations of $\Delta G°$ (Table 13) calculated using $\Delta G° = -RT\ln K$ are reassuring. The standard deviations of $\Delta G°$ are seen to be higher for the measurements made at 22(1) °C than at −65(5) °C. This is caused by the fact that the transitions measured at room temperature have rougly 1/6 of the intensity at −65(5) °C. Measurements of $\Delta G°$ at two temperatures were made for all three equilibria in attempting to derive accurate values not only for $\Delta H°$ but for $\Delta S°$ as well. These two thermodynamic parameters were calculated from the Gibbs-Helmholtz equation.

Unfortunately, no accurate value of $\Delta S°$ could be found using the values of $\Delta G°$ shown in Table 13, as the standard deviation of $\Delta S°$ was found to be larger than $\Delta S°$ itself in all three cases. $\Delta S°$ was therefore estimated using another, and presumable more accurate, procedure. In the case of the II⇄I equilibrium, there are great structural similarities between the two rotamers. The vibrational partition functions of the two conformers are also presumed to be very similar. The quartic contrifugal distortion constants are quite similar for I and II. This is evidence for the assumption that the harmonic force fields of the two conformations are indeed similar. $\Delta S°$ for the II⇄I equilibrium is thus presumed to be very nearly zero. Using this value for $\Delta S°$ in eqn. (3), $\Delta H°$ is estimated to be −0.5(7) kJ/mol for this equilibrium. Conformation I is thus more stable than II by 0.5(7) kJ/mol.

$\Delta S°$ for the III⇄I and III⇄II equilibria was presumed to be $R\ln 2 = 5.8$ J/(mol K) since the statistical weight of I and II in each case is 2 as compared to conformation III. It is thus assumed that the vibrational partition functions are very similar and thus contribute insignificantly to the entropy difference for these two equilibria.

Table 13. Thermodynamic parameters for conformational equilibria of $CHF_2CH_2NH_2$.

Conformational equilibrium	Temp. (K)	Number of obs.	$\Delta G°$ (kJ/mol)[a]	Selected thermodynamic parameters[b] $\Delta H°$ (kJ/mol)[c]	$\Delta S°$ (J/mol K)
II⇄I	208 ± 5	13	−0.32(62)	−0.5(7)	~0
	295 ± 1	24	−0.69(84)		
III⇄I	208 ± 5	23	0.07(62)	1.0(7)	~5.8
	295 ± 1	32	−0.70(79)		
III⇄II	208 ± 5	26	0.30(43)	1.5(7)	~5.8
	295 ± 1	48	−0.09(75)		

[a] Calculated using eqn. (2) and $\Delta G° = -RT\ln K$. Uncertainties represent one standard deviation obtained from the least-squares fit. [b] See text. Uncertainties are estimated standard deviations. [c] Estimated uncertainties.

Table 14. Plausible structural parameters[a] (bond lengths in *pm*, angles in *degrees*) and observed and calculated rotational constants of conformations I, II, and III of $CHF_2CH_2NH_2$.

Assumed structural parameters common for I, II and III

C–F	135.0	∠CCF	110.0	∠HNCC[b] 0.0 or 60.0
C–N	146.9	∠FCF	108.94	
C–C	153.0	∠CCH	109.48	
C–H	109.3	∠HCH	109.48	
N–H	101.7	∠HNC	109.48	
		∠HNH	109.48	
		∠FCH	109.20	

Fitted structural parameters

Conformation	I	II	III
∠FCCN[c] from *syn*	60.0(20)	60.0(20)	60[d]
∠CCN	109.0(10)	114.0(10)	114.0(10)

Hydrogen bond parameters

	I	II	III
N···F	281	290	290
N···H	247	260	260
∠N–H···F[e]	98.4	96.4	96.4
∠C–F, N–H[e,f]	0.3	3.1	3.1

Sum of van der Waals radii[g]

N···F 285 H···F 255

Rotational constants (MHz)

	I		
	Obs.	Obs.–Cal.	Diff. (%)
A	8987.27	−34.51	0.38
B	3699.88	1.29	0.03
C	2828.92	9.84	0.35

	II		
	Obs.	Obs.–Cal.	Diff. (%)
A	8900.80	−16.09	0.18
B	3646.84	4.78	0.13
C	2807.57	1.76	0.06

	III		
	Obs.	Obs.–Cal.	Diff. (%)
A	7125.17	2.76	0.04
B	4185.89	−4.75	0.11
C	3441.17	11.08	0.32

[a] See text. [b] Dihedral angle assumed to be exactly staggered. [c] Dihedral angle involving the fluorine atom engaged in hydrogen bonding. [d] This angle is exactly 60° due to symmetry. [e] Hydrogen atom involved in hydrogen bonding. [f] Angle between C–F and N–H bonds involved in hydrogen bonding. [g] Taken from Ref. 15.

Conformation III is then found to be the most stable of the three conformers. It is favored by enthalpy by 1.0(7) kJ/mol as compared to I and by 1.5(7) kJ/mol as compared to conformation II.

Structures of the three conformations. Only one isotopic species was studied for the three rotamers and only three rotational constants are thus available for each rotamer. A complete geometrical

structure cannot, therefore, be determined for each of the three conformations. A selection of parameters to be fitted must be made. The CCN angle and the FCCN dihedral angle where the fluorine atom is involved in hydrogen bonding, were varied for conformations I and II. Only the CCN angle was fitted for III. These structural parameters were selected because the rotational constants are very sensitive to variations in these angles, because they are chemically interesting, and finally because they are presumed to be among the structural parameters of this molecule most likely to vary from one conformation to another. Further parameters expected to vary in different conformations, namely the HNCC dihedral angle, the HNC and HNH angles, *etc.*, cannot be meaningfully fitted because the rotational constants are relatively insensitive to these angles as a result of the small mass of the amino group hydrogen atoms. The amino group hydrogens were therefore assumed to be in exactly staggered positions. The remaining bond lengths and angles which were kept constant in the fit, were selected from recent accurate structural studies of related compounds. They are shown in Table 14.

The FCCN dihedral angle was varied in steps of 1° and the CCN angle in steps of 0.5°. As shown in Table 14, the rotational constants are reproduced better than 0.4 % by this procedure. The error limits of the FCCN dihedral angles and the CCN angles are assumed to encompass possible differences between the assumed structural parameters and the real ones.

DISCUSSION

2,2-Difluoroethylamine is another example of an amine which takes hydrogen-bonded conformations as its preferred forms. The intramolecular hydrogen bonds are rather weak in all the three conformations as seen by their structural characteristics given in Table 14. The hydrogen bonds are presumably mainly electrostatic in origin since the C – F and N – H bonds are nearly parallel and the corresponding bond dipoles are thus almost antiparallel which is favourable for electrostatic attraction. Covalent forces are hardly of much significance for the hydrogen bonds as the non-bonded distances between the hydrogen and fluorine atoms are approximately equal to the sum of the van der Waals radii of these two atoms.[15]

The fact that the NCCF dihedral angles are 60.0(20)° in both I and II comes as no surprise. Similar values have been found in all hydrogen-bonded amines so far studied.

Important differences exist in the CCN angles of the three conformations. As shown in Table 14, this angle is 109.0(10)° in conformation I and 114.0(10)° in both II and III. Similar findings were made for the two assigned forms of $CH_2FCH_2NH_2$.[4] The identified rotamer of $CF_3CH_2NH_2$[1] was also found to have a CCN angle of 113°50′ ± 1 . This conformation is similar to III of this work. In another related hydrogen-bonded amine, *viz.* ethylenediamine,[2] the average CCN angle of the conformation denoted II was also larger than in rotamer I of this molecule. There is no obvious explanation for these observations. Perhaps repulsion of the 1,3-type is more prevalent in those conformations having the larger CCN angle.

The fact that conformation III of $CHF_2CH_2NH_2$ is the most stable rotamer of the molecule can presumably be explained by the existence of two hydrogen bonds in this form. The slightly higher stability of I as compared to II is paralleled by the findings made for the similar two conformations of $CH_2FCH_2NH_2$.[4]

The three identified rotamers were each found to be more stable than the hypothetical conformations IV and V by at least 2 kJ/mol. Conformation IV has one hydrogen bond, but the probable direction of the amino group lone pair and the other C – F bond not involved in hydrogen bonding are nearly parallel. The resulting repulsion may perhaps explain the instability of IV as compared to the identified rotamers. In V, no hydrogen bonds exist and this may be the reason why this conformation is also less stable than the three rotamers assigned for $CHF_2CH_2NH_2$.

Acknowledgement. The authors are grateful to Professor R. W. Taft, The University of California at Irvine, for donating the sample used in this work.

Note added in proof. A more accurate method of calculating ΔH_0° has now been derived by E. B. Wilson, Jr. and will be presented in a forthcoming paper.

REFERENCES

1. Warren, I. D. and Wilson, E. B., Jr. *J. Chem. Phys.* *65* (1972) 2137.
2. Marstokk, K.-M. and Møllendal, H. *J. Mol. Struct.* *49* (1978) 221.

3. Caminati, W. and Wilson, E. B., Jr. *J. Mol. Spectrosc. 81* (1980) 356.
4. Marstokk, K.-M. and Møllendal, H. *Acta Chem. Scand. A 34* (1980) 15.
5. Smyth, C. P. *Dielectric Behavior and Structure*, McGraw-Hill, New York 1955, p. 244.
6. Esbitt, A. S. and Wilson, E. B., Jr. *Rev. Sci. Instrum. 34* (1963) 901.
7. Marstokk, K.-M. and Møllendal, H. *Acta Chem. Scand. A 34* (1980) 765.
8. Muenter, J. S. *J. Chem. Phys. 48* (1968) 4544.
9. Townes, C. H. and Schawlow, A. L. *Microwave Spectroscopy*, McGraw-Hill, New York 1955, pp. 149 – 173.
10. Ref. 9, p. 84.
11. Herschbach, D. R. and Laurie, V. W. *J. Chem. Phys. 40* (1964) 3142.
12. Braathen, O.-A., Marstokk, K.-M. and Møllendal, H. *Acta Chem. Scand. A 36* (1982) 173.
13. Christen, D. *J. Mol. Struct. 48* (1978) 101.
14. Ellingsen, B. H., Marstokk, K.-M. and Møllendal, H. *J. Mol. Struct. 48* (1978) 9.
15. Pauling, L. *The Nature of the Chemical Bond*, 3rd. Ed., Cornell University Press, New York 1960, p. 260.

Received October 23, 1981.

Acta Chemica Scandinavica A 36 (1982) 535–539

Crystal Structure Refinement of the κ-phase in the Hf–Mo–P System

ANDERS HÅRSTA

Institute of Chemistry, University of Uppsala, Box 531, S-751 21 Uppsala, Sweden

The crystal structure of κ-(Hf–Mo–P) has been determined using X-ray single-crystal diffractometry. κ-(Hf–Mo–P) crystallizes in the space group $P6_3/mmc$ (No. 194) with the cell dimensions: $a=8.6236(4)$ Å, $c=8.6101(6)$ Å. The structure has been refined on F^2 to an $R(F^2)$-value of 0.1286 without excluding any reflexions. κ-(Hf–Mo–P) is isostructural with κ-Hf_9Mo_4Ni but some hafnium substitution occurs on the molybdenum sites. According to the final refinement the composition is $Hf_{9+x}Mo_{4-x}P$ with $x=0.29(4)$.

In a recent communication[1] κ-type phases were reported to occur in the ternary systems Hf–Mo–{Si, P, S} and Hf–Mo–{Ge, As, Se}. It was observed that the unit cell volumes increased in the order κ-(Hf–Mo–Si)→κ-(Hf–Mo–P)→κ-(Hf–Mo–S), and an analogous observation was also made for the Ge, As, Se series. This feature cannot be explained in terms of nonmetal atom size effects, since the normal sizes of the nonmentals concerned decrease for both series of compounds. Vacancies or atomic substitutions in the structure might presumably be responsible for the anomalous cell volume trend, and it was therefore decided to examine some of the κ-phase structures in greater detail by accurate X-ray diffraction methods. In the present paper the results from an X-ray single-crystal refinement of κ-(Hf–Mo–P) are reported.

EXPERIMENTAL

Preparation and phase analysis. The starting materials and the method of synthesis have been described in an earlier paper.[1] Powder photographs showed diffraction lines solely from κ-(Hf–Mo–P), indicating that the sample was a single phase.

Chemical analysis. Phosphorus. The sample was dissolved in a mixture of fuming nitric acid, hydrofluoric acid and sulfuric acid with addition of perchloric acid to complete the oxidation of phosphorus. After evaporation and heating to fumes of sulfuric acid the residue was taken up in water and hydrofluoric acid. In an aliquot of this solution the phosphorus was determined spectrophotometrically according to Murphy and Riley[2] after addition of boric acid.

Molybdenum. The sample was dissolved in a mixture of sulfuric, hydrofluoric, nitric and perchloric acids, the solution evaporated and heated to fumes of sulfuric acid and the residue taken up in water. The precipitate of hafnium phosphate was removed by filtration and molybdenum determined in the filtrate by reduction in a cadmium reductor and titration with permanganate.

Hafnium. The sample was dissolved and treated as for molybdenum, and hafnium was determined separately in precipitate and solution. Hafnium remaining in the solution was precipitated with mandelic acid and the precipitate ignited to and weighed as HfO_2. The hafnium phosphate precipitate was fused with sodium carbonate and the melt extracted with water to remove phosphate. The residue was fused with potassium pyrosulfate, the melt brought into solution and hafnium precipitated with ammonia and ignited to HfO_2. The result for Hf includes Zr and the calculation was based on the assumption of 3 weight percent of Zr in the hafnium as analyzed in the hafnium used for the synthesis.

The result of the analysis was: 80.5(2) % Hf+Zr, 18.14(2) % Mo and 1.48(2) % P.

X-Ray diffraction measurements and data reduction. X-Ray powder photographs were taken using a Guinier-Hägg-type focusing camera with $CrK\alpha_1$ radiation ($\lambda=2.289753$ Å) and Si ($a=5.431065$ Å)[3] as internal standard. The unit cell dimensions were refined using the local program CELNE.[4] After

0302-4377/82/060535-05$02.50

several attempts a small fragment was found which proved to be a single crystal when examined in a Weissenberg camera. A Nonius CAD 4-F diffractometer controlled by a PDP 8/A computer was used to record the intensity data. Graphite-monochromatized Mo$K\alpha$ radiation ($\lambda = 0.71069$ Å) and the $\omega/2\theta$-scan technique were employed. During the data collection four reflexions were used as monitors and checked after every 20th reflexion scanned. The intensity of these monitors had been reduced by about 2.5% at the end of the data collection and a linear correction was applied. F_o^2 and $\sigma_c(F_o^2)$ values were obtained from the integrated peak intensities by applying corrections for background, Lorentz and polarization effects (assuming the monochromator to be ideally imperfect), and for absorption. The crystal was of irregular shape and was approximated with five boundary planes to a polyhedron with dimensions of the order of $0.04 \times 0.03 \times 0.02$ mm. Corrections for absorption were applied using the Gaussian grid method and a calculated linear absorption factor of 874 cm^{-1}. The transmission factors were found to vary from 0.19 to 0.41. In total 2736 reflexions up to 100.0° in 2θ were recorded which included the 24 symmetry related reflexions of the form {2132} which were used to check the absorption correction. After averaging equivalent reflexions 1130 remained.

Calculations. All calculations were performed with a NORD 100 computer using a system of programs described by Lundgren.[5]

STRUCTURE ANALYSIS AND RESULTS

The diffraction symmetry and the systematic absences of reflexions confirmed the space group to be $P6_3/mmc$ (No. 194) as in the case of κ-(Hf–Mo–B)[6] and κ-(Hf–Mo–Ni).[7] The structure was refined using a full-matrix least-squares program using the atomic coordinates of κ-(Hf–Mo–Ni)[7] as initial values for the positional parameters, with phosphorus replacing nickel. The atomic scattering factors for neutral atoms were used and corrected for anomalous dispersion[8] (real as well as imaginary parts). The quantity minimized was $\Sigma w(|F_o^n| - k^n \cdot |F_o^n|)^2$ with $n = 1$ or 2 and the weight w was given by

$$w^{-1} = \sigma_c^2(F_o^n) + (p \cdot |F_o^n|)^2$$

where σ_c is the standard deviation of F_o^n based on counting statistics and p an empirical parameter chosen to obtain a satisfactory weight analysis (p was 0.04 in the final refinement). The agreement indices are defined as

$$R(F^n) = \Sigma(|F_o^n| - |F_c^n|)/\Sigma|F_o^n|$$

$$R_w(F^n) = [\Sigma w(|F_o^n| - |F_c^n|)^2/\Sigma|F_o^n|^2]^{1/2}$$

with $n = 1$ or 2, and where F_o has been multiplied by $1/k^n$.

During a preliminary refinement based on F it was obvious that the strongest observed values F_o were consistently lower than the calculated values F_c. An isotropic extinction correction was therefore applied including the whole material (2736 reflexions). The largest extinction correction was 37%. The internal consistency factor for symmetry related reflexions (defined analogously to the conventional agreement factor) decreased from 4.71% to 3.80%. All subsequent refinements were based on the averaged extinction-corrected F^2 data.

The following refinement was based on the 650 strongest reflexions [$> 3\sigma_c(F_o^2)$] and an $R(F)$-value of 0.1084 was obtained. In order to avoid bias of the input data by the exclusion of "unobserved" reflexions[9,10] all reflexions were included yielding an $R(F)$-value of 0.1330. Since the crystal was rather small, the measured intensities were weak and more than 40% of the reflexions had an intensity less than $3\sigma_c(F_o^2)$. The agreement factors for a refinement omitting observations with $F_o^2 < 3\sigma_c(F_o^2)$ were hence much lower than those for a refinement using the complete material (Table 1). The standard deviations obtained using all reflexions were however about 20% smaller than those based on the restricted material. Introduction of anisotropic temperature factors improved the agreement

Table 1. R-Factors from isotropic and anisotropic refinements on F^2 of κ-(Hf–Mo–P).

No. of refl.	No. of param.	$R(F^2)$	$R_w(F^2)$	$R(F)$
Isotropic refinement				
650($>3\sigma$)	10	0.1084	0.1458	0.0690
1130	10	0.1330	0.1636	0.1234
Anisotropic refinement				
1130	19	0.1303	0.1571	0.1227
1130[a]	21	0.1286	0.1537	0.1216
1130[b]	22	0.1284	0.1537	0.1216
1130[c]	23	0.1284	0.1537	0.1216

[a] Substitution of Hf on the positions 6*h* and 2*a*. [b] P vacancies on the position 2c. [c] Oxygen present on the position 6g.

Table 2. Structure data for κ-$Hf_{9.29}Mo_{3.71}P$. Standard deviations are given in parentheses. Space group $P6_3/mmc$ (No. 194), $Z=2$. Cell dimensions: $a=8.6236(4)$ Å, $c=8.6101(6)$ Å. The anisotropic temperature factor is of the form: $\exp[-2\pi^2(U_{11}h^2a^{*2}+\ldots+2U_{23}klb^*c^*)]$.

Atom	Position	Positional parameters $x(y=2x)$	z	$U_{ij}\times10^4$ (Å^2) U_{11}	U_{22}	U_{33}	U_{12}	U_{13}	U_{23}	Occupancy (%)
Hf(1)	12*k*	0.19879(5)	0.04836(8)	48(2)	56(2)	49(2)	$U_{22}/2$	$U_{23}/2$	−9(2)	100
Hf(2)	6*h*	0.53992(7)	1/4	47(2)	82(4)	54(3)	$U_{22}/2$	0	0	100
Mo(1) Hf(3)	6*h*	0.88991(12)	1/4	31(5)	26(6)	29(5)	$U_{22}/2$	0	0	93.3(1.1) 6.7(1.1)
Mo(2) Hf(4)	2*a*	0	0	39(8)	U_{11}	43(11)	$U_{11}/2$	0	0	91.6(2.2) 8.4(2.2)
P	2*c*	1/3	1/4	29(23)	U_{11}	24(35)	$U_{11}/2$	0	0	100

factors somewhat (see Table 1) and a Hamilton *R*-factor significance test[11] favoured the anisotropic model at the 99.5% confidence level. Due to the experimental difficulties in making a proper geometrical description of the crystal and the very strong absorption, the intensity data could, however, suffer from systematic errors. A ΔR normal probability plot[12] after the refinement, including all 1130 reflexions gave a least-squares line with a slope of 1.33 and an intercept of 0.14 in the interval $|\Delta R|<4.0$ (11 reflexions outside). All points were very close to a straight line. This indicates that the Hamilton test may not be invalidated by the influence of systematic errors.

At this stage of refinement a Fourier difference synthesis was calculated. It indicated excess scattering power associated with both the molybdenum sites. The possibility of hafnium substitution on these sites was therefore tested. Refinement gave the value of 6.7(1.1) % for the occupancy parameter of hafnium on the position 6*h* and the value of 8.4(2.2)% on the position 2*a*. Although no other deviations were detected in the difference synthesis two other modifications of the structure model were tried. First, the possibility of phosphorous vacancies on the site 2*c* was tested and secondly, the site 6*g* was assumed to be partly occupied by oxygen as in κ-(Hf – Mo – Ni).[7] None of these two refinements indicated any deviation from the initial model. *R*-Values for the different refinements are listed in Table 1.

No further improvements were attempted and the results from the final refinement, including Hf/Mo substitution on the sites 6*h* and 2*a* are presented in Table 2. Corresponding interatomic distances are given in Table 3. The total number of parameters varied was 21 (one scale factor, 4 positional parameters, 2 occupancy parameters and 14 anisotropic thermal vibration parameters).

A list of observed and calculated structure factors has been deposited at the Institute of Chemistry, Uppsala, and can be obtained on request.

Table 3. Interatomic distances (Å) for κ-$Hf_{9.29}Mo_{3.71}P$. Distances shorter than 4.00 Å are listed. The estimated standard deviations are less than 0.001 Å for all distances.[a]

Hf(1) – P	2.656	Mo(1) – 2Mo(2)	2.709
Mo(1)	2.890	2Mo(1)	2.848
Mo(2)	2.998	2Hf(1)	2.890
2Hf(1)	3.084	2Hf(2)	2.897
2Mo(1)	3.107	4Hf(1)	3.107
2Hf(2)	3.221		
2Hf(2)	3.228	Mo(2) – 6Mo(1)	2.709
Hf(1)	3.472	6Hf(1)	2.998
2Hf(1)	3.481		
		P – 6Hf(1)	2.656
Hf(2) – 2Mo(1)	2.897	3Hf(2)	3.086
P	3.086		
4Hf(1)	3.221		
4Hf(1)	3.228		
2Hf(2)	3.279		

[a]The sites Mo(1) and Mo(2) are partly occupied by hafnium.

DISCUSSION

As mentioned in the introduction, the purpose of the present investigation was to determine whether crystal defects, such as atomic substitutions or vacancies, might be responsible for the observed cell volume anomaly in the two series of κ-phases: κ-(Hf – Mo – {Si, P, S}) and κ-(Hf – Mo – {Ge, As, Se}). For the only κ-phase structures examined earlier by high-precision diffraction techniques,[7,13] the defects

observed were associated with the nonmetal sublattice. In κ-(W – Co – C) there were vacancies on the 2*c* carbon positions, and in κ-(Hf – Mo – Ni) the 6*g* position was partially occupied by oxygen. In an earlier report [1] it was therefore suggested that the observed cell volume anomaly might be connected with the distribution of the nonmetal atoms in the structure. The present results of the structure refinement indicate, however, that atomic substitutions in the metal sublattice may be the cause of the cell volume anomalies. The 2*c* position is completely occupied by phosphorus (and the 6*g* position is empty), while Hf/Mo substitution occurs on both the 2*a* and the 6*h* molybdenum sites (see Fig. 1). The composition corresponds to the formula $Hf_{9.29(4)}Mo_{3.71(4)}P$. The results of the chemical analysis give the formula $Hf_{9.20(2)}Mo_{3.80(2)}P_{0.96(1)}$, calculated on the basis of thirteen metal atoms per formula unit. Although the powder photographs showed diffraction lines from the κ-phase only, the presence of minor amounts of impurity phases in the sample cannot be excluded. Assuming for instance the presence of 1 % by weight for each of Hf and $HfMo_2$ (which would probably be below the limits of detection), the composition of the κ-phase would be $Hf_{9.27(2)}Mo_{3.73(2)}P_{0.98(1)}$. Accordingly, the results of the structure refinement and the chemical analysis agree to within experimental errors.

It seems very likely that an increasing degree of Hf/Mo substitution in the series κ-(Hf – Mo – Si), κ-(Hf – Mo – P), κ-(Hf – Mo – S) (and analogously in the series containing Ge, As and Se) is entirely responsible for the cell volume anomaly. This hypothesis is supported by a simple estimation of the cell volume effects produced by Hf/Mo substitution. Assuming that the unit cell volumes are proportional to the sums of the atomic volumes of the constituent elements, the calculated unit cell volume for κ-(Hf – Mo – P) (using the occupancy parameters obtained from the present structure refinement) is:

$$(18.57r_{Hf}^3 + 7.43r_{Mo}^3 + 2r_P^3)s = 96.290s,$$

where s is a proportionality constant, $r_{Hf} = 1.58$ Å, $r_{Mo} = 1.40$ Å (Goldschmidt radii for 12-coordination) and $r_P = 1.10$ Å (Pauling covalent radius). For κ-(Hf – Mo – Si) a similar calculation, assuming a completely ordered distribution of all atoms, yields the value

$$(18r_{Hf}^3 + 8r_{Mo}^3 + 2r_{Si}^3)s = 96.148s.$$

This indicates that a greater degree of Hf/Mo substitution in κ-(Hf – Mo – P) may well outweigh the influence of the larger Si atom ($r_{Si} = 1.17$ Å) as compared with P.

In order to substantiate the present hypothesis, a single crystal refinement of the κ-(Hf – Mo – Ge) structure has been started. κ-(Hf – Mo – Si) would be preferable for a study, but unfortunately all attempts to grow single-crystals of this material have been unsuccessful.

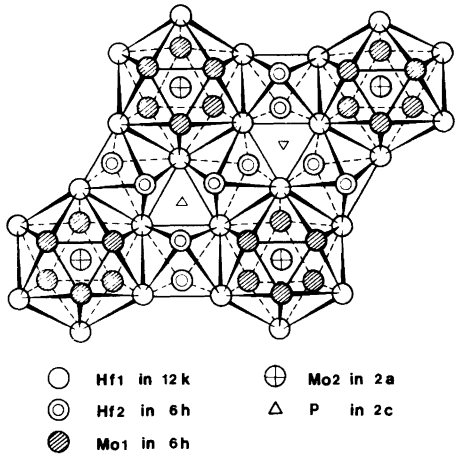

Fig. 1. The structure of κ-(Hf – Mo – P) projected along the hexagonal axis. The sites Mo1 and Mo2 are partly occupied by hafnium.

Acknowledgements. The author is deeply indebted to Professor S. Rundqvist for valuable discussions and criticism of the manuscript, and is most grateful to Professor F. Nydahl and Dr. Lilly Gustafsson, Department of Analytical Chemistry, University of Uppsala, for the careful and methodical way they solved the difficult analytical problems involved in characterizing the κ-phase of this study. Thanks are also due to Dr. T. Gustafsson and Mr. H. Karlsson for assistance with the diffractometer recording. Financial support from the Swedish Natural Science Research Council is gratefully acknowledged.

REFERENCES

1. Hårsta, A. and Wennebo, E. *Acta Chem. Scand. A 35* (1981) 227.
2. Murphy, J. and Riley, J. P. *Anal. Chim. Acta 27* (1962) 31.

3. Deslattes, R. D. and Henins, A. *Phys. Rev. Lett. 31* (1973) 972.
4. Ersson, N.-O. University of Uppsala. *Unpublished.*
5. Lundgren, J.-O., Ed., *Crystallographic Computer Programs*, Institute of Chemistry, University of Uppsala, Uppsala 1975, UUIC-B13-04-2.
6. Rogl, P., Nowotny, H. and Benesovsky, F. *Monatsh. Chem. 104* (1973) 182.
7. Hårsta, A. *Acta Chem. Scand. A 35* (1981) 43.
8. *International Table for X-Ray Crystallography*, Kynoch Press, Birmingham 1974, Vol. 4.
9. Hirschfeld, F. L. and Rabinovich, D. *Acta Crystallogr. A 29* (1973) 510.
10. Wilson, A. J. C. *Acta Crystallogr. A 32* (1976) 781.
11. Hamilton, W. C. *Acta Crystallogr. 18* (1965) 502.
12. Abrahams, S. C. and Keve, K. T. *Acta Crystallogr. A 27* (1971) 157.
13. Hårsta, A., Johansson, T., Rundqvist, S. and Thomas, J. O. *Acta Chem. Scand. A 31* (1977) 260.

Received November 3, 1981.

Acta Chemica Scandinavica A 36 (1982) 541 – 545

The Crystal and Molecular Structure of Bis(1,1-diethyl-3-benzoyl-thioureato)nickel(II)

PEKKA KNUUTTILA,[a] HILKKA KNUUTTILA,[a] HORST HENNIG[b] and LOTHAR BEYER[b]

[a] Department of Chemistry, University of Jyväskylä SF-40100 Jyväskylä 10, Finland and [b] Section of Chemistry, Karl Marx University, DDR-701 Leipzig, German Democratic Republic

The crystal and molecular structure of *cis*-bis(1,1-diethyl-3-benzoyl-thioureato)nickel(II) was determined from three-dimensional X-ray diffraction data. The crystals belong to the monoclinic space group $P2_1/c$ (No. 14). The cell parameters are $a=10.49(1), b=18.47(1), c=14.72(1)$ Å, $\beta=118.80(7)°$, and $Z=4$. The structure was refined to a final R-value of 3.58 %. 1,1-Diethyl-3-benzoyl-thiourea is bidentate and coordinates through its S and O atoms, forming a 6-membered ring. The average Ni–S and Ni–O bond lengths are 2.134 and 1.860 Å, respectively, and the interchelate S–S distance is 2.881(2) Å. Coordination around the nickel atom is square planar. One of the four ethyl groups is disordered. The molecules in the unit cell are arranged in pairs, the Ni–Ni distance being 4.05 Å.

The structures of several metal complexes of thiourea and its derivatives have been determined during the past decades.[1-12] Among these are nickel complexes of substituted thioureas. Depending on the nature of the substituent groups, thiourea acts as a unidentate or bidentate ligand.[1,13-16] The title ligand, 1,1-diethyl-3-benzoylthiourea, acts as a bidentate ligand coordinating through the sulfur atom and the benzoyl oxygen atom. The structures of its palladium and copper complexes have been determined earlier.[17,18] Palladium forms a planar complex, and one modification of the copper complex is tetrahedral.

The present determination of the structure of the nickel complex was carried out to obtain information on the coordination around the nickel atom and on the unusual residual paramagnetism ($\mu=$ 0.61 B.M.) of the complex measured earlier.[19] The only reason for such magnetic behaviour in this type of coordination compounds known from literature[20] is described by the formation of interallogonic systems consisting of planar and tetrahedral structural units in the ratio of 2:1.

EXPERIMENTAL

Data collection. The reddish brown crystals have been synthesized earlier.[19] The compound was recrystallized twice from hot ethanol. A needle-formed crystal was transferred to the Syntex $P2_1$ automatic four-circle diffractometer. Graphite monochromatized Mo$K\alpha$-radiation was used for data collection. The unit cell parameters were calculated by least squares refinement of 15 reflections. The intensities of 2671 independent reflections were collected ($5°<2\theta<50°$) at room temperature using the $\theta/2\theta$-scan technique with the scan rate varying from 1.0 to 15.0° min^{-1} depending on the peak intensity. The intensity of one standard reflection, recorded after every 50 measurements to monitor the crystal stability, remained essentially constant throughout data collection. Out of 2671 measured reflections 1927 were observed on the basis of $I>3\sigma(I)$. The data were corrected for Lorentz and polarization factors but not for absorption (μ(Mo$K\alpha$)=9.66 cm^{-1}).

Structure determination. The phase problem was solved by the MULTAN 78 direct methods.[21] The phases of the 232 E-values larger than 1.3 were calculated. Refinement was carried out with programs of the X-Ray System.[22] The scattering factors for Ni, S, O, N and C were those of Cromer and Mann[23] and for H atoms those of Stewart, Davidson and Simpson.[24] MULTAN gave the coordinates of Ni and the atoms of its coordination circle as well as those of six carbon atoms. During refinement one of the ethyl groups was found to be disordered.

0302-4377/82/060541-05$02.50

The location of its carbon and hydrogen atoms was difficult and one of the hydrogens was not found. The high thermal parameters of C9 and C10 are due to this disorder. The positions of the other atoms could be located satisfactorily. In the final least squares cycles of block-diagonal refinement, non-hydrogen atoms were assigned anisotropic and hydrogen atoms isotropic thermal parameters. After the last cycle the final *R*-value was 3.58 %. The final difference Fourier map showed no peaks above 0.3 e/Å^3. The calculations were carried out on a UNIVAC 1100/60 computer.

DESCRIPTION OF THE STRUCTURE AND DISCUSSION

The molecular structure of bis(1,1-diethyl-3-benzoyl-thioureato)nickel(II) is shown in Fig. 1 and the packing of the molecules in Fig. 2.

The atomic coordinates with their standard deviations for non-hydrogen and hydrogen atoms are given in Table 1. Tables of observed and calculated structure factors and of final thermal parameters are available from the authors on request.

Intramolecular distances and angles with their standard deviations are shown in Table 2.

The central Ni atom is coordinated to two 1,1-diethyl-3-benzoylthiourea molecules through their oxygen and sulfur atoms and the stereochemistry of the complex is *cis*. The coordination around nickel is square planar. The angle between planes (Ni, S1, O1) and (Ni, S2, O2) is 3.33°.

There is no significant difference between the Ni–Sl and Ni–S2 bond lengths of 2.123(2) and 2.144(1) Å, respectively. The The Ni–O1 and Ni–O2 bond lengths of 1.863 and 1.856 Å, respectively, are equal within error limits. Both Ni–S and Ni–O distances are comparable with

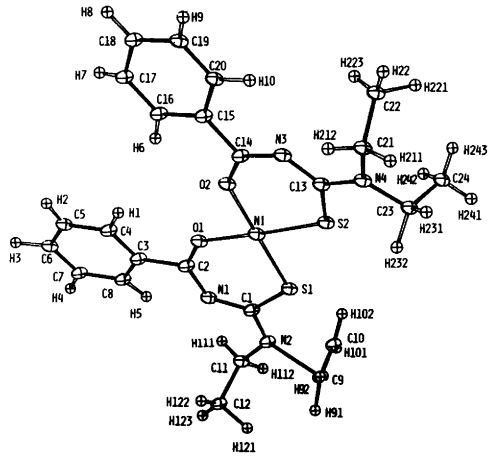

Fig. 1. An ORTEP drawing of bis(1,1-diethyl-3-benzoyl-thioureato)nickel(II), including atomic labeling scheme.

those of the square planar nickel(II)-β-thioxoketonates[25–27] and the Ni–S distances agree with the corresponding distances in bis(dithiobiureato)nickel(II),[10] but are somewhat shorter than those in the dithiolato complex (Ni–S = 2.253–2.338 Å)[28] and the *N,N'*-diallylthiourea complex (Ni–S = 2.221 Å).[1] The chelate ring bond distances show delocalization of π-electrons, and agree with those found in the thiourea complexes determined earlier.[1–12]

The bond distance C–N between the diethylamino substituent and the chelate ring is shorter than a normal single C–N bond length, C1–N2 being 1.332 Å and C13–N4 1.345 Å. This shortening of the C–N bond lengths is in agreement both with the bond distances of thiourea complexes determined earlier[1–12] and with the ^{1}H NMR results

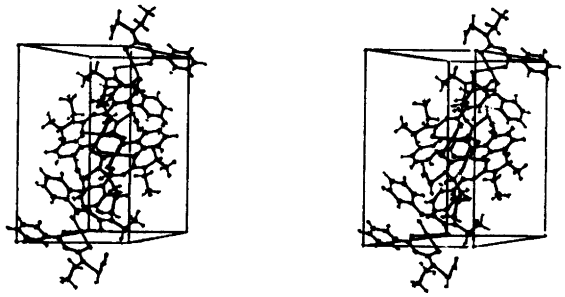

Fig. 2. Stereoview of the packing perpendicular to the *ab* plane.

Table 1. Final positional parameters for $C_{24}H_{30}N_4O_2S_2Ni$ including hydrogen atoms.

Atom	X	Y	Z	Atom	X	Y	Z
Ni	.4902(1)	.0506(0)	.8747(0)	H1	.078(4)	.409(2)	.315(3)
S1	.4745(1)	.0358(1)	1.2057(1)	H2	.832(5)	.391(5)	.259(3)
S2	.7223(1)	.0640(1)	.9486(1)	H3	.367(5)	.951(2)	.386(3)
O2	.7122(3)	−.0419(2)	1.1962(2)	H4	.289(5)	.031(2)	.483(3)
O2	.5383(3)	.8737(1)	.0542(2)	H5	.029(5)	.046(3)	.438(3)
N1	.7750(4)	.0486(2)	.3215(2)	H6	.274(5)	.304(2)	.443(3)
N2	.3647(4)	.6230(2)	.1419(3)	H7	.841(6)	.705(3)	.025(4)
N3	.6919(3)	.1624(2)	.0776(2)	H8	.704(5)	.871(2)	.370(3)
N4	.9199(4)	.1209(2)	.1223(2)	H9	.541(5)	.353(2)	.219(3)
C1	.3595(5)	.5694(2)	.2005(3)	H10	.329(5)	.765(2)	.335(3)
C2	.2000(5)	.4963(2)	.2298(3)	H91	.469(5)	.236(2)	.341(3)
C3	.0418(2)	.4828(2)	.1944(3)	H92	.467(6)	.175(3)	.242(4)
C4	.0029(5)	.4363(2)	.2508(3)	H101	.485(5)	.143(2)	.438(3)
C5	.1423(5)	.9242(2)	.2792(3)	H102	.417(4)	.081(2)	.356(3)
C6	.2518(5)	.9575(2)	.3660(3)	H111	.844(5)	.125(2)	.473(3)
C7	.7869(5)	.5033(3)	.0774(3)	H112	.735(5)	.173(2)	.495(3)
C8	.9322(5)	.5160(2)	.1060(3)	H121	.281(5)	.763(3)	.117(4)
C9	.5403(5)	.6805(4)	.1878(5)	H122	.829(5)	.214(3)	.357(4)
C10	.5454(9)	.6327(4)	.1278(4)	H123	.902(5)	.247(3)	.468(4)
C11	.7658(5)	.1572(3)	.4407(3)	H211	.928(5)	.642(2)	.225(3)
C12	.1874(6)	.7233(3)	.0933(4)	H212	.093(4)	.664(2)	.251(3)
C13	.7758(5)	.1190(2)	.0560(3)	H221	.901(5)	.747(2)	.381(3)
C14	.4521(4)	.6650(2)	.4785(3)	H222	.946(6)	.766(3)	.235(5)
C15	.5236(5)	.7230(2)	.4479(3)	H223	.921(5)	.265(3)	.155(3)
C16	.3259(5)	.2690(2)	.4995(3)	H231	.891(4)	.571(2)	.321(3)
C17	.7417(5)	.7850(3)	.4751(4)	H232	.019(5)	.542(2)	.415(3)
C18	.6576(6)	.8322(2)	.3950(4)	H241	.150(4)	.088(2)	.030(3)
C19	.4927(5)	.3243(2)	.1582(3)	H242	.007(5)	.871(2)	.033(3)
C20	.5596(5)	.2711(2)	.1317(3)	H243	.125(4)	.163(2)	.072(3)
C21	.9750(6)	.1641(2)	.2180(3)				
C22	.0049(6)	.2399(3)	.2039(4)				
C23	.0275(5)	.0795(2)	.1068(3)				
C24	.0789(5)	.1183(2)	.0403(4)				

concerning the hindered rotation of the diethylamino groups about the C−N bond ($\Delta G = 76.1$ kJ mol^{-1}).[29] The atoms of the chelate rings are nearly coplanar. The distances of the atoms from the least squares ring planes are given in Table 3. The angle between these planes is 3.50°.

One ethyl group attached to N2 is disordered. Such disorder was also observed in the previously determined planar palladium complex of the title ligand,[17] but not in the tetrahedral copper complex.[18] This kind of disorder is quite common in terminal alkyl groups of dialkylthiocarbamate complexes.[30-32]

The interchelate distance between S1 and S2 (2.881(2) Å) in the present nickel complex is shorter than the corresponding distance in the palladium and copper complexes (3.12 and 3.14 Å),[17,18] and is much shorter than the sum of van der Waals radii (3.70 Å).[33]

Gray *et al.*[34] have suggested that a relatively short interligand S−S distance (3.18−2.98 Å) could indicate some residual S−S interaction. Also Amma *et al.*[10] have concluded that there is some residual S−S interchelate bonding in bis(dithiobiureato)nickel(II) in which the interchelate S−S distance is 3.220 Å and the intrachelate S−S distance is 2.895 Å. In our nickel complex the interchelate S−S distance is one of the shortest non-bonded S−S distances observed.[2,10,34-40]

In the unit cell the molecules form centrosymmetric pairs. The molecules in the dimers lie almost directly above each other, and the Ni−Ni distance

Table 2. Interatomic distances (Å) and angles (°) with standard deviations.

Ni–S1	2.123(2)	S1–Ni–S2	84.9(1)	C6–C7–C8	121.2(4)
Ni–O1	1.863(3)	S1–Ni–O1	94.5(1)	C3–C8–C7	119.8(5)
Ni–S2	2.144(1)	O1–Ni–O2	86.2(1)	N2–C9–C10	74.2(6)
Ni–O2	1.856(3)	S2–Ni–O2	94.4(1)	N2–C11–C12	113.6(4)
S1–C1	1.731(4)	Ni–S1–C1	109.7(2)	C13–N3–C14	123.6(3)
O1–C2	1.252(4)	Ni–O1–C2	134.1(3)	C13–N4–C21	119.8(4)
N1–C1	1.339(6)	Ni–C2–C13	108.7(2)	C13–N4–C23	123.3(3)
N1–C2	1.327(6)	Ni–O2–C14	133.1(3)	C21–N4–C23	116.9(3)
N2–C1	1.332(7)			S2–C13–N3	127.6(3)
N2–C9	1.940(10)	C1–N1–C2	122.8(3)	S2–C13–N4	115.7(4)
N2–C11	1.465(5)	C1–N2–C9	120.5(3)	N3–C13–N4	116.6(3)
C2–C3	1.496(7)	C1–N2–C11	123.1(4)	O2–C14–N3	130.0(4)
C3–C4	1.386(7)	C9–N2–C11	113.6(4)	O2–C14–N15	115.0(3)
C3–C8	1.397(5)	S1–C1–N1	128.6(4)	N3–C14–C15	115.0(3)
C4–C5	1.381(7)	S1–C1–N2	116.4(4)	C14–C15–C16	120.4(3)
C5–C6	1.384(6)	N1–C1–N2	115.0(3)	C14–C15–C20	120.7(4)
C6–C7	1.379(8)	O1–C2–N1	130.1(4)	C16–C15–C20	118.9(4)
C7–C8	1.388(7)	O1–C2–C3	115.6(4)	C15–C16–C17	121.2(4)
C9–C10	1.274(11)	N1–C2–C3	114.2(3)	C16–C17–C18	119.2(5)
C11–C12	1.489(8)	C2–C3–C4	119.4(3)	C17–C18–C19	119.8(5)
S2–C13	1.732(4)	C2–C3–C8	121.7(4)	C18–C19–C20	120.7(4)
O2–C14	1.265(4)	C4–C3–C8	118.9(4)	C15–C20–C19	120.0(4)
N3–C13	1.335(6)	C3–C3–C5	120.4(4)	N4–C21–C22	113.2(4)
N3–C14	1.324(5)	C4–C5–C6	121.1(5)	N4–C23–C24	113.1(4)
N4–C13	1.345(5)	C5–C6–C7	118.6(5)		
N4–C21	1.475(5)				
N4–C23	1.467(7)				
C14–C15	1.496(6)				
C15–C20	1.393(5)				
C16–C17	1.376(8)				
C17–C18	1.388(6)				
C18–C19	1.386(7)				
C19–C20	1.368(7)				
C21–C22	1.469(5)				
C23–C24	1.508(8)				
S1–S2	2.881(2)				

Table 3. The distance of the chelate ring atoms from the least squares plane.

Atom	Distance (Å)
Ni	0.03
O1	−0.03
C2	0.00
N1	0.02
C1	0.00
S1	−0.02
Ni	−0.11
O2	0.04
C14	0.06
N3	−0.04
C13	−0.08
S2	0.13

is 4.05 Å. The Ni–Ni line forms an angle of 77.6° with the coordination plane (Ni, O1, O2, S1, S2). In *N,N'*-ethylenebis(salicylideneiminato)nickel(II)[41] and *N,N'*-ethylenebis[(2-hydroxo-1-naphtyl)methaniminato]-nickel(II)[42] the very small Ni–Ni distances (3.21 and 3.324 Å, respectively) have led to a pairing of the molecules while an Ni–Ni chain exists in bis(dimethylglyoximato)nickel(II),[43] with an Ni–Ni distance of 3.25 Å.

The unusual paramagnetism of the present compound is not directly explainable from the geometry of the complex molecule.

REFERENCES

1. Chiesi Villa, A., Mangia, A., Nardelli, M. and Pelizzi, G. *J. Cryst. Mol. Struct. 1* (1971) 285.
2. Girling, R. L. and Amma, E. L. *Acta Crystallogr. B 32* (1976) 2903.
3. Battaglia, L. P., Bonamartini Corradi, A., Pelizzi, G. and Vidoni Tani, M. E. *J. Chem. Soc. Dalton Trans.* (1977) 1141.
4. Battaglia, L. P., Bonamartini Corradi, A., Nardelli, M. and Vidoni Tani, M. E. *J. Chem. Soc. Dalton Trans.* (1978) 583.
5. Griffith, E. A. H., Spofford, W. A., III and Amma, E. L. *Inorg. Chem. 17* (1978) 1913.
6. Spofford, W. A. and Amma, E. L. *J. Cryst. Mol. Struct. 6* (1976) 235.
7. Bosman, W. P. and Gal, A. W. *Cryst. Struct. Commun. 5* (1976) 703.
8. Domiano, P. and Tiripicchio, P. *Cryst. Struct. Commun. 1* (1972) 107.
9. Bonamartini Corradi, A., Mangia, A. and Pelizzi, E. *Cryst. Struct. Commun. 2* (1973) 73.
10. Luth, H., Hall, E. A., Spofford, W. A. and Amma, E. L. *J. Chem. Soc. Chem. Commun.* (1969) 520.
11. Belicchi Ferrari, M. and Fava Gasparri, G. *Cryst. Struct. Commun. 5* (1976) 935.
12. Belicchi Ferrari, M. and Fava Gasparri, G. and Montenero, A. *Cryst. Struct. Commun. 4* (1975) 577.
13. Tarantelli, T., Riccieri, P. and Furlani, C. *J. Inorg. Nucl. Chem. 31* (1969) 3585.
14. Furlani, C., Tarantelli, T. and Riccieri, P. *J. Inorg. Nucl. Chem. 33* (1971) 1389.
15. Tarantelli, T. and Furlani, C. *J. Inorg. Nucl. Chem. 34* (1972) 999.
16. Furlani, C. and Tarantelli, T. *Gazz. Chim. Ital. 103* (1973) 951.
17. Firzl, G., Beyer, L., Sieler, J., Richter, R., Kaiser, J. and Hoyer, E. *Z. Anorg. Allg. Chem. 433* (1977) 237.
18. Richter, R., Beyer, L. and Kaiser, J. *Z. Anorg. Allg. Chem. 461* (1980) 67.
19. Beyer, L., Hoyer, E., Hennig, H., Kirmse, R., Hartmann, H. and Liebscher, J. *J. Prakt. Chem. 317* (1975) 829.
20. Uhling, E. *Coord. Chem. Rev. 10* (1973) 227.
21. Main, P., Hull, S. E., Lessinger, L., Germain, G., Declercq, J. P. and Woolfson, M. M. *MULTAN. A System of Computer Programs for the Automatic Solution of Crystal Structures from X-Ray Diffraction Data*, Universities of York, England and Louvain-la-Neuve, Belgium, 1978.
22. *The X-Ray System, Version of 1976*, Technical Report TR-446, Computer Science Center, University of Maryland, College Park 1976.
23. Cromer, D. T. and Mann, J. B. *Acta Crystallogr. A 24* (1968) 321.
24. Stewart, R. F., Davidson, E. R. and Simpson, W. T. *J. Chem. Phys. 42* (1965) 3175.
25. Sieler, J., Uhlemann, E., Thomas, P. and Höhne, E. *Z. Anorg. Allg. Chem. 380* (1971) 160.
26. Siiman, O., Titus, D. D., Cowman, C. D., Fresco, J. and Gray, H. B. *J. Am. Chem. Soc. 96* (1974) 2353.
27. Kutschabsky, L. *Z. Anorg. Allg. Chem. 404* (1974) 239.
28. Bosman, W. P. and van der Linden, H. G. M. *J. Chem. Soc. Chem. Commun.* (1977) 714.
29. Beyer, L., Behrendt, S., Kleinpeter, E., Borsdorf, R. and Hoyer, E. *Z. Anorg. Allg. Chem. 437* (1977) 282.
30. Hesse, R. and Nilson, L. *Acta Chem. Scand. 23* (1969) 825.
31. Hesse, R. and Aava, U. *Acta Chem. Scand. 24* (1970) 1355.
32. Bosman, W. P. and Nieuwpoort, A. *Inorg. Chem. 15* (1976) 775.
33. Pauling, L. *Nature of the Chemical Bond*, Cornell University Press, New York 1960, 3rd Ed., p. 260.
34. Stiefel, E. I., Dori, Z. and Gray, H. B. *J. Am. Chem. Soc. 89* (1967) 3353.
35. Pignedoli, A., Peyronel, G. and Antolini, L. *Gazz. Chim. Ital. 102* (1972) 679.
36. Smith, A. E., Schrauzer, G. N., Mayweg, V. P. and Heinrich, W. *J. Am. Chem. Soc. 87* (1965) 5798.
37. Bennett, M. J., Cowie, M., Martin, J. L. and Takats, J. *J. Am. Chem. Soc. 95* (1973) 7504.
38. Johnston, D. L., Rohrbaugh, W. L. and Horrocks, W. D., Jr. *Inorg. Chem. 10* (1971) 1474.
39. Brown, G. F. and Stiefel, E. I. *Inorg. Chem. 12* (1973) 2140.
40. Leipold, J. G. and Coppens, P. *Inorg. Chem. 12* (1973) 2269.
41. Shkol'nikova, L. M., Yumal, E. M., Shugam, E. A. and Voblikova, V. A. *Zh. Strukt. Khim. 11* (1970) 886.
42. Akhtar, F. *Acta Crystallogr. B 37* (1981) 84.
43. Godycki, L. E. and Rundle, R. E. *Acta Crystallogr. 6* (1953) 487.

Received October 5, 1981.

Acta Chemica Scandinavica A 36 (1982) 547–548

Short Communication

New κ-Phases in the Systems Hf–W–{S,As,Se} and Hf–Re–{Si,P,S,Ge,As,Se,Fe,Co,Ni}

ANDERS HÅRSTA and EVA WENNEBO

Institute of Chemistry, University of Uppsala, Box 531, S-751 21 Uppsala, Sweden

The hexagonal κ-phase has been found to occur in a great number of ternary systems as reported by Rogl and Nowotny [1] and references given therein. In a recent communication,[2] κ-phases were reported in the ternary systems Hf–Mo–{Si,P,S,Ge,As,Se} and Hf–W–P. Studies have now been extended to further combinations and the present communication reports the results from an investigation of the following ternary systems: Hf–Mo–{C,N,Al,Sb}, Hf–W–{S,As,Se}, Hf–Re–{Si,P,S,Ge,As,Se,Fe,Co,Ni} and Sc–Mo–Ni.

Most of the starting materials for the syntheses of the different alloys have been described elsewhere.[2] Additional starting materials are listed in Table 1. Ternary alloys containing Si,Ge,Al,Sb,Fe,Co or Ni were prepared directly by arcmelting mixtures of the constituent elements. Due to the high volatility of the other nonmetals, samples of Hf_3P, Hf_2S, Hf_3As and Hf_2Se were initially prepared in evacuated and sealed silica tubes. These compounds were then mixed with appropriate amounts of the transition metal components and arcmelted. All the arcmelted alloys were subsequently annealed at 1400 °C, except Hf–Re–{Fe,Co,Ni} which were annealed at 1300 °C, and Sc–Mo–Ni which was annealed at 1030 °C. For further experimental details see Ref. 2. The cell dimensions of the new κ-phases are presented in Table 2. Attempts to prepare κ-phases in the other of the above-mentioned ternary systems were unsuccessful.

The unit cell volumes of the new κ-phases show some interesting trends. In the two series of compounds κ-Hf–Re–{Si,P,S} and κ-Hf–Re–{Ge,As,Se}, the unit cell volumes decrease in the order Si→P→S and Ge→As→Se, respectively. This would be in accordance with the normal atomic sizes of these nonmetals, provided that the structures are completely ordered and do not contain vacancies. In contrast, the unit cell volumes increase in the corresponding series of κ-phases containing molybdenum instead of rhenium.[2] Recent results indicate that this effect might be connected with an increasing degree of Hf/Mo substitution on the molybdenum positions.[3] The difference in cell volume trends between the rhenium- and the molybdenum-containing κ-phases may accordingly be due to a much more restricted Hf/Re substitution on the rhenium sites. This hypothesis agrees very well with the substitutional solid solubility behaviour of hafnium in elemental molybdenum and rhenium. In molybdenum, the hafnium solubility extends to over 30 at% [4] while, in rhenium, the maximum solid solubility is at least ten times smaller.[5]

Table 1. Starting materials for the syntheses.

Substance	Supplier	Purity
Re	Hereaus, Hanau, Germany	>99.8%
MoC	Highways International, Baarn, The Netherlands	>99%
Mo_2N+MoN		>99.5%
Si		>99.999%
Al	Gränges SM, Finspång, Sweden	>99.999%
Sb	Johnson & Matthey, London	<1 ppm metallic impurities
Fe		<15 „
Co		<20 „
Ni		<20 „

0302-4377/82/060547-02$02.50

Table 2. Cell dimensions and cell volumes for the new κ-phases. Standard deviations are given in parentheses. The approximate composition is Hf_9M_4X where M = W or Re and X = Si,P,S,Ge,As,Se,Fe,Co or Ni.

Phase	a (Å)	c (Å)	V (Å^3)
κ-Hf–W–S	8.6682(5)	8.5627(5)	557.18(5)
κ-Hf–W–As	8.6741(5)	8.6967(9)	566.67(7)
κ-Hf–W–Se	8.7073(6)	8.6674(5)	569.10(5)
κ-Hf–Re–Si	8.5643(6)	8.6377(10)	548.68(7)
κ-Hf–Re–P	8.5666(5)	8.6221(8)	547.97(6)
κ-Hf–Re–S	8.5907(5)	8.5008(9)	543.32(7)
κ-Hf–Re–Ge	8.5771(5)	8.6642(5)	552.00(5)
κ-Hf–Re–As	8.5968(4)	8.6075(10)	550.91(7)
κ-Hf–Re–Se	8.6050(10)	8.5614(12)	549.00(10)
κ-Hf–Re–Fe	8.5830(5)	8.4178(9)	537.04(7)
κ-Hf–Re–Co	8.6077(2)	8.4281(4)	540.80(3)
κ-Hf–Re–Ni	8.6261(5)	8.4367(5)	543.66(5)

For the three phases κ-Hf–Re–{Fe,Co,Ni}, the unit cell volumes increase in the order Fe→Co→Ni, and this is true also of the κ-Hf–Mo–{Fe,Co,Ni} series. An opposite trend would normally be expected considering the decrease in atomic size of passing from Fe to Co to Ni. A single crystal structure refinement of κ-Hf–Mo–Ni revealed no significant deviations from the ideal crystallographic formula Hf_9Mo_4Ni, except for a minor amount of dissolved oxygen.[6] It would thus appear that atomic substitutions or vacancies must occur to a much greater extent in the cobalt- and iron-containing phases.

Acknowledgements. The authors are indebted to Professor S. Rundqvist for valuable discussions and for criticism of the manuscript. Financial support from the Swedish Natural Science Research Council is gratefully acknowledged.

1. Rogl, P. and Nowotny, H. *Monatsh. Chem. 108* (1977) 1167.
2. Hårsta, A. and Wennebo, E. *Acta Chem. Scand. A 35* (1981) 227.
3. Hårsta, A. *Acta Chem. Scand. A 36* (1982) 535.
4. Garg, S. P. and Ackermann, R. J. *Metall. Trans. A 8* (1977) 239.
5. Ageev, N. V., Ed., *Phase Diagrams of Metallic Systems*, Acad. Sci., Moscow 1969, p. 31.
6. Hårsta, A. *Acta Chem. Scand. A 35* (1981) 43.

Received January 29, 1982.

Acta Chemica Scandinavica A 36 (1982) 549 – 554

Circular Dichroism of [$PtCl_2$(*R*)-pn] and [$PtCl_2$(*S*)-pn] in Solution and in KCl Matrix

KJELD RASMUSSEN and NIELS CHRISTIAN POUL HALD

Chemistry Department A, Building 207, The Technical University of Denmark, DK-2800 Lyngby, Denmark

A technique for quantitative measurement of visible and ultraviolet absorption and circular dichroism spectra of a microcrystalline solid dispersed in an alkali halide matrix is described, and formulae for evaluation of oscillator, dipole and rotatory strengths are given.

The method is applied to [$PtCl_2$(*R*)-pn] and [$PtCl_2$(*S*)-pn], pn = 1,2-propanediamine, which are studied in the range $2-4\times10^6$ m^{-1}.

Absorption and circular dichroism spectra (ABS and CD) of Pd(II)Cl_2 and Pt(II)Cl_2 complexes with (*R*)-1,2-propanediamine ((*R*)-pn or 1-pn) were measured by Ito *et al.*[1] and latter by Sullivan [2] who also studied the solid-state CD in a semi-quantitative manner. We report here ABS and CD of the complexes of Pt(II) with both (*R*)- and (*S*)-pn in aqueous solution and dispersed in KCl matrix. Our measurements cover the frequency range $1.7-4.5\times10^6$ m^{-1}.

These studies were originally undertaken as a prerequisite to similar measurements on [$PtCl_2$en]. One of us proposed on the basis of crystal data,[3] in connection with an infrared study,[4] that [$PtCl_2$en] resolves spontaneously on crystallisation, and that all chelate rings in a single crystal would have identical conformation. This would entail a possibility of studying CD in a *d*-electron system of purely conformational origin. Exploratory studies on tiny single crystals crushed and pressed with KCl indicated that the effect is real but very weak. In order to develop a proper methodology, we undertook the present study wehere the dissymmetric amine would at the same time lock the chelate ring conformation and enhance the CD but would have little effect on the positions of the ABS bands. The original goal was superseded by Jensen's demonstration of the correctness of the original proposal, by single crystal CD measurements,[5] but our study revealed some features which hitherto seem to have escaped detection. Also, our description and evaluation of the measurements may be of some interest; earlier measurements on these or similar compounds in KBr or paraffin oil are either qualitative [2] or not described in any detail.[6-8] Recently, the paraffin oil technique was developed into a quantitative procedure by Taniguchi and Shimura.[9]

EXPERIMENTAL

Preparation. Both complexes were prepared according to Werner.[10] [$PtCl_2$(*R*)-pn]: 0.47 g (1.4 mmol) K_2PtCl_4 was dissolved in 7 ml H_2O, and 0.13 ml (*R*)-pn solution (d = 0.678 g cm^{-3}, 1.2 mmol, $[\alpha]_D^{20} = -31.5°$) was added with stirring. After 24 h the precipitate was recrystallised. Yield: 71%. Analysis: Calc: C 10.62, H 2.95, N 8.26, Cl 20.65, Pt 57.50. Found: C 10.66, H 2.86, N 8.29, Cl 20.85, Pt 57.50, sum 100.16. [$PtCl_2$(*S*)-pn]: Identically, with $[\alpha]_D^{20} = +32.0°$. Yield: 69%. Analyses: Found: C 10.42, H 2.80, N 8.22, Cl 20.73, Pt 57.45, sum 99.62.

Solution spectra. ABS was recorded on a Cary 11 at ~25 °C in 2 and 5 cm silica cells selected for CD. Solutions were ~1 mM in the complex and 60 mM in KCl and in HCl. The same solutions in the same 5 cm cells were used for CD measured with a Roussell-Jouan Dicrographe II.

Solid-state spectra. KCl was used rather than KBr to avoid exchange with the matrix.[11] Preparation of disks: 0.03 – 2 mg substance was milled with 150 mg KCl dried at 150 °C for 16 h in an agate ball mill (RIIC) at speed II for 0.5 min, and then pressed slowly in a 13 mm ø die (RIIC) for 15 min to 6 t under vacuum; if the disk was not satisfactorily clear, it was crushed and the procedure was repeated. A special holder was constructed for use

0302-4377/82/070549-06$02.50

with both instruments; it allowed for rotating the disk around the optical axis in steps of 90°. This was necessary in order to correct for the strain produced in the pressing. CD recordings were made with the disk in four positions, and the averaged spectra were used. If they differed subjectively too much, the disk was re-made as above. The whole procedure was repeated with a second (or higher) preparation; a final CD was accepted only if it, after evaluation (see below), was identical to within the experimental uncertainty for two different preparations.

Evaluation of ABS. In an isotropic disk we write the measured absorbance A as the sum of two quantities, eqn. (1), where g is a constant characterising the disk (the manufacturing), $f(\nu)$ describes the dispersion and $a(\nu)$ is the true absorbance of the disk. In an empty disk with no absorbing material we have eqn. (2) and in another disk containing an absorbing substance eqn. (3).

$$A(\nu) = a(\nu) + f(\nu)g \tag{1}$$

$$A_e(\nu) = f(\nu)g_e \tag{2}$$

$$A_s(\nu) = a(\nu) + f(\nu)g_s \tag{3}$$

If there is a frequency ν_o where $a(\nu)_o = 0$ we have eqns. (4) and (5). The ratio g_s/g_e is thus measurable. From eqns. (5) and (3) we get eqn. (6) and thus eqn. (7).

$$A_s(\nu_o) = f(\nu_o)g_s \tag{4}$$

$$\frac{A_s(\nu_o)}{A_e(\nu_o)} = \frac{g_s}{g_e} \tag{5}$$

$$A_s(\nu) = a(\nu) + f(\nu)\frac{A_s(\nu_o)}{A_e(\nu_o)}g_e = a(\nu) + \frac{A_s(\nu_o)}{A_e(\nu_o)}A_e(\nu) \tag{6}$$

$$a(\nu) = A_s(\nu) - \frac{A_s(\nu_o)}{A_e(\nu_o)}A_e(\nu) \tag{7}$$

It is thus possible to correct for a difference in dispersion between two almost identical disks, provided the dispersion is reasonably unchanged. To test this assumption we measured the absorbance of three disks without sample. In this case, with $a(\nu)=0$ and $f(\nu)$ the same for the three disks, we should have $A_1(\nu)/A_2(\nu) = g_1/g_2$, that is, independent of ν. Plotting the three ratios against σ should then give three horizontal lines. Fig. 1 shows that such is not the case, but that the ratios are constant to within about 30%. We may therefore reckon with an uncertainty of about 50% in the solid state ABS spectra. The crucial assumption that $f(\nu)$ is unchanged from one disk to another is probably the most inaccurate. It is our experience that differences due to the presence of sample are no bigger than between empty disks.

The molar absorbance $\varepsilon = a/cl$ is found as follows. The number of mol in the disk is given by eqn. (8), where m_s, m_{KCl} and m_d are the masses of substance, KCl and the finished disk, and M is the molar weight of the substance. The n mol are dissolved in a volume V, eqn. (9), and the molar absorbance is therefore, as $c = n/V$ and $d = 0.013$ m; $[\varepsilon]$ is $m^2\ mol^{-1}$ if $[m]$ is mg mol^{-1} and $[M]$ g mol^{-1}.

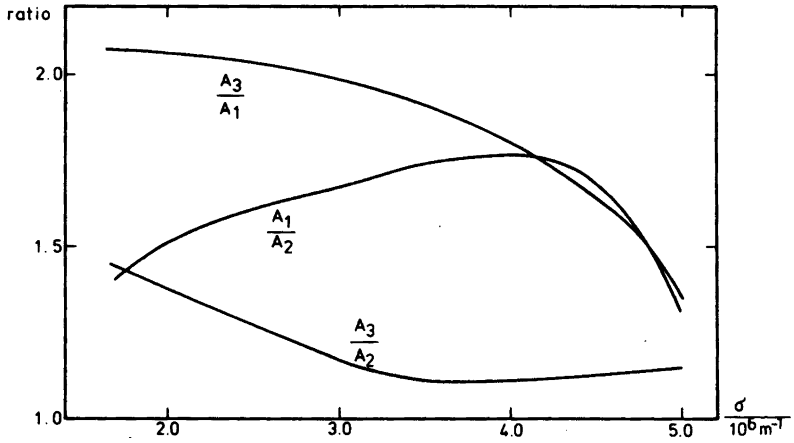

Fig. 1. Ratios of measured absorbances of three KCl disks without sample.

$$n = \frac{m_s m_d}{(m_s + m_{KCl})M} \quad (8)$$

$$V = (d/2)^2 \pi l \quad (9)$$

$$\varepsilon = aV/nl = a\frac{m_s + m_{KCl}}{m_s m_d} M \times 0.1327 \quad (10)$$

In order to get reasonable accuracy for both strong and weak bands, disks containing from 0.1 to 5 mmol substance were prepared.

Evaluation of CD. $\Delta\varepsilon$ is found from Δa precisely as ε from a. Δa is given by the dichrographe, after correction for instrumental sensitivity. The dispersion cancels out, and the strain is corrected for by the averaging procedure of measuring in four positions described above.

$$f = 4\pi\varepsilon_0 m_e c^2 \ln 10/\pi N e^2 \times I = 4\pi m_e \ln 10/\mu_0 \pi N e^2 \times I \quad (11)$$

$$D = \varepsilon_0 3\hbar c \ln 10/\pi N \times a/\sigma_0 \times I = 3\hbar \ln 10/\mu_0 c\pi N \times a/\sigma_0 \times I \quad (12)$$

$$R = 3\hbar \ln 10/4\pi\mu_0 cN \times b/\sigma_0 \times J \quad (13)$$

Evaluation of $\hbar$, D and R. The oscillator, dipole and rotatory strengths are found from the observed ABS and CD using the formulae [12] (11)–(13), where σ_0 is the wavenumber in m^{-1} of the absorption peak, I is the integral (first moment) over the band approximated as $\varepsilon\delta\sigma$, $\delta\sigma$ being the halfwidth, and J is the analogous integral approximated as $\Delta\varepsilon\delta\sigma$. a and b take account of the refractive index of the medium; we use the approximations [12] $a = 9n_0/(n_0^2+2)^2$ and $b = 3/(n_0^2+2)$ with $n_0 = 1.38$ for H_2O [13] and 1.55 for KCl.[14]

The data, as presented in the tables, also include the dissymmetry ratio $g = \Delta\varepsilon/\varepsilon$ and the ratio $4R/D = bJ/aI$, which is a more basic dissymmetry ratio than g, as it is corrected for the influence of the medium.

The unit for both R and D is $m^2s^2A^2$ or $(Cm)^2$, the square of an electric dipole moment. Perhaps a more logical choice for R would be m^3sA^2 or $(Cm)(Am \cdot m)$ or $(Cm)(JT^{-1})$, the product of an electric and a magnetic dipole moment. Because of the wish for the undimensioned dissymmetry ratio R/D the former is chosen; hence the division by c in the formula for R above. The relationships to formerly used units are 1 $Cm = 3 \times 10^{11}$ esu cm and 1 $J\,T^{-1} = 10^3$ erg G^{-1}; in the tables, 1 unit for $D = 9 \times 10^{-38}$ esu and 1 unit for $R = 0.9 \times 10^{-40}$ esu or 0.9 Biot.

RESULTS

Solution spectra. The ABS are presented in Fig. 2 and the CD in Fig. 3. SI units are used for σ, ε and $\Delta\varepsilon$. Overlapping bands are resolved graphically. Within the limits of error, ABS are identical for the two compounds, and CD are mirror images. Uncertainties are very large in regions 2.0–2.5 and $> 3.7 \times 10^6$ m^{-1}.

Numerical data derived from the spectra are given in Table 1; values are averaged over the two compounds and, where possible, over ABS and CD. Signs of $\Delta\varepsilon$, g, R and $R/4D$ are positive overall for the (*R*), negative for the (*S*) compound. The tiny ABS band at 2.37×10^6 m^{-1} is badly determined, and so is the CD band at 3.32×10^6 m^{-1}. If the former is real it has $\Delta\varepsilon < 0.002$ m^2 mol^{-1}.

Solid state spectra. ABS are shown in Figs. 4 and 5. They are not identical, but very much alike; they certainly do not differ within the accuracy of measurement. Three concentrations, here called strong, medium and weak, were used to get also

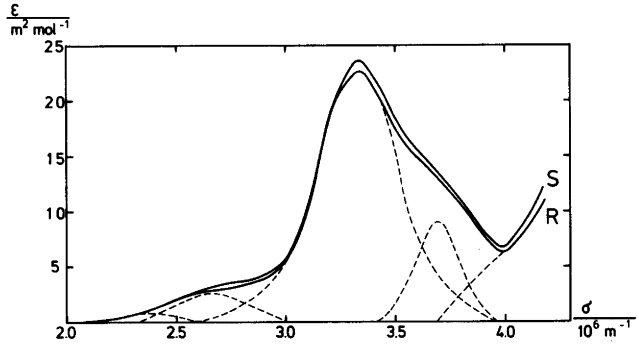

Fig. 2. Absorption spectra of [$PtCl_2$(*R*)-pn] and [$PtCl_2$(*S*)-pn] in aqueous solution.

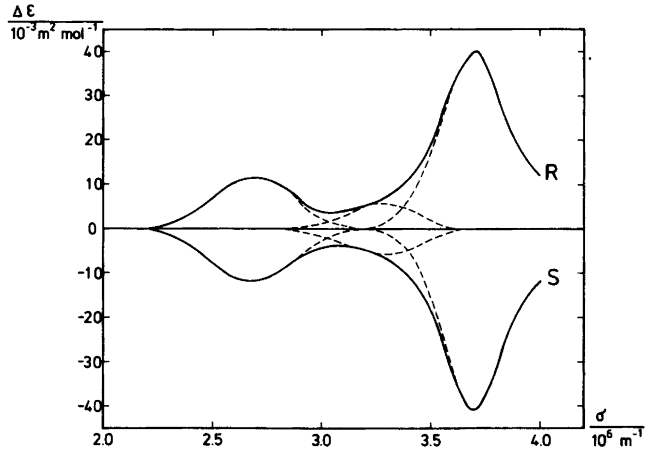

Fig. 3. Circular dichroism spectra of $[PtCl_2(R)\text{-pn}]$ and $[PtCl_2(S)\text{-pn}]$ in aqueous solution.

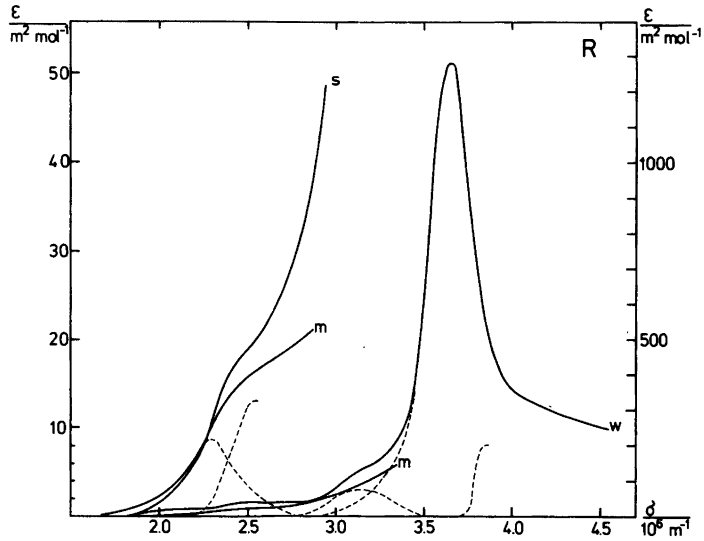

Fig. 4. Absorption spectra of $[PtCl_2(R)\text{-pn}]$ in KCl matrix. s, m and w denote high, medium and low concentration in the disk.

Table 1. Absorption and circular dichroism spectra of $[PtCl_2pn]$ in aqueous solution.

σ_o 10^6 m^{-1}	ε m^2 mol^{-1}	$\Delta\varepsilon$ 10^{-3} m^2 mol^{-1}	g 10^{-3}	f	D 10^{-60} m^2 s^2 A^2	R 10^{-63} m^2 s^2 A^2	$4R/D$ 10^{-3}
2.37	0.8	<2	<2.0	0.0001	0.08		
2.68	2.6	12	4.6	0.00043	0.31	0.38	4.9
3.32	22.6	6	0.27	0.0041	2.36	0.13	0.22
3.70	9.0	40	4.4	0.0009	0.47	0.76	6.5

Table 2. Absorption and circular dichroism spectra of [$PtCl_2$(*R*)-pn] and [$PtCl_2$(*S*)-pn] in KCl matrix.

σ_0 10^6 m^{-1}	ε m^2 mol^{-1}	$\Delta\varepsilon$ 10^{-3} m^2 mol^{-2}	g 10^{-3}	f	D 10^{-60} m^2 s^2 A^2	R 10^{-63} m^2 s^2 A^2	$4R/D$ 10^{-3}
R							
2.30	8.7	−3.65	−0.42	0.0013	0.95	−0.058	−0.24
2.55	13.2	+3.70	+0.28	0.0018	1.22	+0.048	+0.16
3.15	75	−49.5	−0.66	0.014	7.6	−0.63	−0.33
3.64	1285	−2300	−1.79	0.167	78	−13.2	−0.68
3.83	200	+1120	+5.6	0.016	27	+5	+0.7
S							
2.27	8.9	+3.40	+0.38	0.0014	1.01	+0.060	+0.24
2.55	16.0	−3.65	−0.23	0.0026	1.75	−0.053	−0.12
3.14	80	+49.5	+0.62	0.015	8.3	+0.71	+0.34
3.66	1110	+2500	+2.25	0.106	49	+19.1	+1.56
3.89	200	−700	−3.5	0.024	41	−5	−0.5

minor details. CD are given in Fig. 6. They are almost as perfect mirror images as the solution CD.

Numerical data extracted from the graphs are given in Table 2. Wavenumbers are averaged over ABS and CD; otherwise the data are kept separate as the spectra are rather more complicated than for the solutions. The far UV band at about 3.85×10^6 m^{-1} or 260 nm is badly determined in both ABS and CD, but is probably real. It is possible to resolve the solution ABS in an analogous way, but the solution CD does not support this.

For all spectra, D and R are determined through integrals I and J as described above, $\delta\sigma$ being read off the respective graphs.

DISCUSSION

Comparison with earlier work. Ito *et al.*[1] found for $PtCl_2$(*R*)-pn in dilute HCl (σ, ε, $\Delta\varepsilon$, g): (2.73, 3.63, +0.015, 0.00041), (3.31, 23.4, not meas.), (3.7, 12.6, +0.038, 0.00030) for the second, third and fourth

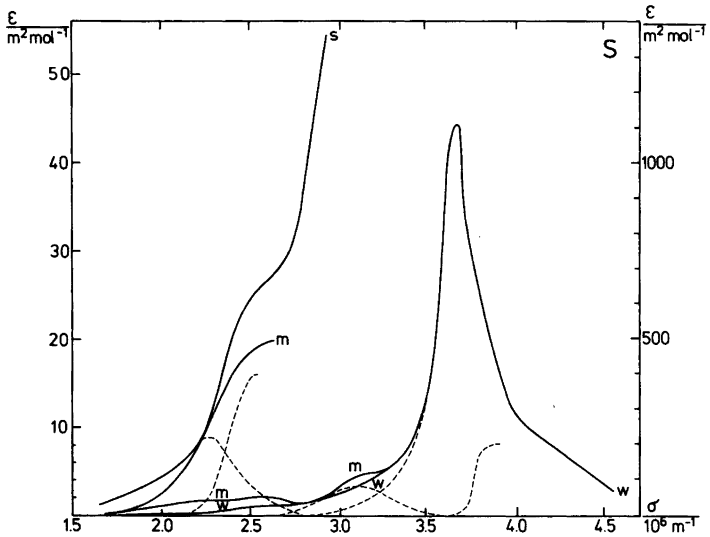

Fig. 5. Absorption spectra of [$PtCl_2$(*S*)-pn] in KCl matrix.

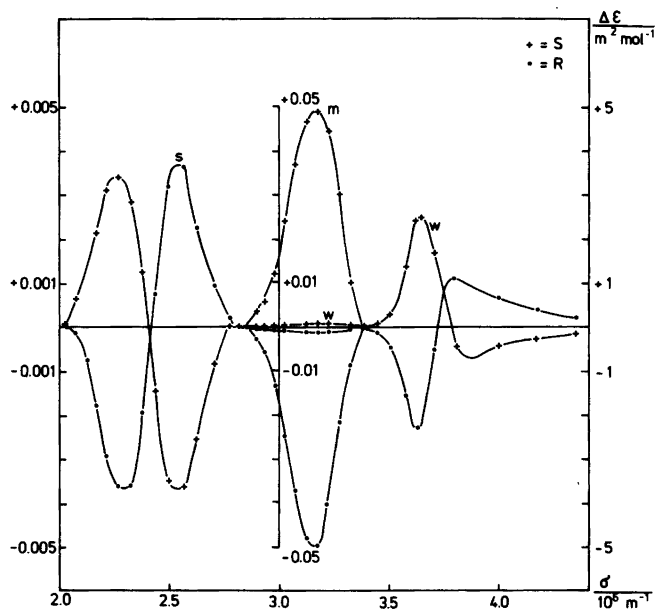

Fig. 6. Circular dichroism spectra of $[PtCl_2(R)\text{-pn}]$ and $[PtCl_2(S)\text{-pn}]$ in KCl matrix.

band. The values are close to ours through not identical.

Sullivan[2] did not give numerical data, but his graphs of ABS in solution and solid and CD in solution are very much like ours. For CD in solid we disagree: Sullivan misses the first band and shows a positive $\Delta\varepsilon$ at $3.4 \times 10^6\ m^{-1}$; we find no indication of this.

Solid versus *solution.* The phenomenological differences are striking. On going from solution to solid there are noticeable bathochromic changes in the wavenumbers of the near UV bands between 2.6 and $3.3 \times 10^6\ m^{-1}$. For the UV bands, extinction and CD increase drastically; and CD changes sign. An interpretation shall not be attempted here.

CONCLUSION

We have demonstrated that it is practicable though tedious to measure and evaluate absorption and circular dichroism spectra of microcrystalline samples. We have, in a quantitative manner, employed the methods to a complete study of the ABS and CD of the title pair of compounds and have derived dipole and rotatory strengths of all observable transitions in the VIS and UV.

Acknowledgements. We thank Dr. H. P. Jensen for providing us with the resolved amines and the Technical Chemistry Fund for a grant supporting part of NH's work.

REFERENCES

1. Ito, H., Fujita, J. and Saito, K. *Bull. Chem. Soc. Jpn. 40* (1967) 2584.
2. Sullivan, E. A. *Can. J. Chem. 57* (1979) 67.
3. Martin, D. S., Jr., Jacobson, R. A., Hunter, L. D. and Benson, J. E. *Inorg. Chem. 3* (1970) 1276.
4. Berg, R. W. and Rasmussen, K. *Spectrochim. Acta A 29* (1973) 319.
5. Jensen, H. P. *Acta Chem. Scand. A 32* (1978) 153.
6. Beddoe, P. G., Harding, M. J., Mason, S. F. and Peart, B. J. *Chem. Commun.* (1971) 1283.
7. Kuroda, R. and Saito, Y. *Bull. Chem. Soc. Jpn. 49* (1976) 433.
8. Kojima, M., Fujita, M. and Fujita, J. *Bull. Chem. Soc. Jpn. 50* (1977) 898.
9. Taniguchi, Y. and Shimura, Y. *Chem. Lett.* (1979) 1091.
10. Werner, A. *Z. Anorg. Chem. 21* (1899) 201.
11. Berg, R. W. and Rasmussen, K. *Spectrosc. Lett. 4* (1971) 285.
12. Moffitt, W. and Moscowitz, A. *J. Chem. Phys. 30* (1959) 648.
13. *Gmelins Handbuch der Anorganischen Chemie*, 8th Ed., System-Nummer 3 Sauerstoff, Lieferung 5, Verlag Chem., Weinheim 1963, p. 1551.
14. *Gmelins Handbuch der Anorganischen Chemie*, 8th Ed., System-Nummer 22 Kalium, Lieferung 1–2, Verlag Chem., Weinheim 1937, p. 378.

Received November 12, 1981.

Acta Chemica Scandinavica A 36 (1982) 555–561

Reaction Rate Studies of the Acid Hydrolysis of Some Chromium(III) Complexes. XIII. Water Exchange of *mer*-Triamminetriaqua- and Amminepentaaquachromium(III). Kinetic *cis* Effect of Ammonia *vs.* Water

L. MØNSTED[a] and O. MØNSTED[b]

[a]Chemistry Department, Royal Veterinary and Agricultural University, Thorvaldsensvej 40, DK-1871 Copenhagen V, Denmark and [b]Chemistry Department I, Inorganic Chemistry, University of Copenhagen, H. C. Ørsted Institute, DK-2100 Copenhagen Ø, Denmark

The rate of water exchange of *mer*-triamminetriaqua- and of amminepentaaquachromium(III) in an acid 1 M perchlorate medium has been investigated. The kinetics of both systems are characterized by two first order processes for which the rate constants at 25 °C are:

mer-$[Cr(NH_3)_3(OH_2)_3]^{3+}$: $(7.6 \pm 1.0) \times 10^{-5}$ s^{-1}, $(1.23 \pm 0.05) \times 10^{-5}$ s^{-1}; and
$[Cr(NH_3)(OH_2)_5]^{3+}$: $(2.8 \pm 0.4) \times 10^{-5}$ s^{-1}, $(0.449 \pm 0.014) \times 10^{-5}$ s^{-1}.

The two types of water ligands in both complexes are exchanged by processes which are largely stereoretentive, and the two larger rate constants are both associated with the reactivity of the water ligand *trans* to an ammonia ligand. Common features in the reactivity pattern for the exchange of water ligands in ammineaquachromium(III) complexes have been established and can be rationalized on the basis of an associative interchange mechanisms.

Few systematic studies of the effect of non-reacting ligands on the reactivity of transition metal complexes have been reported. We have earlier studied the ammonia ligand aquation of the isomeric ammineaquachromium(III) complexes in order to establish data for the kinetic *cis* and *trans* effect of coordinated ammonia *vs.* water.[1] For this system it was not possible, however, to obtain well-defined rate constants for some of the slower reactions because of an unfavourable competition between slow and faster reactions. The water exchange reactions of the same set of complexes are free from this complication. They can all be studied experimentally and the present work describes kinetic water exchange studies of *mer*-triamminetriaqua- and of amminepentaaquachromium(III) which in combination with earlier studies[2,3] completes our work on this series of complexes.

EXPERIMENTAL

Chemicals. *mer*-$[Cr(NH_3)_3(OH_2)Cl_2]Cl$[4,5] and $Cs[Cr(NH_3)(OH_2)_5](SO_4)_2 \cdot 6H_2O$[6,7] were prepared by literature methods. $Ba(tos)_2$* was prepared from warm aqueous solutions of $Ba(OH)_2 + 2H$ tos. The sources of other chemicals have been described earlier.[2,3]

Preparation of oxygen-18 labelled mer-triamminetriaquachromium(III). This cation was labelled with oxygen-18 enriched water by Ag(I) accelerated chloride ligand removal from the *mer*-triammineaqua-*trans*-dichloridochromium(III) cation followed by equilibration in oxygen-18 enriched water, essentially as described for *cis*-diamminetetraaquachromium(III), at method A in Ref. 3. This method was used for experiments 1–4 and 6 in Table 1. Experiment 5 shows an attempt to label the water ligand *trans* to ammonia stereoscpecifically by method C of Ref. 3. The δ'_1/δ'_2

* tos ≡ *p*-toluenesulfonate ≡ p-$CH_3C_6H_4SO_3^-$.

0302-4377/82/070555-07$02.50

ratio was slightly larger and, as found out for *cis*-diamminetetraaquachromium(III),[3] some water ligand isomerization takes place during the purification procedure so that further experiments of this type were not carried out.

Preparation of oxygen-18 labelled amminepentaaquachromium(III). A mixture of 150 mg $Cs[Cr(NH_3)(OH_2)_5](SO_4)_2 \cdot 6H_2O$ + 40 mg tosH + 250 mg $Ba(tos)_2$ was equilibrated in 1.0 ml of oxygen-18 enriched water at 60 °C for 50 min after which excess water was removed by sublimation in vacuum. The remaining solid was treated with 5 ml 0.01 M $HClO_4$ and $BaSO_4$ filtered off. The resulting solution which in addition to the desired $[Cr(NH_3)(OH_2)_5]^{3+}$ mainly contains Ba^{2+} and small amounts of sulphato- and tosylatochromium(III) complexes was purified by ion exchange chromatography as described in detail in Ref. 2. The monoamminepentaaqua ion solution prepared in this way was the basis for experiments 1 and 2 in Table 2. It was also attempted to label a larger fraction of the 'fast' water ligand site by reducing the equilibration time. Experiments 3 and 4 show two such attempts, which significantly reduces the uncertainty of the k_1 rate constant.

Kinetic measurements, methods of analyses, spectrophotometric measurements, mass spectrometric measurements and the *method of calculation* were essentially as described previously.[2,3]

RESULTS AND DISCUSSION

Exchange of oxygen-18 labelled water from *mer*-triamminetriaquachromium(III) takes place with retention of the ammine configuration. For both this cation and amminepentaaquachromium(III) the exchange follows a sum of two exponential functions, *i.e.*:

$$[^{18}O] = [^{18}O]_{t=0} + [Cr(III)] \times \{\delta'_1[1\text{-}\exp(-k_1 t)] + \delta'_2[1\text{-}\exp(-k_2 t)]\} \quad (1)$$

Table 1. Summary of kinetic data for water exchange in *mer*-$[Cr(NH_3)_3(OH_2)_3]^{3+}$ in 0.50 M $HClO_4$ + 0.50 M $NaClO_4$.

Exp.	Temp. [°C]	[Cr(III)] [mM]	δ'_1 [^{18}O/Cr]	δ'_2 [^{18}O/Cr]	$\delta'_1 + \delta'_2$ [^{18}O/Cr]
1	15.1	1.41	0.61 ± 0.14	1.81 ± 0.13	2.43 ± 0.03
2	24.9	1.04	0.80 ± 0.08	1.94 ± 0.08	2.73 ± 0.03
3	24.9_5	0.86	0.72 ± 0.09	1.68 ± 0.09	2.40 ± 0.04
4	24.9_5	1.29	0.73 ± 0.08	1.62 ± 0.08	2.35 ± 0.03
5[a]	24.9_5	1.24	0.11 ± 0.05	0.13 ± 0.05	0.24 ± 0.02
6	35.1	1.57	0.75 ± 0.07	1.60 ± 0.07	2.36 ± 0.03

k_1 (25 °C): $(7.6 \pm 1.0) \times 10^{-5}$ s^{-1} k_2 (25 °C): $(1.23 \pm 0.05) \times 10^{-5}$ s^{-1}

$\rho(k_1, k_2)$: 0.773

[a] See Experimental.

Table 2. Summary of kinetic data for water exchange in $[Cr(NH_3)(OH_2)_5]^{3+}$ in 0.50 M $HClO_4$ + 0.50 M $NaClO_4$ at 25 °C.

Exp.	[Cr(III)] [mM]	δ'_1 [^{18}O/Cr]	δ'_2 [^{18}O/Cr]	$\delta'_1 + \delta'_2$ [^{18}O/Cr]
1	1.08	0.77 ± 0.10	3.28 ± 0.10	4.04 ± 0.04
2	1.17	0.69 ± 0.11	3.45 ± 0.09	4.14 ± 0.05
3[a]	0.39	1.16 ± 0.17	1.78 ± 0.24	2.94 ± 0.12
4[a]	1.41	0.42 ± 0.05	0.27 ± 0.08	0.68 ± 0.03

k_1 (25 °C): $(2.8 \pm 0.4) \times 10^{-5}$ s^{-1} k_2 (25 °C): $(0.449 \pm 0.014) \times 10^{-5}$ s^{-1}
$\rho(k_1, k_2)$: 0.637

[a] See Experimental.

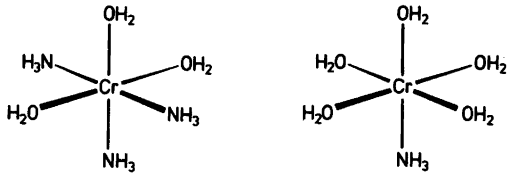

Fig. 1.

For both cations the larger rate constant has the smallest δ'-value as preexponential factor, *cf.* Tables 1 and 2. This clearly identifies this rate constant as that associated mainly with the reactivity of the single water ligand *trans* to an ammonia ligand, in both complexes, *cf.* Fig. 1. The smaller constants consequently describe the reactivity of the two and four remaining water ligands, respectively, in the two complexes. In Ref. 3 the kinetic data for water exchange of the *cis*-diamminetetraaquachromium(III) ion has been analyzed in detail in terms of stereoretentive processes described by k_N and k_O and processes accompanied by water ligand isomerization, k_I, *cf.* Fig. 2. Reactions of the present two complexes, in which also two types of water ligands are present in each, can be analyzed analogously, and from the exact expressions in the Appendix the following approximations are derived:

1. For *mer*-$[Cr(NH_3)_3(OH_2)_3]^{3+}$:

$$k_1 \sim k_N + 4k_I$$

$$k_2 \sim k_O + 2k_I$$

$$\delta'_1 \sim \varkappa_N - \frac{k_I(2\varkappa_N + \varkappa_O)}{k_1 - k_2}$$

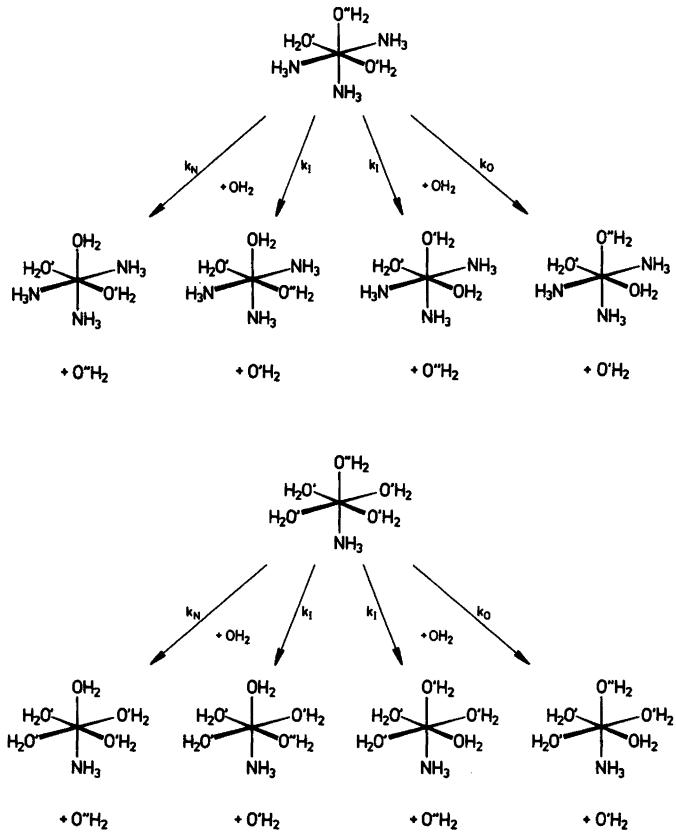

Fig. 2. Water exchange in *mer*-triamminetriaqua- and amminepentaaquachromium(III) by stereoretentive processes, k_N and k_O paths, and by processes accompanied by isomerization, k_I paths.

and

$$\delta'_2 \sim \varkappa_O + \frac{k_I(2\varkappa_N + \varkappa_O)}{k_1 - k_2}$$

Averaged data for the experiments 2 – 4 in Table 1 in combination with the assumption $2\varkappa_N \lesssim \varkappa_O$, *i.e.* assuming that the purification steps mainly reduce the isotopic purity of the 'fast' water ligand site, allow the estimations of the following rate constants at 25 °C:

$$k_I \lesssim (0.16 \pm 0.07) \times 10^{-5}\ s^{-1}$$

$$(7.0 \pm 1.0) \times 10^{-5}\ s^{-1} \lesssim k_N \lesssim (7.6 \pm 1.0) \times 10^{-5}\ s^{-1}$$

and

$$(0.91 \pm 0.15) \times 10^{-5}\ s^{-1} \lesssim k_O \lesssim (1.23 \pm 0.05) \times 10^{-5}\ s^{-1}$$

Similarly for

2. $[Cr(NH_3)(OH_2)_5]^{3+}$:

$$k_1 \sim k_N + 8k_I$$

$$k_2 \sim k_O + 2k_I$$

$$\delta'_1 \sim \varkappa_N - \frac{k_I(4\varkappa_N + \varkappa_O)}{k_1 - k_2}$$

and

$$\delta'_2 \sim \varkappa_O + \frac{k_I(4\varkappa_N + \varkappa_O)}{k_1 - k_2}$$

from which the averaged data for the experiments 1 and 2 in Table 2 and $4\varkappa_N \lesssim \varkappa_O$ allow the estimations for the rate constants at 25 °C:

$$k_I \lesssim (0.03 \pm 0.02) \times 10^{-5}\ s^{-1}$$

$$(2.5 \pm 0.4) \times 10^{-5}\ s^{-1} \lesssim k_N \lesssim (2.8 \pm 0.4) \times 10^{-5}\ s^{-1}$$

and

$$(0.39 \pm 0.04) \times 10^{-5}\ s^{-1} \lesssim k_O \lesssim (0.449 \pm 0.014) \times 10^{-5}\ s^{-1}$$

For both cations the main reactivity is seen to be associated with the k_N and k_O paths. In view of the much smaller maximum value for the two k_I rate

Table 3. Summary of kinetic parameters for water exchange in $[Cr(NH_3)_x(OH_2)_{6-x}]^{3+}$ species, $0 \leq x \leq 5$, classified according to the ligands in *trans* and *cis* position to the reacting water ligand. The data are from this work and Refs. 2 and 3.

cis:	*trans*: NH_3 $10^5\,k$ [s^{-1}]	ΔH^* [kJ mol^{-1}]	ΔS^* [JK^{-1} mol^{-1}]	*trans*: OH_2 $10^5\,k$ [s^{-1}]	ΔH^* [kJ mol^{-1}]	ΔS^* [JK^{-1} mol^{-1}]
$\{(NH_3)_4\}$	5.75 ± 0.06	99.1 ± 1.4	+7 ± 5	1.17 ± 0.03	98.5 ± 2.1	−9 ± 7
$\{(NH_3)_3(OH_2)\}$	5.92 ± 0.13	95.1 ± 1.9	−7 ± 6	1.23 ± 0.05	–	–
$\{cis\text{-}(NH_3)_2(OH_2)_2\}$	5.78 ± 0.09	95.1 ± 1.3	−7 ± 5	1.02 ± 0.09	105 ± 4	+13 ± 14
$\{trans\text{-}(NH_3)_2(OH_2)_2\}$	7.6 ± 1.0	–	–	0.997 ± 0.013	97.0 ± 1.1	−15 ± 4
$\{(NH_3)(OH_2)_3\}$	4.9 ± 0.4	101 ± 3	+11 ± 9	0.449 ± 0.014	–	–
$\{(OH_2)_4\}$	2.8 ± 0.4	–	–	0.246 ± 0.012	109.6 ± 1.3	+16 ± 5

constants it is, therefore, most likely that the present water exchange reactions are dominated by the stereoretentive contributions to the k_N and k_O rate constants, a result which was also arrived at for the *cis*-diamminetetraaquachromium(III) ion.[3]

With the present data in combination with the results in Refs. 2 and 3 the kinetics of water exchange of all ammineaquachromium(III) isomers have been investigated. A summary of these data classified according to the *trans* and *cis* ligands is given in Table 3. It is seen that the reactions are generally faster *trans* to an ammonia ligand than *trans* to a water ligand, and are decelerated by the introduction of *cis* water ligands although not in a regular fashion. This last point is illustrated more clearly in Table 4 where the difference between the observed reactivity of those reactants with from 1 to 3 *cis* water ligands, and that predicted by linear interpolation between the two reactants with 0 and 4 *cis* water ligands, *i.e.*

$$\delta[\Delta G^*(a_{4-i}\,aq_i)] = \Delta G^*(a_{4-i}\,aq_i) - \frac{4-i}{4}\Delta G^*(a_4) - \frac{i}{4}\Delta G^*(aq_4)$$

have been calculated. All numbers in the table are seen to be negative corresponding to an increased reactivity, and are very similar for the two series of reactants, with the average values distributed roughly as 1:2:2:1 as demonstrated on Fig. 3. This result can be rationalized by considering the transition state geometry of Fig. 4, which has earlier been shown to rationalize data for some similar reactions.[8] Fig. 5 demonstrates the possible transition state structures for the present reactions. If a similar geometry is assumed for all these transition states and the major cause of the *cis* effect is the ligand – ligand interactions between the four *cis* ligands and the entering and leaving water

Table 4. 'Excess' *cis*-effect for water exchange in $[Cr(t)\{a_{4-i}\,aq_i\}OH_2]^{3+}$ at 25 °C. Data from Table 3.

$\{a_{4-i}\,aq_i\}$	t=NH_3 $\delta(\Delta G^*)$ [kJ mol^{-1}]	t=OH_2 $\delta(\Delta G^*)$ [kJ mol^{-1}]
$\{(NH_3)_3(OH_2)\}$	-0.51 ± 0.10	-1.09 ± 0.11
$\{cis\text{-}(NH_3)_2(OH_2)_2\}$	-0.91 ± 0.17	-1.60 ± 0.22
$\{trans\text{-}(NH_3)_2(OH_2)_2\}$	-1.59 ± 0.35	-1.54 ± 0.07
$\{(NH_3)(OH_2)_3\}$	-0.97 ± 0.30	-0.53 ± 0.12

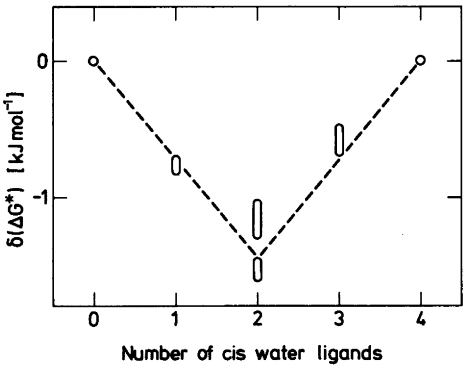

Fig. 3. 'Excess' *cis* effect for complexes with less than tetragonal symmetry of the *cis* ligands. The data are from Table 4, and are drawn with a vertical extent corresponding to ± the estimated uncertainty.

ligands, a linear variation of ΔG^* as function of the number of identical *cis* ligands will be expected. However, for the unsymmetrical transition state structures where the reacting water ligands are closest to two different *cis* ligands, *i.e.* the structures in Fig. 5 which have reacting water ligands marked with a double arrow, this geometry is not that with the minimum energy, and an energy lowered by an amount which will be called $\delta(OH_2)$ can be obtained by distorting this geometry, probably mainly by moving the reacting water ligand in a direction perpendicular to that mirror plane of symmetry of the idealized transition state, *cf.* Fig. 4, which contains the entering and leaving groups. This simple model predicts as a first approximation that the $\delta(\Delta G^*)$ values should be proportional to the number of reacting water ligands which are closest to two different *cis* ligands, *i.e.* should have the values $\delta(OH_2)$, $2\delta(OH_2)$, $2\delta(OH_2)$ and $\delta(OH_2)$. This

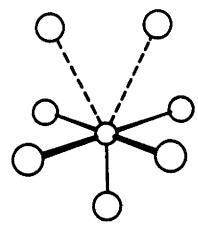

Fig. 4. Idealized transition state geometry used to rationalize kinetic water exchange data. In Fig. 5 this structure is seen from the entering and leaving ligand.

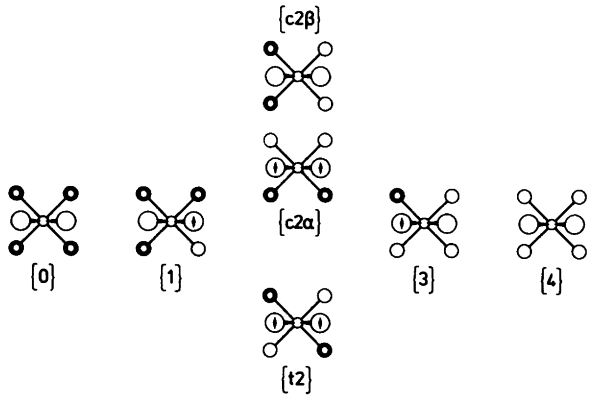

Fig. 5. Transition state geometries, *cf.* Fig. 4, for the series of water exchange reactions with all possible combinations of two different ligands in *cis* position to the reacting ligand. (See also the text).

is seen to be in excellent agreement with the experiments shown in Fig. 3. From the data of this figure it can further be calculated that the lowering in ΔG^* by distortions involving *one* of the reacting water ligands amounts to a value of $\delta(OH_2)$ about -0.7_3 kJ mol^{-1}.

This rationalization of the 'excess' reactivity of complexes with less than tetragonal symmetry may further be tested by analyzing the data for ammonia ligand aquation, which has also been systematically studied for the ammineaquachromium(III) isomers.[1] Table 5 gives data for the reactions *trans* to coordinated ammonia only, as the lack of a well-defined value for the rate constant for the pentaammineaqua- to *trans*-tetraamminediaquachromium(III) reaction prevents the calculation of the similar quantities for the series of reactions *trans* to coordinated water. The four numbers of Table 5 are all seen to be negative and of almost the same magnitude, *i.e.* distributed as 1:1:1:1. An analogous transition state structure to that used for the water exchange reactions can rationalize this result. The

Table 5. 'Excess' *cis*-effect for ammonia ligand aquation in $[Cr(NH_3)\{a_{4-i}aq_i\}(NH_3)]^{3+}$ at 70 °C. Data from Ref. 1.

$\{a_{4-i}aq_i\}$	$\delta(\Delta G^*)$ [kJ mol^{-1}]
$\{(NH_3)_3(OH_2)\}$	-1.05 ± 0.06
$\{cis\text{-}(NH_3)_2(OH_2)_2\}$	-1.06 ± 0.09
$\{trans\text{-}(NH_3)_2(OH_2)_2\}$	-0.81 ± 0.09
$\{(NH_3)(OH_2)_3\}$	-0.92 ± 0.09

various possibilities for transition state structures are similar to those shown in Fig. 5, and in analogy with the arguments just presented it is seen that the $\delta(\Delta G^*)$-values for the $\{c2\alpha\}$- and $\{t2\}$-transition states will be $\delta(OH_2)+\delta(NH_3)$, where $\delta(NH_3)$ is defined analogous to $\delta(OH_2)$. For the $\{1\}$- and $\{3\}$-transition states the model predicts that ΔG^* will be stabilized by either $\delta(OH_2)$ or $\delta(NH_3)$ whichever distortion lowers the transition state energy most. The data in Table 5, interpreted within this model, clearly show that distortions involving either the entering water molecule or the leaving ammonia ligand are energetically without consequent, *i.e.* either $\delta(OH_2)$ or $\delta(NH_3)$ is close to zero. The well-defined negative value for $\delta(OH_2)$ previously obtained makes the last possibility most likely, and gives the set of values $\delta(OH_2) \sim -0.9_2$ kJ mol^{-1} and $\delta(NH_3) \sim 0$ kJ mol^{-1} in good agreement with $\delta(OH_2) \sim -0.7_3$ kJ mol^{-1} obtained from the water exchange data.

The small value for $\delta(NH_3)$ may indicate significantly smaller ligand–ligand interactions when ammonia rather than water ligands are involved. This type of interaction is most likely greater also between the five nonreacting ligands in an associative transition state than in the ground state. The small $\delta(NH_3)$ value can, therefore, be taken as indirect evidence for the hypothesis that such interactions between the nonreacting ligands are also a contributing factor to the *trans* effect for the present series of reactions.

In conclusion, the present analysis of part of the kinetic *cis* effect strongly supports the hypothesis of an associative interchange mechanism, and the

structure shown in Fig. 4 has been demonstrated to be a good approximation to the idealized transition state geometry. This structure has earlier been arrived at through the analysis of the ΔH_X^* *vs.* Δ_X variation as a function of a number of leaving X-ligands,[8] and has now also been applied to the 'excess' reactivity of complexes with less than tetragonal symmetry of the *cis* ligands, and is apparently able to explain this phenomenon for both of the two series of water exchange reactions and also for a series of much slower ammonia ligand aquation reactions.

Acknowledgement. The authors wish to thank the Geophysical Isotope Laboratory at the University of Copenhagen, particularly Dr. Niels Gundestrup, for carrying out the mass spectrometric analyses.

APPENDIX

The elementary reactions shown in Fig. 2 can be used to construct total reaction schemes for irreversible oxygen-18 aquation of labelled *mer*-triamminetriaqua- and ammineпentaaquachromium-(III) as demonstrated in greater detail for the *cis*-diammineteтraaquachromium(III) ion in Ref. 3. In terms of experimentally determined quantities, *cf.* eqn. 1, it can be derived:

1. for *mer*-$[Cr(NH_3)_3(OH_2)_3]^{3+}$:

$$(k_1, k_2) = \tfrac{1}{2}\left[k_N + k_O + 6k_I \pm \sqrt{(k_N + 2k_I - k_O)^2 + 8k_I^2}\right]$$

$$\delta_1' = \frac{(k_O + 4k_I - k_1)(\varkappa_N(k_N + 4k_I - k_2) - \varkappa_O k_I)}{(k_N + 4k_I - k_2)(k_O + 2k_I - k_1) - 2k_I^2}$$

$$\delta_2' = \frac{(k_N + 5k_I - k_2)(\varkappa_O(k_O + 2k_I - k_1) - 2\varkappa_N k_I)}{(k_N + 4k_I - k_2)(k_O + 2k_I - k_1) - 2k_I^2}$$

and

2. for $[Cr(NH_3)(OH_2)_5]^{3+}$:

$$(k_1, k_2) = \tfrac{1}{2}\left[k_N + k_O + 10k_I \pm \sqrt{(k_N + 6k_I - k_O)^2 + 16k_I^2}\right]$$

$$\delta_1' = \frac{(k_O + 6k_I - k_1)(\varkappa_N(k_N + 8k_I - k_2) - \varkappa_O k_I)}{(k_N + 8k_I - k_2)(k_O + 2k_I - k_1) - 4k_I^2}$$

$$\delta_2' = \frac{(k_N + 9k_I - k_2)(\varkappa_O(k_O + 2k_I - k_1) - 4\varkappa_N k_I)}{(k_N + 8k_I - k_2)(k_O + 2k_I - k_1) - 4k_I^2}$$

In both cases $\varkappa_N$ and $\varkappa_O$ are the average number of oxygen-18 labelled water molecules *trans* to ammonia and water, respectively, at the start of the kinetic experiment.

REFERENCES

1. Mønsted, L. and Mønsted, O. *Acta Chem. Scand. A 28* (1974) 569.
2. Mønsted, L. and Mønsted, O. *Acta Chem. Scand. A 34* (1980) 259.
3. Mønsted, L. and Mønsted, O. *Acta Chem. Scand. A 36* (1982) 365.
4. Schlessinger, G. G. *Inorganic Laboratory Preparations*, Chemical Publishing Company, Inc., New York 1962, p. 249.
5. Caldwell, S. M. and House, D. A. *Inorg. Chem. 8* (1969) 151.
6. Ardon, M. and Mayer, B. E. *J. Chem. Soc.* (1962) 2816.
7. Bjerrum, J. and Jørgensen, E. *Acta Chem. Scand. 12* (1958) 1047.
8. Mønsted, O. *Acta Chem. Scand. A 32* (1978) 297.

Received December 1, 1981.

Acta Chemica Scandinavica A 36 (1982) 563 – 570

Ti_7P_4 – Crystal Structure Refinement, and Structural Relationship with $Ti_{11}CuP_8$, Nb_8P_5 and Some Other Compounds

WILDER CARRILLO-CABRERA

Institute of Chemistry, University of Uppsala, Box 531, S-751 21 Uppsala, Sweden

The crystal structure of Ti_7P_4 containing 2.1 atom-% copper has been refined using X-ray single-crystal diffractometry. The symmetry is monoclinic, space group $C2/m$, with lattice parameters: $a=$ 14.474(4) Å, $b=3.4094(3)$ Å, $c=13.616(2)$ Å and $\beta=104.597(16)°$. Ti_7P_4 is isotypic with Nb_7P_4. The refinement indicates a partial substitution of copper for titanium in the M(4) position. The environment of the M(4) atoms has a great similarity to that of the copper atoms in TiCuSi and $Zr_3Cu_4Si_4$. The structural relationships between Ti_7P_4 and some similar silicides, arsenides and phosphides are described.

Work at this institute has established the existence of a series of compounds with composition M_7X_4 isostructural with Nb_7P_4 in the binary Nb – As, Nb – P, Ta – P and Ti – P systems.[1-4] There is also evidence for the occurrence of an Nb_7P_4 type compound in the Hf – As system.[5] Crystals of Ti_7P_4 and other titanium-rich phosphides in ternary Ti – Cu – P samples were found to contain only a few atomic percent copper in solution.[4] The recent structure determination of the $Ti_{11}CuP_8$ phase[6] has stimulated interest in the detailed crystal structures of the other titanium phosphides containing copper. In the present paper the results of the structure refinement of $Ti_{7-x}Cu_xP_4$ with $x=0.23$ are reported.

EXPERIMENTAL

Preparation. A copper-rich ternary alloy of nominal composition $Ti_{0.02}Cu_{0.97}P_{0.01}$ (approx. 2.5 g) was prepared[7] by initially reacting copper (Outokumpu Oy, Pori, Finland; as analyzed better than 99.99 %) and red phosphorus (Kebo, Stockholm, Sweden; better than 99 %) in an evacuated silica ampoule at 800 °C for three days and subsequently melting the reaction products together with lumps of titanium (Koch-Light Laboratories, Colnbrook, England; claimed purity 99.95 %) in a cold-crucible induction furnace. The sample was inhomogeneous even after annealing at 800 °C for 12 days. Small metallic crystals of $(Ti,Cu)_7P_4$ α-Ti_5P_3, $(Ti,Cu)_{14}P_9$ and β-$(Ti,Cu)_5P_3$ were isolated by dissolving the copper matrix in nitric acid.[4]

It was found that all the $(Ti,Cu)_7P_4$ crystals examined were twinned (with (001) as twinning plane). Even after crushing the crystals into smaller fragments it was not possible to select any which were not twinned. Nevertheless, the ratio of the volume of the smaller twin to the larger could be decreased. A crystal with a small satellite in the twin orientation was used for intensity measurements. The crystal was needle-shaped (the long axis coincident with the b axis of the unit cell) with the approximate dimensions $20\times20\times130$ μm. Only the (100) and (001) faces were well-developed.

X-Ray diffraction measurements and data reduction. The single-crystal intensity data were collected using a Nonius CAD 4-F automatic diffractometer, controlled by a PDP 8/A computer. The ω-2θ scan technique was used and reflections from one quarter of the reciprocal sphere were recorded to a maximum in 2θ of 86°. The cell dimensions of the crystal investigated were determined by least-squares refinement of the averages, $\bar{\theta}_i$, of the setting angles of 24 Friedel pairs of reflections with $15°<2\bar{\theta}_i<50°$. Mo$K\alpha$ radiation ($\lambda=0.71069$ Å) was used for this measurement as well as for the intensity data collection. The intensities were corrected for Lorentz, polarization and absorption effects. Absorption correction was carried out using the Gaussian grid method and a linear absorption coefficient of 97.4 cm^{-1} (calculated with mass absorption coefficients from Ref. 8, assuming two atomic percent

0302-4377/82/070563-08$02.50

copper in the crystal). The minimum and maximum transmission factors obtained were 0.778 and 0.856. Correction for absorption in the smaller twin individual could not be applied. The systematic error arising was, however, considered to be negligible due to the small size and low absorption. In total, 2671 reflections were recorded, of which 1979 displayed positive intensities. Due to the twin type the (0*kl*) reflections were completely overlapped by the (0*kl*) reflections of the smaller component crystal. All 57 (0*kl*) reflections were used in the refinement, however, with a separate scale factor. From the two scale factors the ratio of the intensities from the main and "satellite" twin crystal respectively was found to be approximately 5:1. In total 150 reflections were deleted due to overlap with non-equivalent reflections from the smaller twin crystal.

Calculations. All calculations were performed with the computers NORD 100 and IBM 1800 using a system of programs described by Lundgren.[9]

STRUCTURE ANALYSIS AND RESULTS

The preliminary data obtained from Weissenberg films indicated a *C*-centred monoclinic cell. The conditions for (*hkl*) reflections were $h+k=2n$, which is consistent with the space groups *C*2, *Cm* or *C*2/*m*. The centrosymmetric *C*2/*m* (No. 12) space group was chosen and finally confirmed in the refinement.

The structure was refined using a full-matrix least-squares program[9] and the atomic coordinates[2] of Nb_7P_4 as initial values for the positional parameters. The quantity minimized was $\Sigma w(|F_o^2| - k^2|F_c^2|)^2$. Each reflection was assigned a weight w given by eqn. (1), where σ_c is the standard deviation

$$w^{-1} = [\sigma_c(F_o^2)]^2 + (p|F_o^2|)^2 \quad (1)$$

of F_o^2, based on counting statistics, and p and empirical parameter, chosen to obtain a satisfactory weight analysis (p was 0.036 in the final refinement). The agreement indices are defines in eqns. (2) and (3), where F_o^2 has been multiplied by

$$R(F^2) = \Sigma(|F_o^2| - |F_c^2|)/\Sigma|F_o^2| \quad (2)$$

$$R_w(F^2) = [\Sigma w(|F_o^2| - |F_c^2|)^2/\Sigma w|F_o^2|^2]^{1/2} \quad (3)$$

$1/k^2$. Complex neutral-atom scattering factors were used.[8] Extinction effects were hardly dicernible and thus no correction was applied. Initially, the following parameters were refined: 2 scale factors, 20 positional parameters, and 12 isotropic temperature factors. The refinement on F^2, based on 1829 positive reflections, converged rapidly, and the agreement factors obtained were:

$R(F^2) = 0.130$, $R_w(F^2) = 0.131$ and $R(F) = 0.126$

The possibility of Cu/Ti substitution was then examined. Following the principle of good space filling, the smaller metal atoms (Cu) should pref-

Table 1. Structure data for $Ti_{6.77}Cu_{0.23}P_4$ from refinement based on F^2. Space group *C*2/*m* (No. 12), $Z=4$. Standard deviations within parentheses. Cell dimensions: $a=14.474(4)$ Å, $b=3.4094(3)$ Å, $c=13.616(2)$ Å and $\beta=104.597(16)°$. The anisotropic temperature factor is of the form: $\exp[-2\pi^2(U_{11}h^2a^{*2}\cdots+2U_{13}hla^*c^*)]$; $U_{12}=U_{23}=0$.

Atom	Position	Positional parameters			$U_{ij}\times10^4$ (Å^2)				
		x	*y*	*z*	U_{11}	U_{22}	U_{33}	U_{13}	B (Å^2)
Ti(1)	2(a)	0	0	0	–	–	–	–	0.27(2)
Ti(2)	2(d)	0	1/2	1/2	–	–	–	–	0.27(2)
Ti(3)	4(i)	0.42787(10)	0	0.82790(11)	64(5)	14(6)	60(5)	11(4)	(0.39(2))[b]
M(4)[a]	4(i)	0.19672(9)	0	0.31057(11)	59(5)	44(6)	91(5)	10(4)	(0.52(2))[b]
Ti(5)	4(i)	0.20654(10)	0	0.79365(10)	–	–	–	–	0.33(2)
Ti(6)	4(i)	0.33944(9)	0	0.03274(10)	–	–	–	–	0.33(2)
Ti(7)	4(i)	0.00261(9)	0	0.66348(10)	47(5)	20(6)	38(5)	3(4)	(0.29(2))[b]
Ti(8)	4(i)	0.17794(9)	0	0.54059(10)	–	–	–	–	0.28(2)
P(1)	4(i)	0.17847(14)	0	0.10806(15)	–	–	–	–	0.34(3)
P(2)	4(i)	0.37191(14)	0	0.60404(15)	62(8)	20(9)	42(7)	7(6)	(0.35(3))[b]
P(3)	4(i)	0.36957(14)	0	0.34190(15)	54(8)	13(8)	35(7)	0(6)	(0.31(3))[b]
P(4)	4(i)	0.06097(14)	0	0.84898(15)	71(8)	32(9)	20(7)	11(6)	(0.31(3))[b]

[a] M(4) = 0.77(1)Ti + 0.23(1)Cu. [b] Temperature factor from refinement assuming only isotropic thermal vibrations.

erentially occupy the positions which have small coordination numbers *i.e.* M(1), M(2) and M(4). Only in the M(4) site was a significant Cu/Ti substitution found. The least-squares refinement on F^2 gave an occupancy of 0.386 ($\sigma=0.007$) for Ti and 0.114 for Cu (reset), and the following R-values: $R(F^2)=0.124$, $R_w(F^2)=0.122$ and $R(F)=0.122$. A Hamilton R-factor significance test[10] favoured the last model at the 99.5 % confidence level. Refinements under the assumption of Cu/Ti substitution in other metal positions with higher coordination numbers did not reveal any significant copper occupancy. A subsequent refinement with anisotropic temperature factors for all atoms showed that only six atoms could be regarded as anisotropic. The introduction of anisotropic factors for these six atoms led to somewhat improved agreement index. A Hamilton test[10] favoured the model with the six anisotropic atoms at the 99.5 % confidence level. The final refinement on F^2 gave the following agreement values (1829 reflections):

$R(F^2)=0.116$, $R_w(F^2)=0.115$ and $R(F)=0.119$.

The shifts in the final cycle were less than 0.03σ. The total number of parameters varied was 53 (two scale factors, one occupancy factor, 20 positional parameters and 30 temperature factors). The agreement factors for a refinement on F^2 omitting observations with $F_o^2<3\sigma(F_o^2)$ were (1126 reflections): $R(F^2)=0.081$, $R_w(F^2)=0.102$ and $R(F)=0.056$. The standard deviations were, however, on the average 17 % larger than those for the refinement of the more complete intensity material.

A normal probability ΔR-plot[11] after the final refinement displayed a very slightly S-shaped line with a slope of 0.92 and an intercept of -0.16 on the expected ΔR axis (no value fell outside the range $\pm 4\sigma$), indicating that the ΔR are random-normally distributed with some underestimation of $\sigma(F^2)$. The standard deviation of an observation of unit weight,[12] S, was 1.19. A final difference Fourier map exhibited no electron density exceeding 4 % of a phosphorus peak in the F_o synthesis. The results from the final refinement are presented in Table 1. The interatomic distances are given in Table 2.

A list of observed and calculated structure factors can be obtained on request from the Institute of Chemistry, University of Uppsala, Sweden.

Table 2. Interatomic distances (Å) in $Ti_{6.77}Cu_{0.23}P_4$ less than 3.5 Å. Standard deviations within parentheses. M(4) = 0.77 Ti + 0.23 Cu.

Ti(1) – 2P(4)	2.434(2)	Ti(7) – P(4)	2.453(2)
– 2P(1)	2.632(2)	– 2P(2)	2.524(2)
– 4Ti(3)	2.873(1)	– 2P(3)	2.531(2)
– 4Ti(6)	3.005(1)	– 2Ti(2)	2.796(1)
– 2Ti(1)	3.409(0)	– M(4)	2.995(2)
		– Ti(5)	3.037(2)
Ti(2) – 2P(3)	2.480(2)	– 2Ti(3)	3.211(2)
– 2P(2)	2.602(2)	– Ti(8)	3.300(2)
– 4Ti(7)	2.796(1)	– Ti(8)	3.374(2)
– 4Ti(8)	3.022(1)	– 2Ti(7)	3.409(0)
– 2Ti(2)	3.409(0)		
		Ti(8) – 2P(3)	2.548(2)
Ti(3) – 2P(4)	2.534(2)	– 2P(2)	2.562(2)
– 2P(1)	2.591(2)	– P(2)	2.722(2)
– 2M(4)	2.828(2)	– 2M(4)	2.907(2)
– 2Ti(1)	2.873(1)	– 2Ti(2)	3.022(1)
– P(2)	2.950(2)	– 2Ti(8)	3.105(2)
– Ti(5)	3.120(2)	– M(4)	3.211(2)
– 2Ti(7)	3.211(2)	– Ti(7)	3.300(2)
– Ti(6)	3.349(2)	– Ti(5)	3.365(2)
– 2Ti(3)	3.409(0)	– Ti(7)	3.374(2)
– Ti(6)	3.425(2)	– 2Ti(8)	3.409(0)
M(4) – 2P(2)	2.414(2)	P(1) – 2Ti(5)	2.519(2)
– P(3)	2.430(2)	– 2Ti(6)	2.529(2)
– P(1)	2.703(2)	– 2Ti(3)	2.591(2)
– 2Ti(5)	2.808(2)	– Ti(1)	2.632(2)
– 2Ti(3)	2.828(2)	– M(4)	2.703(2)
– 2Ti(8)	2.907(2)	– Ti(6)	2.773(2)
– Ti(7)	2.995(2)	– 2P(1)	3.409(0)
– Ti(8)	3.211(2)		
– 2M(4)	3.409(0)	P(2) – 2M(4)	2.414(2)
		– 2Ti(7)	2.524(2)
Ti(5) – P(4)	2.410(2)	– 2Ti(8)	2.567(2)
– 2P(1)	2.519(2)	– Ti(2)	2.602(2)
– 2P(3)	2.550(2)	– Ti(8)	2.722(2)
– 2M(4)	2.808(2)	– Ti(3)	2.950(2)
– Ti(7)	3.037(2)	– 2P(2)	3.409(0)
– 2Ti(6)	3.119(2)		
– Ti(3)	3.120(2)	P(3) – M(4)	2.430(2)
– Ti(6)	3.338(2)	– Ti(2)	2.480(2)
– Ti(8)	3.365(2)	– 2Ti(7)	2.531(2)
– 2Ti(5)	3.409(0)	– 2Ti(8)	2.548(2)
		– 2Ti(5)	2.550(2)
Ti(6) – 2P(1)	2.529(2)	– P(3)	3.409(0)
– 2P(4)	2.532(2)	– 2P(4)	3.463(2)
– P(1)	2.773(2)		
– 2Ti(1)	3.005(1)	P(4) – Ti(5)	2.410(2)
– 2Ti(6)	3.040(2)	– Ti(1)	2.434(2)
– 2Ti(5)	3.119(2)	– Ti(7)	2.453(2)
– Ti(5)	3.338(2)	– 2Ti(6)	2.532(2)
– Ti(3)	3.349(2)	– 2Ti(3)	2.534(2)
– 2Ti(6)	3.409(0)	– 2P(4)	3.409(0)
– Ti(3)	3.425(2)	– 2P(3)	3.463(2)

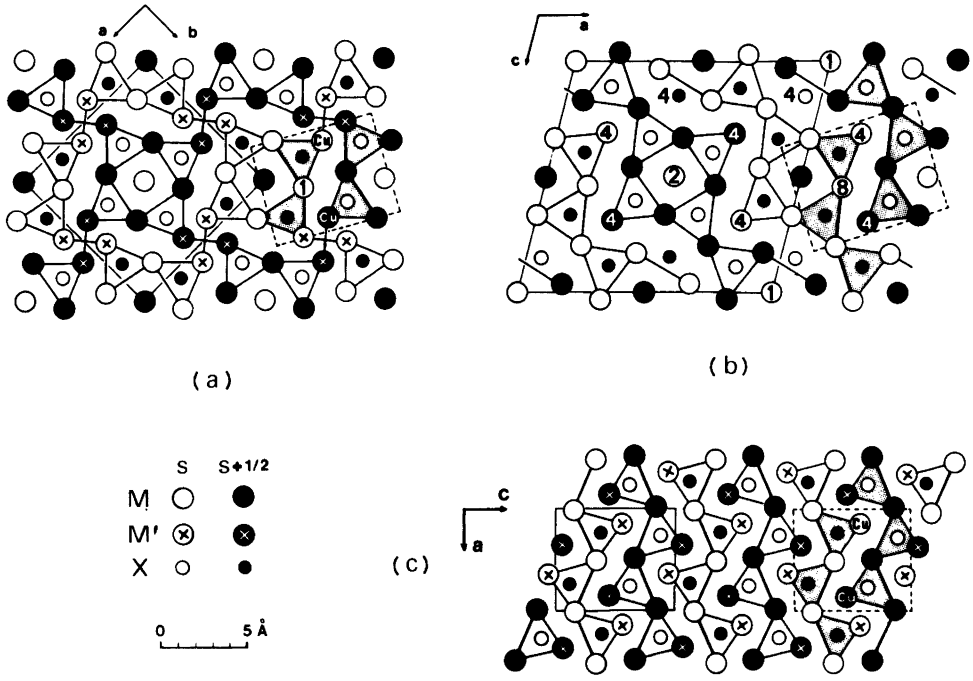

Fig. 1. Projections, along the short axis, of the structures of (a) $Nb_5Cu_4Si_4$ (M′ = Cu, s = 0), (b) Ti_7P_4 (s = 0; Nb_7P_4 type) and (c) TiCuSi (M′ = Cu, s = 1/4; TiNiSi type).

DISCUSSION

The complete single-crystal analysis has shown that Ti_7P_4 is indeed a new member of the Nb_7P_4 structure[2] family. A projection of the Ti_7P_4 structure along the *b*-axis is illustrated in Fig. 1b. There are four non-equivalent phosphorus atoms in the structure. The environment of the phosphorus atoms is triangular prismatic (with metal atoms at the corners of the prism) with 1 – 3 additional metal neighbours outside the quadrilateral faces of the prism. The axis of the triangular prism is perpendicular to the *b*-axis for P(4) and parallel to the *b*-axis for the P(1) – P(3) atoms. Only the triangular prisms about the latter phosphorus atoms, which have high coordination numbers (8, 9), are indicated in Fig. 1b. The structure may thus be described as being built up of M_6P triangular prisms and distorted body-centred cubic M_8M units interconnected to form chains, which are infinite in the [101] direction, with extra phosphorus atoms (P(4)) between the chains. Adjacent chains are displaced by half the unit cell length in the direction of the projection in Fig. 1b.

The Ti_7P_4 structure is closely related to that of the metal richer silicides $Nb_5Cu_4Si_4$[13] and TiCuSi[14] (*E* phase, ordered anti-$PbCl_2$, TiNiSi type[15]) regarding the occurrence of groups of four triangular prisms within a unit indicated by dashed lines in Fig. 1 (coincident with the unit cell of TiCuSi). Furthermore, fragments of two zig-zag chains of trigonal prisms are shaded in Fig. 1 to emphasize the relationships among the structures. The fragment consists of two prisms for $Nb_5Cu_4Si_4$ (Fig. 1a) and three prisms for Ti_7P_4 (Fig. 1b). In the TiCuSi structure, where a zig-zag chain of prisms is infinite in the *a* direction (Fig. 1c), no body-centred metal units occur. However, the coordination of corresponding atoms in the common structural unit (within dashed lines) is similar; *e.g.* the coordination of Nb(1) in $Nb_5Cu_4Si_4$, Ti(8) in Ti_7P_4 and titanium in TiCuSi are almost identical, while the environment of M(4) in Ti_7P_4 is very similar to that of copper in TiCuSi and $Nb_5Cu_4Si_4$ (the positions of the atoms are indicated in Fig. 1). In the present refinement it was found that 23 % of the titanium in the M(4) site of Ti_7P_4 has been replaced by copper. This fact is an indication of the close

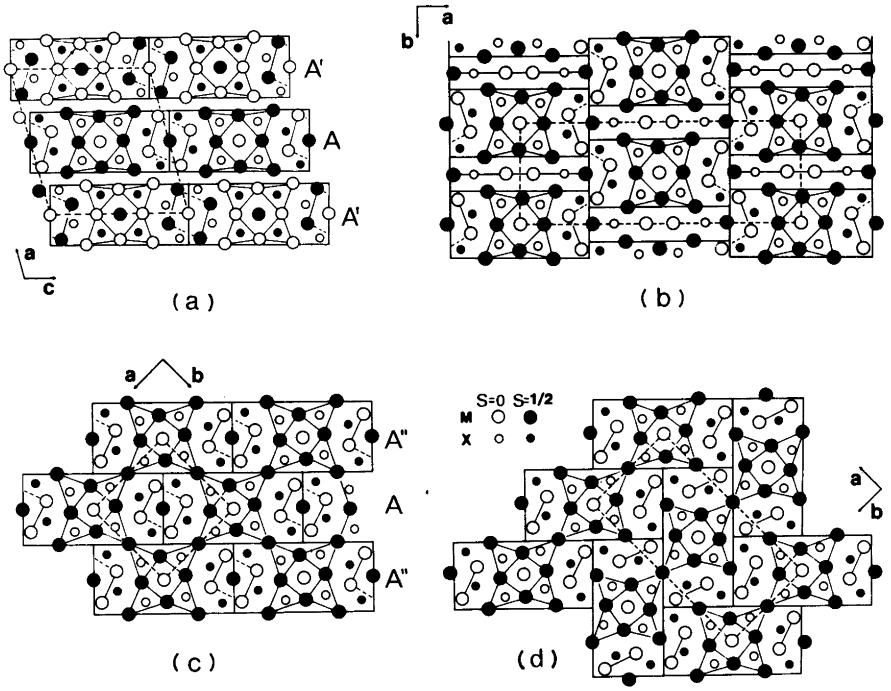

Fig. 2. Comparison among the structures of (a) Ti_7P_4, (b) Nb_8P_5, (c) V_3As_2 and (d) $Ti_{11}CuP_8$ as viewed along the short axis.

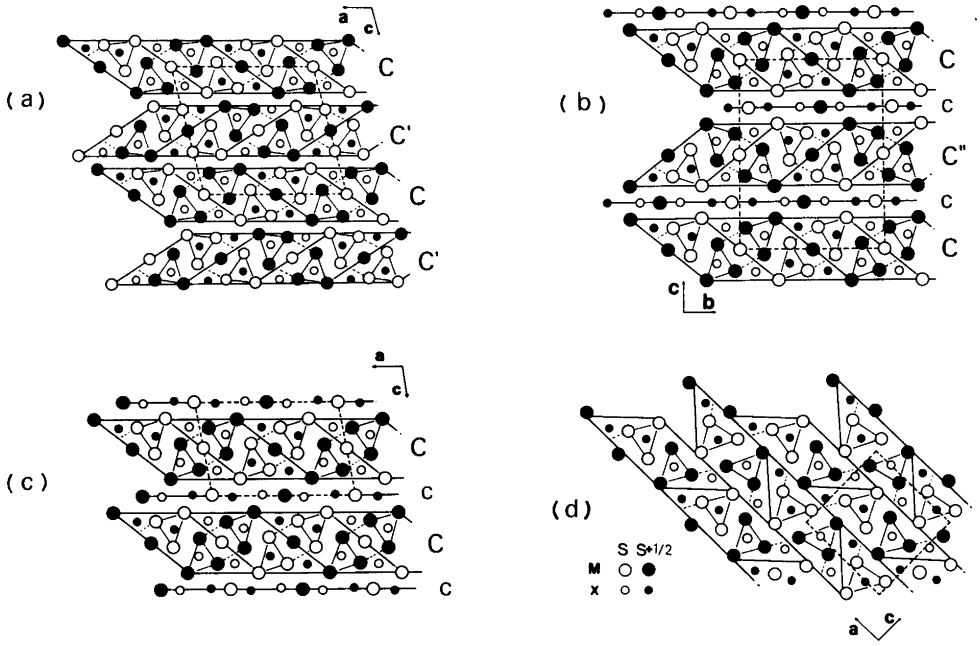

Fig. 3. Relationship between the structures of (a) Ti_7P_4 (s=0), (b) Nb_4As_3 (s=0), (c) Cr_4As_3 (s=0) and (d) Hf_3P_2 (s=1/4) as viewed along the short axis.

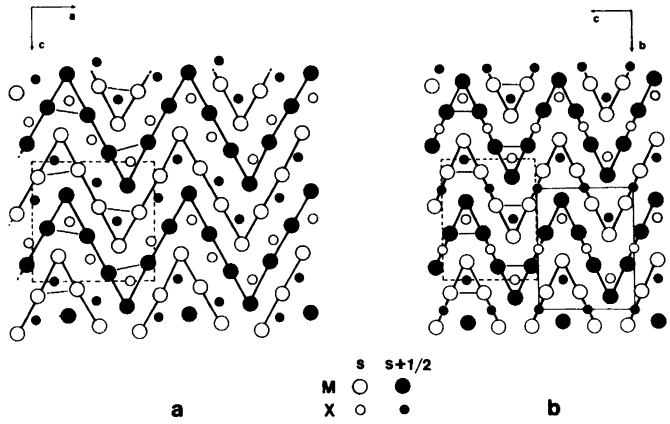

Fig. 4. Comparison of the structure of (a) Hf_3P_2 (s=1/4) with (b) V_3AsC (s=0; filled Re_3B type) projected along the short axis.

similarity of the environment of M(4) in Ti_7P_4 with that of copper in TiCuSi and $Nb_5Cu_4Si_4$. A star-like building block, consisting of a body-centred cubic metal unit with four triangular prisms linked to it, is also discernible in the structures of $Nb_5Cu_4Si_4$ and Ti_7P_4. The sequence of star-like blocks in the $[\bar{1}10]$ direction of $Nb_5Cu_4Si_4$ is identical to that of the blocks in the *a* direction of Ti_7P_4, as shown in Figs. 1a and 1b.

Examination of the manner of packing of the triangular prisms and/or body-centred metal units in the less metal-rich arsenides and phosphides V_3As_2,[16] Nb_4As_3,[17] Cr_4As_3,[18] Nb_8P_5,[19] $Ti_{11}CuP_8$ and Hf_3P_2[20] reveals resemblances with that in Ti_7P_4. This is demonstrated in Figs. 2 and 3, where the structures are shown in projection along the short axis. To make the similarities evident the structure of Ti_7P_4 has been partitioned into slabs and described in two additional ways: as a sequence of slabs packed in the *a* direction (Fig. 2a, slabs type A) or *c* direction (Fig. 3a, slabs type C). A slab of type A is related to one of type A′ by a center of symmetry and a slab of type C is related to one of type C′ by an operation of a pseudo-reflection glide plane. When slabs of type A are allowed to share metal atoms the structure of V_3As_2 is obtained as illustrated in Fig. 2c, where a slab of type A is related to one of type A″ by a slip of $a/\sqrt{2}$ in the $[1\bar{1}0]$ direction. By stacking extra layers of atoms (type c) between the C slabs the structures of Nb_4As_3 (Fig. 3b, C and C″ slabs) and Cr_4As_3 (Fig. 3c, only C slabs) are obtained. A slab of type C is related to one of type C″ by a reflection operation.

Using the notations given, the four structures can be described by the stacking sequence of slabs, or slabs and atom layers:

V_3As_2	A″AA″A...	
Ti_7P_4	A′AA′A...	or C′CC′C...
Nb_4As_3	C″cCcC″cCc...	
Cr_4As_3	CcCcCcCc...	

The structures of $Ti_{11}CuP_8$ (Fig. 2d) and Nb_8P_5 (Fig. 2b) can be described as different arrangements of a rectangular block (fragment of the slab of type A) centred at sites of high point symmetry. In Nb_8P_5 the parallel blocks are tied together by segments of atoms to form thicker slabs, which are stacked in the *a* direction, and adjacent slabs are related by a glide reflection operation. Fragments of the C slabs can be used to describe the structure of Hf_3P_2 as illustrated in Fig. 3d, where the fragments are connected in another manner to form a new type of slabs stacked in the *c* direction. Adjacent slabs are also related by a glide reflection operation. It should be observed as well that the structure of Hf_3P_2 is related to that of V_3AsC[21] (filled Re_3B type[22]). A comparison of Fig. 4a with Fig. 4b shows that the Hf_3P_2 structure can be regarded as a distortion of the filled Re_3B type.

The relationships between Hf_3P_2, $Ti_{11}CuP_8$ and Nb_8P_5, between V_3As_2, $Ti_{11}CuP_8$ and $(Ti,Cu)_{14}P_9$[23] ($Zr_{14}P_9$ type[24]), and between β-V_4As_3 (Cr_4As_3 type) and α-V_4As_3 (Nb_4As_3 type) have also been discussed in Refs. 6, 23 and 25, respectively, using other descriptions of the structures.

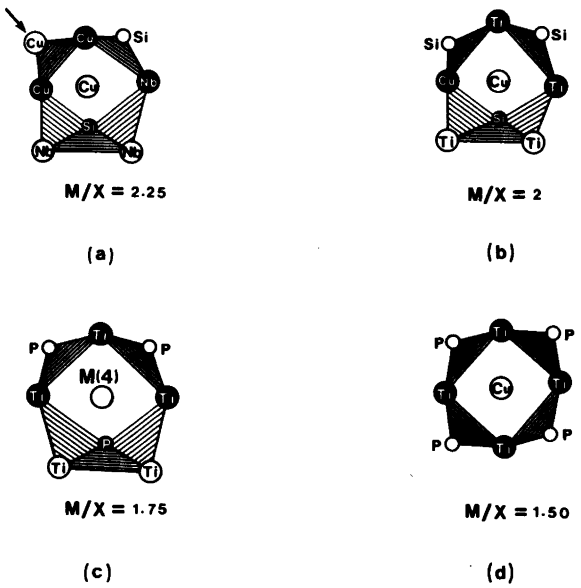

Fig. 5. Projections, as in Fig. 1, of the copper environment in the structures of (a) $Nb_5Cu_4Si_4$, (b) TiCuSi, (c) $Ti_{7-x}Cu_xP_4$ (M(4)=0.77 Ti+0.23 Cu) and (d) $Ti_{11}CuP_8$.

The changes of the atomic arrangement around the copper atom in some transition-metal silicides and phosphides, when the M/X ratio decreases from 2.25 ($Nb_5Cu_4Si_4$) to 1.50 ($Ti_{11}CuP_8$) are illustrated in Fig. 5 in projection along the short axis. The copper atom in these compounds has twelve nearest neighbours (only distances shorter than the length of the short axis are considered). Eight of these are situated at the corners of a quadrangular prism (*corner* atoms) with four further atoms outside the rectangular faces of the prism (*face* atoms). In $Nb_5Cu_4Si_4$ (Fig. 5a) each copper atom is surrounded by three silicon, four niobium and five copper atoms. The arrangement of atoms around copper in TiCuSi is shown in Fig. 5b. The main difference in nearest neighbour environment of copper in $Nb_5Cu_4Si_4$ and TiCuSi is the replacement of a *face* metal atom (indicated by an arrow in Fig. 5a) by a non-metal atom. Half of the *face* atoms and two of the *corner* atoms in TiCuSi are thus non-metals. The coordination of M(4) in Ti_7P_4 (Fig. 5c) and that of copper in TiCuSi are very similar to that of copper in $Zr_3Cu_4Si_4$[14] ($Gd_6Cu_8Ge_8$ type[26]). The difference in environment of copper in these phases is the number of small metal neighbours, being three in $Zr_3Cu_4Si_4$, two in TiCuSi and none in Ti_7P_4. In the metal poorer phase $Ti_{11}CuP_8$ the coordination polyhedron of the copper atom (Fig. 5d) is more regular than that of M(4) in Ti_7P_4. All *corner* atoms are metals and all *face* atoms are non-metals. The difference between the environment of M(4) in Ti_7P_4 and that of copper in $Ti_{11}CuP_8$ can be regarded as an interchange between a *face* metal atom and a *corner* non-metal atom. The slightly distorted capped cubic environment also occurs in Ti_7P_4 around M(1) and M(2) (Fig. 1b), but dissolved copper atoms prefer the M(4) site. However, in the $(Ti,Cu)_{14}P_9$ phase,[23] with a M/X ratio of 1.56, the copper atoms populate a similar site to that of the copper atoms in $Ti_{11}CuP_8$.

The isotropic temperature factors of the atoms in Ti_7P_4 (Table 1) and the Ti–P distances (Table 2) show no great differences from those found in α-Ti_5P_3[7] and $Ti_{11}CuP_8$.[6] A closer look at Table 2 reveals that all the seven P(4)–Ti distances are shorter than the sum of the tetrahedral covalent radius for phosphorus (1.10 Å) and the Goldschmidt metal radius (CN 12). The average distance between the M(4) atom with $r_{M(4)}=0.77r_{Ti}+0.23r_{Cu}$ and its four phosphorus neighbours is 2.490 Å, which is slightly shorter than the radius sum of 2.51 Å (weighted radius for the M(4) atoms used), while the average of the M(4)–Ti distances (2.911 Å) is slightly larger than the radius sum (2.86 Å).

The Ti–Ti interatomic distances are somewhat shorter than the corresponding Nb–Nb distances in Nb_7P_4 owing to the greater size of the niobium atom as compared to titanium.

In the present study the copper content of the crystal investigated was found to be 2.1(1) atom-% (the composition of the crystal is thus $Ti_{6.77}Cu_{0.23}P_4$). There are apparent discrepancies in the cell parameters between the present ternary specimen (single-crystal data, Table 1; copper alloy with nominal Ti/P=2) and that in Ref. 4 (powder data, copper alloy with nominal Ti/P=3) with the same reported copper content. There might be significant differences in copper composition, however, since the ternary specimens had not been in complete equilibrium. Furthermore, the composition of the titanium-richer specimen (Ref. 4) was determined using an electron microprobe and the accuracy of the analysis was relatively low. The unit cell volumes of the above-mentioned ternary specimens are smaller than that reported[4] for binary Ti_7P_4, which was measured on a titanium-rich sample. From the present data it is not possible, however, to establish unambiguously the range of homogeneity of Ti_7P_4 in the Ti–P and Ti–Cu–P systems.

Acknowledgements. The author thanks Doc. Torsten Lundström for his valuable advice and is also indebted to Prof. Stig Rundqvist for his interest in this work. The financial support granted by the Swedish Institute is gratefully acknowledged. This work has been supported by the Swedish Natural Science Research Council.

REFERENCES

1. Rundqvist, S., Carlsson, B. and Pontchour, C.-O. *Acta Chem. Scand. 23* (1969) 2188.
2. Rundqvist, S. *Acta Chem. Scand. 20* (1966) 2427.
3. Björkegren, J. and Andersson, Y. Institute of Chemistry, University of Uppsala, Uppsala 1976, UUIC-B18-53.
4. Carrillo-Cabrera, W. and Lundström, T. *Acta Chem. Scand. A 33* (1979) 401.
5. Rundqvist, S. and Carlsson, B. *Acta Chem. Scand. 22* (1968) 2395.
6. Carrillo-Cabrera, W. and Lundström, T. *Acta Chem. Scand. A 35* (1981) 545.
7. Carrillo-Cabrera, W. and Lundström, T. *Acta Chem. Scand. A 34* (1980) 415.
8. *International Tables for X-Ray Crystallography*, Kynoch Press, Birmingham 1974, Vol. 4.
9. Lundgren, J.-O., Ed., *Crystallographic Computer Programs*, Institute of Chemistry, University of Uppsala, Uppsala 1975, UUIC-B13-04-02.
10. Hamilton, W. C. *Acta Crystallogr. 18* (1965) 502.
11. Abrahams, S. C. and Keve, K. T. *Acta Crystallogr. A 27* (1971) 157.
12. Abrahams, S. C. *Acta Crystallogr. A 25* (1969) 165.
13. Ganglberger, E. *Monatsh. Chem. 99* (1968) 549.
14. Sprenger, H. *J. Less Common Met. 34* (1974) 39.
15. Shoemaker, C. B. and Shoemaker, D. P. *Acta Crystallogr. 18* (1965) 900.
16. Berger, R. *Acta Chem. Scand. A 31* (1977) 287.
17. Carlsson, B. and Rundqvist, S. *Acta Chem. Scand. 25* (1971) 1742.
18. Baurecht, H.-E., Boller, H. and Nowotny, H. *Monatsh. Chem. 101* (1970) 1696.
19. Anugul, S., Pontchour, C.-O. and Rundqvist, *Acta Chem. Scand. 27* (1973) 26.
20. Lundström, T. *Acta Chem. Scand. 22* (1968) 2191.
21. Boller, H. and Nowotny, H. *Monatsh. Chem. 98* (1967) 2127.
22. Boller, H. and Nowotny, H. *Monatsh. Chem. 99* (1968) 721.
23. Carrillo-Cabrera, W. *Acta Chem. Scand. A 36* (1982) 571.
24. Tergenius, L.-E., Noläng, B. I. and Lundström, T. *Acta Chem. Scand. A 35* (1981) 693.
25. Berger, R. *Acta Chem. Scand. A 28* (1974) 771.
26. Rieger, W. *Monatsh. Chem. 101* (1970) 449.

Received September 10, 1981.

Acta Chemica Scandinavica A 36 (1982) 571–578

$Ti_{14-x}Cu_xP_9$ ($x = 0.14$) – Crystal Structure Refinement, and Structural Relationship with $Ti_{11}CuP_8$ and V_3As_2

WILDER CARRILLO-CABRERA

Institute of Chemistry, University of Uppsala, Box 531, S-751 21 Uppsala, Sweden

The crystal structure of $Ti_{14-x}Cu_xP_9$ with $x=0.14$ has been refined using X-ray single-crystal methods. The symmetry is orthorhombic (space group *Pnnm*). The cell dimensions of the crystal investigated were: $a=15.509(4)$ Å, $b=25.564(5)$ Å, $c=3.4718(5)$ Å. The compound is isostructural with $Zr_{14}P_9$. relationship among the V_3As_2, $Ti_{11}CuP_8$ and $Ti_{14-x}Cu_xP_9$ structures is emphasized. A significant quantity of copper was found at the M(14) site. The capped cubic environment around M(14) is identical to that around the copper atom in $Ti_{11}CuP_8$.

Phase-analytical work on the Ti-Cu-P system[1] has revealed the occurrence of an orthothombic phase with the formula $M_{14}P_9$ isostructural with $Zr_{14}P_9$.[2] Using electron micro-probe analysis the phase was found to contain small amounts of copper in solution. The purpose of this paper is to report the results of a single-crystal structure investigation of $Ti_{14-x}Cu_xP_9$ with $x=0.14$.

EXPERIMENTAL

Preparation. Needle-shaped crystals of $Ti_{14-x}Cu_xP_9$ were formed on cooling a copper-rich ternary melt.[1,3] The crystal used for the X-ray intensity measurement was picked from an inhomogeneous ternary sample (crystal A-1, sample A; Table 1). Crystals used for the refinements of the Ti_7P_4 and α-Ti_5P_3 structures[3,4] were also selected from sample A.

Single-crystal diffractometry. The equipment and data collection procedure have been described previously.[3] Up to $2\theta=63.4°$ one octant of the reciprocal lattice (h,k,l, positive) was measured. For $63.4° < 2\theta < 68.0°$ reflections with $0 \leqslant h \leqslant 24$, $0 \leqslant k \leqslant 40$ and $0 \leqslant l \leqslant 2$ were measured. 34 further reflections (higher l-order reflections to some $h\ k\ 0$ and $h\ k\ 1$ strong reflections) with $5 \leqslant l \leqslant 8$ were also measured to improve the values of the temperature factors of the atoms. Instrumental stability and crystal setting were checked by remeasuring four test reflections at regular intervals. In total 2874 reflections were recorded, 37 % of these had $F_o^2 > 3\ \sigma(F_o^2)$. The crystal structure analysis was based on 1952 positive reflections. The cell dimensions of the crystal investigated were determined by least-squares refinement of the average of the setting angles, $\bar{\theta}_i$, of 33 Friedel pairs of reflections with $14° < 2\bar{\theta}_i < 50°$. Graphite-monochromatized Mo$K\alpha$ radiation ($\lambda=0.71069$ Å) was employed for this measurement and for the intensity data collection.

The calculations were performed on IBM 1800 and NORD 100 computers. The intensity data were corrected for Lp and absorption (Gaussian grid technique) effects. The crystal had the approximate dimensions $13 \times 14 \times 254$ μm. The transmission varied between 0.829 and 0.913. The linear absorption coefficient (89.7 cm^{-1}) was calculated using the mass absorption coefficients given in Ref. 5, assuming 0.6 atomic percent copper in the crystal. The crystallographic programs used are described in Ref. 6.

CELL DIMENSION DETERMINATION

The cell dimensions of the $Ti_{14-x}Cu_xP_9$ phase in two ternary samples are given in Table 1. X-Ray single-crystal diffraction (as described above for crystal A-1) was used to determine the cell dimensions of crystal B-1. Sample A is deficient in phosphorus and sample B contains an excess of phosphorus. The samples were, however, inhomogeneous and thus the data of the powder (obtained by crushing agregates of crystals) and single crystal specimens

0302-4377/82/070571-08$02.50

Table 1. Unit cell dimensions for $Ti_{14-x}Cu_xP_9$ in Ti – Cu – P alloys as measured on single crystal and powder specimens. Standard deviations in parentheses. Sample B: high-frequency melted. Sample A: high-frequency melted and annealed at 800 °C for 12d.

Sample (nominal Ti/P)	Specimen	Copper content (at %)	Unit cell data				Ref.
			a(Å)	b(Å)	c(Å)	U(Å^3)	
B(Ti/P = 1.50)	Crystal B-1	0.76(11)	15.515(2)	25.568(4)	3.4816(3)	1381.1(3)	This work
A(Ti/P = 2.00)	Crystal A-1	0.60(6)	15.509(4)	25.564(5)	3.4718(5)	1376.5(5)	This work
	Powder A-2	n.d.[a]	15.529(1)	25.602(2)	3.4796(2)	1383.4(2)	1

[a] The result given in Ref. 1 was measured on a crystal that did not belong to A-2.

in Table 1 are representative for parts of the samples only. Table 1 shows that $Ti_{14-x}Cu_xP_9$ has a range of homogeneity.

STRUCTURE REFINEMENT

Preliminary Weissenberg photographs obtained from rotation of crystals around the c axis showed systematic absences for (h 0 l) and (0 k l) reflections corresponding to the space group *Pnnm* or *Pnn*2. The centrosymmetric *Pnnm* (No. 58) was initially adopted as the space group and confirmed in the refinement.

The structure was refined on F^2 using a full-matrix least-squares program[6] and the atomic coordinates of $Zr_{14}P_9$.[2] The atomic scattering factors, including anomalous dispersion corrections, were taken from Ref. 5. Extinction effects were hardly discernible and thus no correction was applied.

The first refinement converged satisfactorily, but it was noted that the isotropic temperature factor for M(14), which has a low coordination number, was significantly lower than those for the other positions. This indicated a partial occupancy by copper in that position. The Cu/Ti substitution in the M(14) site was then examined. The least-squares refinement yielded a reasonable isotropic temperature factor for M(14) and gave an occupancy of 73(3) % for titanium and 27(3) % for copper (reset). The weighted R_w-value dropped from 0.1004 [$R(F^2)$ = 0.1388] to 0.0978 [$R(F^2)$ = 0.1374]. A significance test[7] favoured the last model at the 99.5 % confidence level. Refinement under the assumption of substitution of copper for titanium in the other low coordinated site, 2(a), did not reveal any significant substitution. At this stage of the refinement the possibility of vacancies in the phosphorus sites with low coordination number, P(1) – P(4), was tested. Only the occupancy of P(3) was found to decrease and was refined to 95.3 % (σ = 1.5 %). The isotropic temperature factor of P(3) decreased from 0.46 to 0.27 Å^2. The agreement factors obtained in the final refinement were (1952 reflections): $R_w(F^2)$ = 0.0976, $R(F^2)$ = 0.1372, and the standard deviation of an observation of unit weight,[8] S, was 1.17. The agreement indices in the text are defined in Ref. 3. The function minimized in the refinements was $\sum w(|F_o^2| - |F_c^2|)^2$. The individual weight of a reflection, w, is defined as: $w^{-1} = [\sigma_c(F_o^2)]^2 + (p.|F_o^2|)^2$, where σ_c is the standard deviation of F_o^2, based on counting statistics, and p modifies the weight to obtain a satisfactory weight analysis (p = 0.020 in all the refinements).

The structure data from the final refinement are presented in Table 2 and the interatomic distances in Table 3. The following parameters were varied: one scale factor, 44 positional parameters, 24 isotropic temperature factors and two occupancy factors. The shifts in the final cycle were less than 0.002σ. No significant features could be found in a difference synthesis based on the final parameters. There were no positive or negative peaks exceeding 4 % of a phosphorus maximum in the corresponding F_o synthesis. The final fit between F_o^2 and F_c^2 was further examined by the ΔR normal probability plot.[9] The plot was essentially linear with slope 0.95 and intercept −0.15 on the expected ΔR axis (four values fell outside the range $\pm 4\sigma$), indicating that the ΔR are random-normally distributed.

The R values for a refinement omitting reflections with $F_o^2 < 3\sigma(F_o^2)$ were (1070 reflections): $R_w(F^2)$ = 0.0856, $R(F^2)$ = 0.0927. The standard deviations were, however, on the average 24 % larger than those for the refinement using the more complete material.

Table 2. Final structural data for $Ti_{13.86}Cu_{0.14}P_{8.95}$ from refinement based on F^2. Space group *Pnnm* (No. 58), $a = 15.509(4)$ Å, $b = 25.564(5)$ Å, $c = 3.4718(5)$ Å; $U = 1376.5(5)$ Å^3; $Z = 4$. Standard deviations are given in parentheses.

Atom	Position	Positional parameters			B (Å^2)
		x	y	z	
Ti(1)	4g	0.05053(15)	0.57814(10)	0	0.35(4)
Ti(2)	4g	0.09966(16)	0.10455(10)	0	0.33(4)
Ti(3)	4g	0.11744(16)	0.75592(10)	0	0.39(4)
Ti(4)	4g	0.13333(16)	0.46936(9)	0	0.34(4)
Ti(5)	4g	0.13822(16)	0.35314(10)	0	0.36(4)
Ti(6)	4g	0.19941(16)	0.99089(9)	0	0.34(4)
Ti(7)	4g	0.20206(16)	0.85716(10)	0	0.44(4)
Ti(8)	4g	0.24642(15)	0.58313(9)	0	0.29(4)
Ti(9)	4g	0.26794(16)	0.18783(9)	0	0.36(4)
Ti(10)	4g	0.33300(15)	0.76277(10)	0	0.30(4)
Ti(11)	4g	0.43146(15)	0.42575(10)	0	0.40(4)
Ti(12)	4g	0.48069(16)	0.17682(9)	0	0.29(4)
Ti(13)	4g	0.48780(16)	0.69692(10)	0	0.36(4)
M(14)[a]	2d	0	1/2	1/2	0.42(7)
Ti(15)	2a	0	0	0	0.38(6)
P(1)	4g	0.13255(24)	0.65708(14)	0	0.37(6)
P(2)	4g	0.34140(23)	0.66558(13)	0	0.26(6)
P(3)[b]	4g	0.04808(23)	0.85831(14)	0	0.27(9)
P(4)	4g	0.26699(22)	0.42227(14)	0	0.38(6)
P(5)	4g	0.27447(24)	0.28585(14)	0	0.32(6)
P(6)	4g	0.04757(23)	0.26705(14)	0	0.38(6)
P(7)	4g	0.43674(23)	0.90775(13)	0	0.33(6)
P(8)	4g	0.34393(23)	0.03780(13)	0	0.27(5)
P(9)	4g	0.39708(24)	0.53245(14)	0	0.36(6)

[a] M(14) = 0.73(3)Ti + 0.27(3) Cu. [b] Occupancy 0.963(15).

A list of observed and calculated structure factors can be obtained on request from the Institute of Chemistry, University of Uppsala, Uppsala, Sweden.

In a preliminary X-ray single-crystal study of $Ti_{14-x}Cu_xP_9$ a very small crystal (crystal B-1, approx. $8 \times 6 \times 188$ μm, sample B, Table 1) was investigated. Of the 2299 independent reflections measured for $2\theta < 60°$, only 25% had $F_o^2 > 3\sigma(F_o^2)$. This affected the refinement resulting in relatively high final R values and estimated standard deviations of the parameters. The final agreement factors for the refinement on F^2 were (1718 positive reflections): $R_w(F^2) = 0.132$, $R(F^2) = 0.221$ and $S = 0.97$. The refinement yielded an occupancy of 65(5) %

Table 3. Interatomic distances and standard deviations for $Ti_{13.86}Cu_{0.14}P_{8.95}$ (Å units). The distances listed are less than 3.48 Å. M(14) = 0.73 Ti + 0.27Cu.

Ti(1) – P(1)	2.385(4)	Ti(2) – P(3)	2.480(4)
– 2P(7)	2.502(3)	– 2P(2)	2.507(3)
– 2P(8)	2.599(3)	– 2P(9)	2.533(3)
– 2M(14)	2.760(2)	– 2Ti(8)	3.002(3)
– Ti(8)	3.041(3)	– Ti(15)	3.087(2)
– Ti(4)	3.063(3)	– 2Ti(11)	3.228(3)
– Ti(4)	3.099(3)	– 2Ti(13)	3.229(3)
– 2Ti(12)	3.100(3)	– Ti(6)	3.292(3)
– Ti(5)	3.414(3)	– Ti(9)	3.368(3)
– 2Ti(1)	3.472(0)	– 2Ti(2)	3.472(0)

Table 3. Continued.

Ti(3) – 2P(5)	2.532(3)
– P(1)	2.538(4)
– P(6)	2.626(4)
– P(3)	2.830(4)
– Ti(7)	2.902(4)
– 2Ti(13)	2.917(3)
– 2Ti(9)	3.034(3)
– 2Ti(12)	3.069(3)
– Ti(10)	3.348(3)
– 2Ti(3)	3.472(0)
Ti(4) – P(4)	2.397(4)
– 2P(8)	2.490(3)
– 2P(7)	2.584(3)
– 2M(14)	2.811(2)
– Ti(5)	2.972(4)
– Ti(1)	3.063(3)
– Ti(1)	3.099(3)
– 2Ti(6)	3.170(3)
– Ti(8)	3.396(3)
– 2Ti(4)	3.472(0)
Ti(5) – 2P(7)	2.513(3)
– P(6)	2.611(4)
– P(4)	2.667(4)
– P(5)	2.725(4)
– 2Ti(10)	2.924(3)
– Ti(4)	2.972(4)
– 2Ti(7)	3.027(3)
– 2Ti(12)	3.093(3)
– Ti(1)	3.413(3)
– 2Ti(5)	3.472(0)
Ti(6) – 2P(4)	2.522(3)
– 2P(9)	2.526(3)
– P(8)	2.542(4)
– 2Ti(8)	3.046(3)
– Ti(15)	3.101(3)
– 2Ti(11)	3.147(3)
– 2Ti(4)	3.170(3)
– Ti(2)	3.292(3)
– Ti(7)	3.419(4)
– 2Ti(6)	3.472(0)
Ti(7) – P(3)	2.388(4)
– 2P(4)	2.452(3)
– 2P(5)	2.543(3)
– Ti(3)	2.902(4)
– 2Ti(5)	3.027(3)
– Ti(10)	3.154(3)
– 2Ti(11)	3.221(3)
– Ti(6)	3.419(4)
– 2Ti(7)	3.472(0)
Ti(8) – 2P(8)	2.514(3)
– P(2)	2.571(4)
– P(1)	2.587(4)
– P(9)	2.672(4)
– 2Ti(2)	3.002(3)
– Ti(1)	3.041(3)
– 2Ti(6)	3.041(3)
– 2Ti(9)	3.198(3)
– Ti(4)	3.396(3)
– 2Ti(8)	3.472(0)
Ti(9) – 2P(1)	2.452(3)
– 2P(2)	2.492(3)
– P(5)	2.508(4)
– 2Ti(10)	3.022(3)
– 2Ti(3)	3.034(3)
– 2Ti(8)	3.198(3)
– Ti(12)	3.312(4)
– Ti(2)	3.368(3)
– 2Ti(9)	3.472(0)
Ti(10) – 2P(5)	2.478(3)
– P(2)	2.488(4)
– 2P(6)	2.541(3)
– 2Ti(5)	2.924(3)
– Ti(13)	2.932(3)
– 2Ti(9)	3.022(3)
– Ti(7)	3.154(3)
– Ti(12)	3.276(3)
– Ti(3)	3.348(3)
– 2Ti(10)	3.472(0)
Ti(11) – 2P(3)	2.467(3)
– P(4)	2.552(4)
– P(9)	2.779(4)
– 2Ti(15)	2.783(2)
– P(9)	2.866(4)
– 2Ti(6)	3.147(3)
– 2Ti(7)	3.221(3)
– 2Ti(2)	3.228(3)
– Ti(13)	3.377(4)
– 2Ti(11)	3.472(0)
Ti(12) – 2P(6)	2.480(3)
– P(7)	2.513(4)
– 2P(1)	2.520(3)
– 2Ti(3)	3.069(3)
– 2Ti(5)	3.093(3)
– 2Ti(1)	3.100(3)
– Ti(13)	3.265(3)
– Ti(10)	3.276(3)
– Ti(9)	3.312(4)
– 2Ti(12)	3.472(0)

Table 3. Continued.

Ti(13) – P(2)	2.408(4)	P(4) – Ti(4)	2.397(4)
– 2P(3)	2.425(4)	– 2Ti(7)	2.452(3)
– 2P(6)	2.555(3)	– 2Ti(6)	2.522(3)
– 2Ti(3)	2.917(3)	– Ti(11)	2.552(4)
– Ti(10)	2.932(3)	– Ti(5)	2.667(4)
– 2Ti(2)	3.229(3)	– P(9)	3.465(5)
– Ti(12)	3.265(3)	– 2P(4)	3.472(0)
– Ti(11)	3.377(4)		
– 2Ti(13)	3.472(0)		
M(14) – 2P(7)	2.554(3)	P(5) – 2Ti(10)	2.478(3)
– 2P(8)	2.606(4)	– Ti(9)	2.508(4)
– 4Ti(1)	2.760(2)	– 2Ti(3)	2.532(3)
– 4Ti(4)	2.811(2)	– 2Ti(7)	2.543(3)
– 2M(14)	3.472(0)	– Ti(5)	2.725(4)
		– 2P(5)	3.472(0)
Ti(15) – 4P(9)	2.500(3)	P(6) – 2Ti(12)	2.480(3)
– 4Ti(11)	2.783(2)	– 2Ti(10)	2.541(3)
– 2Ti(2)	3.087(2)	– 2Ti(13)	2.555(3)
– 2Ti(6)	3.101(3)	– Ti(5)	2.611(4)
– 2Ti(15)	3.472(0)	– Ti(3)	2.626(4)
		– P(1)	3.401(5)
		– 2P(6)	3.472(0)
P(1) – Ti(1)	2.385(4)		
– 2Ti(9)	2.452(3)	P(7) – 2Ti(1)	2.502(3)
– 2Ti(12)	2.520(3)	– 2Ti(5)	2.513(3)
– Ti(3)	2.538(4)	– Ti(12)	2.513(4)
– Ti(8)	2.587(4)	– M(14)	2.554(3)
– P(2)	3.246(5)	– 2Ti(4)	2.584(3)
– P(6)	3.401(5)	– 2P(7)	3.472(0)
– 2P(1)	3.472(0)		
		P(8) – 2Ti(4)	2.490(3)
P(2) – Ti(3)	2.408(4)	– Ti(6)	2.513(3)
– Ti(10)	2.488(4)	– Ti(6)	2.542(4)
– 2Ti(9)	2.492(3)	– 2Ti(1)	2.599(3)
– 2Ti(2)	2.507(3)	– M(14)	2.606(4)
– Ti(8)	2.571(4)	– 2P(8)	3.472(0)
– P(1)	3.246(5)		
– 2P(2)	3.472(0)	P(9) – 2Ti(15)	2.500(3)
		– 2Ti(6)	2.526(3)
P(3) – Ti(7)	2.388(4)	– 2Ti(2)	2.533(3)
– 2Ti(13)	2.425(3)	– Ti(8)	2.672(4)
– 2Ti(11)	2.467(3)	– Ti(11)	2.779(4)
– Ti(2)	2.480(4)	– Ti(11)	2.866(4)
– Ti(3)	2.830(4)	– P(4)	3.46 (5)
– 2P(3)	3.472(0)	– P(9)	3.472(0)

for titanium and 35(5) % for copper in the M(14) site. No indication of any appreciable deviation from the ideal $M_{14}P_9$ formula was obtained from the refinement of the structure of this crystal (B-1) selected from a phosphorus-rich sample. The standard deviations of the parameters on the average were two times larger than those for the crystal A-1, in Table 2. Only one positional parameter differed by 4σ. For the other parameters the difference was less than 2σ (σ is the standard deviation of the

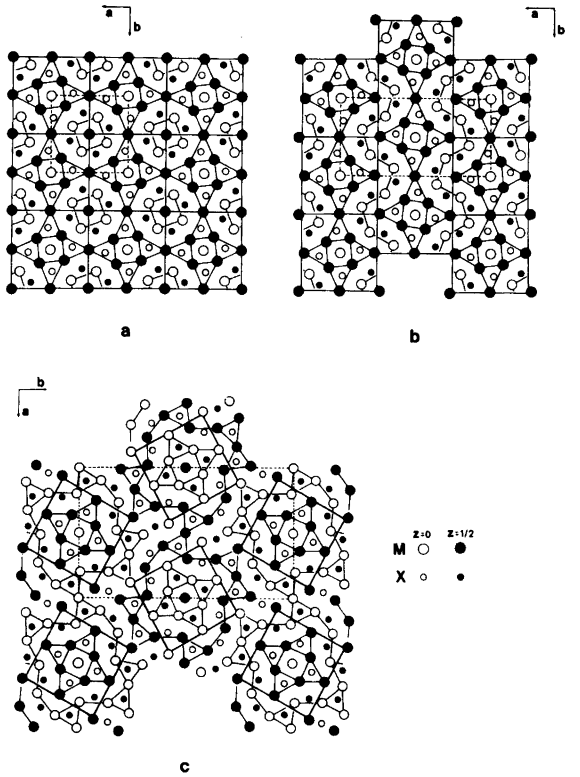

Fig. 1. Relationship between the structure of (a) V_3As_2, (b) $Ti_{11}CuP_8$ and (c)$Ti_{14-x}Cu_xP_9$ ($Zr_{14}P_9$ type) as viewed along the *c* axis.

differences between the parameters for crystal B-1 and the corresponding ones for crystal A-1, in Table 2). Comparison of the interatomic distances gave similar differences, being no greater than 3σ.

DISCUSSION

The present single-crystal refinement confirms that $Ti_{14-x}Cu_xP_9$ is isostructural with $Zr_{14}P_9$.[2] The general structural features of the type have been described in Ref. 2. However, some additional comments, based on structural comparisons, are given here.

A projection of the structure along the *c* axis is shown in Fig. 1c. Examination of the structure reveals resemblances with those of V_3As_2,[10] $Ti_{11}CuP_8$[11] and Nb_5P_3,[12] regarding the manner of packing of the triangular prisms of metals (which surround the non-metal atoms) and the metal body-centred unit as demonstrated in Figs. 1 and 2. In both figures only the triangular prisms around the non-metals atoms, which have high coordination numbers (8 or 9), are indicated. Common structural fragments are also indicated to emphasize relationship and differences between the structures.

The V_3As_2 and $Ti_{11}CuP_8$ structure types are geometrically closely related. Both types can formally be described on the basis of different arrangements of a common sub-unit, which is also discernible in the more complex structure of $Ti_{14-x}Cu_xP_9$, as illustrated in Fig. 1. The sub-unit consists of one unit cell of the tetragonal V_3As_2. The $Ti_{11}CuP_8$ structure can thus be derived from the V_3As_2 type through a glide reflection operation.

The $Ti_{14-x}Cu_xP_9$ structure (Fig. 2c) retains large fragments from $Ti_{11}CuP_8$ (Fig. 2a, block A) and Nb_5P_3 (Fig. 2b, block B), the latter represented by β-$(Ti,Cu)_5P_3$ in the Ti-Cu-P system.[1] The coordination polyhedra for the corresponding atoms within the common blocks (A or B) are thus similar.

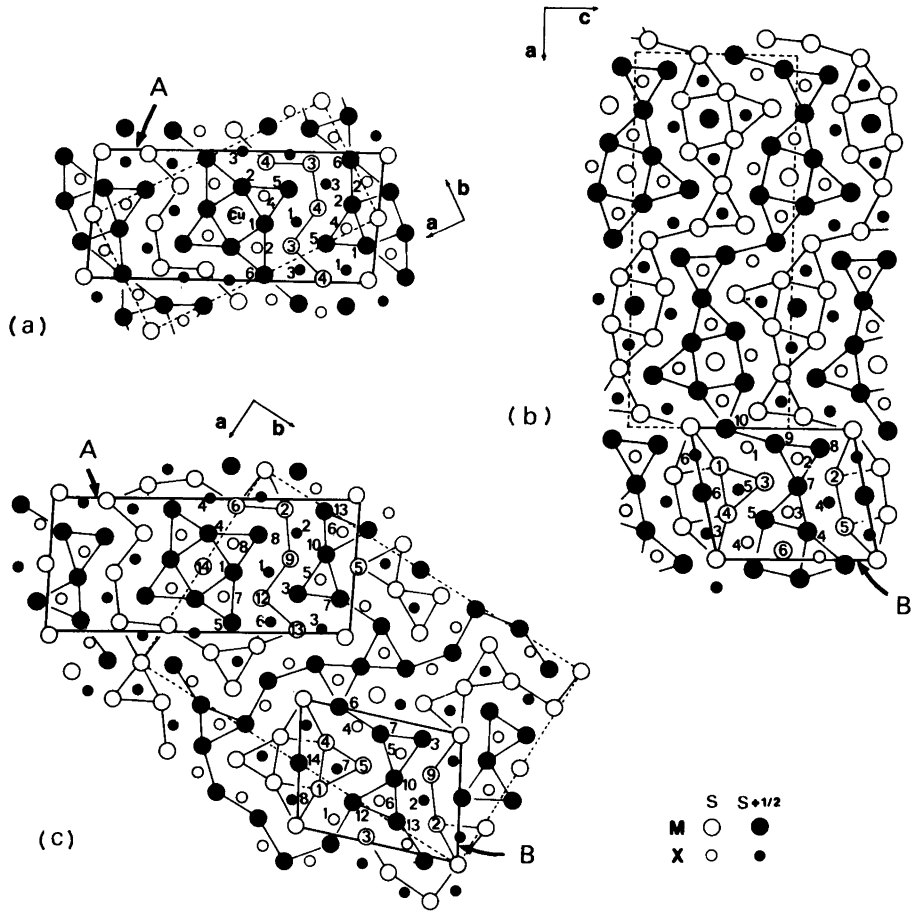

Fig. 2. Comparison among the structures of (a) $Ti_{11}CuP_8$ ($s=0$), (b) Nb_5P_3 ($s=1/4$) and (c) $Ti_{14-x}Cu_xP_9$ ($s=0$) as viewed along the short axis.

However, the environments of Ti(3) and Ti(6) in $Ti_{11}CuP_8$ and those of Nb(8) and Nb(9) in Nb_5P_3 have no counterpart in the structure of $Ti_{14-x}Cu_xP_9$.

The close similarity between $Ti_{11}CuP_8$ and $Ti_{14-x}Cu_xP_9$, which have slightly different compositions, is further substantiated by the fact that the copper atoms in both structures are accommodated in nearly identical crystallographic sites (Cu and M(14) in Figs. 2a and 2c, respectively). The coordination polyhedron around M(14) in $Ti_{14-x}Cu_xP_9$, as well as that around copper in $Ti_{11}CuP_8$, is a distorted capped cube which is situated at the center of the tetragonal sub-unit common to both structures (Figs. 1b and 1c).

Recently[3] it has been found that 23 % of the titanium in the M(4) site of Ti_7P_4 can be replaced by copper. The arrangement of atoms (metals and non-metals) around M(4) in Ti_7P_4 is different from that around M(14) in $Ti_{14-x}Cu_xP_9$, but consists in both cases of eight titanium and four phosphorus atoms. The main difference between the atomic environments of copper in Ti_7P_4, $Ti_{11}CuP_8$ and other compounds in similar systems has been discussed in Ref. 3. Contrary to what is observed in Ti_7P_4 for M(4), in $Ti_{14-x}Cu_xP_9$ the average distance between the M(14) atom and its eight titanium neighbours (2.79 Å) is shorter than the radius sum of 2.85 Å (Goldschmidt CN 12 metal radii and weighted radius $r_{M(14)}=0.73r_{Ti}+0.27r_{Cu}$ used) and the average of the M(14)–P distances (2.58 Å) is larger than the corresponding radius sum of 2.50 Å (tetrahedral covalent radius for

phosphorus used).

The isotropic temperature factors of the atoms in $Ti_{14-x}Cu_xP_9$ (Table 2) are similar to those found in $Ti_{11}CuP_8$, Ti_7P_4 and α-Ti_5P_3.[4] The interatomic distances in $Ti_{14-x}Cu_xP_9$ (Table 3) show a conspicuous feature which has also been observed for the structure of $Ti_{11}CuP_8$: most of the Ti–P distances (75 %) are shorter than the corresponding radius sum of 2.55 Å, whereas the Ti–Ti distances (with the exception of the two Ti(11)–Ti(15) distances of 2.78 Å) are longer than the radius sum of 2.90 Å. In the isostructural $Zr_{14}P_9$, however, about 42 % of the Zr–P distances are longer than the corresponding radius sum of 2.70 Å and twelve Zr–Zr distances are shorter than the radius sum of 3.20 Å.

The number of metal neighbours around the phosphorus atoms in $Ti_{14-x}Cu_xP_9$, as well as in $Zr_{14}P_9$, are seven for P(1)–P(4), eight for P(5)–P(8) and nine for P(9). Nevertheless, a closer examination of the interatomic distances in Table 3 reveals that the trigonal prism around P(3) is very distorted: the distance to one metal atom [Ti(3)] at a corner of this prism is very long (2.83 Å), but the other Ti–P(3) distances are shorter than the radius sum 2.55 Å. The coordination number of P(3) is thus 6(+1) rather than 7. This is also valid for P(3) in $Zr_{14}P_9$.

In the present study the copper content of the two crystals investigated were found to be practically the same (0.60(6) atom-% for A-1 and 0.76(11) atom-% for B-1). The cell volume of the crystal A-1 was, however, significantly smaller than that of the crystal B-1, which was selected from an alloy containing an excess of phosphorus (sample B). Only the short (*c*) axis of A-1 decreased, see Table 1. The decrease in volume (or short axis) might be interpreted in terms of phosphorus vacancies. The structure refinement supported this assumption: the occupancy for P(3) in crystal A-1 (Table 2) refined to 95.3 % ($\sigma = 1.5$ %) while the corresponding one in B-1 converged to 100 %. A comparison between the interatomic distances in the two crystals showed that the largest differences were associated with the atomic environment about P(3). The average of the P(3)–Ti distances was 0.007 Å smaller in the A-1 crystal than in B-1, and all the Ti–Ti distances within the Ti_6 prism surrounding P(3) were shorter in A-1 by amounts corresponding to one or two standard deviations of the differences between A-1 and B-1. It therefore seems likely that the vacancy model is correct and the composition of the crystal A-1 should accordingly be $Ti_{13.86}Cu_{0.14}P_{8.95}$.

The ternary sample A was very inhomogeneous (it contained more than three phases) and specimens from different parts of the sample gave different cell parameters. It can be seen from Table 1 that the cell volume of A-2 powder is bigger than that of crystal A-1.

It has not been possible, as was mentioned in Ref. 1, to prepare a $Ti_{14}P_9$ phosphide in the binary Ti–P system.

Acknowledgements. The author thanks Docent T. Lundström and Professor S. Rundqvist for valuable criticism of the manuscript. Financial support from the Swedish Natural Science Research Council is gratefully acknowledged.

REFERENCES

1. Carrillo-Cabrera, W. and Lundström, T. *Acta Chem. Scand. A 33* (1979) 401.
2. Tergenius, L.-E., Noläng, B. I. and Lundström, T. *Acta Chem. Scand. A 35* (1981) 693.
3. Carrillo-Cabrera, W. *Acta Chem. Scand. A 36* (1982) 563.
4. Carrillo-Cabrera, W. and Lundström, T. *Acta Chem. Scand. A 34* (1980) 415.
5. *International Tables for X-Ray Crystallography*, Kynoch Press, Birmingham 1974, Vol. 4.
6. Lundgren, J.-O., Ed., *Crystallographic Computer Programs*, Institute of Chemistry, University of Uppsala, Uppsala 1975, UUIC-B13-02.
7. Hamilton, W. C. *Acta Crystallogr. 18* (1965) 502.
8. Abrahams, S. C. *Acta Crystallogr. A 25* (1969) 165.
9. Abrahams, S. C. and Keve, K. T. *Acta Crystallogr. A 27* (1971) 157.
10. Berger, R. *Acta Chem. Scand. A 31* (1977) 287.
11. Carrillo-Cabrera, W. and Lundström, T. *Acta Chem. Scand. A 35* (1981) 545.
12. Hassler, E. *Acta Chem. Scand. 25* (1971) 129.

Received September 10, 1981.

Acta Chemica Scandinavica A 36 (1982) 579–582

The Crystal Structure of $Na_4[Ni(NH_3)_4][Ag(S_2O_3)_2]_2 \cdot 0.3NH_3$

ROLF STOMBERG,[a] ING-BRITT SVENSSON,[a] A. A. G. TOMLINSON[b] and INGEBORG PERSDOTTER[a]

[a] Department of Inorganic Chemistry CTH/GU, Chalmers Tekniska Högskola, S-412 96 Göteborg, Sweden and [b] C.N.R. Laboratory for Electronic Structure of Coordination Compounds, Via Montorio Romano 36, 00131 Rome, Italy

The crystals of $Na_4[Ni(NH_3)_4][Ag(S_2O_3)_2]_2 \cdot 0.3 NH_3$ are tetragonal, space group $I4/m$ (No. 87) with $a = 13.996(4)$ Å, $c = 5.709(1)$ Å and $Z = 2$. The structure determination is based on 469 independent reflexions collected with a single crystal X-ray diffractometer using Cu$K\alpha$ radiation. Least-squares refinement of structural and thermal parameters yielded a final R-value of 0.044.

The crystals contain sodium ions, *catena*-di-μ-thiosulfatoargentate(I) ions, square planar tetraamminenickel(II) ions and, to a small extent, octahedral hexaamminenickel(II) ions. Silver is tetrahedrally surrounded by four sulfur atoms [S(2)], one from each of four thiosulfato groups. Each sulfur atom S(2) bridges two silver atoms, thus giving rise to a chain anion parallel to [001]. The thiosulfato group has an almost tetrahedral configuration. Bond distances: Ni–N 1.944(7) and 2.08(6) Å, Ag–S 2.596(2) Å, S–O 1.455–1.459(7) Å and S–S 2.037(3) Å.

Ferrari *et al.* in 1952 claimed to have synthesized $Na_4[Ni(NH_3)_4][Ag(S_2O_3)_2]_2$.[1] The analytical result, however, is more consistent with the formulation $Na_4[Ni(NH_3)_5][Ag(S_2O_3)_2]_2$. The crystal structure and spectra of the product obtained by a diffusion method similar to that described by Ferrari *et al.* has been determined by Stomberg *et al.*[2] That investigation clearly indicated the presence of a fifth ammonia molecule, nickel being both four- and six-coordinated. Since the attempts to remove the fifth ammonia molecule almost completely have been successful, though the preliminary ones were not,[2] it would seem profitable to solve the structure of $Na_4[Ni(NH_3)_4][Ag(S_2O_3)_2]_2$ in order to see the effect of the missing ammonia molecule.

EXPERIMENTAL

Preparation. $Na_4[Ni(NH_3)_4][Ag(S_2O_3)_2]_2 \cdot NH_3$ was prepared according to Stomberg *et al.*[2] The fifth ammonia molecule was removed by keeping the substance over phosphorous(V) oxide *in vacuo* for a long time (months).

Data collection. The collection of data was performed with a SYNTEX $P2_1$ automatic single crystal X-ray diffractometer at room temperature. A crystal with the dimensions $0.088 \times 0.095 \times 0.095$ mm was used.

The cell dimensions were obtained by a least-squares refinement of 15 automatically centred reflexions. The X-ray intensities were measured by the $\theta - 2\theta$ scan technique, using Cu$K\alpha$ radiation ($2\theta < 115°$). The scan rate varied between 2 and 8 °/min. The reflexion checked periodically during the data collection showed no crystal decomposition. A total of 469 independent reflexions with $I > 2\sigma(I)$ were used for the structure analysis. The intensities were corrected for Lorentz factor, polarization and absorption, but not for extinction.

Computing methods. The computational work was performed on an IBM 3033 computer using a set of crystallographic programmes described by Lindgren.[3]

CRYSTAL DATA

$Na_4[Ni(NH_3)_4][Ag(S_2O_3)_2]_2 \cdot 0.3NH_3$; F.W. = 888.1

Space group $I4/m$ (No. 87)

$a = b = 13.996(4)$, $c = 5.709(1)$ Å, $V = 1118.3(5)$ Å^3, $Z = 2$, $D_c = 2.637$ g cm^{-3}, μ(Cu$K\alpha$) = 23.2 mm^{-1}, λ(Cu$K\alpha$) = 1.5418 Å.

A list of observed and calculated structure factors is available from the author R.S. upon request.

0302-4377/82/070579-04$02.50

STRUCTURE DETERMINATION

Approximate atomic coordinates were known from the structure analysis of $Na_4[Ni(NH_3)_4][Ag(S_2O_3)_2]_2 \cdot NH_3$, the only difference being a missing ammonia molecule in $Na_4[Ni(NH_3)_4][Ag(S_2O_3)_2]_2$. These positional parameters, together with anisotropic thermal parameters for nickel, silver and sulfur and isotropic ones for nitrogen and oxygen and and overall scale factor, were refined by the full matrix least-squares method. In a subsequent difference Fourier summation, the largest peak appeared at (0; 0; 0.360) with a peak height of approximately 15 % of that of a nitrogen peak. If significance is to be given to this, it indicates that not all of the more loosely bound ammonia molecules have been removed by the phosphorous(V) oxide. The occupation number for this residual molecule was determined to be 0.16 ± 0.03 by the least-squares method. It was included in the final refinement of the structure using an isotropic thermal parameter. For all other atoms anisotropic thermal parameters were used. The structure factors were weighted according to Cruickshank,[4]

$$w = (a + |F_o| + c|F_o|^2 + d|F_o|^3)^{-1},$$

with $a = 15$, $c = 0.006$ and $d = 0$. The contributions to the structure factors from the hydrogen atoms were not taken into account. A final R-value of 0.044 for 469 observed reflexions was obtained with the parameters given in Table 1. The atomic scattering factors were taken from Ref. 5 as were the dispersion corrections.

DISCUSSION

A stereoscopic view of the unit cell is shown in Fig. 1. Bond distances and angles are given in Table 2 and other interatomic distances in Table 3. In

Table 1a. Atomic coordinates, expressed as fractions of the cell edges, for $Na_4[Ni(NH_3)_4][Ag(S_2O_3)_2]_2 \cdot 0.3NH_3$. Space group $I4/m$, $Z = 2$.

Atom	Position	x	y	z
Ni	2*a*	0	0	0
Ag	4*d*	0	$\frac{1}{2}$	$\frac{1}{4}$
S(1)	8*h*	0.0937(1)	0.2636(1)	$\frac{1}{2}$
S(2)	8*h*	0.1233(2)	0.4061(2)	$\frac{1}{2}$
Na	8*h*	0.2930(3)	0.1664(2)	$\frac{1}{2}$
O(1)	8*h*	−0.0085(5)	0.2442(5)	$\frac{1}{2}$
O(2)	16*i*	0.1405(4)	0.2251(3)	0.292(1)
N(1)	8*h*	0.3660(5)	0.4633(5)	$\frac{1}{2}$
N(2)	4*e*[a]	0	0	0.364(10)

[a] Occupation number = 0.16(3).

Table 1b. Anisotropic thermal parameters U_{ij} for $Na_4[Ni(NH_3)_4][Ag(S_2O_3)_2]_2 \cdot 0.3NH_3$. The expression used is exp $[-2\pi^2(U_{11}h^2a^{*2} + \ldots + 2U_{23}klb^*c^*)]$.

Atom	U_{11} or U_{iso}	U_{22}	U_{33}	U_{12}	U_{13}	U_{23}
Ni	0.016(1)	0.016(1)	0.021(2)	0	0	0
Ag	0.043(1)	0.043(1)	0.025(1)	0	0	0
S(1)	0.017(1)	0.019(1)	0.022(1)	−0.001(1)	0	0
S(2)	0.018(1)	0.020(1)	0.041(1)	0.000(1)	0	0
Na	0.031(2)	0.021(2)	0.037(2)	−0.001(2)	0	0
O(1)	0.022(3)	0.028(4)	0.041(4)	−0.001(3)	0	0
O(2)	0.034(3)	0.032(3)	0.041(3)	−0.004(2)	0.009(2)	−0.010(2)
N(1)	0.020(4)	0.020(4)	0.047(5)	0.001(3)	0	0
N(2)	0.009(12)					

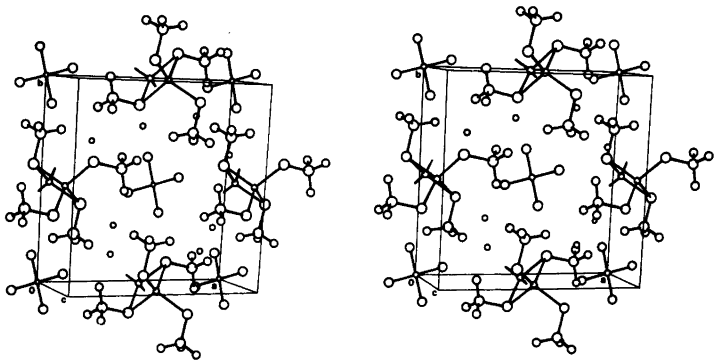

Fig. 1. Stereoscopic drawing of the unit cell of $Na_4[Ni(NH_3)_4][Ag(S_2O_3)_2]_2 \cdot 0.3NH_3$. N(2) is omitted.

Table 2. Bond distances and angles in $Na_4[Ni(NH_3)_4][Ag(S_2O_3)_2]_2 \cdot 0.3NH_3$.

	Distance/Å		Angle/°
Ni – N(1)	1.944(7)	S(2) – Ag – S(2) ($\bar{x}$,1 – y,z)	113.30(5)
Ni – N(2)	2.08(6)	S(2) – Ag – S(2) ($\frac{1}{2}-y,\frac{1}{2}+x,\frac{1}{2}-z$)	107.59(3)
Ag – S(2)	2.596(2)	S(2) – S(1) – O(1)	112.5(3)
S(1) – O(1)	1.455(7)	S(2) – S(1) – O(2)	105.6(2)
S(1) – O(2)	1.459(5)	O(1) – S(1) – O(2)	111.9(3)
S(1) – S(2)	2.037(3)	O(2) – S(1) – O(2) (x,y,1 – z)	108.9(4)
		Ag – S(2) – Ag (x,y,1 – z)	66.70(5)
		Ag – S(2) – S(1)	111.14(9)

$Na_4[Ni(NH_3)_4][Ag(S_2O_3)_2]_2 \cdot 0.3NH_3$ most of the nickel atoms are surrounded by four ammonia molecules in a square planar arrangement, while silver is tetrahedrally coordinated to four sulfur atoms [S(2)], one from each of four thiosulfato groups. Each sulfur atom S(2) bridges two silver atoms, thus giving rise to a chain anion parallel to [001]. The thiosulfato group has an almost tetrahedral configuration. The structure description given by Ferrari *et al.*[6] for $Na_4[Cu(NH_3)_4][Cu(S_2O_3)_2]_2$ is applicable to $Na_4[Ni(NH_3)_4][Ag(S_2O_3)_2]_2 \cdot 0.3NH_3$ (see Figs. 1 and 2 in Ref. 6 and exchange Cu(II) for Ni and Cu(I) for Ag). Notice, however, that there is, in fact, an extra ammonia molecule in the copper compound, not reported by Ferrari *et al.*, but established through the work by Morosin *et al.*[7]

The attempts to remove the fifth ammonia molecule in $Na_4[Ni(NH_3)_4][Ag(S_2O_3)_2]_2 \cdot NH_3$ were, thus, not completely successful. According to the interpretation put forward by Stomberg *et al.*[2] for $Na_4[Ni(NH_3)_4][Ag(S_2O_3)_2]_2 \cdot NH_3$ with both

Table 3. Interatomic distances (Å) other than bond distances in $Na_4[Ni(NH_3)_4][Ag(S_2O_3)_2]_2 \cdot 0.3NH_3$. Distances less than 3.5 Å are included.

Ag – Ag (x, y, $\bar{z}$)	2.855(0)
S(1) – Na	3.103(4)
S(1) – Na ($\frac{1}{2}-x,\frac{1}{2}-y,\frac{1}{2}-z$)	3.410(2)
S(2) – Na($\frac{1}{2}-x,\frac{1}{2}-y,\frac{1}{2}-z$)	3.249(2)
S(2) – O(1)	2.922(7)
S(2) – O(2)	2.807(5)
S(2) – N(1)	3.491(8)
Na – O(1) (y, $\bar{x}$, z)	2.313(7)
Na – O(2)	2.577(6)
Na – O(2) ($\frac{1}{2}-x,\frac{1}{2}-y,\frac{1}{2}-z$)	2.440(6)
O(1) – O(2)	2.414(8)
O(1) – N(1) ($-\frac{1}{2}+y,\frac{1}{2}-x,\frac{1}{2}-z$)	3.268(5)
O(2) – O(2) (x, y, $\bar{z}$)	3.335(11)
O(2) – O(2) (x, y, 1 – z)	2.374(11)
O(2) – O(2) ($\frac{1}{2}-x,\frac{1}{2}-y,\frac{1}{2}-z$)	3.180(10)
O(2) – N(1) ($\frac{1}{2}-x,\frac{1}{2}-y,\frac{1}{2}-z$)	3.122(8)
O(2) – N(1) ($-\frac{1}{2}+y,\frac{1}{2}-x,\frac{1}{2}-z$)	3.249(8)
N(1) – N(1) (y, 1 – x, z)	2.749(10)
N(1) – N(2) ($\frac{1}{2}-x,\frac{1}{2}-y,\frac{1}{2}-z$)	2.85(4)

Table 4. Ni – N distances in some Ni(II) complexes.

Complexes	Distance/Å	Ref.
Octahedral complexes		
$[NiCl_2(meso\text{-}Me_6[14]aneN_4)] \cdot 2CHCl_3$	2.060(3), 2.102(3)	9[a]
$[Ni(ClO_4)_2(C_7H_9N)_4]$	2.093(2)	10
Square planar complexes		
$[Ni(meso\text{-}Me_6[14]aneN_4)]Cl_2 \cdot 2H_2O$	1.957(1), 1.961(1)	9[a]
$[Ni(C_7H_9N)_4(ClO_4)_2$	1.897(3)	11
$[Ni(C_{18}H_{40}N_4)](ClO_4)_2$	1.926(2), 1.931(2)	12

[a] *meso*-$Me_6[14]aneN_4$ = [7*R*(*S*),14*S*(*R*)]-5,5,7,12,12,14-hexamethyl-1,4,8,11-tetraazacyclotetradecane.

square planar and tetragonally distorted octahedra, statistically about 15 % of the nickel atoms are octahedrally coordinated in $Na_4[Ni(NH_3)_4][Ag(S_2O_3)_2]_2 \cdot 0.3NH_3$. This is reflected by the observed in-plane Ni – N distance, 1.944 Å, which ought to be the weighted mean of square planar and octahedral Ni – N distances. In square planar complexes, Ni – N distances usually range between 1.82 and 1.92 Å, while in octahedral complexes Ni – N distances are significantly longer, 2.04 – 2.15 Å (see Table 8 in Ref. 8 and Table 4 in the present investigation). In the parent compound $Na_4[Ni(NH_3)_4][Ag(S_2O_3)_2]_2 \cdot NH_3$, with statistically 50 % of the nickel atoms being six-coordinated and the rest four-coordinated, the in-plane Ni – N distance, 2.01 Å, is significantly longer.

All other bond distances and angles are not significantly different in $Na_4[Ni(NH_3)_4][Ag(S_2O_3)_2]_2 \cdot 0.3NH_3$ and $Na_4[Ni(NH_3)_4][Ag(S_2O_3)_2]_2 \cdot NH_3$.

Acknowledgement. We wish to thank Mrs. Solveig Olson for technical assistance.

REFERENCES

1. Ferrari, A., Cavalca, L. and Coghi, L. *Gazz. Chim. Ital. 82* (1952) 703.
2. Stomberg, R., Svensson, I.-B. and Tomlinson, A. A. G. *Acta Chem. Scand. 27* (1973) 1192.
3. Lindgren, O. *Thesis*, University of Göteborg and Chalmers University of Technology, Göteborg 1977.
4. Cruickshank, D. W. J. *Crystallographic Computing*, Munksgaard, Copenhagen 1970, p. 195.
5. *International Tables for X-Ray Crystallography*, Kynoch Press, Birmingham 1974, Vol. 4.
6. Ferrari, A., Braibanti, A. and Tiripicchio, A. *Acta Crystallogr. 21* (1966) 605.
7. Morosin, B. and Larson, A. C. *Acta Crystallogr. B 25* (1969) 1417.
8. Stomberg, R. *Acta Chem. Scand. 23* (1969) 3498.
9. Ito, T. and Toriumi, K. *Acta Crystallogr. B 37* (1981) 88.
10. Madaule-Aubry, F. and Brown, G. M. *Acta Crystallogr. B 24* (1968) 745.
11. Madaule-Aubry, F., Busing, W. R. and Brown, G. M. *Acta Crystallogr. B 24* (1968) 754.
12. Ito, T., Ito, H. and Toriumi, K. *Acta Crystallogr. B 37* (1981) 1412.

Received November 27, 1981.

Acta Chemica Scandinavica A 36 (1982) 583–588

Copper Complex of α-Aminooxyacetic Acid. The Crystal and Molecular Structure of Diaquo-bis(aminooxyacetate)copper(II) Dihydrate, $[Cu(C_2H_4NO_3)_2(H_2O)_2] \cdot 2H_2O$

JORUNN SLETTEN

Department of Chemistry, University of Bergen, N-5014 Bergen, Norway

The structure of diaquo-bis(aminooxyacetate)copper(II) dihydrate has been determined by X-ray crystallographic methods, using diffractometer data collected at room temperature. The crystals are orthorhombic, space group *Pbca*, with $a = 5.2092(3)$, $b = 18.8395(9)$, $c = 11.1252(6)$ Å. The structure was solved by the heavy atom method, and refined by full-matrix least-squares to an R of 0.023. The copper ion is situated on a centre of symmetry, and has a 4+2 elongated octahedral coordination. Two aminooxyacetate ions coordinate to each copper ion through the amino nitrogen (Cu–N = 1.978 Å) and a carboxylate oxygen (Cu–O1 = 1.967 Å), forming the equatorial plane, while the axial positions are occupied by water molecules (Cu–O4 = 2.545 Å). The six-membered chelate ring is appreciably puckered.

Certain α-aminooxy acids, (I), are known to possess antibacterial properties. Several papers on chemical

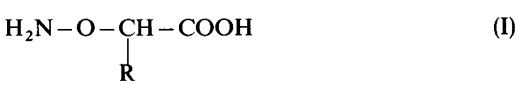

(I)

properties and biological activity of these compounds have been published.[1–5] An early investigation suggested that simple α-aminooxy acids did not form complexes with divalent metals.[6] Shortly afterwards, however, Zilichovsky reported the isolation of a copper(II) complex of α-aminooxyacetic acid[5] and recently a paper on the isolation and characterization of a series of Cu(II), Co(II) and Ni(II) complexes of various α-aminooxy acids appeared.[7] The stability of these complexes in aqueous solutions is reported to be appreciably lower than that of analogous amino acid complexes. This is the first crystal structure to be reported for this class of compounds.

0302-4377/82/070583-06$02.50

EXPERIMENTAL

The compound was synthesized according to the procedure described by Zilichovsky.[5] Bright blue prismatic crystals grew upon recrystallization from water by slow evaporation at room temperature. The crystal used for data collection had dimensions $0.45 \times 0.26 \times 0.30$ mm. Data were recorded at room temperature (20 °C ± 1 °C) on an Enraf-Nonius CAD-4 diffractometer using monochromatized Mo$K\alpha$ radiation and the ω-scan technique. Scan widths were $\Delta\omega = 0.50 + 0.35 \tan\theta$, and the scan speed was varied between 3.3 and 0.4° min.$^{-1}$ depending on peak intensity. Three reference reflections were monitored. The strongest one increased by approximately 25 % in the course of the data collection, indicating extinction. Towards the end of the data collection no further increase was observed. Thus, the strong, low order reflections, up to $\theta = 18°$, were recollected, and replaced the corresponding original measurements. The final data set consists of 1884 independent reflections up to $\theta = 30°$, 1390 of these have $I > 2\sigma_I$, and were used in the refinement. The error in the intensity of any one reflection was estimated as $\sigma_I = [\sigma_c^2 + (0.03N_{net})^2]^{\frac{1}{2}}$. The intensities were corrected for Lorentz and polarization effects and for absorption; the maximum and minimum transmission factors being 0.76 and 0.57, respectively.

CRYSTAL DATA

Diaquo-bis(aminooxyacetate)copper(II) dihydrate, $[Cu(C_2H_4NO_3)_2(H_2O)_2]\cdot 2H_2O$, orthorhombic, *Pbca* (No. 61), $a=5.2092(3)$, $b=18.8395(9)$, $c=11.1252(6)$Å, $V=1091.8(2)$Å^3, $M=315.72$, $Z=4$, $D_m=1.93$ g cm^{-3}, $D_X=1.923$ g cm^{-3}, $\mu(MoK\alpha)=21.36$ cm^{-1}, $\lambda=0.71069$Å.

STRUCTURE DETERMINATION AND REFINEMENT

The structure was solved by the Patterson method. Cu and O1 positions were taken from the Patterson map, the remaining non-hydrogen atoms were localized in subsequent Fourier syntheses. The atoms were refined first isotropically, then anisotropically. Hydrogen atoms were localized in a difference Fourier map and were refined isotropically. In the final cycles of full-matrix least-squares refinement an extinction parameter was included and refined, $g=5.99\times10^{-7}$, $[F_{obs}^{corr}=F_{obs}(1+gI_{obs})]$. The weight assigned to each reflection in the refinement is $w=1/\sigma_F^2$, where $\sigma_F=\sigma_I(I\cdot Lp)^{-\frac{1}{2}}$. The refinement converged at an R of 0.023, the weighted R being 0.040 and the standard deviation of an observation of unit weight 2.03.

Atomic scattering factors used were those of Cromer and Waber.[8] All calculations were carried out on a PDP 11/55 computer using the Enraf-Nonius Structure Determination Programs (SDP).[9]

Final atomic parameters are listed in Table 1. An ORTEP drawing of the formula unit, including atomic numbering scheme, bond lengths and angles are shown in Fig. 1. Lists of structure factors may be obtained from the author.

RESULTS AND DISCUSSION

The copper ion is situated on a centre of symmetry and has a 4+2 elongated octahedral coordination. Two aminooxyacetate ions are coordinated in the equatorial plane, each through the amino nitrogen (Cu–N = 1.978 Å) and a carboxylate oxygen (Cu–O1 = 1.967 Å). Due to symmetry requirements the ligand atoms N, N^i, O1, O1^i and the metal ion Cu(II) are exactly coplanar. The axial positions are occupied by two water molecules (Cu–O4 = 2.545 Å). The observed coordination is similar to that found in a number of α-amino acid– and β-amino acid–Cu(II) complexes, *e.g.* Refs. 10–18; the apical ligands being either water molecules and/or carboxylate groups from neighbouring molecules.

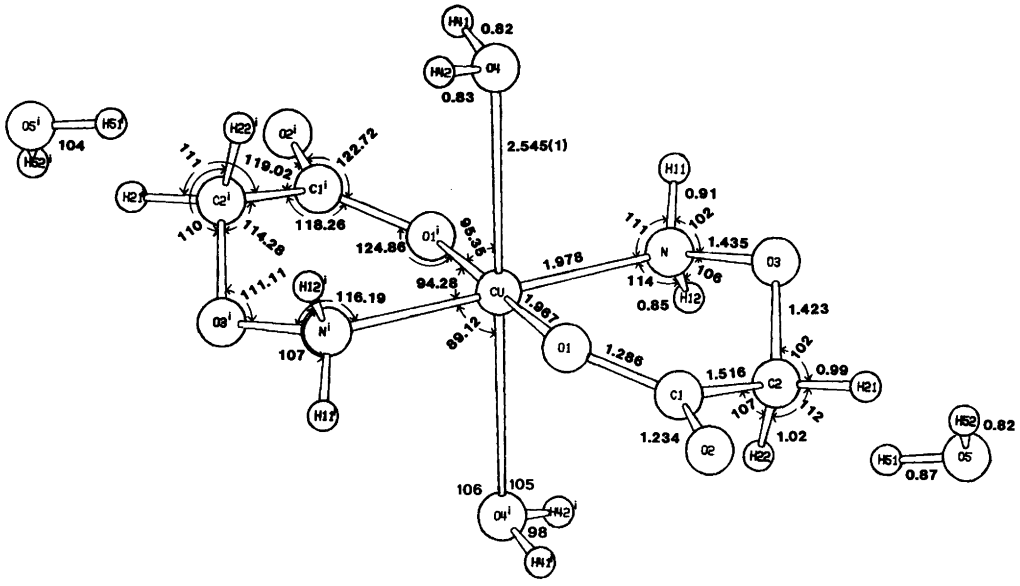

Fig. 1. The formula unit. Standard deviations in bond distances involving non-hydrogen atoms are 0.001 Å, in distances involving hydrogen 0.02 Å. Standard deviations in bond angles at Cu are 0.03°, in other angles involving non-hydrogen atoms 0.05–0.08° and in angles involving hydrogen 1°.

Table 1. Final atomic parameters with standard deviations, as obtained from the inverse least-squares matrix, in parentheses. Anisotropic temperature factor: $\exp[-2\pi^2(U_{11}h^2a^{*2}+\cdots+2U_{23}klb^*c^*)]$. Isotropic temperature factor: $\exp[-B\sin^2\theta/\lambda^2]$.

Atom	X	Y	Z	U(1,1)	U(2,2)	U(3,3)	U(1,2)	U(1,3)	U(2,3)
Cu	0.0000(0)	0.0000(0)	0.0000(0)	0.0207(1)	0.0235(1)	0.0275(1)	−0.00260(7)	0.00462(7)	−0.00509(6)
O1	0.2657(2)	0.07418(6)	0.00523(7)	0.0234(4)	0.0264(4)	0.0394(5)	−0.0023(4)	0.0066(3)	−0.0056(3)
O2	0.3867(2)	0.18604(5)	0.02800(10)	0.0313(5)	0.0292(4)	0.0526(5)	−0.0078(4)	0.0073(4)	−0.0035(4)
O3	−0.0804(2)	0.09816(5)	0.19885(7)	0.0295(4)	0.0342(4)	0.0259(4)	−0.0079(4)	0.0009(4)	−0.0061(3)
O4	0.2881(2)	−0.06499(5)	0.14850(8)	0.0334(4)	0.0307(4)	0.0391(4)	−0.0005(4)	0.0054(4)	−0.0011(4)
O5	0.4148(2)	0.29945(5)	0.18780(9)	0.0418(5)	0.0320(4)	0.0427(5)	0.0005(4)	−0.0032(5)	−0.0023(4)
N	−0.1959(2)	0.03935(6)	0.13705(9)	0.0208(4)	0.0275(4)	0.0270(4)	−0.0019(4)	0.0002(3)	−0.0036(4)
C1	0.2319(2)	0.13751(7)	0.0457(1)	0.0209(4)	0.0247(5)	0.0284(5)	0.0005(4)	−0.0025(4)	−0.0001(4)
C2	−0.0098(2)	0.15287(7)	0.1169(1)	0.0261(5)	0.0237(5)	0.0380(6)	−0.0002(4)	0.0047(4)	−0.0042(5)
				B	Atom	*X*	*Y*	*Z*	*B*
H11	−0.210(3)	0.0069(9)	0.197(2)	2.5(3)	H41	0.227(3)	−0.1047(12)	0.156(2)	4.2(4)
H12	−0.347(3)	0.0521(9)	0.119(1)	3.3(3)	H42	0.417(3)	−0.0757(10)	0.109(2)	3.5(3)
H21	0.015(3)	0.1940(10)	0.172(2)	2.5(3)	H51	0.402(4)	0.2658(12)	0.135(2)	4.9(4)
H22	−0.153(3)	0.1614(9)	0.057(2)	3.4(4)	H52	0.564(4)	0.2972(10)	0.210(2)	3.7(4)

In the α-amino acid complexes the ligands form stable five-membered chelates.[10-15] The introduction of an oxygen atom between the α-carbon and the amino group results in a six-membered chelate ring which is appreciably puckered, C1, C2, O3 being displaced by -.48, -.81 and .14Å, respectively, from the equatorial plane. The ring strain is relieved mainly through rotation around the single bonds C1 – C2, C2 – O3, O3 – N, as seen from the torsional angles listed in Table 2. The puckering is comparable to that found in the six-membered chelate rings of β-amino acid – Cu(II) complexes.[16-19]

The difference in chelate ring geometry between the α-aminooxy acid complex and the α-amino acid complexes apparently does not produce significant differences in the metal – ligand bond distances. In recent structure determinations of α-amino acid complexes[12-15] Cu-$O_{carboxyl}$ distances are found in the range 1.944 – 1.970 Å, and Cu – N_{amino} distances in the range 1.970 – 2.035 Å as compared to 1.967 and 1.978 Å, respectively, in the present structure. *A priori* the introduction of an electron withdrawing group adjacent to the amino nitrogen is expected to reduce the bonding ability of the coordinating lone pair. However, the observed comparatively short Cu – N bond is not in accordance with this simple picture of charge distribution. An accurate low temperature study of the compound is being undertaken in order to determine deformation electron density distribution in the complex.

All internal bond angles are somewhat larger in the α-aminooxy acid chelate than in the α-amino

Table 2. Torsional angles in the chelate ring. Angle *I, J, K, L* is defined as the angle between vectors *J,I* and *K,L* when viewed down *J,K*; positive values denote clockwise rotation of *KL*.

I, J, K, L	Torsional angles (°)
Cu,O1,Cl,O2	−166.6
Cu,O1,C1,C2	12.8
O1,C1,C2,O3	41.0
C1,C2,O3,N	−76.6
C2,O3,N,Cu	52.1
O3,N,Cu,O1	−6.2
N,Cu,O1,C1	−26.9

[a] The asymmetric units are marked as follows:

i:	$1-x,-y,-z$	v:	$-\frac{1}{2}+x,y,\frac{1}{2}-z$
ii:	$1+x,y,z$	vi:	$\frac{1}{2}-x,\frac{1}{2}+y,z$
iii:	$\frac{1}{2}-x,-\frac{1}{2}+y,z$	vii:	$-1+x,y,z$
iv:	$\frac{1}{2}+x,y,\frac{1}{2}-z$	viii:	$-x,y+\frac{1}{2},\frac{1}{2}-z$

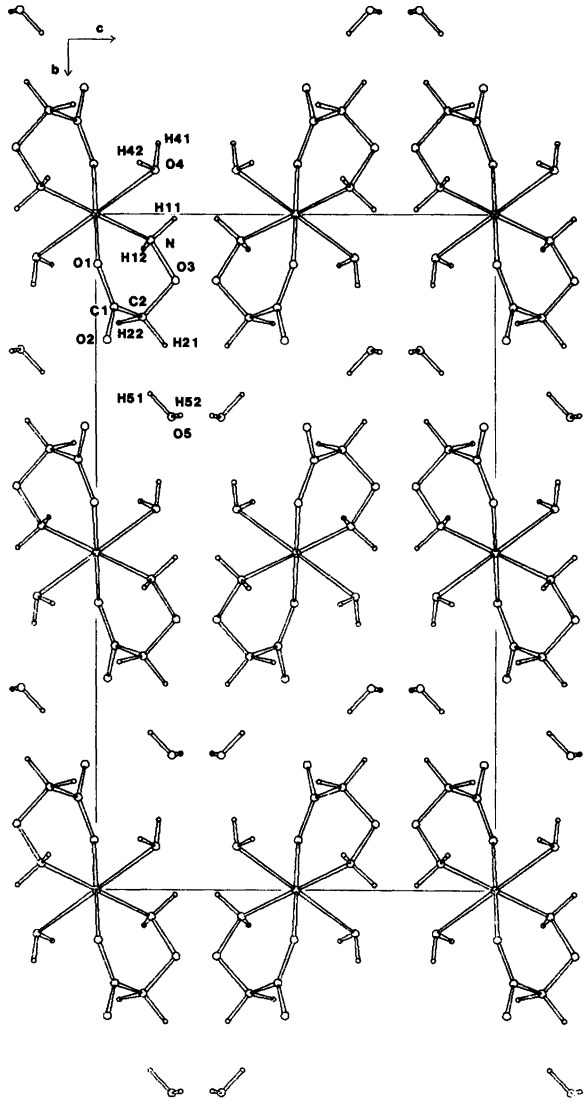

Fig. 2. Crystal packing as viewed down the *a*-axis.

acid chelates, the major differences being in the angles at O1, N and Cu. The N–Cu–O1 angle in the present compound is 94.28° as compared to the range 82.4–86.9° in the α-amino acid complexes referred to above. Corresponding values for Cu–O1–Cl are 124.86 and 112.8–117.7°, and for Cu–N–O3(C2) 116.19 and 105.5–110.3°. In β-amino acid complexes bond angles similar to those in the present structure have been found.[16-19]

The coordinated carboxylic oxygen, O1, participates in two hydrogen bonds, one to the coordinated water molecule and one to the amino group in neighbouring units (Table 3 and Fig. 2). Although the latter contact is rather long (O1---N^{ii} = 3.233 Å), it has been included in the list of hydrogen bonds as the angle at $H12^{ii}$ is 161°. The other carboxylic oxygen, O2, participates in one hydrogen bond to the water of hydration. O3 does not form hydrogen bonds, but has short contacts to symmetry related O3 atoms; O3---$O3^{iv}$ and O3---$O3^{v}$ = 2.843(1)Å),

Table 3. Hydrogen bonds.[a]

	A---H (Å)	A---D (Å)	∠A---H–D (°)
a. Hydrogen bond distances and angles at H-atoms			
O1---H42^{i}–O4^{i}	2.09(2)	2.891(1)	164(1)
O1---H12^{ii}–N^{ii}	2.42(2)	3.233(1)	161(1)
O2---H51–O5	1.92(2)	2.781(1)	175(2)
O4-H41---O5^{iii}	1.98(2)	2.796(1)	175(1)
O4---H11^{iv}–N^{iv}	2.19(2)	3.090(1)	174(1)
O5---H52^{v}–O5^{v}	2.15(2)	2.950(1)	166(1)
b. Hydrogen bond angles at A and D			
∠Cu-N$_H$---O1^{vii}	100.06(2)	∠Cu-O4$_H$---O1^{i}	96.88(2)
∠Cu-N$_H$---O4^{v}	111.74(2)	∠Cu-O4$_H$---O5^{iii}	108.47(3)
∠O3-N$_H$---O1^{vii}	115.12(5)	∠Cu-O4---$_H$N^{iv}	102.18(2)
∠O3-N$_H$---O4^{v}	97.60(5)	∠O1^{i}---$_H$O4$_H$---O5^{iii}	110.00(3)
∠O1^{vii}---$_H$N$_H$---O4^{v}	117.08(5)	∠O1^{i}---$_H$O4---$_H$N^{iv}	118.19(3)
		∠O5^{iii}---$_H$O4---$_H$N^{iv}	118.01(3)
∠Cu-O1---$_H$O4^{i}	120.41(3)		
∠Cu-O1---$_H$N^{ii}	118.71(3)	∠O2---$_H$O5---$_H$O4^{vi}	125.49(4)
∠Cl-O1---$_H$O4^{i}	111.87(5)	∠O2---$_H$O5---$_H$O5^{v}	104.65(4)
∠Cl-O1---$_H$N^{ii}	98.54(5)	∠O2---$_H$O5$_H$---O5^{v}	110.25(4)
∠O4$^{i}_H$---O1---$_H$N^{ii}	63.76(5)	∠O4$^{vi}_H$---O5---$_H$O5^{v}	74.88(3)
		∠O4$^{vi}_H$---O5$_H$---O5^{iv}	114.04(3)
∠Cl-O2---$_H$O5	120.04(5)	∠O5$^{v}_H$---O5$_H$---O5^{iv}	124.09(6)

< O3^{iv}---O3---O3^{v} = 132.84(6)°. The coordinated water molecule participates in three hydrogen bonds, and the water of hydration in four, giving both water molecules somewhat distorted tetrahedral environments.

The hydrogen bonds described above, lace the molecules together in a three-dimensional network. Complex units related by the lattice translation *a* are linked by hydrogen bond O1---H42^{i}–O4^{i}. Units related by the *a*-glide are connected through N1–H11---O4^{v} and through the water of hydration, O2---H51-O5---H52^{v}–O5^{v}–H51^{v}---O2^{v}. Units related by the *b*-glide and the *c*-glide are also connected through water of hydration, by the sequences O2---H51-O5---H41–O4^{vi} and O2---H51-O5---H52^{v}–O5^{v}---H41^{viii}-O4^{viii}, respectively.

REFERENCES

1. McHale, D., Green, J. and Mamalis, P. *J. Chem. Soc.* (1960) 225.
2. Sohár, P., Dancsi, L. and Kisfaludy, L. *Acta Chim. Acad. Sci. Hung. 83* (1974) 391.
3. Undheim, K., Bamberg, P. and Sjöberg, B. *Acta Chem. Scand. 19* (1965) 317.
4. Wood, J. D., Kurylo, E. and Newsbead, J. D. *Can. J. Biochem. 56* (1978) 667.
5. Zvilichovsky, G. *Tetrahedron 22* (1966) 1445.
6. Testa, E., Nicolaus, B. J. R., Mariani, L. and Pogani, G. *Helv. Chim. Acta 46* (1963) 766.
7. Warnke, Z., Wojciechowska, E. and Szyszuk, H. *Metal Ions in Biological, Catalytical and Related Systems*, 10th Summer School-Symposium on Coordination Chemistry, Karpacz, Poland, May 19–27, 1980.
8. Cromer, D. T. and Waber, J. T. *International Tables for X-Ray Crystallography*, Kynoch Press, Birmingham 1974, Vol. 4, p. 99, Table 2.2B.
9. Frez, B. *The SDP User's Guide*, Enraf-Nonius, Delft, Holland 1979.
10. Freeman, H. C., Snow, M. R., Nitta, I. and Tomita, K. *Acta Crystallogr. 17* (1964) 1463.
11. Dijkstra, A. *Acta Crystallogr. 20* (1966) 588.
12. Van der Helm, D., Lawson, M. B. and Enwell, E. L., *Acta Crystallogr. B 27* (1971) 2411.
13. Stephens, F. S., Vagg, R. S. and Williams, P. A. *Acta Crystallogr. B 31* (1975) 841.
14. Ou, C. C., Powers, D. A., Thich, J. A., Felthouse, T. R., Hendrickson, D. N., Potenza, J. A. and Schugar, H. J. *Inorg. Chem. 17* (1978) 34.

15. Fawcett, F. G., Ushay, M., Rose, J. P., Lalancette, R. A., Potenza, J. A. and Schugar, H. J. *Inorg. Chem. 18* (1979) 327.
16. Tomita, K. *Bull. Chem. Soc. Jpn. 34* (1961) 297.
17. Bryan, R. F., Poljak, R. J. and Tomita, K. *Acta Crystallogr. 14* (1961) 1125.
18. Mitsui, Y., Iitaka, Y. and Sakaguchi, H. *Acta Crystallogr. B 32* (1976) 1634.
19. Freeman, H. C. *Advances in Protein Chemistry*, Academic, London 1967, Vol. 22, pp. 257–424.

Received December 3, 1981.

Acta Chemica Scandinavica A 36 (1982) 589 – 593

The Crystal Structure of Bis [benzoato-μ-(2-diethylaminoethanolato-N,μ-O)copper(II)]

KIMMO SMOLANDER

Department of Chemistry, University of Joensuu, SF-80 100 Joensuu 10, Finland

The crystal structure of Cu_2 $[(C_2H_5)_2NC_2H_4O]_2$-$(C_6H_5COO)_2$, $C_{26}H_{38}Cu_2N_2O_6$ is monoclinic with space group $P2_1/c$ and $a=8.721(5)$ Å, $b=8.263(5)$ Å, $c=19.395(7)$ Å and $\beta=100.06(4)°$. The structure was established by Patterson and Fourier methods and refined by least-squares calculations to an R value of 0.056 for 1814 reflections (4240 total).

The structure is dimeric, with two copper(II) ions bridged by 2-diethylaminoethanolato oxygen atoms [Cu···Cu 3.011(1) Å]. The coordination of the copper(II) is slightly distorted square-planar. The basal plane consists of one nitrogen atom, two bridge oxygen atoms and one benzoato oxygen atom with bond lengths 2.042(4), 1.902(4), 1.925(4) and 1.888(4) Å, respectively.

The carbon atoms in the 2-diethylaminoethanolato ligand are disordered having the site occupation factors 0.5. The form A is converted into the form B by rotation around the Cu – N bond, 48.0° on the average. The benzoato ligand is unidentate and almost planar.

The structures of many alkoxo-bridged copper (II) complexes with N,N-dialkylaminoethanols ($R_2NCH_2CH_2OH=R_2LOH$) as the second ligand have been reported.[1] Only one benzoate complex is known, the structure of which contains linear trinuclear oxygen-bridged arrays of copper atoms.[2] Now we have made in the $(C_2H_5)_2LOH$ series the benzoate complex of bis[benzoato-μ-(2-diethylaminoethanolato-N,μ-O)copper(II)].

EXPERIMENTAL

The copper(II) benzoate was made from basic copper(II) carbonate (Merck) and benzoic acid by the method of Bateman and Conrad.[3] Of the salt, 0.01 mol was dissolved in methanol and to this solution 0.01 mol of 2-diethylaminoethanol (Fluka AG) was added with stirring. The solution was filtered and precipitation of the compound was achieved by adding some acetone. After some weeks at ambient temperature, dark blue crystals were obtained.

The unit cell parameters and the orientation matrix were determined by a least-squares refinement from 19 centered reflections measured at ambient temperature on a Nicolet $R3m$ diffractometer. Intensity data were collected ($3°<2\theta<60°$) in the ω-scan mode, using graphite-monochromatized Mo$K\alpha$ radiation. The scan speed varied from 2.0 to 29.3°/min. Two selected reflections were monitored as standards after every 98 measurements. Their intensities showed no significant changes with time. The intensities were corrected for Lorentz and polarisation effects and for absorption from empirical ψ-scan data. Out of 4240 reflections 1814 were retained in subsequent calculations, using an acceptance criterion of $F_o>5\sigma(F_o)$.

CRYSTAL DATA

$Cu(C_6H_{14}NO)(C_7H_5O_2)$, $FW=300.85$
Space group: $P2_1/c$ (No. 14)
$a=8.721(5)$, $b=8.263(5)$, $c=19.395(7)$ Å
$\beta=100.06(4)°$
$V=1376.19$ Å^3, $Z=4$, $F(000)=628$
μ(Mo$K\alpha$)$=16.5$ cm^{-1}, λ(Mo$K\alpha$)$=0.71069$ Å
$D_m=1.44$ g cm^{-3} (flotation technique)
$D_x=1.45$ g cm^{-3}

STRUCTURE DETERMINATION

The positional parameters of the copper atom were obtained from the sharpened Patterson map. The remaining non-hydrogen atoms of the structure were found from successive Fourier syntheses. The

0302-4377/82/070589-05$02.50

Table 1. Fractional atomic coordinates ($\times 10^4$) and thermal parameters ($\times 10^3$) for non-hydrogen atoms with e.s.d. in parentheses. The occupancy factors of A and B positions of carbon atoms are 0.5.

Atom	X	Y	Z	U^a	U_{22}	U_{33}	U_{23}	U_{13}	U_{12}
Cu	−222(1)	1259(1)	535(1)	34(1)	31(1)	41(1)	−5(1)	5(1)	−3(1)
O1	−978(4)	−795(5)	185(2)	39(2)	41(2)	58(3)	−14(2)	17(2)	−14(2)
O2	587(5)	3320(4)	819(2)	45(2)	35(2)	63(3)	−13(2)	−1(2)	−4(2)
O3	2779(6)	2166(5)	1346(3)	76(3)	30(2)	83(4)	0(2)	−13(3)	6(2)
N	−1992(5)	1158(5)	1097(2)	57(3)	54(3)	63(3)	−11(3)	27(3)	−13(3)
C1A	−2228(8)	−1486(13)	460(5)	41(3)					
C1B	−2516(6)	−1194(9)	262(5)	50(3)					
C2A	−2316(28)	−639(14)	1123(9)	114(18)	98(16)	135(19)	−61(14)	96(16)	−72(14)
C2B	−3162(14)	−36(24)	718(13)	62(13)	89(14)	191(25)	−72(17)	72(14)	−23(11)
C3A	−3341(15)	2166(20)	721(11)	48(10)	103(15)	156(21)	−33(16)	53(12)	−7(10)
C3B	−2799(27)	2707(19)	1259(10)	122(18)	94(15)	109(17)	−21(13)	72(15)	45(13)
C4A	−2987(26)	4030(19)	712(11)	80(7)					
C4B	−3228(23)	3657(23)	550(9)	61(5)					
C5A	−1424(21)	1693(20)	1872(7)	152(19)	83(14)	81(13)	−43(11)	90(14)	−31(13)
C5B	−1625(22)	178(21)	1794(8)	118(17)	82(13)	82(13)	27(11)	37(12)	−2(12)
C6A	155(23)	992(36)	2217(12)	102(10)					
C6B	−265(20)	1000(26)	2277(9)	56(5)					
C7	2006(7)	3347(6)	1162(3)	54(4)	29(3)	44(3)	−7(3)	7(3)	−4(3)
C8	2650(7)	5036(7)	1331(3)	46(3)	36(3)	30(3)	−4(2)	4(3)	1(3)
C9	4095(7)	5212(7)	1747(3)	40(3)	39(3)	47(4)	−1(3)	−4(3)	0(3)
C10	4697(7)	6728(8)	1923(4)	44(4)	47(4)	55(4)	−3(3)	−4(3)	−13(3)
C11	3846(8)	8082(7)	1682(4)	66(4)	38(3)	56(4)	−5(3)	12(4)	−16(3)
C12	2432(8)	7913(7)	1259(4)	62(4)	28(3)	64(5)	2(3)	−1(4)	−1(3)
C13	1820(7)	6409(8)	1089(3)	49(3)	36(3)	49(3)	−0(3)	−7(3)	0(3)

[a] U_{11} or U_{iso}.

carbon atoms of 2-diethylaminoethanolato ligand had unusually large thermal motion, and a difference Fourier map proved the structure to be disordered. The carbon atoms of $(C_2H_5)_2LO$ were given site occupation factors 0.5 which were refined, but they showed no significant change and were fixed at 0.5. After some least-squares refinements the A and B forms of the 2-diethylaminoethanolato ligand were

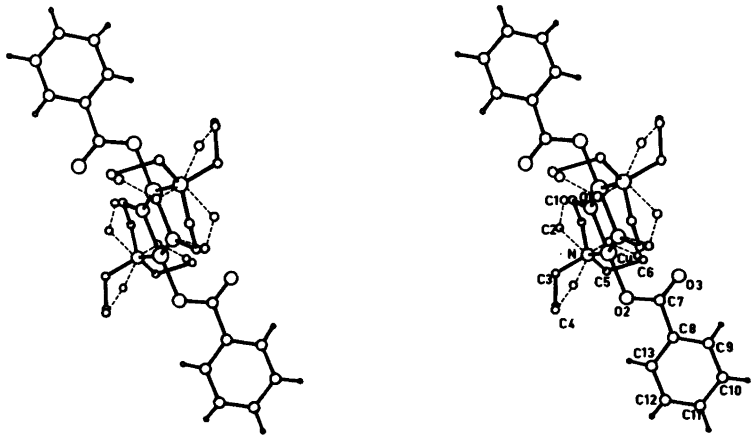

Fig. 1. Stereoview of the structure of $[Cu(C_6H_{14}NO)(C_7H_5O_2)]_2$. The A form in solid lines, the B form in dotted lines. Hydrogen atoms in the disordered part are omitted for clarity.

Table 2. Fractional atomic coordinates ($\times 10^3$) and isotropic thermal parameters ($\times 10^2$) for hydrogen atoms.

Atom	*X*	*Y*	*Z*	*U*
H1(C1A)	−2364	−1120	915	48
H2(C1A)	−2302	−2645	440	48
H1(C1B)	−3094	−1841	−105	59
H2(C1B)	−3155	−315	370	59
H1(C2A)	−1426	−32	1344	109
H2(C2A)	−2742	−1230	1472	109
H1(C2B)	−4244	−170	743	104
H2(C2B)	−2953	1085	643	104
H1(C3A)	−2697	1411	526	102
H2(C3A)	−4376	1738	679	102
H1(C3B)	−3444	2743	1612	123
H2(C3B)	−1766	2380	1467	123
H1(C4A)	−3781	4559	384	87
H2(C4A)	−1990	4488	679	87
H3(C4A)	−3194	4178	1178	87
H1(C4B)	−2508	4044	266	84
H2(C4B)	−4261	3652	279	84
H3(C4B)	−2945	2578	706	84
H1(C5A)	−1209	2296	1477	112
H2(C5A)	−2174	2266	2087	112
H1(C5B)	−602	−282	1912	108
H2(C5B)	−2239	−145	2136	108
H1(C6A)	262	433	2657	99
H2(C6A)	376	2121	2300	99
H3(C6A)	872	547	1945	99
H1(C6B)	−103	372	2700	79
H2(C6B)	−981	445	1923	79
H3(C6B)	−686	2038	2366	79
H1(C9)	4570(63)	4409(71)	1949(29)	53
H1(C10)	5699(66)	6872(71)	2271(30)	59
H1(C11)	4251(65)	9051(72)	1762(30)	62
H1(C12)	1974(67)	8669(73)	1134(30)	64
H1(C13)	863(72)	6284(80)	804(31)	58

derived. The corresponding bond lengths of the A and B forms were given the same value and refined as such.

The structure was refined by the blocked-cascade full-matrix least-squares method[4] with anisotropic temperature factors for non-hydrogen atoms except for the fractional occupancy atoms C1, C4 and C6. The hydrogen atoms were included with fixed bond lengths (C−H=0.96 Å) and constrained angles at calculated positions. The isotropic thermal parameters for the hydrogen atoms were set 1.2 times the equivalent isotropic thermal parameters for the corresponding carbon atom. Finally the positions of the hydrogen atoms in the benzoato ligand were refined.

Table 3. Interatomic distances (Å) and angles (°) with estimated standard deviations in parentheses.

The copper(II) environment

Cu−O1	1.902(4)	O1−Cu−N	84.7(2)
Cu−O2	1.888(4)	O1−Cu−O2	175.7(2)
Cu−N	2.042(4)	O1−Cu−O1^i	76.2(2)
Cu−O1^i	1.925(4)	N−Cu−O2	99.2(2)
Cu...O3	2.907(4)	N−Cu−O^i	159.6(2)
Cu...Cu	3.011(1)	O2−Cu−O1^i	99.7(2)
		Cu−O−Cu^i	103.8(2)

The 2-diethylaminoethanolato ligand

Form A		Form B	
O1−C1	1.42(1)	O1−C1	1.42(1)
C1−C2	1.48(2)	C1−C2	1.48(2)
N−C2	1.52(1)	N−C2	1.52(2)
N−C3	1.52(2)	N−C3	1.52(2)
N−C5	1.56(1)	N−C5	1.56(2)
C3−C4	1.57(2)	C3−C4	1.57(3)
C5−C6	1.54(3)	C5−C6	1.53(2)
Cu−N−C2	102.7(9)	Cu−N−C2	106.0(9)
Cu−N−C3	108.3(8)	Cu−N−C3	119.8(9)
Cu−N−C5	111.1(7)	Cu−N−C5	115.1(8)
C2−N−C3	114.8(10)	C2−N−C3	110.6(10)
C2−N−C5	106.0(9)	C2−N−C5	95.9(11)
C3−N−C5	113.4(10)	C3−N−C5	106.9(10)
N−C2−C1	113.4(12)	N−C2−C1	114.7(9)
N−C3−C4	113.9(11)	N−C3−C4	106.7(15)
N−C5−C6	115.0(15)	N−C5−C6	108.6(13)
O−C1−C2	107.3(10)	O−C1−C2	112.3(8)
C1−O−Cu	117.9(5)	C1−O−Cu	116.5(4)
C1−O−Cu^i	138.2(5)	C1−O−Cu^i	132.5(4)

The benzoato ligand

O2−C7	1.299(7)	Cu−O2−C7	116.1(3)
O3−C7	1.205(7)	O2−C7−O3	124.9(5)
C7−C8	1.518(8)	O2−C7−C8	114.2(5)
C8−C9	1.381(8)	O3−C7−C8	120.9(5)
C9−C10	1.378(9)	C7−C8−C9	119.2(5)
C10−C11	1.378(9)	C7−C8−C13	121.9(5)
C11−C12	1.364(9)	C8−C9−C10	120.7(5)
C12−C13	1.369(9)	C9−C10−C11	119.6(6)
C13−C8	1.383(8)	C10−C11−C12	119.9(6)
		C11−C12−C13	120.7(6)
		C13−C8−C9	118.8(5)
		C12−C13−C8	120.3(5)

i: $-x, -y, -z$

The refinement converged to a conventional *R* of 0.056 and a weighted discrepancy factor of 0.052,

$$R_w = \Sigma||F_o| - |F_c||\sqrt{w}/\Sigma|F_o|\sqrt{w}$$

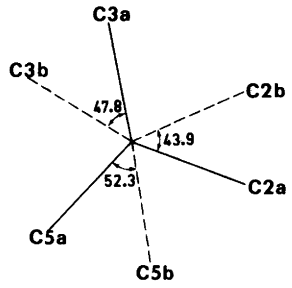

Fig. 2. Projection down the Cu – N bond with the rotation angles between the A and B positions.

with the weighing scheme $w^{-1} = \sigma^2(F_o) + 0.0005F_o^2$.

The neutral atom scattering factors have been taken from *International Tables for X-Ray Crystallography*.[5] The calculations were performed on a Nicolet *R*3m diffractometer system with SHELXTL[4] software for a minicomputer (Nova 3). The final atomic parameters are given in Tables 1 and 2, and bond distances and angles in Table 3.

DISCUSSION

In the unit cell there are two dimeric molecules, which are centrosymmetric and bridged by 2-diethylaminoethanolato oxygen atoms. In the Cu_2O_2 core the Cu···Cu distance of 3.011(1) Å is very similar to that in other dimeric alkoxy-bridged Cu(II) complexes with *N,N*-dialkylaminoethanols where the distances vary from 2.950 Å to 3.026 Å.[1] Also the Cu – O – Cu′ and O – Cu – O′ angles of 103.8(2) and 76.2(2)° agree well with those in other dimers.[1] The deviations from the Cu_2O_2 plane for the benzoato oxygen atom O2 and the nitrogen atom are 0.047 and 0.251 Å, respectively.

The coordination around the copper(II) ion is square-planar and the basal plane consists of two bridging ethanolato oxygen atoms, one benzoato oxygen atom and one nitrogen atom. The bond lengths are Cu – O1 1.902(4) Å, Cu – O1′ 1.925(4) Å, Cu – O2 1.888(4) Å and Cu – N 2.042(4) Å. These are quite normal distances for the coordination bonds.[1] The coordination sphere has slightly tetrahedral distortion where the O1 and O2 atoms lie 0.06 and 0.04 Å above and N and O1′ 0.05 and 0.05 Å below the least-squares plane of atoms O1,O2,N,O1′. The dihedral angle between the Cu,O1,O1′ and Cu,N,O2 planes is 7.5°. The distance between the copper atom and the uncoordinated benzoato oxygen atom O3 is 2.907(4) Å and the angle between the basal plane and the Cu – O3 line is 45.4°.

The structure of 2-diethylaminoethanolato ligand is disordered and there are two forms, A and B, Figs. 1 and 2. In both of them the carbon atoms have the site occupation factors of 0.5. Because some atoms of the A and B forms are quite close to each other (*e.g.* C4a – C4b 0.404 Å), the coordinates were selected such that the angles and bond lengths would be as reasonable as possible. Rotation (av. 48.0°) around the Cu – N bond changes the form from A into B. The rotation angles between the A and B form for atoms C2, C3 and C5 are 43.9, 47.8 and 52.3°, respectively, (Fig. 2). The dihedral angle NClC20 in the five-membered ring is 38.4 and 9.3° in A and B, respectively. Similar disorder has been reported in the $[Cu(C_6H_{14}NO)NCS]_2$[6] complex, where one ethyl group and one ring carbon atom have the occupancy factors 0.5. The rotation angles around Cu – N bond were 45.4° (C ring) and 47.5° (C ethyl).

The benzoato ligand is almost planar, the oxygen atom O2 having (0.008 Å) the largest deviation from the least-squares plane. The dihedral angle between the phenyl ring plane and its carboxyl group is 5.4° and between the phenyl ring and the Cu_2O_2 plane 78.1°. The mean value of the ring C – C bond and C – C – C angle are 1.375 Å and

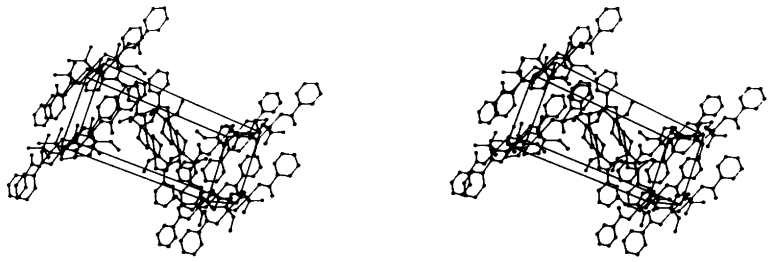

Fig. 3. Stereoview of the packing. The B form is omitted for clarity.

120.0°. The benzoato ligand is unidentate with the C7–O2–Cu angle of 116.1(3)°. The bond lengths and angles agree well with other data reported.[2,7-10] The coordinated C–O bond length is 0.09 Å longer than the uncoordinated one which has more double-bond character. The C–H bond lengths in the phenyl ring vary from 0.76 to 1.01 Å with a mean value of 0.88 Å.

REFERENCES

1. Smolander, K. *Acta Chem. Scand. A 35* (1981) 815 and references therein.
2. Muhonen, H., Pajunen, A. and Hämäläinen, R. *Acta Crystallogr. B 36* (1980) 2790.
3. Bateman, W. G. and Conrad, D. B. *J. Am. Chem. Soc. 37* (1915) 2553.
4. Sheldrick, G. M. *The SHELXTL 1981 (Revision 3) Computer Programs*, Nicolet XRD Corporation, 10061 Bubb Road, Cupertino, California 95014, USA.
5. *International Tables for X-Ray Crystallography*, Kynoch Press, Birmingham 1974, Vol. 4, p. 71.
6. Pajunen, A. and Smolander, K. *Finn. Chem. Lett.* (1977) 99.
7. Muhonen, H. and Hämäläinen, R. *Acta Chem. Scand. A 32* (1978) 121.
8. Borthwick, P. W. *Acta Crystallogr. B 36* (1980) 628.
9. Borel, M. M., Busnot, F. and Leclaire, A. *Z. Anorg. Allg. Chem. 449* (1979) 177.
10. Musaev, F. N., Mamedov, K. S., Movsumov, E. M. and Amiraslanov, I. R. *Koord. Khim. 5* (1979) 119.

Received November 19, 1981.

Acta Chemica Scandinavica A 36 (1982) 595–603

Multicomponent Polyanions. 33. Single Crystal Raman Spectra of $Na_6Mo_7O_{24}(H_2O)_{14}$

LENNART LYHAMN*

Department of Inorganic Chemistry, University of Umeå, S-901 87 Umeå, Sweden

Polarized Raman spectra of an $Na_6Mo_7O_{24}(H_2O)_{14}$ single crystal, containing the anion $Mo_7O_{24}^{6-}$, have been measured. Spectra in the ranges 40–1000 and 2900–3600 cm^{-1} are presented for all the species of point group C_{2v}. Different vibrational activity was observed depending on the geometrical orientation of measurement. Tentative assignments of the vibrational modes are performed by comparing structure and orientation of the Mo_7O_{24} groups within the unit cell. The descriptions of the vibrational modes are also compared with assignments of other Mo-oxo-complexes. From the O–H vibrational modes (1500–1700, 2900–3600 cm^{-1}) two main types of water of crystallization were found, and furthermore that the waters have fixed orientations.

In acidic aqueous solution of Mo(VI) several polynuclear species exist. The complexes established are hepta- and octanuclear species, *e.g.* $Mo_7O_{24}^{6-}$, $H_nMo_7O_{24}^{(6-n)-}$ $(n=1-3)$ and $Mo_8O_{26}^{4-}$.[1-4] Molybdenum(VI) thus easily forms large polyanions with different compositions and structures. Great interest has been shown in identification and characterization of isopolymolybdate complexes using vibrational spectroscopy.[5-12] The Raman technique is particularly useful for obtaining information on species in aqueous solution, since water has only a weak Raman spectrum. An identification method used is to compare the spectrum of a complex in solution with the spectrum of a powdered solid sample.[5,9,11] The interpretation of spectra will, however, become difficult, since spectra of such large complexes in general are incomplete. In order to obtain complementary information, a Raman investigation of a single crystal containing the anion $Mo_7O_{24}^{6-}$ was undertaken. Furthermore, the single crystal spectra will show shifts when transferring the $Mo_7O_{24}^{6-}$ anion from an aqueous solution into the crystal field. It would also be profitable to investigate the extent of correlation splitting effects. Moreover, spectra of single crystals are very valuable, especially for group theoretical interpretations and in theoretical calculations of vibrational modes.[13-16]

EXPERIMENTAL

Polarized single crystal spectra of an $Na_6Mo_7O_{24}(H_2O)_{14}$ phase were recorded with a Spex Ramalog 1401/14018 at the Institute of Inorganic Chemistry, University of Bielefeld, BRD. The Raman spectrophotometer was equipped with a Coherent Radiation Ar^+ laser, and the blue line at 488.0 nm was used for excitation. The scattered light was detected at 90° from that of illumination.

The crystal had natural faces perpendicular to the crystal axes, so no cutting was necessary. After polishing, the size of the crystal was $3 \times 8 \times 11$ mm^3. A goniometer system for the orientation of the crystal was used. The crystal axes were also identified with X-ray diffraction Weissenberg techniques.[17] Since the crystal belongs to an orthorhombic space group $P2_1ab$-C_{2v}^5(No. 29)[18] the optical and crystal axes coincide,[19] which facilitates the experimental work. Spectra of 12 different scattering geometries were recorded, and the wavenumber ranges 40–1000, 1500–1700 and 2900–3600 cm^{-1} were covered.

* Present address: Kursmakarna AB, Skeppsbrogatan 22, S-951 31 Luleå, Sweden.

0302-4377/82/070595-09$02.50

METHOD

An advantage of modern Raman spectroscopy is the use of lasers. The laser beam commonly used is coherent and has a very small cross section, which are useful attributes in investigations of single crystals. There are three ways to orientate the crystal with respect to the laser beam and the spectrometer slit in analyzing the scattered light, and two ways of detection, either parallel or perpendicular to the electric vector of the exciting beam (E). This gives 12 different geometrical orientations of measurement. However, the polarizability tensor $\alpha(I = \alpha \cdot E)$ of an orthorhombic class has only 6 unique components, since $\alpha_{ij} = \alpha_{ji}$.[20] (A rotation of the crystl 180° along each axis gives in all 24 spectra; however, the 12 new orientations are only replicas of the former, but can be used as a control.) In Fig. 1 four different geometrical orientations of the crystal are shown. The equations of the scattered light intensities for the different observations are also given in Fig. 1.

The anion $Mo_7O_{24}^{6-}$ itself has a symmetry very close to C_{2v},[18] and this point group will therefore be adopted. Since the factor group also is C_{2v} and the site symmetry is C_1, there will be a complete correlation splitting of each internal fundamental mode into the four Raman active components A_1, A_2, B_1 and B_2. The interactions between molecules are, however, weak compared with those within molecules.[21]

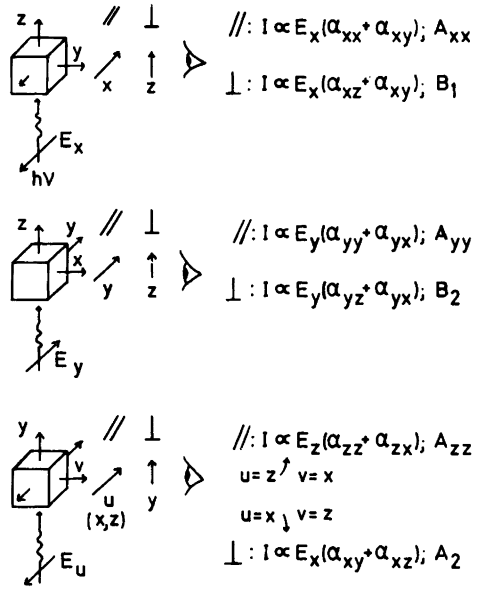

Fig. 1. Different geometrical orientations of the crystal with respect to the exciting laser beam. For each orientation two ways of observation is possible, parallel (//) and perpendicular (⊥). The first polarizability factor (α) is the main term of the scattered light intensity (I), and thus given the point group notation.

The notation of Damen *et al.*[22] is used to indicate the directions of excitation, observation and polarization. The expression $i(xy)j$ thus means that the incident light travels along the i axis and has its electric vector along $x(E_x)$, and the y component of the scattered light is observed along the j axis. Phonons of the symmetric representation A_1 (C_{2v} symmetry) can be observed when the directions of polarization are the same for illumination and observation. For different directions of polarization A_2, B_1 and B_2 phonons can be observed. Thus, using combinations of polarization in different directions, spectra representing the phonons A_1, A_2, B_1 and B_2 can be measured, see Fig. 1.

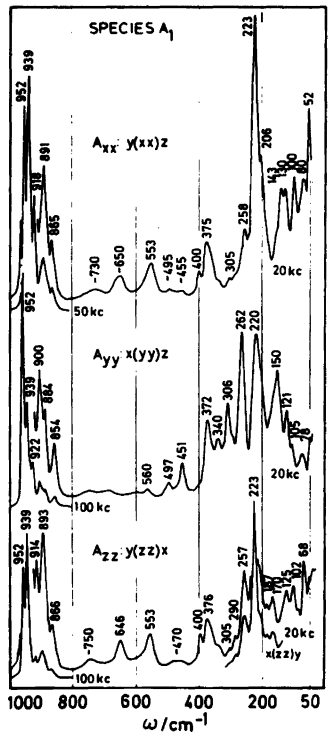

Fig. 2. Polarized Raman spectra of the $Na_6Mo_7O_{24}(H_2O)_{14}$ single crystal, representing the three "symmetric spectra" (A_1) of the anion $Mo_7O_{24}^{6-}$ (kc means 1000 counts).

SPECTRA

Spectral measurements

Spectra of the four different species A_1 (A_{xx}, A_{yy}, A_{zz}), A_2, B_1 and B_2 were recorded in the wavenumber ranges 40–1000, 1500–1700 and 2900–3600 cm^{-1}. In the first range, spectra were taken for all the 12 possible orientations, *i.e.* two independent spectra for each of the 6 different types of representations. Highly reproducible spectra were obtained for each corresponding spectra type. There was sometimes, however, a noticeable change in the intensity of the scattered light, due to a more or less successful alignment of the crystal and the optical devices. Owing to the good reproducibility, it was sufficient to record the 6 spectra types only once within the other wavenumber ranges.

Spectral description. In Fig. 2 the three A_1 spectra (A_{xx}, A_{yy}, A_{zz}) are shown up to 1000 cm^{-1}, and in Fig. 3 the A_2, B_1 and B_2 spectra. These spectra mainly reflect the detectable vibrational modes for the polyanion $Mo_7O_{24}^{6-}$, which will be the main topic of this paper. In Fig. 4 the spectra of the water of crystallization in the range 2900–3600 cm^{-1} are shown. One must, however, be aware that the spectra presented are of the molecules in a crystal field, and that solid state effects may occur.

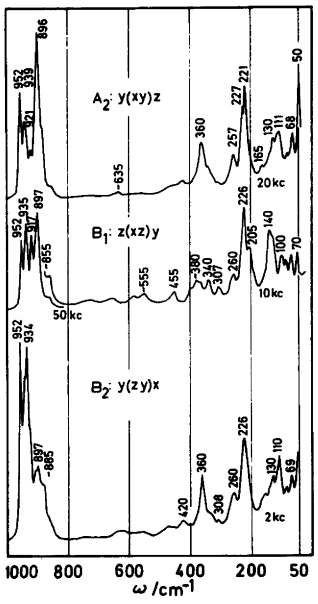

Fig. 3. Polarized Raman spectra of $Na_6Mo_7O_{24}(H_2O)_{14}$, representing the "non symmetric spectra" of the anion $Mo_7O_{24}^{6-}$.

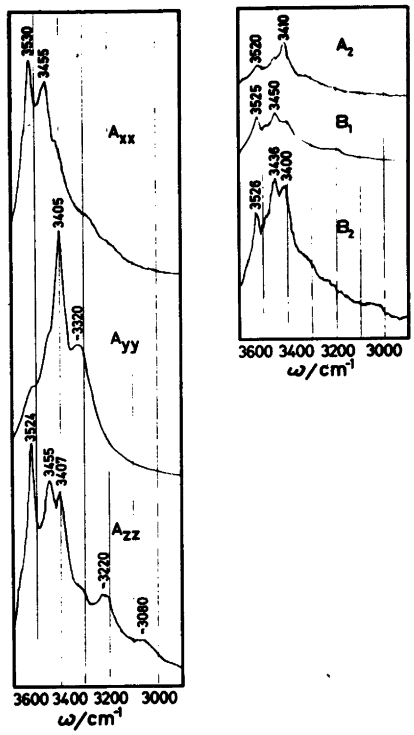

Fig. 4. Polarized Raman spectra of the $Na_6Mo_7O_{24}(H_2O)_{14}$ single crystal, representing the O–H stretch vibrational modes of the water of crystallization.

The difference between the spectra of A_1 phonons ("symmetric spectra") in Fig. 2 and the "nonsymmetric spectra" in Fig. 3 is the greater intensities of the former. The number of peaks is, however, very nearly the same (~15-8) in all the spectra. Owing to the lack of automatic intensity measurements, no depolarization ratio has been calculated. The great similarity of the A_1 to the other spectra thus indicates an almost complete correlation splitting of each fundamental mode of a free anion into the four Raman active components A_1, A_2, B_1 and B_2. Most of the peaks thus seem to represent A_1, *i.e.* symmetrical vibrational modes, since they in general have the highest intensity.

If we compare the A_1 species spectra in Fig. 2 the following observations can be made: (i) that the A_{xx} and A_{zz} have great similarities and thus differ from the A_{yy} spectrum, (ii) that the A_{yy} spectrum has many peaks of high intensity in the range 150–300, where

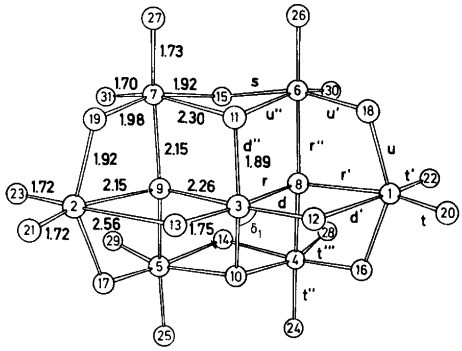

Fig. 5. The structure of the anion $Mo_7O_{24}^{6-}$ with an idealized C_{2v} symmetry. The bond lengths are given in Å, and defined as internal coordinates. The atoms 1 – 7 are Mo, and the other oxygen atoms.

A_{xx} and A_{zz} have only one strong band, (iii) that the A_{xx} and A_{zz} spectra have broad low intensity bands in the range 500 – 800, where A_{yy} shows almost no activity.

The great similarity of A_{xx} and A_{zz} spectra will be discussed below.

Vibrational modes and structure

The low site symmetry and the large extent of correlation splitting diminishes the possibilities for an interpretation of spectra by means of selection rules. Another method will therefore be attempted below.

In order to correlate the spectra of different symmetry with the orientation of the Mo_7O_{24}

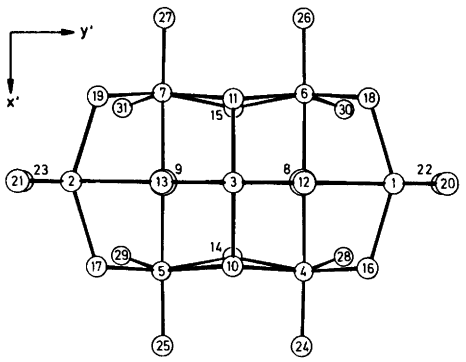

Fig. 6. A top view of the $Mo_7O_{24}^{6-}$ anion, projected on the molecular $x'y'$-plane, *i.e.* the molecular z' axes is perpendicular to the plane of the paper.

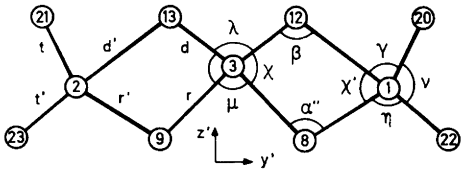

Fig. 7. An Mo_3O_8 fragment, which is the central section of $Mo_7O_{24}^{6-}$, projected on the molecular $y'z'$-plane.

groups within the unit cell, some structural models are depicted in Figs. 5 – 10.

In Fig. 5 an idealized bond model of Mo_7O_{24} with C_{2v} symmetry is depicted, which in Fig. 6 is projected on the molecular $x'y'$-plane. In Fig. 7 the "central section", a Mo_3O_8 fragment of the anion, is projected on the $y'z'$-plane (to show the unit which primarily interacts with the y component of the exciting light, *i.e.* gives A_{yy} spectra). An overall view of several $Mo_7O_{24}^{6-}$ anions linked by sodium ions is depicted in Fig. 8. The "central section" in the y-direction is recognized as the longest part of each polyhedron. This figure shows that the "central section" of a Mo_7O_{24} group is aligned almost parallel with the crystal y-axis, *i.e.* the y' and y axes are almost parallel. The molecular $y'z'$ and crystal yz planes are, however, not parallel. The "molecule" is tilted throughout the crystals so that the angle between the $y'z'$ and xy planes is respectively positive and negative every second time. The molecular x' and z' axes will thus alter while the y' axes will not, compared to the crystal axes. This geometrical phenomenon thus explains the great similarities between the A_{xx} and A_{zz} spectra. Spectral differences would have been expected with the x' and z' axes parallel with the crystal axes.

The Mo_7O_{24} spectra (Figs.2 – 3) can now be examined in conjunction with the orientation of the anion (Figs.5 – 8). For instance, the A_{yy} spectrum will be examined especially in combination with Fig. 7. The notation $x(yy)z$ means that it is the y component of the laser beam which interacts with the anions in the crystal, and that the y component of the scattered light in the z direction is observed. In the spectra the peaks can be divided into three ranges, *viz.* below 400, 400 – 800 and above 800 cm^{-1}.

The characteristic peaks from 150 to 300 cm^{-1} in the A_{yy} spectrum are mainly due to bending vibrational modes, and the main cause is found within the co-planar Mo_2O_2 rings (see Fig. 7). There

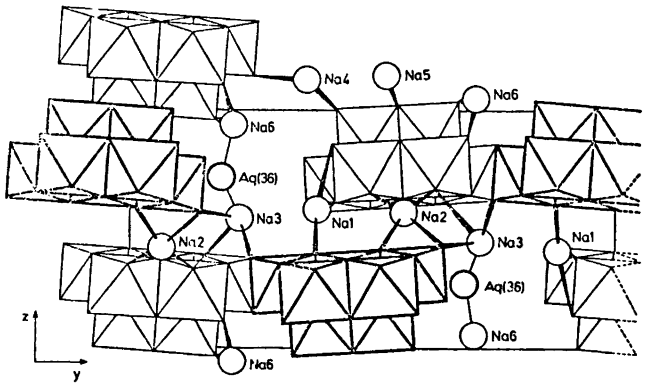

Fig. 8. A schematic drawing of the connection between $Mo_7O_{24}^{6-}$ anions in a crystalline phase.

are, in addition to those in Fig. 7, two Mo_2O_2 rings in Fig. 5 (4-10-5-14 and 6-11-7-15). It is especially the peaks 150, 262 and 306 cm^{-1} which do not occur in the A_{zz} spectrum and they can thus be assigned to bendings such as $\gamma, \eta, \beta, \chi, \alpha''$ and μ (see Fig. 7). In this way peaks occurring only (or with large intensity) in one of the three A_1 spectra can be assigned to a bending mode in one of the *x*-, *y*- or *z*-directions respectively. However, there are too great similarities in the A_{xx} and A_{zz} spectra in this cases to completely allow such assignments. There are some peaks below 150 cm^{-1}, which can be considered as lattice modes. The peak in common at about 220 cm^{-1} for all three spectra must be due to bending of the angle between the terminal oxygen bonds (v, v' *i.e.* ∠24-4-28 *etc.*). These angles have the greatest changes in the *x*- and *z*-directions and the 220 peak is by far the most intense one in the A_{xx} and A_{zz} spectra. There is also a 220 cm^{-1} band with a high intensity, however, little shifted in the three "non-symmetric spectra", see Fig. 3. Since the angles are made up of terminal bonds, the non-symmetric vibrational modes may also have relatively high intensities. It may be noticed that the shift is towards higher wavenumbers compared with the symmetric bendings.

Another band in common is that at about 370 cm^{-1}, which may be a depolarized band. This band can be considered as a "trade mark" of condensed polymolybdates, since it occurs in most other Mo-containing polyanions, even heteropolymolybdates.[11] Since this band occurs in so many different compounds and there is no difference regarding the geometry of detection for Mo_7O_{24}, this band cannot be due to a single type of vibrational mode, *i.e.* one specific bond or angle. One fragment commonly occurring in most polymolybdates is a puckered Mo_3O_3 ring (see Fig. 9). There are four such rings in the $Mo_7O_{24}^{6-}$ anion, which can be considered to give rise to the 370 cm^{-1} band. It is not easy to decide which kind of vibrational mode gives the main contribution to this peak. Most probably there are combinations of bendings and torsions and perhaps even stretchings. The large intensity for the 370 peak in the "non-symmetric spectra" in Fig. 3 supports the idea that it is not a single type of vibrational mode causing this peak.

The 451 peak in the A_{yy} spectrum can be assigned to a bending in the *y*-direction. The most probable candidates are the angles 12-3-13(λ) and 8-3-9(μ). In a theoretical calculation of vibrations, the angle λ obtained the value 554 cm^{-1}.[13] This high value was obtained because the bending force constant was adjusted to give a wavenumber as close as possible to the experimental value at about 555 cm^{-1}.[8,8,11,12] These single crystal spectra (A_{xx} and A_{zz}) show that the 555 peak cannot be a bending in the *y*-direction. The theoretical calculation and assignment is thus incorrect in this sense.

In the range 500 – 800 cm^{-1}, the A_{yy} spectrum has only a small activity, while the A_{xx} and A_{zz} spectra have peaks at about 550, 650 and 750 cm^{-1}. These peaks are to be explained by modes which have no analogues in the *y*-direction. The peaks can be described as being due to "breathings" of the anion, as was found for the anion $Mo_5P_2O_{23}^{6-}$.[16] It means that the dimensions of the anion are changing either in the *x* or the *z*, but not in the *y* direction. It also appears from the structure (see Figs. 5 and 8) that the anion is rather stiff in the *y* direction, while the

two dioctahedra, one on each side of the central Mo_3O_8 section, are less "tightly bonded". In fact they are reminiscent of the wings of a bird. The low peak intensities also indicate some kind of "breathing" modes, which must have very small vibrational amplitudes.

The peaks in the range 800 – 1000 cm^{-1} are due to stretch vibrational modes of short Mo – O bonds. It is obviously the short terminal oxygen bonds which give rise to the most intense peaks. In the A_{yy} spectrum the 952 peak is thus assigned to t and/or t', and in A_{xx} and A_{zz} the 939 peak to t'' and/or t'''. Vibrational modes involving the Mo – O bonds denoted d must be most intense in the A_{yy} spectrum.[13] Because of the short bond length (1.75 Å) the 922 peak is the most probable candidate. The other Mo – O bonds are not easy to assign without any guidance from isotope substituted spectra. The asymmetric spectra have also some high intensity peaks, *e.g.* at about 896, 934 and 952 cm^{-1}. The bonds t, t', d and r' are active only in B_2 except A_1, and d'' is active only in B_1 except A_1.[13] The remainder of the short bonds are active in all four species. These selection rules thus confirm the 952 peak as a t and t' vibrational mode. The 934 peak (B_2) can be an asymmetric vibrational mode of the d bond and the 917 peak (B_1) can be assigned to the d'' bond. The 896 peak appears somewhat shifted in all kinds of spectra, and is thus very difficult to assign. Owing to the very high intensity in A_2 even asymmetric vibrational modes of terminal oxygen bonds (t'', t''') may be involved. Most probably there are several non-resolved peaks in this region, which prevent a more complete description.

The spectra of the crystal waters in Fig. 4 also depend on the orientation of the crystal. In this case differences among all the spectra, and especially among the three A_1 spectra, occur. All the peaks are due to O – H stretch vibrations. This implies that the waters of crystallization have fixed orientations.

The A_{zz} spectrum is the most detailed one, with several well-resolved peaks, and no new peak is found in any of the other spectra in Fig. 4. The two peaks in the A_{xx} spectrum originate most probably from only one type of water molecule, with two different O – H bond lengths. Support for this idea is that there is only one bending vibrational mode [$\delta(H_2O)$, at 1667 cm^{-1}] for the A_{xx} orientation. The three A_1 spectra can thus be considered to represent two different types of water molecules, one represented by the 3455 and 3520 peaks (A_{xx}), and the other by the 3405 peak (A_{yy}). The A_{zz} spectrum has thus contributions from both types of waters. There are also two bending peaks (at 1602 and 1668 cm^{-1}) for the A_{zz} symmetry.

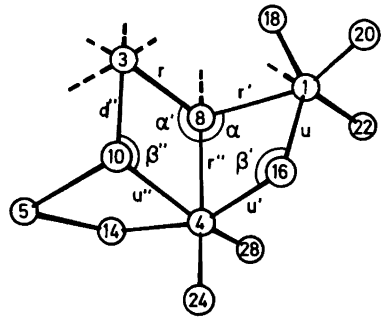

Fig. 9. A fragment of $Mo_7O_{24}^{6-}$ showing one of the puckered Mo_3O_3 rings, *viz.* 1-16-4-10-3-8.

In Figs 8 and 10 one can find two types of waters, namely (i) waters coordinated to only one Na^+, and (ii) waters shared by Na^+ ions. This classification is coarse and there are waters which differ from the two main types, as is also indicated by several shoulders and peaks at lower wavenumbers in the A_{zz} spectrum.

The type of water represented by the 3405 peak (A_{yy}) has identical bond lengths, which should be longer than the bonds in the water represented by the A_{xx} spectrum. For the two-coordinated waters the bonds $Na^+ - O(Aq) - Na^+$ are, in general, different in length, 0.18 Å at the most,[18] which can result in asymmetric O – H bonds, and thus give an A_{xx} type of spectrum. The single coordinated water [Aq(2), Aq(4)],[18] being stronger bonded to Na^+, should thus give the 3405 peak.

The B_2 spectrum has by far the greatest intensity of all the asymmetric spectra. The selection rules for a free water molecule with C_{2v} symmetry allows vibrational modes in B_2, only if the H_2O lies in the yz-plane. B_1 activity corresponds to a molecule in the xz-plane. Accordingly most of the waters thus have the hydrogens orientated in the yz-plane.

DISCUSSION AND CONCLUSION

The similarity of spectra in Figs. 2 and 3 suggests complete correlation splitting. On the other hand the differences in A_{xx} and A_{zz} compared to A_{yy} (Fig. 2) tend to rule out complete correlation splitting. The explanation of this is, as discussed earlier, that the molecular x' and z' axes have a different

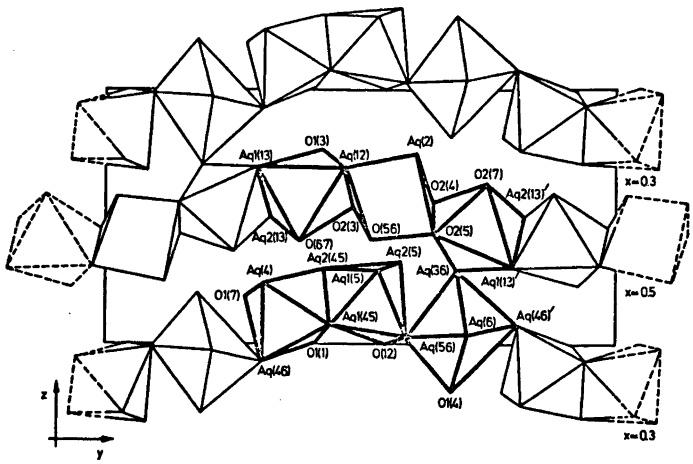

Fig. 10. A schematic drawing of the arrangement of $NaO_x(H_2O_{6-x}$ octahedra.

direction than the crystal axes, while the y' and y axes are almost parallel. The observed correlation splitting is thus not due to intermolecular couplings in the unit cell, but to the geometrical facts mentioned.

Almost all the peaks obtained in this work have been reported for the Raman spectrum of the anion $Mo_7O_{24}^{6-}$ in aqueous solution. However, the intensity relations of the peaks are quite different. Especially the "solution peaks" have much lower intensities than the corresponding peaks obtained for the A_{yy} spectrum. However, the peak positions are not altered much when the anion is transferred from an aqueous to a crystal field. This implies that there exists a lattice of cations also in aqueous solution of high concentration, and that the aqueous and crystal fields are comparable, at least in their effects on $Mo_7O_{24}^{6-}$.

Some comparisons can be made, since several interpretations of vibrational modes of other Mo-oxo-complexes have been reported.[23-25] Table 1 contains a compilation of assignments for mono-

Table 1. A compilation of the assignments for Mo(VI)-oxo-complexes of different nuclearity.

Modes	MoO_2F_4 Ref. 23	$Mo_2O_5(ox)_2(H_2O)_2^{2-}$ I, Ref. 23	$Mo_2O_4(ox)_2(H_2O)_2^{2-}$ II, Ref. 23	$Mo_7O_{24}^{6-}$ Ref. 6	This work
ν^s [$Mo(O_t)_2$]	951	958 R	971	900	952 (t, t')
		919 R			
ν^{as} [$Mo(O_t)_2$]	920	962 IR	975		939 (t'', t''')
		917 IR			
δ[$Mo(O_t)_2$]	385	385		360	224 (ν, ν')
ν^s (Mo–O–Mo)		235		400–600	
ν^{as} (Mo–O–Mo)		851		750–840	
δ (Mo–O–Mo)		130?		219	
ν^s (Mo_2O_2)			499		850–900
ν^{as} (Mo_2O_2)			578		(d, d', d'', r, r')[a]
δ (Mo_2O_2)			224		120–300
					(γ, η, β, α'', μ)
"Mo_3O_3 modes"					370
"Breathing modes" –Mo–O–Mo–					550–750

[a] Interpreted as $Mo-O_b$ stretches.

and dinulcear complexes as well as for the heptamolybdate complex given. The dinuclear Mo complexes found in the solids $K_2Mo_2O_5(Ox)_2(H_2O)_2$ (I)[26] and $BaMo_2O_4(Ox)_2(H_2O)_2$ (II),[27] have one and two oxygen bridges, respectively.

The stretches for the terminal oxygens (O_t) seem to be independent of the nuclearity. There is thus no mixing with other vibrational modes. Griffith[23] assigns peaks at about 360 cm^{-1} to Mo=O bends. The spectra in this work do not support the same assignment for $Mo_7O_{24}^{6-}$, and the 220 peak is assigned to Mo=O bends. It can, however, be noticed that for structures I and II there are peaks at 235 (I) and at 224 (II) cm^{-1}, respectively.

The stretch force constant, *f*, is dependent on the Mo–O bond length, especially for terminal oxygens.[28] Short bond lengths give high *f*-values, which will result in peaks at high wavenumbers. The bridging $Mo-O_b$ bonds for structures I and II are in general shorter than those in $Mo_7O_{24}^{6-}$, *viz.* 1.88 Å (I); 1.88, 1.93 Å (II) compared with 1.75–2.56 Å for $Mo_7O_{24}^{6-}$. Despite this, the $Mo_7O_{24}^{6-}$ anion has several peaks assigned to bridging oxygens at higher wavenumbers, *cf.* $\nu(Mo_2O_2)$ in Table 1. In this case it is most probably the terms of the atomic masses, included in the kinetic energy ($T=\frac{1}{2}mx^2$), which give rise to the peaks at high wavenumbers.

The assignments for the complexes I and II thus differ from those for the heptanuclear $Mo_7O_{24}^{6-}$ complex. One conclusion is thus that one cannot compare large and very condensed structures with smaller ones. This was also clearly shown in a theoretical study of $PMo_{12}O_{40}^{3-}$ and small fragments of the same anion.[29]

Another condensed anion with known structure is $Mo_6O_{19}^{2-}$, of which both Raman and IR spectra are recorded.[25] The reported assignments give Mo $-O_b$ and $Mo-O_t$ vibrational modes in the ranges 470–810 and 950–980 cm^{-1}, respectively. In $Mo_6O_{19}^{2-}$ each Mo has only one terminal oxygen (O_t) and there are only three types of Mo–O bonds in all, whereas in $Mo_7O_{24}^{6-}$ there are 14.[13] Despite that, the reported peaks and assignments are on the whole comparable with those given in this work.

Thus a conclusion is that it is not possible to isolate parts such as

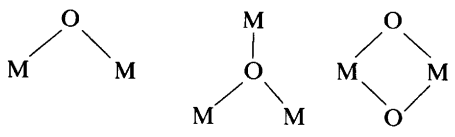

and assign them to unique vibrational modes. The vibrational conditions and peak positions thus depend upon the way in which such units are bonded to the rest of the complex.

There is also a large mixing of the terms for the kinetic energy for multibonded atoms. It is therfore not possible to talk in terms of group frequencies for condensed complexes such as $Mo_7O_{24}^{6-}$. It is thus mostly the outermost atoms, or atoms with few bonds that do have quite assignable vibrational modes.

Acknowledgements. I thank Dr. Britt Hedman for permission to reproduce Figs. 8 and 10 and also for many stimulating discussions. Thanks are also due to Dr. Michael Sharp for correcting the English of the present paper. The work forms part of a program financially supported by the Swedish Natural Science Research Council.

REFERENCES

1. Lindqvist, I. *Ark. Kemi 5* (1951) 568.
2. Sasaki, Y. and Sillén, L. G. *Acta Chem. Scand. 18* (1964) 1014.
3. Sillén, L. G. *Pure Appl. Chem. 17* (1968) 55.
4. Sillén, L. G. In Martell, A. E., Ed., *Coordination Chemistry*, Van Nostrand-Reinhold, New York 1971, Vol. 1, Chapter 9.
5. Aveston, J., Anacher, E. W. and Johnson, J. S. *Inorg. Chem. 3* (1964) 735.
6. Griffith, W. P. and Lesniak, P. J. B. *J. Chem. Soc. A* (1969) 1066.
7. Schönfeld, B. *Untersuchungen am wässerigen Isopolymolybdatlösungen*, Diss., Georg-August-Universität, Göttingen 1973.
8. Hunnius, W.-D. *Habilitationsschrift der Freien Universität Berlin*, Berlin 1977.
9. Tytko, K.-H. and Schönfeld, B. *Z. Naturforsch. B 30* (1975) 471.
10. Tytko, K.-H., Petridis, G. and Schönfeld, B. *Z. Naturforsch. B 35* (1980) 45.
11. Lyhamn, L. and Pettersson, L. *Chem. Scr. 12* (1977) 142.
12. Lyhamn, L. *Chem. Scr. 12* (1977) 153.
13. Lyhamn, L. and Cyvin, S. J. *Z. Naturforsch. A 34* (1979) 867.
14. Lyhamn, L., Cyvin, S. J., Cyvin, B. N. and Brunvoll, J. *Z. Naturforsch. A 31* (1976) 1589.
15. Lyhamn, L., Cyvin, S. J., Cyvin, B. N. and Brunvoll, J. *Spectrosc. Lett. 12* (1979) 101.
16. Lyhamn, L. *Experimental and Theoretical Studies of Some Mo(VI) Polyanion Complexes, with Special Emphasis on the Use of Potentiometric, UV and Raman Methods*, Diss., the University of Umeå, Umeå 1980.

17. Stout, G. H. and Jensen, L. H. *X-Ray Structure Determination – A Practical Guide*, Macmillan, New York 1968.
18. Sjöbom, K. and Hedman, B. *Acta Chem. Scand. 27* (1973) 3673.
19. Gilson, T. R. and Hendra, P. J. *Laser Raman Spectroscopy*, Wiley, London 1970.
20. Loudon, R. *Adv. Phys. 13* (1964) 423.
21. Ross, S. D. *Inorganic Infrared and Raman Spectra*, McGraw-Hill, London 1972.
22. Damen, T. C., Porto, S. P. S. and Tell, B. *Phys. Rev. 142* (1966) 570.
23. Griffith, W. P. *J. Chem. Soc. A* (1969) 211.
24. Griffith, W. P. *Coord. Chem. Rev. 5* (1970) 459.
25. Mattes, R., Bierbüsse, H. and Fuchs, J. *Z. Anorg. Allg. Chem. 385* (1971) 230.
26. Cotton, F. A., Morehouse, S. M. and Wood, J. S. *Inorg. Chem. 3* (1964) 1603.
27. Cotton, F. A. and Morehouse, S. M. *Inorg. Chem. 4* (1965) 1377.
28. Cotton, F. A. and Wing, R. M. *Inorg. Chem. 4* (1965) 867.
29. Lyhamn, L. and Cyvin, S. L. *Spectrosc. Lett. 10* (1977) 907.

Received December 14, 1981.

Acta Chemica Scandinavica A 36 (1982) 605–610

The Crystal Structure of Tetrapyridine Copper(I) Perchlorate and Tetrapyridine Silver(I) Perchlorate at 260 K

KARIN NILSSON and ÅKE OSKARSSON

Inorganic Chemistry 1, Chemical Center, University of Lund, Box 740, S-220 07 Lund 7, Sweden

The crystal structures of $[M(C_5H_5N)_4]ClO_4$, where M = Cu or Ag, have been determined from X-ray intensity data collected at 260 K with a CAD-4 diffractometer. The compounds are isostructural. The space group is $I\bar{4}$ with $Z=2$; $a=12.471(3)$, $c=6.894(2)$ for the Cu and $a=12.874(1)$, $c=6.748(4)$ Å for the Ag compound. The refinements converged to $R=0.040$ (Cu) and $R=0.026$ (Ag). The structure is composed of discrete ions $[M(C_5H_5N)_4]^+$ and ClO_4^-. The coordination geometry is close to tetrahedral with metal–nitrogen distances 2.046(4) (Cu) and 2.322(3) (Ag). The difference between the distances Ag–N and Cu–N is larger than that found between the distances Ag–P and Cu–P in complexes formed by ligands coordinating *via* phosphorous. This indicates that the difference in covalency is larger between the bonds Ag–P and Cu–P than between the bonds Ag–N and Cu–N.

The crystal structure determination of $[Cu(C_5H_5N)_4]ClO_4$ and $[Ag(C_5H_5N)_4]ClO_4$ was undertaken as part of a research programme that deals with complexes formed in pyridine solution. It is of interest to find correlations between thermodynamic parameters, such as the enthalpy and entropy of complex formation in solution, and structural properties such as coordination geometries and steric effects. The latter can be established in the solid state by diffraction methods.

Since the silver compound slowly loses pyridine at room temperature the data collection was made at 260 K. Tetrapyridine copper(I) perchlorate has previously been investigated at room temperature.[1] We have redetermined the structure at 260 K.

0302-4377/82/070605-06$02.50

EXPERIMENTAL

Preparation of crystals. $[Cu(C_5H_5N)_4]ClO_4$ was prepared by treating $[Cu(CH_3CN)_4]ClO_4$ with pyridine.[2] The needle-shaped crystals were light yellow with a slight green tint. Copper was determined by EDTA titration (found 13.2 %, calc. 13.3 %). $[Ag(C_5H_5N)_4]ClO_4$ was prepared by dissolving silver(I) perchlorate in pyridine to a saturated solution. On cooling, colourless crystals were formed. Silver was determined by Volhard titration (found 20.6 %, calc. 20.6 %).

X-Ray data collection. Weissenberg photographs for the Ag-compound taken at 260 K revealed the Laue class $4/m$ and the systematic extinctions hkl, $h+k+l\neq 2n$ consistent with the space groups $I4$, $I\bar{4}$ and $I4/m$. For both compounds, cell dimensions were obtained at 260 K by least squares calculations from θ-values determined as $\theta_{hkl}=(\omega_{hkl}-\omega_{\bar{h}\bar{k}\bar{l}})/2$, (Table 1). A CAD-4 diffractiometer in the bisecting mode, measuring $\omega_{\bar{h}\bar{k}\bar{l}}$ at negative θ angle, was used. The cooling device is described previously.[3]

The intensity data sets were collected at 260 K with the same diffractometer. Zr-filtered Mo$K\alpha$ radiation was used and reflexions $-17\leq h\leq 17$, $-17\leq k\leq 17, 0\leq l\leq 8$ were measured for both compounds. During the data collections three standard reflexions were measured at regular intervals. No systematic variation in their intensities or in the orientation of the crystals was found. Information concerning the collection and reduction of the data sets and the refinements of the crystal structures is given in Table 1. The values of I and $\sigma_c(I)$ were corrected for Lorentz, polarization and absorption effects, the latter by numerical integration. The values of $\sigma_c(I)$ are based on counting statistics. Reflexions with $I\leq 2.5\ \sigma_c(I)$ were considered insignificantly different from the background and excluded from all subsequent calculations. The

Table 1. Crystal data, collection and reduction of intensity data and least-squares refinement.

	$[Cu(C_5H_5N)_4]ClO_4$		$[Ag(C_5H_5N)_4]ClO_4$
Crystal size (mm)	$0.16 \times 0.19 \times 0.25$		$0.64 \times 0.36 \times 0.25$
a(Å)	12.471(3)		12.874(1)
c(Å)	6.894(2)		6.748(4)
V(Å^3)	1072.2		1118.4
D_x(g cm^{-3})	1.48		1.55
Z		2	
$\bar{\lambda}$(Å)		0.7093	
μ(cm^{-1})	12.2		10.3
Range of transmission factor	0.749 – 0.844		0.779 – 0.799
θ interval (°)		3 – 29	
$\omega - 2\theta$ scan width, $\Delta\omega$(°)		1.0 + 0.5 tan θ	
$\sigma_c(I)/I$ requested in a scan		0.030	
Maximum recording time (s)		120	
Number of reflexions measured	1898		2987
Number of reflexions with $I > 2.5\sigma(I)$	1249		1848
Number of independent reflexions with $I > 2.5\sigma(I)$,m	539		539
Number of parameters refined, n	75		75
$R = \Sigma(\|F_o\| - \|F_c\|)/\Sigma\|F_o\|$	0.0396		0.0255
$R_w = [\Sigma w(\|F_o\| - \|F_c\|)^2/\Sigma w\|F_o\|^2]^{1/2}$	0.0469		0.0285
$S = [\Sigma w(\|F_o\| - \|F_c\|)^2/(m-n)]^{1/2}$	2.8		1.5
C (weighting function)	0.010		0.015

intensities of symmetry dependent reflexions were then averaged.

STRUCTURE DETERMINATION AND REFINEMENTS

Of the possible space groups only $I\bar{4}$ gives a reasonable coordination geometry for the metal. The positions of Ag and Cl were deduced from a vector map. The positions of the other non-hydrogen atoms in the silver compound were located in a difference map. The positional and anisotropic thermal parameters were refined by fullmatrix least-squares, minimizing $\Sigma w(|F_o| - |F_c|)^2$ with weights $w = [(\sigma_c^2/4|F_o|)^2 + (C|F_o|)^2]^{-1}$. The constant C was adjusted so that constant values of $\langle w(|F_o| - |F_c|)^2 \rangle$ were obtained in different $|F_o|$and sin θ intervals. The hydrogen atoms were included in the final cycles of refinement. They were placed geometrically (C – H = 1.0 Å) and only the isotropic temperature factor was refined for each H-atom. Scattering factors, with corrections for anomalous dispersion, were taken from the International Tables.[4]

The structure of the Cu-compound was refined using the parameters of the Ag-compound as a starting set. This model for the Cu-compound is essentially the same as the one reported by Lewin *et al.*[1]

Details of the refinements are given in Table 1. The final positional and thermal parameters are given in Tables 2 and 3 and Table 4 gives selected interatomic distances and angles. A list of structure factors may be obtained through the authors.

DESCRIPTION OF THE STRUCTURES

The compounds investigated are isostructural, consisting of discrete $[M(C_5H_5N)_4]^+$ and ClO_4^- ions. The crystal packing is shown in Fig. 1. The complexes are stacked in columns along c and the shortest metal – metal distance is the vector c [Cu···Cu = 6.894(2) and Ag···Ag = 6.748(4) Å]. In this direction the larger silver(I) ion thus gives a more efficient packing of the complexes than the smaller copper(I) ion. The cation, as well as the

Table 2. Atomic coordinates ($\times 10^4$) and thermal parameters $\beta \times 10^4$ and B_{iso} with e.s.d.'s for $[Cu(C_5H_5N)_4]ClO_4$. The form of the temperature factor is exp $(-\beta_{11}h_2 - 2\beta_{12}hk - \ldots)$.

	x	y	z	β_{11},B_{iso}	β_{22}	β_{33}	β_{12}	β_{13}	β_{23}
Cu	5000	5000	5000	58.5(7)	58.5(7)		230(4)		
N	4258(3)	3892(3)	3271(7)	57(3)	52(3)	207(11)	−2(2)	−4(5)	1(5)
Cl	0	5000	2500	58(1)	58(1)	210(7)			
C(1)	3489(5)	4187(4)	2026(9)	92(5)	58(4)	226(15)	−6(3)	−51(7)	23(6)
C(2)	3004(6)	3485(6)	719(10)	104(6)	100(6)	246(16)	−24(5)	−57(8)	22(9)
C(3)	3339(6)	2431(5)	688(9)	105(6)	85(5)	245(17)	−39(4)	−5(8)	15(7)
C(4)	4109(5)	2120(5)	1974(11)	86(5)	55(4)	316(19)	−9(3)	12(8)	−23(7)
C(5)	4540(4)	2853(4)	3239(9)	56(3)	59(4)	277(15)	3(3)	−10(7)	−1(7)
O	154(7)	4115(6)	1381(13)	195(8)	194(8)	777(35)	7(7)	22(15)	−266(15)
H(1)	3252	4955	2030	2030	6(1)				
H(2)	2431	3753	−171	10(2)					
H(3)	3022	1914	−257	6(2)					
H(4)	4359	1355	1999	10(2)					
H(5)	5089	2598	4206	3(1)					

Table 3. Atomic coordinates ($\times 10^4$) and thermal parameters $\beta \times 10^4$ and B_{iso} with e.s.d's for $[Ag(C_5H_5N)_4]ClO_4$. The form of the temperature factor is exp $(-\beta_{11}h^2 - 2\beta_{12}hk - \ldots)$.

	x	y	z	β_{11}, B_{iso}	β_{22}	β_{33}	β_{12}	β_{13}	β_{23}
Ag	5000	5000	5000	75.5(3)	75.5(3)	329(2)			
N	4180(3)	3747(2)	3083(6)	70(2)	61(2)	300(10)	4(2)	−15(4)	2(4)
Cl	0	5000	2500	73(1)	73(1)	232(5)			
C(1)	3460(4)	3990(3)	1760(9)	94(3)	75(3)	403(16)	1(2)	−72(6)	36(6)
C(2)	3094(4)	3288(4)	428(8)	111(4)	117(4)	327(21)	−22(3)	−69(7)	37(7)
C(3)	3479(4)	2285(4)	409(10)	109(3)	103(3)	355(25)	−41(3)	11(7)	−24(7)
C(4)	4188(4)	2036(3)	1799(8)	95(3)	65(3)	375(15)	−7(2)	6(7)	−2(6)
C(5)	4521(3)	2765(3)	3104(7)	73(2)	67(2)	325(13)	3(2)	−23(5)	10(5)
O	230(4)	4144(4)	1311(4)	151(4)	157(4)	599(18)	20(3)	1(8)	−160(8)
H(1)	3130	4700	1910	7(1)					
H(2)	2470	3480	−450	14(3)					
H(3)	3100	1770	−330	9(2)					
H(4)	4480	1310	1830	12(2)					
H(5)	5000	2650	4250	5(1)					

anion, have the symmetry $\bar{4}$. The coordination polyhedra around the metal atoms are tetragonal disphenoids but the deviation from a tetrahedron is small for both compounds as shown by the N−M−N angles (Table 4).

The atoms of the pyridine molecule are designated in Fig. 2. The pyridine molecules are almost planar (Table 4) and the metal ions are situated less than 0.4 Å from this plane. Distance and angles within the pyridine molecule are much the same in both compounds and they agree well with those observed in other pyridine complexes.[5,6] The geometry of the pyridine molecule is not perceptibly influenced by the coordination to a metal ion as judged from a microwave study of pyridine,[7] where the following distances and angles were found: N−C=1.340(1) Å, C−C=1.394(1) and 1.395(1) Å, N−C−C=123.9°, C−N−C=116.8°, C−C−C=118.5 and 118.3°. The smaller C−C distances observed in the solid state are most probably artifacts due to the libration motion of the pyridine molecule.

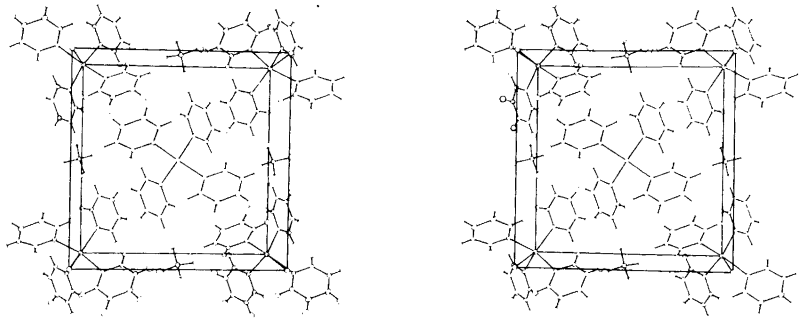

Fig. 1. Stereoscopic view of the unit-cell content.

The perchlorate ion is ordered in both compounds and the geometry is close to tetrahedral (Table 4). The difference observed between the Cl – O distance in the two compounds, 0.034(10) Å, is hardly significant.

DISCUSSION

The Cu – N and Ag – N distances in $[M(C_5H_5N)_4]ClO_4$ are somewhat longer than found in other solvates containing N-donors in a tetrahedral arrangement. In the acetonitrile solvate,[8] $[Cu(CH_3CN)_4]ClO_4$, the average Cu – N = 1.99(1) Å. In the polymeric compounds Cu(NC-

Table 4. Selected interatomic distances (Å) and angles (°) and *r.m.s.* deviation (Å) from the least-squares planes through the pyridine rings.

The superscripts (i)–(iv) denote the following transformation applied to *x,y,z* values given in Tables 2 and 3:

(i) $1-x, 1-y, z$ (ii) $y, 1-x, 1-z$
(iii) $1-x, 1-y, z$ (iv) $1/2-y, 1/2+x, 1/2-z$

	Ag	Cu		Ag	Cu
(a) The coordination polyhedron					
M – N	2.322(3)	2.046(4)	N – M – N^{i}	112.3(2)	108.8(3)
N...N^{i}	3.856(4)	3.326(5)	N – M – N^{ii}	108.1(1)	109.8(1)
N···N^{ii}	3.759(4)	3.349(5)			
(b) The pyridine molecule					
N – C(1)	1.324(6)	1.339(8)	N – C(1) – C(2)	122.1(4)	123.5(5)
C(1) – C(2)	1.359(8)	1.395(9)	C(1) – C(2) – C(3)	120.2(5)	118.5(6)
C(2) – C(3)	1.384(8)	1.379(10)	C(2) – C(3) – C(4)	117.3(5)	118.3(6)
C(3) – C(4)	1.348(8)	1.363(10)	C(3) – C(4) – C(5)	120.1(4)	120.0(6)
C(4) – C(5)	1.356(7)	1.373(9)	C(4) – C(5) – N	122.9(4)	123.4(5)
C(5) – N	1.339(5)	1.342(7)	C(5) – N – C(1)	117.4(4)	116.3(5)
R.m.s. dev	0.0093	0.0085			
(c) The perchlorate ion					
Cl – O	1.394(5)	1.360(8)	O – Cl – O^{iii}	109.8(5)	110.9(7)
			O – Cl – O^{iv}	109.3(2)	108.8(4)

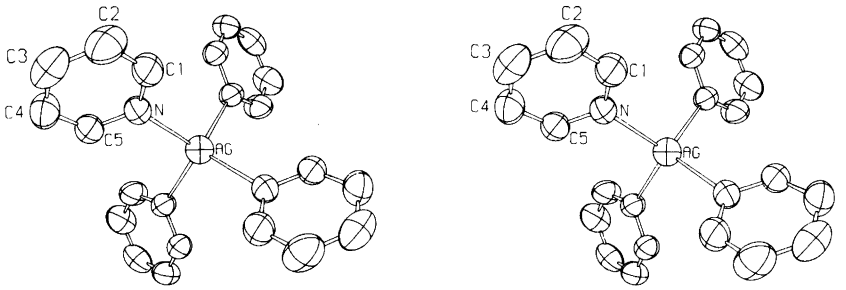

Fig. 2. Stereoscopic view of the $[Ag(C_5H_5N)_4]^+$ ion.

$(CH_2)_4CN)_2NO_3$[9] and $Ag(NC(CH_2)_4CN)_2ClO_4$[10] M–N = 1.98 and 2.28 Å, respectively (Table 5). The difference between the distances Cu–N and Ag–N is almost the same as in the pyridine solvates, however.

For a comparison between Cu–N and Ag–N distances, complexes other than mononuclear tetrahedral ones are also of interest. The cluster compounds $[MIC_5H_{11}N]_4$, M = Cu[11] and Ag,[12] contain an M_4I_4 core. Each metal atom is also coordinated to one nitrogen atom, resulting in a tetrahedral arrangement around M. Again, the difference between the distances Cu–N and Ag–N is almost the same as for the pyridine solvates. Even if the ligands and the coordination geometries are fairly different this difference is evidently close to 0.28 Å (Table 5).

In compounds where Cu(I) and Ag(I) are coordinated to phosphors the difference between the distances Cu–P and Ag–P is considerably smaller. Thus, in cluster compounds with M_4X_4 core, analogous to those discussed above, the difference is only ≃0.20 Å (Table 5). The same difference is found for the pair[13] MClPP, M = Cu or Ag.

The distance between the metal atom, M, and the ligand atom, X, may be regarded as composed of four terms $d_{M-X} = r_M + r_X + \sigma_{rep,X-X} - \sigma_{cov,M-X}$. Here r_M and r_X are the radii for given coordination numbers observed in ionic compounds, $\sigma_{rep,X-X}$ represents repulsive forces between the ligands[14] and $\sigma_{cov,M-X}$ is a function of the covalency of the M–X bond.[15] If two compounds containing the bonds M_1-X and M_2-X are isostructural, the differences for the two ligands X_1 and X_2 are:

$$\Delta_1 = d_{M_1-X_1} - d_{M_2-X_1} = r_{M_1} - r_{M_2} - \sigma_{cov,M_1-X_1} + \sigma_{cov,M_2-X_1}$$

Table 5. Survey of structure containing M–N and M–P bonds (Å).

	d_{Cu-N}	d_{Ag-N}	$d_{Ag-N} - d_{Cu-N}$	Ref.
$[M(C_5H_5N)]_4ClO_4$	2.046(4)	2.322(3)	0.276(6)	This work
$M(NC(CH_2)_4CN)_2A$[a]	1.98(1)	2.28(1)	0.30(1)	9 and 10
$[MIC_5H_{11}N]_4$	2.052(7)	2.329(15)	0.277(17)	11 and 12
Average			0.278(5)	
	d_{Cu-P}	d_{Ag-P}	$d_{Ag-P} - d_{Cu-P}$	
$[PEt_3MCl]_4$	2.176(2)	2.390(2)	0.214(3)	16 and 17
$[PEt_3MBr]_4$	2.199(2)	2.402(5)	0.203(6)	16 and 17
$[PEt_3MI]_4$	2.254(3)	2.438(2)	0.184(4)	19 and 20
MClPP[b]	2.258(2)	2.458(3)	0.200(4)	13
	2.217(4)	2.411(3)	0.194(5)	
Average			0.201(2)	

[a] A = ClO_4 (Ag) and A = NO_3 (Cu). [b] PP = 2,11-bis(diphenylphosphinomethyl)benzo [*c*] phenanthrene.

$$\Delta_2 = d_{M_1-X_2} - d_{M_2-X_2} = r_{M_1} - r_{M_2} - \sigma_{cov,M_1-X_2} + \sigma_{cov,M_2-X_2},$$

if the difference between the terms $\sigma_{rep,X-X}$ can be neglected.

The difference $\Delta = \Delta_1 - \Delta_2$ is given by:

$$\Delta = (\sigma_{cov,M_2-X_1} - \sigma_{cov,M_1-X_1}) - (\sigma_{cov,M_2-X_2} - \sigma_{cov,M_1-X_2}).$$

The size of Δ thus reflects the difference in covalency between the M_2-X_1 and M_1-X_1 bonds as compared to the M_2-X_2 and M_1-X_2 bonds.

The M – N distances obtained in this study may be compared to the M – P distances observed in the cluster compounds $[PEt_3MCl]_4$ and $[PEt_3MBr]_4$.[16,17] In all compounds compared, the closest distance of approach between atoms in the coordination spheres is longer than their van der Waals contact distances. Therefore, it is reasonable to neglect the repulsive forces between the ligands. The simplified expression derived above should thus be valid, *i.e.:*

$$\Delta = (\sigma_{cov,Ag-P} - \sigma_{cov,Cu-P}) - (\sigma_{cov,Ag-N} - \sigma_{cov,Cu-N})$$

with Δ equal to 0.062(7) and 0.073(9) Å for the chloride and bromide compounds, respectively.

Thermodynamic measurements indicate that among the bonds discussed, the covalent interaction is weakest for the Cu – N-bond,[18] *i.e.:* $\sigma_{cov,Ag-N} > \sigma_{cov,Cu-N}$. Then, since $\Delta > 0$, it follows that $\sigma_{cov,Ag-P} > \sigma_{cov,Cu-P}$. This also conforms with the behaviour of these donor – acceptor atoms in solution, where the largest covalent interaction is expected between Ag and P.[18]

As $\Delta > 0$, it may further be concluded that the difference in covalency is larger between the bonds Ag – P and Cu – P than between the bonds Ag – N and Cu – N.

Acknowledgements. We wish to thank Professor Sten Ahrland for valuable help and interest in this work. The financial support given by the Swedish Natural Science Research Council is gratefully acknowledged.

REFERENCES

1. Lewin, A. H., Michl, R. J., Ganis, P., Lepore, U. and Avitabile, G. *Chem. Commun.* (1971) 1400.
2. Chen, K. and Iwamoto, R. T. *Inorg. Nucl. Chem. Lett. 4* (1968) 499.
3. Danielsson, S., Grenthe, I. and Oskarsson, Å. *J. Appl. Crystallogr. 9* (1976) 14.
4. *International Tables for X-Ray Crystallography*, Kynoch Press, Birmingham 1974, Vol. 4.
5. Raston, C. L. and White, A. H. *J. Chem. Soc. Dalton Trans.* (1976) 2153.
6. Schwalbe, C. H., Goody, R. and Saenger, W. *Acta Crystallogr. B 29* (1973) 2264.
7. Bak, B., Hansen-Nygaard, L. and Rostrup-Anderson, J. *J. Mol. Spectrosc. 2* (1958) 361.
8. Csöregh, I., Kierkegaard, P. and Norrestam, R. *Acta Crystallogr. B 31* (1975) 314.
9. Kinoshita, Y., Matsubara, I., Higuchi, T. and Saito, Y. *Bull. Chem. Soc. Jpn. 32* (1959) c 1221.
10. Barnhardt, D. M., Caughlan, C. N. and Mazhar-Ul-Haque *Inorg. Chem. 8* (1969) 2768.
11. Schramm, V. *Inorg. Chem. 17* (1978) 714.
12. Ansell, G. B. *J. Chem. Soc. B* (1971) 443.
13. Barrow, M., Bürgi, H. B., Johnsson, D. K. and Venanzi, L. M. *J. Am. Chem. Soc. 98* (1976) 2356.
14. Pauling, L. *J. Am. Chem. Soc. 49* (1927) 765.
15. Pauling, L. *Z. Kristallogr. 67* (1928) 377.
16. Churchill, M. R., DeBoer, B. G. and Mendak, S. J. *Inorg. Chem. 14* (1975) 2041.
17. Churchill, M. R., Donahue, J. and Rotella, F. J. *Inorg. Chem. 15* (1976) 2752.
18. Ahrland, S. *Pure Appl. Chem. 51* (1979) 2019.
19. Churchill, M. R. and Kalra, K. L. *Inorg. Chem. 13* (1974) 1899.
20. Churchill, M. R. and DeBoer, B. G. *Inorg. Chem. 14* (1975) 2502.

Received December 21, 1981.

Acta Chemica Scandinavica A 36 (1982) 611–622

On the Polynuclear Hydrolysis of the Indium Ion; In^{3+}

GEORGE BIEDERMANN and DIEGO FERRI

Department of Inorganic Chemistry, The Royal Institute of Technology, S-100 44 Stockholm, Sweden

The hydrolysis has been studied in the indium concentration range 0.2 to 0.75 M, by measuring the hydrogen ion concentration, h, in coulometrically alkalified (and reacidified) solutions at 25 °C, with liquid junction-free cells containing a glass electrode. The h data so obtained, as well as the indium amalgam measurements in dilute (5×10^{-4} to 0.1 M) indium solutions reported previously, which were confirmed and refined, may be explained by assuming that only two polynuclear ions are formed: $In_2(OH)_2^{4+}$ and $In_4(OH)_6^{6+}$. Their formation constants in the inert 3 M $NaClO_4$ and in the various $In(ClO_4)_3 - NaClO_4$ media of 3 M $[ClO_4^-]$ level are summarized in Tables 1 and 2. No evidence was found for the formation of hydrolysis products with a higher degree of polymerization.

The indium ion represents an acid of considerable strength, and several mono- and polynuclear bases are formed by its protolysis.[1] The most suitable method to study these equilibria and the interpretation of the data has been the matter of some controversy.[2,3]

A rather comprehensive investigation on this subject was carried out by one of us in 1955.[1] The potentiometric measurements have given clear evidence that for [In(III)] < 1 mM the mononuclear ions $InOH^{2+}$ and $In(OH)_2^+$ are the predominating products of the hydrolysis, while the binuclear species $In_2(OH)_2^{4+}$ and other polynuclear ions of the general composition $In(In(OH)_2)_t^{(3+t)+}$ become increasingly important as the solutions get more concentrated for In(III); t was assumed to represent an integer growing without limit.

This model was criticized[2,3] and the same emf data were subjected to reinterpretation by applying the computerized error square sum minimization techniques developed meanwhile.[4] No definite conclusions could, however, be drawn.[2,3]

One of us (D.F.) has therefore undertaken a new potentiometric study of the hydrolysis. These new amalgam data of a precision of around 0.03 mV have been found to agree with the previous set of emf measurements[1] to within a few tenths of a mV. Thus the steep part of the formation curves which were considered in great detail in the least square calculations[2,3] correspond to homogeneous equilibria.

A new series of systematic computations has been carried out with these recent, precise amalgam data. We preferred especially comparison with normalized model functions, a method originated by Sillén[5] which does not require to guess the magnitude of the formation constant of the species to be tested.

Moreover, we extended the hydrolysis measurements to the indium concentration range 0.2 to 0.75 M, where the highly polymerised species represent the most important hydrolysis products.

These two topics form the main subject of parts I and II of this article. In the light of the present results the hydrolysis equilibria of groups 3a and 3b cations are shortly surveyed in the last, third part.

Notation.

H = proton excess = $[ClO_4^-] - 3[In(III)] - [Na^+] - [Ag^+] - 2[Pb^{2+}]$.
h = hydrogen ion concentration at equilibrium.
B = stoichiometric concentration of indium ions = [In(III)].
b = concentration of In^{3+}.
η = $\log(B/b)$.
w = mol of electrons introduced cathodically or removed by anodic oxidation.
$^*K_1 = [InOH^{2+}]hb^{-1}$.
$^*K_2 = [In(OH)_2^+]h[InOH^{2+}]^{-1}$.
$^*\beta_{qp} = [In_p(OH)_q^{(3p-q)+}]h^q b^{-p}$.

0302-4377/82/070611-12$02.50

In accordance with the nomenclature of the Stability Constants, asterisks are employed to emphasize that H_2O and not OH^- is regarded as the reagent.

I. THE POLYNUCLEAR HYDROLYSIS IN DILUTE INDIUM SOLUTIONS

Interpretation of the amalgam electrode data.

We sought to explain the great number of $\eta(\log h)_B$ data * comprising the B range 0.5 to 100 mM, which are illustrated in Fig. 1, in several stages. In each, a more general and comprehensive model function was introduced based on the results of the preceding step.

Our guiding principle has been to separate, as far as possible, the determination of the composition of the reaction products from the evaluation of the magnitudes of the corresponding formation constants.

(a) Functional analysis at constant acidity levels

We considered first data sets interpolated at a series of *constant* hydrogen ion concentration values, lying in the vicinity of $\log h = -3$. In this region a vertical drawn from the $\log h$ axis is seen from Fig. 1 to cut several η $(\log h)_B$ curves.

Along a vertical, a *single variable b* remains, and an analysis of the $\eta(B)_h$ sets thus obtained should therefore provide straightforward information concerning the number of indium atoms present in the hydrolysis products.

Let's first assume that in addition to $In_2(OH)_2^{4+}$ only another polynuclear ion, $In_p(OH)_Q$, is formed. Then, the ratio of the concentration of indium atoms present as polynuclear species, $\sum_{p\geq 2} p[In_p(OH)_q]$, to b^2 takes the simple form (1), where C_1 and C_2 represent conditional constants depending on the acidity.

$$R_{h,2} = \frac{B - b(1 + {}^*K_1 h^{-1} + {}^*\beta_2 h^{-2})}{b^2} =$$

$$2{}^*\beta_{2,2} h^{-2} + P{}^*\beta_{Q,P} h^{-Q} b^{(P-2)} = C_1 + C_2 b^{P-2} \qquad (1)$$

* The complete set of primary data, considered in this article, is available on request from the authors.

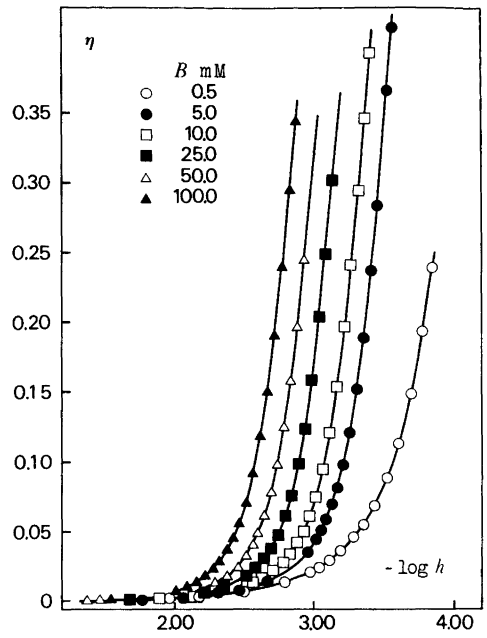

Fig. 1. The hydrolysis of the indium ion in the concentration range 0.5 to 100 mM, $\log(B/b)_B$ as a function of $-\log h$. Symbols represent the amalgam data. For the sake of clarity, about each third point is shown only. The curves have been constructed with the formation constant values summarized in the last column of Table 1.

In eqn. (1) $*K_1$ is the symbol for the formation constant of $InOH^{2+}$ and $*\beta_2 = *K_1 * K_2$ that for its protolysis product $In(OH)_2^+$. Both the new and the old [1] $\eta(\log h)_{5,10-4}$ measurements, that agree to within a few tenths of a mV, were used to evaluate these constants which are needed to calculate the mononuclear correction terms in eqn. (1) and many other formulas which follow.

Comparison of the amalgam data with a normalized model function led to the estimates (2). These values deviate considerably from the previous

$$\log {}^*K_1 = -4.3 \pm 0.1 \text{ and } \log {}^*K_1^* K_2 = -8.6 \pm 0.1 \qquad (2)$$

results [1] ($p^*K_1 = 4.4_2$ and $p^*K_1^*K_2 = 8.3$). The difference is due to the improved method of data treatment not requiring a linearization.

A series of plots $R_{h,2}$ *versus* b^N, $N = P - 2$, were constructed at each acidity level; for the correct

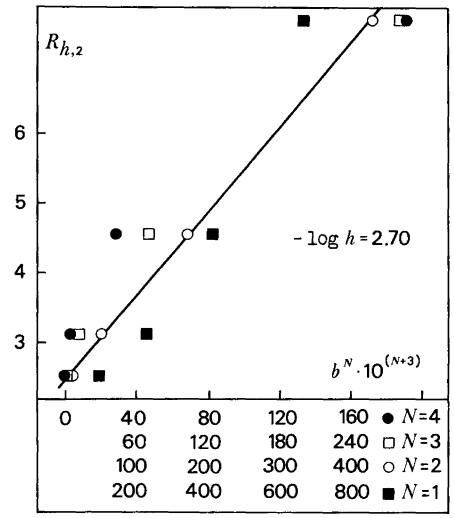

Fig. 2. Determination of the nuclearity in the most polymerized hydrolysis products, $R_{h,2}$ as a function of b^N, *cf.* eqn. (1). The ordinate is common, but for each choice of $N = P\text{-}2$ a special abscissa scale has been taken. The line represents the equation $R_{h,2} = 2.46 + 1.21.10^3 b^2$.

choice of N the plots should, according to (1), be approximable with a straight line.

Typical results are shown in Fig. 2. This affords clear evidence that the additional hydrolysis product is *tetranuclear* as only the $R_{h,2}$ *versus* b^2 data give rise to a plot which is describable with a straight line.

Similar results were obtained in all the other plots covering the log h range -2.4 to -3.0. We know on the basis of the 1955 work, and it was fully corroborated by our recent data, that all the hydrolysis products have the general composition $In_{t+1}(OH)_{2t}$. Hence, the tetranuclear species is likely to be the ion $In_4(OH)_6^{6+}$ as t equals 3.

To test whether the amalgam data are sufficiently accurate to afford an unequivocal reaction mechanism, plots of $R_{h,3}$ against $b^{(P-3)}$ were also made. All of them led to a set of points exhibiting a great curvature.

(b) Comparison with normalized functions

To corroborate these preliminary conclusions further arguments are needed. To this end, *all* the amalgam measurements belonging to the B range 10 to 100 mM have been recalculated to the form (3)

$$\alpha = \log[\{Bb^{-1} - (1 + {}^*K_1 h^{-1} + {}^*\beta_2 h^{-2})\}\ h^2 b^{-1}] \quad \textit{versus} \quad \log(bh^{-2}) \tag{3}$$

and they were compared with the normalized model functions

$$Y_P = Y_P(\log x) = \log(2 + Px^{P-2}) = \alpha - \log {}^*\beta_{2,2} \tag{4}$$

where

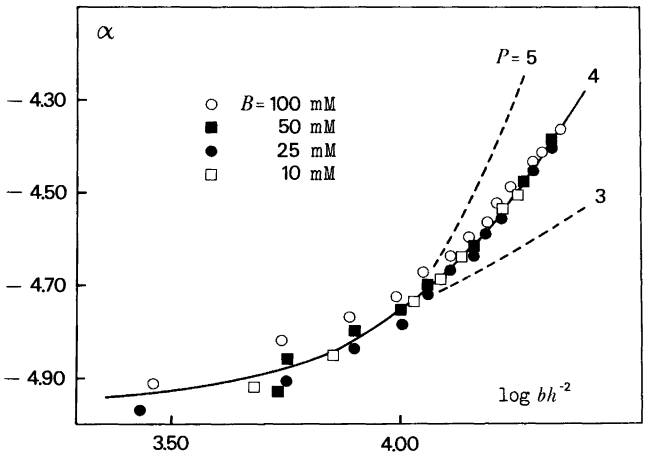

Fig. 3. Determination of the composition of the most polymerized hydrolysis product. Symbols: Data α *versus* $\log(bh^{-2})$, *cf.* eqn. (3). The curves represent the functions $Y_P(\log x)$, eqn. (4), in the position of best fit. For Y_4 this criterion corresponds to $-\log {}^*\beta_{2,2} = 5.25$ and $-\log {}^*\beta_{6,4} = 13.75$. About each third point is included.

$$\log x = \log(bh^{-2}) + \frac{1}{P-2}\left(\log \frac{{}^*\beta_{2(P-1),P}}{{}^*\beta_{2,2}}\right) \qquad (4a)$$

Our results are graphically represented in Fig. 3. This shows that only Y_4 corresponding to the formation of $In_4(OH)_6^{4+}$ fits the data. We get a first estimate for $\log{}^*\beta_{2,2}$ by reading off the ordinate difference, and a first approximation for $\log{}^*\beta_{6,4}$ on the basis of the abscissa difference $\log(bh^{-2}) - \log x$, *cf.* Table 1. Hence this approach is in complete agreement with our preceding conclusions.

(c) Comparison with projection maps. Final estimate of the formation constants

In is seen from eqn. (3) that the magnitudes of the mononuclear formation constants must be known for the calculations. We turned therefore back to the primary data themselves, visualized in Fig. 1, and calculated by interpolation sets of data pairs $(B,h)\eta$ at a series of η levels. These sets were then recalculated to the form $\log(Bh^{-2})$ *versus* $\log(h)_\eta$, and they were compared with a projection map representing the hypothesis that the hydrolysis proceeds through the species $InOH^{2+}$, $In_2(OH)_2^{4+}$ and $In_4(OH)_6^{6+}$.

The map, $\log Y(\log v(u))_{l,\eta}$, was constructed with eqn. (6), where $u = {}^*K_1 h^{-1}$, v represents ${}^*\beta_{2,2}bh^{-2}$, while l denotes ${}^*\beta_{6,4}{}^*\beta_{2,2}^{-3}$.

$$\log Y = \log\{v(1+u+2v+4lv^3)\} = \log(Bh^{-2}) + \log{}^*\beta_{2,2} \qquad (6)$$

An optimal fit was found with $\log l = 2.1$ and by superposition the formation constant values summarized in Table 1 have been deduced.

(d) Least square calculations

We undertook also several series of computations to find the minimum value for the sum

$$U = \sum_{i=1}^{n} (E_i - E_{c,i})^2,$$

where E_i stands for a certain emf value measured with the amalgam cell (I) (see below), and $E_{c,i}$ is its value calculated on the basis of a specified hypothesis. The index i runs to n representing in most cases the total number of amalgam potentials, remeasured in the present work, about 130.

First we wanted to check the visual fit obtained in the preceding sections. By taking as starting values the results of the projection map (*cf.* Table 1), we obtained the formation constants listed under alternative I in the same table. These, corresponding to an average deviation of ± 0.07 mV, show only negligible differences from the graphical calculations.

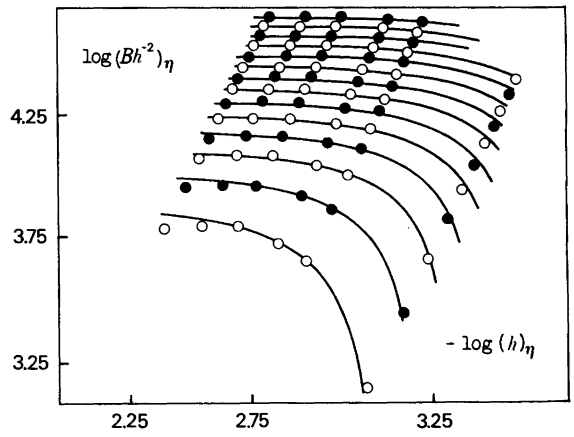

Fig. 4. Comparison of the amalgam measurements with a projection map representing the hypothesis that the hydrolysis proceeds through the formation of the species $InOH^{2+}$, $In_2(OH)_2^{4+}$ and $In_4(OH)_6^{6+}$. Each curve represents an η level that increases in steps of 0.02 units from 0.04 to 0.30 from the lower edge to the top. The curves have been calculated with the formation constants shown in the third column of Table 1.

Next, we started a systematic search for the *minor species* which could have been easily overlooked in our simple graphical treatment. We introduced first as additional reaction product the ion $In_3(OH)_4^{5+}$, which was postulated by Biedermann in 1955 [1] and later by other authors.[2,3]

With this ion the error square sum U could be made to diminish by 3 % but the formation constant $*\beta_{4,3}$ was found to possess an uncertainty equalling its mean value. The magnitudes for the other hydrolysis constants remained practically unchanged as well as the average deviation from the amalgam cell data. Hence this trinuclear ion is not formed in an amount which can be detected with measurements of the present precision.

Then we tested the higher members of the series $In(In(OH)_2)_t$ by taking in each case a starting value for the formation constant on the basis of Biedermanns [1] hypothesis of an unlimited series of hydrolysis products.

Calculations were made up to $t=24$ but no significant improvement in U could be achieved. Thus it appears that no other mechanism consisting of four steps may explain the data better than the simple scheme proposed in the preceding stages of calculations.

Finally we took up the problem of *systematic experimental errors.* The indium concentration values, b, were measured with the cell (I), where

$$\begin{array}{l}(Pt),In-Hg|In(III)\ B,\ H^+\ H,\ Na^+ \\ \quad (0.01\,\%) \\ (3.00\ M-3B-H),\ ClO_4^-\ 3.00\ M|RHC+ \end{array} \qquad (I)$$

RHC:|3.00 M $NaClO_4$|2.99 M $NaClO_4$, 0.0100 M $AgClO_4$|Ag. The emf of this cell at 25 °C can be set equal to eqn. (7), where E_j stands for the small liquid junction potential correction, while E_o represents the sum of the concentration independent terms.

$$E_{am} = E_o - 19.72\ \log[In^{3+}] + E_j(h) \qquad (7)$$

With more concentrated amalgams the overpotential was not sufficient to hinder the dissolution of indium.

Our experiments lasted usually ten to twenty hours and in its course trace amounts of redox impurities (as air or substances dissolved from the stopcock grease) might have easily contaminated the test solution and changed the amalgam concentration. Hence, an average value for E_o reflecting the effect of the contamination, is more correct to use than a value derived by a short series of measurements carried out at the start of the experiment.

Consequently we minimized each series of measurements individually, and we let also E_o represent an adjustable parameter in addition to the equilibrium constants.

The final results, denoted in Table 1 as alternative II, were derived in this way.

The E_o corrections never exceeded 0.13 mV. We attained, however, a great decrease in the error square sum, about 20%. Moreover the average deviation could be suppressed to ± 0.05 mV.

II. THE STUDY OF CONCENTRATED INDIUM SOLUTIONS

Interpretation of the glass electrode measurements.

(a) Method

The hydrolysis in the indium concentration range 0.2 to 0.75 M has been studied with test solutions of the general composition

$$\begin{array}{l}In(III)\ B,\ H^+\ H,\ Ag^+\ A_1,\ Pb^{2+}\ A_2,\ Na^+ \\ (3.00\ M-3B-H-A_1-2A_2),\ \ ClO_4^-\ \ 3.00\ M \end{array}$$

which in the following discussion will be abbreviated by TS.

Table 1. The hydrolysis constants derived by the methods of Part I valid in 3 M $(Na^+)ClO_4^-$ medium.

	Eqn. (1)	Eqn. (3)	Projection map	Letagrop I	Letagrop II [a]
$-\log *K_1$	–	–	4.26 ± 0.05	4.29 ± 0.03	4.23 ± 0.07
$-\log *\beta_{2,2}$	5.3	5.25	5.30 ± 0.05	5.3 ± 0.1	5.27 ± 0.06
$-\log *\beta_{6,4}$	13.7	13.75	13.8 ± 0.1	13.86 ± 0.1	13.79 ± 0.03

[a] Minimization with the adjustment of E_o, *cf.* eqn. (7).

Two *auxiliary ions* Ag^+ and Pb^{2+} are seen to be introduced, both of them represent so weak acids [6,7] that their protolysis can be entirely neglected in the high hydrogen ion concentration range here in question. For reasons which will emerge in the following discussion, their concentrations were kept always at around 0.1 M.

The auxiliary ion Ag^+ was chosen primarily as the reference in the cell (II), which served for the determination of the hydrogen ion concentration in hydrolyzed indium solutions.

glass electrode|TS|Ag+ (II)

$$E_{Ag} = E_{o,Ag} + 59.16 \log([Ag^+]/h) \quad (8)$$

The emf of cell (II) may at 25 °C be put into the simple form (8), where the sum of the concentration independent terms is denoted by $E_{o,Ag}$. Its actual value must be determined in each experiment by measuring E_{Ag} at such high acidities ($\log h \geq -1$) where the indium hydrolysis becomes negligible and consequently h can be set equal to the proton excess, H.

Although the hydrogen ion concentrations of the four stock solutions that were needed to prepare TS were known with some precision, small volumetric errors rendered the starting H value, calculated on the basis of the mixing ratio, rather uncertain. Hence they had to be determined together with $E_{o,Ag}$ by constructing a Gran-diagram.[8] In each case $E_{o,Ag}$ could in this way be evaluated to within ± 0.05 mV, while the starting value for the proton excess could be estimated with an uncertainty of a few tenths of a percent.

In another research project now being carried out in this laboratory[9] evidence was obtained that replacement of the cations of the medium at a constant $[ClO_4^-]$ does not affect the activity factor ratio of the Ag^+ and H^+ ions to an appreciable extent when they are present in the solution at low concentrations. Hence the activity factor ratio term is incorporated into the constant $E_{o,Ag}$ of eqn. (8).

The lead ions were introduced to enable us to vary reversibly the hydrogen ion concentration in TS by coulometric methods. For this purpose we immersed two additional electrodes into TS giving rise to the electrolysis circuit (III), which was connected to a constant current supply.

(Pt)Ag|TS|PbO_2(s),(Pt) (III)

Although the test solution now contains two redox couples $Ag^+ - Ag$ and $PbO_2 - Pb^{2+}$, no spontaneous reaction occurs as the oxidized form of the stronger couple, PbO_2, is kept completely separated from the reduced form of the weaker, Ag, both being solids adhering to a platinum net support. The solubility of PbO_2 is quite negligible in acid solutions. Indeed, the emf of cell (II), E_{Ag}, has always been found (even up to 100 °C) to remain unchanged to within 0.1 – 0.2 mV for several days.

A great number of experiments were made to find the conditions for ensuring theoretical current efficiencies in both directions for the electrode reactions (9) and (10).

$$Ag^+ + e \rightleftharpoons Ag(s) \quad (9)$$

$$PbO_2(s) + 4H^+ + 2e \rightleftharpoons Pb^{2+} + 2H_2O \quad (10)$$

The current efficiency was studied first by neutralizing with the cathodic reduction of PbO_2 and then reacidifying with the anodic oxidation of Pb^{2+} a standardized sample of $HClO_4$. The coulometric analysis was always found to agree to within 0.1 – 0.2% with the value obtained by titration with NaOH.

A similar degree of agreement was obtained when the hydrogen ion concentration in concentrated $AgClO_4$ solutions was determined using a PbO_2 cathode and it was measured by titrating with NaOH.

Many experiments were carried out with cell (II) and the electrolysis circuit (III) to determine the hydrogen ion concentration of $Pb(ClO_4)_2 - AgClO_4$ mixtures which had been also analyzed in divided cells with a glass electrode. The two methods never differed more than 0.2%.

The reversibility of the electrolysis reactions (9) and (10) was checked by acidification – realkalification cycles. The corresponding E_{Ag} values often agreed to within 0.01 mV. Further, in experiments of this kind we also calculated the $E_{o,Ag}$ values ensuing each step of electrolysis by assuming a theoretical current efficiency, eqn. (11). In this

$$E_{o,Ag} = E_{Ag} + 59.16 \log \frac{w^o_{H^+} \pm 2w}{w^o_{Ag^+} \mp w} \quad (11)$$

equation w is the symbol for the number of mol of electrons passed through the test solution, $w^o_{H^+}$ stands for the mol of hydrogen ions present at the start of the experiment, and $w^o_{Ag^+}$ for the initial mol

of Ag^+ ions, We usually obtained $E_{o,Ag}$ values agreeing better than 0.1 mV, when w was varied in both directions by large amounts.

In another experiment we introduced two PbO_2 electrodes, and measured E_{Ag} while current was passed for many hours between them, its strength sometimes was increased to 64 mA. No change in E_{Ag}, exceeding 0.1 mV, could be detected. The same results were obtained when the electrolysis was carried out instead between two silver electrodes immersed into TS.

On the basis of this evidence we concluded, that provided the current density does not exceed 5 mA/cm^2, both electrode reactions (9) and (10) may be considered to proceed with a theoretical current efficiency in both directions. Hence the proton excess could simply be calculated by the equation $H = (w^o_H + \pm 2w)/V$ and the actual concentration of silver ions by $(w^o_{Ag+} \mp w)/V$ where the upper sign refers to acidification and the lower to alkalification. The test solution volume is denoted by V. For the small number of coulombs passed through in a series of measurements, no serious error may arise by assuming V to remain unchanged.

(b) Results

This coulometric approach was primarily chosen to avoid premature precipitation of indium hydroxide due to a local excess of hydroxide ions. Only experiments in which direct evidence could be obtained for the reversibility by the agreement of the alkalification and the reacidification measurements have been considered in the following discussion. A typical experiment satisfying this condition, within the limits of the present precision, is illustrated in Fig. 5.

Our hydrogen ion concentration measurements with cell (II), comprising more than twenty series, are graphically represented in Fig. 6. This shows the average number of hydrogen ions set free per indium ion, Z, eqn. (12), as a function of the

$$Z = \frac{h - H}{B} = Z(\log h)_B \qquad (12)$$

logarithm of the hydrogen ion concentration at the three indium concentration levels 200, 500 and 752

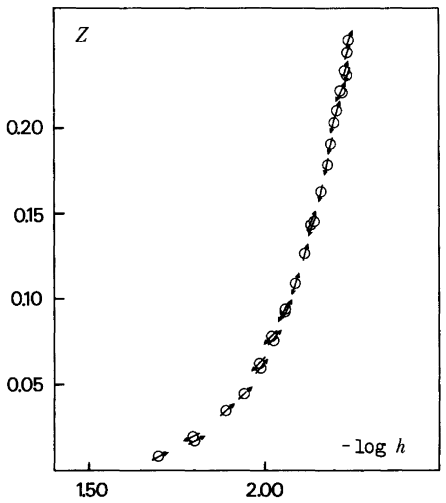

Fig. 5. Reversibility test. The average number of hydrogen ions set free per indium, Z, as a function of $\log h$ at the indium concentration level 0.4967 M. Circles with an upward arrow represent alkalification, with a downward arrow acidification experiments.

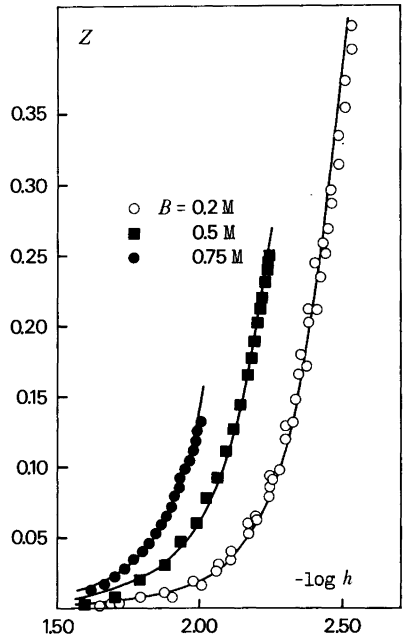

Fig. 6. The hydrolysis of indium(III) in concentrated solutions; $Z = Z(\log h)_B$ at 0.2 (circles), 0.5 (filled squares) and 0.75 M (dots) levels. The curves have been calculated with the $^*\beta_{2,2}$ and $^*\beta_{6,4}$ values summarized in Table 2. About each third experimental point is shown.

mM. For the sake of clarity, about each third of the data is shown only and no distinction is made between alkalification and acidification experiments.

As the replacement of a large portion of the solvent sodium ion with the reacting indium ion influences the activity factors of the reacting species, each B level was interpreted separately.

The sets of $Z(\log h)_B$ data were treated in two stages. First, a comparison was made with model functions representing the hypothesis that only two reaction products are formed in appreciable concentrations: $In_2(OH)_2^{4+}$ and $In_4(OH)_6^{6+}$. On the basis of the results presented in Part I one may easily see that the mononuclear species become quite negligible in the concentrated indium solutions here considered.

We first recalculated the data to the form $Z(\log Bh^{-2})$, and compared each set with the model function (13), where $u = {}^*\beta_{2,2}bh^{-2}$ and x is the symbol for the normalized variant of Bh^{-2}; eqn. (14).

$$Y = \frac{2u + 6lu^3}{1 + 2u + 4lu^3} = Y(\log x)_l \qquad (13)$$

$$\log x = \log(Bh^{-2}) + \log {}^*\beta_{2,2} = \log\{u(1 + 2u + 4lu^3)\} \qquad (14)$$

$$3\ In_2(OH)_2^{4+} \rightleftharpoons In_4(OH)_6^{6+} + 2In^{3+} \qquad (15)$$

The parameter $l = {}^*\beta_{6,4}{}^*\beta_{2,2}^{-3}$ stands for the equilibrium constant of the redistribution reaction (15). By choosing for $\log l$ the value of 2.15, a satisfactory agreement could be obtained at all three B levels. Superimposition of $Y_{2.15}$ yielded in the position of best fit, *cf.* Fig. 6, the $\log {}^*\beta_{2,2}$ and $\log {}^*\beta_{6,4}$ values summarized in Table 2. These results served as the starting point for the least square adjustment.

At each B level we calculated, by employing the recent version of the Letagrop program,[4] the ${}^*\beta_{2,2}$ and ${}^*\beta_{6,4}$ values providing a minimum for the sum

$$\sum_{i=1}^{n} (Z_i - Z_C)^2,$$

where Z_i denotes an experimental datum and $Z_C = Z_C({}^*\beta_{2,2}, {}^*\beta_{6,4})$ a calculated value for the average number of hydrogen ions set free per indium at a certain B level.

Table 2 demonstrates that the two methods of data interpretation afford practically coinciding results. The Letagrop approach enabled us to analyze the fit in more details. At each series of measurements the number of positive and negative deviations was found to differ less than 10%; hence our hypothesis concerning polynuclear hydrolysis may be regarded as a close approximation. The average percentage deviation in Z, $\Delta Z/Z$, varied between 5 and 10%. This is quite reasonable as a large part of the measurements corresponds to a small difference between the hydrogen ion concentration at equilibrium and the proton excess.

We may see by comparing Tables 1 and 2 that the magnitude of $\log {}^*\beta_{2,2}$ is but little influenced by the replacement of a large part of the Na^+ ions with In^{3+} and its hydrolysis products. This result is in accord with the *specific interaction theory*[10] which yields for the medium effect of the equilibrium constant of this reaction the relationship (16), where

$$\log \frac{{}^*\beta_{2,2}(I)}{{}^*\beta_{2,2}(3)} = 2 \log \frac{a_{H_2O}(I)}{a_{H_2O}(3)} \qquad (16)$$

I denotes the ionic strength in an $In(ClO_4)_3 - NaClO_4$ solution and 3 stands for the ionic strength of the inert $NaClO_4$ medium. The water activity is denoted by a_{H_2O}. Its value is not known in indium perchlorate solution.

Table 2. The polynuclear hydrolysis constants in concentrated indium solutions.

Medium	$-\log {}^*\beta_{2,2}$ Eqn. (13)	Letagrop	$-\log {}^*\beta_{6,4}$ Eqn. (13)	Letagrop
0.2 M In(III), 2.4 M $(Na^+ + H^+)$	$5.3_2 \pm 0.05$	5.32 ± 0.08	13.8 ± 0.1	$13.6_5 \pm 0.15$
0.5 M In(III), 1.5 M $(Na^+ + H^+)$	5.25 ± 0.05	5.25 ± 0.08	13.7 ± 0.1	13.7 ± 0.1
0.752 M In(III), 0.74 M $(Na^+ + H^+)$	5.2 ± 0.1	5.23 ± 0.05	13.4 ± 0.1	13.3 ± 0.1

On the other hand, the osmotic coeffient of gallium perchlorate has been carefully studied in a wide concentration range.[11] As the effect of water activity change is small, no serious error is likely to be made by assuming that the water activities in 1 m $Ga(ClO_4)_3$ and 1 m $In(ClO_4)_3$ are equal. Thus we may estimate, with the osmotic coefficient reported in 3.5 m $NaClO_4$[12] as the upper limit for the medium effect, eqn. (16), $2(-0.052+0.053)=0.002$ which is of course far below our experimental precision.

For the medium effect of the tetranuclear species the theory predicts eqn. (17), where $D=D(I)$

$$\log\frac{{}^*\beta_{6,4}(I)}{{}^*\beta_{6,4}(3)} = 6\{D(I)-D(3)\}+6\log\frac{a_{H_2O}(I)}{a_{H_2O}(3)} \quad (17)$$

represents the Debye-Hückel function, equalling at 25 °C $0.5107\sqrt{I}/(1+1.5\sqrt{I})$. We thus obtain that $\log {}^*\beta_{6,4}$ should increase, compared with its value in the inert medium, by 0.04 at $B=0.2$ M, by 0.08 at 0.5 M and by 0.11 units at 0.75 M.

These estimates are seen from Table 2 to be in approximate agreement with our results in the 0.2 and 0.5 M indium perchlorate solutions. However, the increase of 0.3, as we pass to the highest B level, is much larger than expected by the theory.

This discrepancy may in part be ascribed to the experimental uncertainty of our ${}^*\beta_{6,4}$ (0.75 M) value. It arises from the fact that at this B level precipitation occurs already at $Z\sim0.15$, where $[In_4(OH)_6^{6+}]$ is still below $[In_2(OH)_2^{4+}]$. In the more dilute solutions, the tetranuclear species represents the predominant product of hydrolysis in a large part of the accessible acidity range.

Another reason may be that for the correct estimate of the activity factor of the tetranuclear ion, one should make a realistic estimate of the charge distribution, instead of regarding it as a large sphere with uniform charge density.

We checked, however, on the basis of the emf[13,14] and vapor pressure[14] measurements in $LaCl_3-HCl$, $AlCl_3-HCl$ and $LaCl_3-NaCl$[12] mixtures that the specific interaction theory may be safely employed as a useful first approximation in 3 M media containing simple singly and triply charged ions.

DISCUSSION

The main result of the present work is that the polynuclear hydrolysis is explainable by the formation of only two species $In_2(OH)_2^{4+}$ and $In_4(OH)_6^{6+}$ that link the simple ions In^{3+}, $InOH^{2+}$ and $In(OH)_2^+$ with the final reaction product, colloidal indium hydroxide. This hypothesis receives additional support by the preliminary result of an X-ray diffraction study of multimolar indium nitrate and perchlorate solutions. Dr. Georg Johansson with the collaboration of fil.kand. Anita Persson has undertaken in this laboratory this investigation at about the same time as our potentiometric work was started.

The diffraction data at the highest degree of hydrolysis ($Z\sim0.8$) afford evidence for the presence of tetranuclear ions. Moreover, the radial distribution curves hitherto obtained may be explained by assuming that the four octahedrally coordinated indium ions occupy the corners of a tetrahedron and are bound by single hydroxo bridges located at the centers of the six edges.

The question is now arising which types of forces are responsible for the preferential formation of certain hydrolysis products while others, at the first sight equally probable, as $In_3(OH)_4^{5+}$, do not appear to be present in detectable amounts.

The formation constants of the hydrolysis products[15] of the general composition $MeOH^{2+}$ are summarized below together with the electronegativities, χ, of the Me^{3+} ions. The values have been taken from Allred's comprehensive study.[16] For reasons to emerge later, the Fe^{3+} ion is included as well.

p*K_1, χ: Group 3a. Sc^{3+}: 5.1, 1.3_6; Y^{3+}: 9.1, 1.2_2; La^{3+}: 10.1, 1.1_0.

Group 3b. Al^{3+} ~5, 1.6_1; Ga^{3+} ~4, 1.8_1; In^{3+}: 4.30, 1.7_8; Tl^{3+}: 1.14, 2.0_4; Fe^{3+}: 2.9, 1.9_6.

A clear correlation is seen to exist between the strength of the aquo acidity and electronegativity within each group.

Based on Allred's arguments and results[16] we may regard the difference in electronegativity within the same group, including cations of the same charge and of the same coordination number, to provide the difference in the extent of the electron transfer from the ligand oxygen to the central ion.

Oxygen is, of course, more electronegative than hydrogen and therefore a drainage of charge will ensue in the direction hydrogen to oxygen, giving rise to a positive charge density on the periphery of the hydrated ion. The greater the charge density

thus established, the less work needed to remove a proton and transfer it to a water molecule. In other articles to be published soon from this laboratory, evidence will be presented that also within the group 2b and for the lanthanoids the trends in $*K_1$ and in the electronegativity are parallel.

Hence, this model of a hydrated cation, suggested by Pauling,[17] provides an explanation for the trend of the aquo acidity.

Further, it is in accordance with this picture that the solubility in alkalies in group 3b runs opposite to the strength of the aquo acidity. Accumulation of negative charge on the hydroxo complex will promote the solubility, because the degree of hydration increases. For the same reason, strong cation acids, like Fe^{3+} and Bi^{3+}, cannot generally be dissolved in alkali hydroxides.

One may also argue [18] – as a paraphrase – that in a stable complex species the charge on the central cation becomes entirely neutralized by the electrons donated from the ligands. The greater the electronegativity of the central cation, the more negative charge will be transferred from a hydroxide ion, and hence neutralization occurs with a smaller number of ligands. As a consequence, as many as four hydroxide ions will be bound most readily to Al^{3+}.

For In^{3+}, Tl^{3+} and Sc^{3+} even the second step of the mononuclear hydrolysis could be studied. In each case the acid strength of the ion $MeOH^{2+}$ was found [15] to be near to that of the unhydrolyzed species. This somewhat unusual result is probably due to the presence of two coordinated water molecules in antipodal position. The condition $p*K_1 \sim p*K_2$ thus seems to imply a high coordination number. Indeed, the tetracoordinated Be^{2+} ion has been found [19] to be an acid of much higher strength ($p*K_1 = 5.7$) than the $BeOH^+$ ion [20] ($p*K_2 = 8.0$).

Finally, we would like to recall that no evidence could be found either in group 3a or 3b for the formation of the uncharged species $Me(OH)_3$. This is, of course, easy to understand on the basis of an electrostatic model.

It is practical to approach the problem of polynuclear hydrolysis by considering it as polymerization of the mononuclear species.

The polynuclear hydrolysis of the three ions Sc^{3+}, Y^{3+} and In^{3+} has been studied comprehensively, and we may with some confidence use these results as a basis for a general discussion.

Independently of temperature and ionic medium, the main product of the polynuclear hydrolysis for these ions has been found to be the dimer $Me_2(OH)_2^{4+}$. The following table lists the values for the dimerization constant

$$2\ MeOH^{2+} \rightleftharpoons Me_2(OH)_2^{4+};\ K_{2,2} = *\beta_{2,2}(*K_1)^{-2}$$

at 25 °C in 1 and 3 M media:

	$p*K_1$	$p*\beta_{2,2}$	$\log K_{2,2}$
Y^{3+}	9.1	14.3	3.9
In^{3+} (3M NaCl)	6.9_5	10.1_5	3.7_5
Sc^{3+}	5.1	6.1	4.1
In^{3+} (this work)	4.3_0	5.2_7	3.3_3

We may see from this presentation, that although the aquo acidity is greatly increasing as we pass from Y^{3+} to In^{3+}, the $\log K_{2,2}$ values show no trend.

The spread of around ± 0.4 units from the mean, 3.7_5, is only slightly greater than the uncertainty of our $\log K_{2,2}$ calculations which may be estimated to ± 0.3 units.

The Fe^{3+} and Cr^{3+} ions are also of some interest, because the main product of their polynuclear hydrolysis has also been found to be [15] the ion $Me_2(OH)_2^{4+}$. Hedström's precise measurements [15] at 25 °C lead to the $\log K_{2,2}$ estimate of 3.2 for the polymerization of $FeOH^{2+}$. Bjerrums classical investigation [15] of the hydrolysis in dilute chromium (III) chloride solutions yields at 75 °C $\log K_{2,2} = 3.3$ and at 100 °C 3.1. These values are reasonably near to our average 3.7_5.

It appears from this short survey that the extent of dimerization is primarily a property of the oxygen atom and the hydroxide ion. A hydroxide ion bound to a hexahydrated triply charged cation obtains an electrostatic bond strength of 1.5 as defined by Pauling, instead of 2.0 which corresponds to a stable species. When the hydroxide ion joins another coordination sphere, it receives the 0.5 units of electrostatic bond strength needed for stability.

A comparison of the formation constants for the dimerization with a single hydroxo bridge

$$MeOH^+ + Me^{2+} \rightleftharpoons Me_2OH^{3+};$$
$$K_{1,2} = [Me_2OH^{3+}]/([Me^{2+}][MeOH^+])$$

within the group 2b, where the aquo acidity is increased by six logarithmic units from Zn^{2+} to Hg^{2+}, while $K_{1,2}$ remains practically unaffected,

lends further support to our hypothesis. The data will be presented in another publication.

We would also like to mention that polynuclear complex formation has been predominantly found to occur with the ligands of the group 6b elements when they are associated with other atoms of a lower electronegativity, as hydrogen.

Except for indium, too little is known on the more hydrolyzed species, in yttrium and scandium solutions only hydrogen ion concentration data are available. On the other hand, one would like to understand the reason for the preferential formation of $In_4(OH)_6^{6+}$.

In this tetrahedral species, according to Johansson and Persson, the indium ions are bound by single hydroxo bridges, and consequently the average distance between the positive charges is rather long.

The simplest model for the ion $In_3(OH)_4^{5+}$ seems to be an indium coordination octahedron joined to two other indium octahedra by two double hydroxo bridges. Such a configuration involves a shorter distance between the positive charges (distributed as discussed previously), because edges are shared and not corners. As a consequence the formation of this ion would require a greater effort against the electrostatic forces and thus it would less likely be formed. The role of electrostatic forces in polynuclear complex formation will form the subject of a subsequent communication.

EXPERIMENTAL

The *amalgam cell measurements* discussed in Part I were carried out by the technique that has been described in some details by Ferri.[21]

Materials and analysis. The indium, silver and sodium perchlorate solutions, which were employed in Part II for the study of concentrated indium solutions, were prepared and analyzed as usual in this laboratory.[21]

Lead perchlorate solutions were made from lead nitrate preparations of *pro analysi* quality. The nitrate was first recrystallized from 0.1 M HNO_3 and then it was decomposed to PbO at 800 °C. Next the PbO was added in a slight excess to concentrated ($\sim$2M) $HClO_4$ of commercial quality, and the pH of the resulting suspension was adjusted to 6. As a consequence, the heavy metal ion contaminants, originating from the perchloric acid, precipitated slowly as hydroxides or silicates. The excess of PbO was finally removed by filtration through a platinum pad and the filtrate was acidified with dilute $HClO_4$ until pH became 3. This minimum buffer capacity is needed to avoid absorption of CO_2 and reaction with the glass container while the solution is being preserved.

The Pb(II) content of these iron- and chloride-free stock solutions were determined either by titration with an EDTA reagent solution or by precipitating PbO_2 anodically.[22] As the hydrolysis of Pb^{2+} is negligible for pH < 4, the proton excess of the solutions could be determined potentiometrically with a glass electrode using a 10 mM NaOH solution.

Electrodes. These lead perchlorate stock solutions, made first 1 M for $HClO_4$, served also for the preparation of the PbO_2 electrodes of the coulometric circuit. The PbO_2 crystals were precipitated anodically onto a large platinum net, using a current density not exceeding 0.5 mA/cm^2. A slow stream of oxygen was introduced in the vicinity of the platinum cathode to avoid the loss of Pb^{2+} ions.

The silver electrodes, used for the measurement of the silver ion concentration as well as for the electrolysis, were prepared by cathodic reduction from a solution of $KAg(CN)_2$, purified by recrystallization. The silver layers on the platinum net were washed with concentrated ammonia to dissolve AgCN and they were soaked for several days with water.

When several silver electrodes were immersed into a test solution, they never differed more than 0.02 mV from each other or from the silver electrode of the coulometric circuit.

Glass electrodes manufactured by the Beckman Co. and by the Jenaer Glasswerk, Schott & Gen, were employed.

In a series of special experiments we found that the emf of the cell

$$(Pt),H_2(p_{H_2}) \;\Big|\; \begin{array}{l}\text{test solution containing}\\ HClO_4 \text{ or } CH_3COOH\\ \text{and } NaOOCCH_3\end{array} \;\Big|\; \begin{array}{l}\text{glass}\\ \text{electrode}\end{array}$$

remained unchanged to within 0.02 mV or better as the $\log h$ value of the test solution was varied from -1 to -5. Thus, these glass electrodes may under the present experimental conditions be regarded to be equivalent with the hydrogen half-cell.

At the end and start of each potentiometric series of measurements the emf of the glass electrode – silver cell was monitored for several hours. The drift was usually less than 0.01 mV/h and it could therefore be neglected.

Technique of the coulometric experiments. All the emf measurements were carried out in a silicone – oil thermostat kept at 25.00 $\pm$ 0.01 °C.

The recurrent sequence of operations: stepwise change of hydrogen ion concentration by coulometry, determination of the emf and measurement of the bath temperature, was performed with the automatic data acquisition system constructed in this laboratory. The program (current levels, direction of electrolysis and current passage period, duration of waiting time *etc.*) was based on the experience gathered in preliminary experiments. The number of coulombs passed through the test solution could in this way be determined with an uncertainty of $0.01-0.02\%$, while we sought to establish the emf values to within ± 0.02 mV.

Acknowledgements. We would like to thank Dr. Georg Johansson and fil.kand. Anita Persson of this Department for many valuable discussions and for their kindness to communicate their results prior to publication. We are also indebted to Professor Vincenzo Romano of Palermo University, Italy, for his cooperation in the development of the PbO_2 $-$Ag method.

The present work forms part of a research project financially supported by the Swedish Natural Science Research Council *(Svenska Naturvetenskapliga Forskningsrådet)*. One of us (G.B.) would like to express his appreciation to the Consistory of the Royal Institute of Technology, Stockholm, for a research grant.

REFERENCES

1. Biedermann, G. *Ark. Kemi 9* (1955) 277.
2. Sillén, L. G. *Pure Appl. Chem. 17* (1968) 55.
3. Baes, C. F., Jr. and Messmer, R. *The Hydrolysis of Cations*, Wiley, New York 1976.
4. Sillén, L. G. and Warnquist, B. *Ark. Kemi 31* (1969) 315.
5. Sillén, L. G. *Acta Chem. Scand. 10* (1956) 186.
6. Biedermann, G. and Hietanen, S. *Acta Chem. Scand. 14* (1960) 711.
7. Olin, Å. *Acta Chem. Scand. 14* (1960) 126.
8. Gran, G. *Analyst (London) 77* (1952) 661.
9. Biedermann, G., Mizumachi, K. and Ohtaki, H. *To be published.*
10. Harned, H. S. and Robinson, R. A. *Multicomponent Electrolyte Solutions*, Pergamon, Oxford 1968.
11. Petterson, C. S., Tyree, S. Y. and Knox, K. *J. Am. Chem. Soc. 77* (1955) 2195.
12. Rush, R. M. *Osmotic and Activity Coefficients*, ORNL-4402, Report Oak Ridge National Laboratory, Oak Ridge 1969.
13. Harned, H. S. and Owen, B. B. *The Physical Chemistry of Electrolyte Solutions*, 3rd Ed., Reinhold, New York 1958, pp. 625, 626.
14. Lietzke, M. H. and Stoughton, R. W. *J. Phys. Chem. 71* (1967) 662.
15. Sillén, L. G. and Martell, A. E. *Stability Constants of Metal-Ion Complexes*, Chem. Soc. Spec. Publ. *17* (1964);*25* (1971).
16. Allred, A. L. *J. Inorg. Nucl. Chem. 17* (1961) 215.
17. Pauling, L. *J. Chem. Soc. (London)* (1948) 1461.
18. Gillespie, R. J. and Nyholm, R. S. *Quart. Rev. 11* (1957) 339.
19. Schwarzenbach, G. and Wenger, H. *Helv. Chim. Acta 52* (1969) 644.
20. Green, R. W. and Alexander, P. W. *Aust. J. Chem. 18* (5) (1965) 651.
21. Ferri, D. *Acta Chem. Scand. 26* (1972) 733.
22. Hertelendi, L. *Z. Anal. Chem. 122* (1941) 30.

Received November 17, 1981.

Acta Chemica Scandinavica A 36 (1982) 623 – 625

Short Communication

Low-frequency (30 – 400 cm^{-1}) Raman Spectra of Water in Cellulose Gels

O. FAURSKOV NIELSEN,[a] T. LINDSTRÖM[b] and P.-A. LUND[c]

[a] Chemical Laboratory V, The H. C. Ørsted Institute, University of Copenhagen, DK-2100 Copenhagen Ø, Denmark, [b] Swedish Forest Products Research Laboratory, Box 5604, S-114 86 Stockholm, Sweden and [c] Danish National Institute of Occupational Health, Baunegaardsvej 73, DK-2900 Hellerup, Denmark

In a recent paper we studied the structure of water in aqueous agarose and κ-carageenan gels by means of Raman spectroscopy.[1] A transformation of the scattered light called $R(\bar{\nu})$-representation was used.[2] We found this technique powerful in a number of investigations of low frequency Raman spectra,[2-12] where a serious problem is the high intensity of the central Rayleigh line. The $R(\bar{\nu})$-representation and similar representations have been used to avoid this problem or for a comparison with far-IR spectra as discussed in Refs. 1, 2, 11, 13, 14 and references cited therein. In our studies of water,[4] aqueous solutions[5-12] and gels,[1] we found it useful to use a background correction, because these samples always showed an inevitable small fluorescence. This paper presents results on water-swollen cellulose gels. The fluorescence from these gels was intense and consequently a new type of background correction was necessary.

The structure of water near the cellulose interface has been a controversial subject for many years.[15-17] Models proposing both a structuring[16] and a destructuring[15] of water at the phase boundary have been proposed. Goring[16] analyzed the water structure in terms of the cluster model for water[18] and concluded that the cellulose surface reduced the water structure in a layer of water adjacent to the surface, whereas Caulfield[17] proposed a long-range structuring of the water.

There is considerable evidence,[15] mainly from studies on the differential heat of water sorption and investigations on the specific volume and density of moist cellulose, that the first strongly adsorbed water with a high density exhibits properties that are different from those of the rest of the water. In Goring's investigation the high density of the first adsorbed water was interpreted as a perturbation of the water structure rather than as compression or adsorption.

Investigations on the thermoelasticity of the same cellulose gels as used in the present study have previously shown[19] that the enthalpic component (χ_H) of the Flory-Huggins interactive parameter was negative, but that the entropic component (χ_S) was positive (negative residual partial molar entropy of water) thus indicating a structuring of the water absorbed into the cellulose. In these cellulose gels the partial specific volume has been found to be 0.87 cm^3/g for the first 13 % of the sorbed water and 1.00 cm^3/g for the remainder. This suggests that the first 13 % can be classified as bound water, whereas any water in excess of this quantity appears to be normal water. The present investigation was undertaken in order to see whether any long-range ordering of this water can be detected or whether the water should be classified as "normal".

The cellulose gels used here were synthesized by heating cellulose xanthate (viscose) solutions until gelation of the viscose took place, after which regeneration and appropriate washing procedures were employed as previously reported.[19] The gels correspond to the gels denoted O – B for which characteristics and properties have previously been published.[19] The highly swollen (water content: 85 %) gels thus obtained were slowly dried to a range of different water contents and then sealed in glass tubes until used. All results refer to gels in deionized water. A glucose solution was prepared from 1 g D(+)-glucose, H_2O (Riedel-de Haen) and 3 ml redistilled water.

Instrumental details were previously described.[1] The spectral slit width was 4 cm^{-1} and the recording speed 25 cm^{-1} per min. Spectra were obtained from 30 – 400 cm^{-1}. A filter with 10A bandwidth and *ca.* 60 % transmission was used in the laser beam (400 mV, 514.5 nm) to prevent the appearance of laser emission lines in the spectrum. Cylindrical high quality 4 mm (i.d.) NMR tubes were used as cells.

$$R(\bar{\nu}) \propto \bar{\nu}[1 - \exp(-h\bar{\nu}c/kT)]I(\bar{\nu}) \quad (1)$$

0302-4377/82/070623-03$02.50

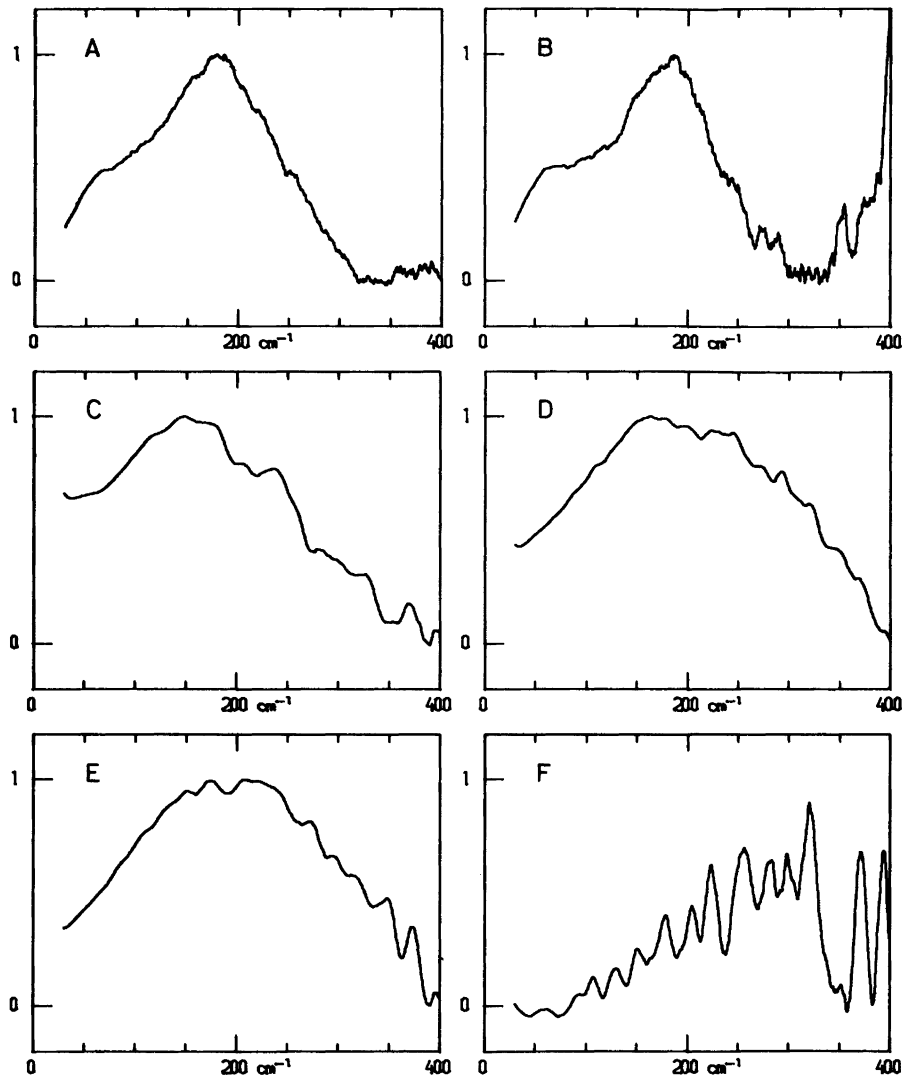

Fig. 1. A, redistilled water. *B*, 1 g D(+)-glucose in 3 ml water. *C*, 3 g water and 1 g cellulose. *D*, 2 g water and 1 g cellulose. *E*, 1.2 g water and 1 g cellulose. *F*, 0.5 g water and 1 g cellulose. The ordinate in each separate figure is the function $R(\bar{\nu})$ which is calculated as described in the text.

$R(\bar{\nu})$-curves were as previously constructed from the intensity in the Stoke's side $[I(\bar{\nu})]$ of the spectrum;[1-12] eqn. (1), where $\bar{\nu}$ is the Raman shift in cm^{-1}, and the other symbols have their usual meaning.

The gels were not transparent, resulting in a very high intensity of the central line, but even worse was the fact that all gels showed a strong fluorescence. Previously, we made corrections in which a mean intensity value around the lowest intensities for water (*ca.* 300 cm^{-1}) was subtracted from all intensities.[1,4-12] A correction in this way was sufficient for liquid water (Fig. 1A) and for the glucose solution (Fig. 1B). The $R(\bar{\nu})$-curves in Fig. 1A – 1B were smoothed by a running mean smoothing procedure.[20] The simple background correction mentioned above was not fruitful for the cellulose gels, because of a very intense fluorescence. We assumed the same band shape of the fluorescence for all gels and to compensate for the fluorescence we

then used the following procedure. $I(\bar{\nu})$-curves from two separate runs for each gel were added and smoothed. The resulting curves are called $I(\bar{\nu})$-sum curves. The intensity of these curves in a 1 cm^{-1} interval at 400 cm^{-1} was normalized to the same value for all gels. The $I(\bar{\nu})$-sum curve for the sample with lowest water content (17%) was then subtracted from the $I(\bar{\nu})$-sum curves of the gels with higher water content. $R(\bar{\nu})$-curves were calculated according to the equation given above from the resulting $I(\bar{\nu})$-curves. In the frequency region investigated (30 – 400 cm^{-1}) liquid water shows a minimum intensity[4,14] at 300 – 400 cm^{-1}, whereas the broad fluorescence band shows maximum intensity at 400 cm^{-1}. The impurities giving rise to the fluorescence should be identical in all samples and the procedure chosen should thus remove the fluoresence.

Finally, the $R(\bar{\nu})$-curves were smoothed in the usual way by the smoothing procedure. The results are shown in Fig. 1C – 1F. The subtraction technique makes the $R(\bar{\nu})$-curves less reliable at higher frequencies and the overall band shapes in Fig. 1C – 1F should not be taken too seriously, but it is evident that the 75% (Fig. 1C), 66.7% (Fig. 1D) and 55% (Fig. 1E) gels show a broad band with a maximum around 200 cm^{-1}, whereas this band was unobservable in a gel containing 33.3% water (Fig. 1F). The low frequency $R(\bar{\nu})$-curve of the glucose solution (Fig. 1B) is dominated by the broad bands from water with maxima at *ca.* 180 cm^{-1} (strong) and at *ca.* 60 cm^{-1} (weak). The spetrum of water in Fig. 1A is included as a reference. The glucose solution in Fig. 1B shows a band at *ca.* 400 cm^{-1}. This band if present in the gels is too weak to be observed in the $I(\bar{\nu})$-curves where the fluorescence is dominating, but the present technique should also compensate for this band and remove it from the difference curves shown. It is therefore plausible to assign the broad bands in Fig. 1C – 1E to the most intense water band with a maximum at 180 cm^{-1}. This band depends upon the local water structure,[4,14] and it can thus be concluded that its structure in the gels is similar to that found in liquid water. No water seems detectable in the gel containing 33.3% water (Fig. 1F), but the signal-to-noise ratio is poor for this sample with the lowest water content.

The main conclusion of this work is that the local water structure in cellulose gels, at least at water concentrations higher than 50%, is identical with that found in liquid water. This result is in accordance with our previous investigations of other polysaccharide gels.[1] Unfortunately no quantitative estimations could be performed due to the very strong fluorescence of the cellulose gels.

Acknowledgement. The authors wish to express their gratitude to the Danish Natural Science Research Council for partially financing the Raman equipment and RC 8000 computer facilities.

1. Nielsen, O. F., Lund, P.-A. and Nicolaisen, F. M. *Acta Chem. Scand. A 34* (1980) 749.
2. Lund, P.-A., Nielsen, O. F. and Praestgaard, E. *Chem. Phys. 28* (1978) 167.
3. Nielsen, O. F., Christensen, D. H., Lund, P.-A. and Praestgaard, E. *Proc. 6th Int. Conf. Raman Spectrosc. Bangalore, India.* Heyden & Son, London 1978, Vol. 2, p. 208.
4. Nielsen, O. F. *Chem. Phys. Lett. 60* (1979) 515.
5. Nielsen, O. F. *Chem. Phys. Lett. 66* (1979) 350.
6. Nielsen, O. F., Lund, P.-A. and Praestgaard, E. *J. Raman Spectrosc. 9* (1980) 286.
7. Nielsen, O. F., Lund, P.-A., Nicolaisen, F. M. and Praestgaard, E. *Proc. 7th Int. Conf. Raman Spectrosc., Ottawa, Canada.* North-Holland, Amsterdam 1980, p. 480.
8. Nielsen, O. F., Lund, P.-A. and Praestgaard, E. *J. Raman Spectrosc. 11* (1981) 92.
9. Nielsen, O. F. and Lund, P.-A. *Chem. Phys. Lett. 78* (1981) 626.
10. Nielsen, O. F., Lund, P.-A. and Petersen, S. B. *J. Raman Spectrosc. 11* (1981) 493.
11. Nielsen, O. F., Lund, P.-A. and Praestgaard, E. *J. Chem. Phys. 75* (1981) 1586.
12. Nielsen, O. F., Lund, P.-A. and Petersen, S. B. *J. Am. Chem. Soc. 104* (1982) 1991.
13. Perrot, M., Brooker, M. H. and Lascombe, J. *J. Chem. Phys. 74* (1981) 2787.
14. Brooker, M. H. and Perrot, M. *J. Chem. Phys. 74* (1981) 2795.
15. Rowland, S. P. *Cellulose: Pores, Internal Surfaces, and the Water Interface* In J. C. Arthur, Ed., *Textile and Paper Chemistry and Technology, ACS Symp. Ser. 49*, Washington, D.C. 1977.
16. Goring, D. A. I. *Fibre-water Interactions in Paper-Making*, Ed. by the Fundamental Res. Comm. Techn. Div. Brit. Paper and Board Ind. Fed., London 1978, Vol. 1, p. 43.
17. Caulfield, D. F. *Fibre-water Interactions in Paper-Making*, Ed. by the Fundamental Res. Comm. Techn. Div. Brit. Paper and Board Ind. Fed., London 1978, Vol. 1, p. 63.
18. Lentz, B. R., Hagler, A. T. and Scheraga, H. A. *J. Phys. Chem. 78* (1974) 1531.
19. Westman, L. and Lindström, T. *J. Appl. Polym. Sci. 26* (1981) 2519, 2533, 2545, 2561.
20. Savitzky, A. and Golay, M. J. E. *Anal. Chem. 36* (1964) 1627.

Received March 29, 1982.

Acta Chemica Scandinavica A 36 (1982) 627–631

Thermochemical Studies on the Formation of Azide Complexes of Gallium(III) and Indium(III)

EFRAIM AVSAR*

Inorganic Chemistry 1, Chemical Center, University of Lund, P.O. Box 740, S-220 07 Lund 7, Sweden

The stabilities and enthalpies of the complexes formed by gallium(III) and indium(III) with azide ion have been determined in an aqueous sodium perchlorate medium of unit ionic strength at 25.0 °C. The stability constants have been determined potentiometrically and the enthalpy changes calorimetrically. In the azide system of gallium(III) only the formation of the first complex could be studied while for the indium(III) azide system studies of four successive steps are possible.

So far, thermochemical studies on the formation of the azide complexes of trivalent ions of the electron configuration d^{10} have not been attempted, except for Tl^{3+} ion, while such data are already available for the corresponding divalent ions,[1-3] *viz.* Zn^{2+}, Cd^{2+} and Hg^{2+}. In this study, among the d^{10} acceptors of group III B Ga^{3+} and In^{3+} are investigated. It is of interest to see how the thermodynamic functions change for divalent and trivalent ions of the same electron configuration.

The equilibrium and enthalpy measurements on the azide systems of gallium(III) and indium(III) show some experimental difficulties. Both acceptors hydrolyze extensively in aqueous medium. In order to suppress the hydrolysis the solutions have thus to be highly acidic.[4] The greater part of the azide will therefore be present as hydrazoic acid which very easily forms explosive corrosion products with various metallic parts of the instrument. Especially in the calorimetric studies, even minute amounts of these corrosion products may cause violent explosions.

All measurements refer to 25.0 °C and a sodium perchlorate medium of unit ionic strength.

EXPERIMENTAL

Chemicals. Gallium(III) perchlorate and indium (III) perchlorate were prepared by dissolving Ga_2O_3 (Fluka, *puriss. C*) and In_2O_3 (Fluka, *purum*) respectively, in perchloric acid (Merck, *p.a.*) and recrystallizing once from an acidic aqueous solution.

Analyses for Ga(III) and In(III) were made gravimetrically by precipitating the oxides.[5] The free acid concentrations in the stock solutions were determined potentiometrically and/or by passing aliquots through columns of Dowex-50 W cation exchange resin in the hydrogen ion form and titrating the eluate with standard sodium hydroxide solutions. Both methods gave the same results.

Sodium azide and sodium perchlorate were prepared and analyzed as described before.[6] The Ag, AgCl electrodes were prepared according to Brown.[7]

Apparatus. A Metrohm E 580 ion activity meter equipped with a Metrohm EA 109 glass electrode was used for the equilibrium measurements. The slope of the glass electrode was checked repeatedly and found to be 59.2 ± 0.2 mV. The titration calorimeter used was described previously.[8,9]

Procedure. The procedures used in the equilibrium measurements have been described before.[10,11] These measurements were arranged as titrations at constant metal ions and acid concentrations, C_M and C_H, respectively.

The emfs of the following cell were measured:

$$+\text{GE}|C_M\text{ M Me}(ClO_4)_3,\ C_H\text{ M HClO}_4,\ C_L\text{M NaN}_3,\ \text{NaClO}_4\text{ to} = 1\text{ M}||\text{RE}-$$

where

$$\text{RE}|| = \text{Ag, AgCl}|0.025\text{ M NaCl, }0.975\text{ M NaClO}_4|1.0\text{ M NaClO}_4|.$$

* Present address: Department of Physical Chemistry, Faculty of Chem. Engineering, Campus of Ayazağa, Emirgăn, Istanbul, Turkey.

0302-4377/82/080627-05$02.50

Here, Me denotes gallium or indium. Each titration was repeated at least four times. Stable emfs were reached in a few minutes. The reproducibility was generally within ± 0.4 mV, and even better for the indium(III) azide system.

The technique of the calorimetric studies has been described elswhere.[10,12] The measurements were carried out as a series of titrations of a solution T into a solution S. Usually the solution S contained the metal ion and T the ligand. In order to reach higher ligand concentrations, however, some titrations were performed where the central ion was added to a ligand solution. The case of indium(III) azide system is a good example. This procedure was not possible for the gallium(III) azide system because of the extensive hydrolysis of gallium(III).

The heats of dilution were determined by similar measurements where either the ligand or the central ion solution had been exchanged for a sodium perchlorate solution of the same ionic strength.

MEASUREMENTS AND RESULTS

Gallium(III) azide. The potentiometric titrations were performed with three different values of C_M, *i.e.* 40, 60 and 80 mM. The acid concentrations, constant during the titrations, were 293, 339 and 386 mM, respectively. A free ligand ion concentration up to $\simeq 3$ mM could be reached in the measurements. Higher concentrations are not possible as most of the ligand is present as undissociated species HN_3.

In this concentration range, only the first mononuclear complex is formed and its formation constant could thus be determined. There is no indication of the formation of other azide complexes beyond the first step. However, hydrolysis of Ga(III) is observed.

In the gaphical calculation of the constant[13] the X_1 *vs.* [L] plot turns out to decrease for increasing values of [L]. From these measurements, only the first formation constant can therefore be calculated. To do this, the free ligand concentration [L] and the average ligand number $\bar{n}$ must first be calculated. Thus, it is necessary to know the ionization constant of hydrazoic acid under the same conditions. This has previously been determined[6] as $K_a = 3.61 \times 10^{-5}$ M. Hence, [L] and $\bar{n}$ can be calculated in the usual way. If only the first complex is formed then eqn. (1) can be written.

$$\frac{1}{\bar{n}} = \frac{1}{\beta_1[L]} + 1 \qquad (1)$$

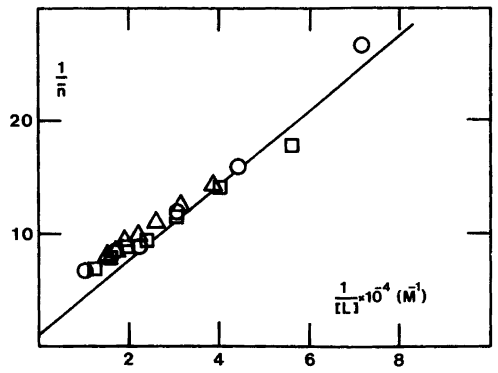

Fig. 1. The determination β_1 for $Ga(Na_3)^{2+}$ [see eqn. (1)]. ○, $C_M = 40$ mM, $C_H = 293$ mM; □, $C_M = 60$ mM, $C_H = 339$ mM; △, $C_M = 80$ mM, $C_H = 386$ mM.

A plot of $1/\bar{n}$ *vs.* $1/[L]$ should therefore give a straight line with intercept 1 and a slope of $1/\beta_1$, Fig. 1. A value of $(3 \pm 1) \times 10^3$ M^{-1} for β_1 could thus be estimated. The errors given correspond to estimated errors from the graphical calculation.

Three different values of C_M, *i.e.* 10,20 and 30 mM, were chosen in the calorimetric measurements. A ligand solution of $C_L = 500$ mM was added. The initial acid concentrations in the metal ion solutions were 43, 100 and 100 mM, respectively. Proton as well as gallium(III) complexes are formed in the calorimetric titrations.

Large exothermic heats are first measured during the titrations. When a certain ligand concentration is reached, however, an abrupt change to large endothermic heats is observed. A white precipitate is finally formed, probably due to hydrolytic reactions.[4] Such side reactions are so extensive that even after a few points in the titrations their influences on the measured heats can be seen. The calorimetric titrations were interrupted at these points.

From the calorimetric data, the value of ΔH_1° can be evaluated. The value of ΔH° of the HN_3 formation must then be known. In an earlier investigation[6] $\Delta H^\circ = -12.76$ kJ mol^{-1} has been found.

Using the value of β_1 found potentiometrically and the values of K ($K = 1/K_a$) and ΔH° for the formation of HN_3, a value of ΔH_1° for $Ga(N_3)^{2+}$ can be estimated by the least squares computer program "Letagrop Kalle".[14] A good fit of the calorimetric data is, however, not possible with $\beta_1 = 3 \times 10^3$ M^{-1}. On the other hand, values of β_1 varying between 10^3 and 10^5 M^{-1} do not give a

Table 1. The overall formation constants and the values of ΔG_j°, ΔH_j° and ΔS_j° for the consecutive steps of the gallium(III) and indium(III) azide systems at 25.0 °C and $I = 1$ M. The errors given correspond to confidence limits on the 99.9 % level of significance or to estimated errors.

System	j	β_j (M^{-j})	$-\Delta G_j^\circ$ (kJ mol^{-1})	$-\Delta H_j$ (kJ mol^{-1})	ΔS_j° (J mol^{-1} K^{-1})
Ga(III)$-N_3^-$	1	$(3\pm1)\times10^3$	20 ± 1	23 ± 6	-10 ± 20
In(III)$-N_3^-$	1	$(1.54\pm0.05)\times10^3$	18.2 ± 0.1	7.4 ± 0.3	36 ± 1
	2	$(4.1\pm0.1)\times10^5$	13.9 ± 0.1	4.0 ± 0.8	33 ± 3
	3	$(1.8\pm0.1)\times10^7$	9.4 ± 0.2	10 ± 1	-2 ± 5
	4	$(2.9\pm0.3)\times10^8$	6.9 ± 0.3	9 ± 2	-6 ± 8

much better fit with the enthalpy data. Some of the results of these calculations are given below:

β_1 (M^{-1})	SIG Y(see Ref. 14)	U (Ref. 14)	$-\Delta H_1^\circ$ (kJ mol^{-1})
1×10^3	0.543	6.78	29.7 ± 4.1
3×10^3	0.454	4.84	22.9 ± 1.8
4×10^3	0.428	4.27	21.8 ± 1.4
5×10^3	0.403	3.74	21.1 ± 1.2
1×10^4	0.320	2.36	19.3 ± 0.7
1×10^5	0.329	2.49	15.7 ± 0.3

The errors given are one standard deviations. As seen, the increasing values of β_1 seem to give a somewhat better fit. However, such large values of β_1 are not computible with the potentiometric data. Since the estimate of the potentiometric data is much more reliable this has been accepted for the value of β_1. Thus, a value of -23 ± 6 k.J. mol^{-1} can be found for ΔH_1°, Table 1.

Indium(III) azide. In the potentiometric measurements four different values of C_M have been chosen for this system. Higher ion concentrations could be used without hydrolysis occurring. For $C_M = 40$ mM, values of C_H 108 and 150 mM, for $C_M = 80$ mM 116 and 159 mM were chosen. In the other two series, the values of C_M were 120 and 160 mM, with the values of C_H 274 and 318 mM, respectively. A free ligand ion concentration of $\simeq 90$ mM could be reached. The formation function is independent of C_M and C_H, in spite of the fairly large variation of both C_M and C_H during the measure-

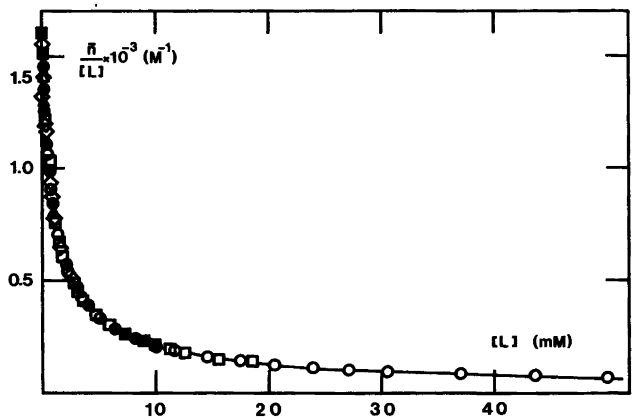

Fig. 2. $\bar{n}/[L]$ as a function of [L] for the indium(III) azide system. Only half of the experimental points, chosen at random, have been plotted. ○, $C_M = 40$ mM, $C_H = 108$ mM; ●, $C_M = 40$ mM, $C_H = 150$ mM; □, $C_M = 80$ mM, $C_H = 116$ mM; ■, $C_M = 80$ mM, $C_H = 159$ mM; △, $C_M = 120$ mM, $C_H = 274$ mM; ▲, $C_M = 160$ mM, $C_H = 318$ mM.

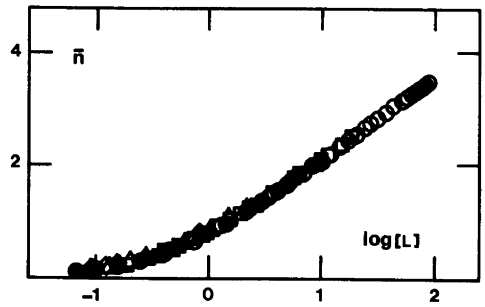

Fig. 3. The complex formation function of the indium(III) azide system. For symbols refer to Fig. 2 ([L] in mM).

ments, which proves that neither polynuclear nor acid complexes are formed, Figs. 2 and 3.

The constants have been evaluated both graphically[13] and numerically.[15] The methods gave concordant values. Four mononuclear complexes are formed in the range studied, Table 1.

In the calorimetric study, ten titration series were performed. In four of these a ligand solution, of C_L = 500 mM, was added to 90.0 ml of indium(III) perchlorate solutions with different values of C_M and C_H. The initial indium(III) concentrations were 10, 20 and 40 mM. For C_M = 10 and 20 mM a value of C_H = 20 mM was used while for C_M = 40 mM values of C_H = 40 and 92 mM were applied. In the other series, an indium solution, of C_M = 100 mM and C_H = 100 mM, was added to both buffered and unbuffered sodium azide solutions.

However, due to precipitation of the hydroxide an unbuffered sodium azide solution could not be used in the measurements. Free ligand ion concentrations >100 mM were reached in the calorimetric titrations.

The enthalpy changes have been calculated by the computer program "Letagrop Kalle"[14] with the values of β_j found in the potentiometric study and the values of K and $\Delta H°$ for the formation of HN_3, determined earlier,[6] as fixed parameters.

The free energy changes $\Delta G_j°$ are calculated from the stepwise formation constants K_j and by combining these with the enthalpy changes $\Delta H_j°$ the entropy changes $\Delta S_j°$ are finally obtained. The results of this investigation are collected in Table 1.

DISCUSSION

The complex GaN_3^{2+} is slightly more stable than InN_3^{2+} though the error of β_1 (GaN_3^{2+}) is so large that a reliable comparison is not really possible. The formation of GaN_3^{2+} is much more exothermic than that of InN_3^{2+}. The entropy change is not large as to be expected for a typically hard acceptor.[16] On the contrary, the values of $\Delta H_1°$ and $\Delta S_1°$ of the gallium(III) azide system give the impression that the interaction has indeed a soft character. Probably the nature of the ligand may play an important role in this connexion. The stability of GaN_3^{2+} is greatly determined by enthalpy change.

Much the same values of the enthalpy changes are found for the successive steps in the azide system of indium(III), except for the second step which has a slightly less exothermic value.

Probably, bonds of nearly the same character are formed. For the first and second steps almost the same values of $\Delta S°$ are obtained. The same is also valid for the third and fourth steps. In this respect, a parallelism can be seen with the corresponding azide complexes of Cd(II)[3]. For the first and second steps, the contributions of the enthalpy and the entropy changes to the decrease of free energy are much the same, while for the last two steps the driving force is evidently the enthalpy decrease, Table 1.

Acknowledgements. The author wishes to thank Prof. Sten Ahrland and Dr. Arvid Sandell for their valuable advice and kind interest in this work. The grant from the Swedish Institute and the permission of the Faculty of Chemical Engineering (I.T.Ü.), which made it possible to carry out the work, are gratefully acknowledged.

REFERENCES

1. Ahrland, S. and Avsar, E. *Acta Chem. Scand. A 29* (1975) 890.
2. Gerding, P. *Acta. Chem. Scand. 20* (1966) 2771.
3. Ahrland, S. and Avsar, E. *Acta Chem. Scand. A 30* (1976) 15.
4. Smith, R. M. and Martell, A. E. *Critical Stability Constants*, Vol. 4, Plenum, New York, London 1976.
5. Hillebrand, W. F., Lundell, G. E. F., Bright, H. A. and Hoffman, J. I. *Applied Inorg. Analysis*, Wiley-Chapman, New York, London 1955.
6. Ahrland, S. and Avsar, E. *Acta Chem. Scand. A 29* (1975) 881.
7. Brown, A. S. *J. Am. Chem. Soc. 56* (1934) 646.
8. Grenthe, I., Ots, H. And Ginstrup, O. *Acta Chem. Scand. 24* (1970) 1067.
9. Ots, H. *Acta Chem. Scand. 26* (1972) 3810.
10. Avsar, E. *Acta Chem. Scand. A 34* (1980) 405.

11. Avsar, E. *J. Inorg. Nucl. Chem. 42* (1980) 881.
12. Ahrland, S. and Kullberg, L. *Acta Chem. Scand. 25* (1971) 3471.
13. Fronaeus, S., In Jonassen, H. B. and Weisberger, A., Eds., *Techniques of Inorg. Chem.*, Interscience, New York, London 1963, Vol. 1, Chapter 1.
14. Arnek, R. *Ark. Kemi 32* (1970) 81.
15. Chandler, J. P. *STEPIT 5, Quantum Chemistry Program Exchange*, Dept. of Chemistry, Indiana University, Bloomington, Indiana, U.S.A. 1965.
16. Ahrland, S. *Struct. Bonding (Berlin) 15* (1973) 167.

Received October 29, 1981.

Acta Chemica Scandinavica A 36 (1982) 633–636

Dissociation, Distribution and Polymerization Constants for Dibutylphenacylphosphonate (HDBPP)

J. P. BRUNETTE,* U. OLOFSSON, A. SELME and B. ALLARD

Department of Nuclear Chemistry, Chalmers University of Technology, S-412 96 Gothenburg, Sweden

The distribution of dibutylphenacylphosphonate between 1 M $(Na,H)ClO_4$ and organic diluents (n-hexane, n-heptane, benzene, toluene) has been studied by a spectrophotometric method, as well as the dissociation in the aqueous phase and the di- and trimerization in the organic phase. The following constants (25 °C) were obtained: Dissociation ($K_a = [H^+][A^-]/[HA]$): 12.30 ± 0.03; distribution ($K_d = [\overline{HA}]/[HA]$): 29.8 ($\Delta H° = 16.8$ kJ/mol, $T\Delta S° = 25.2$ kJ/mol; n-heptane), 35.0 (n-hexane), 1200 ± 200 (benzene) and 1400 ± 200 (toluene); dimerization ($K_n = [(\overline{HA})_n]/[\overline{HA}]^n$, n = 2): 7.95 ($\Delta H° = -11.8$ kJ/mol, $T\Delta S° = -6.6$ kJ/mol; n-heptane), 6.7 (n-hexane), and trimerization (n = 3): 210 (n-heptane), 150 (n-hexane).

Although some metal complexes and metal extraction system using β-ketophosphonates as ligands or extractants have been studied[1-12], very little information is available concerning the properties of these complexing agents in two-phase systems, *i.e.* distribution constants (K_d), dissociation constants (K_a) and possible polymerization constants (K_n). These parameters are required for the interpretation of metal extraction processes. This paper describes a determination of these constants for dibutylphenacylphosphonate [HDBPP; composition $C_6H_5C(O)CH_2P(O)(OC_4H_9)_2$] in aqueous 1 M $NaClO_4$ – n-hexane, n-heptane, benzene and toluene systems.

EVALUATION METHODS

Neglecting any aggregation in the aqueous phase and any dissociation in the organic phase, an acidic extractant HA in a two-phase liquid system can generally be described by the following equilibria:

$$HA \rightleftharpoons H^+ + A^- \quad (K_a, \text{ dissociation constant})$$
$$HA \rightleftharpoons \overline{HA} \quad (K_d, \text{ distribution constant})$$
$$n\overline{HA} \rightleftharpoons (\overline{HA})_n \quad (K_n, \text{ polymerization constant})$$

(overlined symbols refer to species in the organic phase).

The distribution ratio D is defined by

$$D = [\overline{HA}]_{tot}/[HA]_{tot}$$

giving eqn. (1).

$$D = (K_d + \sum_2^n nK_nK_d^n[HA]^{n-1})/(1 + K_a[H^+]^{-1}) \quad (1)$$

K_d and K_n determination. For $pH \ll pK_a$, D is independent of pH and eqn. (1) can be written as eqn. (2). A plot of D *vs.* [HA] permits a determination

$$D = K_d + \sum_2^n nK_nK_d^n[HA]^{n-1} \quad (2)$$

of the constants K_d and K_n with $K_d = D([HA] = 0)$, assuming that K_d is constant, independently of [HA].

K_a determination. For $[HA] \to 0$, the aggregation of HA in the organic phase can generally be neglected and eqn. (1) can be written as

$$D = K_d(1 + K_a[H^+]^{-1})^{-1}$$

or eqn. (3). Thus, pH *vs.* $\log(K_dD^{-1} - 1)$ is a straight line with slope 1 and intercepts pK_a. (It is assumed that K_d is constant in the pH range studied.)

$$pH = \log(K_dD^{-1} - 1) + pK_a \quad (3)$$

*On leave from the Laboratoire de Chimie Minérale, Ecole Nationale Supérieure de Chimie, B.P. 296 R8 67008 Strasbourg Cedex, France.

0302-4377/82/080633-04$02.50

EXPERIMENTAL

Chemicals. Sodium perchlorate was prepared and purified according to conventional methods. HDBPP was prepared, purified and checked as described previously.[9] All other chemicals were of *p.a.* quality and used without further purification.

Distribution measurements. The distribution of HDBPP between an aqueous sodium perchlorate solution and organic phases was studied in a thermostated vessel (±0.1 °C). The two phases (with an initial HDBPP concentration in the organic phase between 10^{-4} and 1.7×10^{-3} M) were vigorously stirred for one hour and then allowed to separate by gravity. For each distribution ratio determination, an aliquot of each phase was withdrawn and diluted with ethanol and the UV spectrum recorded. The UV absorption spectrum of HDBPP in ethanol contains a strong absorption band at 246 nm with a maximum extinction coefficient (ε_{max}) of 13 000 M^{-1} cm^{-1} and a shoulder at 280 nm with $\varepsilon_{max} \sim 1200$ M^{-1} cm^{-1}. The Beer-Lambert law was checked and the 246 nm band used to determine HDBPP concentrations in the two phases. When benzene and toluene were used as solvents, the measurements had to be corrected taking into account the absorption of the solvents themselves (this explains the low relative precision of the corresponding measurements).

In order to check the direct measurements of low HDBPP concentrations in highly dissociated systems, the total aqueous HDBPP concentration was calculated from the difference between the added HDBPP and the measured organic HDBPP concentration. The calculated $[HDBPP]_{tot}$-values were verified by direct UV measurements on the aqueous solutions which were pH adjusted after separation of the phases to suppress the HDBPP dissociation effect.

All UV measurements were performed on a Perkin-Elmer 551 spectrophotometer using 1 cm quartz cells.

Table 1. Distribution and polymerization constants.

Diluent	*t*, °C	K_d	K_2	K_3
	10.0	19.0	10.1	215
n-Heptane	24.9	29.8	7.95	210
	39.4	37.3	6.3	230
n-Hexane	25.0	35.0	6.7	150
Benzene	25.0	1200±200	–	–
Toluene	25.0	1400±200	–	–

RESULTS AND DISCUSSIONS

K_d *and* K_n *determinations.* The determinations of distribution constants and polymerization constants were performed using an aqueous phase of 1 M $(Na,H)ClO_4$ at pH 4, and n-hexane, n-heptane, benzene and toluene as organic diluents. Fig. 1 shows a plot of *D vs.* [HDBPP] at different temperatures for n-heptane and n-hexane. According to

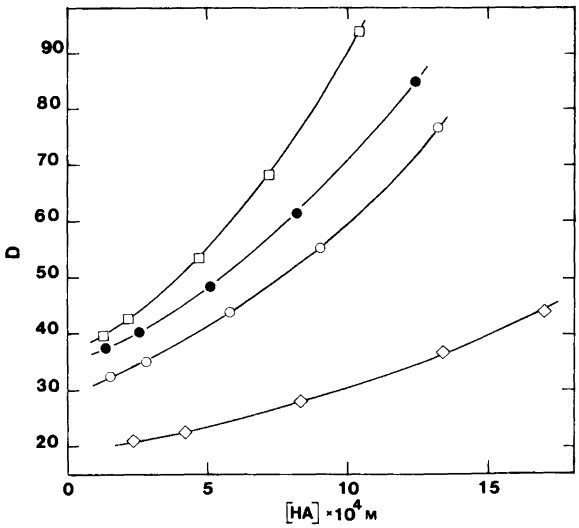

Fig. 1. Distribution ratios of HDBPP in 1 M $(Na,H)ClO_4$ – n-heptane and n-hexane. □, 39.4 °C; ○, 24,9 °C; ◇, 10.0 °C – n-heptane; ●, 25.0 °C – n-hexane.

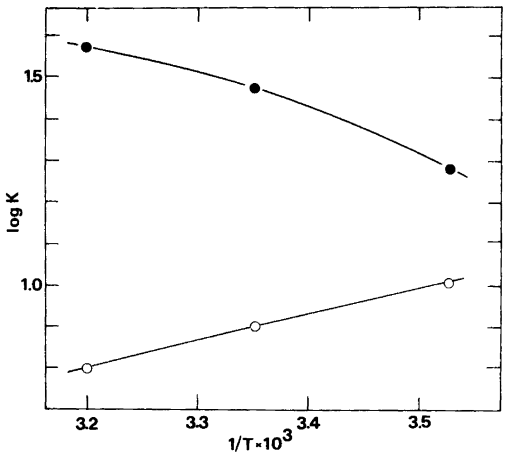

Fig. 2. log K_2 and log K_d *vs.* $1/T$. ○, log K_2; ●, log K_d – n-heptane.

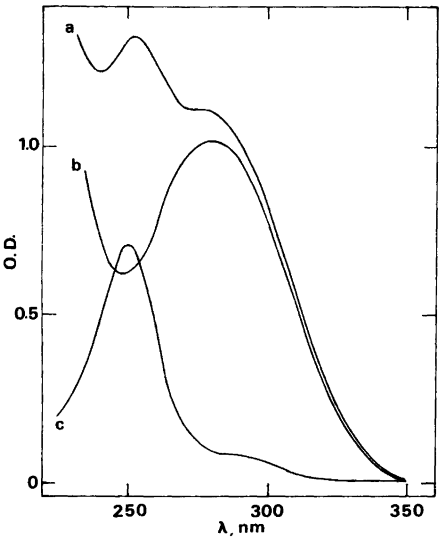

Fig. 3. UV spectra of HDBPP – $DBPP^-$ (optical density, O. D., *vs.* wave length, λ). a. Aqueous phase 1 M (Na,H)ClO_4, pH 12.66, after shaking with a 0.00205 M HDBPP – n-heptane solution. b. $DBPP^-$ in aq, 14.0×10^{-5} M; $\varepsilon_{280} = 7000$ M^{-1} cm^{-1}. c. HDBPP in n-heptane, 6.1×10^{-5} M; $\varepsilon_{250} = 11200$ M^{-1} cm^{-1}.

eqn. (2), the non-linearity of the curves is consistent with a polymerization ($n > 2$). Assuming a trimerization of HDBPP in n-heptane, the experimental results can be well described by eqns. (4)–(6). A similar result is obtained for n-hexane;

$$D(10\,^\circ\text{C}) = 19.0 + 7330[\text{HDBPP}] + 4.38 \times 10^6[\text{HDBPP}]^2 \quad (4)$$

$$D(24.9\,^\circ\text{C}) = 29.8 + 13800[\text{HDBPP}] + 16.3 \times 10^6[\text{HDBPP}]^2 \quad (5)$$

$$D(39.4\,^\circ\text{C}) = 37.3 + 17500[\text{HDBPP}] + 35.8 \times 10^6[\text{HDBPP}]^2 \quad (6)$$

$$D(25.0\,^\circ\text{C}) = 35.0 + 16400[\text{HDBPP}] + 19.5 \times 10^6[\text{HDBPP}]^2 \quad (7)$$

eqn. (7). Using eqns. 2, 4, 5, 6 and 7, K_d, K_2 and K_3 were calculated, Table 1, Fig. 2. For the benzene and toluene systems, the distribution constants were independent of [HDBPP] (in the concentration range $0 < [\text{HDBPP}] < 0.6$ M), which shows that HDBPP is not aggregated in these dilutents. This result is consistent with previous observations from cryoscopic measurements[9] that HDBPP is monomeric in benzene.

The influence of pH on the distribution constant (in the 1 M (Na,H)ClO_4 – n-heptane system, 25 °C) has also been investigated. For $2 < \text{pH} < 10$, other parameters kept constant, the distribution ratio is independent of pH. (The UV spectra of the two phases are constant). For the studied pH range no detectable dissociation of HDBPP occurs.

The hypothesis of extraction of $HClO_4$ by HDBPP as an explanation of the non-linearity of the curves D *vs.* [HDBPP] (Fig. 1) can be eliminated ($HClO_4$ extraction would only occur at lower pH).

pK_a determination. When pH is increased over 10, the UV spectra of the aqueous phases are progressively changed as an effect of HDBPP dissociation. Each spectrum can be decomposed into two spectra corresponding to HDBPP and $DBPP^-$ (Fig. 3). The UV spectrum of $DBPP^-$ has a broad adsorption band at 280 nm with an ε_{max} of 7000 M^{-1} cm^{-1}. If pH is adjusted back to $\text{pH} < 10$, the spectrum of undissociated HDBPP is quantitatively recovered which shows the reversibility of the dissociation and permits quantitatively measurements of aqueous $[\text{HDBPP}]_{tot}$.

The curve pH *vs.* $\log(K_d D^{-1} - 1)$ is given in Fig. 4. The observed slope of 1.03 is close to the theoretical value of 1. The pK_a-value from the intercept is 12.30 ± 0.03, which is higher than for most of the β-diketones (*e.g.* for acetylacetone).[13] Thus, HDBPP would be expected to act as a chelating

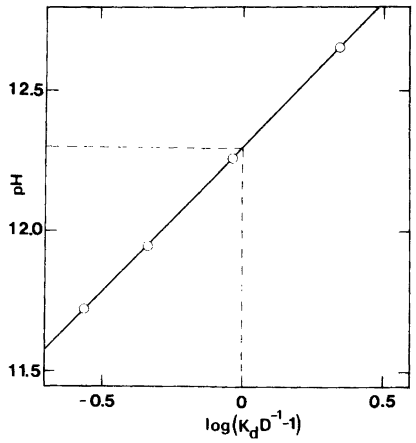

Fig. 4. Dissociation constant of HDBPP at 25 °C. (pH *vs.* $\log(K_dD^{-1}-1)$. Aqueous phase: 1 M (Na,H)-ClO_4; organic phase n-heptane.

extractant in a higher pH-range than *e.g.* acetylacetone.

Temperature effects. From the temperature dependence of K_d and K_2 in the n-heptane system (*cf.* Table 1 and Fig. 2) and according to the relationship $\Delta G^\circ = \Delta H^\circ - T\Delta S^\circ = -RT\ln K$, the following thermodynamic constants were calculated (25 °C):

Distribution: $\Delta H^\circ = 16.8 \pm 1.2$ kJ/mol, $T\Delta S^\circ = 25.2 \pm 1.2$ kJ/mol.

Dimerization: $\Delta H^\circ = -11.8 \pm 1.0$ kJ/mol, $T\Delta S^\circ = -6.6 \pm 1.0$ kJ/mol.

(The uncertainty in the K_3-values is too large to allow any calculation of ΔH°- and $T\Delta S^\circ$-values for the trimerization.) Thus, it is evident that a temperature increase favours a transfer of HDBPP from the aqueous phase to the n-heptane phase, which would be expected, considering the similarity with the β-diketones,[13] but disfavours the dimerization in the organic phase.

Acknowledgement. This work was partly financed by the Swedish Natural Science Research Council (NFR).

REFERENCES

1. Warren, C. J. *J. Inorg. Nucl. Chem. 23* (1961) 103.
2. Cotton, F. A. and Schunn, R. A. *J. Am. Chem. Soc. 85* (1963) 2394.
3. Lestas, C. N. and Truter, M. R. *J. Chem. Soc. A* (1971) 738.
4. Youinou, M. T. and Guerchais, J. E. *Inorg. Chem. Acta 19* (1976) 257.
5. Youinou, M. T., Guerchais, J. E., Louër, M. E. and Grandjea, D. *Inorg. Chem. 16* (1977) 872.
6. Sevdic, D. and Meider-Gorican, H. *J. Less. Common Met. 27* (1972) 403.
7. Bronzan, P. and Meider-Gorican, H. *J. Less Common Met. 29* (1972) 407.
8. Youinou, M. T. and Guerchais, J. E. *J. Chem. Soc. Dalton Trans* (1976) 293.
9. Martin, J. L. and Leroy, M. J. F. *J. Chem. Res. S* (1978) 88.
10. Brunette, J. P., Leroy, M. J. F., Ceccaroli, B. and Alstad, J. *Acta Chem. Scand. A 32* (1978) 415.
11. Alstad, J., Ceccaroli, B., Brunette, J. P. and Leroy, M. J. F. *Proc. Int. Solvent Extraction Conf., ISEC 80*, Liege 1980, p. 80–48.
12. Olofsson, U., Brunette, J. P., Allard, B. and Selme, A. *Proc. Int. Solvent Extraction Conf., ISEC 80*, Liege 1980, p. 80–6.
13. Liljenzin, J. O. *Acta Chem. Scand. 23* (1969) 3592.

Received December 14, 1981.

Acta Chemica Scandinavica A 36 (1982) 637 – 639

On the Molecular Structure of Nitrocyclopropane

ANNE SKANCKE

Department of Chemistry, Institute of Mathematical and Physical Sciences, University of Tromsø, Box 953, N-9001 Tromsø, Norway

Ab initio calculations have been carried out on the title compound. The bisected form is found to be the more stable. Small variations in geometry between the bisected and symmetrical forms may be explained on the basis of symmetry arguments.

The versatile chemistry of cyclopropane and its derivatives has been in the focus of interest for several decades. The bonding aspects have been qualitatively described on the basis of the Walsh model,[1] and for pi interacting systems predictions concerning the interactions between the ring orbitals and substituents may be based on the rationale by Hoffmann.[2] A confirmation of this rationale is found in a survey of microwave spectroscopy data by Penn and Boggs.[3] These authors were able to show a consistent shortening of the C–C bond opposite the substituent, and in the few cases where also the adjacent C–C bond was determined, this was found to be lengthened.

In a series of previous papers[4–8] we have shown that structure parameters for cyclopropane derivatives may be calculated within the Hartree-Fock approximation. Even with moderate basis sets the results were found to be comparable in quality with the results obtained from good experiments.

Such calculations have been greatly simplified with the use of the gradient technique, which has been used throughout the present work. Descriptions of the applied computer programme and basis set (4 – 21 contracted to double zeta) are found elsewhere.[9,10]

We here report on the structure of nitrocyclopropane. This molecule has been investigated by Boggs and coworkers by microwave technique[11] and in a recent vibrational study by Bush and coworkers.[12] Both investigations agree that of the two possible forms (See Fig. 1) the bisected form is the more stable. The barrier height is calculated to be 13.8 ± 6.3 kJ/mol in the microwave work and 19.7 ± 0.6 kJ/mol in the Raman work. This relatively high barrier is of the same order of magnitude as the barrier in nitroethylene[13] and nitrobenzene,[14] in contrast to the barrier of only 0.06 kJ/mol in nitroethane.[15] The substituent to ring interaction has been quantitatively determined in the above-mentioned Raman work where, from a comparison of NO_2 stretching frequencies this molecule has "pseudo-conjugational" properties intermediate between nitro-olefins and nitro-paraffins. The similarity of the cyclopropane compound with the true pi electron systems is thus

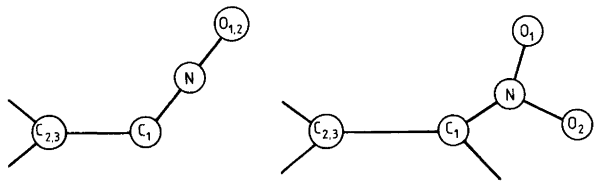

a b

Fig. 1. Projections of the bisected (a) and symmetrical (b) conformations of nitrocyclopropane.

0302-4377/82/080637-03$02.50

found to be striking, and is an indication of the conjugative ability of the extra-annular Walsh orbitals of the ring and unpopulated substituent orbitals. In this case the obvious orbital of choice is the vacant nitrogen p orbital.

RESULTS AND DISCUSSION

The computed parameters are given in Fig. 2.

As is seen from this figure, there is a marked difference between the symmetrical and bisected structures, the former having a lengthened opposite and a shortened adjacent bond, the reverse being the case for the latter form. Although the differences are only of the order of magnitude of a few hundreds of an Ångstrøm, experience from our previous work in this area [4-8] give us reason to believe the differences to be significant.

For instance, in the case of cyclopropyl amine, our predicted C_1-C_2 and C_2-C_3 values were 1.508 and 1.512 Å, respectively, in contrast to existing microwave data [16] yielding 1.535 ± 0.006 Å and 1.513 ± 0.003 Å. However, a reinvestigation of the spectroscopic data [17] gave an unchanged value for C_2-C_3 while the value of C_1-C_2 was changed to 1.486 ± 0.008 Å. Although our computed bond length difference was smaller, the trend of a shorter C_1-C_2 bond and a longer C_2-C_2 bond was predicted in our calculation.

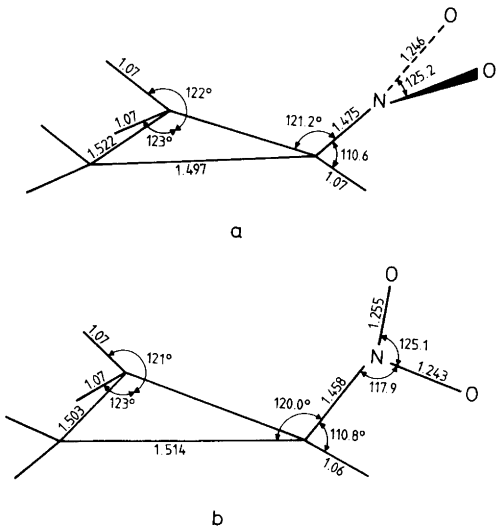

Fig. 2. Geometry parameters resulting from 4-21 optimization.

Other examples are offered in 1,1-dichlorocyclopropane [5] and cyclopropyl cyanide.[7] For both these cases, our calculations were sufficiently reliable to choose between conflicting experimental data.

Direct comparison between experimental and calculated absolute values of bond distances are complicated since the former are normally given as r_a or r_s and the latter as r_e. Also, a limited basis set and neglect of electron correlation may cause significant errors in the absolute values of distances but, in carefully selected cases, these errors cancel when trends in distances or differences between distances are studied. These differences may be either between the corresponding bond in a series of molecules, or, as presently between two C-C bonds in one molecule.

In the particular case of cyclopropyl derivatives we found that our calculations were useful since structure determination by microwave spectroscopy and electron diffraction are difficult (locating C_1 in microwave and resolving close distances in electron diffraction).

In our previous above-mentioned papers, we have emphasized the necessity of invoking symmetry arguments in explaining the induced ring asymmetry. We find that the nitrocyclopropane molecule serves as an excellent illustration of this point. In this case a simple rotation around a single bond leads to different orbital interactions and different ring structures. Both possible forms have an empty *p* orbital perpendicular to the nitro group, for the bisected form this leads to interaction into the antisymmetric component of the occupied Walsh orbital, as suggested by Hoffmann.[2] This leads to a shortening of the opposite bond and a corresponding lengthening of the adjacent bond. For the other conformer, this is a symmetry forbidden interaction, and the only possible mixing is with a totally symmetrical ring orbital, which is the other degenerate *e'* orbital. The relevant orbitals are shown in Fig. 3. The same orbitals are used by Durmaz and Kollmar [18] in a general theoretical

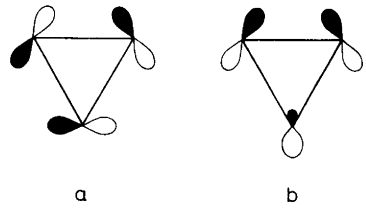

Fig. 3. Walsh MO's of cyclopropane.

discussion of the interaction of cyclopropane with various substituents.

The spectroscopic observables did not suffice for a complete structure determination, but the microwave investigation reports structure data based upon certain assumptions. Although it may be fortuitous, the assumption of the ring being equilateral with C−C bond lengths of 1.511 Å appears to be in good agreement with the results of the present calculation. There is, however, a difference between the reported and computed C−N and N=O bond lengths. The experimental values were 1.488 ± 0.0002 and 1.213 ± 0.0001 Å, respectively. These small standard deviations are a measure of the fit to the rotational constants and, taking the large number of assumptions into account, the authors expect the actual uncertainties to be as large as 0.02 Å for both distance types. In view of this, we find the agreement between this experimental work and the present calculations to be satisfactory. Also, a previous work with the 4−21 basis set [19] gave a lengthening of an N=O bond of 0.02 Å compared to an experimental r_s distance.

The computed energy difference between the two forms is 27,6 kJ/mol, somewhat higher than the experimental values.

As a final point, it may be mentioned that preference for the bisected conformer is also reported in a recent microwave, infrared, Raman and NMR spectroscopic work on cyclopropyldifluoreborane [20] and in a recent infrared and Raman spectroscopy work on the corresponding chlorine compound.[21]

REFERENCES

1. Walsh, A. D. *Trans. Farday Soc. 45* (1949) 179.
2. Hoffmann, R. *Tetrahedron Lett. 33* (1970) 2907.
3. Penn, R. E. and Boggs, J. E. *J. Chem. Soc. Chem. Commun.* (1972) 666.
4. Skancke, A., Flood, E. and Boggs, J. E. *J. Mol. Struct. 40* (1977) 263.
5. Skancke, A. *J. Mol. Struct. 42* (1977) 235.
6. Skancke, A. and Boggs, J. E. *J. Mol. Struct. 50* (1978) 173.
7. Skancke, A. and Boggs, J. E. *J. Mol. Struct. 51* (1979) 267.
8. Skancke, A. and Boggs, J. E. *Acta Chem. Scand. A 32* (1978) 893.
9. Pulay, P. *Theor. Chim. Acta 50* (1979) 299.
10. Pulay, P., Fogarasi, G., Pang, F. and Boggs, J. E. *J. Am. Chem. Soc. 101* (1979) 2550.
11. Mochel, A. R., Britt, C. O. and Boggs, J. E. *J. Chem. Phys. 58* (1973) 3221.
12. Holtzclaw, J. R., Harris, W. C. and Bush, S. F. *J. Raman Spectrosc. 9* (1980) 257.
13. Meyer, R., Gammeter, A., Smith, P., Kuhne, H., Mosberger, P. and Gunthard, H. *J. Mol. Spectrosc. 46* (1973) 397.
14. Høg, J. H., Nygaard, L. and Sørensen, G. O. *J. Mol. Struct. 7* (1971) 111.
15. Groner, P., Meyer, R. and Gunthard, H. *J. Chem. Phys. 11* (1975) 63.
16. Harmony, M. D., Bostrøm, R. E. and Hendricksen, D. K. *J. Chem. Phys. 62* (1975) 1599.
17. Mathur, S. N. and Harmony, M. D. *J. Chem. Phys. 69* (1978) 4316.
18. Durmaz, S. and Kollmar, H. *J. Am. Chem. Soc. 102* (1980) 6942.
19. Cordell, F. R., Boggs, J. E. and Skancke, A. *J. Mol. Struct. 64* (1980) 57.
20. Odom, J. D., Szafran, Z., Johnston, S. A., Li, Y. S. and Durig, J. R. *J. Am. Chem. Soc. 102* (1980) 7173.
21. Durig, J. R., Trowell, P. L., Szafran, Z., Johnston, S. A. and Odom, J. D. *J. Mol. Struct. 74* (1981) 85.

Received January 19, 1982.

Acta Chemica Scandinavica A 36 (1982) 641 – 656

The Vibrational Spectra of Chloro-, Bromo- and Iodocyclohexane

T. WOLDBÆK

Department of Chemistry, University of Oslo, Oslo 3, Norway

The IR spectra of chloro-, bromo- and iodocyclohexane as liquids at various temperatures, as solids and as solutes in different solvents were recorded in the region 4000 – 50 cm^{-1}. High pressure IR spectra of the pure samples (0 – 40 kbar) in a diamond anvil cell were obtained, and dichroism of oriented crystalline films was measured. Raman spectra of the amorphous and crystalline solids at low temperature were recorded, and semiquantitative polarization ratios were measured for liquid chloro- and bromocyclohexane. In addition, FIR spectra (600 – 50 cm^{-1}) of the cyclohexanes as guest molecules in thiourea clathrates were obtained.

A normal coordinate analysis was performed for both conformers of all the three molecules, using a constrained valence force field analogous to that of the *trans*-1,4-dihalocyclohexanes. Tentative assignments of the fundamentals belonging to the *e*- and *a*-conformers are presented in agreement with the results from the normal coordinate calculations.

Chloro-, bromo- and iodocyclohexane have been studied in great detail by a variety of physical methods. In the vapour phase, in solution, in the liquid state and as amorphous solids at 90 K, they exist as equilibrium mixtures of equatorial and axial conformers, although the *e*-conformers are invariably in higher abundance.[1-10] The compounds all crystallize in the *e*-conformer at low temperature [11-14] and under high pressure.[11]

IR and Raman spectra of the three title compounds [11-16] have earlier been obtained of the vapours, liquids and solid phases (at low temperature and under high pressure). Spectra have also been recorded of the halocyclohexane – thiourea clathrates in the Raman effect,[17] in the IR [18,19] and FIR [20] regions. Moreover, the intensities of a few bands in the IR spectra of the liquids have been measured as a function of temperature.[21] Special studies of some IR bands obtained from solutions with different concentrations and solvents [8,9,22] indicate that the vibrational frequencies and the ratio of the amounts of *e*- and *a*-conformers are almost the same for different solutions.

Previous attempts to make normal coordinate analyses for chloro-, bromo- or iodocyclohexane are incomplete.[14,20,23,24] In order to improve the assignments of the fundamental vibrations of both conformers, we have collected new spectral data from solutions in the IR region and from the liquids, crystalline and amorphous solids in the Raman effect as well. Careful inspection of the spectra reveals a number of shoulders and splittings of bands which have not been reported before.[11,12] By comparing the different spectra we have been able to assign the bands to the respective conformer with great reliability. Polarization measurements of oriented crystal of the *e*-conformers under high pressure in the IR region have made the division of fundamentals between the *a'* and *a''* species of the *e*-conformer more certain than in the earlier studies [20,23,24] in which only Raman polarization data for the liquids were available.

In the FIR region we have recorded spectra of the samples at low temperatures, at high pressures, as liquids and as solutes in different solvents and concentrations. FIR spectra were also obtained from the three compounds in thiourea clathrates between 100 and 600 cm^{-1}. These data, as well as the Raman results, give strong criteria with which to interpret the spectra in this region.

Recently we have made a complete normal coordinate analysis of fluorocyclohexane [25] by using a force field slightly modified from that developed for several dihalogenated *trans*-1,4-cyclohexanes.[26] This force field [26] has also been used in the analyses of the chloro-, bromo- and iodocyclohexanes.

0302-4377/82/080641-16$02.50

Table 1. Infrared and Raman spectral data[a] for chlorocyclohexane.

IR			Raman		Assignments	
Solution CCl_4	Crystalline[b]		Liquid	Cryst.[b] 90 K	[e]	[a]
	90 K	~15 kbar				
3021 vw[c,d]	3015 vw			3017 vw	$\nu_3+\nu_{27}$	comb.
2955 s sh	2957 s 2950 s			2957 s 2952 w sh	ν_1 A′	
			2946 s P	2943 s	ν_2 A′	ν_1 A′
~2940 s sh	2937 vs		2935 s sh	2937 s	ν_{28} A″	ν_{28} A″
2925 s sh	2930 s sh 2923 s			2930 m	ν_{29} A″	
			2921 m sh P			ν_2 A′
2907 m	2905 m		2908 s P	2907 m	ν_3 A′	ν_3 A′
2898 m sh	2898 m		2903 m sh	2900 m	ν_4 A′	ν_{29} A″
2889 w sh	2870 w sh		2891 w sh	2859 s sh	ν_5, ν_{30}	ν_4 A′
2866 s sh	2863 m sh					ν_{30} A″
2860 s	2855 s	~2860 s $I_{\parallel}$	2861 s P	2855 s	ν_6, ν_7 ν_{31}	ν_5, ν_6 A′
2844 w sh	*		2845 w sh			ν_7, ν_{31}
2819 vw	2813 w	~2820 w sh $I_{\parallel}$			$2\times\nu_{10}$	
2797 w	2793 w	2796 w $I_{\parallel}$			$\nu_8+\nu_{11}$	
2703 vw	2702 vw		2704 m P	2699 m	$\nu_8+\nu_{13}$	
2677 w	2672 w		2678 m P	2672 m	$2\times\nu_{35}$	
2670 w sh	2662 w				$2\times\nu_{36}$	
2656 w	2655 w		2659 m P	2655 m	$2\times\nu_{12}$	
			2623 w P	2623 w	$\nu_{10}+\nu_{15}$	
2609 vw			2602 w P	2597 w	$\nu_{11}+\nu_{13}$	
1465 m	1466 w 1462 m	1464 s sh $I_{\parallel}$	1466 w sh P	1466 m	ν_8 A′	comb.
1461 m						ν_8 A′
	1456 m	1459 s sh $I_{\parallel}$			$2\times\nu_{22}$	
	1452 s					
1452 s	1448 m	1445 vs bd $I_{\parallel}$	1448 s	1445 s	ν_9, ν_{32}	ν_{32} A″
1449 s	1446 s					
	1443 s					
1441 m sh	1440 m 1437 w				ν_{33} A″	ν_9 A′
1437 vw sh						ν_{33} A″
1430 m	1429 w	1435 m sh	1432 m sh	1431 m	ν_{10} A′	ν_{10} A′
1405 vw	1402 vw	1414 vw sh $I_{\parallel}$	1404 vw P		$\nu_{39}+\nu_{48}$	
1388 vw						comb.
1369 w sh	1363 w	1388 vw $I_{\perp}$		1370 vw sh	ν_{34} A″	
	1361 w	1375 vw sh $I_{\parallel}$			$\nu_{15}+\nu_{27}$	
1359 w sh	*	*				ν_{34} A″
	1351 m					
1354 m	~1350 w sh	1354 s $I_{\parallel}$ 1352 m sh $I_{\perp}$	1355 m sh 1350 m	1351 m	ν_{11}, ν_{35}	ν_{35} A″
	1347 w					
1340 m	1341 m 1338 m	1344 s $I_{\perp}$	1343 s P	1343 m	ν_{36} A″	ν_{11}, ν_{36}
1334 w sh	1333 m 1330 w sh	1334 s $I_{\parallel}$	1333 w sh	1332 m	ν_{12} A′	
1326 w 1321 w	1326 m 1323 m sh	1330 s sh $I_{\parallel}$	1322 vw		$\nu_{18}+\nu_{25}$	ν_{12}, ν_{37}
	1331 vw	1315 vw			$\nu_{19}+\nu_{24}$	
1303 w	1301 m 1299 w sh	1304 s $I_{\perp}$	1302 m	1302 m	ν_{37} A″	

Table 1. Continued.

1272 m sh	1273 w sh 1271 w sh	1285 vw sh			$\nu_{42}+\nu_{48}$	ν_{38} A″
1268 s	1270 m 1268 s	1271 s $I_{\parallel}$	1269 s P	1273 m	ν_{13} A′	ν_{14} A′
	1262 w sh				$\nu_{20}+\nu_{24}$	
1260 s	1259 m 1256 s	1263 s sh $I_{\perp}$ 1260 s $I_{\parallel}$	1261 s P	1261 s	ν_{14}, ν_{38}	ν_{13} A′ .
1245 vw	*					$\nu_{43}+\nu_{47}$
1228 vw	1236 w 1232 w	1240 vw			$\nu_{22}+\nu_{23}$	
1215 s	1218 m 1216 s	1220 s $I_{\parallel}$ 1218 s $I_{\perp}$	1216 s P	1218 m	ν_{15} A′	ν_{15} A′
1185 w	1186 m 1184 m	1189 m $I_{\perp}$	1186 m	1186 m	ν_{39} A″	
1180 vw sh[c]	1177 w	1182 w sh			$\nu_{20}+\nu_{25}$	
1146 w	*	*	1146 w	*		ν_{39} A″
1138 vw sh[c]						$\nu_{26}+\nu_{44}$
1133 w	1134 m 1132 m	1135 m $I_{\parallel}$	1132 s P	1133 m	ν_{16} A′	
	1130 w				comb.	
1119 vw	1121 vw				$\nu_{44}+\nu_{47}$	ν_{40} A″
1099 m	1103 vw sh 1100 w	1102 vw sh	1099 w	*	$\nu_{44}+\nu_{48}$	ν_{16} A′
1089 w	1090 w sh 1088 m	1093 m $I_{\perp}$		1089 vw ?	ν_{40} A″	
1074 vw	1075 w 1073 w	1079 w 1077 w sh $I_{\perp}$	1075 m	1076 m	ν_{41} A″	ν_{41} A″
	1067 w 1062 vw	1073 vw			$\nu_{21}+\nu_{47}$	
1052 w	1052 w sh 1050 m	1053 m $I_{\perp}$	1052 m	1053 m	ν_{42} A″	
	1040 vw				$\nu_{45}+\nu_{47}$	
1031 m 1023 vw	1033 m 1027 w sh 1025 m	1040 w sh $I_{\parallel}$ 1035 w sh 1030 w $I_{\parallel}$	1030 s P	1028 s	$\nu_{45}+\nu_{48}$ ν_{17} A′	ν_{17}, ν_{42}
1015 m	*	*				ν_{18}
1010 vw sh	*	*				$\nu_{22}+\nu_{47}$
994 s	996 s 995 s	999 s $I_{\parallel}$	995 s P	996 s	ν_{18} A′	
	993 s 990 m	997 s sh			$\nu_{20}+\nu_{27}$	
949 vw[c]	948 w	965 vw			$\nu_{22}+\nu_{48}$	
	940 vw sh				$\nu_{23}+\nu_{46}$	
929 w sh	928 vw				$\nu_{23}+\nu_{24}$	$2\times\nu_{24}$
921 w 917 w sh[c]	922 m 919 m	925 w $I_{\perp}$	922 vw	922 w	ν_{43} A″	ν_{43} A″
889 s	892 s 888 s	892 s $I_{\parallel}$	890 w	890 w	ν_{19} A′	
	881 vw sh 876 w sh	879 w sh			ν_{44} A″	
869 m	869 vw	*	869 w sh P	*	$2\times\nu_{46}$	ν_{19} A′
863 w sh	*	*				ν_{44} A″
859 m	*	*				ν_{20} A′

Table 1. Continued.

852 m	850 s	853 m $I_{\parallel}$	853 s P	851 s	ν_{20} A′	
843 vw	846 vw sh 843 vw sh	847 vw ?				$2\times\nu_{24}$
819 s	818 vs 812 m	823 s $I_{\parallel}$	819 s P	819 s	ν_{21} A′	
807 m[c]	809 w sh		809 s P	*		ν_{21} A′
789 w[c]	792 m 789 w sh	795 w $I_{\perp}$	~790 w sh	791 w	ν_{45} A″	
775 vw[c]	*	*	~775 vw sh		ν_{45} A″	
	773 vw				$\nu_{24}+\nu_{25}$	
733 s	728 vs	730 s 725 s sh $I_{\parallel}$	732 s P	726 s	ν_{22} A′	
718 vw sh	721 w sh 718 vw sh				$\nu_{23}+\nu_{48}$	
	713 w 710 w			710 vw sh		
	707 w sh				$\nu_{46}+\nu_{47}$	
686 s	687 vw sh 680 w	~685 w	687 s P	*	$\nu_{24}+\nu_{47}$	ν_{22} A′
	669 w				$2\times\nu_{25}$	
648 vw	659 vw sh 654 w				comb.	$\nu_{46}+\nu_{48}$
613 vw	640 vw 637 vw				$2\times\nu_{26}$	comb.
560 s	*	*	560 s P	*		ν_{23} A′
513 s	513 s 510 s	517 s $I_{\parallel}$	513 s P	513 m	ν_{23}	
	498 w sh				$\nu_{47}+\nu_{48}$	
	485 w	490 vw			$\nu_{25}+\nu_{27}$	
472 m	477 vw 474 w	*	473 m P		$\nu_{26}+\nu_{27}$	ν_{24} A′
455 w	452 vw	467 vw	453 vw		$2\times\nu_{48}$	ν_{46} A″
	441 m	443 w sh $I_{\perp}$	440 m	440 m sh	ν_{46} A″	
435 m[e]	434 m	438 s $I_{\parallel}$	437 s P	436 s	ν_{24} A′	
394 vw sh[e]						$2\times\nu_{48}$
383 w[d]	384 vw	390 vw	383 w P	*	$\nu_{27}+\nu_{48}$	ν_{25} A′
340 s	340 s	348 s	341 s P	342 s	ν_{25} A′	
336 m sh			337 m sh			ν_{47} A″
328 w[e]	330 w	337 s sh	330 w sh	332 w	ν_{26} A′	
307 vw[e]	303 vw				$2\times\nu_{27}$	
286 w[e]	*	*	287 m P	*		ν_{26} A′
258 m	260 m	270 s	260 m	260 m	ν_{47} A″	
222 vw[e]	245 w 236 w	257 w			ν_{48} A″	
199 w[e]	*	*	200 w	*		ν_{48} A″
148 m[e]	166 m 155 m	180 w 167 w	145 w P	167 vw 150 vw	ν_{27} A′	ν_{27} A′

[a] Weak bands in the regions 4000 – 3050 and 2600 – 1500 cm^{-1} are omitted. [b] Anisotropic phase. [c] Liquid. [d] s, strong; m, medium; w, weak; v, very; sh, shoulder; bd, broad; asterisks (*), bands which are absent; P, polarized; $I_{\perp}$ and $I_{\parallel}$, dichroic measurements; comb., combination band. [e] Cyclohexane solution.

EXPERIMENTAL

The samples of chloro-, bromo- and iodocyclohexane were all commercial products from Baker. When checked by gas chromatography idodocyclohexane was 97–98% pure, while chloro- and bromocyclohexane were found to have an even higher purity. All the compounds were treated by preparative gas chromatography, after which several bands disappeared from the spectra of the impure iodocyclohexane. For chloro- and bromocyclohexane no differences were observed in the spectra before and after the preparative gas chromatography.

The Raman spectrometer, the high pressure diamond anvil cell and the low temperature cryostats have been described.[25] Two infrared instruments were used, a Perkin-Elmer model 225 spectrometer (4000–200 cm^{-1}) and a fast scan Fourier transform spectrometer from Bruker (IFS 114c) (3000–50 cm^{-1}).

RESULTS

The Raman spectrum of chlorocyclohexane as an anisotropic solid at 90 K is shown in Fig. 1, and the FIR spectra of bromocyclohexane dissolved in

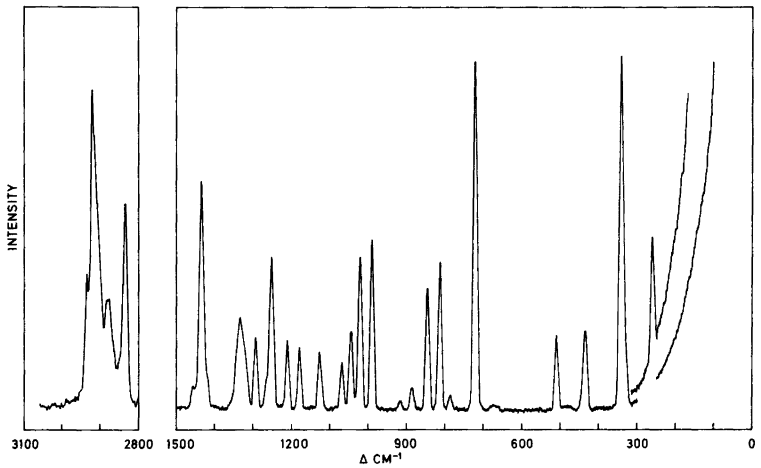

Fig. 1. The Raman spectrum of chlorocyclohexane (anisotropic phase) at 90 K.

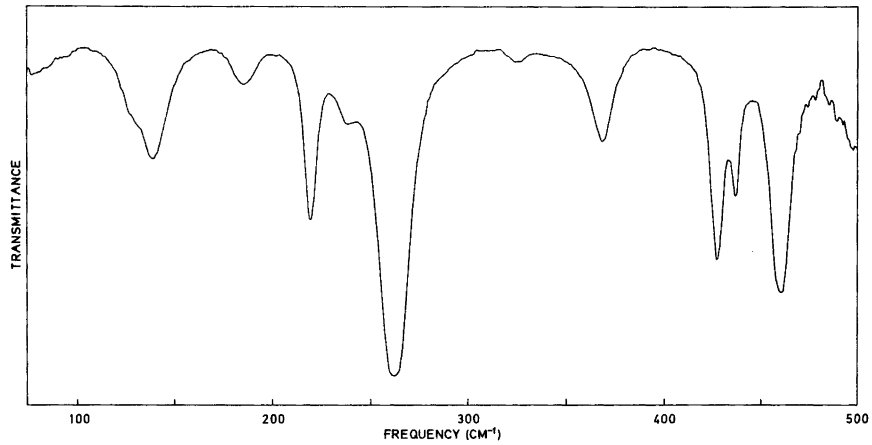

Fig. 2. Far infrared spectrum (75–500 cm^{-1}) of bromocyclohexane dissolved in cyclohexane (~40% solution), 1 mm cell thickness, 6 μm beamsplitter, 1 cm^{-1} resolution.

Table 2. Infrared and Raman spectral data[a] for bromocyclohexane.

IR			Raman		Assignments	
Solution CCl_4	Crystalline[b]		Liquid	Cryst.[b] 90 K	[e]	[a]
	90 K	~15 kbar				
2956 s sh[c]	2962 s	2971 s $I_\perp$		2964 vs	ν_1 A′	
	2951 s	2955 s $I_\parallel$	2943 vs P	2952 s	ν_2 A′	ν_1 A′
2941 s	2936 s, 2930 s	~2945 s		2937 vs, 2926 s	ν_{28} A″	ν_{28} A″
2924 s sh	2920 s	2930 s $I_\perp$	2922 s P	2918 m sh	ν_{29} A″	ν_2 A′
2905 m	~2905 s sh	~2915 s $I_\parallel$	2905 s	2900 s bd	ν_3 A′	ν_3,ν_{29}
2895 w	2891 m	2900 m $I_\parallel$	2896 s P		ν_4 A′	
2886 m	*	*	2885 s P	*		ν_4 A′
2867 s sh	2862 m sh	~2865 m $I_\perp$		2863 w sh	ν_5,ν_{30}	ν_{30} A″
2860 s	2860 s, 2853 s	2860 s $I_\parallel$	2861 s sh, 2857 vs P	2855 vs	ν_6,ν_7,ν_{31}	ν_5,ν_6 A′
2849 s sh[d]	*	*	2840 s P	*		ν_7 A′
2839 m	*	*				ν_{31} A″
2817 w	2817 w				$2\times\nu_{10}$	
2796 w	2794 w	2795 w $I_\parallel$	2803 w P		$\nu_8+\nu_{11}$	
2770 vw sh[e]	2772 w				comb.	
2747 vw	2744 vw, 2738 vw				comb.	
	2709 vw		2710 w sh P		$\nu_{33}+\nu_{37}$	
2701 w	2702 w		2700 m P		$\nu_8+\nu_{13}$	$2\times\nu_{34}$
2676 w	2675 w sh		2678 m P		$2\times\nu_{11}$	$2\times\nu_{35}$
2669 w sh	2667 w		2670 w sh		$2\times\nu_{35}$	
2654 w	2653 w		2654 m P		$2\times\nu_{12}$	$2\times\nu_{11}$
2645 vw sh	2648 vw sh		2645 w sh P		comb.	$2\times\nu_{36}$
2629 vw[e]	2627 vw				comb.	
2616 vw[d]	*		2613 w			$2\times\nu_{12}$
2597 vw	2595 w		2596 w P		$\nu_{11}+\nu_{13}$	
1473 w	1477 w	1484 w $I_\perp$			comb. A″	
1464 m	1466 m, 1465 w sh	1469 m $I_\parallel$	1465 w P	1468 m	ν_8 A′	
1459 w sh[e]	1461 m	1461 m $I_\parallel$			$\nu_{12}+\nu_{27}$	ν_8 A′
1451 s, 1447 s	1453 s sh, 1450 s, 1445 s, 1441 s	1453 s sh $I_\parallel$, 1445 s $I_\perp$	1446 s	1453 m sh, 1441 s	$\nu_{38}+\nu_{47}$, ν_9,ν_{32}	ν_{32} A″
1438 m	1437 m	1439 w sh	1440 m sh P		ν_{33} A″	ν_9,ν_{33}
1433 w sh[d]	*	*				
1429 w sh[e]	*	*	1427 w	*		ν_{10} A′
1425 w sh	1426 w	1425 w sh $I_\parallel$			ν_{10} A′	
1416 w sh[e]	1419 w				$\nu_{27}+\nu_{37}$	
	1370 w				ν_{34} A″	
1358 m	*	*	1357 w sh	*		ν_{34} A″
1351 m sh[e]	1354 m, 1349 w sh	1357 w sh	1350 m	1353 m	ν_{11} A′	
1348 m[e]	1346 m, 1342 m	1348 m, 1345 m sh $I_\perp$		1345 w sh	ν_{35} A″	ν_{35} A″
1337 m	1339 m, 1334 s	1340 m sh $I_\parallel$	1337 s P	1335 s	ν_{12} A′	ν_{11},ν_{36}
1332 vw sh	1332 m sh, 1329 s	1335 s $I_\perp$			ν_{36} A″	

Table 2. Continued.

~1325 w	1323 w	1326 w sh	1325 vw sh	*	$\nu_{15}+\nu_{27}$	ν_{12} A′
1310 w	*	*				ν_{37} A″
1300 m	1301 w sh 1297 m	1309 vw 1299 m $I_\perp$	1299 m	1300 m	ν_{37} A″	$\nu_{20}+\nu_{24}$
	1293 w				comb.	
	1285 vw				$\nu_{24}+\nu_{44}$	
1279 vw[e]	1278 vw				$\nu_{41}+\nu_{48}$	
1273 m	1273 w	*	1273 m	*	comb.	ν_{38} A″
1264 w sh	1265 s 1263 s sh	1268 s 1265 m sh $I_\parallel$	1265 w sh	1266 s	ν_{13} A′	
	1260 w				$\nu_{20}+\nu_{24}$	
1257 s	1257 s	1259 s $I_\parallel$	1257 s P	1257 s	ν_{14},ν_{38}	ν_{13} A′
1254 s	1250 w sh	1254 w sh	1252 m sh P			ν_{14} A′
1225 vw	1226 w				$\nu_{21}+\nu_{24}$	
1215 vw[d]	1217 w				$\nu_{45}+\nu_{46}$	
1193 s	1196 s 1191 w sh	1199 s $I_\parallel$	1193 s P	1187 s	ν_{15} A′	ν_{15} A′
1184 w sh[e]	1184 w 1182 m 1177 m	1185 w sh 1181 m $I_\perp$	1185 m sh	1183 m	$\nu_{22}+\nu_{23}$ ν_{39} A″	
1144 w	1142 vw		1144 w	*	$\nu_{43}+\nu_{47}$	ν_{39} A″
1135 vw	1134 w				$\nu_{19}+\nu_{26}$	
1119 m	1124 m 1120 m	1127 m 1123 m $I_\parallel$	1119 m P	1123 m	ν_{16} A′	ν_{40} A″
	1117 w sh 1114 w				comb.	
1097 vw	1100 vw				$\nu_{22}+\nu_{24}$	
1089 m	1086 m	1091 m $I_\perp$	1087 w	1087 w	ν_{40} A″	ν_{16} A′
1080 vw sh	1081 vw	1086 vw sh				ν_{41} A″
1075 w[e]	1071 w		1076 m	1075 s	ν_{41} A″	
	1066 vw	1074 w $I_\perp$			$\nu_{21}+\nu_{26}$	
1050 w	1052 w 1049 w	1057 w $I_\perp$ 1053 w	1052 m	1051 s	ν_{42} A″	
	1044 w 1035 w	1041 w sh			$\nu_{21}+\nu_{47}$	
1030 m			1030 s			ν_{42} A″
			1026 s sh			ν_{17} A′
1023 w	1027 m 1023 m	1031 m 1026 w sh $I_\parallel$	1023 m sh	1027 s	ν_{17} A′	
1011 m			1014 w sh P	*		ν_{18} A′
1008 w sh[e]	1007 m	1012 w sh $I_\parallel$			$\nu_{45}+\nu_{47}$	
990 s	994 s 989 s	1000 m sh 992 s $I_\parallel$	991 s P	991 s	ν_{18} A′	
992 s sh[d]	986 m 980 w sh				$2\times\nu_{23}$	
963 vw	950 vw	963 vw			$\nu_{21}+\nu_{27}$	$\nu_{23}+\nu_{24}$
931 vw	931 vw	940 vw			$\nu_{22}+\nu_{26}$	
921 m			920 vw			ν_{43} A″
918 w sh	920 m 917 w sh	924 m $I_\perp$		920 vw	ν_{43} A″	
887 s	887 s 883 w	890 s $I_\parallel$	887 m P	888 m	ν_{19} A′	
873 w	876 w sh	873 vw sh ?			ν_{44} A″	
866 m	*	*	865 w P	*		ν_{19} A′
864 m	861 vw	865 vw			$2\times\nu_{46}$	ν_{44} A″
853 m	*	*	854 w sh ?	*		ν_{20} A′

Table 2. Continued.

849 w sh	852 w 845 m	855 w 848 m $I_{\parallel}$	848 s P	852 s ~845 m sh	ν_{20} A′	
	842 w	843 vw sh $I_{\parallel}$			$2\times\nu_{24}$	
811 s	817 w 813 m	816 s $I_{\parallel}$	811 s P	816 s	ν_{21} A′	
804 m[e]	810 m 808 m	812 s sh $I_{\parallel}$	805 s P	*	$\nu_{22}+\nu_{27}$	ν_{21} A′
800 vw sh[e]	798 vw	800 vw $I_{\parallel}$			$\nu_{23}+\nu_{25}$	
789 w[e]	790 m	793 m $I_{\perp}$		791 m	ν_{45} A″	
776 w[e]	*	*	~780 vw sh	*		ν_{45} A″
761 vw[e]	758 vw	770 vw ?	761 vw P		$\nu_{23}+\nu_{26}$	
729 vw[e]	728 w 727 w sh				$\nu_{24}+\nu_{25}$	
	723 vw 720 vw				$\nu_{23}+\nu_{47}$	
705 vw[e]	714 vw 701 vw				$\nu_{23}+\nu_{48}$	
689 vs	~686 vs	689 s $I_{\parallel}$	687 vs P	686 s	ν_{22} A′	
674 vw	671 m	674 m		673 w	$\nu_{24}+\nu_{26}$	
660 s	655 vw	*	658 s P	*		ν_{22} A′
648 vw	*	*				$2\times\nu_{47}$
	638 vw				$\nu_{24}+\nu_{48}$	
549 vw[e]	551 vw	552 vw			$\nu_{25}+\nu_{47}$	$\nu_{27}+\nu_{46}$
541 vw[e]						$\nu_{25}+\nu_{48}$
508 m	523 vw 511 vw	*	~510 m sh P	*	$2\times\nu_{26}$	ν_{23} A′
501 s	499 m 492 s	499 s	502 s P	500 s 490 vw sh	ν_{23} A′	$2\times\nu_{26}$
460 s	*	*	460 s P	*		ν_{24} A′
449 vw sh	*	*				ν_{46} A″
437 m	436 m 434 m	439 m	436 w sh	~440 w sh	ν_{46} A″	
427 m	429 m	431 m	427 s P	429 s	ν_{24} A′	
368 m	*	*	368 m P	*		ν_{25} A′
327 vw						ν_{47} A″
324 vw	331 w	335 w	324 m P	~325 m	ν_{25} A′	
262 s	260 s	264 s	262 s P	262 vs	ν_{26} A′	
251 m sh						ν_{26} A′
237 w	252 s 232 w	239 vw	240 w sh	245 w	ν_{47} A″	
219 m	216 m	219 m	219 m	216 m	ν_{48} A″	
185 w	*	*	185 m	*		ν_{48} A″
138 m	146 m 137 m	153 m 138 m	140 m sh P	~140 w bd	ν_{27} A′	
129 w	*	*	129 s P	*		ν_{27} A′

[a] Weak bands in the regions 4000 – 3000 and 2590 – 1500 cm^{-1} are omitted. [b] Anisotropic phase. [c] For abbreviations, see Table 1. [d] Amorphous solid at 90 K. [e] Liquid.

cyclohexane and as an anisotropic crystal at 90 K are presented in Figs. 2 and 3, respectively. The IR dichroism spectrum of a single crystal of iodocyclohexane under high pressure is given in Fig. 4. Additional spectra of chloro-,[11-13] bromo-[11,12] and iodocyclohexane[12] in the vapour (IR), in the solid (IR) and liquid states (IR, Raman) have previously been reported. The wave numbers of the observed IR and Raman bands are listed in Tables 1 – 3 for chloro-, bromo- and iodocyclohexane, respectively. Data from the vapour phase for chloro- and bromocyclohexane as well as Raman data for

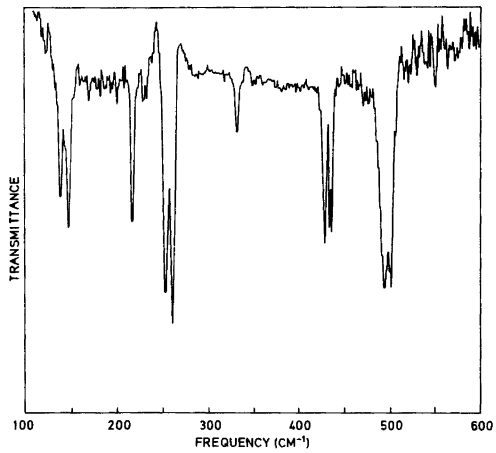

Fig. 3. Far infrared spectrum (100 – 600 cm^{-1}) of bromocyclohexane (anisotropic phase) at 90 K, 3.5 μm beamsplitter, 1 cm^{-1} resolution.

liquid iodocyclohexane can be found in Ref. 11. The present IR and Raman frequencies agree fairly well with the earlier values,[11-13] but a careful inspection of the new IR and Raman spectra has revealed a number of "doublets" and shoulders which were formerly not observed. The data for the FIR region are also much more complete than those reported earlier.[12]

Both conformers of chloro-, bromo- and iodocyclohexane will obviously have C_s symmetry, and the 48 fundamentals of each will accordingly divide themselves into the symmetry species as follows: $27\,a' + 21\,a''$. All the fundamentals are active

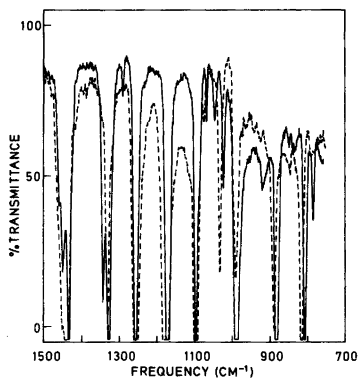

Fig. 4. The infrared dichroism spectrum of a single crystal of iodocyclohexane in the diamond anvil cell at *ca.* 15 kbar pressure and at ambient temperature.

in both IR and Raman; those belonging to species a' will give rise to polarized Raman lines.

Assignments of the fundamental vibrations of the e-conformers. Vibrational spectra of the pure *e*-conformers can easily be obtained since all the compounds crystallize in this conformer both at low temperature and at high pressure. The crystal structures of the three compounds are to our knowledge unknown. However, the Davidov splitting of the bands into two components indicates crystal structures with at least two molecules in the unit cells. The agreement between observed IR and Raman frequencies is usually good, and the unit cells are probably not centrosymmetrical.

Three criteria are used in the assignments of the observed bands to the a' or a'' species:

(1) Raman polarization data, obtained from the liquids.

(2) IR dichroism measurements of the anisotropic crystals under high pressures.

(3) Normal coordinate calculations.

From the Raman polarization data several of the a' fundamentals can easily be identified. Since the liquids consist of an equilibrium mixture of the *e*- and *a*-conformers, the observed Raman bands often belong to fundamentals of both conformers. Moreover, some of the a' fundamentals tend to be very weakly polarized, and the distinction from a depolarized band may be difficult to make. In Tables 1 – 3 only bands which are clearly polarized are marked with a P.

From the molecular structure it is obvious that, for an oriented crystalline film of a monohalogenated cyclohexane, all vibrations belonging to species a'' must have the same dichroistic ratio in the IR spectra. When chlorocyclohexane is compressed in the diamond anvil cell a plastic solid containing both conformers is formed at rather low pressures.[11] When higher pressures are applied, a phase transition between the plastic and the anisotropic phases will occur, and a single crystal of the *e*-conformer can be obtained. For chlorocyclohexane we were not able to grow one single crystal. When the anisotropic crystal was formed as the pressure increased, we obtained at least two or three single crystals. However, the IR spectra gave good dichroistic measurements with the a'' bands almost vanishing in one polarization direction. No plastic crystals have been observed for bromo- and iodocyclohexane,[11,23] and when the pressure was increased an anisotropic single crystal was grown over the entire diamond surface. The spectra

Table 3. Infrared and Raman spectral data[a] for iodocyclohexane.

IR			Raman		Assignments	
Solution CCl_4	Crystalline[b]		Amorphous 90 K	Cryst.[b] 90 K	[e]	[a]
	200 K	~15 kbar				
	2956 s[c]			2958 vs	ν_1 A′	
2944 m sh	2945 m			2946 s	ν_2 A′	ν_1 A′
2936 s			2936 s	2936 s	ν_{28} A″	ν_{28} A″
2920 m sh	2929 s bd		2927 w sh 2918 w sh	2927 vs	ν_{29} A″	ν_2 A′
	2913 s			2918 w sh	$2\times\nu_8$	
2903 w	2898 m		2897 m bd	2900 m bd	ν_3,ν_4	ν_3,ν_{29}
2881 m	2883 w		2884 w	2873 w	$2\times\nu_{32}$	ν_4 A′
2857 s	2860 s sh 2855 s 2851 s sh		2854 s 2850 s sh	2855 vs	ν_5,ν_6,ν_7 ν_{30},ν_{31}	ν_{30} A″ ν_5,ν_6 A′
2833 m	*		2832 m	*		ν_7,ν_{31}
2813 vw	2809 vw	2815 w			$2\times\nu_{10}$	$2\times\nu_{10}$
2796 vw	2794 w	2796 w			$\nu_8+\nu_{11}$	
2782 vw	2787 w				comb.	comb.
2769 vw[d]	2766 w				comb.	
2707 w sh[d]	*					comb.
2698 vw	2698 w	2701 w			$\nu_8+\nu_{13}$	$2\times\nu_{34}$
	2691 w sh				comb.	
2668 w	2673 m 2665 w	2669 m			$2\times\nu_{11}$ $2\times\nu_{35}$	$2\times\nu_{35}$
2652 vw	2652 w	2652 w			comb.	
	2645 w				$2\times\nu_{12}$	
2621 w[d]	2629 vw 2626 vw				$2\times\nu_{36}$	$2\times\nu_{12}$
2597 w[d]	2597 w				$\nu_{11}+\nu_{13}$	
2583 w[d]	2583 w				comb.	
1495 vw[d]	1496 vw				comb.	
1461 m	1464 m	1464 m $I_\parallel$	1461 vw	1467 w	ν_8 A′	
1457 vw ?	1459 w sh 1457 w				$\nu_{14}+\nu_{26}$	ν_8 A′
	1451 m	1457 s $I_\parallel$			$\nu_{12}+\nu_{27}$	
1450 s 1446 m sh	1448 s 1444 s 1441 m	1452 s $I_\perp$ 1445 s $I_\parallel$ 1441 s $I_\parallel$	1440 s	1447 s 1443 s	ν_9,ν_{32}	ν_{32} A″
1437 m 1435 w sh	1437 w sh	1433 w sh $I_\perp$			ν_{33} A″	ν_9 A′ ν_{33} A″
1429 m	*		1425 w sh			ν_{10} A′
1417 w sh[d]	1424 w	1429 vw sh 1424 vw sh			ν_{10} A′	
		1413 vw $I_\parallel$ 1392 vw $I_\parallel$			$\nu_{16}+\nu_{25}$ $\nu_{18}+\nu_{24}$	
1368 vw[d]	1367 vw	1362 vw sh		1362 vw ?	ν_{34} A″	
1355 m	*	*				ν_{34} A″
1352 w sh	1352 m	1352 m $I_\parallel$		1351 w	ν_{11} A′	
1349 m 1337 w sh	1347 m 1342 m	1348 m $I_\perp$ 1344 m sh 1342 m	1347 w 1337 w sh	1339 m	ν_{35} A″ $\nu_{27}+\nu_{38}$	ν_{35} A″ ν_{11} A′
1333 m	1332 s	1337 w sh 1334 s $I_\parallel$	1330 s	1333 s	ν_{12} A′	ν_{36} A″

Table 3. Continued.

1326 w sh[d]	1324 m	1330 s $I_{\perp}$			ν_{36} A″	
1318 w sh[d]	1318 vw	1324 w sh			$\nu_{24}+\nu_{43}$	ν_{12} A′
1303 w	1306 w	1314 w			$\nu_{19}+\nu_{46}$	ν_{37} A″
1298 m	1296 m	1297 w $I_{\perp}$	1296 m	1299 w	ν_{37} A″	
~1290 vw ?	1292 vw 1288 w	1292 w sh			$\nu_{15}+\nu_{27}$	
1278 vw	*	*				$\nu_{20}+\nu_{24}$
1270 w	*	*				ν_{38} A″
1263 w sh	1265 w sh 1259 m	1262 s $I_{\parallel}$	~1265 m sh	1262 s	ν_{13} A′	
1254 s	1254 s	1257 s $I_{\perp}$ 1250 s sh $I_{\parallel}$	1252 s	1251 s	ν_{14},ν_{38}	ν_{13} A′
1246 s	1244 w	1245 w sh $I_{\parallel}$	1241 w sh	*	$\nu_{20}+\nu_{24}$	ν_{14} A′
1224 vw	1229 w 1226 w	1232 w $I_{\perp}$			$\nu_{25}+\nu_{43}$	
1208 vw	1209 vw	1215 vw $I_{\parallel}$			$\nu_{45}+\nu_{46}$	
1191 w	1193 w	1199 vw			comb.	
1181 m sh		1182 s 1178 s		1183 w sh ?	ν_{39} A″	
1174 s	1178 s	1176 m $I_{\parallel}$ 1173 s $I_{\perp}$	1176 s	1178 s	ν_{15} A′	$\nu_{18}+\nu_{48}$
1167 s	1171 m sh	1170 w sh	~1165 m sh	*	$\nu_{27}+\nu_{42}$	ν_{15} A′
	1158 vw				$\nu_{20}+\nu_{25}$	
1144 vw ?	1148 vw				$\nu_{17}+\nu_{27}$	
1139 vw	1138 vw	1136 vw	~1140 vw	*	$\nu_{22}+\nu_{23}$	ν_{39} A″
1128 vw	1129 vw	1128 vw			$\nu_{26}+\nu_{43}$	
1118 w	1119 vw	1118 vw $I_{\parallel}$			$\nu_{21}+\nu_{24}$	ν_{40} A″
1106 w	1106 m	1110 w sh $I_{\parallel}$			$\nu_{43}+\nu_{48}$	
1096 s	1095 s	1101 s sh $I_{\perp}$ 1098 s $I_{\parallel}$ 1094 s sh	1097 m	1100 m	ν_{16} A′ comb.	ν_{16} A′
1082 vw	1082 w	1088 w sh $I_{\perp}$		1082 vw sh	ν_{40} A″	
1075 m	1071 m	1073 w	1075 m	1077 w	ν_{41} A″	ν_{41} A″
1049 w	1049 w 1046 vw	1051 w sh 1049 w $I_{\perp}$	1050 w	1050 w	ν_{42} A″	
1029 m	1038 w 1031 w	1037 w 1033 vw sh	1032 m sh	1032 vw sh	comb.	ν_{17},ν_{42}
1021 w	1023 m	1026 m $I_{\parallel}$ 1024 w sh $I_{\perp}$	1023 s	1024 s	ν_{17} A′	
1006 m	*	1003 vw sh 998 w sh	1006 vw ?	*	comb.	ν_{18} A′
988 s	992 m 987 s	993 s sh $I_{\perp}$ 987 s $I_{\parallel}$	988 s	990 s	ν_{18} A′	
983 m sh	980 m sh	983 m sh $I_{\perp}$			$\nu_{21}+\nu_{48}$	
953 vw	952 vw	954 w $I_{\parallel}$			$\nu_{45}+\nu_{48}$	$2\times\nu_{23}$
917 m	916 w	920 w $I_{\perp}$			ν_{43} A″	ν_{43} A″
884 s	883 s	888 s $I_{\parallel}$ 885 s $I_{\perp}$	886 m	886 m	ν_{19} A′	$2\times\nu_{24}$
	871 w	874 vw sh 870 vw sh			ν_{44} A″	
864 m	*	*	868 w	*		ν_{19} A′
863 m	*	*		*		ν_{44} A″
849 m	843 w	850 vw $I_{\perp}$ 845 w $I_{\parallel}$ 835 vw $I_{\parallel}$	846 s	848 s	ν_{20} A′ $2\times\nu_{24}$	ν_{20} A′

Table 3. Continued.

806 s[d]	807 s 805 m sh	811 s $I_{\parallel}$	806 m	814 m 808 m sh	ν_{21} A′	
801 m sh[d]	802 m	807 m sh $I_{\perp}$			$\nu_{23}+\nu_{25}$	ν_{21} A′
788 w[d]	789 m	790 w $I_{\perp}$		790 w	ν_{45} A″	
779 w[d]	*	*				ν_{45} A″
719 w[d]	721 w				$\nu_{23}+\nu_{47}$	
687 w[d]	*	*				$\nu_{24}+\nu_{26}$
656 s	~655 s	655 s $I_{\parallel}$	656 s	656 s	ν_{22} A′	
640 s	639 m	642 m sh	641 m	641 w sh	$\nu_{24}+\nu_{26}$	ν_{22} A′
621 w		622 vw			$\nu_{46}+\nu_{48}$	
600 vw	*	*				$\nu_{23}+\nu_{27}$
584 vw	*	*				$\nu_{25}+\nu_{26}$
494 m	493 m 485 m	501 m sh 490 m	492 s	495 s	ν_{23} A′	
480 w sh						ν_{23} A′
459 vw	*	*				$2\times\nu_{26}$
446 m	*	448 w	448 s	~445 vw	$2\times\nu_{26}$	ν_{24},ν_{46}
436 w	435 m	439 m			ν_{46} A″	
421 w	423 w 419 w	421 w	422 m	421 m	ν_{24} A′	
402 vw	*	*				$\nu_{26}+\nu_{48}$
359 w	*	*	360 s	*		ν_{25} A′
355 w sh	*	*				$2\times\nu_{48}$
328 vw	334 vw	336 vw	~325 vw	325 w	ν_{25} A′	
314 vw	*	*				ν_{47} A″
260 vw	257 w 250 w	257 w			$2\times\nu_{27}$	
237 w	*	*	240 m	*		ν_{26} A′
235 vw sh	232 vw				ν_{47} A″	
223 m	221 m 220 m	222 m	226 s	223 s	ν_{26} A′	
196 vw	192 vw	~185 vw	188 w	193 m	ν_{48} A″	
175 vw	*	*				ν_{48} A′
133 w	141 vw sh 134 w	138 w	141 vw	140 vw	ν_{27} A′	
121 vw						ν_{27} A′

[a] Weak bands in the regions 4000 – 3000 and 2580 – 1500 cm^{-1} are omitted. [b] Anisotropic crystal. [c] For abbreviations, see Table 1. [d] Liquid.

showed the same trend as for chlorocyclohexane, with the bands belonging to the *a″* species almost vanishing in one of the polarization directions (Fig. 4). Hence all bands having a strong component with this direction must therefore belong to species *a′* and are marked $I_{\parallel}$ in Tables 1 – 3, while the components which are vanishing are designated $I_{\perp}$.

In a few cases, one band of the liquid corresponds to more than two bands of the crystal. This has been taken as a criterion for more than one fundamental at this frequency or for a fundamental overlapping a combination mode. An example is found in chlorocyclohexane where the band at 1354 cm^{-1} of the liquid corresponds to three components of the anisotropic crystal. Hence the three components observed for the crystal are interpreted as two overlapping *e*-fundamentals. For bromo- and iodocyclohexane a similar feature occurs at 1184 and *ca.* 1345 cm^{-1}, respectively, where the three bands in the spectra of the crystals are assigned to a fundamental overlapping a combination band.

Our final assignments of the fundamentals for the *e*-conformers are quite different from those presented earlier [20,23,24] especially in the frequency region above 800 cm^{-1}. By far the most complete normal coordinate analyses for chloro-, bromo- and

Table 4. Observed[a] and calculated fundamental frequencies for chloro- and iodocyclohexane.

	Chlorocyclohexane				Iodocyclohexane			
	e		*a*		*e*		*a*	
	Obs.	Calc.	Obs.	Calc.	Obs.	Calc.	Obs.	Calc.
a'								
ν_1	2955	2956	2946	2956	2955	2955	2944	2955
ν_2	2946	2922	2921	2922	2944	2922	2920	2922
ν_3	2908	2916	2908	2916	2900	2916	2900	2916
ν_4	2903	2914	2889	2914	2900	2914	2879	2914
ν_5	2865	2857	2860	2857	2855	2857	2850	2857
ν_6	2860	2853	2860	2853	2855	2853	2850	2853
ν_7	2860	2851	2845	2851	2855	2851	2832	2851
ν_8	1466	1456	1461	1456	1461	1456	1457	1455
ν_9	1449	1440	1439	1437	1440	1439	1437	1437
ν_{10}	1429	1425	1429	1422	1417	1425	1428	1422
ν_{11}	1353	1351	1343	1345	1352	1346	1337	1344
ν_{12}	1333	1340	1326	1343	1332	1337	1318	1342
ν_{13}	1268	1265	1268	1283	1263	1250	1254	1257
ν_{14}	1259	1251	1260	1251	1254	1241	1244	1234
ν_{15}	1216	1221	1216	1226	1173	1178	1166	1173
ν_{16}	1133	1121	1099	1105	1094	1090	1094	1088
ν_{17}	1026	1020	1030	1026	1021	1019	1029	1024
ν_{18}	994	992	1015	985	987	984	1006	988
ν_{19}	889	892	869	870	883	886	864	859
ν_{20}	852	839	859	853	848	833	848	846
ν_{21}	819	819	807	806	806	800	801	801
ν_{22}	732	733	685	680	655	666	639	627
ν_{23}	512	508	559	552	494	493	482	483
ν_{24}	436	428	473	482	421	418	446	449
ν_{25}	341	342	384	380	328	321	359	349
ν_{26}	328	324	286	290	222	224	236	249
ν_{27}	148	154	148	136	133	129	121	93
a''								
ν_{28}	2943	2918	2943	2917	2936	2917	2936	2917
ν_{29}	2930	2913	2903	2913	2920	2913	2900	2913
ν_{30}	2865	2855	2865	2855	2855	2855	2855	2855
ν_{31}	2860	2852	2845	2851	2855	2852	2832	2851
ν_{32}	1449	1448	1452	1440	1446	1445	1450	1440
ν_{33}	1439	1434	1436	1434	1436	1434	1435	1434
ν_{34}	1366	1383	1358	1368	1368	1380	1355	1367
ν_{35}	1353	1351	1353	1350	1348	1349	1348	1349
ν_{36}	1340	1345	1340	1342	1326	1345	1332	1341
ν_{37}	1302	1299	1321	1320	1296	1298	1303	1309
ν_{38}	1260	1245	1273	1261	1254	1245	1269	1259
ν_{39}	1185	1182	1146	1145	1181	1179	1138	1142
ν_{40}	1089	1100	1119	1144	1082	1090	1117	1137
ν_{41}	1075	1068	1075	1083	1073	1066	1073	1080
ν_{42}	1052	1051	1030	1034	1048	1051	1029	1033
ν_{43}	917	916	921	928	916	913	916	924
ν_{44}	877	886	862	856	873	883	863	854
ν_{45}	789	787	775	792	788	785	779	787
ν_{46}	440	457	454	461	437	456	446	454
ν_{47}	259	263	337	330	235	228	314	286
ν_{48}	240	221	200	182	196	191	175	155

[a] When possible, frequency values for the liquids are given.

iodocyclohexane until now are found in Ref. 23. However, some of the assignments reported[23] are in conflict with our experimental data. As an example, the IR bands at *ca.* 1030 and 890 cm^{-1} observed for all three compounds cannot be assigned to fundamentals of species *a''* as the dichroistic measurements reveal strong components in the $I_{\parallel}$ direction for both bands.

Assignments of the fundamental vibrations of the a-conformers. The earlier attempts at assigning the vibrational spectra of the *a*-conformers of chloro-, bromo- and iodocyclohexane are rather incomplete,[20,23,24] especially in the region above 1000 cm^{-1} where many bands of the *e*- and *a*-conformers are overlapping. New spectral data and the normal coordinate calculations have given a more complete and reliable interpretation of the spectra of the *a*-conformers although some uncertainties still persist.

All attempts to crystallize the *a*-conformers have failed, and no spectra are available of these conformers in the pure state. Since the three halocyclohexanes crystallize in the *e*-conformer, bands vanishing upon crystallization (marked with an asterisk (*) in Tables 1 – 3) mus belong to the *a*-conformer. Hence the pure "axial" bands can be attributed with certainty, but the distinction between "equatorial" bands and bands common to both conformers is in some cases uncertain.

In the liquid phase the *e*-conformer is the more stable, and the ΔG° values are of the order of -2 kJ/mol[1-6] for all three compounds. Upon cooling the liquids, the *e*-conformers should be even more preferred. With a computer-controlled interferometer it has been possible to record IR spectra of the liquids as a function of temperature and to subtract the spectra. When a spectrum obtained at a lower temperature is partially subtracted from a high temperature spectrum, the result should be a spectrum with bands mostly belonging to the *a*-conformer. Although this technique is somewhat hampered by the variations of band widths with temperature, it has been of great value for the interpretation of the IR spectra of the liquids, especially in the regions where several bands overlap.

In thiourea clathrates the *a*-conformer of chloro- and bromocyclohexane are strongly preferred in the channels,[17-20] while iodocyclohexane[17,18] has a certain amount of *e*-conformer in addition. Since the thiourea bands are strongly dominating in the vibrational spectra of the adducts, the information about the *a*-conformers is limited, though in the area below 1000 cm^{-1} some very valuable IR and Raman data have been obtained.[17-20] When these data are compared with the results from the annealing and cooling techniques, it is possible to identify most of the bands belonging to the *a*-conformers even when bands are common to both conformers.

Only the Raman polarization measurements give experimental criteria for assigning the *a*-conformer vibrations to species *a'* and *a''*, and the assignments are based on these data as well as on the normal coordinate calculations. Since our model force field[26] has given excellent agreement between observed and calculated frequencies for a variety of axially substituted cyclohexanes[27,28] including fluorocyclohexane,[25] we believe that this should also be the case for *a*-chloro-, *a*-bromo- and *a*-iodocyclohexane. Moreover, it seems to be a very good approximation to use a similar force field for the *a*- and *e*-conformer of a cyclohexane derivative, and the agreement between observed and calculated frequencies for the *e*-conformer of chloro-, bromo- and iodocyclohexane is quite satisfactory.

Normal coordinate calculations and spectral correlations. Only one torsional force constant had to be adjusted when the force field previously derived for six *trans*-1,4-dihalocyclohexanes,[26] was transferred to the three monohalocyclohexanes. For fluorocyclohexane the force constant, τ_s, for the torsion around the C_1-C_2 bond ($X-\underset{\sim}{C}-C-C_1$ $-C_2-C-\underset{\sim}{C}$) was found to be 0.046 mdyn Å/rad^2.[25] Using the new data from both conformers of chloro- bromo- and iodocyclohexane we have determined τ_s to be 0.0437 mdyn Å/rad^2 when the molecular parameters are the same as in Ref. 26.

The observed and calculated frequencies for chloro- and iodocylohexane are given in Table 4. Corresponding values for bromocyclohexane are listed in Table 5, and for this compound the potential energy distribution (PED) is given in terms of the internal coordinates. The PED of Table 5 is representative also for chloro- and iodocyclohexane although the fundamentals with the same number do not always correspond according to the PED. For example, for the *e*-conformers, ν_{26} of chlorocyclohexane has the same PED as ν_{25} of bromo- and iodocyclohexane, and ν_{25} of chloro- corresponds to ν_{26} of bromo- and iodocyclohexane.

For *e*-bromocyclohexane ν_{47} and ν_{48} at 240 and 219 cm^{-1}, respectively, are strongly coupled and both are observed in the Raman effect, ν_{48} giving rise to the more intense line. ν_{47} of chlorocyclohexane is assigned to a medium intense Raman line as is ν_{48} of

Table 5. Observed[a] and calculated fundamental frequencies for bromocyclohexane.

	e			*a*		
	PED[b]	Obs.	Calc.	PED	Obs.	Calc.
a'						
ν_1	97d(X)[c]	2956	2956	99d(X)	2943	2956
ν_2	96d	2943	2922	96d	2922	2922
ν_3	95d	2905	2916	95d	2905	2916
ν_4	98d	2896	2914	97d	2885	2914
ν_5	96d	2867	2857	94d	2860	2857
ν_6	95d	2860	2853	95d	2860	2853
ν_7	96d	2860	2851	96d	2840	2851
ν_8	$71\delta+18\gamma$	1464	1456	$69\delta+17\gamma$	1459	1456
ν_9	$68\delta+19\gamma$	1447	1439	$66\delta+22\gamma$	1438	1437
ν_{10}	$68\delta+20\gamma$	1426	1425	$71\delta+18\gamma$	1429	1422
ν_{11}	81γ	1350	1347	82γ	1336	1345
ν_{12}	$83\gamma+21$R	1336	1338	$81\gamma+23$R	1323	1343
ν_{13}	76γ	1264	1251	64γ	1257	1262
ν_{14}	63γ	1257	1246	71γ	1252	1239
ν_{15}	$36\gamma+31\theta+18\gamma$(X)	1193	1199	$37\theta+32\gamma+17\gamma$(X)	1193	1207
ν_{16}	$51\gamma+17\theta$	1119	1109	58γ	1088	1097
ν_{17}	50R$+29\gamma$	1023	1020	51R$+29\gamma$	1026	1025
ν_{18}	$41\gamma+31\omega$	989	988	$46\gamma+29\omega$	1011	993
ν_{19}	53R$+39\gamma$	886	890	65R$+25\gamma$	866	864
ν_{20}	47R$+43\gamma$	847	836	$60\gamma+21$R	852	851
ν_{21}	64R$+15\gamma$	811	807	75R	804	804
ν_{22}	49X$+30\gamma+18\omega+16\Xi$	687	696	$31\gamma+29$X$+20\omega+16\ \Xi$	658	648
ν_{23}	$41\omega+41\gamma$	501	499	58X$+27\omega+26\gamma$	510	504
ν_{24}	50ω	427	423	$51\omega+22$X	459	471
ν_{25}	$39\omega+35\tau_s$	324	325	$41\omega+32\tau$	368	362
ν_{26}	49X	261	263	$27\omega+24\Xi+22\tau_s$	251	269
ν_{27}	38τ(X)$+22\Xi+22\omega$	139	141	35τ(X)$+19\Xi$	129	110
a''						
ν_{28}	98d	2941	2917	98d	2941	2917
ν_{29}	98d	2924	2913	98d	2901	2913
ν_{30}	97d	2867	2855	96d	2867	2855
ν_{31}	97d	2860	2852	96d	2839	2851
ν_{32}	$66\delta+16\gamma$	1447	1447	$73\delta+16\gamma$	1451	1440
ν_{33}	$66\delta+21\gamma$	1438	1434	$61\delta+21\gamma$	1438	1434
ν_{34}	$46\gamma+24$R$+23\gamma$(X)	1370	1382	$70\gamma+20$R	1357	1368
ν_{35}	$67\gamma+19$R	1348	1350	83γ	1348	1350
ν_{36}	88γ	1331	1345	$63\gamma+15\gamma$(X)	1336	1342
ν_{37}	76γ	1299	1299	42R$+39\gamma+22\gamma$(X)	1309	1317
ν_{38}	72γ	1257	1245	77γ	1272	1261
ν_{39}	$77\gamma+18$R	1184	1181	95γ	1144	1144
ν_{40}	$57\gamma+42$R	1088	1096	$61\gamma+27$R	1119	1142
ν_{41}	$61\gamma+23$R$+21\gamma$(X)	1075	1068	$57\gamma+27$R	1079	1082
ν_{42}	59R$+24\gamma$	1050	1051	53R$+21\gamma$	1030	1034
ν_{43}	$52\gamma+34$R	918	915	83γ	921	927
ν_{44}	$49\gamma+32$R	873	885	68R$+15\gamma$	864	855
ν_{45}	$78\gamma+15$R	789	788	79γ	776	791
ν_{46}	60ω	436	457	64ω	449	458
ν_{47}	$40\Xi+31\omega+20\tau$	240	237	$58\Xi+24\tau+17\omega$	327	308
ν_{48}	$46\Xi+22\tau+15\omega$	219	211	$31\Xi+24\omega+21\tau$	185	167

[a] When possible, frequency values taken from the liquid spectra are given. [b] The potential energy distribution is defined as $X_{ik}=100F_{ii}L_{ik}{}^2/\lambda_k$. [c] d(X) and γ(X), C–H stretching and C–C–H bending in the Br–C–H group; d and γ, C–H stretchings and C–C–H bendings in the C–CH_2 groups; R, C–C stretchings; X, C–Br stretching; δ, H–C–H bendings; θ, H–C–Br bending; ω, C–C–C bendings; Ξ, C–C–Br bending; τ_s and τ(X), torsions around the C_3-C_4 and the C_1-C_2 bonds (Br$HC^1-C^2H_2-C^3H_2-C^4H_2-C^5H_2-C^6H_2$); τ, the sum of τ_s, τ(X) and the torsion around the C_2-C_3 bond.

iodoctclohexane, while ν_{48} of chloro- and ν_{47} of iodocyclohexane are not observed in the Raman effect at all. Therefore ν_{47} of *e*-chlorocyclohexane corresponds to ν_{48} of iodocyclohexane, and according to the PED can be interpreted as an almost pure C−C−X (X=Cl,I) bending vibration.

For both the *e*- and *a*-conformers ν_{13} and ν_{15} are somewhat coupled, especially for chlorocyclohexane where ν_{13} can be interpreted as the H−C−Cl bending vibration, while for bromo- and iodocyclohexane the H−C−X (X=Br,I) bending seems to be dominating for the ν_{15} mode.

The C−X (X=Cl,Br,I) stretchings of the *a*-conformers are not well-localized vibrations.[14,24] For chlorocyclohexane the bands at 685 and 559 cm^{-1} (ν_{22} and ν_{23}) could both be assigned to this mode according to the PED, while for bromocyclohexane the corresponding vibrations are found at 510 and 658 cm^{-1}, respectively. For iodocyclohexane ν_{24} at 446 cm^{-1} as well as ν_{22} and ν_{23} at 639 and 482 cm^{-1} all have major contributions from stretching of the C−I bond.

Except for the vibrations with strong contribution from C-halogen stretching or bending, the fundamental frequencies are rather similar for the different molecules of the same conformer, while the frequency variations for the different conformers of the same compound are often considerably larger. Especially for species *a″* the differences between the fundamental vibrations of chloro-, bromo- and iodocyclohexane are very small.

Acknowledgements. The author is grateful to P. Klæboe for helpful discussions and to E. Tørneng and A. Horn who recorded parts of the spectra. Financial support from the Norwegian Research Council for Science and the Humanities is acknowledged.

REFERENCES

1. Damiani, D. and Ferretti, L. *Chem. Phys. Lett. 21* (1973) 592.
2. Schneider, H. J. and Hoppen, V. *Tetrahedron Lett. 7* (1974) 579.
3. Subbotin, O. A. and Sergeyev, N. M. *J. Am. Chem. Soc. 97* (1975) 1080.
4. Jensen, F. R. and Bushweller, C. H. *J. Am. Chem. Soc. 91* (1969) 3223.
5. Eliel, E. L. and Martin, R. J. L. *J. Am. Chem. Soc. 90* (1968) 689.
6. Meyer, A. Y. and Allinger, N. L. *Tetrahedron 31* (1975) 1971.
7. Wertz, D. H. and Allinger, N. L. *Tetrahedron 30* (1974) 1579.
8. Dosen-Micovic, L. and Allinger, N. L. *Tetrahedron 34* (1978) 3385.
9. Abraham, R. J. and Siverns, T. M. *J. Chem. Soc. Perkin Trans. 2* (1972) 1587.
10. Agaev, U. Kh., Rizaeva, S. Z. and Khurdaverdieva, E. F. *Azerb. Khim. Zh.* (1973) 25.
11. Klæboe, P. *Acta Chem. Scand. 23* (1969) 2641.
12. Rey-Lafon, M., Rouffi, C., Camiade, M. and Forel, M. T. *J. Chem. Phys. 67* (1970) 2037.
13. Klæboe, P., Lothe, J. J. and Lunde, K. *Acta Chem. Scand. 10* (1956) 1465.
14. Remizov, A. B. and Sverdlov, L. M. *Izv. Vyssh. Uchebn. Zaved. Fiz. 11* (1968) 150.
15. Larnaudie, J. M. *Thesis*, Paris 1953.
16. Chiurdoglu, G., Kleiner, W., Masschelein, W. and Reisse, J. *Bull. Soc. Chim. Belg. 69* (1960) 143.
17. Allen, A., Fawcett, V. and Long, D. A. *J. Raman Spectrosc. 4* (1976) 285.
18. Gustavsen, J. E., Klæboe, P. and Kvila, H. *Acta Chem. Scand. A 32* (1978) 25.
19. Nishikawa, M. *Chem. Pharm. Bull. 11* (1963) 977.
20. Fukushima, K. *J. Mol. Struct. 34* (1976) 67; Fukushima, K. and Sugiura, K. *J. Mol. Struct. 41* (1977) 41.
21. Stokr, J., Schneider, B. and Jakes, J. J. *J. Mol. Struct. 15* (1973) 87.
22. Hallam, H. E. and Ray, T. C. *J. Chem. Soc.* (1964) 2337.
23. Rey-Lafon, M. and Forel, M. T. *J. Mol. Struct. 29* (1975) 193.
24. Opaskar, C. G. and Krimm, S. *Spectrochim. Acta A 23* (1967) 2261.
25. Christian, S. D., Grundnes, J., Klæboe, P., Tørneng, E. and Woldbæk, T. *Acta Chem. Scand. A 34* (1980) 391.
26. Woldbæk, T., Nielsen, C. J. and Klæboe, P. *J. Mol. Struct. 66* (1980) 31.
27. Woldbæk, T., Ellestad, O. H., Gustavsen, J. E. and Klæboe, P. *J. Mol. Struct. 62* (1980) 9.
28. Woldbæk, T. and Klæboe, P. *J. Mol. Struct. 63* (1980) 195.

Received December 17, 1981.

Acta Chemica Scandinavica A 36 (1982) 657–664

Structure and Charge Density of 1,2-Bis(methylsulfonyl)ethane by X-Ray Diffraction

F. MO and Ø. BERG

Institutt for røntgenteknikk, Universitetet i Trondheim-NTH, N-7034 Trondheim-NTH, Norway

The room-temperature structure and charge-density distribution in 1,2-bis(methylsulfonyl)ethane, $H_3C-SO_2-(CH_2)_2-SO_2-CH_3$, has been studied by X-ray diffraction. The space group is $P2_1/c$, $a=6.260(8)$, $b=5.949(3)$, $c=10.643(3)$ Å, $\beta=90.80(1)°$ and $Z=2$. Two equivalent sets of counter data collected to a limit in $(\sin\theta/\lambda)=1.0$ Å^{-1} were corrected for coincidence loss and absorption before averaging. A number of refinements in different shells of reciprocal space have been carried out to investigate the influence on atomic parameters by scattering on the aspherical electron density. Refinement with all data, 2386 F_o, yielded an $R=0.034$; with the 870 F_o below $(\sin\theta/\lambda)=0.65$ Å^{-1} R was 0.029. Oxygen parameters are the most sensitive to data cutoff. In the present study the S–O bonds attain their largest values in the 0.5–1.0 Å^{-1} refinement. Positional and thermal parameters for the non-H atoms were taken from a refinement with $(\sin\theta/\lambda)>0.70$ Å^{-1}. Changes in bond lengths and angles at S relative to the parent sulfoxide are in agreement with the Walsh-Bent rehybridization theory. No significant structural differences were found in the central CH_2-CH_2 moieties of the sulfoxide and sulfone molecules. Deformation density maxima in the SO_2 region are rather broad and the lone-pair density near O is merged with the density in the S–O bonds. Both O atoms exhibit asymmetry in the lone-pair region. The one well-developed lobe near O(1) lies in the O–S–O plane, at O(2) the planes S–O(2)-lobe and O–S–O are nearly orthogonal. The lobes are pointing roughly in the direction of O···H–C contacts, of which one at 2.26 Å is unusually short. In planes defined by pairs of bonds to S there are regions of negative density about S in a trigonal arrangement also found in several related molecules.

Sulfur, a constituent of a variety of inorganic, organic and biological molecules, is characterized by an unusual versatility in bonding. S–S distances are distributed almost continuously from 1.86 Å in SSF_2 to van der Waals distances 3.40–3.60 Å; valency angles at S range between 90 and 180°.[1] Large variations are also seen in the experimental charge-density distribution near sulfur, for instance in compounds like S_8,[2] S_4N_4[3] and the cyclic ion $S_4N_3^+$.[4] The structural flexibility of sulfur is very likely an important prerequisite for some specific functions of S-containing molecules. In particular this element appears to play a significant role for electron transport in such diverse systems as the inorganic semimetal $(SN)_x$, some organic charge-transfer complexes and proteins (*cf.* Ref. 5).

We have undertaken diffraction studies of a family of small S-containing molecules with the general formula $R_1-X_1-(CH_2)_2-X_2-R_2$ where X = S, SO or SO_2, and R = various organic substituents.[5–8] These molecules provide a system allowing a systematic investigation of the effects on electronic structure by changes in the oxidation state and hybridization of sulfur and differences in the electronic properties of the terminal R groups. Some well-diffracting members of the family also appear amenable to charge density studies.

We report here a room-temperature X-ray study of 1,2-bis(methylsulfonyl)ethane, $R_1=R_2=$ Me, $X_1=X_2=SO_2$. Preliminary results have been presented previously.[8,9]

EXPERIMENTAL

Single crystals of 1,2-bis(methylsulfonyl)ethane, hereinafter DION, from ethylacetate were prismatic along b with well-developed pairs of prism faces (100) and (001).

0302-4377/82/080657-08$02.50

Table 1. Crystal data, 1,2-bis(methylsulfonyl)ethane.

Composition	$C_4H_{10}O_4S_2$	T(K)	293.0(5)
M_r	186.25	λ(Å)	0.71069
Space group	$P2_1/c$	Z	2
a(Å)	6.260(8)	D_x(Mg m^{-3})	1.561
b	5.949(3)	μ(mm^{-1})	0.6034[a]
c	10.643(3)	Size(mm)	$\sim 0.36 \times 0.59 \times 0.32$
β(°)	90.80(1)	M.p. (K)	467.0 – 468.0
V(Å^3)	396.3		

[a] Mass absorption coefficients taken from International Tables for X-Ray Crystallography, Vol. IV (1974).

Collection and processing of intensities. Cell dimensions and crystal orientation were measured at the beginning, at the end, and three times during data collection. There was a small but systematic increase in both a and b during this period, ranges 6.254 – 6.268 and 5.946 – 5.951 Å, respectively, other cell parameters did not change. Values given in Table 1 are averages, standard deviations in a and b cover the observed ranges for these parameters.

The intensities of 3517 $+h+k\pm l$ reflections (set I) and 3539 $-h+k\pm l$ (set II) excluding extinctions were measured without attenuators to a limit in $(\sin\theta/\lambda)=s=1.0$ Å^{-1} with Nb-filtered Mo$K\alpha$ radiation on a diffractometer controlled by the Vanderbilt disk-oriented program system.[10] The scan mode was $\omega/2\theta$ at 2° min^{-1} in 2θ, basic scan width was $2\theta(\bar{\alpha})-0.6$ to $2\theta(\bar{\alpha})+0.6$°, and backgrounds were measured for 20 s. Intensities below $2\theta\sim 8$° were remeasured with reduced low-angle scans.[5]

The data were scaled with a best polynomial fit to the averaged curve for three standard intensities measured at intervals of 80 reflections and corrected for coincidence loss.[11,12] A recovery constant 11.3×10^{-8} counts^{-1} was determined for this system. Absorptions in the range 1.185 to 1.253 were calculated as described previously.[5]

Equivalent pairs 0kl and 0k-l and some reflections measured twice were weight-averaged within each data set and the two sets were then weight-averaged to yield 3312 independent F_w^2. The overall agreement $D=\Sigma|F_1^2-F_2^2|/\Sigma F_w^2$ was 0.034 in the range $0<s\leq 0.85$ Å^{-1}. In the high s-range 0.85 – 1.0 Å^{-1}, 55% of the data had $F^2<3\sigma(F^2)$ and D was 0.195. For an individual observation $\sigma(F_i^2)=\sigma(I_i)(\mathrm{Lp})^{-1}$ (scale), where $\sigma^2(I_i)=\sigma_{i\ \mathrm{count}}^2+(SI_{i\ \mathrm{net}})^2$; $i=1,2$. The parameter S was adjusted to 0.030 to obtain a Gaussian distribution of the weighted means of the differences $\Delta_i=|F_i^2-F_w^2|$ within the range $0<s\leq 0.75$ Å^{-1}. This value for S was used for all data and $\sigma(F_w^2)$ were calculated by standard methods. Reflections with $F_w^2<p\sigma(F_w^2)$ were given zero weight, $p=1$, 2 and 3 respectively, for s-ranges 0 – 0.65, 0.65 – 0.85 and 0.85 – 1.0 Å^{-1}. Eight low-angle reflections with very large counting rates could not be properly corrected for coincidence loss and were also weighted zero.

A set of local programs was used for analyses and processing of the data.[13]

Structure solution and refinement. Identification of the S position and subsequent location of the C and O atoms in the asymmetric half molecule was by Patterson and difference Fourier techniques. Following initial isotropic refinement of C, O and S, the H atoms were added with positions from a ΔF map.

The quantity $\Sigma w(|F_o|-k|F_c|)^2$ with $w=\sigma^{-2}(F_o)$ was minimized by the full-matrix least-squares method. Scattering factors were those of Doyle and Turner[14] except for H.[15] Anomalous dispersion values for S were taken from Cromer and Liberman.[16] Anisotropic temperature factors were assigned to C, O and S but not to H.

Least-squares fitting of the isolated spherical-atom model of a molecule to its observed, low-order X-ray transform may introduce significant errors in the atomic parameters. In part to assess the influence on these parameters by deviations from the spherical density due to bonding, several refinements were carried out in different shells of reciprocal space. Table 2 summarizes a selection of these refinements. Corresponding final atomic parameters are given in Table 3. Parameters from the refinements I and II were not different and only those from II are shown in Tables 3 – 5. In all runs with $s\geq 0.60$ Å^{-1} H parameters were fixed at values obtained from the refinement with $s>0.40$ Å^{-1}. A list of structure factors is available from the authors.

Programs for structure solution and refinement were from the X-RAY 76 system,[17] drawings of molecules were made by ORTEP.[18]

Deformation density maps. Deformation density maps can be obtained as the difference between the observed density and that calculated with atomic parameters from a high-angle X-ray refinement satisfying the conditions for the spherical-atom model. In this analysis positional and thermal

Table 2. Survey of refinements.

	Refinement I	II	III	IV	V
$(\sin\theta/\lambda)$ range ($Å^{-1}$)	0–0.65	0–1.00	0.40–1.00	0.50–1.00	0.70–1.00
Number of reflections with $w\neq 0$, NO	870	2386	2188	1982	1307
Number of reflections with $w=0$	36	926	915	912	864
Number of variables, NV	66	66	66	66	46[a]
Scale factor, k	14.52(6)	14.58(3)	14.62(3)	14.74(4)	14.10(9)
$R(F)=\Sigma\|\|F_o\|-k\|F_c\|\|/\Sigma\|F_o\|$	0.029	0.034	0.031	0.032	0.043
$R_w(F)=[\Sigma w(\|F_o\|-k\|F_c\|)^2/wF_o^2]^{\frac{1}{2}}$	0.047	0.045	0.034	0.031	0.036
$R(F^2)=\Sigma\|F_o^2-(kF_c)^2\|/F_o^2$	0.048	0.049	0.035	0.034	0.052
$\mathrm{GOF}=[\Sigma w(\|F_o\|-k\|F_c\|)^2/(\mathrm{NO}-\mathrm{NV})]^{\frac{1}{2}}$	3.94	2.66	1.88	1.58	1.37

[a] Fixed H parameters from refinement III were used.

Table 3. Final atomic parameters. Coordinates are: $\times 10^5$ for S, $\times 10^4$ for C and O, and $\times 10^3$ for H. Thermal parameters, $U_{ij}(Å^2\times 10^4)$ for C, O and S, and $U(Å^2\times 10^4)$ for H are defined by: $\exp[-2\pi^2(U_{11}a^{*2}h^2+\cdots 2U_{12}a^*b^*hk+\cdots)]$ and $\exp[-8\pi^2U(\sin^2\theta/\lambda^2)]$, respectively. For non-H atoms: first row: refinement II(0–1.00 $Å^{-1}$); second row: refinement III(0.40–1.00 $Å^{-1}$); third row: refinement IV(0.50–1.00 $Å^{-1}$); fourth row: refinement V(0.70–1.00 $Å^{-1}$). For H atoms: entries only for three first rows, see text. E.s.d.'s are in parentheses.

Atom	X	Y	Z	U_{11}	U_{22}	U_{33}	U_{12}	U_{13}	U_{23}
S	21172(3)	4158(3)	84116(2)	362(1)	296(1)	259(1)	22(1)	66(1)	14(1)
	21173(3)	4157(3)	84118(1)	362(1)	296(1)	259(1)	22(1)	65(1)	14(1)
	21161(3)	4158(2)	84117(1)	365(1)	299(1)	261(1)	22(1)	66(1)	14(1)
	21152(5)	4161(4)	84113(2)	355(2)	289(1)	253(1)	24(1)	63(1)	17(1)
C(1)	3301(2)	2968(2)	8864(1)	436(5)	395(4)	446(5)	−100(4)	6(4)	61(4)
	3307(2)	2971(2)	8864(1)	441(4)	385(3)	454(4)	−102(3)	6(3)	56(3)
	3307(2)	2967(1)	8862(1)	446(4)	385(3)	452(3)	−105(3)	4(3)	55(3)
	3306(3)	2971(3)	8864(2)	443(6)	385(4)	439(5)	−102(4)	10(4)	53(4)
C(2)	−247(1)	233(2)	9312(1)	337(4)	380(4)	249(3)	−30(3)	28(2)	7(3)
	−252(1)	241(1)	9313(1)	339(3)	385(3)	248(2)	−27(2)	29(2)	5(2)
	−249(1)	243(1)	9313(1)	339(2)	388(3)	246(2)	−27(2)	29(2)	5(2)
	−250(2)	245(2)	9315(1)	332(3)	375(4)	244(2)	−28(3)	25(2)	3(2)
O(1)	1456(1)	557(1)	7108(1)	547(4)	488(4)	253(2)	−18(3)	45(3)	4(2)
	1456(1)	559(1)	7106(1)	565(4)	490(3)	252(2)	−17(3)	53(2)	3(2)
	1455(1)	561(1)	7104(1)	572(3)	492(3)	247(2)	−13(3)	46(2)	6(2)
	1462(3)	559(3)	7107(1)	561(6)	474(4)	245(3)	−8(5)	49(3)	6(3)
O(2)	3512(1)	−1410(1)	8754(1)	522(4)	417(4)	486(4)	175(3)	91(3)	51(3)
	3505(1)	−1421(1)	8757(1)	538(4)	417(3)	482(3)	175(3)	106(3)	54(2)
	3504(1)	−1423(1)	8759(1)	538(4)	417(3)	478(3)	179(3)	103(3)	54(2)
	3506(3)	−1416(3)	8760(1)	526(7)	407(4)	474(5)	168(5)	112(5)	56(4)

Atom	x	y	z	U	Atom	x	y	z	U
H(11)	375(3)	279(3)	953(1)	574(40)	H(21)	−111(2)	−101(3)	890(1)	483(35)
	363(4)	288(4)	963(2)	596(45)		−107(3)	−96(3)	897(2)	442(34)
	362(12)	287(11)	970(7)	869(128)		−92(6)	−111(7)	891(4)	604(64)
H(12)	245(2)	406(3)	871(1)	449(34)	H(22)	−97(2)	154(3)	925(1)	695(46)
	243(4)	410(5)	864(2)	539(41)		−100(3)	160(3)	918(2)	417(31)
	247(6)	420(6)	861(3)	566(58)		−100(5)	159(5)	922(3)	495(49)
H(13)	443(3)	319(3)	854(1)	637(44)					
	447(4)	314(4)	848(2)	589(44)					
	462(7)	325(6)	851(4)	606(65)					

parameters for C, O and S were taken from a refinement with $s>0.70$ Å^{-1} as the best model available. Previous experience has suggested that the best compromise for the *positional* parameters of H in the X-ray case is to normalize the parent bond lengths to neutron diffraction values. This procedure can be rationalized both on theoretical and experimental evidence.[5] In the present case, however, H parameters from the refinement at $s>0.40$ Å^{-1} were used.

Three different sets of maps were calculated with a high cutoff in data 0.65, 0.75 and 1.0 Å^{-1}, respectively. In all cases the scale factor, k, was obtained by refining this parameter alone with atomic parameters fixed at values as described above. For the three distinct cases corresponding values of k and $R(F)$ were: 14.42(3), 0.028; 14.38(2), 0.028; 14.34(1), 0.033, respectively.

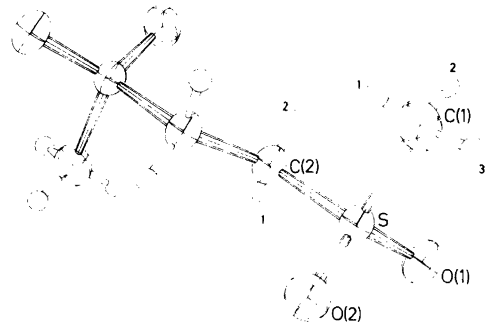

Fig. 1. Molecular conformation and atomic labelling. Sequential numbering of H atoms is given where necessary. Thermal ellipsoids of the non-H atoms correspond to a 50% probability.

RESULTS AND DISCUSSION

The molecular structure. The molecular conformation of DION is shown in Fig. 1. The sequence of bonds C–C–S–C(Me) is oriented *gauche* in contrast with the *trans* arrangement in the deoxygenated analogues *meso*-1,2-bis(methylsulfinyl)-ethane (DIOX)[6] and 1-methylsulfonyl-2-methylsulfinylethane (OXON).[7]

Bond lengths and angles uncorrected for libration effects are given in Tables 4 and 5, respectively. Increase of the lower cutoff in s has a moderate influence on the S–C and C–C lengths. These bonds have their largest values after refinement III (0.40–1.0 Å^{-1}) with shifts 0.001–0.003 Å relative to II (all data). The central C–C bond apparently shortens by 0.004 to 1.515 Å when s_{min} is increased from 0.40 (III) to 0.70 (V) Å^{-1}. However, this bond refined to an intermediate 1.517 Å both with data at $s>0.60$ and $s>0.80$ Å^{-1} (not included in Tables 2–5). The largest changes occur in the S–O bonds. The two bonds are distinctly different after refinement II and expand in a parallel fashion to attain their largest values after refinement IV (0.50–1.0 Å^{-1}). Both bonds contract in refinement V and also become more equal. The difference was reduced further, 1.442 (O(1)) and 1.440 Å (O(2)), in a refinement with $s>0.80$ Å^{-1}, however, parameters from run V are preferred because of their lower e.s.d.'s and unchanged goodness-of-fit (GOF). The observed shifts in the O atoms are in consonance with the different spatial distributions of lone-pair and bonding electron densities. Whereas the latter contribute negligibly to Bragg intensities at the Cu$K\alpha$ limit, ~0.65 Å^{-1}, scattering on the more contracted lone-pair density persists into the region beyond $s=0.75$ Å^{-1},[19] in some cases as far out as 1.0 Å^{-1}, even at room temperature.[20] In a low-temperature study of sulfamic acid, Bats, Coppens and Koetzle[21] obtained the

Table 4. Bond lengths (Å) with standard deviations. For explanation of Roman numerals, see Tables 2 and 3.

	II	III	IV	V
S–C(1)	1.754(1)	1.757(1)	1.755(1)	1.757(2)
S–C(2)	1.778(2)	1.781(2)	1.778(2)	1.779(2)
S–O(1)	1.445(1)	1.447(1)	1.449(1)	1.445(1)
S–O(2)	1.437(1)	1.440(1)	1.442(1)	1.440(2)
C(2)–C(2′)	1.518(1)	1.519(1)	1.518(1)	1.515(1)
C(1)–H(11)	0.77(2)	0.84(3)	0.91(8)	
C(1)–H(12)	0.86(2)	0.89(3)	0.94(4)	
C(1)–H(13)	0.80(2)	0.85(3)	0.93(4)	
C(2)–H(21)	1.01(2)	0.95(2)	1.00(4)	
C(2)–H(22)	0.90(2)	0.94(2)	0.93(3)	

Table 5. Valency angles (°) with standard deviations. For explanation of Roman numerals, see Tables 2 and 3.

	II	III	IV	V
C(1)SC(2)	104.87(6)	104.82(5)	104.84(6)	104.71(8)
C(1)SO(1)	109.12(5)	109.07(5)	109.01(5)	109.04(8)
C(1)SO(2)	109.39(8)	109.56(8)	109.51(8)	109.35(11)
C(2)SO(1)	106.96(7)	106.94(7)	107.03(7)	107.24(9)
C(2)SO(2)	108.94(7)	108.79(7)	108.71(7)	108.80(10)
O(1)SO(2)	116.87(5)	116.95(4)	117.03(5)	116.99(9)
SC(2)C(2')	111.78(8)	111.47(7)	111.68(7)	111.67(9)
SC(1)H(11)	106(1)	108(2)	107(4)	
SC(1)H(12)	110(1)	109(2)	111(2)	
SC(1)H(13)	114(1)	110(2)	115(2)	
H(11)C(1)H(12)	120(2)	116(2)	116(5)	
H(11)C(1)H(13)	96(2)	106(2)	103(5)	
H(12)C(1)H(13)	110(2)	108(2)	104(3)	
SC(2)H(21)	105(1)	107(1)	99(2)	
SC(2)H(22)	109(1)	106(1)	109(2)	
C(2')C(2)H(21)	112(1)	110(1)	110(2)	
C(2')C(2)H(22)	109(1)	114(1)	111(2)	
H(21)C(2)H(22)	110(1)	109(2)	116(3)	

maximum shifts in O coordinates from a refinement with data in the range 0.65 – 0.85 $Å^{-1}$. The magnitude and direction of the asphericity shifts of O atoms will depend both on their hybridization state and the possible polarization of lone-pair density due to interatomic interactions.

Refinement II yielded several short C – H bonds. These and the fairly large spread among the values may indicate some defect in the low-angle data. In runs III and IV all C – H lengths increased except C(2) – H(21) at 1.01 Å and also became more equal. The average lengthening from set II to IV is 0.07 Å. With higher s cutoff, scattering on S becomes more dominant and the small signal from H, which amounts to only about 0.5 % of the S contribution at 0.75 $Å^{-1}$, gradually approaches the noise level in the data. In the various refinements with $s > 0.60$ $Å^{-1}$ the H parameters were unstable. This tendency is beginning to appear in parameter set IV, where some angles are affected.

Except for a significant increase in the U_{11} components of both O atoms and a small reorientation of the vibration ellipsoid of C(1) the thermal parameters of all non-H atoms change very little throughout refinements II – IV. In the runs with $s > 0.70$ (V) and $s > 0.80$ $Å^{-1}$ there was a general decrease in these parameters with a parallel change in the scale factor k.

Minimum corrections for thermal shortening[22] have been applied to the terminal bonds S – O(1) (l_1), S – O(2) (l_2) and S – C(1) (l_3) as obtained from refinement V. They are: $l_1 + 0.001$, $l_2 + 0.003$ and $l_3 + 0.001$ Å. The corrected bond lengths are given in Table 6 with parameters for DIOX,[6] in which

Table 6. Structure parameters of DION, partial structure of $MPSO_2$[5,a] and DIOX.[6]

	Bond lengths (Å)				Valency angles (°)				
	S – O	Central S – C	Central C – C	Terminal S – C	C – S – C	Central C – S – O	Terminal C – S – O	O – S – O	S – C – C
DION	1.446(1)[b]					107.2(1)	109.0(1)		
	1.443(2)[b]	1.779(2)	1.515(1)	1.758(2)[b]	104.7(1)	108.8(1)	109.4(1)	117.0(1)	111.7(1)
	1.452(2)					107.9(1)	108.6(1)		
$MPSO_2$	1.439(3)	1.783(2)	1.525(3)	1.759(3)	103.9(1)	109.0(1)	109.6(2)	117.0(2)	108.1(1)
DIOX	1.501(2)[b]	1.802(2)	1.516(2)	1.788(2)[b]	97.0(1)	106.3(1)	106.8(1)	–	109.4(1)

[a] Data for methyl end of $MPSO_2$ are given in the table. [b] Minimum correction applied.[22]

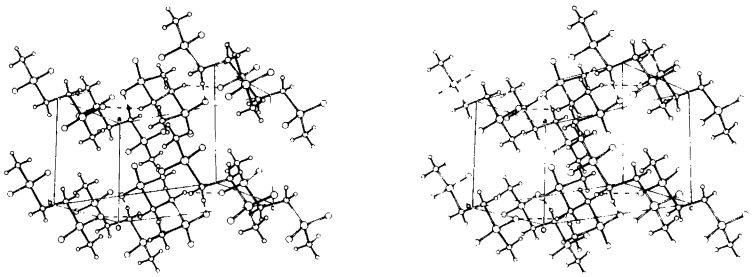

Fig. 2. Stereodrawing of the molecular packing. Short intermolecular distances O(1)···H(21) are shown as broken lines.

$R_1=R_2=$Me and $X_1=X_2=$SO, and 1-methylsulfonyl-2-phenylsulfonylethane, or $MPSO_2$,[5] which has a partial structure identical to the half-molecule of DION. Most pairs or averages of corresponding bond lengths and angles in DION and $MPSO_2$ are in very close agreement. The largest differences appear in the central C–C bonds, 0.010 Å, and in the S–C–C angles, 3.6°.

According to the Walsh-Bent rehybridization theory[23,24] substitution of the lone pair at S in sulfoxide with a second O as in sulfone will reduce the *p* character of all σ-bonds involving S. This implies shorter bonds and larger valency angles at S. All data in Table 6 corroborate these qualitative predictions, bonds S–O and angles C–S–C with changes −0.056 Å and +7.3°, respectively, apparently being the most sensitive parameters. A further result of the theory is that the secondary rehybridization at S will induce a similar but attenuated effect at the other adjacent atoms, thus causing a contraction of the central C–C bond. This relay effect was anticipated to increase in the series sulfide, sulfoxide, sulfone.[6] The C–C bond is shortened in all structures but the results in Table 6 do not indicate any significant difference between sulfoxide and sulfone in this respect. In fact, the averaged difference, 0.004 Å, is probably exaggerated because of the rather long C–C in $MPSO_2$. This bond is 1.515 Å both in DION and OXON[7] and 1.519 Å in the related 1,2-bis(phenylsulfonyl)ethane.[8]

The crystal structure. The molecular packing is shown in Fig. 2. Intermolecular cohesion is mediated largely through the O atoms. There are three O···C and three O···H distances in the normal van der Waals range, 3.257–3.344 and 2.41–2.53 Å, respectively. All contacts with H correspond to C–H lengths normalized to 1.09 Å. A remarkable feature of the crystal structure is a very short distance O(1)···H(21) at $-x$, $1/2+y$, $3/2-z$, 2.26 Å. Assuming 1.52 Å as the appropriate van der Waals radius for O[25] this distance falls in the range between a short van der Waals contact and a long H-bond. It is possible that the different environments of the O atoms involve a stronger polarization of O(1) which would contribute to the apparent lengthening of S–O(1), especially in refinements with low-angle data.

Deformation, density maps. Density maps have been calculated through various sections and bonds. Those shown in Figs. 3 (a)–(e) are based on data with $s<0.65$ Å^{-1}. The standard deviation in the maps away from the nuclear positions was estimated[26] at 0.03 e Å^{-3}.

The aspherical features near the S and O atoms are of particular interest. Compared with the S–C bonds the densities in the S–O bonds, 0.16–0.30 eÅ^{-3} are less regular and lone-pair peaks near O are merged with the density in the bond. Maps calculated with $s<0.75$ Å^{-1} have in general sharper features, and changes due to noise in the data are minor. Figs. 3(a) and 3(f) provide one example of the contribution to $\Delta\rho$ near the SO_2 group from data in the range 0.65–0.75 Å^{-1}. Maps based on the complete data set, $s<1.0$ Å^{-1}, contain significantly more noise than those of lower resolution. This is not surprising in view of the large proportion of weak reflections in the *s*-range 0.85–1.0 Å^{-1}.

Both O atoms are asymmetric in the lone-pair region, each having only one well-developed lobe. On closer inspection one finds that the lone-pair peak near O(1), 0.20 e Å^{-3} (with $s_{max}=0.65$ Å^{-1}), is approximately in the O–S–O plane (Fig. 3 (d)). The peak near O(2) is more dense, 0.31 e Å^{-3}, and describes together with O(2) and S a plane almost orthogonal to the O–S–O plane (Fig. 3(e)). Comparison of the density features in Fig. 3 with

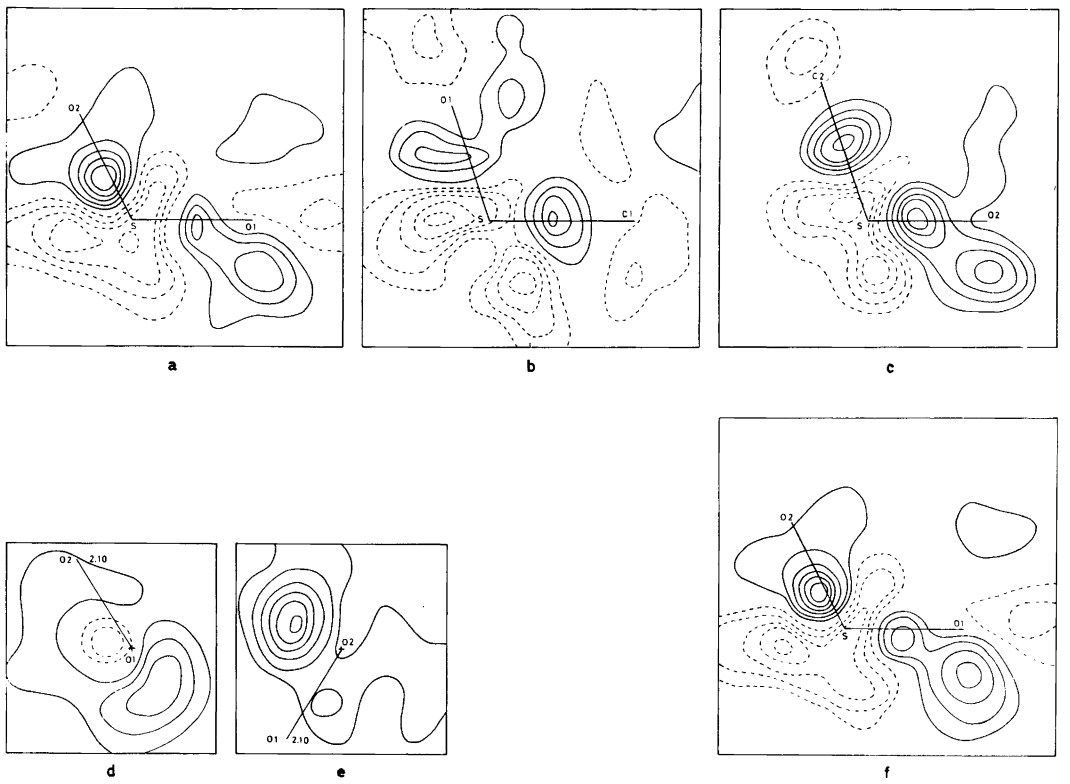

Fig. 3. Deformation density sections. Planes in (a), (b) and (c) are self-explanatory, (d) is plane through O(1) and perpendicular to the S–O(1) bond, (e) is plane through O(2) and perpendicular to S–O(2). In both (d) and (e), projection of bond to the other O atom and its height in Å over plane is given. Maps (a) through (e) are calculated with $s_{max}=0.65$ Å^{-1}. Map (f) is calculated with $s_{max}=0.75$ Å^{-1} and shows density in the same plane as (a). Contours are at 0.05 e Å^{-3} with negative countours broken. Zero contour not shown.

the orientation of molecules in Fig. 2 indicates that the lone-pair peak near O(1) is directed towards the H atom in the short 2.26 Å O(1)···H contact.

A detailed analysis of the deformation density is probably not justified considering that the experimental conditions were not optimal. Positional and thermal parameters of the O atoms in particular are probably still affected by lone-pair scattering at $s>0.70$ Å^{-1}. At room temperature the approximations involved in the harmonic description of atomic thermal motion and the neglect of thermal diffuse scattering may give significant errors. If present, polarization of the core-electron densities at O[27,28] and possibly also at S will contribute to Bragg-scattering at very large angles. Some of these sources of error will become manageable at reduced temperatures. An X-ray study of DION at N_2 liq. temperature has been initiated for a more precise determination of the deformation density.

In the maps of Fig. 3 there are negative lobes in an approximately trigonal arrangement about the S atomic site in planes defined by pairs of bonds to S. Very similar details are present in maps of $MPSO_2$,[5,*] sulfamic acid[21] and sodium sulfanilate.[29] The consistent appearance of such features in all these structures indicates quite large deficiencies in the spherical model of S in tetrahedral bonding.

* Through a computational error, published values for the deformation density in $MPSO_2$ (Ref. 5) are too low by a factor of 1.38. All numbers relating to $\Delta\rho$ in Ref. 5 should be corrected accordingly, and the equidistance in the maps is ~0.07 and not 0.05 e Å^{-3} as given.

Acknowledgement. A grant from *NTH's Fond* is gratefully acknowledged.

REFERENCES

1. Steudel, R. *Angew. Chem. 87* (1975) 683.
2. Coppens, P., Yang, Y. W., Blessing, R. H., Cooper, W. F. and Larsen, F. K. *J. Am. Chem. Soc. 99* (1977) 760.
3. DeLucia, M. L. and Coppens, P. *Inorg. Chem. 17* (1978) 2336.
4. Moss, G., Guru Row, T. N. and Coppens, P. *Inorg. Chem. 19* (1980) 2396.
5. Mo, F. and Gaasdal, A. *Acta Crystallogr. B 36* (1980) 2349.
6. Svinning, T., Mo, F. and Bruun, T. *Acta Crystallogr. B 32* (1976) 759.
7. Berg, Ø., Bruun, T. and Mo, F. *Acta Chem. Scand. A 32* (1978) 163.
8. Mo, F., Berg, Ø., Thorkildsen, G. and Gaasdal, A. *Fifth Eur. Crystallogr. Meeting*, Copenhagen (ECM-5) 1979, Abstr. p. 352, and extended abstract.
9. Berg, Ø. *Hovedoppgave*, Inst. for røntgenteknikk, UNIT-NTH, Trondheim 1976.
10. Lenhert, P. G. *J. Appl. Crystallogr. 8* (1975) 568.
11. Chipman, D. R. *Acta Crystallogr. A 25* (1969) 209.
12. a. Mo, F. and Jensen, L. H. *Acta Crystallogr. B 31* (1975) 2867; b. Mo, F. *Thesis*, Univ. of Trondheim -- NTH, Trondheim 1979.
13. Svinning, T. and Mo, F. *XRDATA, Tekn. Rapport 30-RII-78*, Inst. for røntgenteknikk, UNIT-NTH, Trondheim 1978.
14. Doyle, P. A. and Turner, P. S. *Acta Crystallogr. A 24* (1968) 390.
15. Stewart, R. F., Davidson, E. R. and Simpson, W. T. *J. Chem. Phys. 42* (1965) 3175.
16. Cromer, D. T. and Liberman, D. *J. Chem. Phys. 53* (1970) 1891.
17. Stewart, J. M., Ed., *The X-RAY SYSTEM, Version of 1976*, Technical Report TR-446, Computer Science Center, University of Maryland, College Park 1976.
18. Johnson, C. K. *ORTEP II*, Report ORNL-5138, Oak Ridge National Laboratory, Oak Ridge 1976.
19. Wang, Y., Blessing, R. H., Ross, F. K. and Coppens, P. *Acta Crystallogr. B 32* (1976) 572.
20. Stevens, E. D. *Acta Crystallogr. A 33* (1977) 580.
21. Bats, J. W., Coppens, P. and Koetzle, T. F. *Acta Crystallogr. B 33* (1977) 37.
22. Busing, W. R. and Levy, H. A. *Acta Crystallogr. 17* (1964) 142.
23. Walsh, A. D. *Discuss. Faraday Soc. 2* (1947) 18.
24. a. Bent, H. A. *Chem. Rev. 61* (1961) 275; b. Bent, H. A. *J. Inorg. Nucl. Chem. 19* (1961) 43.
25. Kitaigorodskii, A. I. *Molecular Crystals and Molecules*, Academic, New York 1973, p. 17.
26. Cruickshank, D. W. J. *Acta Crystallogr. 2* (1949) 65.
27. Craven, B. M. and McMullan, R. K. *Acta Crystallogr. B 35* (1979) 934.
28. Kutoglu, A. and Scheringer, C. *Acta Crystallogr. A 35* (1979) 458.
29. Bats, J. W. *Acta Crystallogr. B 33* (1977) 2035.

Received December 4, 1981.

Acta Chemica Scandinavica A 36 (1982) 665–671

Structural Studies on the Phosphorus–Nitrogen Bond. VI. The Crystal Structure of Tris(morpholino)phosphine Oxide

CHRISTIAN RØMMING [a] and JON SONGSTAD [b]

[a] Department of Chemistry, University of Oslo, Oslo 3, Norway and [b] Department of Chemistry, University of Bergen, 5014 Bergen-Univ., Norway

The structure of the title compound, $[O(CH_2CH_2)_2N]_3PO$, has been determined by X-ray methods using diffractometer data collected both at 18 °C and at −150 °C. The crystals are monoclinic, space group $P2_1/n$, with $a = 9.107(1)$ Å; $b = 11.145(1)$ Å; $c = 14.605(1)$ Å and $\beta = 97.03(1)°$ at −150 °C. Full-matrix least-squares refinement gave a final R-value of 0.045 for 4151 reflections.

The average P–N bond length is 1.66 Å and the sum of the nitrogen bond angles ranges from 349.1 to 358.6°. The lone pair of one of the nitrogen atoms has a direction essentially *anti* to the P–O bond; the lone pairs of the two remaining nitrogen atoms are approximately orthogonal to the P=O bond and to each other.

One of the morpholino groups is disordered in the crystal and the resolution of the disorder could only be achieved by the low temperature data set.

It is concluded that tris(dialkylamino)phosphine oxides represent a border case with regard to conformational preference. An increase of the donor ability of the amino groups or the presence of coordinating Lewis acids may change the conformation from the asymmetric *gauche-gauche-anti* one to the fairly symmetric propeller one. The structure of tris(dimethylamino)phosphine oxide is discussed.

In previous studies in this series various tris(dialkylamino)phosphines, $(R_2N)_3P$, together with pentacovalent species and phosphonium salts derived from these phosphines have been studied by X-ray methods; *cf.* Refs. 1 and 2. Generally, these compounds are highly asymmetric with regard to the N–P–N bond angles, the P–N bond lengths and the hybridization of the nitrogen atoms. One of the nitrogen atoms is essentially sp^3 hybridized and its lone pair direction is *anti* to the phosphorus lone pair in the P^{III}-compounds, to the phosphorus–chalcogen bond in $(R_2N)_3PX$ (X = Se or Te) and to the phosphorus–carbon bond in the (Morpholine)$_3P^+$R-cation.[2] In $4\text{-}NO_2\text{–}PhP^+$-(Piperidine)$_3ClO_4$, however, the piperidino groups in the cation are twisted in a propeller-like arrangement with all nitrogen atoms being essentially sp^2 hybridized. Furthermore, Cameron and co-workers[3] have recently shown that in the weak adduct between tris(dimethylamino)phosphine oxide, $[(CH_3)_2N]_3PO$, HMPA, and $Ph_2As(S)$-Me, the three NMe_2 groups are all planar and the HMPA part of the adduct adopts a propeller conformation with three fairly equal O–P–N–C torsion agles. Apparently, for certain substituents, the energy difference between the two conformations in compounds derived from tris(dialkylamino)phosphines, the asymmetric *gauche-gauche-anti* conformation[1,2] and the fairly symmetric propeller one, is fairly small.

Since there have been indications that the polar phosphorus–oxygen linkage in $(R_2N)_3PO$ may alter the conformational preference in favour of the propeller, we have turned to structural studies of this class of compounds in their uncomplexed state. Further knowledge of the preferred conformation may also shed some light upon the unique solvent properties of HMPA, by far the most important compound within this group.[4,5] The exceptional cation solvating properties of this compound is well documented[6] and a large number of metal complexes with HMPA have been prepared.[7,8] Several metal complexes[9] and addition compounds[3,10,11] with HMPA have been studied by X-ray methods. No studies on any uncomplexed tris(dialkylamino)phosphine oxides have so far been

0302-4377/82/080665-07$02.50

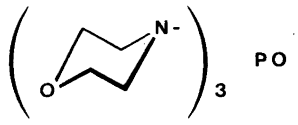

Scheme 1.

reported; HMPA itself is not easily attacked by X-ray methods, being a liquid at room temperature and a glassy substance at low temperature.

In the present study we report the crystal and molecular structure of tris(morpholino)phosphine oxide, Mor_3PO, a nicely crystalline and non-hygroscopic compound. By choosing morpholino groups as substituents a direct comparison could be made with previous results from studies of Mor_3P,[12] Mor_3PSe[1] and Mor_3PTe.[13] Similar to HMPA, Mor_3PO is a powerful ligand toward hard metal cations and a number of complexes have been prepared.[14-18] No structural reports on metal complexes with coordinated Mor_3PO molecules have so far been published.

EXPERIMENTAL

Material. Tris(morpholino)phosphine oxide was prepared as described by Malatesta and Tarantino[19] from $POCl_3$ and morpholine. The compound was repeatedly recrystallized from benzene and ethanol to remove traces of morpholinium hydrochloride, m.p. 187–188 °C (183–185 °C[19]). Crystals suitable for the X-ray study were grown from acetonitrile at room temperature.

X-Ray data. A crystal with dimensions $0.3 \times 0.3 \times 0.4$ mm was used for the X-ray experiments. Data for the measurements of cell dimensions and intensity data were collected on a SYNTEX $P\bar{1}$ diffractometer. Data sets were obtained both at room temperature and with −150 °C at the crystal site using graphite crystal monochromated Mo$K\alpha$ radiation ($\lambda = 0.71069$ Å). Cell parameters were determined by a least-squares fit to the diffractometer settings for 15 general reflections. Intensity data were collected with the $\theta - 2\theta$ scan technique, scan speed 2–4° min^{-1}, scan width 2.2° (2θ). Intensity data in a quadrant of reciprocal space within sin $\theta/\lambda = 0.75$ Å^{-1} were measured. The number of observed reflections [$I \geq 2.5\sigma(I)$] were 2786 for the room temperature data set and 4151 for the low temperature set. The intensities were corrected for Lorentz and polarization effects, but not for absorption.

The refinement procedure followed was as described in Ref. 2.

CRYSTAL DATA

Tris(morpholino)phosphine oxide, $C_{12}H_{24}N_3O_4P$, m.p. 187–188 °C. Monoclinic. $t = 18$ °C: $a = 9.172(1)$ Å; $b = 11.255(2)$ Å; $c = 14.785(2)$ Å; $\beta = 96.73(2)°$; $V = 1515.8$ Å^3. $t = -150$ °C: $a = 9.107(1)$ Å; $b = 11.145(1)$ Å; $c = 14.605(1)$ Å; $\beta = 97.03(1)°$; $V = 1471.3$ Å^3. $M = 305.31$; $Z = 4$;

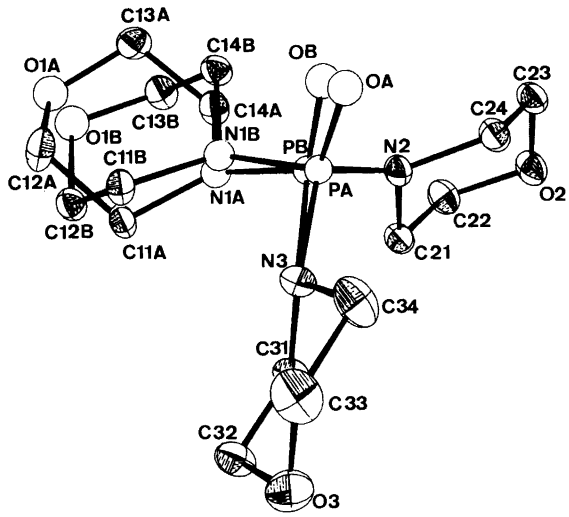

Fig. 1. ORTEP plot of Mor_3PO. Open circles are atoms refined with isotropic thermal parameters.

Table 1. Fractional atomic coordinates and thermal parameters with estimated standard deviations. The anisotropic temperature factor is given by $\exp -2\pi^2(U_{11}a^{*2}h^2+\ldots+2U_{12}a^*b^*hk+\ldots)$.

Atom	X	Y	Z	U_{11}	U_{22}	U_{33}	U_{12}	U_{13}
O2	.4910(1)	.3227(1)	1.0068(1)	.0358(6)	.0236(5)	.0243(5)	−.0008(4)	.0138(4)
O3	1.1930(1)	.1737(1)	.8160(1)	.0165(5)	.0437(7)	.0354(6)	.0025(5)	−.0008(4)
N2	.6281(1)	.1828(1)	.8792(1)	.0245(5)	.0208(5)	.0173(5)	−.0024(4)	.0075(4)
N3	.8865(1)	.1252(1)	.8042(1)	.0189(5)	.0185(5)	.0235(5)	−.0013(4)	.0047(4)
C21	.6323(2)	.3142(1)	.8758(1)	.0235(6)	.0210(6)	.0210(6)	−.0012(5)	.0067(5)
C22	.4977(2)	.3648(2)	.9149(1)	.0269(7)	.0261(7)	.0263(7)	.0037(5)	.0084(5)
C23	.4806(2)	.1944(1)	1.0064(1)	.0292(7)	.0241(7)	.0222(6)	−.0042(5)	.0116(5)
C24	.6162(2)	.1390(1)	.9725(1)	.0275(6)	.0205(6)	.0202(6)	−.0017(5)	.0071(5)
C31	.9401(2)	.2478(1)	.7926(1)	.0176(5)	.0185(6)	.0241(6)	−.0012(4)	.0036(4)
C32	1.0885(2)	.2403(2)	.7554(1)	.0189(6)	.0296(7)	.0297(7)	−.0019(5)	.0060(5)
C33	1.1410(2)	.0554(2)	.8265(1)	.0287(8)	.0368(9)	.0394(9)	.0139(7)	.0054(7)
C34	.9940(2)	.0558(2)	.8659(1)	.0348(8)	.0299(8)	.0320(8)	.0096(6)	.0096(6)
C11A	.7001(3)	.1779(4)	.6178(2)	.0204(13)	.0277(18)	.0153(12)	.0003(12)	.0059(9)
C12A	.6213(4)	.1052(3)	.5386(2)	.0251(13)	.0385(17)	.0180(11)	.0068(12)	.0004(10)
C13A	.4002(3)	.1075(3)	.6037(2)	.0195(11)	0.309(16)	.0251(13)	−.0019(10)	−.0020(10)
C14A	.4667(3)	.1844(4)	.6839(2)	.0147(11)	.0367(20)	.0201(13)	.0025(11)	.0026(9)
C11B	.6997(3)	.1133(4)	.6242(2)	.0184(12)	.0266(18)	.0156(12)	.0033(11)	.0026(8)
C12B	.6300(3)	.2047(3)	.5551(2)	.0200(12)	.0308(15)	.0183(11)	−.0013(10)	.0021(9)
C13B	.4070(3)	.1983(3)	.6218(2)	.0181(11)	.0326(16)	.0240(13)	.0031(11)	.0016(10)
C14B	.4729(3)	.1097(4)	.6940(2)	.0167(11)	.0278(17)	.0206(12)	−.0018(10)	.0019(9)

Atom	X	Y	Z	B	Atom	X	Y	Z
O1A	.4676(3)	.1350(3)	.5234(2)	2.1(0)	O1B	.4720(3)	.1897(3)	.5375(2)
OA	.7068(3)	−.0386(2)	.8439(2)	1.7(0)	OB	.6726(3)	−.0241(2)	.8209(2)
N1A	.6278(3)	.1640(2)	.7025(2)	1.5(0)	N1B	.6335(3)	.1271(3)	.7097(2)
PA	.71738(9)	.08810(7)	.81318(5)	1.2(0)	PB	.69906(9)	.10445(7)	.80046(5)
H211	.631	.341	.810	3.0	H212	.724	.344	.913
H221	.406	.339	.875	3.0	H222	.504	.454	.916
H231	.391	.169	.965	3.0	H232	.474	.166	1.071
H241	.605	.050	.971	3.0	H242	.706	.162	1.014
H311	.952	.290	.853	3.0	H312	.868	.293	.748
H321	1.127	.323	.749	3.0	H322	1.074	.200	.694
H331	1.215	.010	.869	3.0	H332	1.127	.015	.765
H341	1.008	.093	.928	3.0	H342	.958	−.028	.871
A111	.804	.149	.631	3.0	A112	.699	.264	.599
A121	.634	.018	.554	3.0	A122	.668	.124	.482
A131	.416	.021	.620	3.0	A132	.291	.124	.592
A141	.420	.163	.740	3.0	A142	.447	.271	.668
B111	.680	.031	.599	3.0	B112	.809	.128	.636
B121	.674	.194	.495	3.0	B122	.653	.286	.580
B131	.299	.182	.608	3.0	B132	.423	.281	.647
B141	.451	.026	.672	3.0	B142	.429	.124	.752

$F(000)=656$; $D_x(18\,^\circ C)=1.338\ gcm^{-3}$; $D_x(-150\,^\circ C)=1.378\ gcm^{-3}$; $\mu(MoK\alpha)=2.0\ cm^{-1}$. Space group $P2_1/n$ (No. 14).

STRUCTURE DETERMINATION

The structure was determined by direct methods using the program assembly MULTAN and refined by Fourier and least-squares methods. Positions were calculated for hydrogen atoms and these were included as fixed contributors in the least-squares calculations.

One of the morpholino rings turned out to be disordered in a way similar to that found in 4-nitrobenzyl tris(morpholino)phosphonium perchlorate.[2] The two disordered components

correspond to an inversion of the ring and the disorder affects also the P–O part of the molecule. The resolution of the disordered atoms was not possible by means of the room temperature data set; therefore the low temperature data set was collected. The disorder was treated in the way described in Ref. 2 with the splitting of the atoms of the one morpholino ring and also the phosphorus atom with the attached oxygen atom. The two remaining morpholino groups seem to be unaffected by the disorder.

The situation is illustrated in Fig. 1 where the atoms drawn as open cricles had to be treated isotropically whereas the atoms drawn as ellipsoids were given anisotropic thermal parameters. The refinements converged to a conventional R factor of 0.045, $R_w = 0.051$ and the standard deviation of an observation of unit weight, $S = |\Sigma w \Delta F^2/(m-n)|^{\frac{1}{2}}$, was 3.3.

Final atomic parameters are listed in Table 1. Tables of observed and calculated structure factors are available from the authors.

An ORTEP drawing of the molecule is shown in Fig. 1 where the numbering of the atoms is also indicated. In Table 2 are listed the most important structural parameters for the $(C_2N)_3PO$ part of the molecule; sites A and B refer to the two positions of the one disordered morpholino group. The values in the parentheses are the average for the two sites. Also in Table 2 the corresponding structural parameters for the selenide, Mor_3PSe,[1] are given. As mentioned above, it was not possible to resolve the disordered atoms by means of the room temperature data set. However, the refinement based upon this data set (2786 reflections) converged to R and R_w factors of 0.051 and 0.056, respectively, and an S value of 1.81. The calculated torsion angles O–P–N1-lone pair(N1), O–P–N2-lone pair (N2) and O–P–N3-lone pair(N3), 168, −78 and 79°, respectively, are in fair agreement with the torsion angles from the low temperature data set, *cf.* entry 3 in Table 2.

DISCUSSION

As mentioned above, one of the morpholino groups was found to be disordered. In order to obtain a satisfactory resolution, the atoms of this ring together with the phosphorus atom and the attached oxygen atom had to be split. The two "half" morpholino rings are actually inversion forms and are oriented in such a way that the direction of the nitrogen lone pair is approximately retained after the inversion. Thus, this splitting causes only a negligible error in the torsion angle about the P–N bond, *cf.* entry 3 in Table 2. However, since some of

Table 2. A comparison between some structural parameters in tris(monopholino)phosphine, Mor_3PO, and in the corresponding selenide, Mor_3PSe.[1]

	Mor_3PO							Mor_3PSe		
	Site A				Site B					
	N1[a]	N2[b]	N3		N1[a,b]	N2	N3	N1[b]	N2[a]	N3
Σ∠N(°)	351.6	352.1	349.1		358.6	355.2	350.8	354.9	340.1	349.7
Σ∠N(°)		350.9		(352.9)[c]		354.9			348.2	
Tors.angle (°)	167.6	−90.6	82.5		167.4	−74.6	76.2	−77.6	178.9	65.8
	(167.5)[c]	(−83.4)[c]	(79.8)[c]							
P–N (Å)	1.665(3)	1.701(1)	1.616(1)		1.683(3)	1.633(2)	1.717(1)	1.661(2)	1.684(2)	1.670(2)
P–N (Å)		1.66				1.66			1.672	
ΣP–N (Å)		4.982		(4.985)[c]		4.988			5.015	
∠XPN(°)	118.3(1)	114.1(1)	111.4(1)		120.6(1)	106.6(1)	107.9(1)	112.0(1)	115.1(1)	111.4(1)
Σ∠XPN(°)		341.1		(338.1)[c]		335.1			338.5	
∠NPN(°)[d]	114.4(1)	101.3(1)	98.9(1)		112.5(1)	105.0(1)	104.5(1)	101.2(1)	114.1(1)	102.4(1)
Σ∠NPN(°)		314.6		(319.8)[c]		325.0			317.7	
P–X (Å)		1.483(3)		(1.486)[c]		1.489(3)			2.106(1)	

[a] The nitrogen atom with its lone pair *anti* to the P–X bond (X = O,Se). [b] The nitrogen atom with the lowest *p*-character. [c] Values in parenthesis are average values for sites A and B. [d] The bond angle between bonds to nitrogen atoms other than the one heading the column.

the atoms in the two sites, A and B, *cf.* Fig. 1, are fairly close to each other (less than 0.5 Å), their positions could not be determined with satisfactory accuracy. As a result, the calculated P–N bond distances and the bond angles around the phosphorus atom are probably subjected to considerably larger errors than the estimated standard deviations listed in Table 2. The listed values for these parameters, the P–N and the P–O bond lengths and the NPN and the OPN angles are therefore not real and merit no further discussion. The average values for the two sites have been calculated and are the basis for the discussion. They are listed in parenthesis in Table 2.

Compared with Mor_3PSe, the average bond angles around the nitrogen atoms are significantly larger as shown by the sum of the nitrogen bond angles, $\Sigma\angle N$; the average being 348.2° in Mor_3PSe and 352.9° in Mor_3PO. This increment in the *s*-character of the nitrogen atoms is accompanied by a slight but significant decrease in the P–N bond lengths, the average sum being 4.985 Å in the oxide as compared to 5.015 Å in the selenide. The coordination at the phosphorus is in principle tetrahedral but significantly distorted with considerably larger OPN bond angles than NPN bond angles. The average values for the sum of the XPN and NPN bond angles are quite comparable in the oxide and in the selenide. Apparently, the size of the chalcogen atom, X, has negligible influence upon the geometry of the phosphorus atom in $(R_2N)_3PX$.

The morpholino substituents in Mor_3PO are all in the expected chair conformation and are linked to the phosphorus atom approximately equatorially. A survey of the bond lengths and bond angles in these substituents is given in Table 3. All structural parameters, even for the disordered morpholino ring, are as expected.

In the crystal there are no especially short intra- or intermolecular contacts and the crystal packing is apparently dominated by van der Waals' forces. Newman diagrams of the conformation about the P–N bonds are shown in Fig. 2. Regardless the difficulties encountered during the structure determination and hence the uncertainties in some of the structural parameters, there is no doubt that the lone pair of one of the nitrogen atoms, N1A and N1B, is essentially *anti* to the oxygen atom with respect to the phosphorus–nitrogen bond (torsion angle 167.5°). The two remaining morpholino groups are twisted in opposite directions with O–P–N-lone pair (N) torsion agles of approximately −80 and 80°, respectively. The arrangement of the amino substituents in Mor_3PO is thus quite analogous to what has previously been observed in Mor_3PSe,[1] *cf.* Table 2, in the parent aminophosphine, Mor_3P,[12] and its telluride.[13] Owing to the uncertainties in the present structure, no relationship between the *p*-character of the nitrogen atoms and the corresponding P–N bond length could be established, *cf.* the first four entries in Table 2.

It has previously been argued that the *anti*-conformation for one phosphorus–nitrogen bond, and thus a *gauche-gauche-anti* (*g-g-a*) conformation when three nitrogen atoms are linked to a phosphorus atom is only to be anticipated when the nitrogen atoms display a slight or distinct pyramidal configuration.[1,20] The argument is based upon the assumption that the antibonding *sp* hybrid orbital on the phosphorus atom *anti* to the most electronegative substituent may interact with the nitrogen lone pair provided the latter has some *p*-character.[21] Additionally, the *anti* conformation will satisfy the basic assumption of the VSEPR model.[22] By a sufficient drain of electron density from the

Table 3. A survey of some bond lengths and bond angles and various averaged data for the morpholino groups in Mor_3PO.

	N1(A)	N1(B)	N2	N3
∠CNC(°)	111.5(3)	111.1(2)	111.7(1)	110.8(1)
∠COC(°)	109.5(2)	110.3(2)	109.5(1)	110.2(1)
∠PNC1(°)	123.9(2)	127.2(2)	110.6(1)	117.7(1)
∠PNC4(°)	116.5(2)	120.1(2)	123.8(1)	122.3(1)
N–C (Å)	1.479	1.463	1.465	1.465
C–C (Å)	1.517	1.516	1.520	1.521
C–O (Å)	1.426	1.437	1.422	1.421

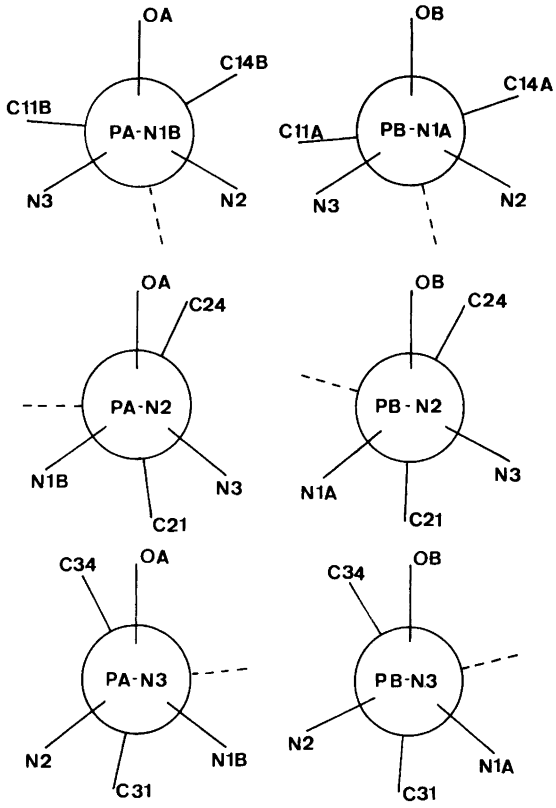

Fig. 2. Newman diagrams of the P−N bonds in Mor_3PO.

nitrogen atoms, either by the substituents as in tris(anilino)phosphine[23] and in tris(pyrazolo)-phosphine[24] or by the phosphorus atom as in the 4-nitrobenzyltris(piperidino)phosphonium cation,[2] the nitrogen atoms will attain an essentially planar coordination and the fairly symmetrical propeller conformation is favoured. An increase in the electronegativity of the chalcogen atom or, alternatively, an increase in the polarity of the P−X bond in $(R_2N)_3PX$ will similarly cause an electron transfer from the nitrogen atoms to the chalcogen atom, *cf.* the average sum of nitrogen bond angles in Mor_3PO and Mor_3PSe in Table 2, second entry. This transfer will be aided by increased donor ability of the dialkylamino group in $(R_2N)_3PX$ and in related compounds. In Mor_3PSe, Pip_3PSe and $(Me_2N)_3PSe$ the average sum of the nitrogen bond angles are 348.2, 353.0 and 352.9°, respectively.[1] The slightly but probably significantly longer P−Se bond length in the two latter compounds substantiates this conclusion. Actually, in phosphonium cations derived from $(R_2N)_3P$, this difference in donor ability of the amino groups may cause the shift from the *g-g-a* conformation in Mor_3P^+R to the propeller one in Pip_3P^+R.[2]

Tervalent compounds derived from simple secondary aliphatic compounds as $(R_2N)_3P$[12] and their selenated or tellurated[13] pentacovalent compounds exclusively prefer the *g-g-a* conformations regardless of the donor ability of the amino groups. However, in the corresponding oxides, $(R_2N)_3PO$, the propeller shaped conformation may be the preferred one with amino groups of better donor ability than the morpholino group. In addition compounds and in metal complexes in which the dipolar nature of the P−O bond is increased and hence the *p*-character of the nitrogen atoms is further decreased, the propeller shaped conformation may be the energetically favoured one.[3] In the majority of the metal complexes with tris(dimethylamino)phosphine oxide, HMPA, as ligand the propeller conformation of the HMPA

molecules is the preferred one. However, in some compounds like the monoclinic form of dioxodichlorobis(HMPA)Mo^{VI} [25] and in the adduct between HMPA and barbital [11] the *g-g-a* conformation of the HMPA molecules is observed. Apparently, weakly coordinated HMPA is a border case with regard to the conformational preference and the crystal lattice forces may be the determining factor for the conformation of HMPA.

REFERENCES

1. Rømming, C. and Songstad, J. *Acta Chem. Scand. A 33* (1979) 187.
2. Rømming, C. and Songstad, J. *Acta Chem. Scand. A 34* (1980) 631.
3. Brown, D. H., Cameron, A. F., Cross, R. J. and McLaren, M. *J. Chem. Soc. Dalton Trans.* (1981) 1459.
4. Normant, H. *Angew. Chem. 79* (1967) 1029.
5. Parker, A. J. *Chem. Rev. 69* (1969) 1.
6. Parker, A. J., Mayer, V., Schmid, R. and Gutmann, V. *J. Org. Chem. 43* (1978) 1843.
7. Schaefer, M. and Curran, C. *Inorg. Chem. 4* (1965) 623.
8. De Bolster, M. W. G. and Groeneveld, W. L. *Recl. Trav. Chim. Pays-Bas. 90* (1971) 477.
9. Sinha, S. P., Pakkanen, T. T., Pakkanen, T. A. and Niinistö, L. *Polyhedron 1* (1982). *In press.*
10. Steudel, R., Rose, F. and Pichardt, J. *Z. Anorg. Allg. Chem. 434* (1977) 99.
11. I-Nan Hsu and Craven, B. M. *Acta Crystallogr. B 30* (1974) 1299.
12. Rømming, C. and Songstad, J. *Acta Chem. Scand. A 32* (1978) 689.
13. Rømming, C., Iversen, A. J. and Songstad, J. *Acta Chem. Scand. A 34* (1980) 333.
14. Donoghue, J. T., Fernandez, E. and Peters, D. A. *Inorg. Chem. 8* (1969) 1191.
15. De Bolster, M. W. G., Kortram, I. E. and Groeneveld, W. L. *J. Inorg. Nucl. Chem. 35* (1973) 1843.
16. De Bolster, M. W. G. *Z. Anorg. Allg. Chem. 404* (1977) 78.
17. Dunstan, P. O. and Matos, F. A. P. *An. Acad. Bras. Cienc. 51* (1979) 211.
18. Schvetz, A. A., Amarskii, E. G. and Moiseeva, O. A. *Koord. Khim. 5* (1979) 1510.
19. Malatesta, P. and Tarantino, B. *Il Farmaco (Pavia) Ed. Sci. 10* (1955) 15.
20. Maartmann-Moe, K., Rømming, C. and Songstad, J. *Acta Chem. Scand. To be published.*
21. Burdon, J., Hotchkiss, J. C. and Jennings, W. B. *J. Chem. Soc. Perkin Trans. 2* (1976) 1052.
22. Gillespie, R. J. *J. Chem. Educ. 47* (1970) 18.
23. Tarassoli, A., Haltiwanger, R. C. and Norman, A. D. *Inorg. Nucl. Chem. Lett. 16* (1980) 27.
24. Cobbledick, R. E. and Einstein, F. W. B. *Acta Crystallogr. B 31* (1975) 2731.
25. Viossat, B., Khodadad, P. and Rodier, N. *Acta Crystallogr. B 33* (1977) 2523, 3793.

Received February 5, 1982.

Acta Chemica Scandinavica A 36 (1982) 673–681

The Crystal and Molecular Structures of 2,5-Diaza-1,6-dioxa-6a-thiapentalene and its 6a-Selena and 6a-Tellura Analogs

FRED A. AMUNDSEN, LARS K. HANSEN and ASBJØRN HORDVIK

Department of Chemistry, Institute of Mathematical and Physical Sciences, University of Tromsø, Box 953, N-9001 Tromsø, Norway

The crystal and molecular structures of 2,5-diaza-1,6-dioxa-6a-thiapentalene (I), 2,5-diaza-1,6-dioxa-6a-selenapentalene (II) and 2,5-diaza-1,6-dioxa-6a-tellurapentalene (III) have been determined by means of X-ray crystallographic methods.

Crystals of I are yellow, space group $P2_1/c$ with $Z=4$ in a unit cell of dimensions $a=6.939(5)$ Å, $b=7.000(5)$ Å, $c=11.013(5)$ Å and $\beta=110.83(7)°$.

Crystals of II are red, space group $P2_1/c$ with $Z=4$ in a unit cell of dimensions $a=6.987(1)$ Å, $b=7.000(2)$ Å, $c=11.379(2)$ Å and $\beta=110.93(2)°$.

Crystals of III are dark red, space group $P2_1/c$ with $Z=4$ in a unit cell of dimensions $a=9.605(4)$ Å, $b=5.006(2)$ Å, $c=12.202(3)$ Å and $\beta=112.94(3)°$.

The structures were solved by direct methods (I), isomorphism (II), and Patterson methods (III), and refined by full-matrix least-squares techniques.

Within experimental errors, the three molecules are planar and symmetric about the respective C(3a)–X(6a) bonds (X=S,Se,Te).

The average values for bond lengths are, O–S= 1.852(2) Å, C–S=1.683(4) Å, O–N=1.350(4) Å, C–N=1.309(6) Å, and C–C= 1.407(5) Å for compound I, O–Se=1.992(6) Å, C–Se=1.827(8) Å, O–N=1.33(1) Å, C–N=1.33(1) Å, and C–C =1.42(1) Å for compound II, and O–Te=2.087(13) Å, C–Te=1.980(15) Å, O–N=1.37(3) Å, C–N= 1.39(3) Å, and C–C=1.36(3) Å for compound III. The bond lengths in I and II have been corrected for libration.

Values of 1.19 Å for Se and 1.39 Å for Te are proposed for the covalent single bond radii of these elements in *cis* planar diselenide and ditelluride groups, respectively. The lengthening of the O–X (6a) bonds in compounds I–III relative to the corresponding sums of covalent radii then become 8.3 %, 7.6 % and 1.8 %, respectively, in agreement with results from ESCA studies and CNDO/2 calculations.

In crystals of I and II there are no intermolecular close contacts shorter than the corresponding van der Waals distances. The crystal structure of III is disordered (50–50) and a series of intermolecular close contacts is possible.

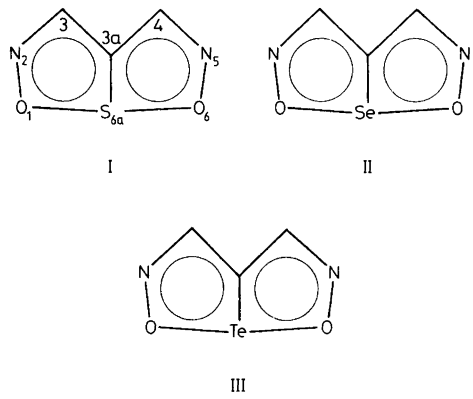

I II III

Compounds I, II and III are related to the 1,6,6a-trithiapentalenes, and the bonding in the O···X···O sequences may be described in terms of three-centre four-electron bonds.[1]

Possible differences between sulfur, selenium and tellurium with respect to such O···X···O bonding might be revealed through the molecular structures of I–III, and the present X-ray studies have therefore been carried out.

STRUCTURE DETERMINATION

Samples of compounds I, II and III were generously supplied by Vialle.[2]

Crystals of I from cyclohexane are yellow plates, which had to be kept in capillaries during the X-ray

0302-4377/82/080673-09$02.50

Table 1. Crystal data for compounds I, II and III.

	I $C_3H_2N_2O_2S$	II $C_3H_2N_2O_2Se$	III $C_3H_2N_2O_2Te$
F.W.	130.12	177.02	225.66
Colour	yellow	red	dark red
Space group	$P2_1/c$	$P2_1/c$	$P2_1/c$
a(Å)	6.939(5)	6.987(1)	9.605(4)
b(Å)	7.000(5)	7.000(2)	5.006(2)
c(Å)	11.013(5)	11.379(2)	12.202(3)
β(°)	110.83(7)	110.93(2)	112.94(3)
V(Å^3)	499.97	519.81	540.30
Z	4	4	4
D_m(g/cm^3)	1.71	2.26	2.74
D_x(g/cm^3)	1.729	2.262	2.774
μ(Mo$K\alpha$)(cm^{-1})	5.27	19.14	14.01

analyses in order to prevent sublimation. Recrystallization of II from a series of different solvents gave twinned crystals. One untwinned prismatic crystal was eventually found in a batch which had been recrystallized from ethanol by slow evaporation; the crystals of II are red. Crystals of III from benzene by slow evaporation are dark red needles elongated along *b*.

Crystal data for compounds I, II and III are given in Table 1. The crystal analyses are based on diffractometer data collected at 22 °C using Mo$K\alpha$ radiation. The intensity data for I and III have been collected on a paper-tape controlled Siemens AED diffractometer using niobium filtered radiation, and the intensity data for II were collected on a Nonius CAD4 computer-controlled diffractometer using graphite monochromatized radiation.

The intensities of the reflections for I and III were measured on the diffractometer by means of the five-value scan technique.[3] Reflections for which the net count was greater than two times the respective standard deviation in the net count were accepted as observed. With this criterion 630 independent reflections for I and 788 for II were accepted as observed in the θ-range $1-26°$; the corresponding numbers of observable reflections are 981 and 1064.

The intensity data for II were collected by the $\omega-2\theta$ scan technique. 2083 reflections were measured in the θ-range $1-33°$, and 1127 of these for which $I>2\sigma(I)$ were accepted as observed. The $0k\bar{l}$ as well as the $0kl$ reflections were measured and included in the data set.

The dimensions in axial directions of the crystals used for intensity measurements were $0.015\times0.52\times0.34$ mm for I, $0.5\times0.5\times0.5$ mm for II and $0.023\times0.42\times0.10$ mm for III. Lp and absorption corrections were applied.[4]

The structure of compound I was solved by direct methods using a program written by Long[5] and the structural parameters were refined by full matrix least squares procedures (see, for example, Ref. 6).

Crystals of I and II are isomorphous and parameters from the refinement of I were used as a start for the refinement of II. The calculations on the latter compound were carried out by means of the X-RAY 76 program system.[7]

Compound III which has a disordered crystal structure was solved by Patterson methods. A careful search for reflections by means of film as well as diffractometer showed that no other reflections are present than those of space group $P2_1/c$. The disorder is therefore 50 – 50.

The Patterson map of III unambiguously showed that there are two tellurium positions per asymmetric unit, and this implies that only 50 % of the molecular positions given by the Patterson map can be occupied.

Due to heavy overlap caused by the disorder, one had to carry out the refinement very carefully. The computer programs used were those mentioned in Ref. 6.

For hydrogen the scattering factor curve given by Stewart *et al.*[8] was used. The other atomic scattering factors were in the case of compounds I and III taken from *International Tables*,[9] and in the case of compound II computed from numerical Hartree-

Table 2. Atomic coordinates (fractional) and temperature parameters (in Å^2) for compounds I and II. The expressions used are $\exp[-8\pi^2 U(\sin^2\theta/\lambda^2)]$ for hydrogen, and $\exp[-2\pi^2(h^2a^{*2}U_{11}\ldots 2hka^*b^*U_{12}+\cdots)]$ for the other atoms. The U_{ij}s have been multiplied by 10^4.

Atom	x	y	z	U_{11}	U_{22}	U_{33}	U_{12}	U_{13}	U_{23}
S(6a)	0.7659(2)	0.0937(1)	0.0747(1)	665(7)	428(5)	438(5)	−61(6)	249(5)	21(5)
O(1)	0.7752(4)	−0.1298(4)	−0.0105(2)	882(21)	695(21)	560(16)	−32(17)	411(16)	−150(15)
O(6)	0.7424(4)	0.2950(3)	0.1752(3)	942(22)	317(15)	680(18)	−13(16)	295(16)	−13(16)
N(2)	0.7626(6)	−0.2858(5)	0.0566(4)	796(26)	500(23)	733(25)	7(21)	350(21)	−154(21)
N(5)	0.7198(6)	0.2421(5)	0.2856(3)	973(31)	499(21)	620(24)	22(21)	346(22)	−71(22)
C(3)	0.7481(6)	−0.2410(5)	0.1663(4)	632(29)	386(22)	593(27)	12(21)	270(22)	−14(21)
C(3a)	0.7456(6)	−0.0446(4)	0.1925(3)	428(22)	378(19)	385(19)	−2(18)	163(16)	−23(16)
C(4)	0.7238(6)	0.0558(5)	0.2949(4)	752(29)	458(25)	428(22)	27(22)	291(21)	22(19)
H(3)	0.731(6)	−0.318(5)	0.225(3)	U=0.078(13)					
H(4)	0.712(5)	0.011(4)	0.369(3)	U=0.056(12)					
Se(6a)	0.7715(1)	0.1140(1)	0.0743(1)	482(5)	476(5)	287(4)	−60(6)	140(3)	30(5)
O(1)	0.7793(10)	−0.1274(10)	−0.0135(6)	741(43)	735(46)	535(34)	−109(44)	339(32)	−199(39)
O(6)	0.7476(10)	0.3084(8)	0.1949(5)	688(45)	354(30)	455(37)	−33(31)	104(34)	17(26)
N(2)	0.7593(12)	−0.2810(13)	0.0467(8)	581(52)	608(53)	689(61)	43(44)	219(49)	−297(45)
N(5)	0.7237(12)	0.2301(10)	0.2955(6)	702(57)	646(46)	514(49)	7(44)	226(44)	−90(39)
C(3)	0.7445(14)	−0.2405(13)	0.1580(10)	420(53)	331(45)	730(65)	50(43)	163(49)	−9(49)
C(3a)	0.7453(13)	−0.0489(10)	0.1911(7)	329(46)	303(38)	380(44)	2(33)	129(38)	4(32)
C(4)	0.7283(15)	0.0455(12)	0.2978(8)	602(61)	468(48)	322(42)	18(45)	170(43)	−4(37)
H(3)	0.768(15)	−0.345(12)	0.220(9)	U=0.101(32)					
H(4)	0.749(13)	−0.035(12)	0.373(7)	U=0.085(27)					

Table 3. Atomic coordinates (fractional) and temperature parameters (in Å^2) for compound III. The expressions used are $\exp[-2\pi^2(h^2a^{*2}U_{11}+\cdots 2hka^*b^*U_{12}+\cdots)]$ for tellurium and $\exp[-8\pi^2 U(\sin^2\theta/\lambda^2)]$ for the other atoms.

Molecule 1					Molecule 2			
Atom	x	y	z	U	x	y	z	U
Te(6a)	−0.0829(1)	0.2141(3)	0.0470(1)		0.5930(2)	−0.0879(3)	0.1200(1)	
O(1)	0.0717(19)	0.0757(34)	0.2126(13)	0.074(4)	0.6657(15)	−0.3464(28)	0.0193(14)	0.053(4)
O(6)	−0.1823(19)	0.2269(34)	−0.1377(19)	0.076(5)	0.4487(23)	0.2028(42)	0.1382(14)	0.068(5)
N(2)	0.1571(27)	−0.1327(54)	0.1982(22)	0.070(8)	0.6011(24)	−0.3164(40)	−0.0985(20)	0.055(5)
N(5)	−0.1302(40)	0.0437(67)	−0.1970(29)	0.103(12)	0.3478(28)	0.3318(45)	0.0379(27)	0.079(6)
C(3)	0.1358(35)	−0.1991(59)	0.0799(29)	0.093(9)	0.4949(33)	−0.1206(55)	−0.1357(23)	0.075(8)
C(3a)	0.0340(20)	−0.0561(39)	−0.0007(19)	0.056(5)	0.4717(19)	0.0248(34)	−0.0447(13)	0.041(4)
C(4)	−0.0170(29)	−0.1031(51)	−0.1245(23)	0.077(6)	0.3717(30)	0.2183(58)	−0.0633(26)	0.079(7)
H(3)	0.217(18)	−0.330(32)	0.068(14)	0.07(5)	0.432(18)	−0.079(31)	−0.215(14)	0.07(5)
H(4)	0.044(19)	−0.238(32)	−0.150(15)	0.06(5)	0.301(19)	0.306(32)	−0.124(15)	0.05(5)

	U_{11}	U_{22}	U_{33}	U_{12}	U_{23}	U_{13}
$Te(6a)_1$	0.0502(7)	0.0608(10)	0.0657(9)	−0.0007(7)	−0.0005(7)	0.0166(6)
$Te(6a)_2$	0.0732(9)	0.0628(9)	0.0411(7)	0.0067(8)	−0.0026(7)	0.0204(6)

Fock wave functions.[10] The final R factors for compound I, II and III are 0.043, 0.061 and 0.049, respectively.

Final atomic coordinates and temperature parameters are listed in Tables 2 and 3. The structure factor lists are available on request.

Rigid body analyses have been carried out for compounds I and II according to the method of

Table 4. Bond lengths l (Å) in compounds I, II and III. The values l' have been corrected for rigid body libration. Standard deviations in parentheses.

	X=S	X=Se		X=Te	Mol. 1 X=Te	Mol. 2 X=Te	Average X=Te
	l	l'	l	l'	l	l	
X(6a)–O(1)	1.838(3)	1.853	1.973(7)	1.987	2.105(14)	2.083(17)	2.094
X(6a)–O(6)	1.835(3)	1.850	1.982(6)	1.997	2.079(21)	2.081(22)	2.080
X(6a)–C(3a)	1.665(4)	1.683	1.810(8)	1.827	1.986(22)	1.973(14)	1.980
O(1)–N(2)	1.339(5)	1.353	1.31(1)	1.32	1.38(3)	1.34(3)	1.36
O(6)–N(5)	1.333(5)	1.347	1.33(1)	1.34	1.38(4)	1.39(3)	1.39)
C(3)–N(2)	1.286(7)	1.299	1.34(1)	1.35	1.42(4)	1.36(3)	1.39
C(4)–N(5)	1.308(5)	1.319	1.29(1)	1.30	1.33(4)	1.46(5)	1.40
C(3)–C(3a)	1.406(5)	1.418	1.39(1)	1.40	1.30(3)	1.42(4)	1.36
C(4)	1.382(6)	1.395	1.42(1)	1.44	1.41(3)	1.32(3)	1.37

Table 5. Bond angles (°) in compounds I, II and III. Standard deviations in parentheses.

			X=S	X=Se	Mol. 1 X=Te	Mol. 2 X=Te	Average X=Te
i	j	k	$\angle ijk$	$\angle ijk$	$\angle ijk$	$\angle ijk$	$\angle ijk$
O(1)	X(6a)	O(6)	171.5(2)	164.3(3)	154.8(7)	152.6(6)	153.7
O(1)	X(6a)	C(3a)	86.0(2)	82.0(3)	77.8(8)	77.1(7)	77.5
O(6)	X(6a)	C(3a)	85.8(2)	82.4(3)	77.0(8)	75.8(7)	76.4
X(6a)	O(1)	N(2)	113.0(2)	114.2(6)	110(2)	116(2)	113
X(6a)	O(6)	N(5)	113.7(2)	112.3(5)	116(2)	120(2)	118
O(1)	N(2)	C(3)	111.2(3)	112.4(8)	117(2)	115(2)	116
O(6)	N(5)	C(4)	110.0(3)	114.8(8)	113(3)	106(2)	110
N(2)	C(3)	C(3a)	116.7(3)	117.8(9)	114(3)	116(2)	115
N(5)	C(4)	C(3a)	116.2(3)	117.1(8)	118(3)	119(2)	119
X(6a)	C(3a)	C(3)	113.5(3)	113.6(7)	120(2)	116(3)	118
X(6a)	C(3a)	C(4)	113.8(3)	113.3(5)	115(2)	119(2)	117
C(3)	C(3a)	C(4)	132.7(3)	133.1(8)	124(3)	125(2)	125

Schomaker and Trueblood.[11] All the calculations were carried out on the UNIVAC 1110 of the University of Bergen.

DISCUSSION

Bond lengths and angles in compounds I, II and III are given in Tables 4 and 5, respectively.

The molecules are planar and, within the experimental error, symmetric about the respective C(3a)–X(6a) bonds. Average O–X(6a) bond lengths and O–X(6a)–O bond angles together with the sums of covalent radii for oxygen and sulfur, 1.71 Å,[13,14] oxygen and selenium, 1.83 Å,[13] and oxygen and tellurium, 2.03 Å[13], are given in Fig. 1. The standard deviations σ_{av} in the average bond lengths and angles are calculated from the individual standard deviations σ_i according to the formula

$$\sigma_{av} = (1/n)\left(\sum_{i=1}^{n} \sigma_i^2\right)^{\frac{1}{2}}$$

One notes from Fig. 1 that the lengthenings of the O–X(6a) bonds relative to the corresponding sums of covalent radii are 8.3, 8.9 and 2.8 %, respectively, for the sulfur, selenium and tellurium compounds. These lengthenings are seen to be smaller than those of 12.5, 10.2 and 10.4 % found for the analogous compounds IV, V and VI, respectively, *cf.* Fig. 2.[15,17]

ESCA studies and CNDO/2 calculations on compounds I–VI[18,19] show that the ground state potential wells for the O–X(6a)–O three-centre

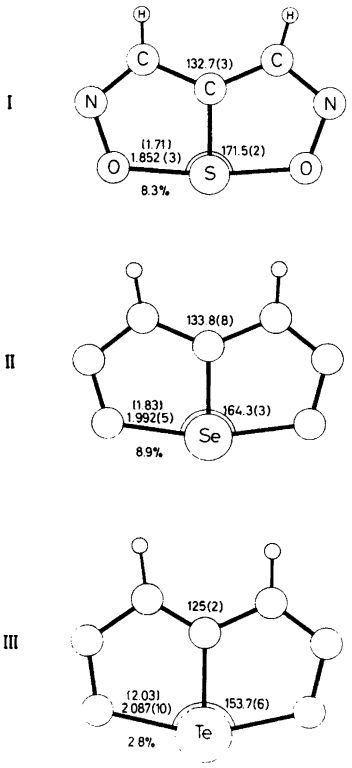

Fig. 1. ORTEP[12] drawings of the molecular structures of compounds I, II and III. The average O–X distances (Å), C–C–C and O–X–O angles (°) are given. The corresponding sums (Å) of covalent radii for O and X are shown in square brackets and the relative lengthening of the O–X bonds are given in percent.

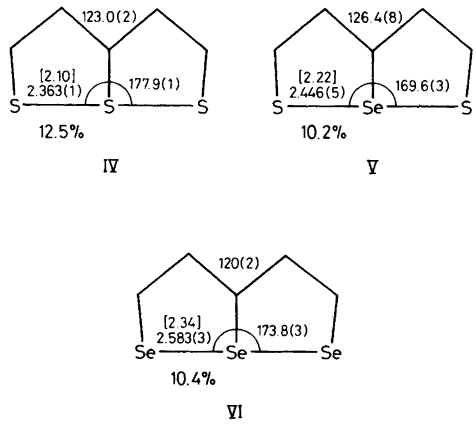

Fig. 2. The structures of 1,6,6a-trithiapentalene (IV) 1,6-dithia-6a-selenapentalene (V) and 1,6,6a-triselenapentalene (VI). The average S–S, S–Se, and Se–Se bond distances (Å) are given together with the corresponding sums of covalent radii (Å) in square brackets. Some bond angles (°), and the relative lengthenings (%) of S–S, S–Se and Se–Se bonds are also given.

bonds in compounds I–III are narrower than that of the S–S–S three-centre bond in compound IV. This implies that the O–X(6a)–O bonding in I–III is stronger than the S–S–S bonding in IV. The lengthening of the O–X(6a) bonds in compounds I–III should therefore, in agreement with the observations, be somewhat smaller than the lengthening of the S–S bonds in compound IV.

The ESCA studies and the CNDO/2 calculations show further that the widths of the ground state potential wells decrease from I–III and from IV–VI, and the bond lengthenings should therefore be expected to decrease in the same order. However, the calculated lengthenings do not decrease as expected, *cf.* Figs. 1 and 2, and a query might be put at the reference values used for the respective single bond lengths, as discussed below.

The length of the S–S single bond in a *cis* planar disulfide group, 2.10 Å,[14] is regarded as a relevant reference value when discussing sulfur–sulfur bonds in planar molecules, and a covalent radius of 1.05 Å for sulfur is accordingly used in the present paper. However, the covalent radii used above for selenium and tellurium do not refer to *cis* planar groups.

It has been shown, empirically and theoretically,[14,20] that the length of the S–S single bond in a disulfide group changes with the dihedral angle; 2.02 Å is a relevant length for the S–S single bond at 90° dihedral angle, and 2.10 Å is a relevant length at 0 and 180° dihedral angles. It is interesting to mention in this connection that the lengths of the S–S bonds in bis(2-pyrimidyl) disulfide at C–S–S–C dihedral angles of 82.5°,[21] 84.6°[22] and 180°,[22] are found to be 2.016(1), 2.019(1) and 2.113(1) Å, respectively.

Calculations on diselenide and ditelluride groups show similar variations of Se–Se and Te–Te bonds with dihedral angle,[20] and the range of the bond length variations are, according to the calculations, almost the same for the Se–Se and Te–Te bonds as for the S–S bond.

A more realistic value for the Se–Se single bond

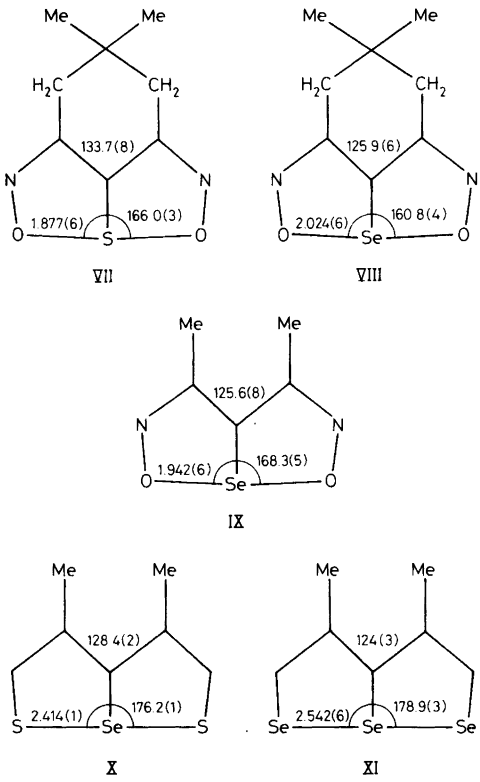

Fig. 3. The structures of derivatives of compounds I, II, V, and VI showing average O–S, O–Se, S–Se, and Se–Se bond lengths (Å) and some bond angles (°).

length in *cis* planar diselenide groups may be obtained if one compares the average Se–Se bond length in Se_8, 2.334(5) Å,[23] with the average bond length in S_8, 2.048(2) Å.[24] The latter is seen to be 0.05 Å shorter than the S–S single bond in *cis* planar groups, and, if this difference is added to the former, one arrives at a value of 2.38 Å for the Se–Se single bond length in *cis* planar diselenide groups. A covalent single bond radius of 1.19 Å may therefore be proposed for Se in such groups. Similarly 1.39 Å may be proposed as a more realistic value than 1.37 Å for the covalent radius of Te in *cis* planar ditelluride groups; the latter value is representative for dihedral angles about 90°.[20] It is realized that the same conclusions have been reached by Sæthre *et al.* from a different view point.[18]

If the values 1.19 and 1.39 Å are used for the covalent radii of Se and Te, respectively, the lengthenings of S–S, S–Se and Se–Se bonds in compounds IV–VI become 12.5, 9.3 and 8.5 %, and the lengthenings of O–S, O–Se and O–Te bonds in compounds I–III become 8.3, 7.6 and 1.8 %, respectively. This agrees with the mentioned ESCA studies and CNDO/2 calculations.

Structures of three derivatives of compounds I and II have been studied earlier, *cf.* Fig. 3.[25–27] One notes that the O–X(6a) bond lengths in these compounds are somewhat different from those in compounds I and II. This illustrates, in fact, to which extent substituents may influence the bonding in compounds I and II. Thus the substituents in VII and VIII have caused lengthenings of the respective O–X(6a) bonds, while the methyl groups in IX have shortened the O–Se(6a) bonds there relative to those in II. The latter effect is also seen if one compares the S–Se and Se–Se bond lengths in X[28] and XI[29] with those in V and VI, respectively, *cf.* Figs. 2 and 3.

Comparison with 1,6,6a-trithiapentalene. A survey of bond lengths in 1,6,6a-trithiapentalenes has been reported.[15] This survey shows that the terminal C(2)–C(3) and C(4)–C(5) bonds are, as a rule, shorter and has more π-character than the central C(3)–C(3a) and C(4)–C(3a) bonds. The same structural feature is found for compounds I and II. Thus the average value of the terminal C–N bonds in I is 1.309(6) Å and in II 1.33(1) Å, and the average values of the central C–C bonds in I and II are 1.407(6) and 1.42(1) Å, respectively, *cf.* Table 4. The C–C and C–N bond lengths in III are not considered accurate enough to be included in this discussion.

The mentioned survey shows further that the central C(3a)–S(6a) bonds in 1,6,6a-trithiapentalenes have a rather constant length of about 1.75 Å, and the terminal C(2)–S(1) and C(5)–S(6) bonds are usually found to be somewhat shorter, about 1.70 Å.

Accepted values for C–S single and double bond lengths are 1.82 and 1.61 Å, respectively.[33] Thus, as a rule, the terminal C–S bonds in 1,6,6a-trithiapentalenes possess more double bond character than the central ones.

The central C(3a)–S(6a) bond in I, 1.683(4) Å, is found to be significantly shorter than that in 1,6,6a-trithiapentalenes. The same applies to the C(3a)–Se(6a) bond in II, 1.827(8) Å, when compared with the average C(3a)–Se(6a) bond length of 1.91(1) Å found for 1,6,6a-triselenapentalenes and 1,6-dithia-6a-selenapentalenes.[16,17,28–32] Accepted

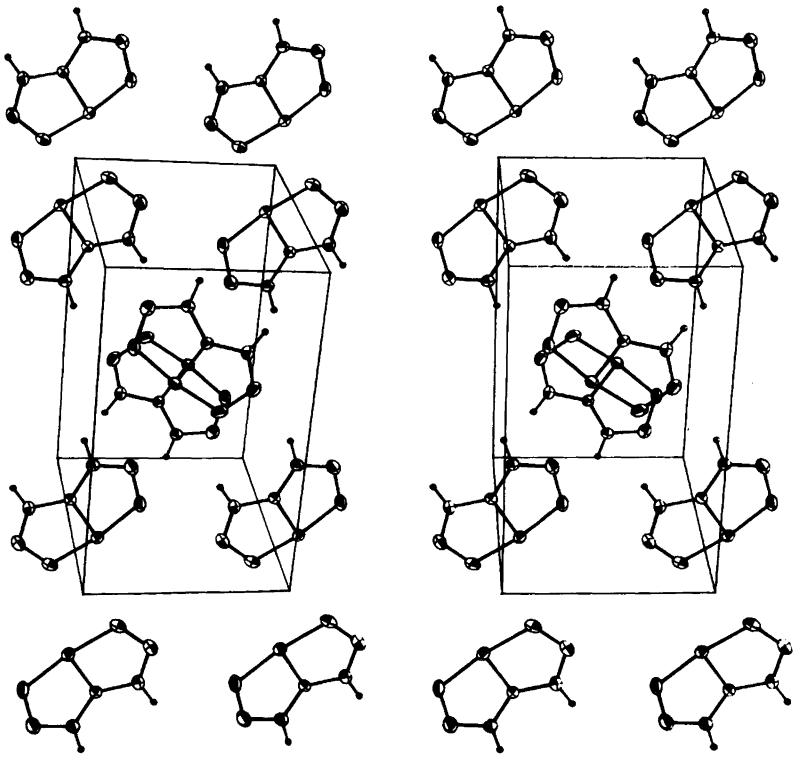

Fig. 4. A stereo view of the crystal structure of I.

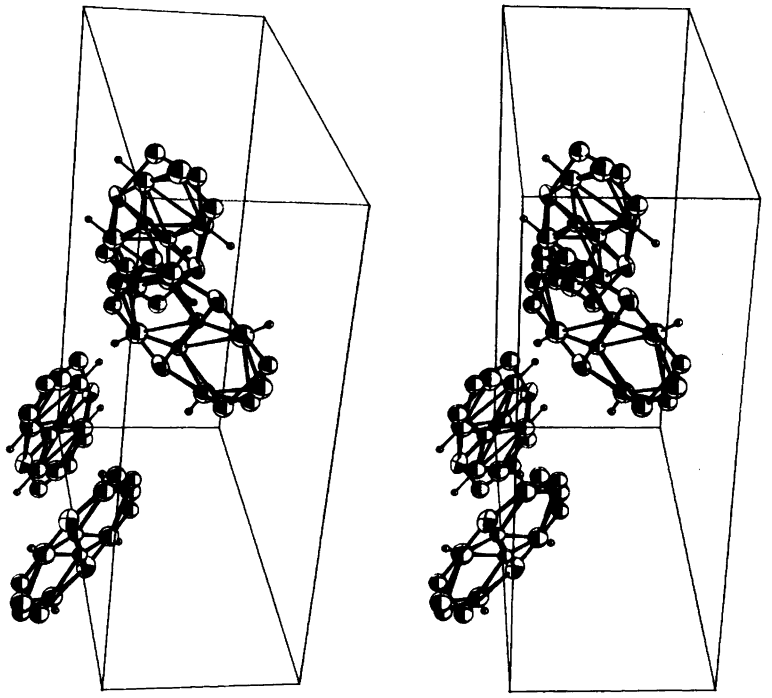

Fig. 5. A stereo view of the crystal structure of III showing the disorder.

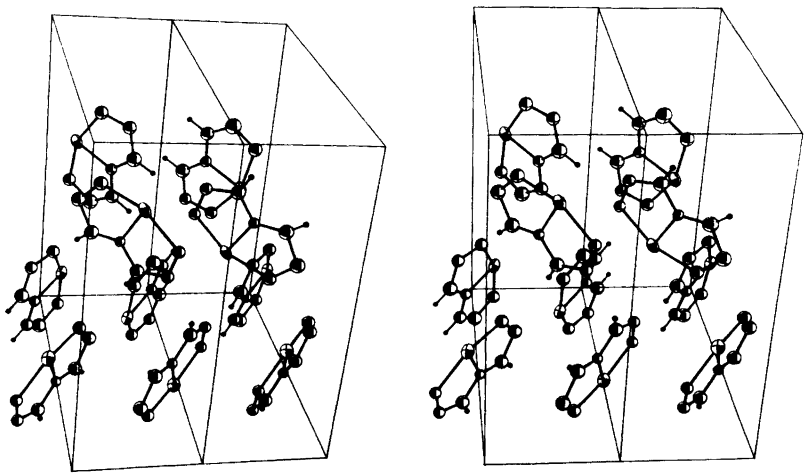

Fig. 6. A stereo view of the crystal structure of III showing an example of the real crystal packing.

values for C–Se single and double bond lengths are 1.94 and 1.74 Å, respectively.[13]

The average N–O bond length is 1.350(5) Å in I and 1.33(1) Å in II, *cf.* Table 4. Accepted lengths for N–O single and double bonds are 1.46 and 1.25 Å, respectively.[13] Thus one may conclude that the double bond characters of the N–O bonds in I and II are about the same as those of the C(3a)–X(6a) bonds in the respective molecules.

Crystal structures. A stereo view of the crystal structure of I is given in Fig. 4. The crystal structure of II is similar since crystals of the two compounds are isomorphous. There are no intermolecular contacts closer than corresponding van der Waals distance in crystals of I and II.

The crystal structure of compound III is disordered. Fig. 5 illustrates the disorder, and Fig. 6 gives one example of real crystal packing. There are a series of possible intermolecular close contacts in the crystal structure of III. These are, two possible Te···Te contacts of 3.67 and 3.86 Å, respectively, five possible Te···O contacts in the range 3.19–3.50 Å and seven possible Te···N contacts in the range 3.26–3.60 Å.

Acknowledgements. The authors are indebted to Dr. J. Vialle, Department de Chimie, Université de Caen, France, for samples of the title compounds. One of us (A. H.) wishes to thank the *Norwegian Research Council for Science and the Humanities for financial aid.*

REFERENCES

1. Hansen, L. K., Hordvik, A. and Sæthre, J. In Stirling, C. J. M., Ed., *Organic Sulphur Chemistry*, Butterworth, London 1975, p. 1.
2. Barillier, D., Rioult, P. and Vialle, J. *Bull. Soc. Chim. Fr.* (1976) 444.
3. Throughton, P. G. H. *Siemens Review XXXVII* (1970) *Fourth Special Issue: X-Ray and Electron Microscopy News.*
4. Coppens, P., Leiserowitz, L. and Rabinovich, D. *Acta Crystallogr. 18* (1965) 1035.
5. Long, R. E. *Ph. D. Dissertation*, University of California at Los Angeles, Los Angeles 1965.
6. Hordvik, A. and Sæthre, L. J. *Acta Chem. Scand. 26* (1972) 3114.
7. *The X-RAY SYSTEM, Version of 1976*, Computer Science Center, University of Maryland, College Park 1976.
8. Stewart, R. F., Davidson, E. R. and Simpson, W. T. J. *Chem. Phys. 42* (1965) 3175.
9. *International Tables for X-Ray Crystallography*, Kynoch Press, Birmingham 1968, Vol. 3, p. 202.
10. Cromer, D. T. and Mann, J. B. *Acta Crystallogr. A 24* (1968) 321.
11. Schomaker, V. and Trueblood, K. N. *Acta Crystallogr. B 24* (1968) 63.
12. Johnson, C. K. *ORTEP-II: A Fortran Thermal-Ellipsoid Plot Program For Crystal Structure Illustrations*, Report ORNL-3794, Oak Ridge National Laboratory, Oak Ridge 1971.
13. Pauling, L. *The Nature of the Chemical Bond*, 3rd Ed., Cornell University Press, New York 1960.
14. Hordvik, A. *Acta Chem. Scand. 20* (1966) 1885.

15. Hansen, L. K. and Hordvik, A. *Acta Chem. Scand. 27* (1973) 411.
16. Hordvik, A. and Julshamn, K. *Acta Chem. Scand. 25* (1971) 1895.
17. Hordvik, A. and Julshamn, K. *Acta Chem. Scand. 25* (1971) 2507.
18. Sæthre, L. J., Mårtensson, N., Svensson, S., Malmquist, P. A., Gelius, U. and Siegbahn, K. *J. Am. Chem. Soc. 102* (1980) 1783.
19. Sæthre, L. J., Malmquist, P. Å., Mårtensson, N., Svensson, S., Gelius, U. and Siegbahn, K. *Inorg. Chem. 20* (1981) 399.
20. Sæthre, L. *Acta Chem. Scand. A 29* (1975) 558; Sæthre, L. *Private communication.*
21. Furberg, S. and Solbakk, J. *Acta Chem. Scand. 27* (1973) 2536.
22. Simmons, C. J., Lundeen, M. and Seff, K. *Inorg. Chem. 18* (1979) 3444.
23. Foss, O. and Janickis, V. *J. Chem. Soc. Dalton Trans.* (1980) 624.
24. Cooper, A. S., Bond, W. L. and Abrahams, S. C. *Acta Crystallogr. 14* (1961) 1008.
25. Llaguno, E. C. and Paul, I. C. *J. Chem. Soc. Perkin Trans. 2* (1972) 2001.
26. Llaguno, E. C. and Paul, I. C. *Tetrahedron Lett.* (1973) 1565.
27. Stevens, E. *Private communication.*
28. Hordvik, A., Rimala, T. S. and Sæthre, L. J. *Acta Chem. Scand. 27* (1973) 360.
29. Jynge, K. *Cand. Real. Thesis,* University of Tromsø, Tromsø (Norway) 1976.
30. Hordvik, A. and Porten, J. A. *Acta Chem. Scand. 27* (1973) 485.
31. Hordvik, A., Rimala, T. S. and Sæthre, L. J. *Acta Chem. Scand. 26* (1972) 2139.
32. Rimala, T. S. *Cand. Real. Thesis,* University of Bergen, Bergen (Norway) 1973.
33. Abrahams, S. C. *Q. Rev. Chem. Soc. 10* (1956) 407.

Received January 7, 1982.

Acta Chemica Scandinavica A 36 (1982) 683–688

The Crystal and Molecular Structure of 2,5-Diphenyl-3,4-dimethylene-1,6,6a-trithiapentalene

BJØRN BIRKNES, ASBJØRN HORDVIK and LEIF J. SÆTHRE

Department of Chemistry, Institute of Mathematical and Physical Sciences, University of Tromsø, Box 953, N-9001 Tromsø, Norway

Crystals of the title compound are orthorhombic, space group *Pnma*, with four molecules in a unit cell of dimensions $a=7.165(1)$ Å, $b=29.704(4)$ Å, and $c=7.372(3)$ Å.

The structure was refined by full-matrix least-squares calculations on 1754 reflections (Mo$K\alpha$) measured within $\theta=27°$.

The molecule lies across the crystallographic mirror plane *m*, the central ring system is almost planar, and the phenyl groups are twisted 30° about their respective connecting bonds.

The S–S bond distances are 2.351(1) Å, and the S(1)–S(6a)–S(6) angle is 173.43(6)°. Other bond lengths in the 1,6,6a-trithiapentalene system are: S(1)–C(2)=1.725(4) Å, S(6a)–C(3a)=1.716(5) Å, C(2)–C(3)=1.374(5) Å, and C(3)–C(3a)=1.407(4) Å.

Bond lengths in the dimethylene bridge are C(3)–C(7)=1.529(5) Å and C(7)–C(8)=1.566(5) Å, and the lengths of the bonds connecting the phenyl groups to the central ring system are 1.489(5) Å. The bond lengths have been corrected for libration.

A relationship between the C(3)–C(3a)–C(4) bond angles (114.1, 122.3, and 126.0°) and the S(6a)–C(3a) bond lengths (1.716, 1.753, and 1.779 Å) in 2,5-diphenyl-3,4-dimethylene-, 2,5-diphenyl-, and 2,5-diphenyl-3,4-dimethyl-1,6,6a-trithiapentalene, respectively, is shown to be consistent with the results from CNDO/2 calculations.

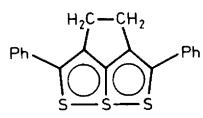

I

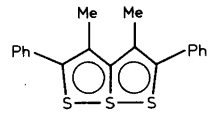

III

II

0302-4377/82/080683-06$02.50

The title compound (I) possesses intramolecular strain caused by the presence of the dimethylene bridge. A structure study of I has been carried out in order to find to which extent this intramolecular strain affects the bonding in the 1,6,6a-trithiapentalene system of I as compared to the bonding in the 1,6,6a-trithiapentalene system of compounds II and III;[1,2] compound II is regarded as a strainless molecule, and in compound III there is a repulsion between the methyl groups.

STRUCTURE ANALYSIS

Crystal data.[3,4]

$C_{19}H_{14}S_3$ F.W.=338.50

Space group *Pnma*

$a=7.165(1)$ Å, $b=29.704(4)$ Å, $c=7.372(3)$ Å

$V=1569.0$ Å^3

$D_x=1.433$ g/cm^3, D_m (flotation)$=1.427$ g/cm^3

$Z=4$

$\mu=4.5$ cm^{-1} (Mo$K\alpha$)

Crystal size, $0.2\times0.1\times0.4$ mm in axial directions.

The unit cell dimensions were determined from the 2θ values of 19 high order reflections measured at room temperature, $t=22$ °C. A least squares procedure gave the values quoted above.

The intensities of the reflections were measured by means of the five-value scan technique.[5] Reflections for which the net count was greater than two times the respective standard deviation in the net count, were accepted as observed. With this criterion 934 out of 1754 observable independent reflections within $\theta=27°$ were regarded as observed.

The scattering factors for sulfur and carbon were taken from the *International Tables*.[6] For hydrogen,

Table 1. Fractional atomic coordinates, and temperature parameters U_{ij}(Å^2) for sulfur and carbon, and U(Å^2) for hydrogen. The expressions used are $\exp[-2\pi^2(h^2a^{*2}U_{11}+\cdots 2hka^*b^*U_{12}+\cdots)]$ and $\exp[-8\pi^2U(\sin^2\theta/\lambda^2)]$, respectively. Standard deviations in parentheses.

Atom	x	y	z	U_{11}	U_{22}	U_{33}	U_{12}	U_{23}	U_{13}
S(1)	0.22633(14)	0.17014(3)	0.03756(15)	.0271(5)	.0452(6)	.0555(7)	.0067(5)	−.0012(6)	−.0051(6)
S(6a)	0.24468(18)	0.25000	0.03357(21)	.0198(7)	.0516(9)	.0450(9)	.0000	.0000	−.0027(8)
C(2)	−0.01204(47)	0.16928(13)	0.01112(49)	.0282(17)	.0467(23)	.0301(25)	.0020(19)	.0015(22)	−.0011(17)
C(3)	−0.09816(45)	0.21029(13)	−0.00687(47)	.0256(16)	.0361(18)	.0293(23)	.0016(18)	.0019(23)	−.0009(17)
C(3a)	0.00810(65)	0.25000	0.00243(74)	.0221(24)	.0358(30)	.0351(37)	.0000	.0000	−.0029(27)
C(7)	−0.30269(44)	0.22366(12)	−0.02591(61)	.0256(18)	.0399(23)	.0435(24)	−.0015(15)	−.0044(21)	−.0008(19)
C(9)	−0.10433(53)	0.12452(11)	0.01239(55)	.0365(21)	.0315(21)	.0323(24)	.0034(18)	−.0032(19)	−.0066(23)
C(10)	−0.26621(64)	0.11585(13)	−0.08533(54)	.0470(25)	.0398(26)	.0504(27)	.0029(25)	.0022(21)	−.0109(26)
C(11)	−0.34525(64)	0.07311(16)	−0.08911(69)	.0517(28)	.0525(30)	.0631(36)	−.0089(24)	.0002(25)	−.0101(25)
C(12)	−0.26354(68)	0.03863(13)	0.00500(59)	.0578(27)	.0376(23)	.0616(32)	−.0035(27)	−.0030(20)	.0077(31)
C(13)	−0.10571(70)	0.04651(15)	0.10617(66)	.0615(31)	.0398(28)	.0607(31)	.0100(25)	.0064(25)	.0008(29)
C(14)	−0.02605(60)	0.08908(14)	0.10858(59)	.0427(25)	.0413(26)	.0525(30)	.0050(22)	−.0006(24)	−.0060(24)

Atom	x	y	z	U	Atom	x	y	z	U
H(10)	−0.3206(49)	0.1394(11)	−0.1537(46)	.043(13)	H(14)	0.0822(51)	0.0954(11)	0.1776(44)	.049(12)
H(11)	−0.4527(60)	0.0686(13)	−0.1635(57)	.080(16)	H(71)	−0.3573(52)	0.2108(13)	−0.1334(46)	.055(13)
H(12)	−0.3193(40)	0.0044(13)	−0.0007(48)	.050(10)	H(72)	−0.3695(47)	0.2109(12)	0.0888(43)	.043(10)
H(13)	−0.0472(53)	0.0233(12)	0.1738(45)	.057(14)					

Table 2. Rigid body libration tensors for the entire molecule (**L**), the three central rings plus C(9) and C(15), ($\mathbf{L}_1$), and the 2-phenyl group plus C(2) ($\mathbf{L}_2$).

	Eigenvalues	Eigenvectors [a]		
	14.50 (°)^2	0	−10000	0
L	3.23	3767	0	−9263
	2.33	9264	0	3766
	15.54	0	−10000	0
$\mathbf{L}_1$	3.87	4434	0	−8963
	0.12	8963	0	4434
	53.56	−3523	−9353	−334
$\mathbf{L}_2$	9.17	−3598	1024	9274
	6.48	−8640	3387	3726

[a] Direction cosines $\times 10^4$ relative to *a*, *b* and *c*, respectively.

the scattering factor curve given by Stewart *et al.*[7] was used.

The refinement procedure is given in Ref. 8. Hydrogen positions were found from a difference map. Corrections for secondary extinction were carried out according to the method of Zachariasen,[9] and the final agreement factors are $R = 0.037$ and $R_w = 0.030$.

Final atomic coordinates and temperature parameters are listed in Table 1. The final structure factor list is available on request.

Rigid body analyses for the entire molecule as well as for certain parts of the molecule have been carried out according to the method of Schomaker and Trueblood.[10] The parts of the molecule treated in this way are the three central rings plus C(9) and

Table 3. Bond lengths *l*(*ij*), bond angles ∠(*ijk*), and deviations Δ_j from least squares plane. Bond lengths *l'*(*ij*) have been corrected according to the librational tensor **L**, and bond lengths *l''*(*ij*) have been corrected according to the librational tensors $\mathbf{L}_1$ and $\mathbf{L}_2$.

Atom *i*	*j*	*k*	Bond lengths (Å) *l''*(*ij*)	*l'*(*ij*)	*l*(*ij*)	Bond angles (°) ∠(*ijk*)	Plane deviations (Å) Δj
C(2)	S(1)	S(6a)	1.725	1.624	1.720(4)	94.8(1)	.015
S(1)	S(6a)	S(6)	2.351	2.351	2.349(1)	173.43(6)	−.031
C(3a)	S(6a)	S(1)	1.716	1.715	1.711(5)	86.92(4)	
S(1)	C(2)	C(3)				115.5(2)	.038
S(1)	C(2)	C(9)				117.9(2)	
C(3)	C(2)	C(9)	1.374	1.374	1.372(5)	126.5(3)	
C(3a)	C(3)	C(2)	1.407	1.408	1.406(4)	119.8(3)	−.015
C(7)	C(3)	C(2)	1.529	1.529	1.525(5)	132.2(3)	
C(3a)	C(3)	C(7)				107.8(3)	
C(3)	C(3a)	C(4)				114.1(3)	−.044
C(3)	C(3a)	C(6a)				122.9(2)	
C(8)	C(7)	C(3)	1.566	1.566	1.565(5)	105.1(3)	.031
C(2)	C(9)	C(10)	1.489	1.487	1.485(5)	122.3(3)	.131
C(14)	C(9)	C(2)	1.398	1.390	1.388(6)	120.2(3)	
C(14)	C(9)	C(10)				117.5(3)	
C(9)	C(10)	C(11)	1.400	1.393	1.390(6)	121.3(3)	−.437
C(10)	C(11)	C(12)	1.394	1.392	1.390(6)	120.0(4)	−.392
C(11)	C(12)	C(13)	1.379	1.371	1.369(6)	120.0(4)	.221
C(12)	C(13)	C(14)	1.386	1.378	1.375(7)	120.0(4)	.818
C(13)	C(14)	C(9)	1.391	1.389	1.387(6)	121.2(4)	.763

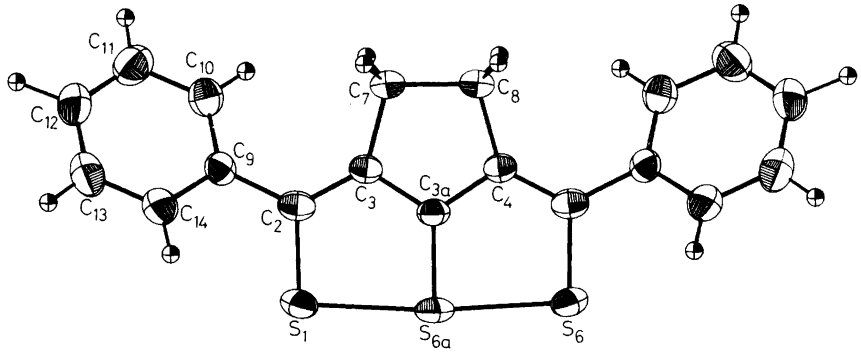

Fig. 1. ORTEP[11] drawing of the molecular structure of the title compound with numbering of atoms.

its symmetry equivalent and the 2-phenyl group plus C(2). The corresponding librational tensors are given in Table 2.

The calculations mentioned above were carried out on an IBM 360/50H computer. The programs, with some exeptions, originate from the Weizmann Institute of Science, Rehovoth, Israel, and have been modified for the 360 by D. Rabinovich, L. M. Milje, K. Maartmann-Moe and K. Åse.

DISCUSSION

Molecular shape and dimensions. The molecular structure of compound I as found in the present study is shown in Fig. 1. Bond lengths and angles are given in Table 3. The molecule lies across the crystallographic mirror plane *m*.

The bond lengths between nonhydrogen atoms have been corrected[12] for rigid-body libration according to the libration tensors given in Table 2. The corrections which give the *l'*-values are based on the libration tensor **L** and the corrections leading to the *l''* values are based on $\mathbf{L}_1$ and $\mathbf{L}_2$. The axis of maximum libration for $\mathbf{L}_2$ runs close to the direction C(2) – C(9) – C(12), and this shows that the phenyl groups librate about the respective connecting bonds. In accordance with this, one notes from Table 3 that the *l''* values for the C – C bonds of the phenyl ring are more realistic than the *l'* values.

Deviations from the least squares plane of the atoms of the 1,6,6a-trithiapentalene system are given in Table 3.

One notes that the two central rings are almost planar, and the phenyl groups point slightly out of this plane. The phenyl groups are twisted 30° about the respective connecting bonds.

A comparison with related molecules is given in Fig. 2. The 3,4-dimethylene bridge in I as well as the 3,4-dimethyl substituents in III introduces strain in the respective molecules, and this strain has caused changes in molecular dimensions. One notes for example for I, when compared with II, that the C(3) – C(3a) – C(4) and the S(1) – S(6a) – S(6) angles as

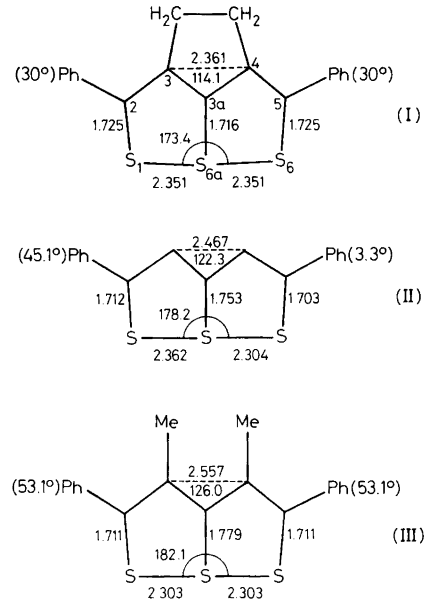

Fig. 2. A comparison of the structure of the present compound (I) with the structures of compounds II and III. Bond lengths are given in Å units and bond angles in degrees.

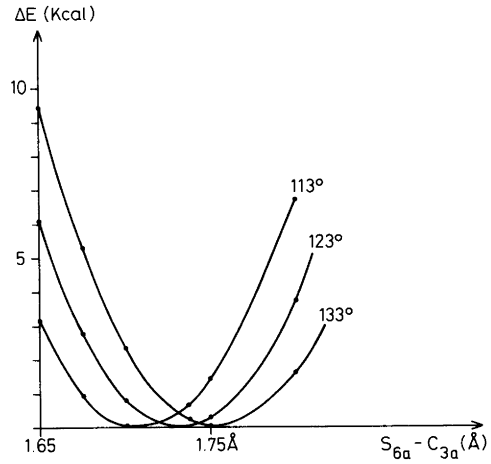

Fig. 3. The change in total energy, ΔE, relative to the minimum energy value, as a function of the S(6a) – C(3a) bond distance for three different molecular models. See the text for further explanation.

well as the C(3)···C(4) and S(6a)–C(3a) distances have decreased, while the sum of the S–S bond lengths have increased; for III the corresponding changes are seen to be the opposite.

It is tempting to point out that the mentioned changes in molecular dimensions are in accordance with what might be expected from "elastic" molecular models, *cf.* Fig. 2. Thus the external sulfur atoms have been pulled out in I and pushed in in III, and the C(3)–C(3a)–C(4) and S(1)–S(6a)–S(6) angles have changed their values accordingly.

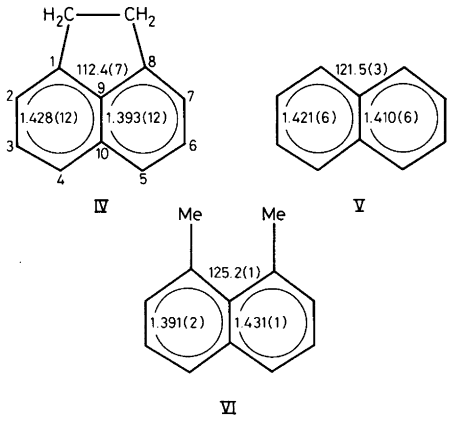

Fig. 4. Some bond distances (Å) and angles (°) from X-ray studies of three naphthalenes.

The most apparent changes have taken place around C(3a). One notes that the difference between the C(3)–C(3a)–C(4) bond angles in I and III and the difference between the S(6a)–C(3a) bond lengths in these compounds are 11.9° and 0.063 Å, respectively. Furthermore, the S(6a)–C(3a) bond in I, 1.716(5) Å, is shorter, and the S(6a)–C(3a) bond in III, 1.779(4) Å, is longer than that of 1.75 Å usually found in 1,6,6a-trithiapentalenes.[8]

There seems to be a relationship between the magnitude of the C(3)–C(3a)–C(4) bond angle and the length of the S(6a)–C(3a) bond, and this relationship is consistent with the results from CNDO/2 calculations as discussed below.

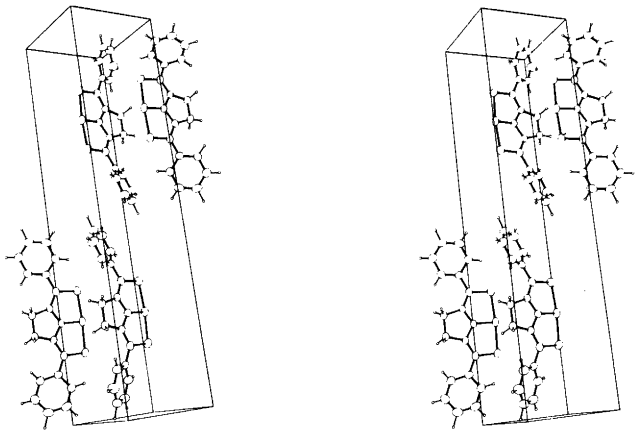

Fig. 5. A stereo view of the crystal structure.

The structure of the mother compound 1,6,6a-trithiapentalene as found by X-ray studies[8] was used as the basic model for the CNDO/2 calculations. Two other model structures were derived from this by changing the C(3)–C(3a)–C(4) angle symmetrically from 123° to 113 and 133°, respectively, keeping the other molecular dimensions, except those involving S–S bonds, constant.

The CNDO/2 total energy[13] has been calculated as a function of the S(6a)–C(3a) bond length for the three model structures. Sulfur *d*-orbitals were included in the calculations, which were carried out using the program CNINDO distributed by the QCPE organization.[14] The change in total energy relative to the minimum energy value as a function of the S(6a)–C(3a) bond distance is given in Fig. 3. One notes that the S(6a)–C(3a) bond distance corresponding to minimum total energy, increases from 1.70–1.75 Å when the C(3)–C(3a)–C(4) bond angle increases from 113–133°. This trend agrees with the experimental results.

The analogy with naphthalenes is illustrated in Fig. 4. Naphthalene and 1,6,6a-trithiapentalene are both aromatic 10π-electron systems. The values given in the figure are taken from the X-ray studies of IV,[15] V,[16] and VI,[17] respectively.

One notes that the 1,8-dimethylene bridge in IV has caused a decrease in the C(1)–C(9)–C(8) angle and the C(9)–C(10) bond distance, and the 1,8-dimethyl groups in VI have caused an increase in these molecular dimensions relative to those in V.

A stereo view of the crystal structure is given in Fig. 5. There are no intermolecular contacts shorter than corresponding van der Waals distances.

REFERENCES

1. Hordvik, A. *Acta Chem. Scand. 25* (1971) 2507.
2. Hordvik, A., Sjølset, O. and Sæthre, L. J. *Acta Chem. Scand. 27* (1973) 379.
3. Birknes, B., Hordvik, A. and Sæthre, L. J. *Acta Chem. Scand. 27* (1973) 382.
4. Stavaux, M. and Lozac'h, N. *Bull. Soc. Chim. Fr.* (1967) 2082.
5. Throughton, P. G. H. *Siemens Review XXX VII* (1970), *Fourth Special Issue: X-Ray and Electron Microscopy News.*
6. *International Tables for X-Ray Crystallography*, Kynoch Press, Birmingham 1968, Vol. III, p. 202.
7. Stewart, R. F., Davidson, E. R. and Simpson, W. T. *J. Chem. Phys. 42* (1965) 3175.
8. Hansen, L. K. and Hordvik, A. *Acta Chem. Scand. 27* (1973) 411.
9. Zachariasen, W. H. *Acta Crystallogr. 16* (1963) 1139.
10. Schomaker, V. and Trueblood, K. N. *Acta Crystallogr. B 24* (1968) 63.
11. Johnson, C. K. *ORTEP-II: A Fortran Thermal-Ellipsoid Plot Program For Crystal Structure Illustrations*, Report ORNL-3794, Oak Ridge National Laboratory, Oak Ridge 1971.
12. Cruickshank, D. W. J. *Acta Crystallogr. 9* (1956) 757; *14* (1961) 896.
13. Santry, D. P. and Segal, G. A. *J. Chem. Phys. 47* (1967) 158.
14. *Quantum Chemistry Program Exchange*, No. 141, Chemistry Department, Indiana University, Bloomington, Indiana 47401.
15. Ehrlich, H. W. W. *Acta Crystallogr. 10* (1957) 699.
16. Cruickshank, D. W. *Acta Crystallogr. 10* (1957) 504.
17. Bright, D., Maxwell, I. E. and deBoer, J. *J. Chem. Soc. Perkin Trans. 2* (1973) 2101.

Received February 8, 1982.

Acta Chemica Scandinavica A 36 (1982) 689–693

Vanadium(V). Part VII.* Kinetics of the Oxidation of Triethanolammonium Ion with Vanadium(V)

M. PUUTIO and P. O. I. VIRTANEN**

Department of Chemistry, University of Oulu, SF-90570 Oulu 57, Finland

The kinetics of the oxidation of triethanolammonium ions with vanadium(V) have been studied in sulfuric and perchloric acidic solutions. The reaction is of first order with respect to the triethanolammonium ion and vanadium(V) concentrations, but of second order with respect to the hydrogen ion concentration. The reaction is faster in sulfuric acid than in a corresponding perchloric acid solution. Both added sodium hydrogen sulfate and perchlorate accelerate the reaction, the effect of the former salt being greater. At a constant hydrogen ion concentration and at constant ionic strength the reaction is of first order with respect to the bisulfate ion concentration. The activation parameters have been determined. The substituent effect of the positively charged ammonium group is very small. A reaction mechanism involving $V(OH)_2^{3+}$ in perchloric acid as well as VO_2HSO_4 and $V(OH)_3HSO_4^+$ in sulfuric acid is suggested.

The kinetics of the oxidation of several aliphatic[2–8] and alicyclic[9,10] as well as benzyl alcohols[1,11] with vanadium(V) have been studied in detail but different oxidizing species and different mechanisms have been suggested for the reactions. Continuing our investigations, we have now studied kinetically the oxidation of triethanolammonium ion in order to obtain information on *e.g.* the positive charge on the rate constant.

EXPERIMENTAL

Ammonium metavanadate was a guaranteed reagent from E. Merck AG. Triethanolamine, diethanolamine and ethanolamine were commercial reagents distilled twice before use.

The method of analyzing the unreacted vanadium(V) was the same as that used earlier.[12]

RESULTS

The rate constants were determined under pseudo first order conditions with ethanolammonium ion in excess. Vanadium is reduced to V(IV) which is seen from the increase of the absorption at 765 nm.[13] All the rate constants reported in this work refer to the oxidation of the first alcohol group and the stoichiometric equation can therefore be expressed as:

$$(HOCH_2CH_2)_3NH^+ + 2V(V) \rightleftharpoons (HOCH_2CH_2)_2NH^+CH_2CHO + 2V(IV) + 2\,H^+ \quad (1)$$

A brief study reveals that the second alcohol group of triethanolamine oxidizes at a rate only slightly slower than that of the first alcohol group. This statistically less favoured side reaction thus cannot affect notably the numerical values of the rate constant observed and the correlation constant found was always close to 1. The oxidation of the aldehyde formed is much slower and does not interfere.[1,11,14]

Table 1 shows that the rate of the oxidation is of first order with respect to both the vanadium(V) and the triethanolammonium ion concentrations.

As seen from Table 2, the addition of sodium perchlorate accelerates the rate. The increase of the rate constant follows the equation $\log \{(k_{obs}/[TEAH^+])/M^{-1}\ s^{-1}\} = (-3.93 \pm 0.01) + (0.208 \pm 0.003) \times [NaClO_4]/M$, $r = 0.9997$.

At a constant ionic strength maintained by variation of the concentrations of sodium perchlorate and bisulfate, the rate is the faster, the more the solution contains the latter salt.

* Part VI, see Ref. 1.

** To whom correspondence should be addressed.

0302-4377/82/080689-05$02.50

Table 1. Variation of the rate constant with the concentration of vanadium(V) and triethanolammonium ion for the oxidation of triethanolammonium ion with vanadium(V) at 60 °C in water.

[V(V)]/M	[TEAH$^+$]/M	[H_2SO_4]/M	k_{obs}/s^{-1}	r	k_{obs}/[TEAH$^+$]/M^{-1} s^{-1}
0.0059	0.394	2.29	1.42×10^{-4}	0.9996	3.60×10^{-4}
0.0118	0.394	2.29	1.55×10^{-4}	0.9996	3.93×10^{-4}
0.0177	0.394	2.29	1.56×10^{-4}	0.9997	3.96×10^{-4}
0.0236	0.394	2.29	1.60×10^{-4}	0.9999	4.06×10^{-4}
0.0296	0.394	2.29	1.61×10^{-4}	0.9998	4.09×10^{-4}
0.0177	0.197[a]	1.74	6.34×10^{-5}	0.9994	3.22×10^{-4}
0.0177	0.394[a]	1.74	1.28×10^{-4}	0.9998	3.25×10^{-4}
0.0177	0.591[a]	1.74	1.99×10^{-4}	0.9991	3.37×10^{-4}
0.0177	0.788[a]	1.74	2.64×10^{-4}	0.9999	3.35×10^{-4}
0.0177	0.985	1.74	3.29×10^{-4}	0.9999	3.34×10^{-4}

[a] NaOH added, [TEAH$^+$] + [Na$^+$] = 0.985 M.

Table 2. Variation of the rate constant with the concentration of sodium perchlorate and bisulfate for the oxidation of triethanolammonium ion with vanadium(V) at 60 °C in water. [V(V)] = 0.0177 M, [TEAH$^+$] = 0.394 M, [$HClO_4$] = 3.09 M.

[$NaClO_4$]/M	[$NaHSO_4$]/M	k_{obs}/s^{-1}	r	k_{obs}/[TEAH$^+$]/m^{-1} s^{-1}
–	–	4.68×10^{-5}	0.9998	1.19×10^{-4}
0.99	–	7.49×10^{-5}	0.9999	1.90×10^{-4}
1.97	–	1.17×10^{-4}	0.9999	2.97×10^{-4}
2.96	–	1.88×10^{-4}	0.9999	4.77×10^{-4}
3.94	–	3.12×10^{-4}	0.9994	7.92×10^{-4}
–	3.94	8.36×10^{-4}	0.9994	2.12×10^{-3}
0.99	2.96	7.16×10^{-4}	0.9999	1.82×10^{-3}
1.97	1.97	6.10×10^{-4}	0.9990	1.55×10^{-3}
2.96	0.97	5.16×10^{-4}	0.9999	1.31×10^{-3}
3.94	–	3.12×10^{-4}	0.9994	7.92×10^{-3}

Table 3. Variation of the rate constant with the concentration of sulfuric and perchloric acid at constant ionic strength for the oxidation of triethanolammonium ion with vanadium(V) at 60 °C. [V(V)] = 0.0177 M, [TEAH$^+$] = 0.394 M.

Acid	H_0[a]	k_{obs}/s^{-1}	r	k_{obs}/[TEAH$^+$]/M^{-1} s^{-1}
0.83 M H_2SO_4[b]	−0.13	3.20×10^{-4}	0.9998	0.81×10^{-3}
1.70 M H_2O_4[b]	−0.68	4.41×10^{-4}	0.9999	1.12×10^{-3}
2.46 M H_2SO_4[b]	−1.09	5.52×10^{-4}	0.9997	1.40×10^{-3}
3.33 M H_2SO_4[b]	−1.54	7.29×10^{-4}	0.9999	1.85×10^{-3}
4.08 M H_2SO_4[b]	−1.89	8.74×10^{-4}	0.9999	2.22×10^{-3}
4.97 M H_2SO_4	−2.27	1.13×10^{-3}	0.9999	2.87×10^{-3}
1.83 M $HClO_4$[c]	−1.78	6.01×10^{-5}	0.9998	1.53×10^{-4}
2.87 M $HClO_4$[c]	−2.10	1.04×10^{-4}	0.9995	2.64×10^{-4}
3.84 M $HClO_4$[c]	−2.40	1.68×10^{-4}	0.9999	4.26×10^{-4}
4.82 M $HClO_4$	−2.72	2.44×10^{-4}	0.9999	6.19×10^{-4}

[a] Ref. 17. [b] $NaHSO_4$ added, I = 4.97 M. [c] $NaClO_4$ added, I = 4.82 M.

Table 4. Solvent effect of acetic acid for the oxidation of triethanolammonium ion with vanadium(V) at 60 °C. [V(V)] = 0.0177 M, [TEAH$^+$] = 0.394 M, [H_2SO_4] = 2.29 M.

AcOH/%(v/v)	k_{obs}/s^{-1}	r	$k_{obs}/[TEAH^+]/M^{-1}s^{-1}$
0	1.56×10^{-4}	0.9997	3.96×10^{-4}
10	2.20×10^{-4}	0.9999	5.58×10^{-4}
20	3.24×10^{-4}	0.9999	8.22×10^{-4}
30	5.01×10^{-4}	0.9999	1.27×10^{-3}
40	8.15×10^{-4}	0.9999	2.07×10^{-3}
50	1.33×10^{-3}	0.9999	3.38×10^{-3}

Table 5. Effect of temperature on the rate constant for the oxidation of triethanolammonium and diethanolammonium ions in water. [V(V)] = 0.018 M, [amineH$^+$] = 0.40 M, [H_2SO_4] = 2.32 M at 25 °C.

Amine	t/°C	k_{obs}/s^{-1}	r	$k_{obs}/[amineH^+]/M^{-1}s^{-1}$
TEA	40	2.36×10^{-5}	0.9999	5.94×10^{-5}
TEA	50	6.31×10^{-5}	0.9998	1.59×10^{-4}
TEA	60	1.56×10^{-4}	0.9997	3.96×10^{-4}
TEA	70	3.91×10^{-4}	0.9999	9.98×10^{-4}
DEA	40	8.86×10^{-6}	0.9998	2.23×10^{-5}
DEA	50	2.26×10^{-5}	0.9995	5.71×10^{-5}
DEA	60	5.37×10^{-5}	0.9997	1.36×10^{-4}
DEA	70	1.16×10^{-4}	0.9998	2.96×10^{-4}

The effect of the acid concentration was studied by diluting 4.97 M sulfuric acid and 4.82 M perchloric acid with sodium hydroxide. The results in Table 3 indicate that for the same concentration of the acid, the rate is faster in sulfuric than in perchloric acid. The rate constant increases with an increasing acetic acid concentration (Table 4).

The effect of temperature on the rate of the oxidation of triethanolammonium and diethanolammonium ions is seen in Table 5. The values of 81.1 ± 0.9 kJ mol^{-1} and 74.4 ± 0.8 kJ mol^{-1} for the enthalpy of activation and the values of -67.4 ± 2.8 J mol^{-1} K^{-1} and -96.6 ± 2.5 J mol^{-1} K^{-1} for the entropy of activation at 50 °C have been evaluated from $k_{obs}/[amineH^+]$ for the oxidation of triethanolammonium and diethanolammonium ions, respectively.

The triethanolammonium ion reacts about three times faster than the diethanolammonium ion. This is about the same as the value obtained for the oxidations with Cr(VI), where $k_{obs}(TEAH^+)\approx 2k_{obs}(DEAH^+)\approx 4k_{obs}(EAH^+)$.[15] The values for ethanolammonium ion are now not reported in the table, because we did not find good first order kinetics for this ion.

DISCUSSION

The addition of triethanolamine to acidic solutions of vanadium(V) deepens the colour of the solutions. This can be taken to indicate a formation of a vanadium(V) – substrate complex, it was as earlier often suggested for the similar oxidations of different alcohols.[2,6,8-10]

The rate constant of the oxidation of ethanol with vanadium(V) in 4 M sulfuric acid at 50 °C is 8.67×10^{-5} M^{-1} s^{-1}.[2] The rate constant of triethanolammonium ion in similar conditions can be approximated to be 2.6×10^{-4} M^{-1} s^{-1} (Tables 5 and 3), which is the statistical value, three times the rate constant of ethanol. Thus the substituent effect of the positively charged ammonium group is very small, which fact clearly excludes the possibility of hydride ion transfer[11,16] or electron transfer from oxygen atom[3] as the rate-determining stage. As the rate increases with the increasing ionic strength (Table 2), ionic species are involved in the rate-determining step. The results are best accordant with a mechanism where a radical is formed in the rate-determining decomposition of a charged complex and either more charges are formed or the

spreading of the charges decreases at the same time.

The decomposing complex may be cyclic or acyclic. A comparison of the values of the rate constants and activation entropies for triethanolammonium and diethanolammonium ions (Table 5) suggests the former alternative, but the available information is far from sufficient.

As seen from Table 3, the reaction is acid-catalyzed. For a correlation of the rates of the oxidations of organic compounds with quinquevalent vanadium, the Hammett acidity function H_o is generally used, although the protonating species here is *e.g.* VO^{2+} cation and organic indicators were used when determining the H_o-scale. For the sake of comparison, we calculated for sulfuric acidic solutions $\log \{(k_{obs}/[TEAH^+])/M^{-1}\ s^{-1}\} = (-3.31 \pm 0.01) + (-0.25 \pm 0.01) \times H_o$, $r = 0.9996$, and for perchloric acidic solutions $\log \{(k_{obs}/[TEAH^+])/M^{-1}\ s^{-1}\} = (-4.96 \pm 0.09) + (-0.65 \pm 0.04) \times H_o$, $r = 0.9964$.[17] Since the H_o-scale is probably not correct for VO_2^+ solutions, no conclusions can be drawn from the numerical values of the slopes. However, the difference of the dependence of $\log \{(k_{obs}/[TEAH^+])/M^{-1}\}$ on H_o of the two system is so marked that factors other than acidity alone have to be considered.

The pK_a's of different alcohols are around -3.[18] Therefore the alcohols studied in strongly acidic solutions are partly protonated. This phenomenon has been discussed in one case to decrease the reactivity,[4] but it seems, on the basis of our results, that the possible protonation does not affect markedly the oxidation and that other effects are dominant. The protonation of alcohols follows fairly well the H_o-scale, but, contrary to it, the Zucker-Hammett plots, $\log k$ *vs.* $-H_o$, found for the oxidation have slopes of less than unity.[1,6,8,10]

The reaction is not of first order with respect to the hydrogen ion concentration. The dependence of the rate constant on the square of the acid concentration is seen in Fig. 1. The linear dependence in perchloric acidic solutions is very good. In sulfuric acidic solutions the dependence is linear in 2.5 – 5.0 M solutions but tends to curve down with a decreasing acid concentration. Both the reactivity and the slope are clearly higher in sulfuric acidic than in perchloric acidic solutions.

There is a linear correlation between the rate and bisulfate concentration at a constant hydrogen ion concentration and at constant ionic strength, $(k_{obs}/[TEAH^+])/M^{-1}\ s^{-1} = (1.02 \pm 0.03) \times 10^{-3} + (2.74 \pm 0.10) \times 10^{-4}[HSO_4^-]/M$, $r = 0.9987$ (Table 2).

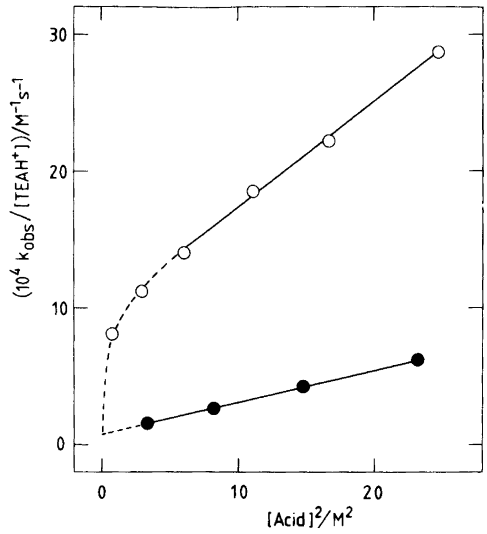

Fig. 1. Dependence of the rate constant $k_{obs}/[TEAH^+]$ on the square of the concentration of perchloric acid (black circles) and sulfuric acid (open circles) at constant ionic strength at 60 °C.

It is well known that vanadium(V) exists in slightly acidic solutions as VO_2^+, $pK_a = 3.70$ at 25 °C.[19] At higher acid concentrations $V(OH)_3^{2+}$ species, and in sulfuric acid also $V(OH)_3HSO_4^+$ are assumed to exist.[9] In yet more acidic concentrations $V(OH)_2^{3+}$ and $V(OH)_2(HSO_4)_2^+$ species have been postulated to exist.[8]

Taking into consideration all the above-mentioned aspects, the following mechanism is assumed to explain well the data on perchloric acidic solutions, where the order of the reaction with respect to the hydrogen ion concentration is two:

$$VO_2^+ + H_3O^+ \rightleftharpoons V(OH)_3^{2+} \quad \text{(fast)} \quad (2)$$

$$V(OH_3^{2+} + H_3O^+ \rightleftharpoons V(OH)_2^{3+} + 2H_2O \quad \text{(fast)} \quad (3)$$

$$VO_2^+ + TEAH^+ \rightleftharpoons \{Complex\}_1^{2+} \quad \text{(fast)} \quad (4)$$

$$V(OH)_2^{3+} + TEAH^+ \rightleftharpoons \{Complex\}_2^{4+} \quad \text{(fast)} \quad (5)$$

$$\{Complex\}_1^{2+} + H_2O \rightarrow (HOCH_2CH_2)_2NH^+CH_2CHOH + H_3O^+ + VO_2 \quad \text{(slow)} \quad (6)$$

$$\{Complex\}_2^{4+} + H_2O \rightarrow (HOCH_2CH_2)_2NH^+CH_2CHOH + H_3O^+ + V(OH)_2^{2+} \quad \text{(slow)} \quad (7)$$

$$(HOCH_2CH_2)_2NH^+CH_2\dot{C}HOH + H_2O + VO_2^+ \rightarrow (HOCH_2CH_2)_2NH^+CH_2CHO + H_3O^+ + VO_2 \quad \text{(fast)} \quad (8)$$

This mechanism leads to the rate law:

$$\text{Rate} = (k_6K_4 + k_7K_5K_3K_2[H_3O^+]^2)[VO_2^+][TEAH^+] \quad (9)$$

The lower line in Fig. 1 follows the equation $(k_{obs}/[TEAH^+])/M^{-1}\,s^{-1} = (7.34 \pm 0.44) \times 10^{-5} + (2.36 \pm 0.03) \times 10^{-5} \times [HClO_4]^2/M^2$, $r = 0.9998$.

In sulfuric acidic solutions the rate law is complicated, as the species VO_2HSO_4, $V(OH)_3HSO_4^+$ and $V(OH)_2(HSO_4)_2^+$ may contribute to the reaction. When considering the concentrations of hydrogen and bisulfate ions, we have assumed that sulfuric acid behaves like a strong monobasic acid. It follows that our results are in favour of a major contribution of $V(OH)_3HSO_4^+$, because the reaction was found to be of first order with respect to the bisulfate ion concentration and because the rate increases linearly in Fig. 1 in the concentration range 2.46–4.97 M. If VO_2HSO_4 or $V(OH)_2(HSO_4)_2^+$ were dominant, the line would curve downwards or upwards, respectively, with an increasing sulfuric acid concentration. This effect would be quite considerable, because the rate is so much higher in sulfuric acidic than in perchloric acidic solutions. If we write eqns. (10)–(12) for

$$V(OH)_3^{2+} + HSO_4^- \rightleftharpoons V(OH)_3HSO_4^+ \quad \text{(fast)} \quad (10)$$

$$V(OH)_3HSO_4^+ + TEAH^+ \rightleftharpoons \{Complex\}_3^{2+} \quad \text{(fast)} \quad (11)$$

$$\{Complex\}_3^{2+} + H_2O \rightarrow (HOCH_2CH_2)_2NH^+CH_2\dot{C}HOH + 2\,H_3O^+ + VO_2 + HSO_4^- \quad \text{(slow)} \quad (12)$$

$$VO_2^+ + HSO_4^- \rightleftharpoons VO_2HSO_4 \quad \text{(fast)} \quad (13)$$

$$VO_2HSO_4 + TEAH^+ \rightleftharpoons \{Complex\}_4^+ \quad \text{(fast)} \quad (14)$$

$$\{Complex\}_4^+ + H_2O \rightarrow (HOCH_2CH_2)_2NH^+CH_2\dot{C}HOH + H_3O^+ + VO_2 + HSO_4^- \quad \text{(slow)} \quad (15)$$

the main reaction, and eqns. (13)–(15) for the probable minor reaction, the rate law is given by eqn. (16).

$$\text{Rate} = (k_6K_4 + k_{15}K_{14}K_{13}[HSO_4^-] + k_{12}K_{11}K_{10}K_2[H_3O^+][HSO_4^-] + k_7K_5K_3K_2[H_3O^+]^2)[VO_2^+][TEAH^+] \quad (16)$$

The solid line in Fig. 1 follows the equation $(k_{obs}/[TEAH^+])/M^{-1}\,s^{-1} = (9.49 \pm 0.41) \times 10^{-4} + (7.77 \pm 0.25) \times 10^{-5} \times [H_2SO_4]^2/M^2$, $r = 0.9989$. Thus $k_{12}K_{11}K_{10}K_2 \approx (5.4 \pm 0.3) \times 10^{-5}\,M^{-3}\,s^{-1}$. Accordingly, the oxidazing ability of $V(OH)_3HSO_4^+$ is about twice of that of $V(OH)_2^{3+}$.

Acknowledgement. The financial support of this work by the Science Research Council of Finland is gratefully acknowledged.

REFERENCES

1. Puutio, M. and Virtanen, P. O. I. *Finn. Chem. Lett.* (1982) 81.
2. Rao, P. V. S., Murty, R. V. S. and Murty, K. S. *Z. Phys. Chem. Leipzig 258* (1977) 7.
3. Saccubai, S. and Santappa, M. *Ind. J. Chem. 8* (1970) 533.
4. Wells, C. F. and Nazer, A. F. M. *J. Chem. Soc. Faraday Trans. 1, 72* (1976) 910.
5. Jones, J. R. and Waters, W. A. *J. Chem. Soc.* (1962) 2068.
6. Mehrotra, R. N. *J. Chem. Soc. B* (1970) 1722.
7. Littler, J. S. and Waters, W. A. *J. Chem. Soc.* (1959) 1299.
8. Mehrotra, R. N. *J. Chem. Soc. B* (1968) 1123.
9. Littler, J. S. and Waters, W. A. *J. Chem. Soc.* (1959) 4046.
10. Kumar, A. and Mehrotra, R. N. *Int. J. Chem. Kinet. 6* (1974) 15.
11. Shanker, R. and Joshi, S. N. *Ind. J. Chem. 1* (1963) 289.
12. Virtanen, P. O. I. and Puutio, M. *Finn. Chem. Lett.* (1981) 49.
13. Sen Gupta, K. K. and Chatterjec, H. R. *Inorg. Chem. 17* (1978) 2429.
14. Lee, D. G. and Spitzer, U. A. *Can. J. Chem. 53* (1975) 3709.
15. Antelo Cortizas, J. M. and Castro Martinez, A. F. *Acta Cient. Compostelana 10* (1973) 87.
16. Rocek, J. *Collect. Czech. Chem. Commun. 25* (1960) 1052.
17. Paul, M. A. and Long, F. A. *Chem. Rev. 57* (1957) 1; Harbattle, G. *J. Am. Chem. Soc. 73* (1951) 4024.
18. Virtanen, P. O. I. and Korpela, J. *Suom. Kemistil. B 41* (1968) 321 and references therein.
19. Yamada, S., Funahashi, S. and Tanaka, M. *J. Inorg. Nucl. Chem. 37* (1975) 835.

Received January 19, 1982.

Acta Chemica Scandinavica A 36 (1982) 695–703

Short Communications

IR Studies of Coordinatively Unsaturated Surface Compounds on Silica Gel. VI. CO Adsorbed on Surface Allyl Chromium

BERND REBENSTORF, BO JONSON and RAGNAR LARSSON

Division of Inorganic Chemistry 1, Chemical Center, University of Lund, Box 740, S-220 07 Lund 7, Sweden

On the basis of IR CO adsorption studies, we have recently put forward the idea that both the Phillips (CrO_3/SiO_2)[1] and the Union Carbide (Chromocene/SiO_2)[2] polyethylene catalysts consist of dinuclear catalytic centres.[3,4] We further concluded that the failure to find homogeneous analogs to the two catalysts was caused by investigating only mononuclear compounds. A system with both homogeneous and heterogeneous activity is, however, available as tris(allyl)chromium[5–8] and tris(allyl)chromium on silica gel.[9–12] An IR CO study should possibly reveal if the latter catalytic centres are related to those of the two commercial chromium catalysts.

Experimental. Tris(allyl)chromium(III) was synthesized following Ref. 13 and stored at −40 °C. One must note that, according to Ref. 12, a bis(allyl)chromium(II) dimer is always present in the pentane solution of allyl chromium. This allylchromium compound is, however, not active as a polymerization catalyst.[8]

Silica gel "Merck 7733"[14] was pressed to a disc and placed in a previously described IR cell.[15] The allyl chromium solution was splashed on to the silica gel disc with the help of a syringe and a 1 mm PVC hose. This procedure was performed under argon (exclusion of oxygen and water). The chromium content of the silica gel disc was not determined analytically, but conversion to chromium(II) with the help of O_2 at 800 °C and CO at 370 °C followed by measuring the CO IR absorption[3] showed that the chromium content was in the range of 0.5 to 1%. The IR spectra were recorded on a Perkin-Elmer 580 B spectrophotometer connected to the IR data station from the same manufacturer.

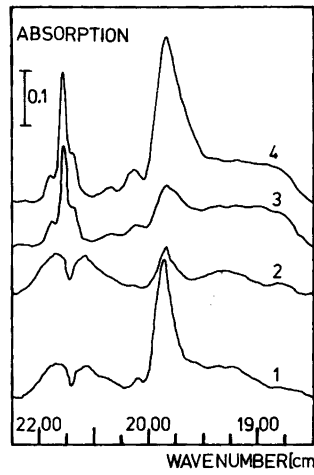

Fig. 1. IR spectra of CO adsorbed on allyl chromium/silica gel. Spectrum 1: Vacuum heat treatment at 600 °C and recorded at 20 °C with 80 Torr CO. Spectrum 2: As 1 but vacuum heat treatment of the silica gel at 300 °C. Spectrum 3: As 2 but 1 Torr CO at −145 °C. Spectrum 4: As 3 but after 16 h.

Results and discussion. Fig. 1 shows the IR spectrum of CO adsorbed on reaction products between allyl chromium and the silica gel surface. Only the band at 1984 cm^{-1} has a noteworthy intensity. A shoulder at 2024 cm^{-1} is coupled to this band and two weak bands at 1920 and 1875 cm^{-1} merge at low temperature (spectra 3 and 4, Fig. 1) to one very broad absorption. The small shoulder at 2184 cm^{-1} in the low temperature spectra is assigned to single bonded CO adsorbed on chromium(II).[3] The two broad bands at 2170 and 2115 cm^{-1} at room temperature (spectra 1 and 2, Fig. 1) are due to CO gas and the band at 2158 cm^{-1}, together with its shoulder at 2136 cm^{-1}, arises from CO adsorbed at surface silanol groups or CO clusters.[16]

The band at 1984 cm^{-1} was found to be air insensitive. This excluded the possibility that this band could be due to an allyl chromium surface compound. In view of recent investigations on the

0302–4377/82/080695-03$02.50

adsorption of $Cr(CO)_6$ on silica gel[17,18] it was concluded that the band at 1984 cm^{-1} and the shoulder at 2024 cm^{-1} belong to $Cr(CO)_6$ physisorbed on the silica gel surface.

Heating the silica gel in vacuum to either 300 or 700 °C prior to admission of allyl chromium had only a minor effect. After relatively low pretreatment temperature (300 °C) the formation of $Cr(CO)_6$ was slower by a factor of at least ten. This might be explained by the assumption that the allyl chromium surface compound, that forms the $Cr(CO)_6$, coordinates with nearby silanol groups.

Fig. 2 shows the CO IR spectrum of chromium(II) CO surface complexes (spectrum 2) obtained after treatment of allyl chromium/SiO_2 with O_2 at 800 °C and CO at 370 °C. The three bands at 2120, 2100 and 2035 cm^{-1} have been assigned previously[3,4] to a *dinuclear* chromium(II) surface complex with three bridging CO molecules adsorbed. These three bands are not present in spectrum 1 (Fig. 2), which shows the IR spectrum of CO adsorbed on allyl chromium/SiO_2. It becomes clear that with allyl chromium on the silica gel surface no dimers are detectable with CO, *i.e.* no coordinatively unsaturated dimers are formed. The small band at 2184 cm^{-1} in spectrum 1, Fig. 2 and the absence of the bands at 2120 and 2100 cm^{-1} in this spectrum (at low temperatures) show that also this chromium(II) CO complex is a mononuclear one. Treatment with H_2 at 600 °C according to Ref. 11 did not give a stronger CO band at 2184 cm^{-1}. The same was the case with heating in vacuum to 300 °C.

Our samples were active for polymerization of ethylene. This can be seen from the spectra in Fig. 3. Bands at 3080 and 1640 cm^{-1} in spectra 2 and 3 are assigned to C–H and C=HO vibrations in olefins, respectively. They may arise from ethylene bonded to surface allyl chromium compounds. These two bands were stable up to 200 °C and vacuum. The band at 1985 cm^{-1} in spectrum 3, Fig. 3, shows that the formation of $Cr(CO)_6$ was not prevented by ethylene.

The colour change of the red allyl chromium solution to light gray on contact with the silica gel is evidence that allyl chromium reacts with silanol groups to form the following surface compound as proposed previously:[8,11] $(C_3H_5)Cr(O-Si-)_2$. A similar complex with the cyclopentadienyl ligand is known to be a stable and rather inert surface compound, which does not adsorb CO.[19] This would explain why we found only relatively weak CO IR bands. In contrast to the cyclopentadienyl ligand the allyl ligand is more reactive and can start the polymerization of ethylene. This can be exemplified by chromocene and tris(allyl)chromium(III), where the former is inactive and the latter is, as noted above, an active polyethylene catalyst.

The preparation of $Cr(CO)_6$ is normally performed by reduction of a chromium salt with a reactive metal and under high CO pressure.[20] We were

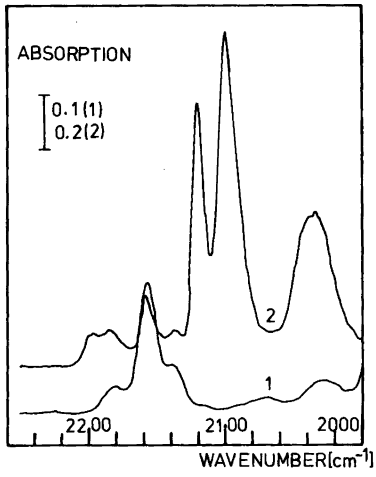

Fig. 2. IR spectra of CO adsorbed on allyl chromium/silica gel and on the dinuclear chromium(II) surface compound. Spectrum 1 is a part of spectrum 4 (Fig. 1). Spectrum 2: Allyl chromium/silica gel converted to chromium(II) with O_2 at 800 °C and CO at 370 °C. Recorded at −145 °C with 1 Torr CO.

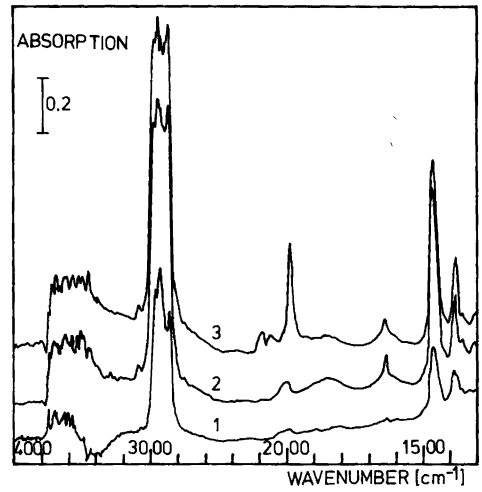

Fig. 3. IR spectra of allyl chromium/silica gel before (spectrum 1) and after polymerization with ethylene (spectrum 2, 650 Torr C_2H_4, 10 min, 100 °C) and evacuation. Spectrum 3: As 2 but addition of 80 Torr CO, 20 °C, 16 h. The silica gel spectrum was subtracted in all three spectra shown.

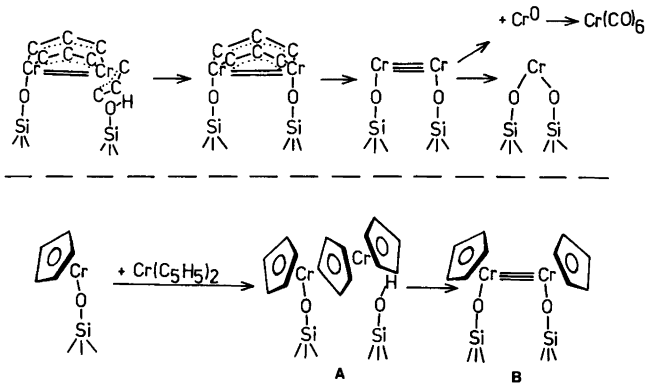

Scheme 1.

unable to find a low pressure process with or without allyl chromium in the literature. In the upper part of Scheme 1 we propose a mechanism for the formation of $Cr(CO)_6$ and of a chromium(II) surface compound from the bis(allyl)chromium(II) dimer.[21] The most important reaction step here is the disproportionation of a chromium(I) surface dimer. Whether chromium metal atoms are really formed as intermediates is not wuite clear.

Why should then chromocene give dinuclear surface compounds? The lower part of the scheme shows a possible mechanism on how this can come about. The cyclopentadienyl chromium surface oxide is highly coordinatively unsaturated (a 12 electron system) and may coordinate to a yet unchanged chromocene molecule *via* a cyclopentadienyl ligand to form a "double" sandwich[22] (A). The coordinated chromocene molecule can thereafter react with the nearby silanol group and form the dimer B shown in Scheme 1. This dimer B can then in turn coordinate four (or three) CO molecules as proposed previously.[4]

Acknowledgement. We thank the Swedish Board for Technical Development (STU) for financial support.

1. Hogan, J. P. *J. Polym. Sci. A-1 8* (1970) 2637.
2. Karol, F. J., Karapinka, G. L., Wu, C., Dow, A. W., Johnson, R. N. and Carrick, W. L. *J. Polym. Sci. A-1 10* (1972) 2621.
3. Rebenstorf, B. and Larsson, R. *Z. Anorg. Allg. Chem. 478* (1981) 119.
4. Rebenstorf, B. and Larsson, R. *J. Mol. Catal. 11* (1981) 247.
5. Wilke, G. *U.S. Pat.* 3 379 706 (1968).
6. Johnson, R. N. and Karol, F. J. *Belgian Pat.* 743 199 (1969).
7. Ballard, D. G. H., Jones, E., Medinger, T. and Pioli, A. J. P. *Makromol. Chem. 148* (1971) 175.
8. Ballard, D. G. H. *Adv. Catal. 23* (1973) 263.
9. Stefanovskaya, N. N., Shmonina, V. L., Tinyakova, E. I. and Dolgoplosk, B. A. *Dokl. Akad. Nauk SSSR 211* (1973) 862, Engl. 619.
10. Dolgoplosk, B. A., Tinyakova, E. I., Stefanovskaya, N. N., Oreshkin, I. A. and Shmonia, V. L. *Eur. Poly. J. 10* (1974) 605.
11. Iwasawa, Y. and Ogasawara, S. *Chem. Lett.* (1980) 127.
12. Johnson, R. N. and Karol, F. J. *J. Polym. Sci. A-1 13* (1975) 1607.
13. *Inorg. Synth. 13* (1972) 73.
14. Krauss, H. L. and Naumann, D. *Z. Anorg. Allg. Chem. 430* (1977) 23.
15. Rebenstorf, B. and Larsson, R. *Z. Anorg. Allg. Chem. 453* (1979) 127.
16. Ghiotti, G., Garrone, E., Morterra, C. and Bocuzzi, F. *J. Phys. Chem. 83* (1979) 2863.
17. Guglielminotti, E. *J. Mol. Catal. 13* (1981) 207.
18. Howe, R. F. *Inorg. Chem. 15* (1976) 486.
19. Krauss, H. L. and Westphal, U. *Z. Naturforsch. Teil B 33* (1978) 1278.
20. Purcell, K. F. and Kotz, J. C. *Inorganic Chemistry*, W. B. Saunders, Philadelphia 1977, p. 856.
21. Aoki, T., Furusaki, A., Tomiie, Y., Ono, K. and Tanaka, K. *Bull. Chem. Soc. Jpn. 42* (1969) 545.
22. Werner, H. *Angew. Chem. 89* (1977) 1.

Received March 19, 1982.

An Ultrasonic Study of Sphere to Rod Transitions in Aqueous Solutions of Hexadecyltrimethylammonium Bromide

SUNE BACKLUND,* HARALD HØILAND, OVE J. KVAMMEN and EVA LJOSLAND

Department of Chemistry, University of Bergen, N-5014 Bergen, Norway

Surfactants are amphiphilic molecules that dynamically associate in aqueous solution above a certain critical concentration, c.m.c., to large molecular aggregates of colloidal dimensions, *i.e.* micelles.[1,2] At surfactant concentrations close to the c.m.c. micelles are spherical, but at increasing concentrations rodlike micelles form.[3]

It has been documented that ultrasound measurements are sensitive to structural changes in solutions. For instance, micelle formation and stacking can be detected by this method.[4-6] In this work we have used the method of ultrasonic measurements to examine aqueous solutions of hexadecyltrimethylammonium bromide (HTAB) in order to gain information about reported changes in the shape of the HTAB micelles with increasing concentration.

In the absence of added electrolyte, HTAB micelles apparently undergo changes from a spherical to a rodlike shape as the concentration exceeds a certain limit. This has been documented by conductivity measurements,[7,8] small angle X-ray scattering,[9] viscosity and light scattering measurements[10] and nuclear magnetic relaxation data.[11,12] It has been suggested that these rod-like micelles have considerable flexibility.[12] The results so far have been summarized in Table 1. It appears that the transition does not occur at a specific molality but takes place over a relatively wide range. The agreement between the various sets of data is not particularly good, but such discrepancies are likely to occur if the transition region is wide.

In Fig. 1, the relative speed of sound (relative to the speed of sound of the solvent) of HTAB solutions has been plotted *versus* molality, m_{HTAB}. In the temperature range 300 – 305 K a transition point, m^t_{HTAB}, can be observed. It appears to be a rather distinct point at 0.27 molal at 300.7 K, increasing to 0.32 at 305.1 K. At 308 K and higher temperatures no transition point could be detected in the concentration range investigated.

The result is in good agreement with the data presented in Table 1. The ultrasonic data, however, do not show a wide transitional region, at least not as wide as indicated by viscosity or ^{81}Br NMR measurements. On the other hand, there is agreement that the transition molality increases with temperature. Note that the aggregation number of spherical ionic micelles decreases with temperature as shown by membrane osmometry.[13,14]

The enthalpy change of transition from spheres to rods has been estimated from the temperature dependence of the transition molality, m^t_{HTAB}. The value thus obtained is -30 ± 1 kJ mol^{-1}.

It is well-known that addition of a third component, electrolyte or nonelectrolyte, can cause structural changes in micelles. Furthermore, this change is highly specific depending on the nature of the additive. Larsen *et al.*[15] thus found from viscosity measurements that while both ethanol and hexane had little or no effect, hexanol caused a pronounced change of structure in a 0.1 M HTAB – 0.1 M NaBr solution. In the absence of NaBr the effect of hexanol on the viscosity of HTAB solutions was small. On the other hand, Tominaga *et al.*[16]

* Present address: Institute of Physical Chemistry, Åbo Akademi, Åbo, Finland.

Table 1. Sphere to rod transition of HTAB micelles in aqueous solution.

T K	m^t_{HTAB} mol kg^{-1}	Method	Ref.
298.2	~0.45	Conductivity	8
308.2	~0.56		
300.2	0.304	Small angle X-ray	9
323.2	0.562		
343.2	0.915		
298.2	0.271 – 0.339	Viscosity, light scattering	10
300 ± 2	0.207 – 0.447	^{81}Br NMR	11
301.2 ± 0.5	0.28	^{14}N NMR	12

0302-4377/82/080698-03$02.50

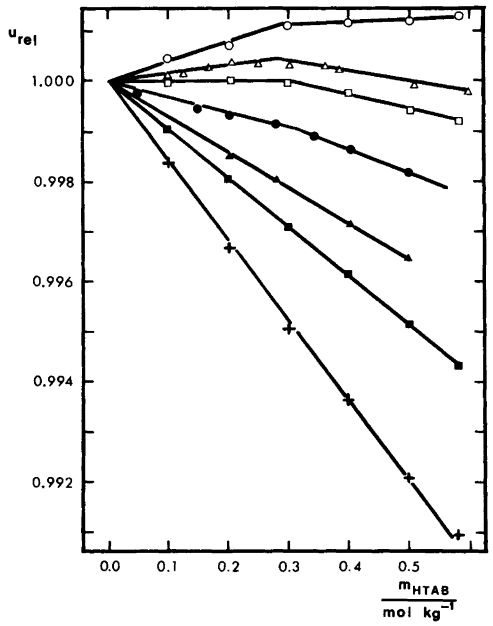

Fig. 1. Relative speed of sound, u_{rel}, in pure HTAB solutions as a function of the HTAB molality at 300.7 (○); 303.1 (△); 303.4 (□); 305.1 (●); 308.2 (▲); 310.7 (■); 315.6 K (+).

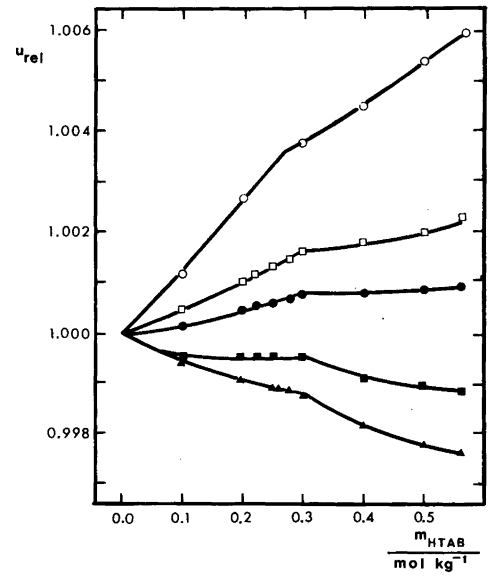

Fig. 2. Relative speed of sound, u_{rel}, in HTAB – 0.01 mol kg^{-1} pentanol solutions as a function of the HTAB molality at 293.2 (○); 298.2 (□); 300.2 (●); 303,.2 (■); 305.2 K (▲).

point out that the viscosity increases rapidly upon addition of hexanol to HTAB solutions suggesting sphere to rod transitions. Lindblom *et al.*[11] also find that small amounts of hexanol appear to promote a sphere to rod transition.

In Fig. 2 the relative speed of sound of HTAB in 0.01 mol kg^{-1} pentanol has been plotted at various temperatures. With pentanol added it was possible to carry out the measurements at lower temperatures, and in this case the temperature ranges from 293.2 – 305.2 K. Otherwise the curves are of a similar character as those in Fig. 1. They show a transition point around 0.30 mol kg^{-1} slightly lower at 293 K. The effect of a little added pentanol is thus small as far as the sphere to rod transition is concerned.

However, the Fig. 3 the same curves have been plotted, the only difference being a pentanol content of 0.05 mol kg^{-1}. At this pentanol content there appears to be a totally different situation. In the HTAB concentration range that has been investigated, there is no longer any sign of changes in micellar structure, at least not any that are signified by abrupt changes in the curvature. Since alcohols apparently promote rods, this result suggests that most of the HTAB molecules are present as rod-like micelles in 0.05 mol kg^{-1} pentanol solutions.

In conclusion, it appears that ultrasound measurements provide a well-suited way to measure changes in micellar structure. As far as HTAB micelles are concerned, a transition takes place

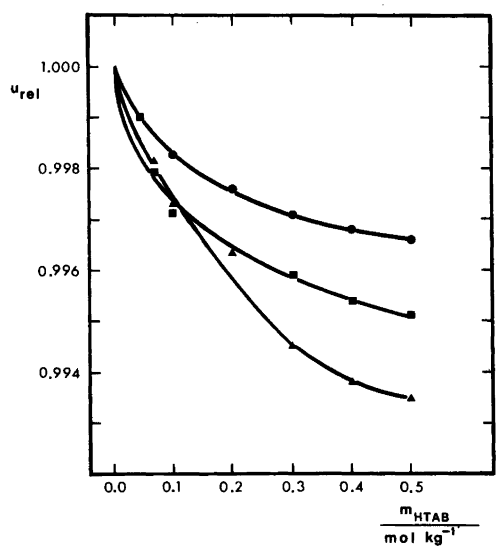

Fig. 3. Relative speed of sound u_{rel}, in HTAB – 0.05 mol kg^{-1} pentanol solutions as a function of the HTAB molality at 303.2 (●); 305.2 (▲); 308.2 K (■).

around 0.3 mol kg^{-1} both in water and in aqueous (0.01 mol kg^{-1}) pentanol. The transition depends on temperature. In pure water no transition can be observed at 308 K and higher temperatures. In aqueous (0.05 mol kg^{-1}) pentanol no transition appears at any of the measured temperatures.

Experimental. Hexadecyltrimethylammonium bromide (HTAB) (purity *ca.* 99 %) was from Sigma. It was dried in an evacuated desiccator and used without further purification n-pentanol (*puriss* quality) was used as supplied by Fluka. The ultrasound measurements were made by the "sing-around" method as previously described.[17] The relative speed of sound, u_{rel}, was calculated as $u_{rel}=f(1-f^*\tau)/f^*(1-f\tau)$. Here τ is the delay time and f and f^* the measured frequencies in solution and solvent, respectively. The temperature in water thermostats were controlled to within ± 0.01 K. The error in the speed of sound is estimated to ± 0.02 m s^{-1}.

Acknowledgement. We wish to thank Dr. Lars Ödberg for suggesting the use of ultrasound on this system, and Professor Ingvar Danielsson for valuable discussions during the preparation of this manuscript. One of us, S.B., thanks *Nordiska Forskarkurser* for financial support.

1. Shinoda, K., Nakagawa, T., Tamamushi, B.-I. and Isemura, T. *Colloidal Surfactants: Some Physicochemical Properties*, Academic, New York 1963, Chapter 1.
2. Tanford, C. *The Hydrophobic Effect: Formation of Micelles and Biological Membranes*, Wiley, New York 1980, Chapters 6–8.
3. Fendler, J. H. *J. Phys. Chem. 84* (1980) 1485.
4. Brun, T. S., Høiland, H. and Vikingstad, E. *J. Colloid Interface Sci. 63* (1978) 89.
5. Hemmes, P., Mayevski, A. A., Buckin, V. A. and Saravazyan, A. P. *J. Phys. Chem. 84* (1980) 699.
6. Palmesen, T., Høiland, H. and Songstad, J. *Acta Chem. Scand. A 35* (1981) 599.
7. Götz, K. G. and Heckmann, K. *J. Colloid Sci. 13* (1958) 266.
8. Götz, K. G. and Heckmann, K. *Z. Phys. Chem. (Frankfurt am Main) 20* (1959) 42.
9. Reiss-Husson, F. and Luzzati, V. *J. Phys. Chem. 68* (1964) 3504.
10. Ekwall, P., Mandell, L. and Solyom, P. *J. Colloid Interface Sci. 35* (1971) 519.
11. Lindblom, G., Lindman, B. and Mandell, L. *J. Colloid Interface Sci. 42* (1973) 400.
12. Henriksson, U., Ödberg, L., Eriksson, J. C. and Westman, L. *J. Phys. Chem. 81* (1977) 76.
13. Birdi, K. S. *Kolloid Z.Z. Polym. 250* (1972) 731.
14. Backlund, S., Rundt, K., Birdi, K. S. and Dalsager, S. *J. Colloid Interface Sci. 79* (1981) 578.
15. Larsen, J. W., Magid, L. J. and Payton, V. *Tetrahedron Lett. 29* (1973) 2663.
16. Tominaga, T., Stem, T. B. and Evans, D. F. *Bull. Chem. Soc. Jpn. 53* (1980) 795.
17. Høiland, H. and Vikingstad, E. *J. Chem. Soc, Faraday Trans. 1, 72* (1976) 1441.

Received March 30, 1982.

Carbon-13 Nuclear Magnetic Resonance Studies on Hexamethylethane

DAGFINN W. AKSNES

Department of Chemistry, University of Bergen, N-5014 Bergen, Norway

Hexamethylethane, $(CH_3)_3CC(CH_3)_3$, referred to hereafter as HME, is the most symmetrical of the octane molecules. The high-temperature plastic phase exists from the transition point at 152.5 K to the melting point at 374 K.[1] The crystal structure of the plastic phase is a body-centered cubic lattice with two molecules per unit cell.[2] At atmospheric pressure the liquid phase exists for a range of only 6 K.

Molecular motion studies carried out by ^1H NMR on the brittle and plastic phases of HME have shown the existence of a variety of motions such as reorientation of methyl and *t*-butyl groups, overall molecular tumbling and self-diffusion.[3-5] However, ^{13}C relaxation measurements are particulary suited to studies of molecular rotations in plastic crystals since intermolecular contributions and dipolar interaction between like spins do not generally complicate the interpretation, unlike the situation for ^1H and ^{19}F.[6] It should also be remembered that the ^1H and ^{13}C NMR techniques are complementary in the sense that they monitor the rotations of different vectors. For these reasons, we have chosen to examine in a direct fashion the NMR spectrum of the dilute ^{13}C nuclei in HME.

The half linewidth, $\Delta\nu_{1/2}$, of the ^{13}C methyl peak has been measured throughout the plastic phase. The line from the quaternary carbon appeared about 212 Hz downfield for the methyl signal. This line exhibited a shoulder on the methyl peak, and thus contributed somewhat to the half linewidth of the main peak, when $\Delta\nu_{1/2} \gtrsim 160$ Hz. The half linewidth of the methyl peak was about 200 Hz from the transition temperature (152 K) to 280 K. A further increase in the temperature resulted in a gradual decrease in $\Delta\nu_{1/2}$ to about 3 Hz in the liquid phase. It is interesting to note that a similar line narrowing has been reported to occur in the same temperature range for the methyl proton signal of HME.[4,5] That line narrowing was attributed to translational self-diffusion of the molecules.

In succinonitrile [7] the ^{13}C linewidth has also been found to increase with decreasing temperature from 4 Hz at 318 K (13 K below the melting point) to a maximum value of 75 Hz. Similarly, in the plastic phase of adamantane [8] a ^{13}C linewidth of about 49 Hz has been reported.

For a unique motional process $\Delta\nu_{1/2}$ is an inverse measure of the spin-spin relaxation time T_2 for the system.[9] In the high-temperature plastic phase this can also be regarded as the equivalent of the spin-lattice relaxation time in the local field $T_{1\rho}$. Whereas T_1 is controlled by the intramolecular dipole-dipole relaxation mechanism in the studied temperature range (*vide infra*), it seems that T_2 (and $T_{1\rho}$) also get significant contributions from intermolecular relaxation processes.

The observed melting point of HME was not sharp and the melting took place over a few degrees. At about 370 K it was possible to observe both a liquid and a solid (plastic) component in the ^{13}C NMR spectrum. The methyl and quaternary ^{13}C signals in the plastic phase were, respectively, 0.57 and 0.45 ppm downfield for the corresponding signals in the liquid phase. In pivalic acid a chemical shift difference of 1.4 ppm between the liquid and solid has been reported.[10] Although the ^{13}C linewidth of the liquid component of HME was distinctly smaller than that of the plastic component, a large change, like that reported to occur in the proton spectrum,[4] was not observed.

The T_1 values of the methyl carbon have been measured in the temperature range 152 to 378 K. It was difficult to obtain accurate values of T_1 just below the melting point due to the presence of the liquid component. A semilog plot of T_1 *versus* the inverse temperature is shown in Fig. 1. It is seen that there is no discontinuity in T_1 in going from the plastic to the liquid phase, indicating a similar mechanism for rotation in both phases. Similar behaviour has been observed for other spherical or approximately spherical molecules.[11,12]

We belleve that the methyl carbon relaxation is dominated by the dipole-dipole (DD) relaxation mechanism throughout the liquid and plastic phases. This assumption is supported by measurements of the nuclear Overhouser enhancement (NOE) factor η which gave maximal NOE within experimental error ($\eta = 1.8 \pm 10\%$ and $\eta = 2.0 \pm 10\%$ in the liquid and plastic phases, respectively). A negligible contribution from the spin-rotation mechanism is consistent with the reported highly hindered correlated reorientation of the methyl and *t*-butyl groups in HME.[4,5] In most organic solids, however, the barriers hindering methyl group rotation are small.[12]

A minimum in T_1 is not reached with falling temperature since the transition point intervenes. However, the temperature variation of T_1 shows an Arrhenius behaviour with an activation enthalpy E_a of 10.3 kJ mol^{-1}. This value is somewhat higher than the value obtained from ^1H NMR studies of HME in the plastic phase (9.2 kJ mol^{-1}).[4,5] Our value is, however, not unusually high for isotropic reorientation in a plastic crystal [12] (for example, 12.9

0302-4377/82/080701-03$02.50

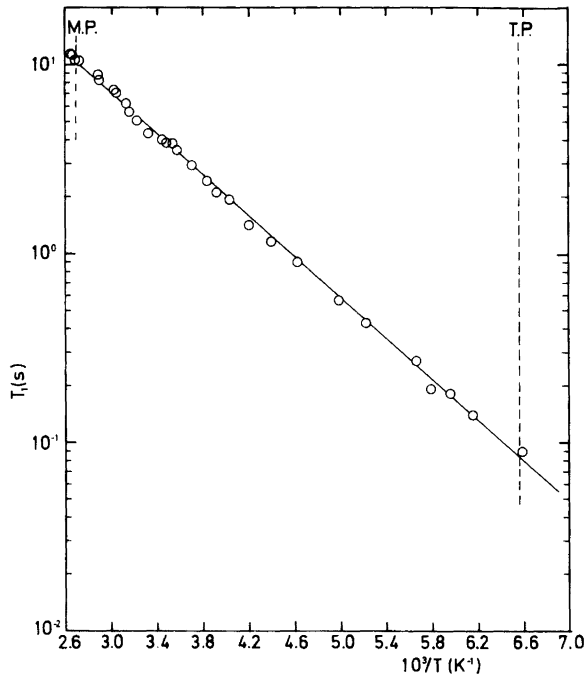

Fig. 1. Carbon-13 spin-lattice relaxation times at 22.63 MHz in hexamethylethane plotted *versus* $10^3/T$.

and 11.7 kJ mol^{-1} in adamantane[11] and *d*-camphor,[13] respectively).

The measured T_1 values are well within the high temperature side of the T_1 minimum, that is, the extreme narrowing condition applies, $(\omega_H + \omega_C)\tau_c \ll 1$ where τ_c is the appropriate correlation time. If contributions from non-bonded protons are ignored, the ^{13}C relaxation time due to the intramolecular C–H dipolar interaction, T_1^{DD}, is given by eqn. (1),[6] where n_H is the number of protons directly attached to the carbon in question, r_{CH} is the C–H bond length and τ_c is the effective isotropic correlation time for molecular reorientation. Assuming that $r_{CH} = 1.10$ Å, as found for ethane, it follows from eqn. (1) that T_1 for the methyl carbon is given by eqn. (2). However, if there is internal

$$1/T_1^{DD} = \hbar^2 \gamma_H^2 \gamma_C^2 n_H r_{CH}^{-6} \tau_c^{eff} \quad (1)$$

$$1/T_1^{DD}{}_{Me} = 6.097 \times 10^{10} \tau_c^{eff} \quad (2)$$

rotation of specific groups, such as a methyl group attached to an isotropically tumbling molecule, one must take into account two correlation times, τ_r for overall rotation and τ_i for internal rotation.[14,15] For $\tau_i \ll \tau_r$ it can be shown that $\tau_c^{eff} = \tau_r/9$. When $\tau_r \ll \tau_i$, however, $\tau_c^{eff} = \tau_r$. Thus, in either limit the dipolar relaxation time is related to the overall tumbling motion alone, whereas for intermediate cases both motions contribute.

By using eqn. (2) it is found that $\tau_c^{eff} \approx 1.5 \times 10^{-12}$ s at the melting point ($T_1 \approx 11.0$ s). On the basis of the above discussion, however, it is reasonable to expect a somewhat larger value for τ_r. Values of τ_r have not been measured for many plastic organic solids, however, according to Boden[12] a value of $\tau_r \simeq 2 \times 10^{-12}$ s at the melting point seems to be a characteristic property of these materials. At the transition point $T_1 \simeq 8.5 \times 10^{-2}$ s, thence $\tau_c^{eff} \simeq 1.9 \times 10^{-10}$ s. This value is quite close to those reported for succinonitrile (*ca.* 2.4×10^{-10} s)[7] and adamantane[8] (*ca.* 1.4×10^{-10} s) at the solid-plastic phase transition temperature.

The proton-coupled methyl carbon quartet has been observed at a series of different temperatures in the plastic and liquid phases of HME. The one-bond proton-carbon coupling constant $^1J_{CH} = 126$ Hz in the liquid phase. The four peaks of the quartet remained quite sharp with a separation of 124 – 126 Hz for temperatures down to about 335 K. When the temperature was reduced further the quartet became rapidly broader with partly overlapped lines and reduced peak separation. At 326 K only the two major peaks of the quartet with a separation of 100 Hz, were observed. The quartet collapsed into a single very broad peak at 320 K. A similar

temperature dependence has also been observed for the corresponding methyl quartet of pivalic acid[10,16] and *t*-butyl chloride.[16] This temperature effect is probably the result of hindered reorientations of the *t*-butyl groups or cooperative intermolecular (medium) effects in the plastic phase. This problem is at present being pursued by means of CNDO/2 calculations in an attempt to elucidate the physical nature of the phenomenon.

Experimental. The sample of HME obtained commercially from EGA-Chemie was purified by sublimation. The ^{13}C NMR spectra were measured at 22.63 MHz on a Bruker CXP 100 spectrometer equipped with external deuterium lock. The sample temperature was regulated and stabilized to within 0.5 K by means of a Bruker B-ST 100/700 c temperature control unit. The longest T_1 values were measured by fast inversion-recovery $(180°-\tau-90°-T)_n$ with T (10–12 s) significantly shorter than $5T_1$,[17] whereas the shorter T_1 values were measured using ordinary inversion-recovery $(180°-\tau-90°-T)_n$ with $T \gtrsim 5T_1$.[6] Short and long τ values were alternated in order to minimize errors in T_1 due to systematic spectrometer performance problems like degrading resolution. The 90° pulse length was 12.4 μs. Throughout the experiment the number of scans varied from 50 to 200, depending on the linewidth.

The T_1's were calculated by means of iterative nonlinear least squares methods[18,19] using 7–18 pairs of experimental points. The estimated accuracy of the T_1 values ranges from ±4 to ±10% depending on the numer of τ values and the signal-to-noise ratio.

1. Scott, D. W., Douslin, D. R., Gross, M. E., Oliver, G. D. and Huffman, H. M. *J. Am. Chem. Soc. 74* (1952) 883.
2. West, C. D. *Z. Kristallogr. 88* (1934) 195.
3. Smith, G. W. *J. Chem. Phys. 54* (1971) 174.
4. Chezeau, J. M., Dufourcq, J. and Strange, J. H. *Mol. Phys. 20* (1971) 305.
5. Albert, S., Gutowsky, H. S. and Ripmeester, J. A. *J. Chem. Phys. 56* (1972) 1332.
6. Lyerla, J. R. and Levy, G. C. *Topics in Carbon-13 NMR Spectroscopy*, Wiley, New York 1974, Vol. 1, Chapter 3.
7. Wasylishen, R. E. and Pettitt, B. A. *Mol. Phys. 36* (1978) 1459.
8. Wasylishen, R. E. and Pettitt, B. A. *Can. J. Chem. 58* (1980) 655.
9. Bladon, P., Lockhart, N. C. and Sherwood, J. N. *Mol. Phys. 20* (1971) 577.
10. Graham, J. D. and Darby, J. S. *J. Magn. Reson. 23* (1976) 369.
11. Resing, H. A. *Mol. Cryst. Liq. Cryst. 9* (1969) 101.
12. Boden, N. In Sherwood, J. N., Ed., *The Plastically Crystalline State*, Wiley, New York 1979, Chapter 5.
13. Anderson, J. E. and Slichter, W. P. *J. Chem. Phys. 41* (1964) 1922.
14. Stejskal, E. O. and Gutowsky, H. S. *J. Chem. Phys. 28* (1958) 388.
15. Woessner, D. E. *J. Chem. Phys. 36* (1962) 1.
16. Aksnes, D. W. and Kimtys, L. L. *Unpublished results.*
17. Levy, G. C. and Peat, I. R. *J. Magn. Reson. 18* (1975) 199.
18. Brunetti, A. H. *J. Magn. Reson. 28* (1977) 289.
19. de Fontaine, D. L., Ross, D. K. and Ternai, B. *J. Magn. Reson. 18* (1975) 276.

Received April 14, 1982.

Acta Chemica Scandinavica A 36 (1982) 705–709

Composition and Molecular Structure of Gaseous Gold Pentafluoride by Electron Diffraction

J. BRUNVOLL,[a] A. A. ISCHENKO,[b] A. A. IVANOV,[b] G. V. ROMANOV,[b] V. B. SOKOLOV,[b] V. P. SPIRIDONOV[b] and T. G. STRAND[c]

[a] Institute of Physical Chemistry, Technical University of Norway, N-7034 Trondheim-NTH, Norway,[b] Department of Chemistry, Moscow State University, Moscow 117 234, USSR and [c] Chemistry Department, University of Oslo, Oslo 3, Norway

Gaseous gold pentafluoride is mostly dimeric at the nozzle temperature of about 220 °C. However, a smaller amount of trimeric molecules is present. In both forms the gold atoms are surrounded by six fluorine atoms in distorted octahedral arrangements. Assuming the two forms to possess D_{2h} and D_{3h} symmetries, respectively, and to have equal Au–F bond distances, and assuming that the estimated root mean-square amplitudes of vibration are correct, least-squares refinements resulted in 81.9(1.0) % of dimers and $R(\mathrm{Au}-\mathrm{F_{a(axial)}})=1.889(9)$, $R(\mathrm{Au}-\mathrm{F_{t(terminal)}})=1.822(8)$ and $R(\mathrm{Au}-\mathrm{F_{b(bridged)}})=2.030(7)$ Å. The angles determined for the dimers and trimers, respectively, were $\angle(\mathrm{F_a}-\mathrm{Au}-\mathrm{F_a})=181.0$ (1.1) and 193.1(3.2), $\angle(\mathrm{F_t}-\mathrm{Au}-\mathrm{F_t})=92.3(1.7)$ and 75.3(6.5) and $\angle(\mathrm{F_b}-\mathrm{Au}-\mathrm{F_b})=80.1(0.5)$ and 115.7 (1.1)°. The least-squares standard deviations are given in parentheses.

Gold in the oxidation state of +V as AuF_6^- salts[1] and as AuF_5[2] has been known for some years. The gaseous pentafluorides of Nb, Ta and Sb are mostly trimeric at nozzle temperatures in the range 20–60 °C.[3] The results of an electron diffraction investigation of gaseous gold pentafluoride at the somewhat higher temperature of about 220 °C are reported in the present paper.

EXPERIMENTAL AND DATA REDUCTION

Gold obtained by reducing Au(III) by formaldehyde in HCl (the Zygmondi method) was oxidized by the stoichiometric quantity of KrF_2 in dry HF. The gold pentafluoride was obtained by distilling off the solvent at 40–50 °C.[4] According to chemical analysis the composition was $AuF_{5.02}$ and the vibrational spectrum agreed with the known one.[5]

The electron diffraction pattern was recorded using the improved apparatus of Moscow State University.[6] No diffraction pattern could be observed below about 220 °C and the gold pentafluoride started to decompose at 250–300 °C. Vapour pressure measurements of the substance do not exist, the electron diffraction experiment indicates a vapour pressure of the magnitude 0.1 mmHg at the applied temperature. The optical densities of the photographic plates were measured by the Joyce-Loebl digital microphotometer of the University of Oslo. The experimental conditions are summarized in Table 1.

The data were treated in the usual way.[7] The first backgrounds were determined by fitting a polynomial to the intensities from each single plate and the first average molecular intensities, $s\,M(s)$, were obtained using these experimental backgrounds. The backgrounds were later adjusted several times according to theoretical molecular intensities.[8]

The atomic scattering factor of F was computed[9] at 74 kV from an analytical representation of the potential[10] and the scattering factor of Au was obtained by interpolation of numerical tables[11] for the same voltage.

ESTIMATES OF *u*- AND *D*-VALUES

The root mean-square amplitudes of vibration *u* and the correction terms between the electron diffraction distances and the distances between the thermal average atomic positions, the *D*-values,

0302-4377/82/090705-05$02.50

Table 1. Experimental conditions for the electron diffraction diagrams of gold pentafluoride at about 74 keV.

Camera distance (mm)	616.465	193.673
Wavelength (Å)[a]	0.04352(4)	0.04350(6)
Beam current (μA)	5.	5.
Nozzle temp. (°C)	225(2)	215(2)
Exposure time (s)	30	80
Blackness interval	0.2 – 0.5	0.4 – 0.2
Applied s-range (Å^{-1})	2.0 – 12.0[b]	8.0 – 29.5[c]
Number of plates	4	4

[a] From zinc oxide diffraction patterns. [b] Intervals of $\Delta s = 0.125$ Å^{-1}. [c] Intervals of $\Delta s = 0.25$ Å^{-1}.

were estimated from simple valence force fields. From the valence force field the symmetry force field and the transformation between symmetry and normal coordinates, the L matrix was obtained.[12] Au – F stretching force constants were adjusted to agree with experimental frequencies.[4,13] The u-and D-values applied in the final least-squares refinement are given in Table 2. Only the the values of the Au – F bond distances have been included.

STRUCTURE INVESTIGATION

The first experimental radial distribution function indicated the presence of dimeric molecules. Least-squares fit of a D_{2h} symmetric dimer resulted in a reasonable geometry. To obtain a satisfactory agreement for only this type of molecules, the u-values of the nonbonded Au···Au and Au···F distances had to be refined and the obtained values turned out to be much too large compared to the estimated ones. Attempts to increase the estimated u-values by reducing the torsional force constants of the ring did not explain the disagreement. However, fixing the u-values of the dimer on the originally estimated values, the experimental and theoretical functions showed large discrepancies in the range 3.0 to 3.7 Å. The theoretical function seemed to be missing a peak at about 3.6 Å. As this distance was somewhat longer than the Au···Au distance of the dimer, the missing peak might be due to the Au···Au distance of a smaller amount of trimeric molecules.

Least-squares refinements of a mixture of dimer and trimer readily converged to about 20 % of trimeric molecules and the agreement improved very much. The u- and D-values of a D_{3h} symmetric trimer were then estimated. The backgrounds were adjusted, and further least-squares refinements showed that the initial constraint of equal Au – F bond distances of the two forms could not be relaxed. Refinement of the u-values of the Au···Au and the nonbonded Au···F distances of the dimer did not improve the agreement significantly and the changes from the estimated u-values were now small.

Results of the final least-squares refinement are given in Table 3 and illustrated in Fig. 1. The D_{2h} and D_{3h} symmetric models were satisfied by the thermal average atomic positions by correcting the

Table 2. Estimated u- and D-values (Å) for the Au – F bond distances of the two forms of gold pentafluoride at 220 °C.

Distance	Dimer D_{2h} u	Dimer D_{2h} D	Trimer D_{3h} u	Trimer D_{3h} D
Au – F_a	0.0464	−0.0125	0.0464	−0.0175
Au – F_t	0.0443	−0.0132	0.0443	−0.0178
Au – F_b	0.0610	−0.0032	0.0618	−0.0027

Table 3. Least-squares results and standard deviations for the composition and the parameters of the thermal average atomic positions of the two forms of gaseous gold pentafluoride at about 220 °C. The axial, terminal and bridged fluorine atoms are denoted F_a, F_t and F_b, respectively.

Parameter[a]	Dimer D_{2h}[b]	Trimer D_{3h}[b]
Percentage	81.9(1.0)	18.1(1.0)[c]
$\Delta R \equiv R(\text{Au}-\text{F}_a) - R(\text{Au}-\text{F}_t)$	0.067(16)	
$R(\text{Au}-\text{F}_a)$[c]	1.889(9)	
$R(\text{Au}-\text{F}_t)$	1.822(8)	
$R(\text{Au}-\text{F}_b)$	2.030(7)	
$\angle(\text{F}_a-\text{Au}-\text{F}_a)$[d]	181.0(1.1)	193.1(3.2)
$\angle(\text{F}_t-\text{Au}-F_t)$	93.3(1.7)	75.3(6.5)
$\angle(\text{F}_b-\text{Au}-\text{F}_b)$	80.1(0.5)	115.7(1.1)
$\angle(\text{Au}-\text{F}_b-\text{Au})$[c]	99.9(0.5)	124.3(1.1)
K_1	0.620(8)	
K_2	0.657(32)	
R_f	4.08	

[a] Distances (Å) and angles (°). K_1 and K_2 are scale factors for the data of the long and short camera distance, respectively, and R_f (%) is a weighted agreement factor (eqn. 16 of Ref. 14). [b] The Au – F bond distances had to be assumed equal in the two forms. [c] Dependent parameters. [d] The angles are defined in Fig. 1.

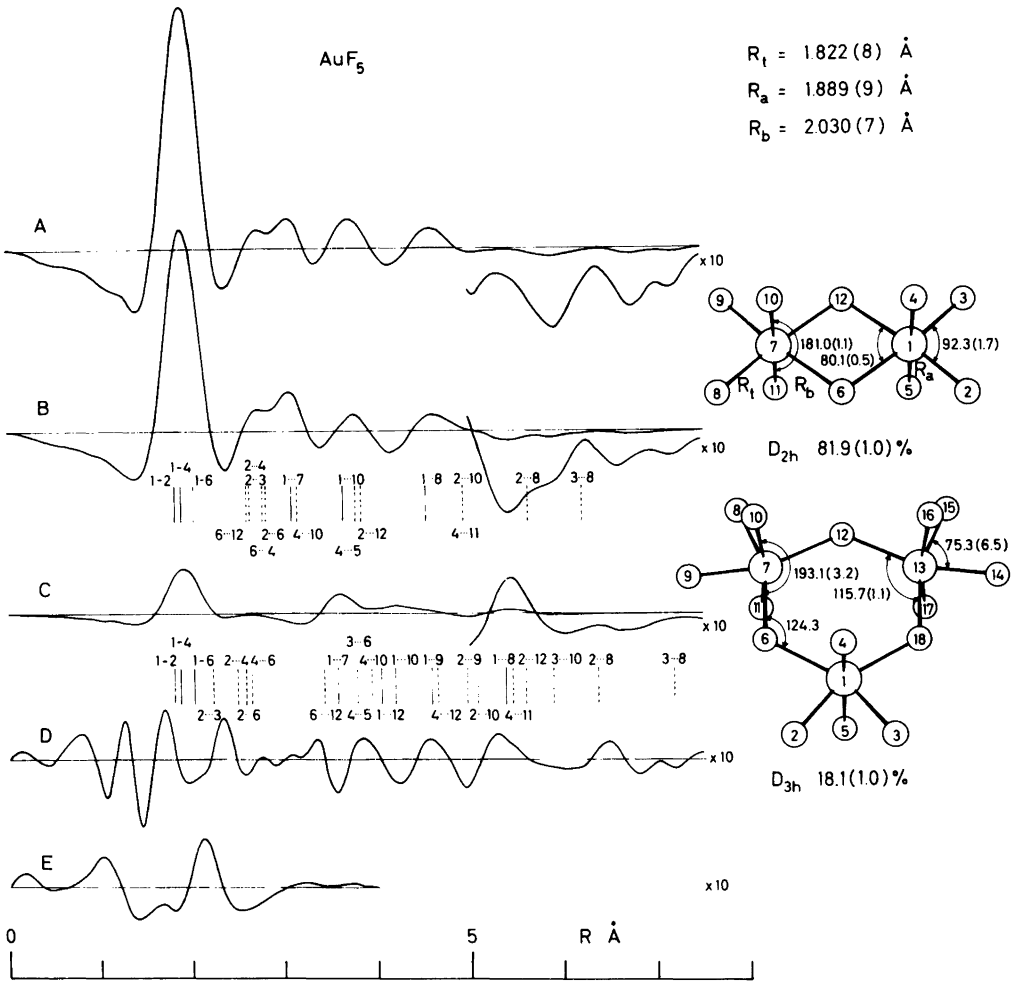

Fig. 1. A, B, C and *E* are radial distribution functions for gold pentafluoride for a damping function of exp $(-0.006s^2)$. Theoretical intensities were added inside $s=2$ Å^{-1} for the experimental function *A*. *B* and *C* are theoretical functions for 81.9 and 18.1 % of the dimer and trimer, respectively, according to the parameters of Table 3. The outer parts of the functions multiplied by a factor of 10 are also illustrated. *D* is the differences between the experimental and theoretical functions, $D=10(A-B-C)$, and *E* is the contribution from three atomic scattering from the dimer multiplied by 10, The different distances of the two forms are indicated with the F···F distances as broken lines.

electron diffraction distances according to the estimated *D*-values. The *u*-values were fixed on the estimated values, and a non-diagonal weighting matrix was applied.[14] The three elements of the correlation matrix with absolute values greater than 0.70 were the elements $\Delta R/R(\mathrm{Au-F_t})$ of −0.94, $R(\mathrm{Au-F_b})/\angle(\mathrm{F_b-Au-F_b})_{\mathrm{dimer}}$ of 0.91 and $R(\mathrm{Au-F_b}/\angle(\mathrm{F_b-Au-F_b})_{\mathrm{trimer}}$ of 0.73.

The theoretical intensities of the final least-squares refinement included contributions of three atomic scattering from the dimer according to the $\mathrm{ITP_2}$ approximation,[15] and the Fourier sine transformation of only these intensities is illustrated in Fig. 1. Leaving out these intensities, R_f increased to 4.85 % for the final parameters.

DISCUSSION

The agreement with the experimental data for the final least-squares refinement is satisfactory as shown by the *R*-factor of Table 3 and the difference curve D of Fig. 1. In the refinement the twelve independent parameters are determined from 168 points and the agreement should to some extent justify the different assumptions of the final refinement.

This agreement could not be obtained without including also a smaller amount of the trimeric form. An additional indication of the presence of this species is the small peak at about 5.4 Å of the experimental radial distribution function which is identified as the Au1···F8 distance of the trimer. The conclusion that gaseous gold pentafluoride at the applied temperature consists of mostly dimeric and a smaller amount of trimeric molecules should be reliable. However, the composition and structure of the two forms may be less accurately determined than indicated by the standard deviations due to uncertainties in the assumptions of the least-squares refinement.

This result for the composition is in agreement with the mass spectrometric investigation of gaseous gold pentafluoride at 85–90 °C.[13]

The axial distances of AuF_5 seem to be longer than the terminal ones, and the average value of 1.856 Å is the same as the corresponding average of $Xe_2F_{11}^+AuF_6^-$.[1b] For the trimeric pentafluorides of Nb and Sb no differences between these distances greater than one standard deviation could be determined while the value found in $(TaF_5)_3$ was 0.023(11) Å.

Assuming that the differences $R_a - R_t$ really are small in $(NbF_5)_3$ and $(SbF_5)_3$, the terminal distances of the four pentafluorides are all in the narrow range from 1.810(2) for NbF_5 to 1.823(5) Å for TaF_5. The bridged distance of 2.030(7) in AuF_5 may be significantly shorter than the $(TaF_5)_3$ value of 2.062(2) Å while these distances of $(NbF_5)_3$ and $(SbF_5)_3$ are in between the two values given.

The metal–metal distances of the three previously investigated trimeric pentafluorides were between 3.95 and 4.04 Å. The Au···Au distances of 3.107(5) Å in the dimer and of 3.589(12) Å of the trimer are significantly shorter. Accordingly, the F_b-Au-F_b angle in the trimer of 115.7(1.1)° is significantly greater than the other four F_b-M-F_b angles with values slightly above 80°.

The axial atoms in $(NbF_5)_3$, $(SbF_5)_3$ and $(TaF_5)_3$ all showed a significant displacement towards the symmetry axis of the ring. This distortion is not observed in the two forms of AuF_5. Here the results indicate that a distortion, if any, is in the opposite direction.

Except for the nonplanar six-membered ring of $(SbF_5)_3$, the structures of the three previously investigated pentafluorides were all very similar. As shown in this discussion, gold pentafluoride differs from these structures in several ways. The most significant difference, at least from an experimental point of view, is the much shorter metal–metal distance in $(AuF_5)_3$.

Acknowledgement. The authors wish to thank cand.real. Svein Samdal for making the background subtraction program applicable also to the *s M(s)* type of molecular intensities.

REFERENCES

1. a. Learly, K. and Bartlett, N. *Chem. Commun.* (1972) 903; b. Learly, K., Zalkin, A. and Bartlett, N. *Inorg. Chem. 13* (1974) 775.
2. Holloway, J. H. and Schrobilgen, G. J. *Chem. Comm.* (1975) 623.
3. a. Brunvoll, J., Ischenko, A. A., Miakshin, I. N., Romanov, G. V., Sokolov, V. B., Spiridonov, V. P. and Strand, T. G. *Acta Chem. Scand. A 33* (1979) 775; b. Brunvoll, J., Ischenko, A. A., Miakshin, I. N., Romanov, G. V., Spiridonov, V. P., Strand, T. G. and Sukhoverkhov, V. F. *Acta Chem. Scand. A 34* (1980) 733.
4. Sokolov, V. B., Prusakov, V. N., Rizkov, A. V., Drobishevski, Y. V. and Khoroshev, S. S. *Dokl. Akad. Nauk SSSR 229* (1976) 884 (in Russian).
5. Sokolov, V. B., Zinaev, V. G. and Rizkov, A. V. *Teor. Eksp. Khim. 16* (1980) 345 (in Russian).
6. Spiridonov, V. P. and Zasorin, E. Z. *Natl. Bur. Stand. Spec. Publ. 561, Proc. 10th Material Res. Symp. on Characterization of High Temperature Vapours and Gases*, NBS 1979.
7. Andersen, B., Seip, H. M., Strand, T. G. and Stølevik, R. *Acta Chem. Scand. 23* (1969) 3224.
8. a. Hedberg, L. *Abstr. 5th Austin Symp. Gas Phase Mol. Struct.*, Austin, Texas 1974, p. 37; b. Gundersen, G. and Samdal, S. *Private communication.*
9. Yates, A. C. *Comput. Phys. Commun. 2* (1971) 175.
10. Strand, T. G. and Bonham, R. A. *J. Chem. Phys. 40* (1964) 1686.
11. Bonham, R. A. and Schäfer, L. *International Tables for X-Ray Crystallography*, Kynoch Press, Birmingham 1974, Vol. 4.

12. Cyvin, S. J. *Molecular Structures and Vibrations*, Elsevier, Amsterdam 1972, p. 95.
13. Vasile, M. J., Richardson, T. J., Stevie, F. A. and Falconer, W. E. *J. Chem. Soc. Dalton Trans.* (1976) 351.
14. Seip, H. M., Strand, T. G. and Stølevik, R. *Chem. Phys. Lett. 3* (1969) 617.
15. Miller, B. R. and Bartell, L. S. *J. Chem. Phys. 72* (1980) 800.

Received March 30, 1982.

Acta Chemica Scandinavica A 36 (1982) 711–718

Tentative Assignments of Fundamental Vibrations of Thio- and Selenoamides. IX. The Influence of Metal Complex Formation on the Characteristic Thioamide Bands in 1,2-Dimethyl-3-pyrazolidinethione

U. ANTHONI,[a] G. BORCH[b] and P. H. NIELSEN[a]

[a] Chemical Laboratory II, The H. C. Ørsted Institute, DK-2100 Copenhagen, Denmark and
[b] Chemistry Department A, The Technical University of Denmark, DK-2800 Lyngby, Denmark

Compounds with a thioamide group often form complexes with metal halides by *S*-coordination. Usually the IR band with maximum CN stretching character moves towards higher frequencies while those with maximum CS stretching character are displaced towards lower frequencies. However, 1,2-dimethyl-3-pyrazolidinethione (DMPT) forms complexes of the type $(DMPT)_2ZnBr_2$, $DMPT \cdot CdI_2$, $(DMPT)_2CdI_2$ and $DMPT \cdot HgCl_2$ in which the frequencies of the CS bands are unchanged or displaced to higher frequencies on complex formation. The IR spectra of these compounds and five deuterated analogues of $DMPT \cdot HgCl_2$ were recorded in the region 4000–180 cm^{-1}. Normal coordinate analysis of $DMPT \cdot HgCl_2$ suggests that one of the reasons for the anomalous shift of the CS stretching bands is due to change in potential energy distribution induced by complex formation. Another reason is an increase in the force constant for CS stretching. From CNDO/2 calculations it is concluded that complex formation increases the weight of the π-character of the thiohydrazide group, $N^+=C-S^-$, with concomitant decrease in the force constant for CS stretching. In addition, the σ-electrons of the CS bond are polarised towards sulfur so as to give an increased σ-density in the CS-region. Apparently the latter effect is pronounced enough to result in an increase in the force constant for CS stretching. The results stress the importance of CNDO/2 calculations as a tool for obtaining qualitative understanding of the changes occurring in ligands on complex formation. An understanding of the importance of the polarisation of the σ-electrons of the CS bond by coordination with metal halides should facilitate future discussions on the structures of related compounds.

In the early study of Jensen and Nielsen[1] and in the review by Gosavi and Rao,[2] attention was drawn to the influence of metal complex formation on IR bands characteristic of the thioamide group. Since then a considerable number of papers have appeared on the subject, the most extensive being those by Devillanova and Verani *et al.* on thio- and selenoureas,[3] Pignedoli and Peyronel *et al.* on dithiobiuret,[4] Desseyn *et al.* on thioamides,[5] and by Kedzia *et al.* on mainly thiocarbazates and thiosemicarbazides.[6] It is generally assumed that *S*-coordination will tend to increase the weight of the canonical structure $N^+=C-S^-$, causing the force constant for νCN (CN stretching) to increase while that for νCS to decrease relative to the free ligand values. As a result, bands with νCN contributions will be displaced towards higher frequencies while bands with νCS character will be displaced to lower frequencies. *N*-coordination, as a first approximation, will have the opposite effects.

Aarts *et al.*[7–9] have pointed out that the frequency shifts of these bands on *S*-coordination may be absent or even occur in the opposite direction to that mentioned above. This was attributed principally to the changes in ligand potential energy distribution (PED) following *S*-coordination. Further, back-donation may occur from the metal ion to the empty sulfur d-orbitals or to low-lying anti-

0302-4377/82/090711-08$02.50

bonding states of the ligand, changing the electron density of the thioamide group. The stereochemistry adopted by the coordination compound[10] or the conformational changes in the ligand[11] (*e.g.* thiosemicarbazides,[12] dithiobiuret[13]) due to complex formation may result in large shifts of the *v*CN and *v*CS frequencies. However, the rules break down when simultaneous *N*,*S*-coordination occur.[14]

In order to assess the relative importance of these factors, reliable normal coordinate analyses (NCA's) of thioamide coordination compounds are needed. This requires that at least (i) the site of coordination (N and/or S) and the conformation of the ligand are known, (ii) the fundamentals are identified, and (iii) the force field is determined by a least-squares iterative procedure for both the ligand and the complex. For example, the force constant for *v*CN increases strongly in *S*-coordinated thioacetamide,[15] but the band with maximum *v*CN character exhibits only a negligible shift. The anomalous small shift can therefore be attributed unambigously to changes in PED following complex formation in this case. Similar investigations have not been reported for metal complexes of thioamides with anomalous shifts of *v*CS bands.

The vibrational spectra of the thiohydrazide 1,2-dimethyl-3-pyrazolidinethione (DMPT) have previously[16] been thoroughly examined. In the coordination complexes of DMPT, $(DMPT)_2ZnBr_2$, $DMPT \cdot CdI_2$, $(DMPT)_2CdI_2$ and $DMPT \cdot HgCl_2$, the *v*CS bands show only very small shifts either towards higher or towards lower frequencies. Since the IR spectra of these coordination compounds are almost identical, $DMPT \cdot HgCl_2$ was selected for closer investigation of the anomalously small CS shift. To eliminate errors and gather sufficient material for the NCA, we have prepared the following deuterated derivatives (*cf.* Ref. 16): (DMPT-1-d_3)$HgCl_2$, (DMPT-2-d_3)$HgCl_2$, (DMPT-d_4)$HgCl_2$, (DMPT-d_6)$HgCl_2$ and (DMPT-d_{10})-$HgCl_2$. The results of the NCA are discussed in relation to the changes in electron density calculated by the CNDO/2 method.

EXPERIMENTAL

The coordination compounds $(DMPT)_2ZnBr_2$, $(DMPT)_2CdI_2$ and $DMPT \cdot HgCl_2$ were prepared by addition of an ethanolic solution of the ligand to a saturated ethanolic solution of the metal halides. $DMPT \cdot CdI_2$ was prepared similarly from a saturated aqueous solution of CdI_2. The solid products were freed from metal halides and ligands by washing with the solvent and drying *in vacuo*. Elemental analysis indicated the crude products to be analytically pure and they were used directly for recording the IR spectra without further purification. The solid state spectra were recorded on a Perkin-Elmer model 580 spectrometer in the range $4000-180$ cm^{-1} in KBr and/or CsI discs. The spectrum of $(DMPT)_2CdI_2$ in $CHCl_3$ and $CDCl_3$ solution was obtained from saturated solutions in KBr cells of 1 mm thickness. The bands in the low-frequency region sensitive to the halide ion were assumed to originate mainly in vibrations involving the metal halide (Table 2).

NORMAL COORDINATE ANALYSIS

The IR spectra of the four coordination compounds of DMPT (Table 2) are almost identical except in the region below 400 cm^{-1} where vibrations due to the metal-ligand bonds and the metal halide are expected to occur. This indicates (i) that ligand vibrations do not couple significantly with the metal halide vibrations in the range $400-4000$ cm^{-1}, (ii) that the ligand spectrum is largely unaffected by the composition (1:1 or 2:1), the symmetry, the crystal structure, and the state of the complex, and (iii) that Zn, Cd and Hg halides coordinate to the same atom(s) of the ligand. These results justify the comparison of the IR results for solid $DMPT \cdot HgCl_2$ with CNDO/2 calculations on a DMPT complex with $ZnBr_2$. Since we were interested only in the influence of complex formation upon the thiohydrazide bands we did not perform a full NCA including the metal halide molecule. Instead we used the calculations reported previously for DMPT[16] and simply replaced the observed fundamentals with the corresponding values for $DMPT \cdot HgCl_2$ and the five deuterated compounds. On the basis of X-ray results for related compounds[17-19] the geometry of DMPT has been assumed to be unchanged upon S-coordination. In summary, a perturbational treatment of the changes in the IR spectrum of DMPT on complex formation is considered adequate for the range $400-4000$ cm^{-1}. From Table 2 it is seen that this approximation is liable to fail only in the case of the force constant for the CS in-plane deformation, which is largely determined by the position of the fundamental ν_{43} below 400 cm^{-1}.

The zeroth order values of the force constants were transferred directly from DMPT.[16] As previ-

Table 1. Valence force constants for DMPT · $HgCl_2$ compared with the values for DMPT.[a]

Symbol	DMPT · $HgCl_2$	DMPT	Symbol	DMPT · $HgCl_2$	DMPT
	CH_3/CH'_3			*Ring*	
K_r	4.76	4.72	K_D	3.85	3.76
F_{rr}	0.01	0.01	K_{L_2}	3.59	3.88
H_α	0.51	0.51	K_{L_1}	4.71	4.59
H_β	0.82	0.76	K_{B_1}	3.77	3.97
F_β	−0.04	−0.04	K_A	5.56	5.35
K'_r	4.77	4.80	K_{B_2}	8.56	7.51
F'_{rr}	−0.08	−0.13	K_{P_1}	4.48	4.64
H'_α	0.51	0.51	K_{P_2}	5.07	5.07
H'_β	0.76	0.72	H_{μ_1}	0.41	0.58
F'_β	−0.03	−0.03	H_{μ_2}	1.59	1.77
	CH_2		H_{μ_3}	0.79	0.82
K_d	4.71	4.80	$H_{\varepsilon_1}=H_{\varepsilon_2}$	1.40	1.27
F_{dd}	0.04	0.03	$H_{\theta_1}=H_{\theta_2}$	2.65	2.42
f'_γ	0.05	0.06	$H_{\varepsilon_3}=H_{\theta_3}$	0.68	0.75
F'_γ	0.08	0.08	H_Δ	0.34	0.35
H_{δ_2}	0.48	0.47	$F_{D\mu_1}=F_{D\mu_2}$	0.55	0.42
$H_{\gamma_3}=H_{\gamma_4}$	0.54	0.59	$F_{L_1\gamma_1}$ *etc.*	0.35	0.35
$H_{\gamma_3^o}=H_{\gamma_4^o}$	0.69	0.69	$F_{L_2w_2}$ *etc.*	0.76	0.74
$F_{\gamma_3\gamma_4}$	−0.31	−0.32	$F_{P_1\beta}=F_{P_2\beta}$	0.65	0.66
$F_{\gamma_3^o\gamma_4^o}$	0.07	0.08			
H_{δ_1}	0.41	0.43			
$H_{\gamma_1}=H_{\gamma_2}$	0.78	0.78			
$H_{\gamma_1^o}=H_{\gamma_2^o}$	0.69	0.66			
$F_{\gamma_1\gamma_2}$	−0.21	−0.14			
$F_{\gamma_1^o\gamma_2^o}$	0.12	0.09			

[a] For interpretation of symbols, units, and force field for DMPT, see Ref. 15. The values of H_τ, F_{DL_2}, F_{DB_2}, $F_{B_2\mu_2}$, $F_{B_2\mu_3}$, $F_{L_2\mu_3}=F_{A\varepsilon_3}$, H_ω, and F_ω are the values of DMPT (see text).

ously, the interaction constants F_{DL_2}, F_{DB_2}, $F_{B_2\mu_2}$ and $F_{B_2\mu_3}$ were fixed. The values of H_τ, H_w and F_w are mainly determined by the fundamentals below 180 cm^{-1}, the position of which have not been recorded for the coordination compounds. Since these force constants can hardly be expected to vary to a significant degree on complex formation they were likewise equated to the values found for DMPT. Inspection of the correlation matrix indicated $F_{L_2\mu_3}=F_{A\varepsilon_3}$ to be highly correlated and therefore they were also transferred from DMPT. A simultaneous least-squares adjustment was then made for DMPT·$HgCl_2$ and its deuterated derivatives. By fitting the remaining 43 force constants to *ca.* 250 observed frequencies, the final set (reported in Table 1) was obtained. The force constants pertaining to the CH_3, CH'_3 and CH_2-CH_2 groups show only small changes. This result supports the expectation that complex formation does not notably influence these parts of the DMPT molecule. The most important changes are observed in the force constants of the thiohydrazide skeleton (N−N−C−S). The force constants for CS in-plane and out-of-plane deformations (H_{μ_1}, H_{μ_2}, H_Δ) decrease on complex formation. This is related to the lowering of ν_{38}, ν_{40} and ν_{43} frequencies which originate to a considerable degree in these modes (Table 2). The upward trends in ν_{11}, ν_{20} and ν_{39} frequencies reflect to a large degree the increase in the force constants for νCS (from 3.76 to 3.85

Table 2. IR spectra (cm^{-1}) of metal complexes $(DMPT)_2ZnBr_2$, $DMPT \cdot CdI_2$, $(DMPT)_2CdI_2$ and $DMPT \cdot HgCl_2$ of 1,2-dimethyl-3-pyrazolidinethione (DMPT). Calculated frequencies, tentative assignments, description of the fundamentals and frequency shift relative to DMPT for the complex $DMPT \cdot HgCl_2$.[a]

$(DMPT)_2ZnBr_2$	$DMPT \cdot CdI_2$	$(DMPT)_2CdI_2$				$DMPT \cdot HgCl_2$				
Observed IR, disc[b]	Observed IR, disc[b]	Observed, IR		DMPT-shift[d]		Observed IR, disc[b]	Calc.[e]	DMPT-shift[d]		Assignment and description (PED, %)[f]
		disc[b]	solution[c]	solid	solut.			obs.	calc.	
2991m	3002m	3003m	3008m	+18	+15	3000m	3001	+15	+13	ν_1, $\nu_{as}CH_3(99)$
							2998	+15	+13	ν_2, $\nu_{as}CH_3(99)$
2971m	2988m 2977m	2987m 2973m	2980m		+15	2971m	2976	+10	+9	ν_3, $\nu_{as}CH'_3(99)$
							2972	+10	+8	ν_4, $\nu_{as}CH'_3(99)$
		2960vw,sh	2965w,sh			2968m,sh	2968	−17	−3	ν_5, $\nu_{as}CH_2(99)$
		2940vw,sh	2945vw,sh	(−21)	(−20)	2949w,sh	2954	−12	−4	ν_6, $\nu_{as}CH_2(99)$
2935w,sh	2935w,sh	2931w,sh	2940w,sh			2931w,sh	2928	+1	−1	ν_7, $\nu_sCH'_3(98)$
							2927	+1	−3	ν_8, $\nu_sCH_2(97)$
2914m	2908m	2908m	2920m	−7	+4	2913m	2915	−2	−3	ν_9, $\nu_sCH_2(99)$
2858m	2867m 2857m	2870w,sh 2861m	2878m	(+9)	+18	2869m	2867	+17	+5	ν_{10}, $\nu_sCH_3(100)$
1560vs,br	1560vs,br	1562vs,br	1550vs,br	+62	+57	1571vs,br	1565	+71	+67	ν_{11}, **$\nu C^3N(81)$**, $\delta_{as}CH'_3(7)$
1459ms	1462m,sh	1461m,sh	1467m,sh	+1	+1	1462m,sh	1462	+2	−3	ν_{12}, $\delta_{as}CH'_3(41)$, $\delta_{as}CH_3(32)$, $\delta CH_2(17)$
1450m,sh	1450ms	1446ms	1454ms	−3	0	1450ms	1457	+1	−2	ν_{13}, $\delta_{as}CH_3(57)$, $\delta_{as}CH'_3(27)$
			1448w,sh		0		1453	+1	−2	ν_{14}, $\delta_{as}CH_3(99)$
1440vw,sh		1438w,sh				1430w	1439	−10	−4	ν_{15}, $\delta_{as}CH'_3(87)$
		1432w,sh					1431	−10	0	ν_{16}, $\delta_{as}CH'_3(15)$, $\delta CH_2(67)$
1420ms	1420ms	1421ms	1418ms	0		1420m,sh	1421	(+4)	+6	ν_{17}, $\delta_sCH_3(68)$, $\delta CH_2(26)$
1416m,sh	1412m,sh	1416w,sh				1413ms	1411	(−9)	−10	ν_{18}, $\delta CH_2(63)$, $\delta_sCH_3(25)$
1389m	1396m	1399m	1401m	+10	+10	1395m	1397	+6	+6	ν_{19}, $\delta_sCH'_3(99)$
1349w	1352w,sh	1354w,sh	1350mw	+6	+6	1354w				
1340w	1347ms	1346ms				1348w	1353	+10	+6	ν_{20}, **$\nu NN(29)$**, ν/δring(54) and $\nu_{34}+\nu_{37}$
1318s	1319s	1319s	1319s	+6	+6	1318s	1324	+5	+7	ν_{21}, $tCH_2(68)$, $\omega CH_2(26)$
		1308w,sh				1308w,sh	1314	+1	+5	ν_{22}, $\omega CH_2(26)$, νring(34), δring (24)
1260w,sh	1253w	1265vw,sh	1260m			1262vw,sh				$\nu_{33}+\nu_{41}$
1246m	1244m	1244m	1248m	−5	+1	1249m		0		$\nu_{35}+\nu_{37}$
1235m,sh	1233mw	1235m,sh	1238w,sh	+4	+5	1233mw	1238	+2	+5	ν_{23}, ν/δring(43), $\omega/tCH_2(35)$, $\rho CH_3(29)$
1192s	1195s	1195s	1193s	+8	+8	1193s	1204	+6	+6	ν_{24}, $tCH_2(37)$, $\omega CH_2(18)$, $\rho CH_3(22)$
1185s,sh						1178m,sh	1164	+2	−4	ν_{25}, $\rho CH_3(56)$, νring(20), $\omega/tCH_2(25)$
1130vs	1133vs	1130vs	1133vs	0	0	1130vs		0		
1115m,sh	1115m,sh	1118s				1120s,sh	1137	+9	0	ν_{26}, $\rho CH_3(30)$, νring(41) and $\nu_{36}+\nu_{38}$

Table 2. Continued.

1092m	1094m	1096m	1098m	+2	+3	1091w	1101	−3	−1	ν_{27}, $\rho CH'_3$(96)
1078m	1080m	1080m	1080mw	+4	+4	1076m	1084	0	−2	ν_{28}, ν_{as}**NCS(13)**, $\rho CH'_3$(41), ν/δring(37)
1063w,sh	1062vw,sh 1048w,sh	1059w,sh	1068w,sh 1049w	0			1063		+3	ν_{29}, νCC(43), ρCH_2(30)
1043w	1042w	1042w	1039vw	−3	−4	1043w	1037	−2	−9	ν_{30}, ν_{as}**NCS(8)**, νring(49), $\rho CH'_3$(24)
1009m	1008m	1010m	1008m	+4	+4	1007m	997	+1 +6	+1	ν_{31}, ρCH_2(64), νCC(16) and $2 \cdot \nu_{38}$
980w	970w	968vw	968w	−2	−3	976vvw				
942m	944m	945m	946m	+3	+6	947m	944	+5 +11	−5	ν_{32}, ρCH_2(59), ν**NN(7)**, νring(24) and $\nu_{37}+\nu_{38}$
930w,sh	932vw,sh	932w,sh				939m				
880m	885m	887m	(890m)	−6	(−1)	882m	899	−11	−5	ν_{33}, ν**NN(15)**), ν**CS(6)**, νring(39), ρCH_2(19)
787m	785m	789m	–			780m	794	−9	−6	ν_{34}, ν**CS(43)**, ν**NN(6)**, ν/δring(60)
688mw	689mw	690mw	–			690mw	694	0	+3	ν_{35}, νC^3N**(8)**, νring(21), δring(54)
638w	635w	640vw	(641w)	0		639w	634	−1 −2	−4	ν_{36}, ν**NN(13)**, ν/δring(100) and $\nu_{39}+\nu_{45}$
592mw	595mw	598mw	600w	0	+1	596mw				
547m	543m	550m	550mw	+2	+8	553m	562	+5 −7	+9	ν_{37}, $\Delta CH_3-N<$(58), νring(23) and $\nu_{42}+\nu_{45}$
515vw	515vw	515vw	518w	−7	+1	515vw				
490m	490m	490m	491m	−1	+4	488m	487	−3	−3	ν_{38}, Δ**CS(23)**, $\Delta CH_3-N<$(26), νring(18)
434m	436ms	435ms	437m	+5	+5	436m	433	+6	+4	ν_{39}, ν**CS(23)**, ν**NN(13)**, Δ**CS(18)**, δring(32)
416m	410m	418m	420ms	−4	−3	413m	414	−9	−7	ν_{40}, Δ**CS(34)**, ν**NCS(16)**, $\Delta CH_3-N<$(43), νring
378vw	375w,sh	378vw		+2		379vw	378	+3	0	ν_{41}, ν/δring(59), ρCH_2(46)
356m	360m	358m	358m			359mw				DMPT-metal halide
	340w,sh	340w,sh	338vw,sh	−10	−11	340m	335	−10	−3	ν_{42}, $\delta CH_3-N</CH'_3-N<$(43), ν/δring(74)
320m	318m	310m	310m			282mw				DMPT-metal halide
248w,sh		255vw,sh		−15		255w,sh	251	−15	−17	ν_{43}, δ**CS(72)**, $\delta CH'_3-N<$(17)
220m	230m	229m				238m				DMPT-metal halide
200m		200vw					199		−3	ν_{44}, $\tau CH'_3$(69)
							170		−1	ν_{45}, τCH_3(91)
							114		−4	ν_{46}, δring
							68		+1	ν_{47}, δring
							21		−1	ν_{48}, δring

[a] The following abbreviations have been used: s, strong; m, medium; w, weak; br, broad; sh, shoulder. Weak and very weak bands not assigned to fundamentals have in many instances been omitted from the table. [b] Best values from KBr/CsI discs. [c] From spectra run in $CHCl_3$ and $CDCl_3$ solutions. [d] Shifts of corresponding bands from DMPT to complex compound in the IR spectra. Approximate values are given in parentheses. The values in bold types are considered significant. [e] Iteration based upon all six isotopic species of DMPT·$HgCl_2$. [f] Abbreviations: ν = stretch; δ = deformation; Δ = out-of-plane deformation; ρ = rock; ω = wag; t = twist; τ = torsion; s = symmetric; as = antisymmetric. Vibrations of the pyrazolidine ring and the attached carbon atoms are designated 'ring' or using the following nomenclature: N^1-CH_3, $N^2-CH'_3$, C^3S. Vibrations believed to originate mainly in the metal halide are designated DMPT-metal halide. The potential energy distribution (PED, $x_{ik} = 100F_{ij}L^2_{ik}/\lambda_k$) is stated only for significant contributions. The PED referring to the thiohydrazide group is given in bold types.

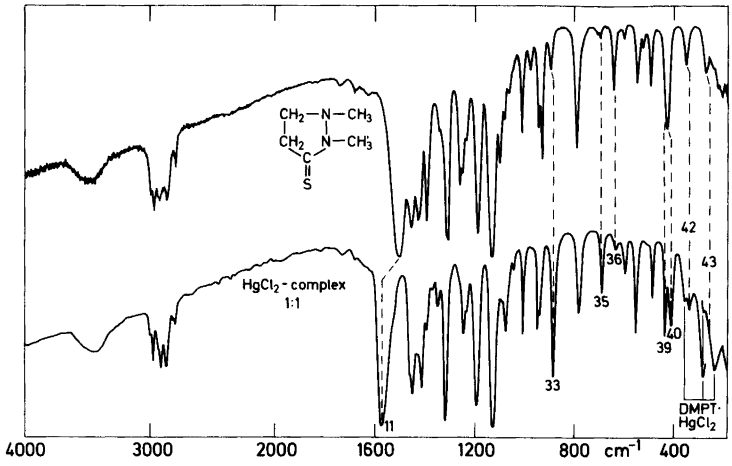

Fig. 1. The IR spectra of 1,2-dimethyl-3-pyrazolidinethione in the liquid state (upper) and the mercury(II) chloride complex in the solid state (lower). Corresponding bands are indicated by dotted lines. The three bands below 400 cm^{-1} (believed to originate from the coordinated $HgCl_2$) are indicated as DMPT·$HgCl_2$.

mdyn/Å), νCN (from 7.51 to 8.56 mdyn/Å) and νNN (from 5.35 to 5.56 mdyn/Å). The force constants for three of the bonds adjacent to the N–N–C–S grouping (K_{L_2}, K_{B_1} and K_{P_1}) decrease on complex formation. This feature appears to be indirectly connected with the decrease in ν_{33}.

RESULTS AND DISCUSSION

The IR spectra of DMPT (liquid) and DMPT · $HgCl_2$ (solid) are compared in Fig. 1. Some of the more important shifts and some shifts which are difficult to observe are indicated with dotted lines. The bands which are believed to originate mainly in vibrations of the coordinated metal halide (below 400 cm^{-1}) have also been indicated on Fig. 1. The frequencies of the vibrational modes of interest are listed in Table 2 in a manner similar to that used for DMPT [16] and the selenium analogue (DMPS) [20] in previous papers in this series. The complete list of the frequencies observed for the isotopic derivatives has been omitted to save space. Generally speaking, the frequencies listed for DMPT · $HgCl_2$ in Table 2 are similar to those of DMPT.[16] Therefore, a systematic description of the spectra can be dispensed with, and the discussion will be restricted to some features of general interest.

In the present context, *i.e.* when the IR spectrum of DMPT · $HgCl_2$ is treated as a perturbed spectrum of DMPT, the following theoretical framework seems appropriate (*cf.* DMPS [20]). Coordination of DMPT involves (i) geometrical change, which is probably small, and (ii) a change in force field due to electronic and steric effects of the metal halide. The complex formation results in (i) a change in position of bands, ν(DMPT · $HgCl_2$) – ν(DMPT) (DMPT-shift in Table 2), (ii) a change in PED of the normal vibrations; and as long as the changes are small we will make use of corresponding bands in DMPT and DMPT · $HgCl_2$, *i.e.* the concept of group frequencies will be applied, (iii) a partial breakdown of the perturbational treatment below 400 cm^{-1} due to coupling effects between DMPT and the metal halide, (iv) changes in intensity and profile of the bands especially as a result of different Fermi interactions with overtones and combination modes.

From the spectra shown in Fig. 1 it appears that there is a close correspondence between DMPT and DMPT · $HgCl_2$ with the following reservations. Firstly, strong intensity changes may occur as in ν_{35}, for example due to the different symmetry of the coordination compounds. Secondly, an intensity reversal may occur between a fundamental and the accompanying Fermi-enhanced combination mode (*e.g.* ν_{36} followed by $\nu_{39}+\nu_{45}$ at slightly lower frequency). Thirdly, some bands which by virtue of their position, form, and intensity seem to be corresponding, have nevertheless quite different PED's (*e.g.* ν_{17} and ν_{18} have interchanged positions, ν_{39} has an increased contribution from ΔCS).

All these complications have been described in some detail in the previous paper[20] and will not be discussed further here.

In qualitative discussions of the vibrational spectra of coordination compounds it is usually assumed that once the above correspondence with the spectrum of the free ligand has been established, the bands which show a frequency shift have important contributions from vibrations of the parts of the ligand involved in complex formation. This assumption is not correct, as can be seen from a comparison of the results in Table 2 with those reported for DMPT.[16] The fundamentals ν_{21} and ν_{24}, for example, display small but definite shifts towards higher frequencies. Nevertheless, the NCA reveals that the shifts arise merely from a change in PED of vibrations of the CH_2 and CH_3 groups. As a matter of fact, most of the shifts observed on complex formation of DMPT are 10 cm^{-1} or less, and without the results of the NCA it would be extremely difficult to locate the contributions from the thiohydrazide group. These results also explain the problems encountered by Devillanova and Verani[21] in identifying the thioamide bands in heterocyclic thiones by complex formation with $CdCl_2$.

The fundamental ν_{11} of DMPT, mainly due to the C^3N stretching vibration, is displaced by 60–70 cm^{-1} towards higher frequencies on complex formation. We therefore expect ν_{34} and ν_{39}, with the highest contributions from CS stretching to shift towards lower frequencies. Nevertheless, ν_{34} shows a downwards shift by only 0–9 cm^{-1} and ν_{39} even shifts 4–6 cm^{-1} towards higher frequencies. The results of the NCA leaves no doubt that one of the reasons for the anomalous shifts of these bands stems from a change in PED. By comparison of the last column in Table 2 with the results published previously for DMPT we can estimate the changes in the composition of the bands following conversion of DMPT · $HgCl_2$. It is seen that the PED of ν_{34} shows an increased contribution from νCS (from 31 to 43 %) at the expense of ring stretching and deformation vibrations. By contrast, the νCS contribution of ν_{39} decreases from 32 to 23 % while ΔCS increases from 4 to 18 %.

However, the NCA also indicates the force constant for CS stretching to increase from 3.76 to 3.85 mdyn/Å. Even if we take all possible errors into account we may safely state that the anomalous shifts of these bands are partly due to the fact that the force constant for CS stretching does not decrease as expected. The reason must be found in the electronic displacements following complex formation, since the phenomenon is observed (Table 2) in Zn, Cd and Hg complexes with different stoichiometry and structure[19] and both in the solid state and in solution. As the metals in question do not have external d-electrons readily available for back-donation to DMPT such an explanation seems excluded.

The possibility remains that the electronic redistribution induced in DMPT on complex formation does not correspond to an increased weight of the structure $N^+=C-S^-$ but is rather associated with an increased electronic density of both the NC and the CS bond. We therefore calculated the electronic density for DMPT and the (hypothetical) complex DMPT · $ZnBr_2$ · H_2O (with the water molecule added in order to retain the tetrahedral structure around Zn) by the CNDO/2 method. The available program did not permit calculations on *e.g.* $(DMPT)_2ZnBr_2$ or DMPT · $HgCl_2$, but there are no grounds for believing that such calculations would significantly alter the conclusions. The principal changes (Fig. 2) are that a density of 0.51e is removed from DMPT mainly from the hydrogen atoms of the CH_2/CH_3 groups (0.15e) and the sulfur atom (0.30e). The Zn–S bond is mainly of the donor-acceptor type and is established between the vacant orbitals of the metal cation and one of the lone-pairs of sulfur (*i.e.* a σ-bond relative to the NCS group of DMPT since the zinc atom is assumed to lie in the NCS plane). In addition weak π-bonding arises as a result of electron donation from the p_π- and d_π-orbitals of sulfur to those of zinc. The calculated bond order and electron density contributions from the individual atomic orbitals show, in line with classical theory, that the electron-deficient sulfur atom induces a change in the π-density of the NCS group corresponding to an increased weight of the structures $N^+=C-S^-$

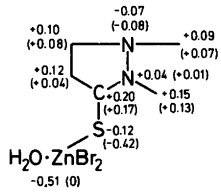

Fig. 2. The CNDO/2 charge density for DMPT · $ZnBr_2$ · H_2O and, in parentheses, for DMPT.

and $C^+ - S^-$, *i.e.* the π-density (and force constant) of the CN bond increases while the π-density (and force constant) of the CS bond decreases. However, in addition to the changes predicted by classical theory, the CNDO/2 calculations also reveal a change in the σ-density of the NCS group. The electron-deficient sulfur atom polarises the CS bond with the result that σ-density is removed from the carbon atom and transferred to the region closer to sulfur with subsequent increase in the σ-bond order (and force constant) of the CS bond. In summary, the changes in the thiohydrazide group amount to an increased strength of the NC bond, while the CS bond (with a decrease in π-density but an increase in σ-density) does not necessarily become weaker on complex formation but may very well be unchanged or become stronger as indicated by the results of the NCA.

Acknowledgement. This research was supported by grants from the Danish Natural Science Research Council.

REFERENCES

1. Jensen, K. A. and Nielsen, P. H. *Acta Chem. Scand. 20* (1966) 597.
2. Gosavi, R. K. and Rao, C. N. R. *J. Inorg. Nucl. Chem. 29* (1967) 1937.
3. Devillanova, F. A. and Verani, G. *J. Inorg. Nucl. Chem. 42* (1980) 623 and references therein.
4. Malavasi, W., Pignedoli, A. and Peyronel, G. *Inorg. Nucl. Chem. Lett. 17* (1981) 101; *Spectrochim. Acta A 37* (1981) 663 and references therein.
5. Desseyn, H. O., Aarts, A. J. and Herman, M. A. *Spectrochim. Acta A 36* (1980) 59 and references therein.
6. Zabokrzycka, A. and Kedzia, B. B. *Bull. Acad. Pol. Sci. Ser. Sci. Chim. 17* (1979) 390 and previous papers in this journal.
7. Aarts, A. J., Desseyn, H. O. and Herman, M. A. *Bull. Soc. Chim. Belg. 85* (1976) 854.
8. Aarts, A. J., Desseyn, H. O. and Herman, M. A. *Bull. Soc. Chim. Belg. 86* (1977) 581.
9. Aarts, A. J., Desseyn, H. O. and Herman, M. A. *Inorg. Chim. Acta 29* (1978) L 197.
10. Manogaran, S. and Sathyanarayana, D. N. *Bull. Soc. Chim. Belg. 90* (1981) 427.
11. Volka, K. and Holzbecher, Z. *Collect Czech. Chem. Commun. 34* (1969) 1353.
12. Geetherani, K. and Sathyanarayana, D. N. *Aust. J. Chem. 30* (1977) 1617.
13. Ray, A. and Sathyanarayana, D. N. *Spectrochim. Acta A 31* (1975) 899.
14. Singh, B. and Singh, R. D. *J. Inorg. Nucl. Chem. 39* (1977) 25.
15. Kharitonov, Y. Y., Tsivadze, A. Y., Smirnov, A. N. and Tsintsadze, G. V. *Sov. J. Coord. Chem. (Engl. Transl.) 1* (1975) 528.
16. Anthoni, U., Borch, G., Klæboe, P., Lerstrup, K. and Nielsen, P. H. *Acta Chem. Scand. A 35* (1981) 767.
17. Bonamico, M., Dessy, G., Fares, V. and Scaramuzza, L. *J. Chem. Soc. A* (1971) 3195.
18. Vega, R., Lopez-Castro, A. and Marquez, R. *Acta Crystallogr. B 34* (1978) 2297.
19. Rolies, M. M. and De Ranter, C. J. *Acta Crystallogr. B 34* 3216.
20. Anthoni, U., Borch, G., Klæboe, P. and Nielsen, P. H. *Acta Chem. Scand. A 36* (1982) 69.
21. Devillanova, F. A. and Verani, G. *Aust. J. Chem. 33* (1980) 279.

Received February 23, 1982.

Acta Chemica Scandinavica A 36 (1982) 719–733

The Conformation and Vibrational Spectra of Cyano- and Isocyanocyclohexane

T. WOLDBÆK, A. BERKESSEL, A. HORN and P. KLÆBOE

Department of Chemistry, University of Oslo, Oslo 3, Norway

The IR spectra of cyano- and isocyanocyclohexane as liquids and as amorphous, plastic and crystalline solids at low temperatures were recorded in the region 4000 – 50 cm^{-1}. High pressure (0 – 40 kbar) IR spectra of the neat samples were obtained in a diamond anvil cell at ambient temperature, and the dichroism of oriented crystalline high pressure crystals was measured. Raman spectra of the liquids, including polarization measurements, and of various low temperature solid phases were recorded.

Both compounds form a mixture of equatorial and axial conformers in the liquid state with nearly equal abundance of the two conformers. Unlike other monosubstituted cyclohexanes, cyanocyclohexane exists as *a*-conformer in the low temperature and high pressure crystals. Isocyanocyclohexane crystallizes in the *a*-conformation at high pressure, whereas both conformers were present in the low temperature solid phases. Plastic phases, with equilibria of *e* and *a* conformers, were observed for both molecules at low temperature as well as under high pressure.

A normal coordinate analysis was carried out for the two molecules, using a constrained valence force field analogous to the one derived for the *trans*-1,4-dihalocyclohexanes. Tentative assignments of the fundamentals belonging to both the *e* and *a* conformers are presented and compared with the results from the normal coordinate analysis.

The conformational equilibria of cyanocyclohexane (cyclohexanecarbonitrile, hereafter abbreviated CCN) and isocyanocyclohexane (CNC) have been carefully studied in solution by proton,[1-3] ^{13}C[4-6] and lanthanide-induced[7] NMR spectroscopy and by equilibration[8,9] technique. The more recent of these studies[6] reveal ΔG° values equal to 0.214 (178 K) and 0.190 kcal/mol (180 K) for CCN and CNC, respectively. These values are the lowest for 22 monosubstituted cyclohexanes studied except for cyclohexaneisocyanate[6] ($\Delta G^\circ = 0.206$ kcal/mol). Unlike other monosubstituted cyclohexanes the equatorial and axial conformers of these compounds are therefore of nearly the same abundance at coalescence temperature (for CCN the *e*-conformer is determined to be of $54.5 \pm 3.1\%$ abundance[7] at 303 K in CCl_4).

Some years ago we studied CCN by IR and Raman technique with special emphasis on the solid state.[10] To our surprise the high pressure crystal consisted of molecules in the axial conformer whereas complete crystallization at low temperature was not achieved.

Later a systematic study of six *trans*-1,4-dihalocyclohexanes[11,12] was completed by means of vibrational spectroscopy. The equatorial and axial conformers of these molecules were separately obtained in the solid state, the spectra interpreted in detail and an extensive force[13] field was developed by the overlay technique. The force constants were transferred with negligible adjustments to the four monohalocyclohexanes[14,15] and to *trans*-1,4-dicyanocyclohexane.[16] It was decided to extend these studies to CCN and to CNC. New vibrational spectra for CCN were recorded in an extended frequency range. Corresponding data were measured for CNC which, apart from an IR survey spectrum,[17] to our knowledge has not previously been studied by vibrational spectroscopy. Our results for both compounds will be given here, while ethynylcyclohexane ($C_6H_{11}C \equiv C-H$) which is isoelectronic with CCN and CNC will be treated in a forthcoming paper.[18]

0302-4377/82/090719-15$02.50

EXPERIMENTAL

The samples of CCN and CNC were commercial products from Fluka and ICN, respectively. They were purified by fractional distillation under reduced pressure, and gas chromatographic analysis showed both to be better than 99% pure.

The IR spectra were recorded on a Perkin-Elmer model 225 spectrometer (4000 – 200 cm^{-1}) and on an evacuable fast scan Fourier transform spectrometer (Bruker 114 C) (4000 – 50 cm^{-1}). Raman spectra were obtained with a modified[19] Cary 81 spectrometer, excited by a CRL model 52 G argon ion laser, using the 4880 and 5145 Å lines.

Conventional IR cells for liquids and solutions were employed, having windows of KBr, CsI and polyethylene. Cryostats cooled by liquid nitrogen with windows of CsI and polyethylene were used in IR; a cooled copper plate was employed for the Raman studies. The temperatures were measured with iron-constantane thermocouples. The high pressure solids were studied in a diamond anvil cell with type II diamonds having spacers of brass and steel coupled to a P.-E. 4× beam condenser.

The various high pressure solid phases were carefully inspected with a polarization microscope and the spectra mostly recorded with the P.-E. 225 equipped with a polarizer. Far IR and mid IR high pressure spectra at better resolution (2 cm^{-1}) were recorded with the Fourier transform spectrometer.

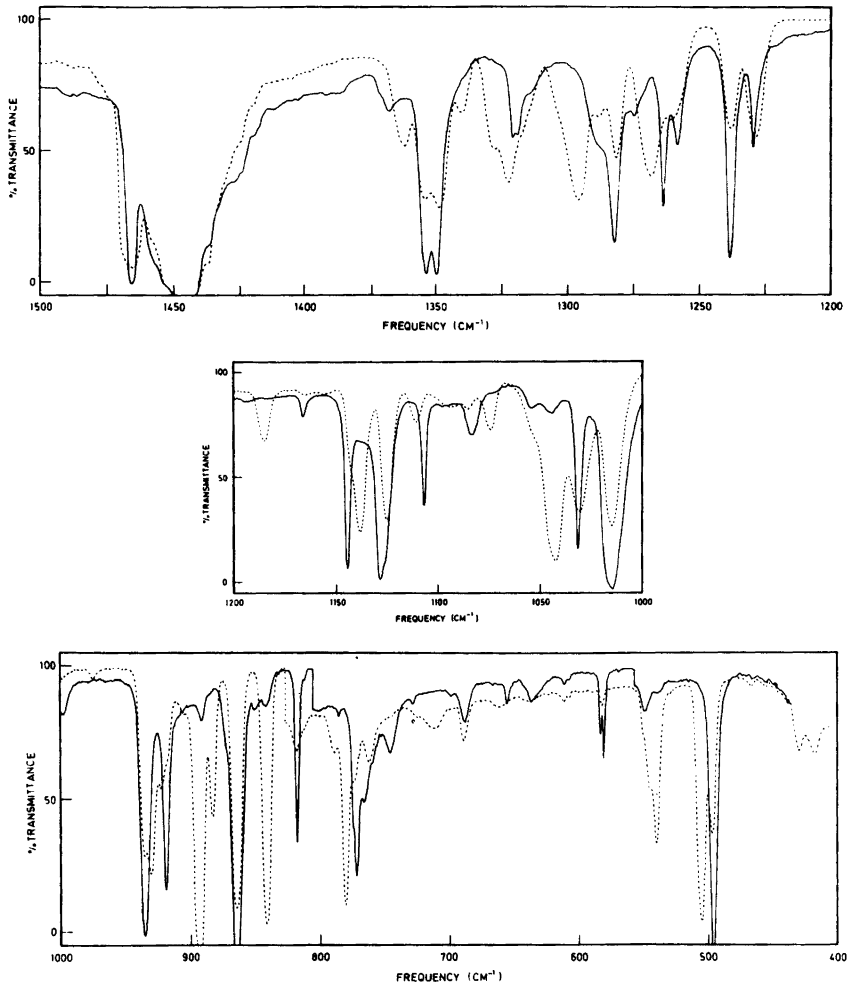

Fig. 1. Infrared spectra of cyanocyclohexane (CCN) as an amorphous solid (dotted curve) and as an anisotropic crystal annealed at 190 K (solid curve) both recorded at 90 K.

IR spectra of the CCN and CNC thiourea clathrates as nujol mulls were recorded using the technique described earlier.[20]

RESULTS

The IR spectra of CCN as a liquid were presented in Ref. 10, the unannealed and annealed solids at 90 K are given in Fig. 1 and the various high pressure curves are shown in Fig. 2. Raman spectra of the

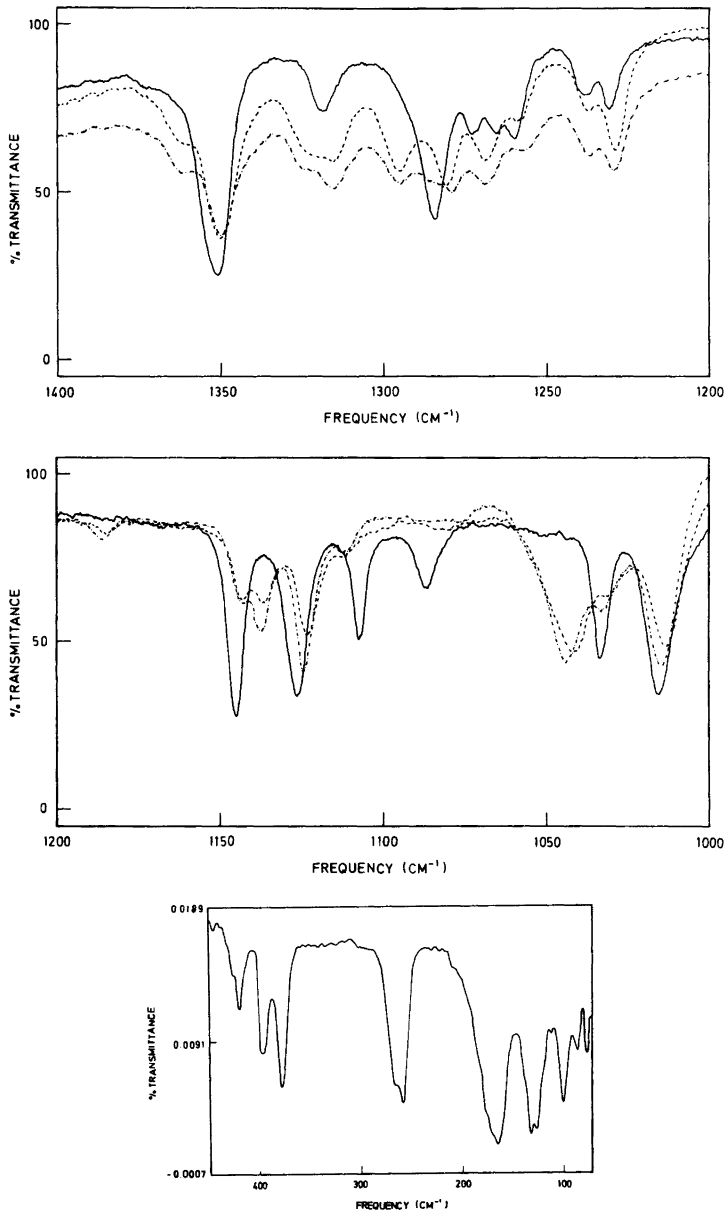

Fig. 2. Infrared spectra of cyanocyclohexane (CCN) in the diamond anvil cell as a liquid at negligible pressure (dashed-dotted curve), as a plastic phase at *ca.* 3 kbar pressure (dashed curve) and as an anisotropic crystal at *ca.* 18 kbar pressure (solid curve).

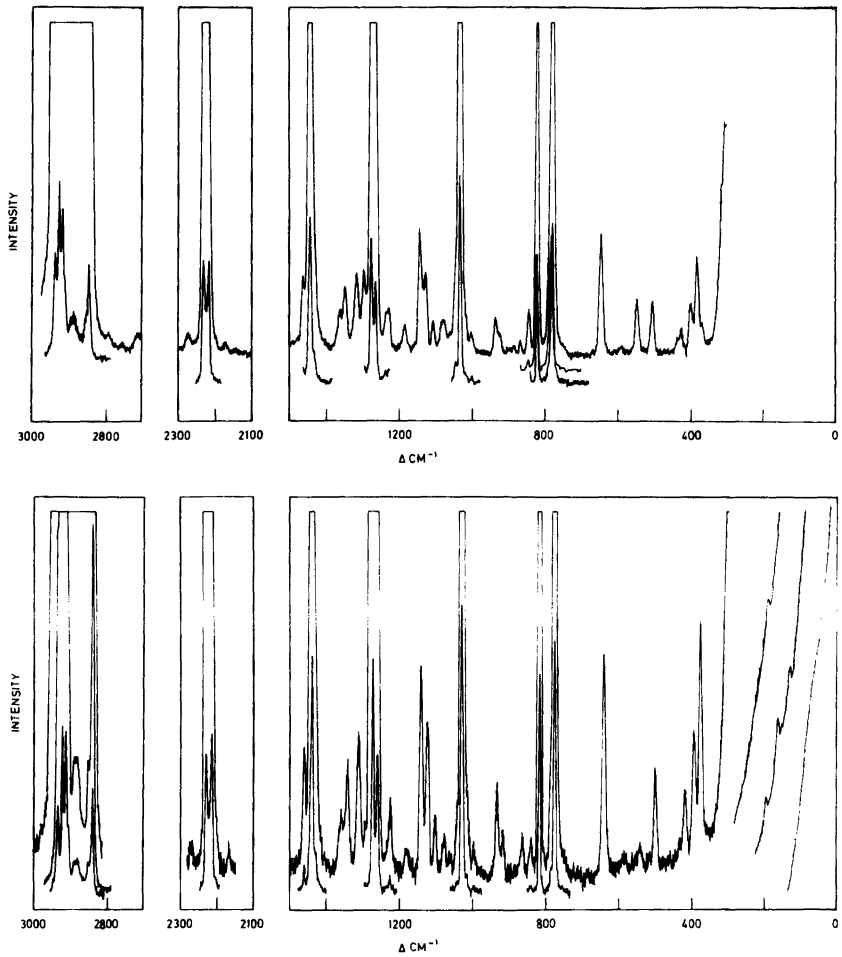

Fig. 3. Raman spectra of cyanocyclohexane (CCN) as an unannealed solid (top) and as a crystalline solid, annealed to 190 K (bottom) both recorded at 90 K.

unannealed and the annealed solids studied at 90 K are reproduced in Fig. 3. The IR and Raman spectra of CNC in the liquid state are given in Figs. 4 and 5, respectively. Low temperature IR curves for CNC appear in Fig. 6 whereas the high pressure spectra recorded with the diamond anvil cell are found in Fig. 7. The wave numbers of the observed IR and Raman bands for the two compounds are listed in Table 1 (CCN) and Table 2 (CNC). Our present CCN data are much more complete than those obtained previously;[10] for CNC our results agree with the limited IR data reported.[17]

Cyanocyclohexane (CCN)

Low temperature solid. Earlier[10] we did not achieve any simplification of the IR and Raman spectra upon solidification, although certain intensity variations were observed after annealing. A large effort was therefore invested in the present cooling of CCN, and various techniques were systematically applied. No success was obtained by cooling the sample from the liquid state. Shock freezing the vapour on a CsI window (IR) or copper block (Raman) at liquid nitrogen temperature and subsequent annealing for 1–2 h at 190 K finally caused crystallization. It appears from Figs. 1 and 3 that a number of bands present in the amorphous,

Table 1. Infrared and Raman spectral data[a] for cyanocyclohexane (CCN).

Liquid		Amorphous		Crystalline				Assignments	
IR	Raman	IR 90 K	Raman 90 K	IR			Raman	equatorial	axial
				Low temp. 90 K	High pressure 4 kbar[b]	High pressure 16 kbar	Low temp. 90 K		
3175 m[c]									comb.
			2955 s				2955 s	ν_1 a'	
2945 vs	2944 vs,P		2944 vs				2943 s		ν_1 a'
		2930 s,sh	2933 vs				2933 s	ν_2 a'	ν_2 a'
	2927 s		2927 m,sh				2927 m,sh	ν_3,ν_{30} a',a''	ν_{30} a''
2905 s,sh		2919 s,sh	2914 m,sh				2911 w	ν_{31} a''	ν_3,ν_{31} a',a''
	2901 m,P	2900 s	2904 m				2904 w	ν_4 a'	ν_4 a'
			2873 m,sh				2873 m,sh		
2860 vs	2860 vs,P	2950 s						ν_5,ν_6,ν_7 a'	ν_5,ν_7,ν_7
			2861 s				2859 s	ν_{32},ν_{33} a''	ν_{32},ν_{33}
2290 w	2283 w,sh	2286 vw	2283 vw	2285 vw,sh				comb.	comb. = 2307 A',A''
				2280 w					comb.
				2265 vw					$2\times\nu_{41}=2286$ A'
2240 s	2242 vs,P	2240 s	2244 s	2240 s			2244 m	ν_8 a'	ν_8 a'
	2237 m	2230 s	2230 s	2226 s			2228 m		$2\times\nu_{17}=2\times\nu_{42}=2246$ A'
1465 s,sh	1465 m,sh,P	1465 s	1470 w	1465 s	1466 m	1470 m$I_\parallel$[d]	1469 m	ν_9 a'	ν_9 a'
1452 vs		1457 m 1454 s,sh		1457 m 1454 s,sh	1459 m	1459 s$I_\parallel$		ν_{10} a'	$\nu_{45}+\nu_{48}=1468$ A'
		1446 vs							
1448 s,sh	1447 s,D		1449 s	1446 vs	1445 vs	1450 vs	1447 vs	ν_{34} a''	ν_{10},ν_{34} a',a''
		1440 s,sh						ν_{35} a''	
		1437 s,sh	1436 w,sh	1437 s,sh	1435 s	1437 s,sh	1436 m,sh	ν_{11} a'	ν_{35} a''
				1426 m,sh		1431 m,sh			ν_{11} a'
1405 vw			1401 vw				*[e]	ν_{12} a'	
1364 w	1365 w,D	1365 m 1362 m	1364 m	1371 vw 1367 w	1373 w 1364 vw		1366 w	ν_{36} a''	ν_{12},ν_{36} a',a''
		1354 m		1354 s		1361 m$I_\perp$			ν_{37} a''
1353 m	1353 w,D	1349 m	1352 m	1350 s	1351 s	1353 s	1350 w	ν_{37} a''	ν_{13},ν_{38} a',a''
		1341 w		*	*	*		ν_{13} a'	
1327 w	1328 w,D	1328 w	1326 w,sh	*			*	ν_{38} a''	
1318 w	1318 vw,P	1322 m 1317 m	1320 m 1318 w	1321 m 1319 w 1314 w	1319 m	1320 w 1315 m$I_\perp$	1318 m	ν_{14} a'	ν_{14},ν_{39} a',a''

Table 1. Continued.

1298 w	1299 s,D	1296 m	1299 m	*	*	*	*	ν_{39} a''	
1287 w		1287 m		1287 m,sh					comb.
1281 w		1281 m	1279 vs	1282 s	1284 s	1289 s$I_\perp$	1279 s		ν_{40} a''
				1275 w	1273 m	1276 w$I_\parallel$			comb.
1270 w	1273 s,D	1268 m	1267 s	*	*	*	*	ν_{15} a'	
				1264 m	1265 m	1263 m$I_\parallel$	1267 s		ν_{15} a'
1258 w	1261 m	1260 w,sh						ν_{40} a''	
				1258 m	1260 m	1259 m$I_\perp$	*		$\nu_{29}+\nu_{41}=1268$ A''
1239 w	1241 w,D	1238 w	1240 w					ν_{16} a'	
1231 w	1232 w,P	1229 m	1233 w,sh	1238 s 1229 m	1238 m 1231 m	1237 m$I_\parallel$ 1227 m$I_\parallel$	1230 m		ν_{16} a'
				1194 vw			1191 vw		comb.
1185 vw	1187 w,D	1185 w	1188 w	*		*		ν_{41} a''	
		1165 vw		1166 w	1168 vw	1169 vw			comb. A''
		1155 vw		*				comb.	
1143 w	1144 w,sh,D	1142 m,sh	1141 m	1144 s	1145 s	1149 s$I_\perp$	1146 m		ν_{41} a''
1136 w	1138 s,P	1138 m		*		*		ν_{17} a'	
1123 m	1125 m,P	1125 s	1129 w,sh	1128 m,sh 1126 vs	1127 s	1131 s$I_\perp$ 1127 s$I_\parallel$	1128 m		ν_{17},ν_{42} a',a''
1111 vw	1114 vs,sh	1110 w	1109 vw	1107 m	1107 m	1105 m$I_\perp$	1108 w		$\nu_{28}+\nu_{46}=1111$ A''
		1094 vw,sh		*				ν_{42} a''	
1083 vw	1085 vw,sh,D	1084 vw	1087 w,sh	1083 w	1087 m	1089 w$I_\perp$	1086 w		ν_{43} a''
1076 vw	1078 w,D	1079 w	1078 w	*		*	*	ν_{43} a''	
1049 w,sh	1048 m,D	1053 w,sh	1047 s	1054 w	1050 vw		*	ν_{44} a''	comb.
1041 s		1043 s		1045 w	1043 vw	*		ν_{18} a'	
1031 m	1033 s,D	1030 m	1036 vs	1032 s 1029 m	1033 s	1036 m$I_\perp$ 1032 m$I_\parallel$	1036 vs 1032 vs	ν_{19}, a'	ν_{18},ν_{44} a',a''
1014 s		1014 s		1015 vs	1016 s	1017 s$I_\parallel$	1020 w		ν_{19} a'
	1002 w,P		1005 vw	997 w,sh			1002 vw		$\nu_{24}+\nu_{27}=1009$ A'
935 m	932 m,P	936 s	935 m	935 vs	938 s	935 s$I_\parallel$	939 m		ν_{20} a'
		931 m		*				ν_{20} a'	
921 w,sh	921 vw,sh	923 w 919 w	922 vw,sh	919 s	924 m	929 s$I_\parallel$	922 w	ν_{45} a''	ν_{45} a''
		905 vw		*				$\nu_{29}+\nu_{47}=913$ A''	
892 vs	892 w,D	896 vs	897 vw	892 w	895 vw	*	*	ν_{46} a''	
882 vw, sh	882 w,P	884 w	886 vw	*			*	ν_{21} a'	
				873 w					
862 s	863 vw,P	865 vs	868 vw	865 vs	869 s	870 s 864 s$I_\perp$	868 w		ν_{21},ν_{46} a',a''
				859 w					

Table 1. Continued.

839 s	842 s,P	841 s	844 m	842 vw	846 vw	*	844 vw	ν_{22} a'	
817 w	819 s,P	819 w	821 s	818 m	822 m	823 m	821 s		ν_{22} a'
	788 s,D?	789 w		786 vw		792 vw $I_\perp$	788 m	ν_{47} a''	ν_{47} a''
779 m	781 vs,P	781 m	779 s	*				ν_{23} a'	
771 w	774 s,P	774 w		776 m 772 s	779 m	778 m$I_\parallel$	778 vs		ν_{23} a'
761 m		764 w		766 w 759 w	762 w 758 w	757 w$I_\parallel$			comb.
737 vw	743 w,sh	746 vw,sh		745 w			750 vw,sh		$\nu_{25}+\nu_{28}=753$ A'
		725 vw		727 vw	732 vw			comb. = 744	$2\times\nu_{27}=742$ A'
689 w		689 w		689 w	690 w			$\nu_{28}+\nu_{49}=699$ A''	$\nu_{49}+\nu_{50}=688$ A'
638 vw	641 m,P	640 vw,bd	644 m	636 w	642 vw	640 vw	644 m		ν_{24} a'
581 vw	583 vw	583 w	585 vw	583 w 581 w	585 w	583 w$I_\parallel$			$\nu_{49}+\nu_{51}=581$ A'
547 vw		551 w,sh 546 w,sh		548 w	552 vw	550 vw		comb.	ν_{48} a''
540 w	542 s,P	541 m	544 m	*			*	ν_{24}, a'	
505 w	506 m,P	506 m	506 w	*	*		*	ν_{25},$\nu_{48}$$a'$,$a''$	
496 w	499 w,sh,P	498 m	500 w,sh	496 vs	503 s	503 s$I_\parallel$	502 w		ν_{25} a'
431 w	433 m,D	432 w	434 w	*			*	ν_{49} a''	
421 w	424 w,sh,D	422 w 417 w	423 w,sh	425 w 417 w	427 w 420 w	432 m 419 w	421 w	$\nu_{28}+\nu_{51}=428$ A''	ν_{49} a''
392 m[f]	389 m,bd,D	392 m	393 w	394 m	396 m	397 m	394 m		ν_{26} a'
385 m		389 m		386 vw	*			ν_{26} a'	
371 s	373 m,P	376 m	378 m	376 m 373 s	379 s	381 s$I_\perp$ 376 m,sh$I_\perp$	377 m		$\nu_{28}+\nu_{29}=382$ A'
358 w,sh	359 s,P	362 w	364 m	*	*		*	ν_{27} a'	
317 vw								$2\times\nu_{51}=320$ A'	
267 m	269 m,D?	273 s 367 m	270 m	267 s	267 m,sh	278 s$I_\perp$		ν_{28} a'	ν_{50} a''
257 m	261 m,P	263 m,sh	260 m	259 s	258 s	265 m	265 w		ν_{28} a'
238 vw,sh		241 w		*				ν_{50} a''	
157 s	162 s,D	172 s 155 s	163 m	162 vs	165 s		162 w	ν_{51} a''	ν_{51} a''
124 s	128 m,D	135 vs	125 m	135 vs	130 s		127 m	ν_{29} a'	ν_{29} a'

[a] Weak bands outside the fundamental regions (4000 – 3100, 2800 – 2300, and 2000 – 1500 cm^{-1}) are omitted. [b] Plastic phase. [c] s, strong; m, medium; w, weak; v, very; sh, shoulder; P, polarized and D, depolarized. [d] $I_\parallel$ and $I_\perp$ dichroic measurements. [e] Asterisks indicate bands which are absent or with strongly reduced intensities in the crystal spectra. [f] Bands below 400 cm^{-1} were observed in benzene solution.

unannealed sample (dotted curves in Fig. 1) vanish in the annealed phase (solid curve). Moreover, the same bands disappeared in the earlier[10] and present high pressure crystals and were assigned as equatorial bands. Therefore, CCN exists as axial conformer in the low temperature as well as in the high pressure crystals, unlike all other mono-substituted cyclohexanes known.

The following observations were made:

(1). The shock frozen sample formed by slowly evaporating CCN on a window at 90 K was amorphous, had a glassy appearance and the conformational equilibrium of the vapour at 300 K was maintained.

(2). Gradual heating to *ca.* 150 K had no effect, but at 170 K the sample appeared frosty and the *e* bands were slightly enhanced relative to the *a* bands.

(3). When the sample was kept at 190 K for 1 – 2 h, the *e*-bands disappeared and the *a*-bands remained.

(4). At 215 K the *e*-bands returned, the sample looked glassy, and the *e*/*a* ratio was close to the value at 150 K. The spectrum remained unchanged until 260 K when the sample evaporated from the window.

(5). When the sample heated above 215 K was recooled to 190 K or lower and kept for two hours no spectral changes occurred.

The observations together with those made under pressure (see below) lead to the following conclusions: (a) CCN is present as a plastic (cubic, rotating) phase between melting and *ca.* 210 K with both conformers in equilibrium, (b) an anisotropic phase exists below *ca.* 210 K consisting of axial molecules, (c) conversion from the plastic to the anisotropic phase "does not occur" (is extremely slow), (d) conversion from the amorphous to the anisotropic phase is very slow, (e) a large similarity is observed between the spectra of the plastic and amorphous samples and (f) the shock frozen solid at 90 K maintains the conformational equilibrium of the vapour (300 K), but thermodynamic equilibrium is achieved at *ca.* 170 K.

High pressure solid. When CCN was compressed in the diamond anvil cell a solid phase was formed at *ca.* 1 kbar pressure. This solid appeared isotropic (plastic) in a polarization microscope, its IR spectrum (dashed curves in Fig. 2) was quite similar to the liquid spectrum (dashed-dotted curves) recorded at ambient pressure. A phase transition occurred fairly slowly at *ca.* 10 – 15 kbar between the plastic and an anisotropic phase. The spectrum of the latter phase (solid curves in Fig. 2) was identical to our earlier[10] results and contained the axial conformer only. Two or three single crystals dominated the sample and a distinct dichroic effect was observed with polarized radiation. The bands enhanced in one preferred direction are designated $I_{\parallel}$ and those enhanced in a direction at right angle to the formed are labelled $I_{\perp}$ in Table 1.

Spectral interpretation. No established correlations are known between the vibrational spectra and the conformations of hydrocarbons containing cyano and isocyano groups similar to the well known relationships for chloro-, bromo- and iodo-substituted hydrocarbons. The high pressure conformer was attributed as axial,[10] based upon various criteria, including band intensity variations with temperature and spectral similarities. Later CCN-thiourea clathrates were made,[20] supporting the earlier conclusions. Moreover, the bands around 640 cm^{-1} assigned to the axial conformer (Tables 1 and 3) agree with the "spectral indicator" recently attributed[21] to the *a* conformer. Finally, our present force constant calculations agree with this assignment.

With 19 atoms in the molecule and C_s symmetry, CCN should have 29 *a'* and 22 *a''* fundamentals for each conformer, of which many will coincide. The bands were assigned on the following criteria: (1) bands present in the low temperature or high pressure crystals should be axial or be common to the axial and equatorial conformers, (2) those present in the liquid and the plastic and amorphous solids, vanishing in the anisotropic crystals, should be equatorial, (3) the polarized Raman bands belong to species *a'*, the depolarized to *a''*; similar conclusions can be drawn from the dichroism of the axial bands in the high pressure crystal.

Force fields for CCN (and CNC) were transferred from *trans*-1,4-dihalocyclohexanes[13] and the monohalocyclohexanes[14,15] and extended with force constants for the side chain. Thus, 30 force constants were transferred and held fixed during the iterations, while 28 parameters for the following molecules, CCN, CNC, ethynylcyclohexane[18] and *trans*-1,4-dicyanocyclohexane,[16] were allowed to vary. The detailed force field and the procedure will be discussed elsewhere,[18] whereas the calculated wave numbers for the *e* and *a* conformers are listed in Table 3. These data were of great help for the assignments and, as is apparent, the agreement between the observed and calculated wave numbers is quite satisfactory.

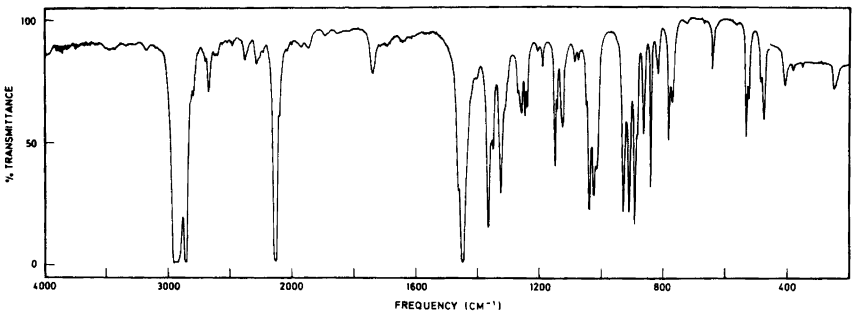

Fig. 4. The infrared spectrum of isocyanocyclohexane (CNC) as a liquid.

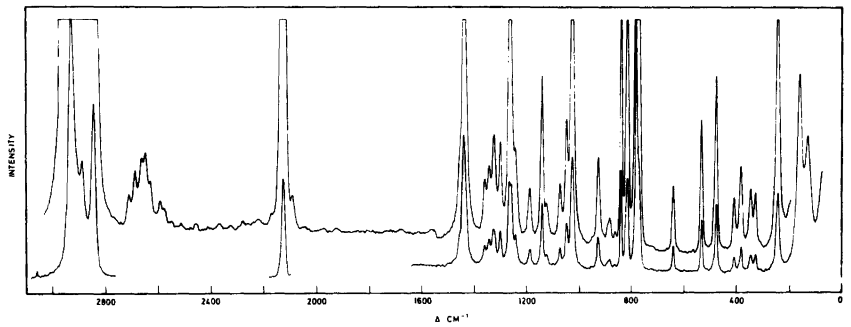

Fig. 5. Raman spectrum of isocyanocyclohexane (CNC) as a liquid.

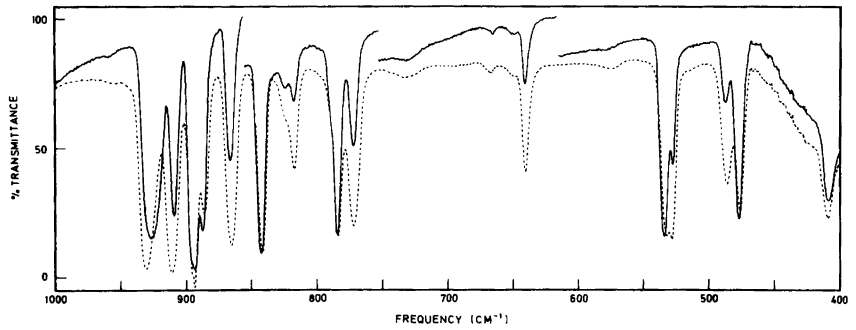

Fig. 6. Infrared spectra of isocyanocyclohexane (CNC) as an unannealed (dashed curve) and annealed solid (solid curve) at 90 K.

As immediately apparent from the columns in Table 3, CCN and CNC have nearly "identical" spectra. Apart from the C≡N and N≇C stretching vibrations (ν_8) observed at 2240 and 2140 cm^{-1}, respectively, the corresponding fundamentals in CCN and CNC are mostly a few cm^{-1} apart. Other exceptions are ν_{25} (*e*) as well as ν_{48} and ν_{49} including both conformers of CCN and CNC, all of these involve bending modes of the side chain.

Isocyanocyclohexane (CNC)

Low temperature solid. CNC was studied in IR and Raman cryostats by the same procedure as

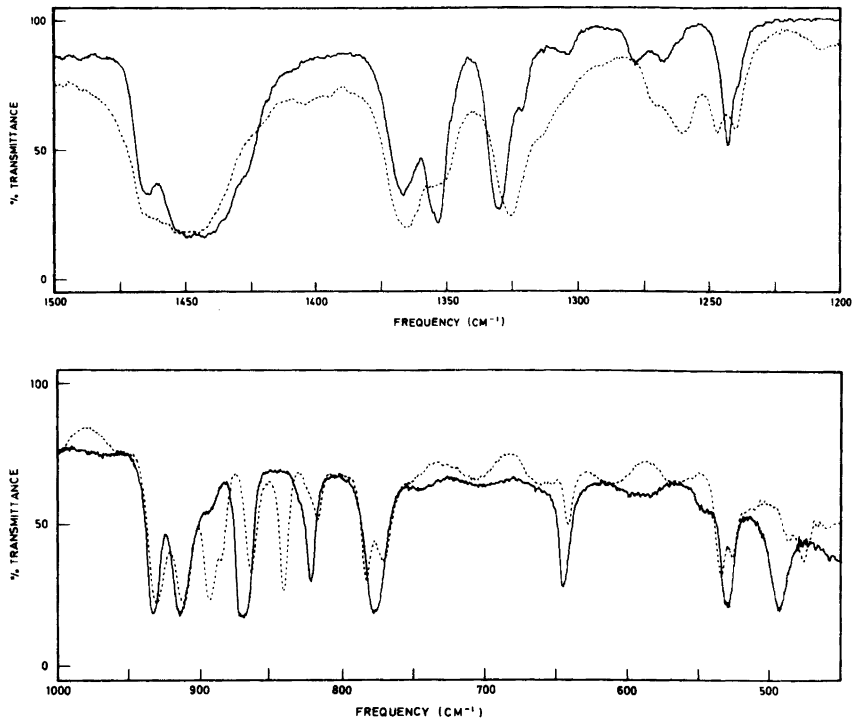

Fig. 7. Infrared spectra of isocyanocyclohexane (CNC) in the diamond anvil cell as a liquid at negligible pressure (dashed curve) and as an anisotropic crystal at *ca.* 20 kbar (solid curve).

described for CCN. In spite of many attempts with prolonged annealing at different temperatures, we were not able to "isolate" one conformer of CNC in the solid phase. Apparently, CNC is still more difficult to crystallize by cooling technique than CCN.

When the shock frozen amorphous solid was heated from 90 K to 170 K the *e/a* ratio increased as observed for CCN. Further heating to 210 K resulted in a small decrease in the *e/a* ratio in agreement with a small negative ΔH value between the conformers. None of the IR curves showed correlation splitting and the band width indicated that the sample was not crystalline in spite of a frosty appearance. At *ca.* 240 K the sample lost its frosty look and the *e/a* ratio increased considerably, in what presumably was a plastic phase. The solid tended to evaporate from the window and the sample was shock frozen to 90 K without any significant change in conformational equilibrium. The region 1000 – 400 cm^{-1} is shown in Fig. 6 giving the unannealed (dashed curve) and annealed (240 K) solid curve; both spectra were recorded at 90 K.

High pressure solid. When compressed, CNC behaved much like CCN, at *ca.* 2 kbar inspection in the polarization microscope suggested the formation of a plastic phase. The spectrum of this phase is not given in Fig. 7 but had slightly stronger *a*-bands than the liquid spectrum (dashed curve). At *ca.* 13 kbar a phase transition took place and an anisotropic crystal was formed in a matter of 10 min (the solid line of Fig. 7). A number of bands vanished in the high pressure crystal and the axial conformer remained as was the case for CCN. High pressure spectra were recorded in the whole spectral region and these data were essential for the spectral assignments.

Thiourea clathrate. CNC-thiourea clathrates were prepared as described [20] and the IR guest bands in the region 1000 – 800 cm^{-1} (representing a window between the host bands) were useful for conformational identification (compare Figs. 1 and 2 of Ref. 20). Distinct IR bands of the clathrate as a nujol mull were observed at 931, 912, 890, 864 and 841 cm^{-1}. The two former bands (931 and 912 cm^{-1}) are both attributed to overlapping *e* and *a*

Table 2. Infrared and Raman spectral data[a] for isocyanocyclohexane (CNC).

Liquid		Amorphous (90 K)		Annealed (238 K)		Crystalline		Assignments	
IR	Raman	IR 90 K	Raman 90 K	IR 90 K	Raman 90 K	IR (High pressure)		equatorial	axial
						10 kbar plastic	15 kbar anisotropic		
2940 vs,bd	2947 sP 2930 s,sh,D?	2940 vs,bd	2945 s	2950 vs 2920 vs	2945 s		2960 vs	ν_1 a' ν_2,ν_3,ν_{30} a',a''	ν_1 a' ν_2,ν_{30} a',a''
2907 s	2909 s,P	2905 s	2905 s	2898 s	2903 s			ν_4,ν_{31} $a'a''$	$\nu_3,\nu_4\nu_{31}$ a',a''
2860 vs	2863 s,P	2860 vs,bd	2859 s	2854 vs	2858 s			ν_5,ν_6,ν_7 a' ν_{32},ν_{33} a''	ν_5,ν_6 a' ν_{32},ν_{33} a''
	2848 w								ν_7 a'
2185 vw	2180 vw,sh	2187 vw		2177 vw				comb.	
2137 vs, bd	2137 s,P	2145 vs,bd	2144 s	2142 vs,bd	2145 s			ν_8 a'	ν_8 a'
2103 w	2103 m,P	2107 w	2105 w	2106 w	2105 w			comb. A'	
1464 m	1465 m,P?	1465 m 1455 m,sh	1462 m	1465 m 1450 s	1463 m	1464 m	1464 m	ν_9 a' ν_{10} a'	ν_9 a'
1450 vs	1447 s,D?		1445 s		1441 s	1445 vs,bd	1445 vs		ν_{34} a''
		1447 vs 1442 m,sh		1445 s				ν_{34} a'' ν_{10} a'	
1436 m,sh	1437 w,sh	1436 m,sh		1436 m				ν_{35} a''	ν_{35} a''
1420 vw		1423 w		1423 w		1418 vw?	1435 w,sh	ν_{11} a'	ν_{11} a'
1404 w		1408 w		1408 w		1404 w	1427 w,sh	ν_{12} a'	comb.
1368 s	1366 m,P	1367 s	1366 m	1366 s	1364 m	1364 s	1367 s	ν_{36} a''	ν_{12},ν_{36} a',a''
1358 w		1354 m		1358 w		1356 m			ν_{37} a''
1352 w	1350 m,D?		1347 m	1352 w 1348 m 1339 w	1348 m	1349 w	1354 s	ν_{37} a'' ν_{13} a'	ν_{13},ν_{38} a',a''
	1334 m,P?			1334 w,sh				ν_{14} a'	
1328 m		1327 s	1331 m		1331 m	1325 s	1330 s	ν_{38} a''	
	1327 w,sh,P			1328 m					ν_{14} a'
1313 w				1317 w		1314 w	1321 w	comb.	$\nu_{45}+\nu_{49}$ A'
1305 vw	1306 m,D?	1305 w	1303 s	1304 w	1303 s	1306 w	1304 w	ν_{39} a''	ν_{39} a''
1272 w	1271 s,D	1272 m	1270 s	1271 w,sh		1270 w	1278 w		ν_{40} a''
1265 w,sh	1266 s,P		1262 s	1264 w,sh	1263 s		1268 w	ν_{15} a'	ν_{15} a'
1260 w	1260 w,sh,D	1261 m		1260 m		1260 m	*	ν_{40} a''	
1248 w	1248 m,D	1248 w	1246 m	1246 w	1246 m	1246 w	*	ν_{16} a'	
1241 w	1240 w,sh,P?	1239 m		1238 w		1239 m	1243 m 1239 w		ν_{16} a'
1209 w		1211 w		1210 w		1210 w	*	$\nu_{29}+\nu_{42}=1219$ A''	
1192 w	1193 m,D	1192 m	1192 m	1192 m	1191 m	1192 w	*	ν_{41} a''	
1169 vw?		1170 vw		1170 vw			1175 vw		comb.
1153 m	1153 w,sh,D?	1153 s		1152 m		1153 s	1157 s 1154 s		ν_{41} a''

Table 2. Continued.

1146 w	1146 s,P	1147 m	1145 s	1147 m	1145 s	1146 m	*	ν_{17} a'	
				1142 vw,sh				comb.	
1133 w,sh		1133 s		1134 w		1135 w,sh	1140 w,sh?		ν_{42} a''
1128 m	1128 m,P	1128 s	1127 w	1128 m		1127 s	1132 s	comb.	ν_{17} a'
1116 vw		1116 w		1117 w		1117 vw,sh		comb.	
1097 vw?		1097 vw					1110 m		comb.
1089 w	1090 vw?	1089 m		1089 m		1089 w	*	ν_{42} a''	
1077 w	1076 m,D	1077 m	1076 m	1077 m	1076 m	1078 w	1085 w	ν_{43} a''	ν_{43} a''
1052 m	1051 m,D	1052 m	1051 s	1051 m	1051 s	1051 m	*	ν_{44} a''	
1041 s		1041 s		1040 s		1041 s	*	ν_{18} a'	
		1033 m		1034 w,sh		1033 w	1033 s		ν_{18},ν_{44} a',a''
1027 s	1029 s,D	1024 s	1029 s	1023 s	1028 s	1025 s	*	ν_{19} a'	
1017 m		1017 s		1016 m,sh		1017 s	1017 s		ν_{19} a'
951 vw	951 vw?	955 vw		959 vw				comb.	
931 s	929 m,P	930 s	926 m	926 s	925 m	930 s	933 s	ν_{20} a'	ν_{20} a'
912 s	913 vw,D?	911 s	911 vw	909 m		911 s	914 s	ν_{45} a''	ν_{45} a''
893 s	893 w,D	893 vs	890 w	893 s	891 m	894 s	894 w	ν_{46} a''	comb.
885 m	884 w,P	886 m		887 m		888 m,sh		ν_{21} a'	
864 m	864 w,P	865 s	864 w	866 m	865 vw	866 s	870 s		ν_{21},ν_{46} a',a''
841 s	841 s,P	841 s	842 s	842 s	843 s	843 s	*	ν_{22} a'	
823 w,sh	823 w,sh,D?	824 w,sh		824 w		827 w,sh		comb.	
817 w	817 s,P	818 m	819 s	818 w	819 m	820 w	822 m		ν_{22} a'
		790 w,sh		790 w,sh			*	ν_{47} a''	
783 m	783 s,P	784 s	783 s	784 s	785 s	785 s	*	ν_{23} a'	
770 m	774 s,sh,P 771 w,sh	772 s	772 s	772 m	772 m,sh	774 m	778 s		ν_{23} a' ν_{47} a''
642 w	642 m,P	641 m	640 m	641 w	640 w	644 w	647 m		ν_{24} a'
536 m	535 s,P	534 s	532 m	536 s	535 m	538 m	*	ν_{24} a'	
528 m		530 s		529 m		529 m	531 s		ν_{48} a''
488 w	488 w,sh	488 m		489 w		490 m	494 s		ν_{25} a'
479 m	480 s,P	478 m	478 s	479 s	480 s	478 m	*	ν_{25},ν_{48} a',a''	
410 m	410 m,D	410 m	411 m	410 m	412 m	413 m	419 vw	ν_{49} a''	ν_{49} a''
384 w	384 m,P	384 w	384 m	382 w	384 m	385 w	402 w	ν_{26} a'	ν_{26} a'
351 w	349 m,P	352 w	353 w		351 m	352 w	352 w	ν_{27} a'	$2\times\nu_{51}=320$ A'
	331 m,P	334 vw	331 m		332 w		339 w	$2\times\nu_{51}$ A'	ν_{27} a'
250 m		254 w					254 w,sh		ν_{28} a'
	243 s,D	246 m	247 m		247 m		246 m	ν_{28},ν_{50} a',a''	ν_{50} a''
							188 m		
170 m	160 s,D		162 m		166 m			ν_{51} a''	ν_{51} a''
							181 m		
150 m	130 m,D		132 m		135 m		140 m	ν_{29} a'	ν_{29} a'

[a] See footnote to Table 1.

Table 3. Observed[a] and calculated fundamental frequencies for cyano- and isocyanocyclohexane.

	Cyanocyclohexane				Isocyanocyclohexane			
	e		*a*		*e*		*a*	
	Obs.	Calc.	Obs.	Calc.	Obs.	Calc.	Obs.	Calc.
a'								
ν_1	2955	2957	2945	2958	2947	2957	2947	2958
ν_2	2933	2922	2933	2922	2930	2922	2930	2922
ν_3	2927	2916	2914	2916	2930	2916	2909	2916
ν_4	2901	2914	2901	2914	2909	2914	2909	2914
ν_5	2860	2857	2860	2857	2860	2857	2863	2857
ν_6	2860	2853	2860	2854	2860	2853	2863	2854
ν_7	2860	2851	2860	2851	2860	2851	2848	2851
ν_8	2240	2240	2240	2240	2137	2140	2137	2140
ν_9	1465	1456	1465	1456	1464	1456	1464	1456
ν_{10}	1452	1439	1447	1437	1450	1440	1442	1437
ν_{11}	1437	1427	1426	1422	1420	1427	1420	1422
ν_{12}	1405	1390	1364	1366	1404	1399	1366	1381
ν_{13}	1341	1343	1353	1346	1339	1343	1350	1346
ν_{14}	1318	1303	1318	1337	1334	1311	1327	1340
ν_{15}	1270	1253	1264	1263	1265	1253	1265	1264
ν_{16}	1239	1232	1231	1231	1248	1233	1241	1233
ν_{17}	1136	1134	1123	1133	1146	1135	1128	1137
ν_{18}	1041	1032	1031	1031	1041	1041	1033	1031
ν_{19}	1031	1023	1014	1005	1027	1023	1017	1005
ν_{20}	931	922	935	927	931	928	931	933
ν_{21}	882	891	862	857	885	891	864	856
ν_{22}	839	934	817	814	841	834	817	815
ν_{23}	779	763	771	776	783	765	774	779
ν_{24}	540	535	638	643	536	530	642	640
ν_{25}	506	505	496	493	479	482	488	490
ν_{26}	385	401	392	391	384	397	384	388
ν_{27}	359	363	371	367	351	351	331	321
ν_{28}	267	283	257	275	243	251	250	254
ν_{29}	124	136	124	110	130	129	130	107
a''								
ν_{30}	2927	2918	2927	2917	2930	2918	2930	2918
ν_{31}	2914	2913	2914	2913	2909	2913	2909	2913
ν_{32}	2860	2855	2860	2855	2860	2855	2863	2855
ν_{33}	2860	2852	2860	2852	2860	2852	2863	2852
ν_{34}	1447	1441	1447	1440	1445	1441	1447	1440
ν_{35}	1440	1432	1437	1433	1436	1432	1436	1433
ν_{36}	1364	1377	1364	1368	1368	1377	1368	1368
ν_{37}	1353	1347	1354	1350	1350	1347	1358	1350
ν_{38}	1327	1344	1350	1340	1328	1344	1350	1340
ν_{39}	1298	1300	1318	1298	1305	1300	1306	1298
ν_{40}	1258	1244	1281	1255	1260	1244	1272	1255
ν_{41}	1185	1188	1143	1156	1192	1188	1153	1156
ν_{42}	1094	1095	1123	1136	1089	1094	1133	1136
ν_{43}	1076	1071	1083	1078	1077	1071	1077	1078
ν_{44}	1048	1052	1031	1035	1052	1053	1033	1035
ν_{45}	921	910	921	933	912	911	912	933
ν_{46}	892	889	862	857	893	889	864	856
ν_{47}	788	788	788	788	790	788	771	788
ν_{48}	505	494	547	542	479	460	528	512
ν_{49}	431	459	421	437	410	430	410	417
ν_{50}	238	228	267	256	243	227	243	234
ν_{51}	162	169	162	147	160	149	160	137

[a] Whenever appropriate wave numbers from the infrared and Raman liquid spectra are given.

bands and therefore give no conformational clue. The 864 cm^{-1} line, assigned as an axial band, was the most intense of the remaining bands whereas 841 cm^{-1} (*e* band) was hardly visible and 890 cm^{-1} (consisting of overlapping *e* bands at 893 and 885 cm^{-1}) was weak. Compared with the intensities of these bands in the liquid (Fig. 4) the *e*/*a* ratio is probably a factor of 10 lower in the clathrate than in the liquid. Thus, the *a* conformer is highly preferred for the CCN and the CNC as well as the chloro- and bromocyclohexane clathrates.[20] For iodocyclohexane [20] the *a* conformer is less preferred and for fluorocyclohexane [14] the clathrate consists of guest molecules in nearly the same conformer mixture as in the liquid.

Spectral interpretations. The IR and Raman bands of CNC were attributed to equatorial and axial conformers using the same criteria as for CCN (although less conclusive for CNC since the isolated *a*-conformer was not obtained in the low temperature IR and Raman spectra). A striking similarity to the CCN spectra was of particular help and the results of the force constant calculations were essential for the spectral interpretations.

DISCUSSION

CCN is to our knowledge the only monosubstituted cyclohexane which is shown to crystallize in the axial conformer at low temperatures. Obviously the conformer adopted by the molecules in the crystal depends upon the $\Delta G°$ between the conformers at the temperature of crystallization as well as specific interactions in the crystal lattice which may favour one or the other conformer. The low $\Delta G°$ for CCN and CNC at the coalescence temperatures (183 – 193 K) means nearly equal concentration of the conformers (although the equatorial is slightly more abundant). Therefore, the crystal interactions will be the deciding factor and apparently favour the axial conformer for CCN.

For crystallizations at higher pressure the conformational equilibrium will be further influenced by the volume difference between the conformer molecules; the smaller volume conformer will be favoured under pressure. It was shown [22] for chloro- and for *trans*-1,4-dihalocyclohexanes in CS_2 solution that the *a*(*aa*) conformer had a partial molar volume ($\Delta\bar{V}$) which was 1.9 – 3.8 cm^3/mol smaller than *e*(*ee*) for these compounds. At least for monohalo-, *trans*-1,2-dihalo- and *trans*-1,4-dihalocyclohexanes, the more spherical, axial (diaxial) conformer always appears to have smaller volume than the more ellipsoidal equatorial (diequatorial) conformer.[23] The *trans*-1,4-dihalocyclohexanes (involving chlorine, bromine and iodine) are converted from an "*ee*-crystal" to an "*aa*-crystal" under 30 – 50 kbar pressure.[11-13] Moreover, *trans*-1,2-bromochlorocyclohexane [24] and isocyanatocyclohexane [10] crystallize in the *ee*(*e*) conformer at low temperature and in the *aa* (*a*) conformer at high pressure, again revealing the preference for the axial conformers under pressure. With this background, the high pressure crystallization of CCN and CNC in the axial form is not surprising.

Large difficulties were encountered in the low temperature crystallization of CCN while for CNC the attempts were not successful. Apparently, the existence of plastic phases in CCN and CNC, common to cyclohexanes with small substituents,[25] made conversion to the anisotropic phase quite difficult.

Similar difficulties were found for fluorocyclohexane [14] also containing a plastic phase, which earlier workers [26] had not been able to crystallize. However, in fluorocyclohexane a reversible transition between the plastic and the anisotropic crystals was obtained by temperature variation, which was not obtained for CCN and CNC. With still more sophisticated cooling and annealing technique an anisotropic crystal of CNC might be grown. In the high pressure diamond anvil cell, however, the various phase transitions took place readily, emphasizing the importance of this technique.

The anomalous stabilization of the diaxial form of *trans*-1,4-dihalocyclohexane compared with the monohalocyclohexane was interpreted [27] as due to 1,3-attractions between the negative halogens and the hydrogens which were calculated to be more positive than usual for these molecules. In *trans*-1,4-dicyanocyclohexane no corresponding stabilization of the diaxial conformer compared with CCN was observed.[16] However, no corresponding electrostatic attraction seems favourable for this molecule.

The cyano and isocyano groups with cylindrical symmetry are found to have low conformational preferences,[1] and their effective van der Waals radii are affected by the electron densities in their outer orbitals.[6] The isoelectronic ethynyl (C≡C–H) cyclohexane has a higher preference [1] for the

equatorial conformer than CCN and CNC (it also crystallizes in the equatorial conformer at low temperature and at high pressure [18]). This difference from CCN was correlated with a high electronic density at the carbon bonded to the ring in ethynylcyclohexane,[6] lowered in CCN due to the electronegative N atom with its lone pair orbital.

Acknowledgement. A student fellowship to A.B. from IAESTE is acknowledged.

REFERENCES

1. Jensen, F. R., Bushweller, C. H. and Beck, B. H. *J. Am. Chem. Soc. 91* (1969). *In press.* Jensen, F. R. and Bushweller, C. H. *Adv. Alicyclic Chem. 3* (1971) 139.
2. Corfield, G. C. and Crawshaw, A. *J. Chem. Soc. B* (1969) 495.
3. Höfner, D., Lesko, S. A. and Binch, G. *Org. Magn. Reson. 11* (1978) 179.
4. Pehk, T. and Lippma, E. *Org. Magn. Reson. 3* (1971) 679.
5. Stephany, R. W., de Bie, M. J. A. and Drenth, W. *Org. Magn. Reson. 6* (1974) 45.
6. Schneider, H.-J. and Hopper, V. *Tetrahedron Lett.* (1974) 579; *J. Org. Chem. 43* (1978) 3866.
7. Raber, D. J., Johnston, M. D. and Schwalke, M. A. *J. Am. Chem. Soc. 99* (1977) 7671.
8. Allinger, N. L. and Szkrybalo, W. *J. Org. Chem. 27* (1962) 4601.
9. Rickborn, B. and Jensen, F. R. *J. Org. Chem. 27* (1962) 4606.
10. Horntvedt, H. T. and Klæboe, P. *Acta Chem. Scand. A 29* (1975) 528.
11. Woldbæk, T. and Klæboe, P. *J. Mol. Struct. 63* (1980) 195 and earlier papers.
12. Klæboe, P., Nielsen, C. J. and Woldbæk, T. *J. Mol. Struct. 60* (1980) 121.
13. Woldbæk, T., Nielsen, C. J. and Klæboe, P. *J. Mol. Struct. 66* (1980) 31.
14. Christian, S. D., Grundnes, J., Klæboe, P., Tørneng, E. and Woldbæk, T. *Acta Chem. Scand. A 34* (1980) 391.
15. Woldbæk, T. *Acta Chem. Scand. A 36* (1982) 641.
16. Ellestad, O. H., Klæboe, P. and Woldbæk, T. *J. Mol. Struct. In press.*
17. Ugi, I. and Meyer, R. *Chem. Ber. 93* (1960) 239.
18. Woldbæk, T., Nielsen, C. J. and Klæboe, P. *Acta Chem. Scand. In press.*
19. Gilbert, B. and Duyckaerts, G. *Spectrochim. Acta A 26* (1970) 2197.
20. Gustavsen, J. E., Klæboe, P. and Kvila, H. *Acta Chem. Scand. A 32* (1978) 25.
21. Zhizhin, G. N. and Sterin, Kh. E. In Durig, J. R., Ed., *Vibrational Spectra and Structure*, Elsevier, Amsterdam 1981, Vol. 9, p. 195.
22. Christian, S. D., Grundnes, J. and Klæboe, P. *J. Am. Chem. Soc. 97* (1975) 3864.
23. Klæboe, P. *Z. Chem. Leipzig 21* (1981) 381.
24. Horntvedt, H. T. and Klæboe, P. *Acta Chem. Scand. 25* (1971) 772.
25. Bailey, R. In Sherwood, J. N., Ed., *The Plastically Crystalline State*, Wiley, New York 1979.
26. Rey-Lafon, M., Rouffi, C., Camiade, M. and Forel, M. T. *J. Chim. Phys. 67* (1970) 2030.
27. Abraham, R. J. and Rosetti, Z. L. *Tetrahedron Lett. 49* (1972) 4965; *J. Chem. Soc. Perkin Trans. 2* (1973) 582.

Received February 23, 1982.

Acta Chemica Scandinavica A 36 (1982) 735–739

Polyol – Water Interactions as Reflected by Aqueous Heat Capacity Values

Y.-N. LIAN, A.-T. CHEN, J. SUURKUUSK and I. WADSÖ

Thermochemistry Laboratory, Chemical Center, University of Lund, P.O. Box 740, S-220 07 Lund, Sweden

Aqueous enthalpies of solution have been determined for D-mannitol, D-sorbitol, *meso*-inositol and α-D-glucose. Heat capacities were determined for the pure compounds leading to partial molar heat capacity values for the dilute aqueous solutions.

Heat capacity values for polyols in aqueous solution are discussed in relation to empirical group additivity parameters. It is concluded that the values for sugars and sugar alcohols are significantly higher than expected from the empirical scheme.

A few years ago we reported a simple group additivity scheme for the prediction of partial molar heat capacities of non-ionic compounds in dilute aqueous solutions, $C_{p,2}$.[1] A very good agreement was obtained between experimental and calculated values for hydrocarbons and monosubstituted alkyl compounds such as alcohols, amines, carboxylic acids, amides and ethers. It was also shown that the scheme could be applied to different types of cyclic compounds and that branching of the alkyl chains had only a small influence on the $C_{p,2}$-values. The results supported the view that solvation effects involving non-ionic groups have the nature of short-range effects.

One important use of such additivity schemes is to detect compounds, or groups of compounds, for which there is a substantial deviation between experimental and calculated values. It is likely that such deviations reflect solute – water interactions which do not exist for the compounds from which the additivity parameters were derived.

It was noted that the scheme predicted quite accurate values for a few simple polyhydroxy compounds, also for those with neighbouring hydroxyl groups. However, a very marked deviation was noted for sucrose for which the experimental value was found to be more than twice the predicted value, suggesting a specific interaction between sucrose and water.[1] Heat capacity values for other sugars and for sugar alcohols point in the same direction.[2–5] Specific interactions between polyols and water have also been inferred from other observations such as dielectric and NMR relaxation[6] and partial molar volumes and compressibilities.[7–9] Substantial differences have been observed for structurally closely related compounds such as mannitol and sorbitol which differ only in the position of one of their six hydroxyl groups.

In order to describe further the thermodynamic properties of polyols, we report here results from calorimetric measurements on D-mannitol, D-sorbitol, *meso*-inositol and α-D-glucose. Aqueous solution enthalpies have been determined at 288.15, 298.15 and 308.15 K, leading to $\Delta C_{p,2}$-values for the solution processes. To arrive at $C_{p,2}$-values [eqn. (1)], heat capacities were also determined for the pure compounds, C_p^*, at 298.15 K.

$$C_{p,2} = \Delta C_{p,2} + C_p^* \quad (1)$$

EXPERIMENTAL

Materials. D-Mannitol was obtained from BDH (organic analytical standard). D-sorbitol, *meso*-inositol and α-D-glucose (anhydrous), of *puriss* quality, were from Fluka. Sorbitol was recrystallized twice from 99.5% ethanol. The other compounds were used without further purification. All samples were dried under vacuum at 80 °C before use in the calorimetric experiments. Reagent-grade water prepared by Milli-Q system was used in the solution calorimetric experiments.

0302-4377/82/090735-05$02.50

Table 1. Solution calorimetric measurements in water for some polyols. n = number of experiments.

Solute	n	ΔH^{∞}_{sol}/kJ mol^{-1} T=288.15	n	T=298.15	n	T=30815	$\Delta C^{\infty}_{p,2}$ (298.15 K) J K^{-1} mol^{-1}
D-Mannitol	6	19.88±0.05	7	21.92±0.03	6	24.12±0.07	212±6
D-Sorbitol	4	17.07±0.03	4	18.66±0.06	5	20.44±0.04	169±5
meso-Inositol	4	14.21±0.05	5	15.29±0.05	5	16.64±0.02	122±5
α-D-Glucose	4	9.67±0.01	6	10.88±0.03	6	12.22±0.03	128±3

Calorimetry. Enthalpy of solution measurements was made with an LKB 8721-1 Precision Calorimeter using a 100 cm^3 glass vessel. Electrical calibrations were made for each solution experiment. Small corrections were applied in order to bring the ΔH_{sol} values to the stated temperature (±0.01 K).

The heat capacity measurements on the pure samples were performed with a micro-drop heat capacity calorimeter.[10] The sample ampoule was charged with *ca.* 0.3 g of material. The ampoules were thermostated at 303 K and were then transferred by free fall to the calorimeter kept at 292 K. The mean temperature in all cases was 298.15 ±0.03 K. The calorimeter was calibrated with water using the C_p-value 75.300 J K^{-1} mol^{-1}. For each compound, measurements were made on 4–5 different ampoule fillings. Measurements on each ampoule were repeated *ca.* 5 times.

RESULTS AND DISCUSSION

Final concentrations in the solution calorimetric determinations were in the range of 0.01 – 0.04 mol dm^{-3}. No consistent trend in ΔH-values *versus* final concentration was observed. Therefore, rather than extrapolating the obtained ΔH-values to zero concentration, average values were calculated and are considered as equal to ΔH^{∞}_{sol}. Results are summarized in Table 1. Uncertainties given for ΔH^{∞}_{sol} are twice the standard deviation of the mean.

Sturtevant[11] has reported a slightly lower value for the enthalpy of solution of α-D-glucose at 298.15 K, 10.71 kJ mol^{-1}, whereas Taylor and Rowlingson[12] found a slightly higher value, 11.00 kJ mol^{-1}, than that reported here. Sturtevant's value obtained at 308.15 K is in exact agreement with the present result.

Fig. 1 shows a plot of the ΔH^{∞}_{sol}-values *versus* T. A weak curvature is observed and the results for ΔH^{∞}_{sol} were represented by eqns. (2) and (3).

$$\Delta H^{\infty}_{sol} = a + bT + cT^2 \quad (2)$$

$$\Delta C^{\infty}_{p,sol} = b + 2cT \quad (3)$$

$\Delta C^{\infty}_{p,sol}$-values are given in Table 1. Uncertainties are estimates.

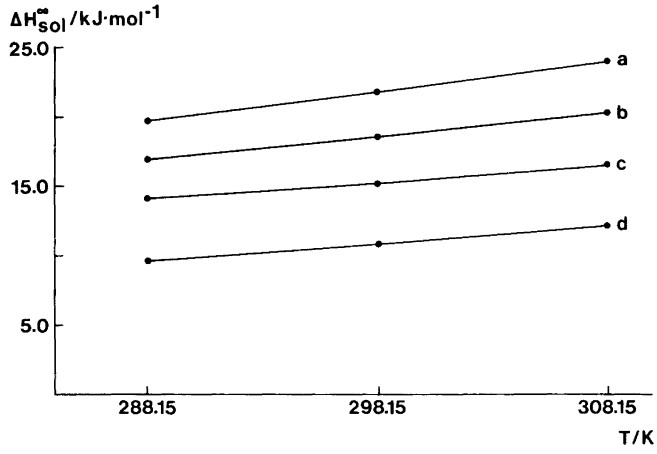

Fig. 1. Enthalpies of solution of some polyols in water. a, D-mannitol; b, D-sorbitol; c, *meso*-inositol; d, α-D-glucose.

Table 2. Heat capacity values for some polyols.

Compound	C_p^*/J K^{-1} mol^{-1}	$C_{p,2}^\infty$/J K^{-1} mol^{-1}
D-Mannitol	239.00±0.16	451±6
D-Sorbitol	241.43±0.31	410±5
meso-Inositol	218.31±0.25	340±5
α-D-Glucose	219.79±0.17	347±3

Results of the heat capacity measurements on the pure samples, C_p^*, and values calculated for the partial molar heat capacities at infinitely dilute aqueous solution, $C_{p,2}^\infty$, are given in Table 2.

Our C_p-value for mannitol is slightly lower than the value which can be derived from the measurements by Spaght *et al.*,[13] 241 J K^{-1} mol^{-1}. For glucose, Kawaizumi *et al.*[4] recently reported the value $C_p = 224 \pm 3$ J K^{-1} mol^{-1} at 298.15 K, which is slightly higher than that obtained here.

In aqueous solution α-D-glucose will form an equilibrium mixture of the α and β forms. However, the main period of the calorimetric solution experiment was short (<2 min), and only a small fraction of the glucose was converted to the β-form (*ca.* 3% at 298 K). The enthalpy change for glucose mutarotation is small, $\Delta H(\alpha \rightarrow \beta) = -1.16$ kJ mol^{-1} at 298.15 K[11] and we therefore consider the enthalpy and heat capacity values reported here for glucose as referring to the pure α-form.

Table 3 summarizes aqueous $C_{p,2}^\infty$-values for some sugar alcohols and sugars. In the table, values are also given which were predicted by our additivity scheme[1] and the corresponding deviations (Δ) from the experimental values. In the last column a value expressing the relative deviation from the experimental value is given, $\Delta_{rel} = [\Delta/C_{p,2}^\infty(\text{exp})] \times 100$. Pentoses and hexoses are considered as cyclic compounds[14] and the cyclization parameter[1] of −20 J K^{-1} mol^{-1} was added to the value calculated from the group parameters. For the disaccharides and for the trisaccharide, −40 and −60 J K^{-1} mol^{-1}, respectively, were added. These latter values

Table 3. Partial molar heat capacities for some polyols in aqueous solution at 298.15 K.

Compound	$C_{p,2}^\infty$/J K^{-1} mol^{-1}				Δ[c]/ J K^{-1} mol^{-1}	Δ_{rel}[c]
	This work	Literature	Preferred value[a]	Calc. value[b]		
Ethanediol		193,[d] 192,[e] 195[f]	193±2	198	−5	−3
Glycerol		279,[g] 226,[g] 240[f]	240±4	230	10	4
meso-Erythriol		310[f]	310±2	262	48	15
D-Xylitol		346[f]	346±2	294	52	15
D-Arabitol		375[f]	375±2	294	81	22
L-Arabitol		373[f]	373±2	294	79	21
Ribitol		376[f]	376±2	294	82	22
D-Xylose		281[h]	281±2	141	140	50
D-Ribose		271[h]	271±2	141	130	48
D-Arabinose		278[h]	278±3	141	137	49
L-Arabinose		270[h]	270±4	141	129	48
D-Mannitol	451	455,[f] 440,[i] 441[j]	452±4	326	126	28
D-Sorbitol	410	423,[f] 413[j]	412±5	326	86	21
meso-Inositol	340		340±5	172	168	49
α-D-Glucose	347	323,[j,l] 331[k,l]	347±3	173	174	50
Fructose		352[k]	352±8	173	179	51
Galactose		324[k]	324±10	173	151	47
Mannose		337[k]	337±5	173	164	49
Lactose		619[k]	619±16	271	348	56
Maltose		614[k]	614±20	271	343	56
Sucrose		649,[f] 655[m]	650±2	271	379	58
Raffinose		931[k]	931±7	369	562	60

[a] Uncertainties are estimates or were taken from the references indicated. [b] Calculated from group parameter scheme.[1] [c] $\Delta = C_{p,2}^\infty(\text{exp}) - C_{p,2}^\infty(\text{calc.})$. $\Delta_{rel} = [\Delta/C_{p,2}^\infty(\text{exp})] \times 100$. [d] Ref. 15. [e] Ref. 16. [f] Ref. 3. [g] Calculated from ΔC_p values given in Ref. 17, *cf.* Ref. 1. [h] Ref. 5. [i] Ref. 18. [j] Calculated from data in Ref. 2. [k] α,β equilibrium mixture. [l] Ref. 4. [m] Ref. 19.

are considered as very uncertain but on a relative basis the cyclization parameters will influence the differences between experimental and calculated values (Δ_{rel}) to only a small extent. For instance, if the cyclization parameter for raffinose is neglected, Δ_{rel} will be 54 rather than 60.

The present $C^{\infty}_{p,2}$-value for mannitol is in excellent agreement with that reported by Di Paola and Bellau,[3] whereas their value for sorbitol is higher than the present result. For this substance our value agrees with that derived from the measurements by Bonner and Cerutti.[2] For glucose the present value is significantly higher than those obtained from heat capacity measurements on glucose solutions, which presumbaly were α,β equilibrium mixtures. From Sturtevant's mutarotation studies[11] the value $\Delta C_p = -9$ J K^{-1} mol^{-1} can be derived for the process

α-D-glucose(aq) = β-D-glucose(aq).

Thus, the $C^{\infty}_{p,2}$-values obtained for the equilibrium mixture (37% α form)[20] should be increased by 5 J K^{-1} mol^{-1} in order to refer to the pure α-form, which will somewhat decrease the difference between the earlier and the present results.

The $\Delta C^{\infty}_{p,2}$-values (Table 1) are all large and positive, suggesting a substantial interaction with the water, as has been pointed out in earlier studies.[2-5] However, we do not consider the ΔC_p-values well-suited for comparison of solute −solvent interactions, as they also will reflect properties of the crystalline compounds. We therefore rather chose to compare the differences between experimental $C^{\infty}_{p,2}$-values and values predicted from our group-parameter scheme, *cf.* recent work by Kawaizumi *et al.*[4,5]

From Table 3 it can be seen that the agreement between predicted and experimental values for ethylene glycol and glycerol is good, which suggests that the presence of neighbouring hydroxyl groups in itself does not impair the additivity scheme. However, for the C_4-C_6 sugar alcohols and for the sugars listed in Table 1, Δ-values are all large. As might be expected, the deviations increase with the size of the solute molecules, but it is interesting to note that there is also a marked relative increase, Δ_{rel}. We note that Δ_{rel} is substantially larger for the pentoses than for the C_5 straight-chain alcohols. The situation is similar for corresponding series of C_6 compounds.

Further, it is interesting to note that the Δ_{rel}-value for the cyclic hexahydroxyl compound *meso*-inositol is much larger than the Δ_{rel}-values for the corresponding open-chain hexahydroxyl compounds mannitol and sorbitol. The value for *meso*-inositol is, in fact, the same as those found for the (cyclic) pentoses and hexoses.

The Δ_{rel}-values for the disaccharides and the trisaccharide are higher than those for the pentoses and the hexoses, but with the uncertain cyclization parameter in mind we do not consider the difference significant. In summary, it seems as if the high $C^{\infty}_{p,2}$-values are partly due to a cooperative effect and that the ring structures give significant contributions. We interpret the observed positive Δ-values as caused by endothermic "melting" processes taking place when extensive interactions (hydrogen bonding) between solutes and water decrease with increasing temperature.

Large negative values for ΔC_p in binding reactions involving *e.g.* proteins are often taken as a sign of hydrophobic interactions. The large $C^{\infty}_{p,2}$-values for polyols suggest that binding reactions involving sugar moieties being transferred from aqueous solution into a water deficient binding site possibly are also characterized by a negative ΔC_p-value.

Acknowledgements. This work has been supported by the Swedish Natural Science Research Council. We gratefully acknowledge the technical assistance of Mrs. G. Gränz.

REFERENCES

1. Nichols, N., Sköld, R., Spink, C., Suurkuusk, J. and Wadsö, I. *J. Chem. Thermodyn. 8* (1976) 1081.
2. Bonner, O. D. and Cerutti, P. J. *J. Chem. Thermodyn. 8* (1976) 105.
3. DiPaola, G. and Belleau, B. *Can. J. Chem. 55* (1977) 3825.
4. Kawaizumi, F., Nishio, N., Nomura, H. and Miyahara, Y. *J. Chem. Thermodyn. 13* (1981) 89.
5. Kawaizumi, F., Kushida, S. and Miyahara, Y. *Bull. Chem. Soc. Jpn. 54* (1981) 2282.
6. Tait, M. J., Suggett, A., Franks, F., Ablett, S. and Quickenden, P. A. *J. Solution Chem. 1* (1972) 131.
7. Franks, F., Ravenhill, J. R. and Reid, D. S. *J. Solution Chem. 1* (1971) 3.
8. Høiland, H. and Holick, H. *J. Solution Chem. 7* (1978) 587.
9. Shahidi, F., Farrel, P. G. and Edward, J. T. *J. Solution Chem. 5* (1976) 807.
10. Suurkuusk, J. and Wadsö, I. *J. Chem. Thermodyn. 6* (1974) 667.

11. Sturtevant, J. M. *J. Phys. Chem. 45* (1941) 127.
12. Taylor, J. B. and Wawlingson, J. S. *Trans. Faraday Soc. 51* (1955) 1183.
13. Spaght, M. E., Thomas, S. B. and Parker, G. S. *J. Phys. Chem. 36* (1932) 882.
14. Angyal, S. J. *Angew. Chem. 81* (1969) 172.
15. Nichols, N., Sköld, R., Spink, C. and Wadsö, I. *J. Chem. Thermodyn. 8* (1976) 993.
16. Jolicouer, C. and Lacroix, G. *Can. J. Chem. 54* (1976) 624.
17. Franks, F., Reid, D. S. and Suggett, A. *J. Solution Chem. 2* (1973) 99.
18. White, C. M. *J. Am. Chem. Soc. 58* (1936) 1620.
19. Gucker, F. T., Jr., Pickard, H. B. and Plenck, R. W. *J. Am. Chem. Soc. 61* (1939) 459.
20. Dawson, R. M., Elliott, D. C., Elliott, W. H. and Jones, K. M. *Data for Biochemical Research*, 2nd Ed., Oxford Univ. Press, London 1969, p. 233.

Received January 29, 1982.

Acta Chemica Scandinavica A 36 (1982) 741 – 750

Hydrophilic Complexes of the Actinides. I. Carbonates of Trivalent Americium and Europium

ROBERT LUNDQVIST

Department of Nuclear Chemistry, Chalmers University of Technology, S-412 96 Göteborg, Sweden

The carbonate complex formation of Am^{3+} and Eu^{3+} has been studied by distribution between 1 M $NaClO_4$ and tributylphosphate (TBP) and by electromigration. The extraction of perchlorate salts as well as the sorption and hydrolysis arising in alkaline solutions have been investigated in some detail.

The distribution data may be explained up to 3 M sodium hydrogencarbonate concentration by assuming the formation of complexes of the type $Me(CO_3)_n^{(3-2n)+}$ with $n=1$ and 2. The following constants have been evaluated at 25 °C:

	Eu^{3+}	Am^{3+}
$\log \beta_1$	5.93 ± 0.05	5.81 ± 0.04
$\log \beta_2$	10.72 ± 0.08	9.72 ± 0.10

Evidence was obtained that the hydrolysis of the Eu^{3+} and Am^{3+} ions is negligible for $pH \lesssim 7$.

One of the most important problem areas of nuclear technology is the safe handling and the storage of spent nuclear fuels. Essential information on actinide chemistry in groundwater is lacking. The complexation of the actinide ions in the various oxidation states with hydrophilic ligands in nearly neutral solutions is especially needed because complexation strongly affects their mobility. Among the most important inorganic ligands for which there is insufficient information available is carbonate. We have therefore undertaken a study of its complexation, beginning with the trivalent americium and europium. Ultra micro quantities of the metals were chosen in order to avoid polynuclear complexes. Distribution between an organic and an aqueous phase was employed as the main technique. Also the migration in an electric field was investigated because it gives complementary information about ionic charges, dimensions and mobilities.

EXPERIMENTAL

Procedures. The solvent extraction experiments were performed in a double glass-walled vessel of approximately 50 ml volume, thermostated to 25 °C. 15 ml of aqueous carbonate-perchlorate solution and of preequilibrated pure tributyl phosphate (100% TBP), plus 10 – 20 μl of ^{241}Am or ^{152}Eu in 0.1 M $HClO_4$ was added. The extraction system was then contacted with CO_2 by bubbling a gas mixture of CO_2 and Ar through the solution. 15 – 20 min stirring periods were found to be sufficient for establishing equilibrium. For some experiments at zero or very low carbonate concentration and near neutral pH, longer stirring times were tested (up to 20 h) in order to follow the kinetics of the loss of activity due to sorption. The sampling, activity and pH measurements were made as described earlier.[1] Total bicarbonate and carbonate concentrations were determined by titration of aqueous samples, to which a known amount of NaOH were added, with $HClO_4$ using a glass electrode and/or methyl red indicator. The TBP was found to not dissolve or extract any appreciable amounts of bicarbonate or carbonate.

The electromigration experiments were carried out, at a field strength of 7.94 V/cm, in aqueous bicarbonate and perchlorate solution, supported by a cellulose filter paper (Whatman 41). In order to be able to account for the increase in viscosity at higher bicarbonate concentrations (up to 3 M $NaHCO_3$) measurements were made with an Ubbelhode viscosimeter. A general description of the method of electromigration has been given earlier.[2]

Chemicals and nuclides. Stock solutions of $NaHCO_3$, $HClO_4$, $NaClO_4$ and NaOH were

0302-4377/82/090741-10$02.50

prepared from *p.a.* quality reagents.[1] TBP (obtained from Fluka *puriss p.a.*) was treated by preextractions with NaOH and fresh perchlorate solutions of a composition corresponding to the actual experiment. For the use as a carrier for the trace concentrations of Am and Eu macro concentrations of Eu or La were sometimes used and therefore stock solutions of 1 M $Eu(ClO_4)_3$ and $La(ClO_4)_3$ were prepared from Eu_2O_3 and La_2O_3 (Merck, *p.a.*). Stock solution of the radioactive isotopes ^{241}Am, ^{152}Eu and ^{22}Na obtained from Amersham were prepared as 0.1 M $HClO_4$ solutions containing about 10^5 Bq/ml.

SOLVENT EXTRACTION STUDIES

Extraction mechanisms. Before employing the TBP solvent extraction system, it was neccesary to analyze the extraction mechanisms with respect to the variables like pH, ionic strength and electrolyte composition (with and without carbonate).

From the obtained information about the distribution D of Am^{3+}, Eu^{3+} and Na^+ (see Fig. 1, showing $D=[M(org)]/[M(aq)]$ *versus* log $[NaClO_4]$), it was found that the distribution values of Am^{3+} and Eu^{3+} were suitable in magnitude at 1 molar ionic strength. At this concentration of $NaClO_4$ there will be an appreciable extraction of $NaClO_4$ into the TBP phase which lowers the free TBP concentration and hence affects the extractibility of other metal perchlorates like $Am(ClO_4)_3$. However, if the $NaClO_4$ concentration is kept constant, there will be no need for any correction of the Eu^{3+} and Am^{3+} distribution values.

Furthermore it was found that the distribution of $NaClO_4$ was rather small anyway, *i.e.* less than 20% reaching its maximum value at about 1–2 M $NaClO_4$. The behaviour of Na^+ agrees well with what has been observed earlier.[3] The extraction of Am and Eu increases sharply with the ionic strength, the log *D vs.* the logarithm of the perchlorate concentration gives a slope of about 2.5. There is region of less steep slope, from 0.3 to 4 M $NaClO_4$, which is most likely the result of a reduction in the extraction capacity of TBP due to the simultaneous maximum in the extraction of $NaClO_4$. Based on the above results, one may suggest that the trivalent metals are extracted by solvation according to relation (1). A detailed knowledge on the extraction mechanism is however not necessary for our purpose.

$$M^{3+} + 3\ ClO_4^- + n\ TBP(\text{organic phase}) \rightleftarrows M(ClO_4)_3 \cdot n\ TBP(\text{organic phase}) \quad (1)$$

Hydrolysis. The versatility of the TBP extraction system is apparent from Fig. 2 where the wide pH region of constant D is shown. The distribution of Am^{3+} and Eu^{3+} between 1 molar perchlorate solutions and TBP is constant between pH 2 and up to at least 6.7 (in the case of Am^{3+}) before sorption of the metals on glass surfaces becomes significant. At still higher pH there is a decrease in the distribution values although unexpectedly high values were

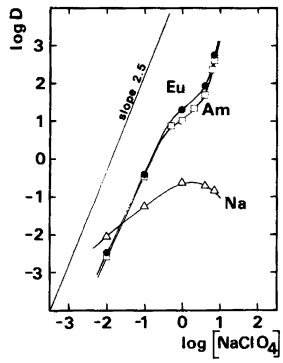

Fig. 1. The effect of the sodium perchlorate concentration on the distribution of Am^{3+}, Eu^{3+} and Na^+ between 100% TBP and aqueous perchlorates solutions at pH 2 and 25 °C. (□) denotes ^{241}Am, (●) ^{152}Eu and (△) ^{22}Na.

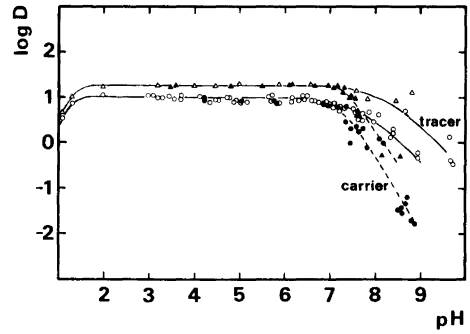

Fig. 2. The effect of pH on the distribution of Am and Eu between 100% TBP and 1 M $NaClO_4$, at 25 °C. The distribution is shown both in the absence and in the presence of Eu carrier (totally 2×10^{-4} M in both phases). (○) Am tracer, (●) Am tracer+Eu carrier, (△) Eu tracer and (▲) Eu tracer+Eu carrier.

Table 1. Change in the distribution values D of Am and Eu at higher pH in presence and absence of europium carrier. Tentative first hydrolysis constants $^*K_1$ ($M^{3+} + H_2O \rightleftarrows MOH^{2+} + H^+$) are derived for 1 M $NaClO_4$, 25 °C.

M(III)	pH (start of decrease in *D*)			pH (50% decrease in *D*)		log K_1*
	tracer	Eu-carrier[a]	La-carrier[b]	tracer	Eu-carrier[a]	tracer
Am	6.7±0.1	6.7±0.1	8.0±0.2	7.5±0.3	7.25±0.08	−7.5±0.3
Eu	7.0±0.1	7.0±0.1		8.1±0.4	7.43±0.08	−8.1±0.4

[a] $0.5-2\times10^{-4}$ M Eu (organic + aqueous phase). [b] $10^{-4}-10^{-3}$ M La (organic + aqueous phase).

occasionally obtained even at a pH as high as 10; in this region the metal sorption was very high (*ca.* 90%), which made the distribution measurements rather uncertain.

It was also noted that if $Eu(ClO_4)_3$ or $La(ClO_4)_3$ was added as a carrier the *D*-values seemed to become more reproducible and they decreased more sharply. The concentration of the carrier, in the concentration range (organic + aqueous phase) from 0.5 to 2×10^{-4} M Eu and from 10^{-4} to 10^{-3} M La, had no effect. However the influence of La and Eu carrier on the distribution of Am^{3+} were different. Whereas for Eu carrier the decrease in the *D*-values began at lower pH, in comparison with carrier free conditions, the opposite was found for La carrier.

In order to avoid or reduce the possible sorption on suspended (colloidal) impurity particles, we tried centrifugation (17000 rpm for one hour) and filtration (pore size 400 nm) of the solutions. However, no remarkable changes compared with the regular solutions were observed. No crucial improvement were obtained either when increasing pH by coulometric electrolysis instead of alkali additions. In Table 1 some data is given on the change in the distribution values at neutral and slightly alkaline conditions. The decreasing extractability is interpreted as due to the onset of hydrolysis of the trivalent metals, and the first hydrolysis constants were estimated from the pH corresponding to a 50% decrease in the extraction at tracer level (see Table 5). Least-squares regression analysis of the distribution data were also performed giving log $^*K_1 = -7.5\pm0.3$ for Am.

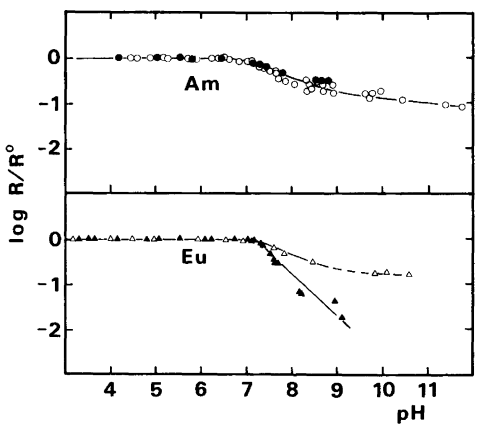

Fig. 3. The effect on the ratio ($R/R°$) due to sorption of Am and Eu in the 100% TBP-1 M $NaClO_4$ extraction system. Experiments were made both in absence and in presence of Eu carrier (totally 2×10^{-4} M in both phases). R = total soluble activity of both phases (Bq/l) and $R°$ = added total activity of both phases (Bq/l). Same symbols as in Fig. 2.

Sorption. Strong sorption at higher pH (*i.e.* over pH 6.7 for Am and pH 7.0 for Eu) introduces a source of uncertainty in the experimental determination of the distribution values. It was found that reproducible distribution values with carbonate were only obtained under conditions of no sorption. Negligible sorption could be achieved either at sufficiently low pH or high enough bicarbonate concentration.

The "safe" concentration area of hydrogen and bicarbonate ions was determined by performing a number of experiments at various conditions while checking the extent of sorption by measuring the ratio $R/R°$. This ratio between the equilibrium activity R (Bq/ml) of the combined organic and aqueous phases and the initially added activity $R°$ is a measure of the mass balance and of the extent of loss of activity due to sorption on the glass vessel. From Fig. 3 one concludes that no sorption occurs for pH lower than about 6.7 and that the sorption process, is affected by the presence of macro concentrations of Eu in case of europium tracer but not americium tracer. The sorption characteristics are collected in Table 2. It can be noted that in the absence of carrier the sorption starts at about the

Table 2. Sorption of Am^{3+} and Eu^{3+} during extraction with TBP from 1 M $NaClO_4$, 25 °C. The extent of sorption is obtained from the ratio R/R° where R is the total activity in both phases and R° the initial activity.

M(III)	pH (sorption starts)			pH (50% sorbed)			max ($\delta \log(R/R^\circ)/\delta$ pH)	
	tracer	Eu-carrier[a]	La-carrier[b]	tracer	Eu-carrier[a]	La-carrier[b]	tracer	Eu-carrier[a]
Am	6.7±0.1	6.7±0.1	7.4±0.2	7.7±0.1	7.8±0.1	8.5±0.3	−0.3	−0.3
Eu	7.0±0.1	7.0±0.1		7.9±0.1	7.5±0.1		−0.3	−1

[a] $0.5-2\times10^{-4}$ M Eu (organic + aqueous phase). [b] $10^{-4}-10^{-3}$ M La.

Table 3. Solubility of CO_2 in 1 M $NaClO_4$ at various pH and at 25 °C. 1 atm of CO_2 (g).[a]

pH	$C=[HCO_3^-]$	log C	$\log[CO_2+H_2CO_3]$ $(=pK_1-pH+\log C)$	$[CO_2+H_2CO_3]$ M
5.04	0.0031	−2.51	−1.51	0.031
5.32	0.0054	−2.27	−1.55	0.028
5.61	0.0109	−1.96	−1.53	0.030
6.09	0.0345	−1.46	−1.51	0.031
6.27	0.0501	−1.30	−1.53	0.030
6.57	0.108	−0.97	−1.50	0.032
6.81	0.181	−0.74	−1.51	0.031
7.13	0.436	−0.36	−1.45	0.036
				mean: 0.031±0.002

[a] $K_1=[H^+][HCO_3^-]/[CO_2+H_2CO_3]=10^{-6.04}$.

same pH value as the hydrolysis.

Carbonate complexing. Introduction of carbon dioxide gas into the extraction system produces carbonate and bicarbonate ions, of which HCO_3^- is the predominating species in the pH interval of interest (from pH 6 to pH 9). The resulting formation

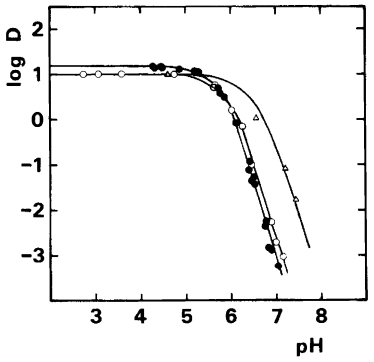

Fig. 4. The distribution D of ^{241}Am and ^{152}Eu between 100% TBP and 1 M $NaClO_4$ saturated with 1 atm. of a gas mixture of CO_2+Ar as a function of pH at 25 °C. (○) Am, 100% CO_2, (●) Eu, 100% CO_2 and (△) Am, 10% $Co_2+90\%$ Ar.

of complexes in the aqueous phase can be described by eqn. (2), where M^{3+} is the trivalent metal (Am or Eu), x and y are system parameters. Assuming that the metal carbonates are not extractable, one can derive an expression, eqn. (3) for the distribution D of the metal, where D° denotes the distribution value ($D=$ [M](organic phase)/[M](aqueous phase) in the absence of the complexing ligands L and OH^-. The influence of pH in the presence of 1 atm of CO_2(g) is shown in Fig. 4 in which the sharp decrease in log D with increased pH above pH 5 is demonstrated. The slope of log D *versus* pH reaches a value of almost −4 at the highest pH. The decrease in D cannot be a hydrolysis effect, because the acidity of the experiments is high enough to prevent interference from hydrolysis or sorption (*i.e.* pH <7 as derived from Figs. 2 and 3 and Tables 1 and 2). One may therefore interpret the diminishment in the extractibility of Am and Eu as a result of complexing with HCO_3^- and CO_3^{2-} which rapidly increases with increased pH.

$$M^{3+}+xHCO_3^- \rightleftarrows M(HCO_3)_xH_{-y}^{(3-x-y)}+yH^+ \quad x\geq y \qquad (2)$$

$$D/D^\circ = [Me^{3+}]/[Me]_{tot} = 1 + \Sigma\beta_n[L]^n + \Sigma\beta_j[OH]^i \quad (3)$$

Separate analysis was made to determine the solubility of CO_2 in 1 M $NaClO_4$ for the used pH range. The titration data are presented in Table 3, showing a constant solubility of CO_2 of about 0.031 M at 25 °C and 1 atm CO_2. In calculating the concentrations of bicarbonate and carbonate ions from the solubility of CO_2 we used the following acid dissociation constants valid for 1 M $NaClO_4$ at 25 °C; log K_1 ($CO_2 + H_2CO_3 \rightleftarrows H^+ + HCO_3^-$) = −6.04 and log K_2 ($HCO_3^- \rightleftarrows H^+ + CO_3^{2-}$) = −9.57.[4]

Despite the fact that the bicarbonate ion HCO_3^- concentration is dominating over CO_3^{2-} in the entire investigated acidity range, it was found that the bicarbonate ion was not participating in the complexing reactions. The D values did not coincide into one curve, log $D = f([HCO_3])$, for different partial pressures of CO_2, *i.e.* the reaction was pH dependent with $y = 1$ to 2 according to eqn. (2). Hence the complexation instead takes place with CO_3^{2-} according to eqn. (4).

$$M^{3+} + n\ CO_3^{2-} \rightleftarrows M(CO_3)_n^{(3-2n)+} \quad (4)$$

This is confirmed by plotting log D against the CO_3^{2-} concentration, see Fig. 5. The maximum slope of log D/D° against log $[CO_3^{2-}]$ is −2 corresponding to n = 2. It can also be noted that the Eu(III) carbonate is somewhat stronger than the Am(III) carbonate. The stability constants for the metal carbonate complexes were derived by least squares regression analysis of the distribution data in the form of eqn. (2).

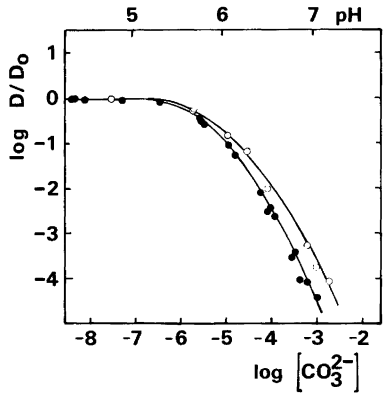

Fig. 5. Normalized distribution (log D/D_0) of Am and Eu between 100% TBP and 1 M $NaClO_4$ as a function of carbonate ion concentration at 25 °C. The aqueous phase was saturated with 1 atm of CO_2 and the corresponding acidity is indicated. (○) Am.

The following values ($\pm\sigma$) were obtained for 1 M $NaClO_4$ and 25 °C; $AmCO_3^+$ (log $\beta_1 = 5.81 \pm 0.04$), $Am(CO_3)_2^-$ (log $\beta_2 = 9.72 \pm 0.10$), $EuCO_3^+$ (log $\beta_1 = 5.93 \pm 0.05$) and $Eu(CO_3)_2^-$ (log $\beta_2 = 10.72 \pm 0.08$).

The utilized extraction system behaves very well under the limited conditions employed for deriving the metal carbonate formation constants. However, deviations are found at higher pH or carbonate concentrations. For instance, the aqueous bicarbonate concentration may be limited because $NaHCO_3$ precipitates out at 1 atm of CO_2 at pH about 8. The TBP extraction system was also tested at very high carbonate concentrations and at 1 M $NaHCO_3$ without any $NaClO_4$. It was possible to estimate a maximum extractability of Am and Eu carbonate due to the fact that the D values did not decrease as much as expected at the highest carbonate concentrations, but levelled off at log $D \sim -4$. This indicates that the metal carbonates might be extractable to this very low extent ($D \leq 10^{-4}$) if not some impurities accounted for the small extraction ("background extraction"). Furthermore, it should be mentioned that the ionic strength increased somewhat at pH > 6.5. However, from previous experience of the TBP system it was not considered relevant to make any corrections in D because of the cancelling influence of β_2 and "salting out" effects.

ELECTROMIGRATION STUDIES

The use of the electromigration method, which is based on the transport properties of the ion in an electrolyte solution, offers the possibility of determining the charge of a metal complex.[2] The relation between the charge z_i and the migration velocity v_i of a metal complex i can be formulated as in relation (5), where g_i is a volume ratio factor and m is the charge of the uncomplexed ion M^{m+}. Since g_i for most of the metal complexes investigated varies only little (within ±20%) one may, as a first approximation, regard the migration velocity as proportional to the charge of the migrating ion.[2]

$$v_i = z_i\ (g_i/m) \quad (5)$$

Table 4. Viscosity of $NaHCO_3 + NaClO_4$ solutions relative to H_2O at 20 °C.

Solution	Viscosity rel. H_2O ($\sigma = \pm 0.03$)	Density g/ml
1 M $NaClO_4$	1.04	1.081
0.1 M $NaHCO_3$ + 0.9 M $NaClO_4$	1.11	1.075
0.2 M $NaHCO_3$ + 0.8 M $NaClO_4$	1.10	1.072
0.4 M $NaHCO_3$ + 0.6 M $NaClO_4$	1.15	1.072
1.0 M $NaHCO_3$	1.31	1.057

The electromigration experiments were carried out in mixtures of $NaHCO_3$ and $NaClO_4$ at 1 M ionic strength and pH about 7.8. In order to improve the accuracy of the migration velocity determinations $^{22}Na^+$ was run simultaneously as a reference ion. Relative migration velocities (v_i/v_{Na^+}) of Am and Eu were calculated and plotted as a function of the total $NaHCO_3$ concentration as shown in Fig. 6. Noticable is the initial increase in migration velocity at low bicarbonate concentrations when sorption and hydrolysis are suppressed by metal carbonate formation. At yet higher bicarbonate concentration (log $[NaHCO_3] > -3.5$ M) there is a continuous decrease in the migration velocities until a plateau value of opposite sign is reached (log $[NaHCO_3] > -0.4$). A possible second plateau corresponding to charge +1 is indicated, but too much emphasis on the shape of the electromigration curve at the lowest $NaHCO_3$ concentrations should not be made because it was difficult to obtain reproducible results for $[NaHCO_3] < 0.01$ M.

The conclusion from the present electromigration study is that the charge of the complexes Am or Eu may become −1, but not more negative (since a plateau of the anionic migration velocities is reached with increasing $NaHCO_3$ concentrations). The "plateau" velocity corresponds to about −32% of the migration velocity of uncomplexed Am or Eu. It is expected to be −33% for charge −1 while for charge −2 it would have been −67%. The absolute migration velocities at the highest bicarbonate concentration is somewhat lower (−27%) because the ions are moving a little slower due to the increase in viscocity. However, the viscosity of the solutions is nearly constant for carbonate concentrations up to about 0.1 M and increases thereafter somewhat; Table 4.

The conclusion is thus that the highest anionic species formed has a charge −1 which agrees well with the solvent extraction studies where the highest carbonate complex was found to be $Am(CO_3)_2^-$ or $Eu(CO_3)_2^-$. Assuming that a mixture of 50% MCO_3^+ and 50% $M(CO_3)_2^-$ moves with zero average speed, which occurs at 0.040 M $NaHCO_3$ and pH about 7.8, one can estimate the formation constant of the second stepwise complex according to eqn. (5); log K_2 becomes 3.2 ± 0.3. This value is

$$AmCO_3^+ + CO_3^{2+} \rightleftarrows Am(CO_3)_2^- \quad (5)$$

somewhat smaller than the log $K_2 = 3.96 \pm 0.09$ derived from the solvent extraction experiments. (The larger uncertainty in the former experiments is due to that the experimental conditions such as pH

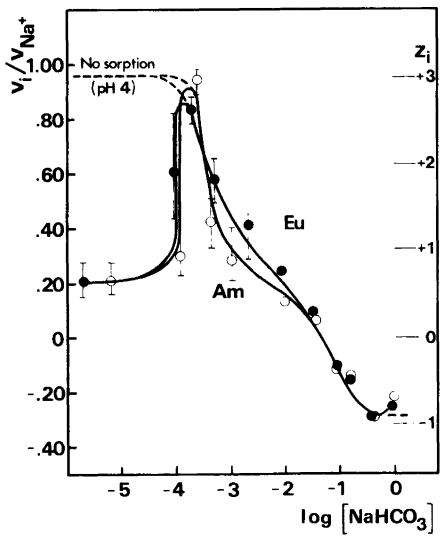

Fig. 6. Electromigration velocities, v_i/v_{Na^+}, relative to Na^+ of Am and Eu in $NaHCO_3 + NaClO_4$ solutions at 1 M ionic strength, pH *ca.* 7.8 and 25 °C. The dashed line shows the migration velosities of the uncomplexed M^{3+} ion obtained in 1 M $NaClO_4$ at pH 4. The charge z_i of the migration complex was estimated by eqn. (5) and is shown for convenience.

and sorption were not controlled as carefully as in the extraction experiments because they were mainly aimed at finding out the maximum anionic charge of the metal carbonates.) A similar deriviation of β_1, although rather uncertain, from the migration curve gives $\log \beta_1 = 5.3 \pm 0.4$ which is not very different from the solvent extraction value ($\log \beta_1 = 5.81 \pm 0.04$).

DISCUSSION

Recently the solubilities of the actinides in neutral or basic solutions were reviewed.[5] Hydrolysis and carbonate complexation were considered to be the two most important systems, in urgent need of reliable data. Our results on hydrolysis and carbonate complexing of Am and Eu will therefore be somewhat extensively discussed and compared with the literature information.

Hydrolysis. The only positively identified hydroxide species of the trivalent actinides or

Table 5. Acid hydrolysis constants K_1^* ($M^{3+} + H_2O \rightleftarrows M(OH)^{2+} + H^+$) of trivalent actinides and lanthanides in $NaClO_4$ solutions at 25 °C. pK_w; 13.80 (1 M $NaClO_4$), 13.79 (0.5 M $NaClO_4$), 13.79 (0.1 M $NaClO_4$), 14.00 (H_2O).

Metal	$\log {}^*K_1$, $\mu=0$	$\log {}^*K_1$, $\mu=0.1$	$\log {}^*K_1$, $\mu=1$ normalized	$\log {}^*K_1$, $\mu=1$	r_c, Å 6-coord[k]	$\log K_s$, $\mu=0$ mol^{-2}
An	-8.0 ± 0.5[a,b]		-8.7 ± 0.5[a,b]			-23.5[a,b]
U	-7 ± 1[a,c]		-8.0 ± 1[a,c]		1.03	-24 ± 3[a,c]
Np	-7.4 ± 0.5[a,c]		-8.7 ± 0.5[a,c]		1.01	-24 ± 2[a,c]
Pu	-6.8 ± 0.5[a,c]		-7.5 ± 0.5[a,c]	-5.54 ± 0.04[l]		-25 ± 2[a,c]
Pu	-8.0 ± 0.5[a,d]		-8.7 ± 0.5[a,d]		1.00	-20[f,i]; -19.7[j]
Pu	-6.95[a,f]		-7.7[a,f]			
Am				-7.03 ± 0.04[l]		
Am		-5.9 ± 0.1[g]	-6.2 ± 0.1[g]	-7.5 ± 0.3 this work	0.99	-24[e]
Am	(−0.5 to 4.0)[h]		(−1.2 to 4.7[h])			
Cm		-5.9 ± 0.1[g]	-6.2 ± 0.1[g]		0.986	
Bk		-5.7 ± 0.1[g]	-6.0 ± 0.1[g]		0.981	
Cf		-5.6 ± 0.1[g]	-5.9 ± 0.1[g]		0.976	
La	-8.5 ± 0.2[a,d]		-9.2 ± 0.2[a,d]		1.061	-21.7 ± 0.6[a,d]
Ce	-8.3 ± 0.2[a,d]		-9.0 ± 0.2[a,d]		1.034	-22.1 ± 0.6[a,d]
Pr	-8.1 ± 0.2[a,d]		-8.8 ± 0.2[a,d]		1.013	-22.5 ± 0.6[a,d]
Nd	-8.0 ± 0.2[a,d]		-8.7 ± 0.2[a,d]		0.945	-23.4 ± 0.6[a,d]
Sm				-8.84 ± 0.02[l]		
Sm	-7.9 ± 0.2[a,d]		-8.6 ± 0.2[a,d]		0.964	-25.5 ± 0.6[a,d]
Eu				-8.12 ± 0.02[l]		
Eu	-7.8 ± 0.2[a,d]		-8.5 ± 0.2[a,d]	-8.1 ± 0.4 this work	0.950	-24.5 ± 0.6[a,d]
Gd	-8.0 ± 0.2[a,d]		-8.7 ± 0.2[a,d]		0.938	-26.4 ± 0.6[a,d]
Tb	-7.9 ± 0.2[a,d]		-8.6 ± 0.2[a,d]		0.923	-25.5 ± 0.6[a,d]
Dy	-8.0 ± 0.2[a,d]		-8.7 ± 0.2[a,d]		0.908	-26.1 ± 0.6[a,d]
Ho	-8.0 ± 0.2[a,d]		-8.7 ± 0.2[a,d]		0.894	-26.6 ± 0.6[a,d]
Er	-7.9 ± 0.2[a,d]		-8.6 ± 0.2[a,d]		0.881	-27.0 ± 0.6[a,d]
Tm	-7.7 ± 0.2[a,d]		-8.4 ± 0.2[a,d]		0.869	-27.0 ± 0.6[a,d]
Yb	-7.7 ± 0.2[a,d]		-8.4 ± 0.2[a,d]		0.858	-27.3 ± 0.6[a,d]
Lu	-7.6 ± 0.2[a,d]		-8.3 ± 0.2[a,d]		0.848	-27.5 ± 0.6[a,d]

[a] Estimated. [b] Ref. 5. [c] Ref. 13. [d] Ref. 8. [e] Ref. 6. [f] Ref. 14. [g] Ref. 15. [h] Ref.9 – 12, see text. [i] 0.069 M HCl. [j] Ref. 26. [k] Ref. 16. [l] Ref. 29.

lanthanides are MOH^{2+}, $M(OH)_3(s)$ and $M(OH)_4^-$, assuming similar behaviour as found for Sc, Y and Ln.[5] In evaluating the information on hydrolysis we chose to examine the first hydrolysis reaction only, written in the form of eqn. (6).

$$M^{3+} + H_2O \rightleftarrows MOH^{2+} + H^+ \quad (6)$$

Table 5 summarizes the information from literature. The value of the stability constant log $*K_1$ of eqn. (6) obtained at different ionic strengths can be related to each other using an empirical relation.[8] It follows that the log $*K_1$ values decrease with increasing ionic strength; by 0.37 units for 0.1 M $NaClO_4$, 0.60 units for 0.5 M $NaClO_4$ and 0.7 units for 1 M $NaClO_4$ at 25 °C in comparison with pure water. Similtaneously the pK_w values decreases from 14.00 in pure water to 13.80 ± 0.02 for any of the above ionic strengths.

It can be seen from Table 5 that the information at large consists of estimates which are based on very few measurements. It is predicted that the value for Am and Eu lies around log $*K_1 = -8.7 \pm 0.5$ and -8.5 ± 0.5, respectively, in 1 M $NaClO_4$.[5,8] This means roughly that 50% hydrolysis would be expected at pH between 8.7 and 8.5. However, our experiments indicate that the hydrolysis values are somewhat higher, the log $*K_1$ being -7.5 ± 0.3 for Am and -8.1 ± 0.4 for Eu. This difference is not surprising, considering that hydrolysis studies generally are complicated by simultaneous occurring disturbing processes like sorption, precipitation and/or formation of polynuclear and colloid species. In the present work the measured distribution values are not affected by the two first processes. (In principle, the distribution values should be independent of loss of material due to sorption or precipitation.) Further, polynuclear or colloid species should be avoided by applying the tracer technique. Precipitation should be no problem because the aqueous phase was undersaturated even when Eu carrier was added, resulting in an aqueous concentration of $0.2 \times 10^{-5} - 4 \times 10^{-4}$ M. The solubility of Am hydroxide would be much higher, around 0.01 – 0.025 M at pH 6.7, where the decrease in the distribution values are observed to begin, as estimated from the solubility product (log $K_s = -24$ and log $K_s = -23.5$ at zero ionic strength).[6,5] It has also been reported that there was no loss of material from a 10^{-5} M Am solution, of about 0.1 M ionic strength, from pH 5 up to about 7.5.[7]

Table 6. Carbonate complexes of trivalent actinides and lanthanides. Stability constants β_n refers to the reaction $M^{3+} + n\ CO_3^{2-} \rightleftarrows M(CO_3)_n^{3-2n}$.

Metal(III)	log β_1	log β_2	log β_3	log β_4	Remarks (solid complexes, ionic media *etc.*)
Pu	9.6 ?	12.8 ?	16.1 ?	–	$\mu = 0$, estimated[18]
Am	5.81 ± 0.04	9.72 ± 0.10	–	–	1 M $NaClO_4$, 25 °C, no higher complexes than 1:2 at pH ≤ 10. This work.
Am					Only Am^{3+}, $Am(CO_3)^+$ and $Am(CO_3)_2^-$ species in in 1 M($NaClO_4 + NaHCO_3$) at pH 3 – 9.[19]
Am					Precipitation of $NaAm(CO_3) \cdot 4H_2O(s)$ from 0.5 M $NaHCO_3$ and $Na_3Am(CO_3) \cdot 3H_2O(s)$ from 1.5 M Na_2CO_3. No evidence for formation of $Am(CO_3)_4^{5-}$.[20]
An	6.5	11.0	14.5	–	$\mu = 0$, estimate.[5]
La	< 6.6				$\mu = 0$, 1 M $NaClO_4$. Recalculated from Ref. 21.
La	5.7				3 M $NaClO_4$[27]
Ce	6.5	10.95	14.5		3 M $NaClO_4$[27]
Nd				1.08 ?	5.35 M KCl[23]
Eu	5.93 ± 0.05	10.72 ± 0.08	–	–	1 M $NaClO_4$, 25 °C. This work.
Eu					Only Eu^{3+}, $Eu(CO_3)^+$ and $Eu(CO_3)_2^-$ in 1 M ($NaClO_4 + NaHCO_3$) at pH 3 – 9.[19]
Eu	–	–	–	15.55 ± 0.09	$\mu = 2.5$, 0.5 M $NaHCO_3$ + 0.5 M Na_2CO_3, pH 10.3. Relative stability to the EDTA complex.[24]
La – Lu	–	–	–	14.4 – 17.1	$\mu = 2.5$, 0.5 M $NaHCO_3$ + 0.5 M Na_2CO_3, pH 10.3. Relative stability to the EDTA complex.[24]

Due to the unknown influence of the sorption and colloid formation on the distribution values the estimated hydrolysis constants for Am and Eu may be more uncertain than indicated from the numeric analysis only (Table 5). Differences in the interpretation of the sorption processes seem to be the reason for the large discrepancies between different investigators. Hence, some authors on the hydrolysis of Am and other actinides have concluded that the hydrolysis starts already in much more acid media. Using an electrophoretic technique Marin and Kikindai found that $\log {}^*K_1 = -2.7$ at $\mu = 0.005$.[9] Shalinets and Stepanov found $\log {}^*K_1 = -3.1$ for Am and $\log {}^*K_1 = -3.2$ for Cm.[10] From various sorption studies Samartseva found that $\log {}^*K_1 \leq -3.5$ to 4.0.[11] Using paper chromatography and cation exchange Korotkin arrives at $\log {}^*K_1 \sim -0.5$, *i.e.* the hydrolysis "starts" already at pH 0.5, which indicates a many orders of magnitude stronger hydrolysis than concluded in the present work.

Recently, the formation and properties of americium colloids in aqueous systems were studied with sorption/centrifugation techniques and with electromigration. True hydroxide colloid were indicated at pH above 12 whereas small fractions of pseudocolloid, *i.e.* Am sorbed on colloidal impurities, could be found even at pH down to 3.[28] Due to these problems, the present technique (and other methods as well) for obtaining hydrolysis constants should be used with caution. Without doubt the soprtion and colloidal properties are very important and deserve more studies.

Finally, two independent corraborative investigations of the hydrolysis of Am have appeared during the completion of this work. Using potentiometric titration Nair and coworkers obtain $\log {}^*K_1 = -7.03 \pm 0.04$ in 1 M $NaClO_4$ and by solvent extraction Choppin and coworkers arrive at $\log {}^*K_1 = -6.93 \pm 0.03$ in 0.7 M NaCl.

Carbonate complexing. Literature about the complexation of trivalent actinides with carbonate is very meager. Comparison can be made with the lanthanides, even here however the material available is small, see Table 6. The complexation with carbonate ions may be considered to occur according to eqn. (4), *i.e.* by consequtive addition of CO_3^{2-} ligands to the metal. No bicarbonate complexes seem to be formed, even in $NaHCO_3$ solutions, where no higher carbonate complexes than the 1:2 metal to ligand have been observed. In Na_2CO_3 solution the activity of the carbonate ion may become high enough to produce a tricarbonate complex.[20] Tetracarbonates have not been observed for the trivalent actinides in contrast to the lanthanides.[24] The stability constant for the 1:1 carbonates was estimated to be $\log \beta_1 = 9.6$ for Pu^{3+} but this value has been regarded to be largely overestimated.[18,5,19,22] The present value for Am, $\log \beta_1 = 5.81 \pm 0.04$, seems more reasonable and agrees well with the expected behaviour for trivalent actinides, which is around $\log \beta_1 = 6$.[5] However the uncertainty ($\pm\sigma$) in the $\log \beta$ values seems to be somewhat small due to that the ratio K_1/K_2 is too different for the two metals. The ratio K_1/K_2 should be rather similar but is around 80 for Am and around 14 for Eu. Hence an additional systematic uncertainty of about the same size as the given error limits is indicated.

The stability of the lanthanide tetracarbonate complexes was derived from measurements of the relative complexing ability of carbonate in comparison with EDTA.[24] However, it seems likely that the reported $\log \beta_4$ values are perhaps 3 orders of magnitude too large because the values (*e.g.* $\log \beta_4 = 15.55 \pm 0.09$ for Eu) imply that the tri- and tetracarbonates would dominate already for carbonate concentrations over 10^{-4} M while this work does not give any indication of these higher complexes at least up to $10^{-2.5}$ M.

Although the stability of the Am carbonate complex is now found to be weaker than expected earlier, it should be realized that the stability is quite sufficient to suppress hydrolysis and sorption. It

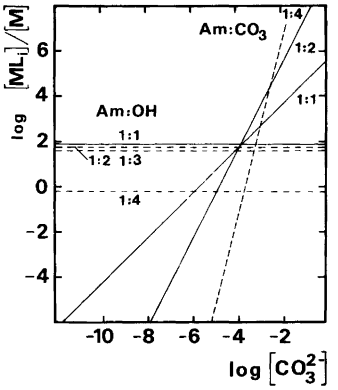

Fig. 7. The ratio $\log [ML_i]/[M]$ for Am(III) as a function of the carbonate concentration in 1 M $NaClO_4$ at pH 9 and 25 °C. Stability constants are from this work (solid lines) and estimated (see Tables 5 and 6, broken lines).

follows that the carbonate ion is a stronger complexing agent, by one order of magnitude, than the hydroxide ion OH^-. This is illustrated in Fig. 7 where $\log [ML_i]/[M]$ is shown as a function of $\log [CO_3^{2-}]$ at pH 9. It follows that the hydrolysis (and sorption) could easily be completely suppressed even at such a high pH.

In this connection one might also comment on the state of Am and Eu in groundwater. Most groundwaters contain 60 – 400 mg HCO_3^- per liter and have a pH in the range from 7.2 to 8.5.[25] As a result of these conditions the carbonates will contribute significantly or even dominate the metal speciation.

Acknowledgements. Many thanks are due to Ing. Theresia Rodinson, Ing. Monica Bengtsson and Miss Marlene Gülich for skilful experimental assistance. The discussions and cooperation with Dr. Jiu Fang Lu, Dr. B. Allard and Prof. J. Rydberg have been very rewarding. This work was supported by the Natural Science Research Council which is gratefully acknowledged.

REFERENCES

1. Lundqvist, R. *Acta Chem. Scand. A 28* (1974) 243.
2. Lundqvist, R. *Acta Chem. Scand. A 35* (1981) 31.
3. Hasegawa, Y., Ishii, T. and Sekine, T. *Bull. Chem. Soc. Jpn. 44* (1971) 275.
4. Dolezal, J. and Novák, J. *Chem. Listy 52* (1958) 582.
5. Allard, B. *Actinides in Perspective, Proc. Actinides-81, Pacific Grove, California, 10 – 15th Sept., 1981*, Pergamon, Oxford 1982, p. 553 and references therein.
6. Starik, I. E. and Ginzburg, F. L. *Radiokhimiya 3* (1961) 685.
7. Edelstein, N., Brown, S. and Silva, R. *Technical Progress Report* ONWI-9(3), 1980, p. 140.
8. Baes, C. F. and Mesmer, R. E. *The Hydrolysis of Cations*, Wiley, New York 1976.
9. Marin, B. and Kikindai, T. *C.R. Acad. Sci. 268* (1969) 1.
10. Shalinets, A. B. and Stepanov, A. V. *Sov. Radiochem. 14* (1972) 290.
11. Samartseva, A. G. *Radiokhimiya 11* (1969) 502.
12. Korotkin, Yu S. *Sov. Radiochem. 15* (1973) 682, 776; Ibid. *16* (1974) 218, 223.
13. Allard, B., Kipatsi, H. and Liljenzin, J. O. *J. Inorg. Nucl. Chem. 42* (1980) 1015.
14. Kraus, K. A. and Dam, J. R. *The Transuranium Elements*, Natl. Nucl. Energy. Ser. Div. IV, 1413, 1949, p. 4. Also in Seaborg, G. T., Katz, J. J. and Mannig, W. M. *The Transuranium Elements*, Pt. 1, McGraw-Hill, New York-Toronto-London 1949, p. 166.
15. Désiré, B., Hussonnois, M. and Guillaumont, R. *C. R. Acad. Sci. Ser. C 269* (1969) 448.
16. Keller, C. *The Chemistry of Transuranium Elements*, Verlag Chemie, Weinheim/Bergstr. 1971, p. 125.
17. Allard, B., Kipatsi, H. and Liljenzin, J. O. *J. Inorg. Nucl. Chem. 42* (1980) 1015.
18. Saltelli, A., Avogadro, A. and Bertozzi, G. *Proc. Workshop on the Migration of Long Lived Radionuclides in the Geosphere*, Brussels Jan. 29 – 31, 1981, p. 147.
19. Lundqvist, R. *Proc. 1ème Journees des Actinides*, Stockholm May 27 – 28, 1980, p. 123.
20. Keller, C. and Fang. O. *Radiochimica Acta 11* (1969) 123.
21. Jordanov, N. and Havezov, I. *Z. Anorg. Allg. Chem. 347* (1966) 101.
22. Skytte-Jensen, B. *Private communication.*
23. Poluektov, N. S. and Kononenko, L. I. *Z. Neorg. Khim. 6* (1961) 1837.
24. Dumonceau, J. *Stabilite des Tetracarbonato-lanthanidates(III), Application a l'Etude des Carbonates Complexes Mixtes*, Thesis, Univ. Reims, 1977.
25. Allard, B. *Proc. Workshop on the Environmental Chemistry of the Actinide Elements*, Warrenton, Oct. 9 – 12, 1978.
26. Degischer, G. and Choppin, G. R. *Complex Chemistry in Aqueous Solutions.* In *Gmelin Handbuch der Anorganischen Chemie, Transurane D1* 1975, p. 129 and references therein.
27. Grenthe, I., as quoted in Ref. 5.
28. Olofsson, U., Allard, B., Andersson, K. and Torstenfelt, B. *Formation and Properties of Americium Colloids in Aqueous Systems.* In *Scientific Bases for Nuclear Waste Management* Elsevier, New York, Vol. 4. *In press.*
29. Nair, G. M., Chander, K. and Joshi, J. K. *Radiochimica Acta 30* (1982) 37.
30. Choppin, G. R. *Private communication.*

Received February 10, 1982.

Acta Chemica Scandinavica A 36 (1982) 751–755

The Crystal Structure of Bis(tetrabutylammonium) Di-μ-iodo-diiododicuprate(I), $[N(C_4H_9)_4]_2[Cu_2I_4]$

MILJA ASPLUND,[a] SUSAN JAGNER[a] and MARTIN NILSSON[b]

[a] Department of Inorganic Chemistry and [b] Department of Organic Chemistry, Chalmers University of Technology and University of Göteborg, S-412 96 Göteborg, Sweden

The crystal structure of the title compound has been determined from single-crystal X-ray diffractometer data collected at 168 K. $[(C_4H_9)_4]_2[Cu_2I_4]$ crystallizes in space group $P2_1/n$ with $a=9.042(3)$, $b=21.231(9)$, $c=11.734(3)$ Å, $\beta=92.88(3)°$ and $Z=2$. Full-matrix least-squares refinement of the 181 structural parameters gave $R=0.058$ for 2088 observed $[I>3.0\sigma(I)]$ independent reflections. The $[Cu_2I_4]^{2-}$ anion is a discrete centrosymmetric dimer containing three-coordinated copper(I). The $Cu-I_{bridging}$ distances are 2.566(2) and 2.592(2) Å; $Cu-I_{terminal}$ is 2.514(2) Å and $Cu\cdots Cu$ 2.726(4) Å.

The structures assumed by dihalocuprate(I) ions appear to be strongly dependent on the nature of the cation, Cu(I) exhibiting linear, tetrahedral, or more seldom, trigonal coordination.[1] As yet, however, relatively little information is available on the geometry of the diiodocuprate(I) ion. Although monomeric $[CuI_2]^-$ ions have been shown to exist in solution,[2-4] there does not appear to be any conclusive evidence for the existence of discrete $[CuI_2]^-$ ions in the solid state. In tetraamminecopper(II) diiodocuprate(I)[5] and bis(1,2-diaminoethane)copper(II) diiodocuprate(I),[6] for example, the anions form infinite chains of edge-sharing Cu(I)–I tetrahedra. The iodocuprate(I) complex $[Cu_2I_3]^-$ has been found as infinite chains of edge- and face-sharing Cu(I)–I tetrahedra in the tetraethylammonium and dimethyl(3-dimethylamino-2-aza-2-propenylidene)ammonium compounds[7] and as double chains of edge-sharing tetrahedra in $Cs[Cu_2I_3]$.[8] With methyltriphenylphosphonium as cation, however, a $[Cu_4I_6]^{2-}$ cluster is obtained in which copper is trigonal-planar coordinated and pairs of copper atoms are bridged by iodine atoms.[9]

The recent preparation[10] of crystalline tetrabutylammonium diiodocuprate(I) has made an investigation of the crystal structure of this compound possible. Apart from providing information on the configuration of the anion and the nature of the copper(I) coordination, it was hoped that the investigation might be instrumental in the elucidation of the nucleophilicity of copper(I) and thus mechanisms of cuprate reactions.[10]

EXPERIMENTAL

Bis(tetrabutylammonium) di-μ-iodo-diiododicuprate(I) was prepared from copper(I) iodide and tetrabutylammonium iodide as described previously.[10] Rotation and Weissenberg photographs showed the crystals to be monoclinic with systematic absences consistent with space group $P2_1/n$.*

Intensities from a crystal, $0.25\times0.07\times0.08$ mm, were measured at 168 K with a Syntex $P2_1$ diffractometer, using graphite-monochromated Mo$K\alpha$ radiation and the $\omega-2\theta$ scan mode. The temperature was maintained by a Syntex LT1 low-temperature device and selected owing to the tendency of the crystals to disintegrate in the radiation at room temperature. Data were collected for $2\theta\leq50°$ with $h\geq0$ and $k\geq0$, the 2θ scan rate being varied between 3.5 and 18.0° min^{-1} depending on the intensity of the reflection. Periodical measurement of the intensities of two reflections showed that the crystal was not subject to decay. A 96-step profile was recorded for each reflection and the Lehmann and Larsen profile-analysis method[12] was used to calculate the intensities.[13] A total of 3895 reflections were measured. Sym-

* Equipoints of general position of $P2_1/n$ (conventional setting,[11a] No. 14, $P2_1/c$): $\pm(x,y,z;\ \frac{1}{2}+x,\frac{1}{2}-y,\frac{1}{2}+z)$.

0302-4377/82/090751-05$02.50

metry-related reflections were merged and systematically absent reflections excluded giving a unique set of 3337 reflections. Of these 2088 had $I > 3.0\sigma(I)$ and were considered to be observed. Data were corrected[14] for Lorentz and polarization effects but not for absorption. The unit-cell parameters at 168 K were determined by least squares from diffractometer setting angles for 15 reflections.

The low-temperature device was removed and unit-cell parameters were determined at 291 K. Intensities were then remeasured at this temperature, a total of 3618 values being obtained, owing to disintegration of the crystal.

CRYSTAL DATA

Bis(tetrabutylammonium) di-μ-iodo-diiododicuprate(I) $[N(C_4H_9)_4]_2[Cu_2I_4]$, $M_r = 1119.6$; monoclinic, space group $P2_1/n$ (No. 14, non-standard setting); $a = 9.042(3)$, $b = 21.231(9)$, $c = 11.734(3)$ Å, $\beta = 92.88(3)°$ at 168 K, $Z = 2$, $D_c = 1.65$ g cm^{-3}, $\mu(MoK\alpha) = 37.7$ cm^{-1}. The compound crystallizes as colourless prisms. At 291 K the unit-cell dimensions are: $a = 9.140(4)$, $b = 21.152(10)$, $c = 12.020(5)$ Å, $\beta = 95.25(3)°$.

STRUCTURE DETERMINATION AND REFINEMENT

The structure was solved from Patterson and successive electron density maps.[14] Block-diagonal and finally full-matrix least-squares refinement[14] of the positional and anisotropic thermal parameters and a scale factor yielded $R = 0.058$ for 181 parameters (2088 reflections); when the 1249 unobserved reflections were included $R = 0.095$. The F_o values were weighted[15] according to $w = (32.0 + F_o + 0.010\,F_o^2)^{-1}$. The scattering factors were those of Doyle and Turner[16] for the uncharged atoms, those of I and Cu being corrected[11b] for the real part of the anomalous dispersion. Since C(12) had a rather large temperature factor, attempts were made to assign this atom to two partially occupied sites, but this did not improve the model. Atomic coordinates and thermal parameters are listed in Table 1. Structure factors can be obtained from the authors on request. A final difference map showed no unusual features and had diffuse peaks in probable hydrogen atom positions. No attempt was made to include the hydrogen atoms in the calculations.

The data collected at room temperature yielded essentially the same structural model but with

Table 1. Fractional coordinates and thermal parameters ($U_{ij} \times 10^3$). Estimated standard deviations are given in parentheses. The anisotropic temperature factor is $\exp[-2\pi^2(U_{11}a^{*2}h^2 + \cdots + U_{23}b^*c^*kl)]$.

Atom	x	y	z	U_{11}	U_{22}	U_{33}	U_{12}	U_{13}	U_{23}
I(1)	0.21778(11)	−0.00919(4)	0.08880(9)	52.0(6)	37.7(5)	59.8(6)	0.0(9)	−40.5(9)	−11.9(9)
I(2)	0.00424(10)	0.18162(4)	0.03164(8)	39.8(6)	36.8(5)	56.2(6)	0.1(8)	−16.5(8)	6.1(8)
Cu	0.0096(2)	0.0637(1)	0.0119(1)	49(1)	38(1)	43(1)	−2(2)	−8(2)	−2(1)
N	0.4869(12)	0.1722(5)	0.1790(9)	40(6)	46(7)	34(6)	−28(11)	14(9)	−14(10)
C(1)	0.4503(15)	0.1535(7)	0.0547(11)	40(7)	53(8)	29(7)	−20(13)	−5(11)	−19(12)
C(2)	0.5622(15)	0.1780(7)	−0.0294(11)	41(8)	79(11)	29(7)	3(16)	12(11)	9(14)
C(3)	0.5097(16)	0.1584(9)	−0.1510(12)	44(9)	102(13)	32(8)	−34(18)	14(13)	−16(16)
C(4)	0.3723(21)	0.1933(11)	−0.1968(15)	70(12)	141(19)	55(10)	−77(25)	−14(18)	−63(24)
C(5)	0.6335(17)	0.1420(7)	0.2226(13)	51(9)	57(9)	58(10)	5(15)	−58(16)	−5(15)
C(6)	0.6334(19)	0.0690(7)	0.2240(14)	75(12)	49(9)	68(11)	40(17)	−20(18)	16(16)
C(7)	0.7926(19)	0.0506(8)	0.2671(14)	70(12)	67(11)	61(11)	55(18)	−12(17)	15(17)
C(8)	0.7979(25)	−0.0254(11)	0.2673(17)	110(17)	97(15)	69(13)	58(27)	29(23)	72(23)
C(9)	0.3569(16)	0.1473(7)	0.2462(11)	60(9)	46(8)	28(7)	−31(14)	12(12)	−13(12)
C(10)	0.3703(20)	0.1591(9)	0.3740(14)	81(12)	78(11)	50(10)	−74(20)	13(17)	−47(17)
C(11)	0.2313(27)	0.1392(10)	0.4304(15)	135(19)	95(15)	43(10)	−59(27)	38(22)	−28(20)
C(12)	0.1870(37)	0.0748(14)	0.4217(18)	250(36)	177(27)	49(13)	−264(53)	115(34)	−79(29)
C(13)	0.5049(15)	0.2435(6)	0.1939(11)	41(8)	35(7)	41(8)	−31(12)	−10(12)	−21(12)
C(14)	0.3673(17)	0.2805(6)	0.1429(15)	54(10)	30(7)	84(12)	2(14)	0(17)	−13(15)
C(15)	0.3996(22)	0.3498(7)	0.1642(16)	99(14)	38(8)	74(12)	12(18)	−22(20)	4(16)
C(16)	0.2740(26)	0.3905(8)	0.1019(15)	151(19)	44(9)	53(10)	74(22)	16(22)	27(16)

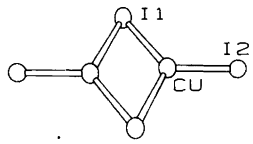

Fig. 1. The di-μ-iodo-diiododicuprate(I) anion showing the atomic numbering.[17]

large temperature factors for iodine and copper ($B \sim 6.5$ Å^2) and exceedingly large for some of the carbon atoms. It was not therefore considered profitable to refine the structure using this data set. The difference between the unit-cell parameters at the two temperatures can undoubtedly be ascribed to orientational disorder at room temperature of the tetrabutylammonium ion, in particular.

DISCUSSION

In bis(tetrabutylammonium) di-μ-iodo-diiododicuprate(I) the anion is a centrosymmetric dimer (Fig. 1) containing three-coordinated copper(I). The structure of the analogous $[Cu_2Br_4]^{2-}$ has recently been reported[18] but to our knowledge this is the first structural determination of $[Cu_2I_4]^{2-}$. The configuration of iodine atoms about copper(I) is approximately trigonal planar (Table 2), with the copper atom 0.03(3) Å from the plane defined by the three iodine atoms [I(1), I(1:$\bar{x},\bar{y},\bar{z}$) and I(2)]. As is seen from Table 2, the bridging Cu–I(1) distances differ slightly from one another and both are longer than the terminal Cu–I(2). The Cu–I(1) distances, the angle subtended at I(1) by the copper atoms [63.8(1)°], the Cu···Cu contact [2.726(4) Å] and the closest distance of approach of the bridging iodine atoms [I(1)···I(1)=4.380(3) Å] all agree closely with the corresponding values in the $[Cu_4I_6]^{2-}$ cluster, as determined in methyltriphenylphosphonium hexaiodotetracuprate(I).[9]

Table 2. Interatomic distances (Å) and angles (°) within the $[Cu_2I_4]^{2-}$ ion. Estimated standard deviations are given in parentheses. The superscript (*i*) denotes an atom in $-x,-y,-z$.

Cu–I(1)	2.566(2)	I(1)–Cu–I(2)	125.8(1)
Cu–I(1^i)	2.592(2)	I(1^i)–Cu–I(2)	117.9(1)
Cu–I(2)	2.514(2)	I(1)–Cu–I(1^i)	116.2(1)
Cu···Cu	2.726(4)	Cu–I(1)–Cu	63.8(1)

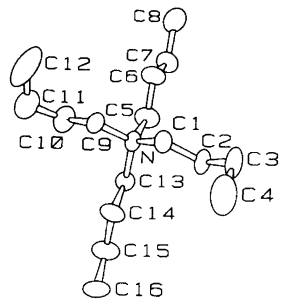

Fig. 2. The tetrabutylammonium ion showing the atomic numbering.

The configuration of $[Cu_2I_4]^{2-}$ is similar to that of $[Cu_2Br_4]^{2-}$ in the tetrathiotetracene salt.[18] There is, however, a somewhat larger difference between the copper(I)-terminal and copper(I)-bridging ligand distances in $[Cu_2Br_4]^{2-}$ than is the case for $[Cu_2I_4]^{2-}$, *i.e.* $Cu-Br_{terminal}=2.328(2)$ Å, $Cu-Br_{bridging}=2.490(2)$ and 2.472(3) Å. Moreover, $[Cu_2Br_4]^{2-}$ shows distortion from planarity, the copper atom lying 0.196 Å out of the plane through the three bromide ligands. There are also Cu–S contacts of 2.684 and 3.062 Å to tetrathiotetracene cations such that the copper(I) coordination can be described as being approximately trigonal bipyramidal.[18]

It would seem that the Cu···Cu distance is determined largely by the stereochemical demands of the bridging ligands[9,19] but that the value 2.726(4) Å in $[Cu_2I_4]^{2-}$ may indicate a weak attractive Cu(I)–Cu(I) interaction.[19] As expected, the Cu···Cu contact in $[Cu_2Br_4]^{2-}$, 2.660(3) Å,[18] is shorter than that in di-μ-iodo-diiododicuprate(I).

The cation is depicted[17] in Fig. 2 and a stereoscopic view[17] of the unit cell is shown in Fig. 3. The large thermal parameters of some of the carbon atoms, in particular those of the terminal atoms of the chains, would suggest some orientational disorder, which is also borne out by the data collected at room temperature. In consequence, bond distances and angles within the cation are associated with relatively large standard deviations (Table 3). The connectivity relationships show, however, good general agreement with values found in other tetrabutylammonium derivatives. Orientational disorder and/or large thermal parameters associated with the tetrabutylammonium ion appear to be not uncommon, *e.g.* $[N(C_4H_9)_4]IO_4$,[20] $[N(C_4H_9)_4]_2[Mo_2O_3S(C_4O_2S_2)_2]$,[21] $[N(C_4H_9)_4]$-

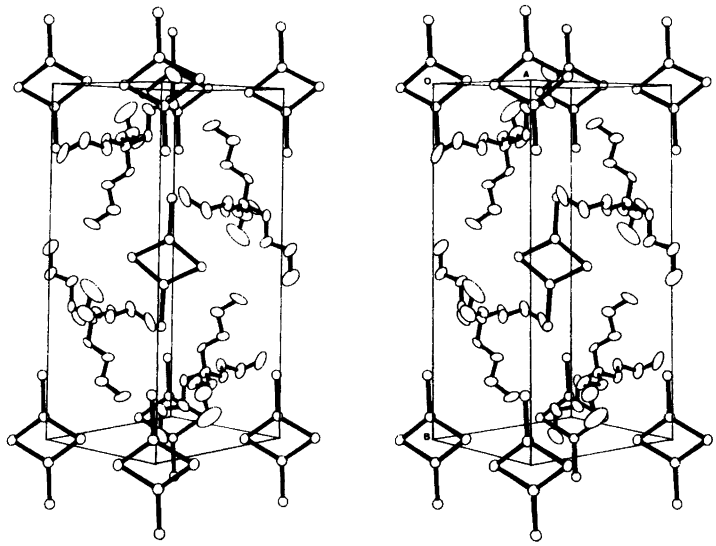

Fig. 3. Stereoscopic view of the unit cell.

Table 3. Bond lengths (Å) and angles (°) within the tetrabutylammonium ion. Estimated standard deviations are given in parentheses.

N–C(1)	1.53(2)	C(1)–N–C(5)	111(1)
C(1)–C(2)	1.54(2)	C(1)–N–C(9)	105(1)
C(2)–C(3)	1.54(2)	C(1)–N–C(13)	112(1)
C(3)–C(4)	1.52(2)	C(5)–N–C(9)	111(1)
N–C(5)	1.54(2)	C(5)–N–C(13)	107(1)
C(5)–C(6)	1.55(2)	C(9)–N–C(13)	111(1)
C(6)–C(7)	1.55(2)	N–C(1)–C(2)	114(1)
C(7)–C(8)	1.62(3)	C(1)–C(2)–C(3)	109(1)
N–C(9)	1.54(2)	C(2)–C(3)–C(4)	114(1)
C(9)–C(10)	1.52(2)	N–C(5)–C(6)	115(1)
C(10)–C(11)	1.51(3)	C(5)–C(6)–C(7)	105(1)
C(11)–C(12)	1.43(4)	C(6)–C(7)–C(8)	106(1)
N–C(13)	1.53(2)	N–C(9)–C(10)	115(1)
C(13)–C(14)	1.56(2)	C(9)–C(10)–C(11)	111(1)
C(14)–C(15)	1.52(2)	C(10)–C(11)–C(12)	118(2)
C(15)–C(16)	1.58(3)	N–C(13)–C(14)	112(1)
		C(13)–C(14)–C(15)	106(1)
		C(14)–C(15)–C(16)	109(1)

$[Ag_3I_4]$.[22] The closest non-bonded approach distances between carbon and copper(I) and carbon and iodide in $[N(C_4H_9)_4]_2[Cu_2I_4]$ are C(7)···Cu 3.67(2) Å and I(1)···C(9) 3.98(1) Å.

Acknowledgements. Financial support from the Swedish Natural Science Research Council (NFR) and the National Swedish Board for Technical Development (STU) is gratefully acknowledged.

REFERENCES

1. Jardine, F. H. *Adv. Inorg. Chem. Radiochem. 17* (1975) 116.
2. Specker, H. and Pappert, W. *Z. Anorg. Allg. Chem. 341* (1965) 287.
3. Mahfooz Khan, M., Zaidi, S. A. A. and Malik, A. U. *Z. Anorg. Allg. Chem. 375* (1970) 291.
4. Waters, D. N. and Basak, B. *J. Chem. Soc. A* (1971) 2733.

5. Baglio, J. A., Weakliem, H. A., Demelio, F. and Vaughan, P. A. *J. Inorg. Nucl. Chem. 32* (1970) 795.
6. Freckmann, B. and Tebbe, K.-F. *Z. Naturforsch. Teil B 35* (1980) 1319.
7. Hartl, H. and Mahdjour-Hassan-Abadi, F. *Angew. Chem. 93* (1981) 804.
8. Jouini, N., Guen, L. and Tournoux, M. *Rev. Chim. Miner. 17* (1980) 486.
9. Bowmaker, G. A., Clark, G. R. and Yuen, D. K. P. *J. Chem. Soc. Dalton Trans.* (1976) 2329.
10. Nilsson, M. *Acta Chem. Scand. B 36* (1982) 125.
11. a. *International Tables for X-Ray Crystallography*, Kynoch Press, Birmingham 1952, Vol. 1, p. 99; b. *Ibid.* 1974, Vol. 4, p. 149.
12. Lehmann, M. S. and Larsen, F. K. *Acta Crystallogr. A 30* (1974) 580.
13. Lindqvist, O. and Ljungström, E. *J. Appl. Crystallogr. 12* (1979) 134.
14. Lindgren, O. *An Integrated Set of Crystallographic Programs.* In *On the Oxygen Coordination of Cerium in Some Sulfates and Chromates*, Thesis, Department of Inorganic Chemistry, Chalmers University of Technology and University of Göteborg, Göteborg 1977.
15. Cruickshank, D. W. J. *Crystallographic Computing*, Munksgaard, Copenhagen 1970, p. 195.
16. Doyle, P. A. and Turner, P. S. *Acta Crystallogr. A 24* (1968) 390.
17. Johnson, C. K. *ORTEP*, Report ORNL-3794, Oak Ridge National Laboratory, Oak Ridge 1965.
18. Shibaeva, R. P. and Kaminskii, V. F. *Kristallografiya 26* (1981) 332.
19. Mehrotra, P. K. and Hoffmann, R. *Inorg. Chem. 17* (1978) 2187.
20. Carpy, A., Goursolle, M., Léger, J.-M. and Nivaud, E. *C. R. Acad. Sci. Paris C 285* (1977) 311.
21. Altmeppen, D. and Mattes, R. *Acta Crystallogr. B 36* (1980) 1942.
22. Gilmore, C. J., Tucker, P. A. and Woodward, P. *J. Chem. Soc. A* (1971) 1337.

Received February 22, 1982.

Acta Chemica Scandinavica A 36 (1982) 757–765

Structural Studies on the Phosphorus–Nitrogen Bond. VII. The Crystal Structure of *P,P*-Dimorpholinophenylphosphine Selenide and *P,P*-Diphenylmorpholinophosphine Selenide

KNUT MAARTMANN-MOE,[a] CHRISTIAN RØMMING[b] and JON SONGSTAD[a]

[a] Department of Chemistry, University of Bergen, N-5014 Bergen-Univ., Norway and [b] Department of Chemistry, University of Oslo, Oslo 3, Norway

The structure of the title compounds, $[O(CH_2CH_2)_2N]_2P(Se)C_6H_5$, I, and $O(CH_2CH_2)_2NP(Se)(C_6H_5)_2$, II, have been determined from X-ray data. Full-matrix least-squares refinements for the non-hydrogen atoms led to final conventional R-values of 0.033 (3849) for I and 0.032 (2087) for II; the number of observed reflections in parentheses. I crystallizes in the monoclinic system with the following unit cell dimensions at 20 °C: $a=10.266(2)$ Å; $b=17.286(5)$ Å; $c=9.706(2)$ Å; $\beta=112.06(2)°$. The crystals of II are orthorhombic with cell dimensions at 20 °C: $a=7.874(2)$ Å; $b=14.099(2)$ Å; $c=14.539(2)$ Å. The space groups are $P2_1/c$ (I) and $P2_1cn$ (II) and both compounds have four molecules in the unit cell.

The sums of the bond angles at the nitrogen atoms are 342.9 and 348.2° in I and 344.4° in II. In I, the lone pair of the nitrogen atom of highest *p*-character is *antiperiplanar* to the P–Se bond; the lone pair of the other nitrogen atom is roughly orthogonal to the P–Se bond. In II the lone pair of the nitrogen lone pair is strictly *antiperiplanar* to the P–Se bond.

The P–N bond lengths are 1.669(2) and 1.662(2) Å in I and 1.672(4) Å in II. The P–Se bond lengths are 2.097(1) and 2.102(1) Å in I and II, respectively.

In several studies in the present series tervalent and pentacovalent phosphorus compounds containing three dialkylamino groups, $(R_2N)_3P$ and $(R_2N)_3PX$, (X = Se and Te), have been examined by X-ray methods.[1–3] In all the compounds one of the nitrogen atoms is essentially sp^3 hybridized and its lone pair is *anti* to the phosphorus lone pair in the tervalent compounds[1] and to the phosphorus chalcogen bond in the pentacovalent compounds.[2,3] The remaining two nitrogen atoms are generally sp^2 hybridized or close to sp^2 hybridized and their lone pairs are *synclinal* to the phosphorus lone pair or to the chalcogen atom.

In phosphorus compounds containing one or two dialkylamino groups in addition to aryl groups the question arises which conformations of the P–N bonds are the energetically favoured ones. In R'_2PNR_2 and in $R'_2P(X)NR_2$ two conformers are possible when neglecting the various *skew* conformers; the nitrogen lone pair may be *antiperiplanar* or *synclinal* to the phosphorus lone pair or to the X atom. Likewise, with two dialkylamino groups present as in $R'P(NR_2)_2$ and in $R'P(X)(NR_2)_2$, two conformations are conceivable; both the nitrogen lone pairs may be in *synclinal* positions or one of them may be *antiperiplanar* relative to the phosphorus lone pair or to the X atom in the tervalent and in the pentacovalent species, respectively.

In an attempt to obtain information with regard to the preferential conformation of the P–N bond in compounds where the phosphorus atom also has aryl substituents, we want to report on the structure of *P,P*-dimorpholinophenylphosphine selenide, $Mor_2P(Se)Ph$, I, and *P,P*-diphenylmorpholinophosphine selenide, $MorP(Se)Ph_2$, II. Admittedly,

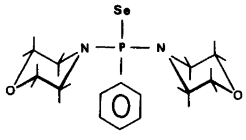

I

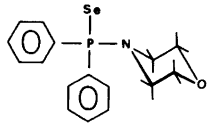

II

0302-4377/82/090757-09$02.50

the unselenated species of I and II were the compounds of choice; however, owing to difficulties in getting suitable crystals of $MorPPh_2$ and its extreme sensitivity to moisture the selenated compounds were chosen. The close similarity between the structure of aminophosphines and their corresponding selenides[1,2] may allow one to draw some conclusions with regard to the structure of Mor_2PPh and $MorPPh_2$ from structural studies of I and II.

EXPERIMENTAL

Materials. *P,P*-Dimorpholinophenylphosphine selenide, I, was made from the corresponding phosphine, Mor_2PPh,[4] 2.8 g, dissolved in 50 ml dry benzene and 1.2 g black selenium powder (50% excess). The mixture was refluxed for 30 min, cooled and filtered, and the product precipitated with light petroleum (40–60 °C) at −20 °C. After two crystallizations from methanol, 2.6 g, 72 %, was obtained, m.p. 121 °C (122–124 °C[5]). Suitable crystals for the X-ray experiments were grown from a very dilute ethanolic solution by slow cooling to 0 °C.

P,P-Diphenylmorpholinophosphine selenide, II, was formed by slow addition of 3.5 g, 2 eq., morpholine in 50 ml benzene to 6.0 g, 1 eq., freshly distilled *P*-chlorodiphenylphosphine selenide, $Ph_2P(Se)Cl$, dissolved in 100 g benzene. The mixture was stirred for 1 h at room temperature, cooled and filtered, whereupon the solvent was removed *in vacuum*. The oily residue solidified upon addition of cold methanol in which the compound is only slightly soluble. A yield of 3.8 g, 54 %, m.p. 118 °C, was obtained after two crystallizations from methanol. The crystals from methanol were suitable for the X-ray experiments.

X-Ray data. The dimensions of the crystals used were 0.08 × 0.18 × 0.35 mm (I) and 0.30 × 0.30 × 0.50 mm (II). An ENRAF-NONIUS CAD 4 diffractometer with graphite monochromated Mo$K\alpha$ radiation was used for the determination of cell parameters and recording of intensity data. The cell parameters were determined by least squares fits to the diffractometer settings of 25 general reflections for both I and II. Mo$K\alpha$-radiation ($\lambda_{\alpha 1}$ = 0.70926 Å, $\lambda_{\alpha 2}$ = 0.71354 Å) gives reflection peaks with the center of gravity displaced relative to a theoretical center of gravity due to $\lambda_{\alpha 1}$ alone. The experimentally found centers of gravity were corrected for this offset and the cell parameters were calculated on the basis of $\lambda_{\alpha 1}$.

Intensity data were recorded at room temperature (19–20 °C) using the ω-scan technique with variable scan speed, 0.4–1.5° min^{-1} for I and 0.5–3° min^{-1} for II. Minimum scan width was 1.5° for both I and II, including the background scans of 0.25° at the beginning and at the end of the scans. The orientation of the crystals was checked at intervals of 100 recordings. Three standard reflections were remeasured every 2 h and the intensity data later corrected according to the variation of these. Maximum corrections were 6 % for I and 3 % for II. All crystallographically independent reflections with $\sin\theta/\lambda < 0.66$ $Å^{-1}$ were recorded, 3849 for I and 2087 for II. Reflections with $I < 2\sigma(I)$ were excluded, leaving 2632 reflections for I and 1090 for II.

All computer programs used belong to the ENRAF-NONIUS Structure Determination Pack, version 16, 1979. Atomic form factors and anomalous scattering coefficients were taken from Ref. 6.

CRYSTAL DATA

I. *P,P*-Dimorpholinophenylphosphine selenide, $C_{14}H_{21}N_2O_2PSe$, m.p. 121 °C. Monoclinic, a = 10.266(2) Å; b = 17.286(5) Å; c = 9.706(2) Å; β = 112.06(2)°; V = 1596.3 $Å^3$ (~20 °C); M = 359.27; Z = 4; $F(000)$ = 736; μ(Mo$K\alpha$) = 26.3 cm^{-1}; D_x = 1.495 g cm^{-3}. Space group $P2_1/c$ (No. 14).

II. *P,P*-Diphenylmorpholinophosphine selenide, $C_{16}H_{18}NOPSe$, m.p. 118 °C. Orthorhombic, a = 7.874(2) Å; b = 14.099(2) Å; c = 14.539(2) Å; V = 1614.1 $Å^3$ (~20 °C); M = 350.26; Z = 4; $F(000)$ = 712; μ(Mo$K\alpha$) = 26.0 cm^{-1}; D_x = 1.441 g cm^{-3}. Space group $P2_1cn$ (No. 33).

STRUCTURE DETERMINATIONS

The intensity data were corrected for Lorentz and polarization effects and for absorption. Both structures were solved by interpretation of Patterson and difference Fourier density maps.

From the systematically absent reflections, the space group of II may be $P2_1cn$ (No. 33) or $Pmcn$ (No. 62). The choice of the former is justified by the final solution and refinement. The enantiomorph to the presented structure was refined and the result gave unambiguous reason for its exclusion.

Positions for the hydrogen atoms were calculated with a C–H distance of 0.95 Å and fixed; their thermal parameters were refined, averaged and accordingly given the value 5.0 $Å^2$ and kept fixed in the final refinements. The non-hydrogen atoms were refined anisotropically. The full-matrix least squares refinement program applied minimizes the quantity $\Sigma w\Delta F^2$; the weights were the inverse of the variance in the observation calculated from

Table 1. Fractional atomic coordinates.

	I			II			
ATOM	X	Y	Z	ATOM	X	Y	Z
SE	0.19259(3)	0.45050(2)	0.28192(3)	SE	0.00000(0)	-0.00772(4)	0.15755(4)
P	0.21515(6)	0.56335(4)	0.36694(7)	P	-0.1682(2)	0.0817(1)	0.2288(1)
O1	0.3308(2)	0.5482(1)	0.8599(2)	O	-0.5153(7)	0.2259(3)	0.0283(3)
O2	-0.1600(2)	0.7167(1)	0.1572(3)	N	-0.3112(6)	0.1414(3)	0.1665(3)
N1	0.2595(2)	0.5718(1)	0.5503(2)	C11	-0.4499(8)	0.0885(4)	0.1223(4)
N2	0.0684(2)	0.6152(1)	0.2985(2)	C12	-0.5812(10)	0.1571(5)	0.0895(5)
C11	0.1508(3)	0.5615(2)	0.6136(3)	C13	-0.3841(10)	0.2749(5)	0.0693(5)
C12	0.2094(3)	0.5899(2)	0.7718(3)	C14	-0.2435(10)	0.2118(4)	0.1010(4)
C13	0.4365(3)	0.5573(2)	0.8002(3)	C21	-0.2990(7)	0.0201(3)	0.3127(4)
C14	0.3868(3)	0.5280(2)	0.6417(3)	C22	-0.2659(9)	-0.0737(4)	0.3338(4)
C21	0.0766(3)	0.6985(2)	0.3343(4)	C23	-0.3623(10)	-0.1175(4)	0.4026(4)
C22	-0.0671(3)	0.7294(2)	0.3060(4)	C24	-0.4868(10)	-0.0710(4)	0.4477(4)
C23	-0.1699(3)	0.6366(2)	0.1247(4)	C25	-0.5205(10)	0.0216(4)	0.4260(4)
C24	-0.0303(3)	0.6022(2)	0.1452(3)	C26	-0.4281(8)	0.0663(4)	0.3589(4)
C31	0.3500(2)	0.6176(1)	0.3325(3)	C31	-0.0616(7)	0.1770(3)	0.2908(3)
C32	0.3567(3)	0.6134(2)	0.1918(3)	C32	0.1058(8)	0.1690(4)	0.3149(4)
C33	0.4529(3)	0.6575(2)	0.1584(3)	C33	0.1836(8)	0.2410(4)	0.3629(4)
C34	0.5463(3)	0.7043(2)	0.2641(3)	C34	0.0963(8)	0.3202(4)	0.3882(4)
C35	0.5414(3)	0.7085(2)	0.4033(3)	C35	-0.0715(9)	0.3286(4)	0.3663(4)
C36	0.4425(3)	0.6667(2)	0.4368(3)	C36	-0.1536(8)	0.2566(4)	0.3179(4)
H111	0.1269	0.5083	0.6114	H111	-0.4992	0.0461	0.1654
H112	0.0695	0.5904	0.5577	H112	-0.4066	0.0537	0.0715
H121	0.1397	0.5841	0.8134	H121	-0.6278	0.1888	0.1414
H122	0.2332	0.6430	0.7722	H122	-0.6682	0.1228	0.0589
H131	0.5175	0.5290	0.8594	H131	-0.4277	0.3082	0.1210
H132	0.4596	0.6106	0.8016	H132	-0.3394	0.3189	0.0262
H141	0.3650	0.4745	0.6393	H141	-0.1585	0.2488	0.1304
H142	0.4586	0.5355	0.6035	H142	-0.1955	0.1800	0.0498
H211	0.1161	0.7253	0.2739	H22	-0.1795	-0.1077	0.3023
H212	0.1344	0.7057	0.4361	H23	-0.3395	-0.1817	0.4180
H221	-0.0605	0.7835	0.3252	H24	-0.5506	-0.1023	0.4941
H222	-0.1036	0.7045	0.3710	H25	-0.6080	0.0548	0.4574
H231	-0.2318	0.6293	0.0244	H26	-0.4532	0.1304	0.3439
H232	-0.2064	0.6109	0.1890	H32	0.1681	0.1139	0.2985
H241	0.0051	0.6258	0.0781	H33	0.3003	0.2353	0.3787
H242	-0.0408	0.5482	0.1261	H34	0.1521	0.3694	0.4211
H32	0.2948	0.5799	0.1187	H35	-0.1326	0.3837	0.3840
H33	0.4546	0.6556	0.0612	H36	-0.2710	0.2618	0.3035
H34	0.6138	0.7336	0.2411				
H35	0.6064	0.7404	0.4770				
H36	0.4378	0.6717	0.5323				

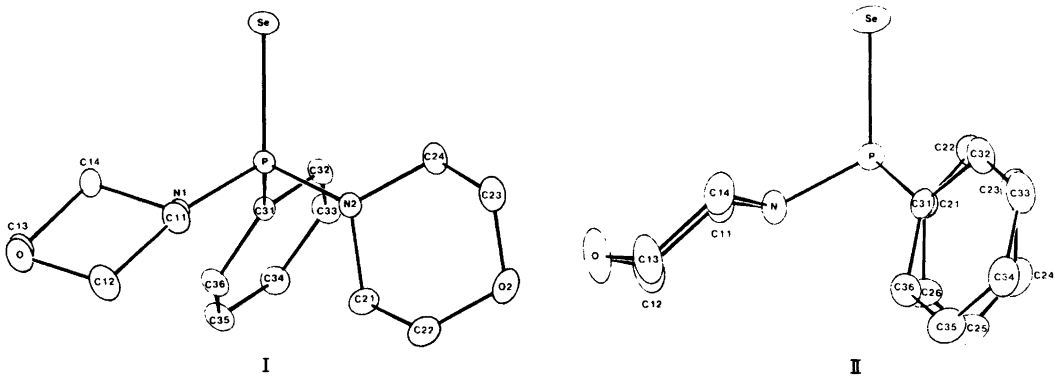

Fig. 1. ORTEP drawings of *P,P*-dimorpholinophenylphosphine selenide (I) and *P,P*-diphenylmorpholinophosphine selenide (II).

counting statistics plus 2 % of the net intensity.

The refinements converged to conventional R factors of 0.033(I) and 0.032(II); the R_w-values were 0.033(I) and 0.033(II). The standard deviation of an observation of unit weight, $[\Sigma w\Delta F^2/(m-n)]^{\frac{1}{2}}$, was 1.41 (I) and 1.60 (II).

Final atomic parameters are listed in Table 1. Tables of thermal parameters, observed and calculated structure factors are available from the authors.

ORTEP drawings of the molecules are shown in Fig. 1 where the numbering of the atoms is included.

Table 2. Structural data.

Bond lengths (Å)

I			II		
P	Se	2.097(1)	P	Se	2.102(1)
P	N1	1.669(2)	P	N	1.672(4)
P	N2	1.662(2)	P	C21	1.817(5)
P	C31	1.805(2)	P	C31	1.822(5)
N1	C11	1.472(3)	N	C11	1.470(6)
C11	C12	1.506(3)	C11	C12	1.494(8)
C12	O1	1.414(3)	C12	O	1.415(8)
O1	C13	1.418(3)	O	C13	1.379(8)
C13	C14	1.515(3)	C13	C14	1.493(9)
C14	N1	1.482(3)	C14	N	1.474(7)
N2	C21	1.475(3)	C21	C22	1.383(6)
C21	C22	1.495(4)	C22	C23	1.399(8)
C22	O2	1.418(3)	C23	C24	1.349(9)
O2	C23	1.415(3)	C24	C25	1.369(7)
C23	C24	1.494(4)	C25	C26	1.371(7)
C24	N2	1.469(3)	C26	C21	1.382(7)
C31	C32	1.395(3)	C31	C32	1.369(6)
C32	C33	1.380(3)	C32	C33	1.376(8)
C33	C34	1.374(3)	C33	C34	1.362(9)
C34	C35	1.372(3)	C34	C35	1.365(8)
C35	C36	1.380(3)	C35	C36	1.394(8)
C36	C31	1.388(3)	C36	C31	1.393(8)
C–H (Assumed)		0.95	C–H (Assumed)		0.95

Table 2. Continued.

Bond angles (°)

I				II			
Se	P	N1	116.5(1)	Se	P	N	117.3(2)
Se	P	N2	113.3(1)	Se	P	C21	113.7(2)
Se	P	C31	112.9(1)	Se	P	C31	113.3(2)
N1	P	N2	102.8(1)	N	P	C21	102.9(2)
N1	P	C31	103.4(1)	N	P	C31	102.0(2)
N2	P	C31	106.8(1)	C21	P	C31	106.4(2)
P	N1	C11	119.2(1)	P	N	C11	118.8(3)
P	N1	C14	114.8(2)	P	N	C14	116.4(4)
P	N2	C21	118.0(2)	P	C21	C22	120.0(4)
P	N2	C24	120.0(2)	P	C21	C26	121.2(4)
P	C31	C32	118.5(2)	P	C31	C32	120.7(5)
P	C31	C36	123.0(2)	P	C31	C36	119.6(4)
C11	N1	C14	108.9(2)	C11	N	C14	109.1(4)
N1	C11	C12	108.1(2)	N	C11	C12	109.0(4)
C11	C12	O1	112.0(2)	C11	C12	O	113.0(6)
C12	O1	C13	109.4(2)	C11	O	C13	110.2(4)
O1	C13	C14	111.1(2)	O	C13	C14	113.0(5)
C13	C14	N1	108.8(2)	C13	C14	N	109.4(5)
C21	N2	C24	110.2(2)	C26	C21	C22	118.8(4)
N2	C21	C22	109.9(2)	C21	C22	C23	118.6(5)
C21	C22	O2	111.8(2)	C22	C23	C24	121.8(5)
C22	O2	C23	110.1(2)	C23	C24	C25	119.5(5)
O2	C23	C24	112.0(2)	C24	C25	C26	120.0(5)
C23	C24	N2	109.6(2)	C25	C26	C21	121.3(5)
C36	C31	C32	118.4(2)	C36	C31	C32	119.7(6)
C31	C32	C33	120.2(2)	C31	C32	C33	120.0(6)
C32	C33	C34	120.7(2)	C32	C33	C34	121.1(6)
C33	C34	C35	119.6(2)	C33	C34	C35	119.8(6)
C34	C35	C36	120.5(2)	C34	C35	C36	120.3(7)
C35	C36	C31	120.7(2)	C35	C36	C31	119.2(6)

Various derived and averaged data

	I			II		
	N1	N2	C	N	C21	C31
$\overline{N-C}$ (Å)	1.477	1.472		1.472		
$\overline{C-C}$ (Å)	1.510	1.495	1.382	1.493	1.376	1.377
$\overline{C-O}$ (Å)	1.416	1.417		1.397		
Deviation of N from plane PCC (Å)	0.373	0.309		0.355		
Torsion angle (°):						
Se–P–N-lone pair N	−167.5	−77.7		−177.4		
Se–P–C-ring normal			48.8		−81.9	−69.4
Sum of N bond angles (°)	342.9	348.2		344.4		
Cone angle at P (°)		313.0			311.3	

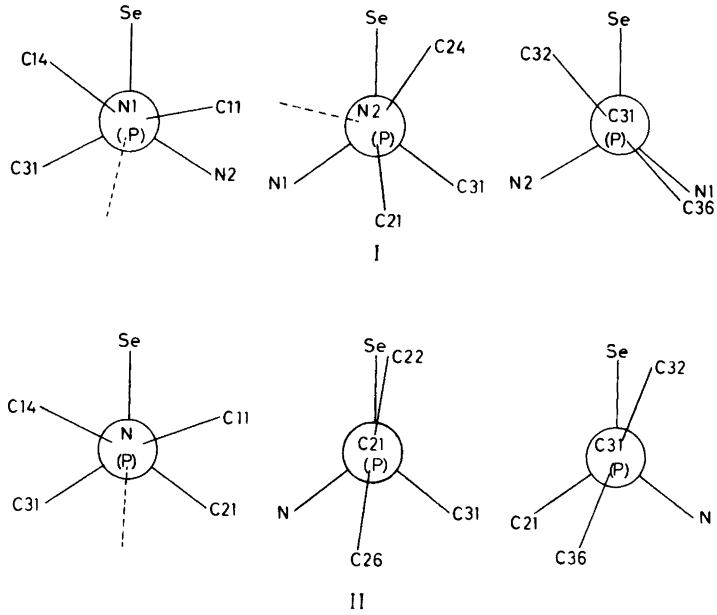

Fig. 2. Newman projections along the P–N and the P–C bonds in *P,P*-dimorpholinophenylphosphine selenide (I) and *P,P*-diphenylmorpholinophosphine selenide (II).

RESULTS AND DISCUSSION

Bond lengths, bond angles and various other structural data are listed in Table 2. The estimated standard deviations were calculated from the correlation matrices. In Fig. 2 are shown Newman projections of the P–N and P–C bonds where broken lines indicate the nitrogen lone pair directions as defined in Ref. 1. In Table 3 is presented a comparison of pertinent structural parameters in tris(morpholino)phosphine selenide,[1] in I and II from the present study and in triphenylphosphine selenide.[7]

Conformational considerations. From NMR studies of acyclic aminophosphines of the general type X_2PNR_2 (X = F and Cl) and related substances there is considerable evidence that the *synclinal* conformation, *i.e.* the lone pairs of the nitrogen and phosphorus atoms being orthogonal, is the best representation of the ground state geometry.[8,9] This observation is in agreement with the so-called "*gauche*-effect".[10] For the corresponding pentacovalent compounds in solution considerably less is known. NMR experiments are generally far less conclusive owing to the smaller rotational barriers around the P^V-N bonds combined with the effect of other exchange processes such as pseudorotation.[11–15] With regard to the preferred conformation of the P–N bond in pentacovalent compounds in the crystalline state, a number of X-ray studies have shown that the nitrogen lone pair is generally orthogonal to the P–X bond; *cf.* Ref. 15 for a survey of references. Furthermore, planarity or near planarity of the bonds to the nitrogen atom is fairly common in aminophosphorus compounds.

In triphenylphosphine[16] and trimesitylphosphine[17] and also in triphenylphosphine oxide[18] the phenyl groups form a propeller-formed arrangement with the normal to the phenyl rings *synclinal* to the phosphorus lone pair or to the oxygen atom. The average torsion angle as defined by normal phenyl-C-P-O (or lone pair P) is about 55° for $Ph_3P=O$ and Ph_3P and 45° for $((CH_3)_3Ph)_3P$. In the mixed dimethylamino and phenyl phosphine selenides there seems to be a competition of the groups for the *synclinal* conformation and that the phenyl groups have no inclination to take a position where the normal is pointing *antiperiplanar* to the P–Se direction. In both compounds the nitrogen atoms are intermediate between sp^2 and sp^2 hybridized, the sum of the nitrogen bond angles

Table 3. Comparison between some structural parameters in Mor_3PSe, $Mor_2P(Se)Ph$, $MorP(Se)Ph_2$ and Ph_3PSe.

Mor_3PSe[a]	$Mor_2P(Se)Ph$[b]	$MorP(Se)Ph_2$[b]	Ph_3PSe[c]
P=Se (Å)			
2.106(1)	2.097(1)	2.102(1)	2.106
Cone angle at P (°)			
317.7	313.0	311.3	318
Se–P–N-lone pair N (°)			
−77.6	−77.7		
−178.9	−167.5	−177.5	
65.8			
Σ∠N (°)			
354.9 *sc*[d]	348.2 *sc*		
340.1 *ap*[d]	342.9 *ap*	344.4 *ap*	
349.7 *sc*			
P–N, (P–C) (Å)			
1.659(2) *sc*	1.662(2) *sc*	(1.817(5))	
1.681(2) *ap*	1.669(2) *ap*	1.672(4) *ap*	(1.83(1))[e]
1.668(2) *sc*	(1.805(2))	(1.822(5))	
∠SePN, (∠SePC) (°)			
112.0 *sc*	113.3 *sc*	(113.7)	
115.1 *ap*	116.5 *ap*	117.3 *ap*	(113.1)[e]
111.4 *sc*	(112.9)	(113.3)	

[a] Ref. 2. [b] This study. [c] Ref. 7. [d] *sc* and *ap* refer to the direction of the nitrogen lone pair being essentially *synclinal* or *antiperiplanar*, respectively, relative to the P=Se bond [e] Average values, *cf.* Ref. 7.

being 342.9° and 348.2° in I and 344.4° in II. In I the lone pair of the nitrogen atom of highest *p*-character is essentially *antiperiplanar* to the P–Se bond with a torsion angle of −167.5° while the lone pair of the remaining nitrogen atom is approximately *synclinal* to the P–Se bond (torsion angle −77.7°). The torsion angle Se–P–C-ring normal is 48.8°. In II, the lone pair of the one nitrogen atom is strictly *antiperiplanar* with a torsion angle of 177.4°; the Se–P–C-ring normal torsion angles are −81.9 and −69.4°, respectively, *cf.* Table 2 and Fig. 2.

The phosphorus – nitrogen bond lengths. The P–N bond lengths are 1.669 and 1.662 Å in I and 1.672 Å in II. In the previous structural study on several tris(dialkylamino)phosphine selenides, a fairly good linear correlation between the sum of the nitrogen bond angles and the P–N bond lengths was observed.[2] The P–N bond lengths observed in the present study are slightly but significantly below this line. Apparently, the introduction of phenyl groups into this class of compounds causes a contraction of the P–N bond of approximately 0.01 Å. However, the effect of the phenyl groups does not appear to be additive since the bond length in II, 1.672(4) Å, is quite comparable to the length of the bond linking the phosphorus atom to the one nitrogen atom with its lone pair being *antiperiplanar* to the P–Se bond in I, 1.669(2) Å.

Likewise, there is apparently no significant effect of the number of phenyl groups upon the hybridization of the *antiperiplanar* nitrogen atoms; the sum of the bond angles for these atoms being 342.9 and 344.4° in I and II, respectively. In compounds with three dimethylamino groups, $(R_2N)_3PSe$, *cf.*

Ref. 2 and Table 3, the P–N bonds to the *antiperiplanar* nitrogen atoms are significantly longer than the remaining two P–N bonds. In I the two P–N bond lengths are 1.662(2) and 1.669(2) Å, the latter to the nitrogen atom with its lone pair *antiperiplanar* to the P–Se bond. These two bond lengths may not be significantly different; the trend, however, is in accordance with previous findings.[1-3] Presumably the small difference in the hybridization of the two nitrogen atoms in I, $\Sigma\angle N$ being 342.9 and 348.2°, is the cause for the small or negligible effect upon the observed P–N bond lengths.

The phosphorus–carbon bond lengths. The P–C bond length in I may at first sight appear to be slightly shorter than in II, 1.805(2) Å in I and 1.817(5) and 1.822(5) Å in II. However, owing to the lower accuracy in the structural parameters in II, these bond lengths may be equal within the limit of errors. The P–C bond lengths observed in the present study appear to be of the expected magnitude and are possibly slightly longer than that observed in phosphonium salts.[19,20] A further discussion of these bond lengths has to be postponed until sufficient data on $P-C_{Ar}$ bond lengths with three reliable digits, as in I, are made available.

In compound II, one of the phenyl rings lies almost parallel to the P–Se bond; the torsion angle Se–P–C–C being only 8.1°, *cf.* Fig. 2. This conformation of one phenyl ring being fairly parallel to the P–X bond appears to be quite common in compounds of the general type Ar_3PX.[7,18,21,22] Presumably this conformation facilitates an efficient packing of the molecules.

The phenyl rings in both compounds are strictly planar. The angle between the phenyl ring planes in II is 71.6°.

Bond angles around the phosphorus atom. The cone angles at phosphorus, 313.0° in I and 311.3° in II, are significantly smaller than both in Mor_3PSe[2] and in Ph_3PSe,[7] *cf.* Table 3. Three morpholino substituents and three twisted phenyl groups are thus more space demanding than a mixture of these substituents. Both compounds are fairly asymmetric with regard to the PN_2C and PNC_2 moieties. In I the angle between the P–C bond and the bond linking the *synclinal* nitrogen atom to the central phosphorus atom is larger than the other NPC angles, 106.8 and 103.4°, respectively. As in Mor_3PSe, the angle between bonds to *synlinal* and *antiperiplanar* nitrogen atoms is approximately 102°. The CPC bond angle in II, 106.4°, is comparable to the average CPC bond angle in Ph_3PSe.[7] It is interesting to note that both I and II are significantly asymmetric with regard to the SePN and SePC bond angles, *cf.* the last entry in Table 3. Apparently, in all compounds studied in this series, the angle between the phosphorus–chalcogen bond and the bond to the nitrogen atom having its lone pair *antiperiplanar* to the P–X bond is 3–4° larger than the remaining two bond angles.[2,3]

The phosphorus–selenium bond lengths. P–Se bond lengths in the series $Mor_{3-n}Ph_nPSe$ (n= 0,1,2 and 3) are highly similar, *cf.* Table 3. Thus, the morpholino group and the phenyl group appear to influence the P–Se bond length to a similar extent. Only in I, $n=1$, is the P–Se bond slightly but significantly shorter than in the three remaining compounds in the series. The P–Se bond length is known to range from 2.055 Å in 2-seleno-2-methoxy-5,5-dimethyl-1,3,2-dioxaphosphorinane[23] to 2.120 Å in tris(dimethylamino)phosphine selenide.[2] The variations observed are generally regarded to be related to the contribution of the dipolar form $\equiv P^{\delta+}-Se^{\delta-}$.

The morpholino substituents. These substituents are, in both compounds, in the expected chair conformation and are linked to the phosphorus atom in an approximately equatorial direction. All bond angles and lengths are within the expected range.[1-3] The part of these substituents made up from the four carbon atoms forms strictly a plane within experimental errors. The CNC and the COC planes form angles of 54.0 and 53.6° (N1 ring in I), 50.5 and 52.6° (N2 ring in I) and 51.8 and 50.8° in II with the planes defined by the four carbon atoms. These plane angles in the morpholino rings appear to be related to the hybridization of the nitrogen atoms.

Intramolecular contacts. In both I and II the packing in the crystals is of the normal van der Waals' type, the contacts being mainly between hydrogen atoms.

REFERENCES

1. Rømming, C. and Songstad, J. *Acta Chem. Scand. A 32* (1978) 689.
2. Rømming, C. and Songstad, J. *Acta Chem. Scand. A 33* (1979) 187.
3. Rømming, C., Iversen, A. J. and Songstad, J. *Acta Chem. Scand. A 34* (1980) 333.
4. Stangeland, L. J., Austad, T. and Songstad, J. *Acta Chem. Scand. 27* (1973) 3919.

5. Konieczny, M. and Sosnovsky, G. *Z. Naturforsch. B 33* (1978) 1040.
6. *International Tables for X-Ray Crystallography*, Kynoch Press, Birmingham 1974, Vol. 4.
7. Codding, P. W. and Kerr, K. A. *Acta Crystallogr. B 35* (1979) 1261.
8. Cowley, A. H., Dewar, M. J. S., Jackson, W. R. and Jennings, W. B. *J. Am. Chem. Soc. 92* (1970) 1085, 5206.
9. Cowley, A. H., Cushner, M. C. and Szobota, J. S. *J. Am. Chem. Soc. 100* (1978) 7784.
10. Wolfe, S. *Acc. Chem. Res. 5* (1972) 102.
11. Burdon, J., Hotchkiss, J. C. and Jennings, W. B. *J. Chem. Soc. Perkin Trans. 2* (1976) 1052.
12. Martin, J. and Robert, J. B. *Tetrahedron Lett.* (1976) 2475.
13. Cowley, A. H., Braun, R. W. and Gilje, J. W. *J. Am. Chem. Soc. 97* (1975) 434.
14. Emsley, J. and Williams, J. K. *J. Chem. Soc. Dalton Trans.* (1973) 1576.
15. Keat, R., Rycroft, D. S. and Thompson, D. G. *J. Chem. Soc. Dalton Trans.* (1980) 1858.
16. Daly, J. J. *J. Chem. Soc.* (1964) 3799.
17. Blount, J. F. *Tetrahedron Lett.* (1975) 913.
18. Ruban, G. and Zabel, V. *Cryst. Struct. Commun.* (1976) 671.
19. Schiemenz, G. P. *Angew. Chem. Int. Ed. Engl. 13* (1974) 351.
20. Henrick, K., Hudson, H. R. and Kow, A. *Chem. Commun.* (1980) 226.
21. Codding, P. W. and Kerr, K. A. *Acta Crystallogr. B 34* (1978) 3785.
22. Dreissig, W. and Plieth, K. *Acta Crystallogr. B 28* (1972) 3478.
23. Galdecki, Z., Glowka, M. L., Michalski, J., Okruszek, A. and Stec, W. J. *Acta Crystallogr. B 33* (1977) 2322.

Received February 23, 1982.

Acta Chemica Scandinavica A 36 (1982) 767–772

The Crystal and Molecular Structures of Diaquabis(picolinato *N*-oxido) Complexes of Mn(II), Co(II), Ni(II) and Cu(II)

PEKKA KNUUTTILA

Department of Chemistry, University of Jyväskylä, SF-40100 Jyväskylä 10, Finland

The picolinato *N*-oxido complexes of Mn^{2+}, Co^{2+} and Ni^{2+} ions form an isostructural series belonging to the space group $P2_1/c$. The corresponding Cu^{2+} complex crystallizes in the space group $P\bar{1}$.

All four complexes are octahedral, with picolinate *N*-oxide coordinating through the N–O oxygen and one of the (COO) oxygens. The average bond distances between the metal ions and the organic ligand oxygens are 2.13, 2.07 and 2.03 Å for Mn^{2+}, Co^{2+} and Ni^{2+} complexes, respectively, and 1.94 Å for the copper(II) complex. The corresponding M–O(aqua) distances are 2.23, 2.15, 2.09 and 2.49 Å. All structures were refined to final *R*-values of 0.030–0.049.

The present investigation is a continuation of the X-ray studies on 3*d* metal complexes of pyridine monocarboxylic acid *N*-oxides being carried out in this laboratory.[1-3] Pyridine monocarboxylic acid *N*-oxides are interesting from a coordination point of view since they include two different coordinating groups, the carboxylate group and the *N*-oxide group. In all these complexes the picolinic acid *N*-oxide coordinates to the metal ion through the N–O oxygen and one of the (COO) oxygens forming a stable six-membered chelate ring.

The coordination of pyridine monocarboxylic acids with 3*d* metals through the N–O oxygen has been observed for these complexes and for di-aquadi-μ-hydroxobis-μ-(nicotinato *N*-oxide)bis-μ-(nicotinato *N*-oxido)tricopper(II).[1] The study confirms the coordination of these complexes proposed earlier on the basis of IR-spectra and magnetic properties.[4-8]

EXPERIMENTAL

Preparation of the compounds. All the metal complexes of picolinic acid *N*-oxide with metal salts were prepared according to instructions given in the literature[4,8] except that solutions were more dilute.

Data collection. The crystal and intensity data were measured on a SYNTEX $P2_1$ automatic four-circle diffractometer using graphite monochromatized Mo$K\alpha$-radiation. The details of the data collection are seen in Table 1. The data were corrected for Lorentz and polarization factors but not for absorption effects.

Structure determination. The structure of triclinic diaquabis(picolinato *N*-oxido)copper(II) was solved by assuming the compound to be centrosymmetric

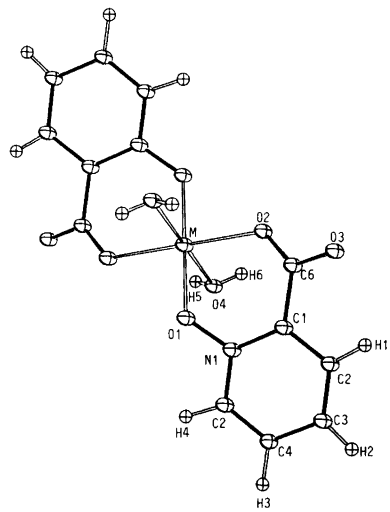

Fig. 1. The atomic labeling scheme of $[M(N\text{-picO})_2(H_2O)_2]$ complexes, $M = Mn^{2+}, Co^{2+}, Ni^{2+}$ and Cu^{2+}.

0302-4377/82/090767-06$02.50

Table 1. Details of the data collection for $[M(N\text{-picO})_2(H_2O)_2]$ complexes, M = Mn^{2+}, Co^{2+}, Ni^{2+} and Cu^{2+}.

	Mn^{2+}	Co^{2+}	Ni^{2+}	Cu^{2+}
(a) Crystal data				
Space group	$P2_1/c$	$P2_1/c$	$P2_1/c$	$P\bar{1}$
a (Å)	6.682(2)	6.673(3)	6.618(3)	6.634(11)
b	15.812(4)	15.729(13)	15.713(10)	7.302(14)
c	7.006(3)	6.993(2)	6.930(2)	7.968(9)
α (°)	90.0	90.0	90.0	80.5(1)
β	114.15(2)	115.29(3)	115.38(3)	89.4(1)
γ	90.0	90.0	90.0	61.4(1)
V (Å^3)	675.4	663.6	651.0	333.1
d_c (gcm^{-3})		1.98		1.87
d_o		1.82		1.83
Z	2	2	2	1
μMoKα (cm^{-1})	8.35	14.20	15.63	17.78
M	363.14	367.14	366.91	371.75
(b) Intensity measurements				
$\theta-2\theta$ Scan range		$4° < 2\theta < 55°$		
Scan rate		1° to 29.3° min^{-1}		
Refl.meas.	1795	1768	1617	1636
Criteria		$I > 3\sigma(I)$		
Refl.obs.	1307	1324	1617	2636
$R\left(\frac{\Sigma\|\|F_o\|-\|F_c\|\|}{\Sigma\|F_o\|}\right)$	0.033	0.030	0.049	0.039

with the central metal ion occupying the special position 1*a* of the space group $P\bar{1}$. All other atoms, including hydrogen atoms, were located from the difference Fourier map.

The structures of diaquabis(picolinato *N*-oxido)Mn(II), Co(II) and Ni(II) were solved with the MULTAN 78 program.[9] The central metal ions were located at the special position 2*a* of the space group $P2_1/c$.

Block-diagonal refinements was carried out with programs of the X-Ray System.[10] The scattering factors for the metal ions and O, N and C atoms were those of Cromer and Mann[11] and for H atoms those of Stewart, Davidson and Simpson.[12]

In the final least-squares refinement, non-hydrogen atoms were assigned anisotropic and hydrogen atoms isotropic thermal parameters. Unit weights were used. The final difference Fourier

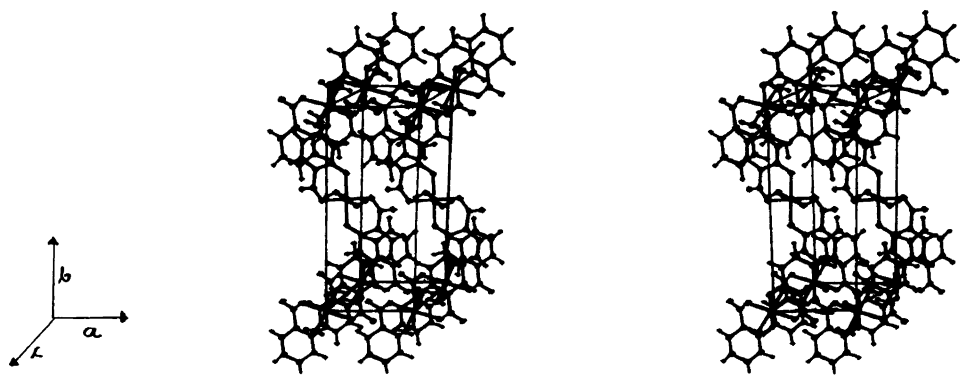

Fig. 2. A stereoview of the packing of the $[M(N\text{-picO}_2)(H_2O)_2]$ molecules in the unit cell, M = Mn^{2+}, Co^{2+} and Ni^{2+}.

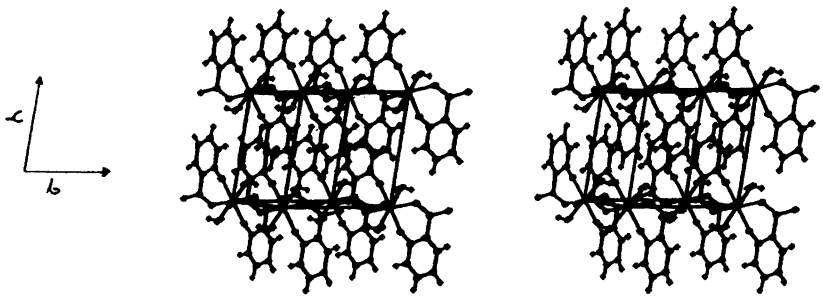

Fig. 3. A stereoview of the packing of the $[Cu(N\text{-picO})_2(H_2O)_2]$ molecules in the unit cell.

Table 2. Selected bond distances (Å) and bond angles (°) with their standard deviations for $[M(N\text{-picO})_2(H_2O)_2]$, $M = Mn^{2+}$, Co^{2+}, Ni^{2+} and Cu^{2+}.

	Mn^{2+}	Co^{2+}	Ni^{2+}	Cu^{2+}
M–O1	2.154(1)	2.061(1)	2.035(3)	1.947(4)
M–O2	2.113(1)	2.079(1)	2.015(3)	1.922(3)
M–O4	2.226(1)	2.148(1)	2.094(3)	2.488(5)
O1–N1	1.322(1)	1.341(1)	1.329(5)	1.330(2)
O2–C6	1.252(1)	1.274(1)	1.249(4)	1.266(2)
O3–C6	1.246(1)	1.271(1)	1.232(4)	1.229(2)
C6–C1	1.512(1)	1.507(2)	1.510(6)	1.500(2)
O1–M–O2	97.17(3)	94.03(3)	92.3(1)	90.19(9)
O1–M–O4	89.50(4)	89.99(5)	90.1(1)	87.1(2)
O2–M–O4	88.79(3)	87.43(3)	88.1(1)	92.8(1)
N1–O1–M	120.88(6)	120.18(6)	118.6(3)	116.1(1)
C6–O2–M	128.43(6)	125.94(7)	126.2(3)	124.93(6)
O2–C6–O3	125.31(8)	124.41(9)	123.1(4)	124.77(9)

Table 3. Hydrogen bonding data for $[M(N\text{-picO})_2(H_2O)_2]$ complexes, $M = Mn^{2+}$, Co^{2+}, Ni^{2+} and Cu^{2+}.

	Mn^{2+}	Co^{2+}	Ni^{2+}	Cu^{2+}
O4–H5(*i*)	0.51(1)	0.78(2)	1.0(1)	0.74(1) (*viii*)
O4–H6(*ii*)	0.93(1)	0.86(1)	0.95(4)	0.66(1) (*viii*)
O4···O3 (*iii*)	2.729(1)	2.788(1)	2.737(3)	2.768(5) (*viii*)
O4···O3 (*ii*)	2.751(1)	2.745(1)	2.736(5)	2.834(6) (*ix*)
O3···H6 (*iv*)	2.361(1)	1.97(1)	1.80(4)	2.215(8) (*x*)
O3···H5 (*i*)	2.26(1)	1.97(2)	1.71(7)	2.051(8)
(*v*)O4–H5–O3 (*v*)	167(2)	175(1)	172(5)	163.5(6) (*viii*)
(*vi*)O4–H6–O3 (*vii*)	165(1)	160(1)	165(6)	156.9(7) (*x*),(*viii*)

Symmetry code:
(*i*) $2-x,y,-\frac{1}{2},\frac{1}{2}+z$
(*ii*) x,y,z
(*iii*) $-x,1-y,-z$
(*iv*) $2-x,\frac{1}{2}-y,-z$
(*v*) $1-x,\frac{1}{2}+y,\frac{1}{2}-z$
(*vi*) $1-x,1-y,-z$
(*vii*) $1+x,y,z$
(*viii*) $1-x,-y,-z$
(*ix*) $x,y-1,z$
(*x*) $1-x,1-y,-z$

Table 4. Final positional parameters for non-hydrogen atoms with *e.s.d.*'s in parentheses and U_{eq} (Å^2 × 10^3).

	x	*y*	*z*	U_{eq} [a]
Mn	0.0000	0.5000	0.5000	18.13(7)
O1	0.90919(9)	0.61570(4)	0.32255(10)	27.5(3)
O2	1.34338(9)	0.51779(3)	0.62314(9)	24.8(3)
O3	0.32470(9)	0.50704(4)	0.13018(9)	25.9(3)
O4	0.00425(10)	0.43197(4)	0.22350(9)	28.3(3)
N1	0.73912(11)	0.66063(4)	0.31496(10)	20.2(3)
C1	0.54090(13)	0.62508(5)	0.27754(12)	20.7(4)
C2	0.36646(14)	0.67665(6)	0.25875(14)	27.8(4)
C3	0.39042(16)	0.76344(6)	0.27607(15)	33.5(5)
C4	0.59428(17)	0.79760(5)	0.31644(15)	34.0(5)
C5	0.76534(15)	0.74594(5)	0.33407(14)	27.9(5)
C6	0.50856(13)	0.53026(5)	0.25941(13)	21.0(4)
Co	0.0000	0.5000	0.5000	17.7(1)
O1	0.92226(9)	0.61084(4)	0.32999(9)	26.2(3)
O2	1.33588(9)	0.52275(4)	0.62530(9)	24.3(3)
O3	0.32515(9)	0.50590(4)	0.13252(9)	26.0(3)
O4	0.00775(10)	0.43432(4)	0.23461(9)	26.5(3)
N1	0.75281(10)	0.65806(5)	0.32331(10)	20.2(4)
C1	0.55210(12)	0.62254(6)	0.28404(12)	19.7(4)
C2	0.37864(13)	0.67638(6)	0.26505(13)	26.1(5)
C3	0.40743(15)	0.76336(7)	0.28360(14)	32.1(5)
C4	0.61465(16)	0.79700(6)	0.32587(14)	32.9(5)
C5	0.78353(15)	0.74283(6)	0.34480(13)	25.7(4)
C6	0.51522(12)	0.52834(6)	0.26183(12)	21.1(4)
Ni	0.0000	0.5000	0.5000	18.5(3)
O1	0.9296(4)	0.6108(2)	0.3319(4)	27.3(2)
O2	1.3317(5)	0.5224(2)	0.6275(4)	26.3(1)
O3	0.3268(4)	0.5067(2)	0.1338(4)	26.0(1)
O4	0.0091(5)	0.4362(2)	0.2386(4)	27.0(2)
N1	0.7589(5)	0.6577(2)	0.3241(4)	18.7(2)
C1	0.5554(6)	0.6227(3)	0.2821(6)	23.0(2)
C2	0.3831(6)	0.6767(3)	0.2618(6)	26.0(2)
C3	0.4108(7)	0.7629(3)	0.2785(6)	32.3(2)
C4	0.6212(7)	0.7964(3)	0.3255(6)	31.3(2)
C5	0.7874(6)	0.7429(3)	0.3427(6)	23.7(2)
C6	0.5180(6)	0.5277(2)	0.2584(6)	20.7(2)
Cu	0.0000	0.0000	0.0000	27.28(3)
O1	−0.11135(5)	0.20219(5)	−0.21436(4)	32.1(2)
O2	0.20304(6)	0.10617(5)	0.05112(3)	35.0(2)
O3	0.30192(6)	0.35767(5)	−0.00766(4)	40.8(2)
O4	0.28714(6)	−0.25767(5)	−0.16340(4)	39.1(2)
N1	−0.04880(6)	0.78083(5)	0.30683(4)	24.4(1)
C1	0.21757(7)	0.24269(6)	−0.23912(5)	24.2(2)
C2	0.62610(8)	0.73226(7)	0.34171(5)	31.6(2)
C3	0.35644(9)	0.26986(8)	−0.51541(6)	37.0(2)
C4	0.18179(10)	0.24704(7)	−0.57980(5)	37.1(2)
C5	0.97055(9)	0.77794(7)	0.47536(5)	31.8(2)

[a] $U_{eq} = \frac{1}{3} \Sigma_i U_{ii}$.

maps showed no peaks above 0.5 e $Å^{-3}$. All calculations were carried out on a UNIVAC 1100/60 computer.

RESULTS AND DISCUSSION

The atomic labeling is shown in Fig. 1 and the packing of the molecules in Figs. 2 and 3. Final atomic coordinates and thermal parameters with their standard deviations are presented in Tables 4 and 5. Tables of observed and calculated structure factors and anisotropic temperature factors are available from the author on request.

The octahedral coordination geometry about the central metal atom in the Mn^{2+}, Co^{2+} and Ni^{2+} complexes is not very much distorted, but in the Cu complex clearly elongated. In the latter case, the Jahn-Teller effect causes an extension of the Cu −O4(aqua) bond to 2.488(5) Å, which in the other complexes is between 2.09(1) and 2.26(1) Å. The most important bond distances and bond angles of the complexes are presented in Table 2. The bond distances between the metal atoms and the picolinato *N*-oxido ligand oxygens range from 2.154(1) to 1.922(3) Å in order of decreasing metal ion radius. The M−O4 bond distance becomes shorter, too, on moving from the Mn^{2+} complex to the Ni^{2+} complex [2.226(1)−2.094(3)].

The change of the central metal ion has only a slight influence on the bond distances in the picolinate *N*-oxide ligand. The bond distances N1 −O1 vary from 1.337(1) to 1.322(1) Å, whereas the same distance is 1.329(1) Å in the "free" nicotinic acid *N*-oxide.[13] The bond distance between the coordinated oxygen and the carbon atom, O2−C6, varies between 1.252(1) and 1.266(1) Å, and the uncoordinated oxygen carbon distance O3−C6 varies between 1.229(1) and 1.247(1) Å in the carboxylato group of the complexes. The corresponding distances in the free acid are 1.301(1) and 1.198(1) Å.[13] The angle of the carboxylato group, O2−C6−O3, is 125.3(1)−123.1(4)°, compared with 125.15(4)° in the free acid.[13] Thus coordination does not cause any noticeable opening of the carboxylato group angle.

The hydrogen bonds connecting the molecules with each other through the aqua oxygen atom, O4, and the uncoordinated carboxylate oxygen atom, O3, are shown in Table 3. The hydrogen bonds are so oriented that one connects the molecules in the direction of the *a* axis and the other in the direction of the *b* axis. In the Mn−Ni complex series there is also a diagonal hydrogen bond in the *ab* plane, (Figs. 2 and 3). The observed bond distances between the hydrogen and carbon or oxygen atoms vary from 0.5 to 1.1 Å, with the shortest values in the coordinated water molecule (Table 3).

According to earlier X-ray structure determinations of pyridine *N*-oxide metal complexes, the angle N−O−M varies between 116.7 and 134° when the central metal ion is Fe(II),[14] Co(II),[14-16] Ni(II)[17,18] or Cu(II).[14,19-22] In the present complexes the same angle varies from 116.1(1) to 120.9(1)°. As in the published pyridine *N*-oxide complexes it is found that the angle N−O−M is smallest for the copper complex. If it is assumed that

Table 5. $[M(N\text{-picO})_2(H_2O)_2]$, M = Mn^{2+}, Co^{2+}, Ni^{2+} and Cu^{2+}. Final positional parameters and isotropic thermal parameters ($\times 10^2$) for hydrogen atoms with their standard deviations.

	x	*y*	*z*	U_{iso}
$[Mn(N\text{-picO})_2(H_2O)_2]$				
H1	0.264(2)	0.798(1)	0.275(2)	5.3(4)
H2	0.225(2)	0.649(1)	0.347(1)	3.2(3)
H3	0.374(2)	0.359(1)	0.134(2)	8.9(5)
H4	0.908(2)	0.764(1)	0.343(2)	5.0(3)
H5	0.928(2)	0.941(1)	0.284(2)	7.1(4)
H6	0.874(2)	0.448(1)	0.109(2)	4.8(3)
$[Co(N\text{-picO})_2(H_2O)_2]$				
H1	0.245(2)	0.647(1)	0.233(2)	5.1(3)
H2	0.296(2)	0.805(1)	0.264(2)	5.2(4)
H3	0.357(2)	0.363(1)	0.153(2)	4.4(3)
H4	0.937(2)	0.762(1)	0.377(2)	4.4(3)
H5	0.896(2)	0.440(1)	0.129(2)	7.6(4)
H6	0.898(2)	0.955(1)	0.295(2)	8.1(5)
$[Ni(6\text{-picO})_2(H_2O)_2]$				
H1	0.262(8)	0.648(3)	0.329(7)	4(1)
H2	0.324(7)	0.801(3)	0.256(6)	2(1)
H3	0.358(8)	0.366(3)	0.163(7)	5(1)
H4	0.931(10)	0.762(4)	0.373(8)	7(2)
H5	0.880(10)	0.968(4)	0.305(8)	7(2)
H6	0.876(8)	0.455(3)	0.120(7)	3(1)
$[Cu(N\text{-picO})_2(H_2O)_2]$				
H1	0.501(1)	0.729(1)	0.293(1)	2.5(1)
H2	0.486(1)	0.266(1)	0.413(1)	4.4(2)
H3	0.174(1)	0.233(1)	0.312(1)	5.8(2)
H4	0.888(1)	0.215(1)	0.489(1)	3.5(1)
H5	0.599(1)	0.274(1)	0.135(1)	4.6(2)
H6	0.740(1)	0.333(1)	0.142(1)	5.7(2)

the *N*-oxide oxygen uses its sp^2 orbitals for bonding with the nitrogen and the metal atom, and the N – O bond is pure double bond, then the theoretical M – O – N angle is 120°.

REFERENCES

1. Knuuttila, H. *Inorg. Chim. Acta 50* (1981) 221.
2. Knuuttila, P. *Inorg. Chim. Acta 52* (1981) 141.
3. Knuuttila, P. *Inorg. Chim. Acta 58* (1982) 201.
4. Lever, A. B. P., Lewis, J. and Nyholm, R. S. *J. Chem. Soc* (1962) 5262.
5. Delia, T. J., Little, M. A. and West, D. X. *J. Inorg. Nucl. Chem. 35* (1973) 1400.
6. Boyd, S. A., Kohrman, R. E. and West, D. X. *Inorg. Nucl. Chem. Lett. 12* (1976) 603.
7. Boyd, S. A., Kohrman, R. E. and West, D. X. *J. Inorg. Nucl. Chem. 38* (1976) 607.
8. Iaconianni, F. J., Gelfand, L. S., Pytlewski, L. L., Nikulski, C. M., Speca, A. N. and Karayannis, N. M. *Inorg. Chim. Acta 36* (1979) 97.
9. Main, P., Hull, S. E., Lessinger, L., Germain, G., Declercq, J. P. and Woolfson, M. M. *MULTAN. A System of Computer Programs for the Automatic Solution of Crystal Structures from X-Ray Diffraction Data*, Universities of York, England and Louvain-la-Neuve, Belgium 1978.
10. Stewart, J. M. *The X-Ray System, Version of 1976*, Technical Report TR-446, Computer Science Center, University of Maryland, College Park 1976.
11. Cromer, D. T. and Mann, J. B. *Acta Crystallogr. A 24* (1968) 321.
12. Stewart, R. F., Davidson, E. R. and Simpson, W. T. *J. Chem. Phys. 42* (1965) 3175.
13. Knuuttila, H. *Unpublished work.*
14. Taylor, D. *Aust. J. Chem. 31* (1978) 713.
15. Bergendahl, T. J. and Wood, J. S. *Inorg. Chem. 14* (1975) 338.
16. Coyle, B. A. and Ibers, J. A. *Inorg. Chem. 9* (1970) 767.
17. VanIngen Schenau, A. D., Verschoor, G. C. and Romers, C. *Acta Crystallogr. B 30* (1980) 1686.
18. Horrocks, de W. W., Templeton, D. H. and Zallkin, A. *Inorg. Chem. 7* (1968) 1552.
19. O'Connor, C. J., Sinn, E. and Carlin, R. L. *Inorg. Chem. 16* (1977) 3314.
20. Lee, J. D., Brown, D. S. and Melsom, B. G. A. *Acta Crystallogr. B 25* (1969) 1378.
21. Watson, H. W. *Inorg. Chem. 8* (1969) 1879.
22. Williams, R. J., Cromer, D. T. and Watson, W. H. *Acta Crystallogr. B 27* (1971) 1619.
23. Coyle, B. A. and Ibers, J. A. *Inorg. Chem. 9* (1970) 767.

Received February 8, 1982.

Acta Chemica Scandinavica A 36 (1982) 773–777

Calculation of Fundamental Frequencies of 2,5-Dimethyl-2,3,4-hexatriene

ASTRI ROGSTAD * and CLAUS J. NIELSEN

Department of Chemistry, University of Oslo, Blindern, Oslo 3, Norway

Tetramethylbutatriene has been analyzed using force constant calculations, which demonstrated that force constants may be transferred from structurally related compounds such as butatriene and tetramethylethylene.

Recently, the vibrational spectra of tetramethylbutatriene were analyzed by one of us.[1] The ambiguities in the assignments due to incomplete vibrational spectral data suggested to us that we use force constant calculations as a tool for obtaining more reliable assignments. Further, tetramethylbutatriene has recently been subjected to a gas electron-diffraction investigation by the Oslo group[2] and mean amplitudes of vibration are needed in the analysis. The scope of this paper is to demonstrate that the approximate, transferred force constants may be applied in studying fundamental modes of vibration for tetramethylbutatriene.

Some of the constants of an approximate internal valence force field for tetramethylbutatriene can be transferred from butatriene and tetramethylethylene. Previously, Cyvin and Hagen[3] established a force field for butatriene by transferring initial force constants from ethylene and allene and producing a final force field by adjusting the force constants to fit exactly the observed frequencies of butatriene. Different types of force fields have been reported for propene,[4] *cis*-2-butene[5] and *trans*-2-butene,[6] but no force field has been published for tetramethylethylene.

VIBRATIONAL ASSIGNMENTS

Butatriene. The vibrational spectra of butatriene have been published by Miller *et al.*[7] and by Cyvin *et al.*[8] The assignment of the fundamental modes of vibration given by the former, was later modified by Cyvin and Hagen.[3] The reassignment was in part confirmed by our calculations. However, there are no experimental criteria to distinguish between the $\nu_7(b_{2g})$ mode at 544 cm^{-1} and the $\nu_{10}(b_{3g})$ mode at 459 cm^{-1}, as was stated by Cyvin and Hagen.[3] For tetramethylbutatriene the normal coordinate calculations give better results if the values of ν_7 and

* Permanent address: Department of Food Hygiene, Veterinary College of Norway, Oslo 1, Norway.

Table 1. Structural parameters used in normal coordinate calculations.

	Ethylene	Tetramethyl-ethylene	Butatriene	Tetramethyl-butatriene
C=C (Å)	1.34	1.34	1.33 1.27	1.33 1.27
C–C (Å)		1.51		1.51
C–H (Å)	1.085	1.09	1.085	1.09
C=C–H C=C–C (°)	121	122	121	122
C–C–H (°)		109.47		109.47

0302-4377/82/090773-05$02.50

ν_{10} are interchanged. It also seems reasonable to assume that the out-of-plane mode will appear at a lower frequency than the corresponding in-plane mode.

2,3-Dimethyl-2-butene. Several research groups have analyzed the vibrational spectra of tetramethylethylene.[9-12] Apart from the uncertainty in the assignment of the methyl torsional modes $\nu_{17}(b_{1g})$, $\nu_{22}(b_{2g})$ and $\nu_{48}(b_{3u})$ some inconsistencies appear in the assignments of $\nu_6(a_g)$, $\nu_{12}(b_{2g})$, $\nu_{43}(b_{2u})$ and $\nu_{47}(b_{3u})$. We have assigned the latter modes to bands at 947, 505, 272 and 308 cm^{-1}, respectively, as first suggested by Scott *et. al.*[9] The alternative assignments[12] of these modes do not agree with our calculations.

FORCE CONSTANT CALCULATIONS

In the present work, the force field for tetramethylbutatriene was constructed by transferring a common force field for ethylene, butatriene and tetramethylethylene, derived by the overlay technique. The structural parameters used in the normal coordinate analyses, are given in Table 1. Definitions of the internal valence coordinates are shown in Fig. 1. The methyl torsions have been defined as the normalized sum of the three C=C−C−H torsions, while the C=C torsions were defined as the normalized sum of the two *trans* X−C=C−X torsions.

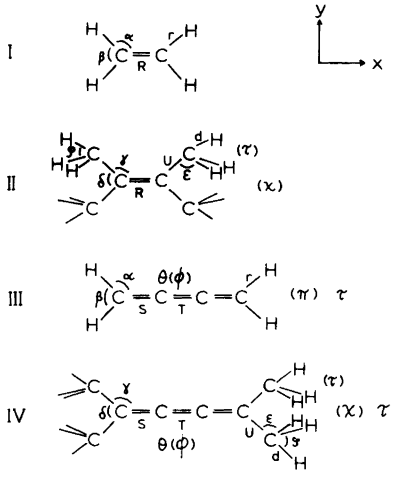

Fig. 1. Definition of the internal coordinates in ethylene (I), tetramethylethylene (II), butatriene (III) and tetramethylbutatriene (IV). The out-of-plane deformations are in the direction of the *z*-axis.

Table 2. Suggested valence force constants, with reference to Fig. 1, for ethylene (I), tetramethylethylene (II), butatriene (III) and tetramethylbutatriene (IV).

Constant	Value[a]	Used in molecule
K_R	9.63	I, II
K_S	9.25	III, IV
K_T	10.83	III, IV
K_U	4.40	II, IV
K_r	5.06	I, III
K_d	4.62	II, IV
H_α	0.551	I, III
H_β	0.383	I, III
H_θ	0.437	III, IV
H_ϕ	0.328	III, IV
H_γ	1.09	II, IV
H_δ	1.24	II, IV
H_ε	0.614	II, IV
H_ζ	0.530	II, IV
H_π	0.198	III
H_χ	0.267	II, IV
H_τ	0.139	III, IV
F_{ST}	0.68	III, IV
F_{RU}, F_{SU}	0.96	II, IV
F_{dd}	0.05	II, IV
$F_{R\alpha}$, $F_{S\alpha}$	0.30	I, III
$F_{R\gamma}$, $F_{S\gamma}$	0.53	II, IV
$F_{U\gamma}$	0.48	II, IV
$F_{U\varepsilon}$	0.33	II, IV
$F_{d\varepsilon}$	0.10	II, IV
$f^t_{\alpha\alpha}$	0.06	I
$f^c_{\alpha\alpha}$	−0.04	I
$f_{\theta\theta}$	−0.04	III, IV
$f_{\phi\phi}$	0.02	III, IV
$f^t_{\gamma\gamma}$	0.33	II
$f^c_{\gamma\gamma}$	0.60	II
$f_{\varepsilon\varepsilon}$	−0.02	II, IV
$f_{\varepsilon\zeta}$	−0.01	II, IV
$f_{\theta\gamma}$	−0.05	IV
$f_{\phi\chi}$	−0.05	IV
$f_{\chi\chi}$	−0.045	II
$H_{\tau-Me}$	0.018	II, IV

[a] Stretching force constants in mdyn/Å, bending force constants in mdyn · Å and stretch−bend interactions in mdyn.

Table 3. Observed and calculated frequencies (cm^{-1}) for tetramethylethylene.[a]

Species	Obs.	Calc.	Species	Obs.	Calc.
a_g ν_1	2930	2934	b_{1u} ν_{30}	2930	2932
ν_2	2860	2870	ν_{31}	2879	2870
ν_3	1683	1684	ν_{32}	1460	1457
ν_4	1456	1455	ν_{33}	1382	1386
ν_5	1397	1380	ν_{34}	1172	1169
ν_6	947	954	ν_{35}	902	874
ν_7	690	699	ν_{36}	417	410
ν_8	411	411			
			b_{2u} ν_{37}	2930	2930
b_{1g} ν_{14}	2930	2928	ν_{38}	2879	2870
ν_{15}	1456	1454	ν_{39}	1453	1457
ν_{16}	947	965	ν_{40}	1382	1386
ν_{17}	–	172	ν_{41}	1165	1175
			ν_{42}	972	961
b_{2g} ν_{18}	2930	2929	ν_{43}	272	265
ν_{19}	1456	1458			
ν_{20}	1071	1057	b_{3u} ν_{44}	2930	2929
ν_{21}	505	510	ν_{45}	1460	1458
ν_{22}	–	152	ν_{46}	1028	1033
			ν_{47}	308	277
b_{3g} ν_{23}	2930	2930	ν_{48}	–	164
ν_{24}	2862	2870			
ν_{25}	1456	1456			
ν_{26}	1374	1383			
ν_{27}	1269	1264			
ν_{28}	947	948			
ν_{29}	505	506			

[a] Experimental data from Refs. 9 – 12.

Table 4. Observed and calculated frequencies (cm^{-1}) for butatriene[a] and tetramethylbutatriene.[b]

Species	Butatriene No.	Obs.	Calc.	Tetramethylbutatriene No.	Obs.	Calc.
a_g	ν_1	2995	2995	ν_1	2904	2932
	ν_2	2079	2079	ν_2	2850	2870
	ν_3	1430	1450	ν_3	2064	2073
	ν_4	878	877	ν_4	1459	1459
				ν_5	1377	1383
				ν_6	1280	1296
				ν_7	966	902
				ν_8	595	606
				ν_9	291	344
b_{1g}	ν_5	736	736	ν_{15}	2924	2928
				ν_{16}	1436	1454
				ν_{17}	948	965
				ν_{18}	177	172
b_{2g}	ν_6	878	871	ν_{19}	2924	2929
	ν_7	459	459	ν_{20}	1459	1457
				ν_{21}	1059	1044

Table 4. Continued.

				ν_{22}	528	541
				ν_{23}	329	303
				ν_{24}	130	157
b_{3g}	ν_8	3059	3097	ν_{25}	2924	2929
	ν_9	1090	1081	ν_{26}	2860	2870
	ν_{10}	546	544	ν_{27}	1436	1456
				ν_{28}	1364	1384
				ν_{29}	1280	1224
				ν_{30}	948	952
				ν_{31}	748	728
				ν_{32}	275	269
b_{1u}	ν_{11}	2994	2994	ν_{33}	2934	2931
	ν_{12}	1608	1605	ν_{34}	2863	2870
	ν_{13}	1370	1393	ν_{35}	1661	1629
				ν_{36}	1447	1455
				ν_{37}	1374	1383
				ν_{38}	1010	1037
				ν_{39}	808	826
				ν_{40}	401	442
b_{2u}	ν_{14}	3080	3097	ν_{41}	2918	2932
	ν_{15}	1060	1049	ν_{42}	2863	2870
	ν_{16}	215	215	ν_{43}	1447	1456
				ν_{44}	1374	1384
				ν_{45}	1211	1216
				ν_{46}	956	952
				ν_{47}	533	576
				ν_{48}	85	83
b_{3u}	ν_{17}	854	861	ν_{49}	2918	2929
	ν_{18}	215	215	ν_{50}	1459	1458
				ν_{51}	1063	1045
				ν_{52}	433	456
				ν_{53}	–	161
				ν_{54}	100	110

[a] Experimental data from Refs. 7 and 8. [b] Experimental data from Ref. 1.

A total of 35 force constants was fitted to reproduce the vibrational fundamental modes of the three molecules: ethylene, butatriene and tetramethylethylene (Table 2). All interaction constants between valence coordinates not involving common atoms were assumed vanishingly small. Two additional interaction constants, $f_{\theta\gamma}$ and $f_{\theta\chi}$, were introduced for tetramethylbutatriene in order to reproduce the lowest bending modes.

The observed and calculated vibrational frequencies for tetramethylethylene are given in Table 3, while the corresponding results for butatriene and tetramethylbutatriene are given in Table 4. In general the agreement is within 1 %. The magnitudes of the force constants of Table 2 seem to be physically reasonable. The fact that the interaction constants are refined to fit several molecules increases our confidence in the force constants.

REFERENCES

1. Rogstad, A. *Spectrochim. Acta A 36* (1980) 131.
2. Aanensen, J. E. and Gundersen, G. *To be published.*
3. Cyvin, S. J. and Hagen, G. *Acta Chem. Scand. 23* (1969) 2037.
4. Silvi, B., Labarbe, P. and Perchard, J. P. *Spectrochim. Acta A 29* (1973) 263.

5. Levin, I. W. and Pearce, R. A. R. *J. Mol. Spectrosc. 49* (1974) 91.
6. Levin, I. W., Pearce, R. A. R. and Harris, W. C. *J. Chem. Phys. 59* (1973) 3048.
7. Miller, F. A. and Matsubara, I. *Spectrochim. Acta 22* (1966) 173.
8. Cyvin, S. J., Cyvin, B. N., Klæboe, P. and Augdahl, E. *Acta Chem. Scand. 19* (1965) 883.
9. Scott, D. W., Finke, H. L., McCullough, J. P., Gross, M. E., Messerly, F. F., Pennington, R. E. and Waddington, G. *J. Am. Chem. Soc. 77* (1955) 4993.
10. Kimmel, H. S. and Snyder, W. H. *J. Mol. Struct. 4* (1969) 473.
11. Durig, J. R., Hawley, C. W. and Bragin, J. *J. Chem. Phys. 57* (1972) 1426.
12. Sverdlov, L. M., Kevner, M. A. and Krainov, E. P. *Vibrational Spectra of Polyatomic Molecules*, Wiley, New York 1974, Chapter 5.

Received February 18, 1982.

Acta Chemica Scandinavica A 36 (1982) 779–781

Short Communication

A Small Angle Neutron Scattering Investigation on Aluminium Hydroxide

A. NØRLUND CHRISTENSEN,[a]
M. S. LEHMANN[b] and A. WRIGHT[b]

[a] Department of Inorganic Chemistry, Aarhus University, DK-8000 Aarhus C, Denmark and [b] Institut Max von Laue – Paul Langevin, B.P. 156, F-38042 Grenoble Cedex, France

In the hydrolysis of aluminium solutions with bases, the polynuclear complex $Al_{13}O_4(OH)_{24}(H_2O)_{12}^{7+}$ is formed.[1] A small angle X-ray scattering investigation on hydrolyzed aluminium nitrate solutions with OH – Al ratios up to 2.25 showed the presence of a particle with a 4.3 Å radius of gyration in good agreement with that calculated for the polynuclear complex.[2] When the OH – Al ratio exceeds 2.7, an amorphous aluminium hydroxide gel is formed, and a small angle X-ray scattering investigation of the gel shows it to be polydisperse with particles of sizes from at least a few hundred Å to 25 Å or possibly less than 25 Å,[3,4] In a recent small angle neutron scattering investigation of the aging of iron(III) hydroxide gels it was found that the particle diameters were in the range 700 – 1000 Å, and all the systems investigated showed a clear polydispersity.[5] In order to study the early stages of the formation of a gel it was decided to make an on-line small angle neutron scattering experiment of the homogeneous hydrolysis of an aluminium solution with urea. In addition, the aging of aluminium hydroxide gels should be studied by small angle neutron scattering to compare the aging process with that of iron(III) hydroxide gels.

Hydrolysis of Me(III) solutions. In a previous investigation it was found that solutions of iron(III) nitrate on heating were hydrolyzed to α-Fe_2O_3.[6] The Me(III) solutions listed in Table 1 were sealed in thick-walled pyrex ampoules and kept at the indicated experimental conditions. By this treatment only the iron(III) solution and the indium(III) solution yielded solid products of hydrolyses. The solids were identified from Guinier photographs taken with a Guinier camera using Cu$K\alpha_1$ radiation.

Solutions of urea, NH_2CONH_2, in water can be used in a homogeneous hydrolysis of Me(III) solutions. When a solution of urea is heated to temperatures above 85 °C, NH_3 (and CO_2) is produced at a convenient rate for hydrolysis. Table 2 shows a selection of solutions of Me(III) salts hydrolyzed by urea in sealed pyrex ampouls at 94 °C. It is interesting to note the hydrolysis product of the iron(III) nitrate solution is crystalline α-FeOOH formed at low pH conditions in the solution, and that the product of hydrolysis of the aluminium nitrate solution is an amorphous gel.

Heat treatment of aluminium hydroxide gels. The gel of aluminium hydroxide was made from a 1 M solution of $Al_2(SO_4)_3.18H_2O$ (Merck) and a 3 M solution of NaOH (Merck). The base was added dropwise to the aluminium sulfate solution and pH was measured simultaneously with a Radiometer PHM 64 pH-meter. The precipitation was

Table 1. Hydrolysis of 1 M metal salt solutions at 180 °C for 6 h.

Solution of	pH before	pH after	Product
$Fe(NO_3)_3.6H_2O$	0.62	−0.22	α-Fe_2O_3
$In_2(SO_4)_3$	1.05	0.59	$InOHSO_4$
$Cr(NO_3)_3.9H_2O$	1.66	0.71	No solid
$Al(NO_3)_3.9H_2O$	1.70	1.60	No solid
$La(NO_3)_3.6H_2O$	4.57	4.62	No solid

Table 2. Hydrolysis of metal solutions with urea at 94 °C for 24 h. The solutions are 4.5 M with respect to urea and 0.75 M with respect to the metal ions.

Solution of	pH before	pH after	Product
$Fe(NO_3)_3.6H_2O$	1.87	7.24	α-FeOOH
$In_2(SO_4)_3$	2.39	6.94	$In(OH)_3$[a]
$Cr(NO_3)_3.9H_2O$	2.60	7.71	Gel
$Al(NO_3)_3.9H_2O$	2.70	7.90	Gel

[a] Contains $In(OH)_3$ and an unidentified compound.

0302-4377/82/090779-03$02.50

interrupted when pH of the solution was 4.77, and 15 ml samples of the aluminum hydroxide with the mother liquid were sealed in pyrex ampouls and kept at 94 °C for up to 24 h.

Small angle neutron scattering experiments. The small angle neutron scattering experiments were performed at the Institut Max von Laue – Paul Langevin in Grenoble with the instrument D11, using 10 Å neutrons and a sample detector distance of 20 m. The specimens were housed in cuvettes of quartz placed in a rack where a temperature of up to 100±0.5 °C could be obtained during the diffraction experiment. The scattered neutrons were measured with a two dimensional multi detector and the data reduction was performed as described previously.[5] The scattering curves show that the particles belong to a polydisperse size distribution, and a simple model has been used for analysis. This model has been developed for analysis of small angle scattering curves from colloidal systems.[7] At the present time, it is limited to describing scattering from spherical particles with a hard sphere exclusion potential exceeding the radius of the particle. Therefore, the interparticle interference effects can be described by including in the fit the effective volume fraction of the extended sphere. Cleary, the use of a spherical particle model to describe a gel system is a coarse approximation, but it is not possible at the present time to calculate the particle function for lower symmetry particles. The other parameters in the least-squares analysis were the particle size (S), the size distribution function (σ) and the intensity of forward scattering [$I(Q_o)$].

When a solution containing Al^{3+} ions and urea is heated to temperatures above 85 °C, pH of the solution will increase with time, and the faster the higher the temperature and the concentration of urea. At a pH value of approximately 6 a gel is

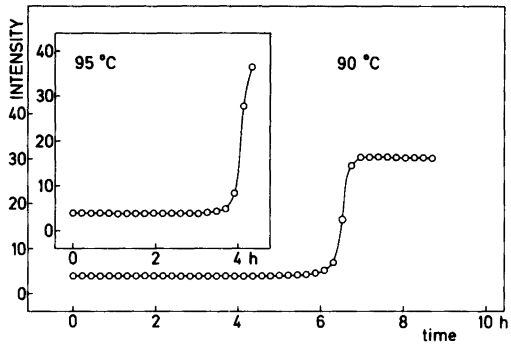

Fig. 1. Total scattering intensity of a solution that is 0.74 M Al^{3+} and 4.50 M urea *vs.* The formation of the gel results in an increase in the scattering intensity.

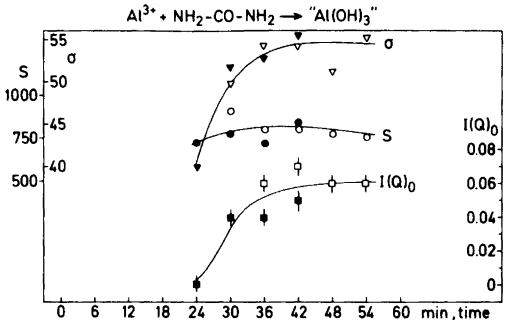

Fig. 2. $I(Q_o)$, S, and σ for gels of aluminium hydroxide formed by the hydrolysis of urea.

formed. At this pH value the dominant species is the $Al_{13}O_4(OH)_{24}(H_2O)_{12}^{7+}$ ion[8] and the formation of the gel is so fast that it has the character of a polymerization. Fig. 1 displays the total scattering (on an arbitrary scale) *vs.* time for a solution that was 0.74 M with respect to Al^{3+} and 4.50 M with respect to urea. After approximately 4 h at 95 °C or 6 h at 90 °C, the total scattering of the specimens increases and reaches a maximum value within 1 h. Fig. 2 shows $I(Q_o)$, the particle size, S, and the standard deviation of the size distribution function, σ, for gels of aluminium hydroxide formed by the hydrolysis with urea. The solutions were pre-heated for 6 h in a thermostat kept at 90 °C, and the diffraction experiments were then performed with the cuvettes at a temperature of 90 °C. It is interesting to note that the values, apparently, reach a constant maximum in the homogeneous hydrolysis process. Fig. 3 displays $I(Q_o)$, σ, and S for specimens of aluminium hydroxide gels aged at 94 °C for up to 24 h.

The measurements show that the polycondensation appears to be a two stage process. Within a narrow pH range the abrupt appearance of large particles is observed. There is no evidence of a small particle precursor. Within the time period of the experiment the particles do not grow significantly in size (Fig. 2). However, the growth in forward scattering observed for long time aging at room temperature or at elevated temperatures (Fig. 3) shows an increase in scattering contrast between particles and the solution which is interpreted as elimination of protons from the precipitate.

Whilst a moderately good fit to the scattering curves can be obtained without introduction of interparticle interference effects, the fit in the middle scattering range can be improved by using the volume fraction as a parameter in the least-squares analysis. However, we do not consider that the volume fraction so obtained is a reliable value in the

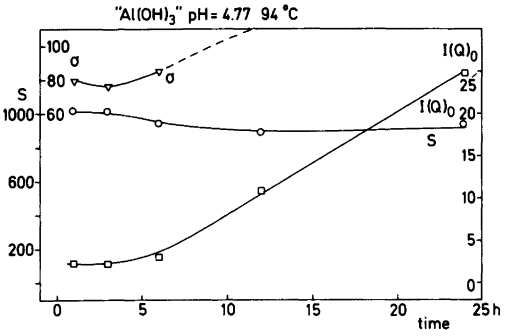

Fig. 3. $I(Q_o)$, S, and σ for gels of aluminium hydroxide aged at 94 °C for up to 24 h.

absence of a marked interference peak. It is equally likely that the use of spherical particles in the model is a poor approximation to the real particle scattering function in this range of Q. Small angle scattering patterns of silica gel show a shoulder in $I(Q)$ which can be interpreted according to a model of agglomerated spherical particles in which a dimer of two spheres in contact gives the best particle scattering function.[9] This model is consistent with a process in which independently formed particles stick together in contact without rearranging to form a more compact cluster. Further analysis of the iron(III) data [5] will be made to test this hypothesis.

Acknowledgements. The Danish Natural Science Research Council is acknowledged for financial support to one of us (ANC). We are indebted to Dr. H. Haesslin and R. Oberthür for the loan of the sample heater used in the scattering experiment.

1. Johansson, G. *Acta Chem. Scand. 14* (1960) 771.
2. Rausch, W. V. and Bale, H. D. *J. Chem. Phys. 40* (1964) 3391.
3. Bale, H. D. and Schmidt, P. W. *J. Chem. Phys. 62* (1958) 1179.
4. Bale, H. D. and Schmidt, P. W. *J. Chem. Phys. 31* (1959) 1612.
5. Christensen, A. N., Lehmann, M. S. and Wreight, A. *Acta Chem. Scand. A 37* (1983). *In press.*
6. Christensen, A. N., Convert, P. and Lehmann, M. S. *Acta Chem. Scand. A 34* (1980) 771.
7. Hanis, N. *Thesis.* Institut Laue–Langevin, Grenoble 1980.
8. Öhman, L.-O. and Forsling, W. *Acta Chem. Scand. A 35* (1981) 795.
9. Hayter, J. and Wright, A. *To be published.*

Received May 27, 1982.

Acta Chemica Scandinavica A 36 (1982) 783–795

Compounds with Intermediate Spin. 6.* Structure and Magnetic Properties of Tris(*N*,*N*-dipropionitriledithiocarbamato)iron(III) Hemichloroform

J. ALBERTSSON, Å. OSKARSSON and K. STÅHL

Inorganic Chemistry 1 and 2, Chemical Center, University of Lund, P.O.B. 740, S-220 07 Lund, Sweden

$Fe[S_2CN(C_3H_4N)_2]_3 \cdot \frac{1}{2}CHCl_3$, $M_r = 710.38$, has a temperature dependent magnetic moment which varies from $\mu_{eff} = 1.50$ at 5 K to 4.09 at 315 K. Its crystal structure has been determined with direct and Fourier methods from X-ray intensities collected with a four-circle single-crystal diffractometer at 210 and 297 K. At both temperatures the crystals are triclinic with space group $P\bar{1}$, $Z = 2$; $a = 10.676(4)$, $b = 12.038(5)$, $c = 14.034(5)$ Å, $\alpha = 70.36(4)$, $\beta = 74.61(3)$, $\gamma = 67.26(3)°$, $V = 1547(1)$ Å^3, $D_x = 1.525$ g cm^{-3} and $\mu_{eff} = 3.19$ at 210 K; $a = 10.756(5)$, $b = 12.062(6)$, $c = 14.113(6)$ Å, $\alpha = 70.14(5)$, $\beta = 74.98(3)$, $\gamma = 67.59(4)°$, $V = 1574(1)$ Å^3, $D_x = 1.499$ g cm^{-3} and $\mu_{eff} = 3.94$ at 297 K. The least-squares refinements converged to $R = 0.048$ (210 K) and 0.061 (297 K). The structure comprises mononuclear complexes of pseudosymmetry D_3. They are van der Waals packed with statistically distributed chloroform molecules. The magnetic properties were investigated with the Faraday method in the temperature range 5–315 K using a microcomputer controlled balance together with $N_2(l)$ and He(l) cryostats. Above 225 K, the effective changes of enthalpy and entropy for the low to high-spin transition can be obtained from a ln K *vs.* T^{-1} plot: $\Delta H_{eff} = 8.4(3)$ kJ mol^{-1}, $\Delta S_{eff} = 22(1)$ J K^{-1} mol^{-1}. The spin transition appears to be non-cooperative.

Most complexes formed between iron(III) and substituted dithiocarbamate ligands have properties that are characteristic of a thermal equilibrium between the low-spin $^2T_2$ and high-spin $^6A_1$ states of iron(III) (assuming O_h symmetry of the FeS_6 core).[1,2] The present series of investigations [3,4] aims at correlating the magnetic behaviour of various $Fe(S_2CNR_2)_3$ complexes with their geometrical features: (*i*) the size, symmetry and distortion of the FeS_6 core at different temperatures, (*ii*) bond distances, bond angles and conformations of the ligand molecules, especially the S_2CNC_2 part, and (*iii*) the crystal packing of the complexes. Thermal smearing prevents the resolution of high and low-spin complexes except at very low temperatures,[5] but there are still relatively large changes in the geometry of the FeS_6 core between the two spin states since the difference between the high and low-spin radii of Fe^{3+} is about 0.15 Å.[4] Thus the spin transition may readily be affected by changes in the structure as the crystal must be able to accommodate the two types of complex simultaneously.

It has been suggested that the transformation from high to low-spin would involve the formation of small regions of low-spin complexes in a high spin crystallite and the subsequent growth of these low-spin domains.[6,7] In this description, crystal defects are preferred sites for nucleation of the minority spin domain, but they can also inhibit further growth by increasing the activation energy. For some materials one way to increase the number of crystal defects is to grind the sample thoroughly. Solid solvates may have additional crystal defects caused by disorder and loss of the solvent molecules.

In this paper we report the crystal structure of tris(*N*,*N*-dipropionitriledithiocarbamato)iron(III) hemichloroform at 210 and 297 and its magnetic properties in the temperature range 5–315 K. The propionitrile substituent was chosen because the

* For part 5 in this series see Ref. 4.

0302-4377/82/100783-13$02.50

corresponding secondary amine has a smaller pK_a value than those corresponding to the other substituents we have investigated: $pK_a \approx 5.3$ for dipropionitrile amine in aqueous solution[8] as compared to 10.9 for dimethylamine.[9] Thus, there might be a change in the FeS_2CN part of the complex caused by the changed inductive effect of the substituents on the nitrogen atom.

EXPERIMENTAL

An ethanol solution with 0.1 mol l^{-1} sodium *N,N*-dipropionitriledithiocarbamate was prepared by mixing equal amounts of carbon disulfide, dipropionitrile amine and sodium hydroxide:

$$CS_2 + HN(C_3H_4N)_2 + NaOH \rightarrow Na^+ + S_2CN(C_3H_4N)_2^- + H_2O$$

The Fe(III) complex was precipitated by adding an ethanol solution of anhydrous $FeCl_3$. Black, platelike single-crystals were grown from a chloroform solution of the precipitate by slow evaporation at room temperature. All preparative work was made in nitrogen atmosphere.

Preliminary Weissenberg photographs at 295 K indicated the Laue class $\bar{1}$ and other photographs at 120 K revealed that there is no phase transition on cooling. Cell dimensions (Table 1) were derived by least squares from 50 reflexions measured with graphite monochromated Mo$K\alpha$ radiation on a CAD4 diffractometer ($\lambda\alpha_1 = 0.70930$ Å). The diffractometer was equipped with a gas-stream apparatus working with $N_2(l)$.[10] The single-crystal used was tabular c and bound by the forms {320} and {2$\bar{1}$0}. The size was $0.27 \times 0.34 \times 0.06$ mm^3. Almost full spheres of reciprocal space with radii $\sin\theta/\lambda = 0.60$ Å^{-1} were then measured at 210 and 297 K.* The intensities were collected using $\omega - 2\theta$ scans with $\Delta\omega = 1.00° + 0.50° \tan\theta$. Maximum

* The originally intended low temperature was 150 K but due to an error in the regulating system the actual temperature became 60 K higher.

Table 1. Unit cell dimensions of $Fe(S_2CN(C_3H_4N)_2)_3 \cdot \frac{1}{2}CHCl_3$ in the interval 195–297 K.

T/K	*a*/Å	*b*/Å	*c*/Å	*α*/°	*β*/°	*γ*/°	*V*/Å^3
195	10.635(4)	12.022(7)	14.025(7)	70.34(5)	74.56(3)	67.27(3)	1538(1)
210	10.676(4)	12.038(5)	14.034(5)	70.36(4)	74.61(3)	67.26(3)	1547(1)
225	10.687(4)	12.044(6)	14.035(6)	70.37(4)	74.64(3)	67.32(3)	1551(1)
240	10.719(3)	12.036(5)	14.051(5)	70.33(4)	74.70(2)	67.29(2)	1556(1)
255	10.710(6)	12.039(9)	14.073(10)	70.28(8)	74.81(5)	67.31(5)	1558(2)
270	10.740(4)	12.050(6)	14.093(6)	70.21(4)	74.92(3)	67.35(3)	1566(1)
297	10.756(5)	12.062(6)	14.113(6)	70.14(5)	74.98(3)	67.59(4)	1574(1)

Table 2. Crystal data of $Fe(S_2CN(C_3H_4N)_2)_3 \cdot \frac{1}{2}CHCl_3$ and the least-squares refinements. Unit cell dimensions are given in Table 1.

M_r ($C_{21}H_{24}FeN_2S_6 \cdot \frac{1}{2}CHCl_3$) = 710.38		
Triclinic space group $P\bar{1}$ (No. 2), $Z = 2$		
Temperature (K)	210	297
D_x (g cm^{-3})	1.525	1.499
μ(Mo$K\alpha$) (cm^{-1})	10.36	10.18
Range of transmission factor	0.78–0.95	0.77–0.95
No. of reflexions recorded	11059	11567
No. of reflexions with $I < 2\sigma_c(I)$	3489	4329
No. of reflexions in LS refinement, *m*	3868	3786
No. of parameters refined, *n*	456	433
$R = \Sigma\|\Delta F\|/\Sigma\|F_o\|$ [a]	0.048	0.061
$R_w = [\Sigma w(\Delta F)^2/\Sigma w\|F_o\|^2]^{1/2}$	0.068	0.080
$S = [\Sigma w(\Delta F)^2/(m-n)]^{1/2}$	0.938	1.015
C_1 (weighting function)	0.030	0.048
C_2 (weighting function)	2.50	1.00

[a] $\Delta F = |F_o| - |F_c|$.

counting times of 120 (210 K) and 180 s (297 K) resulted in that most reflexions had $\sigma_c(I)/I \lesssim 0.030$ and 0.020, respectively [$\sigma_c(I)$ is based on counting statistics]. The intensities of three standard reflexions were measured every two hours. They showed no systematic variations. Corrections were made for Lorentz, polarization and absorption effects (Table 2). The crystal structure was solved using one independent half of the room temperature data but, before the refinement commenced, the intensities of each pair of centrosymmetrically related reflexions were averaged for both data sets.

Magnetic susceptibilities were measured on polycrystalline samples using the Faraday principle. The apparatus consists of a medium-sized electromagnet,[11] with constant gradient pole caps and a Cahn TG electrobalance. It is similar to a Faraday balance described by Blom and Hörlin[12] but the weighing procedure is controlled by an Intel 8080 microcomputer. Temperatures below 77 K were reached using a Leybold-Heraeus He(*l*) vaporization cryostat VNK 3 – 300. The apparatus was calibrated with $HgCo(SCN)_4$.[13] In order to check saturation effects the measurements were repeated at different field strengths, 0.6 and 0.8 T. Effects caused by crystal size and perfection were investigated by also repeating the measurements after carefully grinding the sample with agate mortar and pestle.

SOLUTION AND REFINEMENT OF THE STRUCTURE

The FeS_6 core of the complex was located with MULTAN.[14] The intensity statistics indicated a centric distribution (*i.e.* space group $P\bar{1}$). The rest of the non-H ligand atoms were found in a difference electron density map. The positions of the H atoms in the CH_2 groups were calculated assuming tetrahedral C atoms and C – H = 1.0 Å. These atoms were assigned fixed isotropic thermal parameters $B = 5.0$ Å^2 at 210 K and 8.0 Å^2 at 297 K while the other ones were assumed to vibrate anisotropically within the simple harmonic approximation. A least-squares refinement of the room temperature structure gave no better value of R than 0.13. A new difference map revealed a chloroform molecule located at either of two centrosymmetrically related positions near $\frac{1}{2},\frac{1}{2},0$. A disorder was also detected in one of the ligands. The dissordered group, $-C(6)H_2-C(7)\equiv N(3)$, was subsequently treated as statistically distributed over two sets of positions, *A* and *B*, at both temperatures.

The function $\Sigma w(\Delta F)^2$ was minimized with full-matrix least-squares refinement (Table 2). The weights w were calculated from $w^{-1} = \sigma_c^2(|F_o|) + (C_1|F_o|)^2 + C_2$ with C_1 and C_2 so adjusted that constant values of $<w(\Delta F)^2>$ were obtained in different $|F_o|$ and $\sin\theta$ intervals. Because of the large number of parameters in the structure model, the $Fe(S_2CN)_3$ group was refined separately from the non-H atoms of the ligand substituents and the chloroform molecule until all the shifts were well below their esd's. The occupancies of the chloroform molecule and of positions *A* of the disordered propionitrile group were also included. The thermal motion of the chloroform molecule had to be treated as isotropic in the room-temperature model with the same parameter assigned to each Cl atom. The thermal parameters of C(7*A*), N(3*A*), C(7*B*) and N(3*B*) at room temperature and of C(7*B*) and N(3*B*) at 210 K could not be refined. The positions of the methylene H atoms were varied in some least-squares cycles towards the end of each refinement. The final difference map of the room-temperature structure showed some peaks with height about 1 e Å^{-3} in the vicinity of the chloroform molecule but the 210 K model gave only spurious peaks of hight less than 0.6 e Å^{-3}.

Atomic scattering factors and dispersion correction factors were taken from *International Table for X-Ray Crystallography*.[15] Atomic parameters are given in Table 3. Data and final models are compared in Fig. 1 by probability plotting of ordered values of $\delta R_i = \Delta F_i/\sigma(|F_o|_i)$ *vs.* those expected for ordered normal deviates [$\sigma(|F_o|_i) = w_i^{-1/2}$].[16] The slopes and intercepts of the curves indicate that the systematic errors are small and that $\sigma(|F_o|)$ is on average rather well estimated (*cf.* the related *S* values of Table 2). The shape of the 210 K curve does though point towards some residual errors in the model or data. The observed and calculated structure amplitudes and anisotropic thermal parameters are available on request.

DESCRIPTION OF THE STRUCTURE

The structure of $Fe[S_2CN(C_3H_4N)_2]_2 \cdot \frac{1}{2}CHCl_3$ comprises mononuclear complexes of pseudosymmetry D_3 van der Waals packed with chloroform molecules. Fig. 2 shows stereoscopic pairs of drawings of the complex at 210 and 297 K. Interatomic distances and angles are given in Table 4 and some geometrical characteristics of the FeS_6 polyhedron in Table 5.

Neither the temperature nor the effective magnetic moment changes much between the two

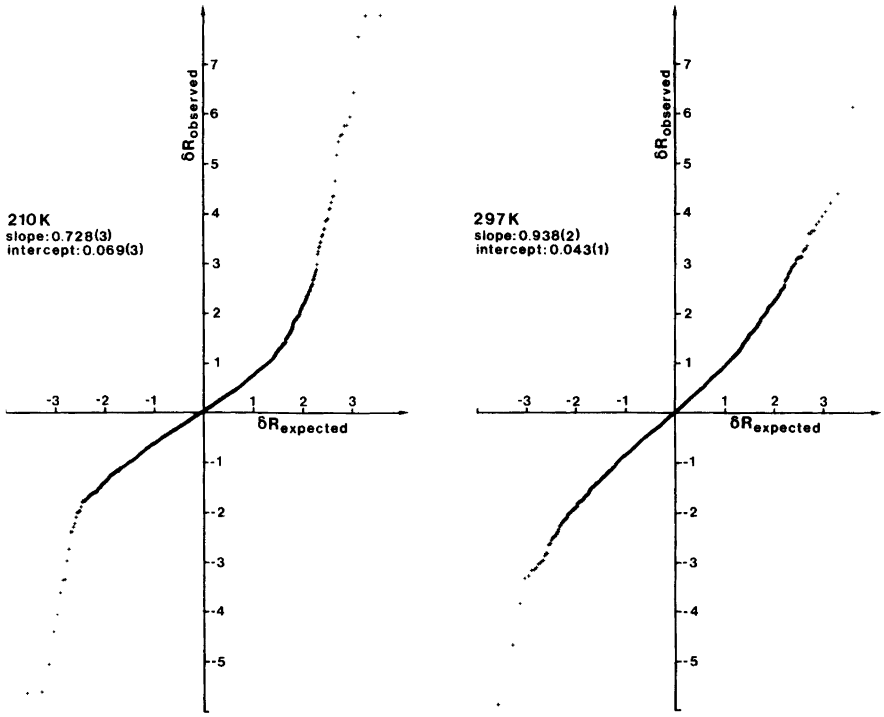

Fig. 1. δR-plot comparison of data and models of $Fe[S_2CN(C_3H_4N)_2]_3 \cdot \frac{1}{2}CHCl_3$ at 210 and 297 K.

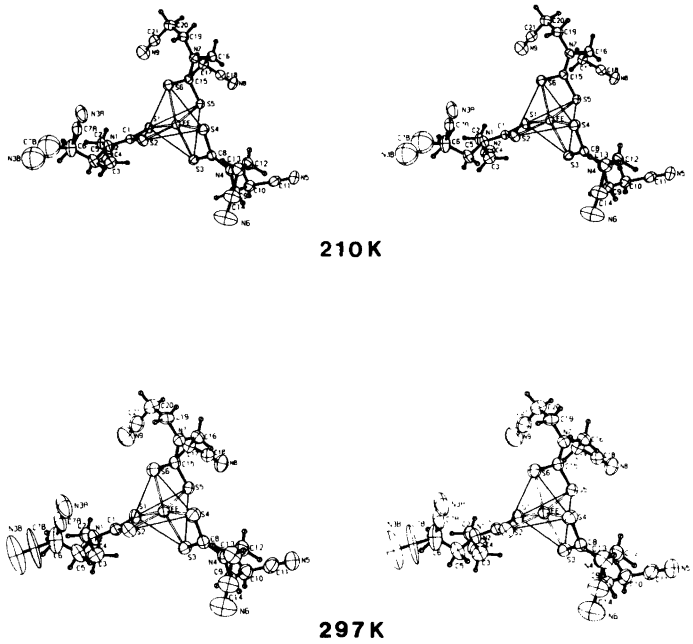

Fig. 2. Stereoscopic pairs of drawings of the complex at 210 and 297 K. The thermal ellipsoids of the non-H atoms are scaled to include 50% probability.

Table 3. Final atomic coordinates with estimated standard deviations of $Fe[S_2CN(C_3H_4N)_2]_3 \cdot \frac{1}{2}CHCl_3$. The B values of the non-H atoms were calculated from the anisotropic temperature factor coefficients. For the H atoms $B = 5.0$ Å^2 at 210 K and 8.0 Å^2 at 297 K.

	x	y	z	B/Å^2	Occupancy
(*a*) 210 K					
Fe	.31585(8)	.24787(7)	.45149(6)	2.3(1)	
S(1)	.43821(14)	.13669(14)	.33271(10)	2.5(1)	
S(2)	.16126(14)	.29665(14)	.34380(11)	2.8(1)	
C(1)	.29162(55)	.19763(51)	.27931(39)	2.4(2)	
N(1)	.28337(47)	.17048(45)	.19625(35)	2.7(2)	
S(3)	.24981(15)	.08692(14)	.57255(11)	2.7(1)	
S(4)	.15919(16)	.34128(14)	.57385(11)	3.0(1)	
C(8)	.15293(55)	.19349(56)	.64038(40)	2.6(2)	
N(4)	.08020(47)	.16779(47)	.73459(34)	2.8(2)	
S(5)	.50963(14)	.20321(13)	.52075(10)	2.4(1)	
S(6)	.39196(14)	.41618(14)	.36856(11)	2.7(1)	
C(15)	.52377(52)	.34089(49)	.43869(38)	2.2(2)	
N(7)	.62520(44)	.38387(41)	.43055(33)	2.3(1)	
C(2)	.40298(64)	.08614(59)	.14768(43)	2.9(2)	
C(3)	.41518(66)	−.04908(62)	.20620(51)	3.6(2)	
C(4)	.54683(70)	−.14029(62)	.17284(50)	3.5(2)	
N(2)	.64634(68)	−.20803(58)	.14786(52)	5.1(2)	
C(5)	.15022(69)	.20074(63)	.16606(51)	3.6(2)	
C(6)	.13012(83)	.29831(76)	.06563(54)	4.7(3)	
C(7A)	.11292(88)	.42140(81)	.07576(58)	3.5(3)	.81(2)
N(3A)	.09675(110)	.51634(106)	.08408(69)	5.5(4)	.81(2)
C(7B)	.053(10)	.381(8)	−.011(7)	12.0	.19
N(3B)	−.039(10)	.398(9)	−.045(7)	12.0	.19
C(9)	.07609(68)	.04246(69)	.78246(48)	3.7(2)	
C(10)	.19728(70)	−.04251(62)	.84113(48)	3.5(2)	
C(11)	.18799(73)	−.01128(72)	.93677(52)	4.1(3)	
N(5)	.17997(74)	.01296(71)	1.01027(45)	5.3(3)	
C(12)	.00939(62)	.26478(63)	.78985(46)	3.2(2)	
C(13)	−.12300(66)	.35480(64)	.75597(50)	3.5(2)	
C(14)	−.22369(74)	.29868(66)	.76601(62)	4.3(3)	
N(6)	−.30115(78)	.25439(72)	.76770(76)	7.3(4)	
C(16)	.72858(57)	.31253(55)	.50100(43)	2.7(2)	
C(17)	.83345(58)	.19449(57)	.46904(44)	2.8(2)	
C(18)	.87250(59)	.09147(63)	.56126(49)	3.0(2)	
N(8)	.89890(61)	.01386(56)	.63105(43)	4.1(2)	
C(19)	.63785(63)	.50008(58)	.35762(47)	3.1(2)	
C(20)	.76789(65)	.48030(61)	.27797(51)	3.4(2)	
C(21)	.78400(65)	.38849(62)	.22598(49)	3.4(2)	
N(9)	.79966(63)	.31233(67)	.18763(51)	5.0(3)	
Cl(1)	.45956(69)	.44072(71)	.11421(42)	6.1(2)	.46(1)
Cl(2)	.46609(57)	.38970(46)	−.07242(35)	6.2(2)	.46(1)
Cl(3)	.53463(102)	.60006(91)	−.08119(61)	9.2(4)	.46(1)
C(22)	.43296(161)	.50968(143)	−.01248(105)	3.9(5)	.46(1)
H(1C2)	.4845(71)	.1013(65)	.1424(52)		
H(2C2)	.4045(72)	.0979(66)	.0800(52)		
H(1C3)	.3385(70)	−.0575(65)	.1872(51)		
H(2C3)	.4172(70)	−.0573(65)	.2816(51)		
H(1C5)	.0793(71)	.2190(66)	.2258(52)		
H(2C5)	.1576(70)	.1308(65)	.1500(51)		

Table 3. Continued.

H(1AC6)	.0462	.3032	.0433		.81(1)
H(2AC6)	.2123	.2743	.0131		.81(1)
H(1BC6)	.1587	.3600	.0804		.19
H(2BC6)	.2077	.2504	.0215		.19
H(1C9)	.0787(76)	.0073(68)	.7312(55)		
H(2C9)	−.0167(76)	.0484(68)	.8363(55)		
H(1C10)	.2976(72)	−.0475(66)	.7984(52)		
H(2C10)	.2048(72)	−.1085(65)	.8544(51)		
H(1C12)	.0597(70)	.2914(66)	.7803(53)		
H(2C12)	−.0107(71)	.2201(66)	.8725(52)		
H(1C13)	−.0819(71)	.3649(66)	.6947(52)		
H(2C13)	−.1753(70)	.4150(65)	.8016(52)		
H(1C16)	.6796(71)	.2984(66)	.5567(52)		
H(2C16)	.7751(71)	.3655(66)	.4993(52)		
H(1C17)	.9131(72)	.1964(65)	.4232(51)		
H(2C17)	.7921(72)	.1668(66)	.4339(51)		
H(1C19)	.6260(71)	.5676(65)	.3925(51)		
H(2C19)	.5561(70)	.5449(65)	.3260(52)		
H(1C20)	.8643(70)	.4547(65)	.3120(51)		
H(2C20)	.7549(71)	.5685(66)	.2254(52)		
H(C22)	.3347	.5642	−.0128		.46(1)
(b) 297 K					
Fe	.31692(8)	.24666(8)	.45060(6)	3.5(1)	
S(1)	.43730(15)	.13465(15)	.33293(11)	3.9(1)	
S(2)	.16425(15)	.29602(15)	.34026(13)	4.4(1)	
C(1)	.29186(57)	.19656(53)	.27789(41)	3.6(2)	
N(1)	.28408(50)	.16997(48)	.19713(37)	4.3(2)	
S(3)	.25011(16)	.08520(14)	.57241(12)	4.2(1)	
S(4)	.16079(18)	.33989(15)	.57206(13)	4.7(1)	
C(8)	.15329(59)	.19363(56)	.63855(42)	3.8(2)	
N(4)	.08434(49)	.16577(47)	.73128(36)	4.1(2)	
S(5)	.51020(15)	.20199(14)	.52053(11)	3.9(1)	
S(6)	.39387(16)	.41603(15)	.36794(12)	4.3(1)	
C(15)	.52407(55)	.34001(50)	.43914(40)	3.4(2)	
N(7)	.62539(48)	.38173(43)	.43139(35)	3.7(2)	
C(2)	.40248(69)	.08639(60)	.14798(48)	4.4(2)	
C(3)	.41244(75)	−.04903(65)	.20434(59)	5.5(3)	
C(4)	.54057(87)	−.13725(72)	.16904(62)	5.9(3)	
N(2)	.63944(85)	−.20556(75)	.14414(71)	8.6(3)	
C(5)	.15407(78)	.20423(76)	.16253(61)	5.8(3)	
C(6)	.1380(11)	.3033(10)	.0675(7)	8.6(4)	
C(7A)	.1133(14)	.4194(11)	.0786(9)	5.7	.60(1)
N(3A)	.0918(18)	.5165(12)	.0874(11)	8.9	.60(1)
C(7B)	.0481(35)	.3499(34)	.0050(24)	15.0	.40
N(3B)	−.0317(27)	.3939(33)	−.0442(23)	14.9	.40
C(9)	.07894(69)	.04025(66)	.78115(47)	4.6(2)	
C(10)	.19710(79)	−.04411(70)	.84155(53)	5.5(3)	
C(11)	.18973(81)	−.01297(78)	.93448(60)	5.9(3)	
N(5)	.17877(98)	.01202(92)	1.00806(57)	8.8(4)	
C(12)	.01502(70)	.26216(68)	.78733(50)	4.8(2)	
C(13)	−.11661(76)	.35245(71)	.75226(62)	5.6(3)	
C(14)	−.21479(83)	.29464(73)	.76438(70)	6.1(3)	
N(6)	−.29321(92)	.25291(80)	.76718(82)	9.3(4)	
C(16)	.72717(64)	.31038(59)	.50090(50)	4.3(2)	

Table 3. Continued.

C(17)	.83207(63)	.19389(64)	.47037(49)	4.6(2)	
C(18)	.87202(65)	.09416(69)	.56073(54)	4.7(2)	
N(8)	.89986(72)	.01435(68)	.63086(52)	6.5(3)	
C(19)	.63584(68)	.49889(56)	.35897(52)	4.5(2)	
C(20)	.76426(79)	.48108(71)	.27996(59)	5.6(3)	
C(21)	.78120(85)	.38632(85)	.23085(62)	6.1(3)	
N(9)	.79982(88)	.31106(89)	.19431(69)	8.7(4)	
Cl(1)	.4499(11)	.4469(10)	.1130(8)	11.4(2)	.39(1)
Cl(2)	.4773(10)	.3927(10)	−.0691(8)	11.4(2)	.39(1)
Cl(3)	.5248(11)	.6106(10)	−.0852(8)	11.4(2)	.39(1)
C(22)	.4421(24)	.5141(24)	−.0113(19)	7.3(5)	.39(1)
H(1C2)	.4780(85)	.1085(77)	.1448(62)		
H(2C2)	.3903(86)	.1031(77)	.0755(62)		
H(1C3)	.3336(84)	−.0785(75)	.2120(62)		
H(2C3)	.4189(85)	−.0706(76)	.2902(62)		
H(1C5)	.0728(86)	.2166(77)	.2240(63)		
H(2C5)	.1299(85)	.1494(78)	.1430(63)		
H(1AC6)	.0598	.3037	.0396		.60(1)
H(2AC6)	.2163	.2837	.0151		.60(1)
H(1BC6)	.1547	.3598	.0839		.40
H(2BC6)	.2119	.2499	.0243		.40
H(1C9)	.0857(85)	−.0010(77)	.7375(63)		
H(2C9)	−.0064(85)	.0433(77)	.8271(64)		
H(1C10)	.2708(84)	−.0232(78)	.7897(62)		
H(2C10)	.1789(85)	−.1114(77)	.8561(62)		
H(1C12)	.0885(84)	.2869(77)	.7798(62)		
H(2C12)	−.0053(84)	.2106(76)	.8630(62)		
H(1C13)	−.0943(85)	.3933(76)	.6721(64)		
H(2C13)	−.1552(84)	.4073(76)	.7833(64)		
H(1C16)	.6677(83)	.2860(77)	.5675(61)		
H(2C16)	.7757(85)	.3714(77)	.4944(62)		
H(1C17)	.8903(87)	.2138(78)	.4231(62)		
H(2C17)	.7837(86)	.1623(77)	.4305(61)		
H(1C19)	.6288(84)	.5541(75)	.3881(61)		
H(2C19)	.5610(85)	.5383(77)	.3209(63)		
H(1C20)	.8582(85)	.4460(76)	.3130(61)		
H(2C20)	.7601(86)	.5618(78)	.2235(63)		
H(C22)	.3548	.5770	−.0222		.39(1)

structure determinations. The Fe−S bond distance, the S−C−S bond angle and the trigonal twist of the coordination polyhedron are strongly correlated to the effective magnetic moment as shown by an analysis of a number of accurate structure determinations (the Fe−S bond length and the S−C−S bond angle both increase while the trigonal twist decreases when μ_{eff} increases).[17] In the present structure these quantities have values expected for complexes with low μ_{eff}. The mean observed increase in the Fe−S distance between 210 and 297 K is only 0.016(1) Å while the changes in the S−C−S and twist angles are insignificant.

There are 33 bonds between non-H ligand atoms in the complex, excluding C(7*B*) and N(3*B*). The apparent bond lengths do not decrease when the temperature increases, the average decrease being 0.0038(40) Å between 210 and 297 K. Half-normal probability plotting [3,16] of $\delta d_i = \Delta d_i/\sigma(\Delta d_i)$ where Δd_i is the difference in bond lengths between the two temperatures, resulted in a correlation coefficient of 0.992, a slope of 1.35(3) and an intercept of −0.03(2). Thus the interatomic distances may have somewhat underestimated standard deviations. Another half-normal plot, this time comparing all interatomic distances less than 2.90 Å in the ligands at 210 and

Table 4. Selected interatomic distances (Å), bond angles (°) and torsion angles (°) in the $Fe[S_2CN(C_3H_4N)_2]_3$ complex and r.m.s. deviations (Å) from the least-squares planes through the S_2CNC_2 groups.

	210 K	297 K
(*a*) The FeS_6 core		
Fe–S(1)	2.295(2)	2.310(2)
Fe–S(2)	2.309(2)	2.329(2)
Fe–S(3)	2.312(2)	2.327(2)
Fe–S(4)	2.309(2)	2.324(2)
Fe–S(5)	2.317(2)	2.331(2)
Fe–S(6)	2.303(2)	2.321(2)
S(1)–S(2)	2.833(2)	2.836(3)
S(3)–S(4)	2.837(3)	2.846(3)
S(5)–S(6)	2.822(3)	2.833(3)
S(1)–S(3)	3.423(2)	3.443(3)
S(1)–S(5)	3.339(2)	3.363(2)
S(3)–S(5)	3.381(2)	3.404(3)
S(2)–S(4)	3.440(2)	3.476(3)
S(2)–S(6)	3.433(2)	3.458(3)
S(4)–S(6)	3.387(2)	3.412(3)
S(1)–S(6)	3.397(3)	3.434(3)
S(2)–S(3)	3.448(3)	3.489(3)
S(4)–S(5)	3.444(2)	3.473(3)
(*b*) Ligand 1		
S(1)–C(1)	1.707(5)	1.718(6)
S(2)–C(1)	1.718(6)	1.713(6)
C(1)–N(1)	1.344(7)	1.314(7)
N(1)–C(2)	1.458(8)	1.469(8)
C(2)–C(3)	1.528(9)	1.530(10)
C(3)–C(4)	1.484(9)	1.472(11)
C(4)–N(2)	1.114(9)	1.126(12)
N(1)–C(5)	1.466(8)	1.463(9)
C(5)–C(6)	1.505(10)	1.459(13)
C(6)–C(7A)	1.472(12)	1.379(16)
C(7A)–N(3A)	1.130(14)	1.147(18)
C(6)–C(7B)	1.396(91)	1.312(34)
C(7B)–N(3B)	1.125(132)	1.101(43)
S(1)–C(1)–S(2)	111.7(3)	111.5(3)
S(1)–C(1)–N(1)	122.7(4)	122.7(4)
S(2)–C(1)–N(1)	125.6(4)	125.8(5)
C(1)–N(1)–C(2)	120.0(5)	120.8(5)
C(1)–N(1)–C(5)	121.2(5)	121.9(5)
N(1)–C(2)–C(3)	109.7(5)	109.6(5)
C(2)–C(3)–C(4)	113.1(5)	112.1(6)
C(3)–C(4)–N(2)	179.2(7)	178.4(9)
C(2)–N(1)–C(5)	117.4(5)	116.6(5)
N(1)–C(5)–C(6)	113.2(6)	113.4(7)
C(5)–C(6)–C(7A)	110.8(6)	113.7(9)
C(6)–C(7A)–N(3A)	178.5(1.0)	179.5(1.6)
C(5)–C(6)–C(7B)	153.9(3.9)	133.0(1.8)
C(6)–C(7B)–N(3B)	141.4(9.3)	175.8(3.8)

Table 4. Continued.

S(1)–C(1)–N(1)–C(2)	−0.3(8)	−1.2(9)
S(1)–C(1)–N(1)–C(5)	166.1(5)	168.4(5)
S(2)–C(1)–N(1)–C(2)	179.0(5)	177.8(5)
S(2)–C(1)–N(1)–C(5)	−14.7(8)	−12.6(9)
C(1)–N(1)–C(2)–C(3)	81.2(7)	82.9(8)
N(1)–C(2)–C(3)–C(4)	−170.2(6)	−171.0(6)
C(1)–N(1)–C(5)–C(6)	114.0(7)	109.7(9)
N(1)–C(5)–C(6)–C(7A)	−70.2(9)	−74.0(1.2)
N(1)–C(5)–C(6)–C(7B)	−173.1(9.4)	170.1(2.5)
R.m.s. deviation	0.0366	0.0309
(*c*) Ligand 2		
S(3)–C(8)	1.701(6)	1.719(6)
S(4)–C(8)	1.727(6)	1.716(6)
C(8)–N(4)	1.346(7)	1.328(7)
N(4)–C(9)	1.443(9)	1.453(9)
C(9)–C(10)	1.541(9)	1.537(10)
C(10)–C(11)	1.481(9)	1.458(11)
C(11)–N(5)	1.137(9)	1.143(11)
N(4)–C(12)	1.467(8)	1.480(9)
C(12)–C(13)	1.491(9)	1.502(10)
C(13)–C(14)	1.431(10)	1.420(11)
C(14)–N(6)	1.136(11)	1.122(12)
S(3)–C(8)–S(4)	111.7(3)	112.0(3)
S(3)–C(8)–N(4)	125.1(5)	123.5(5)
S(4)–(8)–N(4)	123.3(5)	124.5(5)
C(8)–N(4)–C(9)	119.4(5)	121.2(5)
C(8)–N(4)–C(12)	120.6(5)	120.1(5)
N(4)–C(9)–C(10)	113.2(5)	113.6(6)
C(9)–C(10)–C(11)	113.3(6)	114.2(6)
C(10)–C(11)–N(5)	179.6(8)	177.4(9)
C(9)–N(4)–C(12)	120.1(5)	118.7(5)
N(4)–C(12)–C(13)	114.6(5)	113.8(6)
C(12)–C(13)–C(14)	114.4(6)	113.2(7)
C(13)–C(14)–N(6)	175.7(9)	175.3(1.0)
S(3)–C(8)–N(4)–C(9)	−3.2(9)	−4.3(9)
S(3)–C(8)–N(4)–C(12)	174.8(5)	173.7(5)
S(4)–C(8)–N(4)–C(9)	177.3(5)	177.7(5)
S(4)–C(8)–N(4)–C(12)	−4.8(8)	−4.4(9)
C(8)–N(4)–C(9)–C(10)	86.4(7)	87.7(8)
N(4)–C(9)–C(10)–C(11)	71.6(8)	71.3(9)
C(8)–N(4)–C(12)–C(13)	78.5(8)	77.7(8)
N(4)–C(12)–C(13)–C(14)	59.4(8)	60.9(9)
R.m.s. deviation	0.0184	0.0213
(*c*) Ligand 3		
S(5)–C(15)	1.707(9)	1.707(6)
S(6)–C(15)	1.709(5)	1.713(6)
C(15)–N(7)	1.335(7)	1.331(7)
N(7)–C(16)	1.486(7)	1.472(8)
C(16)–C(17)	1.551(8)	1.544(9)
C(17)–C(18)	1.481(9)	1.451(10)
C(18)–N(8)	1.113(9)	1.132(10)
N(7)–C(19)	1.460(8)	1.461(8)

Table 4. Continued.

C(19)–C(20)	1.527(9)	1.528(10)
C(20)–C(21)	1.453(9)	1.461(12)
C(21)–N(9)	1.151(10)	1.121(13)
S(5)–C(15)–S(6)	111.4(3)	111.8(3)
S(5)–C(15)–N(7)	124.1(4)	123.7(4)
S(6)–C(15)–N(7)	124.5(4)	124.5(4)
C(15)–N(7)–C(16)	118.8(4)	119.0(5)
C(15)–N(7)–C(19)	123.3(5)	122.2(5)
N(7)–C(16)–C(17)	111.8(5)	113.0(5)
C(16)–C(17)–C(18)	110.0(5)	110.1(6)
C(17)–C(18)–N(8)	178.4(7)	177.4(8)
C(16)–N(7)–C(9)	117.9(4)	118.8(5)
N(7)–C(19)–C(20)	113.1(5)	112.9(5)
C(19)–C(20)–C(21)	112.9(5)	112.0(6)
C(20)–C(21)–N(9)	177.4(7)	176.9(9)
S(5)–C(15)–N(7)–C(16)	−3.8(8)	−4.3(8)
S(5)–C(15)–N(7)–C(19)	178.0(5)	178.4(5)
S(6)–C(15)–N(7)–C(16)	176.2(4)	176.9(5)
S(6)–C(15)–N(7)–C(19)	−1.9(8)	−0.5(8)
C(15)–N(7)–C(16)–C(17)	76.3(7)	77.4(7)
N(7)–C(16)–C(17)–C(18)	−144.3(5)	−145.7(6)
C(15)–N(7)–C(19)–C(20)	−116.4(7)	−117.7(7)
N(7)–C(19)–C(20)–C(21)	52.1(8)	50.8(9)
R.m.s. deviation	0.0143	0.0120

297 K, was also made. For this plot the correlation coefficient is 0.997, the slope 1.47(2) and the intercept 0.01(1). We conclude that also the bond angles are quite similar at both temperatures. The dimensions of the S_2CNC_2 groups are within the ranges expected from previsouly determined dithiocarbamate structures.[17] The S–C and C–N bonds have partial double bond character indicating some degree of Fe–S π-bonding.[18] There is no evidence of any effects on these bonds caused by the ligand substituents. At both temperatures all three S_2CNC_2 groups are slightly non-planar as shown by the torsion angles and the r.m.s. deviations from the least-squares planes through them.

The C–C≡N part of the propionitrile substituents are nearly linear except the disordered C(6)–C(7)≡N(3). Excluding the latter group we find the average values C–C = 1.454(4) Å, C–N = 1.131(3) Å and C–C–N = 188.8(3)° in good agreement with the dimensions of α-acetonitrile at 215 K.[19] Acceptable dimensions are found for C(6)–C(7A)≡N(3A) but not for C(6)–C(7B)≡N(3B). There is probably a further disorder, at least of the *B* positions, as is also indicated by the large thermal parameters. Neglecting this, we can use the occupancies x_A and x_B at 210 and 297 K and calculate a formal equilibrium constant $K = x_B/x_A$ for $A \rightleftarrows B$ at both temperatures. By using eqn. (1) we

$$\ln K = -\Delta H^\circ/RT + \Delta S^\circ/R \qquad (1)$$

then estimate the order of magnitudes $\Delta H^\circ \approx 6$ kJ mol^{-1} and $\Delta S^\circ \approx 20$ J K^{-1} mol^{-1} for $A \rightleftarrows B$ (*cf.* the thermodynamic treatment of the magnetic data below).

The packing of the iron complexes and the chloroform molecules is shown in Fig. 3. Table 6 gives the dimensions of the chloroform molecule. Its occupancy converged to a value well below $\frac{1}{2}$ at room temperature but this might be an artefact caused by the strong correlation to the chlorine temperature factor. The molecules are located on either side of the symmetry centres $\frac{1}{2},\frac{1}{2},0$ resulting in overlapping electron densities. The apparent distortions are caused by this overlap.

Selected packing distances are given in Table 7. The shortest distance is about 3.04 Å, between the

Table 5. The geometry of the coordination polyhedron.

	210 K	295 K
μ_{eff}	3.19	3.94
Fe–S (Å)	2.308(3)	2.324(3)
Ligand bite (S–S) (Å)	2.831(4)	2.840(3)
Edge of riangular face (Å)	3.400(16)	3.426(17)
Height of prism (Å)	2.424(2)	2.439(3)
Torsion angle (trigonal twist) (°)	43.7(5)	43.1(4)
Tilt angle between triangular faces (°)	0.9(2)	0.8(2)
Fe – centroid of prism (Å)	0.027(2)	0.026(2)

Table 6. Bond distances (Å) and angles (°) in the chloroform molecule.

	210 K	297 K
C(22)–Cl(1)	1.739(16)	1.672(28)
C(22)–Cl(2)	1.784(16)	1.783(28)
C(22)–Cl(3)	1.716(18)	1.648(27)
Cl(1)–C(22)–Cl(2)	108.7(9)	106.9(1.5)
Cl(1)–C(22)–Cl(3)	113.3(9)	124.8(1.6)
Cl(2)–C(22)–Cl(3)	109.2(8)	108.6(1.5)

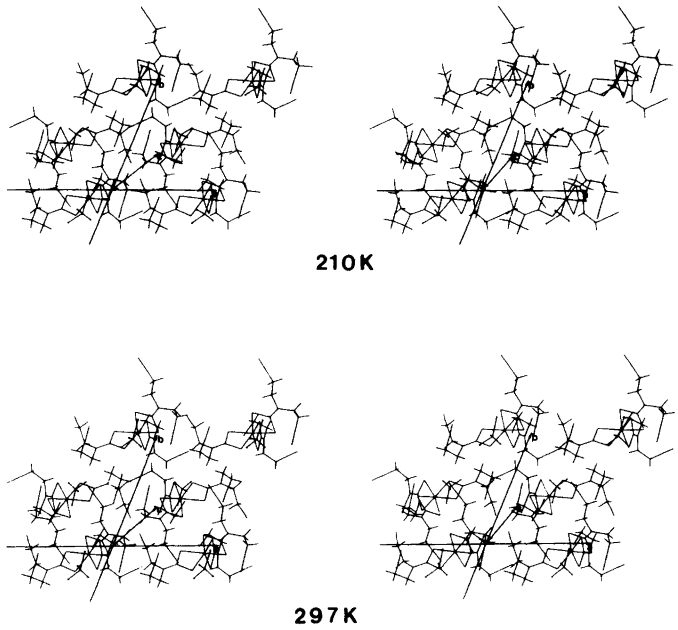

Fig. 3. Stereoscopic pairs of drawings of the crystal packing of the complexes and the chloroform molecules at 210 and 297 K. For the disordered $C(6)H_2-C(7)\equiv N(3)$ only the *A* positions are included. The chloroform molecules may also occupy centrosymmetrically related positions.

methylene C(3) and nitrile N(6) atoms. The packing of the complexes becomes more efficient when the vibration amplitudes decrease. The averaged decrease in the nitrile N contact distances is $\Delta = 0.046(5)$ Å between 297 and 210 K. The packing geometry is such that the quantity $\Delta + 2\delta(Fe-S)$

Table 7. The packing of the complexes; interatomic distances (Å) less than 3.5 Å from nitrile N atoms to atoms in neighbouring complexes and the five shortest Fe–Fe distances. The superscripts (*i*)–(*x*) denote the following transformations of the *x*, *y*, *z* values given in Table 3:

(*i*)	$1-x, \bar{y}, 1-z$	(*vi*)	$\bar{x}, \bar{y}, 1-z$
(*ii*)	$\bar{x}, 1-y, \bar{z}$	(*vii*)	$x-1, y, 1+z$
(*iii*)	$\bar{x}, 1-y, 1-z$	(*viii*)	$2-x, \bar{y}, 1-z$
(*iv*)	$x, y, z-1$	(*ix*)	$1+x, y, z$
(*v*)	$x-1, y, z$	(*x*)	$1-x, 1-y, 1-z$

	210 K	297 K
$N(2)-C(11^{i})$	3.449(10)	3.494(12)
$N(2)-N(5^{i})$	3.399(13)	3.433(13)
$N(3A)-C(6^{ii})$	3.260(13)	3.330(19)
$N(3A)-C(7A^{ii})$	3.293(13)	3.332(21)
$N(3A)-C(12^{iii})$	3.334(13)	3.375(15)
$N(3A)-C(13^{iii})$	3.246(19)	3.280(16)
$N(3B)-C(6^{ii})$	3.33(10)	3.31(4)
$N(3B)-C(7B^{ii})$	2.96(13)	3.25(5)
$N(3B)-C(12^{iv})$	3.07(9)	3.12(3)
$N(3B)-C(13^{iv})$	3.40(9)	3.47(3)
$N(3B)-N(9^{v})$	3.29(9)	3.40(3)
$N(6)-C(3^{vi})$	3.034(10)	3.053(11)
$N(6)-C(4^{vi})$	3.212(10)	3.251(12)
$N(6)-Cl(2^{vii})$	3.198(10)	3.286(14)
$N(8)-N(1^{i})$	3.436(8)	3.457(9)
$N(8)-C(5^{i})$	3.220(8)	3.295(11)
$N(8)-C(17^{viii})$	3.335(8)	3.383(10)
$N(8)-C(18^{viii})$	3.356(9)	3.400(10)
$N(9)-C(5^{ix})$	3.419(9)	3.485(12)
$N(9)-C(7B^{ix})$	3.464(9)	3.301(34)
$N(9)-C(10^{i})$	3.392(10)	3.412(12)
$Fe-Fe^{i}$	5.671(3)	5.675(4)
$Fe-Fe^{iii}$	7.294(4)	7.407(5)
$Fe-Fe^{x}$	9.001(3)	9.044(4)
$Fe-Fe^{vi}$	10.185(4)	10.208(5)
$Fe-Fe^{v}$	10.676(3)	10.756(4)

Table 7. Continued.

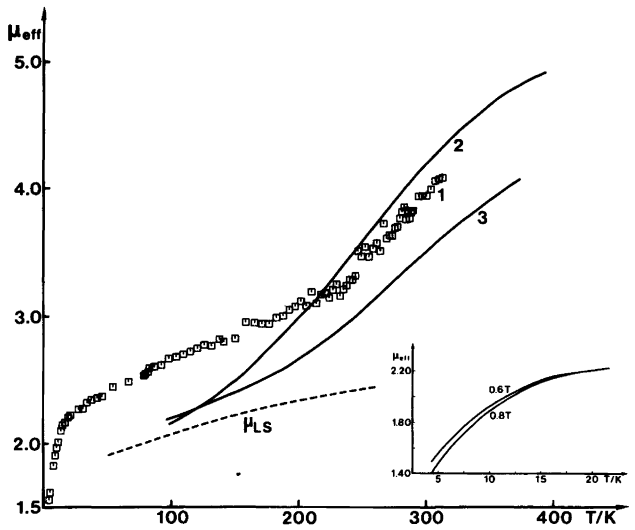

Fig. 4. The effective magnetic moment of $Fe[S_2CN(C_3H_4N)_2]_3 \cdot \frac{1}{2}CHCl_3$ (*1*) as a function of temperature compared with the corresponding curves for $Fe[S_2CN(CH_3)_2]_3$ (*2*) and $Fe[S_2CN(CH_2C_6H_5)_2]_3$ (*3*). The inset shows the effect of the external field when $T < 20$ K.

approximately should equal the mean decrease in unit cell dimensions. We find $\Delta(V^{1/3}) = 0.067(3)$ Å in rather good agreement with $\Delta + 2\delta(Fe-S) = 0.078(6)$ Å.

MAGNETIC PROPERTIES AND THE NATURE OF THE SPIN TRANSITION

Fig. 4 shows the effective magnetic moment μ_{eff} as a function of temperature (μ_{eff} is the number of Bohr magnetons; 1 B M $= 9.274 \cdot 10^{-24}$ J T^{-1}). The plot can be divided into three parts: (*i*) $T > 225$ K, (*ii*) $20\text{ K} < T < 225$ K and (*iii*) $T < 20$ K. Above 225 K the

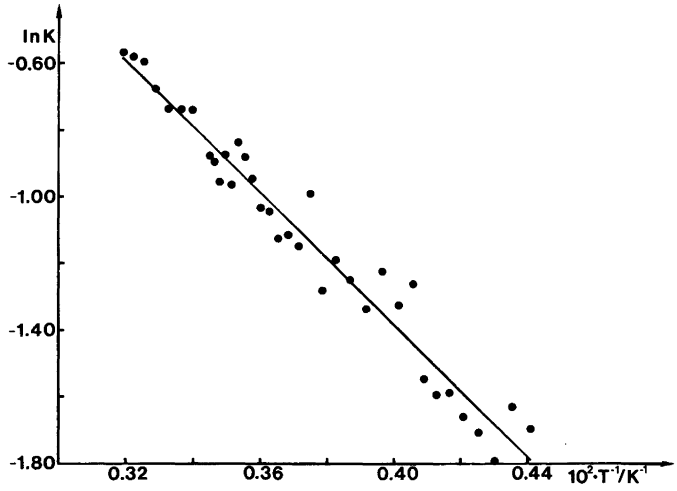

Fig. 5. A plot of ln K *vs.* T^{-1} ($T > 225$ k) where $K = x_{HS}/(1 - x_{HS})$ and x_{HS} the fraction of the complexes in high-spin state.

plot is intermediate to that of the methyl substituted iron(III) dithiocarbamate complex ($pK_a = 11.9$ for dimethylamine[9]) and that of the benzyl substituted ($pK_a = 8.5$ for dibenzylamine[20]). Obviously the inductive effect from the substituents is of minor importance compared to steric factors, crystal defects and other solid state effects.

We presume that above 225 K we have an equilibrium between high and low-spin complexes. We denote the fraction of high-spin complexes with x_{HS} defined by eqn. (2), where $\mu^2_{HS} = 35$ and μ^2_{LS} as given in eqn. (3) with $y = \lambda/RT$ and $\lambda = -5000$ J

$$\mu^2_{eff} = x_{HS}\mu^2_{HS} + (1 - x_{HS})\mu^2_{LS} \quad (2)$$

$$\mu^2_{LS} = \frac{8 + (3y - 8)e^{-3y/2}}{y(2 + e^{-3y/2})} \quad (3)$$

mol^{-1}.[21] The trigonal distortion of the complex will only cause minor deviations in μ_{LS} compared to eqn. (3) above ~100 K.[22] A simple thermodynamic treatment of the crossover region $T > 225$ K is shown in Fig. 5, where ln K is plotted *vs.* T^{-1}. $K = x_{HS}/(1 - x_{HS})$ is the formal equilibrium constant for the $S = \frac{1}{2} \rightleftarrows S = \frac{5}{2}$ transition. The spin equilibrium is independent of the disorder $A \rightleftarrows B$ discussed above. Following Ref. 23 we evaluate the straight line in Fig. 5 using eqn. (1). The resulting effective changes in enthalpy and entropy are related to the standard changes by $\Delta H_{eff} = n\Delta H^\circ$ and $\Delta S_{eff} = n\Delta S^\circ$. The quantity n is a function of the intermolecular interactions, sometimes expressed as a domain size. ΔH_{eff} and ΔS_{eff} are then changes associated with the transition of 1 mol LS domains to HS domains, each domain containing n complexes. The line in Fig. 5 gives us $\Delta H_{eff} = 8.4(3)$ kJ mol^{-1} and $\Delta S_{eff} = 22(1)$ J K^{-1} mol^{-1}. The spin contribution to ΔS° is $R \cdot \ln(2 \cdot \frac{5}{2} + 1)/(2 \cdot \frac{1}{2} + 1) = 9.1$ J K^{-1} mol^{-1} and the contributions from intermolecular and lattice vibrations are positive.[23] We conclude that ΔS_{eff} and ΔS° are of the same order of magnitude and set an upper limit of n to ~2. Repeated measurements after careful grinding of the sample gave the same result. Thus, the spin transition appears to be non-cooperative in the region above 225 K. The appreciable amount of $A \rightleftarrows B$ disorder in this range and the solvate molecules give almost one site per complex for nucleation of a spin-changed domain.

Since the disorder and spin transition are similarly affected by the temperature ($x_B \approx x_{HS}$ at 225 and 300 K) the two processes show approximately the same enthalpy and entropy changes.

At 225 K and below there is a residual occupancy of the high-spin state; $x_{HS} = 0.15$ at 225 K, which slowly decreases as the temperature is lowered. In this low-temperature region there are small thermal vibration amplitudes and little occurrence of $A \rightleftarrows B$ disorder. The effect of the solid state on the spin transition may be quite different here compared to the high-temperature region. However, the main part of the decrease in effective magnetic moment in part (*ii*) of the μ_{eff} *vs.* T plot is the decrease in the value of μ_{LS}. The dashed curve in Fig. 4 shows μ_{LS} *vs.* T using eqn. (3).

The sharp decrease in μ_{eff} below 20 K is as can be expected from more complete calculations of the magnetic properties of the d^5 electron system made by Figgis[22] and König and Kremer.[24] The effect should be further enhanced by zero field splitting caused by the trigonal distortion of the FeS_6 core from O_h symmetry.[21] There is a noticeable effect on μ_{eff} from the external magnetic field when $T < 15$ K as can be seen in the inset of Fig. 4.[24].

Acknowledgements. We are indebted to Dr. Mats Nygren, University of Stockholm, for many discussions during the construction of the Faraday balance and to Ms. Lena Timby for help with part of the experimental work and for preparation of the illustrations. The Swedish Natural Science Research Council gave financial support.

REFERENCES

1. White, A. H., Roper, R., Kokot, E., Waterman, H. and Martin, R. L. *Aust. J. Chem. 17* (1964) 294.
2. Ewald, A. H., Martin, R. L., Sinn, E. and White, A. H. *Inorg. Chem. 8* (1969) 1837.
3. Albertsson, J., Elding, I. and Oskarsson, Å. *Acta Chem. Scand. A 33* (1979) 703.
4. Albertsson, J., Oskarsson, Å., Ståhl, K., Svensson, C. and Ymén, I. *Acta Crystallogr. B 37* (1981) 50.
5. Leipoldt, J. G. and Coppens, P. *Inorg. Chem. 12* (1973) 2269.
6. Haddad, M. S., Lynch, M. W., Federer, W. D. and Hendrickson, D. N. *Inorg. Chem. 20* (1981) 123.
7. Haddad, M. S., Federer, W. D., Lynch, M. W. and Hendrickson, D. N. *Inorg. Chem. 20* (1981) 131.
8. Stevensson, G. W. and Williamson, D. *J. Am. Chem. Soc. 80* (1958) 5943.

9. Everett, D. H. and Wynne-Jones, W. F. K. *Proc. R. Soc. London A 177* (1941) 499.
10. Danielsson, S., Grenthe, I. and Oskarsson, Å. *J. Appl. Crystallogr. 9* (1976) 14.
11. Bodforss, S. *Kungl. Fysiogr. Sällsk. Lund Förh. 7* (1938) No. 16.
12. Blom, B. and Hörlin, T. *Chem. Commun. Univ. Stockholm* (1977) No. 5.
13. Mulay, L. N. and Mulay, I. N. *Anal. Chem. 46* (1974) 4912.
14. Main, P., Hull, S. E., Lessinger, L., Germain, G., Declercq, J.-P. and Woolfson, M. M. *MULTAN, A Program for the Automatic Solution of Crystal Structures from X-Ray Diffraction Data*, Univs. of York, England and Louvain, Belgium, 1978; Woolfson, M. M. *Acta Crystallogr. A 33* (1977) 219.
15. *International Tables for X-Ray Crystallography*, Kynoch Press, Birmingham 1974, Vol. 4.
16. Abrahams, S. C. and Keve, E. T. *Acta Crystallogr. A 27* (1971) 157.
17. Ståhl, K. and Ymén, I. *To be published;* Oskarsson, Å., Ståhl, K. and Ymén, I. *Abstract to XXII ICCC*, Budapest 1982, August 23rd – 27th.
18. Albertsson, J. and Oskarsson, Å. *Acta Crystallogr. B 33* (1977) 1871.
19. Barrow, M. I. *Acta Crystallogr. B 37* (1981) 2239.
20. Christensen, J. J., Izatt, R. M., Wranthall, D. P. and Hansen, L. D. *J. Chem. Soc. A* (1969) 1212.
21. Ballhausen, C. J. *Introduction to Ligand Field Theory*, McGraw-Hill, New York 1962, pp. 111 – 149.
22. Figgis, B. N. *Trans. Faraday Soc. 57* (1961) 204.
23. Gütlich, P., Köppen, H., Link, R. and Steinhäuser, H. G. *J. Chem. Phys. 70* (1979) 3977.
24. König, E. and Kremer, S. *Ber. Bunsenges. Phys. Chem. 78* (1974) 269.

Received March 22, 1982.

Acta Chemica Scandinavica A 36 (1982) 797–804

Tentative Assignments of Fundamental Vibrations of Thio- and Selenoamides. X. The Influence of *S*-Methylation on the Characteristic Thioamide Bands in 1,2-Dimethyl-3-pyrazolidinethione

U. ANTHONI,[a] G. BORCH[b] and P. H. NIELSEN[a]

[a] Chemical Laboratory II, The H. C. Ørsted Institute, DK-2100 Copenhagen, Denmark and [b] Chemistry Department A, The Technical University of Denmark, DK-2800 Lyngby, Denmark

Recent efforts to extract information on the molecular vibrations of a cyclic thiohydrazide, 1,2-dimethyl-3-pyrazolidinethione (DMPT), have involved donor–acceptor reactions with group IIb metals and substitution of sulfur with selenium. The present investigation deals with *S*-methylation. The IR spectra of DMPT-*S*-CH_3I and eight differently deuterated derivatives have been recorded in the range 180–4000 cm^{-1}. Based on a normal coordinate analysis tentative assignments of the fundamental vibrations of these compounds are given. In agreement with results obtained from CNDO/2 calculations, indicating an increased weight of the π-resonance structure $N^+=C-S^-$ on *S*-methylation it is inferred that the force constant for CN stretching of the thiohydrazide group increases while that for CS stretching decreases. The use of *S*-methylation as a method for empirical classification of vibrations of the thioamide cannot be recommended.

A useful clue to the selection of IR bands originating in the thioamide group is provided [1] by comparison with the spectra of *S*-methiodides, metal complex compounds, and the corresponding selenoamides. The present status of the two latter methods has been summarized in the preceeding papers.[2,3] In this paper we describe the origin and significance of the IR shifts following conversion of the thioamide group into the *S*-methiodide.

It was originally proposed [1] (and is still assumed a suitable model [4]) that *S*-methylation is followed by an increased CN bond order and a decreased CS bond order of the thioamide group. As a result, the force constants for CN and SC stretching will increase and decrease, respectively. In the vibrational spectra an increase in frequency is observed for bands assigned mainly to CN stretching and a downward shift for bands originating from the CS stretching. In some instances (*e.g.* 1,3-dimethylthiourea [5]) upwards frequency shifts have also been reported for the CS in-plane and out-of-plane deformation bands, but rationalizations do not seem to have been attempted. In studies of thioamides, thioureas, and thiocarbamates, it was noted by Devillanova and Verani [4] and by Sathyanarayana *et al.*[5] that in some cases the shifts of the thioamide bands on *S*-methylation were much smaller than expected. In addition, frequency shifts sometimes occur in bands without contributions from vibrations of the thioamide group. These anomalies can either arise from changes in the composition of the potential energy distribution (PED) of the thioamide bands or from electronic displacements influencing the bond orders of the thioamide group. The absence of any full normal coordinate analyses (NCA) on *S*-methylated thioamides precludes definite conclusions to be made regarding this interesting point. A perturbational NCA treatment [6] of the changes in the spectrum of tetramethylthiourea on *S*-methylation not only suggests that the question may be settled in this way, but also that the changes in force constants can be correlated to the charge redistribution of the thioamide group as calculated by the CNDO/2 method.

0302-4377/82/100797-08$02.50

As an extension of our study of the vibrational spectra of 1,2-dimethyl-3-pyrazolidinethione (DMPT)[7] and its derivatives, we have measured the IR spectra in the range 180–4000 cm^{-1} of the methiodide, DMPT-*S*-CH_3I, and the trideutero-methiodide, DMPT-*S*-CD_3I. In order to obtain the amount of data necessary to carry out a full NCA, the IR spectra of the following deuterated compounds were recorded (*cf.* Ref. 7): DMPT-1-D_3-*S*-CH_3I, DMPT-1-D_3-*S*-CD_3I, DMPT-D_4-*S*-CH_3I, DMPT-D_4-*S*-CD_3I, DMPT-D_6-*S*-CH_3I, DMPT-DMPT-D_{10}-*S*-CH_3I and DMPT-D_{10}-*S*-CD_3I. An attempt is made to correlate the change in force field on *S*-methylation with the corresponding bond orders or change densities calculated by the CNDO/2 method.

EXPERIMENTAL

The methiodides were prepared in almost quantitative yield by addition of excess of methyl iodide (or CD_3I) to an alcoholic solution of DMPT (parent or deuterated). The precipitate was isolated by filtration or centrifugation and washed with small amounts of ice cold solvent. All compounds gave correct elemental analyses and had an isotopic purity exceeding 95%. The spectra were recorded on a Perkin-Elmer model 580 spectrometer in KBr and/or CsI discs. No signs of halide vibrations were observed in the spectra.

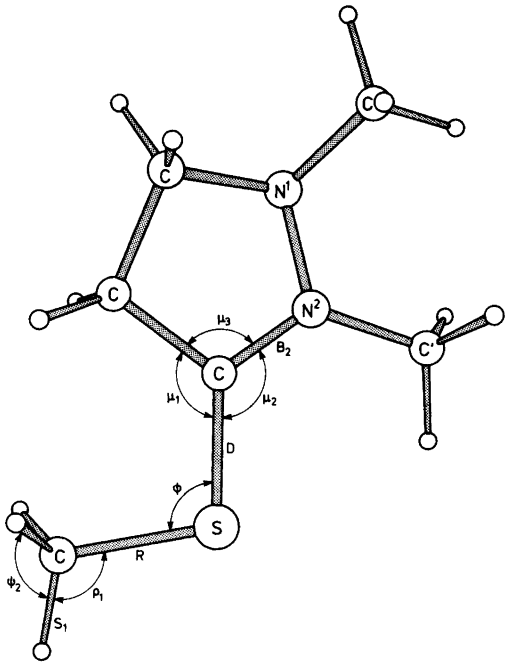

Fig. 1. Internal coordinates in the neighbourhood of the CH_3-S group of DMPT·CH_3S. Other coordinates are not shown on the figure: τ_3, $^{C}_{N}>C-S$ torsion, τ_4, $S-CH_3$ torsion.

NORMAL COORDINATE ANALYSIS

Crystal data on the *S*-methylisothiuronium ion[8] and the *S*-methyl isothiocarbonohydrazidium cation[9] suggest that the structure of DMPT is hardly altered on *S*-methylation except for a small elongation of the CS bond of the thioamide group. The available data also suggest that the *S*-methyl carbon atom is located approximately in the plane of the thioamide group. For these reasons we used a model with the *S*-methyl group situated *trans* to the N^2-CH_3 group in the N^2CS plane (see Fig. 1). The bond angles and distances for the CH_3-S-C group were taken from *S*-methylated thiocarbonohydrazide.[9] The secular equation was set up for the *S*-methyl-1,2-dimethyl-3-pyrazolidinethionium cation taking all 22 atoms into account and the calculations carried out using internal coordinates (or simple linear combinations) as symmetry coordinates in a manner identical to that used previously for DMPT.[7] The internal coordinates necessary for describing the vibrations of the CH_3-S-C group are chosen as shown in Fig. 1.

The final force constants, which are listed in Table 1, have been determined as follows. An initial set of valence force constants was taken from previous studies of DMPT,[7] methanethiol[10] and alkanethiols and thioalkanes.[11] Attempts to adjust the force constants by taking into account the values of the Jacobian matrix gave discrepancies (of some of the low-frequency vibrations related to CS in-plane deformation) which could not be removed despite various adjustments of the force constants. Therefore an interaction force constant between the $C-C-S$ and $C-S-CH_3$ deformations of the $CH_2-C-S-CH_3$ chain was introduced to obtain a satisfactory fit. As stated in the footnote of Table 1, several interaction force constants were also fixed to the values found for DMPT to ensure convergence to physically reasonable values. From this point a simultaneous least-squares adjustment was made for all the compounds by fitting 50 force constants to approximately 450 observed frequencies. The vibrational frequencies calculated by the final force field had an average standard error below 1% for

Table 1. Final valence force constants for DMPT·CH_3I compared with DMPT.[a]

Symbol	Value		Symbol	Value	
	DMPT·CH_3I	DMPT		DMPT·CH_3I	DMPT
CH_3/CH'_3			Ring		
K_r	4.732	4.722	K_D	3.384	3.758
F_{rr}	0.003	0.008	K_{L_2}	3.829	3.883
H_α	0.518	0.515	K_{L_1}	4.555	4.590
H_β	0.805	0.763	K_{B_1}	3.924	3.974
F_β	−0.041	−0.037	K_A	5.367	5.354
K'_r	4.748	4.802	K_{B_2}	8.727	7.507
F'_{rr}	−0.086	−0.134	K_{P_1}	4.639	4.642
H'_α	0.506	0.512	K_{P_2}	4.900	5.070
H'_β	0.754	0.723	H_{μ_1}	1.799	0.585
F'_β	−0.034	−0.031	H_{μ_2}	2.209	1.766
CH_2			H_{μ_3}	0.603	0.820
K_d	4.716	4.722	$H_{\varepsilon_1}=H_{\varepsilon_2}$	1.265	1.270
F_{dd}	0.030	0.035	$H_{\theta_1}=H_{\theta_2}$	2.474	2.422
f^t_γ	0.055	0.058	$H_{\varepsilon_3}=H_{\theta_3}$	0.748	0.754
F'_γ	0.072	0.081	H_Δ	0.267	0.351
H_{δ_2}	0.472	0.470	$F_{L_1\gamma_1}$ *etc.*	0.344	0.353
$H_{\gamma_3}=H_{\gamma_4}$	0.588	0.592	$F_{L_2\omega_2}$ *etc.*	0.860	0.738
$H^o_{\gamma_3}=H^o_{\gamma_4}$	0.663	0.693	$F_{P_1\beta}=F_{P_2\beta}$	0.639	0.660
$F_{\gamma_3}=F_{\gamma_4}$	−0.346	−0.321	CH_3-S		
$F_{\gamma_3\gamma^o_4}$	0.030	0.077	$K_R=3.158$, $H_\phi=2.282$, $K_S=4.843$, $F_{SS}=0.054$, $H_\rho=0.554$, $F_\rho=-0.069$, $H_\psi=0.519$, $H_{\tau_3}=H_{\tau_4}=0.03$, $F_{\mu_1\phi}=0.684$		
H_{δ_1}	0.446	0.432			
$H_{\gamma_1}=H_{\gamma_2}$	0.803	0.780			
$H_{\gamma^o_1}=H_{\gamma^o_2}$	0.645	0.657			
$F_{\gamma_1\gamma_2}$	−0.105	−0.136			
$F_{\gamma^o_1\gamma^o_2}$	0.092	0.086			

[a] For interpretation of symbols, units, and force field for DMPT, see Ref. 7. The values of H_τ, $F_{DL_2}=F_{DB_2}$, $F_{B_2\mu_2}$, $F_{B_2\mu_3}$, $F_{L_2\mu_3}=F_{A\varepsilon_3}$, $F_{D\mu_1}=F_{D\mu_2}$, H_ω, and F_ω were transferred and held fixed.

each of the 9 isotopic species of DMPT$-S-CH_3$ included in the NCA.

The resulting force field is listed in Table 1. The differences between the force constants found for DMPT and DMPT·CH_3I are, in most instances, small and demonstrate convincingly that *S*-methylation indeed leaves most of the molecule largely unchanged. In accordance with simple resonance theory we observe the force constant for CS stretching, K_D, to decrease from 3.76 to 3.38 mdyn/Å and that for CN stretching, K_{B_2}, to increase from 7.51 to 8.73 mdyn/Å on *S*-methylation. The increase in the force constants related to NCS in-plane deformation, H_{μ_1} and H_{μ_2}, and the decrease in the force constant of the corresponding out-of-plane deformation, H_Δ, suggest an increased electron density in the plane of the NCS group at the expense of the π-density. The results pertaining the CH_3S group are remarkable in that an interaction constant $F_{\mu_1\phi}$ of 0.684 mdyn Å/(rad)^2 is necessary to account for the position of the fundamentals ν_{52} and ν_{53} (see Table 2). A similar interaction force constant (with opposite sign) has been found necessary to describe the spectrum of methanethiol.[10]

CNDO/2 CALCULATIONS

More information of the nature and the extent of the electron densities of DMPT and DMPT$-S-CH_3$ was obtained from CNDO/2 calculations. The electronic density changes in the plane of the NCS group (σ-plane) and in a parallel plane 0.85 Å

Table 2. Observed and calculated frequencies (cm^{-1}) of the methiodide (DMPT·CH_3I) and trideuteromethiodide (DMPT·CD_3I) of 1,2-dimethyl-3-pyrazolidinethione (DMPT). Tentative assignment of the IR spectrum of DMPT·CH_3I, description of the fundamentals and frequency shift relative to DMPT.[a]

Observed, IR		Calculated[b]		DMPT-shift[c]		DMPT·CH_3I Assignment and description (PED, %)[d]
DMPT·CH_3I	DMPT·CD_3I	DMPT·CH_3I	DMPT·CD_3I	Obs.	Calc.	
2998w,sh	2247m	**3002**	**2240**	–	–	ν_1, $\nu_{as}CH_3$(S) (99)
		3000	**2235**	–	–	ν_2, $\nu_{as}CH_3$(S) (100)
2983m	2987m	2988	2988	−2	0	ν_3, $\nu_{as}CH_3$(99)
		2985	2985	−2	0	ν_4, $\nu_{as}CH_3$(99)
2968m,sh	2870m,sh	2971	2971	(−17)	−1	ν_5, $\nu_{as}CH_2$(99)
2960m	2962m	2966	2966	−1	−2	ν_6, $\nu_{as}CH_3'$(99)
		2962	2962	−1	−2	ν_7, $\nu_{as}CH_3'$(99)
		2958	2958	−1	0	ν_8, $\nu_{as}CH_2$(98)
2925w,sh	2122w	**2932**	**2112**	–	–	ν_9, ν_sCH_3(S) (100)
	2930w,sh	2928	2928	−3	−2	ν_{10}, ν_sCH_2(98)
		2924	2924	−3	−5	ν_{11}, ν_sCH_3'(99)
2918m	2920m	2914	2914	+3	−4	ν_{12}, ν_sCH_2(99)
2872m	2878m	2869	2869	+20	+7	ν_{13}, ν_sCH_3(100)
1606vs	1608vs	1606	1606	**+106**	**+103**	ν_{14}, **νC^3N(78)**
1466m,sh	1467m,sh	1464	1464	(+17)	+5	ν_{15}, $\delta_{as}CH_3$(90)
1455m	1458m	1460	1460	−5	−4	ν_{16}, $\delta_{as}CH_3'$(42), $\delta_{as}CH_3$(37)
		1459	1459	+6	+4	ν_{17}, $\delta_{as}CH_3$(62), $\delta_{as}CH_3'$(26)
1437m,sh	1446w,sh	1441	1441	−3	−2	ν_{18}, $\delta_{as}CH_3'$(54), δCH_2(20)
	1038m,sh	**1437**	**1036**	–	–	ν_{19}, $\delta_{as}CH_3$(S) (97)
		1436	**1033**	–	–	ν_{20}, $\delta_{as}CH_3$(S) (100)
	1439w,sh	1435	1435	−3	+4	ν_{21}, $\delta_{as}CH_3'$(54), δCH_2(28)
1424m	1426m	1419	1419	+3	+4	ν_{22}, δ_sCH_3(99)
1405m	1412m	1411	1411	**−16**	**−10**	ν_{23}, δCH_2(77)
1388m,sh	1387m,sh	1387	1387	−1	−4	ν_{24}, δ_sCH_3'(98)
1350mw	1351mw	1353	1352	**+10**	**+6**	ν_{25}, **νNN(25)**, ν/δ ring(58)
1320s	1320s	1320	1319	+7	+2	ν_{26}, ωCH_2(58), tCH_2(19), νring(16)
1310s	1068w,sh	**1312**	**1072**	–	–	ν_{27}, δ_sCH_3(S) (86)
1308m,sh	1305vw,sh	1309	1309	+1	0	ν_{28}, ωCH_2(18), tCH_2(33), ring(22)
1249mw	1251w,sh	1237	1237	0		
1236mw	1238mw			+6	+4	ν_{29}, ω/tCH_2(45), ν/δring(38), ρCH_3(23) and $\nu_{41}+\nu_{50}$
1200ms	1204m	1206	1206	**+13**	**+10**	ν_{30}, ω/tCH_2(66), ρCH_3(20)
1175w,sh	1175w,sh	1171	1171	−1	+3	ν_{31}, νring(35), ω/tCH_2(30), ρCH_3(36)
1129vs	1133vs	1141	1141	−1	+4	ν_{32}, ρCH_3(59), νring(24)

1099m	1100mw	1101	1101	+5	+1	ν_{33}, $\rho CH'_3(96)$
1076m	1080mw	1092	1092	0	+4	ν_{34}, ν_{as}**NCS(6)**, $\rho CH'_3(41)$, ν/ring(41)
1060w,sh	1068w,sh	1063	1061	+1	+3	ν_{35}, **νCS(4)**, νCC(35), $\rho CH_2(37)$
1041w	1043w	1043	1042	−4	−3	ν_{36}, ν_{as}**NCS(4)**, $\rho CH'_3(24)$, νring(61)
993m	1000m	995	995	−13	−1	ν_{37}, $\rho CH_2(54)$, νCC(21) and $\nu_{46}+\nu_{48}$
975w,sh	980w,sh					
956m	730w	968	732	–	–	ν_{38}, $\rho CH_3(S)$ (90)
	723w,sh	952	718	–	–	ν_{39}, $\rho CH_3(S)$ (100)
940m	943m	939	940	−2	−10	ν_{40}, **νNN(9)**, $\rho CH_2(52)$, νring(24) and $\nu_{47}+\nu_{48}$
920w,sh						
876ms	880ms	895	898	**−17**	**−9**	ν_{41}, **νNN(16)**, νCS(8), νring(33), $\rho CH_2(22)$
781m	788m	788	806	**−8**	**−12**	ν_{42}, **νCS(27)**, ν/δring(76) and $\nu_{49}+\nu_{50}$
760w,sh	776m					
706w	688w	**738**	**709**	–	–	ν_{43}, $\nu CH_3-S(46)$, ν/δring(40)
	670w					
689mw	637w	**685**	**638**	–	–	ν_{44}, $\nu CH_3-S(36)$, ν/δring(45) and $\nu_{50}+\nu_{52}$
662w,sh						
632vw	638vw	625	615	(−8)	−13	ν_{45}, **νNN(10)**, νring(62), δring(37) and $\nu_{48}+\nu_{55}$
595mw	596mw			(−3)		
548m	548m	563	561	(0)	+10	ν_{46}, $\Delta CH_3-N<^{N}_{C}(58)$, νring(30) and $\nu_{52}+\nu_{53}$
525w,sh	536w,sh					
477w	479w	470	467	**−14**	**−20**	ν_{47}, **νCS(11), ΔCS(10), δCSC((5)**, ν/δring(55)
434m	432m	438	429	**+4**	**+9**	ν_{48}, **νCS(12))$_n$, νNN(14), ΔCS(12))$_n$**, δCSC(22), ring(49)
396m	400m	396	395	**−26**	**−25**	ν_{49}, **ΔCS(33)**, $\Delta CH_3-N<^{N}_{C}(37)$, δring(32)
367m	370m	373	372	**−9**	**−5**	ν_{50}, **ΔCS(12)**, ν/δring(60), $\rho CH_2(26)$
355w,sh	350w,sh	341	339	+5	+3	ν_{51}, **δCS(16), δCSC(9)**, ν/δring (90)
302m	300m	302	292	–	–	ν_{52}, **δCS(17), δCSC(29), νCS(17)**, δring(31)
240m	230m	245	227	–	–	ν_{53}, **δCS(33)), δCSC(25)**, ν/δring(22)
202w	197mw	200	199	(−4)	−2	ν_{54}, $\tau CH'_3(66)$
		171	171	–	0	ν_{55}, $\tau CH_3(92)$
		123	**89**	–	–	ν_{56}, $\tau S-CH_3(88)$
		110	112	–	−8	ν_{57}, δring
		72	70	–	+5	ν_{58}, δring
		38	36	–	–	ν_{59}, $\tau C-SCH_3$
		20	19	–	−2	ν_{60}, δring

[a] The following abbreviations have been used: s, strong; m, medium; w, weak; br, broad; sh, shoulder. Weak and very weak bands not assigned to fundamentals have mostly been omitted from the table. [b] These values have been obtained by iteration based upon all isotropic species, both deuterated in the DMPT and the CH_3I part of the molecule. Calculated values for vibrations mainly originating in the CH_3S/CD_3S group are in bold types. [c] Shifts of the IR bands of solid DMPT on conversion to the methiodide compared with the calculated changes. Shifts considered to be significant are in bold types. [d] Abbreviations: ν = stretch; δ = deformation: Δ = out-of-plane deformation; ρ = rock; ω = wag; t = twist; τ = torsion; s = symmetric; as = antisymmetric. Vibration of the pyrazolidine ring and the attached heavy atoms are designated 'ring' or using the following nomenclature: N^1-CH_3; $N^2-CH'_3$; C^3S. The potential energy distribution (PED, $x_{ik}=100F_{ii}L^2_{ik}/\lambda_k$) is stated only for significant contributions. The PED referring to the thiohydrazide group is underlined.

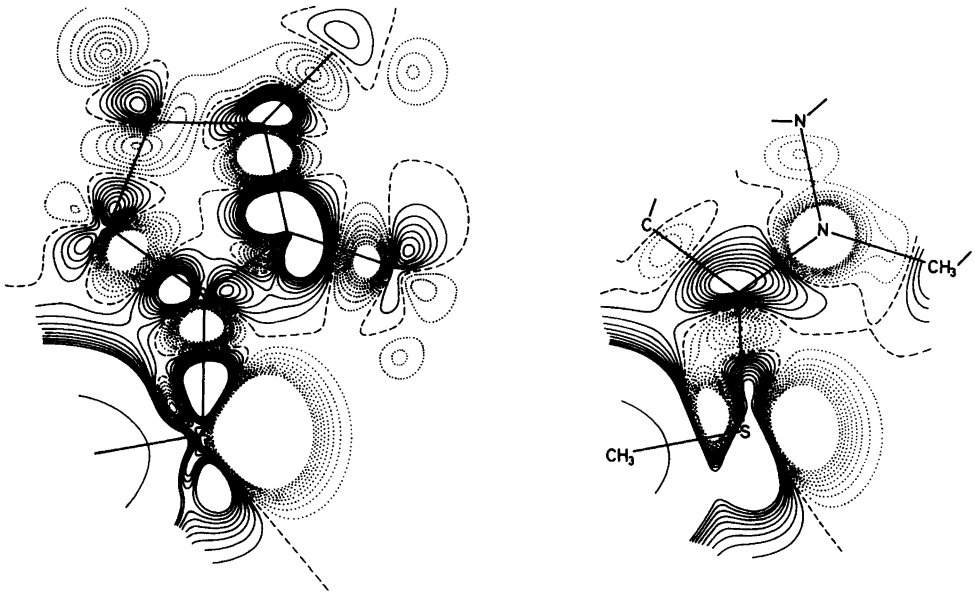

Fig. 2. Difference map (DMPT · CH_3I – DMPT) of the total molecular density in the NCS plane (left) and in a parallel plane 0.85 Å above this plane (right) as calculated by the CNDO/2 method. Solid, dashed and dotted lines represent positive, zero and negative difference densities, respectively, plotted linearly with a spacing of 0.001 electron/Å^3.

apart (π-plane) are illustrated in Fig. 2. The difference-density maps are calculated by substracting the density of DMPT from that of DMPT·CH_3I.

The density of the sulfur *p*-orbital directed towards the methyl group decreases from 1.98 to 1.05 on *S*-methylation. This means that bonding between sulfur and methyl takes place essentially by sharing of the electrons of one of the sulfur lone-pairs. This leaves the sulfur atom with a fractional positive charge which may be compensated by different displacements of the σ- and π-electrons of the thiohydrazide group. The π-changes are mainly confined to the NCS group, and may be described by the classical resonance structure $N^+=C-S^-$. Thus, the π-density of the nitrogen atoms decreases from 1.58 to 1.38, while the π-bond order of the neighbouring CN bond increases from 0.66 to 0.80 on *S*-methylation. At the same time the π-bond order of the CS bond decreases from 0.57 to 0.35 and the π-density of the sulfur atom increases from 1.69 to 1.88. In addition a small increase from 0.70 to 0.75 in the π-density of the carbon atoms is calculated, but this hardly invalidates the main conclusion. In total, the π-density changes tend to increase the force constant for CN stretching and decrease that for CS stretching.

The changes in the σ-density are illustrated on the left-hand side of Fig. 2. An increase in the electron-attracting properties of sulfur on *S*-methylation is clearly revealed by the polarization induced in the $S-C^3-C^4-C^5$ chain. Thus, the sulfur atom polarizes the $S-C^3$ bond, which in turn polarizes the C^3-C^4 bond and so on. The polarization diminishes with the distance from the sulfur atom. However, proceeding in the same way along the $S-C^3-N^2-N^1$ chain seems to indicate a similar increase in the electron-attracting properties of the N^2-atom on *S*-methylation. The C^3N bond in the thioamide group is under both influences and the result is very weak polarization. (The increased electron attraction by N^2 may be due to the fact that nitrogen is not sp^2-hybridized but slightly pyramidal. The orthogonality of σ- and π-electrons of the NCS group therefore breaks down, and the decreased π-density of the N^2 atom is transmitted to the σ-core.) Though the σ-core is strongly polarized the changes in σ-densities and σ-bond orders on *S*-methylation are only small. They can be summarized as a slight increase in the total σ-

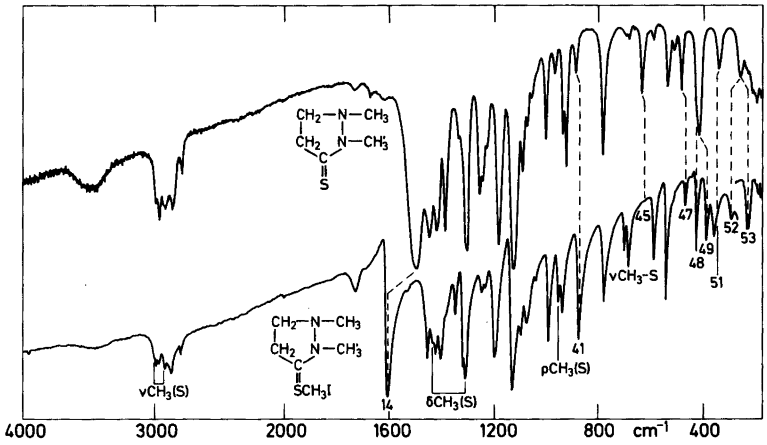

Fig. 3. The IR spectra of 1,2-dimethyl-3-pyrazolidinethione in the liquid state (top) and the *S*-methiodide in the solid state (bottom). Corresponding bands (see text) are indicated by dotted lines. The bands originating mainly from the *S*-methyl group are indicated separately in the figure.

density of the CS bond polarized in the direction C^+S^-. In total the σ-density changes therefore result in a small increase of the force constant for CS stretching.

The changes described here on *S*-methylation of DMPT are almost the same as those described previously for complex formation with metal halides.[3] In both cases, attack on the sulfur atom is followed by a π-change rationalized as $N^+=C-S^-$ and a polarization of the σ-electrons of the CS bond corresponding to C^+-S^-. Nevertheless an important difference should be noted. When DMPT is *S*-methylated, the force constant for CS stretching will decrease because the changes in π-density exceed those in the σ-core. However, on conversion to metal complex compounds the polarization of the σ-electrons of the CS bond exceeds the changes in the π-density with the result that the force constant for CS stretching increases slightly.

DISCUSSION OF THE S-METHYLATION EFFECTS ON THE SPECTRUM OF DMPT

Survey spectra of DMPT and DMPT·CH_3I at room temperature are shown in Fig. 3. The IR spectrum of DMPT refers to the liquid state, but is virtually unchanged from that of crystalline DMPT. To facilitate comparison of the bands, dotted lines are added on the figure. If the bands originating from the CH_3-S group are disregarded there is a fair, but not striking, similarity of the spectra, and several shifts would indeed be difficult to establish without the results of the NCA. In Table 2 the observed frequencies of DMPT are tabulated, together with those of DMPT·CD_3I, as an example of the changes arising from deuteration of the *S*-methyl group. The table includes an assignment of the spectrum based upon the calculated frequencies of the fundamentals. The fundamentals are described in terms of the PED of the internal coordinates. Finally, the frequencies shifts of corresponding bands in DMPT and DMPT·CH_3I(DMPT-shift) are tabulated. Since it is precisely these shifts which form the basis of the diagnostic use of *S*-methylation for revealing bands with contributions from vibrations of the thioamide group, they will be the main subject of the following discussion.

Firstly, it should be noted that in spite of the close similarity between DMPT and DMPT·CH_3I it is not possible to establish a one-to-one correspondence visually, *i.e.* merely by comparing the position, form, and intensity of the bands. Three of the reasons (intensity changes, intensity reversal and changes in PED) have been discussed in some detail in the preceeding papers[2,3] and examples documenting their operation on *S*-methylation are easily found from Table 2. A fourth reason is the occurrence of coupling between the vibrations of DMPT and the attached *S*-methyl group. From Table 2 it is seen that the stretching, deformation and rocking vibrations of the $S-CH_3$ group do not couple significantly with the vibrations of DMPT.

On the other hand, the CH_3-S stretching vibrations couple strongly with the fundamental ν_{35} of DMPT near 690 cm^{-1} to give the doublet ν_{43} and ν_{44} around 700 cm^{-1} in DMPT·CH_3I. The CS in-plane deformation vibration which is the main component of the fundamental ν_{43} near 270 cm^{-1} in DMPT also couples strongly with the $C-S-CH_3$ deformation vibration to give two new bands (ν_{52} and ν_{53}) in DMPT·CH_3I near 240 and 300 cm^{-1}. Since similar couplings probably arise on *S*-methylation of other thioamides the latter results may have general significance and may be useful in qualitative work.

Secondly, our results demonstrate that it is not possible to distinguish between bands with and without contributions from the thiohydrazide group by the shifts obtained on *S*-methylation even in cases where the one-to-one correspondence can be proved. The fundamentals ν_{23} and ν_{30} are examples of bands which display a definite shift in frequency relative to the corresponding bands in DMPT. However, the origins of the shifts are to be found in changes in PED, not in contributions from vibrations of the thiohydrazide group. On the contrary, ν_{48} and ν_{51} are examples of bands which have significant contributions from vibrations of the thiohydrazide grouping, but nevertheless hardly shift on *S*-methylation. A quite similar conclusion for heterocyclic thioamides was reached empirically by Devillanova and Verani.[4] For these reasons, *S*-methylation cannot be recommended as a tool for assignment of bands due to the NCS group.

However, in the light of the results of the NCA it is possible to comment briefly on the shifts on the bands of DMPT as a result of *S*-methylation. The very strong fundamental ν_{16} near 1500 cm^{-1} in DMPT mostly due to CN stretching of the thiohydrazide group is shifted *ca.* 100 cm^{-1} towards higher frequencies in DMPT·CH_3I (ν_{14}) mainly as a result of an increase in the force constant for CN stretching, K_{B_2}. The weak fundamental ν_{20} near 1340 cm^{-1} in DMPT has a substantial contribution from NN stretching. On *S*-methylation the polarity and transition moment of the NN bond will increase (due to the structure $N-N^+=C-S-CH_3$) and the corresponding fundamental ν_{25} near 1350 cm^{-1} in DMPT·CH_3I consequently increases in intensity.

The two prominent bands, ν_{33} and ν_{34} near 890 and 790 cm^{-1} in DMPT, have considerable CS stretching character and are both displaced towards lower frequencies in DMPT·CH_3I (ν_{41} and ν_{42}) partly as a result of the lower force constant for CS stretching. A third band, ν_{39} at 430 cm^{-1} in DMPT with 32% CS stretching character, has no close counterpart in DMPT·CH_3I since the bands ν_{47} and ν_{48} now share this contribution. The fundamental ν_{40} in DMPT near 420 cm^{-1} has a 44% contribution from CS out-of-plane deformation. As a result of a decrease in the corresponding force constant, H_Δ, the counterpart ν_{49} in DMPT·CH_3I is found at 26 cm^{-1} lower frequencies, and some of the CS out-of-plane character is even transferred to the next lower fundamental ν_{50}.

Acknowledgement. This research was supported by grants from the Danish Natural Science Research Council.

REFERENCES

1. Jensen, K. A. and Nielsen, P. H. *Acta Chem. Scand. 20* (1966) 597.
2. Anthoni, U., Borch, G., Klæboe, P. and Nielsen, P. H. *Acta Chem. Scand. A 36* (1982) 69.
3. Anthoni, U., Borch, G. and Nielsen, P. H. *Acta Chem. Scand. A 36* (1982) 711.
4. Devillanova, F. A. and Verani, G. *Aust. J. Chem. 33* (1980) 279 and references therein.
5. Devi, K. R. G. and Sathyanarayana, D. N. *Bull. Chem. Soc. Jpn. 53* (1980) 2990 and references therein.
6. Borch, G., Klæboe, P., Nielsen, P. H. and Pedersen, L. M. *Acta Chem. Scand. A 32* (1978) 259.
7. Anthoni, U., Borch, G., Klæboe, P., Lerstrup, K. and Nielsen, P. H. *Acta Chem. Scand. A 35* (1981) 767.
8. Stam, C. H. *Acta Crystallogr. 15* (1962) 317.
9. Bigoli, F., Leporati, E. and Pellinghelli, M. A. *Cryst. Struct. Commun. 7* (1978) 527.
10. May, I. W. and Pace, E. L. *Spectrochim. Acta 24* (1968) 1614.
11. Scott, D. W. and El-Sabban, M. Z. *J. Mol. Spectrosc. 30* (1969) 317.

Received March 16, 1982.

Acta Chemica Scandinavica A 36 (1982) 805–811

Molecular Force Fields and Bonding in Methylchlorogallate and Methylchloroindate Ions: $|R_{4-n}M^{III}Cl_n|^-$; R=CH_3 or CD_3; M^{III}=Ga or In; n=0–4

ARNE HAALAND[a] and JOHANN WEIDLEIN[b]

[a]Department of Chemistry, University of Oslo, Blindern, Oslo 3, Norway and [b]Institut für Anorganische Chemie, Universität Stuttgart, D-7000 Stuttgart 80, Germany

The infrared and Raman spectra of the deutero-methylchlorometallates $|(CH_3)_4As||(CD_3)_{4-n}M^{III}Cl_n|$; M^{III}=Ga or In and n=1 to 3 have been recorded for the solid state and interpreted on the basis of C_{3v} or C_{2v} symmetry for the metallate ions. Simple valence molecular force fields for the series have been determined by least squares calculations on these spectra and the spectra of the undeuterated analogues previously reported. Both M–Cl and M–C stretching force constants increase markedly and monotonically with increasing chlorine substitution across the series $|(CH_3)_{4-n}M^{III}Cl_n|^-$; n=0 to 4. These variations are correlated with observed changes in M–Cl and M–C bond distances, and rationalized as a combination of inductive and resonance effects.

The preparation and the vibrational spectra of the solid compounds $[(CH_3)_4M^V][(CH_3)_{4-n}M^{III}Cl_n]^-$, where M^V=As or Sb, M^{III}=Ga or In and n=0, 1, 2, 3 or 4 have been described by us some years ago.[1] A number of these compounds have also been studied by X-ray crystallography,[2–7] and the average bond distances and valence angles of the anions are listed in Table 2. As pointed out by Hausen and coworkers,[4–6] the average M–Cl bond distance in the anions decreases monotonically with increasing Cl substitution: The decrease on going from $[(CH_3)_3MCl]^-$ to $[MCl_4]^-$ is about 0.21 Å when M=Ga and about 0.22 Å when M=In. The variation of the M–C bond distances is less clear, both because the error limits of the M–C bond distances are larger, and because the variation of the M–C bond distances with increasing Cl substitution is smaller. But comparison of the structures of the ions $[(CH_3)_4In]^-$ and $[(CH_3)InCl_3]^-$ suggests that the total change of the M–C bond distance across the series is about 0.06 Å.

We have previously carried out normal coordinate analysis of the isoelectronic species $[(CH_3)_4M^{III}]^-$, M^{III}=Al, Ga and In, $(CH_3)_4M^{IV}$, M^{IV}=Si, Ge and Sn and $[(CH_3)_4M^V]^+$, M^V=P, As and Sb[8] and discussed variations in the force fields. We were now interested in investigating how the force fields vary across the series $[(CH_3)_{4-n}M^{III}Dl_n]^-$ and have supplemented the IR and Raman spectra quoted in Ref. 1 with spectra of the fully deuterated species before carrying out normal coordinated analysis.

EXPERIMENTAL

The deuterated starting materials $(CD_3)_3Ga \cdot O(C_2H_5)_2$ and $(CD_3)_3In$ were prepared by Grignard reactions from CD_3I and Ga/Mg or In/Mg alloys in diethyl ether. Both compounds were purified by vacuum distillation. Reaction of these deuterated derivatives with stoichiometric amounts of $GaCl_3$ or $InCl_3$ yielded $(CD_3)_2GaCl$ or $(CD_3)_2InCl$ of high purity.

The deuterated methylchlorometallates were prepared by the following reactions as described in Ref. 1:

$$(CH_3)_3AsCl_2 + (CD_3)_2M^{III}Cl \rightarrow [(CH_3)_3As(CD_3)]^+[(CD_3)M^{III}Cl_3]^-$$

$$(CH_3)_4AsCl + (CD_3)_2M^{III}Cl \rightarrow [(CH_3)_4As]^+[(CD_3)_2M^{III}Cl_2]^-$$

0302-4377/82/100805-07$02.50

$(CH_3)_4AsCl + (CD_3)_3In \rightarrow$
$[(CH_3)_4As]^+[(CD_3)_3InCl]^-$
$(CH_3)_4AsCl + (CD_3)_3Ga \cdot O(C_2H_5)_2 \rightarrow$
$[(CH_3)_4As]^+[(CD_3)_3GaCl]^- + O(C_2H_5)_2$
$M^{III} = Ga, In$

The products were purified by one recrystallization from CH_2Cl_2.

Elemental analysis for C, H and Cl were performed by usual methods, the Ga or In content was determined by titration with Titriplex III. The yields listed in Table 1 refer to the alkyl metal component. IR spectra were taken of Nujol or Hostaflon mulls, pressed as capillary films between CsBr plates, and recorded with a Perkin-Elmer PE 283 spectrometer. Raman spectra were measured on a PH O spectrophotometer of Coderg, Inc.; for excitation, the bluegreen (4880 Å) line of an Argon laser was employed.[9]

NORMAL COORDINATE ANALYSIS

For each of the species under consideration a valence force field was defined using the pertinent members of the following set: Stretching force constants $f(M-C)$ and $f(M-Cl)$ and stretch/stretch interaction force constants $f(MC/MC')$, $f'(MC/MCl)$ and $f'(MCl/MCl')$; Bending force constants $f(CMC)$, $f(CMCl)$ and $f(ClMCl)$; Methyl group force constants $f(C-H)$ (stretch), $f(MCH)$ and $f(HCH)$ (bend) and $f'(MCH/MCH')$ (interaction). The framework bond distances and valence angles are listed in Tables 2a and 2b. All C–H bond distances were fixed at 1.08 Å and all M–C–H angles were assumed to be tetrahedral.

Normal coordinate analysis was carried out using a program written by Hilderbrandt[10] which allows the force constants to be refined by least-squares calculations on the observed vibrational frequencies by an iterative procedure. The best values for the force constants are listed in Tables 2a and 2b, and observed and calculated frequencies are compared in Tables 3a and 3b. In Tables 2a and 2b we also include the values for the force constants previously obtained for the species $[(CH_3)_4M]^-$,[8] and the force constants obtained for $[GaCl_4]^-$ and $[InCl_4]^-$ using the observed frequencies of Chemouni[11] and Contreras and Tuck.[12]

DISCUSSION

Inspection of the M–Cl and M–C stretching force constants in Tables 2a and 2b, reveals that the

Table 1. Preparation and elemental analysis data.

Starting materials $(CD_3)_2M^{III}Cl$ or $(CD_3)_3M^{III}$ g (mmol)		$(CH_3)_3AsCl_2$ or $(CH_3)_4AsCl$ g (mmol)		Product	Yield (%)	Elemental analysis, found (calc.) (%) Metal	C	H + 1/2D	Cl
0.46	(3.26)	0.62	(3.25)	$[(CH_3)_3AsCD_3][CD_3GaCl_3]$	92	21.22 (20.99)	18.01 (18.08)	4.60 (4.55)	31.95 (32.01)
0.57	(3.06)	0.58	(3.04)	$[(CH_3)_3AsCD_3][CD_3InCl_3]$	88	30.1 (30.43)	16.01 (15.92)	4.08 (4.01)	28.21 (28.19)
0.44	(3.11)	0.52	(3.05)	$[(CH_3)_4As][(CD_3)_2GaCl_2]$	80	22.41 (22.36)	23.30 (23.11)	5.86 (5.82)	22.81 (22.74)
0.68	(3.65)	0.62	(3.64)	$[(CH_3)_4As][(CD_3)_2InCl_2]$	84	31.98 (32.17)	20.28 (20.19)	5.11 (5.08)	19.9 (19.87)
1.12[a]	(5.65)	0.90	(5.28)	$[(CH_3)_4As][(CD_3)_3GaCl]$	68	23.91 (23.68)	28.17 (28.56)	6.98 (7.19)	11.92 (12.04)
1.06	(6.27)	1.07	(6.27)	$[(CH_3)_4As][(CD_3)_3InCl]$	74	33.6 (33.82)	24.81 (24.76)	6.30 (6.23)	10.56 (10.44)

[a] As $(CD_3)_3Ga \cdot O(C_2H_5)_2$.

Table 2a. Bond distances (in Å), stretching force constants (in mdyn/Å), valence angles (in deg) and bending force constants (in mdyn Å) for the ions $|(CH_3)_{4-n}GaCl_n|^-$.[a]

	$[(CH_3)_4Ga]^{-2,8}$	$[(CH_3)_3GaCl]^{-1}$	$[(CH_3)_2GaCl_2]^{-3}$	$[CH_3GaCl_3]^{-3}$	$[GaCl_4]^{-4}$
R(Ga–C)	2.2(2)	2.053(23)	1.980(13)	1.934(8)	
f(Ga–C)	1.87	2.24	2.56	2.80	
R(Ga–Cl)		2.381(8)	2.277(4)	2.222(3)	2.172(2)
f(Ga–Cl)		0.74	1.16	1.51	1.96
∠(CGaC)	109.5	115.2(10)	125.3(6)		
f(CGaC)	0.10	0.18	0.09		
∠(CGaCl)		102.9(10)	107.2(4)	114.3(6)	
f(CGaCl)		0.65	0.45	0.46	
∠(ClGaCl)			99.7(1)	104.3(2)	109.5
f(ClGaCl)			0.48	0.47	0.54
f'(GaC/GaC')	0.12	0.14	0.12		
f'(GaC/GaCl)		0.17	0.16	0.12	
f'(GaCl/GaCl')			0.11	0.18	0.18
f(C–H)	4.75	4.72	4.75	4.82	
f(HCH)	0.45	0.38	0.39	0.39	
f(GaCH)	0.28	0.35	0.36	0.38	
f'(GaCH/GaCH')	−0.0045	−0.003	−0.0008	−0.011	

[a] The bond distances and valence angles have been averaged to yield species of T_d ($[(CH_3)_4Ga]^-$ and $[GaCl_4]^-$), C_{3v} ($[(CH_3)_3GaCl]^-$ and $[CH_3GaCl_3]^-$) and C_{2v} symmetry ($[(CH_3)_2GaCl_2]^-$). The estimated standard deviations listed are the average e.s.d's of crystallographically independent bond distances and valence angles.

Table 2b. Bond distances (in Å), stretching force constants (in mdyn/Å), valence angles (in deg) and bending force constants (in mdyn Å) for the ions $|(CH_3)_{4-n}InCl_n|^-$.[a]

	$[(CH_3)_4In]^{-5,8}$	$[(CH_3)_3InCl]^{-1}$	$[(CH_3)_2InCl_2]^-$	$[CH_3InCl_3]^{-6}$	$[InCl_4]^{-7}$
R(In–C)	2.239(3)	2.23(3)	(2.20)[b]	2.183(16)	
f(In–C)	1.57	1.94	2.19	2.41	
R(In–Cl)		2.551(7)	(2.45)[b]	2.400(3)	2.33(2)
f(In–Cl)		0.66	0.98	1.38	1.78
∠(ClnC)	109.5	116.4(10)	(135)[b]		
f(ClnC)	0.06	0.12	0.09		
∠(CInCl)		101.0(10)	(105.9)[b]	116.3	
f(CInCl)		0.58	0.45	0.36	
∠(ClInCl)			(99.0)[b]	102.0	109.5
f(ClInCl)			0.50	0.54	0.39
f(InC/InC')	0.09	0.09	0.08		
f'(InC/InCl)		0.12	0.11	0.09	
f'(InCl/InCl')			0.13	0.15	0.12
f(C–H)	4.75	4.78	4.76	4.77	
f(HCH)	0.45	0.35	0.36	0.36	
f(InCH)	0.25	0.33	0.34	0.38	
f'(InCH/InCH')	−0.050	−0.003	−0.007	−0.078	

[a] See comments Table 2a. [b] Estimated values, see also data for $[(CH_3)_4As][(CH_3)_2InBr_2]$ in Ref. 13.

Table 3a. Observed and calculated frequencies (in cm^{-1}) for the ions $[(CH_3)_{4-n}GaCl_n]^-$ and $[(CD_3)_{4-n}GaCl_n]^-$ with $n = 1$, 2 or 3.

$[(CH_3)_4As]^+$ $[(CH_3)_3GaCl]^-$ obs.[1,22]	calc.		$[(CH_3)_4As]^+$ $[(CD_3)_3GaCl]^-$ [a] obs.[9]	calc.	$[(CH_3)_4As]^+$ $[(CH_3)_2GaCl_2]^-$ obs.[1,22]	calc.		$[(CH_3)_4As]^+$ $[(CD_3)_2GaCl_2]^-$ obs.[9]	calc.	$[(CH_3)_4Sb]^+$ $[CH_3GaCl_3]^-$ obs.[1]	calc.		$[(CH_3)_3AsCD_3]^+$ $[CD_3GaCl_3]^-$ obs.[9]	calc.	Assignment (C_{3v} or C_{2v})
2950	2976		2208	2213	2959	2986		2212	2221	2990	3003		2238	2234	$\nu_{as}CH_3(CD_3)$
2846	2862		2115	2056	2891	2871		2110	2063	2894	2887		2118	2076	$\nu_sCH_3(CD_3)$
1182 1178	1236 to 1164		943	933 to 892	1206 1200	1245 to 1171		950 (925)	948 to 898	1212 1204	1258 to 1189		943	967 to 908	$\delta_sCH_3(CD_3)$
734 724	723 to 713		539	545 to 530	740 725	744 to 738		568 545	560 to 551	758 740	761		598 578	573	$\rho CH_3(CD_3)$
541	547		490	481	582	591		532	518	591	598		535	522	ν GaC, A_1
513	525		n.o.	452	547	551		482	476						$\nu_{as}GaC_3(GaC_2)$,
242	238		230	234											$\nu_sGaC_3(GaC_2)$,
					286	291		285	289	328	333		339	331	νGaCl, A_1
					301	292		289	291	334	331		333	329	$\nu_{as}GaCl_3(GaCl_2)$
172	170	E	n.o.	157	165	157	B	153	148	162	163	E	152	149	$\nu_sGaCl_3(GaCl_2)$
148	147	A_1	n.o.	135	144	148 A_2 / 145 B		127	136 / 132	130	139	A_1	125	138	δ CGaC / δ CGaCl
118	118	E	n.o.	105	133	122	A_1	107	114	118	115	E	119	115	δ ClGaCl
					119 / 107	111	A_1	95	106						

[a] In the case of $[(CH_3)_4As][(CD_3)_3GaCl]$ only the IR spectra could be measured.

Table 3b. Observed and claculated frequencies (in cm^{-1}) for the ions $[(CH_3)_{4-n}InCl_n]^-$ and $[(CD_3)_{4-n}InCl_n]^-$ with $n=1$, 2 or 3.

$[(CH_3)_4As]^+$ $[(CH_3)_3InCl]^-$ obs.[1]	calc.		$[(CH_3)_4As]^+$ $[(CD_3)_3InCl]^-$ obs.[9]	calc.	$[(CH_3)_4Sb]^+$ $[(CH_3)_2InCl_2]^-$ obs.[1]	calc.		$[(CH_3)_4As]^+$ $[(CD_3)_2InCl_2]^-$ obs.[9]	calc.		$[(CH_3)_4Sb]^+$ $[CH_3InCl_3]^-$ obs.[1]	calc.		$[(CH_3)_3AsCD_3]^+$ $[CD_3InCl_3]^-$ obs.[9]	calc.		Assignment (C_{3v} or C_{2v})
2965	2995		2218	2226	2976	2988		2210	2222		2980	2995		2208	2226		$\nu_{as}CH_3(CD_3)$
2891	2875		2120	2068	2880	2873		2098	2064		2885	2875		2121	2069		$\nu_sCH_3(CD_3)$
1150 1140	1191 to 1121		885	893 to 860	1166 1156	1206 to 1132		904 898	910 to 871		1159 1155	1202 to 1145		898	924 to 866		$\delta_sCH_3(CD_3)$
685	694 to 689		517	519 to 511	704	714 to 711		549 512	533 to 529		741	757		557	566		$\rho CH_3(CD_3)$
											530	537		481	469		νInC, A_1
480	487		436	431	522	525		468	462								$\nu_{as}InC_3(InC_2)$
467	480		421	417	490	501		442	435								$\nu_sInC_3(InC_2)$,
215	205		197	204													ν_sInCl, A_1
					241	239		235	238		293	288		290	287		$\nu_{as}InCl_3(InCl_2)$
					257	258		252	258		308	308		307	307		$\nu_sInCl_3(InCl_2)$
144	146	E	135	136	134	136	B_1	130	129	A_1	130	129	A_1	123	122		δ CInC
						135	A_2		124						118		
130	128	A_1	119	115	128	125	B_2	114	114		120	122	E				δ CInCl
n.o.	90	E	n.o.	80	116	112	A_1	96	104		110	108	E	106	108		δ ClInCl
					106	101	A_1	86	96								

decrease of M–Cl and M–C bond distances with increasing Cl substitution is accompanied by a monotonic *increase* of the M–Cl and M–C force constants. And just as the decrease of M–Cl bond distances across the series is more than twice as large as the decrease of the M–C bond distances (0.20 Å *versus* about 0.06 Å), so the f(M–Cl) force constants are found to increase by a factor of about 2.6, while the f(M–C) force constants increase with a factor of about 1.5. Closer inspection shows that f(M–Cl) change with nearly constant steps of 0.32 to 0.42 mdyn Å^{-1} across both series, while the change in f(M–C) is particularly large when the first Cl atom is introduced into $[(CH_3)_4M]^-$, 0.40 and 0.37 mdyn Å^{-1}, while the two following Cl atoms bring about changes ranging from 0.21 to 0.29 mdyn Å^{-1}.

It is well known that increased halogen substitution in derivatives of Group IV elements of the type $(CH_3)_{4-n}M^{IV}Cl_n$ leads to a shortening of the bond distances. In the present context it is pertinent to recall the bond distances obtained for the series with M^{IV} = Sn, which is isoelectronic with the series $[(CH_3)_{4-n}InCl_n]^-$:

	R(M–C)m(Å)	R(M–Cl) (Å)
$(CH_3)_4Sn$[14]	2.144(3)	
$(CH_3)_3SnCl$[15]	2.106(6)	2.351(2)
$(CH_3)_2SnCl_2$[16]	2.109(9)	2.327(4)
$(CH_3)SnCl_3$[15]	2.104(16)	2.304(3)
$SnCl_4$[17]		2.281(4)

The M–Cl bond distance is seen to decrease monotonically down the series, though the total change (0.07 Å) is only about one third of that observed for the isoelectronic ions $[(CH_3)_{4-n}InCl_n]^-$. The variation of the M–C distances is again less clear, but the total change appears to be about 0.04 Å, not very different from that found for the Group III complex ions.

Donor–acceptor bonds in complexes formed by derivatives of Group III and V elements are, however, known to be very sensitive to inductive effects. Thus the Ga–N bond distance in $(CH_3)_3GaN(CH_3)_3$ is 2.20(3) Å,[18] in $H_3GaN(CH_3)_3$ 2.111(2) Å[19] and in Cl_3GaNH_3 2.057(11) Å.[20] The Ga–P bond distance in $(CH_3)_3GaP(CH_3)_3$ is 2.52(2) Å[18] and in $Cl_3GaP(CH_3)_3$ 2.353(2) Å,[21] a change of 0.17 Å.

We have previously described the anionic complexes $[(CH_3)_3MCl]^-$ as donor acceptor complexes between $(CH_3)_3M$ and Cl^-: $(CH_3)_3M{\leftarrow}Cl^-$.[22] This description seems reasonable when the Ga–Cl bond distance in this complex is compared to the Ga–P bond distance in $(CH_3)_3GaP(CH_3)_3$: 2.38 *versus* 2.52 Å. It is also in agreement with the similarity of the Ga–C stretching force constant in the complex ion and in free $(CH_3)_3Ga$:[23] 2.27 *versus* 2.29 mdyn Å^{-1}.

The structure of the ion $[GaCl_4]^-$ may be discussed in terms of four resonance structures of the type $Cl_3Ga{\leftarrow}Cl^-$. The three "normal", "covalent" Ga–Cl bonds should then be similar to the Ga–Cl bonds in $Cl_3GaP(CH_3)_3$ which are 2.17 Å long.[21] The donor acceptor bond would be expected to be about 0.17 Å shorter than in the complex $[(CH_3)_3GaCl]^-$, that is about 2.21 Å. Resonance between the four canonical forms gives a tetrahedral ion when each Ga–Cl bond distance is equal to $(3/4)\cdot 2.17$ Å $+(1/4)\cdot 2.21$ Å $= 2.18$ Å.

The structure of $[(CH_3)_2GaCl_2]^-$ may be rationalized in terms of two resonance structures of the type $(CH_3)_2ClGa{\leftarrow}Cl^-$. By analogy with the series $(CH_3)_{4-n}SnCl_n$ the presence of two methyl groups is expected to increase the covalent Ga–Cl bond with about 0.04 to 2.21 Å, and the donor acceptor bond by $(2/3)\cdot 0.17$ Å from 2.21 to 2.32 Å. The average bond distance obtained by resonance is $(1/2)\cdot 2.21$ Å $+(1/2)\cdot 2.32$ Å $= 2.27$ Å. A similar argument applied to $[(CH_3)GaCl_3]^-$ leads to a predicted average Ga–Cl bond distance of 2.22 Å, again in agreement with the experimental value.

In our discussion of M–Cl bonding we have implicitly assumed that the M–C bonds in the species $[(CH_3)_3MCl]^-$, $[(CH_3)_2MCl]^-$ and $[(CH_3)MCl_3]^-$ are essentially normal covalent bonds. These bonds would be expected to change with increasing Cl substitution much in the same way as the Sn–C bond distances in the series $(CH_3)_{4-n}SnCl_n$, that is with 0.01 or 0.02 Å per Cl atom.

The structure of the ions $[(CH_3)_4M]^-$ must be discussed in terms of resonance structures of the type $(CH_3)_3M{\leftarrow}CH_3^-$. Each M–C bond would then be 75% covalent and 25% dative. We would therefore expect the largest change in M–C bond distance on going from $[(CH_3)_3MCl]^-$ to $[(CH_3)_4M]^-$. Unfortunately the M–C bond distances have not been determined with sufficient accuracy to allow these predictions to be tested. But it is gratifying that the greatest increase in M–C stretching force constants occurs on going from $[(CH_3)_4M]^-$ to $[(CH_3)_3MCl]^-$.

Finally we wish to point out that the largest angle bend force constants are found for the species $[(CH_3)_3MCl]^-$ which are the only ones that we have described in terms of a single resonance structure.

REFERENCES

1. Widler, H.-J., Schwarz, W., Hausen, H.-D. and Weidlein, J. *Z. Anorg. Allg. Chem. 435* (1977) 179 and references therein.
2. Wolfrum, R., Sauermann, G. and Weiss, E. *J. Organomet. Chem. 18* (1969) 18.
3. Hausen, H.-D., Guder, H. J. and Schwarz, W. *J. Organomet. Chem. 132* (1977) 37.
4. Hausen, H.-D., Binder, H. and Schwarz, W. *Z. Naturforsch. B 33* (1978) 567.
5. Hoffmann, K. and Weiss, E. *J. Organomet. Chem. 50* (1973) 17.
6. Guder, H. J., Schwarz, W., Weidlein, J., Widler, H.-J. and Hausen, H.-D. *Z. Naturforsch. Teil B 31* (1976) 1185.
7. Trotter, J., Einstein, F. W. B. and Tuck, D. G. *Acta Crystallogr. B 25* (1969) 603.
8. Tatzel, G., Schrem, H. and Weidlein, J. *Spectrochim. Acta A 34* (1978) 549.
9. Ehrmann, T. *Zulassungsarbeit*, Universität Stuttgart, Stuttgart 1980.
10. Hilderbrandt, R. L. and Wieser, J. D. *J. Chem. Phys. 55* (1971) 4648.
11. Chemouni, E. *J. Inorg. Nucl. Chem. 33* (1971) 2325.
12. Contreras, J. G. and Tuck, D. G. *Inorg. Chem. 11* (1972) 2967.
13. Schwarz, W., Guder, H. J., Prewo, R. and Hausen, H.-D. *Z. Naturforsch. Teil B 31* (1976) 1427.
14. Nagashimi, M., Fujii, H. and Kimura, M. *Bull. Chim. Soc. Jpn. 46* (1973) 3708.
15. Beagley, B., McAloon, K. and Freemann, J. M. *Acta Crystallogr. B 33* (1974) 444.
16. Fujii, H. and Kimura, M. *Bull. Chem. Soc. Jpn. 44* (1971) 2643.
17. Fujii, H. and Kimura, M. *Bull. Chem. Soc. Jpn. 43* (1970) 1933.
18. Golubinskaya, L. M., Golubinskii, A. V., Mastryukov, V. S., Vilkov, L. V. and Bregadze, V. I. *J. Organomet. Chem. 117* (1976) C4.
19. Durig, J. R., Chatterjee, K. K., Li, Y. S., Jalilian, M., Zozulin, A. J. and Odom, J. D. *J. Chem. Phys. 73* (1980) 21.
20. Hargittai, M., Hargittai, I. and Spiridonov, V. P. *J. Mol. Struct. 30* (1976) 31.
21. Carter, J. C., Jugie, G., Enjalbert, R. and Galy, J. *Inorg. Chem. 17* (1978) 1248.
22. Widler, J. G. *Thesis*, Universität Stuttgart, Stuttgart 1977 and *unpublished results.*
23. Durig, J. R. and Chatterjee, K. K. *J. Raman Spectrosc. 11* (1981) 168.

Received March 23, 1982.

Acta Chemica Scandinavica A 36 (1982) 813–818

The Crystal and Molecular Structure of 3,4-Dimethyl-1,6-diphenyl-1,2,5,6-tetra-aza-6a-thiapentalene

BJØRN BIRKNES and ASBJØRN HORDVIK

Department of Chemistry, Institute of Mathematical and Physical Sciences, University of Tromsø, Box 953, N–9001 Tromsø, Norway

Crystals of the title compound $C_{17}H_{16}N_4S$ are orthorhombic, space group *Pbca*, with unit cell dimensions $a=12.393(4)$ Å, $b=8.560(3)$ Å, $c=29.024(5)$ Å, and $Z=8$. The structure was solved by direct methods and refined by full-matrix least-squares.

The central ring system is almost planar with bond distances, N(1)–S(6a) = 1.895(4), N(6)–S(6a) = 1.873(4), N(1)–N(2) = 1.340(6), N(2)–C(3) = 1.330(6), C(3)–C(3a) = 1.398(6), C(3a)–S(6a) = 1.738(4), C(3a)–C(4) = 1.411(6), C(4)–N(5) = 1.351(6), and N(5)–N(6) = 1.329(5)Å; the N(1)–S(6a)–N(6) angle is 167.4(2)°.

The 1- and 6-phenyl groups are twisted 18 and 15° about the respective connecting bonds, and the N(1)–C(15)–C(18) and the N(6)–C(9)–C(12) sequences point slightly out to opposite sides of the central ring plane. The methyl carbons C(7) and and C(8) lie 0.09 and −0.13 Å off this plane.

The 1,6,6a-trithiapentalene system (Ia) has now been known for more than twenty years,[1] and its interesting structure has been thoroughly studied, *e.g.* by X-ray crystallography, electron diffraction, ESR, and ESCA, as well as by theoretical methods.[2–4]

Since the beginning of 1958 several new compounds, *e.g.* Ib–Id, analogous to Ia, have been synthesized,[5–10] and for a series of these the structures have been determined.[2]

The molecular structure of a compound which contains the ring system Ic, with A = S and X = N · Ar, has not been reported so far, and the present study of II was therefore carried out.

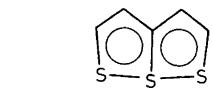

(Ia)

A	X
Se	Se, S
Se, S	O
Se, S	N·R

(Ib)

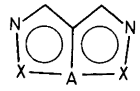

A	X
Se, S	N·Ar
Te, Se, S	O

(Ic)

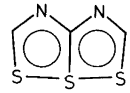

(Id)

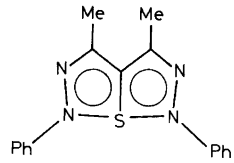

(II)

STRUCTURE ANALYSIS

Crystals of II were generously supplied by D.H. Reid.[10] The crystals are dark red.

0302-4377/82/100813-06$02.50

Table 1. Fractional atomic coordinates for compound II with temperature parameters U_{ij}(Å^2) for sulfur, nitrogen and carbon, and U(Å^2) for hydrogen. The expressions used are $\exp[-2\pi^2(h^2 a^{*2}U_{11} + \cdots 2hka^*b^*U_{12} + \cdots)]$ and $\exp[-8\pi^2 U(\sin^2\theta/\lambda^2]$, respectively. Standard deviations in parantheses.

Atom	x	y	z	U_{11}	U_{22}	U_{33}	U_{12}	U_{13}	U_{23}
S(6a)	0.23214(8)	0.17578(13)	0.12454(3)	.0509(6)	.0619(6)	.0587(6)	.0033(5)	−.0015(5)	−.0012(6)
N(1)	0.1179(3)	0.2534(4)	0.08778(12)	.0605(22)	.0636(24)	.0660(24)	.0037(19)	−.0032(19)	−.0010(20)
N(2)	0.1479(3)	0.3426(4)	0.05217(12)	.0704(24)	.0637(25)	.0608(22)	−.0020(20)	−.0032(19)	.0000(20)
N(5)	0.4523(3)	0.1590(4)	0.12770(13)	.0507(19)	.0645(24)	.0738(24)	−.0020(18)	.0048(18)	−.0054(21)
N(6)	0.3643(2)	0.1195(4)	0.15098(12)	.0461(19)	.0659(24)	.0624(21)	.0034(17)	.0000(17)	−.0050(18)
C(3)	0.2548(4)	0.3440(5)	0.04899(14)	.696(28)	.0587(27)	.0583(23)	.0003(23)	.0012(23)	−.0031(22)
C(3a)	0.3122(3)	0.2631(5)	0.08285(14)	.0636(26)	.0460(24)	.0599(26)	−.0016(21)	.0057(21)	−.0057(21)
C(4)	0.4237(3)	0.2414(5)	0.08998(16)	.0630(27)	.0557(28)	.0654(29)	−.0022(23)	.0031(23)	−.0055(23)
C(7)	0.3031(4)	0.4382(6)	0.01032(16)	.0950(35)	.0798(36)	.0735(30)	.0000(29)	.0095(27)	.0101(29)
C(8)	0.5136(4)	0.2933(6)	0.05872(17)	.0649(29)	.1006(41)	.0819(33)	−.0060(28)	.0108(26)	−.0017(30)
C(9)	0.3764(3)	0.0187(5)	0.19019(14)	.0496(22)	.0578(27)	.0586(25)	.0029(20)	−.0042(20)	−.0077(22)
C(10)	0.4729(3)	−0.0520(5)	0.20006(15)	.0508(24)	.0725(31)	.0709(28)	.0054(22)	.0021(22)	−.0013(26)
C(11)	0.4797(3)	−0.1522(6)	0.23767(17)	.0587(27)	.0910(37)	.0862(36)	.0134(27)	−.0026(26)	.0076(30)
C(12)	0.3909(4)	−0.1788(6)	0.26528(16)	.0700(29)	.0868(36)	.0717(30)	.0074(28)	.0001(25)	.0114(28)
C(13)	0.2953(3)	−0.1073(6)	0.25492(16)	.0566(26)	.0924(35)	.0705(29)	.0028(25)	.0048(23)	.0067(28)
C(14)	0.2873(3)	−0.0062(6)	0.21780(15)	.0472(24)	.0896(34)	.0661(27)	.0104(23)	−.0006(20)	.0025(26)
C(15)	0.0066(3)	0.2445(5)	0.09882(15)	.0595(26)	.0607(27)	.0573(26)	.0025(23)	−.0083(22)	−.0075(23)
C(16)	−0.0261(4)	0.1330(5)	0.12999(16)	.0665(29)	.0700(32)	.0818(33)	−.0025(24)	−.0120(25)	.0115(27)
C(17)	−0.1333(4)	0.1267(6)	0.14255(18)	.0685(32)	.0942(40)	.0799(32)	−.0081(29)	−.0091(26)	.0103(30)
C(18)	−0.2085(4)	0.2261(6)	0.12492(17)	.0616(29)	.0996(42)	.0781(32)	−.0029(27)	−.0002(27)	.0027(32)
C(19)	−0.1755(4)	0.3361(6)	0.09367(17)	.0610(29)	.0956(40)	.0782(32)	.0131(28)	−.0108(25)	−.0105(31)
C(20)	−0.0674(4)	0.3468(6)	0.08025(14)	.0675(28)	.0751(33)	.0582(27)	.0049(26)	−.0090(22)	−.0037(24)

Atom	x	y	z	U	Atom	x	y	z	U
H(10)	0.534(3)	−0.024(5)	0.1831(15)	.080(15)	H(19)	−0.230(4)	0.413(6)	0.0804(16)	.100(18)
H(11)	0.553(4)	−0.209(6)	0.2460(18)	.113(19)	H(20)	−0.040(3)	0.429(5)	0.0583(15)	.073(15)
H(12)	0.393(4)	−0.258(6)	0.2898(18)	.105(20)	H(71)	0.339(4)	0.358(7)	−0.0083(18)	.097(19)
H(13)	0.228(3)	−0.125(5)	0.2736(14)	.076(14)	H(72)	0.245(5)	0.484(7)	−0.0001(19)	.123(25)
H(14)	0.220(3)	0.043(4)	0.2106(12)	.055(11)	H(73)	0.356(4)	0.532(7)	0.0211(18)	.117(21)
H(16)	0.027(4)	0.061(6)	0.1422(18)	.105(19)	H(81)	0.513(3)	0.244(5)	0.0336(17)	.072(16)
H(17)	−0.153(4)	0.044(7)	0.1639(20)	.112(24)	H(82)	0.514(4)	0.418(7)	0.0561(19)	.123(24)
H(18)	−0.291(4)	0.223(5)	0.1338(16)	.093(17)	H(83)	0.585(4)	0.249(6)	0.0694(16)	.089(18)

CRYSTAL DATA

$C_{17}H_{16}N_4S$; F.W. = 308.40
Space group *Pbca*
$a = 12.393(4)$ Å, $b = 8.560(3)$ Å, $c = 29.024(5)$ Å
$V = 3079.0$ Å^3
$D_c = 1.330$ g/cm^3, D_m(flotation) = 1.34 g/cm^3
$Z = 8$
$\mu = 18.22$ cm^{-1} (Cu$K\alpha$)

All the X-ray measurements were carried out on a paper-tape controlled Siemens AED diffractometer using Cu$K\alpha$ radiation. The unit cell dimensions were determined from the 2θ values of high order reflections measured at room temperature, $t = 22$ °C, $\lambda\alpha_1 = 1.5404$ Å. A least-squares procedure gave the values quoted above.

The intensities were measured by means of the five-value scan technique.[11] Reflections for which the net count was greater than two times the respective standard deviations in the net count, were accepted as observed. With this criterion 2270 independent reflections within $\theta = 71°$ were accepted as observed. The data set comprises in addition the 696 unobserved reflections.

Lp corrections and absorption corrections[12] were applied. The dimensions of the crystal were $0.3 \times 0.5 \times 0.3$ mm in the three axial directions; a grid of $8 \times 16 \times 8$ points was used.

The scattering factors for sulfur, nitrogen and carbon were taken from *International Tables*.[13] For hydrogen, the scattering factor curve given by Stewart *et al.*[14] was used.

The structure was solved by a symbolic addition procedure programmed by Long.[15] Only parts of the molecule showed up in the *E*-map, but a subsequent *F*-map with signs calculated on the basis of these parts, showed all the nonhydrogen atoms. The positions of the phenyl hydrogens were calculated, and the positions of the methyl hydrogens were found from a difference map. The atomic parameters were refined by full-matrix least-squares (see for example Ref. 16) to an R of 0.070.

Final atomic coordinates and temperature parameters are listed in Table 1. The final structure factor list is available on request.

Rigid body analysis has been carried out according to the method of Schomaker and Trueblood.[17] In this analysis the central ring system plus C(7), C(8), C(9) and C(15), *cf.* Fig. 1, were regarded as a rigid body. The corrections in bond lengths due to libration are small, less than the corresponding standard deviations, *cf.* Table 2. The corrections have been carried out according to the method of Cruickshank.[18]

The calculations mentioned above were carried out on an IBM 360/50H computer. The programs,

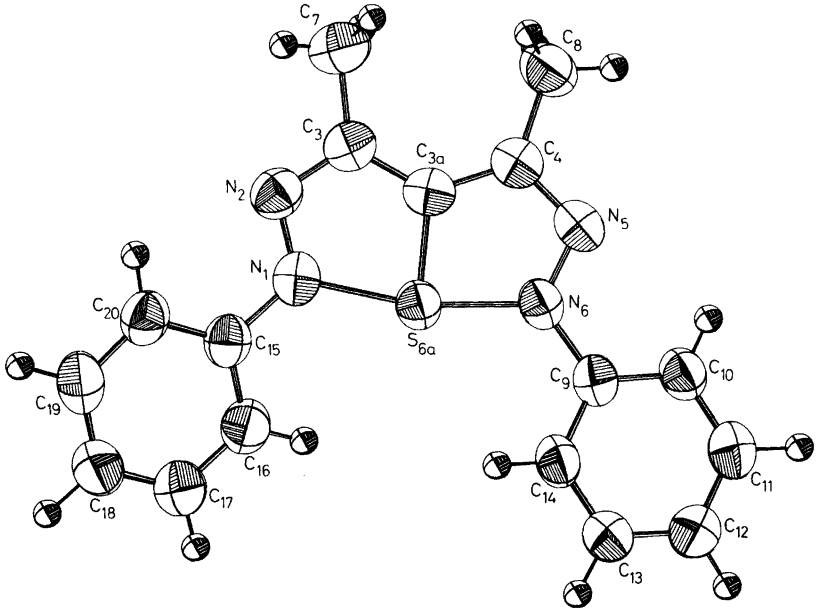

Fig. 1. The molecular structure of compound II with numbering of atoms. ORTEP[20] drawing.

Table 2. Bond lengths $l(jk)$ and $l'(jk)$, bond angles $\angle(ijk)$, and deviations Δ from least-squares plane for compound II. Standard deviations in parentheses. The bond lengths $l'(jk)$ have been corrected for libration. The deviations for atoms which are included in the least-squares plane calculations are printed in italics.

Atoms			Bond lengths (Å)		Bond angles (°)	Plane deviations (Å)	
i	*j*	*k*	*l*(*jk*)	*l'*(*jk*)	∠(*ijk*)	Δ*j*	Δ*k*
N(1)	S(6a)	N(6)			167.4(2)	*−.001*	
C(3a)	S(6a)	N(1)	1.893(4)	1.895	83.3(2)		
C(3a)	S(6a)	N(6)	1.872(4)	1.873	84.0(2)		
S(6a)	N(1)	N(2)	1.338(6)	1.340	115.3(3)	*−.050*	
N(2)	N(1)	C(15)	1.418(6)	1.421	118.5(3)		
S(6a)	N(1)	C(15)			125.5(3)		
N(1)	N(2)	C(3)	1.328(6)	1.330	109.6(3)	*.037*	
N(2)	C(3)	C(3a)	1.397(6)	1.398	117.1(4)	*.023*	
N(2)	C(3)	C(7)	1.506(9)	1.510	117.2(4)		
C(3a)	C(3)	C(7)			125.7(5)		.088
C(3)	C(3a)	C(4)	1.410(6)	1.411	131.8(4)	*−.011*	
C(3)	C(3a)	S(6a)	1.734(4)	1.738	114.4(3)		
S(6a)	C(3a)	C(4)			113.8(3)		
C(3a)	C(4)	N(5)	1.350(6)	1.351	116.3(4)	*−.028*	
C(3a)	C(4)	C(8)	1.504(9)	1.508	126.9(4)		−.132
C(8)	C(4)	N(5)			116.8(4)		
C(4)	N(5)	N(6)	1.327(5)	1.329	109.4(3)	*−.016*	
N(5)	N(6)	S(6a)			116.3(3)	*.044*	
N(5)	N(6)	C(9)	1.436(6)	1.438	118.2(3)		
S(6a)	N(6)	C(9)			124.8(2)		
N(6)	C(9)	C(10)			121.6(4)		
N(6)	C(9)	C(14)			118.1(3)		
C(14)	C(9)	C(10)			120.3(4)	−.060	
C(9)	C(10)	C(11)	1.388(8)		119.6(4)	−.394	
C(10)	C(11)	C(12)	1.379(8)		120.5(5)	−.511	
C(11)	C(12)	C(13)	1.370(8)		119.3(5)	−.287	
C(12)	C(13)	C(14)	1.385(8)		120.8(4)	.038	
C(13)	C(14)	C(9)	1.380(6)		119.5(4)	.174	
C(16)	C(15)	N(1)			118.3(4)		
N(1)	C(15)	C(20)			121.6(4)		
C(20)	C(15)	C(16)	1.375(7)		120.1(4)	.034	
C(15)	C(16)	C(17)	1.379(8)		119.0(5)	−.284	
C(16)	C(17)	C(18)	1.358(8)		122.7(5)	−.156	
C(17)	C(18)	C(19)	1.374(9)		118.0(5)	.261	
C(18)	C(19)	C(20)	1.398(7)		121.1(5)	.567	
C(19)	C(20)	C(15)	1.379(7)		119.1(4)	.457	

with some exceptions, originate from the Weizmann Institute of Science, Rehovoth, Israel, and have been modified for the 360 by D. Rabinovich, L. M. Milje, K. Maartmann-Moe and K. Åse.

DISCUSSION

The molecular structure of compound II as found in the present study is shown in Fig. 1. Bond lengths and angles with standard deviations, calculated from the values in Table 1, are listed in Table 2. A more realistic estimate of the standard deviations might probably be obtained by multiplying those given by a factor of two.[19]

Deviations of atoms from a least-squares plane through the atoms of the central rings are given in Table 2. Weights equal to atomic weights were used in this calculation. One notes from Table 2 that the central ring system is nearly planar and that the N(1)−C(15)−C(18) and the N(6)−C(9)−C(12) sequences point slightly out to opposite sides of this

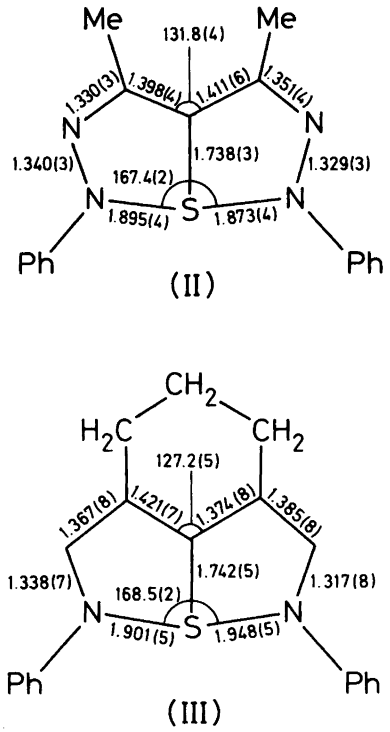

Fig. 2. Bond lengths (Å) and angles (°) in the central ring system of the present compound (II) and it the central ring system of 1,6-diphenyl-3,4-trimethylene-1,6-diaza-6a-thiapentalene (III).

plane. The methyl carbons C(7) and C(8) lie 0.09 and −0.13 Å, respectively, off the plane of the central rings.

The 1- and 6-phenyl groups are twisted 18 and 15° about the respective connection bonds, *cf.* Fig. 3. The twist angle about N(1)−C(15) was taken as the angle between the normal to the least-squares plane through C(15), N(1), N(2) and S(6a) and the normal to the least-squares plane through C(20, C(16), C(15) and N(1); the twist about N(6)−C(9) was calculated similarly.

Calculations show that the environments of N(1) and N(6) are slightly pyramidal. Thus, N(1) lies −0.051 Å out from the plane through C(15), N(2), and S(6a), and N(6) lies 0.072 Å off the plane through C(9), N(5) and S(6a).

A comparison of bond lengths and angles in the central ring system of the present compound with bond lengths and angles in the central ring system of 1,6-diphenyl-3,4-trimethylene-1,6-diaza-6a-thiapentalene (III)[21] is given in Fig. 2. One notes that the sum of the N−S distances is 3.768 Å in II and 3.849 Å in III; the difference of 0.081 Å is significant. It should be mentioned in this connection that the difference between the sum of S−S bond lengths in 2,5-diphenyl-1,6,6a-trithiapentalene,[22] 4.666 Å, and the sum of S−S bond lengths in 2,5-diphenyl-3,4-dimethyl-1,6,6a-trithiapentalene,[23] 4.606 Å, is 0.060 Å, and this difference as well as that mentioned above should be seen in relation to the repulsion

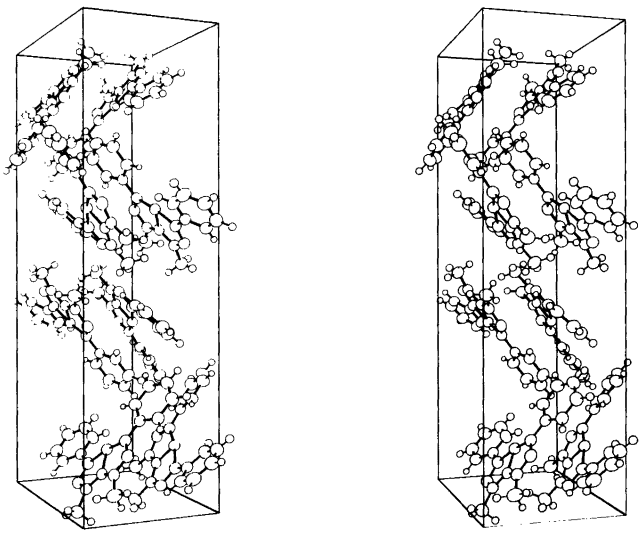

Fig. 3. A stereoscopic view of the crystal structure of compound II in *a*-axis direction.

between the methyl groups in 3- and 4-positions. A discussion of this effect has recently been reported.[24]

The lengths of other bonds in II are normal. Apart from the N–S bonds one notes that the double bond characters of equivalent bonds in the central ring systems of molecules II and III agree within the experimental error.

A stereoscopic view of the molecular packing in the unit cell is given in Fig. 3. There are no intermolecular contacts shorter than corresponding van der Waals distances.

REFERENCES

1. Bezzi, S., Mammi, M. and Garbuglio, C. *Nature 182* (1958) 247.
2. Hansen, L. K., Hordvik, A. and Sæthre, L. J. In Stirling, C. J. M., Ed., *Organic Sulphur Chemistry*, Butterworth, London 1975.
3. Gleiter, R. and Gygax, R. *Topics in Current Chemistry*, Springer, Berlin 1976, Vol. 63, p. 49.
4. Pedersen, C. Th. *Sulfur Reports*, Hardwood, New York 1980, Vol. 1. p. 1.
5. Klingsberg, E. *Q. Rev. Chem. Soc. 23* (1969) 537.
6. Lozac'h, N. *Adv. Heterocycl. Chem. 13* (1971) 161.
7. Reid, D. H. *Organic Compounds of Sulphur, Selenium and Tellurium*, Specialist Periodical Reports, Chem. Soc., Letchworth 1970, Vol. 1, p. 321.
8. a. Beer, R. J. S. *Organic Compounds of Sulphur, Selenium and Tellurium*, Specialist Periodical Reports, Chem. Soc., Letchworth 1973, Vol. 2, p. 497; b. *Ibid.* 1975, Vol. 3, p. 494; c. *Ibid.* 1977, Vol. 4, p. 300.
9. Leaver, D. *Organic Compounds of Sulphur, Selenium and Tellurium*, Specialist Periodical Reports, Chem. Soc., Letchworth 1979, Vol. 5, p. 306.
10. Christie, R. M., Reid, D. H., Walker, R. and Webster, R. G. *J. Chem. Soc. Faraday Trans. 1* (1978) 195.
11. Throughton, P. G. H. *Fourth Special Issue: X-Ray and Electron Microscopy News, Siemens Rev. XXXVII* (1970).
12. Coppens, P., Leiserowitz, L. and Rabinovich, D. *Acta Crystallogr. 18* (1965) 1035.
13. *International Tables for X-Ray Crystallography*, Kynoch Press, Birmingham 1968, Vol. 3, p. 202.
14. Stewart, R. F., Davidson, E. R. and Simpson, W. T. J. *Chem. Phys. 42* (1965) 3175.
15. Long, R. E. *Dissertation*, University of California, Los Angeles 1965.
16. Hordvik, A. and Sæthre, L. J. *Acta Chem. Scand. 26* (1972) 3114.
17. Schomaker, V. and Trueblood, K. N. *Acta Crystallogr. B 24* (1968) 63.
18. Cruickshank, D. W. J. *Acta Crystallogr. 9* (1956) 757; *Ibid. 14* (1961) 896.
19. Hamilton, W. C. and Abrahams, S. C. *Acta Crystallogr. A 26* (1970) 18.
20. Johnson, C. K. ORTEP-II: *A Fortran Thermal Ellipsoid Plot Program For Crystal Structure Illustrations*, Report ORNL-3794, Oak Ridge National Laboratory, Oak Ridge 1971.
21. Hordvik, A. and Julshamn, K. *Acta Chem. Scand. 26* (1972) 343.
22. Hordvik, A. *Acta Chem. Scand. 25* (1971) 2507.
23. Hordvik, A., Sjølset, O. and Sæthre, L. J. *Acta Chem. Scand. 27* (1973) 379.
24. Birknes, B., Hordvik, A. and Sæthre, L. J. *Acta Chem. Scand. A 36* (1982) 683.

Received March 11, 1982.

Acta Chemica Scandinavica A 36 (1982) 819–824

Metal Complexes with Mixed Ligands. 25. Complex Formation in the Ag(I) – Tris(hydroxymethyl)aminomethane – OH^- System in 3.0 M (Na)ClO_4 Medium

INGER GRANBERG, WILLIS FORSLING and STAFFAN SJÖBERG

Department of Inorganic Chemistry, University of Umeå, S-901 87 Umeå, Sweden

Three-component equilibria between silver(I), tris(hydroxymethyl)aminomethane ($H_2NC(CH_2OH)_3$, L, THAM) and OH^- were studied by means of emf titrations at 25 °C in an ionic medium of 3.0 M (Na)ClO_4. In the measurements, glass as well as Ag,AgCl electrodes were employed. The total concentrations of silver(I), B, and HL^+, C, were varied within the limits $0.002 \leq B \leq 0.08$ M and $0.005 \leq C \leq 0.160$ M, respectively, and the ratio C/B between $0.5 \leq C/B \leq 12$. With $C/B > 4$ data could be explained with the complexes AgL^+ and AgL_2^+ with $\log \beta_1 = 3.406 \pm 0.002$ and $\log \beta_2 = 7.198 \pm 0.002$. At low ratios of C/B, a ternary hydroxy THAM complex, AgOHL with $\log K$ ($Ag^+ + L + H_2O \rightleftarrows AgOHL + H^+$) $= -6.40 \pm 0.05$, is formed. Data have been analyzed with the least-squares computer program LETAGROPVRID.

The ability of different metal – imidazole complexes to form ternary species with the ligands OH^- and Cl^- has been demonstrated in preceding papers of this series.[1-5] The results have clearly shown that the ternary $Me^{z+} - L - X^-$ complexes ($Me^{z+} = Co^{2+}$,[1] Ni^{2+}, Cu^{2+},[3] Zn^{2+},[2] Cd^{2+},[4] Hg^{2+},[3] Ag^+,[5] $X^- = OH^-$, Cl^-) are of greater stability than the corresponding $Me^{z+} - X^-$ complexes. These findings indicate that coordinated imidazole ligands enhance the affinity for the anions Cl^- and OH^-. An explanation for this behaviour is given by Sigel,[6] who claims that the high stability of ternary metal complexes with aromatic nitrogen containing ligands is mainly caused by back-donation from the metal ion into the unsaturated π-orbitals of the ligands which lowers the electron concentration near the central ion.

0302-4377/82/100819-06$02.50

As a test of this hypothesis, Forsling[7] exchanged imidazole for the aliphatic *N*-ligand tris(hydroxymethyl)aminomethane (TRIS or THAM, L) and complexation in the nickel(II) system was investigated. It was found that THAM forms a proton series of tetrameric hydroxy complexes, *viz.* $Ni_4(OH)_4(L)_4^{4+}$, $Ni_4(OH)_4(L)_3(H_{-1}L)^{3+}$ and $Ni_4(OH)_4(L)_2(H_{-1}L)_2^{2+}$ as well as the trimer $Ni_3(OH)_3(L)_2^{3+}$. All these ternary species were found to predominate in slightly alkaline solutions (pH 7–9). It was also concluded that THAM as ligand enhances the affinity for OH^- as second ligand; however, a direct comparison with the corresponding imidazole system could not be made as no ternary polynuclear hydroxy complex was formed in this system.

The aim of the present investigation is to interpret complexation in the $Ag^+ - THAM - OH^-$ system, with special reference to the formation of probable ternary hydroxy complexes and compare the results with those corresponding to the imidazole system.

EXPERIMENTAL

Chemicals and analysis. Tris(hydroxymethyl)-aminomethane, L, $H_2NC(CH_2OH)_3$ (SIGMA, reagent grade) was used without further purification after drying at 80 °C. Stock solutions of HL^+ were prepared by dissolving a weighed amount of L in excess of standardized $HClO_4$. The total concentrations of HL^+, C, were determined potentiometrically and were found to agree within 0.2% with the amounts weighed. Stock solutions of *sodium perchlorate* and *silver perchlorate* as well as the dilute *perchloric acid* and the *sodium hydroxide* were prepared and standardized as earlier.[5]

Apparatus. The cell arrangement and the experimental details of the emf measurements have been described earlier.[5]

Electrodes. Ag, AgCl electrodes were prepared and tested as described earlier.[5] Glass electrodes (Ingold type 201-NS) were tested against the hydrogen electrode and were found to give a constant and reproducible potential with $-\log[H^+] \lesssim 9.1$.

Method. The present investigation has been carried out as a series of titrations in which both $[H^+]$, h and $[Ag^+]$, b were measured using a glass electrode and an Ag,AgCl electrode, respectively.

The total concentrations of Ag^+, B and HL^+, C, were varied within the limits $0.002 \leq B \leq 0.040$ M and $0.005 \leq C \leq 0.160$ M. h and b were varied by adding hydroxide or hydrogen ions. For quotients $C/B \leq 2.5$, the available $-\log h$ range was restricted due to the formation of a precipitate. With $C/B > 2.5$, no precipitates were observed and the titrations could be continued as long as the glass electrode functioned properly ($-\log h < 9.1$). In general, most of the titrations were performed at constant C/B ratio, and the following were studied: 0.5, 1, 1.5, 2, 2.5, 3, 4, 6, 8 and 12.

The reproducibility and reversibility of equilibria were tested by performing both forward (increasing $-\log h$) and backward (decreasing $-\log h$) titrations. As a test of the reversibility, dilution experiments at different C/B ratios and at constant Z values were performed (Z is defined as $(h-H)/B$).

h and b were determined by measuring the emf of the cell (1), where ME denotes the measuring electrode (glass electrode and Ag,AgCl electrode)

$$-\text{RE}\|\text{equilibrium solution}|\text{ME}+ \quad (1)$$

and RE denotes Ag,AgCl|0.01 M Ag^+, 2.99 M Na^+, 3.00 M ClO_4^-||3.00 M $NaClO_4$.

Assuming the activity coefficients to be constant, the expressions (2a) and (2b) are valid for the measured emf. E_{OH} and E_{OB} are constants determined in acidic (H^+, Ag^+, HL^+) solutions of known composition, where complex formation can be neglected ($-\log h \leq 3$).

$$E_H = E_{OH} + 59.16 \log h + E_j \quad (2a)$$

$$E_B = E_{OB} + 59.16 \log b + E_j \quad (2b)$$

It has been found that E_{OH} is dependent on the Ag^+, b, HL^+, c and L ($k_a ch^{-1}$) contents. Investigations show that the change in E_{OH}, due to changes in b, c and $ck_a h^{-1}$ could be described by the linear function (3), where $\Delta E_{Ag} = 2.0 \pm 0.1$ mV M^{-1}, $\Delta E_{HL}{}^2 = 5.3$ mV M^{-1} and $\Delta E_L{}^2 = 8.7$ mV M^{-1}. The magnitude of ΔE_{OH} caused by concentration changes during the titrations used in the final calculations, was estimated. ΔE_{OH} did not exceed 0.1 mV, which will hardly cause any changes in the equilibrium model.

$$\Delta E_{OH} = \Delta E_{Ag}\Delta b + \Delta E_{HL}\Delta c + \Delta E_L \Delta(ck_a h^{-1}) \quad (3)$$

Data treatment. We will assume the presence of three component equilibria of the general type (4) together with the two component equilibria (5) and (6).

$$pH^+ + qAg^+ + r\,HL^+ \rightleftarrows (H^+)_p(Ag^+)_q(HL^+)_r;\ \beta_{pqr} \quad (4)$$

$$HL^+ \rightleftarrows L + H^+;\ k_a \quad (5)$$

$$pH^+ + q\,Ag^+ \rightleftarrows (H^+)_p(Ag^+)_q;\ \beta_{pqo} \quad (6)$$

For reaction (5) Forsling [7] reported $\log(k_a \pm 3\sigma) = -8.646 \pm 0.002$. For reaction (6) two complexes have been reported. Biedermann and Hietanen [8] found the complex AgOH to predominate at high B (1 M $AgNO_3$) giving $\log \beta_{-110} \lesssim -11.1$. At low B (< 1 mM in 3 M $NaClO_4$) Antikainen and Dyrssen [9] found $Ag(OH)_2^-$ to be the main hydrolytic species with $\log \beta_{-210} = -24.84$.

These results on the two-component equilibria will be considered as known in the following and no attempts will be made to adjust their equilibrium constants.

The search for a model (pqr) and corresponding equilibrium constants β_{pqr} that give the best fit to experimental data was carried out using the least-squares computer program LETAGROPVRID [10] (version ETITR).[11]

The different standard deviations given were defined and calculated according to Sillén.[12] The computations were performed on a CD 6600 computer.

CALCULATIONS AND RESULTS

The analysis of data was started by making $\bar{n}(\log[L])$, (E_H-data) and $\eta(\log[L])$, [($E_B + E_H$)-data] plots which are given in Fig. 1 and Fig. 2, where $\bar{n}$ and η are defined as in Ref. 5. According to these figures, $\bar{n}$ as well as η seem to be independent of B and C for quotients > 4, thus indicating formation of a series of mononuclear complexes AgL_n^+. Data fulfilling these conditions will be denoted Data 1. However, with $C/B \leq 4$ and $B \leq 0.010$ M, systematic deviations from the mononuclear $\bar{n}$ as well as η curves were observed, which implies that additional species are formed. These data will be treated separately and denoted as Data 2. In the

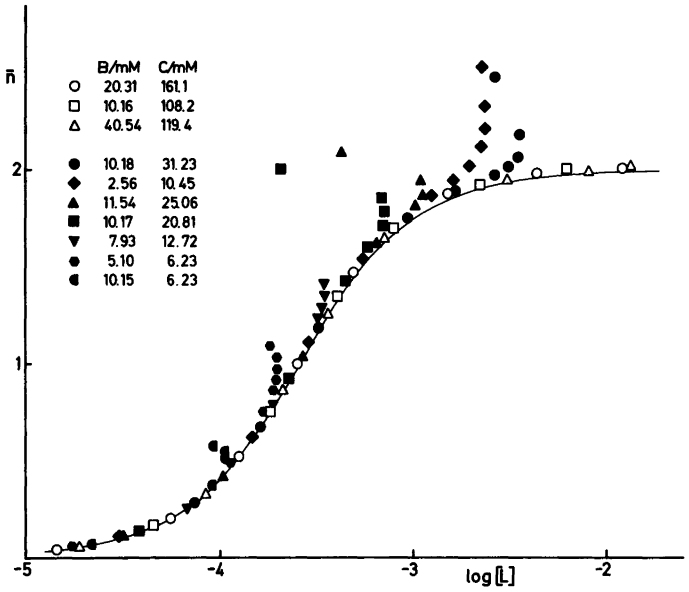

Fig. 1. Experimental data plotted as curves $\bar{n}$ log[L]. In order to make the figure clear, only a few titrations have been plotted. The full drawn curve has been calculated with the proposed constants for AgL^+ and AgL_2^+.

LETAGROP calculations different data sets were used (*cf.* Table 2). This procedure enabled us to compare results obtained from the different calculations and thus to obtain information about the reliability of the different electrodes as well as of eventual errors in the analytical concentrations.

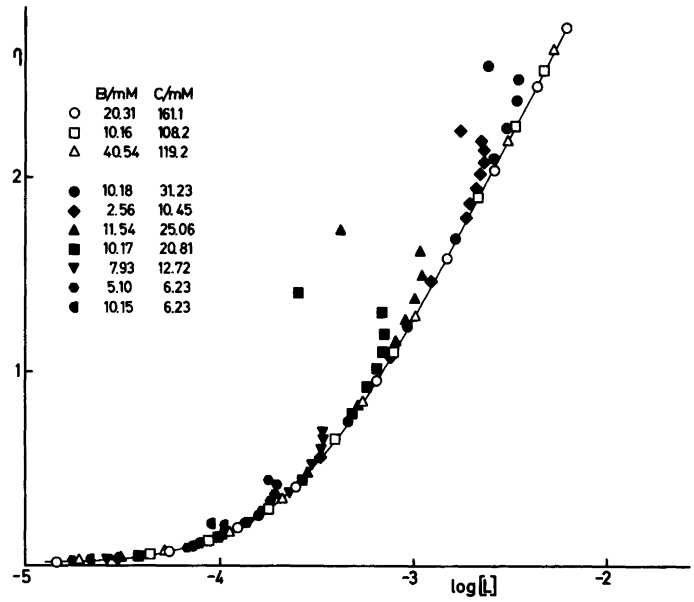

Fig. 2. Experimental data plotted as curves η log[L].

Data 1. A LETAGROP analysis showed that E_H, E_B as well as E_H+E_B data could be well explained with the complexes AgL^+ and AgL_2^+. Details of these calculations are given in Table 1. According to this table the agreement in $\beta_{-1,1,1}$ and $\beta_{-2,1,2}$, independent of data sets or minimizing function, is very good, the spread being less than 0.023 and 0.012 logarithmic units, respectively.

The values, $\log \beta_{-111} = -5.242 \pm 0.002$ and $\log \beta_{-212} = -10.102 \pm 0.002$, obtained from calculations on the combined E_H+E_B data, are considered as the most reliable ones and are final proposals.

Data 2. In the search for the ternary species, it was assumed that the formation constants for the species AgL^+ and AgL_2^+ had the values proposed above. Furthermore, formation constants for the hydrolytic species AgOH and $Ag(OH)_2^-$ were those given by Biedermann and Dyrssen, respectively. The analysis of Data 2 was started with a *pqr* analysis of the residuals at $C/B<4$, *i.e.* a systematic trial and error procedure which tests complexes with different composition $(H^+)_p(Ag^+)_q(HL^+)_r$ one by one. The test was carried out with a representative part of data including 16 titrations and 216 experimental points. The result of the analysis is shown in Fig. 3. It is seen from these data that the lowest error squares sum is obtained for the complex $(H^+)_{-2}(Ag^+)_1(HL^+)_1$ with $\log \beta_{-2,1,1} = -15.05 \pm 0.05$ giving $\sigma(E_B)$ is somewhat higher than one could expect from the calculations with Data 1 and depends largely on a systematic deviation at pH 8.5. This deviation did not exceed 0.5 mV and a covariation of β_{-212} with β_{-211} explained the systematic deviations by changing the formation constants for AgL_2^+ by 0.006 in $\log \beta_{-2,1,2}$ (*cf.* Table 1). The formation constant for the complex $(H^+)_{-2}(Ag^+)_1(HL^+)_1$ was found to be $\log \beta_{-2,1,1} = -15.14 \pm 0.06$ giving $\sigma(E_B) = 0.20$ mV. As the ternary complex is formed in slightly alkaline solution ($-\log h \gtrsim 9$) supplementary measurements were performed where the $-\log h$ range was extended to $-\log h \lesssim 10.5$. As the glass electrode provides too uncertain data to be of any use within this range, only E_B data were treated and the result of a calculation on these is also given in Table 1. As can be seen, β_{-211} was in very good agreement with that obtained from E_H+E_B data at a lower $-\log h$ range ($\log \beta_{-211} = -15.07 \pm 0.05$, $\sigma(B) = 0.04$ mM.

Although this ternary complex is formed in small amounts (*cf.* Fig. 4), there is consistency in E_H as well as E_B data, which makes the evaluated equilibrium model trustworthy.

DISCUSSION

The present investigation of the silver(I) – THAM $-OH^-$ system was carried out by measuring two free concentrations, h and b. In the LETAGROP calculations one of the quantities h, b, H or B was excluded, thus yielding four different types of data

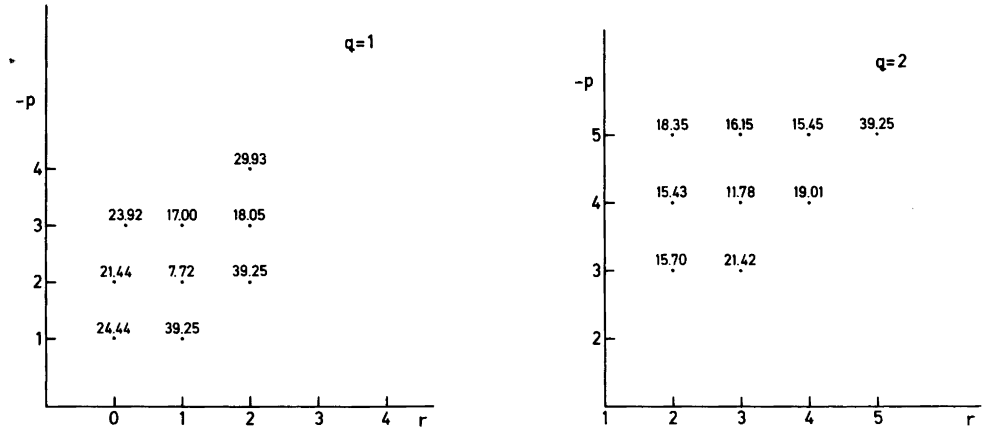

Fig. 3. LETAGROP search for ternary $H_pAg_q(HL)_r^{(p+q+r)+}$ complexes. The diagram gives error square sums $U(pr)_q$, where $U = \Sigma(E_{BCALC} - E_{BEXP})$ assuming only one complex. In the calculation the hydrolytic species and the binary species AgL^+ and AgL_2^+ have been assumed to be known. The calculation is based on 216 experimental points, chosen to cover as great concentration ranges as possible.

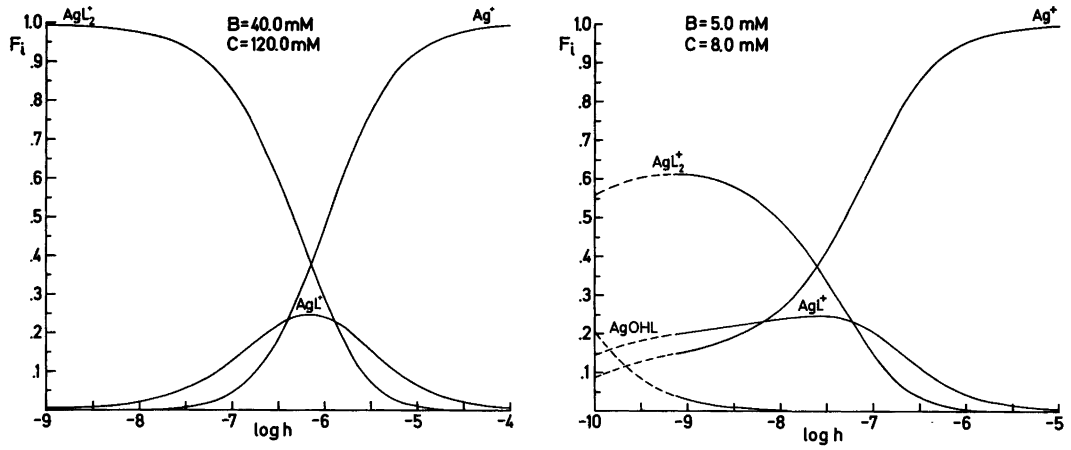

Fig. 4. Distribution diagrams $F_i(\log h)_{BC}$. F_i is defined as the ratio between silver(I) in the species and the total silver(I). The computer program SOLGASWATER [19] was used for the calculations with the set of proposed constants. Broken lines denote ranges where no measurements have been performed due to precipitation (extrapolated range).

sets (*cf.* Table 1).* Results of these calculations have shown that the agreement in the evaluated formation constants was good, which is an indication that systematic or occasional errors in H and B as well as h and b are negligible.

*A complete list of the experimental data is available from this department.

The calculations gave clear evidence for the existence of a ternary complex $H_{-1}AgL$, besides the two binary complexes AgL^+ and AgL_2^+. There was no indication for the existence of any polynuclear species. The ternary complex $H_{-1}AgL$ is formed in small amounts ($\sim 4\%$ of B) at low C/B ratios (≤ 4). It is not possible from the potentiometric data to deduce whether this is a hydroxy complex Ag(OH)L

Table 1. Results of LETAGROP calculations on different data sets. The formation constants β_{pqr} are defined according to the equilibria $pH^+ + q\,Ag^+ + r\,HL^+ \rightleftarrows H_pAg_q(HL)_r^{(p+q+r)+}$. The errors 3σ ($\log \beta_{pqr}$) are given when the corresponding equilibrium constant has been varied.

Data	Number of titr./number of points	AgL^+ $\log(\beta_{-111} \pm 3\sigma)$	AgL_2^+ $\log(\beta_{-212} \pm 3\sigma)$	AgOHL $\log(\beta_{-211} \pm 3\sigma)$	σ(Y)	Data set used
E_H	17/226	−5.233 ±0.004	−10.094 ± 0.002		0.033[a]	*h*, *H*, *B*, *C*
E_B	17/226	−5.256 ±0.004	−10.106 ± 0.007		0.024[b]	*b*, *H*, *B*, *C*
E_H+E_B	17/226	−5.231 ±0.004	−10.100 ± 0.002		0.037[a]	*h*, *b*, *H*, *C*
E_H+E_B	17/226	−5.242 ±0.002	−10.102 ± 0.002		0.063[c]	*h*, *b*, *B*, *C*
E_H+E_B	19/250	−5.242	−10.102	−15.05 ± 0.05	0.24[c]	*h*, *b*, *B*, *C*[d]
E_H+E_B	19/250	−5.242	−10.096 ± 0.002	−15.14 ± 0.06	0.20[c]	*h*, *b*, *B*, *C*
E_B	20/252	−5.242	−10.111 ± 0.008	−15.07 ± 0.05	0.042[b]	*b*, *H*, *B*, *C*

[a] $Y = H_{CALC} - H_{EXP}$/mM. [b] $Y = B_{CALC} - B_{EXP}$/mM. [c] $Y = E_{B\ CALC} - E_{B\ EXP}$/mV. [d] Proposed constants.

or a complex where THAM acts as a chelate, $Ag(H_{-1}L)$.

Due to steric reasons the first alternative is most likely. Furthermore, if one of the hydroxy groups in the THAM molecule loses one proton and the ligand acts as a chelate, it must be reflected in the magnitude of the corresponding stability constant. In an investigation of the $Cu^{2+}-THAM-OH^-$ system, Bai and Martell[13] found a series of ternary complexes, *e.g.* $Cu(H_{-1}L)^+$, $Cu(H_{-1}L)L^+$, $Cu(H_{-1}L)_2$ and $Cu_2(H_{-1}L)_2^{2+}$. According to a structure determination[14] of the complex $Cu(H_{-1}L)_2$, L acts as a bidentate chelate through the amino group and one of the OH groups. This behaviour was assumed to be likely for the other ternary species as well. By considering the equilibria

$$CuL^{2+} \rightleftarrows Cu(H_{-1}L)^+ + H^+$$

Bai and Martell found $\log K_a(CuL^{2+}) = -6.0$, which can be compared with the values $\log K_a(Cu^{2+}) = -8.0$[15] and $\log K_a(Cu(imidazole)^{2+}) = -7.2$.[3] This means that the chelate complex $Cu(H_{-1}L)^+$ is more stable than the hydroxy species $CuOH^+$ and $Cu(imidazole)OH^+$.

If a similar interpretation is made in the $Ag^+-THAM-OH^-$ system, $\log K_a(AgL^+) = -9.88$ indicates that this complex is a mixed hydroxy species, as $\log k_a(Ag\ imidazole^+) = -8.11$ and $\log K_a(Ag^+) \lesssim -11.1$.

If we compare the acidity constants for the ternary complexes with AgL^+ and OH^- we find that all complexes between silver and an aliphatic nitrogen compound give an acidity constant somewhat stronger than the corresponding value for the hydrated silver ion. This is valid for the complex AgL^+, where L stands for THAM, ethylenediamine,[16] 1,2-propanediamine,[16] 1,3-propanediamine[17] and 1,4-butanediamine[17] with the acidity constants $\log k_a = -9.9$, -10.0, -9.6, -10.1 and -10.8 respectively. The corresponding complex with an aromatic amine such as imidazole[4] differs from those mentioned above with $\log k_a = -8.11$, which confirms the hypothesis that mixed hydroxy complexes with aromatic *N*-ligands are more stable than corresponding species with aliphatic *N*-ligands. Furthermore, the presence of an aliphatic *N*-ligand seems to enhance the affinity for OH^- compared with the hydrated silver ion. Forsling found similar behaviour for polynuclear mixed complexes in the $Ni^{2+}-THAM-OH^-$ system, while Sigel[18] reported the opposite tendency for $M-THAM-ATP$ where M stands for (Co^{2+}, Ni^{2+}, Cu^{2+}, Zn^{2+}, Cd^{2+}, Pb^{2+}) and ATP stands for Adenosine 5′-Tri-phosphate). This is an indication that the size of the oxygen donor is important for the formation of ternary mixed complexes, due to steric hindrance.

The present investigation has also given further evidence for the compositional connection between the binary metal hydrolysis and the ternary hydrolytic species (*cf.* AgOH and AgOHL).

Acknowledgements. We thank Professor Nils Ingri for much valuable advice, for his great interest and for all the facilities placed at our disposal. The English of the present paper has been corrected by Dr. Michael Sharp. The work forms a part of a program financially supported by the Swedish Natural Science Research Council.

REFERENCES

1. Forsling, W., Granberg, I. and Sjöberg, S. *Acta Chem. Scand. A 35* (1981) 473.
2. Forsling, W. *Thesis*, Umeå, Sweden 1978.
3. Sjöberg, S. *Thesis*, Umeå, Sweden 1976.
4. Granberg, I. and Sjöberg, S. *Acta Chem. Scand. A 35* (1981) 193.
5. Granberg, I. and Sjöberg, S. *Acta Chem. Scand. A 33* (1979) 531.
6. Sigel, H. *Inorg. Chem. 19* (1980) 1411.
7. Forsling, W. *Acta Chem. Scand. A 32* (1978) 857.
8. Biederman, G. and Hietanen, S. *Acta Chem. Scand. 14* (1960) 711.
9. Antikainen, P. J. and Dyrssen, D. *Acta Chem. Scand. 14* (1960) 86.
10. Ingri, N. and Sillén, L. G. *Ark. Kemi 23* (1964) 97.
11. Arnek, R., Sillén, L. G. and Wahlberg, O. *Ark. Kemi 31* (1969) 353; Brauner, P., Sillén, L. G. and Whiteker, R. *Ark. Kemi 31* (1969) 365.
12. Sillén, L. G. *Acta Chem. Scand. 16* (1962) 159; Sillén, L. G. and Warnqvist, B. *Ark. Kemi 31* (1969) 341.
13. Bai, K. S. and Martell, A. E. *J. Inorg. Nucl. Chem. 31* (1969) 1697.
14. Ivarsson, G. *To be published.*
15. Berecki-Biedermann, C. *Ark. Kemi 9* (1956) 175.
16. Ohtaki, H. and Ito, Y. *J. Coord. Chem. 3* (1973) 131.
17. Ohtaki, H. and Cho, K. *Bull. Chem. Soc. Jpn. 50* (1977) 2764.
18. Fischer, B. E., Häring, U. K., Tribolet, R. and Sigel, H. *Eur. J. Biochem. 94* (1979) 523.
19. Eriksson, G. *Anal. Chim. Acta 112* (1979) 375.

Received March 22, 1982.

Acta Chemica Scandinavica A 36 (1982) 825–827

Structure of an Unsymmetrical Tetradentate Schiff Base Complex of Copper(II) as Obtained from UV Absorption and Circular Dichroism Spectra

HANS PETER JENSEN

Chemistry Department A, Building 207, Technical University of Denmark, DK-2800 Lyngby, Denmark

Absorption and circular dichroism spectra from the copper(II) complex of the Schiff base derivative from (*R*)-1,2-propanediamine, one molecule of acetylacetone and one molecule of salicylaldehyde, have been studied. The results are interpreted by means of exciton theory in order to give stereochemical information about configurational deviations from square-planar complexation of copper(II) ions.

Through the use of exciton theory the molecular structure of various optically active Schiff bases of β-diketones and diamines, together with their transition metal complexes, have been studied extensively. As far as Schiff base derivatives of acetylacetone are concerned, the theoretical framework for a treatment within an exciton formalism was given by Larsen.[1] The $\pi\rightarrow\pi^*$ transitions, expected to be polarized in the N–O direction of the planar en-amine chromophores, may at small distances split due to a purely coulombic interaction. In the case of optically active compounds, such couplets exhibit Cotton effects (CD-bands) of numerically equal rotatory strengths, but of opposite signs. Since the absolute configuration of the rigid compound $(-)_D$-(*R*,*R*)-*trans*-1,2-cyclohexanediamine (*R*-chxn) is known, the characteristic circular dichroism envelope of the Schiff base derivative of this diamine with acetylacetone [*R*-chxn(acacH)$_2$] has been used in the correlation of molecular structures of similar compounds.[2–5]

Bosnich attacked the interpretation of circular dichroism spectra from optically active Schiff base derivatives of salicylaldehyde and their transition metal complexes in a similar fashion.[6] The CD spectrum of *N*,*N*′-bis(salicylidene)-$(-)_D$-(*R*)-1,2-propanediamine [*R*-pn(salH)$_2$] exhibits two regions of interest for the present purpose, a band around 25×10^3 cm^{-1} and a band around 30×10^3 cm^{-1}. As indicated by Bosnich the first band may be assigned as an $n\rightarrow\pi^*$ transition, whereas the second corresponds to a $\pi\rightarrow\pi^*$ transition involving the azomethene group, a transition which is also polarized in the N–O direction of the chromophore.[7] It is, as indicated above, well known that two $\pi\rightarrow\pi^*$ transitions distributed helically possess the power of showing exciton splitting,[1,7–10] and it is immediately seen from spectra of *R*-pn(salH)$_2$ that such a coupling exists in the benzoic transition region,[11] analogous, by the way, to the coupling observed with enantiomers of 1,3-diphenylallene.[12]

As mentioned by Smith *et al.*, it is puzzling that the negative circular dichroism band at 30×10^3 cm^{-1}, assignable to $\pi\rightarrow\pi^*$ transition involving the azomethene groups of *R*-pn(salH)$_2$, does not show any sign of exciton coupling.[7] This may, however, as proposed by Mason *et al.*,[13] be a consequence of configuration interaction. Under absorptions exhibiting exciton coupling, two bands in the circular dichroism spectrum are expected of equal magnitude, but of opposite signs.[1] However, inequality in the areas of the two bands may arise from the mixing with excited states. Thus configuration interactions will mix out-of-phase (antisymmetric, *B*) transitions and in-phase (symmetric, *A*) transitions among themselves. Accordingly it is conceivable, as may also be seen from the formulas presented by Mason *et al.*,[13] that configurational interactions may increase the

0302-4377/82/100825-03$02.50

absolute magnitude of the *B* transition mode and decrease the magnitude of the *A* transition mode to such an extent that only a single negative CD-band is observed. In the case of complexation, however, configurational interactions are of lesser importance as may be seen from the spectra of the Zn(II) complex of *N,N'*-bis(salicylidene)-(−)$_D$-(*R*)-1,2-propanediamine [Zn *R*-pn(sal)$_2$], which clearly exhibit exciton splitting under the $\pi \rightarrow \pi^*$ transition band.[6]

In this paper we shall, observing the points of view presented above, discuss and interprete spectra of the compound *R*-pn(acacH)(salH), *i.e.* the Schiff base derived from one molecule of (−)$_D$-(*R*)-1,2-propanediamine, one molecule of acetylacetone and one molecule of salicylaldehyde together with the inner-sphere Cu(II) complex of this particular ligand.

EXPERIMENTAL

The ligand *R*-pn(acacH)(salH) was prepared according to a modification of a procedure described earlier for *R*-pn(acacH)$_2$ by Martell *et al.*[14] To a mixture of 1 mol of salicylaldehyde and 1 mol of acetylacetone, 1 mol of (−)$_D$-(*R*)-1,2-propanediamine was added slowly and with stirring. After evolution of heat had ceased, stirring was continued for another hour and the reaction mixture finally dissolved in acetone. On addition of water in which solvent *R*-pn(acacH)$_2$ is soluble[14] an oil is developed and subsequently separated. According to the procedure published by Kwiatkowski and Kwiatkowski[15] the oil is then extracted several times with hot *n*-hexane in which solvent *R*-pn(salH)$_2$ is fairly insoluble. The collected extracts yield on standing *R*-pn(acacH)(salH) as an oil, which crystallizes below temperature (m.p.: 5 °C). The identity of the compound has been confirmed through chemical analysis. (Calc. for $C_{15}H_{20}N_2O_2$: C, 69.23%; H, 7.70%; N, 10.76%. Found: C, 69.50%; H, 7.38%; N, 10.24%). The copper(II) complex Cu *R*-pn(acac)(sal) may be prepared from solutions of the ligand and a convenient copper(II) salt, either acetate or carbonate.[16,17] The identity of the compound has been confirmed through chemical analysis. (Calc. for $C_{15}H_{18}N_2O_2Cu,H_2O$: C, 53.01%; H, 5.93%; N, 8.23%. Found: C, 53.73%; H, 6.01%; N, 8.07%).

RESULTS AND DISCUSSION

We may start by considering the spectra of the free ligand *R*-pn(acacH) (Fig. 1). Two bands in the non-benzoic transition region and of negative rotational strength are observed in the CD spectrum. It is obvious that the spectrum resemples that of *R*-pn(salH)$_2$ (Fig. 1 of Ref. 6), and may be assigned similarly, *i.e.* the peak at 25×10^3 cm^{-1} to a $n \rightarrow \pi^*$ transition and the band at 31×10^3 cm^{-1} as an enforced out-of-phase exciton couplet from $\pi \rightarrow \pi^*$ transitions in the two chromophoric parts of *R*-pn(acacH)(salH). Thus the negative sign of this peak in the circular dichroism spectrum reflects stereochemical dominance from the *R*-1,2-propanediamine bridge.[1-5]

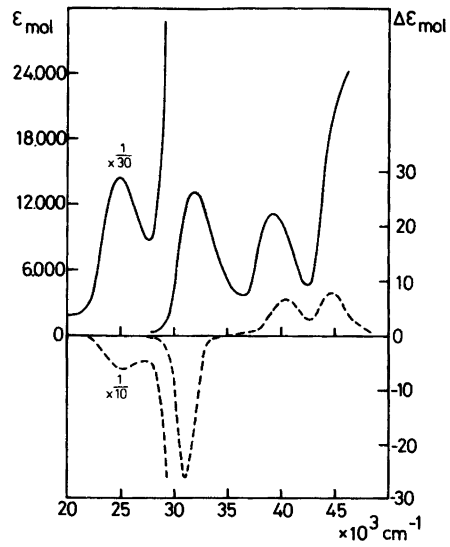

Fig. 1. Molar absorption (−) and circular dichroism spectra (---) of *R*-pn(acacH)(salH) dissolved in CH_3OH.

Turning our attention to the copper(II) complex it might first of all be appropriate to recollect the spectra of Cu *R*-pn(acac)$_2$ and Cu *R*-pn(sal)$_2$. The former shows in the internal ligand transition region an exciton couplet with a positive rotational strength and a circular dichroism maximum of ~60 M^{-1} cm^{-1} at 30×10^3 cm^{-1}.[18] The latter shows in the same region a circular dichroism maximum of ~15 M^{-1} cm^{-1} at 25×10^3 cm^{-1}.[19] From this information it is easily seen, in comparison with the circular dichroism spectrum of Cu *R*-pn(acac)(sal) Fig. 2), that we are not dealing with just a mixture of Cu *R*-pn(acac)$_2$ and Cu *R*-pn(sal)$_2$. We furthermore notice that the $\pi \rightarrow \pi^*$ transition region of the mixed-ligand complex shows circular dichroism bands of relatively low intensity. It is true, however, as may be seen from the $d \rightarrow d$ transition region of the mixed-

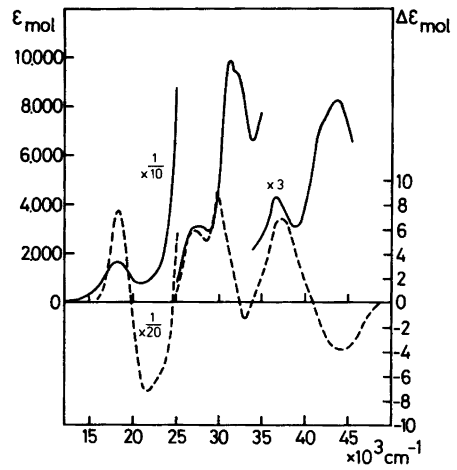

Fig. 2. Molar absorption (—) and circular dichroism spectra (---) of Cu *R*-pn(acac)(sal) dissolved in CH_3OH.

ligand complex that the two possible isomers of formula Cu *R*-pn(acac)(sal) are non-planar and that the configurational deviation from planarity must be of the same sign as that of Cu*R*-pn(acac)$_2$ (*cf.* Fig. 2 of Ref. 18).

As mentioned, the $\pi \rightarrow \pi^*$ transition region in the circular dichroism spectrum of the mixed-ligand complex does not distinctly show the characteristics of exciton couplets. This is due to the relatively large energy separation of the $\pi \rightarrow \pi^*$ transitions of salicylaldehyde and acetylacetone, respectively, occurring by complexation. It is known that the $\pi \rightarrow \pi^*$ transition of an acetylacetone Schiff base is found at 32×10^3 cm^{-1} with a shift towards 32.5 $\times 10^3$ cm^{-1} by complexation to a Cu(II) ion,[1,18] whereas a Schiff base of salicylaldehyde shows its $\pi \rightarrow \pi^*$ transition at 31.5×10^3 cm^{-1} with a shift towards 28.5×10^3 cm^{-1} by complexation.[6,19] Thus the two $\pi \rightarrow \pi^*$ transitions interact only to a minor extent in the mixed-ligand complex and will accordingly not give rise to strong exciton bands in absorption and circular dichroism spectra.

Acknowledgement. The author wishes to acknowledge the skillful technical assistance of Mrs. L. Penzien.

REFERENCES

1. Larsen, E. *Acta Chem. Scand. 23* (1969) 2158.
2. Jensen, H. P. and Larsen, E. *Acta Chem. Scand. A 29* (1975) 157.
3. Jensen, H. P. and Larsen, E. *Gazz. Chim. Ital. 107* (1977) 143.
4. Jensen, H. P. *Acta Chem. Scand. A 32* (1978) 149.
5. Jensen, H. P. *Acta Chem. Scand. A 36* (1982) 167.
6. Bosnich, B. *J. Am. Chem. Soc. 90* (1968) 627.
7. Smith, H. E., Neergaard, J. R., Burrows, E. P. and Chen, F.-M. *J. Am. Chem. Soc. 96* (1974) 2908.
8. Schellman, J. A. *Acc. Chem. Res. 1* (1968) 144.
9. Bosnich, B. *Acc. Chem. Res. 2* (1969) 266.
10. Hug, W. and Wagniére, G. *Tetrahedron 28* (1972) 1241.
11. Gullotti, M., Pasini, A., Fantucci, P., Ugo, R. and Gillard, R. D. *Gazz. Chim. Ital. 102* (1972) 855.
12. Mason, S. F. and Vane, G. W. *Tetrahedron Lett. 21* (1965) 1593.
13. Gottarelli, G., Mason, S. F. and Torre, G. *J. Chem. Soc. B* (1970) 1349.
14. McCarthy, P. J., Hovey, R. J., Ueno, K. and Martell, A. C. *J. Am. Chem. Soc. 77* (1955) 5820.
15. Kwiatkowski, E. and Kwiatkowski, M. *Inorg. Chim. Acta 42* (1980) 197.
16. Pfeiffer, P., Christeleit, W., Hesse, F., Pfitzner, H. and Thielert, H. *J. Prakt. Chem. 150* (1938) 261.
17. Kuska, H. A., Farona, M. F., Pappas, P. and Potterton, S. *J. Coord. Chem. 1* (1971) 259.
18. Jensen, H. P. and Larsen, E. *Acta Chem. Scand. 25* (1971) 1439.
19. Pasini, A., Cullotti, M. and Ugo, R. *J. Chem. Soc. Dalton Trans.* (1977) 346.

Received March 31, 1982.

Acta Chemica Scandinavica A 36 (1982) 829–839

The Crystal Structure of Bis(triphenylphosphine)iminium Halocyano-4-nitrobenzyltellurates(II), [PNP][4-NO_2-$PhCH_2Te(CN)X$], X = Cl, Br and I

KNUT MAARTMANN-MOE and JON SONGSTAD

Department of Chemistry, University of Bergen, N-5014 Bergen, Norway

The structures of $[(Ph_3P)_2N][4\text{-}NO_2\text{-}PhCH_2Te(CN)X]$, I: X = Cl, II: X = Br, III: X = I, have been determined by X-ray methods using diffractometer data collected at room temperature. Full-matrix least-squares refinements led to final conventional *R*-values of 0.048 (3589) for I, 0.051 (3166) for II and 0.036 (5256) for III. (The number of observed reflections in parentheses.)

The compounds crystallize in the triclinic system with the following unit cell dimensions: I: a = 9.833(2) Å, b = 14.435(2) Å, c = 16.307(2) Å, α = 66.09(2)°, β = 78.63(2)°, γ = 71.77(2)°; II: a = 9.902(2) Å, b = 14.464(2) Å, c = 16.392(1) Å, α = 65.95(1)°, β = 78.57(1)°, γ = 71.97(1)°, III: a = 12.578(2) Å, b = 12.730(3) Å, c = 14.258(2) Å, α = 77.68(2)°, β = 79.05(2)°, γ = 69.92(2)°. All three compounds have space group $P\bar{1}$(No. 2), Z = 2; I and II are isomorphous.

Tellurium and the arrangement of the atoms bonded to tellurium are T-shaped and of the three-center-two-electron type. The halogen atoms are linked to the tellurium atom approximately *trans* to the cyano group with fairly short Te–X bond distances; Te–Cl is 2.923(2) Å in I, Te–Br is 3.100(1) Å in II and Te–I is 3.299(0) Å in III. A comparison with the sum of the van der Waals' radii and with the sum of the covalent distances of the atoms indicates the bond order of the Te–X bonds to be Te–Cl > Te–Br > Te–I. This bond order sequence suggests that symbiosis may play an important role with regard to bond lengths in Te(II)-complexes. In I and II there are weak intermolecular bonds to neighbouring oxygen atoms of 3.449(3) Å (I) and 3.435(5) Å (II). In III the tellurium atom is strictly three-coordinated.

The Te–C(CN) bond lengths are significantly longer, ~0.08 Å, than in the parent organic tellurocyanate while the other bond lengths, bond angles and torsion angles remain essentially the same.

The [PNP]-cations have the non-linear form with a P–N–P bond angle of 137.1(4)° in I, 136.8(4)° in II and 142.8(2)° in III.

Alkyl thiocyanates, RSCN, and alkyl selenocyanates, RSeCN, are readily prepared from the corresponding halides and alkali metal thiocyanates and selenocyanates by the Finkelstein reaction, eqn. (1). The limited solubility of the alkali metal

$$RX + KSCN(KSeCN) \rightarrow RSCN(RSeCN) + KX \quad (1)$$

halides in the usual dipolar organic solvents, protic and aprotic ones, allows the products to be isolated in high yield.[1]

The preparation of organic tellurocyanates, RTeCN, is more difficult since alkali metal tellurocyanates cannot be prepared.[2] Cava and coworkers,[3] however, have recently shown that by employing alkali metal tellurocyanates in dimethyl sulfoxide, made *in situ*, organic tellurocyanates may be formed as depicted by eqn. (1). So far, only substituted benzyl tellurocyanates have been prepared by this method.[3–6]

When using stable onium tellurocyanates[2,7,8] when attempting to prepare organic tellurocyanates according to eqn. (1) in dipolar aprotic solvents in which the tellurocyanate ion is stable,[2] the product is not the expected one but a salt.[9] The anion of this salt was proposed to be the addition compound between the first formed organic tellurocyanate and the displaced halide ion, an alkylcyanohalotellurate(II) anion,[9] eqn. (2). Apparently, an equilibrium between this anion and the organic tellurocyanate exists, eqn. (3).

0302-4377/82/100829-11$02.50

$$RX + O^+NCTe^- \rightarrow O^+[RTe(CN)X]^- \quad (2)$$

$$[RTe(CN)X]^- \rightleftarrows RTeCN + X^- \quad (3)$$

In the presence of alkali metal cations this equilibrium is completely shifted to the right due to the limited solubility of the alkali metal halides in dipolar aprotic solvents which is the key to Cava's preparation[3] according to eqn. (1). When using tetraphenylarsonium tellurocyanate, $Ph_4AsTeCN$, the yield of the complex anion, eqn. (2), is moderate.[9] This is due to the fairly limited solubility of the Ph_4As^+-halides and of Ph_4As^+-tellurocyanate as compared with the extreme solubility of the Ph_4As^+-salts of the complex tellurate anions in the usual dipolar aprotic solvents. By addition of diethyl ether to the reaction mixture, the equilibrium, as depicted by eqn. (3), is readily displaced to the right and a mixture of Ph_4As^+-salts is obtained.[9]

However, when using the bis(triphenylphosphine)iminium ion, $[PNP]^+$, as cation, the difference in the solubility of the [PNP]-halides and of the [PNP]-tellurates is greatly diminished allowing the latter salts to be isolated in almost quantitative yield. In the present study we want to report the crystal structures of three such salts:

$[PNP][4\text{-}NO_2\text{-}PhCH_2Te(CN)X]$
$([PNP]^+ = [(Ph_3P)_2N]^+)$

I:X=Cl II:X=Br III:X=I

The 4-nitrobenzyl group was chosen since the structure of the parent organic tellurocyanate, $4\text{-}NO_2\text{-}PhCH_2TeCN$, has recently been described[6] allowing a direct comparison. Furthermore, the high stability of this tellurocyanate allowed an alternative and facile synthesis of the adducts in acetone or acetonitrile according to eqn. (4) as a proof of their composition.

$$4\text{-}NO_2\text{-}PhCH_2TeCN + [PNP]X \rightarrow [PNP][4\text{-}NO_2\text{-}PhCH_2Te(CN)X] \quad (4)$$

EXPERIMENTAL

Solvents. All solvents used were purified and dried according to standard procedures and distilled in an argon atmosphere prior to use.

Materials. The preparation and purification of [PNP]X (X=Cl^-, Br^-, I^- and $TeCN^-$) has been described.[1] The 4-nitrobenzyl halides were crystallized from cyclohexane prior to use and stored dark in the cold. The corresponding tellurocyanate was prepared as reported[6] and crystallized from dichloromethane prior to use. All operations involving [PNP]TeCN and the [PNP]-tellurates in solution were carefully performed in argon-flushed solvents. In the solid state, however, these compounds are stable for months without any precautions with regard to moisture, oxygen or light.

I. *Bis(triphenylphosphine)iminium chlorocyano-4-nitrobenzyltellurate(II)*, $[PNP][4\text{-}NO_2\text{-}PhCH_2Te(CN)Cl]$. To 0.5 g (0.003 M) 4-nitrobenzyl chloride in 40 ml acetone was added 1.73 g (0.0025 M) [PNP]-tellurocyanate dissolved in 20 ml acetone. The mixture was stirred for 24 h at room temperature in a closed bottle. Traces of Te and TeO_2 was removed by filtration whereupon nearly all the solvent was removed *in vacuum*. A fairly large amount of diethyl ether was added until turbidity and the first crop of precipitate, essentially [PNP]Cl, was discarded. After two days at ~ -20 °C the yellowish product was isolated in close to quantitative yield. This purification procedure was repeated once and 1.60 g, 76 %, was finally obtained. This compound could be prepared in about the same yield from 4-nitrobenzyl tellurocyanate and [PNP]Cl in acetone or acetonitrile according to eqn. (4). M.p. ~120 °C (dec.). (Found: C 61.61; H 4.34; N 4.95. Calc. for $C_{44}H_{36}ClN_3O_2P_2Te$: C 61.18; H 4.20; N 4.86). IR(KBr): The spectrum (400–4000 cm^{-1}) was as the sum of the spectra of [PNP]Cl and the parent organic tellurocyanate except that no peak due to C≡N stretch in the 2000–2200 cm^{-1} region could be detected. UV(8×10^{-4} M in MeCN, 1 cm path length): A shoulder to the NO_2-peak at ~355 nm, shifted some 15 nm toward higher wave length as compared with 4-nitrobenzyl tellurocyanate[6] but with essentially unaltered extinction coefficient, log ε~3.3. NMR (MeCN): 4.36(s,2H), as in the organic tellurocyanate.[6]

II. $[PNP][4\text{-}NO_2\text{-}PhCH_2Te(CN)Br]$. From 0.24 g (0.0011 M) $4\text{-}NO_2\text{-}PhCH_2Br$ and 0.69 g (0.001 M) [PNP]TeCN a yield of 0.75 g. 83 %, was obtained according to the procedure described for the corresponding chloro compound, I. This compound could also be prepared from [PNP]Br and $4\text{-}NO_2\text{-}PhCH_2TeCN$ in more than 70 % yield. Yellow needles, m.p. ~120 °C (dec). (Found: C 58.76; H 4.09; N 4.45. Calc. for $C_{44}H_{36}BrN_3O_2P_2Te$: C 59.19; H 4.19; N 4.62). IR(KBr): As for I. UV(MeCN): A less distinct shoulder than for I at ~350 nm. NMR(MeCN): 4.40 (s, 2H).

III. $[PNP][4\text{-}NO_2\text{-}PhCH_2Te(CN)I]$. From 0.70 g (0.0027 M) $4\text{-}NO_2\text{-}PhCH_2I$ and 1.75 g (0.0025 M) [PNP]TeCN 1.92 g (80 %) was obtained as described for I. An identical product was prepared from $4\text{-}NO_2\text{-}PhCH_2TeCN$ and [PNP]I in aceto-

nitrile. Yellow-brownish needles, m.p. ~120 °C. (dec.) (Found: C 55.83; H 3.88; N 4.23. Calc. for $C_{44}H_{36}IN_3O_2P_2Te$: C 55.32; H 3.80; N 4.40). IR(KBr): As for I. UV(MeCN): No distinct shoulder in the 330–360 nm region; the spectrum appears as a smooth curve which above 360 nm is shifted some 15 nm toward higher wavelength as compared with the parent organic tellurocyanate but with a tail toward 450 nm. NMR(MeCN): 4.46 (s, 2H).

Instrumental. A Perkin-Elmer UV-VIS Spectrophotometer Model 555 was used for the UV measurements. A Perkin-Elmer 399 B Infrared Spectrophotometer was used for the recording of the IR spectra. The proton chemical shifts were determined with a Varian EM 360 A NMR Spectrometer at ~25 °C.

X-Ray data and structure determination. The crystals of I, II and III from acetone–diethyl ether were suitable for the X-ray study. An Enraf-Nonius CAD4 diffractometer with graphite-monochromated Mo$K\alpha$ radiation was used for the determination of cell parameters, and for recording of intensity data. Cell parameters were in each case based upon least square fits to the diffractometer settings of 25 independent reflections ($\lambda(\alpha_1)=0.70926$ Å, $\lambda(\alpha_2)=0.71354$ Å).[10]

Intensity data ($\lambda=0.71073$ Å) were recorded at room-temperature using the ω-scan technique with variable scan speed; I: 0.8–4 min^{-1}; II: 0.8–2.5 min^{-1}; III: 1.7–7 min^{-1}. Minimum scan width was 1.5° including $2\times0.25°$ background scans. The orientation of the crystals was checked at intervals of 100 recordings. Three standard reflections were measured every 2 h and the intensity data later corrected according to the variation of these. Maximum corrections (average corrections in parentheses); I: 4 % (1 %); II: 8 % (3 %); III: 5 % (0 %). All crystallographically independent reflections with $\theta<25°$ were recorded.

The intensity data were corrected for Lorentz, polarization, and absorption effects. The absorption corrections were based on crystal faces and dimensions. The structure of I and III were solved by interpretation of Patterson and Fourier density maps. Since I and II are isomorphous, initial atomic coordinates for II were taken from I and showed to be satisfactory for the subsequent refinement.

Atomic form factors and anomalous dispersion

Table 1. Crystal data and structural parameters.

Compound	I	II	III
Mp. °C	~120(dec)	~120(dec)	~120(dec)
Recryst. from	Acetone/ether[a]	As I	As I
Cryst. system	Triclinic	Triclinic	Triclinic
a(Å)	9.833(2)	9.902(2)	12.578(2)
b(Å)	14.435(2)	14.464(2)	12.730(3)
c(Å)	16.307(2)	16.392(1)	14.258(2)
α(°)	66.09(2)	65.95(2)	77.68(2)
β(°)	78.63(2)	78.57(2)	79.05(2)
γ(°)	71.77(2)	71.97(2)	69.92(2)
Volume (Å^3)	2003.2(5)	2031.7(4)	2077.7(8)
Temp. °C	Room temp. (~19 °C)	As I	As I
Space group	$P\bar{1}$ (No. 2)	$P\bar{1}$ (No. 2)	$P\bar{1}$ (No. 2)
M	863.80	908.25	955.25
Z	2	2	2
F(000)	872	908	944
D_c (gcm^{-3})	1.432	1.485	1.527
Abs. coeff. (cm^{-1})	9.595	19.23	16.12
Cryst.dim. (mm)	$0.23\times0.60\times0.07$	$0.23\times0.08\times0.05$	$0.1\times0.1\times0.2$
Fudge factor	0.020	0.020	0.020
Scale factor	1.9545	2.3566	0.6363
No. of refl.	7051	7142	7285
No. of refl. $>2\sigma$	3589	3166	5256
R	0.048	0.051	0.036
R_w	0.046	0.046	0.037
S	1.136	1.197	1.385
Diff. Four. max. eÅ^{-3}	0.21	0.23	0.46

[a] Diethyl ether.

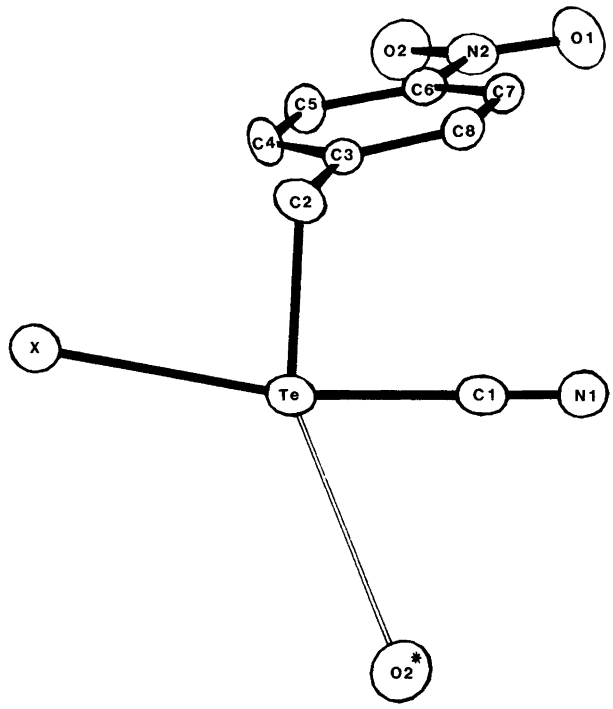

Fig. 1. ORTEP drawing of the $[4\text{-}NO_2\text{-}PhCH_2Te(CN)X]^-$-anion, *cf.* text. (When X = I no Te-O_2* bond is observed).

coefficients were taken from Ref. 11. Hydrogen atoms were placed geometrically at C–H = 0.95 Å and fixed, their thermal parameters refined and averaged, then attributed rounded values in the full matrix least square iterations to follow. The function minimized is $\Sigma\omega\Delta F^2$; the attributed weights correspond to the counting statistics plus 2 % of the net intensity (fudge factor of 0.02).

Reflections with $I < 2\sigma(I)$ were excluded and considered unobserved in the least square refinement.

All computer programs used belong to the Enraf-Nonius Structure Determination Pack, version 17-1980.

Table 1 summarizes the crystal data and other relevant information. Final atomic coordinates together with tables of observed and calculated structure factors are available from the authors, and have been made available to the crystallographic Data Center at Cambridge (GB).

RESULTS

An ORTEP drawing of the anion in I, the $[4\text{-}NO_2\text{-}PhCH_2Te(CN)Cl]$-anion, including numbering of the atoms, is shown in Fig. 1. For clarity the hydrogen atoms are omitted. In this drawing the tellurium atom, Te, the cyano carbon, C1, and the methylene carbon atom, C2, are in the plane of the paper. Since the anions in the two isomorphous compounds, I and II, are most similar except for the Te–Cl and the Te–Br bond distances, the drawing in Fig. is representative also for the $[4\text{-}NO_2\text{-}PhCH_2Te(CN)Br]$-anion and the halogen atom is therefore termed X.

In these two anions the tellurium atom forms a weak intermolecular "secondary bond"[12] to an oxygen atom, O2*, from a neighbouring nitro group of 3.449(5) Å (I) and 3.435(7) Å (II). In the anion of III, the $[4\text{-}NO_2\text{-}PhCH_2Te(CN)I]$-anion, no such weak intermolecular bond to an oxygen atom or to any other atom (< 4.5 Å) could be observed. In this anion the tellurium atom is thus strictly three-coordinated. The rest of the anion, however, is most similar to the anions in I and II. With the exception of the weak Te–O2* interactions as shown in Fig. 1, Fig. I may thus also illustrate the anion in III. In the accompanying table to Fig. 1, Table 2, the

Table 2. Distances of the various atoms from the C1 – Te – C2-plane in the anions as shown in Fig. 1 together with bond lengths and bond angles for the tellurium part of the anions.

	I	II	III
Distance from C1TeC2-plane (Å)			
X	−0.342(2)	−0.392(1)	−0.230(0)
O2*	+0.958(6)	+0.984(7)	
N1	−0.099(8)	−0.077(10)	−0.046(5)
C3	−1.293(7)	−1.319(9)	−1.341(4)
C4	−2.368(8)	−2.365(10)	−2.350(4)
C5	−3.616(8)	−3.623(10)	−3.567(5)
C6	−3.781(7)	−3.775(9)	−3.768(4)
C7	−2.745(7)	−2.728(9)	−2.790(5)
C8	−1.502(8)	−1.500(10)	−1.579(5)
N2	−5.108(6)	−5.114(8)	−5.064(4)
O1	−5.237(6)	−5.206(8)	−5.223(4)
O2	−6.047(6)	−6.031(7)	−5.914(4)
Bond lengths (Å)			
Te – X	2.923(2)	3.100(1)	3.299(0)
Te – Cl	2.140(10)	2.130(12)	2.144(5)
Te – C2	2.159(8)	2.155(10)	2.154(4)
Te – O2*	3.449(5)	3.435(7)	
C1 – N1	1.128(10)	1.120(12)	1.086(5)
Bond angles (°)			
C1 – Te – C2	87.4(3)	87.8(4)	88.7(2)
X – Te – C1	167.9(2)	167.6(3)	170.9(1)
X – Te – C2	82.5(2)	82.2(3)	83.1(1)
X – Te – O2*	122.8(7)	120.2(1)	
C1 – Te – O2*	68.7(2)	71.5(3)	
Te – C1 – N1	174.8(9)	176.0(10)	176.5(5)
Te – C2 – C3	110.6(5)	110.8(6)	112.5(2)

distances of the various atoms from the C1TeC2-plane for all three anions are listed together with the bond lengths and the bond angles which characterize the coordination of the tellurium atoms. The structural data for the remaining part of the anions, the 4-nitrobenzyl part, are listed in Table 3. Fig. 2 shows the projections of the unit cells along the *a*-axes for I and III.

The phenyl rings in the anions and in the cations are all planar within experimental error. In all three anions, particularly in the anions in I and II, the methylene carbon atom, C2, and the nitrogen atom, N2, do not lie in the plane of the phenyl ring. The distances of these two atoms and of the oxygen atoms, O1 and O2, from the plane formed by the phenyl carbon atoms, C3 to C8, are summarized in Table 4. In the anions the C6N2O1O2 part is planar within experimental error. In I and II the nitro group is bent out of the phenyl plane toward the tellurocyanate group by 2.8 and 3.0°, respectively, but is not twisted. In III the nitro group is not bent out of this phenyl plane but is slightly twisted, 0.7°; *cf.* Table 4.

Conformationally the three anions are quite similar; *cf.* Fig. 3 which shows general Newman projections for the three anions along the Te – C2 bond and along the C2 – C3 and the C3 – C6 bonds. For clarity of the latter projection, the distance of C2 from the phenyl plane is disregarded and the nitro group in the rear of the phenyl ring is omitted.

Table 3. Structural data for the 4-nitrobenzyl part of the anions.

	I	II	III
Bond lengths (Å)			
C2–C3	1.466(10)	1.501(12)	1.503(5)
C3–C4	1.394(10)	1.374(12)	1.376(5)
C4–C5	1.375(10)	1.393(13)	1.372(5)
C5–C6	1.370(10)	1.359(13)	1.375(5)
C6–C7	1.360(9)	1.371(12)	1.365(6)
C7–C8	1.382(10)	1.369(12)	1.374(6)
C8–C3	1.388(9)	1.377(12)	1.382(5)
C6–N2	1.471(9)	1.486(11)	1.476(5)
N2–O1	1.211(8)	1.215(10)	1.208(5)
N2–O2	1.228(8)	1.212(9)	1.200(5)
Bond angles (°)			
C2–C3–C4	120.9(7)	119.3(9)	121.1(3)
C3–C4–C5	121.9(7)	119.9(9)	121.3(4)
C4–C5–C6	118.3(7)	119.1(9)	118.8(4)
C5–C6–C7	122.0(7)	121.6(9)	121.4(4)
C6–C7–C8	119.3(7)	119.1(9)	119.1(4)
C7–C8–C3	120.9(7)	120.7(9)	120.9(4)
C8–C3–C2	121.6(7)	121.1(9)	120.3(4)
C8–C3–C4	117.5(7)	119.5(9)	118.6(4)
C5–C6–N2	120.1(7)	120.3(9)	119.4(4)
C7–C6–N2	118.0(7)	118.1(9)	119.2(4)
C6–N2–O1	119.1(7)	117.8(9)	117.7(5)
C6–N2–O2	117.9(7)	117.0(10)	118.0(4)
O1–N2–O2	122.9(8)	125.2(10)	124.1(5)

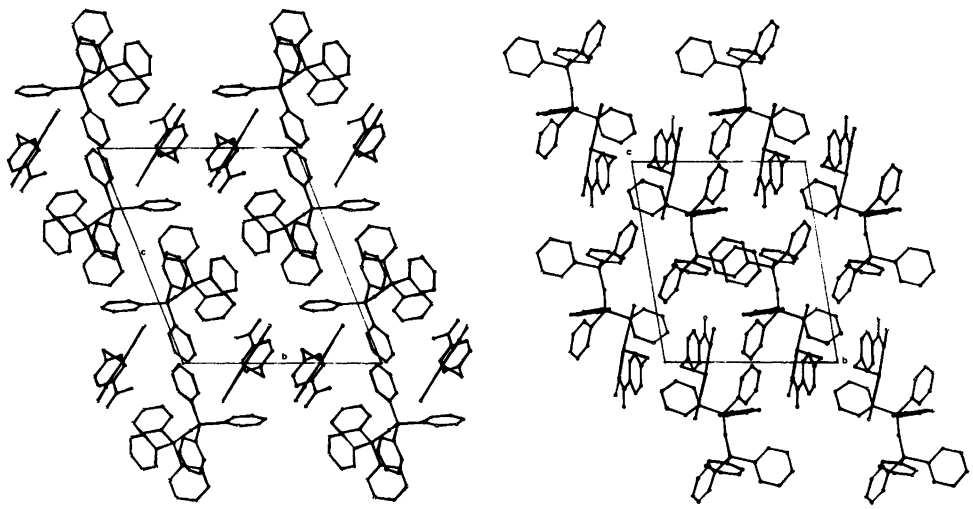

I III

Fig. 2. The projection of the unit cell along the *a*-axes for I (left) and for III (right).

Table 4. The distance of C2, N2, O1 and O2 from the phenyl ring plane. Negative value is defined as the same side as the [Te(CN)X]-part of the anions, *cf.* Fig. 1.

	I	II	III
C2	−0.108(8)	−0.104(10)	+0.035(4)
N2	−0.076(6)	−0.081(8)	+0.020(4)
O1	−0.113(6)	−0.111(8)	−0.016(4)
O2	−0.128(6)	−0.110(7)	+0.010(5)

DISCUSSION

The UV and the ^1H NMR spectra, *cf.* Experimental, readily suggest that products are formed when ionic halides are added to an organic tellurocyanate, RTeCN, in solution. The present crystallographic study serves as the final proof for the existence of complex anions of the general type $[RTe(CN)X]^-$. A number of experiments were performed during the present study in order to prepare similar anions from various alkyl selenocyanates, RSeCN, by varying the cation, n-But_4N^+, Ph_4As^+ or $[PNP]^+$, and also the solvent. However, all attempts failed and not even spectroscopic evidence for any interaction between RSeCN and X^- could be obtained. Apparently, the formation and existence of $[RTe(CN)X]^-$ is unique for tellurium in the *VI* main group. Presumably, the ability of this element to make very stable Te(II)-complexes is the cause for this observation, complexes in which the bonding in the linear three-center system is of the two-electron type.[13]

Bonding to the tellurium atom in the anions. In all the three anions the halogen atom is approximately *trans* to the cyano group with X−Te−Cl bond angles of 167.9(2)°(I), 167.6(3)°(II) and 170.9(1)°(III). This observation is as anticipated in view of the *trans* effect of the 4-nitrobenzyl group, particularly its *σ-trans* effect, which is known to be far greater than that of the cyano group.[14] Due to this bonding between the central tellurium atom and the halogen

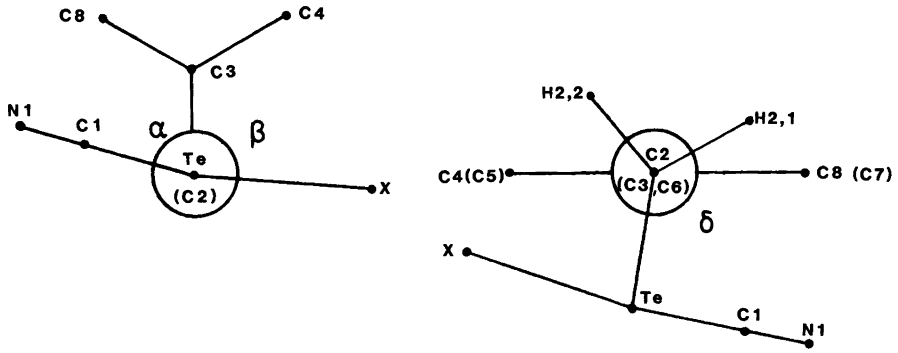

	I	II	III	RTeCN[6]
α°	70.5	70.1	74.9	77.4
β°	102.8	102.6	101.0	
δ°	96.7	97.2	100.1	98.0

Fig. 3. General Newman projections for the anions in I, II and III; along the Te−C2 bond (left) and along the C2−C3 and the C3−C6 bond (right).

Table 5. A comparison between the Te–X bond distances in $[RTe(CN)X^-]^-$, $Te-X_{obs}$, with the sum of the van der Waals' radii of tellurium and the halogens, ΣR_{vdW}, and the sum of the covalent single bond distances, ΣR_{cov}. (Bond distances in Å.)

	I(X = Cl)	II(X = Br)	III(X = I)
ΣR_{vdW}	3.81	3.91	4.04
ΣR_{cov}	2.31	2.43	2.60
$Te-X_{obs}$	2.923(2)	3.100(1)	3.299(0)
$\Sigma R_{vdW}-(Te-X)_{obs}$	0.89	0.81	0.74
$(Te-X)_{obs}-\Sigma R_{cov}$	0.61	0.67	0.70

atoms *trans* to the cyano group, the Te–C(CN) bond lengths are significantly elongated from what was observed in the parent organic tellurocyanate, 2.060(4) Å,[6] to 2.140(10) Å in I, 2.130(12) in II and 2.144(5) Å in III. Actually, this elongation of the Te–C(CN) bond causes the two Te–C bonds in the anions, the Te–C(CN) bond and the Te–$C(CH_2)$ bond, to be fairly similar, 2.13–2.16 Å, when taking the experimental uncertanties into account, *cf.* Table 2. This range is the expected one for tellurium–carbon single bonds.[15] Significantly shorter Te–C bond lengths as in 4-nitrobenzyl tellurocyanate[6] have been observed in the tellurocyanate ion,[16] in phenoxatellurine[17] and especially in Te=C=S.[18]

A comparison is given in Table 5 between the Te–X bond lengths in the anions and the sum of the covalent single bond distances, ΣR_{cov}, and the sum of the van der Waals' radii, ΣR_{vdW}.[12,19] The Te–X bond distances in the anions are clearly significantly longer than Te–X single bonds by 0.6 to 0.7 Å but are from 0.7 to 0.9 Å shorter than the sum of the van der Waals' distances. It is notable that the Te–Cl bond length is closer to ΣR_{cov} and further from ΣR_{vdW} than is the length of the Te–I bond. This suggests the bond order of the Te–X bonds in the anions to be Te–Cl > Te–Br > Te–I, a bond order sequence which at first sight is surprising in view of the fact that Te(II) is a typical soft acid.[13,20] However, since the halogen atoms are *trans* to a very electronegative group, the cyano group, the more electronegative halogen will be favoured. Apparently, symbiosis[21] has to be taken into account when considering bonding in Te(II)-complexes. When halogen atoms are linked to Te(II) *trans* to a soft atom as in PhTe(tu)X (tu = thiourea) the bond prder is the expected one, Te–I > Te–Br > Te–Cl.[22] Owing to the strength of the Te–I bond in these Te(II)-complexes the *trans*-bond-lengthening effect upon the Te–S bond of iodine is superior to that of bromine and chlorine causing the Te–S bond length in PhTe(tu)I to be ~0.09 Å longer than in the corresponding chloro and bromo compounds.[22] As mentioned above, the Te–C(CN) bonds in the $[4\text{-}NO_2\text{-}PhCH_2Te(CN)X]^-$ anions are independent upon the halogen atom when taking the experimental error into account, *cf.* Table 2.

In spite of the apparent weakness of the Te–I bond in the anion in III, the iodine atom in this anion is closer to the C2TeCl plane than are the chlorine atom and the bromine atom in I and II, respectively; *cf.* Fig. 1 and Table 2, first entry. The anion in III is thus closer to an idealized T-shaped anion than are the anions in I and II. In I and II the tellurium atom may be considered as tetracoordinated owing to the closeness of an oxygen atom from a neighbouring nitro group, *cf.* Fig. 1. Presumably the electronegativity of the chlorine and the bromine atoms will cause some positive charge to reside on the central tellurium atom enabling this atom to interact with the slightly negatively charged oxygen atoms. It should be emphasized, however, that this interaction is very weak; the observed bond distances of 3.449(5) Å (I) and 3.435(7) Å (II) are only slightly less than the van der Waals distance, 3.58 Å.[19] Furthermore, the oxygen atoms are close to 1 Å away from the C1TeC2 plane, *cf.* Table 2. It is notable, however, that the C1TeO2* bond angles in I and II, 68.7 and 71.5°, are most similar to the corresponding bond angle in 4-nitrobenzyl tellurocyanate, 68.9°, in which a considerably shorter Te–O* bond distance of 3.182(3) Å is observed.[6] In III, the iodo compound, the anion is strictly three-coordinated. In this respect this anion resembles PhTe(tu)I;[22] the corresponding chloro and bromo compounds are tetracoordinated in the solid state.[22]

The bond angles around the tellurium atom are in the three anions most similar, *cf.* Table 2. The

C1–Te–C2 bond angles are slightly but significantly smaller by 2–3° than in the parent organic tellurocyanate in which this bond angle is 90.6°.[6] Presumably, this bond angle decrease is caused by repulsion between the lone pairs on the tellurium atom in accordance with the VSEPR theory.[23] The same argument applies to the X–Te–Cl bond angles which in all three anions are significantly less than 180°.

The TeCN group. As mentioned above the Te–C(CN) bonds are longer in the anions than in the organic tellurocyanate from which they are derived.[6] This elongation appears to be accompanied by a slight but distinct deviation from linearity of the TeCN group; the Te–C1–N1 bond angles being 174.8(9)° in I, 176.0(10)° in II, 176.5(5)° in III as compared with 179.3(4)° in 4-nitrobenzyl tellurocyanate.[6] In all three anions, and especially in the anions of I and II, the N1-nitrogen atom is significantly below the C1–Te–C2 plane; *cf.* Fig. 1 and Table 2. The C1–Te–C2 plane and the Te–C1–N1 plane are almost perpendicular in all three anions.

The non-linearity of the TeCN groups in the anions is small and may be caused by packing effects, but it is interesting in view of the fact that numerous examples of bent SCN groups are known, both in inorganic[24] and in organic compounds.[25] This non-linearity of the thiocyanate group has been suggested to be due to some contribution of the $-S=C=N$ form giving rise to fairly short S–C bond lengths. For a critical survey of bonding in the thiocyanate group, *cf.* Ref. 26. The anticipated elongation of the C–N bond has not been observed.

Actually, in the three anions the opposite appears to be the case with fairly long Te–C1 bond lengths and short C1–N1 bond lengths, especially in III. A very short C1–N1 bond length, significantly less than the accepted C1–N1 bond length of 1.14–1.15 Å has previously been observed in the tellurocyanate ion.[16] This raises the general question whether the short C1–N1 bond length, ~1.09 Å, as observed in the [4-NO_2PhCH_2Te(CN)I]-anion and in the $TeCN^-$ anion[16] is real or is a result of the experimental method. For a detailed discussion regarding the electron density in a linear molecule and the effect of thermal vibration upon bond lengths, *cf.* Ref. 27. Presently, it seems as if a critical discussion of bond angles and bond lengths in the tellurocyanate group has to be postponed until low-temperature data are made available.

Table 6. Structural data for the $[Ph_3P-N-PPh_3]^+$-cations.

	I	II	III
Bond lengths (Å)			
N3–P1	1.581(5)	1.581(6)	1.578(3)
N3–P2	1.581(5)	1.576(6)	1.569(3)
P–C	1.796	1.794	1.798
C–C	1.385		
Bond angles (°)			
P1–N3–P2	137.1(4)	136.8(4)	142.8(2)
C111–P1–C121	107.7(3)	106.4(4)	107.2(2)
C111–P1–C131	107.7(3)	107.9(4)	107.9(2)
C121–P1–C131	107.4(3)	107.5(4)	107.6(2)
C211–P2–C221	108.7(3)	108.7(4)	108.3(2)
C211–P2–C231	107.6(3)	107.2(4)	106.7(2)
C221–P2–C231	108.0(3)	107.4(4)	106.4(2)
N3–P1–C111	113.8(3)	114.5(4)	108.7(2)
N3–P1–C121	107.7(3)	107.7(4)	115.2(2)
N3–P1–C131	112.2(3)	112.5(4)	110.0(2)
N3–P2–C211	110.3(3)	110.7(4)	114.7(2)
N3–P2–C221	107.8(3)	108.3(4)	111.7(2)
N3–P2–C231	114.2(3)	114.4(4)	108.7(2)
C–P–C	107.8	107.5	107.4
N–P–C	111.0	111.3	111.5

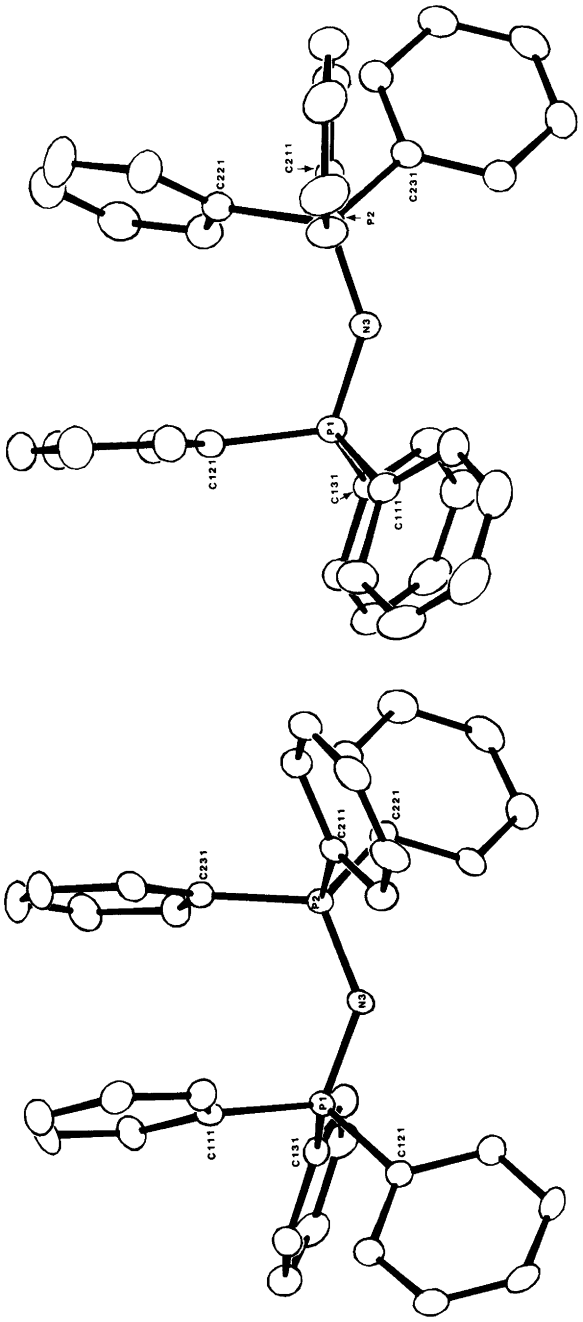

I III

Fig. 4. ORTEP drawing of the $[PNP]^+$-cations in I (left) and in III (right). The P1, the N3 and the P2 atoms are in the plane of the paper.

The Newman projections in Fig. 3 clearly indicate that the TeCN-group is *synclinal (gauche)* to the C2–C3 bond in all three anions. The torsion angle is in all anions most similar to the one observed in the parent organic tellurocyanate, 77.4°.[6] Fig. 3 shows that the TeC2C3 planes make angles of ~ 100° with the benzene ring in all three anions which is quite comparable with the corresponding angle in 4-nitrobenzyl tellurocyanate, 98.0°.[6] It is apparent that no significant conformational changes take place when 4-nitrobenzyl tellurocyanate is complexed with halide ions.

The 4-nitrobenzyl group. All bond lengths and bond angles as listed in Table 3 are as expected. The C2–C3 bond length in the anion of I is fairly small but we cannot offer a satisfactory explanation for this observation. The N–O bond lengths and the C6–N–O bond angles in the anions of I and II are similar since the intermolecular contact between the tellurium atom and O2 is very weak. This observation contrasts what was found in the case of 4-nitrobenzyl tellurocyanate.[6]

The $[PNP]^+$-cations. ORTEP drawings of the cations in I and III together with naming of the central atoms are shown in Fig. 4. Table 6 summarizes the most important structural data for the cations in the three salts. The P1 – N3 – P2 bond angle in III is seen to be significantly larger than in I and II, *cf.* Table 6. However, bond angles in this cation, when bent, are known to range from 135 to 145° depending upon packing. The C–P–C bond angles in the cations are close to an average value of 107.5°. The cations are less symmetrical with regard to the N–P–C bond angles which range from 107 to 115° with an average value of 111.3°.

REFERENCES

1. Maartmann-Moe, K., Sanderud, K. A. and Songstad, J. *Acta Chem. Scand. B 36* (1982) 211.
2. Austad, T., Songstad, J. and Åse, K. *Acta Chem. Scand. 25* (1971) 331.
3. Spencer, M. K., Lakshmikantham, M. V. and Cava, M. P. *J. Am. Chem. Soc. 99* (1977) 1470.
4. Engman, L. and Cava, M. P. *J. Org. Chem. 46* (1981) 4194.
5. Suzuki, H., Miyoshi, K. and Osuka, A. *Nippon Kagaku Kaishi 1981*, 472; *Chem. Abstr. 95* (1981) 80371 w.
6. Maartmann-Moe, K., Sanderud, K. A. and Songstad, J. *Acta Chem. Scand. A 35* (1981) 151.
7. Downs, A. *Chem. Commun.* (1968) 1290.
8. Martinsen, A. and Songstad, J. *Acta Chem. Scand. A 31* (1977) 645.
9. Austad, T., Esperås, S. and Songstad, J. *Acta Chem. Scand. 27* (1973) 3594.
10. Maartmann-Moe, K., Rømming, C. and Songstad, J. *Acta Chem. Scand. A 36* (1982) 757.
11. *International Tables for X-Ray Crystallography*, Kynoch Press, Birmingham 1962, Vol. 4, p. 86.
12. Alcock, N. W. *Adv. Inorg. Chem. Radiochem. 15* (1973) 1.
13. Foss, O. *Pure Appl. Chem. 24* (1970) 31.
14. Basolo, F. and Pearson, R. G. *Mechanism of Inorganic Reactions*, Wiley, New York 1967, p.375.
15. Dewan, J. C. and Silver, J. *J. Chem. Soc. Dalton Trans.* (1977) 644.
16. Foust, A. *Chem. Commun.* (1979) 414.
17. Smith, M. R., Mangion, M. M., Zingaro, R. A. and Meyers, E. A. *J. Heterocycl. Chem. 10* (1973) 527.
18. Callomon, J. H., Hirota, E., Kuchitsu, K., Lafferty, W. J., Maki, A. G. and Pole, C. S. *Structure Data on Free Polyatomic Molecules*, Landold-Bornstein, New Series, Springer, Berlin 1976.
19. Bondi, A. *J. Phys. Chem. 68* (1964) 441.
20. Pearson, R. G. and Songstad, J. *J. Am. Chem. Soc. 89* (1967) 1827.
21. Jørgensen, C. K. *Inorg. Chem. 3* (1964) 1201.
22. Vikane, O. *Thesis*, University of Bergen, Bergen 1975.
23. Gillespie, R. J. *J. Chem. Educ. 47* (1970) 18.
24. Burmeister, J. L. In Newman, A. A., Ed., *Chemistry and Biochemistry of Thiocyanic Acid and Its Derivatives*, Academic, London 1975, p. 68.
25. Corfield, G. C. In Patai, S., Ed., *Chemistry of Cyanates and their Thio Derivatives*, Wiley, Chichester 1977, p. 131.
26. Wittel, K., Meeks, J. L. and McGlynn, S. P. In Patai, S., Ed., *Chemistry of Cyanates and Their Thio Derivatives*, Wiley, Chichester 1977, p. 1.
27. Hargittai, I. and Paul, I. C. In Patai, S., Ed., *Chemistry of Cyanates and Their Thio Derivatives*, Wiley, Chichester 1977, p. 69.

Received April 2, 1982.

Acta Chemica Scandinavica A 36 (1982) 841 – 845

The Crystal and Molecular Structure of Bis(N^1-isopropyl-2-methyl-1,2-propanediamine)[(*S*)-lactato]zinc(II) (*S*)-Lactate Monohydrate

MARKKU AHLGRÉN, URHO TURPEINEN and REIJO HÄMÄLÄINEN

Department of Inorganic Chemistry, University of Helsinki, SF-00100 Helsinki 10, Finland

The structure of bis(N^1-isopropyl-2-methyl-1,2-propanediamine)[(*S*)-lactato]zinc(II) (*S*)-lactate monohydrate has been determined from three-dimensional X-ray data and refined by full-matrix least-squares to a final *R* value of 0.049 for 1795 reflections. The crystals are monoclinic, space group $P2_1$, with $a=8.818(3)$, $b=18.887(5)$, $c=8.500(2)$ Å and $\beta=102.13(2)°$. The zinc coordination is distorted trigonal bipyramidal with a carboxyl oxygen atom [2.009(5) Å] and two nitrogen atoms [2.004(8) and 2.095(6) Å] forming the equatorial coordination plane and with the nitrogen atoms bonded to isopropyl groups in the axial positions [2.234(8) and 2.264(7) Å]. Complex cations, (*S*)-lactate ions and water molecules form a hydrogen bonding network.

Complex formation in aqueous solution between copper(II) and 1,2-propanediamine and substituted 1,2-propanediamine has recently been investigated in this laboratory.[1] Crystallographic analyses of some mono- and bis(N^1-isopropyl-2-methyl-1,2-propanediamine)copper(II) carboxylates have also been carried out.[2-5] In all bis(N^1-isopropyl-2-methyl-1,2-propanediamine)copper(II) carboxylates so far examined, the coordination sphere of Cu(II) is square pyramidal with the apical position occupied by the oxygen atom of a carboxyl group. The apical Cu – O distances of 2.23 Å in tartrate[5] and malate[6] complexes and 2.16 Å in succinate,[6] fumarate[6] and lactate[4] complexes are only 0.1 – 0.2 Å longer than the basal Cu – N distances and the Cu atoms are appreciably lifted (0.19 – 0.33 Å) from the basal planes.

To investigate further N^1-isopropyl-2-methyl-1,2-propanediamine transitio-metal carboxylates, we prepared the bis(N^1-isopropyl-2-methyl-1,2-propanediamine)zinc(II) (*S*)-lactate. Preliminary X-ray work indicated that the zinc(II) compound is isomorphous with the copper(II) compound. Likewise the IR-spectra of the two compounds are very similar. A slight increase in the separation of the antisymmetric and symmetric stretching frequencies of the unidentate carboxyl group in the zinc(II) compound may be due to stronger bonding of the lactate group.[7] To investigate this supposition we have made an X-ray structural analysis of the zinc(II) compound and report the results in this paper.

EXPERIMENTAL

Colourless crystals were obtained by slow evaporation of a water – ethanol solution containing zinc(II) oxide, L-lactic acid and N^1-isopropyl-2-methyl-1,2-propanediamine in molar ratio 1:2:3. A single crystal of dimensions $0.3 \times 0.3 \times 0.5$ mm was selected for the X-ray investigation.

Lattice parameters were obtained from least-squares refinement of eighteen well-centered reflections measured on a Syntex $P2_1$ diffractometer using graphite monochromatized Mo$K\alpha$ radiation ($\lambda=0.71069$ Å). Crystal data: $a=8.818(3)$, $b=18.887(5)$, $c=8.500(2)$ Å, $\beta=102.13(2)°$, $Z=2$, $D_m=1.25(1)$, $D_c=1.25$ g cm^{-3}, space group $P2_1$, μ(Mo$K\alpha$) $=9.6$ cm^{-1}.

Intensity data were collected ($5<2\theta<50°$) at room temperature using the ω-scan technique and a scan rate varying from 2.0 to 30.0° min^{-1} depending upon the peak intensity. The intensity of one check reflection, recorded after every 99 measurements, remained essentially constant throughout the data collection. Out of 2521 independent reflections measured, 1795 had $I>3\sigma(I)$, and were used in the structure determination. The data were corrected

0302-4377/82/100841-05$02.50

for Lorentz and polarization factors and for absorption from ϕ-scan data.

STRUCTURE DETERMINATION AND REFINEMENT

The initial positions of the nonhydrogen atoms were taken from the corresponding copper(II) compound,[4] with Cu replaced by Zn, and five cycles of least-squares refinement were run on these positions using isotropic thermal parameters. The conventional agreement factor $R=\Sigma||F_o|-|F_c||/\Sigma|F_o|$ was 0.092.

Anomalous dispersion corrections were included for Zn[8] and refinement with anisotropic temperature factors for nonhydrogen atoms gave $R=0.060$. The function minimized was $\Sigma w(|F_o|-|F_c|)^2$ with $w=1/\sigma^2(F_o)$. At this stage the hydrogen atoms were included in the calculated positions (X–H = 1.0 Å and $U_{iso}=0.06$ Å^2) and not refined since all hydrogen atoms could not be found unambiguously from a difference Fourier map. A full-matrix refinement based on 1795 reflections and 289 variables yielded $R=0.049$, the average shift/error ratio in the last cycle being 0.09. Scattering factors for nonhydrogen atoms were from Cromer & Mann[9] and for H atoms from Stewart, Davidson and Simpson.[10] The largest peak on a final difference map was close to Zn and had a density of 0.5 eÅ^{-3}. The computations were performed on a Univac 1108 computer with the X-RAY 76 program system.[11]

RESULTS AND DISCUSSION

The atomic coordinates and isotropic thermal parameters with their standard deviations are given

Table 1. Fractional atomic coordinates ($\times10^4$) and isotropic thermal parameters for non-hydrogen atoms.

	x	y	z	B_{eq} (Å^2)
Zn	−902(1)	2500	1248(1)	3.78(3)
O1	1116(6)	3029(3)	1813(6)	4.0(3)
O2	620(7)	3877(4)	−44(8)	5.8(4)
O3	3103(8)	4578(3)	1135(9)	7.8(4)
O4	6740(7)	1926(4)	5288(9)	7.7(4)
O5	5162(6)	2576(4)	3509(7)	5.9(3)
O6	2633(7)	2027(4)	4247(8)	6.0(4)
O7	2684(12)	6074(5)	2255(10)	10.6(6)
N1	−95(8)	1525(4)	180(9)	4.6(4)
N2	−961(8)	1832(4)	3067(9)	4.3(4)
N3	−2358(7)	3338(3)	2135(7)	3.0(3)
N4	−2244(8)	2861(4)	−935(8)	5.3(4)
C1	12(12)	989(5)	1443(13)	6.1(6)
C2	−1134(14)	1087(5)	2491(14)	6.2(6)
C3	−816(17)	584(6)	3924(19)	10.0(9)
C4	−2769(16)	993(6)	1556(16)	8.2(8)
C5	1302(11)	1588(5)	−521(12)	5.3(5)
C6	1874(15)	893(6)	−1032(15)	8.7(8)
C7	993(12)	2090(7)	−1879(12)	6.4(6)
C8	−3111(11)	3741(6)	683(12)	4.8(5)
C9	−3646(11)	3264(7)	−759(11)	5.8(6)
C10	−4289(13)	3713(9)	−2229(14)	9.8(9)
C11	−4869(11)	2755(6)	−519(11)	6.9(7)
C12	−1604(9)	3809(5)	3446(11)	3.5(4)
C13	−2783(12)	4308(5)	3973(11)	5.7(6)
C14	−778(10)	3386(5)	4870(10)	4.6(5)
C15	1392(10)	3612(4)	1157(11)	4.0(4)
C16	2847(10)	3987(5)	2060(12)	4.5(5)
C17	2741(12)	4207(6)	3730(13)	6.2(6)
C18	5431(11)	2120(5)	4557(12)	5.2(5)
C19	4046(11)	1730(5)	4989(12)	5.3(5)
C20	4088(15)	966(6)	4505(21)	10.3(9)

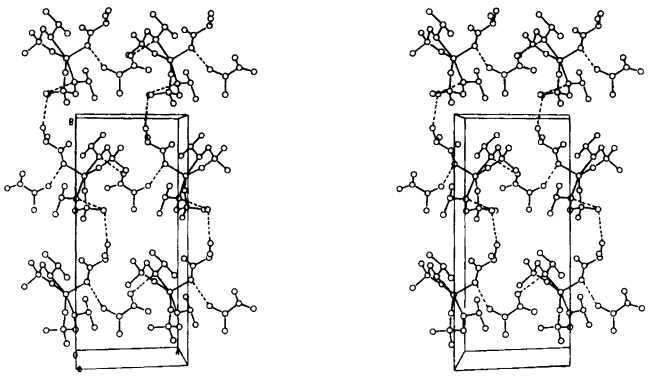

Fig. 1. Stereoscopic view along the c-axis of the packing.

Table 2. Bond lengths (Å) and angles (°) with standard deviations in parentheses.

Zn–O1	2.009(5)	O1–Zn–N2	107.1(2)	N1–Zn–N4	94.4(3)
Zn–N2	2.004(8)	O1–Zn–N4	110.9(3)	N1–Zn–N3	164.3(3)
Zn–N4	2.095(6)	N2–Zn–N4	141.9(3)	N3–Zn–O1	96.2(3)
Zn–N1	2.234(8)	N1–Zn–O1	99.5(3)	N3–Zn–N2	94.3(3)
Zn–N3	2.264(7)	N1–Zn–N2	81.8(3)	N3–Zn–N4	79.2(3)
N1–C1	1.466(13)	Zn–N1–C1	104.4(6)	N2–C2–C3	109.8(9)
C1–C2	1.492(18)	Zn–N1–C5	117.4(6)	N2–C2–C4	107.9(9)
C2–N2	1.487(12)	C1–N1–C5	114.8(7)	C3–C2–C4	110.0(10)
C2–C3	1.524(18)	N1–C1–C2	113.8(8)	Zn–N2–C2	111.0(6)
C2–C4	1.504(17)	C1–C2–N2	106.3(9)	N1–C5–C6	113.8(9)
N1–C5	1.481(13)	C1–C2–C3	111.4(10)	N1–C5–C7	109.5(8)
C5–C6	1.504(17)	C1–C2–C4	111.4(10)	C6–C5–C7	110.7(9)
C5–C7	1.474(15)				
N3–C8	1.483(11)	Zn–N3–C8	105.6(5)	N4–C9–C10	112.2(9)
C8–C9	1.514(14)	Zn–N3–C12	118.5(5)	N4–C9–C11	108.9(10)
C9–N4	1.486(14)	C8–N3–C12	111.8(7)	C10–C9–C11	108.5(8)
C9–C10	1.518(16)	N3–C8–C9	112.2(8)	Zn–N4–C9	113.9(5)
C9–C11	1.491(16)	C8–C9–N4	105.2(7)	N3–C12–C13	111.5(6)
N3–C12	1.471(10)	C8–C9–C10	109.5(11)	N3–C12–C14	110.8(7)
C12–C13	1.538(14)	C8–C9–C11	112.6(8)	C13–C12–C14	109.5(8)
C12–C14	1.504(12)				
C15–O1	1.281(10)	Zn–O1–C15	124.3(5)	C15–C16–O3	107.6(7)
C15–O2	1.210(10)	O1–C15–O2	126.7(8)	C15–C16–C17	113.0(8)
C15–C16	1.524(11)	O1–C15–C16	113.4(7)	C17–C16–O3	110.9(8)
C16–O3	1.410(12)	O2–C15–C16	119.9(8)		
C16–C17	1.501(15)				
C18–O4	1.246(11)	O4–C18–O5	125.9(9)	C18–C19–O6	112.3(8)
C18–O5	1.226(12)	O4–C18–C19	116.1(8)	C18–C19–C20	109.2(9)
C18–C19	1.535(14)	O5–C18–C19	118.0(8)	C20–C19–O6	109.5(8)
C19–O6	1.391(11)				
C19–C20	1.504(16)				

in Table 1. Lists of structure factors and anisotropic thermal parameters can be obtained from the authors. The bond lengths and angles are listed in Table 2.

The structure consists of bis(N^1-isopropyl-2-methyl-1,2-propanediamine)[(*S*)-lactato]zinc(II) cations, (*S*)-lactate ions and water molecules held together by hydrogen bonds and electrostatic forces (Fig. 1). The complex cation with the atomic labelling is shown in Fig. 2.

The coordination geometry around the zinc(II) ion can be considered as distorted trigonal bipyramidal with two nitrogen atoms and a carboxyl oxygen atom in the equatorial sites and two nitrogen atoms bonded to the isopropyl groups in the axial positions. The zinc(II) atom deviates only 0.03(1) Å from the equatorial plane (N2–N4–O1) and the axial bonds [2.234(8) and 2.264(7) Å] are 0.14–0.26 Å longer than the equatorial ones [2.004(8)–2.095(6) Å], as has been suggested for trigonal-bipyramidal coordination.[12] Both equatorial and axial bond angles show marked distortion towards a square-pyramidal geometry due to the out-of trigonal-plane chelation of the diamine ligands and nonbonding interactions. Similar geometry about the zinc(II) ion is found in Zn(acetylacetone)$_2$H$_2$O [13] and in Zn(L-serinato)$_2$ [14] where acetylacetone and L-serinate groups form six- and five-membered rings, respectively, with Zn.

The two diamine rings in the complex cation assume an asymmetric *gauche* configuration. The asymmetry in the ring Zn–N1–C1–C2–N2, where the carbon atoms C1 and C2 deviate 0.08 and −0.57 Å from the plane N1–Zn–N2, is

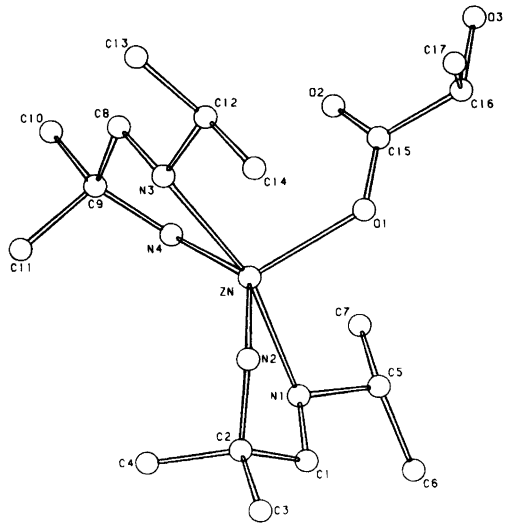

Fig. 2. View of the complex cation.

greater than in the ring Zn−N3−C8−C9−N4, where C8 and C9 deviate 0.30 and −0.40 Å from the plane N3−Zn−N4. It is not immediately obvious why the former ring is so buckled but it is likely that different hydrogen-bonding patterns involving the amine nitrogen atoms are responsible for the phenomenon. The two diamine chelate rings are in the same conformation (λ) as in the corresponding copper(II) compound[4] and in bis(N^1-isopropyl-2-methyl-1,2-propanediamine)copper(II) succinate[6] and fumarate,[6] where *trans* chelation by diamine ligands slightly favours the $\lambda\lambda$ or $\delta\delta$ arrangement.[15] However in bis(N^1-isopropyl-2-methyl-1,2-propanediamine)copper(II) tartrate[5] and malate[6] the $\delta\lambda$ configuration is found, owing to intramolecular interactions caused by the apical dicarboxylates.

Both the coordinated and uncoordinated carboxylate groups (C−COO) are planar within experimental error and the α-hydroxyl oxygen atoms O3 and O6 deviate 0.15 Å from the C−COO planes. It should be noted that an intramolecular hydrogen bond between the α-hydroxyl oxygen atom and a carboxyl oxygen atom is highly unfavourable although the O2···O3 and O5···O6 distances are 2.575(9) and 2.651(9) Å, respectively.[16] The carboxyl C−O bond lengths [1.281(10) and 1.210(10) Å] and C−C−O angles [113.4(7) and 119.9(8)°] of the monodentate lactate group are significantly different and indicate double-bond character for the nonbonded carboxyl oxygen atom. This is consistent with the observation that in α-hydroxy carboxylic acids and their salts the α-hydroxyl group is almost coplanar with the C−COO plane and in an eclipsed position relative to the double-bonded carboxyl oxygen atom.[16] The carboxyl C−O bond lengths of the ionic lactate group are equal within experimental error but the C−C−O angles still retain an inequivalency, the larger being towards the α-hydroxyl group.

Complex cations and (*S*)-lactate ions appear to be connected by hydrogen bonds to chains parallel to the a axis (Fig. 1). The O1···O6 distance of 2.913(8) Å and the O5···N3 ($1+x$, y, z) distance of 3.048(9) Å indicate weak hydrogen bonding between these atoms. In addition the N2···O6 distance of 3.139(9) Å can be considered as indicating a very weak hydrogen bond. The O4···N2 ($1+x$, y, z) distance of 3.051(11) Å represents a purely electrostatic interaction rather than a hydrogen bond since this interaction is directed out of the plane of the carboxyl group and below the oxygen lone-pair lobe assuming sp^2 hybridization for carboxyl oxygen atoms). Water molecules join the chains together in the *b* and *c* directions. The O3···O7 distance of 3.030(12) Å indicates a very weak and the O7···N1 ($-x$, $1/2+y$, $-z$) distance of 2.870(11) Å a weak hydrogen bond between chains in the direction of the *b* axis. The The O7···O4 ($1-x$, $1/2+y$, $1-z$) distance of 2.601(12) Å is the shortest hydrogen-

bond distance in the structure and it joins layers represented in Fig. 1 together in the direction of the *c* axis.

The packing of the complex cations, (*S*)-lactate ions and water molecules in the present structure is similar to that in the corresponding copper(II) compound. Neither compound has any unusual feature in the bond lengths abd angles of the diamine ligands or lactate groups. The main difference arises from the stereochemistry of the metal ions. In the copper(II) compound the geometry about the metal atom is a distorted square pyramid with the basal Cu – N bond distances on average 0.10 Å shorter than the apical Cu – O distance of 2.16 Å. Similar coordination geometry around zinc(II) is found in [5,10,15,20-tetrakis(4-pyridyl)porphinato]-(pyridine)zinc(II)[17] and [5-{2-{[2-(3-pyridyl)ethyl]-carbonylamino}phenyl}-10,15,20-triphenylporphinato]zinc(II)[18] where basal Zn – N bond distances are also 0.10 Å shorter than the apical Zn – N bond distances of 2.15 Å. Gillespie[12] has shown in terms of the theory of valency-shell electron-pair repulsion that trigonal-bipyramidal geometry is slightly preferred to square-pyramidal for transition elements with d^{10} configuration. In the above two zinc(II) porphin complexes, however, polydentate ligands prevent the formation of a trigonal bipyramid. In the present zinc(II) compound the preferred trigonal-bipyramidal configuration is found, though markedly distorted.

REFERENCES

1. Näsänen, R., Tilus, P., Lindell, E. and Eskolin, E. *Suom. Kemistil. B 45* (1972) 111.
2. Kansikas, J. and Hämäläinen, R. *Finn. Chem. Lett.* (1977) 118.
3. Kansikas, J. and Pajunen, A. *Acta Crystallogr. B 36* (1980) 2423.
4. Ahlgrén, M. and Hämäläinen, R. *Finn. Chem. Lett.* (1975) 211.
5. Kansikas, J. and Hämäläinen, R. *Finn. Chem. Lett.* (1978) 54.
6. Kansikas, J. *Private communication.*
7. Ahlgrén, M. *Ann. Acad. Sci. Fenn. Ser. A 2 No. 187* (1979) 23.
8. *International Tables for X-Ray Crystallography*, Kynoch Press, Birmingham 1974, Vol. 4, p. 149.
9. Cromer, D. T. and Mann, J. B. *Acta Crystallogr. A 24* (1968) 321.
10. Stewart, R. F., Davidson, E. R. and Simpson, W. T. *J. Chem. Phys. 42* (1975) 3175.
11. Stewart, J. M., Ed., *The X-Ray System, Version of 1976*, Technical Report TR-446, Computer Science Center, University of Maryland, College Park 1976.
12. Gillespie, R. J. *J. Chem. Soc.* (1963) 4679.
13. Lippert, E. L. and Truter, M. R. *J. Chem. Soc.* (1960) 4996.
14. Van Der Helm, D., Nicholas, A. F. and Fisher, C. G. *Acta Crystallogr. B 26* (1970) 1172.
15. Corey, E. J. and Bailar, J. C. *J. Am. Chem. Soc. 81* (1959) 2620.
16. Kanters, J. A., Kroon, J., Peerdeman, A. F. and Schoone, J. C. *Tetrahedron 23* (1967) 4027.
17. Collins, D. M. and Hoard, J. L. *J. Am. Chem. Soc. 92* (1970) 3761.
18. Bobrik, M. A. and Walker, F. A. *Inorg. Chem. 19* (1980) 3383.

Received March 24, 1982.

Acta Chemica Scandinavica A 36 (1982) 847–851

Structural Studies of Hexagonal Mg_2NiH_x

DAG NORÉUS[a] and PER-ERIK WERNER[b]

[a]Royal Institute of Technology, Department of Reactor Physics, S-100 44 Stockholm, Sweden and [b]Department of Structural Chemistry, Arrhenius Laboratory, University of Stockholm, S-106 91 Stockholm, Sweden

X-Ray and neutron powder diffraction measurements have been used to study the structural changes when a small amount of hydrogen is absorbed in the hexagonal alloy Mg_2Ni, $a=5.2107$ Å and $c=13.2437$ Å. The unit cell dimensions for saturated Mg_2NiH_x ($x\simeq0.3$) are $a=5.2315$ Å and $c=13.404$ Å. It is shown that the most significant structural change caused by the hydrogenation is an increase in one Mg – Mg distance from 3.062 Å to about 3.73 Å, indicating a hydrogen site between the two Mg-atoms. The result is also in agreement with the assumption that fully ionized H^- is present in $Mg_2NiH_{0.3}$.

The reaction between hydrogen and Mg_2Ni to form the ternary hydride Mg_2NiH_4, proposed as a possible hydrogen storage material, occurs in two consecutive steps, (I) and (II).

$$Mg_2Ni+(\tfrac{x}{2})H_2 \rightleftarrows Mg_2NiH_x \quad (x\simeq0.3) \qquad (I)$$

$$Mg_2NiH_x+(2-\tfrac{x}{2})H_2 \rightleftarrows Mg_2NiH_4 \qquad (II)$$

In the first reaction hydrogen dissolves in hexagonal Mg_2Ni with minor expansions of the unit cell dimensions, primarily of the c-axis (*cf.* Table 1).[1] In the second reaction a complete phase transition takes place, and if the reaction occurs above 235 °C a cubic Mg_2NiH_4(HT) structure, $a=6.490$ Å, of antifluorite type is formed.[2]

It has been proposed in a recent study by Hirata, Matsumoto, Amano and Sasaki [3] that the HT phase is tetragonal, with $a=6.533$ Å and $c=7.499$ Å. An examination of their published data, however, gives scant support for this conclusion. Although the deviations of observed from calculated diffraction angles are smaller for the proposed tetragonal cell than for a cubic cell, the De Wolff figure of merit,[4] M_{20}, is higher for a cubic indexing in an F-centered space group than for the tetragonal indexing. Interestingly, the 9 first lines ($2\theta<85°$) of the 11 measured reflections show positive differences between observed and calculated diffraction angles in a cubic refinement, thus indicating a possible zero point error.

Table 1. Crystal data.

	Mg_2Ni	Mg_2NiH_x ($x\approx0.3$)
Space group	$P6_222$	$P6_222$
Z	6	6
FW	107.33	107.67
a (Å)	5.2107(2)	5.2315(6)
c (Å)	13.2437(5)	13.404(3)
V (Å^3)	311.41	317.70
d_{calc} (g/cm^3)	3.434	≈3.37
M_{20}	193	26

The transformations of Mg_2NiH_4(HT) below 235 °C have been studied by Genossar and Rudman,[5] by Darnaudery, Pezat, Darriet and Hagenmuller [6] and by Noréus and Werner.[7] Although the reaction is not yet fully understood, it seems clear that at 20 °C a monoclinic low-temperature modification Mg_2NiH_4(LT) exists. The unit cell dimensions proposed by the present authors are $a=6.497$ Å, $b=6.414$ Å, $c=6.601$ Å and $\beta=93.23°$, although it was stated that the interpretation of weak lines in the pattern as superstructure lines could not be completely ruled out.[7] Independently, a similar conclusion was drawn by Genossar and Rudman.[5] Darnaudery *et al.*[6] claim that the a-axis should be doubled, 12.99 Å. They have also found an orthorhombic

0302-4377/82/100847-05$02.50

Mg_2NiH_4(LT) phase with $a=6.499$ Å, $b=6.415$ Å and $c=6.589$ Å. Unfortunately, however, we have not found it possible to index all diffraction lines in patterns from Mg_2NiH_4 obtained at 20 °C solely by these two unit cells.

The present work was undertaken in an attempt to provide information about the first reaction step, I, in the transformation of Mg_2Ni to a hydrogen containing material. The second reaction, II, will be the subject of a forthcoming study.

EXPERIMENTAL

The Mg_2Ni used in the present study was supplied by MPD-Technology Corp.; it is commercially available as their hydrogen storage alloy, Hystore 301. It contains a slight excess of free magnesium metal in order to prevent the formation of $MgNi_2$ during its preparation.

A sample of 2 g of Mg_2Ni was cycled several times at 400 °C with hydrogen pressures up to 100 bar. Then the pressure was slowly decreased. By monitoring the temperature in the sample, the onset of dehydrogenation could be determined. About 20% of the expected hydrogen content was then very slowly withdrawn. The temperature was lowered to the ambient value, and a sample of a few mg was taken out for X-ray analysis. The hydride was then cycled a few more times to reduce surface oxide contamination. The above procedure was repeated, and each time about 20% more hydrogen was removed from the hydride. Thus, a set of 5 samples with various hydrogen contents was obtained.

The diffraction patterns yielded by the samples contained lines of $Mg_2NiH_{0.3}$, MgH_2 and Mg_2NiH_4(LT). The unit cell dimensions of the constituents remained the same within the standard deviations throughout the set. A number of elusive lines could, however, not be indexed. Their intensities were always very weak, and they diminished at approximately the same rate as those belonging to the monoclinic Mg_2NiH_4(LT). Some of these lines also showed small positional variations, which made it difficult to interpret them as superstructure lines in a simple way. The last sample was used in the subsequent profile refinement.

DATA COLLECTION

The X-ray powder photographs were taken in a subtraction-geometry Guinier-Hägg focussing camera of 80 mm diameter, with strictly monochromatized Cu$K\alpha_1$ radiation ($\lambda=1.5405981$ Å).[8] Single-coated film (CEA Reflex 15) was used in order to avoid superposition of front- and back-layer intensity profiles, and to reduce the background. All measurements of the films were made by means of a computer-controlled single-beam microdensitometer specially designed for X-ray powder diffraction photographs.[9] The slit opening of the collimator was 0.040×2.0 mm and the corresponding measuring step length in the θ-direction on the photographs was about 0.0143°. The θ scale was calibrated by the internal standard technique, using a parabolic correction curve. Silicon [$a=5.430880(35)$ Å at 25 °C] [10] was chosen as standard substance.

The neutron diffraction pattern of Hystore 301 was recorded using one of the diffractometers at the R2 reactor in Studsvik.[11] The incoming wavelength was selected to be 1.1562 Å, allowing a wave vector transfer from 1.0 to 8.4 $Å^{-1}$. To avoid preferred orientation effects the target was rotated during the measurements.

RESULTS AND DISCUSSION

a. Mg_2Ni. Diffraction data from Mg_2Ni, with a slight excess of Mg, was collected by neutron and X-ray powder techniques. Both data sets were refined by the Rietveld profile analysis procedure [12] using program versions for simultaneous refinement of two phases present in a powder sample.[13] Unit cell dimensions for Mg_2Ni, $a=5.2107(2)$ Å and $c=13.2437(5)$ Å, were taken from Ref. 7. The fractional atomic coordinates in space group $P6_222$ used as starting parameters in the refinements were those derived by Schubert and Anderko.[14] No significant differences between the coordinates obtained by the two techniques were found, but the most accurate results were obtained from the neutron diffraction data. The R_F ($=\Sigma|\sqrt{I_{obs}}-\sqrt{I_{calc}}|/\Sigma\sqrt{I_{obs}}$) values obtained from this data set were 0.031 and 0.051 for Mg_2Ni and Mg, respectively. Final position and isotropic thermal parameters are given in Table 2a. Interatomic distances are listed in Table 3a.

b. $Mg_2NiH_{0.3}$. The $Mg_2NiH_{0.3}$ sample, also containing a small amount of MgH_2, was investigated by X-ray diffraction technique. The diffraction patterns obtained were of low quality, however, because of disorder in the structure, caused by the non-stoichiometric hydrogen content. The half-widths of the diffraction lines varied in an

Table 2. Positional and isotropic thermal parameters.

Atom	Site	x	y	z	B (Å^2)
Positional and isotropic thermal parameters for Mg_2Ni					
Ni1	3(b)	0.0	0.0	0.5	0.73(4)[a]
Ni2	3(d)	0.5	0.0	0.5	0.82(4)
Mg1	6(f)	0.5	0.0	0.1158(2)	0.69(5)
Mg2	6(i)	0.1626(6)	0.3252(12)	0.0	0.53(5)
Mg position parameters for $Mg_2NiH_{0.3}$					
Mg1	6(f)	0.5	0.0	0.1391(9)	
Mg2	6(i)	0.160(3)	0.320(6)	0.0	

[a] Estimated standard deviations are given within parantheses.

irregular way. Thus, the prerequisite for a Rietveld refinement, that the half-widths should be described by a second-order polynomial in tg θ, was not well fullfilled. Furthermore, the background was seriously affected by a large amount of amorphous material. It was supposed, however, that because of the simplicity of the structure a refinement could be made, albeit with limited accuracy. Most of the positional coordinates are fixed by the space group symmetry, $P6_222$. The only refinable coordinates are z for Mg1 and x for Mg2 (*cf.* Table 2), as y for Mg2 equals $2x$.

It was found in a number of refinements, using the complete data set up to $2\theta = 88°$, as well as using partial data sets from selected 2θ intervals, that although the R_F values usually were as high as about 0.2, the magnesium coordinates varied only within one standard deviation. Furthermore, if z for Mg1 was fixed at the start value 0.1158 (*cf.* Table 2a), the R_F values increased about 0.1. Therefore, it can be concluded that the transition of Mg_2Ni to $Mg_2NiH_{0.3}$ causes a significant shift in the Mg1 position. It should be realized, however, that the coordinates and distances listed in Tables 2b and 3b, respectively, are derived from a somewhat disordered structure. They should be interpreted as

Table 3. Interatomic metal-metal distances (Å) less than 4.0 Å. Estimated standard deviations are given within parentheses.

(a) Mg_2Ni			
Ni1 – Ni2	2.605(1)		
Ni1 – Mg1	2.691(1)		
Ni1 – Mg2	2.648(3)		
Ni2 – Mg1	2.691(1)		
Ni2 – Mg2	2.679(1)		
Mg1 – Mg1	2.932(2)	3.062(4)	
Mg1 – Mg2	3.255(2)	3.360(2)	3.408(4)
Mg2 – Mg2	2.936(7)	3.045(5)	
(b) $Mg_2NiH_{0.3}$			
Ni1 – Ni2	2.620(1)		
Ni1 – Mg1	2.66(2)		
Ni1 – Mg2	2.646(2)		
Ni2 – Mg1	2.718(8)		
Ni2 – Mg2	2.646(2)		
Mg1 – Mg1	2.722(6)	3.73(3)	
Mg1 – Mg2	3.02(2)	3.53(2)	3.61(3)
Mg2 – Mg2	2.90(4)	3.09(3)	

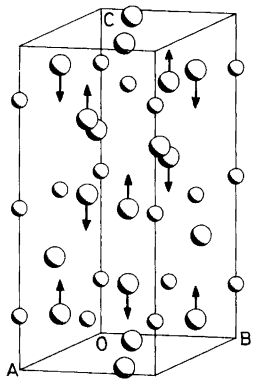

Fig. 1. View of the Mg_2Ni structure. The arrows denote the main directions of distortions induced when hydrogen enters the structure.

Table 4. Observed and calculated 2θ values for $Mg_2NiH_{0.3}$.

$2\theta_{obs}$	$2\theta_{calc}$	$\Delta 2\theta$	d_{obs}	I_{obs}	(*hkl*)
19.603	19.578	0.025	4.525	2354	(100)
19.908	19.855	0.053	4.456	5421	(003)
20.694	20.678	0.016	4.289	3484	(101)
23.717	23.685	0.032	3.7484	1948	(102)
28.072	28.025	0.047	3.1761	890	(103)
34.925	34.920	0.005	2.5670	762	(111)
36.872	36.857	0.015	2.4358	7314	(112)
39.068	39.008	0.060	2.3038	7150	(105)
39.756	39.759	−0.003	2.2655	8725	(200)
{	40.340	0.032			(006)
{ 40.372	40.347	0.025	2.2323	638	(201)
43.912	43.873	0.039	2.0602	1081	(114)
44.783	44.822	−0.039	2.0221	11745	(203)
45.219	45.219	0.000	2.0037	547	(106)
48.628	48.591	0.037	1.8708	179	(115)
51.837	51.791	0.046	1.7623	169	(107)
53.430	53.466	−0.367	1.7135	194	(210)
{ 53.920	53.930	−0.010	1.6991	663	(116)
{	53.936	−0.016			(211)
55.331	55.328	0.003	1.6590	369	(212)
57.600	57.598	0.002	1.5989	190	(213)
57.947	57.930	0.017	1.5902	1205	(206)
58.662	58.704	−0.042	1.5725	115	(108)
60.703	60.685	0.018	1.5244	85	(214)
61.759	61.767	−0.008	1.5009	195	(301)
62.252	62.291	−0.039	1.4902	177	(009)
63.033	63.048	−0.015	1.4736	1627	(302)
64.546	64.522	0.024	1.4426	3602	(215)
65.167	65.151	0.016	1.4304	342	(303)
66.170	66.182	−0.012	1.4111	736	(118)
68.062	68.038	0.024	1.3764	212	(304)
72.147	72.168	−0.021	1.3082	4105	(220)
75.698	75.713	−0.015	1.2554	1163	(223)

giving an average picture of the structure.

The unit cell dimensions of $Mg_2NiH_{0.3}$ determined by the profile refinement are listed in Table 1. An indexed pattern is given in Table 4.

As can be seen from Table 3, the most significant difference between Mg_2Ni and $Mg_2NiH_{0.3}$ is that one short Mg1 – Mg1 distance is increased from 3.062(4) Å in Mg_2Ni to 3.73(3) Å in $Mg_2NiH_{0.3}$. This is symbolized by arrows in Fig. 1, and it may be concluded that the hydrogen enters the structure at the midpoint between these Mg-atoms. In Fig. 2, the assumed hydrogen position is indicated. Interestingly, this point (0,0,1/2), position 3(c) in $P6_222$,[15] is the point in the structure located at maximum distance from the Ni-atoms. Considering that the Mg1 – Mg1, 3.73 Å, in $Mg_2NiH_{0.3}$ represents an average distance because of the disorder, and that Mg – D in MgD_2 is 1.95(2) Å,[16] it may be concluded that hydrogen in $Mg_2NiH_{0.3}$ is present as fully ionized H^-. This is also in agreement with the increase in volume of about 4 Å^3 per H-atom entering Mg_2Ni.

It was concluded by Genossar and Rudman [5] that Mg_2NiH_4 is a weakly ionized structure $Mg_2^{+2\delta}NiH_4^{-\delta}$ with $\delta \rightarrow 0$. Thus, reaction II (see above) should be accompanied by a distribution of the electric charge on H^- over more hydrogen atoms, although the total charge may remain the same.

Acknowledgements. The authors wish to thank Profs. P. Kierkegaard and K. E. Larsson for their kind interest in this work. Our sincere thanks are due to Mr. Lars Göthe and Mr. L. E. Karlsson for their skilful technical assistance. This investigation

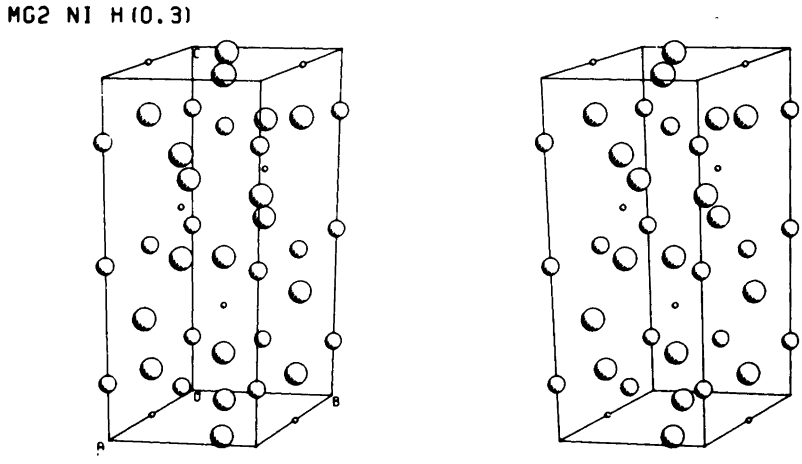

Fig. 2. Stereo view of the $Mg_2NiH_{0.3}$ structure. Small circles = assumed hydrogen sites (occupation factor ≈0.6), medium circles = Ni and large circles = Mg.

has received financial support from the Swedish Natural Science Research Council.

REFERENCES

1. Schefer, J., Fischer, P., Hälg, W., Stucki, F., Schlapbach, L., Didisheim, J. J., Yvon, K. and Andresen, A. F. *J. Less Common Met. 74* (1980) 65.
2. Gavra, Z., Mintz, M. H., Kimmel, G. and Hadari, Z. *Inorg. Chem. 18* (1979) 3595.
3. Hirata, T., Matsumoto, T., Amano, M. and Sasaki, Y. *J. Phys. F 11* (1981) 521.
4. De Wolff, P. M. *J. Appl. Crystallogr. 1* (1968) 108.
5. Genossar, J. and Rudman, P. S. *J. Phys. Chem. Solids 42* (1981) 611.
6. Darnaudery, J.-P., Pezat, M., Darriet, B. and Hagenmuller, P. *Mater. Res. Bull. 16* (1981) 1237.
7. Noréus, D. and Werner, P.-E. *Mater. Res. Bull. 16* (1981) 199.
8. Deslattes, R. D. and Henins, A. *Phys. Rev. Lett. 31* (1973) 972.
9. Johansson, K. E., Palm, T. and Werner, P.-E. *J. Phys. E 13* (1980) 1289.
10. Hubbard, C. R., Swanson, H. E. and Mauer, F. A. *J. Appl. Crystallogr. 8* (1975) 45.
11. Stedman, R. and Nilsson, G. *Rev. Sci. Instr. 39* (1968) 637.
12. Rietveld, H. M. *J. Appl. Crystallogr. 2* (1969) 65.
13. Werner, P.-E., Salomé, S., Malmros, G. and Thomas, J. O. *J. Appl. Crystallogr. 12* (1979) 107.
14. Schubert, K. and Anderko, K. *Z. Metallkd. 42* (1951) 321.
15. *International Tables for X-Ray Crystallography*, Kynoch Press, Birmingham 1969, Vol. 1.
16. Zachariasen, W. H., Holley, C. E., Jr. and Stamper, J. F., Jr. *Acta Crystalogr. 16* (1963) 352.

Received March 30, 1982.

Acta Chemica Scandinavica A 36 (1982) 853–860

Short Communications

Nickel Chelates of Trithione- and Isotrithionedithiolate – A New Class of 1,2-Dithiolates. Part II.* The Crystal Structure of Tetramethylammonium Bis(isotrithionedithiolato)nickelate(II)

OLIVER LINDQVIST,[a] LENNART SJÖLIN,[a] JOACHIM SIELER,[b] GÜNTER STEIMECKE[b] and EBERHARD HOYER[b]

[a] Department of Inorganic Chemistry, Chalmers University of Technology and the University of Göteborg, S-412 96 Göteborg, Sweden and [b] Sektion Chemie der Karl-Marx-Universität Leipzig, 701 Leipzig, Liebig Str. 18, German Democratic Republic.

A mixture of dimethylformamide (DMF), alkali metals and carbondisulfide reacts to give 1,3-dithiole-2-thion-4,5-dithiolate:[1,2]

$$4K + 4CS_2 \rightarrow C_3S_5^{2-} + CS_3^{2-} + 4K^+$$

On heating the products to 120–140 °C in the presence of dimethylformamide, the "isotrithionedithiolate" ion rearranges to form an isomeric $C_3S_5^{2-}$ ion which has different physical and chemical properties. A nickel chelate complex of this ion with the composition $[N(C_4H_9)_4]_2[Ni(C_3S_5)_2]$, has been isolated.[3] The structure analysis of this compound will provide valuable information concerning the nature of the rearrangement within the $C_3S_5^{2-}$ ion and of the coordination properties of the new isomer system. The compound crystallizes in space group $P2_1/n$ with parameters: $a = 14.670(3)$ Å, $b = 8.611(2)$ Å,** $\beta = 105.15(6)°$, $D_x = 1.31$ g cm^{-3}, $\mu = 4.6$ mm^{-1}, $Z = 2$ and M.W. = 936.4.

The intensity data were collected on a Syntex $P2_1$ four-circle diffractometer using graphite monochromatized Cu$K\alpha$ radiation to $2\theta = 100°$. A total of 1346 reflexions were collected, and those 937 reflexions with $I > 3\sigma(I)$ were considered significant and used in the subsequent calculations. The background and integrated intensities were obtained from the Lehmann-Larsen profile analysis method.[4] The intensities were corrected for Lorentz and polarisation effects, but not for absorption or extinction. The full-matrix least squares refinement of an overall scale factor, positional and anisotropic thermal parameters for all non-hydrogen atoms, isotropic thermal parameters for the hydrogen atoms gave a final $R = 0.054$. A list of structure factors, thermal parameters and coordinates of the hydrogen atoms is available from the authors on request. The positional parameters of the non-hydrogen atoms are given in Table 1.

Table 1. Positional parameters with standard deviations, $\times 10^4$, and isotropic thermal parameters.

	x/a	y/b	z/c	B Å^{-2}
Ni(1)	0	0	0	3.7(1)
S(1)	1346(3)	−44(6)	−779(2)	6.3(1)
S(2)	658(3)	800(5)	−801(2)	4.7(1)
S(3)	3316(3)	596(6)	736(2)	7.4(1)
S(4)	3696(3)	1379(7)	−120(2)	8.2(1)
S(5)	2455(3)	1940(6)	−1481(2)	6.0(1)
C(1)	2126(10)	476(8)	339(7)	4.9(4)
C(2)	1839(11)	894(9)	−364(7)	5.2(4)
C(3)	2534(10)	1349(6)	−678(7)	4.5(4)
N(1)	5718(8)	−1178(3)	3175(5)	4.2(4)
C(4)	5700(10)	−1361(7)	3937(7)	4.3(4)
C(5)	6254(10)	−179(20)	4403(7)	5.5(5)
C(6)	6395(12)	−755(22)	5156(9)	7.5(6)
C(7)	6879(12)	489(20)	5657(8)	6.6(5)
C(8)	5302(10)	385(17)	2907(7)	4.5(5)
C(9)	4255(10)	607(18)	2873(7)	5.6(5)
C(10)	3926(10)	2194(18)	2601(7)	5.2(5)
C(11)	2895(12)	2471(23)	2522(9)	7.6(6)
C(12)	6747(10)	−1088(18)	3102(7)	4.4(4)
C(13)	7279(13)	−2526(24)	3402(9)	8.2(5)
C(14)	8353(14)	−2070(24)	3391(10)	9.4(5)
C(15)	9117(17)	−2977(31)	3833(12)	13.5(6)
C(16)	5169(10)	−2546(17)	2770(7)	4.6(4)
C(17)	5064(10)	−2463(19)	2016(7)	5.6(5)
C(18)	4555(13)	−3913(22)	1670(9)	7.7(5)
C(19)	4438(15)	−3855(26)	886(10)	10.6(6)

* For part I, see Ref. 2.
** $c = 20.140(3)$ Å.

0302-4377/82/100853-02$02.50

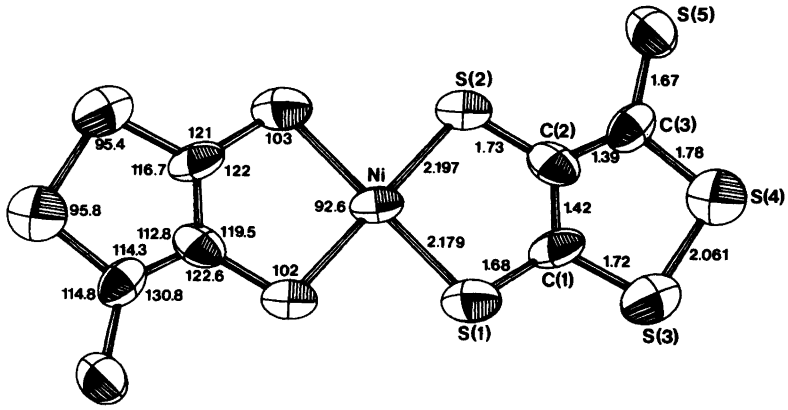

Fig. 1. The planar $Ni(C_3S_5)_2^{2-}$ ion. The standard deviations in the Ni – S, C – S and C – C bond distances are 0.004, 0.01 and 0.02 Å, respectively.

The structure of the $[Ni(C_3S_5)_2]^{2-}$ ion is shown in Fig. 1. The structure analysis shows that the 1,3-dithiole-2-thion-4,5-dithiolate has transformed to the thermodynamically more stable 1,2-dithiole-3-thion-4,5-dithiolate (trithionedithiolate) by heating. The trithionedithiolate ion is stabilized in relation to the isotrithionedithiolate by resonance in the ring system:

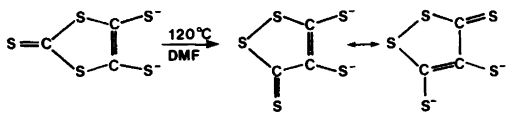

As expected the $[Ni(C_3S_5)_2]^{2-}$ anion is planar. None of the atoms deviates by more than one standard deviation from the plane. The two Ni – S distances (Fig. 1) are significantly shorter than the corresponding distances, 2.211(4) and 2.221(4) Å, in the nickel(II) isotrithionedithiolate compound,[2] but are comparable with the distances found in other 1,2-ditriolates.[5,6] The S(3) – S(4) distance corresponds to a single bond which is also consistent with the C(1) – S(3) – S(4) and S(3) – S(4) – C(3) angles of 95.4 and 95.8°, respectively.

The atoms in the $[N(C_4H_9)_4]^+$ cation show considerable thermal motions and the standard deviations of the bond lengths are therefore high. Two $[N(C_4H_9)_4]^+$ cations are centrosymmetrically arranged around the $Ni[(C_3S_5)_2]^{2-}$ anion. The shortest contact between the ions are S – H bridges with distances of 2.8 – 2.9 Å. Similar S – H contacts have been observed previously in nickel-1,1 dithiolate structures.[7]

1. Steimecke, G., Sieler, J., Kirmse, R. and Hoyer, E. *Phosphorus Sulfur* 7 (1979) 49.
2. Sjölin, L., Lindqvist, O., Sieler, J., Steimecke, G. and Hoyer, E. *Acta Chem. Scand. A 33* (1979) 445.
3. Steimecke, G., Sieler, J., Kirmse, R., Dietzsch, W. and Hoyer, E. *Phosphorus Sulfur 12* (1982) 237.
4. Lehmann, M. S. and Larsen, F. K. *Acta Crystallogr. A 30* (1974) 580.
5. Eisenberg, R. E. *Prog. Inorg. Chem. 12* (1970) 295.
6. Eisenberg, R. E. and Ibers, J. A. *Inorg. Chem. 4* (1965) 605.
7. Newman, P. W. G. and White, A. H. *J. Chem. Soc. Dalton Trans. 4* (1972) 1460.

Received June 29, 1982.

Nickel Chelates of Trithione- and Isotrithionedithiolate – a New Class of 1,2-Dithiolates. Part III. The Crystal Structure of Tetrabutylammonium Bis(isotrithionedithiolato)nickelate(III)

OLIVER LINDQVIST,[a] LEIF ANDERSEN,[a] JOACHIM SIELER,[b] GÜNTER STEIMECKE [b] and EBERHARD HOYER [b]

[a] Department of Inorganic Chemistry, Chalmers University of Technology and the University of Göteborg, S-412 96 Göteborg, Sweden and [b] Sektion Chemie der Karl-Marx-Universität Leipzig, 701 Leipzig, Liebig Str. 18, German Democratic Republic

When alkali metals react with carbon disulfide in a solution of dimethylformamide (DMF), a new type of sulfur-rich dithiolene ligand is formed: 1,3-dithiole-2-thion-4,5-dithiolate.[1,2] Its chelate complex with nickel shows characteristic reversible electron-transfer reactions. In a solution of acetone, it is possible to oxidize the nickel(II) complex with iodine to a nickel(III) complex [1] of the composition $[N(C_4H_9)_4]Ni(C_3S_5)_2$:

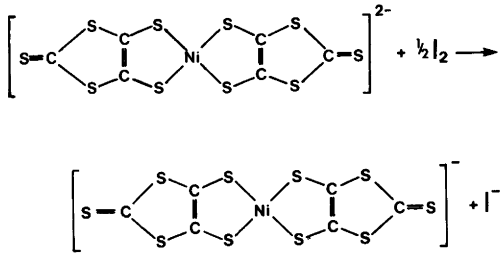

The structure analysis of the nickel(III) complex should provide information about the change in bonding character compared to the corresponding nickel(II) complex.[2]

The nickel(III) compound, $[N(C_4H_9)_4]Ni(C_3S_5)_2$, crystallizes in space group $P2_1/c$ with parameters $a=14.649(3)$ Å, $b=13.497(3)$ Å, $c=16.383(4)$ Å, $\beta=91.14(6)°$, $D_x=1.42$, $\mu=1.2$ mm^{-1}, $Z=4$, and M.W. = 693.8. Small crystals, $\leqq 0.1$ mm in cross section, are green and transparent, while larger crystals appear to be black and opaque. The x-ray data were collected on a Syntex $P2_1$ diffractometer, using graphite monochromated Mo$K\alpha$ radiation. Three-dimensional data (6848 reflections with $2\theta \leqq 100°$) were measured using the $\omega/2\theta$ scan technique. Integrated intensity values were obtained from the Lehmann-Larsen profile analysis method.[3,4] Those 2349 reflections having $I > 3\sigma(I)$ were used for the structure determination and refinement. The intensities were corrected for Lorentz and polarization effects, using the program GECOR,[5] but not for absorption or extinction, since these effects were small. The structure was solved from the Patterson function. Positional and thermal parameters were subjected to several cycles of block-diagonal least squares refinement.[5] The final refinement included anisotropic temperature factors for the non-hydrogen atoms and isotropic temperature factors for the hydrogen atoms, and the

Table 1. Positional parameters and standard deviations, $\times 10^4$.

Atom	x/a	y/b	z/c	B_{eq} Å^2
Ni	1601(1)	1389(1)	1588(1)	3.4(1)
S(1)	1665(2)	2921(2)	1232(2)	4.2(1)
S(2)	132(2)	1353(2)	1551(2)	4.8(1)
S(3)	168(2)	4433(2)	918(2)	5.0(1)
S(4)	−1247(2)	2983(3)	1164(2)	5.3(1)
S(5)	−1779(3)	5008(3)	657(3)	7.7(1)
S(6)	3079(2)	1434(2)	161(2)	4.5(1)
S(7)	1567(2)	−122(2)	2008(2)	5.2(1)
S(8)	4474(2)	−62(2)	2208(2)	5.1(1)
S(9)	3092(2)	−1503(2)	2565(2)	5.5(1)
S(10)	5036(2)	−2022(3)	2872(2)	6.4(1)
C(1)	529(7)	3227(7)	1177(6)	3.6(2)
C(2)	−138(7)	2558(8)	1288(6)	3.8(2)
C(3)	−992(8)	4188(9)	890(6)	5.1(3)
C(4)	3355(7)	286(7)	2005(6)	3.9(2)
C(5)	2707(7)	−389(8)	2186(6)	4.3(2)
C(6)	4259(7)	−1241(9)	2581(6)	4.6(2)
Tetrabutylammonium ion				
N	2368(6)	4151(6)	3739(5)	4.1(2)
C(7)	2916(7)	3216(8)	3558(6)	4.1(2)
C(8)	3149(8)	2568(9)	4266(6)	5.1(3)
C(9)	2708(9)	1707(9)	4013(7)	5.9(3)
C(10)	4025(9)	1091(11)	4706(9)	7.8(4)
C(11)	1461(7)	3903(8)	4137(6)	4.4(2)
C(12)	832(8)	3205(9)	3675(7)	5.3(3)
C(13)	5(9)	2982(12)	4155(7)	6.8(3)
C(14)	−671(10)	2332(10)	3761(8)	7.1(4)
C(15)	2157(7)	4697(8)	2942(6)	4.0(2)
C(16)	2984(8)	5078(8)	2490(6)	4.7(2)
C(17)	2695(8)	5661(9)	1741(8)	5.8(3)
C(18)	3477(10)	6044(9)	1274(7)	7.1(3)
C(19)	2928(8)	4808(7)	4332(6)	4.6(2)
C(20)	2575(9)	5809(10)	4493(7)	7.3(3)
C(21)	3191(12)	6338(12)	5112(9)	8.5(4)
C(22)	4106(11)	6547(17)	4866(13)	12.6(6)

0302-4377/82/100855-02$02.50

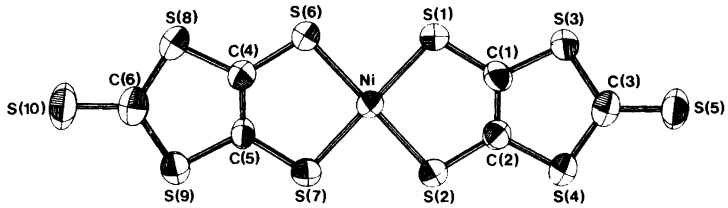

Fig. 1. The $Ni^{III}(C_3S_5)_2^-$ ion. The notation is in accordance with Tables 1 and 2.

resulting R $(=\Sigma||F_o|-|F_c||/\Sigma F_o)$ value was 0.054. Lists of structure factors, thermal parameters and refined coordinates of the hydrogen atoms are available from the authors on request. The positional parameters of the non-hydrogen atoms are given in Table 1. Bond distances and angles of the $Ni^{III}(C_3S_5)_2^-$ ion are given in Table 2, and its structure together with atom identifications is shown in Fig. 1.

Table 2. Bond lengths (Å) and angles (°) within the $Ni^{III}(C_3S_5)_2^-$ ion.

Bond distances		Bond angles	
Ni–S(1)	2.151(3)	S(1)–Ni–S(2)	93.4(1)
Ni–S(2)	2.160(3)	S(6)–Ni–S(7)	93.1(1)
Ni–S(6)	2.158(3)	S(1)–Ni–S(6)	86.1(1)
Ni–S(7)	2.154(3)	S(2)–Ni–S(7)	87.4(1)
S(1)–C(1)	1.72(1)	Ni–S(1)–C(1)	101.6(4)
S(2)–C(2)	1.73(1)	Ni–S(2)–C(2)	102.1(4)
S(3)–C(1)	1.76(1)	Ni–S(6)–C(4)	102.0(4)
S(3)–C(3)	1.73(1)	Ni–S(7)–C(5)	102.7(4)
S(4)–C(2)	1.73(1)		
S(4)–C(3)	1.73(1)	S(1)–C(1)–C(2)	122.5(8)
S(5)–C(3)	1.64(1)	S(1)–C(1)–S(3)	121.5(6)
S(6)–C(4)	1.72(1)	C(2)–C(1)–S(3)	115.9(8)
S(7)–C(5)	1.73(1)	S(2)–C(2)–S(4)	123.4(6)
S(8)–C(4)	1.73(1)	S(2)–C(2)–C(1)	120.2(8)
S(8)–C(6)	1.74(1)	S(4)–C(2)–C(1)	116.4(8)
S(9)–C(5)	1.72(1)	C(1)–S(3)–C(3)	96.9(5)
S(9)–C(6)	1.74(1)	C(2)–S(4)–C(3)	97.8(5)
S(10)–C(6)	1.62(1)	S(3)–C(3)–S(4)	112.9(7)
C(1)–C(2)	1.35(1)	S(3)–C(3)–S(5)	124.3(7)
C(4)–C(5)	1.35(1)	S(4)–C(3)–S(5)	122.8(7)
		S(6)–C(4)–S(8)	122.0(6)
		S(6)–C(4)–C(5)	121.9(8)
		C(5)–C(4)–S(8)	116.1(8)
		S(7)–C(5)–S(9)	123.6(6)
		S(7)–C(5)–C(4)	120.1(8)
		C(4)–C(5)–S(9)	116.2(8)
		C(4)–S(8)–C(6)	98.0(5)
		C(5)–S(9)–C(6)	98.2(5)
		S(8)–C(6)–S(9)	111.4(6)
		S(8)–C(6)–S(10)	124.7(6)
		S(9)–C(6)–S(10)	123.8(7)

The most significant differences between the Ni(II) and the Ni(III) complexes are found for the Ni–S bond distances. In the $Ni^{II}(C_3S_5)_2^{2-}$ complex, these distances were found to be 2.221(4) and 2.211(4) Å,[2] while the average value in $Ni^{III}(C_3S_5)_2^-$ is 2.156(3) Å (*cf.* Table 2). This difference in ionic radius of Ni shows that the redox process within the nickel-dithiolene complexes has taken place at the central nickel atom. The C–S and the C–C bond lengths are of comparable magnitudes in the two complexes. The C(3)–S(5) and C(6)–S(10) distances of 1.64 and 1.62 Å are slightly shorter than the corresponding value in the $Ni^{II}(C_3S_5)_2^{2-}$ ion, being 1.68 Å, *i.e.* showing more double bond character in the oxidized form. The ring systems have a high degree of electron delocalization in both complexes, the C–S and C–C bond lengths being intermediate between double and single bond values. The previous structure determination showed that the $Ni^{II}(C_3S_5)_2^{2-}$ ion is planar,[2] while the planes containing Ni, S(1)–S(5), C(1)–C(3) and Ni, S(6)–S(10), C(4)–C(6), respectively, in the $Ni^{III}(C_3S_5)_2^-$ ion have an inclination of 6.1°. Normally, MS_4 complexes should be planar for a d^8 configuration of M, and the present deviation may be due to packing effects.

The bond distances and angles within the tetrabutylammonium ion have normal values.

1. Steimecke, G., Sieler, J., Kirmse, R. and Hoyer, E. *Phosphorus Sulfur 7* (1979) 49.
2. Sjölin, L., Lindqvist, O., Sieler, J., Steimecke, G. and Hoyer, E. *Acta Chem. Scand. A 33* (1979) 445.
3. Lehmann, M. S. and Larsen, F. K. *Acta Crystallogr. A 30* (1974) 580.
4. Lindqvist, O. and Ljungström, E. *J. Appl. Crystallogr. 12* (1979) 134.
5. Sjölin, L. *Thesis*, University of Göteborg, Göteborg 1979.
6. Mazid, M. A., Razi, T. and Sadler, P. J. *Inorg. Chem. 20* (1981) 2872.

Received June 29, 1982.

Polymorphism in $IrSi_3$

INGVAR ENGSTRÖM and ERIK ZDANSKY

Institute of Chemistry, University of Uppsala, Box 531, S-751 21 Uppsala, Sweden

The iridium – silicon system has earlier been studied by Finnie,[1] Bhan and Schubert [2] and Engström and Zackrisson.[3,4] Finnie found a hexagonal compound $IrSi_{3\pm0.5}$, the structure of which was proposed to be of the *anti*-Na_3As-type. However, it was pointed out by Finnie and later by Pearson [5] that the *c*/*a*-ratio deviated considerably from what could be expected for an *anti*-Na_3As-type compound.

A single-crystal study of $IrSi_3$ by White and Hockings [6] showed that the compound was hexagonal, but the atomic arrangement did not correspond to the *anti*-Na_3As-type. The Si–Si-distances found were much shorter than those in other platinum-metal silicides;[3] the proposed structure is therefore probably only an approximative description of the real atomic arrangement.

The present paper describes an X-ray powder characterization of two new phases closely related to the hexagonal $IrSi_{\sim3}$ discussed above [here denoted $IrSi_{\sim3}(h)$].

Experimental. Polycrystalline samples were made by arc-melting iridium sponge (Specpure J & M) and silicon powder (3N); unfortunately, it has not been possible to obtain single crystals. They were then heat-treated in evacuated silica tubes at various temperatures and quenched. The compositions of the samples given below are nominal.

X-Ray powder photographs were taken with Guinier-Hägg cameras (diam. = 100 mm) using $CuK\alpha_1$- ($\lambda = 1.540589$ Å) or $CrK\alpha_1$-radiation ($\lambda = 2.289753$ Å). Silicon was used as an internal calibration standard ($a = 5.431065$ Å). Some investigations were also made using the high-temperature Guinier-Hägg camera described in Ref. 7. Intensities were measured using a film-scanner. The powder data presented in Tables 1 and 2 were

Table 1. X-Ray diffraction powder pattern of the orthorhombic modification of $IrSi_{\sim3}$.

hkl	d_{obs} (Å)	Q_{obs} (Å^{-2})	Q_{calc} (Å^{-2})	I_{obs}
200	3.782	.06992	.06992	18
110	3.769	.07038	.07040	16
002	3.312	.09114	.09117	30
201	3.284	.09272	.09272	100
111	3.276	.09318	.09320	100
202	2.492	.16110	.16109	45
112	2.488	.16155	.16157	40
310	2.181	.21023	.21025	30
020	2.174	.21169	.21169	15
203 / 113	1.906	.27530	.27505 / .27553	80
400	1.891	.27961	.27970	vw[a]
220	1.884	.28157	.28162	10
312	1.822	.30141	.30142	70
401 / 022	1.817	.30276	.30249 / .30286	45
221	1.812	.30448	.30441	45
004	1.656	.36479	.36467	vw[a]
402	1.641	.37126	.37086	vw[a]
222	overlap with Si-line		.37278	vw[a]

[a] Non-measurable intensity.

Table 2. X-Ray diffraction powder pattern of the monoclinic modification of $IrSi_{\sim3}$.

hkl	d_{obs} (Å)	Q_{obs} (Å^{-2})	Q_{calc} (Å^{-2})	I_{obs}
200	3.848	.06753	.06756	10
110	3.806	.06904	.06909	18
$\bar{2}01$	3.358	.08869	.08870	30
$\bar{1}11$	3.310	.09130	.09133	55
201	3.277	.09314	.09312	
002 / 111	3.270	.09349	.09340 / .09354	100
$\bar{2}02$	2.528	.15647	.15654	2
$\bar{1}12$	2.498	.16025	.16028	10
112	2.464	.16468	.16470	14
202	2.459	.16535	.16538	6
310	2.213	.20418	.20421	25
020	2.188	.20881	.20879	14
400	1.924	.27026	.27024	16
$\bar{1}13$ / 220	1.903	.27603	.27593 / .27635	30
113	1.881	.28258	.28256	20
$\bar{2}03$	1.875	.28437	.28434	8
$\bar{4}01$	1.860	.28920	.28917	10
$\bar{3}12$	1.854	.29101	.29098	25
$\bar{2}21$	1.834	.29737	.29749	35
401	1.832	.29795	.29801	
221 / 022	1.820	.30202	.30191 / .30219	45
$\bar{3}12$	1.813	.30426	.30424	25
$\bar{4}02$	1.680	.35436	.35480	vw[a]
$\bar{2}22$	1.655	.36513	.36534	vw[a]
402			.37248	
004	1.635	.37393	.37360	vw[a]
222			.37417	

[a] Non-measurable intensity.

0302-4377/82/100857-02$02.50

Table 3. Unit cell dimensions of $IrSi_{\sim 3}$-polymorphs (in Å and degr.).

	Unit cell	$a/\sqrt{3}b$	γ_P	V
$IrSi_{\sim 3}(m)$	$a=7.6976(3)$ $b=4.3770(3)$ $c=6.5467(4)$ $\beta=91.594(4)$	1.015	120.75	220.5
$IrSi_{\sim 3}(o)$	$a=7.5634(11)$ $b=4.3469(2)$ $c=6.6238(10)$	1.0046	120.23	217.8
$IrSi_{\sim 3}(h)$[a]	$a=7.5410(16)$ $b=4.3538(9)$ $c=6.6277(15)$	1	120	217.6

[a] Unit cell dimensions from Ref. 4 transformed to an *ortho*-hexagonal unit cell.

obtained from investigations with $CrK\alpha_1$-radiation. Least-squares refinements of unit cell dimensions were performed with the computer program CELNE.[8]

Phase-analytical results. In a sample of composition $Ir_{23}Si_{77}$ (*i.e.* 23 at % Ir), silicon was found as well as $IrSi_{\sim 3}$; and in a sample of composition $Ir_{30.5}Si_{69.5}$ a more Ir-rich phase was found as well as $IrSi_{\sim 3}$. A sample of composition $Ir_{26}Si_{74}$ consisted almost exclusively of $IrSi_{\sim 3}$.

In arc-melted samples, the $IrSi_{\sim 3}$ phase was found to be orthorhombic, $IrSi_{\sim 3}(o)$ but, after heat-treatment for one week at 900 °C, it had transformed to monoclinic, $IrSi_{\sim 3}(m)$. The phase transition could be reversed by a subsequent heat-treatment at 1000 °C. The phase transition could also be confirmed by an investigation of the sample in a high-temperature X-ray camera. The existence of the hexagonal form, $IrSi_{\sim 3}(h)$, could not be confirmed by this investigation, which was confined to the temperature region 900 – 1000 °C.

The unit cell dimensions (Table 3) of $IrSi_{\sim 3}(o)$ are very close to those of $IrSi_{\sim 3}(h)$ (ortho-hexagonal unit cell); the latter are also cited [4] for comparison. The unit cell dimensions of the monoclinic form deviate slightly more from those of $IrSi_{\sim 3}(h)$. The deviation from the hexagonal symmetry can also be illustrated by the ratio $a/\sqrt{3}b$ and $\gamma_P = 2\text{arctg}(a/b)$, which is the γ-angle of the primitive cell. These two quantities given in Table 3 are, of course, interrelated.

The unit cell dimensions of the monoclinic modification were determined from a sample which was arc-melted and heat-treated for one week at 900 °C. The orthorhombic unit cell was determined from an arc-melted sample. The diffraction photographs were taken with $CrK\alpha_1$-radiation.

Both polymorphs of $IrSi_{\sim 3}$ show *C*-centering extinctions, as could be expected for *pseudo*-hexagonal phases. The observed *Q*-values for the powder patterns are given in Tables 1 and 2. In the least-squares refinement of the cell dimensions the reflections were given individual weights between 0 and 1 depending on the quality of the diffraction lines and the degree of overlap.

The figures of merit were calculated according to the rules in Ref. 9. For the powder diffraction data in Table 1 the result was $M_{17}=89$ ($F_{17}=88$) and for the data in Table 2 the result was $M_{20}=82$ ($F_{25}=87$). The *C*-centering, discussed above, was taken into account when the figures of merit were calculated. The high numerical values of the figures indicate that the indexing and thus the unit cell dimensions are reliable.

Acknowledgements. The authors thank Prof. S. Rundqvist for the facilities put at their disposal. One of the authors (E. Zdansky) also wishes to thank Docent T. Lundström and Dr. N.-O. Ersson for valuable advice during the work. Financial support from the Swedish Natural Science Research Council is gratefully acknowledged.

1. Finnie, L. N. *J. Less Common Met. 4* (1962) 24.
2. Bhan, S. and Schubert, K. *Z. Metallkd. 51* (1960) 327.
3. Engström, I. *Structural Chemistry of Platinum Metal Silicides, Acta Univ. Ups. 156* (1970).
4. Engström, I. and Zackrisson, F. *Acta Chem. Scand. 24* (1970) 2109.
5. Pearson, W. B. *A Handbook of Lattice Spacing and Structures of Metals and Alloys 2*, Pergamon, New York 1967, p. 1093.
6. White, J. G. and Hockings, E. F. *Inorg. Chem. 10* (1971) 1934.
7. Hägg, G., Ersson, N.-O., Rudenholm, G. and Sellberg, B. *J. Appl. Crystallogr. 12* (1979) 221.
8. Ersson, N.-O. Institute of Chemistry, University of Uppsala, Uppsala, Sweden. *Unpublished.*
9. Smith, G. S. and Snyder, R. L. *J. Appl. Crystallogr. 12* (1979) 60.

Received April 30, 1982.

Magnetic Properties of the Chromium(III) Dimer $\Delta(-)_{546}$-Di-μ-hydroxo(*S,S,S,S*)-tetrakis(L-prolinato)dichromium(III) Tetrahydrate

SOLVEIG KALLESØE and ERIK PEDERSEN

Chemistry Department I (Inorganic Chemistry), University of Copenhagen, H. C. Ørsted Institute, Universitetsparken 5, DK-2100 Copenhagen Ø, Denmark

The magnetic properties of dimeric chromium(III) complexes of the type $[CrL_m(OR)]_2^{n+}$ where L is a mono-, bi-, tri-, or tetradentate ligand and R is a hydrogen atom or an alkyl group have recently been intensely studied.[1-9] A model (the GHP model) has been proposed[1] which quantitatively relates the magnitude of the superexchange coupling with the Cr–O–Cr bridging angle, ϕ, the Cr–O bond length, r, and the dihedral angle between the bridging plane and the OR vector of the bridging group, θ. According to this model the exchange parameter J in the Hamiltonian, eqn. (1), is given as competing antiferro- and ferromagnetic contributions according to eqn. (2), where the values of the constants a, b, and c have been determined from a set of experiments based on magnetic and structural data for fifteen dimers.

$$\mathcal{H} = JS_1S_2 \tag{1}$$

$$J = J_{af} - J_f = e^{-a(r-1.8)} \cdot [b\cos^4\theta / \left\{1 - \sin^2\theta / \tan^2\left(\frac{\phi}{2}\right)\right\} - c\sin^2\phi / \{1-\cos\phi\}^2] \tag{2}$$

The structural parameters for one of the isomers of the title complex $[Cr(L\text{-pro})_2OH]_2 \cdot 4\,H_2O$ were recently determined,[2] and we thus have the possibility for another control of the GHP model since all the values of r, θ, and ϕ were determined.

Another set of data may be available for a corresponding bis(ethylenediamine-*N,N'*-diacetato) complex whose structural[3] and magnetic parameters[4] have recently been determined. The two samples investigated[3,4] were not shown to be identical and, since our repeated preparations inevitably gave an inseparable mixture of several of the many possible isomers, we excluded these data from further consideration.

The title complex was prepared according to the literature method.[2] $[Cr(C_4H_8NCOO)_2OH]_2 \cdot 4H_2O$ was analyzed for Cr, C, H, N. The product was also analyzed by Guinier X-ray technique. Fifteen lines in the range $\sin^2(\theta) \leq 0.034$ (θ is in this case the diffraction angle) for copper radiation were measured, and their positions were found to be in complete agreement with the structural data available for one of the many isomers possible.[2]

The magnetic susceptibility of powdered samples

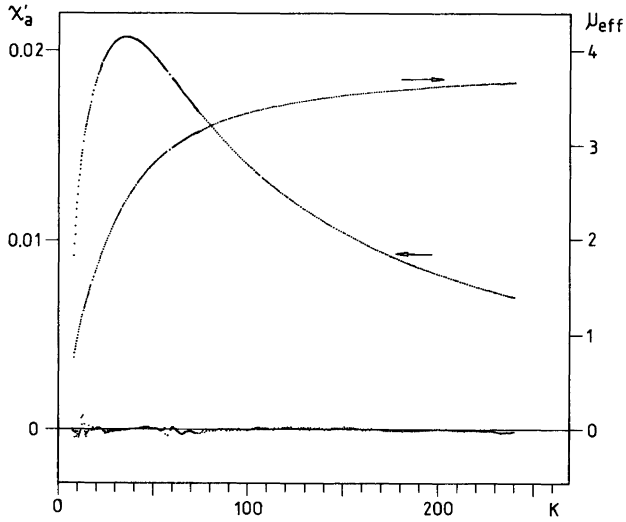

Fig. 1. Magnetic susceptibility (left scale in c.g.s. units) and effective magnetic moment (right scale in Bohr magnetons) of $\Delta(-)_{546}$-di-μ-hydroxo(*S,S,S,S*)tetrakis(L-prolinato)dichromium(III) tetrahydrate. The lower set of points indicate $(\chi_{obs} - \chi_{calc.}) \times 50$ as obtained from fitting of the results to model 3, *cf.* Table 1.

0302-4377/82/100859-02$02.50

was measured by the Faraday method at a field of 12.000 Ø in the temperature range 4–300 K. A typical result is shown in Fig. 1. The susceptibility data were fitted by a least squares technique to the expression (3), where E_i are the energies of the 16 components of the ground state manifold. Details of the fitting procedure are found elsewhere.[5] The fitting was performed by application of three different models for the exchange Hamiltonian. Model 1 assumed the simple Heisenberg Hamiltonian eqn. (1). Model 2 included a biquadratic exchange term according to eqn. (4). Finally Model 3 assumed independent energies of the triplet, quintet and septet states.

$$\chi'_A = -\frac{N}{H}\frac{\sum_i \left(\frac{\partial E_i}{\partial H}\right) e^{-E_i/kT}}{\sum_i e^{-E_i/kT}} \quad (3)$$

$$\mathcal{H} = JS_1S_2 + j(S_1S_2)^2 \quad (4)$$

Some of the results of the data fittings are displayed in Table 1. It is obvious that the data are not sufficiently well described by model 1. Inclusion of the biquadratic exchange term (model 2) markedly improved the fit, lowering the variance per degree of freedom (*var/f*) from 17 to 1.6. Moreover inclusion of the additional variable in model 3 led to a further but small improvement; *var/f* was reduced to 1.2. It is seen from Table 1, however, that the Landé rule for splitting of the ground state manifold as implied by eqn. (1) is followed rather closely, the singlet–triplet separation being 15 cm^{-1}.

The structural parameters for the bridging system were derived from the crystallographic data available.[2] Since the space group is $P2_12_12_1$ and Z = 4 no symmetry requirements are imposed on the molecules, and in the comparison with the theoretical expresseion eqn. (2) average values of r, θ and ϕ were used. This is reasonable because the deviations are small. The values used were r = Cr–O = 1.948(15) Å, ϕ = Cr–O–Cr = 100.0(6)°, and θ = 34°. The out-of-plane angle, θ, was calculated from the positional parameters *via* the angles between the O–O vector and the O–H vectors. The estimated standard deviations for r and ϕ are two times those estimated by the crystallographers.[2] The standard deviation for θ was estimated to be 5°.

Table 1. Parameters derived from magnetic susceptibility data for $[Cr(L\text{-pro})_2OH]_2.4H_2O$.

	Model 1	Model 2	Model 3
J(cm^{-1})	14.53(5)	13.29(2)	–
j(cm^{-1})	–	−0.41(1)	–
$E(1)$[a](cm^{-1})	14.53(5)[b]	15.96(3)[b]	15.06(11)
$E(2)$(cm^{-1})	43.5(2)[b]	45.4(1)[b]	45.01(9)
$E(3)$(cm^{-1})	87.2(4)[b]	83.4(2)[b]	81.6(2)
g	2.023(3)	1.977(1)	1.970(1)
var/f[c]	17.3	1.60	1.27
f	425	424	423

[a] $E(1-3)$ refer to triplet, quintet and septet energies. [b] Values calculated from J and j for comparison with model 3. [c] Variance per degree of freedom.

These crystallographic results, together with the estimated triplet energy of 15.1(1) cm^{-1}, were used for an expansion of the data set already used in fitting eqn. (2). The calculated values a = 19(1) $Å^{-1}$, b = 611(38) cm^{-1} and c = 172(54) cm^{-1} were found to be identical to their old values.[1] The calculated value of the triplet energy of the title complex was $J = J_{af} - J_f = 26 - 7 = 19$ cm^{-1} in excellent agreement with the experimental result considering the estimated standard deviation (e.s.d) of 8 cm^{-1}. The main contribution to this rather large e.s.d. is related to the e.s.d.'s of r and θ.

These results reconfirm the validity of the GHP exchange model[1] as expressed in eqn. (2) and illustrate that the exhange parameter in this case is rather small compared to other di-μ-hydroxo complexes, with similar r values as expected when the hydrogen atoms of the μ-hydroxo groups are displaced so much out of the bridging plane.

Acknowledgement. We are grateful to the Danish Natural Science Research Council for grants Nos. 511-742, 511-3993 and 511-10516.

1. Glerup, J., Hodgson, D. J. and Pedersen, E. *Acta Chem. Scand. A 37* (1983). *Submitted*, and references therein.
2. Oki, H. and Yoneda, H. *Inorg. Chem. 20* (1981) 3875.
3. Srdanov, G., Herak, R., Radanović, D. J. and Veselinović, D. S. *Inorg. Chim. Acta 38* (1980) 37.
4. Hatfield, W. E., MacDougall, J. J. and Shepherd, R. E. *Inorg. Chem. 20* (1981) 4216.
5. Michelsen, K. and Pedersen, E. *Acta Chem. Scand. A 32* (1978) 847.
6. Decurtins, S., Güdel, H. U. and Pfeuti, A. *Inorg. Chem. 21* (1982) 1101.
7. Scaringe, R. P., Hodgson, D. J. and Hatfield, W. E. *Transition Met. Chem. 6* (1981) 340.
8. Michelsen, K., Pedersen, E., Wilson, S. R. and Hodgson, D. J. *Inorg. Chim. Acta 63* (1982). *In press.*
9. Michelsen, K. and Pedersen, E. *Acta Chem. Scand. A 37* (1983). *In press.*

Received July 12, 1982.